Modern Acoustics and Signal Processing

Antoine Chaigne
Jean Kergomard

Acoustics of Musical Instruments

Foreword by
Murray Campbell

Modern Acoustics and Signal Processing

More information about this series at http://www.springer.com/series/3754

The ASA Press

The ASA Press imprint represents a collaboration between the Acoustical Society of America and Springer dedicated to encouraging the publication of important new books in acoustics. Published titles are intended to reflect the full range of research in acoustics. ASA Press books can include all types of books published by Springer and may appear in any appropriate Springer book series.

ASA Press

Antoine Chaigne • Jean Kergomard

Acoustics of Musical Instruments

Foreword by Murray Campbell

ASA Press

Springer

Antoine Chaigne
Institute of Music Acoustics
University of Music and Performing Arts Vienna (MDW)
Vienna, Austria

Jean Kergomard
CNRS Laboratoire de Mécanique et d'Acoustique (LMA)
Marseille, France

Original edition: Acoustique des instruments de musique, Second Edition

ISSN 2364-4915 ISSN 2364-4923 (electronic)
Modern Acoustics and Signal Processing
ISBN 978-1-4939-3677-9 ISBN 978-1-4939-3679-3 (eBook)
DOI 10.1007/978-1-4939-3679-3

Library of Congress Control Number: 2016933347

Printed on acid-free paper

This Springer imprint is published by Springer Nature
The registered company is Springer-Verlag New York

Acoustical Society of America

The mission of the **Acoustical Society of America** (www.acousticalsociety.org) is to increase and diffuse the knowledge of acoustics and promote its practical applications. The ASA is recognized as the world's premier international scientific society in acoustics, and counts among its more than 7,000 members, professionals in the fields of bioacoustics, engineering, architecture, speech, music, oceanography, signal processing, sound and vibration, and noise control.

Since its first meeting in 1929, The Acoustical Society of America has enjoyed a healthy growth in membership and in stature. The present membership of approximately 7,500 includes leaders in acoustics in the United States of America and other countries. The Society has attracted members from various fields related to sound including engineering, physics, oceanography, life sciences, noise and noise control, architectural acoustics; psychological and physiological acoustics; applied acoustics; music and musical instruments; speech communication; ultrasonics, radiation, and scattering; mechanical vibrations and shock; underwater sound; aeroacoustics; macrosonics; acoustical signal processing; bioacoustics; and many more topics.

To assure adequate attention to these separate fields and to new ones that may develop, the Society establishes technical committees and technical groups charged with keeping abreast of developments and needs of the membership in their specialized fields. This diversity and the opportunity it provides for interchange of knowledge and points of view has become one of the strengths of the Society.

The Society's publishing program has historically included the *Journal of the Acoustical Society of America,* the magazine *Acoustics Today,* a newsletter, and various books authored by its members across the many topical areas of acoustics. In addition, ASA members are involved in the development of acoustical standards concerned with terminology, measurement procedures, and criteria for determining the effects of noise and vibration.

Series Preface for Modern Acoustics and Signal Processing

In the popular mind, the term "acoustics" refers to the properties of a room or other environment—the acoustics of a room are good or the acoustics are bad. But as understood in the professional acoustical societies of the world, such as the highly influential Acoustical Society of America, the concept of acoustics is much broader. Of course, it is concerned with the acoustical properties of concert halls, classrooms, offices, and factories—a topic generally known as architectural acoustics, but it is also concerned with vibrations and waves too high or too low to be audible. Acousticians employ ultrasound in probing the properties of materials, or in medicine for imaging, diagnosis, therapy, and surgery. Acoustics includes infrasound—the wind-driven motions of skyscrapers, the vibrations of the earth, and the macroscopic dynamics of the sun.

Acoustics studies the interaction of waves with structures, from the detection of submarines in the sea to the buffeting of spacecraft. The scope of acoustics ranges from the electronic recording of rock and roll and the control of noise in our environments to the inhomogeneous distribution of matter in the cosmos.

Acoustics extends to the production and reception of speech and to the songs of humans and animals. It is in music, from the generation of sounds by musical instruments to the emotional response of listeners. Along this path, acoustics encounters the complex processing in the auditory nervous system, its anatomy, genetics, and physiology—perception and behavior of living things.

Acoustics is a practical science, and modern acoustics is so tightly coupled to digital signal processing that the two fields have become inseparable. Signal processing is not only an indispensable tool for synthesis and analysis but it also informs many of our most fundamental models about how acoustical communication systems work.

Given the importance of acoustics to modern science, industry, and human welfare Springer presents this series of scientific literature, entitled Modern Acoustics and Signal Processing. This series of monographs and reference books is intended to cover all areas of today's acoustics as an interdisciplinary field. We expect that scientists, engineers, and graduate students will find the books in this series useful in their research, teaching, and studies.

William M. Hartmann

Foreword

For more than 40,000 years, human beings have been making and playing musical instruments. Although Greek philosophers of the Pythagorean school carried out pioneering studies on stringed instruments, it is only in the last few centuries that advances in physics and mathematics have made it possible to develop a reasonably comprehensive scientific understanding of how musical instruments function. By the mid-twentieth century, the basic principles of classical mechanics, fluid dynamics and acoustics had been successfully applied to explain many aspects of the behaviour of musical instruments. In recent decades, however, there has been a remarkable acceleration in the scope and pace of research in musical acoustics, leading to fresh insights into musically important features of instrumental behaviour which are not captured by simplified models. Experimental studies have benefited from the ready availability of highly sophisticated instrumentation devices, while the rapid growth in computational power has made numerical modelling an increasingly important resource. In parallel with these technological advances, there have been theoretical developments which have clarified the often complex physical processes whose interaction is responsible for the generation of sound in musical instruments.

The time is therefore ripe for a textbook which provides a systematic presentation of the current state of our understanding of the physics of musical instruments. Antoine Chaigne and Jean Kergomard are the ideal authors to present such an overview, since each has an outstanding record of research leadership and publication in this field. Where appropriate they have invited authoritative contributions from other experts, including Xavier Boutillon, Jean-Pierre Dalmont, Benoit Fabre, Joël Gilbert and Cyril Touzé. A notable feature of this book, which makes it particularly valuable as a textbook for advanced students, is its systematic exposition of the mathematical treatments, with full derivations of the crucial equations. This provides an excellent pedagogical introduction to the research literature, for which extensive references are given. The book is structured to facilitate a gradual unfolding of different formalisms. Modal theory, for example, is introduced in Chap. 3 for the case of undamped normal modes; complex modes which include

dissipation are discussed in Chap. 5; and the increasingly important theory of nonlinear modes is presented in Chap. 8. In each case the relevance to musical examples is made clear.

This book will undoubtedly become the standard reference text for postgraduate students and teachers of musical instrument acoustics. The mathematical level required to engage fully with the theoretical derivations is that of an undergraduate degree in physics, mathematics or engineering. Readers without a formal scientific education will also gain many fascinating and important insights, since the mathematical treatments are usually introduced and framed by non-technical discussions and explanations. The authors display a deep understanding of the musical significance of the scientific discussions and are able to convey this in a language which is readily accessible to performers and musical instrument makers. There are many aspects of the sound production and playability of instruments which are musically important, but which depend on subtle details of the underlying physics. The study of such subtleties has been a hallmark of much recent work in musical instrument acoustics, and this textbook leads the reader from basic physical principles to the current research frontier with a unique and admirable combination of scientific rigour and musical sensibility.

Edinburgh, UK
1 February 2016

Murray Campbell

Preface

Objectives of the Book

This book is devoted to the acoustics of musical instruments. Its prime aim is to highlight the physical principles that govern the production and radiation of sound by these complex sources. It is the result of several years of work which would not have been possible without the active and enthusiastic contribution of colleagues to whom we wish to extend our sincere thanks and gratitude. We should also mention that Chap. 10 on the flute was written by Benoît Fabre and Chap. 11 on the violin by Xavier Boutillon. Jean-Pierre Dalmont, Joël Gilbert and Cyril Touzé wrote some paragraphs in the third part.

The book is meant primarily as a textbook for students at master's and doctorate levels. This is the reason why it includes a large number of significant equations where the mathematical derivations are presented in detail. In addition, we thought that it was necessary to account for the most recent results of research in musical acoustics. Therefore, a large number of references can be found at the end of each chapter. N. Fletcher and T. Rossing's famous book *Physics of Musical Instruments (Springer)* was published in 1991, and ever since this field of research has benefitted from plenty of new discoveries. One can cite, for example, the essential contribution of fluid dynamics and aeroacoustics for the comprehension of wind instruments, the interest of nonlinear structural models for describing the behaviour of cymbals and gongs and, more generally, the application of the theory of dynamical systems to every class of instruments.

In fact, this book is intended not only for students but also to researchers, engineers and other physicists with a strong interest in music. We also hope that musicians, instrument makers and music lovers who wish to acquire some basic knowledge on the physics of musical instruments will be able to read it profitably, even if they cannot follow all mathematical aspects in detail. In this view, the links between physical phenomena, instrument making and playing are explained as clearly as possible.

How much remains unknown in the realm of musical instruments? Is it worth putting so much attention to the instrument itself, given the somewhat fundamental role of the player in the subtleties of musical sound? Our belief is that a number of phenomena still remain to be elucidated with regard to the production and radiation of sound in musical instruments, despite the contribution of famous acousticians over the last four centuries. It is remarkably difficult to find the physical basis of musical instruments in a single book, due to the great variety of the subjects involved.

Basically, all musical instruments are governed by fundamental laws of fluid and solid mechanics, including acoustics and vibrations. Today, the main outlines of these laws are well known. However, musical instruments are very subtle sound sources that need to be described with great accuracy, in view of the ability of the players and sensitivity of the human ear. In the case of a violin, for example, the sound results from continuous friction of a bow on a stretched string, one end of which is connected to a bridge attached to the soundboard. In Chap. 11, we will see that even the melding properties of the rosin play an important role in the origin of the oscillations of the string and, in turn, of the violin sound.

Two main aspects must be considered with regard to the perception of a musical instrument. First, we need to understand the causes that influence the perception of the instrument by the player: the so-called playability of the instrument. Second, we want to identify the factors influencing the perception of sound by the listeners, including the player, which can be referred to as "sound quality". Today, the science has not found an entirely satisfying answer to these questions. In this context, this book attempts to review and to describe the physical phenomena related to these problems. The auditory perception is sometimes mentioned in this book, and this seems to be natural in view of the normal function of an instrument. However, its prime objective is to analyse the instrument and its playing from the point of view of the physics.

Contents of the Book

In the first part "Basic Equations and Oscillators", the main continuous models of the elementary constitutive parts of the instruments are described: strings, bars, plates, tubes, etc. In addition, models of the excitation mechanisms (finger, mallet, etc.) are presented, which are specific to musical instruments. The single degree of freedom (SDOF) oscillator is presented in detail in the second chapter, since its properties are essential and serve as references for the rest of the book.

The fundamental concepts of sound waves and modes of vibrations are presented in the second part "Waves and Modes", starting from the simple case of 1-D waves. The concepts are illustrated by examples which are directly linked to musical instruments: plucked string, wind and percussive instruments. Emphasis is put on the equivalences between temporal and modal representations, since the transition from time to modal domain is of high interest in musical acoustics. For pedagogical

reasons, dissipation phenomena are ignored in this presentation. However, Chap. 5 is entirely devoted to these mechanisms. This chapter is important, since decay and damping due to losses are essential parameters of musical sounds. In this chapter, the main mechanisms of dissipation both in the air and in the structural components of the instruments are described. As a consequence, it is shown how the properties of waves and modes are modified, due to damping. The concept of *complex modes* is introduced, which is relatively new in the context of musical acoustics. This part ends with a description of some coupling situations in string instruments (Chap. 6), followed by the presentation of the main characteristics of wind instrument tubes (variable section, discontinuities, bells, toneholes, etc.) which are essential for understanding their functioning (Chap. 7). The general idea of this part is thus to model complete instruments starting from basic concepts with progressive refinements.

These first two parts belong to the fields of linear acoustics and linear vibrations. The basic results are presented within the framework of musical instruments. However, some presentations are relatively original and could probably be used in other contexts.

In the real world, musical instruments are most often governed by nonlinear phenomena, and this might explain why numerous physicists today are interested in their behaviour. For percussive instruments such as gongs and cymbals, the nonlinearity is due to the large amplitude of the motion following the impact. This forms the heart of Chap. 8 whose goal is also to introduce the main models and methods applicable to nonlinear oscillations. On the other hand, a nonlinear element is mandatory for bowed strings and wind instruments, since it is necessary here to convert a continuous (or slowly varying) source of energy, such as blowing pressure or bow velocity, into a rapidly oscillating acoustic source. Three chapters are devoted to the corresponding families of instruments: reed instruments (including brass instruments), flute-like instruments and bowed string instruments.

Obviously, the ultimate purpose of musical instruments is to radiate sound, and thus, Part IV is entirely dedicated to radiation. In fact, references to radiation can be found in the previous parts, but, in most cases, radiation does not influence the production of sound significantly which, therefore, authorizes such an apparently paradoxical splitting.

An extensive list of references can be found in the literature with regard to sound radiation, particularly within the context of noise reduction: in this case, most applications have the objective to reduce sound power. For musical instruments, the goal is to enhance the radiated sound though without affecting the tone quality and the function of the instrument. It will be seen in Chap. 13, for example, that it is not always appropriate to increase the transfer of energy from the strings to the soundboard in a piano, since it causes at the same time a decrease in tone duration, which is also a determining quality of piano sound. In order to be able to explain numerous examples such as this one, we believe that it is worth recalling the main results of radiation theory, through the viewpoint of musical acoustics. As a consequence, Part IV starts with the description of elementary sound sources,

continues with the fundamentals of structural acoustics with applications to stringed and percussive instruments and ends with more complex systems involving fluid-structure interaction.

Organization of the Book

One main feature of the book lies in the progressive description from elementary systems to complete instruments. Except for some particular cases (reed instruments, flute, violin), the chapters do not refer explicitly to a given family of instruments. Our strategy consists rather in grouping the presentation of concepts and results applicable to all instruments whenever possible. This is particularly true for the first two parts of the book. In the first chapter, for example, emphasis is put on the analogies between strings and pipes.

The index has been built so as to identify the sections dealing with one particular instrument. Thus, the reader interested in the acoustics of the piano, for example, will find information on strings in Chap. 3 and on damping in Chap. 5. A detailed discussion on coupled piano strings follows in Chap. 6 and considerations on piano radiation in Chap. 13. Similarly, the reader interested in the clarinet will benefit from reading Chaps. 4, 7 and 9.

Due to constraints of size, we also had to make choices, and thus this book does not pretend to be exhaustive: the instruments are rather described in terms of physical principles and in great detail. Some important instruments, such as the singing voice, are not presented at all. The book is also restricted to "acoustic" instruments, as opposed to "electronic" instruments where the sound has an electronic origin and where the reproduction of sound is made through loudspeakers or headphones.

It is our hope that this book will help the reader to get a better understanding of the physical phenomena involved in musical instruments. It is also aimed at illustrating how to take advantage of instrument modelling for practical applications in sound recording and instrument making. During the last 20 years, more and more sophisticated models were used for application in sound synthesis, either for the validation of a physical description or for musical applications, sometimes in conjunction with elaborated signal processing techniques. These sound synthesis applications are probably today one of the key milestones in the recent scientific research on musical instruments.

Acknowledgements

Besides the co-workers mentioned above, many other colleagues provided us with valuable help, either through proofreading or by giving us high-quality figures and illustrations. We wish to thank, in particular, Olivier Thomas, Nicolas Quaegebeur,

Grégoire Derveaux, François Gautier, Vincent Doutaut, Alexandre Garcia, Danielle Ribouillaut, Bruno Marlat, Etienne Balmès, the Company Rythmes et Sons, Mico Hirschberg, Christophe Vergez, Fabrice Silva, Philippe Guillemain, Didier Ferrand, Patrick Sanchez, Thierry Voinier, Thomas Guimezanes, Sami Karkar, Franck Laloë, Alain Léger, René Caussé, Joe Wolfe, Michele Ducceschi, Earl Williams, Bill Hartmann, Samy Missoum, Karim Sabra, Dan Russell, David Sharp, Jonathan Kemp, Andrew Norris, Stephen Thompson, Nick Giordano, Murray Campbell, David Wagg, Kerem Ege and Denis Matignon.

We warmly thank James Cottingham and the Acoustical Society of America for their interest in this book. We also wish to acknowledge the following institutions for their support: the Laboratoire de Mécanique et d'Acoustique de Marseille (UPR 7051 CNRS); the Agence Nationale de la Recherche, within the framework of the "CONSONNES" project, that brought up a number of significant results mentioned in this book; and the French Ministère de la Culture et de la Communication.

Vienna, Austria — Antoine Chaigne
Marseille, France — Jean Kergomard
July 2015

Contents

List of Contributors

Xavier Boutillon Laboratory for Solid Mechanics, CNRS and École Polytechnique, Palaiseau, France

Antoine Chaigne Institute of Music Acoustics, University of Music and Performing Arts Vienna (MDW), Vienna, Austria

Jean-Pierre Dalmont Laboratoire d'Acoustique de l'Université du Maine (LAUM), Le Mans, France

Benoît Fabre Laboratoire LAM – Lutherie Acoustique Musique, and IJLRA – Institut Jean le Rond d'Alembert, Université Pierre-et-Marie-Curie, CNRS, ministère de la culture et de la communication, Paris, France

Joël Gilbert Laboratoire d'Acoustique de l'Université du Maine (LAUM), Le Mans, France

Jean Kergomard CNRS Laboratoire de Mecanique et d'Acoustique (LMA), Marseille, France

Cyril Touzé Institute of Mechanical Sciences and Industrial Applications (IMSIA), ENSTA ParisTech, Université Paris-Saclay, Palaiseau, France

Part I
Basic Equations and Oscillators

Basic differential and partial differential equations of current use in vibrations and acoustics of musical instruments are reviewed in this first part. The main source terms of the instruments are also presented. The analogies between strings and tubes are summarized in Table 1.1, which should be of help throughout the book. Chapter 2 is devoted to the presentation of free and forced oscillations of the Single Degree Of Freedom (SDOF) oscillator. This oscillator is the elementary component of the modal decomposition, also used permanently throughout this book.

Chapter 1
Continuous Models

Antoine Chaigne and Jean Kergomard

Abstract The aim of this introductory chapter is to summarize the main mechanical models which describe the physics of musical instruments and of their constitutive parts. These models derive from the general principles of the mechanics of continuous media (solids and fluids). In this framework, the phenomena are described at a scale of the so-called *particle*, or *element*, whose dimensions are infinitesimal in the sense of differential calculus. Particular emphasis is given to the bending of structures and to the equations of acoustic waves in air, because of their relevance in musical acoustics. One section is devoted to the excitation mechanisms of musical instruments. Analogies between vibrations of solids (such as strings) and fluids (in pipes) are underlined. Elementary considerations on the numerical formulation of the models are also given. This chapter should be considered as a summary which contains reference results to help in reading the rest of the book. It focuses on the origin of the equations and on their underlying assumptions, living aside the complete demonstrations.

1.1 Strings, Membranes, Bars, Plates, and Shells

1.1.1 Introduction

In this chapter, we present *linear* models. This means, in particular, that we limit ourselves to the case of *small displacements* (geometric linearity) and to materials whose constitutive stress–strain relations are linear (material linearity).

A. Chaigne (✉)
Institute of Music Acoustics, University of Music and Performing Arts Vienna (MDW), Anton-von-Webern-Platz 1, 1030 Vienna, Austria
e-mail: antchaigne@gmail.com

J. Kergomard
CNRS Laboratoire de Mecanique et d'Acoustique (LMA), 4 impasse Nikola Tesla CS 40006, 13453 Marseille Cedex 13, France
e-mail: kergomard@lma.cnrs-mrs.fr

A. Chaigne, J. Kergomard, *Acoustics of Musical Instruments*, Modern Acoustics and Signal Processing, DOI 10.1007/978-1-4939-3679-3_1

Conversely, in Chap. 8, several examples of nonlinearity will be examined. For the time being, the dissipative phenomena in solids are ignored. Chapter 5 will be specifically devoted to damping.

We study here the class of *elastic* solids. If such a solid is deformed under the effect of a given load, the deformation disappears as the load is gradually removed until the solid returns to its initial state. For example, if we hit the bar of a vibraphone with a soft mallet, and if we touch the bar after a few seconds in order to suppress the sound, we find that the state of the bar is unchanged. However, if a xylophone wooden bar is hit with a hard mallet, irreversible *plastic* deformations may appear locally on the bar. A hard stroke might even break it!

In order to excite the structures used in musical acoustics, it is often necessary to apply a *prestress* to some of them. This is, for example, the case of strings and membranes subjected to a static tension field at rest. A piano (or a guitar) soundboard is also subjected to a strong prestress due to the tension of the strings attached to, or passing over, the bridge (see Fig. 1.1) [7, 40]. The prestress works only if the structure departs from its equilibrium. It is sometimes called *geometric stiffness*.

The dynamics of structures which are vibrating parts of musical instruments are governed by both elasticity and geometric stiffness. If only elasticity is present, we are in the extreme case of bars and plates. Geometric stiffness dominates in the case of strings and membranes. In practice, a structure with zero elasticity can never be found. Systems with geometric stiffness, such as ideal strings and membranes, where the intrinsic elasticity is ignored, should be considered as theoretical limiting cases (see Sect. 1.1.2).

The case of shells is more complex and will be considered separately. This book is limited to the study of thin shallow shells. Such structures are found both in percussion (cymbals, gongs, etc.) and string instruments (soundboard of bowed string instruments, for example). The presence of curvature has several important

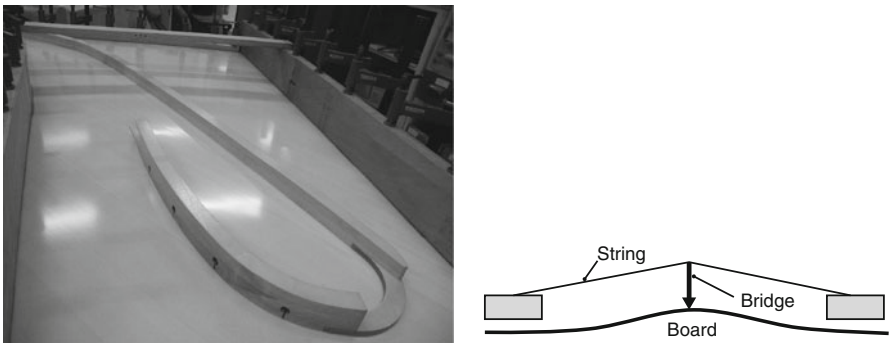

Fig. 1.1 (*Left*) A grand piano soundboard with its bridge (© Pleyel). (*Right*) Simplified diagram of the prestress supported by a piano soundboard. The soundboard is initially curved. Under the influence of string tension, the bridge presses on the soundboard. This transverse force is partially converted into longitudinal stress in the soundboard

effects: change of the radiation properties compared to flat plates (see Chap. 13), increase of the maximum static load supported by the soundboard, easier starting nonlinear behavior for large amplitude of vibration for shells with free edges such as gongs (see Chap. 8).

A common feature between membranes, plates, and thin shells follows from the fact that their models involve only two spatial dimensions. If the vibration wavelength is large compared to the thickness, it is justified to integrate the stress along this dimension and neglect the thickness strain. As a consequence, the "3D" model is reduced to a "2D" one. In addition, to obtain string and bar equations, it is assumed that these structures are *slender*, where one dimension (the length) is large compared to the other two. This leads then to a "1D" model where the integration of the stress is now made along the two dimensions of a cross-section.

1.1.2 Membranes and Strings

Preamble For a complete demonstration of the membrane equation, the reader can consult the literature devoted to the mechanics of continuous media (see [51]). The presentation is limited here to the heterogeneous membrane equation in orthonormal Cartesian coordinates.

We consider an infinitesimal element of membrane with coordinate vector $\mathbf{x}$ and density $\rho(\mathbf{x})$, for which the elastic stiffness is ignored. At equilibrium, the membrane is located in the plane $(\mathbf{e}_x, \mathbf{e}_y)$ and subjected to a tension field. This tension field is described by a symmetrical tensor of order 2

$$\underline{\underline{\tau}} = \begin{bmatrix} \tau_{11} & \tau_{12} \\ \tau_{12} & \tau_{22} \end{bmatrix}, \tag{1.1}$$

where the τ_{ij} are the components of the tensor (see Fig. 1.2). From this tensor, we can derive the tensional forces acting on a membrane elements:

$$\begin{cases} \text{on the surfaces with normal vector oriented along } \mathbf{e}_x : \boldsymbol{\tau}_x = \tau_{11}\mathbf{e}_x + \tau_{21}\mathbf{e}_y, \\ \text{on the surfaces with normal vector oriented along } \mathbf{e}_y : \boldsymbol{\tau}_y = \tau_{12}\mathbf{e}_x + \tau_{22}\mathbf{e}_y, \end{cases} \tag{1.2}$$

A tension field is measured in force per unit length, and its unit is thus in $\mathrm{N\,m^{-1}}$. Integrating this tension along the perimeter of a given surface gives the total external force which is necessary to apply at the periphery to balance the internal tension field.

The off-diagonal tension components have the symmetry property $\tau_{12} = \tau_{21}$ to ensure equilibrium of the moments on the membrane element (reciprocity principle). Each component τ_{ij} is a function of the coordinate vector $\mathbf{x}$. It is assumed that the membrane can move freely along $\mathbf{e}_z$ so that its vertical displacement $\xi(x, y, t)$ at time t is governed by the equilibrium between the inertial forces and the restoring

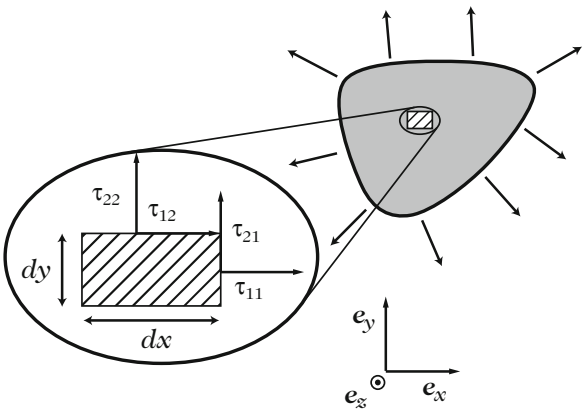

Fig. 1.2 Tension field exerted on a membrane element. $\mathbf{e}_x$, $\mathbf{e}_y$, and $\mathbf{e}_z$ are the unit vectors in Cartesian coordinates

forces due to the tension field. Gravity is ignored. With the assumptions of small displacements, the rotations θ_x and θ_y of the membrane element on both planes $(\mathbf{e}_x, \mathbf{e}_z)$ and $(\mathbf{e}_y, \mathbf{e}_z)$ are given by:

$$\begin{cases} \theta_x \approx \sin\theta_x \approx \tan\theta_x \approx \dfrac{\partial \xi}{\partial x}, \\ \theta_y \approx \sin\theta_y \approx \tan\theta_y \approx \dfrac{\partial \xi}{\partial y}\,. \end{cases} \tag{1.3}$$

Similarly, for any function $G(x, y)$ on the membrane, a first-order expansion yields

$$\begin{cases} G(x+dx, y) = G(x, y) + \dfrac{\partial G}{\partial x} dx, \\ G(x, y+dy) = G(x, y) + \dfrac{\partial G}{\partial y} dy\,. \end{cases} \tag{1.4}$$

Balancing the forces applied on each sides of the element, and projecting them on the vertical axis $\mathbf{e}_z$, we obtain the equation of transverse motion of a heterogeneous membrane:

$$\rho(\mathbf{x}) h \ddot{\xi} = \frac{\partial}{\partial x}\left(\tau_{11}\frac{\partial \xi}{\partial x} + \tau_{12}\frac{\partial \xi}{\partial y}\right) + \frac{\partial}{\partial y}\left(\tau_{12}\frac{\partial \xi}{\partial x} + \tau_{22}\frac{\partial \xi}{\partial y}\right), \tag{1.5}$$

where h is the thickness. Denoting:

$$\mathbf{grad}\xi = \frac{\partial \xi}{\partial x}\mathbf{e}_x + \frac{\partial \xi}{\partial y}\mathbf{e}_y, \tag{1.6}$$

we can write this equation in a more compact form:

$$\rho(\mathbf{x})h\ddot{\xi} = \text{div}\left(\underline{\underline{\tau}}.\mathbf{grad}\xi\right) . \tag{1.7}$$

If the membrane is also subjected to external pressure forces that cannot be neglected, as for drums and timpani, then the projection of Newton's second law along the vertical axis $\mathbf{e}_z$ leads to the equation with a "source" term:

$$\rho(\mathbf{x})h\ddot{\xi} = \text{div}\left(\underline{\underline{\tau}}.\mathbf{grad}\xi\right) + p(x,y,0^-,t) - p(x,y,0^+,t) . \tag{1.8}$$

In Eq. (1.8), the source term corresponds to a *pressure jump* across the membrane. For timpani, this pressure jump is equal to the difference between the sound pressure in the cavity and the sound pressure in the external air, in the membrane plane $z = 0$. More generally, the membrane may be subjected to a distribution of external forces localized or distributed on its surface. This surface distribution of forces $f_s(x,y,t)$ (with dimension of a pressure) is due, for example, to the action of a timpani mallet or of a drum stick. In this case, the equation of motion becomes[1]

$$\rho(\mathbf{x})h\ddot{\xi} = \text{div}\left(\underline{\underline{\tau}}.\mathbf{grad}\xi\right) + p(x,y,0^-,t) - p(x,y,0^+,t) + f_s(x,y,t) . \tag{1.9}$$

1.1.2.1 1D Approximation: Transverse Motion of Strings

The string length of musical instruments are large compared to the radius of the cross-section, so that it is justified to neglect the deformation in both transverse dimensions. Rewriting Eq. (1.5) through integration of inertial and tension forces along $\mathbf{e}_y$ yields the 1D approximation of the transverse motion equation (along $\mathbf{e}_z$) for a heterogeneous string:

$$\mu(x)\ddot{\xi} = \frac{\partial}{\partial x}\left[T(x)\frac{\partial \xi}{\partial x}\right], \tag{1.10}$$

where $\mu = \rho_s S$ is the linear density of the string and T the tension at rest (in N). S is the cross-sectional area of the string.

If the string is subjected to external forces along its length (linear density of forces $f_{\text{ext}}(x,t)$ in $\text{N}\,\text{m}^{-1}$) the equation of motion, including the source term, becomes

$$\mu(x)\ddot{\xi} = \frac{\partial}{\partial x}\left[T(x)\frac{\partial \xi}{\partial x}\right] + f_{\text{ext}}(x,t) . \tag{1.11}$$

[1]Equation (1.9), written here in Cartesian coordinates, can be generalized to other coordinate systems.

Since we are dealing here with a 1D model, there is no need to consider air pressure forces here.

Comments

1. Another transverse motion $\eta(x,t)$ oriented along $\mathbf{e}_y$ exists on the string. The equation of motion for $\eta(x,t)$ is analogous to (1.10). In general, both *polarizations* are excited.
2. In the absence of coupling terms in the model, ξ and η are independent of each other. In stringed musical instruments, however, this coupling does exist: it is mainly due to motion of the bridge at the end and to the existence of nonlinear terms for large amplitude motion (see Chap. 8).
3. Strings (and membranes) are also subjected to *longitudinal* vibrations. Such vibrations arise because fluctuations in length induce stress fluctuations. As a consequence, the stress becomes a function of the amplitude (and thus a function of time). This transverse–longitudinal coupling is usually neglected under the assumption of small amplitude. Nevertheless, it can be easily observed in piano strings, for example. This point will be clarified in Chap. 8.

1.1.2.2 Homogeneous Membranes and Strings Under Uniform Tension

For a uniformly stretched membrane made of a homogeneous material, the tension tensor $\underline{\underline{\tau}}$ becomes isotropic, which can be written as $\underline{\underline{\tau}} = \tau \underline{\underline{\mathbb{1}}}$, where $\underline{\underline{\mathbb{1}}}$ denotes the unit tensor. Equation (1.7) becomes

$$\tau \mathrm{div}\,(\mathbf{grad}\xi) = \tau \Delta\xi = \rho h \ddot{\xi}, \tag{1.12}$$

where the Laplacian in Cartesian coordinates is

$$\Delta\xi = \frac{\partial^2 \xi}{\partial x^2} + \frac{\partial^2 \xi}{\partial y^2}\,. \tag{1.13}$$

For timpani and drums, the most easier way to obtain a uniform tension is to choose a circular geometry for the membrane. In this case, the use of polar coordinates (r,θ) is preferable and Eq. (1.12) is written:

$$\rho h \ddot{\xi} = \tau \left(\frac{\partial^2 \xi}{\partial r^2} + \frac{1}{r}\frac{\partial \xi}{\partial r} + \frac{1}{r^2}\frac{\partial^2 \xi}{\partial \theta^2} \right)\,. \tag{1.14}$$

Homogeneous String Under Uniform Tension

With a uniform tension T, Eq. (1.11) reduces to:

$$\mu \ddot{\xi} = T \frac{\partial^2 \xi}{\partial x^2} + f_{\mathrm{ext}}(x,t)\,. \tag{1.15}$$

This partial differential equation of order 2 can be rewritten in the form of a system of two equations of order 1 involving force and velocity:

$$\begin{cases} \dfrac{\partial f}{\partial t} = T\dfrac{\partial v}{\partial x}, \\ \mu\dfrac{\partial v}{\partial t} = \dfrac{\partial f}{\partial x} + f_{\text{ext}}(x,t) \;\text{ with }\; v = \dfrac{\partial \xi}{\partial t}\,. \end{cases} \tag{1.16}$$

The latter formulation is useful in numerical analysis and sound synthesis, where it is often easier to solve systems of equations of lower order. It also helps in highlighting formal analogies with electrical transmission lines (see Chap. 4).

1.1.3 Stress and Strain

Before starting to examine the deformation of elastic solids, it is necessary to briefly recall the concepts of *strain* and *stress* that form the basis of continuum mechanics. For more details the reader may refer to specialized textbooks (see, for example, [49]).

1.1.3.1 Strain

General Formulation

The concept of strain can be introduced by writing the variation of length of an elementary vector $\mathbf{ds}_1$, whose both ends are subjected to the displacements $\boldsymbol{\xi}$ and $\boldsymbol{\xi} + \mathbf{d\xi}$, respectively (see Fig. 1.3).

Starting from the general formula giving the length of sides in a triangle, we get the length of the vector $\mathbf{ds}_2$, noting that:

$$ds_2^2 - ds_1^2 \;\simeq\; 2\,\mathbf{ds}_1.\mathbf{d\xi} \;=\; 2\,[d\xi_1 dx_1 + d\xi_2 dx_2 + d\xi_3 dx_3], \tag{1.17}$$

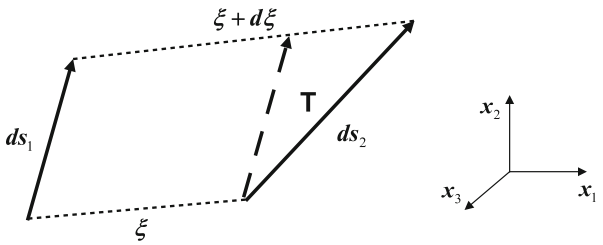

Fig. 1.3 Displacement of a vector in a deformable solid. The length of the vector $\mathbf{ds}_2$ is calculated from the length of sides in triangle T

where the second-order terms in $d\xi^2$ are neglected, and where x_i (i = {1,2,3}) denote the coordinates of the initial vector $\mathbf{ds}_1$. The displacement $\boldsymbol{\xi}(x)$ depends on the coordinates x_i, therefore the differential of each of its components is written:

$$d\xi_i = \sum_{j=1}^{3} \frac{\partial \xi_i}{\partial x_j} dx_j \, . \tag{1.18}$$

The subscript j in (1.18) is called *summation index* (or *dummy index*), since it appears in both the partial derivative and differential form. In continuum mechanics, we use the *Einstein convention* which consists in ignoring the summation sign ($\sum$) when it applies to a dummy index, in order to simplify the notation. In these conditions, Eq. (1.17) becomes

$$ds_2^2 - ds_1^2 \simeq 2 \frac{\partial \xi_i}{\partial x_j} dx_j dx_i \, . \tag{1.19}$$

In addition, one can show the following property of symmetry:

$$\frac{\partial \xi_i}{\partial x_j} = \frac{\partial \xi_j}{\partial x_i}. \tag{1.20}$$

Therefore, each term in (1.19) can be written as follows:

$$ds_2^2 - ds_1^2 \simeq \varepsilon_{ij} dx_j dx_i \text{ with } \varepsilon_{ij} = \frac{1}{2}\left(\frac{\partial \xi_i}{\partial x_j} + \frac{\partial \xi_j}{\partial x_i}\right) \, . \tag{1.21}$$

The quantities ε_{ij} form a set of six distinct components called *strain tensor*, which is written $\underline{\underline{\varepsilon}}$. It is a tensor of rank 2, since it depends on two indices. This tensor is symmetrical since $\varepsilon_{ij} = \varepsilon_{ji}$. Its six components fully characterize the strain of a continuous medium in three dimensions.

1.1.3.2 Stress

In the mechanics of rigid bodies, a general load is represented by a set of *forces* and *moments*. In fluid mechanics, it is necessary to also introduce the concept of *pressure*. However, these notions are not sufficient to represent the internal constraints acting in a deformable solid. It is observed first that the contact load exerted by an infinitesimal element on its neighbors inside the deformable medium cannot be reduced to a simple set of forces and moments. Secondly, the resulting forces are not oriented normally to each contact surface, as it is the case for perfect fluids. It is therefore necessary to introduce the concept of *stress* reflecting the fact that, on each elementary surface of contact between two particles, the *surface force*

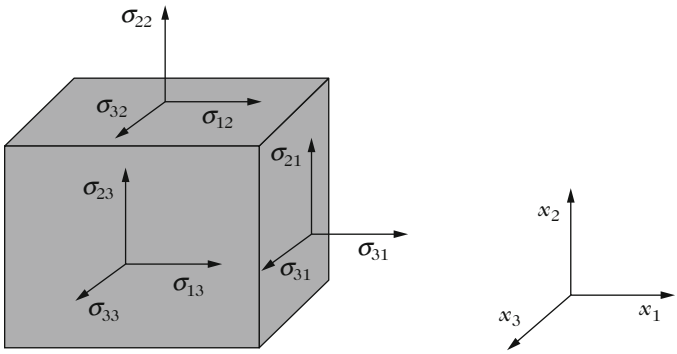

Fig. 1.4 Stress components exerted on a small elementary cubic volume

density vector is defined by three components. To clarify this, the concept of stress is illustrated on a small elementary cubic volume, with edges parallel to the axes (see Fig. 1.4).

The elementary forces applied on each surface dS_j ($j = \{1, 2, 3\}$) can be decomposed into three components dF_i ($i = \{1, 2, 3\}$). The surface density of force is defined as:

$$\sigma_{ij} = \frac{dF_i}{dS_j} . \tag{1.22}$$

The balance of moments leads to the symmetry property:

$$\sigma_{ij} = \sigma_{ji} . \tag{1.23}$$

In total, on each side of the elementary volume, we get nine components σ_{ij} which reduce to six components, due to symmetry. This set, denoted $\underline{\underline{\sigma}}$, is the *stress tensor* for the continuous medium. It is a symmetric tensor of rank 2, as for the strain tensor. In vector and tensor notation, we write the resulting force on a surface dS with normal vector $\boldsymbol{n}$:

$$\boldsymbol{dF} = \underline{\underline{\sigma}}.\boldsymbol{n} dS . \tag{1.24}$$

$\boldsymbol{T} = \underline{\underline{\sigma}}.\boldsymbol{n}$ is the *stress vector* on the surface. Finally, in the presence of a body force field $\boldsymbol{f}$, and taking further the inertial forces into account, the local equilibrium equation in a given solid element of density ρ is written:

$$\rho \ddot{\boldsymbol{\xi}} = \mathrm{div} \underline{\underline{\sigma}} + \boldsymbol{f}, \tag{1.25}$$

where $\ddot{\boldsymbol{\xi}}$ is the local acceleration.

1.1.4 Constitutive Equations of Materials: Linear Elasticity

In the dynamics of rigid bodies, the motion reduces to a set of translations and rotations, as a result of the application of forces and moments. In this case, inertial quantities such as the masses and the moments of inertia of the body make the links between load and motion. In continuum mechanics, we need a finer description of the internal properties of the deformable body to interpret static and dynamic strain and stress. The applied load results in a distribution of stress in the body. In the example discussed in the following subsection, a tensile force along the axis of a specimen leads to an almost uniaxial stress. As a result of stress, the structure will deform more or less according to its internal properties. We call *constitutive equations of materials* all properties (elasticity, viscosity, and thermal expansion) that make the link between stress and strain. We restrict ourselves to the particular class of linear elastic materials.

1.1.4.1 A One-Dimensional Traction Experiment

Let us perform a simple traction experiment on an homogeneous cylinder with cross-section S, whose length at rest L_0 is significantly larger than $\sqrt{S}$. It is observed that the relative extension $\frac{L-L_0}{L_0} \approx \varepsilon_{xx}$ linearly varies with the surface density of force $\sigma_{xx} \approx \frac{F}{S}$, as long as it does not exceed the yield strength σ_e (see Fig. 1.5).

In addition, it is observed that the experiment is reversible and that the sample recovers its initial form when the tensile force is removed. As a consequence, we write

$$\sigma_{xx} = E\,\varepsilon_{xx}, \tag{1.26}$$

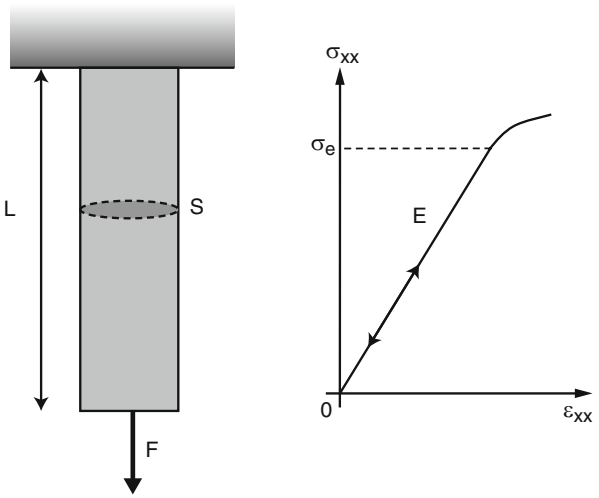

Fig. 1.5 Tension experiment. The force F is applied along the axis of the cylinder with initial cross-section S and length L_0. The relative extension $\frac{L-L_0}{L_0} \approx \varepsilon_{xx}$ is measured for increasing and decreasing values of the stress $\sigma_{xx} \approx \frac{F}{S}$. As long as σ_{xx} is less than the yield strength σ_e (which depends on the material) the curve $\sigma_{xx} = f(\varepsilon_{xx})$ is linear and reversible. The slope is the Young's modulus E

where E (in N/m^2) is the Young's modulus of the material. One important point here is that the stress is proportional to the strain: we are in the situation of a *linear* elastic behavior. This relationship, based on experimental facts, is also called *Hooke's law*.

Comment The relation (1.26) does not take the variation of the cross-section in the body consecutive to elongation (or compression) into account. This can only be done with the 3D generalization of Hooke's law (see the next section).

1.1.4.2 Elasticity Tensor

In a deformable body, one stress component σ_{ij} is likely to generate several components of strain ε_{kl}. Assume a linear constitutive law, we can generalize Eq. (1.26) to:

$$\sigma_{ij} = A_{ijkl}\,\varepsilon_{kl}, \tag{1.27}$$

where A_{ijkl} represents the *elasticity tensor* of the material, also denoted $\underline{\underline{\underline{\underline{A}}}}$. It is a fourth rank tensor. In theory, this tensor should have $3^4 = 81$ distinct components. However, if we recall that $\underline{\underline{\sigma}}$ and $\underline{\underline{\varepsilon}}$ are symmetrical, it reduces to 36, which is the maximum number of independent components for $\underline{\underline{\underline{\underline{A}}}}$. Because of additional energetic considerations, this number is reduced to 21 in the case of an anisotropic material [8]. Finally, taking also the symmetry of the material into account allows to reduce again the number of elasticity components.

Isotropic Material

In an *isotropic* material, all directions are equivalent. In this particular case, only 12 components A_{ijkl} are non-zero, and they are defined as function of two independent elasticity coefficients only, λ and μ, called *Lamé parameters* [49]. For such a material, the stress–strain relations are written:

$$\begin{pmatrix} \sigma_{xx} \\ \sigma_{yy} \\ \sigma_{zz} \\ \sigma_{zx} \\ \sigma_{yz} \\ \sigma_{xy} \end{pmatrix} = \begin{pmatrix} \lambda+2\mu & \lambda & \lambda & 0 & 0 & 0 \\ \lambda & \lambda+2\mu & \lambda & 0 & 0 & 0 \\ \lambda & \lambda & \lambda+2\mu & 0 & 0 & 0 \\ 0 & 0 & 0 & 2\mu & 0 & 0 \\ 0 & 0 & 0 & 0 & 2\mu & 0 \\ 0 & 0 & 0 & 0 & 0 & 2\mu \end{pmatrix} \begin{pmatrix} \varepsilon_{xx} \\ \varepsilon_{yy} \\ \varepsilon_{zz} \\ \varepsilon_{zx} \\ \varepsilon_{yz} \\ \varepsilon_{xy} \end{pmatrix}, \tag{1.28}$$

which can be written equivalently using the following compact tensor form:

$$\underline{\underline{\sigma}} = \lambda(\mathrm{tr}\underline{\underline{\varepsilon}})\underline{\underline{\underline{\underline{\mathbb{1}}}}} + 2\mu\underline{\underline{\varepsilon}}, \tag{1.29}$$

where $\mathrm{tr}\underline{\underline{\varepsilon}}$ is nothing but the divergence of the displacement field: $\mathrm{div}\boldsymbol{\xi}$. We also call it *dilatation*. In order to derive the strain tensor from the stress tensor, it is sufficient to invert Eq. (1.29), which leads to:

$$\underline{\underline{\varepsilon}} = \frac{1+\nu}{E}\underline{\underline{\sigma}} - \frac{\nu}{E}(\mathrm{tr}\underline{\underline{\sigma}})\underline{\underline{\mathbb{1}}}, \tag{1.30}$$

with

$$E = \frac{\mu\,(3\lambda + 2\mu)}{\lambda + \mu} \quad \text{et} \quad \nu = \frac{\lambda}{2(\lambda + \mu)}\,. \tag{1.31}$$

We recognize here the Young's modulus E and the Poisson's ratio ν. The latter is a dimensionless coefficient such that $-1 < \nu < 1/2$. By inverting the system (1.31), we obtain the expression of the Lamé parameters as function of E and ν:

$$\lambda = E\frac{\nu}{(1+\nu)(1-2\nu)} \quad ; \quad \mu = \frac{E}{2(1+\nu)}\,. \tag{1.32}$$

For a uniaxial stress field σ_{xx} applied (see the previous experiment of tension) to a "3D" specimen, we get from (1.29): $\varepsilon_{xx} = \sigma_{xx}/E$, $\varepsilon_{yy} = -\nu\sigma_{xx}/E$, and $\varepsilon_{zz} = -\nu\sigma_{xx}/E$ (see Fig. 1.6).

We can conclude that the Poisson's ratio gives a measure of the lateral compression of a specimen along the axes $\mathbf{e}_y$ and $\mathbf{e}_z$ under the effect of a traction along $\mathbf{e}_x$. This property is called "Poisson's effect."

Orthotropic Material

Unlike isotropic materials, anisotropic materials do not show identical elastic properties in all directions. Wood, for example, is an orthotropic material, which is a special case of anisotropy. To be convinced of such a behavior, a simple experiment can be made which consists in bending a guitar soundboard in Spruce with the hands. The experienced rigidity is higher when the bending is applied in the direction of the fibers compared to the case where the bending moment is applied in a direction perpendicular to them. More generally, for an orthotropic material, we can distinguish three orthogonal directions: longitudinal (L), radial (R), and tangential (T) (see Fig. 1.7).

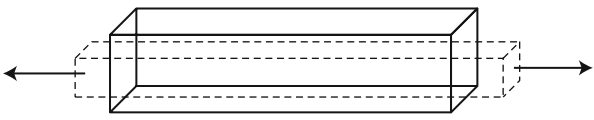

Fig. 1.6 Tension of a 3D bar and lateral compression (Poisson's effect)

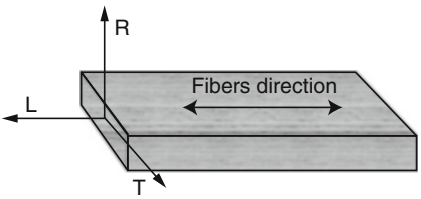

Fig. 1.7 Orthotropic material. A sample made from an orthotropic material (such as wood) has different elastic properties depending on whether the longitudinal direction (L), the radial direction (R), or the tangential direction (T) is considered

For a system of axes with coordinates (x, y, z) corresponding to these directions, the strain tensor in such a material is expressed as follows [28]:

$$\begin{pmatrix} \varepsilon_{xx} \\ \varepsilon_{yy} \\ \varepsilon_{zz} \\ \varepsilon_{zx} \\ \varepsilon_{yz} \\ \varepsilon_{xy} \end{pmatrix} = \begin{pmatrix} \frac{1}{E_L} & -\frac{\nu_{RL}}{E_R} & -\frac{\nu_{TL}}{E_T} & 0 & 0 & 0 \\ -\frac{\nu_{LR}}{E_L} & \frac{1}{E_R} & -\frac{\nu_{TR}}{E_T} & 0 & 0 & 0 \\ -\frac{\nu_{LT}}{E_L} & -\frac{\nu_{RT}}{E_R} & \frac{1}{E_T} & 0 & 0 & 0 \\ 0 & 0 & 0 & \frac{1}{2G_{LT}} & 0 & 0 \\ 0 & 0 & 0 & 0 & \frac{1}{2G_{TR}} & 0 \\ 0 & 0 & 0 & 0 & 0 & \frac{1}{2G_{RL}} \end{pmatrix} \begin{pmatrix} \sigma_{xx} \\ \sigma_{yy} \\ \sigma_{zz} \\ \sigma_{zx} \\ \sigma_{yz} \\ \sigma_{xy} \end{pmatrix} \tag{1.33}$$

where the Poisson's ratios ν_{ij} correspond to a contraction in direction j consecutive to an extension applied in direction i. As an example, ν_{LR} corresponds to a contraction in the radial direction consecutive to an extension in the longitudinal direction.

The symmetry properties of the material lead to the following equalities:

$$\frac{\nu_{LR}}{E_L} = \frac{\nu_{RL}}{E_R} \; ; \; \frac{\nu_{LT}}{E_L} = \frac{\nu_{TL}}{E_T} \; ; \; \frac{\nu_{RT}}{E_R} = \frac{\nu_{TR}}{E_T} \; . \tag{1.34}$$

In summary, the elastic properties of an orthotropic material are defined by nine independent coefficients:

- Three Young's moduli (or elasticity moduli): E_L, E_R, andE_T,
- Three Poisson's ratios: ν_{LR}, ν_{RT}, and ν_{TL},
- Three shear moduli: G_{LT}, G_{TR}, and G_{RL}.

Comment For a guitar soundboard made of Spruce, the ratio E_L/E_T usually lies between 10 and 20. The directions of the fibers correspond to those of the strings so that the board resists to the shear induced by the bridge. Flexibility in the tangential direction is partially compensated by stiffeners glued on the inferior face of the board. Using more recent materials, such as carbon fiber and composites, it is possible to control the elastic properties in all three directions [8]. Today, a number of soundboards of stringed instruments are made by mixing, in various proportions, wood and carbon fibers [9]. It will be seen in Chap. 13 that the choice of materials in instrument making is not only governed by static considerations but also by radiation criteria, which is fully understandable for musical instruments.

1.1.5 Bars and Plates

We are now interested in the case of elastic solids without prestress. As previously done for the membranes, dissipation phenomena are ignored. The bar model can be applied to elastic solids whose one dimension is of a higher order of magnitude than the two others (slender solid), and for which a one-dimensional model can thus be developed. Plates correspond to 2D plane solids where the order of magnitude of the thickness is lower than the length of the sides. For a bar subjected to small perturbations it is justified to decouple the different regimes of vibrations: traction, torsion, and bending [39]. For pedagogical reasons, we will examine these limiting cases in the order of increasing difficulty. Thus, traction and torsion will be presented before the bending, although this does not correspond to the relative significance of these regimes in musical acoustics. In xylophones and other mallet instruments, for example, bending vibrations are responsible for the essential part of the sound. Torsional vibrations are also present, but are usually unwanted. Finally, longitudinal motion is unsignificant.

1.1.5.1 Traction (or Compression) of a Bar

Consider an isotropic elastic bar loaded along its main axis (denoted $\mathbf{e}_x$) (see Fig. 1.8). In this case, the displacement $\boldsymbol{\xi}(x,t)$ at each point is axial (or longitudinal). In musical acoustics, the axial vibrations of piano strings play a major role, especially during the attack transient [5].

The strain in the bar is $\varepsilon_{xx} = \varepsilon = \frac{\partial \xi}{\partial x}$. The axial stress is $\sigma_{xx} = \sigma = E\varepsilon$ where E is the Young's modulus. For a bar of length L and cross-section S, the elastic potential energy is given by:

$$E_p = \frac{1}{2}\int_0^L ES\left(\frac{\partial \xi}{\partial x}\right)^2 dx, \tag{1.35}$$

and the kinetic energy is

$$E_c = \frac{1}{2}\int_0^L \rho S\left(\frac{\partial \xi}{\partial t}\right)^2 dx\,. \tag{1.36}$$

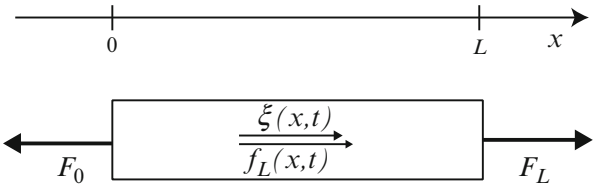

Fig. 1.8 Traction (or compression) of a bar. One-dimensional model

Application of Hamilton's principle yields the equation of motion:

$$\rho S \frac{\partial^2 \xi}{\partial t^2} - \frac{\partial}{\partial x}\left(ES\frac{\partial \xi}{\partial x}\right) = f_L(x,t) \tag{1.37}$$

where $f_L(x,t)$ is the force per unit length applied to the bar.

Comment. *Unless otherwise specified, quantities E, ρ, and S defined above are functions of the abscissa x. Thus, the present model allows to treat the case of heterogeneous bars and/or bars of variable thickness.*

Denoting F_0 and F_L the forces applied at both ends $x = 0$ and $x = L$ (see Fig. 1.8), the boundary conditions are written:

$$\begin{cases} \left(ES\dfrac{\partial \xi}{\partial x}\right)_{x=0} = -F_0, \\ \left(ES\dfrac{\partial \xi}{\partial x}\right)_{x=L} = F_L\ . \end{cases} \tag{1.38}$$

In this book, we will have to consider general boundary conditions (BC) of the type:

$$\alpha ES\frac{\partial \xi}{\partial x} + \beta \xi = F \quad \text{with} \quad (\alpha,\beta) \in \mathbb{R}, \tag{1.39}$$

These general conditions include the two following simple cases:

$$\frac{\partial \xi}{\partial x} = 0 \quad \text{(free BC)} \quad ; \quad \xi = 0 \quad \text{(fixed BC)}\ . \tag{1.40}$$

1.1.5.2 Torsion of a Bar

The bars of keyboard percussion instruments often show a torsional motion around the main axis, especially when they are struck near the edge. The amplitude of this motion can be significant if the bar is cut in its central part since, in this case, the torsional stiffness decreases notably (see below for an accurate definition of torsional stiffness). The torsional vibrations can be musically annoying, because the corresponding frequencies are generally not in harmonic correspondence with the main components of the bending vibrations (see the next section) that mainly contribute to the sound of the instrument.

Bowed strings (which can be considered as prestressed bars) are also subjected to a torsional moment induced by the bow. Woodhouse and colleagues have shown that these vibrations, particularly through their dissipative function, have an important role in the stability of the motion of the bowed string [23, 56, 57] (see Chap. 11).

To model torsional vibrations, we consider the simple case of a cylinder with a circular cross-section of radius a (see Fig. 1.9).

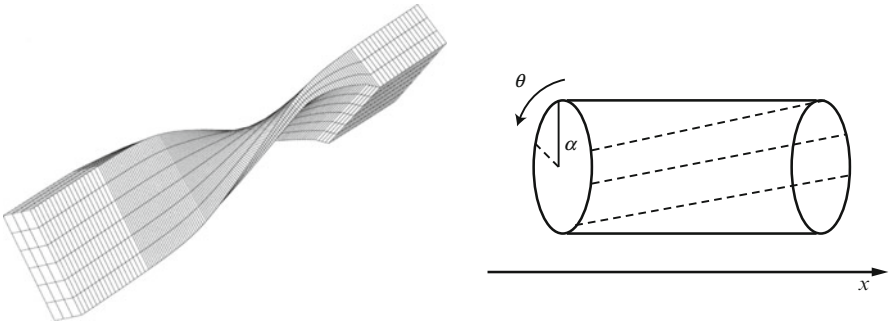

Fig. 1.9 (*Left*) Torsional motion of a marimba bar. Such a motion, which can be musically very annoying, often appears when a bar with an undercut is struck near the edge. For such a bar of complex geometry, the equations that govern the torsional motion can only be solved numerically. (*Right*) Torsion of a cylindrical bar with a circular cross-section of radius a. We assume that, under the effect of a torsional torque, each cross-section of the cylinder of abscissa x rotates with an angle $\theta(x,t)$. The *dashed lines* show the deformation of the generatrices of the cylinder, consecutive to the rotation $\theta(x,t)$. The cylinder can be viewed as a kind of "spaghetti" bundle where each generatrix remains straight in the rotation

We note $\theta(x,t)$ the angular displacement of a cross-section of abscissa x, $dS = rdrd\theta$ a surface element in this section, σ the modulus of the torsional stress, G the torsional modulus of the cylinder's material, and ϕ the angular displacement of a generatrix initially parallel to the x axis. First, we can write

$$\phi = r\frac{\partial\theta}{\partial x}\,. \tag{1.41}$$

According to the definition of the torsional modulus, we have $\sigma = G\phi$. In this case, the relation between the moment $M(x)$ applied to the cross-section S of the cylinder and the rotation is given by:

$$M = \int_S \sigma r dS = \int_S Gr^2\frac{\partial\theta}{\partial x}dS = GJ\frac{\partial\theta}{\partial x}, \tag{1.42}$$

where $J = \int_S r^2 dS$ is *the rotational inertia of the section*. This quantity has the dimension of a length to the fourth power. It is equal to $J = \pi a^4/2$ for a circular cross section of radius a.

Newton's second law (or law of conservation of angular momentum) applied to an element dx of the bar leads to the balance of moments:

$$I\frac{\partial^2\theta}{\partial t^2} = \frac{\partial M}{\partial x} + m_e, \tag{1.43}$$

where I is here the mass moment of inertia with respect to the axis x and per unit length of the cylinder; m_e is the density per unit length of the external momenta applied to the cylinder. Combining (1.43) and (1.42), we obtain the partial differential equation governing θ:

$$I\frac{\partial^2\theta}{\partial t^2} = \frac{\partial}{\partial x}\left(GJ\frac{\partial\theta}{\partial x}\right) + m_e, \tag{1.44}$$

which, in the case of a uniform cylinder of constant cross-section, reduces to:

$$I\frac{\partial^2\theta}{\partial t^2} = GJ\frac{\partial^2\theta}{\partial x^2} + m_e \,. \tag{1.45}$$

In the particular case of a homogeneous beam of constant circular cross-section (and in this case, only!), we also have $I = \rho J$. We formally obtain a wave equation with the same form as for the vibrating string (or for the longitudinal vibrations of a bar), but notice that the physical phenomena at the origin of these equations are fully different.

1.1.5.3 Bending of an Isotropic Bar

We now consider the bending of a slender bar in the plane $(\mathbf{e}_x, \mathbf{e}_y)$ with the following assumptions:

1. One dimension (along the main axis) is large compared to the other two.
2. The material is elastic and linear.
3. The cross-sections are symmetrical so that we make no distinction between the mean fiber (locus of the center of gravity of the cross-sections) and the neutral fiber (locus of the points which are not subjected to bending stress during the deformation).
4. The Poisson's effect (lateral contraction–extension) is ignored.
5. Each point of a cross-section at abscissa x moves vertically in the direction of the axis $\mathbf{e}_y$ with amplitude $v(x)$ small compared to the bar's thickness.
6. The cross-sections are subjected to a rotation θ_z around the axis $\mathbf{e}_z$ so that they remain straight and perpendicular to the mean fiber during the motion.
7. The rotations are small, so that we can perform a first-order approximation $\theta_z \approx \frac{\partial v}{\partial x}$. In addition, we neglect the rotational kinetic energy of the sections.

Within the framework of these *Euler–Bernoulli assumptions*, a displacement field is of the form:

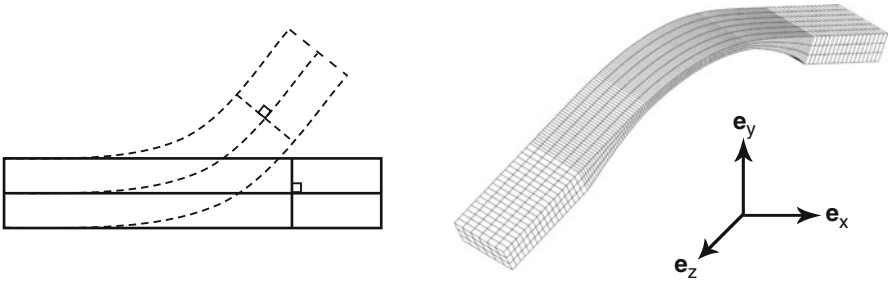

Fig. 1.10 (*Left*) Euler–Bernoulli kinematics. During the motion, the cross-sections remain straight and perpendicular to the neutral fiber. (*Right*) Bending motion of a marimba bar. The bending of such a bar is well described by a model of a bar with variable cross-section

$$\xi_x = -y\theta_z \approx -y\frac{\partial v}{\partial x} \;\; ; \;\; \xi_y = v \;\; ; \;\; \xi_z = 0, \tag{1.46}$$

from which we get, from (1.21), the strain tensor:

$$\begin{cases} \varepsilon_{xx} = \dfrac{\partial \xi_x}{\partial x} = -y\dfrac{\partial^2 v}{\partial x^2}, \\ \varepsilon_{xy} = \varepsilon_{yx} = \dfrac{1}{2}\left(\dfrac{\partial \xi_x}{\partial y} + \dfrac{\partial \xi_y}{\partial x}\right) = 0, \\ \varepsilon_{yy} = \dfrac{\partial \xi_y}{\partial y} = 0\,. \end{cases} \tag{1.47}$$

The hypothesis of isotropic material yields the stress tensor. Here, we write [see Eq. (1.26)] $\sigma_{xx} = E\varepsilon_{xx}$, since the Poisson's effect is neglected.

Let us now express *the elastic potential energy*, also called *strain energy*, of the bending bar. For an elementary spring of stiffness k, the elastic energy stored under the effect of a traction (or compression) of elongation x from equilibrium is $E_p = \frac{1}{2}kx^2$. By analogy, the elementary force dF_x applied to an element of length dx of the bar with cross-section dS is, according to (1.22): $dF_x = \sigma_{xx}dS$. Therefore, the elementary elastic potential energy is: $dE_p = \frac{1}{2}\sigma_{xx}\varepsilon_{xx}\, dx\, dS$. By integrating this expression on the complete volume of the bar of length L, we get

$$E_p = \frac{1}{2}\int_S\int_0^L Ey^2\left(\frac{\partial^2 v}{\partial x^2}\right)^2 dx\, dS = \frac{1}{2}\int_0^L EI_z(x)\left(\frac{\partial^2 v}{\partial x^2}\right)^2 dx \tag{1.48}$$

where $I_z(x) = \int_S y^2 dS$ is the *principal moment of inertia along the axis 0z* of the cross-section S. The quantity $\mathscr{M} = EI_z\frac{\partial^2 v}{\partial x^2}$ is the bending moment and $\mathscr{C} = \frac{\partial^2 v}{\partial x^2}$ is the curvature.

The kinetic energy E_c of the beam of density ρ is written:

$$E_c = \frac{1}{2}\int_S\int_0^L \rho\dot{\xi}^2 dx dS = \frac{1}{2}\int_S\int_0^L \rho\left[y^2\left(\frac{\partial \dot{v}}{\partial x}\right)^2 + \dot{v}^2\right] dx\, dS\,. \tag{1.49}$$

This energy can be rewritten as:

$$E_c = \frac{1}{2}\int_0^L \rho I_z\dot{\theta}_z^2 dx + \frac{1}{2}\int_0^L \rho S\dot{v}^2 dx, \tag{1.50}$$

which shows that the kinetic energy is the sum of both a rotational and a translational energy. Under the Euler–Bernoulli framework, the rotational inertia is neglected, so that we get

$$E_c \simeq \frac{1}{2}\int_0^L \rho S\dot{v}^2 dx\,. \tag{1.51}$$

Starting from the energetic quantities, we obtain the equation of motion through application of Hamilton's principle. Denoting $f(x,t)$ the density per unit length of non-conservative external forces applied to the bar, and δv a cinematically acceptable virtual displacement (test function), we get the virtual mechanical work δW_{nc} of these forces from the expression:

$$\delta W_{nc} = \int_0^L f(x,t)\ \delta v\ dx\ . \tag{1.52}$$

The method consists in deriving the equation of motion and the boundary conditions that must be verified by the displacement field $v(x,t)$ to ensure that the following integral is equal to zero between two arbitrary moments of time t_1 and t_2 [21, 25]:

$$\int_{t_1}^{t_2} \left(\delta E_c - \delta E_p + \delta W_{nc}\right) dt = 0\ . \tag{1.53}$$

The variations of both kinetic and potential energy are given by:

$$\delta E_c = \frac{\partial E_c}{\partial v}\delta v + \frac{\partial E_c}{\partial \dot{v}}\delta \dot{v} = -\frac{d}{dt}\left(\frac{\partial E_c}{\partial \dot{v}}\right)\delta v = -\int_0^L \rho S \ddot{v}\ \delta v\ dx, \tag{1.54}$$

and

$$\delta E_p = \frac{\partial E_p}{\partial v''}\delta v'' = \left[EI_z \frac{\partial^2 v}{\partial x^2}\delta v'\right]_0^L - \left[\frac{\partial}{\partial x}\left(EI_z \frac{\partial^2 v}{\partial x^2}\right)\delta v\right]_0^L + \int_0^L \frac{\partial}{\partial x}\left(EI_z \frac{\partial^2 v}{\partial x^2}\right)\delta v\ dx, \tag{1.55}$$

where $v'' = \frac{\partial^2 v}{\partial x^2}$ and $v' = \frac{\partial v}{\partial x}$.

By inserting (1.55) and (1.54) in (1.53), we derive the bending equation of motion of the bar, within the simplified framework of Euler–Bernoulli assumptions:

$$\rho S \ddot{v} + \frac{\partial^2}{\partial x^2}\left(EI_z \frac{\partial^2 v}{\partial x^2}\right) = f, \tag{1.56}$$

with the boundary conditions:

$$\left[EI_z \frac{\partial^2 v}{\partial x^2}\delta v'\right]_0^L = 0 \quad \text{and} \quad \left[\frac{\partial}{\partial x}\left(EI_z \frac{\partial^2 v}{\partial x^2}\right)\delta v\right]_0^L = 0\ . \tag{1.57}$$

Equation (1.56) is of fourth-order in space. Therefore, four boundary conditions, two conditions at each end, are necessary to properly define the problem. From (1.57), we see that only four combinations are possible at each end:

$$\begin{cases} \text{Simply supported edge: } v = 0 \text{ and } \mathscr{M} = EI_z \dfrac{\partial^2 v}{\partial x^2} = 0, \\ \text{Clamped edge : } \dfrac{\partial v}{\partial x} = 0 \text{ and } v = 0, \\ \text{Free edge: } \mathscr{T} = \dfrac{\partial}{\partial x}\left(EI_z \dfrac{\partial^2 v}{\partial x^2}\right) = 0 \text{ and } \mathscr{M} = EI_z \dfrac{\partial^2 v}{\partial x^2} = 0, \\ \text{Guided edge: } \mathscr{T} = \dfrac{\partial}{\partial x}\left(EI_z \dfrac{\partial^2 v}{\partial x^2}\right) = 0 \text{ and } \dfrac{\partial v}{\partial x} = 0\,. \end{cases} \tag{1.58}$$

The quantity $\mathscr{T} = \dfrac{\partial}{\partial x}\left(EI_z \dfrac{\partial^2 v}{\partial x^2}\right)$ is the *shear force*.

- In musical acoustics, the Euler–Bernoulli model gives satisfactory results provided that the ratio between the length and a characteristic dimension of the cross-section (radius or side length) is greater than or equal to about 10. For keyboard percussion instruments (xylophone, vibraphone, and marimba), this model is valid for the lowest bars only. As the length of the bar decreases, it is necessary to choose a kinematic model accounting for the fact that the cross-sections do not remain perpendicular to the neutral axis during the motion. It becomes also necessary to take the rotational inertia of the sections into account (Timoshenko model) [19]. For a detailed comparison of different models of bars, the reader can refer to [27].

1.1.5.4 Bending of Thin Elastic Plates

The "thin plate" hypotheses (or Kirchhoff–Love model) generalize for plates the Euler–Bernoulli assumptions applied to the bars (see Sect. 1.1.5.3). A detailed presentation of the equation of bending plates is beyond the scope of this book. We can refer, for example, to the work by Yu [58] or Geradin and Rixen [21].

Here, only the main steps of the modeling are summarized, using the same approach as for bars in the previous paragraph. The case of orthotropic plates is selected as an illustration. It is particularly useful in musical acoustics since it can be applied to wooden plates used in lutherie [13, 55]. The problem is treated in Cartesian coordinates, and the transverse displacement is denoted $w(x, y, t)$. We assume that the coordinates coincide with the symmetry axes of the material and that $\boldsymbol{e}_z$ is the transverse direction. We therefore consider that the displacement field $\boldsymbol{\xi}$ in the plate is of the form:

$$\xi_x = -z\frac{\partial w}{\partial x} \;\; ; \quad \xi_y = -z\frac{\partial w}{\partial y} \;\; ; \quad \xi_z = w, \tag{1.59}$$

from which we get the strain tensor, assumed to be plane:

$$\begin{cases} \varepsilon_{xx} = \dfrac{\partial \xi_x}{\partial x} = -z\dfrac{\partial^2 w}{\partial x^2}, \\ \varepsilon_{yy} = \dfrac{\partial \xi_y}{\partial y} = -z\dfrac{\partial^2 w}{\partial y^2}, \\ \varepsilon_{xy} = \varepsilon_{yx} = \dfrac{1}{2}\left(\dfrac{\partial \xi_x}{\partial y} + \dfrac{\partial \xi_y}{\partial x}\right) = -z\dfrac{\partial^2 w}{\partial x \partial y}\,. \end{cases} \tag{1.60}$$

The orthotropy of the material leads to the following relations between plane stress and strain:

$$\begin{pmatrix} \sigma_{xx} \\ \sigma_{yy} \\ \sigma_{xy} \end{pmatrix} = \begin{pmatrix} \dfrac{E_x}{1-\nu_{xy}\nu_{yx}} & \dfrac{\nu_{yx}E_x}{1-\nu_{xy}\nu_{yx}} & 0 \\ \dfrac{\nu_{yx}E_x}{1-\nu_{xy}\nu_{yx}} & \dfrac{E_y}{1-\nu_{xy}\nu_{yx}} & 0 \\ 0 & 0 & 2G_{xy} \end{pmatrix} \begin{pmatrix} \varepsilon_{xx} \\ \varepsilon_{yy} \\ \varepsilon_{xy} \end{pmatrix} \tag{1.61}$$

where the coefficients ν_{ij} are such that $1 - \nu_{ij}\nu_{ji} > 1$ [13].

The bending moments are obtained by integration of the elementary moments on the plate thickness h:

$$\mathscr{M}_x = \int_{-h/2}^{h/2} z\sigma_{xx}dz\,;\ \mathscr{M}_y = \int_{-h/2}^{h/2} z\sigma_{yy}dz\,;\ \mathscr{M}_{xy} = \mathscr{M}_{yx} = \int_{-h/2}^{h/2} z\sigma_{xy}dz, \tag{1.62}$$

from which we derive the relations between moments and curvatures:

$$\begin{pmatrix} \mathscr{M}_x \\ \mathscr{M}_y \\ \mathscr{M}_{xy} \end{pmatrix} = -\begin{pmatrix} D_1 & D_2/2 & 0 \\ D_2/2 & D_3 & 0 \\ 0 & 0 & D_4/2 \end{pmatrix} \begin{pmatrix} \dfrac{\partial^2 w}{\partial x^2} \\ \dfrac{\partial^2 w}{\partial y^2} \\ \dfrac{\partial^2 w}{\partial x \partial y} \end{pmatrix}, \tag{1.63}$$

where

$$D_1 = \frac{E_x h^3}{12(1-\nu_{xy}\nu_{yx})}\,; \qquad D_2 = \frac{E_x \nu_{yx} h^3}{6(1-\nu_{xy}\nu_{yx})} = \frac{E_y \nu_{xy} h^3}{6(1-\nu_{xy}\nu_{yx})}, \tag{1.64}$$

$$D_3 = \frac{E_y h^3}{12(1-\nu_{xy}\nu_{yx})}\,; \qquad D_4 = \frac{G_{xy} h^3}{3}\,. \tag{1.65}$$

The equation of motion is again obtained from the Hamilton integral [Eq. (1.53)]. The variation of the kinetic energy resulting from a virtual displacement δw is written:

$$\delta E_c = -\int_S \rho_p h \ddot{w}\, \delta w\, dS\,. \tag{1.66}$$

The variation of the potential energy that generalizes the case of bars is

$$\delta E_p = \int_S \left[\mathscr{M}_x \delta w''_{xx} + \mathscr{M}_y \delta w''_{yy} + 2\mathscr{M}_{xy} \delta w''_{xy}\right] dS\,. \tag{1.67}$$

Finally, for a surface density of transverse force $f(x, y, t)$, the virtual mechanical work is written:

$$\delta W_{nc} = \int_S f(x, y, t)\, \delta w\, dx\,. \tag{1.68}$$

Applying Hamilton's principle to the set of Eqs. (1.66)–(1.68), we derive the bending equation of the plate:

$$\rho_p h \frac{\partial^2 w}{\partial t^2} = \frac{\partial^2 \mathscr{M}_x}{\partial x^2} + \frac{\partial^2 \mathscr{M}_y}{\partial y^2} + 2\frac{\partial^2 \mathscr{M}_{xy}}{\partial x \partial y} + f(x, y, t)\,. \tag{1.69}$$

Equation of Motion of Plates in Terms of Displacement

We eliminate the bending moments from Eqs. (1.63) and (1.69) to get the equation describing the transverse displacement of the orthotropic plate:

$$\begin{aligned}\rho_p h \frac{\partial^2 w}{\partial t^2} &+ \frac{\partial^2}{\partial x^2}\left(D_1 \frac{\partial^2 w}{\partial x^2} + \frac{D_2}{2}\frac{\partial^2 w}{\partial y^2}\right) + \frac{\partial^2}{\partial y^2}\left(D_3 \frac{\partial^2 w}{\partial y^2} + \frac{D_2}{2}\frac{\partial^2 w}{\partial x^2}\right) \\ &+ \frac{\partial^2}{\partial x \partial y}\left(D_4 \frac{\partial^2 w}{\partial x \partial y}\right) = f(x, y, t)\,.\end{aligned} \tag{1.70}$$

which becomes, in the particular case of a homogeneous plate:

$$\rho_p h \frac{\partial^2 w}{\partial t^2} + D_1 \frac{\partial^4 w}{\partial x^4} + D_3 \frac{\partial^4 w}{\partial y^4} + (D_2 + D_4)\frac{\partial^4 w}{\partial x^2 \partial y^2} = f(x, y, t)\,. \tag{1.71}$$

For an isotropic plate, we have $E_x = E_y = E$ and $\nu_{xy} = \nu_{yx} = \nu$, so that the rigidity constants are written:

$$\begin{aligned} D_1 = D_3 &= \frac{Eh^3}{12(1-\nu^2)} = D\,;\; D_2 = 2\nu D, \\ D_4 &= \frac{\mu h^3}{3} = \frac{Eh^3}{6(1+\nu)} = 2(1-\nu)D\,. \end{aligned} \tag{1.72}$$

In conclusion, we obtain the classical equation of homogeneous and isotropic thin plates under Kirchhoff–Love assumptions:

$$\rho_p h \frac{\partial^2 w}{\partial t^2} + D\left[\frac{\partial^4 w}{\partial x^4} + \frac{\partial^4 w}{\partial y^4} + 2\frac{\partial^4 w}{\partial x^2 \partial y^2}\right] = f(x, y, t)\ . \tag{1.73}$$

More generally, we assume the following notation, which is independent of the coordinate system:

$$\rho_p h \frac{\partial^2 w}{\partial t^2} + D\nabla^4 w = f, \tag{1.74}$$

where ∇^4 represents the bi-Laplacian. The symbol Δ^2 is also used for designating this operator.

Boundary Conditions

In Sect. 1.1.5.3, Eq. (1.55) has shown that the boundary conditions are the results of integration by parts carried out to express the variation of elastic potential energy as a function of the virtual displacement (noted δv for bars). We proceed here in a similar manner for the variation of potential energy in plates written in (1.67). Here the integration is performed on a surface, and thus the results and the number of possible boundary conditions depend on the geometry of the plate. For rectangular plates, for example, Leissa lists 21 possible cases for the boundary conditions [36]. For a given edge (at $x = x_0$ for example), the most commonly encountered conditions are the following:

1. Clamped edge: displacement $w = 0$ and rotation $\frac{\partial w}{\partial x} = 0$,
2. Simply supported edge: displacement $w = 0$ and bending moment $\mathscr{M}_x = 0$,
3. Free edge: bending moment $\mathscr{M}_x = 0$ and shear force $\mathscr{T}_x = \frac{\partial \mathscr{M}_x}{\partial x} + 2\frac{\partial \mathscr{M}_{xy}}{\partial y} = 0$.

The boundary conditions for a free edge are written in Cartesian coordinates:

$$\begin{cases} \mathscr{M}_x = D_1 \dfrac{\partial^2 w}{\partial x^2} + \dfrac{D_2}{2}\dfrac{\partial^2 w}{\partial y^2} = 0, \\ \mathscr{T}_x = \dfrac{\partial}{\partial x}\left(D_1 \dfrac{\partial^2 w}{\partial x^2} + \dfrac{D_2}{2}\dfrac{\partial^2 w}{\partial y^2}\right) + \dfrac{\partial}{\partial y}\left(D_4 \dfrac{\partial^2 w}{\partial x \partial y}\right) = 0\ . \end{cases} \tag{1.75}$$

For a corner at the intersection of two free edges, we must add the condition:

$$\mathscr{M}_{xy} = 0, \quad \text{or} \quad \frac{\partial^2 w}{\partial x \partial y} = 0\ . \tag{1.76}$$

Fig. 1.11 The vibrations of bells are described by models of shells. © Australian-Dream.Fotolia.com

For an isotropic and homogeneous material, the conditions (1.75) become

$$\begin{cases} \dfrac{\partial^2 w}{\partial x^2} + \nu \dfrac{\partial^2 w}{\partial y^2} = 0 \quad \text{and} \\ \dfrac{\partial^3 w}{\partial x^3} + (2-\nu) \dfrac{\partial^3 w}{\partial x \partial y^2} = 0 \,. \end{cases} \tag{1.77}$$

1.1.6 Equation of Shells

A *shell* is a continuous medium which is completely defined by a surface and a thickness (see, as an example, the bells on Fig. 1.11). A plate corresponds to the special case of a shell with a plane surface. In musical acoustics, models of shells can be applied to a large number of percussion instruments (gongs, cymbals, bells, etc.) and to soundboards of string instruments. Here, we restrict our study to a brief presentation of the theory of *thin* elastic shells (the *thin shell theory*).[2] This theory, due to Love, is applicable when the thickness of the shell is small compared to other dimensions [51].

As for the Kirchhoff–Love model previously applied to plates, we assume that the local displacement field in the cross-sections consists in a translation and a rotation, so that each cross-section remains plane during the motion (see Figure 1.12). Translations and rotations differ from one section to another, otherwise, we would

[2]Here, we do not treat the cylindrical shells theory, which naturally applies to wind instruments, because it requires significant developments that are beyond the scope of this book. Nevertheless, we provide valuable references in Chap. 13 which deals with sound–structure interaction.

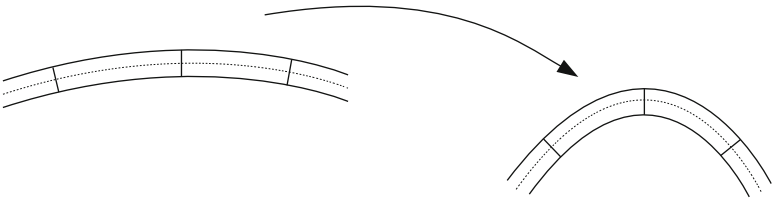

Fig. 1.12 Deformation of a thin shell. Each cross-section is subjected to a combination of translation and rotation

simply get a rigid body global displacement for the shell and, consecutively, no strain. In what follows, rotational inertia and transverse shear are ignored.

The main difference between strain tensors of plate and shell, respectively, is that, because of the non-zero curvature, the deformation induced by a transverse load is not only of the *bending* type as in the case of bars and plates, but also includes a *membrane-like* deformation. This means that a strain normal to the load exists in the thickness of the shell. The strain tensor is therefore formed by the sum of two contributions (see in the following Section the example of the spherical cap).

The Love model can be further simplified under the assumption that the shells are *slightly curved, or shallow,* and excited along their transverse dimension. The resulting model is traditionally called "Donnell–Mushtari–Vlasov model" (or DMV model) and is one of the most often used in shell theory. The fundamental assumptions of this model are

1. The membrane displacement is neglected in the bending strain.
2. Inertia of the membrane displacement is neglected.

To solve the problem it is convenient to introduce an auxiliary variable called *force function* or *Airy function*. Consequently, the motion equations take the form of a system of partial differential equations with two unknowns: the transverse displacement and the force function. For more details, the reader is invited to read the specialized literature on shells [3, 37, 51].

1.1.6.1 Thin Shallow Spherical Shells

In order to illustrate its general concepts, the main features of the DMV model are applied to the particular case of thin shallow spherical shells. This example has the advantage of being simple enough, while showing the influence of the curvature. In addition, it allows to properly explain the dynamics of cymbals and gongs.

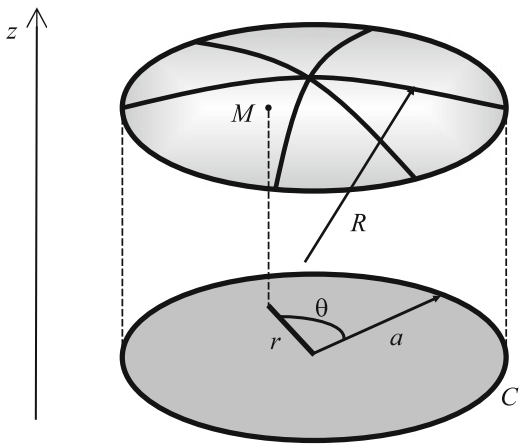

Fig. 1.13 Geometry of a thin spherical cap

Presentation

We are interested in a thin spherical cap of constant thickness h small compared to the radius a of the circle $\mathscr{C}$ obtained by projecting the cap on the horizontal plane (see Fig. 1.13).

We assume that the cap is slightly curved (shallow shell), which is expressed by the condition $a \ll R$, where R is the radius of curvature of the shell. It is supposed that the Kirchhoff–Love conditions are fulfilled: rigid body displacement for each cross-section, shear and rotational inertia neglected. Only the case of a homogeneous and isotropic shell is considered. Because of the rotational symmetry, we use the polar coordinates (r, θ, z) where (r, θ) are the coordinates of the projection of a current point M of the shell on the disk of radius a, and z its vertical coordinate in the shell thickness, with $-h/2 \leq z \leq h/2$.

Displacement Field

With the Kirchhoff–Love assumptions, the components of the displacement field $\boldsymbol{\xi}$ in the shell are written:

$$\begin{cases} \xi_r = u(r,\theta) + z\beta_r(r,\theta), \\ \xi_\theta = v(r,\theta) + z\beta_\theta(r,\theta), \\ \xi_z = w(r,\theta), \end{cases} \tag{1.78}$$

where (u, v, w) are the components of a translation vector and where β_r and β_θ are the elementary rotations of a cross-section of the shell along r and θ. First-order expansions of these rotations are written [51]:

$$\begin{cases} \beta_r(r,\theta) = \dfrac{u}{R} - \dfrac{\partial w}{\partial r}, \\ \beta_\theta(r,\theta) = \dfrac{v}{R} - \dfrac{1}{r}\dfrac{\partial w}{\partial \theta}. \end{cases} \tag{1.79}$$

Strain Tensor

We obtain the strain tensor by calculating the elongation of a small vector under an elementary displacement [see Eq. (1.19)]. In the case of thin shallow shells, the strain tensor can be put on the form:

$$\underline{\underline{\varepsilon}} = (\underline{\underline{\varepsilon}})_m + z(\underline{\underline{\varepsilon}})_f \tag{1.80}$$

where $(\underline{\underline{\varepsilon}})_m$ is a *membrane* type tensor that expresses the strains in the thickness of the shell, and where $(\underline{\underline{\varepsilon}})_f$ is a *bending* type tensor with components representing the changes of curvature consecutive to the displacement. These components are written:

$$\begin{cases} (\varepsilon_{rr})_m = \dfrac{\partial u}{\partial r} + \dfrac{w}{r}, \\ (\varepsilon_{\theta\theta})_m = \dfrac{u}{r} + \dfrac{1}{r}\dfrac{\partial v}{\partial \theta} + \dfrac{w}{R}, \\ (\varepsilon_{r\theta})_m = (\varepsilon_{\theta r})_m = \dfrac{1}{r}\dfrac{\partial v}{\partial \theta} + r\dfrac{\partial}{\partial r}\left(\dfrac{v}{r}\right), \end{cases} \tag{1.81}$$

and

$$\begin{cases} (\varepsilon_{rr})_f = -\dfrac{\partial^2 w}{\partial r^2}, \\ (\varepsilon_{\theta\theta})_f = -\dfrac{1}{r}\left(\dfrac{\partial w}{\partial r} + \dfrac{1}{r}\dfrac{\partial^2 w}{\partial \theta^2}\right), \\ (\varepsilon_{r\theta})_f = (\varepsilon_{\theta r})_f = -2\dfrac{\partial}{\partial r}\left(\dfrac{1}{r}\dfrac{\partial w}{\partial \theta}\right). \end{cases} \tag{1.82}$$

The other components of the tensor $\underline{\underline{\varepsilon}}$ are equal to zero.

Stress–Strain Relation

For a homogeneous and isotropic material, characterized by its Young's modulus E and Poisson's ratio ν, the non-zero components of the stress tensor are written:

$$\begin{cases} \sigma_{rr} = \dfrac{E}{1-\nu^2}\left(\varepsilon_{rr} + \nu\varepsilon_{\theta\theta}\right), \\ \sigma_{\theta\theta} = \dfrac{E}{1-\nu^2}\left(\varepsilon_{\theta\theta} + \nu\varepsilon_{rr}\right), \\ \sigma_{r\theta} = \sigma_{\theta r} = \dfrac{E}{2(1+\nu)}\varepsilon_{r\theta}\,. \end{cases} \tag{1.83}$$

Resulting Forces and Moments

As for bars and plates (see Sect. 1.1.5.4), the resulting forces applied to each elementary volume of the shell are obtained through integration of the stress vector over the thickness:

$$N_r = \int_{-h/2}^{h/2} \sigma_{rr}\, dz \;;\; N_\theta = \int_{-h/2}^{h/2} \sigma_{\theta\theta}\, dz \;;\; N_{r\theta} = N_{\theta r} = \int_{-h/2}^{h/2} \sigma_{r\theta}\, dz\,. \tag{1.84}$$

Similarly, the resulting moments are obtained by calculating:

$$M_r = \int_{-h/2}^{h/2} \sigma_{rr} z\, dz \;;\; M_\theta = \int_{-h/2}^{h/2} \sigma_{\theta\theta} z\, dz \;;\; M_{r\theta} = M_{\theta r} = \int_{-h/2}^{h/2} \sigma_{r\theta} z\, dz\,. \tag{1.85}$$

As a result, we get

$$\begin{cases} N_r = \dfrac{Eh}{1-\nu^2}\left[(\varepsilon_{rr})_m + \nu(\varepsilon_{\theta\theta})_m\right], \\ N_\theta = \dfrac{Eh}{1-\nu^2}\left[(\varepsilon_{\theta\theta})_m + \nu(\varepsilon_{rr})_m\right], \\ N_{r\theta} = N_{\theta r} = \dfrac{Eh}{2(1+\nu)}(\varepsilon_{r\theta})_m\,. \end{cases} \tag{1.86}$$

and

$$\begin{cases} M_r = \dfrac{Eh^3}{12(1-\nu^2)}\left[(\varepsilon_{rr})_f + \nu(\varepsilon_{\theta\theta})_f\right], \\ M_\theta = \dfrac{Eh^3}{12(1-\nu^2)}\left[(\varepsilon_{\theta\theta})_f + \nu(\varepsilon_{rr})_f\right], \\ M_{r\theta} = M_{\theta r} = \dfrac{Eh^3}{24(1+\nu)}(\varepsilon_{r\theta})_f\,. \end{cases} \tag{1.87}$$

These expressions show that the resulting forces applied by an element of shell on its neighboring elements are entirely due to membrane deformations. The resulting moments are the consequence of changes in curvature, as in the case of plates.

Equations of Motion

The equations of motion for the shell are obtained by writing down the balance of forces and moments on a shell element, and applying Newton's second law. After some calculations, we get

$$\begin{cases} D\nabla^4 w + \dfrac{N_r + N_\theta}{R} + \rho h \dfrac{\partial^2 w}{\partial t^2} = f \quad \text{with } D = \dfrac{Eh^3}{12(1-\nu^2)}, \\ \dfrac{\partial (rN_r)}{\partial r} + \dfrac{\partial N_{r\theta}}{\partial \theta} - N_\theta = 0, \\ \dfrac{\partial (rN_{r\theta})}{\partial r} + \dfrac{\partial N_\theta}{\partial \theta} + N_{r\theta} = 0\,. \end{cases} \tag{1.88}$$

These three spherical shells Eq. (1.88) are expressed in terms of transverse displacement w and force components N_r, N_θ, and $N_{r\theta}$. These four unknowns are not independent since the three force components depend on the coordinates u, v, and w [see Eq. (1.86)]. The first equation in (1.88) shows that the additional term $(N_r + N_\theta)/R$ is due to membrane forces and tends to zero when the radius of curvature tends to infinity: it corresponds to the case of plates (Eq. 1.74). In most cases, we are primarily interested in the vertical component w of the displacement. The variables u and v can be eliminated in Eq. (1.88) by introducing a force function (or Airy function) F such that:

$$N_r = \frac{1}{r}\frac{\partial F}{\partial r} + \frac{1}{r^2}\frac{\partial^2 F}{\partial \theta^2} \;\; ; \;\; N_\theta = \frac{\partial^2 F}{\partial r^2} \;\; ; \;\; N_{r\theta} = N_{\theta r} = \frac{1}{r^2}\frac{\partial F}{\partial \theta} - \frac{1}{r}\frac{\partial F}{\partial r \partial \theta}, \tag{1.89}$$

As a result, we obtain

$$\nabla^2 F = N_r + N_\theta\,. \tag{1.90}$$

Finally, the system (1.88) is written:

$$\begin{cases} D\nabla^4 w + \dfrac{\nabla^2 F}{R} + \rho h \dfrac{\partial^2 w}{\partial t^2} = f, \\ \nabla^4 F = \dfrac{Eh}{R}\nabla^2 w\,. \end{cases} \tag{1.91}$$

If necessary, the Airy function F can be further eliminated, in order to derive an equation in terms of w. However, in most cases, and, in particular, in the context of numerical resolution, it is more appropriate to keep a formulation based on a system with two unknowns, which offers the advantage to involve differential operators of lower orders.

Boundary Conditions

The boundary conditions for the thin shallow shell are obtained from Hamilton's principle using the same method as for bars and plates (see Eq. 1.57). This yields the following possibilities at the periphery of the shell (in $r = a$):

$$\begin{cases} N_r = 0 \quad \text{or} \quad u = 0, \\ N_{r\theta} + \dfrac{M_{r\theta}}{R} = 0 \quad \text{or} \quad v = 0, \\ \dfrac{1}{r}\dfrac{\partial M_{r\theta}}{\partial \theta} = 0 \quad \text{or} \quad w = 0, \\ M_r = 0 \quad \text{or} \quad \beta_r = 0\,. \end{cases} \tag{1.92}$$

A shell clamped at its edge, for example, has the following four boundary conditions:

$$u = v = w = 0 \ \text{ and } \ \beta_r = 0, \tag{1.93}$$

while the boundary conditions for a spherical shell with free edges are written:

$$N_r = 0 \ ; \ N_{r\theta} + \frac{M_{r\theta}}{R} = 0 \ ; \ \frac{\partial M_{r\theta}}{\partial \theta} = 0 \ ; \ M_r = 0 \ . \tag{1.94}$$

1.2 3D Acoustic Waves

The equation of three-dimensional (3D) acoustic waves in a non-dissipative medium at rest, at low level, forms the basis of each book of acoustics. The knowledge of the solution allows at least deriving a first approximation of the eigenfrequencies of wind instruments, known since Bernoulli to be very close to the played frequencies, or the frequencies of cavity appearing in string and percussion instruments. Further in this book, we need to partially remove the above-mentioned restrictions, particularly concerning dissipation. Conversely, we will start by studying cases much simpler than the 3D problem. We now establish the three-dimensional equation to set the framework of many following chapters. For more details on this subject, we refer the reader to some basic textbooks on acoustics [12, 41, 44, 48], but also on fluid mechanics [6].

Under the above-defined conditions, the acoustic wave equation is the result of the elimination of two acoustic variables, the velocity $\mathbf{v}$ and the density ρ. Only the acoustic pressure, which is a scalar quantity, is kept from two conservation equations and a state equation. For a given physical quantity, the corresponding

acoustic quantity is defined as the variation of the quantity around an average value, considered as time invariant. This variation is assumed to be small, which allows to use linear approximations of phenomena (see the comments in the box below). The propagation of a sound wave in a fluid mainly depends on the fact that this fluid has a mass and a compressibility. It can therefore be seen as a combination of masses and springs, or rather springs with a certain mass, that are modeled in continuum mechanics as infinitesimal objects, called "particles." The compressibility of the fluid makes an acoustic motion different from a regular, incompressible flow, with a density remaining constant. Some results presented here are summarized and detailed further in Chap. 5 where the dissipation effects are studied.

Acoustic Quantities and Decibels
The variation of the acoustic quantities is small, but its magnitude can vary considerably, by a factor 10^7, from the lowest audible sound to the sound of a taking off airplane: this is the reason why the decibel scale is used. For a given acoustic pressure amplitude (i.e., the root-mean-square pressure), p, we define $N_{\text{dB}} = 20\log(p/p_0)$, where p_0 is the reference value equal to 2×10^{-5} Pa. This value is almost the lowest sound level perceived by the ear at 1000 Hz. For a musical instrument playing *piano*, the sound level is approximately 60 dB, or 0.02 Pa, and for a *fortissimo* play, the sound hardly exceeds 100 dB, or 2 Pa, which is very far from the atmospheric pressure, equal to 10^5 Pa. However, it will be seen in Part III that the pressure at the input of a wind instrument can reach 170 dB, or 6000 Pa (this value still remains well below the atmospheric pressure, although it will produce new phenomena which be discussed in Part III of the book). Finally, to take into account that hearing perceives frequencies between 1000 and 3000 Hz much better than other frequencies, a weighted decibel, the dBA [20, 59] has been defined.

1.2.1 State Equation of a Gas

At equilibrium, the gas has a density ρ_0, expressed in kg m^{-3}, a uniform temperature T, expressed in °K, and a pressure p_0, expressed in N m^{-2} or Pascals (Pa). If we consider a volume V equal to nM/ρ, nM being the mass of the fluid[3] in the volume V, these quantities are linked by a state equation, $f(P, V, T) = 0$. As there are only two independent thermodynamic variables, we can express any variations of the quantities defining the fluid in terms of two of them.

Thus for the specific heat received by a fluid element $dQ = TdS$, (where S is the entropy per unit mass, which is a state function), we can express it in terms of the variations dP and dV (or dP and $d\rho = -\rho dV/V$). For acoustic motions of

[3] n is number of moles, and M the molar mass.

a sufficiently high frequency, it is assumed that motions are isentropic ($dQ = 0$), i.e., there is no heat exchange between the fluid elements (dissipation is discussed in Chap. 5). We derive a proportionality relation between pressure variations and density variations, which gives the first of the three sought equations. It is written:

$$dP = c^2 d\rho, \tag{1.95}$$

where $c \triangleq \sqrt{(\partial P/\partial \rho)_S}$ is a coefficient which will be later identified as the speed of sound waves. We note that c is simply related to the isentropic compressibility

$$\chi_S \triangleq \frac{1}{\rho}\left(\frac{\partial \rho}{\partial P}\right)_S = \frac{1}{\rho c^2}. \tag{1.96}$$

- If we write that pressure $P = p_0 + p$ and density $\rho = \rho_0 + \rho'$ slightly vary around their equilibrium values,[4] p_0 and ρ_0, we obtain from (1.95):

$$p = \frac{1}{\rho_0 \chi_S}\rho' = c^2 \rho'. \tag{1.97}$$

We note also that for constant entropy, as for the density variation, the temperature variation is proportional to the pressure variation. So if we write $T = T_0 + \tau$, the acoustic temperature τ is proportional to the acoustic pressure p. We find the expression of the corresponding coefficient in Chap. 5, as well as the values of the compressibility and the speed of sound for a given gas law, including temperature. We will show that if $PV = n\mathrm{R}T$, or $MP = \mathrm{R}T\rho$, where R is the constant of an ideal gas, we have

$$\chi_T \triangleq \frac{1}{\rho}\left(\frac{\partial \rho}{\partial P}\right)_T = \frac{1}{p_0} \text{ which leads to } \chi_S = \frac{1}{\gamma p_0} \text{ and } c^2 = \frac{\gamma p_0}{\rho_0} = \gamma \frac{\mathrm{R}T_0}{M}, \tag{1.98}$$

where $\gamma = C_p/C_v$, the ratio of specific heats at constant pressure and volume. This allows calculating the theoretical value of the speed of sound with respect to the temperature. Numerical values of the speed of sound, density, and other constants of air are given in Chap. 5.

1.2.2 Momentum Conservation

Here we write the conservation of momentum, i.e., the Newton's second law. We use the Eulerian variables, which are best suited for this study: these are the variables that an observer sees when he is looking at the fluid evolution from a fixed point in space, **r**, instead of following the evolution of a fluid element (Lagrangian description).

[4] This difference in notation for pressure and density, although it is apparently illogical, is convenient for the following of the statement.

- Considering a given quantity f depending on space and time, its time variation depends on the infinitesimal motion with velocity $\mathbf{v} = d\mathbf{r}/dt$. We write

$$\begin{aligned} df &= f(\mathbf{r}+\mathbf{dr}, t+dt) - f(\mathbf{r}, t) \\ &= f(\mathbf{r}+\mathbf{dr}, t+dt) - f(\mathbf{r}, t+dt) + f(\mathbf{r}, t+dt) - f(\mathbf{r}, t) \\ &= \mathbf{grad} f(\mathbf{r}, t+dt).d\mathbf{r} + [\partial f(\mathbf{r}, t)/\partial t]\ dt, \end{aligned}$$

or at the first order

$$df = \mathbf{grad} f(\mathbf{r}, t).d\mathbf{r} + [\partial f(\mathbf{r}, t)/\partial t]\ dt = \mathbf{grad} f(\mathbf{r}, t).\mathbf{v}dt + [\partial f(\mathbf{r}, t)/\partial t]\ dt. \tag{1.99}$$

Thus, we can define in general the following operator:

$$\frac{d}{dt} = (\mathbf{v}.\mathbf{grad}) + \frac{\partial}{\partial t}. \tag{1.100}$$

- Now we write the Newton's second law for an infinitesimal volume:

$$\rho \frac{d\mathbf{v}}{dt} = -\mathbf{grad} P + \rho \mathbf{F} \tag{1.101}$$

where $\mathbf{F}$ is an external force per unit mass. In one dimension, it is read as follows: the product of the acceleration by the mass of the fluid element is equal to the pressure difference at both sides added to an external force. The $-$ sign on the right-hand side comes from the fact that, at position $(x + dx)$, a positive pressure applies a force along the negative x-axis, in contrast to what happens at position x.

Equation (1.101) is the equation of the momentum conservation $\rho\mathbf{v}$. For a finite volume D bounded by a surface S, it can be written in the following integral form:

$$\iiint_D \rho \frac{d\mathbf{v}}{dt} dD = -\iint_S P d\mathbf{S} + \iiint_D \rho \mathbf{F} dD. \tag{1.102}$$

The derivative with respect to time of the momentum in the volume D is equal to the outflow, which is simply the pressure force applied on the surface, added to the effect of forces external to the fluid.

- In linear acoustics, we can now linearize Eq. (1.101) to the first order, which is the Euler equation. For a fluid at rest, the total velocity $\mathbf{v}$ is the acoustic velocity, which is small, i.e., of the first order, and we obtain

$$\rho_0 \frac{\partial \mathbf{v}}{\partial t} = -\mathbf{grad} p + \rho_0 \mathbf{F}. \tag{1.103}$$

Equation (1.101) implies that the zeroth order of $\mathbf{F}$ is zero (because ρ_0 is not zero): thus, $\mathbf{F}$ is of the first order. We obtain here the second vector equation connecting p, ρ, and $\mathbf{v}$, this time with a source external to the fluid.[5]

Bernoulli's Law

Returning to the non-linearized Euler Equation (1.101), it is seen that if the force $\mathbf{F}$ is irrotational, this is also the case for the velocity, and they both derive from a potential, written $-V$ and φ: $\mathbf{F} = -\mathbf{grad}V$ and $\mathbf{v} = \mathbf{grad}\varphi$. If the motion is isentropic (i.e., adiabatic and reversible), the pressure P depends on ρ only, and we can write

$$\frac{1}{\rho}\mathbf{grad}P = \frac{1}{\rho}\frac{dP}{d\rho}\mathbf{grad}\rho = \mathbf{grad}\int \frac{1}{\rho}\frac{dP}{d\rho}d\rho = \mathbf{grad}\int \frac{dP}{\rho}.$$

In addition $(\mathbf{v}.\mathbf{grad})\mathbf{v} = \frac{1}{2}\mathbf{grad}v^2 - (\mathbf{v} \times \mathbf{rot}\mathbf{v}) = \frac{1}{2}\mathbf{grad}v^2$, and we obtain from (1.101):

$$\mathbf{grad}\left[\frac{\partial \boldsymbol{\varphi}}{\partial t} + \frac{1}{2}v^2 + \int \frac{dP}{\rho} + V\right] = 0.$$

We can integrate this equation in space: by calculating the scalar product of this quantity and $\mathbf{v}$, and noting that the quantity $\mathbf{v}.\mathbf{grad} = v\partial/\partial_n$ is the derivative in the direction of $\mathbf{v}$, i.e., along a streamline. We obtain the Bernoulli's law by integrating along such a line:

$$\frac{\partial \boldsymbol{\varphi}}{\partial t} + \frac{1}{2}v^2 + \int \frac{dP}{\rho} + V = \text{function}(t). \tag{1.104}$$

We can include the right-hand side function in the potential φ, which is defined apart from a space-independent function, and we obtain a right-hand side equal to zero. The quasi-static version of (1.104), in homogeneous medium and without external force, will be useful to describe the flow at the input of a reed instrument. It is written:

$$P + \frac{1}{2}\rho v^2 = \text{constant}. \tag{1.105}$$

Concerning the version obtained in linear acoustics for a homogeneous medium at rest, it is simply written: $p = -\rho_0 \partial\varphi/\partial t$, where φ is the velocity potential.

[5] We could also add a source to Eq. (1.97): it would be a heat source, varying in time, which does not occur in musical instruments.

1.2.3 Conservation of Mass

We need another equation to link the quantities p, ρ, and $\mathbf{v}$: it is the conservation of mass, that we first write in an integral form. The mass entering a domain D bounded by a surface S per unit of time, to which we possibly add the one produced by a density of source mass ρq, is equal to the increase in fluid mass in the domain per unit of time:

$$-\iint_S \rho \mathbf{v}.\mathbf{dS} + \iiint_D \rho q(\mathbf{r},t) dD = \frac{\partial}{\partial t} \iiint_D \rho \, dD, \tag{1.106}$$

if $\mathbf{dS}$ is the outgoing normal of the volume. We will see examples of sources $q(\mathbf{r},t)$, which are flow sources per unit volume, especially for reed instruments. By using the divergence theorem, we get

$$\iiint_D \left[\mathrm{div}(\rho \mathbf{v}) + \frac{\partial \rho}{\partial t} \right] dD = \iiint_D \rho q(\mathbf{r},t) dD.$$

This expression is valid for any domain D and can therefore be written in a differential form:

$$\mathrm{div}(\rho \mathbf{v}) + \frac{\partial \rho}{\partial t} = \rho q(\mathbf{r},t). \tag{1.107}$$

For the same reasons as those given for $\boldsymbol{F}$ (see Sect. 1.2.2), q is of order 1, and the linearization gives for a homogeneous medium at rest:

$$\rho_0 \mathrm{div}\mathbf{v} + \frac{\partial \rho'}{\partial t} = \rho_0 q(\mathbf{r},t). \tag{1.108}$$

1.2.4 Acoustic Wave Equation

- In summary, the three linearized equations (1.97), (1.103), and (1.108) *(from here, we omit the subscript 0 for the average density)*, where only two of them have an external source, are written:

$$\begin{aligned} p &= \frac{1}{\rho \chi_S} \rho' = c^2 \rho', \\ \rho \mathrm{div}\mathbf{v} + \frac{\partial \rho'}{\partial t} &= \rho q(\mathbf{r},t), \\ \rho \frac{\partial \mathbf{v}}{\partial t} &= -\mathbf{grad} p + \rho \mathbf{F}. \end{aligned}$$

- Eliminating the acoustic density ρ', we derive two equations for the two most usual quantities, acoustic pressure and particle velocity:

$$\mathrm{div}\mathbf{v} + \chi_S \frac{\partial p}{\partial t} = q(\mathbf{r}, t)\ ; \tag{1.109}$$

$$\mathbf{grad}p + \rho \frac{\partial \mathbf{v}}{\partial t} = \rho \mathbf{F}. \tag{1.110}$$

- The mass-spring fluid system is finally characterized by two main parameters, its density ρ and its compressibility χ_S. If we remove the velocity, using a cross derivation, we obtain the wave equation for the pressure:

$$\Delta p - \frac{1}{c^2}\frac{\partial^2 p}{\partial t^2} = \rho \left(\mathrm{div}\mathbf{F} - \frac{\partial q}{\partial t} \right) \tag{1.111}$$

where $\Delta = \nabla^2$. The choice of the pressure as the unique acoustic variable is very common, because, on the one hand, the pressure is a scalar quantity, and, on the other hand, the pressure is, to a first approximation, the quantity to which the ear is sensitive. We see that the production of sound is due to the time variation of the flow q. If the flow is constant, there is no sound.

1.2.5 Simple Solutions: Traveling and Standing Waves

We consider the particular case of a plane wave, where all quantities vary in the x direction, only. After the change of variables $(x, t) \rightarrow (x - ct, x + ct)$, the general solution is of the form:

$$p = f^+(x - ct) + f^-(x + ct), \tag{1.112}$$

which is the sum of two traveling waves, an outgoing one and an incoming one, of any shape. The wave speed is c, the square of which is the inverse of the product of the two parameters ρ and χ_S [see Eq. (1.95)]. Notice that when there is no term in the right-hand side in the equation, the velocity potential is governed by the same equation as the pressure (provided that it has been adequately chosen). This is also the case for the acoustic velocity. Therefore, in one dimension, the general solution for both the potential and velocity has an expression similar to Eq. (1.112).

For the outgoing wave, we have $\partial f^+/\partial t = -c\partial f^+/\partial x$, and we deduce $p = \rho c v_x$. The quantity p/v is the *specific acoustic impedance*, which, for both waves, is called the *characteristic impedance*. It is equal to $Z_S = \rho c = \sqrt{\rho/\chi_S}$,

while $c = 1/\sqrt{\rho\chi_S}$. The pair of parameters of our fluid-spring system, ρ and χ_S, is equivalent to another pair, which characterizes a plane traveling wave: the speed of sound c and the specific characteristic impedance, or impedance of the medium, Z_S. We can alternatively use one pair or the other, depending on the context.

- There is another simple general solution of the wave equation, which separates the space and time variables. If we search for a solution of the form $p(\mathbf{r}, t) = R(\mathbf{r})T(t)$, Eq. (1.111) without sources becomes

$$c^2 \frac{\Delta R}{R} = \frac{1}{T} \frac{d^2 T}{dt^2}. \tag{1.113}$$

The left-hand side is a function of space only, and the right-hand side a function of time only. Therefore, each side is a constant, known as the separation constant, that we denote $-\omega^2$ if it is negative.[6] The function of time depends on two constants, A and φ:

$$T(t) = A\cos(\omega t + \varphi).$$

For plane waves, we can also find the function of space, and finally write:

$$p(\mathbf{r}, t) = (a\cos kx + b\sin kx)\cos(\omega t + \varphi),$$

where a and b are two constants. $k = \omega/c$ is the wavenumber. It is related to the spatial period λ, i.e., the wavelength, by $k = 2\pi/\lambda$. The solution is a *standing wave* solution, since all points of the space are vibrating in phase (or in antiphase, depending on the sign of the spatial solution): the phase is equal to φ or $\varphi + \pi$. They are clearly distinguishable from traveling waves (1.112), which are not separable into functions of space and time.

Complex Notation: Fourier and Laplace Transforms

If a quantity varies sinusoidally, for example, $p(t) = A\cos(\omega t + \varphi)$, it is very convenient to associate a complex quantity to it:

$$p_c(t) = ae^{j\omega t}\ , \text{where } a = Ae^{j\varphi}. \tag{1.114}$$

The interesting quantity is the real part of this complex quantity $p(t) = \Re e\,[p_c(t)]$. a is called *complex amplitude*. This simplifies all linear calculations, such as addition, scalar multiplication, derivation, and integration. For

(continued)

[6] Exponentially time-increasing or time-decreasing solutions may also exist if the constant is positive (but this is rare). The case of complex values is treated in the following section. Furthermore we can continue this operation by separating the variables of space. This will happen several times in this book.

example,

$$p_1(t) + p_2(t) = \Re e\left[p_{c1}(t) + p_{c2}(t)\right].$$

Thus we can use this method for the wave equation (1.111). Most often, the c subscript is omitted because there is no confusion. The solution with separate variables $p(\mathbf{r}, t) = R(\mathbf{r})T(t)$ can also be written using complex quantities. It can happen that the constant ω is complex, thus the functions $R(\mathbf{r})$ and $T(t)$ are complex (a complete problem must include the boundary conditions, which are governing the possible values of the separation constant). For this case there are no standing waves, as it can be easily verified by taking the real part: the phase varies in space.

Looking for solutions with sinusoidal variation is usual. Therefore we use a complex formulation, with a time dependence in $\exp(j\omega t)$. This means that we look for particular solutions, related to the time variation of the source.

This search for particular sinusoidal solutions should be distinguished from the search for *general* solution using a Fourier transform. For the latter, we will choose the definition:

$$P(\mathbf{r}, \omega) = \int_{-\infty}^{+\infty} p(\mathbf{r}, t) e^{-j\omega t} dt, \text{ with} \tag{1.115}$$

$$p(\mathbf{r}, t) = \frac{1}{2\pi} \int_{-\infty}^{+\infty} P(\mathbf{r}, \omega) e^{j\omega t} d\omega. \tag{1.116}$$

In these expressions, $p(\mathbf{r}, t)$ is the real physical general solution, which implies $P(\mathbf{r}, -\omega) = P^*(\mathbf{r}, \omega)$. Thus, if the pressure at one given point is $p(t) = a\cos(\omega_0 t + \varphi)$, we have

$$* P(\omega) = (a/2)\left[\delta(\omega - \omega_0)\exp(j\varphi) + \delta(\omega + \omega_0)\exp(-j\varphi)\right], \tag{1.117}$$

* where δ is the delta function. Recall that, for any function $g(x)$, and for any interval $[a, b]$ including the origin, the delta function satisfies

$$\int_a^b g(x)\delta(x)dx = g(0).$$

For example, the wave equation (1.111) without sources becomes, in the Fourier domain, the Helmholtz equation: $\left(\Delta + k^2\right) P(\mathbf{r}, \omega) = 0$.

For initial values problems, we also use the Laplace transform, where $s = \sigma + j\omega$ has a positive real part:

(continued)

$$P(\mathbf{r},\mathbf{s}) = \int_0^{+\infty} p(\mathbf{r},t)e^{-st}dt \text{ with} \tag{1.118}$$

$$p(\mathbf{r},t) = \frac{1}{2\pi j}\int_{-j\infty+\varepsilon}^{j\infty+\varepsilon} P(\mathbf{r},s)e^{st}ds. \tag{1.119}$$

As a reminder, the derivation rules for this transform are

$$\text{If } f(t) \to F(s), \text{ then } f'(t) \to sF(s) - f(0) \text{ and } f''(t) = s^2F(s) - sf(0) - f'(0). \tag{1.120}$$

1.3 Energy, Intensity, and Power

In this section, two simple examples are treated in parallel: the vibrating string and the acoustic waves, in order to emphasize some interesting analogies.

1.3.1 Example of the Vibrating String

We consider an ideal homogeneous vibrating string without external source. In view of the results presented in Sect. 1.1.2, the equation of motion is written:

$$\mu\frac{\partial^2\xi}{\partial t^2} - T\frac{\partial^2\xi}{\partial x^2} = 0\,. \tag{1.121}$$

An energy-based formulation of the problem is obtained by multiplying this equation by the speed $v = \frac{\partial\xi}{\partial t}$ and integrating the resulting expression over the entire length of the string. After an integration by parts, we find

$$\int_0^L \mu\frac{\partial^2\xi}{\partial t^2}\frac{\partial\xi}{\partial t}dx + \int_0^L T\frac{\partial^2\xi}{\partial x\partial t}\frac{\partial\xi}{\partial x}dx + \left[-T\frac{\partial\xi}{\partial x}\frac{\partial\xi}{\partial t}\right]_0^L = 0 \tag{1.122}$$

The first two integrals in (1.122) correspond to the time variation of the total energy $E = E_c + E_p$ of the string, where

$$\begin{cases} E_c = \displaystyle\int_0^L e_c \, dx \quad \text{where} \quad e_c = \frac{1}{2}\mu \left(\frac{\partial \xi}{\partial t}\right)^2, \\ E_p = \displaystyle\int_0^L e_p \, dx \quad \text{where} \quad e_p = \frac{1}{2} T \left(\frac{\partial \xi}{\partial x}\right)^2. \end{cases} \tag{1.123}$$

In these expressions, e_c is the kinetic energy per unit length and e_p the elastic potential energy per unit length. For the total energy per unit length, $e = e_c + e_p$, Eq. (1.122) is simply rewritten as:

$$\int_0^L \frac{\partial e}{\partial t} dx + \left[-T \frac{\partial \xi}{\partial x} \frac{\partial \xi}{\partial t} \right]_0^L = 0, \tag{1.124}$$

which can be alternatively formulated in the form:

$$\int_0^L \left(\frac{\partial e}{\partial t} + \frac{\partial}{\partial x} \left[-T \frac{\partial \xi}{\partial x} \frac{\partial \xi}{\partial t} \right] \right) dx = 0 \, . \tag{1.125}$$

The quantity $\Pi = -T \frac{\partial \xi}{\partial x} \frac{\partial \xi}{\partial t}$ has the dimension of an instantaneous power at point M with abscissa x. It is the product of the force $f = -T \frac{\partial \xi}{\partial x}$ by the velocity $\frac{\partial \xi}{\partial t}$ of the string at point M. For a wave traveling to the right, this power is imparted to the points situated at the right-hand side of M (see Fig. 1.14).

Finally, the fact that the integral in (1.125) vanishes implies that we can write at any point:

$$\frac{\partial e}{\partial t} + \frac{\partial \Pi}{\partial x} = 0 \, . \tag{1.126}$$

Equation (1.126) is a classical example of conservation law. It links the time variation of a density (here e) to the spatial variation of a flow (here Π). This equation shows that wave propagation corresponds to a continuous energy transfer from one point to another in the medium.

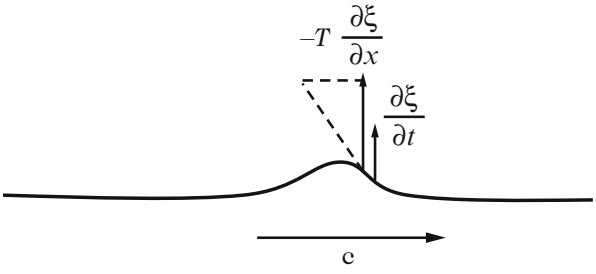

Fig. 1.14 Energy transfer on a string

1.3.2 Example of Linear Acoustic Waves

In linear acoustics, writing an equation for energy as a corollary of linearized equations is questionable, since the goal is to calculate quantities of order 2. However, it can be shown from the non-linearized equations that the following result is correct. Using (1.109) and (1.110), the quantity div($p\mathbf{v}$), can be calculated. Since div($p\mathbf{v}$) = $p$div($\mathbf{v}$) + $\mathbf{v}$.**grad**p, we obtain

$$\text{div}\,\mathbf{I} = -\frac{\partial}{\partial t}[E] + pq + \rho\mathbf{v}.\mathbf{F}, \tag{1.127}$$

$$\text{where } \mathbf{I} = p\mathbf{v}\ ;\ E = \frac{1}{2}\left[\chi_s p^2 + \rho\mathbf{v}.\mathbf{v}\right]. \tag{1.128}$$

The quantity E is the total energy per unit volume: it can be shown that $E_p = \frac{1}{2}\chi_s p^2$ is the potential energy density, and $E_c = \frac{1}{2}\rho\mathbf{v}.\mathbf{v}$ the kinetic energy density. The vector $\mathbf{I} = p\mathbf{v}$ is *the acoustic intensity*. It is connected to the power per unit area by $dP = \mathbf{I}.\mathbf{n}dS$, where $\mathbf{n}$ is the unit vector in the velocity's direction.

By integrating on a volume V and using the divergence theorem, Eq. (1.127) can be interpreted as follows: the power $\iint_S p\mathbf{v}.\mathbf{dS}$ going out the volume V through the surface S is equal to the total energy decrease in the volume added to the power supplied by sources. In periodic regime, averaged over a period, the term containing E vanishes (the average of the time derivative of a periodic quantity is zero), and in the absence of a source, the average outgoing power is zero. This is due to the fact that we assume the system to be conservative.

1.3.3 Power and Impedance

1.3.3.1 Instantaneous and Average Acoustic Power: Acoustic Impedance

With the previous definition of the acoustic power, we consider the *instantaneous* power through the surface of area S in harmonic regime: $\mathscr{P} = Sp(t)v(t) = p(t)u(t)$, where $u(t) = Sv(t)$ is the flow rate. We assume that the pressure and velocity are uniform on this surface, and that $p_c(t) = A\exp j(\omega t + \varphi)$. With the complex variables, we define also the *acoustic impedance* $Z = p_c/u_c$ and the *acoustic admittance* $Y = u_c/p_c$, thus and $u_c = Yp_c$. We get

$$u(t) = \Re e\left[u_c(t)\right] = \Re e\left[YAe^{j\omega t+\varphi}\right] = A\Re e(Y)\cos(\omega t + \varphi) - A\Im m(Y)\sin(\omega t + \varphi),$$

and the instantaneous acoustic power is written as follows:

$$\mathscr{P} = p(t)u(t) = \mathscr{P}_m + \frac{1}{2}A^2\left[\Re e(Y)\cos 2(\omega t + \varphi) - \Im m(Y)\sin 2(\omega t + \varphi)\right]. \tag{1.129}$$

The term $\mathscr{P}_m = \frac{1}{2}A^2\Re e(Y)$ is the power averaged over a period. The second term, of zero mean value, is called "fluctuating power," as the system restores during a half-period the energy it has received in the previous half-period.[7]

In complex notation (see Sect. 1.2.5), the calculation of quadratic quantities turns out to be rather tricky. However, in practice, as previously, we often calculate the average values of some variables over a period T, only. The general result for two variables p_1 and p_2 is

$$\frac{1}{T}\int_0^T p_1(t)p_2(t)dt = \frac{1}{2}\Re e\left[p_{c1}(t)p_{c2}^*(t)\right] = \frac{1}{4}\left[p_{c1}(t)p_{c2}^*(t) + p_{c1}^*(t)p_{c2}(t)\right],$$

where $*$ is the conjugate quantity. With these expressions, we can write the most useful formulas:

$$\mathscr{P}_m = \frac{1}{2}\Re e(p_c u_c^*) = \frac{1}{2}\left|u_c\right|^2\Re e(Z) = \frac{1}{2}\left|p_c\right|^2\Re e(Y) \tag{1.131}$$

1.3.3.2 Power Supplied to a Passive System

- The power is either provided to a system, or provided by this system, depending on the sign of the real part of the impedance (resp. admittance). Consider a simple example in mechanics: a force **f** is applied to a passive system, it performs the mechanical work **f**.**x**, where **x** is the displacement of the system. The generated power, i.e., the work per unit time, is therefore **f**.**v**. This scalar product is equal to the provided power, which is also the power dissipated in the passive system, and it is, by definition, positive.
- By convention we define the impedance as the ratio of a quantity providing energy to a quantity characterizing a passive system (we can see that if we choose the reaction force of the passive system on the excitation, equal to $-\mathbf{f}$, we would have a definition leading to a negative real part for the impedance). An example of such a system is a volume of air excited by a vibrating wall: the definition of the impedance is the ratio between the force applied by the wall on the air and the velocity (either of the wall or of air, because these velocities are identical for a perfectly reflecting wall). The opposite convention would be to use the force exerted by air on the wall. If the passive system is not dissipative, i.e., conservative, the impedance is purely imaginary.

[7] The average power $\mathscr{P}_m$ is also called *active* power. A "reactive" power is also defined by

$$\mathscr{P}_r = \frac{1}{2}\Im m(pv^*) = -\frac{1}{2}\left|p\right|^2\Im m(Y) = \frac{1}{2}\left|v\right|^2\Im m(Z). \tag{1.130}$$

We choose arbitrarily its sign, which will be positive or negative depending on whether the system is dominated by stiffness or mass (we do not go further here, because the chosen quantities are formal).

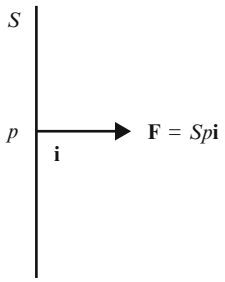

Fig. 1.15 Acoustic pressure force

- A special case is that of the force of acoustic pressure, because pressure is a scalar quantity. Let us consider a passive surface S on which the pressure p is applied (see Fig. 1.15). We choose, by convention, to define the specific impedance as p/v, where v is the projection of the velocity onto the normal to the surface in the direction of the force due to the pressure (and the acoustic impedance as $p/(Sv)$). We see that this convention is consistent with the previous choice. It is also the case for the input impedance of a wind instrument: as the resonator is passive, if a pressure is applied at its input, the input impedance of the resonator is always defined by choosing the velocity projection along the axis directed towards the exit of the pipe.

1.3.3.3 Standing Waves

In sinusoidal regime, for the complex quantity corresponding to a standing wave, we can write: $p_c = f(\mathbf{r})\exp(j\omega t + \varphi)$, where φ does not depend on the spatial dimension. Using the Euler equation (1.110), we derive that the velocity is in phase quadrature with the pressure, since $\partial/\partial t = j\omega$. Therefore, the impedance is purely imaginary for the three velocity components, thus the admittance vector $\mathbf{Y} = \mathbf{v}/p$ is purely imaginary, and the average acoustic intensity over a period is zero in all directions. It is noticeable that standing waves do not carry any energy averaged over a period. It is (almost) the case for the oscillation of the air column of a wind instrument or, similarly, for the vibration of a string.

1.4 Sources in Musical Acoustics: Excitation Mechanisms

In the previous sections, a number of differential equations were written to describe the structures used in musical instruments. To use them, we must know the sources, which can be introduced either in the differential equation itself, such as for Eq. (1.9) or Eq. (1.111), or in the boundary and initial conditions. In this section, some type of sources found in musical acoustics are presented.

1.4.1 Generalities About Sources and Types of Oscillations

To build a model, we need to consider that one or more physical quantities are imposed in a region of space and time, and that they are insensitive to the medium in which they are imposed. These quantities play the role of sources, or generators. Thus in a linear circuit, it is often assumed that one can impose a voltage (possibly with an internal impedance, according to Thevenin and Norton's theorems). All quantities in the circuit are proportional to the magnitude of this source. The power supplied to the circuit depends on the circuit, i.e., on the impedance viewed at the source. Thus a source term not only implies a notion of imposed magnitude, but also a notion of supplied power.

In musical acoustics, we have to consider sources that produce oscillations and, in turn, sounds. Different types of oscillations can be encountered:

- The oscillations are *linear* if the result is proportional to the cause, or, in case of multiple causes, if the result is a linear combination of these causes (superposition principle). If a source is sinusoidal, a result proportional to the cause is also sinusoidal with the same frequency. Otherwise, the oscillations are nonlinear.
- Oscillations are *free* after extinction of the sources, and are *forced* during application of the sources.

Musical instruments enter into two main categories:

- Instruments with a *transient* excitation, followed by free oscillations. In this case, the sound usually lasts longer than the excitation: this is the case for percussion and string instruments, except for bowed strings. For these instruments, the free oscillations can be either linear or nonlinear (piano, timpani, cymbals,...). The excitation is produced by means of an impact (hammer, stick, and mallet), or a pluck (plectrum and finger).
- Instruments with a *continuous* excitation, which is often constant or slowly varying. Oscillations arising from a constant or slowly varying excitation are necessarily nonlinear, and are called "self-sustained oscillations." This is the case for bowed string instruments excited by a continuous bow-string friction process, and for all wind instruments, where the excitation is the result of jet–edge interaction (flute-like instruments) or air–structure interaction (vocal folds, lips, and reed).

Some constitutive parts of an instrument can be regarded as steady-state oscillating sources generating *forced* oscillations: a string fixed at the bridge of a soundboard (or soundbox), for example, acts as a source of oscillations for the board. Such a source generally has a low internal impedance, which means that the string transmits to the board the *force* developed at the point of coupling, almost entirely. Conversely, the soundboard (or soundbox) is an oscillating source that induces forced oscillations to the surrounding air. This source is generally of high internal impedance: the board transmits its *velocity* to the ambient fluid.

For wind instruments, the air in the pipe plays the same role for the external air as the soundboard. It can be assumed, especially at low frequencies, that the flow produced at the holes is not affected by radiation.

For most models expressed in the form of differential equations, such as acoustic waves, source terms appear in the right-hand side of the conservation equations. In some cases, however, the sources are included in the boundary conditions, or even in initial conditions. In a number of cases, both formulations are equivalent. A simple example is the one of a plucked string released from its initial position at the origin of time: the problem can be either treated as an initial value problem, or as a problem with a second member that contains a plucking force (see Chap. 3).

1.4.2 Acoustic Sources

1.4.2.1 Flow Source

Equations (1.109) and (1.110) show two types of acoustic sources, referred to as sources of type 1 (flow sources) and type 2 (force sources). We will reexamine these concepts in Chap. 12 devoted to radiation in free space. Let us now illustrate Eq. (1.109) with the example of a vibrating body that imposes its velocity to the fluid (at rest). One can imagine the membrane of a small loudspeaker, with displacement $\xi(t)$, acting at a given point $\mathbf{a}$ in space. This loudspeaker is assumed to be a point-source, which means in practice that its dimensions are much smaller than the wavelength (see the following Sect. 1.5). The speaker is located in an enclosure, to avoid a short-circuit between both sides of the membrane. In three dimensions, the speaker can be viewed as a "pulsating" sphere, radiating uniformly in all directions (see Fig. 1.16).

This source, which is well-known in acoustics, is obviously an idealized object, only conceivable in "thought experiments." The displacement per unit volume is $\xi(t)\delta(\mathbf{r}-\mathbf{a})$, where δ is the Dirac delta function (integrating this quantity on any volume yields $\xi(t)$). Consequently, the velocity per unit volume is $\delta(\mathbf{r}-\mathbf{a})\partial[\xi(t)]/\partial t$,

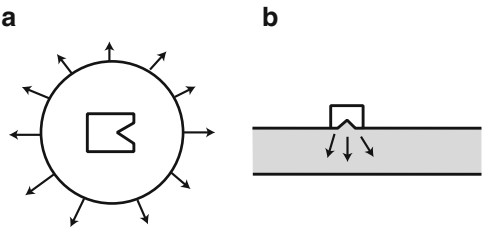

Fig. 1.16 "Punctual" speaker, located in an enclosed space, radiating: (**a**) in free space; (**b**) in a pipe

and the flow per unit volume is $q = S_m \delta(\mathbf{r}-\mathbf{a}) \partial [\xi(t)] / \partial t$, where S_m is the membrane area.[8]

- Let us now turn back to wind instruments, assuming a cylindrical cross-section. The elementary acoustic solutions are plane waves. We put the little speaker on the side of the pipe (Fig. 1.16), and we study the case of a sinusoidal excitation with angular frequency ω. A flow $u_s(t) = S_m \, \partial [\xi(t)] / \partial t = S_m j\omega \xi$ is produced, at point $x = a$. For a pipe of cross-section S, the projection of the velocity vectors on the x axis yields

$$u_s = S [v_x(x + dx) - v_x(x)] = S \left[v_x(a^+) - v_x(a^-) \right]. \tag{1.132}$$

  It is assumed further that the speaker does not disturb the pressure field, which remains plane and continuous at the position of the speaker (this question will be discussed in more details in Chap. 7 with regard to the effects of side holes). The law of dynamics: $dp/dx = -j\omega\rho v_x$ (1.110) applies here. Therefore, the pressure p is continuous at position $x = a$ whereas its derivative is discontinuous. This gives for the wave equation:

$$\frac{d^2p}{dx^2} + \frac{\omega^2}{c^2} p = -\frac{j\omega\rho}{S} u_s \delta(x-a). \tag{1.133}$$

  (We can verify this result by integrating this equation between a^- and a^+: it is the discontinuity of the derivative that brings the Dirac delta function on the right-hand side).
- If we now return to an arbitrary dependence in time $u_s(t)$, we obtain

$$\frac{\partial^2 p}{\partial x^2} - \frac{1}{c^2} \frac{\partial^2 p}{\partial t^2} = -\frac{\rho}{S} \frac{du_s(t)}{dt} \delta(x-a). \tag{1.134}$$

  This is consistent with what was obtained in three dimensions. The presence of the cross-section S here is a consequence of the unidimensional character of the Dirac delta function which is inversely proportional to a length, and not to a volume. We can imagine a practical illustration by considering the key of an instrument with side holes that are instantaneously closed. The flow is almost a

[8] Assuming a given function of time for the displacement, the source term in Eq. (1.111) is entirely known. A "realistic" simple function is, for example, $hH(t)$, where h is the amplitude and $H(t)$ the unit step function (or Heaviside step function). In practice, this means that the membrane is suddenly moved, then blocked. In this case, the source term in (1.111) becomes $-\rho h S_m \delta(\mathbf{r}-\mathbf{a}) \partial [\delta(t)] / \partial t$, since $\delta(t)$ is the derivative of $H(t)$. In the next chapters, a particular case of elementary source called Green's function, where the source is written $\delta(\mathbf{r}-\mathbf{a})\delta(t-t_0)$, will be examined in details. To achieve it in our "thought experiment," the velocity should be a step function, and therefore, the displacement should increase indefinitely, which is not realistic! Another way to obtain this Green's function is to write the acoustic wave equation in terms of velocity potential [see Eq. (1.105)]. In this latter case, the source term becomes $hS_m \delta(\mathbf{r}-\mathbf{a})\delta(t)$.

pulse, but as the closure is not instantaneous, the pulse is not perfect. However, we clearly hear a sound with definite pitch.

Since we impose a displacement, we can also consider a problem without a source, but rather with imposed boundary conditions.[9] Several problems exist with imposed flow, or rather with flow function $u_s = F(p)$ of the pressure, particularly for reed instruments. At the origin of the transients, this function is linear, and we can write $u_s = F_0 + Ap$. Since we are interested in the derivative only, the source term is written $-\frac{\rho}{S}Ap\delta(x-a)$. As the oscillation starts, growing exponentially, the source must provide energy, and the coefficient A must be negative. Otherwise, it would not be a source, but a dissipating system.

1.4.2.2 Relation Between Applied Force and Acoustic Force Strength

What happens if the membrane of the speaker, which is now supposed to be free on both sides, is set perpendicular to the pipe, thus preventing any continuous flow? It exerts a force **f** on the fluid, which has to be balanced by the pressure. By projecting this force on the x-axis, we obtain

$$f + S\left[p(a^-) - p(a^+)\right] = 0\,.$$

With an imposed force, we obtain a source of pressure difference and not the difference of its derivative. We can write an expression similar to (1.134), by interchanging the roles of pressure and velocity, i.e., by using the conservation of mass instead of Euler equation:

$$\frac{\partial^2 v_x}{\partial x^2} - \frac{1}{c^2}\frac{\partial^2 v_x}{\partial t^2} = -\frac{\chi_S}{S}\frac{df(t)}{dt}\delta(x-a).$$

Taking the derivative of both terms with respect to x, and integrating with respect to time, we get

$$\frac{\partial^2 p}{\partial x^2} - \frac{1}{c^2}\frac{\partial^2 p}{\partial t^2} = \frac{1}{S}f(t)\frac{d}{dx}\delta(x-a). \tag{1.135}$$

In Chap. 10, it will be shown that the production of sound in flute-like instruments can be represented by such an aeroacoustical force strength.

[9] A wave equation or a boundary condition including a source is called *heterogeneous*. It can be shown that it is always possible to transform a heterogeneous boundary condition into a homogeneous one by changing the wave equation.

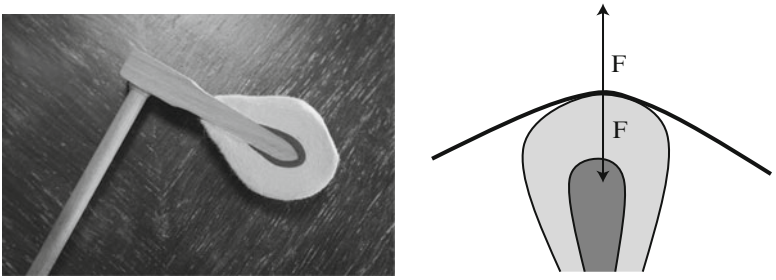

Fig. 1.17 (*Left*) A piano hammer (© Itemm). (*Right*) Interaction between an exciter and the vibrating system. Example of the piano hammer. As a result of the motion of the key pressed by the pianist, the hammer strikes the string(s) and transmits a force F that depends on time and impact velocity. According to the principle of action and reaction, the string exerts an equal and opposite force that leads to push the hammer back after an interaction time of a few milliseconds

1.4.3 Transient Mechanical Excitation

We describe here the transient vibrations of strings and percussion instruments subjected to impact or friction (plucking). During such transients, the energy of the exciter is transmitted to the vibrating system during a finite duration. In this time interval, the interaction between the exciter and the system can be rather complex and it is generally not possible to ignore the reaction of the structure on the exciter. In the case of the piano, for example, the impact force is not imposed: it is the result of the temporal evolution of the strings in contact with the hammer (see Fig. 1.17).

1.4.3.1 Friction and Plucking

Transient excitation by friction, or plucking, occurs in plucked string instruments such as guitar, lute, harp or harpsichord. In most works, the plucking action is simply viewed as an initial condition for the displacement of the string (see [45]). This model provides a first approximation of the spectral content of the free vibration of the string. However, it does not account for the interaction with the exciter or the player. This initial stage is essential since it contributes to determine the timbre of the produced sound. Auditory experiments performed with recorded sounds where the initial transients are truncated show that the listeners are not able to recognize the instruments anymore. Some elements to consider for a better physical description of the plucking are given below.

- The string is moved from its initial position by a force localized on a small portion of the string, that we can write as $F(\mathbf{x}, t) = F(t)\delta(\mathbf{x}-\mathbf{x_o})$. As long as the frictional force exerted by the finger (or plectrum) on the string remains below a given threshold F_M, it stays stuck to the exciter: this corresponds to the *stick* phase. The amplitude of F then continues to increase and is balanced by the restoring

force resulting from the angle formed by the two sides of the string on both sides of the exciter. During this phase, the motion of the string might contain a torsional component.

- When the restoring force reaches the threshold F_M, then the string slides under the finger and begins to produce free oscillations. During this *slip* phase, which is relatively short compared to the stick phase, the finger (or plectrum) is likely to introduce a damping which decreases as the relative velocity between exciter and string at the contact point increases. We will find again such a succession of stick and slip phases in the mechanics of the bowed string (see Chap. 11). In the latter case, the essential difference follows from the fact that such transitions occur repeatedly with a cadence that gradually synchronizes with the oscillation of the string.

  A detailed description of the excitation of a guitar string by the friction of the finger was done by Pavlidou [43]. More recently, a similar model has been developed for a plucked harp string [14, 15, 34]. We briefly recall here some principles of the Pavlidou model. The two transverse polarizations and torsional waves are taken into account on the string. We also consider the motion of the bridge at one end. The tension T of the string is assumed to be constant during the motion. The finger model first includes a muscle, represented by a nonlinear spring with a spring force $S(\xi)$ which is a hyperbolic function of its elongation ξ (see Fig. 1.18) written as:

$$S(\xi) = \begin{cases} \dfrac{\sigma_1 \xi}{\sigma_2 - \xi} & \text{for} \quad \sigma_2 > \xi \geq 0, \\ \dfrac{\sigma_1 \xi}{\sigma_2 + \xi} & \text{for} \quad -\sigma_2 < \xi < 0, \end{cases} \tag{1.136}$$

  where σ_1 and σ_2 are constants derived from experimental measurements. The model also includes the upper part of the finger, considered as a lever arm with a speed imposed by the guitarist, and the nail, circular, in direct contact with the string. The interaction with the pulp of the finger is not considered here (see Fig. 1.19).

  During the three phases of the motion, the model is obtained by considering:

1. **During the stick phase**: (a) the translational motion of the string element interacting with the exciter, (b) the rotational motion of the fingertip, (c) the rotational motion of the string element, and (d) the relative velocity between string and finger.
2. **During the slip phase**: the friction coefficient μ depends on the relative velocity V_{rel} between string and nail. Typically, such a function is of the form (see Fig. 1.20):

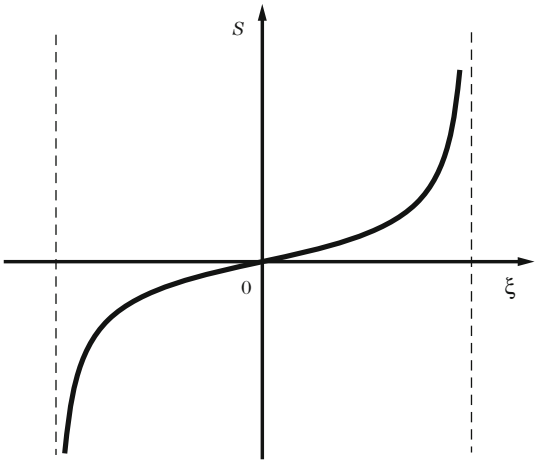

Fig. 1.18 Force-elongation diagram of a muscle (from Pavlidou [43])

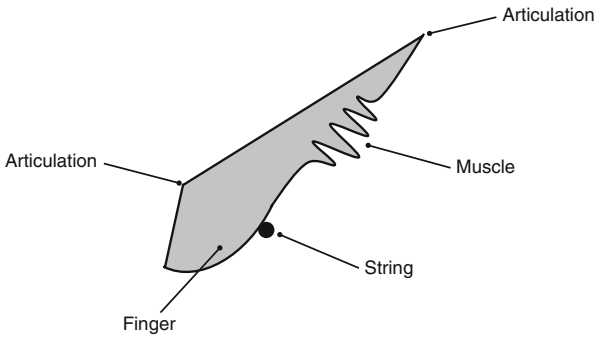

Fig. 1.19 Finger model (from Pavlidou [43]). This diagram shows the two last phalanges of the finger. The last one is in direct contact with the string, and its motion is guided by both the articulation and muscle that connect it to the upper phalanx

$$\mu = \begin{cases} \dfrac{(-V_0\mu_s - \mu_d V_{\text{rel}})}{V_{\text{rel}} + V_0} & \text{for} \quad V_{\text{rel}} > 0, \\ \dfrac{(V_0\mu_s - \mu_d V_{\text{rel}})}{V_0 - V_{\text{rel}}} & \text{for} \quad V_{\text{rel}} < 0\,. \end{cases} \tag{1.137}$$

In this equation μ_s is the static friction coefficient, μ_d the dynamic friction coefficient, and V_0 the initial velocity of the finger impacting the string. A similar model accounts for the friction of the rosin on a violin bow (see, for example, [50], and Chap. 11 of this book). For more information on friction models, the reader can refer to [1].

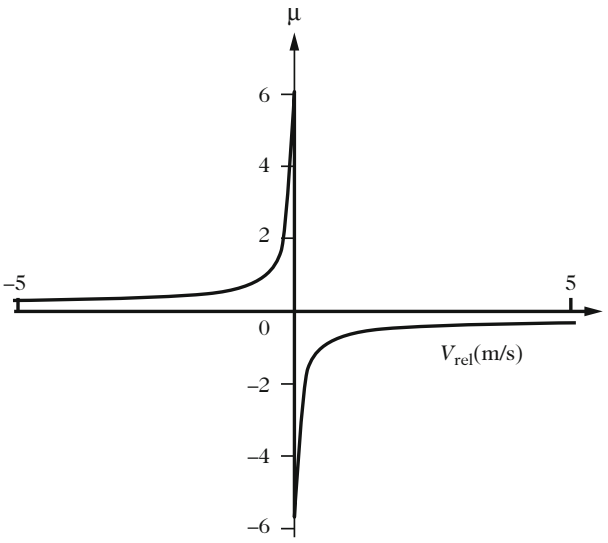

Fig. 1.20 Friction model during the slip phase

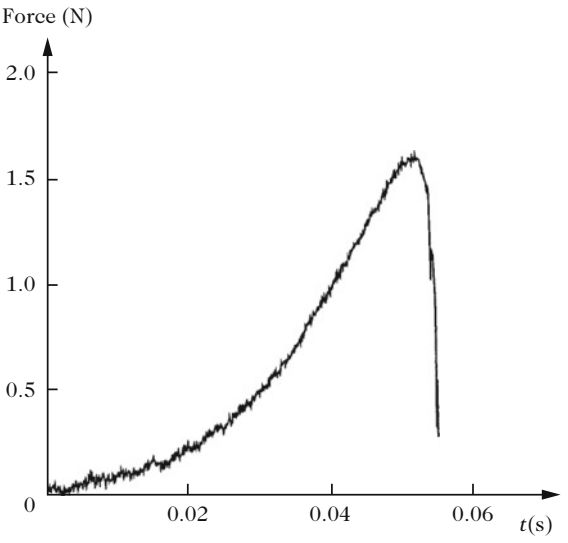

Fig. 1.21 String–plectrum interaction force of a harpsichord note

3. **During the free oscillations**: the motion of the string is completely defined by three equations (two transverse polarizations and one torsional oscillation) with initial conditions obtained from the equations of the stick phase.

Giordano and Winans measured the string–plectrum interaction force for a harpsichord string (see Fig. 1.21). They showed a gradual increase of the force during the stick phase followed by a rapid decrease during the slip phase [24].

For plucked strings, there is an average rise time of about 20 ms followed by a rapid decrease (<1 ms), after which the free oscillation starts. Systematic variations of interaction parameters show that the sound quality primarily depends on the following properties:

- The characteristics of the finger-string friction, mostly during the slip phase. This mainly affects the relaxation phase.
- The elastic properties of the finger muscle.
- The input admittance of the string at the bridge. This admittance affects the transmission rate of energy from string to soundboard. The reaction force exerted by the string on the exciter depends on this rate: the player says that he "feels" his instrument under his finger.
- The initial direction of the finger motion (angle of attack). This parameter affects the initial polarizations of the string that are coupled at the bridge [32].

Finally, the plucking velocity primarily affects the amplitude of vibration (and sound), and weakly the timbre, as long as the assumption of linear vibrations of the string is valid.

1.4.3.2 Elastic Hertzian Impact

Impact excitation concerns the piano and almost all percussion instruments. Musical experience shows that the sound produced depends, among other things, on the properties of the exciter: the thickness of the felt varies among the piano hammers, and timpani mallets show a large variety of rigidity (see Fig. 1.22). The head of xylophone mallets also differs from each other in terms of weight and stiffness. To be convinced of the relevance of exciter properties, just look at percussionists in an orchestra: they change their sticks and mallets several times during a performance.

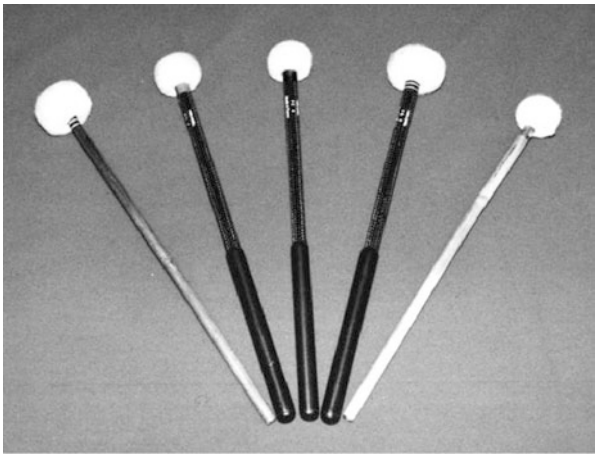

Fig. 1.22 Examples of kettledrum mallets. They differ from each other through the stiffness of the felt and the elasticity of the stick

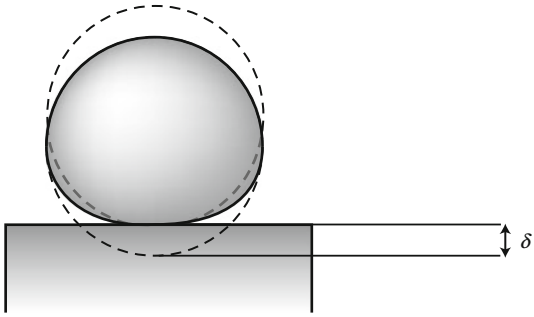

Fig. 1.23 Contact between an elastic sphere and an infinite rigid plane. The quantity δ indicates the *compression* of the sphere, which represents its change in thickness consecutive to the impact

During the impact, an interaction force is generated between the impactor and the struck structure, as a result of the deformation of both elastic solids in contact. Historically, the first theory of contact between two semi-infinite elastic solids is due to Hertz and was published in 1882 [29]. This theory predicts, in particular, the stress distribution in the contact area. One of the most famous result of this theory is the expression of the interaction force F:

$$F = K\delta^{3/2}, \tag{1.138}$$

where δ is the *compression* or, in other words, the summation of strains on both surfaces (see Fig. 1.23), and K is a constant which depends on both the curvature and elastic coefficients of the solids. This constant is given by [33]:

$$\frac{1}{K} = \frac{3}{4}\left[\frac{1-\nu_1^2}{E_1} + \frac{1-\nu_2^2}{E_2}\right]\sqrt{\frac{1}{R_1} + \frac{1}{R_2}} = \frac{3}{4}\frac{1}{E_{\text{eq}}}\frac{1}{\sqrt{R_{\text{eq}}}}, \tag{1.139}$$

where E_1 and E_2 are the Young's moduli, ν_1 and ν_2 the Poisson's ratios, R_1 and R_2 the radii of curvature of the solids at the contact point. The quantities E_{eq} and R_{eq} are equivalent Young's modulus and radius, respectively, often used to simplify the formula.

The formula (1.139) can be applied to the case of a sphere impacting an infinite rigid plane, as $R_2 \to \infty$. If, in addition, $E_1 \gg E_2$, which means that the impactor is significantly more rigid than the impacted surface. As a consequence, the coefficient K becomes

$$K = \frac{4}{3}\frac{E_2}{1-\nu_2^2}\sqrt{R_1} \quad \text{in} \quad \text{N m}^{-3/2}\,. \tag{1.140}$$

In other words, the softer solid imposes the main properties of the impact.

- Hertz's contact theory remains valid as long as the dimensions of the contact area remain small compared to both the dimensions of the solids and radii of

curvature. It does not predict good results for head materials subjected to large deformations as, for example, rubber (see [16]). Hertz's theory also ignores the effects of inertia and elastic waves in the media in contact. However, if the contact time is small compared to the period of the studied phenomena, this theory reasonably accounts for experimental observations, which explains its wide use.

Pulse Duration and Maximum Impact Force

Based on Hertz's law, an estimation for both the pulse duration and maximum of the impact force can be derived. If V_0 is the initial velocity of the impactor on the solid surface at rest, and denoting $m_r = m_1 m_2/(m_1 + m_2)$ the reduced mass of the two solids, the conservation of the total energy of the system (without dissipation) is written [33]:

$$\frac{1}{2} m_r \dot{\delta}^2 + \frac{2}{5} K \delta^{5/2} = \frac{1}{2} m_r V_0^2 \,. \tag{1.141}$$

The maximum of the compression is obtained when $\dot{\delta} = 0$, which provides

$$\delta_{\text{Max}} = \left(\frac{5 m_r}{4K} \right)^{2/5} V_0^{4/5} \,. \tag{1.142}$$

The duration τ of the force impulse is obtained by integrating (1.141):

$$\tau = 2 \int_0^{\delta_{\text{Max}}} \frac{d\delta}{\sqrt{V_0^2 - \dfrac{4K}{5m_r} \delta^{5/2}}} = 2 \left(\frac{25 m_r^2}{16 K^2 V_0} \right)^{1/5} \int_0^1 \frac{d\xi}{\sqrt{1 - \xi^{5/2}}}, \tag{1.143}$$

which yields finally:

$$\tau = 3.218 \left(\frac{m_r^2}{K^2 V_0} \right)^{1/5} \,. \tag{1.144}$$

Equation (1.144) shows, in particular, that the pulse duration only weakly depends on the impact velocity. This result is in agreement with measurements made on a large number of mallets [11]. From an experimental point of view, the constant can be derived K from measurements of the maximum impact force and pulse width using Eqs. (1.138), (1.142), and (1.144). We find

$$K = 35.4 \frac{1}{\tau^3} \sqrt{\frac{m_r^3}{F_{\text{Max}}}} \,. \tag{1.145}$$

1.4.3.3 Empirical Generalization of Hertz's Law

Since Ghosh in 1927 [22], several authors proposed a generalization of Hertz's law for piano hammers, on the form:

$$F = K\delta^p, \tag{1.146}$$

where the superscript p is between 2.0 and 4.0 approximately [26]. This expression has been also used for modeling the impact of timpani mallets [46]. The power law (1.146) is essentially empirical and is not based on an accurate analysis of stress and strain, in contrast with Hertz's law. This expression fairly accounts for the compression of the felt (a porous material) wrapped around the wooden tip. It offers the practical advantage to identify experimental force-compression laws with two parameters only.

1.4.3.4 Impact with Dissipation

In practice, the contact force is not purely elastic. Due to their rheological properties, hammer and mallet materials are subjected to internal dissipation. Moreover, impacts can be strong and lead to additional dissipation due to plastic deformation. We can, for example, easily observe proofs of impacts on wooden xylophone bars.

Viscous Dissipation

N.B. In this section, plastic deformation is ignored.

As a consequence of viscous dissipation, the force-deformation curve $F(\delta)$ shows a hysteresis loop (see Fig. 1.24). This loop is due to the viscoelasticity of the material, a "memory effect" which produces a relaxation (decrease) of stress over time after application of strain. The first attempt to extend Hertz's law to viscoelastic media was made by Pao [42]. His theory leads to a modified expression of the form:

$$F = F_0\left[\delta^{3/2} - \int_0^t \Psi(\xi - t)\delta^{3/2}(\xi)d\xi\right], \tag{1.147}$$

where $\Psi(t-\xi)$ is a relaxation function which can be represented by a sum of exponentials. This expression was revisited by Stulov [53] for piano hammers:

$$F = F_0\left[\delta^p - \frac{\varepsilon}{\tau_o}\int_0^t \exp\left(\frac{\xi - t}{\tau_o}\right)\delta^p(\xi)d\xi\right], \tag{1.148}$$

where ε is a dimensionless coefficient that reflects the hysteresis area, i.e., the energy lost per cycle, and where τ_o is the relaxation time. In the case of piano hammer felt, τ_o is approximately 1–2 ms.

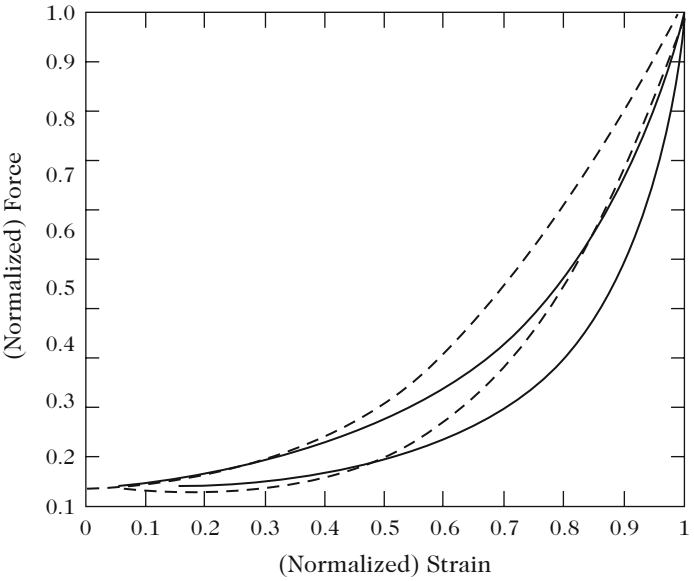

Fig. 1.24 Force-compression curve for a dissipative mallet with hysteresis loop. *Solid line*: experimental curve; *dotted line*: differential model (1.149)

For piano and percussion instruments, the contact pressure on the felt is applied relatively slowly, since the impact velocities do not exceed 5 m/s. This allows writing $F \gg \tau_o \frac{dF}{dt}$. Calculating $\frac{dF}{dt}$ from (1.148), we find

$$F_{tot} \simeq F + \tau_o \frac{dF}{dt} = K\left[\delta^p + R\frac{d\delta^p}{dt}\right], \tag{1.149}$$

where $K = F_0(1-\varepsilon)$ is the stiffness coefficient and $R = \frac{\tau_o}{1-\varepsilon}$ the coefficient of viscous dissipation. The differential formulation (1.149) has been used in models of piano and drums [31]. An estimation for the coefficient R can be obtained by energetic considerations [17]. This differential expression is simpler to use than the integral formulation (1.148), though it remains valid for medium or low impact velocities only. Figure 1.24 shows a comparison between an experimental curve and a differential model of type (1.149) for a timpani mallet.

Plastic Strain

By definition, a plastic solid shows stable residual strains, after cessation of the excitation. This behavior does not depend explicitly on time (see, for example, [38]). For an elastic, *perfectly plastic* solid, strain ε is linear (and characterized by a Young's modulus E) below the yield stress (or threshold) of plasticity σ_s.

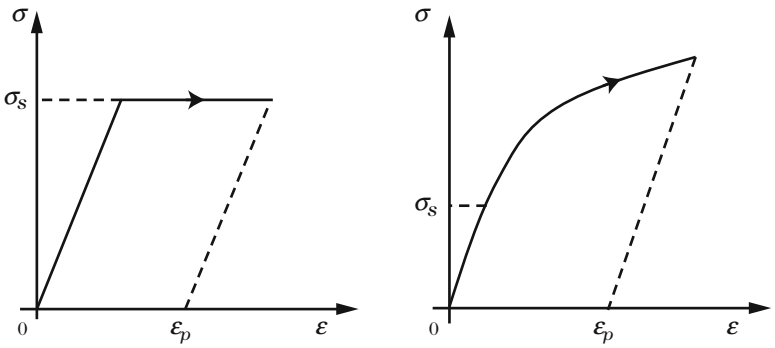

Fig. 1.25 (*Left*) Behavior law for an elastic perfectly plastic solid. (*Right*) Behavior law for an elastoplastic solid

The stress then remains constant as ε increases above σ_s/E. As the stress then decreases, another curve is drawn, distinct from the linear part, showing a permanent deformation ε_p at $\sigma = 0$ (see Fig. 1.25).

In the case of an *elastoplastic* solid, the stress continues to increase beyond the threshold of plasticity σ_s, generally in a nonlinear manner with respect to ε. Again, we note the existence of a permanent deformation after cessation of the loading (see Fig. 1.25).

In the case of contact between two spheres, Johnson showed that the impact becomes plastic when the average pressure between the two solids is about $p_m = 1.1\sigma_s$ [30]. From this property, this author deduced that the velocity of contact above which plastic deformations are likely to occur is about $V_l = 0.14\,\mathrm{m\,s^{-1}}$ for a steel of medium hardness and $V_l < 0.08\,\mathrm{m\,s^{-1}}$ for aluminum. The important point indicated by these values is that plasticity is present in most of the common impacts, even at low speed. For an impact between two solids made of the same material of density ρ, with a threshold of plasticity σ_s and for which the the relative velocity of impact is V, the following table, due to Johnson [30], provides a good order of magnitude:

- $\frac{\rho V^2}{\sigma_s} < 10^{-6}$ $\rightarrow$ elastic behavior.
- $10^{-6} < \frac{\rho V^2}{\sigma_s} < 10^{-3}$ $\rightarrow$ elastoplastic behavior
- $10^{-3} < \frac{\rho V^2}{\sigma_s} < 10^{-1}$ $\rightarrow$ perfectly plastic behavior.

One effect of plasticity is that the force-compression curve again shows a hysteresis loop (see Fig. 1.26).

This curve shows a maximum at point A (of coordinates F_c, δ_c). We see that there is a non-zero residual deformation δ_p as the interaction force equals zero, corresponding to the situation where the two solids move away from each other (point B on the curve). As a consequence, the energy restored during the decrease of the force, which corresponds to the area below the curve AB, is less than the

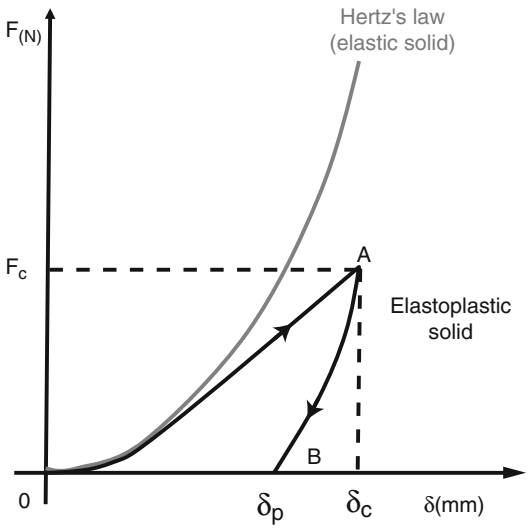

Fig. 1.26 Force-compression curve for an impact between two elastoplastic solids. From [54]

energy stored during the impact, corresponding to the area below the curve OA. The *restitution coefficient* is the ratio between these two energies. It is less than unity for a plastic impact.

Several formulations were proposed to extend Hertz's law to elastoplastic or perfectly plastic case. Stronge [52] suggests to model the loading curve OA using Hertz's law, and the unloading curve AB with an equation of the form:

$$F = \frac{4}{3} E_{\text{eq}} \sqrt{R^*_{\text{eq}}} (\delta - \delta_p)^{3/2}. \tag{1.150}$$

where R^*_{eq} is a curvature radius greater than R_{eq}, due to plastic deformation.

Vu-Quoc and Zhang developed a numerical model of impact between two elastoplastic spheres whose central idea is based on the decomposition of the contact radius into an elastic part and a plastic part [54]. The detailed presentation of this theory is beyond the scope of the present book. The results show that this model is able to predict the variations of the coefficient of restitution with the impact velocity accurately. This represents a significant advance over previous models in the sense that most of the parameters of this model can be directly related to material and geometric properties of the solids. Impact modeling still remains an open field of study, especially in the field of granular media.

1.5 Lumped Elements; Helmholtz Resonator

Having established the differential equations and discussed about the sources, we study a very particular case, usually encountered at low frequencies. Under certain conditions, the acoustic wave equation can be simplified. Leaving aside the sources

in (1.111), there are conditions for which the term containing the time derivative (of order two) of the pressure is very small compared to that containing the spatial derivative. To establish these equations we make a dimensional analysis, assuming that there is a length L and a time τ by which we make dimensionless distance and time. If we note these quantities $\overline{x}, \overline{y}, \overline{z}, \overline{t}$, we get

$$\frac{\partial^2 p}{\partial \overline{x}^2} + \frac{\partial^2 p}{\partial \overline{y}^2} + \frac{\partial^2 p}{\partial \overline{z}^2} = (\mathrm{He})^2 \frac{\partial^2 p}{\partial \overline{t}^2},$$

where $\mathrm{He} = \frac{L}{c\tau}$ is the Helmholtz number, which is mostly written with an angular frequency $\omega = 1/\tau$:

$$\mathrm{He} = \frac{\omega L}{c} = kL = \frac{2\pi L}{\lambda}, \tag{1.151}$$

where λ is the wavelength. We see that at the limit of low frequencies, spatial variations become predominant and we can solve the Laplace equation $\Delta p = 0$, valid for an incompressible (not viscous) fluid. This occurs particularly near singularities such as the open end of a pipe, when considering only a "compact" area, i.e., an area of dimensions small compared to the wavelength c/ω: such a zone is called "lumped zone." In fact we can go a step further by examining the two first order equations involving pressure and velocity, (1.109) and (1.110).

- In Eq. (1.109) without right-hand side, the time-derivative term becomes very small under the following conditions: at low frequencies—in fact at low Helmholtz number, as it has been seen—or if the pressure is small, which also occurs near the end of a pipe, or if the compressibility is low (the fluid is close to incompressibility). Then, by integrating the term div$\mathbf{v}$ in the considered zone, we see that the flow rate is zero. Thus, in one dimension, the incoming flow rate is equal to the outgoing one, and it is the same for the velocity. The two equations can be reduced to an acoustic "Ohm's law" [10]:

$$v_x(x) = v_x(x + \delta x) = v \;\; ; \;\; p(x) - p(x + \delta x) = \rho(\partial v_x/\partial t)\, \delta x = \rho c(\partial v_x/\partial \overline{t})\mathrm{He}\,. \tag{1.152}$$

- In the second Eq. (1.110), the time-derivative term becomes very small under the following conditions: at low frequencies, if the velocity is small, or if the fluid is very light (small ρ). This occurs in particular near a rigid wall, where the velocity is zero, and, in turn, the term **grad**p is zero: the pressure is uniform in the

[10] The electroacoustic analogy called "acoustic impedance" associates acoustic pressure and velocity to electric voltage and current, respectively. Ohm's law states that between two points the difference in one of the quantities is proportional to the other quantity.

considered area, and using the divergence theorem, the total flow rate entering the zone of volume V is equal to $V\chi_S \partial p/\partial t$. In one dimension this gives the second Ohm's law[11]:

$$p(x) = p(x+\delta x) = p \;\; ; \;\; v_x(x) - v_x(x+\delta x) = \chi_S(\partial p/\partial t)\,\delta x = c\chi_S(\partial p/\partial \overline{t})\text{He}. \tag{1.153}$$

- A physical system exists that combines these two effects: the Helmholtz resonator. It is made of a rigid cavity of volume V with a neck of length ℓ and section S (see Fig. 1.27), the neck being open onto a large space imposing a low pressure at the exit of the neck.

In order to model the resonator at wavelengths much greater than its dimensions, taking the sources into account, we have to consider the connection between the neck and the volume. Using again the divergence theorem, the flow rate u entering the cavity, where the pressure is uniform p_V, is written:

$$u = C_a \partial p_V/\partial t - u_{\text{source}}, \tag{1.154}$$

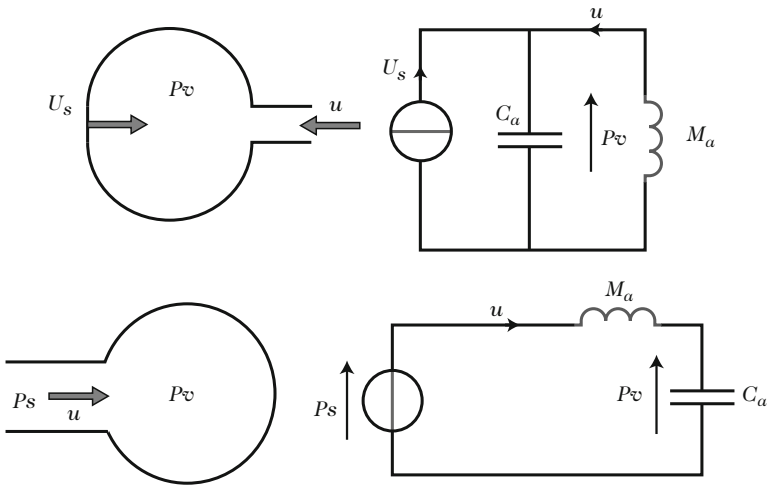

Fig. 1.27 Helmholtz resonator: its behavior is that of a system with localized constants at its resonance frequency. The volume of the cavity is V, the length and thickness of the neck are ℓ and S. We have: $C_a = \chi_S V$ and $M_a = \rho\ell/S$. The case shown on the *top* of the figure is that of a flow rate excitation [first Eq. (1.156)], the *lower one* corresponds to a pressure excitation [second Eq. (1.156)]

[11] We will encounter several times this concept of lumped-element systems. Notice that the finite difference calculation (Sect. 1.7.1) is based upon the division of a continuous system into lumped elements.

where $C_a = \chi_S V$ is the *acoustic compliance* and $u_{\text{source}} = \iiint_V q(\mathbf{r}, t)dV$ [see Eq. (1.109)]. In the neck, the flow entering from outside is equal to the flow rate u entering the cavity. As the transverse dimension of the neck is small compared to the wavelength, we assume that the pressure is uniform (i.e., plane) in a slice of fluid. We will see later (Chap. 7) how to connect the pressure at the exit of the neck with that of the cavity. For now, we assume that they are equal. Using the equation obtained above in one dimension, we derive

$$-p_V = M_a \frac{\partial u}{\partial t} - p_{\text{source}}. \tag{1.155}$$

where $M_a = \rho\ell/S$ is the *acoustic mass* and $p_{\text{source}} = p_e + \rho \int_{\text{neck}} F_x dx$. In this last expression the incoming pressure is added to the acoustic force strength.

- We will see that the correct matching leads to the same equation with a modified length ℓ (Chap. 7). We can then distinguish the two problems depending on whether the source is a source of flow in the cavity or a source of pressure in the neck, and write the second-order differential equations:

$$\begin{aligned} C_a \frac{\partial^2 p_V}{\partial t^2} + \frac{1}{M_a} p_V &= \frac{\partial u_{\text{source}}}{\partial t} \quad \text{and} \\ M_a \frac{\partial^2 u}{\partial t^2} + \frac{1}{C_a} u &= \frac{\partial p_{\text{source}}}{\partial t}. \end{aligned} \tag{1.156}$$

These equations are similar to those of electric circuits which are well known: if we choose the "acoustic impedance" analogy (pressure, flow, mass and compliance are analog of voltage, current, inductance, capacitance, respectively), the first equation is that of an antiresonant circuit (mass and compliance in parallel), while the second is that of a resonant circuit (mass and compliance in series). Of course, we expect to find in these equations a derivative of order 1, associated with damping. We will formally introduce damping in Chap. 2 to study the behavior of these equations. However in most situations, damping is frequency dependent, the modeling as a derivative of order 1 being a rough approximation.

Another way to model approximately an acoustic (or mechanical) system is to calculate a modal expansion, and to truncate the modal series to the first mode, as it is often done in this book.

1.6 Vibrating Strings-Sound Pipes Analogies

The analogy between longitudinal waves in solids and fluids is obviously very natural. It is so true that the term analogy can be discussed. However, it is not really useful in musical acoustics. As previously noticed, we are most often interested in transverse vibrations of solids, mainly in 2D, while for the fluid we are mainly

concerned with 1D and 3D models. We therefore limit this section to the analogy between lumped elements ("0D") and the analogy between vibrating strings and sound pipes, considered as 1D systems. Notice that, in all cases, we choose a pair of main quantities whose product gives the power, and whose ratio gives the impedance. Thus *the mechanical impedance is the ratio force/velocity*, and the admittance (or mobility) the inverse ratio. For a fluid, several pairs may be chosen.

- Let us start by lumped elements: we consider a fluid element of surface S moving with a velocity v and subjected to a pressure force $f = Sp$, which are the projection of vectors on the same axis. If we consider these two quantities, the acoustic system appears to be a mechanical system. But this choice of basic quantities is not the most useful for a main reason: as seen in Sect. 1.5, at the junction between ducts, the conserved quantity is the flow rate $u = Sv$. This is similar to the forces at the junction of several elementary mechanical elements, such as springs, having an identical velocity. For joined ducts, we will show that, at the lowest frequencies, the pressure is uniform. An important example for wind instruments is the junction between the main pipe and the "chimney" of a tonehole. Flow conservation at a junction is a major reason for which the most used impedance for a fluid is the impedance called "acoustic impedance," based upon the equivalence between pressure p and velocity of a mechanical system v, and between acoustic flow rate $u = Sv$ and force f, respectively. We consider here scalar quantities obtained by projecting a vector on an axis. Thus the *acoustic impedance*[12] *is defined as the ratio pressure/flow rate* $Z = p/Sv$. Notice that the power through a section S of pipe is given by the product of these two quantities, whatever the chosen pair $(f = Sp, v)$ or $(p, u = Sv)$.
- This analogy is presented in Table 1.1 for vibrating strings and sound pipes in one dimension.[13] We call it "reverse" analogy, because it reverses potential and kinetic energies. However, it is the most useful in practice. It can be extended, in particular, to continuous sources of self-sustained oscillations: velocity for bowed strings, pressure for reed instruments. On the other hand, for flutes, because of the nature of the source of self-sustained oscillations, it is preferable to choose the direct analogy, where the pair (f, v) matches the pair (p, Sv). For this reason, Table 1.1 also mentions this analogy.

[12]Sometimes we will also use an acoustic impedance called *specific* defined by the ratio pressure/velocity (see Sect. 1.2.4). This choice is convenient for some problems of unbounded media, or for energy transmission between two media with different sound speed or density.

[13]This table has some specificity with regard to the dimensions. The quantity f_{ext}, for example, is a force per unit length, whereas the quantity F in Eq. (1.110) is a force per unit mass. In addition, the equation of vibrating strings is written in terms of velocity: this is rather unusual, but it allows to easily highlight some analogies. Finally, the wave equations are written here for a homogeneous medium, although we will have to deal with heterogeneous strings and horns, for which the analogies remain valid.

Table 1.1 Reverse and direct analogies for strings and pipes

	Strings	Pipes (reverse analogy)	Pipes (direct analogy)
Variable 1	$f(x,t) = -T\partial\xi/\partial x =$ force applied to the right of x by the tension T (towards the $x > 0$)	$u =$ flow rate	$p =$ pressure
Variable 2	$v =$ velocity	$p =$ pressure	$u = Sv =$ flow rate
Equation 1	$\frac{\partial v}{\partial x} = -\frac{1}{T}\frac{\partial f}{\partial t}$	$\frac{\partial p}{\partial x} = -\frac{\rho}{S}\frac{\partial u}{\partial t}$	$\frac{\partial u}{\partial x} = -S\chi_S\frac{\partial p}{\partial t}$
Equation 2	$\frac{\partial f}{\partial x} = -\rho S\frac{\partial v}{\partial t} + f_{\text{ext}}$	$\frac{\partial u}{\partial x} = -S\chi_S\frac{\partial p}{\partial t} + q$	$\frac{\partial p}{\partial x} = -\frac{\rho}{S}\frac{\partial u}{\partial t} + \frac{1}{S}f_{\text{ext}}$
Source	$f_{\text{ext}} =$ external force per unit length	$q =$ flow rate per unit length	$f_{\text{ext}} =$ external force per unit length
Parameter 1	$T =$ tension	$S/\rho =$ cross-section/density	$1/\chi_s S =$ 1/(compressibility × section)
Parameter 2	$\rho S =$ density × cross-section	$\chi_S S =$ compressibility × cross-section	$\rho/S =$ density/cross-section
Element 1	$C =$ compliance $= 1/K$ ($K =$ stiffness)	$M_a = \rho\ell/S =$ acoustic mass	$C_a = \chi_S V =$ acoustic compliance
Element 2	$M = \rho\ell S =$ mass	$C_a = \chi_S V =$ acoustic compliance	$M_a = \rho\ell/S =$ acoustic mass
Wave speed	$c = \sqrt{T/\rho S}$	$c = 1/\sqrt{\rho\chi_s}$	$c = 1/\sqrt{\rho\chi_s}$
Ratio	$Y =$ mechanical admittance $= v/f$	$Z =$ acoustic impedance $= p/u$	$Y =$ acoustic admittance $= u/p$
Wave characteristic	$Y_c = \frac{1}{\sqrt{T\rho S}} = c/T$	$Z_c = \sqrt{\rho/\chi_S S^2} = \rho c/S$	$Y_c = \sqrt{S^2\chi_s/\rho} = S/\rho c$
Additional variable	$\xi =$ displacement $= \int v dt$	$\varphi =$ velocity potential $= -\int p/\rho dt$	volume displacement $= \int u dt$
Wave equation	$\rho S\frac{\partial^2 v}{\partial t^2} - T\frac{\partial^2 v}{\partial x^2} = \frac{\partial f_{\text{ext}}}{\partial t}$	$S\chi_S\frac{\partial^2 p}{\partial t^2} - \frac{S}{\rho}\frac{\partial^2 p}{\partial x^2} = \frac{\partial q}{\partial t}$	$\frac{\rho}{S}\frac{\partial^2 u}{\partial t^2} - \frac{1}{\chi_s S}\frac{\partial^2 u}{\partial x^2} = \frac{1}{S}\frac{\partial f_{\text{ext}}}{\partial t}$

1.6.1 Note on the Definition of Impedances for Forced Oscillations

A definition was given in Sect. 1.3.3.1 for the impedance in case of forced oscillations. This concept can be slightly extended, considering a simple situation with a point excitation of linear and sinusoidal forced oscillations, for example a source of acoustic flow, so that we can define:

- a *transfer impedance* as the ratio of the pressure response P at a point b to the flow source U provided at point a: $Z_t = P(b)/U(a)$;
- a *driving-point impedance* as the previous quantity for the particular case $a = b$: $Z = P(a)/U(a)$.

Of course, the inverse ratio is called admittance. When we use mechanical quantities, both are vectors, so that impedance and admittance become matrices. Similarly if there are multiple sources and multiple receivers, we can have an impedance matrix, and if there are continuous sources and receivers, we have an operator. These concepts are developed in Chap. 3 extensively.

Here we used the frequency domain. In the time domain, we would write equivalent equations, for example:

$$p(b) = \widehat{Z(t)} * u(a),$$

where $\widehat{Z(t)}$ is an impulse response, i.e., the inverse Fourier transform of the impedance. If the impedance is a pressure response to a unit flow, the corresponding impulse response is the pressure response to a flow pulse $\delta(t)$. In addition, there are other concepts of impedance:

- in the case of one-dimensional waves, *the local impedance*: we consider a pipe excited by several sources, and a point a downstream the sources. The part downstream of the point a is therefore passive. Then, the impedance $Z = P(a)/U(a)$ at point a is determined by the characteristics of the downstream medium, and has the same value as the impedance at the driving-point a. This is the typical case of the input impedance of a wind instrument, and, by extension, of the admittance matrix imposed by a soundboard or a sound box to the string. This concept can be generalized to one or more dimensions, but it will not be treated here.
- *the impedance of an element*: if between two points of a pipe a and b, the flow rate u is constant, the pipe element has an impedance $Z = [P(a) - P(b)]/U$ (we can define something similar if the pressure is constant, see Sect. 1.5). Thus, in the table of analogies 1.1, the impedances $Z = j\omega M, Z = 1/j\omega C, \ldots$, correspond to the impedances of a mass, the compliance of a spring, etc.

1.7 Numerical Methods

Analytical methods for solving the wave equation will be presented in Chaps. 3 and 4. As this equation becomes more complex through addition of extra terms (damping, stiffness, interaction with an exciter, etc.) which are needed to properly model an instrument, then the use of numerical methods becomes necessary.

A detailed description of the numerical techniques used for solving partial differential equations involved in models of musical instruments is beyond the scope of this book. However, we find it useful to say a few words about two of the most common techniques used, namely the finite difference and the finite element methods. To introduce and illustrate the foundations of these methods, the simple example of the ideal wave equation, without source terms, is selected. Emphasis is put on time-domain numerical modeling. For more information on the application of finite differences to simulations in musical acoustics, one can refer to the book by Bilbao [10].

1.7.1 Finite Difference Methods

In order to illustrate the use of finite difference methods we discuss the typical example of the wave equation where the initial conditions are given in explicit form. The objective is to solve the following system numerically:

$$\begin{cases} \dfrac{\partial^2 \xi}{\partial t^2} = c^2 \dfrac{\partial^2 \xi}{\partial x^2} \quad \forall x, \quad \forall t > 0, \\ \xi(x,0) = \xi_0(x) \quad ; \quad \dfrac{\partial \xi}{\partial t}(x,0) = \xi_1(x)\,. \end{cases} \tag{1.157}$$

Here, the variable $\xi(x,t)$ might designate, for example, the transverse oscillation of a string, the longitudinal motion of a bar, or the sound pressure in a 1D pipe. The resolution method consists in replacing this continuous variable by a discrete variable $\xi_j^n = \xi(x_j, t^n)$ which is defined at some discrete spatial points x_j, and for a discrete series of instants t^n only. Equally spaced points $x_j = j\Delta x$ are generally selected, where Δx is the spatial step. Similarly, the simplest methods use constant time steps Δt, so that we can write $t^n = n\Delta t$. Variable step methods are also used, particularly when it is needed to refine a subdomain of the meshing [2].

In what follows, we limit ourselves to the case of a uniform mesh in space and time. The basic principle of finite difference methods is to approximate the partial derivatives in time and space by linear combinations of ξ_j^n. Thus, for example, if we want to make a second-order approximation of the partial derivatives appearing in (1.157), we write

$$\begin{cases} \dfrac{\partial^2 \xi}{\partial t^2}(x_j, t^n) \approx \dfrac{\xi_j^{n+1} - 2\xi_j^n + \xi_j^{n-1}}{\Delta t^2}, \\ \dfrac{\partial^2 \xi}{\partial x^2}(x_j, t^n) \approx \dfrac{\xi_{j+1}^n - 2\xi_j^n + \xi_{j-1}^n}{\Delta x^2} \end{cases} \tag{1.158}$$

The resulting difference equation can be rewritten:

$$\xi_j^{n+1} = 2(1-\alpha^2)\xi_j^n + \alpha^2(\xi_{j-1}^n + \xi_{j+1}^n) - \xi_j^{n-1} \quad \text{with} \quad \alpha = c\frac{\Delta t}{\Delta x}. \tag{1.159}$$

In (1.159), a recurrence equation is obtained that allows to explicitly calculate the future value ξ_j^{n+1} as a function of the values taken by the same variable at earlier instants, at the same point and at neighboring points. This is called an *explicit* finite difference scheme. Equation (1.159) is initialized at both instants ($n = 0$ and $n = 1$) by means of the initial conditions in displacement and velocity defined in (1.157).

The number of spatial steps included in a recurrence equation depends on the order of the scheme. For a better accuracy, it might be necessary to use higher order approximations. As an example, the following approximation:

$$\frac{\partial^2 \xi}{\partial x^2}(x_j, t^n) \approx \frac{1}{\Delta x^2}\left(-\frac{1}{12}\xi_{j-2}^n + \frac{4}{3}\xi_{j-1}^n - \frac{5}{2}\xi_j^n + \frac{4}{3}\xi_{j+1}^n - \frac{1}{12}\xi_{j+2}^n\right) \tag{1.160}$$

is of the fourth-order in space. The explicit scheme presented in (1.159) is a special case. If ξ_j^{n+1} cannot be directly expressed as a function of the values of the variable at earlier instants, an *implicit* scheme is obtained [4].

1.7.1.1 Stability of the Discretization Scheme

With a given discrete approximation, cumulative errors might propagate during the calculation over time, causing the "explosion" of the solution because of numerical instability. Each numerical scheme thus requires a prior analysis of its stability properties. Such an analysis can be performed by energy methods or by Fourier techniques. Some guidance on this latter method are given below. The reader is invited to consult the specialized literature for more details [2, 47].

In the Fourier method, discrete solutions of the form $\xi_j^n = \hat{\xi}^n \exp(-ikx_j)$ are tested, where $i = \sqrt{-1}$ and k the wavenumber. Within the framework of our reference example (1.159), this leads to the equation:

$$\hat{\xi}^{n+1} - 2(1-2\beta)\hat{\xi}^n + \hat{\xi}^{n-1} = 0 \quad \text{where} \quad \beta = 2\alpha^2 \sin^2 \frac{k\Delta x}{2}. \tag{1.161}$$

The resulting scheme will be stable provided that the solutions do not contain terms whose amplitude grows continuously with time. It is known that the general

solution of (1.161) is $\hat{\xi}^n = a_1 d_1^n + a_2 d_2^n$ where d_1 and d_2 are solutions of the associated characteristic equation $d^2 - 2(1-2\beta)d + 1 = 0$. If $\beta > 2$, either the modulus of d_1, or the modulus of d_2 is greater than unity, and instability occurs. Therefore, the stability condition imposes here $\beta \leq 2$. This result must be true for any k, thus leading to the condition:

$$\alpha = c\frac{\Delta t}{\Delta x} \leq 1 \,. \tag{1.162}$$

This last condition is called Courant–Friedrichs–Levy (or CFL) condition. It shows that, for stability reasons, time and space steps cannot be selected independently. A specific condition of stability corresponds to each scheme. Some implicit schemes can guarantee an unconditional stability, but at the cost of lower accuracy, for a given order of approximation [18].

1.7.1.2 Numerical Dispersion

Numerical schemes also have dispersive properties, which means that the propagation velocities are not correctly estimated. The dispersion properties of a given scheme are analyzed on the basis of the Fourier transform, which states that the solution can be represented as a superposition of plane waves of the form $\xi(x_j, t^n) = \xi_j^n \exp i(\omega t^n - k x_j)$. By introducing this form in the recurrence equation (1.159), it is found that the relation of numerical dispersion between angular frequency ω and wavenumber k, is given by:

$$D_{\text{num}}(\omega, k) = \sin^2 \frac{\omega \Delta t}{2} - \frac{c^2 \Delta t^2}{\Delta x^2} \sin^2 \frac{k \Delta x}{2} = 0 \,. \tag{1.163}$$

Equation (1.163) shows that the numerical phase velocity is equal to:

$$c_{\text{num}} = \frac{\omega}{k} = \frac{c}{\alpha K} \arcsin\left[\alpha \sin K\right] \quad \text{with} \quad K = \frac{k \Delta x}{2} = \frac{\pi \Delta x}{\lambda} \,. \tag{1.164}$$

As K tends to zero in (1.164), i.e., when the spatial step is small compared to the wavelength λ, then c_{num} tends to the continuous phase velocity c. Thus, if we want to numerically reproduce a wave propagation with good accuracy, it is necessary to discretize the equation with a large number of points per wavelength. Figure 1.28 shows the ratio $R = c_{\text{num}}/c$ as a function of the parameter K for different values of the stability parameter α. It can be seen that the dispersion properties of the scheme are degraded as α decreases. Notice that the ideal wave equation shows a remarkable result for the limiting stability value $\alpha = 1$. In this case, Eq. (1.164) shows that the numerical phase velocity is strictly equal to c, whatever the wavelength. This limiting condition of stability therefore provides the exact solution of the wave equation for the particular centered explicit scheme selected here. This result is due

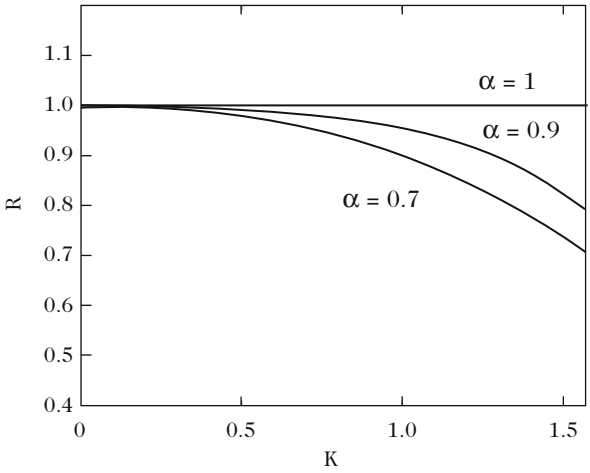

Fig. 1.28 Numerical dispersion of a second-order centered finite difference scheme applied to the wave equation, for different values of the stability parameter$\alpha = c\Delta t/\Delta x$

to the particular form of this equation. We could show, for example, that with a fluid damping term introduced in (1.157), then it is not anymore possible to find a value of α giving the exact solution of the problem.

1.7.2 Finite Element Method

The ideal wave equation with simple boundary conditions (equation of the ideal string of length L fixed at both ends) is now solved by means of the finite element method. The main idea is that the solution $\xi(x,t)$ is now approximated by a linear combination of *basic functions* $\phi_i(x)$ [35]:

$$\xi(x,t) \simeq \sum_{i=1}^{N} q_i(t)\phi_i(x), \tag{1.165}$$

where N is the number of discrete points with abscissa x_i on the string and $q_i(t)$ the unknown functions of time which are expected to provide the *best possible approximation* for $\xi(x,t)$.

The method is illustrated using *hat* functions for $\phi_i(x)$. Hat functions (or triangular functions) are equal to 1 for x_i and show linear slopes from 0 to 1 between x_i and its adjacent points x_{i-1} and x_{i+1} (see Fig. 1.29). The 2D equivalent of such piecewise linear functions are *triangle functions* and, in 3D, *tetrahedron functions*. These basic functions are the most commonly used.

Figure 1.30 shows that we can achieve a discrete approximation of the string motion at each time using a linear combination of *hat* functions.

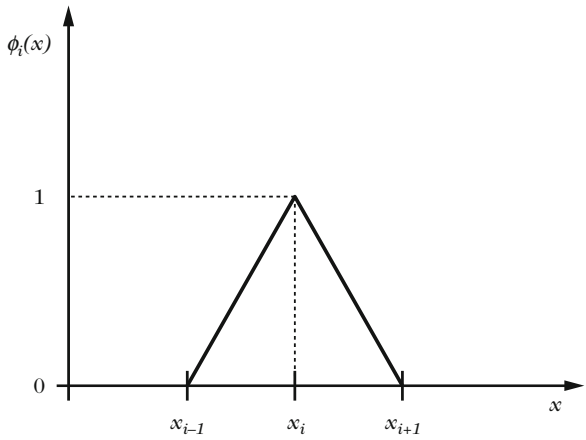

Fig. 1.29 "Hat" function (or triangular function)

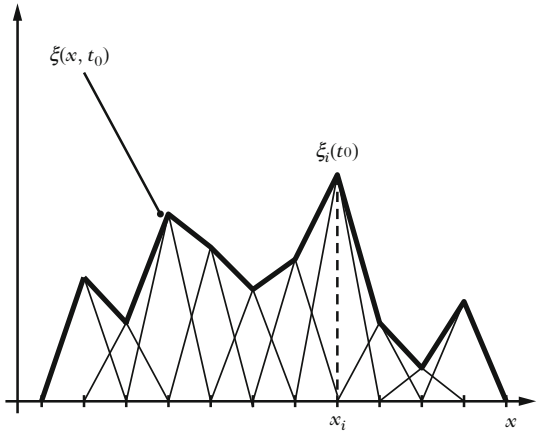

Fig. 1.30 Discrete approximation of a string motion using *hat* functions

Variational Formulation of the Wave Equation

The finite element method is based on a variational formulation (or *weak* formulation) of the motion equations. Let us note $c^{-2}\xi_{tt} - \xi_{xx} - f = 0$ the wave equation, where the subscripts are the partial derivatives with respect to time and space. Considering $v(x)$ as a continuous *test-function*, at least differentiable once, and bounded on the interval $[0, L]$, that satisfies the boundary conditions at both ends of the string. We can check that

$$\int_0^L (c^{-2}\xi_{tt} - \xi_{xx} - f)v \, dx = 0 \, . \tag{1.166}$$

After integration by parts, and taking the boundary conditions into account, (1.166) is written:

$$\int_0^L c^{-2}\xi_{tt} v \, dx + \int_0^L \xi_x v_x \, dx - \int_0^L f v \, dx = 0 \, . \tag{1.167}$$

The discrete formulation of the problem is done by replacing $\xi(x,t)$ in (1.167) by its approximation (1.165). Considering that every hat function $\phi_k(x)$ satisfies all conditions imposed to $v(x)$, the following system of differential equations is obtained

$$c^{-2} \sum_{i=1}^{N} \ddot{q}_i \int_0^L \phi_i(x)\phi_k(x) \, dx + \sum_{i=1}^{N} q_i \int_0^L \frac{d\phi_i}{dx}\frac{d\phi_k}{dx} \, dx = \int_0^L f\phi_k \, dx, \tag{1.168}$$

that can be written as

$$\mathbb{M}\ddot{\mathbf{Q}} + \mathbb{K}\mathbf{Q} = \mathbf{F} \tag{1.169}$$

where $\mathbf{Q}$ is the vector whose components are the $q_i(t)$ and where $\mathbf{F}$ is the vector whose components are the projection of the excitation f on the discrete string.

The parameter $h = L/(N+1)$ is the space step. The following results for the coefficients of mass $\mathbb{M}$ and stiffness matrices $\mathbb{K}$ can be verified, in case of *hat* functions:

$$\begin{cases} \displaystyle\int_0^L \phi_i^2 dx = \frac{2h}{3} \, ; & \displaystyle\int_0^L \left(\frac{d\phi_i}{dx}\right)^2 dx = \frac{2}{h} \quad \forall i = 1, 2, \ldots N, \\ \\ \displaystyle\int_0^L \phi_i\phi_{i+1} dx = \frac{h}{6} \, ; & \displaystyle\int_0^L \frac{d\phi_i}{dx}\frac{d\phi_{i+1}}{dx} dx = -\frac{1}{h} \quad \forall i = 1, 2, \ldots N-1, \end{cases} \tag{1.170}$$

which leads to

$$\mathbb{M} = c^{-2}h \begin{pmatrix} 2/3 & 1/6 & 0 & \ldots & 0 & 0 & 0 \\ 1/6 & 2/3 & 1/6 & 0 & \ldots & 0 & 0 \\ 0 & 1/6 & 2/3 & 1/6 & 0 & \ldots & 0 \\ & & & \ldots\ldots\ldots\ldots & & & \\ 0 & 0 & \ldots & 0 & 1/6 & 2/3 & 1/6 \\ 0 & 0 & 0 & \ldots & 0 & 1/6 & 2/3 \end{pmatrix} \tag{1.171}$$

and

$$\mathbb{K} = \frac{1}{h} \begin{pmatrix} 2 & -1 & 0 & \ldots & 0 & 0 & 0 \\ -1 & 2 & -1 & 0 & \ldots & 0 & 0 \\ 0 & -1 & 2 & -1 & 0 & \ldots & 0 \\ & & & \ldots\ldots\ldots\ldots & & & \\ 0 & 0 & \ldots & 0 & -1 & 2 & -1 \\ 0 & 0 & 0 & \ldots & 0 & -1 & 2 \end{pmatrix} . \tag{1.172}$$

Therefore, for $i \neq 1$ and $i \neq N$, the discrete variable $q_i(t)$, which represents here the displacement $\xi_i(t)$ at point $x_i = ih$ of the string, since $\phi_i(x_i) = 1$, is governed by the equation:

$$\left(\frac{1}{6}\frac{d^2\xi_{i-1}}{dt^2} + \frac{2}{3}\frac{d^2\xi_i}{dt^2} + \frac{1}{6}\frac{d^2\xi_{i+1}}{dt^2}\right) - c^2\frac{\xi_{i+1} - 2\xi_i + \xi_{i-1}}{h^2} = F_i\,. \tag{1.173}$$

Comparing this finite element approximation (1.173) with the second-order centered finite difference method approximation (1.159), one can see that the second-order partial derivative in space is identical in both cases:

$$\frac{\partial^2\xi}{\partial x^2}(x_i) \simeq \frac{\xi_{i+1} - 2\xi_i + \xi_{i-1}}{h^2}\,. \tag{1.174}$$

However, the approximation of the second-order partial derivative in time is not punctual here, since it involves three spatial points:

$$\frac{\partial^2\xi}{\partial t^2}(x_i) \simeq \frac{1}{6}\frac{d^2\xi_{i-1}}{dt^2} + \frac{2}{3}\frac{d^2\xi_i}{dt^2} + \frac{1}{6}\frac{d^2\xi_{i+1}}{dt^2}\,. \tag{1.175}$$

Without going into details, let us mention here the existence of techniques known as "mass lumping" which consists in the simplification:

$$\frac{\partial^2\xi}{\partial t^2}(x_i) \simeq \frac{d^2\xi_i}{dt^2}, \tag{1.176}$$

which is equivalent to replacing the matrix $\mathbb{M}$ by $c^{-2}h\mathbb{I}$ where $\mathbb{I}$ is the identity matrix [18].

References

1. Akay, A.: Acoustics of friction. J. Acoust. Soc. Am. **111**(4), 1525–1548 (2002)
2. Ames, W.F.: Numerical Methods for Partial Differential Equations. Academic Press, New York (1992)
3. Axisa, F., Trompette, P.: Modelling of Mechanical Systems: Structural Elements. Elsevier, Oxford (2005)
4. Bamberger, A.: Elastic and Electromagnetic Waves (in French). Cours de l'Ecole polytechnique, Palaiseau (1996)
5. Bank, B., Sujbert, L.: Generation of longitudinal vibrations in piano strings: from physics to sound synthesis. J. Acoust. Soc. Am. **117**(4), 2268–2278 (2005)
6. Batchelor, G.: An Introduction to Fluid Dynamics. Cambridge University Press, Cambridge (1976)
7. Berthaut, J., Ichchou, M.N., Jézéquel, L.: Piano soundboard: structural behavior, numerical and experimental study in the modal range. Appl. Acoust. **64**(11), 1113–1136 (2003)
8. Berthelot, J.M.: Composites Materials. Springer, New York (1999)

9. Besnainou, C.: From wood mechanical measurements to composite materials: new technologies for instruments makers. MRS Bull. **20**(3), 34–36 (1995)
10. Bilbao, S.: Numerical Sound Synthesis: Finite Difference Schemes and Simulation in Musical Acoustics. Wiley, Chichester (2009)
11. Bork, I.: Measuring the acoustical properties of mallets. Appl. Acoust. **30**, 207–218 (1990)
12. Bruneau, M.: Fundamentals of Acoustics. Wiley, London (2006)
13. Bucur, V.: Acoustics of Wood, 2nd edn. Springer, Berlin (2006)
14. Chadefaux, D., Le Carrou, J.L., Fabre, B., Daudet, L.: Experimentally based description of harp plucking. J. Acoust. Soc. Am. **131**(1), 844–855 (2012)
15. Chadefaux, D., Le Carrou, J.L., Fabre, B.: A model of harp plucking. J. Acoust. Soc. Am. **133**(4), 2444–2455 (2013)
16. Chaigne, A., Doutaut, V.: Numerical simulations of xylophones. I. Time-domain modeling of the vibrating bars. J. Acoust. Soc. Am. **101**, 539–557 (1997)
17. Chaigne, A., Ramdane, A.: Numerical simulations of membrane-mallet interaction in kettledrums. Tech. Rep. 98D010, ENST Paris (1998)
18. Cohen, G.C.: Higher-Order Numerical Methods for Transient Wave Equations. Springer, Berlin (2002)
19. Doutaut, V.: Experimental study and numerical simulation of keyboard percussion instruments (in French). Ph.D. thesis, ENST Paris (1996)
20. Fastl, H., Zwicker, E.: Psychoacoustics: Facts and Models. Springer, Berlin (1990)
21. Géradin, M., Rixen, D.: Mechanical Vibrations: Theory and Application to Structural Dynamics. Wiley, Chichester (1999)
22. Ghosh, R.: A note on the elastic impact of the pianoforte hammer. Proc. Phys. Soc. **40**, 224–225 (1927)
23. Gillan, F.S., Elliott, S.J.: Measurement of the torsional modes of vibration of strings on instruments of the violin family. J. Sound Vib. **130**(2), 347–351 (1989)
24. Giordano, N., Winans, J.: Plucked strings and the harpsichord. J. Sound Vib. **224**, 455–473 (1999)
25. Guyader, J.L.: Vibrations in Continuous Media. Wiley, London (2006)
26. Hall, D.E., Askenfelt, A.: Piano string excitation V: spectra for real hammers and strings. J. Acoust. Soc. Am. **83**(4), 1627–1638 (1988)
27. Han, M., Benaroya, H., Wei, T.: Dynamics of transversely vibrating beams using four engineering theories. J. Sound Vib. **225**(5), 935–988 (1999)
28. Hearmon, R.F.S.: An Introduction to Applied Anisotropic Elasticity. Oxford University Press, Oxford (1961)
29. Hertz, H.: Ueber die Beruehrung fester elasticher Koerper. J. Reine Angew. Math. **92**, 156–171 (1882)
30. Johnson, K.: Contact Mechanics. Cambridge University Press, Cambridge (1987)
31. Joly, P., Rhaouti, L.: A qualitative analysis of a simplified model for the nonlinear membrane-mallet interaction. Tech. Rep. 3234, INRIA (1997)
32. Lambourg, C., Chaigne, A.: Measurements and modeling of the admittance matrix at the bridge in guitars. In: Proceedings of the SMAC 93, pp. 448–453 (1993)
33. Landau, L., Lifchitz, E.: Theory of Elasticity, 2nd edn. Pergamon Press, Oxford (1970)
34. Le Carrou, J.L.: Vibro-acoustics of the concert harp. Ph.D. thesis, Ecole doctorale de l'Université du Maine, Le Mans (2006). http://tel.archives-ouvertes.fr/
35. Lehtinen, J.: Time-domain numerical solution of the wave equation. Tech. rep., Helsinki University of Technology (2003)
36. Leissa, A.: Vibrations of Plates. Acoustical Society of America, Melville (1993)
37. Leissa, A.: Vibrations of Shells. Acoustical Society of America, Melville (1993)
38. Lemaitre, J., Chaboche, J.: Mechanics of Solid Materials. Cambridge University Press, Cambridge (1994)
39. Le Tallec, P.: Introduction to the Dynamics of Structures (in French). Ellipses, Paris (1996)

40. Mamou-Mani, A.: Prestresses and vibration of a soundboard: towards the modelling of the know-how of the musical instruments makers (in French). Ph.D. thesis, Université Paris 6 (2007)
41. Morse, P.M., Ingard, K.: Theoretical Acoustics. McGraw Hill, New York (1968)
42. Pao, Y.: Extension of the Hertz theory of impact to the viscoelastic case. J. Appl. Phys. **26**, 1083 (1955)
43. Pavlidou, M.: A physical model of the string-finger excitation on the classical guitar. Ph.D. thesis, University of Cardiff (1997)
44. Pierce, A.D.: Acoustics: An Introduction to Its Physical Principles and Applications. Acoustical Society of America, Melville (1989)
45. Rao, S.S.: Mechanical Vibrations. Pearson Prentice Hall, Upper Saddle River (2004)
46. Rhaouti, L.: Fictitious domains for the modeling of a fluid-structure interaction problem. simulation of a kettledrum (in French). Ph.D. thesis, Université Paris Dauphine (1999)
47. Richtmyer, R., Morton, K.W.: Difference Methods for Initial-Value Problems, 2nd edn. Interscience/Wiley, New York (1967)
48. Rienstra, S., Hirschberg, A.: An introduction to acoustics. Eindhoven University of Technology (2006)
49. Salençon, J.: Hankbook of continuum mechanics: General concepts, thermoelasticity. Springer-Verlag, Berlin (2001)
50. Serafin, S.: The sound of friction: real-time models, playability and musical applications. Ph.D. thesis, Department of Music, Stanford University, Stanford (2004)
51. Soedel, W.: Vibrations of shells and plates, 3rd edn. Marcel Dekker Inc., New York (2004)
52. Stronge, W.J.: Contact problems for elasto-plastic impact in multi-body systems. In: B. Brogliato (ed.) Impact in mechanical systems. Springer (2000)
53. Stulov, A.: Dynamic behavior and mechanical features of wool felt. Acta Mechanica **169**, 13–21 (2004)
54. Vu-Quoc, L., Zhang, X.: An elastoplastic contact force-displacement model in the normal direction: displacement-driven version. Proc. R. Soc. Lond. A **455**, 4013–4044 (1999)
55. Wegst, U.G.K.: Wood for sound. American Journal of Botany **93**(10), 1439–1448 (2006)
56. Weinreich, G., Caussé, R.: Elementary stability considerations for bowed-string motion. J. Acoust. Soc. Am. **89**(2), 887–895 (1991)
57. Woodhouse, J., Loach, A.: Torsional behaviour of cello strings. Acustica Acta Acustica **85**(5), 734–40 (1999)
58. Yu, Y.Y.: Vibrations of elastic plates. Springer, New York (1996)
59. Zenatti, A.: Psychology of music (in French). Presses Universitaires de France, Paris (1994)

Chapter 2
Single-Degree-of-Freedom Oscillator

Antoine Chaigne and Jean Kergomard

Abstract Single-degree-of-freedom oscillators are often found as such in musical acoustics. It is important to understand their behavior because they are elementary building blocks of more complicated (discrete or continuous) systems in the context of the modal theory. In this chapter, a number of basic results are summarized. Fundamental methods, based on the use of Green's functions, are introduced and applied to the harmonic oscillator. Their relevance and efficiency for treating more complex systems will appear throughout this book. Whenever possible, conclusions are drawn concerning practical examples. Two important notions, that are not always intuitively well understood by musicians, are addressed: resonance and reverberation. In addition, three different definitions of the quality factor are given, and the analysis of the harmonic oscillator in terms of energetic quantities is emphasized.

2.1 Introduction

For this introductory chapter, the most common example of a standard mechanical oscillator is chosen. We have seen how to switch from mechanical to acoustical resonators by means of analogies (see Table 1.1). The example of the Helmholtz resonator without dissipation, in particular, has been studied in Chap. 1 (Sect. 1.5). Consider a mechanical oscillator of mass M, stiffness K, and with a viscous damping coefficient R, driven by a force $f(t)$ and whose moving part has a velocity $v(t)$ (see Fig. 2.1). The motion of this oscillator is described by the differential equation:

$$M\frac{dv}{dt} + Rv + K\int v dt = f, \tag{2.1}$$

A. Chaigne (✉)
Institute of Music Acoustics, University of Music and Performing Arts Vienna (MDW), Anton-von-Webern-Platz 1, 1030 Vienna, Austria
e-mail: antchaigne@gmail.com

J. Kergomard
CNRS Laboratoire de Mecanique et d'Acoustique (LMA), 4 impasse Nikola Tesla CS 40006, 13453 Marseille Cedex 13, France
e-mail: kergomard@lma.cnrs-mrs.fr

A. Chaigne, J. Kergomard, *Acoustics of Musical Instruments*, Modern Acoustics and Signal Processing, DOI 10.1007/978-1-4939-3679-3_2

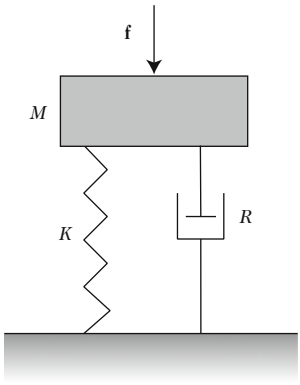

Fig. 2.1
Single-degree-of-freedom mechanical oscillator

which can be written equivalently with respect to displacement $y(t)$ ($v(t) = dy(t)/dt$) and usual scaled parameters:

$$\frac{d^2y}{dt^2} + 2\alpha_0 \frac{dy}{dt} + \omega_0^2 y = \frac{f}{M}, \tag{2.2}$$

where

$$\omega_0^2 = \frac{K}{M} \quad \text{and} \quad \alpha_0 = \zeta_0 \omega_0 = \frac{\omega_0}{2Q_0} = \frac{R}{2M}. \tag{2.3}$$

The *resonance* angular frequency is denoted by ω_0, which, because of the damping coefficient R, is not necessarily equal to the *eigen* (or natural) angular frequency: both angular frequencies will be defined later in this chapter. Q_0 is the second basic parameter describing the sharpness of the resonance: it is called "quality factor," and plays an essential role in several properties of the oscillator. One should remember that its limit is infinite when damping approaches zero. It may appear cumbersome to define three quantities to express damping, α_0, ζ_o, and Q_0. However, each quantity has its own meaning and use, as it will be seen later.

The damping model has not been discussed yet. In Chap. 5 it will be shown that damping often depends on frequency, which of course strongly modifies the time-domain equation (2.2). It is assumed that it is not the case here. Similarly, the damping coefficient is chosen positive so that free oscillations decrease exponentially: in fact, for self-oscillating instruments (see Part III), the sound starts with an exponential growth, because the energy source is proportional to the term R, which can be either positive or negative.

2.2 Solution With and Without a Source: Green's Function

2.2.1 Solution Without a Source; Eigenfrequency

The first step is to write the solutions of Eq. (2.2) without source terms, i.e., after the extinction ($f(t) = 0$). This corresponds therefore to the case of *free oscillations*. Complex solutions in the form $Ae^{j\omega t}$ are sought, where ω is the angular *eigenfrequency*.[1] The equation to be solved is derived from Eq. (2.2):

$$\left[\frac{\omega}{\omega_0}\right]^2 - j\frac{1}{Q_0}\frac{\omega}{\omega_0} - 1 = 0, \tag{2.4}$$

and the solutions are given by:

$$\omega_0^{\pm} = j\alpha_0 \pm \omega_p \text{ where } \omega_p = \omega_0\delta_0, \text{ with } \delta_0 = \sqrt{1-\zeta_0^2} = \sqrt{1-\frac{1}{4Q_0^2}}. \tag{2.5}$$

If ζ_0 is greater or equal to unity, i.e., if Q_0 is lower or equal to $1/2$, the two solutions $\omega_0^{\pm}$ are purely imaginary, and there is no oscillations. Discarding this case, two complex eigenfrequencies are found, which have the same real part ω_p, in absolute value. The real part is often called (angular) eigenfrequency of the oscillator, even if the signal is pseudo-periodic, when it is attenuated. In the following, the term *"eigenfrequency"* will be used for ω_0^+ and ω_0^- as well as for ω_p, because there is generally no ambiguity. The general solution is written as:

$$y(t) = e^{-\alpha_0 t}\left[A^+ e^{j\omega_p t} + A^- e^{-j\omega_p t}\right] \quad \text{or} \quad y(t) = Ae^{-\alpha_0 t}\sin(\omega_p t + \varphi). \tag{2.6}$$

The first expression involves two complex coefficients, $A^{\pm}$, but only the real part is of interest for us. The second expression involves two real coefficients: A and φ. The signal has a pseudo-period $T = 2\pi/\omega_p$, and is exponentially attenuated, the exponent being proportional to ζ_0. During a pseudo-period, the amplitude of the signal is divided by a factor:

[1] What does "eigen" mean? The German word *eigen* can be translated as "own," or "natural." For a physicist, it means that the eigenfrequency is characteristic of the oscillator, thus independent of external excitation. For a mathematician, it is linked to the eigenvalues of an operator. Thus, if (2.2) is written as:

$$\frac{d}{dt}\begin{pmatrix} y \\ dy/dt \end{pmatrix} = \begin{pmatrix} 0 & 1 \\ -\omega_0^2 & -2\alpha_0 \end{pmatrix}\begin{pmatrix} y \\ dy/dt \end{pmatrix}.$$

The operator is a usual matrix and it can be shown that its eigenvalues are $j\omega_0^{\pm}$ and its eigenvectors $\begin{pmatrix} 1 \\ j\omega_0^{\pm} \end{pmatrix}$.

Table 2.1 Some typical values of the quality factor Q in musical acoustics

Instrument	Frequency domain	Q-factor
Clarinet	150 Hz–3 kHz	10–50
Wooden guitar soundboard	50 Hz–5 kHz	10–100
Acoustic modes of a violin sound box	100 Hz–10 kHz	50–150
Kettledrum drumhead	50 Hz–1 kHz	10–300
Guitar string (Nylon)	100 Hz–5 kHz	100–1000
Piano string	20 Hz–15 kHz	10^2–10^4
Metal harpsichord string	20 Hz–20 kHz	10^3–10^4

To a first approximation, each resonance can be viewed as a single resonator with its own Q-factor (see Chap. 3). The Q-factors are usually decreasing with frequency, but this decrease is not monotonous in general

$$e_T = \exp\left[-\frac{2\pi}{\delta_0}\zeta_0\right] = \exp\left[-\frac{\pi}{Q_0\delta_0}\right]. \tag{2.7}$$

The larger the quality factor, the longer the oscillation. If it is large enough ($\delta_0 \simeq 1$), an approximate definition for the oscillation to decrease by a factor $e = 2.7$ is given by the number of pseudo-periods, divided by π. Table 2.1 gives some typical values of quality factors encountered in some musical instruments.

The coefficients A and φ in (2.6) can be found provided that initial values of the function $y(t)$ and its first derivative $v(t)$ are known. The following results are obtained by setting $t = 0$ in Eq. (2.6) and in the corresponding expression for dy/dt:

$$y(t) = e^{-\alpha_0 t}\left[\frac{1}{\omega_p}\left[v(0) + \alpha_0 y(0)\right]\sin\omega_p t + y(0)\cos\omega_p t\right], \tag{2.8}$$

and

$$v(t) = e^{-\alpha_0 t}\left[v(0)\cos\omega_p t - \delta_0^{-1}\left[\zeta_0 v(0) + \omega_0 y(0)\right]\sin\omega_p t\right]. \tag{2.9}$$

A special case of initial conditions, which is important for future considerations, is the case where the oscillator is released without initial velocity and with an initial displacement $y(0)$. This means that a force $f^-(t) = F^- = Ky(0)$ was applied during negative time. The velocity (see Fig. 2.2) is expressed by:

$$v(t) = -\frac{F^-}{M\omega_p}e^{-\alpha_0 t}\sin(\omega_p t). \tag{2.10}$$

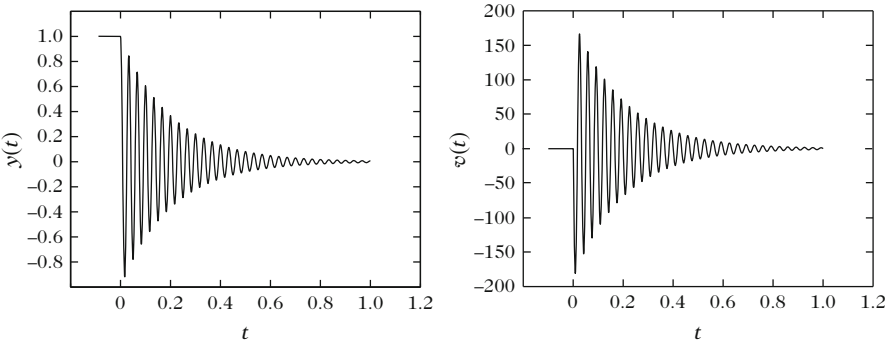

Fig. 2.2 Oscillator released at $t = 0$ without initial velocity. On the *left* the displacement and on the *right* the velocity. $y(0) = 1$; $f_0 = 30\,\text{Hz}$; $Q_0 = 18.85$. In this case it takes 6 pseudo-periods for the oscillation to decrease by a factor e

and the displacement:

$$y(t) = y(0)e^{-\alpha_0 t}\left[\cos(\omega_p t) + \frac{\zeta_0}{\delta_0}\sin(\omega_p t)\right] = \frac{y(0)}{\delta_0}e^{-\alpha_0 t}\cos(\omega_p t + \varphi) \qquad (2.11)$$

where $\tan\varphi = -\zeta_0/\delta_0$ (or $\cos\varphi = \delta_0$).

2.2.2 Solution with an Elementary Source: Green's Function

Expression (2.11) is a first illustration of an oscillator with a source switched off at $t = t_0$. Looking also at negative times, it can be written as a solution of the following equation, with a source term:

$$\frac{d^2y}{dt^2} + 2\alpha_0\frac{dy}{dt} + \omega_0^2 y = \frac{F^-}{M}H(t_0 - t), \qquad (2.12)$$

where $H(t)$ is the Heaviside step function. The velocity is a solution of the following equation:

$$\frac{d^2v}{dt^2} + 2\alpha_0\frac{dv}{dt} + \omega_0^2 v = -\frac{F^-}{M}\delta(t - t_0).$$

It is therefore, to within the multiplicative factor $-F^-/M$, a solution of the equation with an elementary source $\delta(t-t_0)$. The solution is called *Green's function*. This function and its first derivative are assumed to be equal to zero at time $t < t_0$. It allows expressing a solution for any source (see the following section). The Green's function is denoted $g(t|t_0)$, and is a solution of the following equation:

$$\left[\frac{d^2}{dt^2} + 2\alpha_0 \frac{d}{dt} + \omega_0^2\right] g(t|t_0) = \delta(t - t_0), \tag{2.13}$$

and, according to (2.10), is equal to:

$$g(t|t_0) = \frac{1}{\omega_p} H(t - t_0) e^{-\alpha_0 (t - t_0)} \sin[\omega_p (t - t_0)]. \tag{2.14}$$

t_0 is the pulse emission time, and t is the observation time. Note that the Green's function is a function of $(t - t_0)$: it does not change if the emission time t_0 is changed to $-t$, and the observation time from t to $-t_0$. This is the property of *temporal reciprocity*.[2] Except for a multiplying factor, its shape is that of the velocity in Fig. 2.2, if $t_0 = 0$.

A direct solution of Eq. (2.13) is now shown. To simplify the problem it is assumed that t_0 is zero. The method is similar to the one developed for the solution without a source (2.8), by matching solutions at $t = 0$. It is known that, for $t > 0$, the solution has the form (2.6). Both coefficients A and φ are found by matching this solution to the solution for negative time, which is equal to zero, as it is the case for its first derivative. It can be shown, and at least it can be a posteriori checked, that the presence of the Dirac delta function in Eq. (2.13) implies the continuity of the solution at $t = 0$, hence $\varphi = 0$, and the discontinuity of its first derivative. By integrating Eq. (2.13) between $t - \varepsilon$ and $t + \varepsilon$, the following results are obtained:

$$\left[\frac{d}{dt} g(t, 0)\right]_{t-\varepsilon}^{t+\varepsilon} = 1 \quad \text{hence} \quad A = \frac{1}{\omega_p},$$

and Eq. (2.14) is obtained again for $t_0 = 0$.

2.2.3 General Solution with a Source Term

2.2.3.1 Solution by Fourier Transform

From the Green's function, the general equation (2.2) can be solved. We first derive the Fourier transforms of the equation with $y(t)$ and of the Green's function equation:

$$\left[-\omega^2 + 2\alpha_0 j\omega + \omega_0^2\right] \mathscr{Y} = \frac{F}{M} \tag{2.15}$$

[2] Notice that the Green's function does not have the dimension of a mechanical quantity but only of a time [the dimension of the Dirac delta function is the inverse of a time, which can be seen immediately when integrating the 2nd term of Eq. (2.13)]. An equation with physical meaning is obtained by multiplying the source term by a factor with the right dimensions.

$$\left[-\omega^2 + 2\alpha_0 j\omega + \omega_0^2\right] G = 1 \tag{2.16}$$

where $\mathscr{Y}(\omega)$, $F(\omega)$, *and* $G(\omega)$ are the Fourier transforms of $y(t)$, $f(t)$, and $g(t|0)$. Calculating the ratio of the two previous equations yields

$$\mathscr{Y}(\omega) = \frac{F(\omega)}{M} G(\omega). \tag{2.17}$$

Therefore, by returning to the time domain, and considering that the convolution product is the inverse Fourier transform of the ordinary product in the frequency domain, we get

$$y(t) = \frac{1}{2\pi M} \int_{-\infty}^{+\infty} F(\omega) G(\omega) e^{j\omega t} d\omega = \frac{1}{M} \int_{-\infty}^{+\infty} f(t') g(t - t'|0) dt',$$

$$\text{or } y(t) = \frac{1}{M} \int_{-\infty}^{+\infty} f(t') g(t|t') dt' = \frac{1}{M} \int_{-\infty}^{t} f(t') g(t|t') dt'. \tag{2.18}$$

In fact, because the Green's function $g(t|t')$ is a function of $(t-t')$, the convolution becomes a simple product, and the Green's function is equal to zero for $t' > t$.

2.2.3.2 Solving by Laplace Transform

For a source starting at a given time, the force can be written $f(t) = H(t)\tilde{f}(t)$, and the previous result (2.18) is applicable. But it is often more convenient to use the Fourier transform of the product rather than the convolution product. It is then easier to use the Laplace transform, which involves the initial conditions [see Eq. (1.118)]. Equation (2.17) is replaced by:

$$\mathscr{Y}(s) = G(s) \left[F(s)/M + (s + 2\alpha_0) y(0) + v(0)\right] \tag{2.19}$$

and the integral equation (2.18) becomes

$$y(t) = \frac{1}{M} \int_0^t f(t') g(t|t') dt' + \left[2\alpha_0 y(0) + v(0)\right] g(t|0) + y(0) \frac{dg(t|0)}{dt}. \tag{2.20}$$

If there is no source $f(t)$, the solution without a source (2.8) is found again, which can be verified.[3]

[3] This is the standard form of an integral equation which makes use of an elementary solution such as the Green's function. If the initial conditions are identical to those of the Green's function, only the integral term remains. This kind of equations can be generalized to a problem with variables depending on both space and time, but the initial conditions can be chosen for the Green's function: if it satisfies the same initial conditions as the unknown, there will be no terms linked to these conditions, which would not be the case otherwise.

2.3 Examples of Free and Forced Oscillations

This section aims at studying some examples of solutions, in the case of a steady-state excitation, or for an excitation which is either starting or stopping at a given time. One can easily imagine a vibrating string, acting as an oscillating source for a sound box that would have a single-degree-of-freedom: the starting and stopping of the sound box's vibration is of great interest, even if the present study will provide qualitative results only. Similarly one can easily transpose these simple situations to any instrument producing a sound in a room: it also acts as an oscillating source. This illustration implies that the oscillation produced is not influenced by the room itself; this is reasonable, except maybe in the case of an organ (because of the size of the pipes).

2.3.1 Displacement of a System from Equilibrium

We first treat the case of the displacement of a system from equilibrium, because it is very simple and complementary to the case of a system released without initial velocity [Eq. (2.11)]. Let the force be $f(t) = F_M H(t)$, the system being at equilibrium at $t = 0$: $y(0)$ and $v(0)$ are zero. We do not discuss the method for producing such a force. We can use the linearity of the problem, and therefore the superposition principle, and observe that $f(t) + f^-(t) = F_M$, if $f^-(t) = F_M H(-t)$, which is a case we have already described in Eq. (2.11). Now the solution for $f(t) = F_M$ (constant) is known: it is $y(t) = F_M/M\omega_0^2$. Subtracting the solution (2.11) from this result, we obtain the complete solution:

$$y(t) = \frac{F_M}{M\omega_0^2}\left[1 - e^{-\alpha_0 t}\left(\cos(\omega_p t) + \frac{\zeta_0}{\delta_0}\sin(\omega_p t)\right)\right]. \tag{2.21}$$

The expected initial conditions are satisfied. However, we find that it was not needed to use them for this new problem! In fact all the information is contained in the evolution of the force from $t = -\infty$ to $+\infty$: $f(t) = F_M H(t)$. The important fact is that a sudden change of excitation in one direction or the other produces a free oscillation which is attenuated exponentially, in addition to the steady term $F_M/M\omega_0^2$ (see Fig. 2.3).

2.3.2 Excitation (Forced) by a Steady Sinusoidal Force

Consider, for example, $f(t) = F_M \cos\omega t$. The solution is the real part of the solution for $f(t) = F_M e^{j\omega t}$. For steady forced oscillations, the solution can be sought in the form $A(\omega)e^{j\omega t}$. The derivatives are then derived in a straightforward

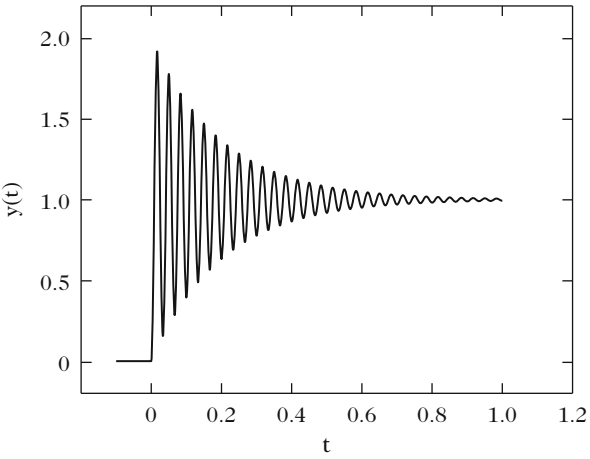

Fig. 2.3 Displacement of the system from equilibrium: the displacement is calculated with the same parameters as in Fig. 2.2, but $y(0) = 0$

way. The oscillating response has the same frequency as the excitation. Now, the eigenfrequency intervenes in the amplitude only: this point will be discussed in detail later. Using Eq. (2.16), one obtains

$$y(t) = F_M M^{-1} G(\omega) e^{j\omega t}. \tag{2.22}$$

Taking the real part of this result yields

$$y(t) = \frac{F_M}{M} \Re e \left[\frac{e^{j\omega t}}{-\omega^2 + 2j\alpha_0\omega + \omega_0^2} \right] = \frac{F_M}{MD^{1/2}(\omega)} \sin(\omega t + \varphi) \tag{2.23}$$

where

$$D(\omega) = \left[(\omega^2 - \omega_0^2)^2 + 4\alpha_0^2\omega^2 \right] \; ; \; \tan\varphi = (-\omega^2 + \omega_0^2)/2\alpha_0\omega. \tag{2.24}$$

The velocity is given by:

$$v(t) = A\cos(\omega t + \varphi) \text{ where } A = \frac{\omega F_M}{MD^{1/2}(\omega)}. \tag{2.25}$$

2.3.3 *Excitation by a Sinusoidal Force Starting at $t = 0$*

Consider now the particular case when the starting time of the source is taken into account. Let us roughly suppose that it starts abruptly: the force is, for example, $f(t) = F_M H(t) \cos\omega t$. We now calculate the velocity by using the Laplace Transform. The transform of the force is $F(s) = F_M s/(s^2 + \omega^2)$, and that of the derivative is $F_M s^2/(s^2+\omega^2) - f(0^+) = -F_M\omega^2/(s^2+\omega^2)$. Since the initial velocity

and the acceleration are zero (velocity is zero for all negative times), the transform of the velocity is

$$V(s) = -\frac{F_M}{M}\frac{\omega^2}{(s^2+\omega^2)(s^2+2\alpha_0 s+\omega_0^2)}. \tag{2.26}$$

The standard method for calculating the inverse transform is the partial fractions expansion in terms of the form $(s-s_n)^{-1}$, which leads to simple poles. It is actually more efficient to group the conjugate poles (we expect to find the combination of two signals of angular frequency ω and ω_p). We are therefore looking to write $V(s)$ as:

$$V(s) = \frac{as+b}{s^2+\omega^2} + \frac{a's+b'}{s^2+2\alpha_0 s+\omega_0^2}. \tag{2.27}$$

The result is obtained, after identification and inverse transform, but the calculation remains heavy. A lighter approach is based on the observation that, given the form of Eq. (2.27), the solution is of the type:

$$v(t) = H(t)\left[A\cos(\omega t+\varphi) + A_p e^{-\alpha_0 t}\cos(\omega_p t+\varphi_p)\right], \tag{2.28}$$

and thus only the first term remains when time goes to infinity. In other words, the first term is equal to the solution (2.25), multiplied by $H(t)$. To find the other two parameters, we can simply use the initial conditions (zero velocity and acceleration), which gives

$$\omega\tan\varphi = \alpha_0 + \omega_p\tan\varphi_p\ ;\ A\cos\varphi = -A_p\cos\varphi_P,$$

and, after some calculations, $A_p = A\omega/\omega_p$.

The second term in the right-hand side of (2.28) is not negligible compared to the first as long as the observation period is small compared to the characteristic damping time α_0^{-1}. For some weakly damped structural modes of musical instruments, this characteristic time can be of the order of magnitude of 0.1 ms or higher. Therefore, assuming that the exponential becomes negligible after a time of five to ten times larger, it appears that this second term cannot be neglected for 0.5 to 1 s after the excitation has started, if we want to correctly estimate the average power dissipated.

2.3.4 *Excitation by a Sinusoidal Force Stopping at $t = 0$*

What happens for a force stopping at $t = 0$, i.e., $f(t) = F_M H(-t)\cos\omega t$? One can use the Fourier Transform, with the necessary precautions concerning the function $H(-t)$, but a simpler method exists. We use the principle of superposition applied

to the previous problem, which gives a sinusoidal steady source, and we derive by simple subtraction between (2.25) and (2.28):

$$v(t) = AH(-t)\cos(\omega t + \varphi) - A_p H(t) e^{-\alpha_0 t}\cos(\omega_p t + \varphi_p). \tag{2.29}$$

The form (2.29) is interesting because it exhibits the reverberation: after the pulsation source ω stops, the oscillator vibrates at its eigenfrequency, with free oscillations. The phenomenon that occurs when the source starts [see Eq. (2.28)] can also be called reverberation: however, it overlaps with the oscillation produced by the source. The reverberation is a phenomenon triggered by the non-stationarity of a source: it is an oscillation whose frequency is the eigenfrequency of the system, and which decreases because of damping. These results are qualitatively very general, since they can be extended to any vibrating system with several degrees of freedom (DOF). The only phenomenon that cannot occur with a single DOF (i.e., a single mode) is the phenomenon of echo, due to delays: in a room, there is a very large number of modes (or DOF), which combine together and produce successive reflections on the walls. In Chap. 4 the relationship between modes and waves will be presented.

2.4 Forced Oscillations: Frequency Response

Forced sinusoidal motions are often used in experimental devices, in order to estimate the mechanical losses of a structure, in particular. It is therefore necessary to understand their main aspects and their theoretical limitations. In a steady sinusoidal regime, it is convenient to use the complex notation, what we adopt hereafter. We wish to study the response of the displacement (Eq. 2.15), and, above all, the velocity due to a sinusoidal force $f(t) = F_M \exp(j\omega t)$, since the product of force by velocity determines the power. We must therefore consider the response, called mechanical admittance, when the frequency varies

$$Y(\omega) = \frac{V(\omega)}{F(\omega)} = \frac{1}{M}\frac{j\omega}{-\omega^2 + 2j\omega\alpha_0 + \omega_0^2}, \tag{2.30}$$

the Fourier Transform of $f(t)$ being $F(\omega') = F_M \delta(\omega' - \omega)$. A function of ω of this form is often called "Lorentzian." We are interested in the quantities: modulus, argument (which is a phase difference), real and imaginary parts of the admittance, for which the evolution versus frequency can be seen in Figs. 2.4 and 2.5. We limit the study to the response in velocity, because in musical acoustics the input admittance (or impedance) is the most useful response. However the responses in displacement or in acceleration are interesting too, and show other variations with frequency.

It will be shown in Chap. 3 that for any discrete or continuous system, under certain conditions, the response is simply the sum of quantities of the type (2.30),

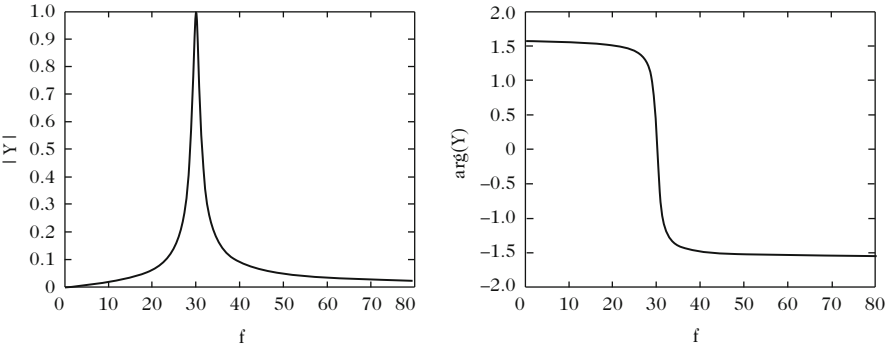

Fig. 2.4 Oscillator's admittance modulus and argument versus frequency, for $Q_0 = 18.85$; $f_0 = 30\,\text{Hz}$, $M = 1$

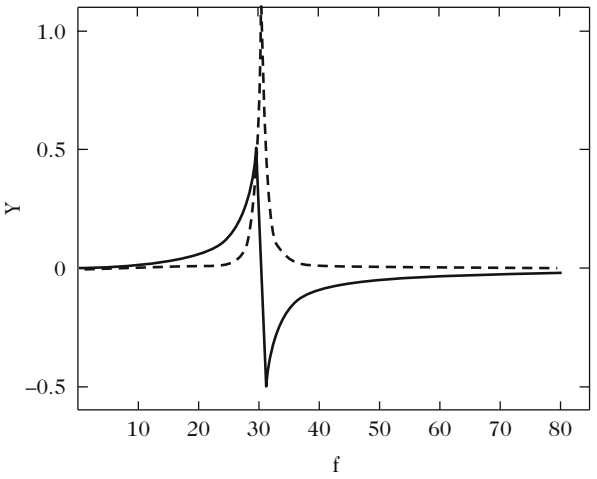

Fig. 2.5 Real (*dotted line*) and imaginary part (*solid line*) of the oscillator's admittance versus frequency, for $Q_0 = 18.85$; $f_0 = 30\,\text{Hz}$, $M = 1$

each corresponding to a mode. For forced oscillations, we are interested in the maximum of this quantity; for self-sustained oscillations, our interest is in the zeros of the imaginary part (this will be explained in Chap. 9), the two kinds of frequencies being very close. For the present case (single mode), they are identical.

To study the admittance variation versus frequency, the easiest way is to start by considering the inverse quantity, i.e., the impedance

$$Z(\omega) = j\omega M + R + \frac{K}{j\omega} = M\omega_0 \left[j\frac{\omega}{\omega_0} - j\frac{\omega_0}{\omega} + \frac{1}{Q_0} \right]. \tag{2.31}$$

Z is real when $\omega = \omega_0$, which implies that the admittance also is real. For $\omega > \omega_0$, the leading term is the mass term, otherwise it is the stiffness term $M\omega_0^2/j\omega$. The real parts of Z and Y are always positive for a passive system, as explained in Chap. 1. The imaginary part is either positive or negative.

The modulus Z is minimum when $\omega = \omega_0$, the so-called *resonance* angular frequency. For a given amplitude of excitation F (the cause), it corresponds to the angular frequency for which the amplitude of the response V (the effect) is maximum.[4] It differs from the angular eigenfrequency ω_p, unless the damping is low [large Q_0, see Eq. (2.5)]. If Q_0 is large, impedance and admittance are almost purely imaginary at any frequency, except very close to the resonance.

Two other frequencies are interesting[5]: these are those for which the imaginary part is equal or opposite to the real part (the argument of Z is then $\pm\pi/4$). This gives the following values:

$$\frac{\tilde{\omega}^{\pm}}{\omega_0} = \sqrt{1 + \frac{1}{4Q_0^2}} \pm \frac{1}{2Q_0} = 1 \pm \frac{1}{2Q_0} + O\left(\frac{1}{Q_0^2}\right). \tag{2.32}$$

For very large Q_0, they are very close to the resonance frequency. It is easy to show that they correspond to extrema of the imaginary part of admittance, which can be written as:

$$Y = \frac{1}{M\omega_0} Q_0 \frac{1 - j\mu Q_0}{1 + \mu^2 Q_0^2} \text{ where } \mu = \frac{\omega}{\omega_0} - \frac{\omega_0}{\omega}. \tag{2.33}$$

At these frequencies, the modulus of Y is thus equal to its value at the resonance ($\mu = 0$), divided by $\sqrt{2}$. We note that

$$\frac{\tilde{\omega}^{+} - \tilde{\omega}^{-}}{\omega_0} = \frac{1}{Q_0}\sqrt{1 + \frac{1}{4Q_0^2}}. \tag{2.34}$$

This quantity is the *relative width of the peak of the quantity* $|Y|^2$ *at half maximum*: for large Q_0, it is close to $1/Q_0$. This is a second definition of the quality factor, the first one being the decay rate by period for free oscillations [see (2.7)]. However the two definitions only coincide at the third order of Q_0^{-1}. We still have to examine the variation of the real part of the admittance: Equation (2.33) shows that it reaches a maximum at the resonance, and it is then equal to:

$$\Re e(Y) = |Y| = \frac{Q_0}{M\omega_0} = \frac{1}{R}. \tag{2.35}$$

[4] ω_0 is also the angular eigenfrequency of the undamped system, obtained for $R = 0$.

[5] They are called quadrantal frequencies.

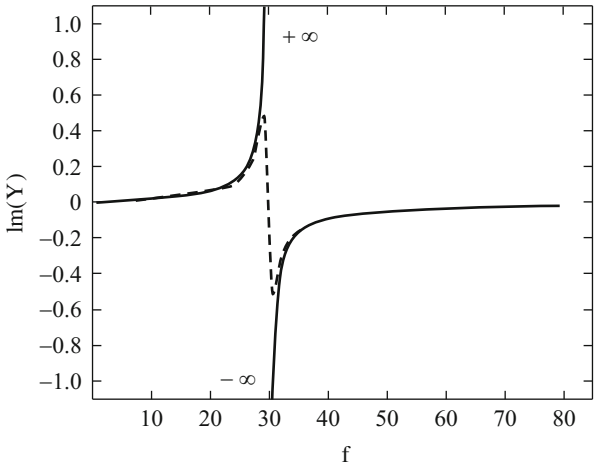

Fig. 2.6 Imaginary part of the admittance when Q_0 tends to infinity: there is no zero-crossing. The *dotted curve* represents the case $Q_0 = 18.85$. The two curves merge far from resonances

2.4.1 Remarks on the Determination of the Resonance Frequency

We notice that the resonance frequency ω_0 does not depend on the quality factor. This is why in the case where we are only interested in resonance frequencies, the quality factor can be taken to be infinite, i.e., the damping equal to zero. We then have a purely imaginary admittance, which approaches $\pm\infty$ when the frequency approaches the resonance. In this case, the shape of the curve of the imaginary part of Y becomes very different, since the two extrema are infinite, and it does not cross 0 (Fig. 2.6). If we consider Eq. (2.33), we see that the limit of the imaginary part of Y when $Q_0 \longrightarrow \infty$ is not straightforward for small μ. On the other hand, the modulus of the impedance Z shows little change.

It turns out that the imaginary part of the impedance is a very good candidate for determining the resonance frequency by interpolation. A simple calculation shows that if $\Im m(Z)$ is known at two angular frequencies ω_1 and ω_2, the resonance is given by:

$$\omega_0^2 = \frac{\omega_1\omega_2\left[\omega_2\Im m(Z_1) - \omega_1\Im m(Z_2)\right]}{\omega_1\Im m(Z_1) - \omega_2\Im m(Z_2)}. \tag{2.36}$$

This method can be used even if other modes are present, since the admittance is then the sum of terms of type (2.33). In the presence of modes, some of them may have an amplitude such that the imaginary part of Y does not vanish anymore. Nevertheless if we ignore the damping terms, each term goes to infinity at resonance, and this problem does not arise. Ignoring damping to find the resonance frequencies is therefore very usual and this approximation is very useful in musical acoustics, regardless of the number of modes. Finally, what happens when damping,

and therefore the quality factor depends on frequency (in this case, the initial time-domain equation can be greatly modified)? If we look at the cancelation of the imaginary part, the resonance frequency remains independent of the variation of damping with frequency, as seen in the expression of the impedance (2.31). Conversely if we look at the maximum of the modulus of Y for forced oscillations, it is a bit more complicated but it can be shown that the variation of $Q_0(\omega)$ leads to a variation of magnitude $1/Q_0^2$ only, for both the resonance frequency and the maximum.

Simplification of the response around the resonance: "simple" modes
We saw in Sect. 2.2.1 that a single-degree-of-freedom oscillator has two complex eigenfrequencies denoted $\omega_0^{\pm}$ [Eq. (2.5)]. These frequencies are the (simple) poles of the admittance (2.30). We have

$$\omega^2 - j\omega\omega_0/Q_0 - \omega_0^2 = (\omega - \omega_0^+)(\omega - \omega_0^-).$$

Hence if $Y_{M0} = Q_0/M\omega_0$ is the maximum of the modulus of Y:

$$Y = \frac{1}{M}\frac{j\omega}{\omega_0^2 - \omega^2 + j\omega\omega_0/Q_0} = -\frac{j}{2}\frac{Y_{M0}}{Q_0\delta_0}\left[\frac{\omega_0^+}{\omega - \omega_0^+} - \frac{\omega_0^-}{\omega - \omega_0^-}\right]. \tag{2.37}$$

Each term can be seen as a mode that we will call "simple mode."[6] Around $\omega = \omega_0$, we can ignore the term of negative eigenfrequency (more specifically the term with a negative real part), which gives, if $Z_{m0} = 1/Y_{M0}$ is the minimum of the impedance:

$$Z = 1/Y \simeq 2jQ_0\delta_0 Z_{m0}\left[\frac{\omega - \omega_0^+}{\omega_0^+}\right] = \frac{1}{1 + j/(2Q_0\delta_0)} Z_{m0}\left[1 + 2jQ_0\frac{\omega - \omega_0\delta_0}{\omega_0}\right]. \tag{2.38}$$

If the quality factor Q_0 is large enough, this reduces to:

$$Z \simeq Z_{m0}\left[1 + 2jQ_0\frac{\omega - \omega_0}{\omega_0}\right] \simeq 2jZ_{m0}Q_0\frac{\omega - \omega_0^+}{\omega_0}. \tag{2.39}$$

(continued)

[6] One can also write $s_0 = j\omega_0^+ = (j\omega_0^-)^*$

$$Y = -\frac{j}{2}\frac{Y_{M0}}{Q_0\delta_0}\left[\frac{s_0}{j\omega - s_0} - \frac{s_0^*}{j\omega - s_0^*}\right],$$

hence $Y(-\omega) = Y^*(\omega)$ for ω real.

This highlights that such an approximation is convenient for representing a Lorentz resonance near its maximum, at the cost of a first-order approximation in $1/Q_0$. A more direct approximation method is to write $\omega = \omega_0(1 + \varepsilon)$ in Eq. (2.37) and expand it to the first order in ε. This approximation is justified as well as the truncation of a modal series to a single mode, under the condition that the frequency is close to the resonance of this mode, with a high quality factor.

2.5 Energy, Power, and Efficiency

2.5.1 Energy and Power

The *instantaneous mechanical power* $p_m(t)$ of the oscillator is given by the scalar product of f and v (see Chap. 1), which leads to:

$$p_m = \frac{d}{dt}\left[\frac{1}{2}Mv^2 + \frac{1}{2}Ky^2\right] + Rv^2 \,. \tag{2.40}$$

The three terms on the right-hand side of (2.40) represent the temporal variations of the kinetic energy of mass M, the elastic energy of spring K, and the power dissipated in the resistance R, respectively.

In most applications, the time average of $p_m(t)$, i.e., its slow fluctuations, is more interesting than its fine details and rapid evolution in time. In audible acoustics, for instance, the human ear is sensitive to the sound level which is well correlated to the average value of the sound power, after integration over a period of 50 ms. This is typically the kind of information that can be read on a sound level meter. In room acoustics, the reverberation time is defined in the same way as the decay of the slow fluctuations of the energy density in the room after the excitation has stopped.

We define below an integration time T whose selection criteria will be discussed later. Using Eq. (2.40) we calculate the average mechanical power $\mathscr{P}_m(T)$:

$$\mathscr{P}_m(T) = \frac{1}{2T}\left[Mv^2(T) + Ky^2(T) - Mv^2(0) - Ky^2(0)\right] + \frac{1}{T}\int_0^T Rv^2(t)dt \,. \tag{2.41}$$

For free oscillations the average power $\mathscr{P}_m(T)$ is zero. We derive

$$\frac{1}{2}\left[Mv^2(T) + Ky^2(T)\right] = \frac{1}{2}\left[Mv^2(0) + Ky^2(0)\right] - \int_0^T Rv^2(t)dt, \tag{2.42}$$

which quantifies the average power $\mathscr{P}_s(T) = \int_0^T Rv^2(t)dt$ dissipated during the given time interval T. This power $\mathscr{P}_s(T)$ is also the power needed by the system to ensure a periodic motion of period T. We notice, in this case, that the quantity between brackets in (2.41) vanishes.

2.5.1.1 Special Case: Steady Sinusoidal Movement

For an excitation force $f(t) = F_M \cos \omega t$, it has been shown in Eq. (2.25) that the velocity is given by $v(t) = V_M \cos(\omega t + \varphi)$. Therefore, the average power is written as follows:

$$\mathscr{P}_m(T) = \frac{1}{T} \int_0^T F_M V_M \cos \omega t \cos(\omega t + \varphi) dt \tag{2.43}$$

The oscillation period is denoted $\tau = \frac{2\pi}{\omega}$. The integration time is then given by $T = n\tau + \tau_o$, where n is a positive integer. The average power becomes

$$\mathscr{P}_m(T) = \frac{1}{2} F_M V_M \cos \varphi + \frac{F_M V_M}{4(2\pi n + \tau_o \omega)} \left[\sin(2\omega\tau_o + \varphi) - \sin \varphi\right] . \tag{2.44}$$

Discussion

- Equation (2.44) shows that the average power $\mathscr{P}_m(T)$ is approximately equal to $\frac{1}{2} F_M V_M \cos \varphi$ only if the average integration period involves a sufficiently large number n of oscillation periods. For the special case where T equals τ, the equality is strict. In what follows, we consider that this condition is satisfied, so that the dependence of the terms of the average power on the integration period is suppressed.
- For a given force, the expression of the velocity was found (see Sect. 2.3.2). The average power can be written using complex quantities:

$$\mathscr{P}_m = \frac{1}{2} \Re e \left[f(t) v^*(t)\right] = \frac{1}{2} F_M^2 \Re e(Y). \tag{2.45}$$

  This result, which is consistent with Eq. (1.131), confirms the well-known result that the maximum of dissipated power is obtained when the excitation frequency is equal to the resonance frequency of the oscillator, namely for $\omega = \omega_0$. Then, following Eq. (2.35) we can write:

$$\text{Max}\left\{\mathscr{P}_m\right\} = \frac{F_M^2}{2R} . \tag{2.46}$$

  As a consequence, from Eq. (2.46), if F_M is known, we can easily derive R by power measurements.

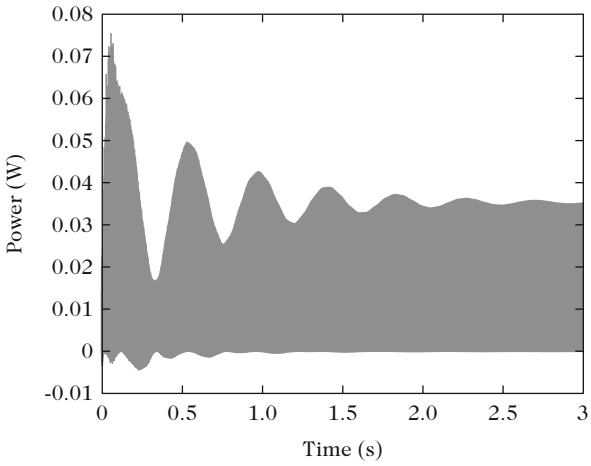

Fig. 2.7 Variation with time of the average dissipated power for an excitation angular frequency ω close to the angular eigenfrequency ω_0

- For forced oscillations with angular frequency ω, the calculation of the power $\mathscr{P}_m$ exhibits terms in $\omega + \omega_0\delta_0$ and $|\omega - \omega_0\delta_0|$, where δ_0 is defined in Eq. (2.5). Consequently, the average power exhibits low frequency variations before the steady state emerges (see Fig. 2.7). Experimentally, this transient state may take some time if ω is close to ω_0, which might pose some difficulty for practical measurements of the average power.

2.5.1.2 Third Definition of the Quality Factor

It is possible to link the average power supplied to the energy of the system, averaged over a period, through the quality factor Q_0. The total energy, which is the sum of kinetic energy and potential energy, is given in Eq. (2.40). Using complex quantities for force and velocity, we have $f(t) = F_M \exp(j\omega t)$ and $v(t) = V_M \exp(j\omega t + \varphi)$. Using the results of Chap. 1, the power and the total energy averaged over a period are given by:

$$\mathscr{P}_m = \frac{1}{2} R\,|v|^2 \quad \text{et } \mathscr{E} = \frac{1}{4}\left[M\,|v|^2 + K\,|y|^2\right] .$$

We get the ratio

$$\frac{\mathscr{E}}{T\mathscr{P}_m} = \frac{\omega}{4\pi}\frac{M\,|v|^2 + K\,|y|^2}{R\,|v|^2} = \frac{Q_0}{4\pi}\frac{\omega}{\omega_0}\left[1 + \frac{\omega^2}{\omega_0^2}\right].$$

This shows that at the resonance, it is equal to $Q_0/2\pi$. This definition complements the definitions based on the decay rate (2.7) and on the relative width of the resonance peak (2.34). These three definitions coincide for small damping values

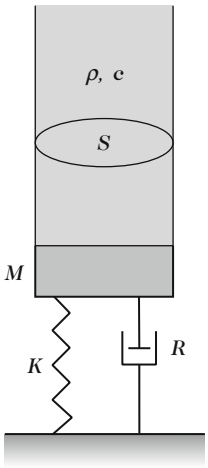

Fig. 2.8 Mechanical single-degree-of-freedom oscillator loaded by air

only. When a more general response is considered, expressed as the sum of several modes, the situation becomes even more complicated. Finally, at the resonance, the average energy is equally distributed between potential and kinetic energy.

2.5.2 *Mechanical Air Loaded Oscillator*

The following example is the simplest model of acoustic radiation by a structure with a single-degree-of-freedom. As in the previous paragraph, we examine its properties in terms of energy, and we define its efficiency in terms of power.

To illustrate the model, imagine a mechanical single-degree-of-freedom oscillator loaded by a semi-infinite tube of cross section S, filled with air of density ρ and where the sound speed is denoted c (see Fig. 2.8). A wave travels in the tube whose specific characteristic impedance ρc was found in Chap. 1 (Sect. 1.2.4). The pressure force is simply proportional to velocity. The equation of this oscillator is written as:

$$f = M\frac{dv}{dt} + Rv + K\int v\,dt + R_a v \quad \text{with} \quad R_a = \rho c S. \tag{2.47}$$

The instantaneous power supplied to the system is written as follows:

$$p_m(t) = \frac{d}{dt}\left[\frac{1}{2}Mv^2 + \frac{1}{2}Ky^2\right] + (R + R_a)v^2. \tag{2.48}$$

Hence the average power (per period) is

$$\mathscr{P}_m(T) = \frac{1}{T}\int_0^T Rv^2(t)dt + \frac{1}{T}\int_0^T R_a v^2(t)dt = \mathscr{P}_s(T) + \mathscr{P}_a(T), \tag{2.49}$$

where $\mathscr{P}_a(T)$ is the average acoustic power radiated into the tube. We define the *acoustical efficiency* by:

$$\eta = \frac{\mathscr{P}_a(T)}{\mathscr{P}_m(T)} = \frac{\mathscr{P}_a(T)}{\mathscr{P}_s(T) + \mathscr{P}_a(T)} = \frac{R_a}{R + R_a}\,. \tag{2.50}$$

This last result requires some comments.

- We observe in (2.50) that the efficiency is independent of T.
- Although the form of η here appears to be very simple, its experimental determination is not straightforward because it requires to estimate R, for example, through measurements in vacuo.
- In the academic example presented above, R_a is obtained analytically, which is rarely the case for structures with complex materials and geometry such as musical instruments. In the general case, $\mathscr{P}_a(T)$ is obtained experimentally (or numerically) by computing the flow of the acoustic intensity vector over a closed surface surrounding the source.
- In general, the efficiency may depend on frequency, which is not the case here, but when there are no losses (this corresponds here to setting $R = 0$) it is always, by definition, equal to unity! Conversely, we have seen that the response of a resonant system always depends on frequency, especially when the losses are small (see, for example, Fig. 2.4). Efficiency and response are therefore quantities whose physical meaning is very different.

2.5.2.1 Link Between Radiated Power and Damping Factor

For a radiating single-degree-of-freedom system, it is possible to estimate the sound power from the measurement (or numerical simulation) of the damping factor, in free oscillations. In Chap. 13, we will examine the conditions for extending this result to systems with multiple DOF. The equation of the mechanical oscillator loaded by air can be written in a reduced form:

$$\frac{d^2y}{dt^2} + 2\zeta\omega_0\frac{dy}{dt} + \omega_0^2 y = 0 \quad \text{with} \quad \zeta = \frac{R + R_a}{2M\omega_0}, \tag{2.51}$$

for which it is known that the solution is written as (assuming $\zeta < 1$):

$$y(t) = \exp(-\zeta\omega_0 t)\left[\cos(\omega_0\sqrt{1-\zeta^2}t) + \frac{\zeta}{\sqrt{1-\zeta^2}}\sin(\omega_0\sqrt{1-\zeta^2}t)\right]. \tag{2.52}$$

Equation (2.52) shows that the *damping factor* (equal to the inverse of the time constant) is equal to:

$$\alpha = \zeta\omega_0 = \frac{R + R_a}{2M} . \tag{2.53}$$

In conclusion, considering the definition (2.3), we note that, for the simple case of a single-degree-of-freedom oscillator, the acoustical efficiency can be estimated in the time domain by using the expression:

$$\eta = \frac{\alpha - \alpha_0}{\alpha} . \tag{2.54}$$

Note It should, however, be emphasized that one of the damping effects is to slightly modify the frequency of the oscillator, compared to the in vacuo case. This effect has no consequence here because, concerning a "monochromatic" signal, the determination of α from the exponential envelope is independent of the oscillation frequency. Furthermore, in the present example, the air load is considered as purely resistive. If, however, we are in a situation where the fluid load also includes a mass or elastic component, we could not obtain the efficiency from a formula as simple as Eq. (2.54). This point of view will be developed in more detail in Chap. 13.

Part II
Waves and Modes

This second Part of the book is devoted to the linear vibrations of musical instruments. The "modal" and "wave" approaches are described in Chaps. 3 and 4, respectively, for non-dissipative structures of simple shapes. Dissipation phenomena are presented in Chap. 5. Coupled systems are addressed in Chap. 6, whereas Chap. 7 is devoted to the resonators of wind instruments. For these instruments, the exact shape of the bore (flaring, toneholes) has an essential function. Leaving aside the radiation, which will be presented in the fourth part of the book, this part is aimed at presenting a global approach of free linear oscillations, eigenfrequencies and eigenmodes of musical instruments.

Chapter 3
Modes

Antoine Chaigne and Jean Kergomard

Abstract The concept of mode (or eigenmode) is ubiquitousin musical acoustics, since the behavior of musical instruments, as many other mechanical systems, is fairly described by boundary value models, for which the modes are the eigensolutions, in the strict mathematical sense. In this chapter, the basic properties of the eigenmodes are reviewed, for both discrete and continuous non dissipative systems. The efficiency of the modal description is illustrated by numerous examples taken from the physics of strings and percussive instruments. In addition, most of the results presented in this chapter will be used in Chap. 7 devoted to wind instruments. It is shown, in particular, to what extent the geometry, material, and conditions of excitation determine the vibrational properties of the instruments. Fundamental results on the vibrations of strings, beams, membranes, plates, and shells are demonstrated, which will be used throughout the book. The links with experimental modal analysis are also emphasized.

3.1 Introduction

The concept of *modes* is widely used in musical acoustics. Experimentally, one can gain a visual appreciation of modes through the so-called *Chladni patterns* (see Fig. 3.1). Such patterns are obtained by sprinkling sand on a plane or on a slightly curved structure (plate and soundboard) which is being continuously excited (using, for example, a bow, or a loudspeaker driven by a sinusoidal input signal).[1]

[1]Chladni patterns on drumheads were obtained by Worland [43].

A. Chaigne (✉)
Institute of Music Acoustics, University of Music and Performing Arts Vienna (MDW), Anton-von-Webern-Platz 1, 1030 Vienna, Austria
e-mail: antchaigne@gmail.com

J. Kergomard
CNRS Laboratoire de Mecanique et d'Acoustique (LMA), 4 impasse Nikola Tesla CS 40006, 13453 Marseille Cedex 13, France
e-mail: kergomard@lma.cnrs-mrs.fr

A. Chaigne, J. Kergomard, *Acoustics of Musical Instruments*, Modern Acoustics and Signal Processing, DOI 10.1007/978-1-4939-3679-3_3

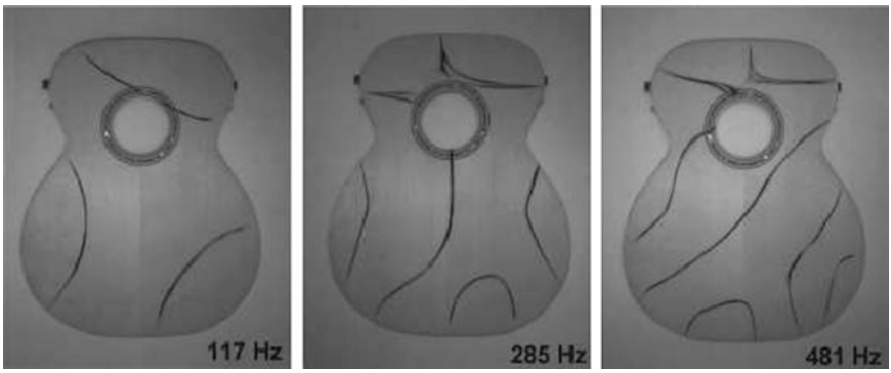

Fig. 3.1 Chladni patterns showing the modes of vibration of a guitar soundboard, at 117, 285 and 481 Hz, respectively. According to [41]. © Thomas Erndl

It is observed that the grains gather together on continuous lines, or nodal lines, corresponding to points with zero amplitude of vibration. The resulting figure is the *mode shape* corresponding to the excited *eigenfrequency*. One can clearly hear the associated sound when the structure is weakly damped, as it is the case for a metallic plate. In what follows, *eigenmodes*, or simply *modes*, designate the set of eigenfrequencies and mode shapes of a continuous, or of a discrete, system for a given geometry and material.

In the previously described experiment, different modes can be successively excited if the excitation point, or the excitation frequency, is modified. If the boundary conditions are changed, then the eigenmodes and eigenfrequencies also change. This result has important consequences in lutherie: it shows that the violin soundboard, once glued to the instrument, does not exhibit the same eigenmodes as it did when it was free to vibrate at the edge.

From a theoretical point of view, the concept of modes is of great interest. Because of their mathematical orthogonality, it is possible to expand any linear solution of vibratory or acoustic phenomena onto a basis of eigenmodes. In Chap. 8, it will be shown under which conditions such expansions can be applied to weakly nonlinear systems.

Strictly speaking, the concept of eigenmodes can be applied to any undamped, linear system of finite dimensions involving both kinetic and elastic energy, when the dynamics of the system are observed over a time scale which is large compared with the "characteristic time" of the system. The characteristic time corresponds to the time taken by a wave to propagate from an internal excitation point to the edges of the finite domain defined by the system. In Chap. 5 this notion will be extended to damped systems by introducing the concept of complex modes.

In the present chapter, the discussion is restricted to real modes. The basic mathematical properties of modes are presented, as well as general methods to calculate them. We illustrate these concepts using some examples linked to

string and percussion instruments. The acoustics of wind instrument resonators is considered in Chap. 7, where some results of the present chapter are used, drawing on the analogies outlined in Table 1.1 in Chap. 1.

3.2 Time Scale: Transition from Wave to Mode

When a continuous elastic medium (either solid or fluid), of finite size, is perturbed by an external stimulus, then the disturbance propagates away from the excitation point. The propagation speed of the disturbance depends on the inertial properties (density) and elasticity (compressibility, Young's moduli, and Poisson's ratios) of the medium. As long as the disturbance does not reach the boundaries of the medium, a *wave* approach such as the one outlined in Chap. 1 and developed in Chap. 4 is a suitable means of describing the phenomenon. Taking L as being a characteristic dimension of the medium, and c as the propagation speed, we can define a *characteristic time* $t_c = L/c$, where this wave approach remains valid (see Fig. 3.2). When the disturbance reaches the boundaries of the domain, part of the energy is generally transmitted to the external medium, the remaining part being reflected inside. Two situations can occur

1. The interference between incident and reflected waves at the boundaries is *constructive*. This happens at frequencies for which the incident and reflected waves are in phase. In this case, the total energy for these frequencies tends to increase with time. Only energy losses due to absorption or transmission at the boundaries, and during the propagation through the medium itself, limit this growth. In the absence of dissipation, the energy increases indefinitely in the medium.
2. The interference between incident and reflected waves at the boundaries is *destructive*. In this case, the phase relationship is such that no energy growth is possible over time in the medium. Because of absorption, the amplitudes of the corresponding frequencies gradually decrease.

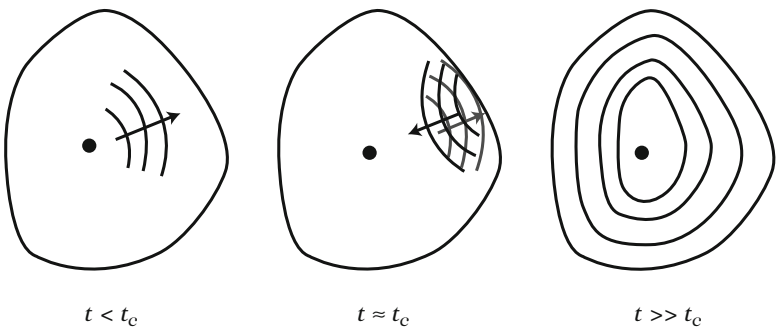

Fig. 3.2 Local vs. global approach of dynamic phenomena. t_c is the *characteristic time*

If the observation time is significantly larger than the characteristic time t_c of the medium, then the initial disturbance travels back and forth several times between the excitation point and the boundaries of the domain. In this scenario, it is therefore more useful to describe the phenomenon in a way that accounts for the fact that the energy of the system is distributed over a set of discrete frequencies. In the absence of dissipation, these frequencies are the "eigenfrequencies" of the finite medium. In the following paragraph, a rigorous definition will be introduced. As stated in the introduction, if a single eigenfrequency can be isolated (this can be achieved with a monochromatic excitation spectrum), then the spatial profile of the medium corresponds to an eigenshape.

It is always possible to describe the dynamics in terms of waves. We will show some applications of this approach in the next chapter. However, this wave approach quickly becomes very cumbersome and does not always provide a clear understanding of the physics. It is worth noting, finally, that, strictly speaking, the growth of an eigenmode needs a significant number of round-trips. Therefore, there is a definite intermediate period of time (between one and "a number of" t_c), where both the "wave" approach and the "mode" approach are acceptable.

3.3 Definitions and Basic Properties of the Eigenmodes

An eigenmode, for a discrete system or for a continuous medium with finite dimensions, is an eigensolution of a boundary value problem without a source (in the mathematical sense). In practice, this means that they are solutions of the equations describing the system without external excitation. If the system is conservative, these solutions are sinusoidal in time and are in phase (or in anti-phase): "standing waves" are obtained. The restriction to conservative media at this stage may be surprising as dissipation is essential for musical instruments, but before we consider musical instruments it is first important to understand the properties of the eigenmodes for this limiting reference case.

3.3.1 Discrete System

A discrete system has a finite number of degrees of freedom. In linear dynamics, the equations of motion of a discrete conservative system can be written in the general form:

$$\mathbb{M}\ddot{\boldsymbol{\xi}} + \mathbb{K}\boldsymbol{\xi} = 0, \tag{3.1}$$

where $\boldsymbol{\xi}$ is a vector containing the variables which describe the motion of the system, $\mathbb{M}$ is the mass matrix, and $\mathbb{K}$ the stiffness matrix. Each component of $\boldsymbol{\xi}$ is a function

of time. Matrices $\mathbb{M}$ and $\mathbb{K}$ are symmetrical. The general form of Eq. (3.1) is the same as that obtained for a discretized continuous medium, using finite element or finite difference methods (see Chap. 1).

In Chap. 2, it was shown how the eigenvectors and eigenfrequencies of an SDOF oscillator can be found. Let us now define the vector $\boldsymbol{w}$ and the matrix $\mathbb{M}_K$:

$$\boldsymbol{w} = \begin{pmatrix} \boldsymbol{\xi} \\ \dot{\boldsymbol{\xi}} \end{pmatrix} \; ; \; \mathbb{M}_K = \begin{pmatrix} \mathbf{0} & \mathbb{I} \\ -\mathbb{M}^{-1}\mathbb{K} & \mathbf{0} \end{pmatrix} , \tag{3.2}$$

so that Eq. (3.1) becomes: $\dot{\boldsymbol{w}} = \mathbb{M}_K \boldsymbol{w}$.

By definition, the eigenvectors of $\mathbb{M}_K$ must fulfill the condition: $\mathbb{M}_K \boldsymbol{w} = \lambda \boldsymbol{w}$, or

$$\dot{\boldsymbol{\xi}} = \lambda \boldsymbol{\xi} \; ; \; -\mathbb{M}^{-1}\mathbb{K}\boldsymbol{\xi} = \lambda \dot{\boldsymbol{\xi}} \text{ , from which } \mathbb{K}\boldsymbol{\xi} = -\lambda^2 \mathbb{M}\boldsymbol{\xi} . \tag{3.3}$$

Denoting $\lambda^2 = -\omega^2$, the eigenfrequencies are the roots ω_n of the characteristic polynomial:

$$\det\left[-\omega^2\mathbb{M} + \mathbb{K}\right] = 0 . \tag{3.4}$$

The number of roots is finite. These roots are real for a conservative system [16]. The eigenvectors (or *eigenshapes*) $\boldsymbol{\Phi}_n$ are therefore the nonzero solutions of the following equation:

$$\left[-\omega_n^2\mathbb{M} + \mathbb{K}\right]\boldsymbol{\Phi}_n = 0 . \tag{3.5}$$

Important Property Since Eq. (3.5) is indeterminate, the components of $\boldsymbol{\Phi}_n$ are defined up to a multiplying factor.

The set $(\omega_n, \boldsymbol{\Phi}_n)$ defines the eigenmodes of the system. The mathematical theory of spectral analysis shows that the shapes $\boldsymbol{\Phi}_n$ form an $\mathbb{M}$- and $\mathbb{K}$-orthogonal basis of the vector space corresponding to the small motion of the system, which means

$${}^t\boldsymbol{\Phi}_m\mathbb{M}\boldsymbol{\Phi}_n = 0 \text{ and } {}^t\boldsymbol{\Phi}_m\mathbb{K}\boldsymbol{\Phi}_n = 0 \quad \text{for} \quad m \neq n , \tag{3.6}$$

where ${}^t\boldsymbol{V}$ represents the transpose of vector $\boldsymbol{V}$.

Demonstration

Let us write (3.5) for two specific eigenmodes n and m. We obtain

$$\omega_n^2\mathbb{M}\boldsymbol{\Phi}_n = \mathbb{K}\boldsymbol{\Phi}_n \quad \text{and} \quad \omega_m^2\mathbb{M}\boldsymbol{\Phi}_m = \mathbb{K}\boldsymbol{\Phi}_m . \tag{3.7}$$

(continued)

Multiplying both sides of the first expression by ${}^t\boldsymbol{\Phi}_m$ and, similarly, both sides of the second expression by ${}^t\boldsymbol{\Phi}_n$, we obtain

$$ {}^t\boldsymbol{\Phi}_m \omega_n^2 \mathbb{M} \boldsymbol{\Phi}_n = {}^t\boldsymbol{\Phi}_m \mathbb{K} \boldsymbol{\Phi}_n \quad \text{and} \quad {}^t\boldsymbol{\Phi}_n \omega_m^2 \mathbb{M} \boldsymbol{\Phi}_m = {}^t\boldsymbol{\Phi}_n \mathbb{K} \boldsymbol{\Phi}_m \, . \tag{3.8} $$

We now transpose the second expression, which leads to:

$$ \omega_m^2 \, {}^t\boldsymbol{\Phi}_m \, {}^t\mathbb{M} \boldsymbol{\Phi}_n = {}^t\boldsymbol{\Phi}_m \, {}^t\mathbb{K} \boldsymbol{\Phi}_n \, . \tag{3.9} $$

Given the symmetry properties of $\mathbb{M}$ and $\mathbb{K}$, the last equality becomes

$$ {}^t\boldsymbol{\Phi}_m \omega_m^2 \mathbb{M} \boldsymbol{\Phi}_n = {}^t\boldsymbol{\Phi}_m \mathbb{K} \boldsymbol{\Phi}_n \, . \tag{3.10} $$

By comparing the first expression of (3.8) with (3.10), we find

$$ \left(\omega_n^2 - \omega_m^2\right) {}^t\boldsymbol{\Phi}_m \mathbb{M} \boldsymbol{\Phi}_n = 0, \tag{3.11} $$

from which the expressions (3.6) are derived, since the eigenfrequencies are different.[2]

The orthogonality properties mean that the inertia and stiffness forces involved in a given eigenmode do not develop energy in the motion of the other modes. A mechanical independence exists between two distinct modes.

In theory, one can take advantage of this orthogonality to expand any solution of this problem onto the eigenmodes of the system. Thus, if the system is excited by a distribution of forces f, its motion is described as:

$$ \mathbb{M} \ddot{\boldsymbol{\xi}} + \mathbb{K} \boldsymbol{\xi} = \boldsymbol{f} \, . \tag{3.12} $$

The spectral theory shows that the eigenmodes form a *complete* system. As a consequence any solution of Eq. (3.12) yields a unique projection on the eigenmodes basis [15]. This projection can be written as:

$$ \boldsymbol{\xi} = \sum_n \boldsymbol{\Phi}_n q_n(t) \, . \tag{3.13} $$

The functions $q_n(t)$ are referred to as the *generalized displacements* or the *modal participation factors*. By substituting (3.13) into (3.12), and by making a inner product on both sides with any eigenvector $\boldsymbol{\Phi}_m$, we find, (after eliminating the zero products when $m \neq n$):

$$ \langle \boldsymbol{\Phi}_n, \mathbb{M} \boldsymbol{\Phi}_n \rangle \ddot{q}_n + \langle \boldsymbol{\Phi}_n, \mathbb{K} \boldsymbol{\Phi}_n \rangle q_n = \langle \boldsymbol{\Phi}_n, \boldsymbol{f} \rangle \, , \tag{3.14} $$

[2] It is shown, see, e.g., [18], that the orthogonality properties can be extended to the case of multiple eigenvalues.

where the notation $\langle\ ,\ \rangle$ represents the inner product: $\langle \boldsymbol{x}, \boldsymbol{x}' \rangle = {}^t\boldsymbol{x}\boldsymbol{x}'$. Equation (3.14) expresses the decoupling of generalized displacements. Each of these displacements is described by the differential equation of an independent SDOF oscillator. The quantity

$$m_n = \langle \boldsymbol{\Phi}_n, \mathbb{M}\boldsymbol{\Phi}_n \rangle \tag{3.15}$$

is the *modal mass* of the mode n. Like the eigenshapes, the modal masses are defined up to a constant multiplicative factor. Similarly, the quantities

$$\kappa_n = \langle \boldsymbol{\Phi}_n, \mathbb{K}\boldsymbol{\Phi}_n \rangle \tag{3.16}$$

are the modal stiffnesses. Note that:

$$\kappa_n = m_n {\omega_n}^2 . \tag{3.17}$$

Finally, the quantity

$$f_n = \langle \boldsymbol{\Phi}_n, \boldsymbol{f} \rangle \tag{3.18}$$

represents the projection of the external forces onto the mode n. In practice, if the inner product is zero, it is not possible to excite the corresponding mode. This occurs, for example, if a string is attached at a position corresponding to a node of a soundboard mode: in this case, the string cannot excite this mode.

In view of these definitions, we can rewrite the equation of each oscillator in the following generic form:

$$\ddot{q}_n + \omega_n^2 q_n = \frac{f_n}{m_n} . \tag{3.19}$$

The Fourier transform of $\boldsymbol{\xi}$ [Eq. (3.13)] becomes

$$\boldsymbol{\Xi}(\omega) = \sum_n \boldsymbol{\Phi}_n \frac{f_n}{m_n} \frac{1}{\omega_n^2 - \omega^2} . \tag{3.20}$$

The right-hand side of this expression is a sum of resonant terms. Consequently, if the system is forced at a frequency ω close to one particular eigenfrequency ω_n, the amplitude of that term will tend to infinity. In such a situation, the assumption of linearity for the system is no longer justified, and other tools for describing the nonlinear phenomena must be used (see Chap. 8).

Note 1: Since the eigenvectors are defined up to a constant multiplicative factor C, (3.15) shows that the modal mass is proportional to C^2. Consequently, (3.18) shows that f_n is proportional to C and (3.19) indicates that q_n is proportional to C^{-1}. In summary, (3.13) shows that the solution $\boldsymbol{\xi}$ is independent of C.

Note 2: The expression *normal mode* is sometimes used to designate an eigenmode *normalized* by an arbitrary constant. This constant can either be the modal mass of the mode n, or any other appropriate constant (the total energy of the system, the modal mass of the fundamental...), depending on the physical context.

3.3.1.1 Energy Approach

The total kinetic energy of the system is

$$\begin{aligned}\mathscr{E}_c = \frac{1}{2}\langle\dot{\boldsymbol{\xi}}, \mathbb{M}\dot{\boldsymbol{\xi}}\rangle &= \frac{1}{2}\langle\sum_n \boldsymbol{\Phi}_n\dot{q}_n(t), \mathbb{M}\sum_m \boldsymbol{\Phi}_m\dot{q}_m(t)\rangle \\ &= \frac{1}{2}\sum_n\sum_m\langle\boldsymbol{\Phi}_n, \mathbb{M}\boldsymbol{\Phi}_m\rangle\dot{q}_n(t)\dot{q}_m(t) \\ &= \frac{1}{2}\sum_n m_n\dot{q}_n^2(t).\end{aligned} \tag{3.21}$$

Similarly, the elastic potential energy is

$$\mathscr{E}_p = \frac{1}{2}\langle\boldsymbol{\xi}, \mathbb{K}\boldsymbol{\xi}\rangle = \frac{1}{2}\sum_n \kappa_n q_n^2(t)\ . \tag{3.22}$$

Therefore, the total energy of the system is the sum of the modal energies:

$$\mathscr{E} = \mathscr{E}_c + \mathscr{E}_p = \frac{1}{2}\sum_n m_n\dot{q}_n^2(t) + \kappa_n q_n^2(t) = \sum_n \mathscr{E}_n\ . \tag{3.23}$$

3.3.2 Extension to Continuous Systems

Extending the results obtained for discrete systems to continuous (conservative) systems, within the framework of linear approximation, shows that an *infinite* set of eigenmodes exists with orthogonality properties related to mass and stiffness operators. These eigenmodes form a complete basis for any linear motion of the system. In this case, the eigenvectors $\boldsymbol{\Phi}_n$ defined for discrete systems become continuous eigenfunctions of space $\Phi(\boldsymbol{x})$ and the inner products are expressed in the form of integrals over the entire structure.

The equation of motion for linear continuous systems can be written as:

$$\mathscr{L}(y) + \ddot{y} = s(\boldsymbol{x}, t)\ , \tag{3.24}$$

where $y(\boldsymbol{x}, t)$ is the displacement (or one of its derivatives), $\mathscr{L}(y)$ a linear operator, function of y and of its derivatives, and $s(\boldsymbol{x}, t)$ a source term. It is necessary to add boundary and initial conditions to define a well-posed problem.[3]

3.4 Application to Vibrating Strings

As the name suggests, the basic sound generation mechanism in any string instrument is the vibration of the strings attached to the neck and soundboard. The soundboard is set into motion by the strings, which act as vibratory sources, and the vibrations of the soundboard are transformed into an acoustic pressure (see Fig. 3.3).

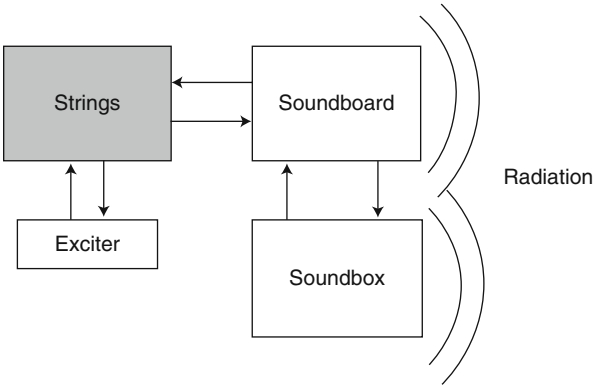

Fig. 3.3 Basic principles of string instruments. An exciter (finger, plectrum, hammer, and bow) sets one or more strings into vibration. This results in a string-exciter coupling which is either limited in time (plucked or struck strings) or permanent (bowed). The vibrations of the strings are transmitted to the soundboard via the bridge. The motion of the soundboard modifies the vibration of the strings slightly, especially if it is light and flexible, since it provides a moving end for the strings. The soundboard is usually coupled to an air cavity with sound holes (rose, f-holes). The radiation of the instrument is primarily due to the soundboard and soundholes and, to a lesser extent, to the back plate. The other parts of the instrument (neck, ribs) do not radiate much sound in general

[3] One can also define a vector $\boldsymbol{w} = \begin{pmatrix} y \\ \dot{y} \end{pmatrix}$ and separate time and space. Thus for the wave equation $\mathscr{L}(y) = -c^2 \frac{\partial^2 y}{\partial x^2}$, the equation to be solved can be written:

$$\dot{\boldsymbol{w}} = \boldsymbol{A}\boldsymbol{w} \text{ , where } \boldsymbol{A} = \begin{pmatrix} 0 & 1 \\ -c^2 \frac{\partial^2 y}{\partial x^2} & 0 \end{pmatrix} .$$

We therefore have a matrix operator $\boldsymbol{A}$, for which we can determine the eigenvectors and eigenvalues.

The same basic principles apply for all string instruments, though a wide variety of sounds and tone colors exist in this family. Variations in the excitation mechanisms and the material properties of the body are largely responsible for this diversity, although significant differences between the properties and regimes of vibration of the strings themselves are observable from one instrument to another. As an illustration, we will present some properties of bowed strings at the end of this section. These properties will be discussed in more detail in Chap. 11.

The experimental study of vibrating strings is a hard task, mainly because it is difficult to mechanically isolate them from their supporting frame: it is, for example, extremely hard in practice to obtain perfectly fixed boundary conditions. Moreover, the motion of a real string does not remain planar: there are always conditions of excitation, heterogeneities, and/or coupling conditions at the fixed ends that induce two polarizations and thus a resulting 3D motion. Finally, a coupling exists between the (dominant) transverse vibration and the longitudinal vibration (see Chap. 8).

In what follows, the fundamental behavior of string motion is reviewed, in the context of musical acoustics. The discussion is limited to the case of a planar transverse motion.

3.4.1 Heterogeneous String

For a one-dimensional string with density $\rho(x)$, tension $T(x)$, length L, and cross-section $S(x)$ (case of a heterogeneous string with variable diameter), the equation that describes the transverse displacement $y(x,t)$ is [see Eq. (1.11)]:

$$\rho(x)S(x)\frac{\partial^2 y}{\partial t^2} - \frac{\partial}{\partial x}\left[T(x)\frac{\partial y}{\partial x}\right] = f(x,t)\ , \tag{3.25}$$

where $f(x,t)$ is a linear density of force applied to the string, which can even be propagative, for example, in the case of a sliding finger. A variable tension $T(x)$ can be obtained if, for example, one hangs a string vertically, because of gravity. We deliberately choose this example of a heterogeneous string to highlight the general properties of the eigenmodes.

We limit ourselves in this section to cases where the boundary conditions are characterized either by a zero displacement or by a zero force. In Sect. 3.4.5 the extension to more complex situations will be examined, such as the cases (important in musical acoustics) of mass or elastic ends.

Let $\Phi_n(x)$ be the set comprising the eigenshapes of the string, for given boundary conditions. We expand a solution onto this basis by writing

$$y(x,t) = \sum_n \Phi_n(x) q_n(t)\ . \tag{3.26}$$

Multiplying both sides of (3.25) by any mode $\Phi_m(x)$, and integrating over the entire string, yields

$$\sum_n \ddot{q}_n(t) \int_0^L \Phi_n(x)\Phi_m(x)\rho(x)S(x)dx - \sum_n q_n(t) \int_0^L \Phi_m(x)\frac{d}{dx}\left(T(x)\frac{d\Phi_n(x)}{dx}\right)dx = \int_0^L \Phi_m(x)f(x,t)dx\,, \tag{3.27}$$

which can be rewritten in a symbolic form:

$$\mathscr{M}\,(\ddot{y}, \Phi_m) + \mathscr{K}\,(y, \Phi_m) = \langle f, \Phi_m \rangle\,. \tag{3.28}$$

Equation (3.28) is very general and can be applied to any continuous conservative system. The symbol $\mathscr{M}$ designates the mass operator, and $\mathscr{K}$ is the stiffness operator.

3.4.1.1 Orthogonality of the Eigenmodes

Consider a given eigenmode $\Phi_n(x)$. It must satisfy Eq. (3.25) for the case where the source term $f(x,t) = 0$:

$$-\omega_n^2\rho(x)S(x)\Phi_n(x) = \frac{d}{dx}\left[T(x)\frac{d\Phi_n(x)}{dx}\right]\,. \tag{3.29}$$

Using a similar method as used previously for discrete systems, we multiply both sides by $\Phi_m(x)$ and we integrate over the string's length. This gives

$$\omega_n^2 \int_0^L \Phi_n(x)\Phi_m(x)\rho(x)S(x)dx + \int_0^L \Phi_m(x)\frac{d}{dx}\left(T(x)\frac{d\Phi_n(x)}{dx}\right)dx = 0\,. \tag{3.30}$$

To simplify the working, the following notation is used:

$$\mathscr{P}_M(m,n) = \int_0^L \Phi_n(x)\Phi_m(x)\rho(x)S(x)dx \tag{3.31}$$

and

$$\mathscr{P}_T(m,n) = \int_0^L T(x)\frac{d\Phi_m(x)}{dx}\frac{d\Phi_n(x)}{dx}dx\,. \tag{3.32}$$

After integration by parts of the second term, the equality (3.30) becomes

$$\omega_n^2 \mathscr{P}_M(m,n) = \mathscr{P}_T(m,n) - \left[\Phi_m(x)T(x)\frac{d\Phi_n(x)}{dx}\right]_0^L . \tag{3.33}$$

Writing the same equation for both indices (n,m) yields

$$(\omega_m^2 - \omega_n^2)\mathscr{P}_M(m,n) = \left[\Phi_m(x)T(x)\frac{d\Phi_n(x)}{dx} - \Phi_n(x)T(x)\frac{d\Phi_m(x)}{dx}\right]_0^L , \tag{3.34}$$

and

$$(\omega_m^2 - \omega_n^2)\mathscr{P}_T(m,n) = \left[\omega_m^2\Phi_m(x)T(x)\frac{d\Phi_n(x)}{dx} - \omega_n^2\Phi_n(x)T(x)\frac{d\Phi_m(x)}{dx}\right]_0^L . \tag{3.35}$$

With the assumptions made on the boundary conditions (i.e., zero displacement or zero force), the terms between brackets are zero. Therefore, if $m \neq n$, the orthogonality of the eigenmodes with regard to mass and stiffness can be written as:

$$\mathscr{P}_M(m,n) = 0 \;\; ; \;\; \mathscr{P}_T(m,n) = 0 . \tag{3.36}$$

The kinetic and potential energies can be expressed as functions of these quantities:

$$E_c = \frac{1}{2}\sum_{n,m}\mathscr{P}_M(m,n)\,\dot{q}_n\dot{q}_m \;;\; E_p = \frac{1}{2}\sum_{n,m}\mathscr{P}_T(m,n)\,q_n q_m . \tag{3.37}$$

Since the products $\mathscr{P}_M$ and $\mathscr{P}_T$ are zero for $m \neq n$, the energy is thus the sum of the energy of the modes (see Sect. 3.3.1.1).

Notes The orthogonality properties (3.36) are not related to any particular form of the solutions $\Phi(x)$ (sinusoidal or other). The demonstration here is valid for a heterogeneous string, for which the eigenfunctions are not explicitly known.

The previous results are also valid for a mode with a zero eigenfrequency. Equation (3.29) then shows that we must have $Td\Phi/dx =$ constant, which occurs when both boundary conditions are of "zero force" type. We then obtain $\Phi =$ constant as one of the solutions to the problem (this corresponds to a globally undeformed displacement, also known as a *rigid body mode*). To achieve such boundary conditions in the case of strings, we can think of rings sliding on rails orthogonal to the string, but it is a little bit exotic in the context of musical applications. However, an equation of the form (3.25) can be found in other contexts (longitudinal vibrations of bars and sound pipes) where the present remark then makes full sense.

3.4.1.2 Generalized Displacements

As a consequence of the orthogonality of the eigenmodes, and by taking Eq. (3.29) into account, (3.28) becomes

$$\ddot{q}_n(t) + \omega_n^2 q_n(t) = \frac{f_n(t)}{m_n}\,, \tag{3.38}$$

where the modal mass of the mode n is

$$m_n = \int_0^L \Phi_n^2(x)\rho(x)S(x)dx, \tag{3.39}$$

and where

$$f_n(t) = \int_0^L f(x,t)\Phi_n(x)dx \tag{3.40}$$

is the projection of the force density on the mode n. The modal stiffness is equal to:

$$\kappa_n = m_n\omega_n^2 = \int_0^L T\left(\frac{d\Phi_n}{dx}\right)^2 dx\,. \tag{3.41}$$

N.B. *In general, finding the modal mass m_n is easier than finding the modal stiffness κ_n. Since ω_n is known, the modal stiffness is most often determined using the first equality in Eq. (3.41).*

A set of oscillator equations is obtained for the generalized displacement of a continuous system, in the same way as for discrete systems. The main difference is that, for a continuous system, the number of independent differential equations is infinite in theory. In practice, however, a truncation of modes is made, depending on the frequency range under examination. In musical acoustics, we are primarily interested in the frequency domain corresponding to the audible range. This range might be further restricted in view of other considerations, such as damping or the spectral width of the excitation.

To solve the problem related to each generalized displacement, the methods and results presented in Chap. 2 devoted to the oscillator are of direct relevance. Damping phenomena will be introduced later in Chap. 5. The differential equations to be solved require a knowledge of the initial conditions. In the broad sense, these initial conditions include cases where the excitation is known starting from $t = -\infty$ (see Chap. 2).

Consider the case where the string is set into motion at a particular instant of time ($t = 0$) with initial profile $y(0,t)$ and initial velocity $\dot{y}(0,t)$. We can write as:

$$y(0,t) = \sum_n \Phi_n(x)q_n(0). \tag{3.42}$$

A similar expression can be written for the initial velocity. The mass and stiffness orthogonality of the modes yields the initial conditions for the displacements $q_n(t)$:

$$q_n(0) = \frac{1}{m_n} \int_0^L \rho(x) S(x) y(0,t) \Phi_n(x)\, dx$$

and (3.43)

$$\dot{q}_n(0) = \frac{1}{m_n} \int_0^L \rho(x) S(x) \dot{y}(0,t) \Phi_n(x)\, dx\,.$$

This leads to the result:

$$q_n(t) = \frac{1}{m_n \omega_n} \int_0^t f(\theta) \sin \omega_n (t-\theta)\, d\theta + q_n(0) \cos \omega_n t + \dot{q}_n(0) \frac{\sin \omega_n t}{\omega_n}\,. \tag{3.44}$$

Denoting $g_n(t) = \frac{\sin \omega_n t}{\omega_n}$, the first term of $q_n(t)$ is the convolution $f_n(t) \star g_n(t)$, where $g_n(t)$ is the Green's function of the oscillator corresponding to the nth-mode of the string (Note: see Chap. 2 and compare (3.44) with (2.20)).

3.4.1.3 Impulse Response of a String

In the particular case where $f_n(t)$ is a Dirac delta function of the form $f_{n0}\ \delta(t)$, its Laplace transform is a constant $F_n(s) = f_{n0}$. The expression (3.44) can then be reduced to:

$$q_n(t) = \frac{f_{n0}}{m_n} \frac{\sin \omega_n t}{\omega_n} + q_n(0) \cos \omega_n t + \dot{q}_n(0) \frac{\sin \omega_n t}{\omega_n}\,. \tag{3.45}$$

The *impulse response for the nth-mode of the string* is obtained. Some remarks can be made

1. An equivalence exists between the expressions of $q_n(t)$ obtained for the impulse excitation and the initial velocity condition, respectively. In other words, the string motion is identical, if the vibration is generated with an initial velocity profile or with a spatial distribution of forces whose time dependence is a Dirac delta function.
2. If the excitation also occurs at an infinitesimally small point in space, i.e., located at the point $x = x_0$, it is written $f(x,t) = A\delta(x - x_0)\delta(t)$. In this case, the result is $f_n(t) = \langle f(x,t), \Phi_n(x) \rangle = A\Phi_n(x_0)\delta(t)$. The magnitude of the the contribution of the nth mode to the string motion therefore depends on the value of the mode shape at the excitation point. In other words, the mode n of the string cannot be excited if the force is applied on one of its vibration nodes.

3. The Green's function for Eq. (3.25) can be defined as the function for which the applied force is[4]:

$$f(x,t) = T(x_0)\delta(t-t_0)\delta(x-x_0)\,.$$

The solution is:

$$g(x,t|x_0,t_0) = H(t-t_0)T(x_0)\sum_n \frac{\Phi_n(x)\Phi_n(x_0)}{m_n}\frac{\sin\omega_n(t-t_0)}{\omega_n}\,. \tag{3.46}$$

This solution illustrates the reciprocity between the source (at position x_0) and the receiver (at position x). For the constant mode $\Phi(x) = 1$ (when it exists), one must replace the last ratio with $(t-t_0)$. In this case, the growth over time is compensated in practice by the damping.

3.4.2 Ideal String Fixed at Both Ends

The simplest case to be considered is the so-called *ideal* string rigidly fixed at both ends. An *ideal* string is homogeneous with density ρ, constant cross-section S, and uniform tension T. It is assumed that vibrations occur without damping and restricted to a single plane. This situation is far from a real string, but it can be considered as a reference case. The transverse displacement $y(x,t)$ of the string is then described by the wave equation:

$$\frac{1}{c^2}\frac{\partial^2 y}{\partial t^2} = \frac{\partial^2 y}{\partial x^2}\,, \tag{3.47}$$

where $c = \sqrt{\frac{T}{\rho S}}$ is the propagation speed of the transverse waves. For a harmonic wave of the form $y(x,t) = e^{j(\omega t - kx)}$, Eq. (3.47) yields *the dispersion equation* $D(\omega,k)$ which expresses the relationship between angular frequency ω and wavenumber k. We obtain

$$D(\omega,k) = \omega^2 - c^2k^2 = 0\,, \tag{3.48}$$

showing that the ratio between angular frequency and wavenumber is constant and equal to c, a general property of *non-dispersive* medium. For a string of length L rigidly fixed at both ends, the eigenmodes must fulfill the conditions:

$$\frac{d^2\Phi_n}{dx^2} + \frac{\omega^2}{c^2}\Phi_n = 0 \quad \text{with} \quad \Phi_n(0) = \Phi_n(L) = 0\,. \tag{3.49}$$

[4]The factor $T(x_0)$ is written here in the applied force term to be consistent with other Green's functions which will appear in later chapters of this book.

As a consequence, the solutions for the eigenfunctions are

$$\Phi_n(x) = \sin k_n x \,, \tag{3.50}$$

where the wavenumber values correspond to the discrete set:

$$k_n = \frac{n\pi}{L}. \tag{3.51}$$

Using Eq. (3.48), the discrete set of angular frequencies is

$$\omega_n = \frac{n\pi c}{L}, \quad \text{i.e., for the eigenfrequencies: } f_n = \frac{nc}{2L} \,. \tag{3.52}$$

According to Eq. (3.39), the modal mass is $m_n = \frac{\rho SL}{2} = \frac{M_s}{2}$, where M_s is the total mass of the string. In this particular case, all modal masses are equal. It is worth remembering that the value of the ratio $m_n/M_s = 1/2$ is purely arbitrary, since the modal masses are defined up to a multiplicative factor. On the contrary, the multiplicative constants are suppressed in Eq. (3.21) showing that the kinetic energy $\mathscr{E}_n = \frac{1}{2} m_n \dot{q}_n^2$ has a physical meaning.

3.4.3 Initial Conditions and Starting Transients

Traditionally, string instruments are divided into three main families: plucked strings (guitar, harpsichord, harp, etc.), struck strings (piano, hammered dulcimer, etc.), and bowed strings (violin, viola, cello, and double bass). This classification is based directly on the different excitation mechanisms of the string. In Chap. 1, a detailed physical description of the pluck was presented. In this chapter, the main focus is on vibration modes, and we will thus restrict ourselves in Sect. 3.4.4 with a simplified description of the pluck excitation.

In Sect. 3.4.7 there is some discussion on struck strings, with emphasis on the interaction between piano hammer and string. Finally, in Sect. 3.4.9, some properties of bowed strings are presented. The bow–string interaction is presented in detail in Chap. 11, focusing on the violin.

3.4.4 Plucked String

When plucked by a finger or a plectrum, the string is moved away from its initial equilibrium position. During the stick phase, a contact exists between the exciter and the string. When the restoring force due to tension (see Fig. 3.4) becomes slightly higher than the frictional force, the string slips under the finger (see Sect. 1.4.3.1 in Chap. 1).

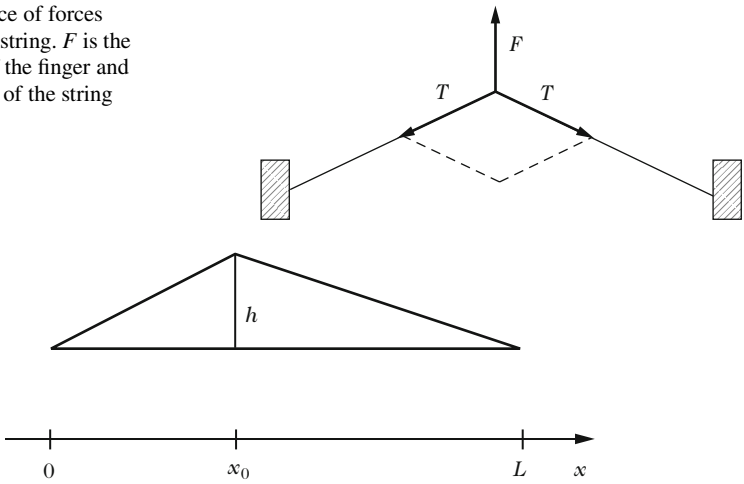

Fig. 3.4 Balance of forces for the plucked string. F is the pulling force of the finger and T is the tension of the string

Fig. 3.5 Simplified model of initial profile for a plucked string without stiffness

A simplified model for the starting transient of the string is presented below. It is assumed that the string leaves the exciter without initial velocity at string position x_0 with the initial profile (see Fig. 3.5):

$$y(0,t) = \begin{cases} \frac{hx}{x_0} & \text{for} \quad 0 \le x \le x_0, \\ \frac{h(L-x)}{L-x_0} & \text{for} \quad x_0 \le x \le L\,. \end{cases} \tag{3.53}$$

Note The string shape here is a perfect triangle, which is not realistic because of the intrinsic stiffness of the string. If stiffness terms are added to the string equation, then this initial string shape will have to be revisited.

The modal method involves searching for solutions of the form indicated in Eq. (3.26). This equation must be satisfied in particular at time $t = 0$, which leads to Eq. (3.43). Since the initial string velocity is taken equal to zero, we get $\dot{q}_n(0) = 0$, and the remaining unknown variables of the problem are the initial generalized displacements $q_n(0)$. Using the orthogonality properties of the modes, we find

$$q_n(0) = \frac{1}{m_n}\int_0^L \rho S y(0,t)\Phi_n(x)\,dx = \frac{1}{m_n}\int_0^L \rho S y(0,t)\sin k_n x\,dx\,, \tag{3.54}$$

from which we derive[5]

[5]In the particular case considered here, the constant term ρS can be moved out of the integrals in Eq. (3.54), and the orthogonality properties of the modes are reduced to:

$$q_n(0) = \frac{2hL^2}{n^2\pi^2 x_0(L-x_0)} \sin k_n x_0 \,. \tag{3.56}$$

The expression for $q_n(t)$ is provided by the equation of an oscillator with no applied force:

$$\ddot{q}_n + \omega_n^2 q_n = 0 \,, \tag{3.57}$$

which, given the initial displacement and velocity conditions, leads to $q_n(t) = q_n(0)\cos\omega_n t$. In summary, the general expression of the transverse displacement of the string is given by:

$$y(x,t) = \sum_n \frac{2hL^2}{n^2\pi^2 x_0(L-x_0)} \sin k_n x_0 \sin k_n x \cos\omega_n t \,. \tag{3.58}$$

Despite its simplicity, this last expression is very informative:

1. For an ideal plucked string rigidly fixed at both ends, the eigenfrequencies are integer multiples of a *fundamental* frequency $f_1 = c/2L$ which corresponds to the inverse of the period of vibration (Fig. 3.6). We obtain a *harmonic* spectrum.
2. The amplitudes of the modal components decrease as $1/n^2$ (see Fig. 3.7). As a consequence of this rapid decrease with regard to the rank n of the mode, one can consider representing the vibration with a limited number of components. In fact, the modal truncation depends on the problem under examination. In practice, a note played on the low E-string of the guitar (83 Hz fundamental) may contain 60–100 audible components, whereas notes produced on the high E-string (fundamental 330 Hz) only contain about 10–20 audible components.
3. The fact that the amplitude of mode n is proportional to $\sin k_n x_0$ shows that it is possible to suppress a given spectral component ω_n by exciting the string at points $(x_0)_p = \frac{pL}{n}$ where p is an integer $< n$.
4. The respective roles of the excitation position x_0 and observation position x are exchangeable in (3.58). This property is a consequence of the *principle of reciprocity*.
5. As x_0 tends to 0, $y(x,t)$ tends to

$$y(x,t) = \sum_n \frac{2h}{n\pi} \sin k_n x \cos\omega_n t \,. \tag{3.59}$$

$$\int_0^L \Phi_n(x)\Phi_m(x)\,dx = \begin{cases} 0 & \text{for } m \neq n, \\ \frac{L}{2} & \text{for } m = n \,. \end{cases} \tag{3.55}$$

This expression is a particular case. The formulation (3.54) is more general and this is the reason why we have kept it.

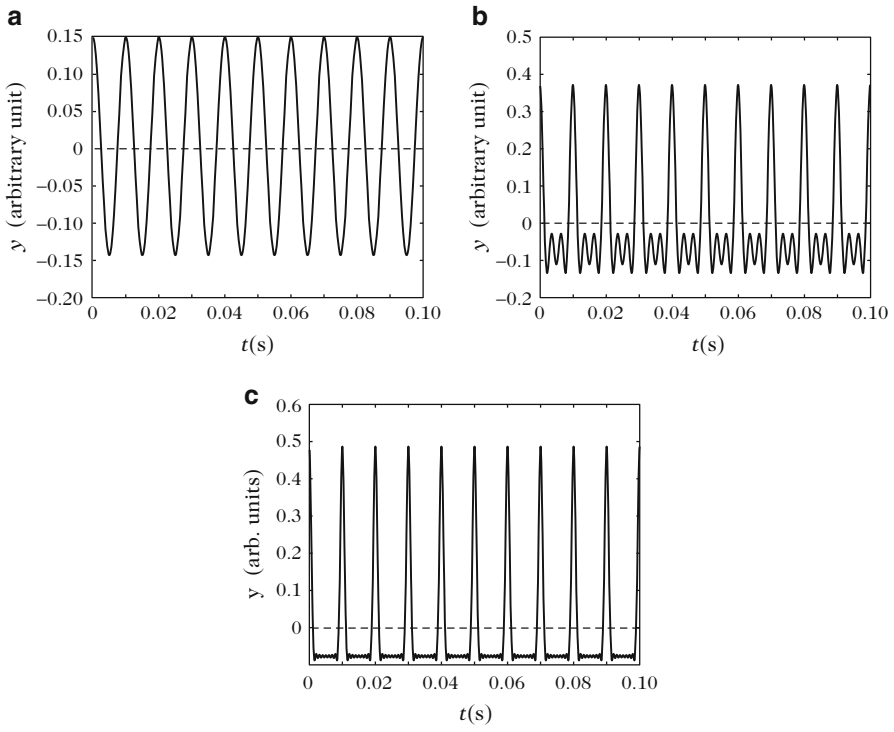

Fig. 3.6 Waveform of the displacement for an ideal string plucked at 7/8th of its length and observed at the same point. (**a**) One component; (**b**) three components; (**c**) ten components. As the number of components increases, the solution converges to a piecewise linear function, which corresponds to the exact solution (see Chap. 4)

The magnitudes of the components now vary as $1/n$, which means that if the excitation point is close to one end, then more harmonics are excited with significant amplitude. The corresponding sound will be "brighter".[6] By symmetry, the same argument can be made in the case where x_0 tends to L.

[6]The *brightness* of a sound is one of the perceptual attributes that characterize its timbre. A number of studies show that it is highly correlated to the *spectral centroid*, or *SC*, of the sound (indicating the "center of gravity of the spectrum"). If A_k is the amplitude of the frequency spectral component f_k of a sound containing N components, the SC is defined by $SC = \frac{\sum_{k=1}^{N} f_k A_k}{\sum_{k=1}^{N} A_k}$. This quantity characterizes the balance between bass and treble: a *dull* sound has a low *SC*, whereas a *bright* sound contains many high frequency components and therefore has a high *SC*.

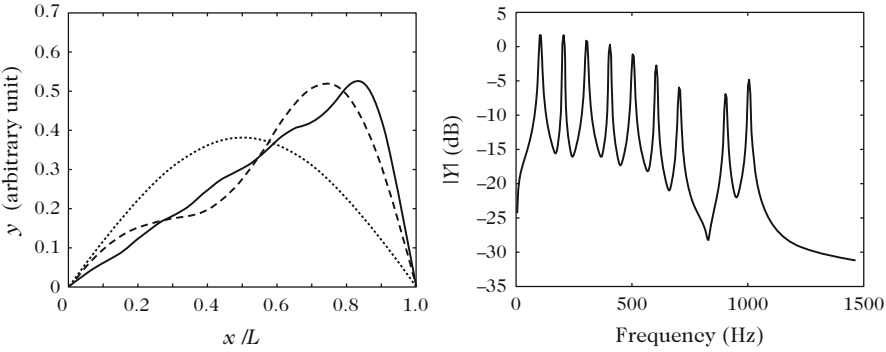

Fig. 3.7 *Left*: spatial shape of the string plucked at 7/8th of its length for a fixed time t. (*Dotted*) One mode; (*dashed*) three modes; (*solid line*) ten modes. *Right*: spectrum of the displacement of the string shown in Fig. 3.6 (ten components)

3.4.4.1 Force Transmitted by the String to the Bridge

As the string is moving, it exerts a time-dependent transverse force at both ends. To a first-order, we can assume that this force is proportional to the spatial derivative of the displacement, i.e., given the orientation of the x-axis (see Fig. 3.5):

$$F(0,t) = T\left(\frac{\partial y}{\partial x}\right)_{x=0} \quad \text{and} \quad F(L,t) = -T\left(\frac{\partial y}{\partial x}\right)_{x=L} . \tag{3.60}$$

In what follows, the bridge is arbitrarily taken as being located at $x = L$. The force transmitted by the string to the bridge can then be written as:

$$F(L,t) = -T\left(\frac{\partial y}{\partial x}\right)_{x=L} = -T\sum_n \frac{2hL}{n\pi x_0(L-x_0)} \cos k_n L \sin k_n x_0 \cos \omega_n t \, . \tag{3.61}$$

The amplitudes of the spectral components of the force vary as $1/n$, and tend towards a constant value when the excitation position x_0 gets closer to one of the ends. Thus, they decrease less rapidly with n than the displacement components do. Through sound synthesis, one can verify that the simulated sound of a "force" is "brighter" than the sound of the corresponding "displacement."

We will verify in Chap. 4 that, for an ideal string, the displacement waveform is piecewise linear (exact solution). The force waveform is therefore piecewise constant. Experimentally, it is observed that the force pulses are rounded, a consequence of string stiffness, limited bandwidth of the excitation, and damping. The truncation to ten modes shown here illustrates the resulting error on force and displacement waveforms (see Figs. 3.6 and 3.8).

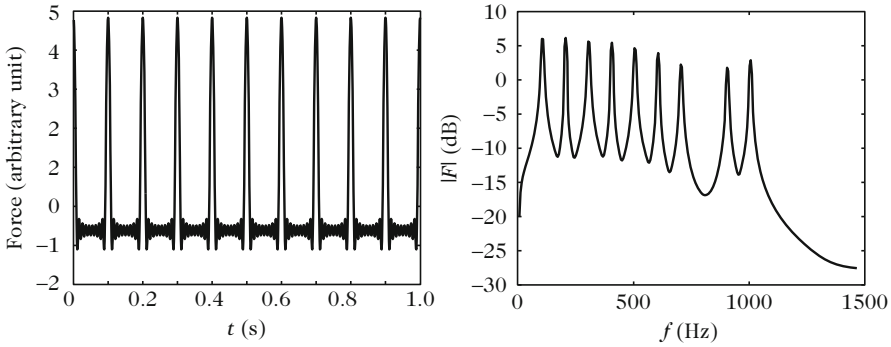

Fig. 3.8 Force transmitted by the string to the bridge. (*Left*) waveform (ten components); (*right*) corresponding spectrum. The force eigenfrequencies are identical to those of the displacement, but the comparison with Fig. 3.7 shows that the amplitudes of the force components with high order n (around 1000 Hz) are less attenuated compared to the components with lower order (around 100 Hz) than it is the case for the displacement component

3.4.5 String with a Moving End

In a string instrument, the strings do not radiate any significant acoustic energy, because their diameter is small compared to the acoustic wavelength (see Chap. 12). As an empirical proof, it is easy to carry out a simple experiment: stretch a string between your fingers and pluck it. You will only hear a sound when the string is brought close to your ear.

To radiate acoustic energy efficiently, the string needs to be coupled to a resonator with a large surface. This is the main role of the soundboard. As a consequence, the assumption of zero displacement at both ends of the string is unrealistic. It would imply that the soundboard is rigidly fixed and does not produce any sound.

We shall therefore now consider that at least one of the string's ends is moving. This boundary condition corresponds to the coupling of two continuous systems (string and soundboard), each of them presenting an infinite number of modes. A comprehensive model of such coupled systems will be presented in Chap. 6. Here, the effect of one particular mode (a single oscillator) of the soundboard on the string will be examined.

It is well-known (see Chap. 2) that such an oscillator behaves either like a spring or like a mass, depending on the ratio between the excitation frequency and the eigenfrequency of the oscillator. These two limiting cases will be studied, leaving the particular case where the oscillator behaves as a pure damper temporarily aside. This latter case will be studied in detail in Chap. 5. In actual fact, the soundboard itself is subjected to dissipation, because of internal losses and radiation, which we will also ignore for the moment.

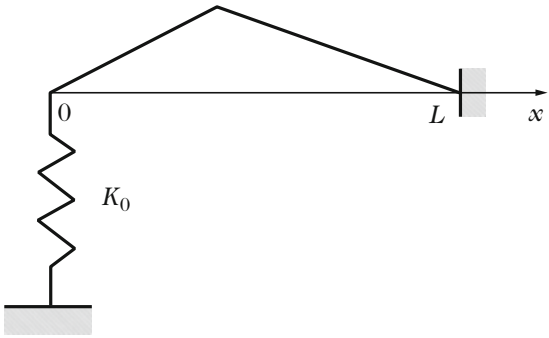

Fig. 3.9 String fixed at one of its ends (at position $x = 0$) to a spring of stiffness K_0

3.4.5.1 Purely Elastic End

Consider first the situation of a homogeneous string fixed to a spring of stiffness K_0 at point $x = 0$ (see Fig. 3.9). The balance of forces yields the boundary condition:

$$T\left(\frac{\partial y}{\partial x}\right)_{x=0} = K_0\, y(0,t)\ . \tag{3.62}$$

It is assumed that the displacement of the string remains equal to zero at the other end, i.e., $y(L,t) = 0$. To calculate the eigenmodes, we search for solutions of the form $y(x,t) = \Phi(x)\cos\omega t$. According to Eq. (3.47), the functions $\Phi(x)$ must satisfy the equation:

$$\frac{d^2\Phi}{dx^2} + k^2\Phi = 0 \tag{3.63}$$

and the two boundary conditions. Equation (3.63) with the condition $\Phi(L) = 0$ gives

$$\Phi_n(x) = \sin k_n(x - L). \tag{3.64}$$

The condition at $x = 0$ yields

$$\tan k_n L = -\frac{k_n T}{K_0}\ . \tag{3.65}$$

The index n in Eq. (3.65) shows that the condition is fulfilled for a discrete set of values of the variable k only. Equation (3.63) is, in turn, only satisfied for a discrete set[7] of functions $\Phi_n(x)$. Using Eq. (3.65), we can write:

[7]The solution $k_n = 0$ is excluded here, since it leads through (3.63) to the degenerate solution $\Phi_n(x) = 0\ \ \forall x$, because of the condition of zero displacement in $x = L$.

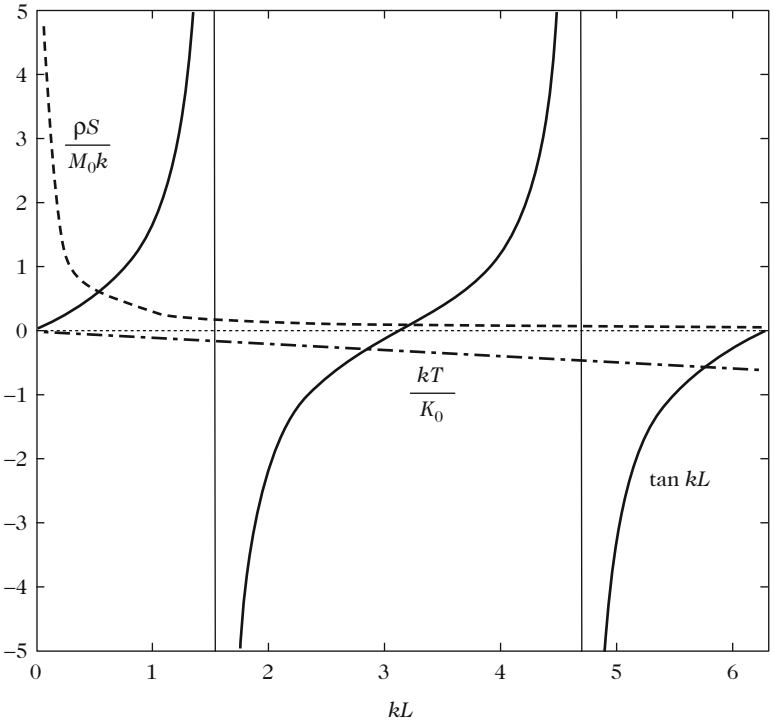

Fig. 3.10 Graphical representation of Eq. (3.65) for the case of a moving end. *Dotted line*: elastic end. *Dashed line*: string with a mass at one end

$$\Phi_n(x) = \sin k_n x + \frac{k_n T}{K_0} \cos k_n x \,. \tag{3.66}$$

The graphical representation of (3.65) (see Fig. 3.10) shows that the roots k_n are no longer multiples of k_1, as it was the case for the ideal string with fixed ends. As a consequence, the motion of the string is not periodic. The roots depart more and more from the ideal harmonic series as the rank n of the partial increases. The presence of a spring at one end of the string systematically leads to a *decrease* in the eigenfrequencies in comparison with the ideal case. This is not surprising as it corresponds to introducing a finite stiffness into the system, compared with the perfectly rigid case (equivalent to an infinite stiffness). Introducing flexibility in a system leads to a lowering of its eigenfrequencies.[8]

[8] One can also consider the introduction of a spring as an apparent increase in the length of the string, but with the condition that the length correction depends on the rank n of the partial. If one writes $k_n \Delta\ell = \arctan [k_n T/K_0]$, the roots are solutions of the equation $\tan k_n(L + \Delta\ell) = 0$. For the first modes, we have $\Delta\ell \simeq T/K_0$. This approach is very convenient for wind instruments.

Once the modes are determined, the initial values $q_n(0)$ of the generalized displacements can be derived from the integral expressed in Eq. (3.54). Equations (3.34) and (3.35) show that, for an isolated string, the modes are orthogonal with respect to mass, but are no longer orthogonal with respect to stiffness. However, one can generalize the concept of orthogonality to the whole system (string + spring) by considering the total potential energy.[9]

According to Eqs. (1.124), (3.62), and (3.37):

$$E_p = \frac{1}{2}\int_0^L T\left(\frac{\partial y}{\partial x}\right)^2 dx + \frac{1}{2}K_0 y^2(0,t)$$
$$= \frac{1}{2}\sum_{n,m}\left[\mathscr{P}_T(m,n) + K_0\Phi_n(0)\,\Phi_m(0)\right] q_n q_m \,.$$

However, according to Eq. (3.35), $\mathscr{P}_T(m,n) = -K_0\Phi_n(0)\,\Phi_m(0)$ for $n \neq m$. So, finally we get[10]

$$\mathscr{E}_p = \frac{1}{2}\sum_n \left[\kappa_n + K_0\Phi_n^2(0)\right] q_n^2 \quad \text{where} \quad \kappa_n = \mathscr{P}_T(n,n)\,. \tag{3.67}$$

3.4.5.2 String with a Mass at One End

The case of a homogeneous string with a mass at one end is now examined. It is assumed that the mass M_0 is located at position $x = 0$. The following boundary condition must then be satisfied[11]:

$$T\left(\frac{\partial y}{\partial x}\right)_{x=0} = M_0\,\frac{\partial^2 y}{\partial t^2}(0,t)\,. \tag{3.68}$$

[9] In (1.124), the term within the brackets corresponds to the input power at both ends. We get:

$$T\frac{\partial y}{\partial x}\frac{\partial y}{\partial t} = K_0 y\frac{\partial y}{\partial t} = \frac{\partial e_0}{\partial t} \quad \text{where} \quad e_0 = \frac{1}{2}K_0 y^2 \text{ in } x = 0.$$

[10] A similar problem will be tackled in Chap. 4 for a pipe loaded by a radiation impedance at low frequencies. We will see that, assuming $k_n\Delta\ell << 1$, where $\Delta\ell = T/K_0$, the moving end can be replaced by a fixed termination for the pipe with an end correction $\Delta\ell$ at the end $x = 0$. The calculations of the modes are simplified, and we can recover the term $K_0\Phi_n^2(0)$, considering the energy located between $x = -\Delta\ell$ and $x = 0$. This means that, instead of considering a boundary condition corresponding to a lumped element at $x = 0$, we consider a longer medium, with some particular parameters ρ, S, and T in the extension, and with a simple boundary condition, $y(-\Delta\ell, t) = 0$.

[11] We obtain identical results with the mass located at position $x = L$. In this latter case, there is a change of sign in the boundary condition.

It is assumed that the other end is fixed, i.e., $y(L,t) = 0$. The condition (3.68) involves time derivatives, which makes the resolution by Fourier transform difficult (see below). The method used here is the separation of variables. It involves testing the existence of standing waves of the form $y(x,t) = \Phi(x)w(t)$ and searching for those conditions under which the equations of the problem are verified. Inserting $y(x,t)$ in Eq. (3.47), we obtain:

$$\frac{\Phi}{c^2}\frac{d^2w}{dt^2} = w\frac{d^2\Phi}{dx^2} \,. \tag{3.69}$$

By grouping the terms involving the same variables, we derive

$$\frac{1}{c^2 w}\frac{d^2w}{dt^2} = \frac{1}{\Phi}\frac{d^2\Phi}{dx^2} = -\alpha^2, \tag{3.70}$$

where $-\alpha^2$ is a constant. The only way to satisfy the first equality of Eq. (3.70) is for both sides of the equality to be set as constant, since they involve a different variable (resp. t and x). Due to the boundary conditions, it will be now shown that the constant α is real.

The resolution of both differential equations in (3.70) yields the general solutions:

$$w(t) = A\cos c\alpha t + B\sin c\alpha t \quad \text{and} \quad \Phi(x) = C\cos\alpha x + D\sin\alpha x \,. \tag{3.71}$$

The boundary conditions for $x = 0$ and $x = L$ imply that:

$$\begin{aligned} &\Phi(L) = C\cos\alpha L + D\sin\alpha L = 0 \\ &\text{and} \quad T\frac{d\Phi}{dx}(0) = -\alpha^2 c^2 M_0 \Phi(0) \,. \end{aligned} \tag{3.72}$$

Thus α must fulfill the condition:

$$\tan\alpha L = \frac{\rho S}{\alpha M_0} \,, \tag{3.73}$$

and is therefore real.

Figure 3.10 shows that this equality can be obtained for a discrete set of wavenumbers only:

$$k_1 < k_2 < \ldots < k_n. \tag{3.74}$$

This leads to the eigenvalue equation:

$$\tan k_n L = \frac{\rho S}{M_0 k_n} \,. \tag{3.75}$$

The mass loading leads to an *increase* in the eigenfrequencies of the string and in turn to an *apparent decrease* in its length (see Fig. 3.10). The ideal case is obtained as M_0 tends to infinity in Eq. (3.75).

In the case of a mass-loaded end, the modes of the string are orthogonal with regard to stiffness, but not with regard to mass. For the string+mass system, the orthogonality can be extended by considering the total kinetic energy:

$$\mathscr{E}_c = \frac{1}{2}\sum_n \left[m_n + M_0\Phi_n^2(0)\right]\dot{q}_n^2 \quad \text{where} \quad m_n = \mathscr{P}_M(n,n). \tag{3.76}$$

Note The first consequence of the coupling between string and soundboard is to modify its eigenfrequencies. This is one cause of *inharmonicity* in the sound produced by the instrument. The coupling affects the lowest eigenfrequencies primarily, i.e., those for which the amplitude of the soundboard motion is the strongest, and thus where the assumption of perfect rigidity is the least satisfied.

Orthogonality Properties of a Heterogeneous String

Turning back to the general case of a heterogeneous string of length L (Eq. (3.25) without an applied force term), the goal is now to find the orthogonality properties of the eigenmodes when one end is fixed while the other end is connected to a mass M_L. With boundary conditions of the problem:

$$y(0,t) = 0 \quad \text{and} \quad -T(x)\frac{\partial y}{\partial x} = M_L\frac{\partial^2 y}{\partial t^2}, \ \text{at } x = L\,, \tag{3.77}$$

we obtain

$$\mathscr{P}_M(m,n) = \frac{t_n}{\omega_n^2}\delta_{mn} - M_L\Phi_m(L)\Phi_n(L), \tag{3.78}$$

where

$$t_n = \mathscr{P}_M(n,n) = \int_0^L T(x)\left[\frac{d\Phi_n(x)}{dx}\right]^2 dx\,. \tag{3.79}$$

This shows that the modes are orthogonal with regard to stiffness, but not with regard to mass. In conclusion, Eq. (3.38) becomes

$$\begin{aligned}\ddot{q}_n(t) + \omega_n^2 q_n(t) &= \frac{1}{t_n}\int_0^L \frac{\partial}{\partial x}\left(\frac{f(x,t)}{\rho(x)S(x)}\right)T(x)\frac{d\Phi_n(x)}{dx}dx \\ &= \frac{1}{t_n}\left[\frac{f(L,t)}{\rho(L)S(L)}M_L\Phi_n(L) + \omega_n^2\int_0^L f(x,t)\Phi_n(x)dx\right]\,.\end{aligned} \tag{3.80}$$

Fourier Domain Approach
Eigenmode decomposition can also be applied in the Fourier (or in the Laplace) domain. To illustrate this, the case of a homogeneous string with a mass at one end is presented. In the Fourier domain, the condition at the mass-loaded end (3.68) is

$$T\frac{d\mathscr{Y}}{dx} = M\omega^2\mathscr{Y}\ . \tag{3.81}$$

The Fourier transform of the wave equation (3.25) is the Helmholtz equation:

$$\frac{d^2\mathscr{Y}(\omega)}{dx^2} + \frac{\omega^2}{c^2}\mathscr{Y}(\omega) = -\frac{1}{T}F(x,\omega). \tag{3.82}$$

Let us now examine the case of a localized excitation, e.g., a Green's function $F(x,\omega) = T(x_0)\delta(x-x_0)$. The solution is expanded onto the *eigenfunctions* ψ_p of the equation:

$$\frac{d^2\psi_p}{dx^2} + \frac{\omega_p^2}{c^2}\psi_p = 0\ , \tag{3.83}$$

with the boundary conditions: $\psi(0) = 0$, and (3.81). In Eqs. (3.81) and (3.82), *ω is a parameter. Thus the eigenfunctions and their corresponding eigenfrequencies ω_p depend on frequency:* As a consequence, we do not get modes in the strict sense. Finally, we write: $\psi_p = \sin(\omega_p x/c)$, where

$$\tan\frac{\omega_p(\omega)L}{c} = \frac{T}{Mc}\frac{\omega_p(\omega)}{\omega^2}. \tag{3.84}$$

For a given ω, there is an infinite set of values for ω_p. The solution can then be expressed as a sum of functions $\psi_p(x)$:

$$\mathscr{Y}(\omega) = \sum_p \psi_p(x)Q_p(\omega). \tag{3.85}$$

These functions are orthogonal with regard to the mass, i.e., for a homogeneous string:

$$\int_0^L \psi_p(x)\psi_q(x)dx = \Lambda_p\delta_{pq}, \tag{3.86}$$

(continued)

where Λ_p is a constant and δ_{pq} the Kronecker symbol. All these functions satisfy Eq. (3.81) with a fixed ω. One can therefore write

$$\mathscr{Y}(\omega) = c^2 \sum_p \frac{\psi_p(x)\psi_p(x_0)}{\Lambda_p \left[\omega_p^2(\omega) - \omega^2\right]} . \tag{3.87}$$

If (3.84) is solved for a given frequency, (3.87) enables the calculation of the Fourier transform of $y(t)$, that is $\mathscr{Y}(\omega)$ and, by inverse Fourier transform, $y(t)$ itself. This approach is often used in acoustics, especially in room acoustics [27]. It is also systematically used in sound synthesis based on physical models by Rabenstein and Trautmann [37].

Note 1: The previously described orthogonality is *simple* for this conservative problem. In general, depending on the end impedances, one must build an adjoint problem, with an adjoint modes basis denoted $\overline{\psi_p}$. The *bi-orthogonality* between both families of modes is written:

$$\int_0^L \psi_p(x)\overline{\psi_q}(x)dx = \Lambda_p \delta_{pq} . \tag{3.88}$$

It turns out that the adjoint family is the family of the conjugates, which implies $\int_0^L \psi_p(x)\psi_q(x)dx = \Lambda_p \delta_{pq}$, even if the functions $\psi_p(x)$ are complex.

Note 2: Inverse transformation to the time domain, and therefore to the modes, is possible in the case studied above, but it is subtle. In the series (3.87), for a given frequency ω, only two functions $\psi_p(x)$ are resonant, which means that some terms of the series may have a zero denominator. Denoting their indices by n and $-n$, we have: $\omega_n = \pm\omega$ and both correspond to the same shape $\psi_n(x)$. By inserting $\omega_n = \pm\omega$ in (3.84), it can be seen that the two values of ω_n satisfy Eq. (3.75). As a consequence, both resonant terms of the series (3.87) have an infinite number of poles. Finally, one can check that $\psi_n(x) = \Phi_n(x)$. The residues theorem is used to return to the time domain (see the appendix at the end of this chapter). First, the Taylor expansion of the denominator $D(\omega) = \Lambda_n(\omega_n^2 - \omega^2)$ is written in the form $D(\omega) = D(\omega_n) + (\omega - \omega_n)D'(\omega_n)$, with:

$$\begin{aligned} D'(\omega_n) = \left[\frac{dD(\omega)}{d\omega}\right]_{\omega=\omega_n} &= \Lambda_n \left[2\omega_n \frac{d\omega_n}{d\omega} - 2\omega\right]_{\omega=\omega_n} \\ &= 2\Lambda_n\omega_n \left[\left(\frac{d\omega_n}{d\omega}\right)_{\omega=\omega_n} - 1\right]. \end{aligned} \tag{3.89}$$

(continued)

To calculate $d\omega_n/d\omega$ in ω_n, one needs to derive Eq. (3.84) with respect to ω. It is also necessary to explicitly calculate Λ_n. After some tedious calculations, we get

$$\Lambda_n \left[\left(\frac{d\omega_n}{d\omega} \right)_{\omega=\omega_n} - 1 \right] = -\frac{L_n}{2} \quad \text{with}$$

$$L_n = L + \frac{\Delta\ell}{1 + \left(\frac{\omega_n \Delta\ell}{c} \right)^2} \quad \text{where} \quad \Delta\ell = \frac{M}{\rho S} . \tag{3.90}$$

In addition, we find $t_n = TL_n\omega_n^2/(2c^2)$. By adding both terms with poles of Eq. (3.87), we finally obtain $\mathscr{Y}(\omega) = \sum \psi_n(x) Q_n(\omega)$, with:

$$-\omega^2 Q_n + \omega_n^2 Q_n = 2c^2 \psi_n(x_0)/L_n = T\psi_n(x_0)\omega_n^2/t_n. \tag{3.91}$$

This is in agreement with the expression (3.80), when $f(x,t) = T\delta(x - x_0)\delta(t)$.

3.4.6 *Influence of Spatial Width and Duration of the Excitation*

In practice, the excitation of a string is distributed over a segment of finite length. One can think, for example, of the width of a violin bow, of a piano hammer, or of a player's finger. Many string instruments (piano, guitar, harp, violin played pizzicato, etc...) are also excited over a finite time interval, corresponding to the duration of the interaction with the exciter. In this section, the effect of both the spatial width and finite duration of the excitation on the string's response are examined.

Note For simplicity, only the example of the ideal string fixed at both ends is treated here. In this case, we know that the eigenmodes are $\Phi_n(x) = \sin k_n x$. Nevertheless, the method developed here remains valid in the general case.

We first consider the situation presented in Fig. 3.11 where the string is excited by a force term comprising a Dirac delta function in time, and distributed over a string segment of width $2a$ centered at position x_0. We write[12]

$$f(x,t) = B\delta(t)g(x) \quad \text{with} \quad g(x) = \begin{cases} 1 & \text{if } x_0 - a \le x \le x_0 + a, \\ 0 & \text{elsewhere .} \end{cases} \tag{3.92}$$

[12]The coefficient B in this expression has the dimension of a mass divided by time ($[M][T]^{-1}$) because of the presence of the Dirac delta function.

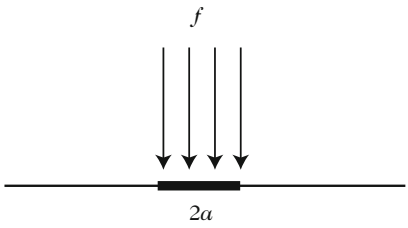

Fig. 3.11 Spatial width of the excitation of a string. The force f exerted on a string by a finger, a plectrum, a hammer, or a bow, is distributed over a finite width, here denoted $2a$

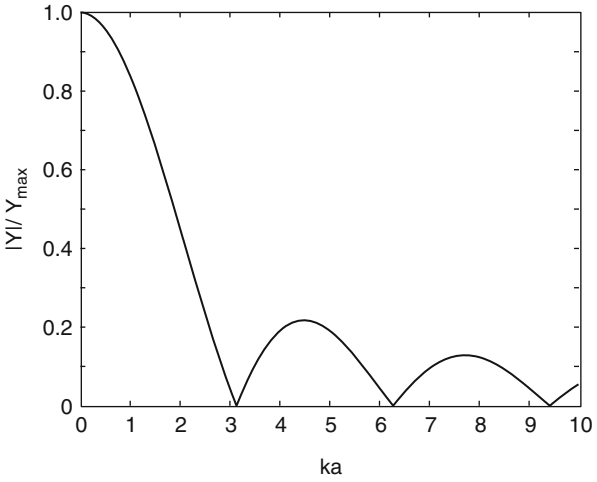

Fig. 3.12 Low pass filtering of the string displacement due to the width $2a$ of the exciter

We derive the projection of the applied force term on the mode n:

$$f_n = \langle f, \Phi_n \rangle = B\delta(t) \int_{x_0-a}^{x_0+a} \sin k_n x \, dx = 2aB\delta(t) \sin k_n x_0 \frac{\sin k_n a}{k_n a} \,. \tag{3.93}$$

Hence, for a string initially at rest, the displacement is

$$y(x,t) = 2aB \sum_n \frac{\sin k_n x \sin k_n x_0}{m_n} \frac{\sin k_n a}{k_n a} \frac{\sin \omega_n t}{\omega_n} \,. \tag{3.94}$$

The expression (3.94) shows that, compared to the case of a point excitation, the spatial width induces a *low pass filtering* of the string response, through the term in $\frac{\sin k_n a}{k_n a}$ (see Fig. 3.12). The first cutoff frequency f_c of this filter occurs when $ka = \pi$, i.e., $f_c = \frac{c}{2a}$.

Numerical Example For a piano wire of length $L = 62\,\text{cm}$, corresponding to the note C4 (fundamental $f_1 = 262\,\text{Hz}$), the propagation speed of the transverse

Fig. 3.13 Pulse of finite duration

waves is $c = 2Lf_1 = 325$ m/s. Taking $2a = 2$ cm as an order of magnitude estimate for the spatial window of excitation by the hammer, we find $f_c = 16$ kHz, which approximately corresponds to the upper limit of the audible spectrum.

- Now the effect of the finite duration of the interaction between string and exciter is investigated. We assume a spatially localized force density of the form:

$$f(x,t) = C\delta(x - x_0)h(t) \tag{3.95}$$

with

$$h(t) = \begin{cases} 1 & \text{for } 0 \le t \le 2\tau, \\ 0 & \text{for } t > 2\tau, \end{cases}$$

where C has a dimensions $[M][L][T]^{-2}$, and where 2τ represents the duration of the interaction between string and exciter (see Fig. 3.13).

From Eq. (3.44), and under the assumption of a string initially at rest, the generalized displacement of mode n is

$$q_n(t) = \frac{C\Phi_n(x_0)}{m_n\omega_n} \int_0^{2\tau} \sin\omega_n(t-\theta)d\theta, \tag{3.96}$$

which gives the string displacement:

$$\begin{cases} \text{For} \quad 0 \le t \le 2\tau \quad y(x,t) = 2\tau C \sum\limits_n \dfrac{\sin k_n x \sin k_n x_0}{m_n} \dfrac{1-\cos\omega_n t}{\omega_n^2 \tau}, \\ \text{For} \quad t > 2\tau \quad y(x,t) = 2\tau C \sum\limits_n \dfrac{\sin k_n x \sin k_n x_0}{m_n} \dfrac{\sin\omega_n \tau}{\omega_n \tau} \dfrac{\sin\omega_n(t-\tau)}{\omega_n}. \end{cases} \tag{3.97}$$

As for the spatial width analysis, the finite duration of the interaction force results in a low pass filtering of the response $y(x,t)$ through the term $\frac{\sin \omega_n \tau}{\omega_n \tau}$. Returning back to the example of the piano wire, we notice that the calculation of the cutoff frequency, defined by the first zero of the previous function, yields here $f_c = \frac{1}{2\tau}$. By taking $2\tau = 1$ ms as an order of magnitude typically observed on piano wires, (see, for example, [3]), we find $f_c = 1$ kHz. This cutoff frequency is significantly lower than the one resulting from the spatial width of the excitation.

3.4.7 Struck String

The previous considerations give some understanding of the effects of finite width and duration on the string spectrum. Returning now to a more accurate description of the piano string, we must take the mass M_h of the hammer and its initial impact velocity V_0 into account. This description will be refined later with the introduction of damping mechanisms both in the string and in the hammer's felt, as shown in Chap. 5.

During the contact phase between hammer and string, some of the initial kinetic energy is transformed into elastic compression energy of the felt (see Fig. 3.14).

The resulting compression force is imparted to the string and gives rise to transverse traveling waves. These waves are initiated on both sides of the impact position. As a result of the magnitude of the propagation speed of the bending wave on the string, and the small distance between the impact position and one of its ends (the agraffe side), the waves propagating on this "shorter side" of the string reach the hammer before it leaves the string (see Figs. 3.14 and 3.15). As a consequence, the action of the wave modifies the compression force, resulting in a modulation of the interaction force between hammer and string. These modulations can be intense enough to cause the hammer to bounce back and, in turn, a discontinuity of the force in the lower range of the instrument can be observed (see Fig. 3.16).

An abundance of literature on the analytical and numerical modeling of the hammer–string interaction is available; see, for example, [7, 11, 22]. We will see a similar 2-D example in Chap. 14: the mallet-membrane interaction in timpani.

3.4.8 Driving-Point and Transfer Admittance

The motion of the end of the string that is fixed to the bridge induces vibrations in the soundboard. The modal approach is an appropriate tool to characterize this transfer, both theoretically and experimentally. In order to study this coupling, which is essential for the understanding of string instruments, we start by defining the concept of mechanical *admittance* (or mobility) (see also Sect. 1.6 in Chap. 1), before studying its frequency behavior in detail.

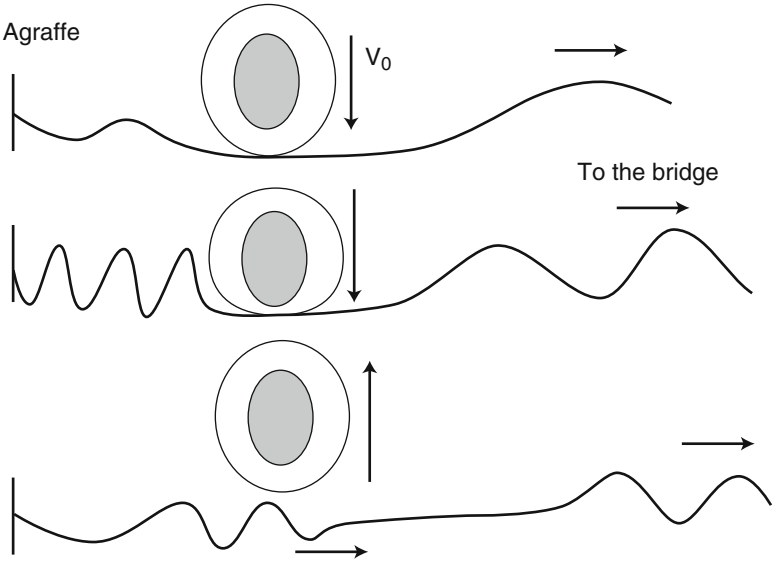

Fig. 3.14 Hammer–string interaction. (*1*) The hammer with initial impact velocity V_0 comes into contact with the string. The felt is compressed and a force is imparted to the string. Transverse waves are developed on the string on both sides of the hammer. (*2*) As long as string and hammer stay in contact, the waves developed on the shorter side of the string stay confined between the agraffe and the hammer, which prevents propagation towards the bridge. (*3*) After a few milliseconds, the reaction of the string pushes the hammer back and these waves are free to propagate

Consider a continuous structure, a piano soundboard, for example, subjected to forces and moments. In general, for numerical and/or experimental reasons, it is necessary to work on a discretized version of this structure, i.e., on a mesh containing a finite number N of areas whose dimensions are small in comparison with the wavelength. These small areas are commonly referred to as"points." This amounts to considering the structure as a discrete system with N degrees of freedom (see Fig. 3.17).

At each point of the mesh, the motion is characterized by three translation components and three rotation components. In what follows, the velocity is treated as a variable. Similarly, the external actions at each point reduce to three force components and three moment components [9].

Admittances are defined in the frequency domain. At each point, the velocity components of the motion (V_k) are linked through a 6×6 matrix to the force and moment components, denoted F_l. The *admittance matrix at one point* $\mathbb{Y}$ is defined as:

$$\boldsymbol{V} = \mathbb{Y}\boldsymbol{F}\,. \tag{3.98}$$

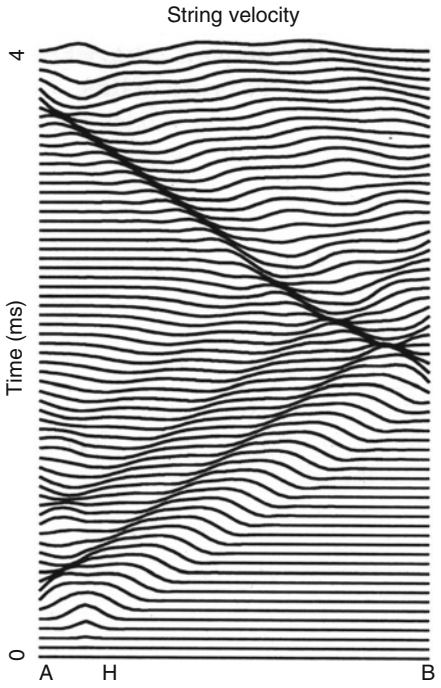

Fig. 3.15 Simulation of the wave propagation on a piano wire just after the hammer impact. The letter H marks the position of the hammer, A is the agraffe, and B is the bridge. For about 1 ms, waves are "trapped" on the shorter side (between A and H). There are then released and follow the main front which propagates towards B. At bridge B, the waves are reflected and their sign changes, according to [10]

Consider now the complete structure, composed of N points. For each action component at a given point j, denoted $F_{j|l}$, a motion is induced at any point i. If $V_{i|k}$ represents one component of this motion, we define for the pair $(V_{i|k}, F_{j|l})$ the *transfer admittance*:

$$Y_{ij|kl} = \frac{V_{i|k}}{F_{j|l}} \quad \text{with} \quad 1 \leq i, j \leq N \quad \text{and} \quad 1 \leq k, l \leq 6\,. \tag{3.99}$$

In total, we obtain for the *transfer admittance matrix* a group of $6N \times 6N$ coefficients such as $Y_{ij|kl}$ to characterize the structural response to external stimuli.

As an application of the concept of transfer admittance, one can think of the sympathetic excitation of the strings of an instrument through the bridge: the point j refers to the attachment point at the bridge of the excited string, while the point i refers to the attachment point of the sympathetic string (see Fig. 3.18). The sympathetic string vibrates if some frequencies of the excitation signal in j are close to eigenfrequencies of string i and, in addition, if the admittance coefficient Y_{ij} at this frequency is sufficiently high and does not correspond, for example, to a vibration node of the bridge at this frequency. The concept of admittance is essential for understanding the behavior of coupled strings in the piano [39] (see Chap. 6).

Notation. In what follows, the indices (k, l) used for designating the components of force and velocity are removed for simplicity. The coefficients of the transfer

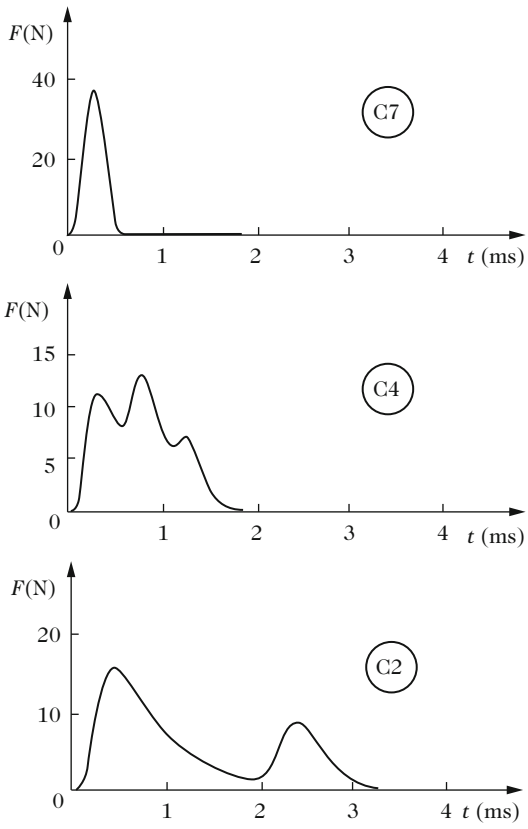

Fig. 3.16 Simulations of the interaction force between hammer and string. (*Top*) String C7 (2093 Hz); (*Middle*) String C4 (262 Hz); (*Bottom*) String C2 (65.4 Hz). The amplitude modulations of the envelope are due to the waves returning from the agraffe to the hammer, according to [11]

admittance matrix are written Y_{ij}, which can be reduced to Y_{ii} (or simply to Y_i through index contraction) in the case of the admittance coefficients at the driving-point. Emphasis is put on force and translation velocity, though the results can be generalized to moments and rotations.

The frequency behavior of the transfer admittance coefficients Y_{ij} are now examined. The force excitation is located at the coordinate x_j. The displacement at a given point x_i on the structure is: $\xi_i = \sum \Phi_n(x_i) q_n(t)$. To be consistent with the notation used for a continuous medium, we write: $\xi(x_i) = \xi_i, f(x_j) = f_j$. The corresponding vector component is written $\Phi_n(x_j)$. According to (3.18), we derive: $f_n = \Phi_n(x_j) f(x_j)$. Equation (3.19) can be rewritten as:

$$\ddot{q}_n(t) + \omega_n^2 q_n(t) = \frac{\Phi_n(x_j) f(x_j)}{m_n} \,. \tag{3.100}$$

In the frequency domain (using the convention of writing the variables in capital letters), the generalized displacements $Q_n(\omega)$ are

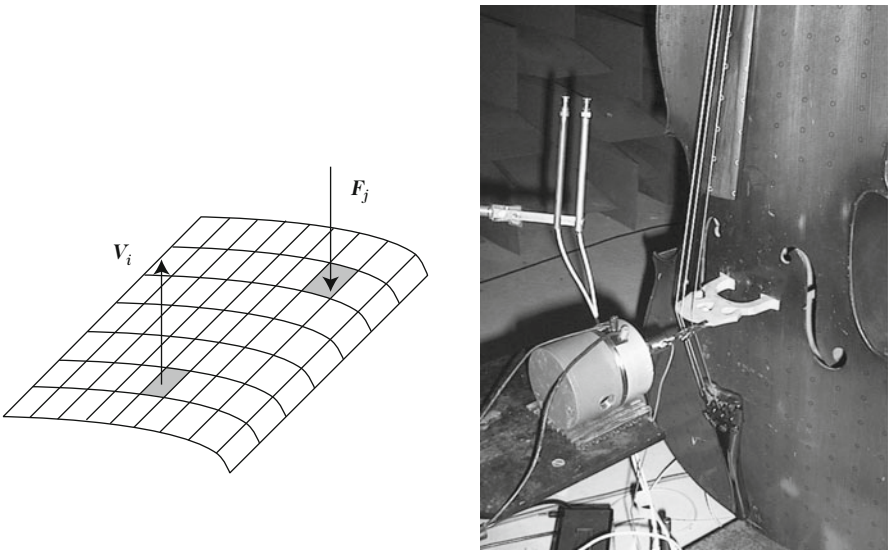

Fig. 3.17 (*Left*) Transfer admittance for a structure with N degrees of freedom. For each pair of points $1 \leq i,\ j \leq N$, the transfer admittance $Y_{ij|kl}$ is the ratio between the velocity component $V_{i|k}$ at point i and the force component $F_{j|l}$ at point j. (*Right*) Vibratory and acoustic analysis of a cello. We note on the cello soundboard the presence of circles marking positions of excitation or response in modal analysis experiments (© A. Garcia, CNAM)

$$\left(\omega_n^2 - \omega^2\right) Q_n = \frac{\Phi_n(x_j) F(x_j)}{m_n} \,. \tag{3.101}$$

Through modal projection, the displacement at point x_i is

$$\Xi(x_i) = \sum_{n=1}^{N} \frac{\Phi_n(x_i)\Phi_n(x_j)}{m_n\left(\omega_n^2 - \omega^2\right)} F(x_j), \tag{3.102}$$

where N corresponds to the number of discrete points on the structure (and thus to the number of modes). The quantity $\Xi(x_i)$ in Eq. (3.102) represents the shape of the structure (commonly referred to as the *Operating Deflection Shape or ODS*) for a forced excitation with frequency ω located at point x_j, from which the transfer admittance between points x_i and x_j is derived:

$$Y_{ij}(\omega) = j\omega \sum_{n=1}^{N} \frac{\Phi_n(x_i)\ \ \Phi_n(x_j)}{m_n\left(\omega_n^2 - \omega^2\right)} \,. \tag{3.103}$$

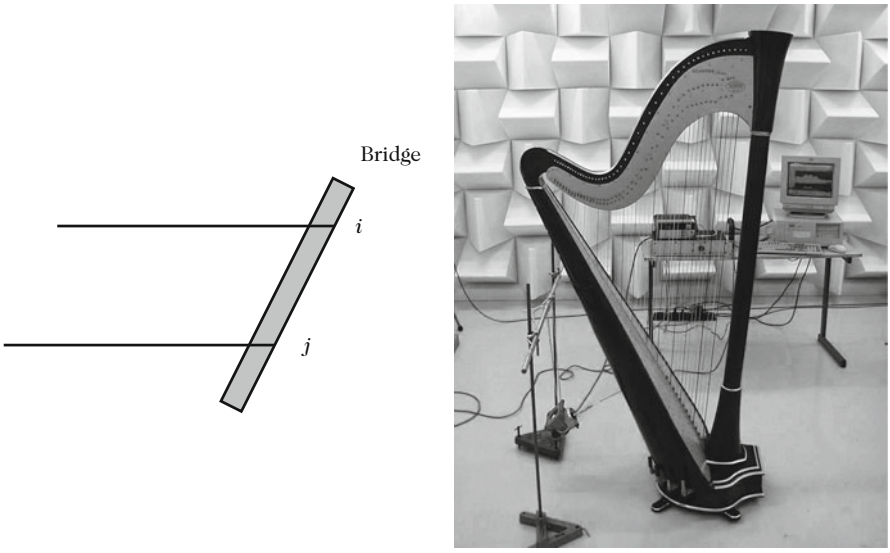

Fig. 3.18 (*Left*) Excitation of sympathetic strings. Several strings which have one end fixed to a moving bridge are likely to vibrate in sympathy. Such a phenomenon requires two conditions: the transfer admittance between i and j should not be zero, and the strings must have at least one eigenfrequency in common. (*Right*) The harp is an example of instrument where sympathetic vibrations are observed, because of the coupling of the strings through the mounting bar located on the axis of the soundboard [24]

N.B. *The symbol j in the previous expression refers to the complex root of unity, and should not be confused with the index "$_j$" which appears in the spatial coordinates and the mechanical variables.*

The driving-point admittance at point x_i is

$$Y_i(\omega) = j\omega \sum_{n=1}^{N} \frac{\Phi_n^2(x_i)}{m_n \left(\omega_n^2 - \omega^2\right)} \,. \tag{3.104}$$

Note Both expressions (3.103) and (3.104) were obtained within the framework of the modal theory for conservative systems, i.e., with no damping. In practice, it is more realistic if account is taken of dissipation in the structure. It will be shown in Chap. 5 that, under some particular assumptions, the modal shapes remain unchanged in the presence of damping, so that one can write:

$$Y_{ij}(\omega) = j\omega \sum_{n=1}^{N} \frac{\Phi_n(x_i)\ \ \Phi_n(x_j)}{m_n \left(\omega_n^2 + 2j\zeta_n\omega_n\omega - \omega^2\right)} \,, \tag{3.105}$$

where ζ_n is a one-dimensional modal damping coefficient, with the assumption $\zeta_n \ll 1$. As a result, the admittance can be considered as being a sum of damped SDOF oscillators (see Chap. 2).

3.4.8.1 Frequency Analysis of Admittances

The modulus of $Y_{ij}(\omega)$ reaches its maximum at frequencies close to the eigenfrequencies of the structure. These maxima are sometimes difficult to detect, especially if the modes are closely spaced in frequency, and with significantly different amplitudes. The imaginary part of the admittance vanishes for frequencies equal to the eigenfrequencies of the structure, and the slope of the phase is maximum (see Figs. 3.19 and 3.20). In the presence of modal damping, a better accuracy is often obtained by using the imaginary part (rather than the magnitude) to determine the eigenfrequencies from experimental admittance measurements.

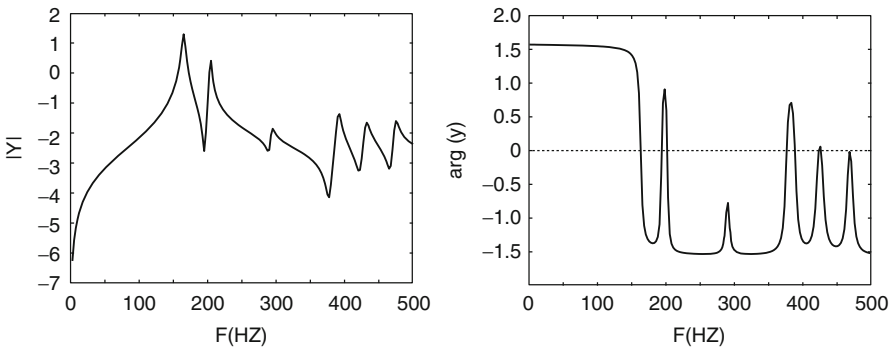

Fig. 3.19 Example of a typical admittance, highlighting the dependence of magnitude and phase on frequency

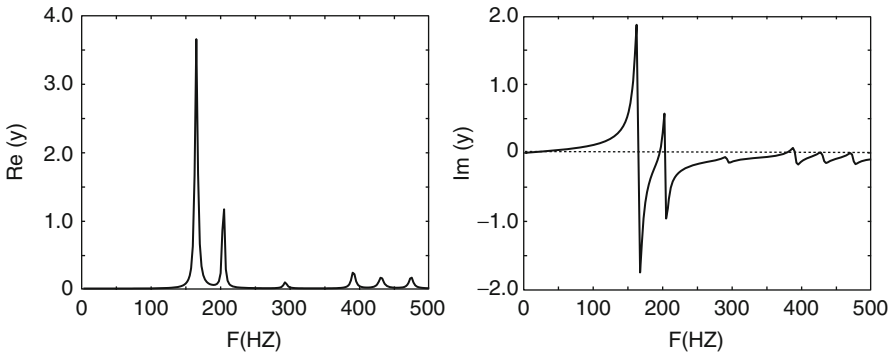

Fig. 3.20 Example of a typical admittance, highlighting the dependence of real and imaginary parts on frequency

- When $\omega \simeq \omega_n$, the main term of $Y_{ij}(\omega)$ is equal to $j\omega \dfrac{\Phi_n(x_i)\ \Phi_n(x_j)}{m_n\left(\omega_n^2 - \omega^2\right)}$.
- When $\omega \gg \omega_n$, the coefficients become

$$Y_{ij} \simeq j\omega \sum_{l>n} \frac{\Phi_l(x_i)\ \Phi_l(x_j)}{-m_l\omega^2} \simeq \frac{1}{j\mathsf{M}\omega} \quad \text{with} \quad \frac{1}{\mathsf{M}} = \sum_{l>n} \frac{\Phi_l(x_i)\ \Phi_l(x_j)}{m_l} \,. \tag{3.106}$$

  All modes with a rank higher than a given value n play the role of a mass M whose value depends on the modal masses and modal shapes at points x_i and x_j. The value of M depends on rank n.
- Similarly, considering the modes with rank lower than n, we find

$$Y_{ij} \simeq j\omega \sum_{l<n} \frac{\Phi_l(x_i)\ \Phi_l(x_j)}{m_l\omega_l^2} \simeq \frac{j\omega}{\mathsf{K}} \quad \text{with} \quad \frac{1}{\mathsf{K}} = \sum_{l<n} \frac{\Phi_l(x_i)\ \Phi_l(x_j)}{m_l\omega_l^2} \,. \tag{3.107}$$

  The contribution of these modes is equivalent to a stiffness K. In summary, in the vicinity of a given mode n, the transfer admittance can be written approximately as:

$$Y_{ij}(\omega) \simeq j\omega \frac{\Phi_n(x_i)\ \Phi_n(x_j)}{m_n\left(\omega_n^2 - \omega^2\right)} + \frac{j\omega}{\mathsf{K}} + \frac{1}{j\mathsf{M}\omega} \,. \tag{3.108}$$

  In summary, Eq. (3.108) shows that one cannot generally consider the term of rank n only in the expansion of Y_{ij}; it is also necessary to take both the mass and stiffness residues M and K into account. These two terms represent the influence of the other modes in the vicinity of the n-th mode.

3.4.9 Strings of Bowed Instruments

Bowed strings are either single wires (like the *E*-string of a modern violin) or wrapped strings, where a central wire core is overwound with some form of fine wire. Pickering [29] and Schumacher [34] investigated the mechanical behavior of strings for bowed instruments in detail. In the case of wrapped strings, the core can either be made of a monofilament (steel, tungsten or aluminum) or made of many threads (generally nylon, but sometimes also steel). The winding is a metallic ribbon or a thread (different kinds of aluminum, silver, copper, or tungsten alloys) twisted around the core.

Each string of the instrument is stretched with tension T during the initial tuning. During normal playing, the length L is changed for each note. These two parameters will be considered as constant in what follows, although this is not totally true in

practice. In fact, the use of vibrato (a modulated motion of a finger, resulting in four to eight oscillations per second) affects both the actual length of the string and its tension, and probably also the mobility at the bridge. The amplitude of this motion varies during a note interval, however, on average, it results in an increase in tension.[13]

Three main types of waves are observed in a vibrating string.

- Longitudinal waves can generally be ignored in the motion of bowed strings.
- (Transverse) bending waves are predominant. Since the main component of the bowed string motion occurs in the plane formed by the direction Ox of the string at rest and the direction Oy of the bow velocity, only this polarization plane will be considered for transverse waves in the following sections.
- Torsional waves involve the angular displacement $\psi(x,t)$ of each section of the string, with regard to the string axis Ox. Since the bow excites the string at its outer surface, these waves are always present in a bowed string.

3.4.9.1 Bending Waves

When a string is deflected from its rest position, it tends to return back under the combined effects of two restoring forces oriented in the Oy-direction: one due to the tension T and the other due to the intrinsic stiffness of the string. The restoring force on a portion of string of length dx is $T\dfrac{\mathrm{d}^2\xi}{dx^2}$, where ξ is the displacement along Oy. For a single string with Young's modulus E and geometric moment of inertia of a cross-section I_g, the restoring force due to the finite elasticity of the string is $-EI_g\dfrac{\mathrm{d}^4\xi}{dx^4}$ (see Chap. 1).

Bowed strings are only single wires; most often they present very complex wrapped structures. However, assuming that the structure remains invariant during the deformation (which means that there is no aggregation of the threads in the neutral plane, for example), we can homogenize the cross-section of the string and consider an equivalent single string. The stiffness force then keeps the same formal expression $-\langle EI_g\rangle\dfrac{\mathrm{d}^4\xi}{dx^4}$, where $\langle EI_g\rangle$ is an equivalent bending modulus. For a string with linear density[14] ϵ, the equation of motion becomes

$$-\langle EI_g\rangle\frac{\mathrm{d}^4\xi}{dx^4}+T\frac{\mathrm{d}^2\xi}{dx^2}-\epsilon\frac{\mathrm{d}^2\xi}{dt^2}=0 \quad . \tag{3.109}$$

This equation is dispersive because of the presence of the stiffness term (see the example of a prestressed bar in Sect. 3.5.1.4). The dispersion is low if the

[13] The period of a vibrato is typically 125 ms whereas the largest period of a violin note is only 5 ms (up to 25 ms for the double bass). In view of this duration, it is justified to consider the *average* tension increase in the string.

[14] ϵ is denoted ρS for a homogeneous single wire string.

perturbation term $\varepsilon = \langle EI_g \rangle / TL^2$ is small compared with unity (see Eq. 3.138), which is the case for bowed instruments. The important point here is that the eigenfrequencies of the string are inharmonic. However, for a bowed string, we will see in Chap. 11 that the motion is composed of self-sustained oscillations and is thus quasi-periodic. As a consequence, the components of the bowed string motion *do not coincide* with the eigenfrequencies of the string. In contrast, in the case of free oscillations, like those resulting from a "pizzicato" pluck, the sound spectrum consists of the eigenfrequencies predicted by Eq. (3.138).

One effect of string end mobility is a modification of the string's eigenfrequencies compared with the case where the ends are rigidly fixed (see Sect. 3.4.5). To a first-order, the relative change is equal to (see Eq. 6.54):

$$\frac{\delta f_n}{f_1} \approx \frac{jZ_{c,T}Y}{\pi}, \tag{3.110}$$

where $Z_{c,T}$ is the characteristic impedance of the bending waves and Y the mobility at one end of the string (either in $x = 0$ or $x = L$) assuming that the other end is fixed. The end mobility usually has a reactive component which modifies the eigenfrequencies and a dissipative component which introduces damping in the eigenmodes or, equivalently, a finite width in the resonance curve.

During the coupling with the bow, a transverse string mode can be excited if the inharmonicity resulting from both the stiffness and finite end mobility remains lower than the width of the resonance curve related to dissipation.

3.4.9.2 Torsional Waves

Like the bar of circular cross-section described in Chap. 1, the string has a torsional stiffness GJ, so that the relationship between the moment $\mathscr{M}(x,t)$ exerted on a section and its angular displacement ψ is given by [see Chap. 1, Eq. (1.42)]:

$$\mathscr{M}(x,t) = GJ\frac{\mathrm{d}\psi}{dx}\,. \tag{3.111}$$

The string also has a rotational inertia with regard to its axis, with moment I per unit length. The equation for torsional waves (see Chap. 1, Eq. (1.45)) can then be written as:

$$\frac{\mathrm{d}^2\psi}{dx^2} - \frac{1}{c_R^2}\frac{\mathrm{d}^2\psi}{dt^2} = 0 \quad , \tag{3.112}$$

where the propagation speed c_R is $\sqrt{GJ/I}$. This speed is about five times higher than the propagation speed for transverse waves. Torsional waves have an important intrinsic damping: their associated Q-factor is typically a few tens, an order of

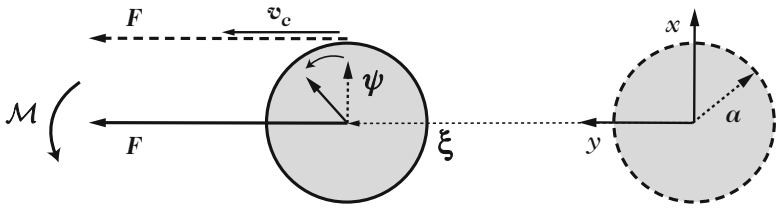

Fig. 3.21 Transverse displacement ξ combined to the rotation ψ of a string section consecutive to a horizontal force F applied at its surface by the bow. *Right*: string at rest; *left*: string in motion

magnitude below that for bending waves [20, 42]. Torsional waves also have a characteristic impedance which links $\mathscr{M}$ and $\dot{\psi}$ for a traveling wave:

$$\mathscr{M} = \pm\sqrt{JGI}\,\dot{\psi}\ . \tag{3.113}$$

Finally, a force F applied at the string's curved outer surface is equivalent to the following combination (see Fig. 3.21):

- a force F applied at the center generating a bending wave and
- a moment $\mathscr{M} = aF$ (where a is the string's radius) which generates the torsional wave $\psi(x,t)$.

The expression of the velocity v_c at the string's surface combines together the torsional and the bending waves:

$$v_c = \dot{\xi} + a\dot{\psi}, \tag{3.114}$$

It is generally more convenient to use the variables (v_c, F) for describing the combination of both traveling waves:

$$v_c = Y_{c,T}F + a^2\frac{F}{\sqrt{JGI}} = Y_c F, \tag{3.115}$$

where

$$Y_c = Y_{c,T} + \frac{a^2}{I\,c_R} \tag{3.116}$$

is the resulting mobility of the string at its surface. In this expression, the characteristic impedance of the torsional waves, seen from the outer curved surface of the string, is

$$Z_R = \pm\frac{F}{a\dot{\psi}} = \frac{I\,c_R}{a^2}. \tag{3.117}$$

The characteristic mobility Y_c will be used to describe the dynamics of the string in Chap. 11.

3.5 Application to Percussion Instruments

Percussion instruments are characterized by a short excitation, followed by free oscillations. In the linear range, the spectral content of the sound during decay is composed of the eigenfrequencies of the excited system. In the first chapter of this book, the basic equations describing the vibrations of elementary structures such as bars, plates, membranes, and shells were presented. A number of percussion instruments are made up of such structures. In Chap. 1, the main impact mechanisms were also described. Using the general properties of modes, we are now able to apply these results to percussive instruments.

3.5.1 Vibration of Beams

Beam models are well suited to the description of tuned mallet percussion instruments with keyboard such as the xylophone, vibraphone, marimba, glockenspiel, etc. For these instruments, the bending transverse vibrations are dominant, and deserve careful attention. However, other modes, including torsional modes, can also be excited. This is particularly true in the upper frequency range of these instruments, when the length of the beam becomes comparable to the other dimensions, and therefore treating the beam as a "slender solid" is no longer valid.[15]

In this section we restrict ourselves to the case of transverse bending vibrations. We first examine the analytical reference solution provided by the case of bars with constant cross-section. We then study the case of bars of variable cross-section, which better correspond to real instruments. Finally, the particular case of prestressed bars allows us to establish a comparison with the transverse vibrations of strings discussed in Sect. 3.4.

As shown in Chap. 1, the basic equation describing the transverse bending vibrations of bars, assuming Euler–Bernoulli assumptions and isotropic material, is written:

$$\frac{\partial^2}{\partial x^2}\left(EI(x)\frac{\partial^2 y}{\partial x^2}\right) + \rho(x)S(x)\frac{\partial^2 y}{\partial t^2} = 0\,, \tag{3.118}$$

where $y(x,t)$ is the transverse vertical displacement (in the $\boldsymbol{e}_y$ direction). The eigenmodes $y(x,t) = \Phi(x)\cos\omega t$ are the sinusoidal solutions of (3.118) which satisfy the equation:

[15] In musical acoustics, the word *bar* is often used to designate xylophone beams. Both terms are used in this book. In structural dynamics, the term *beam* is used to designate slender solids in bending regime, while the term *bar* is used in the context of longitudinal vibrations. We do not make such a distinction here.

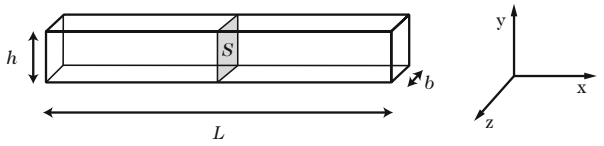

Fig. 3.22 Geometry of a bar with a constant cross-section

$$\frac{d^2}{dx^2}\left(EI(x)\frac{d^2\Phi}{dx^2}\right) - \omega^2\rho(x)S(x)\Phi = 0\,. \tag{3.119}$$

Equation (3.119) cannot be solved analytically, except in a small number of cases such as a bar of constant cross-section, discussed in Sect. 3.5.1.1 below. For variable cross-section bars, we must use approximate resolution techniques (see Sect. 3.5.1.2).

3.5.1.1 Free-Free Bars of Constant Cross-Section

Consider the reference case of an homogeneous, isotropic bar of length L, width b, thickness h, constant cross-section $S = bh$, whose moment of inertia with respect to the neutral plane at $z = h/2$ (see Fig. 3.22) is $I = bh^3/12$.

In this case, Eq. (3.118) reduces to:

$$EI\frac{\partial^4 y}{\partial x^4} + \rho S\frac{\partial^2 y}{\partial t^2} = 0\,. \tag{3.120}$$

Searching eigensolutions of the form $y(x,t) = \Phi(x)\cos\omega t$ leads to [19]:

$$\Phi(x) = A\cosh kx + B\sinh kx + C\cos kx + D\sin kx$$
$$\text{with}\quad k = \tfrac{\omega}{v}\quad\text{where}\quad v = \sqrt{\omega}\sqrt[4]{\tfrac{EI}{\rho S}}\,. \tag{3.121}$$

This expression shows that the *phase velocity* v of the bending waves varies as the square root of the angular frequency ω. The waves are therefore dispersive, the high frequencies propagating faster than the low frequencies. The associated dispersion equation is

$$EIk^4 - \rho S\omega^2 = 0, \tag{3.122}$$

from which we obtain v as a function of wavenumber k:

$$v = \frac{\omega}{k} = k\sqrt{\frac{EI}{\rho S}}\,. \tag{3.123}$$

However, in terms of energy transportation, the appropriate velocity to consider is not the phase velocity, but the group velocity (see, for example, [21]). For a "wave packet" localized in time, the group velocity is the velocity of the envelope, which can be calculated by:

$$v_g = \frac{\partial \omega}{\partial k} = 2k\sqrt{\frac{EI}{\rho S}} = 2v = 2\sqrt{\omega}\sqrt[4]{\frac{EI}{\rho S}}\,. \tag{3.124}$$

The group velocity here is twice the phase velocity. This result reveals a paradoxical phenomenon, namely that the group velocity of elastic bending waves in the bar tends to infinity with frequency. This is in disagreement with the basic laws of physics since if would mean that some bending waves could propagate faster than light! This apparent paradox is a result of the simplified model of Euler–Bernoulli which ignores the effects of rotational inertia of the bar and the shear of the cross-sections. Introducing these two corrections into the bar model (Timoshenko model [18]), shows that the velocity of the bending waves actually varies as $\sqrt{\omega}$ at low frequencies and then tends to a constant asymptotic value as the frequency increases, which is more realistic (see Fig. 3.23).

Continuing the calculation, we introduce the free boundary conditions (Fig. 3.24), which amount to nullifying moments and forces exerted by the external environment on the ends of the bar (see Chap. 1), which yields

$$\begin{aligned} &\frac{\partial^2 y}{\partial x^2}(0,t) = \frac{\partial^2 y}{\partial x^2}(L,t) = 0, \\ \text{and}\quad &\frac{\partial^3 y}{\partial x^3}(0,t) = \frac{\partial^3 y}{\partial x^3}(L,t) = 0\,. \end{aligned} \tag{3.125}$$

Finally, the eigenfrequency equation for a bar of constant cross-section free at both ends (see Fig. 3.26) is

$$\cos kL \cosh kL = 1\,. \tag{3.126}$$

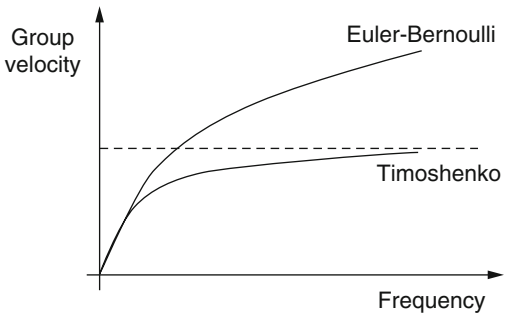

Fig. 3.23 Group velocity of bending waves in a bar, for different models

Fig. 3.24 On tuned keyboard percussion instruments, the "free-free" boundary conditions are obtained by attaching the bars together with a light and flexible cord. The attachment points of the cord on the bar are approximately located at the position of the nodes of the fundamental mode in order to minimize damping. We see on this figure the example of a balafon or African xylophone

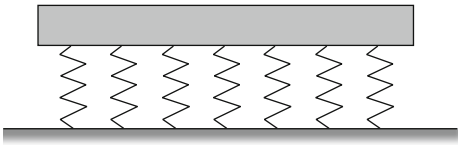

Fig. 3.25 Xylophone bar with its suspension

Note 1: In (3.126), the solution $k = 0$ does not hold: it would correspond to the case where the free bar goes to infinity after the impact. Imagine, for example, striking a bar with a hockey stick on a frozen lake: it will take a rigid body motion made of the combination of translation and rotation, and you will have to run far away to recover it!

Note 2: In practice, the boundary conditions are satisfied by flexible suspensions.[16] These suspensions, combined with the total mass of the bar, provide an extra rigid body mode (see Sect. 3.4.1.1). This mode usually has an eigenfrequency of a few Hz, which is very low as compared with the first eigenfrequency of the transverse motion (see Fig. 3.25).

The graphical resolution of Eq. (3.126) in Fig. 3.26 shows that the roots are such that $k_n L \simeq (2n + 1)\pi/2$. From the dispersion equation (3.122), we derive the eigenfrequencies f_n (in Hz):

[16]The arrangement of bars of ascending pitch is, for example, maintained by a thin cord which passes through all bars.

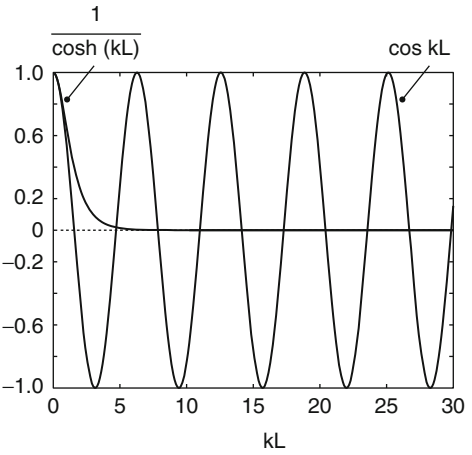

Fig. 3.26 Graphical solution of the eigenfrequency equation for a free homogeneous bar of constant cross-section: the solutions are found at the intersections of the curves $\cos kL$ and $\frac{1}{\cosh kL}$

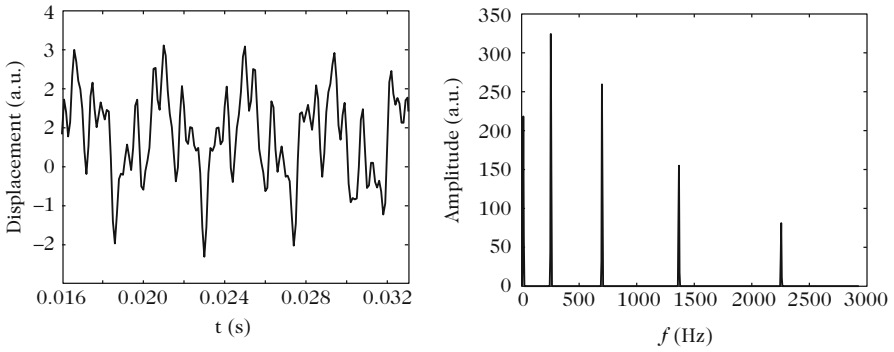

Fig. 3.27 Waveform and amplitude spectrum for a bar of constant cross-section. The waveform is not periodic and the spectral components are not integer multiples of the fundamental

$$f_n \simeq \sqrt{\frac{EI}{\rho S}} \frac{\pi}{8L^2} \left[3^2, 5^2, 7^2, \ldots, (2n+1)^2\right] . \tag{3.127}$$

Unlike for the case of an ideal string, the bending eigenfrequencies for a bar of constant cross-section are inharmonic, i.e., they are not integer multiples of a fundamental. This property is apparent in Fig. 3.27 which shows the amplitude spectrum for the vibration of a bar of constant cross-section. On the same figure, an extra peak close to zero (a few Hertz) can be seen which corresponds to the suspension resonance of the bars. This resonance, which is not predicted by Eq. (3.126), does not produce any sound.

From a musical point of view, the major shortcoming of an inharmonic spectrum is that the perceived pitch is not well defined. For this reason, the bars are cut on their lower side. The eigenfrequencies of bars with an undercut can be calculated from Eq. (3.119). In this case, there is no analytical solution and one has to use

numerical approximations. It is possible to optimize the width and depth of the cut (while respecting other criteria such as, for example, the non-appearance of torsional vibrations and the elasticity limit of the bar) in order to ensure that the partials of higher rank will be close to multiples of the fundamental.

3.5.1.2 Bars of Variable Cross-Section

The Galerkin method of solving the eigenvalue problem for the bending vibrations in a bar of variable cross-section is now briefly explained [26]. This method applies to conservative and non-conservative problems. It is an approximation method where the eigenmodes $\Phi(x)$ are sought in the form of a finite sum of p terms:

$$\Phi^{(p)}(x) = \sum_{j=1}^{p} a_j \phi_j(x) \,, \tag{3.128}$$

where the functions $\phi_j(x)$ are arbitrary with the restriction that they must fulfill the boundary conditions: they are said to be *kinematically admissible*. Combining Eqs. (3.128) and (3.119), and defining $\lambda^{(p)} = (\omega^2)^{(p)}$ (the approximate eigenvalues of order p), we obtain the *Galerkin's residue*:

$$\mathscr{R}\left[\Phi^{(p)}(x)\right] = \frac{d^2}{dx^2}\left(EI(x)\frac{d^2\Phi^{(p)}}{dx^2}\right) - \lambda^{(p)}\rho(x)S(x)\Phi^{(p)} \,, \tag{3.129}$$

which can be written, given Eq. (3.128):

$$\mathscr{R}\left[\Phi^{(p)}(x)\right] = \sum_{j=1}^{p} a_j \left\{\frac{d^2}{dx^2}\left(EI(x)\frac{d^2\phi_j(x)}{dx^2}\right) - \lambda^{(p)}\rho(x)S(x)\phi_j(x)\right\} \,. \tag{3.130}$$

The functions $\phi_j(x)$ are now used to obtain a *weak formulation* for the eigenvalue problem, i.e., after multiplication by a function ϕ_i and integration over the entire length of the bar:

$$\int_0^L \phi_i(x) \sum_{j=1}^{p} a_j \left\{\frac{d^2}{dx^2}\left(EI(x)\frac{d^2\phi_j(x)}{dx^2}\right) - \lambda^{(p)}\rho(x)S(x)\phi_j(x)\right\} dx = 0 \,. \tag{3.131}$$

The problem is equivalent to searching those coefficients a_j which cancel the residue $\mathscr{R}\left[\Phi^{(p)}(x)\right]$. The formulation (3.131) can then be written as:

$$\sum_{j=1}^{p} k_{ij}a_j - \lambda^{(p)} \sum_{j=1}^{p} m_{ij}a_j = 0 \quad \text{for} \quad i = 1, 2, .., p \,, \tag{3.132}$$

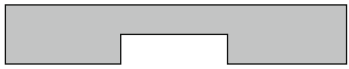

Fig. 3.28 Bar with an undercut

where the mass and stiffness coefficients are given by:

$$k_{ij} = \int_0^L \phi_i(x) \frac{d^2}{dx^2} \left(EI(x) \frac{d^2 \phi_j(x)}{dx^2} \right) dx,$$

$$\text{and} \quad m_{ij} = \int_0^L \phi_i(x) \rho(x) S(x) \phi_j(x) \, dx \, . \tag{3.133}$$

Equation (3.132) can be written in matrix form:

$$[\mathbb{K} - \lambda \mathbb{M}] \boldsymbol{a} = 0 \, , \tag{3.134}$$

where $\boldsymbol{a}$ is a vector of dimension p, and where $\mathbb{K}$ and $\mathbb{M}$ are matrices of dimensions $p \times p$. The method presented is thus equivalent to solving an eigenvalue problem similar to those encountered for discrete systems.

A simple example of a bar of variable cross-section is depicted in Fig. 3.28 which shows a bar with reduced height in its central part. Removing material near the center decreases the inertia (proportional to thickness), but also the stiffness in higher proportion (since the stiffness is proportional to the third power of the thickness), and therefore the eigenfrequencies whose corresponding eigenshapes reach a maximum near the center decrease, which is the case for odd modes. This simple example shows that it is possible to control the spacing of the eigenfrequencies with an appropriate undercut.

3.5.1.3 Application to Xylophone and Keyboard Instruments

In practice, bar shapes similar to the one shown in Fig. 3.28 should be avoided since high internal stress is concentrated near the sharp corners, which weakens the structure. It is preferable to design bar profiles with a high radius of curvature and without slope discontinuities.

Today, the design of bars for keyboard percussion instruments still remains largely empirical. Cutting the bar near its center lowers the frequency f_1 of the first partial, while keeping the frequency f_2 of the second partial approximately constant, and lowering the frequency f_3 of the third partial slightly. Instrument makers usually adjust the ratios $R_1 = f_2/f_1$ and $R_2 = f_3/f_1$. In practice, it becomes difficult to independently adjust the partials of higher rank, and so the focus usually remains on these two parameters only. The depth of the undercut is limited by the resistance of the bar to shocks and by the fact that, if the bar becomes too thin in the center, torsional vibrations might become important. According to Eq. (3.127), the initial values of the two frequency ratios (before starting the undercut) are

$$R_{10} = \frac{25}{9} = 2.754 \quad \text{and} \quad R_{20} = \frac{49}{9} = 5.404\,. \tag{3.135}$$

From experience, it is known that the target for R_1 usually lies between 3 and 4, and between 6 and 10 for R_2. The standard values used by makers are the following:

- $R_1 = 3$ and $R_2 = 6$,
- $R_1 = 4$ and $R_2 = 8$,
- $R_1 = 3$ and $R_2 = 9$,
- $R_1 = 4$ and $R_2 = 10$.

On real tuned mallet percussion instruments, these ratios can only be obtained for the lower notes. In the middle register, the second and third partials are not in harmonic ratio with the fundamental anymore. This is due to the fact that the assumption that a bar behaves as a 1D slender solid is less justified as the length of the bars decreases. Orduña-Bustamante suggests to cutting parabolic profiles in the bars [28]. The idea is to adjust the depth h_c and width x_c of the undercut to obtain appropriate values for R_1 and R_2. This idea has been extended by Doutaut who suggests polynomial profiles of order 4 and 8, enabling a larger range of possible modifications for the eigenfrequencies (see Fig. 3.29) [12].

In order to tune the complete range of bars in a mallet percussion instrument, it is necessary to adjust both the shape of the undercut and the length of the bars. For an instrument with four octaves, the ratio between the higher and the lower fundamental is $f_{\max}/f_{\min} = 2^4 = 16$. Since the eigenfrequencies of the bars vary as the inverse of the square of the length [see Eq. (3.127)], in principle, it might be considered that the length of the bars should be adjusted such that $D = L_{\max}/L_{\min} = 4$. However, measuring actual bar lengths on most real instruments shows that D is close to 3. There are several reasons for this: the first reason is with respect to the playability of the instrument; the player would encounter difficulties in playing on very short bars in the high frequency range. At the other end of the instrument, long bars at low frequencies would be more difficult to produce, would take more space and would use more material. The second reason is linked to manufacturing, because of the constraints associated with the attachment of the bars. Finally, as mentioned

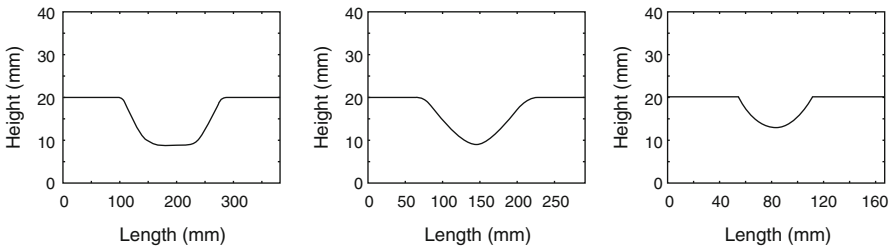

Fig. 3.29 Examples of undercut shapes for xylophone bars. (*Left*) Polynomial of order 8 for bar C4 (f_1 = 262 Hz); (*Middle*) Polynomial of order 4 for bar C5 (f_1 = 524 Hz; (*Right*) Polynomial of order 2 for bar C7 (f_1 = 2093 Hz), according to [12]

above, it is preferable to have longer bars at high frequencies for tuning reasons. In practice, to make a chromatic instrument where fundamental frequencies vary by 6 % from one note to the next, about 5 % of the variations are obtained by modifying the lengths of the bars and the remaining 1 % by adjusting the cuts. Makers tend to start by using the most usable length of bar for the high frequency notes, and then make greater and greater undercuts as they work towards the lower notes.

3.5.1.4 Prestressed Bars and Stiff Strings

Strings of musical instruments are made of elastic materials that have a finite Young's modulus. As a consequence, it is impossible to create any discontinuity of slope by bending the string. This is particularly true for metallic strings, such as piano wires. If such a string is fixed at one end, when undisturbed it remains almost straight, like a bar. Therefore, it is necessary to refine the previous ideal string model, to take both the axial prestress (due to tension T) and bending stiffness into account. The equation that describes the transverse bending vibrations of a stiff string (or, equivalently, of a prestressed bar), assuming an Euler–Bernoulli behavior, becomes

$$\rho S \frac{\partial^2 y}{\partial t^2} = T \frac{\partial^2 y}{\partial x^2} - EI \frac{\partial^4 y}{\partial x^4} \,. \tag{3.136}$$

For a traveling wave of the form $y(x,t) = e^{j(\omega t - kx)}$, we obtain the dispersion equation:

$$\omega^2 = k^2 c^2 \left(1 + \frac{EI}{T} k^2\right) \,. \tag{3.137}$$

For a string of length L, the usual orders of magnitude are such that it is justifiable to define a dimensionless coefficient $\varepsilon = \frac{EI}{TL^2}$, small compared to unity, so that Eq. (3.137) becomes

$$\omega^2 = k^2 c^2 \left(1 + \varepsilon k^2 L^2\right) \,. \tag{3.138}$$

For the case of a stiff string simply supported at both ends, the displacement and moment are both zero at these points, which yields the condition for the wavenumbers:

$$\sin kL = 0 \quad \text{i.e.} \quad k_n L = n\pi \,. \tag{3.139}$$

From Eq. (3.138), the eigenfrequencies of the stiff string are given by:

$$\omega_n \simeq \frac{n\pi c}{L} \left(1 + \varepsilon \frac{n^2 \pi^2}{2}\right) \,. \tag{3.140}$$

Due to bending stiffness, the eigenfrequencies of the stiff string are higher than those of the corresponding ideal string. This difference increases with the rank n of the partial. This property is observed on piano wires [30]. The inharmonicity due to stiffness for the nth-partial of the string is defined as:

$$i_n = \frac{\omega_n - \omega_{no}}{\omega_{no}} , \tag{3.141}$$

where ω_{no} is the angular frequency in the case of no stiffness. The application of this definition to the present case leads to:

$$i_n = \varepsilon \frac{n^2 \pi^2}{2} . \tag{3.142}$$

In real instruments, the inharmonicity due to stiffness should be added to the inharmonicity due to the coupling with the soundboard, as studied in Sect. 3.4.5.

Time Domain: Precursor

For stiff strings, the dispersion equation (3.138) shows that the phase velocity $v_\phi = \omega/k$ and the group velocity $v_g = \frac{d\omega}{dk}$ are both monotonic increasing functions of frequency. In the time domain, rapidly varying oscillations preceding steep wavefronts can be seen on force waveforms (see Fig. 3.30). These oscillations were called "precursors" by Cuesta and Valette [38]. These authors also highlighted the modifications of the precursor due to amplitude nonlinearity (see Chap. 8) and their perceptual significance.

3.5.2 *Vibrations of Membranes In Vacuo*

A similar distinction can be made for 2D systems as it has been previously made for strings and bars. In what follows, an *ideal membrane* refers to a thin structure, i.e., whose thickness is small compared with the other dimensions, and where the elastic

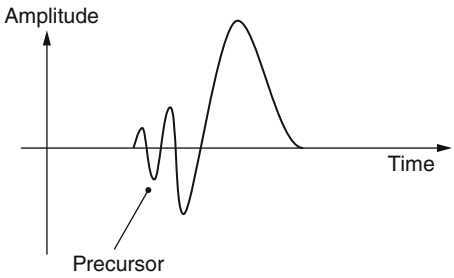

Fig. 3.30 Precursor due to stiffness in linear regime

restoring forces are due to prestress, i.e., to a surface tension applied at its periphery. Conversely, a *plate* is a thin, two-dimensional structure where the restoring forces are due to the intrinsic elasticity of the material. As for strings, real membranes have a nonzero modulus of elasticity. Finally, we also find prestressed plates in musical acoustics, such as the soundboard of a piano. For almost all string instruments, the body of the instrument is prestressed by the tension of the strings. In membranes, in addition, the presence of both the surrounding air and the cavity influences the vibrations. This is due to both the large surface in contact with the fluid and the small thickness of the membrane. In this section, only the case of membrane vibrations in vacuo will be addressed, keeping in mind that this reference case has no practical interest in musical acoustics. However, it will be used in Chap. 14 for building a kettledrum model.

3.5.2.1 Transverse Free Vibrations of a Circular Membrane

Membranes are used in percussion instruments (timpani, drums, bass drum, etc.) and in a number of string instruments (banjo [31], African kora, etc.). A circular geometry is usually preferred so as to obtain homogeneous tension across the membrane (Fig. 3.31). Membranes are usually excited by impact and therefore the oscillations are free after the mallet (or stick) has left the membrane. The discussion here is restricted to free oscillations. Assuming small displacements (which might not be justified during the excitation phase in the case of strong impacts), one can assume that the free transverse displacement $z(r, \theta, t)$ of a membrane in vacuo with surface density σ (in $\mathrm{kg\,m^{-2}}$) and tension per unit length τ (in $\mathrm{N\,m^{-1}}$) is described by the 2D wave equation (see Chap. 1):

$$\sigma \frac{\partial^2 z}{\partial t^2} = \tau \Delta z = \tau \left[\frac{\partial^2 z}{\partial r^2} + \frac{1}{r} \frac{\partial z}{\partial r} + \frac{1}{r^2} \frac{\partial^2 z}{\partial \theta^2} \right] . \tag{3.143}$$

A standard method of solving Eq. (3.143) is to use separation of variables [21]. A condition of zero displacement at the edge $z(r = a, \theta, t) = 0$ is imposed. In real instruments (in a kettledrum, for example), energy losses occur at the edge of the membrane because of both the presence of absorbing material (such as rubber) and the transmission of vibrations to the kettle. Such dissipation will be ignored in this chapter. For an ideal circular membrane, the transverse displacement can be written as [21]:

$$\begin{aligned} z(r, \theta, t) = \sum_{m=1}^{\infty} \Bigg\{ \sum_{n=0}^{\infty} Z_{mn}(r, \theta) \left(A_{nm} \cos \omega_{mn} t + B_{nm} \sin \omega_{mn} t \right) \\ + \sum_{n=1}^{\infty} \tilde{Z}_{mn}(r, \theta) \left(\tilde{A}_{nm} \cos \omega_{mn} t + \tilde{B}_{nm} \sin \omega_{mn} t \right) \Bigg\} . \end{aligned} \tag{3.144}$$

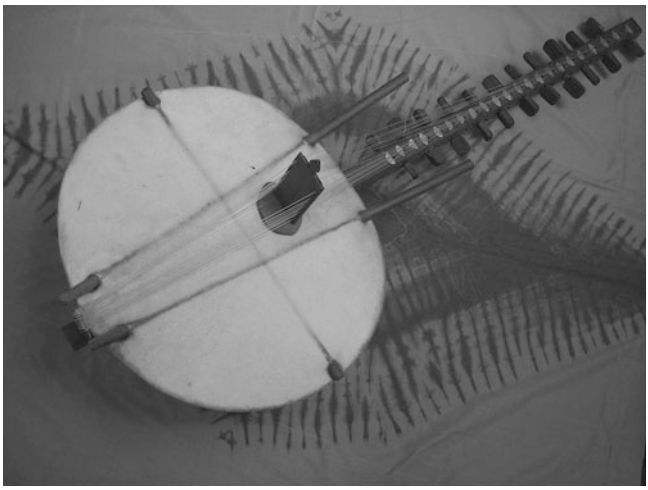

Fig. 3.31 Kora (African harp). The string vibrations are transmitted to a skin (or membrane) coupled to a cavity (a gourd) with a hole on the back

In Eq. (3.144), the eigenshapes of the membrane are given by:

$$Z_{mn}(r,\theta) = J_n(\beta_{mn} r)\cos n\theta \quad \text{and} \quad \tilde{Z}_{mn}(r,\theta) = J_n(\beta_{mn} r)\sin n\theta \,, \tag{3.145}$$

where the functions J_n are the *Bessel functions of the first kind of order n* [1]. Indices m and n correspond to the number of nodal circles and diameters, respectively (see Fig. 3.32). The discrete values of the wavenumber β_{mn} are determined by the boundary conditions at the edge. For a fixed edge, we get

$$J_n(\beta a) = 0 \,. \tag{3.146}$$

For each value of n, we obtain an infinite series β_{mn} of roots of Eq. (3.146). For $n = 0$, for example, we find that $J_0(\beta a) = 0$ yields the solutions $\beta_{m0}a = 2.405,\ 5.520,\ 8.654,\ 11.792,\ 14.931, \ldots$. Similarly, the roots of $J_1(\beta a) = 0$ are given by $\beta_{m1}a = 3.832,\ 7.016,\ 10.173,\ 13.324,\ 16.471, \ldots$.

The first nodal circle ($m = 1$) corresponds to the edge of the membrane. The *symmetrical* modes correspond to the cases where $n = 0$, i.e., with no nodal diameter. In these cases, only the shapes of type $Z_{mn}(r,\theta)$ remain. These modes are excited for a membrane struck near its center. In all other cases, we get twin modes with the same dependence with regard to r but which differ from each other by an angular shift equal to $\pi/2n$. The modes $m1$ are strongly excited when the player strikes near the edge, and are the most important from a musical point of view (see Chap. 14). The eigenfrequencies ω_{mn} are derived from the 2D wave equation (3.143):

$$\omega_{mn} = c\beta_{mn} \quad \text{where} \quad c = \sqrt{\frac{\tau}{\sigma}} \,. \tag{3.147}$$

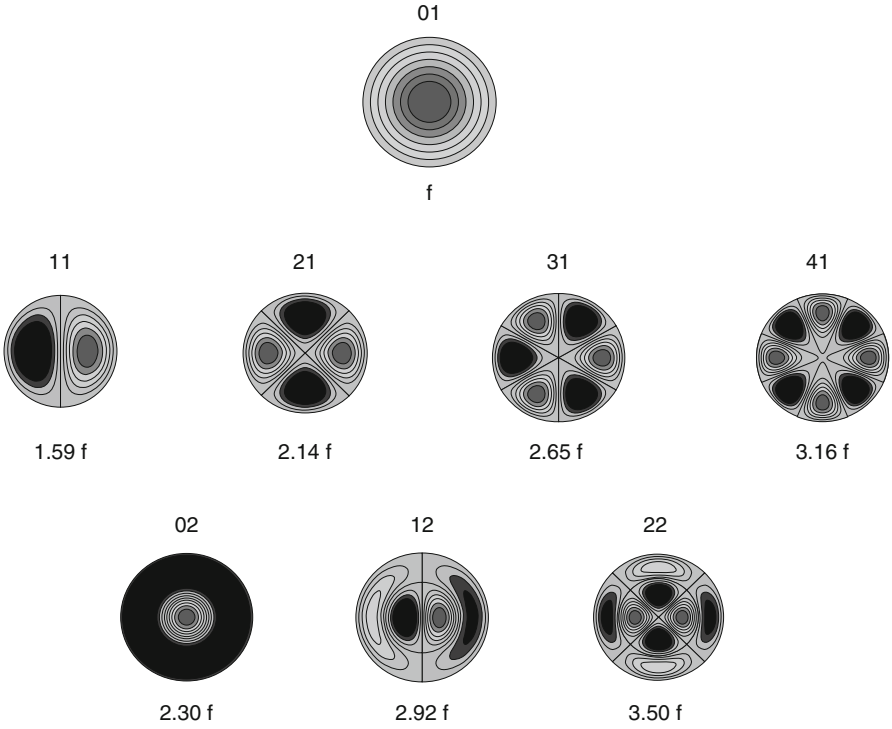

Fig. 3.32 Modal shapes of a circular membrane in vacuo. Each mode is designated by *nm* where *n* is the number of nodal diameters and *m* the number of nodal circles. The corresponding eigenfrequencies are indicated below each shape

In contrast to ideal strings, the eigenfrequencies of a membrane in vacuo are not harmonically related. We will see in Chap. 14, however, that the first modes of the *m*1 family can become almost harmonic under the combined loading effects of surrounding air and cavity. As a consequence, in this situation, a defined pitch can be produced when the membrane is struck near the edge.

3.5.2.2 Modal Density of a Membrane

The transverse vibrations of a membrane in vacuo can be viewed as a 2D generalization of the vibrations of ideal strings. One main difference between these two systems lies in the *modal density* (or number of modes per Hz) observed in their respective spectra.

In this book, we will have several opportunities to discuss the concept of modal density. This quantity influences linear and nonlinear couplings, acoustic radiation, and the statistical representation of vibration phenomena at high frequencies. The modal density of an ideal string stretched between two rigid supports is compared below with the modal density of a rectangular membrane rigidly fixed

at its edges. The rectangular geometry is chosen here only for the sake of simplicity, but the results obtained can be generalized to other geometries. We start by calculating the number of modes $N(f)$ with eigenfrequencies lower than a given frequency f. On a wavenumber scale, the successive modes of a string are equally spaced with an interval equal to π/L. Therefore we have

$$N(f) = \frac{k}{\frac{\pi}{L}} = \frac{2Lf}{c} . \tag{3.148}$$

The modal density is, by definition:

$$D(f) = \frac{dN}{df} = \frac{2L}{c} = \frac{1}{f_1} . \tag{3.149}$$

We find that the number of modes per Hz for an ideal string is equal to the inverse of the fundamental, which is a fairly obvious result. A similar method is now used for a rectangular membrane of length L_x and width L_y. The eigenfrequencies can be obtained by the method of separation of variables. The wavenumbers are now given by:

$$k_{mn} = \sqrt{k_m^2 + k_n^2} = \sqrt{\frac{m^2\pi^2}{L_x^2} + \frac{n^2\pi^2}{L_y^2}} \quad \text{with} \quad m, n \geq 1 . \tag{3.150}$$

In the k-plane, each discrete wavenumber k_{mn} with components (k_m, k_n) is represented by a vector of origin O and whose end is one of the nodes of the mesh with spatial steps $\pi/L_x, \pi/L_y$ (see Fig. 3.33). The number $N(f)$ is obtained by dividing the area of the quarter circle of radius k by the area of one element of the mesh:

$$N(f) = \frac{\pi}{4}\frac{4\pi^2 f^2}{c^2}\frac{L_x L_y}{\pi^2} = \pi\frac{Sf^2}{c^2}, \tag{3.151}$$

where S is the membrane surface area. We derive, in turn, the modal density:

$$D(f) = \frac{dN}{df} = \frac{2\pi S}{c^2} f . \tag{3.152}$$

The modal density of a membrane is proportional to the frequency. We will see in Chap. 5 that, for timpani membranes and for drumheads, the damping also increases with frequency. This leads to a modal overlap, so that it is not possible to discriminate the modes anymore. The spectrum becomes almost continuous.

3.5.3 *Transverse Vibrations of Thin Plates*

Flat plates can be viewed as two-dimensional bars, the third dimension (thickness) being considered as small compared with length and width. A piano (or a guitar)

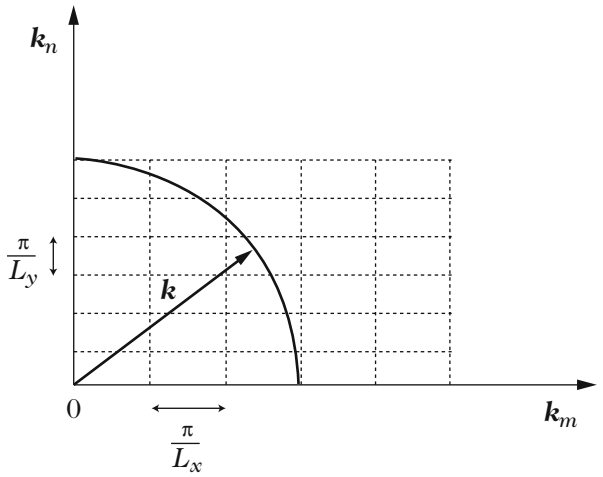

Fig. 3.33 Determining the number of modes and modal density for a two-dimensional system

soundboard is fairly well represented by a plate model. This is also the case for other string instruments, such as harps or lutes. Freely suspended metallic plates can also be used as percussion instruments [33].

In what follows, the transverse plate displacement is assumed to be small enough so that the equation of motion is linear. The thickness is also assumed to be small and the frequency range under study is such that transverse shear and rotational inertia can both be ignored. The transverse vibrations of the plates are then described by the Kirchhoff–Love model (see Chap. 1). This model is a generalization of the Euler–Bernoulli model (previously introduced for bars) to the case of plates.

The modes of simply supported rectangular plates are briefly reviewed below, in the context of musical acoustics. Emphasis is put on orthotropic plates, since most soundboards of string instruments are made of wood. Isotropic plates are thus considered as limiting cases. The effects of boundary conditions are discussed. As for membranes, we limit ourselves to the case of plates in vacuo. The structural-acoustic coupling between vibrating plate and air will be studied in Chap. 13.

3.5.3.1 Simply Supported Rectangular Orthotropic Plates

For a homogeneous orthotropic plate in Cartesian coordinates, with the axes oriented in the principal directions of orthotropy, and under Kirchhoff–Love assumptions, the equation that describes the transverse bending displacement w is (see Chap. 1):

$$\rho_p h \frac{\partial^2 w}{\partial t^2} + D_1 \frac{\partial^4 w}{\partial x^4} + (D_2 + D_4) \frac{\partial^4 w}{\partial x^2 \partial y^2} + D_3 \frac{\partial^4 w}{\partial y^4} = 0 \,. \tag{3.153}$$

For a simply supported rectangular plate of dimensions a and b, the displacement and bending moment are zero at the edges:

$$w(0,y,t) = w(a,y,t) = w(x,0,t) = w(x,b,t) = 0$$
$$\mathscr{M}_x(0,y,t) = \mathscr{M}_x(a,y,t) = \mathscr{M}_y(x,0,t) = \mathscr{M}_y(x,b,t) = 0\,. \tag{3.154}$$

The eigenmodes are

$$\Phi_{mn}(x,y) = \sin\frac{m\pi x}{a}\sin\frac{n\pi y}{b}, \tag{3.155}$$

and the wavenumbers take the discrete values:

$$k_{mn}^2 = k_m^2 + k_n^2 = \frac{m^2\pi^2}{a^2} + \frac{n^2\pi^2}{b^2}. \tag{3.156}$$

Using the dispersion equation, the associated angular eigenfrequencies are obtained

$$\omega_{mn} = \pi^2\sqrt{\frac{1}{\rho_p h}}\sqrt{D_1\frac{m^4}{a^4} + D_3\frac{n^4}{b^4} + (D_2+D_4)\frac{m^2n^2}{a^2b^2}}\,. \tag{3.157}$$

In these expressions, m and n are positive integers.[17] As previously shown for strings in Sect. 3.3.2, the eigenmodes Φ_{mn} are orthogonal with respect to mass and stiffness, which means here:

$$\int_0^a\int_0^b \rho_p h\Phi_{mn}(x,y)\Phi_{m'n'}(x,y)dx\,dy = \begin{cases} 0 & \text{if } m\neq m' \text{ or } n\neq n',\\ M_{mn} & \text{if } m=m' \text{ and } n=n'.\end{cases} \tag{3.158}$$

where M_{mn} is the modal mass for the mode (m,n). The eigenfrequencies of the orthotropic plate are distributed in an area located between two limiting dispersion curves (see Fig. 3.34).

3.5.3.2 Isotropic Case

For an isotropic material, one needs to substitute in the previous equations:

$$D_1 = D_3 = D = \frac{Eh^3}{12(1-\nu^2)} \quad \text{and}$$
$$D_4 = \frac{Eh^3}{6(1+\nu)}\;;\; D_2 = 2D_1 - D_4 = \frac{E\nu h^3}{6(1-\nu^2)}\,. \tag{3.159}$$

[17] They can also be zero in case of free boundary conditions.

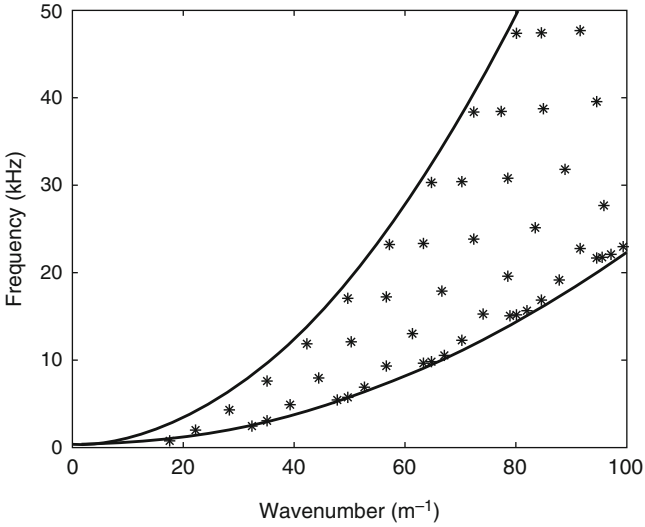

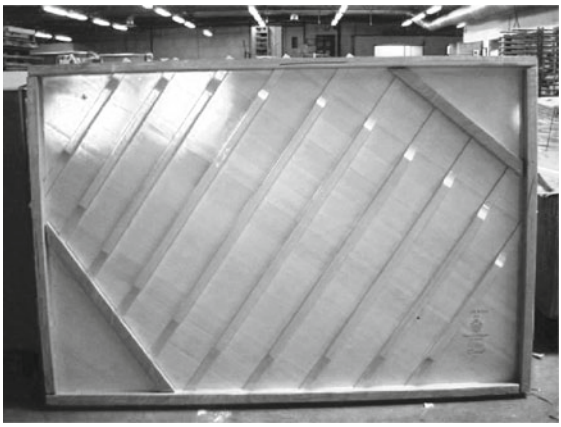

Fig. 3.34 (*Top*) Example of dispersion curves for an orthotropic plate. The eigenfrequencies (*asterisk*) are located between two limiting curves corresponding to the highest and lowest elasticity modulus, respectively. (*Bottom*): The soundboard of an upright piano is an example of an orthotropic plate. The ribs oriented perpendicularly to the fibers increase the transverse stiffness significantly. (© Itemm)

Here, the elastic behavior of the material is entirely determined by two constants: the Young's modulus E and the Poisson's ratio ν. The equation of motion of the plate becomes

$$\rho_p h \frac{\partial^2 W}{\partial t^2} + D\left(\frac{\partial^4 W}{\partial x^4} + 2\frac{\partial^4 W}{\partial x^2 \partial y^2} + \frac{\partial^4 W}{\partial y^4}\right) = 0\,. \tag{3.160}$$

The mode shapes $\Phi_{mn}(x,y)$ have the same form as in Eq. (3.155). However, the eigenfrequencies are now given by:

$$\omega_{mn} = \pi^2 \sqrt{\frac{D}{\rho_p h}} \left[\frac{m^2}{a^2} + \frac{n^2}{b^2} \right] . \tag{3.161}$$

Prestressed Isotropic Plate

For a prestressed plate, under the combined effects of a tension T_x applied in the plane of the plate in the direction Ox and a tension T_y applied along Oy, then the isotropic plate equation is modified in the following way [4]:

$$\rho_p h \frac{\partial^2 W}{\partial t^2} + D \left(\frac{\partial^4 W}{\partial x^4} + 2 \frac{\partial^4 W}{\partial x^2 \partial y^2} + \frac{\partial^2 W}{\partial y^4} \right) - T_x \frac{\partial^2 W}{\partial x^2} - T_y \frac{\partial^2 W}{\partial y^2} = 0 . \tag{3.162}$$

In this case, the eigenfrequencies become

$$\omega_{mn} = \sqrt{\frac{1}{\rho_p h}} \sqrt{D \left(\frac{\pi^2 m^2}{a^2} + \frac{\pi^2 n^2}{b^2} \right)^2 + T_x \frac{m^2 \pi^2}{a^2} + T_y \frac{n^2 \pi^2}{b^2}} . \tag{3.163}$$

3.5.3.3 Modal Density of a Plate

Because of their 2D geometry, plates show higher modal density than bars. As a consequence of damping, especially in wood, a high density of modes leads to a modal overlap (as in membranes), which means that it becomes difficult, or even impossible, to isolate a particular mode.

The case of a simply supported isotropic plate is considered here as an example. Its eigenfrequencies are given by (3.161). Taking the square root of this expression, we obtain $\sqrt{\omega_{mn}} = \sqrt{C} \sqrt{\frac{m^2}{a^2} + \frac{n^2}{b^2}}$, where $C = \pi^2 \sqrt{\frac{D}{\rho_p h}}$. In the k-plane (see Fig. 3.33), the quantity $\sqrt{\omega_{mn}/C}$ is represented by a vector pointing from the origin to the coordinates $(m/a, n/b)$.

As previously done for membranes, the number of modes $N(f)$ contained in the interval $[0, f]$ is calculated. For this purpose, a circle arc of radius $R = \sqrt{\omega/C}$ is drawn in the k-plane. The number of discrete points contained in a quarter of this circle of area $\pi R^2/4 = \frac{\pi \omega}{4C}$ is determined. Since the area of a single rectangular element is $1/ab$, the total number of modes below a given frequency f is given by:

$$N(f) = \frac{ab}{2} \sqrt{\frac{\rho_p h}{D}} f, \tag{3.164}$$

from which we derive the modal density:

$$D(f) = \frac{ab}{2}\sqrt{\frac{\rho_p h}{D}} = \frac{ab}{h}\sqrt{\frac{3\rho_p(1-\nu^2)}{E}}\,. \tag{3.165}$$

In summary, the modal density for a simply supported isotropic plate is constant. This constant is a function of both the geometry and elastic properties of the material. The modal density increases as the plate becomes more flexible, or thinner, and when its surface area increases. For an orthotropic plate whose rigidity constants have the property $D_2+D_4 = 2\sqrt{D_1 D_3}$, we obtain the same expression as Eq. (3.165) for the modal density, provided that D is replaced by D_1 and b by $\beta = b\left(\frac{D_1}{D_3}\right)^{1/4}$. For a given plate geometry and material, orthotropy leads to an increase in the modal density compared to the isotropic case [32].

Particular Case of a Prestressed Isotropic Plate

The influence of prestress on the eigenfrequencies of a plate can be discussed with the help of Eq. (3.163). In this equation, the terms of highest degrees in m and n are modified by the respective factors $1+\frac{T_x}{\pi^2 D}\frac{a^2}{m^2}$ and $1+\frac{T_y}{\pi^2 D}\frac{b^2}{n^2}$. If T_x and T_y are positive (tensile case), the eigenfrequencies increase compared to the non-prestressed case. If T_x and T_y are negative, the overall stiffness decreases, and the eigenfrequencies decrease. The consequences in terms of modal density are not straightforward. The analytical calculation was made by Wilkinson [40] who showed that the effects of prestress are essentially noticeable on the lowest modes, and that the modal density of the prestressed plate tends asymptotically to modal density of a plate without tension as the frequency increases. In addition, the modal density is a function of the squared tension, so that it is independent of its sign. As shown in the PhD manuscript by Ege [17, p. 151], the modal density of a plate decreases with the prestress, whatever its sign. One can also show that the modal density of a plate under high tension becomes close to the modal density of a membrane: this is coherent from a physical point of view.

3.5.3.4 Other Boundary Conditions for Plates

The general determination of eigenmodes for plates under complex boundary conditions will not be discussed in this book. One can refer, for example, to books by Yu [44] and Graff [21] for more information. Only the case of an isotropic rectangular plate is briefly presented below. The standard method used is separation of variables. It involves testing in Eq. (3.160) solutions of the form:

$$w(x,y,t) = X(x)Y(y)e^{j\omega t}\,. \tag{3.166}$$

As a result X and Y must obey:

$$X^{iv}Y + 2X''Y'' + XY^{iv} - \beta^4 XY = 0 \quad \text{with} \quad \beta^4 = \frac{\omega^2 \rho_p h}{D} . \tag{3.167}$$

The variables can be separated under the conditions:

$$\begin{aligned} &Y'' = -\gamma^2 Y \ \text{ and } \ Y^{iv} = \gamma^4 Y \\ &\text{or, alternatively} \\ &X'' = -\alpha^2 X \ \text{ and } \ X^{iv} = \alpha^4 X . \end{aligned} \tag{3.168}$$

In a third case, both conditions can be satisfied simultaneously. In Eq. (3.168), α^2 and γ^2 are real positive numbers given by the boundary conditions. Let us suppose that the conditions of the second group (those relating to X) are satisfied. We then derive from Eq. (3.167) the condition for Y, for each value α_n of α defined by the boundary conditions on X:

$$Y^{iv} - 2\alpha_n^2 Y'' - (\beta^4 - \alpha_n^4) Y = 0 . \tag{3.169}$$

Equation (3.169) has different types of solution, depending on the value of β compared to α. For $\beta > \alpha$, we get

$$\begin{aligned} &Y(y) = A \sin k_2 y + B \cos k_2 y + C \sinh k_1 y + D \cosh k_1 y \\ &\text{with} \quad k_1 = \sqrt{\beta^2 + \alpha_n^2} \quad \text{and} \quad k_2 = \sqrt{\beta^2 - \alpha_n^2} . \end{aligned} \tag{3.170}$$

The constants A, B, C, and D are then determined by the boundary conditions in y. For a plate clamped at $y = 0$ and $y = b$, for example, we have the conditions:

$$Y(0) = Y'(0) = Y(b) = Y'(b) = 0 . \tag{3.171}$$

The eigenfrequencies are given by the roots of the determinant of the system of equations that governs the constants, which yields

$$k_1 k_2 \left[\cos k_2 b \cosh k_1 b - 1\right] - \alpha_n^2 \sin k_2 b \sinh k_1 b = 0 . \tag{3.172}$$

For each value of n, Eq. (3.172) provides the m successive values of β (and, in turn, the eigenfrequencies ω). The same equations can then be used to calculate the eigenshape associated with each mode.

3.5.3.5 Piano Soundboard and Ribbed Structures

Ribbed plates and shells can be found in numerous vehicles (planes and ships) and in architecture. The prime function of ribs is to increase the rigidity of a given structure without increasing its mass too much. In Chap. 13, it will be shown that such a property also is desirable for enhancing the radiation efficiency of stringed instruments. For this reason, guitar and piano soundboards, for example, are reinforced by ribs (see Fig. 3.34). Another reason follows from static considerations. As mentioned in Chap. 1, wood is an orthotropic material. As a consequence, wooden plates are more rigid in the direction of the fibers than in the direction perpendicular to them, where they can break more easily. Therefore, if the purpose is to globally stiffen the soundboard, for dynamical and acoustical reasons, as well as to increase its breaking strength, then a good strategy consists is to glue the ribs perpendicular to the fibers.

In the case of the piano, the soundboard is also stiffened by the bridges, which are fixed on the upper side, where the strings are attached (see Fig. 1.1 in Chap. 1). The combination of the ribs and bridges has pronounced effects on the sound quality of a piano, as underlined by several studies and patents in the past decades [6, 14]. The exact nature of these effects was identified and quantified more accurately in recent studies [8, 13]. Let us consider, first, the simplified example of a ribbed plate whose geometry and material are comparable to those of an upright piano soundboard. As long as the modal frequencies remain lower than, say, 1 kHz, then the way the ribs are spaced has little effect on the global patterns of the modal shapes (see Fig. 3.35).

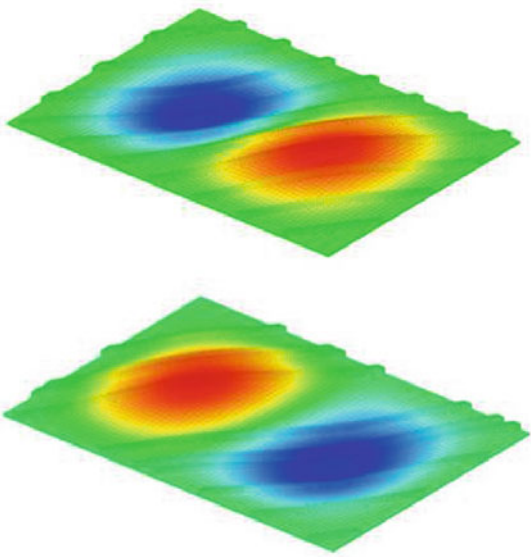

Fig. 3.35 Influence of the ribs on the modal shapes of the lowest modes of a ribbed soundboard. (*Top*) Regularly spaced ribs; (*Bottom*) Irregularly spaced ribs

For such an example, one can prove mathematically, with the help of homogenization techniques, that an equivalent homogeneous plate can be defined in this frequency range, with similar properties to the ribbed plate [5]. However, above a certain cutoff frequency (which is near 1.1–1.2 kHz for most upright pianos), the elastic half wavelength becomes of the same order of magnitude as the mean inter-rib distance. As a consequence, the soundboard zones between the ribs behave like "waveguides" bounded by the ribs, as seen on the modal shapes (see Fig. 3.36). At this stage, it is worth noting that the rib distance usually varies slightly on a soundboard. The calculation of the modes then shows that, even for slightly irregular rib spacing, the parts of the soundboard with significant amplitudes are restricted to a few inter-ribs zones only (see Fig. 3.36). This is the so-called localization of modes. Such localization effects resulting from small departures from exact periodicity are frequently encountered in physics. They have been intensively studied by Anderson [2]. These phenomena are often referred to as "Anderson's localization effects." On a piano soundboard, the localization is further enhanced by the presence of the bridges. As shown in Fig. 3.36d, only a section of one inter-rib spacing, situated in the region above the main bridge, vibrates significantly. For the frequency shown here (2149 Hz), the bridge appears to act as a supplementary boundary condition. Thus, the vibrational energy is confined in a section of one inter-rib zone

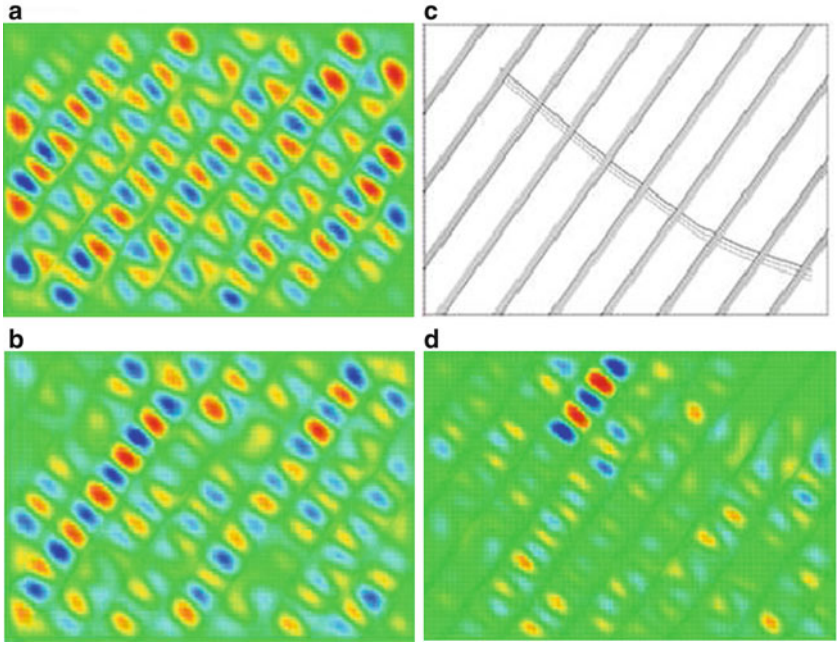

Fig. 3.36 Influence of rib spacing and bridge on the localization of modes for an upright piano soundboard. (**a**) Regular rib spacing; (**b**) Slightly irregular rib spacing; (**c**) Sketch of soundboard with bridge and ribs; (**d**) Increased localization of modes due to the bridge

only. It will be seen in Chap. 7 that the phenomenon is slightly different for wind instruments. Finally, in Chap. 14, the effects of mode localization on piano radiation and, particularly, on the directivity of the radiated field, will be presented.

3.5.4 Vibrations of Shells

As indicated for plates, a detailed study of the vibrations of shells is beyond the scope of this book. The interested reader will find more information in specialized books, such as [35].

3.5.4.1 Spherical Caps

In this section, the vibrations of a thin and shallow spherical cap are investigated. This structure illustrates the effect of a finite radius of curvature, compared with the case of thin circular plates. To a first approximation, it can be assumed that some percussion instruments, such as cymbals and gongs, can be modeled by such shells. We consider here that the vibrations are linear, so that we can use a modal approach. As a consequence, the presentation is restricted to the case of low stress, low strain, and small displacements compared with the shell thickness. As the displacement field of the shell becomes comparable or larger than the shell thickness, nonlinear vibrations will have to be considered, as developed in Chap. 8. In order to account for cymbals and gongs, the particular case of free boundary conditions is treated below. This problem is not commonly addressed in the literature [25].

We consider a spherical cap of thickness h, radius of curvature R, and whose plane projection is a circle of radius a (see Fig. 3.37). The hypotheses of Donnell–Mushtari–Vlasov (see Chap. 1) applied to the case of a thin ($h \ll a$) and shallow ($a \ll R$) shell yield the equation describing the free transverse bending motion $w(r, \theta, t)$ of the cap [35]:

$$D\nabla^4 w + \frac{Eh}{R^2} w + \rho h \ddot{w} = 0 \,, \tag{3.173}$$

where E is the Young's modulus, ρ the density, ν the Poisson's ratio, and $D = \frac{Eh^3}{12(1-\nu^2)}$ the rigidity factor. Equation (3.173) is equivalent to Eq. (1.88) shown in Chap. 1, but with the force function F removed. It is convenient to express this equation in a dimensionless form, through introduction of the reduced variables $\overline{w} = w/w_o$, $\overline{r} = r/a$ and $\overline{t} = t/t_o$ with $t_o = a^2\sqrt{\frac{\rho h}{D}}$. We get

$$\nabla^4 \overline{w} + \chi \overline{w} + \ddot{\overline{w}} = 0 \;\text{ where }\; \chi = 12(1-\nu^2)\frac{a^4}{R^2 h^2} \,. \tag{3.174}$$

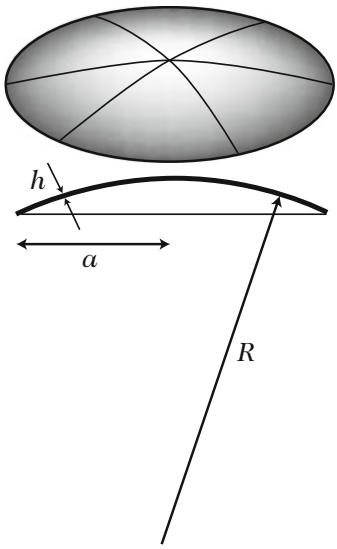

Fig. 3.37 A thin shallow spherical cap. R is the radius of curvature, a is the radius of the circle obtained by projection of the cap on a plane, and h is the thickness. The assumption of *thin* shell means $h \ll a$, and a *shallow* shell is such that $a \ll R$

Note 1: In the linear case, w_o can be chosen arbitrarily. This will not be the case for nonlinear vibrations, as seen in Chap. 8.
Note 2: In what follows, only the dimensionless equation is solved, but the overlines on the variables are omitted, for the sake of clarity.

3.5.4.2 Eigenmodes of a Spherical Cap with Free Edges

We look for solutions of Eq. (3.174) of the form $w(r,\theta,t) = \Phi(r,\theta)q(t)$. These solutions must satisfy one of the following conditions [23]:

$$\begin{cases} \text{If } \omega^2 - \chi = \zeta^4 > 0 \quad \text{then } \left[\nabla^4 - \zeta^4\right]\Phi = 0 \quad \textbf{case 1} \\ \text{If } \omega^2 - \chi = -\zeta^4 < 0 \text{ then } \left[\nabla^4 + \zeta^4\right]\Phi = 0 \quad \textbf{case 2} \end{cases} \tag{3.175}$$

In **case 1**, the eigenfunctions are given by:

$$\Phi_{nm}(r,\theta) = \left[A_n r^n + B_n J_n(\zeta_{nm} r) + C_n I_n(\zeta_{nm} r)\right] \begin{vmatrix} \cos m\theta \\ \sin m\theta \end{vmatrix} . \tag{3.176}$$

where A_n, B_n, and C_n are constants, ζ_{nm} are determined by the boundary conditions, J_n are the Bessel functions of the first kind, and I_n are the modified Bessel functions of the first kind [1].

In **case 2**, the eigenfunctions are given by:

$$\Phi_{nm}(r,\theta) = \left[A_n r^n + B_n \mathrm{ber}_n(\zeta_{nm} r) + C_n \mathrm{bei}_n(\zeta_{nm} r)\right] \begin{vmatrix} \cos m\theta \\ \sin m\theta \end{vmatrix} . \tag{3.177}$$

where ber_n and bei_n are the Kelvin's functions defined by [1]:

$$\mathrm{ber}_n(x) + j\mathrm{bei}_n(x) = J_n(x \exp(3j\pi/4)) \,. \tag{3.178}$$

For a free edge, the eigenvalues ζ_{mn} are determined by the boundary conditions (1.94) at $r = a$. Four different situations may occur [36]:

$$\begin{cases} \text{for } n \in \{0,1\}, \quad \forall m \geq 1 \quad \omega_{nm} = \sqrt{\chi + \omega_{nm}^{(0)2}} \\ \text{for } n \geq 2, \quad m = 0 \quad \text{and } \chi < \chi_n^{\lim} \quad \omega_{n0} = \sqrt{\chi + \zeta_{n0}^4} \\ \text{for } n \geq 2, \quad m = 0 \quad \text{and } \chi > \chi_n^{\lim} \quad \omega_{n0} = \sqrt{\chi - \zeta_{n0}^4} \\ \text{for } n \geq 2, \quad m \geq 1, \quad \omega_{nm} = \sqrt{\chi + \zeta_{nm}^4} \end{cases} \tag{3.179}$$

where $\omega_{nm}^{(0)}$ are the eigenfrequencies of a circular plate with free edges of radius a, corresponding to the limiting case of a cap with zero curvature (infinite radius of curvature). Figure 3.38 shows how the different eigenfrequencies of the cap vary as a function of the curvature parameter χ.

The limiting value of the parameter χ that makes the difference between "Bessel" modes and axisymmetric "Kelvin" modes is given by Johnson and Reissner [23]:

$$\chi_n^{\lim} = \frac{(1-\nu)(3+\nu)n^2(n^2-1)}{1 + \frac{1}{4}(1-\nu)(n-2) - \frac{n^2(n-1)(1-\nu)(4n-\nu+9)}{16(n+2)^2(n+3)}} \,. \tag{3.180}$$

Appendix: Modal Decomposition Using the Residue Calculus

One often needs to expand a transfer function $G(\omega)$ in the frequency domain onto a modal basis. In this case residue calculus is a powerful tool. It yields, in turn, the inverse Fourier transform $g(t)$ as a sum of damped sinusoids. We restrict ourselves to the simple, though frequently encountered, case where the poles of the function $G(\omega)$ are simple. These poles ω_n are generally complex. It is assumed here that their imaginary part is positive, so that the function $\exp(j\omega_n t)$ is decreasing for $t > 0$. The poles are therefore located in the upper complex half-plane. The result, shown below, is the following:

$$g(t) = j \sum_n R_n e^{j\omega_n t} \quad \text{for } t > 0, \tag{3.181}$$

with $g(t) = 0$ for $t < 0$. The quantities R_n are the residues defined for simple poles by:

$$R_n = \lim_{\omega \longrightarrow \omega_n} (\omega - \omega_n) G(\omega). \tag{3.182}$$

(continued)

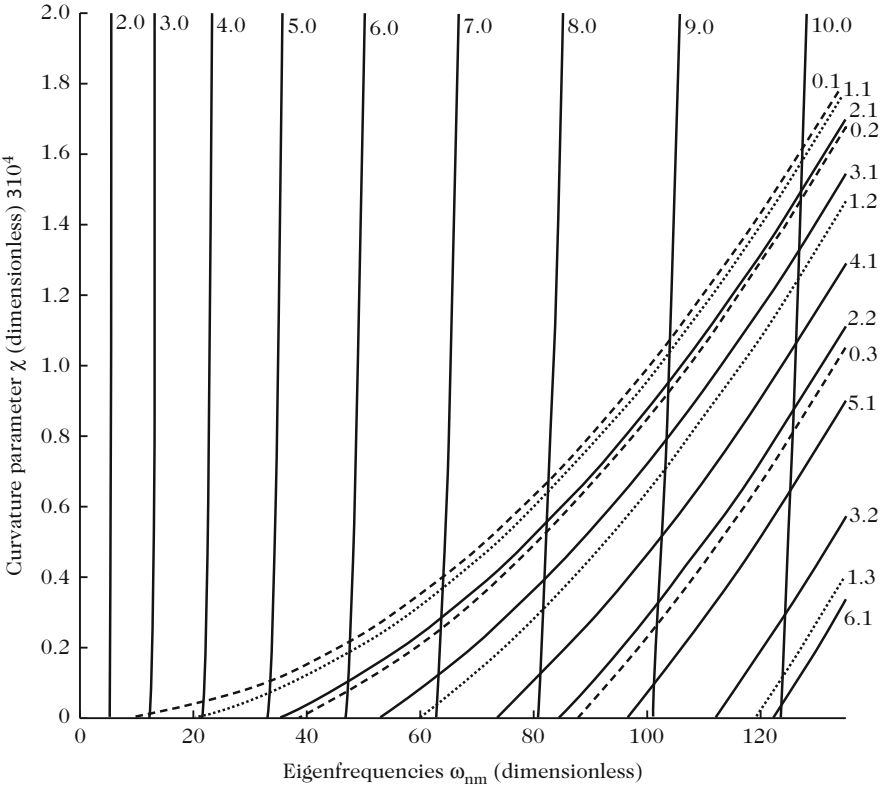

Fig. 3.38 Variations of the eigenfrequencies for a spherical cap with curvature parameter χ. Notice that the eigenfrequencies increase with χ, except for the modes ω_{n0} which remain almost unchanged

If $G(\omega) = N(\omega)/D(\omega)$, in order to calculate the residues, one only needs to write the denominator in the form[18] $D(\omega) \simeq (\omega - \omega_n)D'(\omega_n)$. As a consequence, we get

$$R_n = \frac{N(\omega_n)}{D'(\omega_n)}. \tag{3.183}$$

For the proof, we start from the definition of $g(t)$ [see Eq. (1.116)] :

$$g(t) = \frac{1}{2\pi}\int_{-\infty}^{+\infty} G(\omega)e^{j\omega t}d\omega. \tag{3.184}$$

(continued)

[18]We make sure that the numerator $N(\omega)$ and the denominator $D(\omega)$ have only zeros and no poles. Thus, the tangent function is written as the ratio sine/cosine.

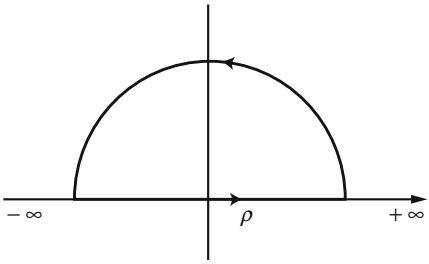

Fig. 3.39 Contour of the integral (3.185), equivalent to the integral on the real axis. The equivalence applies when the radius of the circle ρ tends to infinity, since the function to integrate on the circle tends to 0

The integration is carried out for a real ω, from $-\infty$ to $+\infty$, but we can convert it to a contour integral: as a consequence the integral on the contour presented in Fig. 3.39 is equal to the integral (3.184), when $t > 0$. The coordinate of a point located on the semi-circle of the complex plane can be written: $z = \rho\cos\theta + j\rho\sin\theta$, with $\sin\theta > 0$. When t is positive, and when the radius ρ of the circle tends to infinity, the quantity $G(z)e^{jzt}$ tends to 0, provided that the modulus of the function $G(z)$ tends sufficiently quickly to 0 as z tends to infinity (Jordan's lemma). The value of the contour integral on the semi-circle tends to 0, and this contour integral is the result that we were searching for.

The residue theorem states

$$\oint F(z)dz = 2\pi j \sum \text{Residues}(F(z)). \tag{3.185}$$

In this formula, the contour goes counterclockwise. We obtain

$$g(t) = j\sum \text{Residues}(G(\omega)e^{j\omega t}) = j\sum_n R_n e^{j\omega_n t}.$$

For $t < 0$, we can use the symmetrical contour with regard to the real axis. This contour is located in the lower half-plane, and since there are no poles in this half-plane, it is equal to 0. Given the choice made for the poles of $G(\omega)$, we find that $g(t)$ is causal.

In addition, since the function $g(t)$ is real, the poles are grouped by pairs: the existence of terms of the form $jR_n\exp(j\omega_n t)$ implies terms $-jR_n^*\exp(-j\omega_n^* t)$. Similarly, the existence of poles ω_n implies the poles $-\omega_n^*$ (which are also located in the upper half-plane).

Finally, taking the Fourier transform of (3.181) yields

$$G(\omega) = \sum_n \frac{R_n}{\omega - \omega_n} = \sum_n \frac{N(\omega_n)}{(\omega - \omega_n)D'(\omega_n)}. \tag{3.186}$$

(continued)

To prove this, we can apply the formula (3.181) to the function $R_n/(\omega - \omega_n)$, whose residue is R_n! When ω tends towards ω_n, only the nth-term of the series is relevant, since we have: $G(\omega) = N(\omega_n)/\left[(\omega - \omega_n)D'(\omega_n)\right] = N(\omega)/D(\omega)$.

A difficulty remains for the poles located on the real axis: the formula given for the poles located in the upper half-plane is valid, but the proof is more difficult (it uses the necessary causality of the function $g(t)$).

References

1. Abramowitz, M., Stegun, I.A.: Handbook of Mathematical Functions, with Formulas, Graphs, and Mathematical Tables. Dover, New York (1972)
2. Anderson, P.: Absence of diffusion in certain random lattices. Phys. Rev. **109**, 1492–1505 (1958)
3. Askenfelt, A., Jansson, E.V.: From touch to string vibrations. III: String motion and spectra. J. Acoust. Soc. Am. **93**(4), 2181–2196 (1993)
4. Axisa, F., Trompette, P.: Modelling of Mechanical Systems: Structural Elements. Elsevier, Oxford (2005)
5. Berthaut, J., Ichchou, M., Jézéquel, L.: Piano soundboard: structural behavior, numerical and experimental study in the modal range. Appl. Acoust. **64**, 1113–1136 (2003)
6. Bilhuber, P.H., Johnson, C.A.: The influence of the soundboard on piano tone quality. J. Acoust. Soc. Am. **11**(3), 311–320 (1940)
7. Boutillon, X.: Model for piano hammers: experimental determination and digital simulation. J. Acoust. Soc. Am. **83**(2), 746–754 (1988)
8. Boutillon, X., Ege, K.: Vibroacoustics of the piano soundboard: reduced models, mobility synthesis, and acoustical radiation regime. J. Sound Vib. **332**(18), 4261–4279 (2013)
9. Boutillon, X., Weinreich, G.: Three-dimensional mechanical admittance: theory and new measurement method applied to the violin bridge. J. Acoust. Soc. Am. **105**(6), 3524–3533 (1999)
10. Chaigne, A., Askenfelt, A.: Numerical simulations of piano strings. I. A physical model for a struck string using finite difference methods. J. Acoust. Soc. Am. **95**(2), 1112–1118 (1994)
11. Chaigne, A., Askenfelt, A.: Numerical simulations of piano strings. II. Comparisons with measurements and systematic exploration of some hammer-string parameters. J. Acoust. Soc. Am. **95**(3), 1631–1640 (1994)
12. Chaigne, A., Doutaut, V.: Designing and building a xylophone prototype (in French). Research report, ENST (1997)
13. Chaigne, A., Cotté, B., Viggiano, R.: Dynamical properties of piano soundboards. J. Acoust. Soc. Am. **133**(4), 2456–2466 (2013)
14. Conklin, H.A.: Soundboard construction for stringed musical instruments. US Patent 3866506 (1975)
15. Courant, R., Hilbert, D.: Methods of Mathematical Physics, vol. 1. Interscience Publishers, New York (1966)
16. Dautray, R., Lions, J.: Mathematical analysis and numerical methods for science and technology. In: Evolution Problems II, vol. 6. Springer, Berlin (2000)
17. Ege, K.: The piano soundboard: modal studies in the low- and mid-frequency range (in French). Ph.D. thesis, Ecole polytechnique, Palaiseau (2009)
18. Géradin, M., Rixen, D.: Mechanical Vibrations: Theory and Application to Structural Dynamics. Wiley, Chichester (1999)

19. Gibert, R.J.: Vibrations of Structures. Interaction with Fluids. Random Excitation Sources (in French). Eyrolles, Paris (1988)
20. Gillan, F.S., Elliott, S.J.: Measurement of the torsional modes of vibration of strings on instruments of the violin family. J. Sound Vib. **130**(2), 347–351 (1989)
21. Graff, K.F.: Wave Motion in Elastics Solids. Dover, New York (1991)
22. Hall, D.E.: Piano string excitation. VI: Nonlinear modeling. J. Acoust. Soc. Am. **92**(1), 95–105 (1992)
23. Johnson, M.W., Reissner, E.: On transverse vibrations of spherical shells. Q. Appl. Math. **15(4)**, 367–380 (1956)
24. Le Carrou, J.L.: Vibro-acoustics of the concert harp. Ph.D. thesis, Ecole doctorale de l'Université du Maine, Le Mans (2006). http://tel.archives-ouvertes.fr/
25. Liew, K.M., Lim, C.W., Kitipornchai, S.: Vibrations of shallow shells: a review with bibliography. Trans. ASME Appl. Mech. Rev. **8**, 431–444 (1997)
26. Meirovitch, L.: Fundamentals of Vibrations. McGraw-Hill, New York (2001)
27. Morse, P.M., Ingard, K.: Theoretical Acoustics. McGraw-Hill, New York (1968)
28. Orduna-Bustamante, F.: Nonuniform beams with harmonically related overtones for use in percussion instruments. J. Acoust. Soc. Am. **90**(6), 2935–2941 (1991)
29. Pickering, N.: Problems in string making. J. Catgut Acoust. Soc. **2**(3), 1–4 (1993)
30. Podlesak, M., Lee, A.R.: Dispersion of waves in piano strings. J. Acoust. Soc. Am. **83**(1), 305–317 (1988)
31. Politzer, D.: Banjo timbre from string stretching and frequency modulation. Acta Acust. United Acust. **101**(1), 1–4 (2015)
32. Renji, K., Nair, P., Narayanan, S.: Modal density of composite honeycomb sandwich panels. J. Sound Vib. **195**(5), 687–699 (1996)
33. Rossing, T.D.: Science of Percussion Instruments. World Scientific, Singapore (2000)
34. Schumacher, R.: Measurements of some parameters of bowing. J. Acoust. Soc. Am. **96**(4), 1985–1998 (1994)
35. Soedel, W.: Vibrations of Shells and Plates, 3rd edn. Marcel Dekker Inc., New York (2004)
36. Thomas, O., Touzé, C., Chaigne, A.: Non-linear vibrations of free-edge thin spherical shells: modal interaction rules and 1:1:2 internal resonance. Int. J. Solid Struct. **42**(1), 3339–3373 (2005)
37. Trautmann, L., Rabenstein, R.: Digital Sound Synthesis by Physical Modeling Using the Functional Transformation Method. Kluwer, New York (2003)
38. Valette, C., Cuesta, C.: Mechanics of the Vibrating String (in French). Hermès, Paris (1993)
39. Weinreich, G.: Coupled piano strings. J. Acoust. Soc. Am. **62**, 1474–1484 (1977)
40. Wilkinson, J.P.D.: Modal densities of certain shallow structural elements. J. Acoust. Soc. Am. **43**(2), 245–251 (1968)
41. Wolfe, J.: Music acoustics web page, the University of New South Wales. http://www.phys.unsw.edu.au/music/ (2007)
42. Woodhouse, J., Loach, A.: Torsional behaviour of cello strings. Acust. Acta Acust. **85**(5), 734–740 (1999)
43. Worland, R.: Chladni patterns on drumheads: a "physics of music" experiment. Phys. Teach. **49**(1), 24–27 (2011)
44. Yu, Y.Y.: Vibrations of Elastic Plates. Springer, New York (1996)

Chapter 4
Waves

Antoine Chaigne and Jean Kergomard

Abstract Wave analysis of the acoustic pressure field is shown to be a useful complement to modal analysis. In this chapter, many intuitive results are directly obtained in the time domain, by considering an impulse source and successive wave reflections at boundaries, for a one-dimensional medium. In the frequency domain, it is shown that the concept of input impedance (or admittance), of current use in musical acoustics, can be viewed as a generalized frequency response to a sinusoidal source. Furthermore, it is shown how infinite series of modes (resp. waves) can be avoided by using a closed-form of the responses, both in the time and frequency domain. For the sake of simplicity, 2D and 3D media are not considered, but the direct relationship between modes and waves is established for the particular case of a 1D medium. The chapter is mainly based on the example of a cylindrical tube, but all the results can be transposed to the case of a homogeneous string.

4.1 Introduction

Solutions of numerous differential equations encountered in musical acoustics have been given as modes in Chap. 3. In a *bounded* medium such as those studied (strings, pipes, bars, membranes, etc.), another way of studying the phenomena is to decompose the variables into expressions featuring successive reflected waves. Due to the very high number of reflections, such a decomposition would be heavy in a general medium with 2 or 3 dimensions; that is why the present chapter deals only with one-dimensional media. The aim of this chapter is to show how, for this simple case, we can go from one decomposition to another, which is often useful in musical acoustics. A particular case is that of periodic reflections, which correspond

A. Chaigne
Institute of Music Acoustics, University of Music and Performing Arts Vienna (MDW), Anton-von-Webern-Platz 1, 1030 Vienna, Austria
e-mail: antchaigne@gmail.com

J. Kergomard (✉)
CNRS Laboratoire de Mecanique et d'Acoustique (LMA), 4 impasse Nikola Tesla CS 40006, 13453 Marseille Cedex 13, France
e-mail: kergomard@lma.cnrs-mrs.fr

A. Chaigne, J. Kergomard, *Acoustics of Musical Instruments*, Modern Acoustics and Signal Processing, DOI 10.1007/978-1-4939-3679-3_4

to modes with harmonically related eigenfrequencies. The emphasis will be put on the time-domain representation. While it is less usual, it is essential for some applications such as calculation by multi-convolution (see [1]), or, in its discrete time version, for sound synthesis.

We still search for responses to a given source, with particular attention to two types of idealized excitations: pulse and sine function. Acoustic waves are chosen as illustrating examples. We limit ourselves to a homogeneous medium, keeping for Chap. 7 some examples of heterogeneous media or non-cylindrical tubes like horns. However, we will again take interest in the boundary conditions, which already lead to a great variety of situations. These boundary conditions can be absorbing, but the medium itself is supposed to be non absorbing (the case of absorbing media will be treated in Chap. 5). Finally, in addition to both the modal expansion and the decomposition into successive reflections, another general solution expressed in a closed-form, i.e., not in the form of an infinite series, will be presented.

4.2 Solutions Without Source, First Reflection

In Sect. 1.2.4 (Chap. 1) the general solution of the equation without a source has been written as the superposition of outgoing and incoming traveling waves:

$$p(x,t) = f^+(t - x/c) + f^-(t + x/c). \tag{4.1}$$

Actually, the reality here is described only in a quite abstract way. Generally, there is an infinity of incoming and outgoing waves because an infinity of reflections appear in a bounded medium. Mathematically, the sum of outgoing waves is again an outgoing wave, and similarly for the incoming waves. More precisely, it can be written[1] $f^+(t - x/c) = f^+(t) * \delta(t - x/c)$: thus every convolution of an outgoing wave by a function of time, independent of x, always leads to an outgoing wave. This is, for example, the case of a simple delay $\delta(t - \tau)$, or of a delay followed by two reflections, at each end.

- Conversely, a reflection at only one end (let us choose the right one, called ℓ) must transform an outgoing wave into an incoming wave (or vice versa for the left one), and a *reflection function* $r(x,t)$ appears such as:

$$\begin{aligned} r(x,t) * f^+(t) * \delta(t - x/c) &= f^-(t) * \delta(t + x/c) \quad \forall x, \\ \text{hence} \quad f^-(t) &= r(x,t) * f^+(t) * \delta(t - 2x/c). \end{aligned} \tag{4.2}$$

[1]The mathematically accurate notation would be $f^+(t - x/c) = \left[f^+ * \delta_{x/c}\right](t)$, but for numerous successive reflections, it would be very heavy. Let us highlight also that the FT of this expression is $F^+(\omega)\exp(-j\omega x/c)$.

If $f^+(t)$ is a pulse $\delta(t)$, the reflection function $r(x,t)$ is

$$r(x,t) = f^-(t) * \delta(t + 2x/c) = f^-(t + 2x/c). \tag{4.3}$$

We can define it as *the response in incoming wave to a pulse of outgoing wave*.

At the extremity $x = \ell$, the reflection function is known if the external medium is passive (it is equivalent to the termination impedance, the relation between the two quantities will be seen later): it will be denoted $r_\ell(t)$. By definition:

$$f^-(t + \ell/c) = r_\ell(t) * f^+(t - \ell/c) \ \ \forall t\,, \text{ or} \tag{4.4}$$

$$f^-(t) = r_\ell(t) * f^+(t) * \delta(t - 2\ell/c) \ \forall t\,. \tag{4.5}$$

Thus, with (4.2), as the convolution integral is commutative:

$$r(x,t) = r_\ell(t) * \delta\left[t - 2(\ell - x)/c\right]. \tag{4.6}$$

This result can be interpreted very easily: the outgoing wave in x propagates until the extremity ℓ, thus over the length $(\ell - x)$, where it is reflected according to $r_\ell(t)$, and propagates again in the other direction on the length $(\ell - x)$. This calculation can be done again in the frequency domain as an exercise.

Finally, it can be noticed that the reflection function for the flow rate is the opposite of the reflection function for the pressure. Actually, using the Euler equation, we have to differentiate the pressure (4.1) with respect to x, then integrate the result with respect to t: the general solution for the flow is linked to the one for the pressure through

$$u(x,t) = Z_c^{-1}\left[f^+(t - x/c) - f^-(t + x/c)\right]. \tag{4.7}$$

This expression is again written as a sum of incoming and outgoing waves, but the incoming function is different, implying the difference in reflection functions for pressure and flow. Thus, for a zero pressure at every moment at the end $\ell, f^- = -f^+$ at this point, and there is a (local) doubling of acoustic flow (and vice versa). Here $Z_c = \rho c/S$, because it is defined as the ratio of pressure/flow rate. It is the acoustic impedance, which differs from the specific acoustic impedance defined in Sect. 1.2.5 of Chap. 1.

4.3 Successive Reflections of Waves Produced by a Pulse Source

4.3.1 General Expression

In Chap. 1 it has been seen that an impulsive point source of flow can be created by a small piston placed on the pipe side in $x = x_s$ and moved suddenly at $t = 0$ from a height h [Eq. (1.134)]. The piston location is $hH(t)$, and the flow is $u_s(t) = S_m h\delta(t) = u_s\delta(t)$ (see Fig. 4.1). We will see that this is the Green's function's derivative with respect to time, and what its equivalent is for a plucked string.

- In an infinite pipe, this piston creates a plane pressure wave $Z_c u(t)$, where $Z_c = \rho c/S$ (S is the section of the pipe); but as the piston sees both parts (right and left) of the pipe indifferently, the flow is divided in two equal parts, and the pressure created in the pipe is

$$p_{\text{dir}}(x,t) = \frac{1}{2} Z_c u_s \delta(t - |x - x_s|/c). \tag{4.8}$$

  In this expression, the delay depends on the absolute value of the distance to the source only. Obviously, on the right of the source ($x > x_s$), this is an outgoing wave. On the other side, ($x < x_s$,) it is a "incoming" wave, with our nomenclature linked to the direction of the x-axis. The two waves (4.8) will be called *direct* waves.

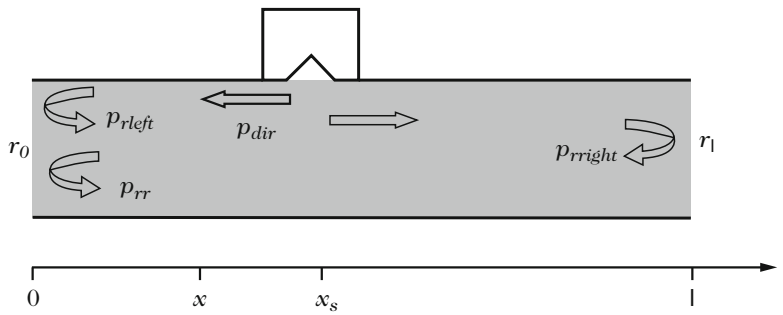

Fig. 4.1 Source of flow rate $u_s(t)$ located on a pipe side; it produces two direct pressure waves in opposite directions. These reflect at the ends characterized by the reflection functions, $r_0(t)$ and $r_\ell(t)$, linked to termination impedances, $Z_0(\omega)$ and $Z_\ell(\omega)$. The *labeled arrows* point out the four "primary" waves, which form the pattern reflecting periodically at each back and forth on the length ℓ, and are linked to the spatial form of modes (see Sect. 4.6.2)

- The direct left wave, p_{dir}, reflects in $x = 0$ (see Fig. 4.1), with the reflection function $r_0(t)$, and creates a reflected wave, p_{left}, which comes back to x:

$$p_{\text{left}}(x,t) = p_{\text{dir}}(0,t) * r_0(t) * \delta(t - x/c) = \frac{1}{2} Z_c u_s r_0(t) * \delta[t - (x + x_s)/c]. \tag{4.9}$$

- The direct right wave also reflects, in $x = \ell$, with the function $r_l(t)$, and comes back to x:

$$p_{\text{right}}(x,t) = p_{\text{dir}}(\ell,t) * r_\ell(t) * \delta[t - (\ell - x)/c] = \frac{1}{2} Z_c u_s r_\ell(t) * \delta[t - (2\ell - x - x_s)/c]. \tag{4.10}$$

- All the delays included in the three previous waves are lower than the time of a round trip in the pipe ($\tau = 2\ell/c$). Another wave remains, which reaches x before this time τ: the one that reflects at both ends. If $x < x_s$, it is the wave traveling to the right, and reflected first in $x = \ell$ then in $x = 0$. It is written:

$$p_{rr}(x,t) = p_{\text{right}}(x,t) * r_0(t) * \delta(t - 2x/c) = \frac{1}{2} Z_c u_s r_\ell(t) * r_0(t) * \delta[t - (2\ell + x - x_s)/c]. \tag{4.11}$$

In the case where $x > x_s$, the result is obtained by inverting x and x_s, i.e., by replacing $(x - x_s)$ by its absolute value. All the other reflections are obtained by considering each of these four "primary" waves, shifted by a round trip, two round trips, etc. Now a complete round trip acts as a convolution by the following function, independent of both the source and receiver positions,

$$g_{\text{RT}}(t) = r_\ell(t) * r_0(t) * \delta(t - 2\ell/c). \tag{4.12}$$

Finally, for a finite pipe the response to a flow pulse is found to be:

$$p(x,t) = p_{\text{primary}}(x,t) * \sigma(t) \tag{4.13}$$

where

$$\sigma(t) = \delta(t) + g_{\text{RT}}(t) + [g_{\text{RT}} * g_{\text{RT}}](t) + [g_{\text{RT}} * g_{\text{RT}} * g_{\text{RT}}](t) + \cdots \tag{4.14}$$

and

$$\begin{aligned} p_{\text{primary}}(x,t) = \frac{1}{2} Z_c u_s [&\delta(t - |x - x_s|/c) + r_0(t) * \delta[t - (x + x_s)/c] \\ &+ r_\ell(t) * \delta[t - (2\ell - x - x_s)/c] \\ &+ r_\ell(t) * r_0(t) * \delta[t - (2\ell - |x - x_s|)/c]]. \end{aligned} \tag{4.15}$$

The symmetry between the source and receiver abscissae can be noticed. We will see that it is possible to factorize the term of primary waves, resulting in the spatial dependency of modes.

4.3.2 Reflections and Modes Periodicity

The infinite series of round trips in the function $\sigma(t)$ (4.13) corresponds to a series of reflections occurring at periodic instants. For simple cases, we can deduce harmonically related eigenfrequencies, which are multiples of the lowest one. For example, for the case where $r_\ell(t) = r_0(t) = -\delta(t)$, the pipe being open at both ends,[2] this series is periodic, and is written

$$\sigma(t) = \sum_{n=0}^{+\infty} \delta(t - 2n\ell/c).$$

For negative times, $\sigma(t) = 0$, and the series can be written also:

$$\sigma(t) = H(t) \sum_{n=-\infty}^{+\infty} \delta(t - 2n\ell/c)$$

as the function $\delta(x)$ is null for strictly negative x. The infinite series is a Dirac comb, which is a periodic function; the Poisson formula enables to develop it in Fourier series:

$$\sigma(t) = \frac{c}{2\ell} H(t) \sum_{n=-\infty}^{+\infty} \exp(j\omega_n t) = \frac{c}{\ell} H(t) \sum_{n=0}^{+\infty} \cos(\omega_n t). \tag{4.16}$$

where $\omega_n = n\pi c/\ell$. We converted from waves to modes, because, by convoluting $\sigma(t)$ by the term of primary waves (i.e., the term between brackets, see Eq. (4.15)), which depends on x and x_s, the spatial dependency $p(x, t)$ can be found. Here is the result:

$$p(x, t) = \frac{c}{2\ell} H(t) \sum_{n=-\infty}^{+\infty} P_{\text{primary}}(x, \omega_n) \exp(j\omega_n t). \tag{4.17}$$

The calculation of $P_{\text{primary}}(x, \omega_n)$ is not given here: we simply wanted to illustrate in a simple way the change from waves into modes. We will see further more general

[2] This means that radiation impedance is ignored. The equivalent is a string fixed on a perfectly rigid support, acoustic pressure and string velocity being analogous.

methods to realize this kind of change when there is no periodicity. Using the present method, we see that Formula (4.17) remains valid for the case $r_\ell(t) = r_0(t) = \delta(t)$, which corresponds to a pipe closed at both ends, but with a different term $P_{\text{primary}}(x, \omega_n)$.

- Regarding the case $r_\ell(t) = -\delta(t)$, $r_0(t) = \delta(t)$, which corresponds to a closed–open pipe, we remark that the periodicity is different: the period is double, and the infinite series in (4.14) must be written as:

$$\sigma(t) = [\delta(t) - \delta(t - 2\ell/c)] * \sum_{n=0}^{+\infty} \delta(t - 4n\ell/c).$$

  The following mode decomposition is deduced, if $\omega_n = n\pi c/2\ell$:

$$p(x,t) = \frac{c}{4\ell} H(t) \sum_{n=-\infty}^{+\infty} P_{\text{primary}}(x, \omega_n) \left[1 - \exp(-2j\omega_n \ell/c)\right] \exp(j\omega_n t).$$

  It appears that the term between brackets is cancelled for even harmonics, and that again Formula (4.17) is found, but is limited to the odd harmonics. Let us note that the round trip function $g_{\text{RT}}(t)$ is important for the evolution of the system: Eq. (4.12) exhibits that no essential difference exists between the dissipation occurring at extremities, in the reflections, and the one occurring during propagation, modifying the Dirac function.

What has just been studied is the impulse response in pressure (at a pulse in flow rate); this is nothing other, more or less, than the Green's function, which will be studied now. This is a useful tool in many situations.

4.3.3 Remark on the Reflection Function (4.3)

If, at a given point, the excitation is a pulse of outgoing wave $f^+(t) = \delta(t)$, this means namely that the outgoing wave is null at this point for all positive times. This pulse reflects, for instance, at $x = \ell$, and the reflection function (4.3) simply is the incoming wave at the x point: there is only an incoming wave. No other successive reflections occur, otherwise the outgoing wave would not be impulsive! In other words, a termination without echo has been put at the pipe entry, which produces the impedance of an incoming wave[3](the acoustic impedance is $\rho c/S$) .

[3]This impulsive outgoing wave cannot be realized with a small lateral piston, as the flow pulse divides into two: an outgoing wave (or more generally right wave) and an incoming one (or more generally left one). Thus the response to the outgoing wave must include the incoming wave coming back from $x = \ell$, but also the incoming wave directly from the source (about this matter, see [1]).

4.4 One-Dimensional Green's Function

4.4.1 Expression of the Green's Function

Equation (1.134) has been solved, and can be written as follows:

$$\frac{\partial^2 p}{\partial x^2} - \frac{1}{c^2}\frac{\partial^2 p}{\partial t^2} = -\frac{\rho}{S}u_s \frac{d\delta(t)}{dt}\delta(x - x_s). \tag{4.18}$$

Now the Green's function, the solution of the wave equation for an elementary source, is solution of the following equation:

$$\left[\frac{\partial^2}{\partial x^2} - \frac{1}{c^2}\frac{\partial^2}{\partial t^2}\right] g(x, t|x_s, 0) = -\delta(t)\delta(x - x_s), \tag{4.19}$$

if the source emission time is $t_0 = 0$ (otherwise, t can just be replaced by $t - t_0$ in this equation). Up to the constant multiplicative factor $\rho u_s/S$, the solution for the time derivative of the Green's function in a finite pipe has been found above. In order to obtain the Green's function itself, Eq. (4.13) must be integrated, i.e., one of the convolution integral factors must be integrated: thus the functions δ are replaced by step functions H in (4.15). Doing this, a condition is imposed on the Green's function: it needs to be null for negative times as must its first derivative, as already shown in Chap. 2. Its value can be written as:

$$g(x, t|x_s, 0) = g_{\text{primary}} * \left[\delta(t) + g_{\text{RT}}(t) + \left[g_{\text{RT}} * g_{\text{RT}}\right](t) + \ldots\right], \tag{4.20}$$

where

$$\begin{aligned} g_{\text{primary}} = \frac{c}{2}[&H(t - |x - x_s|/c) + r_0(t) * H[t - (x + x_s)/c] \\ &+ r_\ell(t) * H[t - (2\ell - x - x_s)/c] \\ &+ r_\ell(t) * r_0(t) * H[t - (2\ell - |x - x_s|)/c]]. \end{aligned} \tag{4.21}$$

It is the one-dimensional Green's function. Two other very useful expressions can be found: the first one is a closed-form expression, see Sect. 4.6, and the second one is the modal expansion, already studied above.

4.4.2 Approximated "Practical" Realization

An intuitive idea of the Green's function, or at least of its first derivative, is easily obtained with the excitation on the pipe side [Expression (4.13)]. Figure 4.2 shows this derivative for the case $x = x_s = 0$, which is the response of a cylinder-shaped

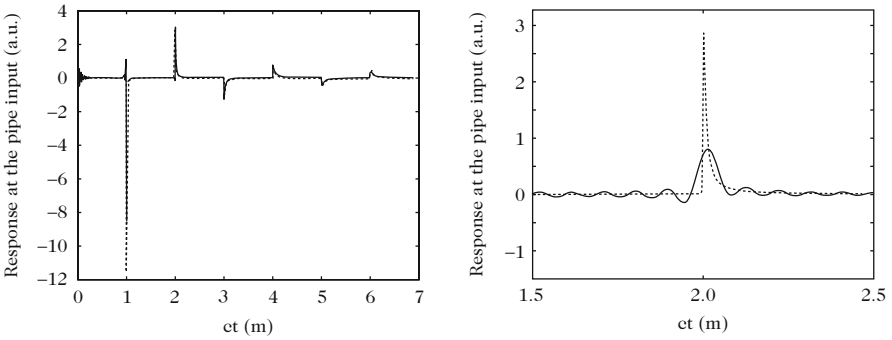

Fig. 4.2 Example of a pressure response in a tube to a sudden closing at input; the pipe is open at the output, where the pressure wave reflects with a change in sign, and closed at the input (after excitation), where the pressure signal is received. Visco-thermal effects, studied in Chap. 5, are taken into account for better realism, by replacing the functions $\delta(t)$ in (4.13) by the functions given by (5.148). The first pulse $\delta(t)$ at $t = 0$, unaffected by dissipation, has been omitted. The *dotted line* corresponds to (4.13); the *solid line* corresponds to the modal expansion, derived from (4.53) when losses are ignored (the expression will be given in Chap. 5). The modal series being truncated (to the first 200 modes), oscillations appear before each peak, corresponding to the Gibbs phenomenon. This phenomenon is well known in the sum of Fourier series. It is even clearer on the *right figure*, showing a zoom of the second peak, for a summation over ten modes only. The pipe dimensions are: radius 4 mm and length $\ell = 50$ cm

instrument to a sudden closing at the entry. This response is the inverse Fourier transform of the input impedance. In order to make it more realistic, dissipation has been taken into account. This kind of response can also be realized approximatively at any point x_s by closing suddenly a hole placed at this point: because of dissipation, the obtained sound decreases quickly, but it is possible to hear the frequency clearly. It is familiar to the instrumentalists, and is the equivalent of pizzicato for bowed-string instruments. The obtained frequency corresponds roughly to $c/4\ell_{\text{eff}}$, where ℓ_{eff} is the pipe length upstream to the first open hole.

Turning our attention to strings, this intuitive idea is also very simple. The string can be regarded as plucked by a force applied at point x_s, and stopped at $t = 0$, as shown before for a single- degree-of-freedom oscillator in Chap. 1. The only difference is that the excitation now is a force per unit length. The equation of strings with a source term can be used [see Eq. (3.25)]:

$$\left[\frac{\partial^2}{\partial x^2} - \frac{1}{c^2}\frac{\partial^2}{\partial t^2}\right] y(x,t) = -\frac{h}{\ell\beta(1-\beta)} H(-t)\delta(x - x_s), \tag{4.22}$$

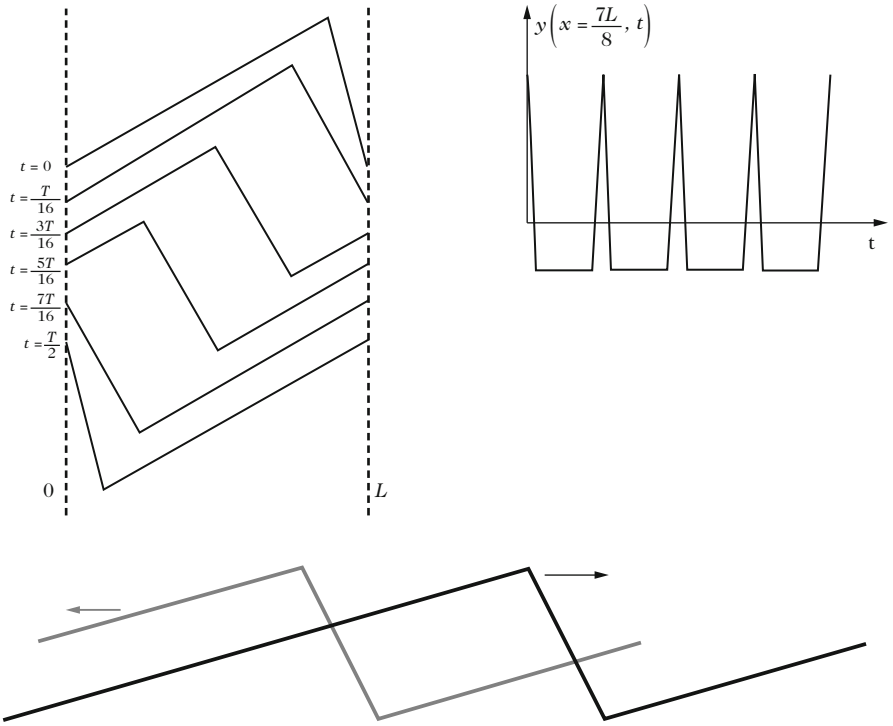

Fig. 4.3 The shape of a string plucked at the 7/8th of its length and released without initial velocity is shown at successive times $t = 0,\ T/16,\ 3T/16,\ 5T/16,\ 7T/16$, and $T/2$ (*left, top*). To obtain these lines in the interval $[0, L]$ bounding the string, at each chosen time, the contributions of the two waves propagating in opposite direction from each others, and reflecting with a change in sign at the ends, are added (see *bottom figure*). By plotting as a function of time the successive values taken by the string at a given position (here in $x = 7L/8$), the shape of the displacement wave is obtained for this position (*right, top*) and can be compared to Fig. 3.6 of Chap. 3

where $\beta = x_s/\ell$ (in the static regime, the force must compensate for the unbalanced tension force in x_s). Thus, up to a constant, the string velocity is the Green's function in this problem, and the acceleration is the time derivative of the Green's function: the string-tube analogy (see Table 1.1) works here only up to a time derivative for the source. Thus the acceleration is a succession of pulses, velocity is a succession of steps, and displacement is a succession of corners (see Fig. 4.3).

The Case of an Infinite String: D'Alembert Equation

The above section is concerned with a string of finite length and an impulsive excitation. An interesting calculation, due to d'Alembert, enables us to easily

(continued)

determine the displacement of an infinite string whose initial conditions, $y_0(x)$ and $v_0(x)$, are known. A method consists in putting the Green's function into an integral equation. Another simpler method is the following: when there is no source, the displacement can be written as [see (4.1)]:

$$y(x,t) = f^+(x-ct) + f^-(x+ct).$$

hence, by differentiating with respect to time:

$$v(x,t) = -c\dot{f}^+(x-ct) + c\dot{f}^-(x+ct).$$

At time $t = 0$, the displacement is

$$y_0(x) = f^+(x) + f^-(x)\ ;\ v_0(x)/c = -\dot{f}^+(x) + \dot{f}^-(x).$$

The second relation gives

$$\frac{1}{c}\int_{-\infty}^{x} v_0(x_0)dx_0 = -f^+(x) + f^-(x).$$

Hence:

$$2f^{\pm}(x) = y_0(x) \mp \frac{1}{c}\int_{-\infty}^{x} v_0(x_0)dx_0$$

and finally

$$y(x,t) = \frac{1}{2}\left[\frac{1}{c}\int_{x-ct}^{x+ct} v_0(x_0)dx_0 + y_0(x-ct) + y_0(x+ct)\right]. \tag{4.23}$$

4.5 Solutions Without Source in the Frequency Domain; Transmission Lines

Before calculating the Green's function in the frequency domain, some classical notions and results, namely the concept of *projected impedance* from one point to another, are reviewed. We start from Eq. (4.1) written in the frequency domain:

$$P(x,\omega) = P^+(\omega)e^{-jkx} + P^-(\omega)e^{jkx}. \tag{4.24}$$

There are two complex coefficients, $P^{\pm}(x)$, depending on frequency, which will be shown[4] to be the Fourier transforms of $f^{\pm}(t)$. The ratio between the two waves is called *reflection coefficient* $R(\omega)$:

$$R(x,\omega) = \frac{P^-}{P^+} e^{2jkx}. \tag{4.25}$$

This coefficient's amplitude is independent of x, contrary to its argument. If each member is multiplied by P^+, this equation is none other than the Fourier transform of Eq. (4.2): $R(x,\omega)$ is the transform of $r(x,t)$. The solution can also be written for the velocity (which is itself the solution of the same equation as for the pressure), or for the flow [see Eq. (4.7)]:

$$U(x,\omega) = Z_c^{-1}\left[P^+ e^{-jkx} - P^- e^{jkx}\right]. \tag{4.26}$$

Equivalently, general solutions for pressure and flow can be rewritten by replacing P^+ and P^- (which depend only on frequency and are constant in x) by the flow and pressure values in $x = 0$, denoted $P_0 = P(0,\omega)$ and $U_0 = U(0,\omega)$, and using a simple expansion of the exponential functions in sine and cosine:

$$\begin{cases} P(x,\omega) = P_0 \cos kx - U_0 Z_c j \sin kx \\ U(x,t) = -P_0 Z_c^{-1} j \sin kx + U_0 \cos kx. \end{cases} \tag{4.27}$$

A generalization to x_1 and x_2 abscissae, with obvious notations, leads to the following formula:

$$\begin{pmatrix} P_1 \\ U_1 \end{pmatrix} = \begin{pmatrix} \cos\left[k(x_2 - x_1)\right] & Z_c j \sin\left[k(x_2 - x_1)\right] \\ Z_c^{-1} j \sin\left[k(x_2 - x_1)\right] & \cos\left[k(x_2 - x_1)\right] \end{pmatrix} \begin{pmatrix} P_2 \\ U_2 \end{pmatrix}. \tag{4.28}$$

This relation is of the "*transfer matrix*" kind: if the (flow, pressure) vector is known at a point x_2, it is known everywhere else. Instead of two constants for one scalar quantity, there is only one constant for a vector quantity. This formalism is called "transmission line" formalism: it is based upon first-order differential equations [see Eqs. (1.109) and (1.110)], for a vector quantity. It will be used efficiently when the damping in pipes is treated. In particular it allows us to write a relation for the impedance:

$$Z_1/Z_c = \frac{j \tan\left[k(x_2 - x_1)\right] + Z_2/Z_c}{1 + j \tan\left[k(x_2 - x_1)\right] Z_2/Z_c} = j \tan\left[k(x_2 - x_1) + \eta_2\right] \tag{4.29}$$

where

[4]The Fourier transform of Eq. (4.1) is calculated by doing the following variable change in the integral: $t' = t \mp x/c$.

$$\eta_2 = -\arctan(jZ_2/Z_c), \text{ hence } j\tan\eta_2 = Z_2/Z_c. \tag{4.30}$$

The impedance at point x_1 is called the impedance *projected* from point x_2. If the impedance is purely imaginary at a point, it is purely imaginary everywhere, because of energy conservation: if there is no power at a point, there is power nowhere. A similar equation is obtained for the admittance, replacing Z/Z_c by Y/Y_c. For a cylinder-shaped pipe, the duality is perfect between pressure and flow rate (similarly for a homogeneous string, duality is perfect between velocity and force exerted on one side). Equations (4.24) and (4.26) also show that the impedance depends on one constant only, which is none other than the reflection coefficient:

$$\frac{Z(x,\omega)}{Z_c} = \frac{1+R(x,\omega)}{1-R(x,\omega)}. \tag{4.31}$$

The inverse relationship is found to be:

$$R(x,\omega) = \frac{Z(x,\omega)/Z_c - 1}{Z(x,\omega)/Z_c + 1}. \tag{4.32}$$

The result (4.29) is important: in a medium without source, if the impedance is known at a point, it is known everywhere. Thus, for a wind instrument, whose source is at the input, the impedance seen by the source is easily deduced when the termination impedance is known. For instance, if the radiation impedance in infinite space[5] is simplified in $Z_\ell = 0$, the input impedance is $Z_c j\tan k\ell$. The input impedance of an open cylinder is shown in Figs. 4.4 and 4.5: because of losses the maxima are not infinite; this will be explained in Chap. 5. If, as a first rough estimate, the frequencies of a cylindrical clarinet can be said to correspond to the input impedance maxima,[6] they are found to be: $(2n+1)c/4\ell$. For a cylinder-shaped flute, they correspond to minima, and are $nc/2\ell$. For a closed flute, such as bourdon pipes of organs or panpipes, the termination impedance is infinite, and the frequencies are the same as for a cylindrical clarinet. It can finally be noted that calculating the *upstream* reflection coefficient is very easy, thanks to (4.24):

$$R_1 = R_2 e^{-jk(x_2-x_1)}. \tag{4.33}$$

This section does not detail all classical results for pressure and velocity maxima and minima, impedance measurement, especially using Kundt's tube, Smith chart, etc. (see, e.g., [5]).

[5] At the open end of a pipe, the impedance is set by the fact that the external medium is passive. It is called radiation impedance. We will come back to this quantity in the fourth part of the book, but for now it is supposed to be zero for the sake of simplicity: the external medium is so huge compared to the pipe that the pressure does not vary much there.

[6] Actually, Chap. 9 will explain more precisely that there are frequencies canceling the imaginary part of admittance.

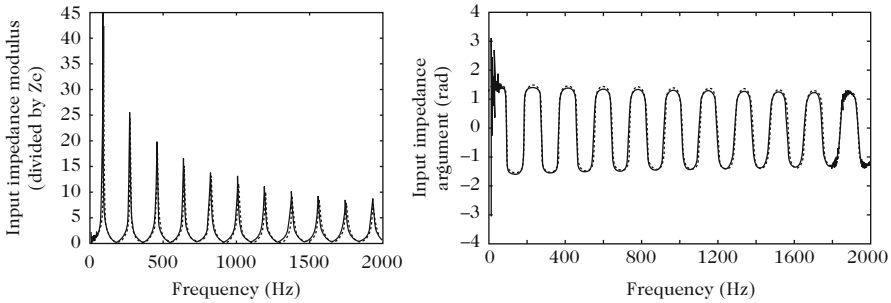

Fig. 4.4 Input impedance of a cylinder (the *left plot* shows the modulus and the *right plot* shows the argument). Experimental (*solid line*) and theoretical (*dotted line*) results. The radius is 10.7 mm and the length is 92.8 cm

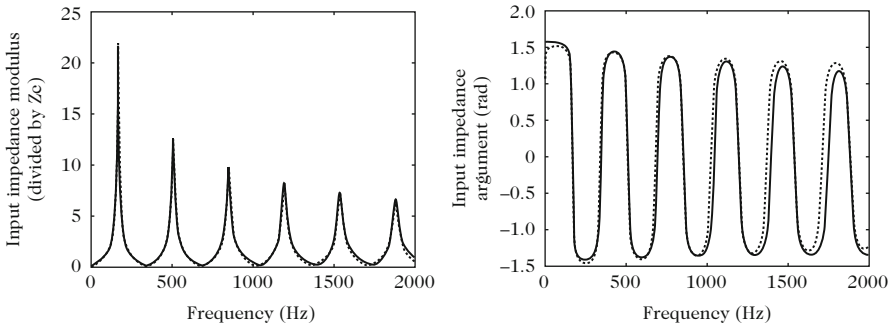

Fig. 4.5 Input impedance of a cylinder: theoretical results, without radiation ($Z_2 = 0$). This figure represents the Fourier transform of the response for the same pipe as this of Fig. 4.2. *Dotted line* corresponds to the closed-form expression (4.29), visco-thermal effects being taken into account (see Eq. (5.144) at first order). *Solid line* corresponds to the sum of ten modes [see Eq. (5.168)]. The *left plot* shows the modulus and the *right plot* shows the argument

4.6 Green's Function in Sinusoidal Regime: the Particular Case of the Input Impedance

4.6.1 Closed-Form Solution of the Green's Function

Results presented in the previous section show that the pipe input impedance is known thanks to the passive character of the pipe, and with the hypothesis that only plane waves propagate in it, or more generally, that propagation is one-dimensional. Using an impedance projected towards the source can seem to be odd, as causality suggests the calculation of the acoustic quantities from the source, but it must be recalled that the sinusoidal regime is a steady state, and not a transient one: therefore, there is energy in the whole space. The impedance, and all transfer

functions between input and output quantities, are known as soon as the termination impedance is known, as it can be remarked by observing the matrix equation (4.28). Then, if the input quantities are known, the output flow can also be calculated, and it gives access to the sound radiated outside. All that is written here applies even if the source is located upstream of abscissa x_1, and whatever else is upstream of x_1, such as discontinuities or side holes: all the transfer functions between any pair of abscissae are set by the fact that the pipe is passive, and the termination impedance is set by the fact that the surrounding space is passive.

- A flow rate source is now considered on the pipe side at a point x_s, as it has been done for the impulse regime (see Fig. 4.1). For that purpose, the Fourier transform of Eq. (4.18) is calculated

$$\frac{\partial^2 P(x,\omega)}{\partial x^2} + \frac{\omega^2}{c^2} P(x,\omega) = -j\omega \frac{\rho}{S} U_s(\omega)\delta(x - x_s). \tag{4.34}$$

  For the case where $u_s(t) = u_s\delta(t)$, this gives $U_s(\omega) = u_s$ (the source amplitude is constant, independent of frequency): $P(x,\omega)$ is the Green's function in the frequency domain $G_\omega(x, x_s)$, apart from the multiplicative factor $j\omega\frac{\rho}{S}U_s$, and $G_\omega(x, x_s)$ is the Fourier transform of $g(x, t|x_s, 0)$ [Eq. (4.19)].

The flow U_s is divided into two flows, $U_s = U_s^+ - U_s^-$, the minus sign coming from the fact that the flows are calculated towards a surface whose outside normal is in the positive x direction. These flow rates depend on the boundary conditions at both ends, linked to the reflection coefficients $R_0(\omega)$ and $R_\ell(\omega)$, which are the Fourier transforms of the reflection functions $r_0(t)$ and $r_\ell(t)$. In other words, these coefficients are linked to the termination impedances, satisfying conditions like (4.32). Using the matrix relation (4.28) between x_s and x, for the case where $x > x_s$, and projecting the termination admittance back to x, then gives

$$\frac{P}{U_s^+} = \frac{Z_c}{j\sin\left[k(x - x_s)\right] + \cos\left[k(x - x_s)\right] Y/Y_c} \text{ with } Y/Y_c = \frac{j\tan\left[k(\ell - x)\right] + Y_\ell/Y_c}{1 + j\tan\left[k(\ell - x)\right] Y_\ell/Y_c}. \tag{4.35}$$

It remains to calculate the same ratio P/U_s^-, and to deduce P/U_s, but the calculation using impedances is stopped here, because it is easier to use reflection coefficients in order to make the link to the time domain. On both sides of the source, the solution is written as in (4.24), but the constants are different. For the sake of simplicity, the constants are chosen as follows:

$$P(x,\omega) = A^+\left[e^{-jkX} + B^+ e^{jkX}\right], \quad \text{where } B^+ = R_\ell e^{-2jk(\ell - x_s)} \text{ if } X > 0\,; \tag{4.36}$$

$$P(x,\omega) = A^-\left[B^- e^{-jkX} + e^{jkX}\right], \quad \text{where } B^- = R_0 e^{-2jkx_s} \quad \text{if } X < 0. \tag{4.37}$$

where $X = x - x_s$. At $x = x_s$, pressure continuity and flow conservation $U_s = U_s^+ - U_s^-$ can be written. After some calculations[7] the following result is obtained:

$$P = \frac{P_{\text{primary}}}{1 - g_{\text{RT}}(\omega)}, \tag{4.38}$$

$$\text{where } g_{\text{RT}}(\omega) = R_\ell R_0 \exp(-2jk\ell) \tag{4.39}$$

$$\text{and } P_{\text{primary}}(\omega) = \frac{1}{2} Z_c U_s e^{-jk\ell} \times \left[e^{jk(\ell - x)} + R_\ell e^{-jk(\ell - x)}\right]\left[e^{jkx_s} + R_0 e^{-jkx_s}\right] \text{ if } x > x_s. \tag{4.40}$$

Similarly, it can be shown that inverting x and x_s is sufficient to obtain the result for the case where $x < x_s$. It can be verified that P_{primary} is the Fourier transform of $p_{\text{primary}}(x, t)$ [see Eq. (4.15)] when $U_s(\omega) = u_s$. It may be noted that a factorization of the square brackets involved in (4.15) has been found. This factorization distinguishes two cases corresponding to the respective positions of source and receiver.

- It remains to be checked that the result (4.38) is indeed the Fourier transform of the result expressed in (4.13). $g_{\text{RT}}(\omega)$ is the transform of $g_{\text{RT}}(t)$. For the case where $|g_{\text{RT}}(\omega)|$ is less than unity,[8] the factor including $g_{\text{RT}}(\omega)$ can be replaced by:

$$\frac{1}{1 - g_{\text{RT}}(\omega)} = 1 + g_{\text{RT}}(\omega) + g_{\text{RT}}^2(\omega) + g_{\text{RT}}^3(\omega) + \cdots \tag{4.41}$$

  Reflections for a complete round trip are found again.

  Another equivalent expression for Eq. (4.38) is useful:

$$P(x, x_s) = jZ_c U_s \frac{\sin\left[k(\ell - x) + \eta_\ell\right] \sin\left[kx_s + \eta_0\right]}{\sin\left[k\ell + \eta_0 + \eta_\ell\right]} \text{ if } x > x_s, \tag{4.42}$$

[7] At $x = x_s$, it is written:

$$P(x_s, \omega) = A^+\left[1 + B^+\right] = A^-\left[B^- + 1\right]; Z_c U_s^+(\omega) = A^+\left[1 - B^+\right]; Z_c U_s^-(\omega) = A^-\left[B^- - 1\right].$$

The total admittance at the source point is the sum of the upstream admittances on both sides:

$$Z_c \frac{U_S}{P_S} = \frac{1 - B^+}{1 + B^+} - \frac{B^- - 1}{B^- + 1}.$$

This leads to the value of $P_s = A^+\left[1 + B^+\right]$ as a function of U_S. This yields A^+, and the final result thanks to (4.36).

[8] This condition assumes that one of the ends is absorbing: thus, either $|R_0|$ or $|R_\ell|$ is smaller than unity. Equation (4.38) remains valid when damping occurs during propagation (This is studied in details in the next chapter), i.e., when jk is replaced by $jk + \alpha$, where α is positive. This is a third case, where $|g_{\text{RT}}(\omega)| < 1$. If there is an energy source at one extremity, or during propagation, this condition implies that globally the round trip must be dissipative, damping prevailing over energy supply.

with

$$R_\ell = -e^{-2j\eta_\ell} \quad \text{where} \quad Z_\ell/Z_c = j\tan\eta_\ell \tag{4.43}$$
$$\text{and } R_0 = -e^{-2j\eta_0} \quad \text{where} \quad Z_0/Z_c = -j\tan\eta_0.$$

For a zero termination impedance, the quantity η is zero; for an infinite impedance $\eta = \pi/2$. Generally η is real if the impedance is purely imaginary. If both terminal impedances are purely imaginary (energy conservation), the ratio P/U_s is purely imaginary whatever x is. In other words all pressures are in phase or in anti-phase. The waves are thus standing waves in the sense that they do not transport any energy from one point to another: the power supplied by the source $\frac{1}{2}\Re e\left[P_s U_s^*\right]$ is zero.

- It is also possible to deduce the Green's function in the frequency domain, which is the solution of the Fourier transform of Eq. (4.19):

$$\left[\frac{\partial^2}{\partial x^2} + k^2\right] G_\omega(x, x_s) = -\delta(x - x_s). \tag{4.44}$$

Dividing the result (4.38) by $j\omega\frac{\rho}{S}U_s$, yields[9]

$$G_\omega(x, x_s) = \frac{G_{\omega,\text{primary}}}{1 - R_\ell R_0 \exp(-2jk\ell)}, \tag{4.45}$$

where

$$G_{\omega,\text{primary}} = \frac{1}{2jk} e^{-jk\ell}\left[e^{jk(\ell-x)} + R_\ell e^{-jk(\ell-x)}\right]\left[e^{jkx_s} + R_0 e^{-jkx_s}\right] \quad \text{if } x > x_s. \tag{4.46}$$

Finally, we get

$$G_\omega(x, x_s) = \frac{1}{k}\frac{\sin\left[k(\ell - x) + \eta_\ell\right]\sin\left[kx_s + \eta_0\right]}{\sin\left[k\ell + \eta_0 + \eta_\ell\right]} \text{ if } x > x_s. \tag{4.47}$$

If both termination impedances are purely imaginary (energy conservation), the Green's function is real. This closed-form solution (4.47), which is not decomposed in terms of modes or successive reflections, is very useful; it will be used, for example, in the calculation of a modal expansion with absorbing end conditions (through residue calculus), and its time domain version presented

[9] This calculation is equivalent to write the solution at both the right and left side of the source, together with the continuity of the solution at $x = x_s$, and the jump of the first spatial derivative due to the function $\delta(x - x_s)$, as it has been done for the time variable of the single-degree-of-freedom oscillator (Chap. 2 Sect. 2.2.2).

in Sect. 4.6.4 will be used for the transient calculations of violins and wind instruments (see Part III of this book). Unfortunately, this closed-form exists only when the problem depends on a unique space coordinate.

4.6.2 Modal Expansion

Returning back to the modal expansion can be made in several ways: either using mode orthogonality, when the modes are proved to be orthogonal (see Chap. 3), or using the residue calculus (by calculating the inverse Fourier transform), or using the Poisson formula, which will not be developed here. The present section will be limited to three canonical cases for which the use of three methods is possible: open–open pipe, closed–closed pipe, and closed–open pipe (or the equivalent for a string).

4.6.2.1 Mode Orthogonality

This section begins with the use of mode orthogonality, as previously used to obtain Eq. (3.46), however, considering the Fourier domain first (both are equivalent, as the boundary conditions studied here are independent of frequency). Modes $\Phi_n(x)$ are solutions of Eq. (4.44) without the right-hand side member, and with the same boundary conditions as the Green's function, which are written according to the Euler equation:

$$\frac{Z_0}{Z_c}\frac{\partial G_\omega}{\partial x} = jkG_\omega \text{ and } \frac{Z_\ell}{Z_c}\frac{\partial G_\omega}{\partial x} = -jkG_\omega. \tag{4.48}$$

The differential equation and the condition at $x = 0$ impose

$$\Phi_n(x) = \sin(k_n x + \eta_0) \tag{4.49}$$

and the condition at $x = \ell$ implies that, if n is an integer, eigenfrequencies satisfy

$$k_n \ell = -\eta_0 - \eta_\ell + n\pi. \tag{4.50}$$

For the studied cases, only positive or zero values of n are considered.

- For an *open–open* pipe, $\eta_0 = \eta_\ell = 0$, and the mode $-n$ is the same as the mode n (it should be recalled that modes have an amplitude defined up to a multiplicative factor!), and there is no mode 0 here ($k_0 = 0$), because of the boundary conditions implying the nullity of the studied physical quantity. For that case, the eigenfrequencies are $nc/2\ell$.

- For a *closed–open* pipe, $\eta_0 = \pi/2$, $\eta_\ell = 0$, the mode $-n$ is the same as the mode $n+1$: the negative or zero indices give the same modes as the positive indices, and the eigenfrequencies are $(2n-1)c/4\ell$.
- For a *closed–closed* pipe, $\eta_0 = \pi/2$, $\eta_\ell = \pi/2$, modes $-n$ and $n+2$ are identical, the eigenfrequencies are the same as for the open–open case (this is due to the symmetry of the problem) but here the constant mode exists ($k_1 = 0$).

The orthogonality of modes is very simple here, because the pipe is homogeneous:

$$\int_0^\ell \Phi_n(x)\Phi_m(x)dx = \frac{\ell}{2}\delta_{nm}. \tag{4.51}$$

(The norm is ℓ for the constant mode). Seeking the solution of (4.44) in the form $G_\omega(x,x_s) = \sum_n A_n\Phi_n(x)$, orthogonality gives, in a way similar to that of Chap. 3:

$$G_\omega(x,x_s) = \frac{2c^2}{\ell}\sum_{n>0}\frac{\Phi_n(x)\Phi_n(x_s)}{\omega_n^2-\omega^2} + \left[-\frac{c^2}{\ell\omega^2}\right]. \tag{4.52}$$

The term in brackets corresponds to the constant mode that exists only in the closed–closed case. In Chap. 2, the inverse transform of the Green's function (2.16) was given in (2.14), hence:

$$g(x,t|x_s,0) = \frac{2c^2}{\ell}H(t)\sum_{n>0}\Phi_n(x)\Phi_n(x_s)\frac{\sin\omega_n t}{\omega_n} + \left[\frac{c^2}{\ell}tH(t)\right]. \tag{4.53}$$

which is indeed Eq. (3.46). For the constant mode, the method is the same, because both the Green's function and its first derivative vanish at negative times.

4.6.2.2 Residue Calculus

Starting from the closed-form formula (4.47), it can be noticed that the poles are given by the denominator zeros, and indeed give the eigenfrequencies (4.50): but all poles must be considered, with either positive or negative frequencies. If the zero pole is discarded for now, all poles are simple. Residues are calculated by first-order expansion of the inverse of the function $G_\omega(x,x_s)$ around the poles ω_n. This gives without difficulties, for small $(\omega-\omega_n)$:

$$G_\omega(x,x_s) \simeq -\frac{c^2}{\ell}\frac{1}{\omega_n}\frac{\sin(k_n x+\eta_0)\sin(k_n x_s+\eta_0)}{\omega-\omega_n}. \tag{4.54}$$

The residue theorem indicates that the inverse Fourier transform is, for positive times, j times the sum of the residues, hence [see Eq. (3.181)]:

$$g(x,t|x_s,0) = -j\frac{c^2}{\ell}\sum_{n=-\infty}^{+\infty}\sin(k_n x+\eta_0)\sin(k_n x_s+\eta_0)\frac{e^{j\omega_n t}}{\omega_n}, \tag{4.55}$$

To find Eq. (4.53), the two modes with the same shape $\Phi_n(x)$ must be added (the reader can do this calculation, e.g., for the open–open case). It can also be deduced that $G_\omega(x,x_s)$ is simply given by the sum of terms like (4.54):

$$G_\omega(x,x_s) = -\frac{c^2}{\ell}\sum_{n=-\infty}^{+\infty}\frac{1}{\omega_n}\frac{\sin(k_n x+\eta_0)\sin(k_n x_s+\eta_0)}{\omega-\omega_n}. \tag{4.56}$$

When the terms due to the poles ω_n and $-\omega_n$ are added, (4.52) is obtained. This remark is important, because it can lead to another definition of the modes: in Chap. 3, it has been said that they are real functions varying sinusoidally with time (for a non dissipative system). Modes with a complex dependency $e^{j\omega_n t}$ against time could also be sought, which leads to two modes instead of one, with frequencies ω_n and $-\omega_n$. They are called "single" modes in Chap. 2 (Sect. 2.4.1).

The zero pole remains: the study of (4.47) for each studied case confirms that it exists for the closed–closed case only (for the other cases the numerator vanishes too), and that the pole is double: for ω near 0, $G_\omega(x,x_s) = -c^2/(\ell\omega^2)$. It is indeed the constant term of (4.52), and its inverse transform has already been calculated.

4.6.2.3 Transfer Impedances and Transfer Functions

As explained earlier, we do not need the Green's function itself, but its derivative, corresponding to impedances at one point and transfer impedances. Equation (4.42) gives the transfer impedance $P(x)/U_s$. Its modal expansion is written as [see Eqs. (4.49) and (4.52)]:

$$P(x,x_s) = Z_c U_s\frac{2c}{\ell}j\omega\sum_{n>0}\frac{\Phi_n(x)\Phi_n(x_s)}{\omega_n^2-\omega^2} + \left[Z_c U_s\frac{1}{j\omega}\frac{c}{\ell}\right]. \tag{4.57}$$

Using the Euler equation, the transfer function for the flow rate can also be found:

$$U(x,x_s) = U_s\frac{\cos\left[k(\ell-x)+\eta_\ell\right]\sin\left[kx_s+\eta_0\right]}{\sin\left[k\ell+\eta_0+\eta_\ell\right]} \text{ if } x>x_s\,; \tag{4.58}$$

$$U(x,x_s) = -U_s\frac{\sin\left[k(\ell-x)+\eta_\ell\right]\cos\left[kx_s+\eta_0\right]}{\sin\left[k\ell+\eta_0+\eta_\ell\right]} \text{ if } x<x_s. \tag{4.59}$$

It can be checked that $U(x_s^+, x_s) - U(x_s^-, x_s) = U_s$. For $x \neq x_s$, the modal expansion of the flow transfer function is therefore written as:

$$U(x, x_s) = -U_s \frac{2c^2}{\ell} \sum_{n>0} \frac{\Phi_n(x_s) d\Phi_n(x)/dx}{\omega_n^2 - \omega^2}. \tag{4.60}$$

4.6.3 The Particular Case of a Source at the Input: Input Impedance

What happens if the source position tends towards one of the limits, for example, $x_s = 0$, which is the most frequent case for reed instruments? All quantities at every position in the pipe are thus perfectly determined, using the second equation of the matrix relation (4.29), and with $x_1 = 0$ and $U_1 = u_s$. This consists in solving the equation without source with the so-called inhomogeneous boundary condition, i.e., including a source term:

$$\frac{dP}{dx} = -j\omega \frac{\rho}{S} U_s. \tag{4.61}$$

Can the general calculation of the Green's function still be used? The answer is yes, if $U_s = U_s^+$, thus $U_s^- = 0$, hence $R_0 = 1$, $\eta_0 = \pi/2$, $Z_0 = \infty$. A boundary condition must therefore be imposed, as well as a source term, and this gives the right result (the justification demands long explanation, see [2]). The result will easily be shown to be correct by inserting $x_s = 0$ and $\eta_0 = \pi/2$ into Eq. (4.47)

$$G_\omega(x, 0) = \frac{1}{k} \frac{\sin[k(\ell - x) + \eta_\ell]}{\cos[k\ell + \eta_\ell]},$$

thus

$$P(x, 0) = Z_c U_s j \frac{\sin[k(\ell - x) + \eta_\ell]}{\cos[k\ell + \eta_\ell]}. \tag{4.62}$$

It is sufficient to use a formula like (4.35) to check this result. It must be remembered that *the input impedance is a Green's function, up to the multiplicative factor $j\omega\rho/S$ if an infinite impedance is imposed at the input*, which is not intuitive. The flow rate transfer function is also written:

$$U(x, 0) = U_s \frac{\cos[k(\ell - x) + \eta_\ell]}{\cos[k\ell + \eta_\ell]}. \tag{4.63}$$

4.6.4 Closed-Form Expression: Back to the Time Domain

It has been seen how, in the frequency domain, the closed-form expression leads to successive reflections, using Eq. (4.41). A closed-form expression can also be found in the time domain, which is useful for calculating the Helmholtz motion for wind and bowed-string instruments (see Part III). It will be done here for the transfer impedance P/U_s. Equation (4.38) must be multiplied by the denominator $[1 - g_{\mathrm{RT}}(\omega)]$, then expressed in the time domain. Thus for a source $u_s(t)$:

$$p(x,t) - r_0(t) * r_\ell(t) * p(x, t-\tau) = p_{\mathrm{primary}}(x,t), \tag{4.64}$$

where

$$\begin{aligned} 2Z_c^{-1} p_{\mathrm{primary}}(x,t) = {} & u_s(t - |x - x_s|/c) + r_0(t) * u_s[t - (x + x_s)/c] \\ & + r_\ell(t) * u_s[t - \tau + (x + x_s)/c] \\ & + r_\ell(t) * r_0(t) * u_s[t - \tau + |x - x_s|/c]. \end{aligned}$$

with $\tau = 2\ell/c$. This expression can be obtained directly in the time domain but the calculation is less straightforward: the two terms of the left-hand side of (4.64) must be replaced by their decomposition as successive reflections, and it can be checked that infinite series disappear.

An interesting example is the Raman model (see [7]) for a bowed-string. It is assumed that $r_\ell(t) = r_0(t) = -\lambda$, hence λ is a positive and real coefficient, which represents a particular damping model (independent of frequency). This model enables a stability study much more useful than the model without losses. The situation where the source is at the same place as the receiver is considered, $x = x_s = \ell_a$, where lies the nonlinearity that produces the oscillation. The equation for the mechanical quantities is

$$v(t) - \lambda^2 v(t-\tau) = \frac{Y_c}{2}\left[f_s(t) - \lambda f_s[t - 2\ell_a/c] - \lambda f_s[t - \tau + 2\ell_a/c] + \lambda^2 f_s(t-\tau)\right]. \tag{4.65}$$

Let us suppose that the bow excites the string with a ratio $a/b = \ell_a/(\ell - \ell_a)$, where a and b are integers such as $a < b$, and that the time step is defined as $\Delta = \tau/N = 2\ell/cN$, where $N = a + b$. Because $\ell_a = a\ell/N$, a difference equation is obtained (if we denote $v_n = v(n\Delta)$ and $f_n = f(n\Delta)$):

$$v_n - \lambda^2 v_{n-N} = \frac{Y_c}{2}\left[f_n - \lambda f_{n-a} - \lambda f_{n-b} + \lambda^2 f_{n-N}\right]. \tag{4.66}$$

This equation simplifies the calculation, avoiding the infinity of successive reflections.

Length Correction and Modal Decomposition

Chapter 3 has dealt with strings with moving ends or mass ends. This section will discuss for the case where the termination impedance is the radiation impedance of a pipe at low frequencies. The impedance is of mass type (this will be studied in Chap. 12):

$$Z_R = Z_c jk\Delta\ell \text{ where } Z_R = j\omega\rho S^{-1}\Delta\ell. \tag{4.67}$$

where $\Delta\ell \simeq 0.6R$, R being the radius. The real part has not been written, i.e., damping is ignored.

If the low frequencies assumption is still considered, $k\Delta\ell$ being small, it can be written as: $Z_R \simeq Z_c j \tan k\Delta\ell$, where $\eta_\ell = k\Delta\ell$ [see Eq. (4.43)]. This assumption is consistent with Eq. (4.67), obtained using a Taylor series approximation. Everything that has been written previously can be applied, and happens as if the pipe length was increased by a *length correction* $\Delta\ell$. This can be used for the closed-form expression, as for the modal or successive reflection expansions, but only if low frequencies alone are considered. Thus the transfer and input impedances are obtained using the formulas

$$P(x,0) = Z_c U_s j \frac{\sin k(\ell+\Delta\ell-x)}{\cos k(\ell+\Delta\ell)} = Z_c U_s j\omega \frac{2c}{\ell+\Delta\ell} \sum_{n>0} \frac{\cos k_n x}{\omega_n^2 - \omega^2} \tag{4.68}$$

$$Z_0/Z_c = j \tan k(\ell+\Delta\ell) = j\omega \frac{2c}{\ell+\Delta\ell} \sum_{n>0} \frac{1}{\omega_n^2 - \omega^2}, \tag{4.69}$$

where

$$\omega_n = \left[n - \frac{1}{2}\right] \pi \frac{c}{\ell+\Delta\ell}. \tag{4.70}$$

For the flow rate transfer functions this leads to:

$$U(x,0) = U_s \frac{\cos k(\ell+\Delta\ell-x)}{\cos k(\ell+\Delta\ell)} = -U_s \frac{2c^2}{\ell+\Delta\ell} \sum_{n>0} k_n \frac{\sin k_n x}{\omega_n^2 - \omega^2}. \tag{4.71}$$

The former modal expansion is not valid at $x = 0$, at the source. However, for x as small as wanted, the infinite series does not tend to 0, because quantities $k_n x$ are not small for higher modes.

(continued)

Some Remarks

1. In the following, the assumption leading to Expressions (4.68)–(4.71) will be used often, with the total pipe length equal to be $L = \ell + \Delta\ell$. This poses a small problem at the end, because it should not be forgotten that at the end, $x = \ell$ and not L. However for $U_\ell = U(\ell, 0)$, which is the main quantity for the radiation calculation, $\cos k\Delta\ell$ can be approximated by 1 at the same order of approximation. This is equivalent to writing $x = L$!
2. All these equations have been detailed to fully understand the meaning of modal expansion. Now the approximation $k\Delta\ell \simeq \tan k\Delta\ell$ is not made anymore. Then a boundary condition appears similar to the "moving end" condition (see Chap. 3, Sect. 3.4.5): $\Delta\ell\partial p/\partial x = -p$ at $x = \ell$, which does not depend on frequency (the quantity T/K_0 can be seen as a length correction). Since we are interested in the input impedance, the modes are different from those calculated earlier: $\Phi_n(x) = \cos k_n x$, where $\cot k_n\ell = k_n\Delta\ell$. Applying the method described in Sect. 4.6.2.1, the modal norm being $\Lambda_n = \frac{1}{2}\left[\ell + \Delta\ell/(1 + k_n^2\Delta\ell^2)\right]$, the following result is obtained:

$$P(x, x_s) = 2Z_c U_s j\omega c \sum_{n>0} \frac{1}{\ell + \Delta\ell/(1 + k_n^2\Delta\ell^2)} \frac{\cos k_n x \cos k_n x_s}{\omega_n^2 - \omega^2} \tag{4.72}$$

hence for the input impedance:

$$Z_0/Z_c = \frac{j\tan k\ell + jk\Delta\ell}{1 - k\Delta\ell\tan k\ell} = 2j\omega c \sum_{n>0} \frac{1}{\ell + \Delta\ell/(1 + k_n^2\Delta\ell^2)} \frac{1}{\omega_n^2 - \omega^2}. \tag{4.73}$$

The comparison of this expression with Eq. (4.69) shows that the two expressions are equivalent if $k\Delta\ell << 1$. If $k_n\Delta\ell << 1$, the two modal expansions are also identical (with the same eigenfrequencies), because $k_n\Delta\ell = \tan k_n\Delta\ell$. This can be explained as follows: in the low frequency range, only the first terms for which the condition $k_n\Delta\ell = \tan k_n\Delta\ell$ is valid intervene significantly. However making approximations in an infinite series generally requires some precautions. It is better to make them on the closed-form formula.
3. Modal expansions were written in the form of series. No details will be given on the decomposition in terms of a product of modes. Nevertheless, this decomposition is useful for the study of an elementary model of singing voice, called the "source-filter" model (see [3, 4, 6]). In this model, the glottis is a flow source at the input of the vocal tract. We are interested

(continued)

again in the transfer function U_ℓ/U_s. For the case where the vocal tract is cylindrical, it can be shown that:

$$U(L,0) = \frac{U_s}{\cos kL} = U_s \frac{2c^2}{L} \sum_{n>0} \frac{(-1)^n k_n}{\omega_n^2 - \omega^2} = \frac{U_s}{\prod_n (1 - \omega^2/\omega_n^2)}. \qquad (4.74)$$

References

1. Agulló, J., Barjau, A., Martinez, J.: Alternative to the impulse response h(t) to describe the acoustical behavior of conical ducts. J. Acoust. Soc. Am. **84**, 1606–1612 (1988)
2. Bensoam, J.: Integral representation applied to sound synthesis by physical modeling (in French). Ph.D. thesis, Université du Maine, France (2003)
3. Fant, G.: Acoustic Theory of Speech Production: With Calculations Based on X-Ray Studies of Russian Articulations, 2nd edn. Mouton, The Hague, Paris (1970)
4. Flanagan, J.L.: Speech Analysis, Synthesis and Perception. Springer, Berlin (1965)
5. Léwy, S.: Industrial acoustics and aeroacoustics (in French). Hermès (2001)
6. Sundberg, J.: The Science of the Singing Voice. Northern Illinois University Press, DeKalb, IL (1987)
7. Woodhouse, J.: Idealised models of a bowed string. Acustica **79**, 233–250 (1993)

Chapter 5
Dissipation and Damping

Antoine Chaigne and Jean Kergomard

Abstract This chapter examines the dissipation of sound and vibration into heat, which, in turn, yields a damping of the amplitudes. One consequence of dissipation is that the quality factors of the resonances decrease. This decrease usually depends on frequency. In addition, dissipative phenomena are likely to modify the nature of the modes, which can become a combination of traveling and standing waves, called complex modes. This happens if the internal damping is said to be "non-proportional," i.e., when the damping coefficients depend on space. It also occurs as a consequence of acoustic radiation into an "infinite" space, outside the instruments. Various causes of dissipation are examined in solid materials and in air. In solid materials, thermoelasticity and viscoelasticity are the main mechanisms of internal damping mechanisms. In some situations, air viscosity should also be considered as a pertinent cause of energy loss, as in the case of thin strings. In wind instruments, heat diffusion and viscosity are the main causes of damping. They appear near the walls of a tube. The theory of Kirchhoff, following that of Stokes and simplified by Zwikker and Kosten, is particularly relevant for describing these phenomena.

5.1 Introduction: Dissipative Phenomena in Musical Acoustics

Like in any physical systems, dissipative phenomena are present in musical instruments. This means that part of the mechanical energy imparted to the instrument through impact, blow or air, or continuous excitation by a bow, is transformed into heat. These losses result from viscous phenomena in fluids and solids, from coupling between thermal and elastic properties in materials, or from dissipation at

A. Chaigne (✉)
Institute of Music Acoustics, University of Music and Performing Arts Vienna (MDW), Anton-von-Webern-Platz 1, 1030 Vienna, Austria
e-mail: antchaigne@gmail.com

J. Kergomard
CNRS Laboratoire de Mecanique et d'Acoustique (LMA), 4 impasse Nikola Tesla CS 40006, 13453 Marseille Cedex 13, France
e-mail: kergomard@lma.cnrs-mrs.fr

A. Chaigne, J. Kergomard, *Acoustics of Musical Instruments*, Modern Acoustics and Signal Processing, DOI 10.1007/978-1-4939-3679-3_5

the boundaries imposed by the player. One can think, for example, of the dissipation due to the finger on a string, or due to the lips at the mouthpiece of a saxophone. In addition, and this is rather good news, a part of the mechanical energy is transformed into acoustical energy which propagates to the far-field, thus allowing us to hear the radiated sounds (see Part IV of this book).

For instruments generating free oscillations (plucked and struck strings, percussion instruments), the dissipation phenomena have a *damping* effect on the oscillations, which results in a decrease of the amplitude of the radiated sound. From a theoretical point of view, if a modal expansion is made onto the basis of the associated conservative system, then the damping is often responsible of an intermodal coupling. However, under some assumptions that will be detailed later in this chapter, it is possible to use approximate modal descriptions of the system, and, even in some cases, an exact modal description, though with extension of the modal properties (see the next section devoted to complex modes).

For instruments generating self-sustained sounds (bowed strings and wind instruments), dissipation phenomena are essential to ensure the stability of the system. Here, the sounds produced strongly depend on the balance between input and dissipated energies. For instruments based on free oscillations, the timbre of the sound largely depends on its spectral distribution, i.e., on all excited eigenmodes and eigenfrequencies. Experiences of sound synthesis carried out for more than 50 years have shown that the timbre strongly depends on the time history of the partials. In short, the dissipation phenomena are not only essential from a physical point of view, but are also critical in the context of musical sound perception (see, for example, the book by Castellengo, with numerous sound examples [8]). Therefore, these phenomena are of prime importance in musical acoustics.

In this chapter, the consequences of dissipation on the theoretical results related to eigenmodes in Chap. 3 are presented. These general considerations are necessary to understand the examples treated in subsequent parts of this book. The main damping mechanisms encountered in musical instruments are also briefly reviewed. For the sake of brevity, the important questions related to measurements of damping are not reviewed here, and the reader is invited to consult the specialized literature [3, 17].

5.2 Generalizing the Concept of Mode

Comment. *Some developments presented in this section were directly inspired by the book by Géradin and Rixen [19] to which the reader can refer for more details.*

In continuity with Chap. 3, the consequences of damping mechanisms on the eigenmodes obtained in the conservative case will be first examined. The advantages and drawbacks of this formulation will be highlighted. A more general approach leading to the definition of complex modes is then presented.

5.2.1 Dissipative Discrete System

In a linear system with a finite number of degrees of freedom (DOF), the dissipated energy can be written as a quadratic function of the velocity:

$$\mathscr{E}_D = \frac{1}{2}\, {}^t\dot{\boldsymbol{\xi}}\mathbb{C}\dot{\boldsymbol{\xi}}, \tag{5.1}$$

where $\mathbb{C}$ is a symmetrical damping matrix whose elements are positive or null (non-negative matrix). This class of functions corresponds to a large number of situations encountered in the physics of musical instruments. Under this assumption, the equations of motion (3.12) obtained for a conservative system can be transformed into the matrix equation:

$$\mathbb{M}\ddot{\boldsymbol{\xi}} + \mathbb{C}\dot{\boldsymbol{\xi}} + \mathbb{K}\boldsymbol{\xi} = \boldsymbol{F}\,. \tag{5.2}$$

As in Chap. 3, ω_n and $\boldsymbol{\Phi}_n$ are the eigenfrequencies and eigenshapes of the associated conservative system. To take advantage of the orthogonality properties of the eigenmodes, $\boldsymbol{\xi}$ is developed in this basis, as[1]:

$$\boldsymbol{\xi} = \sum_m \boldsymbol{\Phi}_m q_m(t)\,. \tag{5.3}$$

Through scalar multiplication of Eq. (5.2) by $\boldsymbol{\Phi}_n$, we get

$$\langle \boldsymbol{\Phi_n}, \mathbb{M}\boldsymbol{\Phi_n}\rangle \ddot{q}_n + \sum_m \langle \boldsymbol{\Phi_n}, \mathbb{C}\boldsymbol{\Phi_m}\rangle \dot{q}_m + \langle \boldsymbol{\Phi_n}, \mathbb{K}\boldsymbol{\Phi_n}\rangle q_n = \langle \boldsymbol{\Phi_n}, \boldsymbol{F}\rangle, \tag{5.4}$$

thus, using the conventional notations, and defining further:

$$\langle \boldsymbol{\Phi_n}, \mathbb{C}\boldsymbol{\Phi_m}\rangle = 2\zeta_{nm} m_n \omega_n, \tag{5.5}$$

where ζ_{nm} are the *inter-modal damping coefficients*, it is finally found that the generalized coordinates satisfy the system of equations:

$$\ddot{q}_n + 2\omega_n \sum_m \zeta_{nm}\dot{q}_m + \omega_n^2 q_n = \frac{f_n}{m_n}, \tag{5.6}$$

which can be rewritten as:

$$\ddot{q}_n + 2\omega_n\zeta_n\dot{q}_n + \omega_n^2 q_n = \frac{f_n}{m_n} - 2\omega_n \sum_{m\neq n} \zeta_{nm}\dot{q}_m, \tag{5.7}$$

[1] Selecting n, or m, as index in the expression of $\boldsymbol{\xi}$ has no consequence, since they are *dummy* indices.

where ζ_n is the *modal damping coefficient* for the mode n. In general, the matrix $\mathbb{C}$ cannot be diagonalized, so that the ζ_{nm} are not all equal to zero. As a consequence, the generalized displacements are coupled. This is due to the fact that we are not dealing here with the "true" eigenmodes. However, this method has the advantage of showing the links with the modes of the associated conservative system. It can be used in the case of weak damping, when approximated solutions are sufficient (see the next section).

5.2.1.1 Systems with Weak Damping

It is, in fact, possible to simplify the formulation (5.7) for systems with weak damping. In musical acoustics, this corresponds to the case of strings and metallic percussion instruments. However, the condition of weak damping is generally not fulfilled for wooden soundboards or timpani heads, especially in the high frequency range.

In the case of weak damping, a first-order expansion of the eigenfrequencies and eigenshapes can be done in the form:

$$\omega_n' = \omega_n + \Delta\omega_n \quad ; \quad \boldsymbol{\Phi}_n' = \boldsymbol{\Phi}_n + \Delta\boldsymbol{\Phi}_n, \tag{5.8}$$

where $\Delta\omega_n$, $\Delta\boldsymbol{\Phi}_n$ and all the coefficients of the matrix $\mathbb{C}$ are supposed to be of the same order (i.e., in $\mathcal{O}(\varepsilon)$). Inserting these expressions in Eq. (5.2) without right-hand side, and ignoring the second-order terms, yields

$$\left(\mathbb{K} - \omega_n^2\mathbb{M}\right)\Delta\boldsymbol{\Phi}_n + \omega_n\left(-2\Delta\omega_n\mathbb{M} + j\mathbb{C}\right)\boldsymbol{\Phi}_n \simeq 0\,. \tag{5.9}$$

Through scalar multiplication of (5.9) by Φ_n, we get

$$\Delta\omega_n \simeq j\zeta_n\omega_n\,. \tag{5.10}$$

This last expression shows two major results:

1. The correction in frequency due to damping is purely imaginary. As a consequence, the eigensolution now becomes a *damped sinusoid* of the form $\exp(j\omega_n t)\exp(-\zeta_n\omega_n t)$, which is slowly decreasing if the damping is weak.
2. Under the assumption of weak damping, the inter-modal damping coefficients have no influence on the first-order frequency correction. This is equivalent to the approximation of a diagonal matrix for $\mathbb{C}$.

In a second step, Eq. (5.9) is used to determine the influence of damping on the eigenshapes. This amounts to searching for the coefficients α_m in the expansion $\Delta\boldsymbol{\Phi}_n$ defined by:

$$\Delta\boldsymbol{\Phi}_n = \sum_{m\neq n}\alpha_m\boldsymbol{\Phi}_m\,. \tag{5.11}$$

Injecting this expression in (5.9) and multiplying this quantity by any other eigenshape, taking further the orthogonality properties of $\boldsymbol{\Phi}_m$ into account, yields to first-order:

$$\alpha_m = 2j\zeta_{mn}\frac{m_n\omega_n^2}{m_m\left(\omega_n^2-\omega_m^2\right)}\,. \tag{5.12}$$

Consequently, the eigenshapes with weak damping become, still to the first-order:

$$\boldsymbol{\Phi}'_n = \boldsymbol{\Phi}_n + 2jm_n\omega_n^2\sum_{m\neq n}\boldsymbol{\Phi}_m\frac{\zeta_{mn}}{m_m\left(\omega_n^2-\omega_m^2\right)}\,. \tag{5.13}$$

The expression (5.13) shows that:

1. If the eigenfrequencies of the associated conservative system are *sufficiently separated from each other*, the corrective terms on the shapes are of the order of magnitude of the inter-modal reduced damping ζ_{mn}. Otherwise, as a consequence of the presence of the factor $\omega_n^2-\omega_m^2$ in the denominator, the shapes can be significantly modified.
2. As for the eigenfrequencies, the corrective terms of the eigenshapes are purely imaginary. Therefore, these shapes are no longer in phase (or in anti-phase) as in the ideal limiting case of the conservative system.

In summary, if the inter-modal damping coefficients ζ_{mn} are sufficiently weak, and if, at the same time, the eigenfrequencies of the associated conservative system are sufficiently separated from each other, then it is legitimate to decouple the equations of the generalized displacements, which are then written:

$$\ddot{q}_n + 2\omega_n\zeta_n\dot{q}_n + \omega_n^2 q_n \simeq \frac{f_n}{m_n}. \tag{5.14}$$

In addition, we can admit that the eigenshapes remain unchanged compared to the conservative case.

5.2.1.2 Proportional Damping

Examining Eq. (5.2) carefully shows that a family of particular cases exists where the damping matrix is diagonal and can be written in the form $\mathbb{C} = \alpha\mathbb{M} + \beta\mathbb{K}$, where α and β are two real constants. In this case, (5.4) becomes

$$\begin{aligned}&\langle\boldsymbol{\Phi_n},\mathbb{M}\boldsymbol{\Phi_n}\rangle\ddot{q}_n + \alpha\langle\boldsymbol{\Phi_n},\mathbb{M}\boldsymbol{\Phi_n}\rangle\dot{q}_n\\ &\quad+\beta\langle\boldsymbol{\Phi_n},\mathbb{K}\boldsymbol{\Phi_n}\rangle\dot{q}_n + \langle\boldsymbol{\Phi_n},\mathbb{K}\boldsymbol{\Phi_n}\rangle q_n = \langle\boldsymbol{\Phi_n},\boldsymbol{F}\rangle\,.\end{aligned} \tag{5.15}$$

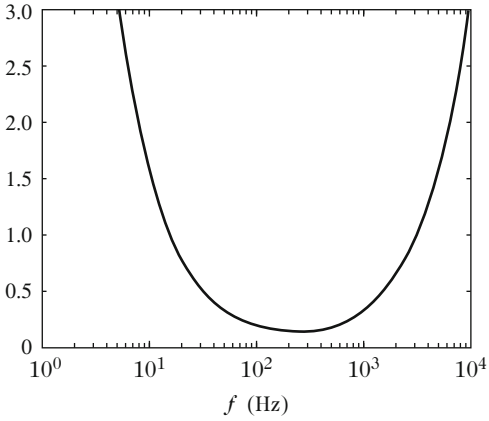

Fig. 5.1 Example of a modal damping factor as a function of the frequency in case of proportional damping ($\alpha = 100, \beta = 0.0001$)

This can be written in a reduced form:

$$\ddot{q}_n + 2\omega_n \zeta_n \dot{q}_n + \omega_n^2 q_n = \frac{f_n}{m_n} \quad \text{with} \quad \zeta_n = \frac{\alpha}{2\omega_n} + \frac{\beta\omega_n}{2} \,. \tag{5.16}$$

In this case, the eigenmodes have the same shapes as in the conservative case, but the eigenfrequencies become *complex*. A modal damping factor is obtained, which is a function of frequency (see Fig. 5.1). With positive values for α and β, the damping decreases approximately as $1/\omega$ up to $\omega = \sqrt{\frac{\alpha}{\beta}}$, and increases then linearly. This type of damping rarely corresponds to a particular physical phenomenon. It is most often selected for mathematical reasons of convenience, to allow the decoupling of the differential equations of the generalized displacements. However, such a frequency dependence can be reasonably used for approximating damping laws observed experimentally, at least in a restricted frequency range. One example will be presented later in this chapter, for the particular case of viscoelastic strings.

5.2.1.3 Discrete Systems: First Notions on Complex Modes

For more general damping laws, it has been shown in Sect. 5.2.1 that the matrix $\mathbb{C}$ cannot be diagonalized with the matrices $\mathbb{K}$ and $\mathbb{M}$ only. The goal is now to obtain exact solutions, and not approximated ones which are no longer valid, and a new method is necessary. After defining $\boldsymbol{v} = \dot{\boldsymbol{\xi}}$, the matrix equation (5.2) is rewritten in the form of a system of two first-order differential equations, as follows:

$$\begin{Bmatrix} \dot{\boldsymbol{\xi}} \\ \dot{\boldsymbol{v}} \end{Bmatrix} + \begin{bmatrix} 0_{N\times N} & -\mathbb{I}_N \\ \mathbb{M}^{-1}\mathbb{K} & \mathbb{M}^{-1}\mathbb{C} \end{bmatrix} \begin{Bmatrix} \boldsymbol{\xi} \\ \boldsymbol{v} \end{Bmatrix} = \begin{Bmatrix} 0 \\ \mathbb{M}^{-1}\boldsymbol{F} \end{Bmatrix} , \tag{5.17}$$

where $0_{N\times N}$ is the null matrix and $\mathbb{I}_N$ the identity matrix of dimension N. N is the number of DOF in the system. If $\mathbb{C} = 0$ in (5.17), the conservative solution is found. The characteristic equation then yields purely *imaginary* conjugate solutions, and the eigenmodes analysis made in Chap. 3 can be carried out.

In the general case, the roots of the characteristic equation solutions are complex, with non-zero real parts. The general solution of the equation (without right-hand side) is searched in the form:

$$\boldsymbol{\xi}(t) = 2\boldsymbol{\psi_r}\, e^{-\alpha t}\cos\omega t - 2\boldsymbol{\psi_i}\, e^{-\alpha t}\sin\omega t\ . \tag{5.18}$$

This solution is *real*. However, it is convenient to do all calculations in the complex space, and return to the real expressions of the results only at the end. It is the reason why *complex modes* of the form:

$$\boldsymbol{\psi} = \boldsymbol{\psi_r} + j\boldsymbol{\psi_i}, \tag{5.19}$$

are introduced, as well as *complex generalized displacements*:

$$q(t) = e^{-\alpha t}\left[\cos\omega t + j\sin\omega t\right] = e^{st} \quad \text{with} \quad s = -\alpha + j\omega\ . \tag{5.20}$$

The main results with regard to complex modes are now developed briefly, so that differences and analogies with the real modes defined in Chap. 3 are enhanced. Equation (5.17) is written in the form:

$$\dot{\boldsymbol{\Xi}} - \mathbb{A}\boldsymbol{\Xi} = \mathscr{F} \quad \text{with} \quad \mathbb{A} = -\begin{bmatrix} 0_{N\times N} & -\mathbb{I}_N \\ \mathbb{M}^{-1}\mathbb{K} & \mathbb{M}^{-1}\mathbb{C} \end{bmatrix}\ . \tag{5.21}$$

$\mathbb{A}$ is independent of time. Then, the eigenvalues problem corresponds to finding the eigenvalues λ_n and the associated eigenvectors $\boldsymbol{\Psi_n}$, such as:

$$\mathbb{A}\boldsymbol{\Psi_n} = \lambda_n\boldsymbol{\Psi_n}. \tag{5.22}$$

The orthogonality conditions for the complex modes can be simply obtained by rewriting first Eq. (5.17) in the form:

$$\begin{bmatrix} \mathbb{C} & \mathbb{M} \\ \mathbb{M} & 0 \end{bmatrix}\begin{Bmatrix} \dot{\boldsymbol{\xi}} \\ \dot{\boldsymbol{v}} \end{Bmatrix} + \begin{bmatrix} \mathbb{K} & 0 \\ 0 & -\mathbb{M} \end{bmatrix}\begin{Bmatrix} \boldsymbol{\xi} \\ \boldsymbol{v} \end{Bmatrix} = \begin{Bmatrix} \boldsymbol{F} \\ 0 \end{Bmatrix} \tag{5.23}$$

or, equivalently, in compact matrix form:

$$\boldsymbol{D}\begin{Bmatrix} \dot{\boldsymbol{\xi}} \\ \dot{\boldsymbol{v}} \end{Bmatrix} + \boldsymbol{B}\begin{Bmatrix} \boldsymbol{\xi} \\ \boldsymbol{v} \end{Bmatrix} = \begin{Bmatrix} \boldsymbol{F} \\ 0 \end{Bmatrix}\ . \tag{5.24}$$

The eigenvectors must then fulfill:

$$(\lambda_n \boldsymbol{D} + \boldsymbol{B})\boldsymbol{\Psi_n} = 0 \tag{5.25}$$

which, in the case of distinct eigenvalues ($\lambda_m \neq \lambda_n$) leads to the orthogonality conditions:

$${}^t\boldsymbol{\Psi_m} \boldsymbol{D} \Psi_n = 0 \quad \text{and} \quad {}^t\boldsymbol{\Psi_n} \boldsymbol{B} \boldsymbol{\Psi_m} = 0 \quad \text{for} \quad m \neq n. \tag{5.26}$$

The solution of (5.17) is written:

$$\boldsymbol{\Xi} = \sum \boldsymbol{\Psi_n} q_n(t) \tag{5.27}$$

where the generalized displacements satisfy the differential equations:

$$A_n \left[\dot{q}_n - \lambda_n q_n\right] = {}^t\boldsymbol{\Psi_n} \mathbb{A} \mathscr{F} \quad \text{with} \quad A_n = {}^t\boldsymbol{\Psi_n} \mathbb{A} \boldsymbol{\Psi_n} \, . \tag{5.28}$$

Finally, the initial conditions yield

$$A_n q_n(0) = {}^t\boldsymbol{\Psi_n} \mathbb{A} \boldsymbol{\Xi}\,(0) \, . \tag{5.29}$$

The two components of the vector $\boldsymbol{\Psi}$ are written explicitly:

$$\boldsymbol{\Psi} = \begin{pmatrix} \boldsymbol{\psi} \\ \widetilde{\boldsymbol{\psi}} \end{pmatrix} \, . \tag{5.30}$$

With (5.22), the relations governing the eigenvectors are

$$\widetilde{\boldsymbol{\psi}}_{\boldsymbol{n}} = \lambda_n \boldsymbol{\psi_n} \;\; ; \;\; \lambda_n^2 \mathbb{M} \boldsymbol{\psi_n} + \lambda_n \mathbb{C} \boldsymbol{\psi_n} + \mathbb{K} \boldsymbol{\psi_n} = 0 \, . \tag{5.31}$$

Expressing now the orthogonality conditions (5.26) explicitly yields

$${}^t\boldsymbol{\psi_m} \mathbb{K} \boldsymbol{\psi_n} = \lambda_m \lambda_n \, {}^t\boldsymbol{\psi_m} \mathbb{M} \boldsymbol{\psi_n} \;\; ; \;\; {}^t\boldsymbol{\psi_m} \mathbb{C} \boldsymbol{\psi_n} + (\lambda_m + \lambda_n) \, {}^t\boldsymbol{\psi_m} \mathbb{M} \boldsymbol{\psi_n} = 0 \, . \tag{5.32}$$

Notice that the orthogonality conditions for real modes can be retrieved by canceling the damping matrix $\mathbb{C}$ in (5.32). As soon as the eigenvalues and eigenvectors are known, the displacement $\boldsymbol{\xi}$ and the velocity $\boldsymbol{v}$ are expanded onto this basis, yielding finally:

$$\boldsymbol{\xi}(t) = \sum \boldsymbol{\psi_n} q_n(t) \;\; ; \;\; \boldsymbol{v}(t) = \sum \lambda_n \boldsymbol{\psi_n} q_n(t) \, . \tag{5.33}$$

5.2.2 *Continuous Systems*

The results obtained for discrete damped systems can be generalized to the continuous case, as it has been done for conservative systems in Chap. 3. The example of a string vibrating is treated here (see also Sect. 3.3.2 in Chap. 3). As for discrete systems, we consider the case of weak damping and start by looking for solutions expanded onto the basis of the conservative modes of the form:

$$y(x,t) = \sum_n \Phi_n(x) q_n(t) \ . \tag{5.34}$$

As a consequence, the equations for the generalized displacements can be written in a symbolic form as[2]:

$$\mathscr{M}\ (\ddot{y}, \Phi_m) + \mathscr{C}\ (\dot{y}, \Phi_m) + \mathscr{K}\ (y, \Phi_m) = \langle f, \Phi_m \rangle \tag{5.35}$$

where $\mathscr{C}$ represents the damping operator. Recall that Eq. (5.35) is obtained after multiplication of both sides of the partial differential equations by an arbitrary eigenshape $\Phi_m(x)$, followed by an integration on the string length. This operation generalizes the scalar product used for discrete systems. This formulation has the advantage to take the boundary conditions into account, due to the use of integrations by parts, as it has been shown, for example, for moving ends in Sect. 3.4.5 of Chap. 3.

One reason for expanding the solution in the basis of eigenmodes $\Phi_n(x)$, *even in the case of damped systems*, is to take advantage of their mathematical orthogonality properties. As shown in the discrete case, the damping operator induces a coupling of the generalized displacements $q_n(t)$, except in some particular cases, such as the proportional damping. These general ideas are now illustrated with some examples of practical relevance in musical acoustics.

5.2.2.1 A Simple Example of Proportional Damping: The Homogeneous String

i) Damping Independent of Frequency

A string with damping independent of space is considered. For simplicity, the study is limited to the case of a homogeneous string. The unrealistic, though useful, reference case of a damping independent of frequency is treated. We start with

[2] See Chap. 3, Sects. 3.3 and 3.4, for the definition of the notations (a, b) used for a continuous operator, and $\langle a, b \rangle$ for the scalar product.

Eq. (3.25) in which a damping term is added in the form of a proportional force with opposite sign with regard to velocity:

$$\rho S\frac{\partial^2 y}{\partial t^2} + 2\alpha\rho S\frac{\partial y}{\partial t} - T\frac{\partial^2 y}{\partial x^2} = f(x,t), \tag{5.36}$$

where, for convenience, the damping coefficient is written $2\alpha\rho S$. The method presented in Sect. 3.3.2 can be fully applied here, since α does not vary with x, and, therefore, no mode coupling exists. Again, the selected basis of modes here is that of the conservative case. Searching for solutions of the form $y(x,t) = \sum_n \Phi_n(x)q_n(t)$, a generalization of Eq. (3.38) is obtained

$$\ddot{q}_n + 2\alpha\dot{q}_n + \omega_n^2 q_n = f_n/m_n\ . \tag{5.37}$$

The notations are identical to those used in Chap. 3. Similar equations were solved in Chap. 2. Thus, for a Green's function such as $f(x,t) = T\delta(x-x_0)\delta(t)$, we get $f_n(t) = T\Phi_n(x_0)\delta(t)$, and Eq. (2.14) is used

$$g(x,t) = H(t)T\sum_n \frac{\Phi_n(x)\Phi_n(x_0)}{m_n}e^{-\alpha t}\frac{\sin\omega_{pn}t}{\omega_{pn}},$$

where $\omega_{pn} = \omega_n\sqrt{1-\alpha^2/\omega_n^2}$ (in most usual cases, it can be written as $\omega_{pn} \simeq \omega_n$, since damping is weak). For Dirichlet boundary conditions (fixed ends), we have $\Phi_n(x) = \sin k_n x$, $k_n = n\pi/L = \omega_n/c$, $m_n = \rho SL/2$. Thus:

$$g(x,t) = H(t)\frac{2c^2}{L}\sum_n \sin k_n x \sin k_n x_0 e^{-\alpha t}\frac{\sin\omega_{pn}t}{\omega_{pn}},$$

that can be compared to Eq. (4.53). Here, the eigenfrequencies are complex.[3]

For a damped plucked string with no initial velocity, we derive from (2.11) and (3.58) the expression of the displacement:

$$y(x,t) = \sum_n \frac{2hL^2}{n^2\pi^2 x_0(L-x_0)}\sin k_n x \sin k_n x_0 e^{-\alpha t}\frac{\cos(\omega_{pn}t+\varphi_n)}{\delta_n} \tag{5.38}$$

where $\tan\varphi_n = -\alpha/\omega_{pn}$ and $\delta_n = \omega_{pn}/\omega_n$. The Green's function $G(x)$ in the frequency domain is derived

[3] What is the connection between the present case and the proportional damping in discrete systems seen in Sect. 5.2.1.2? To answer this question, assume that the string is discretized in small elements of the same length, similar to the use of spatial finite differences. The mass and damping matrices are diagonal, with equal elements: they are thus proportional, with proportionality coefficient 2α, from (5.36). By writing $\alpha = \omega_n\zeta_n$ for all elements, Eq. (5.16) is found again, up to a factor 2, since we had $\mathbb{C} = \alpha\mathbb{M}$, and not $\mathbb{C} = 2\alpha\mathbb{M}$.

$$G(x) = \frac{2c^2}{L} \sum_n \frac{\sin k_n x \sin k_n x_0}{\omega_n^2 - \omega^2 + j\omega\omega_n/Q_n} \tag{5.39}$$

with $Q_n = \omega_n/2\alpha$. This formula can be compared to (4.52).

ii) Frequency-Dependent Damping

If the damping phenomena depend on frequency, the partial differential equation (5.36) can often take a very complicated form, as it will be seen later in Sect. 5.4 in this chapter for the damping in tubes.[4] It is thus more convenient to return to the frequency domain, where a decomposition remains simple as long as the boundary conditions do not depend on frequency. For boundary conditions similar to the previous case of the string, Eq. (5.39) remains valid when $\alpha(\omega)$ depends on ω. Notice that we write ω, which is a continuous variable, and not ω_n which corresponds to the discrete series of the string modes. Thus we can write $Q_n = \omega_n/2\alpha(\omega)$ for the quality factor. What changes here, compared to the standard oscillator, is that the variations with frequency of the magnitude are not given by a Lorentzian function anymore (see Chap. 2). However, it is often the case that, since the effects of the damping are significant near $\omega = \omega_n$ only, one can approximately write $Q_n \simeq \omega_n/2\alpha(\omega_n)$. Under this assumption, $G(x)$ in Eq. (5.39) can be approximated by a series of Lorentzian terms, which enables us to return to the time domain using (5.38). This question will be addressed again for tubes (Sect. 5.6).

5.2.2.2 Example of Non-proportional Damping: Localized Damping

A vibrating string of length L is now considered with eigenfrequencies ω_n and associated eigenshapes $\Phi_n(x)$ in the conservative case (no damping).[5] A "fluid" localized damping is introduced at a point of abscissa $x = x_o$, with $0 < x_o < L$, in the form of a mechanical resistance R (see Fig. 5.2). This simple model is a rough, though relevant, description of the type of damping that occurs when a player presses his (or her) finger against the fingerboard.

In terms of energy, the mechanical resistance yields a quadratic function of string velocity. Its action is described by a force proportional to velocity, with an opposite sign, of the form $-R\dot{y}(x,t)\delta(x - x_o)$. Using the notations of Sect. 3.3.2 in Chap. 3, the equation of motion of the string becomes

[4] In some cases, it is possible to search for equivalent time-domain formulations of damping terms, as shown later in this chapter for damping in plates (see Sect. 5.3). However, such formulations usually are rather complicated.

[5] These assumptions are valid for heterogeneous strings with non-dissipative impedance-like boundary conditions. The case of dissipative boundary conditions is addressed in Sect. 5.2.2.3.

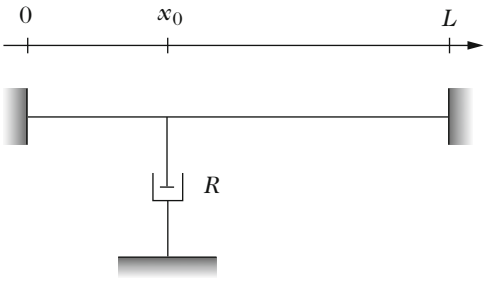

Fig. 5.2 String with a localized damping, represented by a mechanical resistance R at a fixed point $x = x_0$

$$\rho(x)S(x)\frac{\partial^2 y}{\partial t^2} + R\frac{\partial y}{\partial t}\delta(x - x_o) - \frac{\partial}{\partial x}\left[T(x)\frac{\partial y}{\partial x}\right] = f(x,t) \tag{5.40}$$

which, after standard use of the scalar product, leads to:

$$\sum_m \ddot{q}_m(t)\int_0^L \Phi_m(x)\Phi_n(x)\rho(x)S(x)dx + \sum_m \dot{q}_m(t)\int_0^L R\delta(x - x_o)\Phi_m(x)\Phi_n(x)dx$$
$$-\sum_m q_m(t)\int_0^L \Phi_n(x)\frac{d}{dx}\left(T(x)\frac{d\Phi_m(x)}{dx}\right)dx = \int_0^L \Phi_n(x)f(x,t)dx\,. \tag{5.41}$$

As a consequence, taking advantage of the orthogonality properties of the eigenshapes $\Phi_n(x)$, the generalized coordinates satisfy the differential equations:

$$\ddot{q}_n + 2\omega_n\sum_m \zeta_{nm}\dot{q}_m + \omega_n^2 q_n = \frac{f_n}{m_n} \tag{5.42}$$

where the inter-modal damping coefficients are written:

$$\zeta_{nm} = \frac{R\Phi_n(x_o)\Phi_m(x_o)}{2m_n\omega_n}\,. \tag{5.43}$$

Again, it is observed that the damping leads to a coupling between the modes of the conservative system. However, as it has been shown in Sect. 5.2.1.1, these equations can be decoupled, using first-order approximations for weak damping, which leads to the simplified equation:

$$\ddot{q}_n + 2\omega_n\zeta_n\dot{q}_n + \omega_n^2 q_n \simeq \frac{f_n}{m_n} \tag{5.44}$$

where the modal damping coefficient is now defined by:

$$\zeta_n = \frac{R\Phi_n^2(x_o)}{2m_n\omega_n}\,. \tag{5.45}$$

Application To illustrate the practical importance of this example, the simplified case of an homogeneous string fixed rigidly at both ends is taken, for which $\Phi_n(x) = \sin k_n x$ and $\omega_n = ck_n = \frac{n\pi c}{L}$. The damper (finger) is supposed to be applied at the middle of the string at position $x_o = L/2$. In this case, Eq. (5.45) shows that the modal damping coefficient is written $\zeta_n = \frac{R \sin^2(\frac{n\pi}{2})}{2m_n\omega_n}$. Based on this expression, one has to consider two cases:

1. For odd values of n, $\sin^2(\frac{n\pi}{2}) = 1$ and $\zeta_n = \frac{R}{2m_n\omega_n}$.
2. For even values of n, $\zeta_n = 0$.

As a conclusion, we see that, in this particular example, only the odd modes of the string are damped. In other words, the damper has no action on the modes if its location corresponds to a nodal point. This result is coherent with the fact that the damper cannot dissipate energy if the velocity of the string at its attachment point is zero.

5.2.2.3 String with a Dissipative End

A string with a dissipative end is the simplest case for which the concept of complex modes can be generalized to continuous systems. Such as system yields time-varying modal shapes, among other results. Intuitively, one can easily imagine that some difficulties may occur to maintain a stable eigenshape, since some energy is dissipated at one end. This section presents the simple example of a homogeneous string without a source term, rigidly fixed at one end, and attached to a mechanical resistance at the other (see Fig. 5.3). The model is the following:

$$\rho S \frac{\partial^2 y}{\partial t^2} - T \frac{\partial^2 y}{\partial x^2} = 0, \tag{5.46}$$

with boundary conditions:

$$y(0,t) = 0 \quad \text{and} \quad T \frac{\partial y}{\partial x}(L,t) = -R \frac{\partial y}{\partial t}(L,t). \tag{5.47}$$

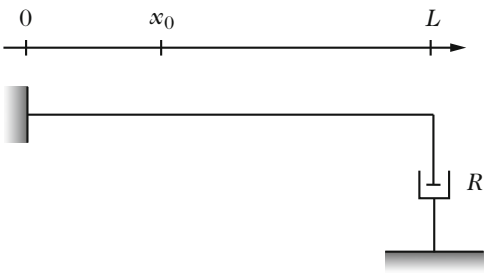

Fig. 5.3 String with a damper at one end

The method used here consists in searching for the general solution in separated variables $y(x,t) = f(x)g(t)$. This method will be detailed in Chap. 7, Sect. 7.6. Due to the dissipative condition in $x = L$, it is convenient to search for the general solution in the complex space.[6] Thus, solutions are sought in $\mathbb{C}$-space of the form:

$$g(t) = Ae^{-st} + Be^{st}, \tag{5.48}$$

with A, B and $s \in \mathbb{C}$. The function $f(x)$ satisfies

$$\frac{d^2f(x)}{dx^2} = \frac{s^2}{c^2}f(x) \quad \text{with} \quad c = \sqrt{\frac{T}{\rho S}}\,. \tag{5.49}$$

Using the boundary condition in $x = 0$, it is found that the spatial dependency $f(x)$ is

$$f(x) = \sinh sx/c. \tag{5.50}$$

It can be shown (though not demonstrated here) that both terms in (5.48) give the same modes. Thus, for the sake of simplicity, the resolution of the problem continues from here with $g(t) = \exp(st)$ only. The boundary condition at $x = L$ yields

$$\cosh sL/c = -r \sinh sL/c \tag{5.51}$$

where $r = R/Z_c$, with $Z_c = T/c$ the characteristic impedance of the string. With $s = j\omega + \alpha$, two families of solutions are found, depending on whether the resistance R is larger than Z_c or not.

1. For $r < 1$, Eq. (5.51) gives the conditions:

$$\cos\frac{\omega L}{c} = 0 \;\; ; \;\; \tanh\frac{\alpha L}{c} = -r\,. \tag{5.52}$$

2. For $r > 1$, Eq. (5.51) gives the conditions:

$$\sin\frac{\omega L}{c} = 0 \;\; ; \;\; \tanh\frac{\alpha L}{c} = -\frac{1}{r}\,. \tag{5.53}$$

In what follows, only the case $r > 1$ will be considered. This situation corresponds to string instruments, where the real part of the impedance at the bridge is significantly larger than the characteristic impedance of the strings. The angular eigenfrequencies are complex. Their real parts $\omega_n = n\pi c/L$ are unchanged, compared to the case of a string rigidly fixed at both ends. Denoting α^+ the positive value of α, so that $\tanh \alpha^+ L/c = 1/r$, then we get

[6] Nevertheless, as shown at the end of this section, the "physical" solution obtained after considering the initial conditions will be expressed in the real space.

$$g(t) = \exp\left[jn\pi c/L - \alpha^+\right] t.$$

where n can be either positive or negative. The general solution can be written as: $g(t) = \exp\left[j\omega_n - \alpha^+\right] t$. Finally, the following decomposition of $y(x,t)$ is obtained, (denoting now $\alpha^+ = \alpha$) :

$$y(x,t) = e^{-\alpha t} \sum_n a_n \sinh\left[(j\omega_n - \alpha)x/c\right] e^{j\omega_n t}, \tag{5.54}$$

which can be rearranged under the following form, where the factor $1/2$ is inserted in the amplitude a_n:

$$y(x,t) = e^{-\alpha t}\left[e^{-\alpha x/c} \sum_n a_n e^{j\omega_n(t+x/c)} - e^{\alpha x/c} \sum_n a_n e^{j\omega_n(t-x/c)}\right] \tag{5.55}$$

or in closed form:

$$y(x,t) = e^{-\alpha t}\left[e^{-\alpha x/c} F\left(t + \frac{x}{c}\right) - e^{\alpha x/c} F\left(t - \frac{x}{c}\right)\right], \tag{5.56}$$

with

$$F(t) = \sum_n a_n e^{j\omega_n t}\,. \tag{5.57}$$

The complex constants a_n are determined by the initial conditions. It can be shown that the result leads to a real function $F(t)$.

A number of interesting remarks can be derived from Eq. (5.56):

1. The presence of the resistance R results in an exponentially decreasing oscillation, with time constant $\tau = 1/\alpha$ independent of frequency.
2. The term between [ ] corresponds to two traveling waves in opposite direction and with different amplitudes, except in $x = 0$ where both terms cancel at any time, according to the boundary condition. Consequently, *no standing wave* can exist on the string.

In conclusion, as shown in Fig. 5.4, traveling waves exist on the string with a dissipative end. Strictly speaking, one cannot describe the phenomena in terms of modes, nodes, and antinodes, since all these quantities are moving with time. In the frequency domain, we will refer to such dynamics as "complex" modes. Chapter 13 deals with a similar example, since the radiation in space can be viewed as a 3D generalization of a string with a resistive end. The "complex" modes are not orthogonal for the usual scalar products seen in Chap. 3, exhibiting mass and stiffness orthogonality. However, we will present in Sect. 5.2.3 below another scalar product with specific orthogonality properties. With this scalar product, the complex

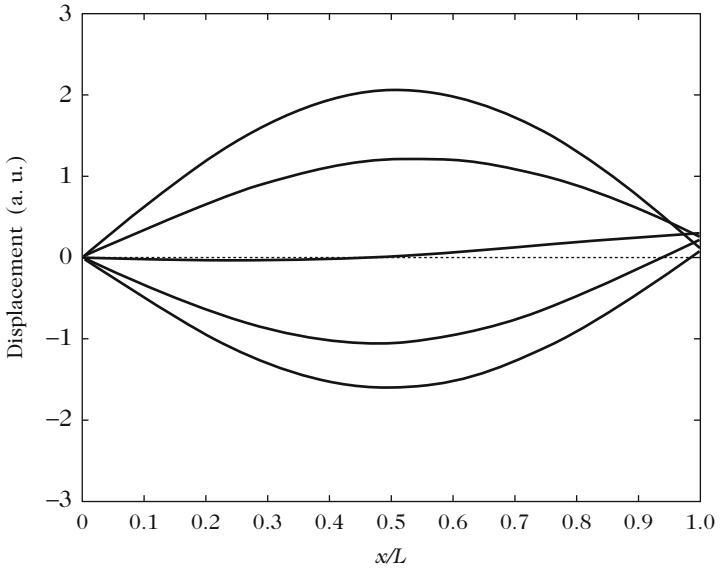

Fig. 5.4 Snapshots of a string with a dissipative end, at successive instants of time

modes form a complete basis for the solutions, which enables to solve general problems with initial values and source terms [28].

For continuous systems, as for discrete systems, first-order approximations are possible in the case of weakly dissipative systems, where the modal shapes are almost stationary. In the particular case of the string with dissipative end presented above, the problem gives an exact solution, and no approximations are necessary. This solution shows, in the time domain, the consequences of phase shift due to dissipation between the eigenmodes, as shown in Sect. 5.2.1.1.

5.2.3 Continuous Complex Modes

This section deals with the general case of continuous systems where the damping operator cannot be diagonalized. For simplicity, only one-dimensional systems, such as bars or strings, are considered for which the equation of motion is written in the form [31]:

$$\mathscr{L}(w) + \mathscr{C}(\dot{w}) + \rho S\ddot{w} = f(x,t), \tag{5.58}$$

where $w(x,t)$ is the displacement. As for the discrete case, the velocity variable $v = \dot{w}$ is introduced, so that (5.58) can be written in state variables:

$$\begin{bmatrix} \mathscr{L} & 0 \\ 0 & -\rho S \end{bmatrix} \begin{Bmatrix} w \\ v \end{Bmatrix} + \begin{bmatrix} \mathscr{C} & \rho S \\ \rho S & 0 \end{bmatrix} \begin{Bmatrix} \dot{w} \\ \dot{v} \end{Bmatrix} = \begin{Bmatrix} f \\ 0 \end{Bmatrix} . \tag{5.59}$$

It is further assumed that the stiffness $\mathscr{L}$ and damping $\mathscr{C}$ operators are *self-adjoints*. This property implies some restrictive conditions on the boundary conditions, However, it is applicable to a large class of problems in dynamics. In practice, it means that, given two displacements w and w' that fulfill the boundary conditions, we can write [35]:

$$\int_L \mathscr{L} w \, w'^{\star} \, dx = \int_L w \mathscr{L} w'^{\star} \, dx, \tag{5.60}$$

where the $\star$ sign indicates the complex conjugate.

5.2.3.1 Solution of the Eigenvalue Problem

Defining

$$\boldsymbol{W} = \begin{Bmatrix} w \\ v \end{Bmatrix} \;\; ; \;\; \boldsymbol{F} = \begin{Bmatrix} 0 \\ (\rho S)^{-1} f \end{Bmatrix} \;\; \text{and} \;\; \mathbb{A} = \begin{bmatrix} 0 & 1 \\ -(\rho S)^{-1} \mathscr{L} & -(\rho S)^{-1} \mathscr{C} \end{bmatrix} \tag{5.61}$$

the system (5.59) is written in the same way as for the discrete case seen in Sect. 5.2.1.3:

$$\dot{\boldsymbol{W}} - \mathbb{A} \boldsymbol{W} = \boldsymbol{F} \, . \tag{5.62}$$

Consequently, the eigenvalue problem is written:

$$\mathbb{A} \boldsymbol{W_n} = \lambda_n \boldsymbol{W_n} \;\; ; \;\; \lambda_n w_n = v_n \;\; ; \;\; \mathscr{L} w_n + \lambda_n \mathscr{C} w_n + \rho S \lambda_n^2 w_n = 0 \, . \tag{5.63}$$

The orthogonality relations can also be generalized. We obtain

$$\begin{cases} \displaystyle\int_L w_r \left[\mathscr{L} - \lambda_r \lambda_n \rho S \right] w_n dx = A_n \delta_{rn}, \\ \displaystyle\int_L w_r \left[\mathscr{C} + \rho S (\lambda_r + \lambda_n) \right] w_n dx = B_n \delta_{rn} \, . \end{cases} \tag{5.64}$$

Notice that the constants A_n and B_n are not independent. In fact, combining the two relations in (5.64) for $r = n$, we have $A_n = -\lambda_n B_n = -2\lambda_n^2 m_n$, where m_n is

the modal mass generalized to complex modes. This quantity can be equivalently written:

$$m_n = \frac{1}{2}\int_L w_n \left[\rho S - \frac{1}{\lambda_n^2}\mathscr{L}\right] w_n dx$$
$$= \int_L w_n \left[\rho S + \frac{1}{2\lambda_n}\mathscr{C}\right] w_n dx\,. \tag{5.65}$$

Using both the orthogonality properties and the expressions of the modal masses allows us to expand the solution in terms of the eigenmodes[7]:

$$\begin{bmatrix} w(x,t) \\ v(x,t) \end{bmatrix} = \sum_n q_n(t) \begin{bmatrix} w_n(x) \\ \lambda_n w_n(x) \end{bmatrix}, \tag{5.66}$$

where the $q_n(t)$ are functions of time with complex amplitudes. Substituting these expansions in the equation of motion (5.59), and taking advantage of the orthogonality properties of the eigenmodes, the equations governing the generalized coordinates are obtained:

$$A_n q_n + B_n \dot{q}_n = f_n \quad \text{with} \quad f_n = \int_L w_n f(x,t) dx, \tag{5.67}$$

which can be alternatively expressed in terms of modal mass m_n and eigenvalue λ_n:

$$\dot{q}_n - \lambda_n q_n = \frac{1}{2\lambda_n m_n} f_n\,. \tag{5.68}$$

Finally, a set of first-order decoupled differential equations is obtained, that can be compared to the system of second-order differential equations obtained in the conservative case (see Chap. 3).

As for real modes, the integration constants are obtained through the introduction of initial conditions for both the displacement and velocity:

$$\begin{bmatrix} w(x,0) \\ v(x,0) \end{bmatrix} = \sum_n q_n(0) \begin{bmatrix} w_n(x) \\ \lambda_n v_n(x) \end{bmatrix}\,. \tag{5.69}$$

Using again the orthogonality relations, we have

[7] Since $\mathscr{L}$ and $\mathscr{C}$ are self-adjoints operators, the adjoint operator of $\mathbb{A}$ is equal to its transpose and its eigenvalues are the same as for $\mathbb{A}$. It can then be shown that *bi-orthogonality* relations exist between these two families of modes that guarantee the uniqueness of the solution. These very technical considerations will not be developed further.

$$q_n(0) = -\frac{1}{2\lambda_n^2 m_n}\int_L w_n\left[\mathscr{L}w(x,0) - \lambda_n \rho S v(x,0)\right]dx$$
$$= \frac{1}{\lambda_n m_n}\int_L w_n\left[(\mathscr{C} + \lambda_n \rho S)w(x,0) + \rho S v(x,0)\right]dx\,. \tag{5.70}$$

In contrast with the real mode case, $q_n(0)$ depends on both displacement and velocity conditions. To illustrate the method of complex modes, an example of application is given in the next section.

5.2.3.2 Application: String with a Localized Damping

In Sect. 5.2.2.2, the example of a string with a localized damping has been presented with details (see Fig. 5.2). It has been shown that the eigenmodes of the conservative system are generally coupled, and that only a few particular cases can be found where decoupling is possible. This example is used again below in order to show how to tackle the problem when the damping operator $\mathscr{C}$ cannot be diagonalized, and, in addition, when simplifying assumptions cannot be made. The following example has been solved by Krenk [31]. In the particular case where the damper is put at the end of the string, then the reader will recognize some of the results obtained in Sect. 5.2.2.3. However, the method used below is by far more general.

The case of a homogeneous string with two fixed ends is investigated. It is described by the well-known equations:

$$\begin{cases} T\dfrac{\partial^2 y}{\partial x^2} - \rho S\dfrac{\partial^2 y}{\partial t^2} = 0 \quad \text{for} \quad x \neq x_0, \\ y(0,t) = y(L,t) = 0\,. \end{cases} \tag{5.71}$$

As shown in Fig. 5.2, a damper with resistance R is attached to the string at position $x = x_0$. In this point, the solution must satisfy the discontinuity relation:

$$T\left[\frac{\partial y}{\partial x}\,|_{x_0+} - \frac{\partial y}{\partial x}\,|_{x_0-}\right] = R\frac{\partial y}{\partial t}\,|_{x=x_0}\,. \tag{5.72}$$

Free vibrations are sought in the form $y(x,t) = Y(x)\exp(j\omega t)$, where Y and ω are complex. The dispersion equation then gives the complex wave number $k = \omega/c$. Because of the discontinuity in $x = x_0$, the general form of the complex modes is given by:

$$Y_n(x) = \begin{cases} Y_n(x_0)\dfrac{\sin k_n x}{\sin k_n x_0} \quad \text{for} \quad 0 \le x \le x_0, \\ \\ Y_n(x_0)\dfrac{\sin k_n (L-x)}{\sin k_n (L-x_0)} \quad \text{for} \quad x_0 \le x \le L, \end{cases} \tag{5.73}$$

where the k_n are obtained by the discontinuity condition (5.72):

$$\cot k_n x_0 + \cot k_n (L - x_0) = j \frac{R}{Z_c} \,. \tag{5.74}$$

where Z_c is the characteristic impedance of the string. Using the general results obtained in the first part of this section, the modal mass is found to be equal to:

$$m_n = \frac{1}{2} \rho S Y_n^2(x_0) \left\{ \frac{x_0}{\sin^2 k_n x_0} + \frac{L - x_0}{\sin^2 k_n (L - x_0)} \right\} \,. \tag{5.75}$$

Finally, in the case of a forced regime with, for example, a force of amplitude F applied at $x = x_1$ for $t \geq 0$, the generalized coordinate is obtained

$$q_n(t) = -\frac{F Y_n(x_1)}{2 \lambda_n^2 m_n} \left[1 - e^{jck_n t} \right] . \tag{5.76}$$

From the knowledge of $Y_n(x)$ and $q_n(t)$, the solution $y(x, t)$ is obtained, using (5.66).

5.3 Damping Mechanisms in Solid Materials

5.3.1 Introduction

The analysis and modeling of damping in solid materials is difficult, due to the existence of many different mechanisms. Any irreversible process in materials dissipates energy. Figure 5.5 shown below illustrates three common processes:

- (a) A straight line is drawn in the stress–strain plane, consecutive to a traction test on a sample made of *elastic* material. During the release, it it observed that

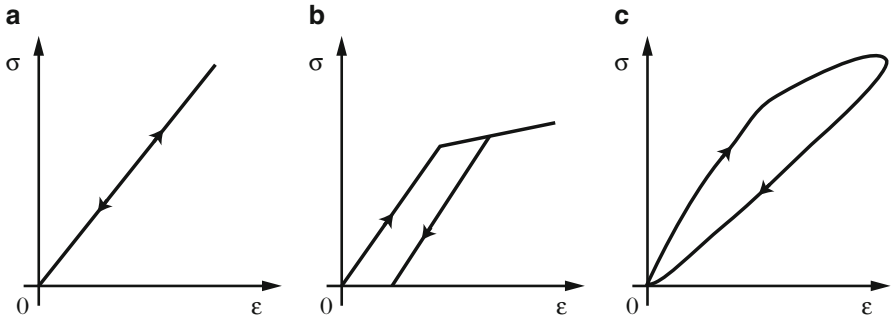

Fig. 5.5 Reversible and irreversible processes. (**a**) Elastic, non-dissipative behavior. (**b**) Anelastic behavior. (**c**) Linear viscoelastic behavior

the same line is drawn and that the final state corresponds to the initial state at the origin of the axes. The process is said to be reversible and no energy is dissipated during the experiments.

- (b) If the same test is made on a glass fiber, for instance, a curve is obtained showing that a part of the mechanical energy is transformed into heat at each cycle. This dissipation is due to an internal reorganization of the solid. As a consequence, the particles do not go over the same equilibrium states, for increasing and decreasing stress, respectively. The behavior is said *anelastic*.
- (c) Some materials exhibit reversible processes, provided that they remain in the linear domain, but are sensitive to strain velocity. This is the case for *viscoelastic* materials. Wood and polymers enter in this category of materials, which are largely used in musical acoustics. The viscoelastic damping also depends strongly on the temperature.

For metals, which are conductors of heat, it is necessary to also take the coupling between elastic waves and heat diffusion into account. Everybody can easily reproduce the experience of bending a metallic rod and noticing that a warm-up occurs, especially in the zone of maximum strain. This mechanism is a consequence of *thermoelastic* losses that also occur in metallic strings or in structures used in percussion (bars, plates, and shells). Dislocations, i.e., motions of defects lines that are hindered by impurities present in the crystal lattice, also occur in metals. These motions induce losses whose amplitude and spectrum depend on the metallurgical treatment undergone by the metal. In this context, Valette reports important results with regard to losses in harpsichord strings [43].

In what follows, special consideration is given to the description of thermoelastic and viscoelastic damping, which are the predominant dissipative mechanisms in the materials used for making musical instruments. Hysteretic damping will also be mentioned, since it is widely used in the context of structural dynamics. In addition, the viscous damping of a string vibrating in the air will be briefly presented, and the reader should refer to Valette for more developments [43]. For bars, plates, and shells, these viscosity effects are often negligible compared to the other causes of damping. The damping due to acoustic radiation will be presented in the fourth part of this book.

5.3.2 String Damping Due to Air Viscosity

The main reference model of viscosity losses for a string vibrating in air was given by Stokes in 1851 [41]. He shows that the mechanical resistance per unit length r_m for a cylinder with diameter d and oscillation frequency f in a fluid such as air with *viscosity coefficient* μ and density ρ, is equal to:

$$r_m = \pi^2 \rho f \frac{d^2}{2}\left(\frac{\sqrt{2}}{M} + \frac{1}{2M^2}\right) \quad \text{with} \quad M = \frac{d}{4}\sqrt{\frac{2\pi f}{\nu_a}}, \tag{5.77}$$

where $\nu_a = \mu/\rho$ is the fluid *kinematic viscosity*.

For air, we have $\mu = 1.832 \times 10^{-5}\,\mathrm{kg/m\,s}$ and $\nu_a = 1.52 \times 10^{-5} \times \mathrm{m^2/s}$. For typical strings of musical instruments, in the medium frequency range, the dimensionless coefficient M is of the order of unity.

The power $\mathscr{P}_v$ dissipated by viscosity is obtained by summing the scalar product of the elementary viscosity forces $df = -r_m v dx$ and transverse string velocity v over the total length of the string. The kinetic energy decreases as a consequence of viscosity losses. In total, we can write

$$\mathscr{P}_v = \frac{d\mathscr{E}_c}{dt} = -r_m \int_L v^2 dx\,. \tag{5.78}$$

Denoting ρ_s the string density, its kinetic energy is written

$$\mathscr{E}_c = \frac{\rho_s S}{2}\int_L v^2 dx, \quad \text{with} \quad S = \pi d^2/4.$$

Equation (5.78) can be put in the form:

$$\frac{d\mathscr{E}_c}{dt} = -\frac{\mathscr{E}_c}{\tau_e} \text{ with } \tau_e = \frac{\rho_s}{2\pi f \rho}\left(\frac{M^2}{2\sqrt{2}M+1}\right), \tag{5.79}$$

where τ_e is the time constant. The energy is proportional to the square of the amplitude, therefore the viscosity time constant τ of the string motion is equal to:

$$\tau = 2\tau_e = \frac{\rho_s}{\pi f \rho}\left(\frac{M^2}{2\sqrt{2}M+1}\right). \tag{5.80}$$

Equation (5.80) shows that the viscosity time constant decreases roughly as $1/\sqrt{f}$ for $f \gg \nu_a/4\pi r^2$, which corresponds approximately to $f \gg 5\,\mathrm{Hz}$ for the numerical data shown in Fig. 5.6. Viscosity losses can be significant for high frequencies. They can be reduced with the use of dense materials. One can also check that τ increases (hence losses decreases) with radius r.

5.3.3 *Thermoelasticity in Orthotropic Plates*

The thermoelastic damping is a consequence of the coupling between elastic strain and heat diffusion. It affects the vibrations of solids with a noticeable thermal conductivity, such as metals. This type of damping is adequately described by

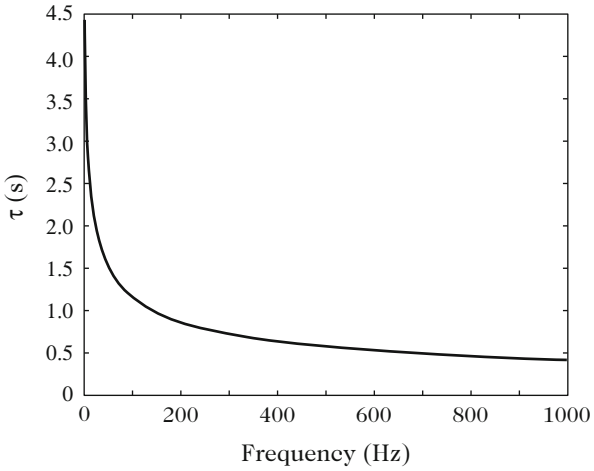

Fig. 5.6 Viscosity time constant for a Nylon string as a function of the frequency. Numerical values: $\rho_s = 10^3\,\mathrm{kg/m^3}$; $\rho = 1.29\,\mathrm{kg/m^3}$; $d = 1.0\,\mathrm{mm}$

a coupling between the dynamics of the structure under consideration and heat diffusion [5, 44]. In this section, it will be shown how to represent this damping by adding an imaginary part to the stiffness constants. The method is illustrated by the example of orthotropic plates. The thermoelastic damping in isotropic plates and bars is then deduced as particular cases. The case of thermoelastic damping in prestressed bars (or stiff strings) was done by Valette and Cuesta [43].

The variations of temperature θ in the materials are supposed to be reasonably weak so that the constitutive equations relating stress σ_{ij} and strain $W_{,ij}$ can be linearized (the symbols ij represent here the partial derivative of the transverse displacement W with respect to the coordinates). The symbol s is the Laplace variable. In Cartesian coordinates, the three stress components in the plate are written [10]:

$$\begin{aligned}
\sigma_{xx} &= -12z\big(D_1 W_{,xx} + \frac{D_2}{2} W_{,yy}\big) - \phi_x \theta, \\
\sigma_{yy} &= -12z\big(D_3 W_{,yy} + \frac{D_2}{2} W_{,xx}\big) - \phi_y \theta, \\
\sigma_{xy} &= -6z D_4 W_{,xy}\ ,
\end{aligned} \tag{5.81}$$

where ϕ_x and ϕ_y are the thermal coefficients of the material. For the particular case of an isotropic material, $\phi_x = \phi_y = \phi$, and this coefficient is related to the thermal dilatation coefficient α by the relationship [39]:

$$\phi = \alpha \frac{E}{1-2\nu}\ . \tag{5.82}$$

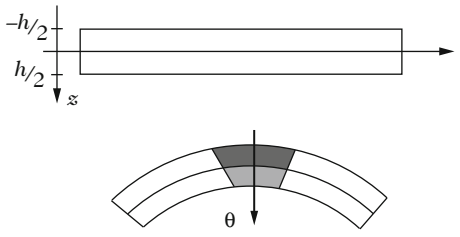

Fig. 5.7 Thermoelastic plate. The temperature θ increases from the stretched to the compressed fibers

The system (5.81) is complemented by the heat diffusion equation, where it is assumed that θ depends on the coordinate z of the plate thickness only (see Fig. 5.7):

$$\kappa\theta_{,zz} - \rho Cs\theta = -zT_0 s\left(\phi_x W_{,xx} + \phi_y W_{,yy}\right), \tag{5.83}$$

In (5.83), T_0 is the absolute temperature, C is the specific heat for constant strain, and κ is the thermal conductivity. Following the method used by Cremer [15], $\theta(z)$ is supposed to be of the form:

$$\theta(z) = \theta_0 \sin\frac{\pi z}{h} \quad \text{for} \quad z \in \left[-\frac{h}{2}, \frac{h}{2}\right]. \tag{5.84}$$

This expression accounts for the fact that the thermal exchange between plate and air is small. Integrating $z\sigma_{ij}$ along the plate thickness h, one obtains the expressions that connect the bending and torsion moments M_{ij} to the spatial derivatives of the transverse displacement W. After some calculations, it is found that the stiffness factors are written [10]:

$$\begin{aligned}
\tilde{D}_1(s) &= D_1 + \phi_x^2 \frac{s\zeta}{1+\tau s},\\
\tilde{D}_2(s) &= D_2 + 2\phi_x\phi_y \frac{s\zeta}{1+\tau s},\\
\tilde{D}_3(s) &= D_3 + \phi_y^2 \frac{s\zeta}{1+\tau s},\\
\tilde{D}_4(s) &= D_4.
\end{aligned} \tag{5.85}$$

The thermal relaxation time constant τ and the parameter ζ are defined as follows:

$$\tau = \frac{\rho C h^2}{\kappa\pi^2} \quad \text{and} \quad \zeta = \frac{8T_0 h^2}{\kappa\pi^6}. \tag{5.86}$$

Table 5.1 Thermal constants for some usual materials

	Wood	Steel	Glass	Aluminum	Nylon
C (J/kg °C)	2000	460–625	700	900	1500
α ($\times 10^{-6}$ K^{-1})	4	14	6–10	22	10^3
κ (W/m K)	0.04–0.4	11–46	1.1	105–250	0.1–0.3

The thermoelastic losses are proportional to the imaginary part of the stiffness constants $\tilde{D}_i(j\omega)$. From (5.85), these losses are shown to increase with frequency and reach an asymptotic value proportional to ζ/τ^2. In practice, this means that the thermoelastic losses increase proportionally to $1/h^2$.

It can also be noticed that D_4 is real. As a consequence, the modes of the plates subjected to a torsional strain, involving D_4, are less affected by the thermoelastic damping than the other modes. In fact, the thermoelastic damping depends on the modal shapes, so that, from one mode to another, the graphs showing the evolution of the modal damping factors in s^{-1} as a function of frequency have an apparent erratic behavior (see Fig. 5.8). This behavior is a direct consequence of the theory of thermoelasticity, and is not the result of errors in measurements.

In some cases, it might be appropriate to write the complex stiffnesses under the following form:

$$\tilde{D}_i(s) = D_i\left[1 + \tilde{d}_{it}(s)\right] = D_i\left[1 + \frac{sR_i}{s + c_1/h^2}\right],\ i = [1, 2, 3]$$
$$\tilde{D}_4(s) = D_4, \tag{5.87}$$

in order to highlight their dependency upon thickness. Considering the order of magnitude of the thermal constants for usual materials (see Table 5.1), the norm of the term $\tilde{d}_{it}(s)$ can be considered to be small compared to unity, so that it appears as a perturbation term. In (5.87), the coefficients R_i are defined as:

$$R_1 = \frac{8T_0\phi_x^2}{\pi^4 D_1 \rho C}\ ;\ R_2 = \frac{16T_0\phi_x\phi_y}{\pi^4 D_2 \rho C}\ ;\ R_3 = \frac{8T_0\phi_y^2}{\pi^4 D_3 \rho C}\ . \tag{5.88}$$

Thermoelastic damping is not the only dissipation mechanism present in vibrating structures. For non metallic plates and shells, the viscoelastic damping is often predominant. The radiation damping must also be considered. However, thermoelastic damping remains the primary cause of dissipation at low frequencies for metals.

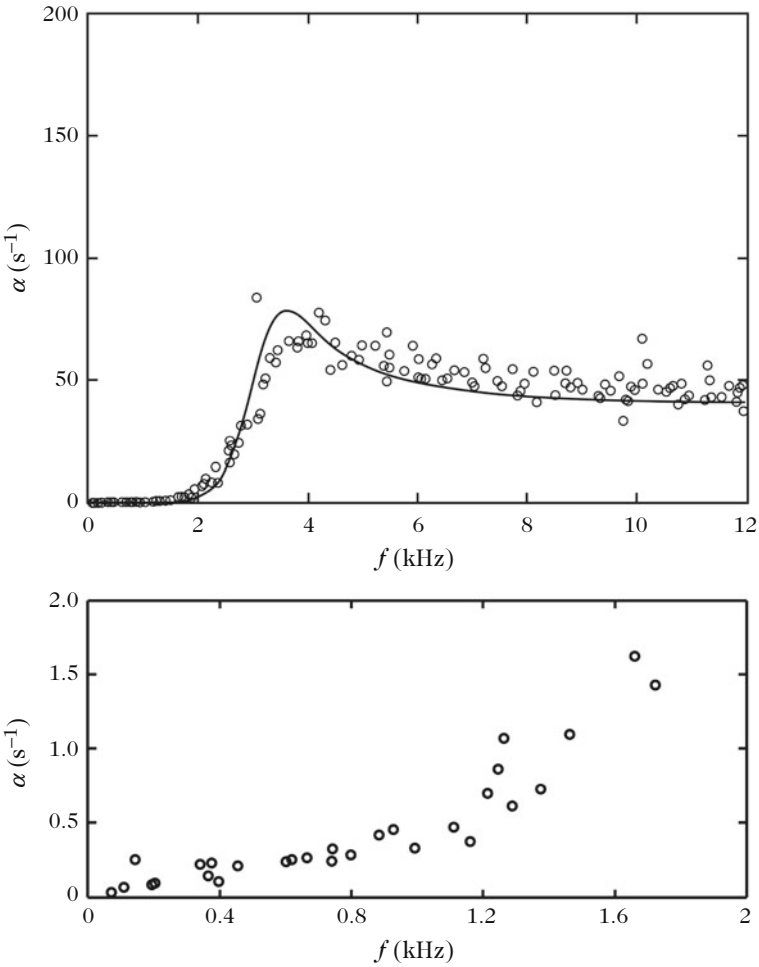

Fig. 5.8 (*Top*) Damping factors (in s^{-1}) of a rectangular aluminum plate, as a function of frequency (in kHz). Comparison between theory (*solid line*) and experiments (*open circle*). (*Bottom*) Zoom of the previous figure in the lower part of the spectrum, showing the apparent erratic behavior of the thermoelastic damping due to the influence of the modal shapes. From [10]

5.3.4 Viscoelasticity

The viscoelastic models used in vibration theory are based on a macroscopic approach to dissipation phenomena and are most often derived from experiments. In their general form, these laws can be expressed as a function relating stress, strain, time, and temperature, as follows [11]:

$$\mathscr{F}\left(\mathscr{D}_1(\sigma), \mathscr{D}_2(\varepsilon), t, T\right) = 0 \tag{5.89}$$

where $\mathscr{D}_1$ and $\mathscr{D}_2$ are integral or differential operators that are assumed to be linear throughout this section.

5.3.4.1 Preliminary Experiments: Viscoelastic String

Each string instrument player has experienced the fact that a newly stretched string does not keep its tension, and that it is necessary to wait for a couple of days to get stability of the pitch. This effect of *stress relaxation* is due to viscoelasticity, which is the main cause of thermal dissipation in non heat conducting materials (such as nylon, or catgut, which are materials largely used for strings). One approach for modeling this phenomenon is to consider that if the string is abruptly subjected to a variation of length (or of *strain* $\varepsilon = \frac{L-L_o}{L_o}$, where L_o is the initial string length), then the tension divided by the section S of the string (or axial *stress* $\sigma = \frac{T}{S}$) is described by the differential equation [16]:

$$\dot{\sigma} + \frac{\sigma}{\tau} = E\dot{\varepsilon}, \tag{5.90}$$

where E is the Young's modulus of the string, and τ a relaxation constant. By turning the peg at one end of the string, a strain $\varepsilon(t) = \varepsilon_1 H(t)$ is imposed, where $H(t)$ is the Heaviside function. As a consequence, the axial stress decreases exponentially with time: $\sigma(t) = E\varepsilon_1 e^{-\frac{t}{\tau}}$. Therefore, the string tension also decreases with time, which is confirmed by daily experiments (see Fig. 5.9).

During playing, the string is constantly subject to variations of tension, associated with the flexural vibrations, and thus the viscoelasticity phenomenon is present. Here, one can consider that these fluctuations of stress lead to variations of strain according to the equation:

$$\sigma = E\left(\varepsilon + \tau\dot{\varepsilon}\right) . \tag{5.91}$$

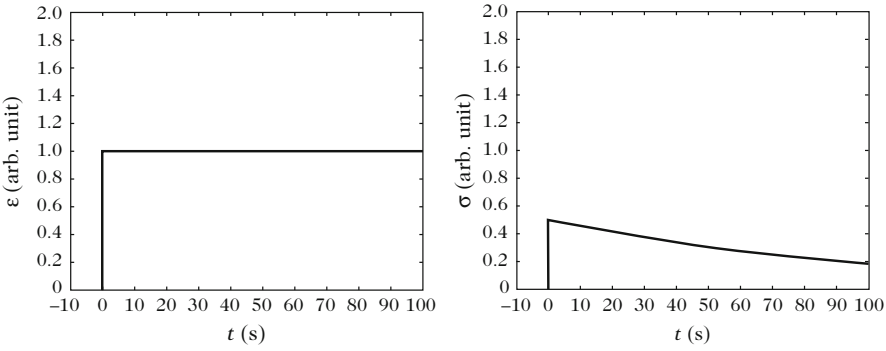

Fig. 5.9 Relaxation of a stretched string, after a sudden variation of strain (arbitrary units)

Introducing (5.91) in the vibrating string Eq. (3.47), we get

$$\frac{1}{c^2}\frac{\partial^2 y}{\partial t^2} = \frac{\partial^2 y}{\partial x^2} + \tau \frac{\partial^3 y}{\partial x^2 \partial t} \,. \tag{5.92}$$

Consider now the propagation of a harmonic wave of the form $y(x,t) = e^{j(kx-\omega t)}$ in this damped string. The string is supposed to be infinite in length (this is equivalent to considering the propagation of the waves before they reach the ends). The dispersion equation becomes

$$\omega^2 = c^2(1 - j\omega\tau)k^2 \,. \tag{5.93}$$

For an imposed wavenumber k, and considering further that $\tau \ll \frac{2}{kc}$, the displacement can be written as:

$$y(x,t) = e^{-\frac{\tau k^2 c^2}{2}t} e^{jk(x \pm ct)} \,. \tag{5.94}$$

The large wave numbers are found to be damped faster than the small ones, which induces a deformation of the wave during its propagation.

The solution of Eq. (5.92) is now expressed as an expansion onto the basis of the eigenmodes of the ideal string. Using the orthogonality properties as shown in Sect. 3.3.2, the equations satisfied by the generalized coordinates are obtained

$$\ddot{q_n} + \tau\omega_n^2 \dot{q}_n + \omega_n^2 q_n = 0 \,. \tag{5.95}$$

With $\tau \ll \frac{2}{\omega_n}$, a condition that is usually fulfilled for the strings of musical instruments in their usual frequency range, and with zero initial velocity, we have

$$q_n(t) \approx q_n(0) e^{-\frac{\tau\omega_n^2}{2}t} \cos\omega_n t \,. \tag{5.96}$$

In the time domain, the viscoelastic damping introduced in (5.92) consequently leads to a time constant which is proportional to the square of frequency. This simple model is in accordance with the phenomena observed in Nylon strings.

Remark. With the viscoelastic damping term introduced here in the string equation, it is observed that the differential equations of the generalized coordinates remain decoupled. This is a particular case of *proportional damping* presented in Sect. 5.2.1.2, where the damping matrix is written here $\mathbb{C} = \tau\mathbb{K}$.

5.3.4.2 General Viscoelastic Models

Both examples (5.90) and (5.91) represent particular cases of a general differential formulation of viscoelasticity combining stress, strain, and their time derivatives. These simple examples provide a reasonable interpretation of some phenomena

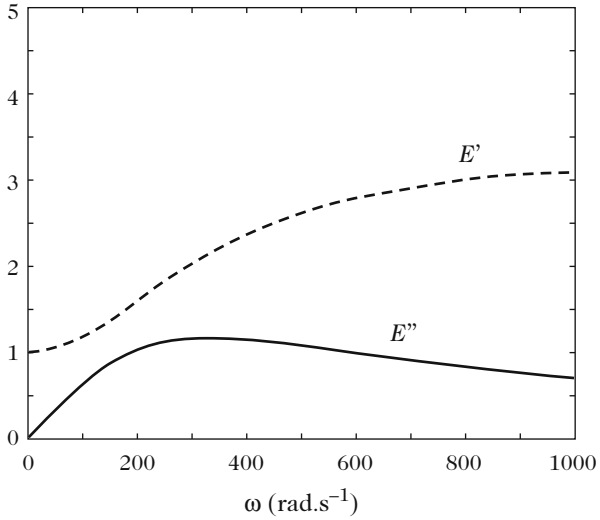

Fig. 5.10 Linear standard model (or Zener model). Variation of the real part E' (*dotted line*), and imaginary part E'' (*solid line*) of the complex Young's modulus as a function of the angular frequency ω. Ordinate units are arbitrary

observed in stringed instruments. One generalization of these models is the so-called standard viscoelastic linear model (or Zener model):

$$\sigma + \tau_1 \dot{\sigma} = E\,(\varepsilon + \tau_2 \dot{\varepsilon}) \tag{5.97}$$

which includes three parameters (E, τ_1, and τ_2). If Eq. (5.97) is written in the frequency domain, for solutions of the form $\sigma = \sigma_0 e^{j\omega t}$ and $\varepsilon = \varepsilon_0 e^{j\omega t}$, a complex Young's modulus can be expressed as:

$$E(\omega) = \frac{\sigma}{\varepsilon} = E^{'}(\omega) + jE^{''}(\omega) = E\left[\frac{1+\omega^2\tau_1\tau_2}{1+\omega^2\tau_1^2} + j\frac{\omega(\tau_2-\tau_1)}{1+\omega^2\tau_1^2}\right]. \tag{5.98}$$

Variations of real ($E^{'}$) and imaginary($E^{''}$) parts of the complex Young's modulus vs. frequency are shown in Fig. 5.10. Even if it is conceptually and qualitatively interesting, the main drawback of this model is that the commonly observed variations of the Young's modulus with frequency are less pronounced. As a consequence, it is often difficult to adjust the constants of the model E, τ_1, and τ_2 to fit the experimental data.

Because of these limits to this use, several authors have proposed to extend the standard model to a generalized differential formulation such as:

$$\sigma + \sum_{i=1}^{n} a_i \frac{d^i\sigma}{dt^i} = E\left(\varepsilon + \sum_{i=1}^{n} b_i \frac{d^i\varepsilon}{dt^i}\right). \tag{5.99}$$

This formulation enables a better fit to observed phenomena, compared to the Zener case. The price to pay is that a larger number of parameters need to be adjusted, which implies to collecting a larger number of measured data. In the frequency domain, the complex Young's modulus becomes

$$E(\omega) = E\frac{1 + \sum_{i=1}^{n} a_i (j\omega)^i}{1 + \sum_{i=1}^{n} b_i (j\omega)^i} \,. \tag{5.100}$$

In (5.100), n is an integer, which limits the model to moduli exhibiting flat slopes vs. frequency. For that reason, recent developments use fractional values of n for representing smoothly varying frequency dependence [34].

5.3.4.3 Integral Formulation

The previous section has shown some limits of the differential models for describing linear viscoelasticity. In some cases, an integral continuous formulation is preferred, such as [11]:

$$\sigma(t) = \int_{-\infty}^{t} E(t-\tau) d\varepsilon(\tau), \tag{5.101}$$

where $E(t-\tau)$ is a relaxation function. Physically, this formulation, in the form of a convolution integral, means that the stress depends on the history of material strain. With $E(t) = E_0 + E_r(t)$, and assuming further that $E_r(t)$ tends to zero as time t tends to ∞, an equivalent formulation is found

$$\sigma(t) = E_0 \varepsilon(t) + \int_{-\infty}^{t} E_r(t-\tau) \frac{d\varepsilon(\tau)}{d\tau} d\tau \,. \tag{5.102}$$

The obtained formulation can be easily handled with Fourier or Laplace analysis.

5.3.5 Hysteretic Damping

Hysteretic damping accounts for energetic losses observed in phenomena with hysteresis loops. It is frequently encountered in the dynamics of structures. By defining the *loss factor* as the ratio between the energy dissipated in the system during one period of oscillation, and the maximum of the potential energy [13], the hysteretic damping is shown to represent a loss factor independent of frequency. The equation of motion of a one DOF oscillator with hysteretic damping is written in the frequency domain:

$$[-M\omega^2 + K\,(1 + j\eta\ \mathrm{sgn}(\omega))]\Xi(\omega) = F(\omega) \,. \tag{5.103}$$

Such a formulation accounts for stationary oscillations of the system. However, its dual formulation in the time domain is not causal. In fact, the inverse Fourier transform of the damping term $F_d(\omega) = j\omega R(\omega)\Xi(\omega) = jK\eta \operatorname{sgn}(\omega)\Xi(\omega)$ is written [13]:

$$f_d(t) = \frac{jK\eta}{2\pi} \int_{-\infty}^{+\infty} \operatorname{sgn}(\omega) e^{j\omega t} d\omega \int_{-\infty}^{+\infty} \xi(\tau) e^{-j\omega\tau} d\tau \ . \tag{5.104}$$

The mass displacement expression is then:

$$\xi(t) = \frac{1}{2\pi K\eta} \int_{-\infty}^{+\infty} \frac{e^{j\omega t}}{j\operatorname{sgn}(\omega)} d\omega \int_{-\infty}^{+\infty} f_d(\tau) e^{-j\omega\tau} d\tau. \tag{5.105}$$

As an example, let us impose $f_d(t) = \delta(t)$. Equation (5.105) yields

$$\xi(t) = \frac{1}{\pi K\eta} \frac{1}{t} \qquad -\infty < t < +\infty. \tag{5.106}$$

The expression (5.106) is clearly non causal, since the response precedes the excitation. As a conclusion, this calculation shows that hysteretic damping does not constitute an appropriate formulation for losses in the time domain, and that other strategies should be then used to model a loss factor independent of frequency.

5.4 Damping Mechanisms in Cylindrical Pipes

5.4.1 Introduction

There are several types of attenuation mechanisms for an acoustic wave in air, and their relative importance varies significantly with both the frequency and limits of the spatial domain. In pipes, two mechanisms clearly dominate at audible frequencies: viscosity and thermal conduction effects. Both occur primarily near the walls. This means that the plane waves that are assumed to occur in a pipe cannot be truly plane, because the velocity tangential to a wall must be zero. Physical arguments have been found from experimental observations (a theory based on the analysis of molecular motion would be very complex): then if the velocity parallel to walls is zero at the wall, and non-zero near the walls, friction occurs because of air viscosity (see Fig. 5.11).

The complete theory of attenuation and dispersion (the dispersion is the variation of the phase velocity with frequency) is due to Kirchhoff [30]. It takes the viscosity and thermal conduction effects into account, and is valid both in free space and near the walls.

In free space, attenuation increases as the square of frequency: it is the mechanism responsible for the dissipation by radiation (this is true for all musical

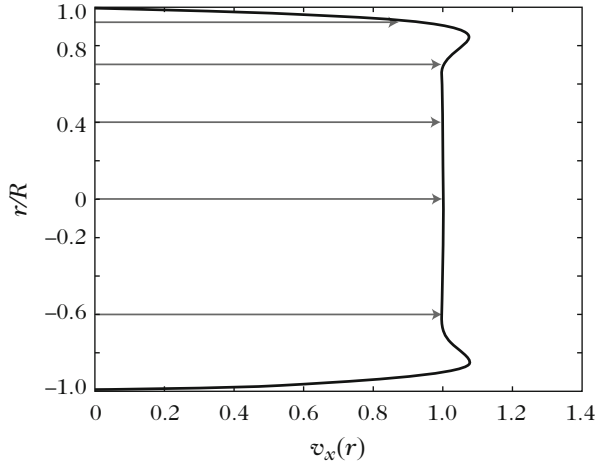

Fig. 5.11 Axial velocity profile in a cylindrical pipe, for a Stokes number equal to 21: the velocity is zero on the walls and uniform in the central part of the pipe. The ordinate axis shows the radial coordinate r, normalized by its value R on the wall

instruments!). The radiated energy is never reflected in free space, because it is dissipated before reaching any obstacle; nevertheless, it is not needed to know the dissipation mechanism precisely as it is sufficient to write that no wave returns back from infinity (see Chap. 12).

Near the walls attenuation increases as the square root of frequency. It is the dominant attenuation mechanism in pipes, and thus needs to be well understood. At the wall, Kirchhoff suggested to add two supplementary conditions to the model with zero velocity perpendicular to a rigid wall: the vanishing of both tangential velocity and acoustic temperature. A first method consists of simplifying Kirchhoff results to observe what occurs near the walls. However, this approach can be cumbersome, and here a simple theory is preferred: it is a simplification of Kirchhoff's theory, and it enables a better understanding of the phenomena encountered in wind instruments. This approach due to Zwikker and Kosten [45], forms the basis of the theory of absorbing materials with rigid skeleton, seen as a set (or bundle) of narrow rigid pipes. Its knowledge is useful for wide pipes (it is defined later what is meant by "wide"), and for very narrow pipes such as a small slit leading to leaks. This theory is largely sufficient for the study of wind instruments. Let us add that damping is essential for the sound production, as it determines the threshold of self-sustained oscillations (see Chap. 9).

The Zwikker and Kosten theory enables replacing the propagation equations of a plane wave by one-dimensional equations obtained by averaging the acoustic quantities over a pipe cross section. A great advantage is that it separates the viscous effects and the thermal conduction effects, and leads to a transmission line

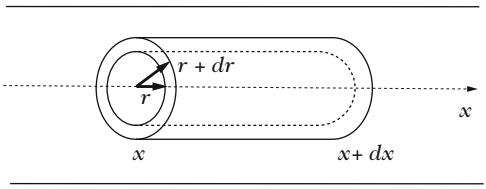

Fig. 5.12 Geometry of a ring in a pipe slice

formulation for averaged quantities. The case of a cylindrical pipe of radius R is chosen, and polar coordinates will be used. Similar results have been obtained for rectangular pipes [2, 27].

N.B. ***If readers prefer to skip the proof, they can continue to read this chapter from Sect. 5.5.***

5.4.2 Viscous Effects

5.4.2.1 Simplified Navier–Stokes Equation

The equation of momentum conservation is now written including viscosity. By doing so, the Navier–Stokes equation is obtained, that replaces Euler Equation [see Eq. (1.101)]. In fact, this equation is simplified straightaway, assuming that there is no average flow, and making some other assumptions, such as axisymmetry. Let us consider a fluid slice between abscissae x and $x+dx$, and in this slice, a ring between radius r and $r + dr$ (see Fig. 5.12). Without viscosity, the force equilibrium is

$$-(2\pi r dr)\frac{\partial p}{\partial x}dx = \rho(2\pi r dr)dx\frac{\partial v_x(r,x)}{\partial t}\ . \tag{5.107}$$

where $v_x(r,x)$ is the axial velocity. The pressure difference between x and $x + dx$, on the surface $2\pi r dr$ is on the left-hand side. The friction forces, linked to the viscosity coefficient μ, must be added to the pressure force. They are, by definition, proportional to μ, to the wall surface area, and to the derivative of the axial velocity. On the internal and external faces of the ring, their values are respectively:

$$-\mu(2\pi r dx)\frac{\partial v_x(r,x)}{\partial r} \text{ and } \mu[2\pi(r+dr)dx]\frac{\partial v_x(r+dr,x)}{\partial r}.$$

The choice of signs can be explained as follows: the axial velocity must decrease from $r = 0$ to $r = R$, where it is zero, thus $\partial v_x/\partial r$ is negative, and the force must speed up the slower fluid layer, and slow down the faster fluid layer. On the internal face, the layer outside of the ring (radius lower than r) moves faster than the layer inside the ring, and thus the latter should speed up (positive force); it is the opposite for the external face. Dividing by $(2\pi r dx dr)$, the force equilibrium yields

$$\frac{\mu}{r}\frac{\partial}{\partial r}\left[r\frac{\partial v_x}{\partial r}\right]-\frac{\partial p}{\partial x}=\rho\frac{\partial v_x}{\partial t}. \tag{5.108}$$

It can be verified that this is the linearized Navier–Stokes equation, for the $\boldsymbol{x}$ direction, i.e.:

$$\rho\frac{\partial \boldsymbol{v}}{\partial t}+\text{grad}p=\mu\Delta\boldsymbol{v}+\left[\eta+\frac{\mu}{3}\right]\text{graddiv}\boldsymbol{v}$$

where the leading term of the axial velocity Laplacian is assumed to be the radial one. Furthermore, the velocity divergence is assumed to be essentially longitudinal ($\partial v_x/\partial x \gg r^{-1}\partial\left[rv_r\right]/\partial r$). Moreover, second viscosity effects have been neglected (linked to rotation and vibration movements of molecules, coefficient η) relative to shear effects (linked to the translation movements of molecules, with coefficient μ). It can also be shown that the velocity $\boldsymbol{v}$ can be decomposed as the sum of an irrotational component and a solenoidal one, with zero divergence. Thus, for the x-component, $v_x = v_{xa} + v_{xt}$, and, with the approximations leading to Eq. (5.108),

$$\frac{\partial p}{\partial x}=-\rho\frac{\partial v_{xa}}{\partial t}\ \text{ and }\ \Delta v_x\simeq\frac{1}{r}\frac{\partial}{\partial r}\left[r\frac{\partial v_{xt}}{\partial r}\right]=\frac{\rho}{\mu}\frac{\partial v_{xt}}{\partial t}. \tag{5.109}$$

The term v_{xa} corresponds to the acoustic velocity of a plane wave, which is known to be a solution of a propagation equation, whereas velocity v_{xt} is a solution of a diffusion equation (the time derivative term is a single derivative with respect to time, as for the heat equation): this term is crucial near the wall, as it must have equal magnitude and opposite sign to the plane wave at the wall, and very be small far from the wall, as it is seen below.

5.4.2.2 Solving of the Equation

Equation (5.108), is solved in the frequency domain,[8] and an additional assumption is made, that is legitimated by a comprehensive calculation of the Kirchhoff theory. The assumption is that the pressure remains plane, the term $\partial p/\partial x$ being independent of r. The following equation can be solved in r:

$$\frac{1}{r}\frac{\partial}{\partial r}\left[r\frac{\partial V_x}{\partial r}\right]+k_v^2V_x=\frac{1}{\mu}\frac{dP}{dx}\quad\text{where}\quad k_v=\left[-\frac{j\omega\rho}{\mu}\right]^{1/2}. \tag{5.110}$$

k_v is the wavenumber of the diffusion wave for viscous effects. The general solution of this equation is the sum of a particular solution and of the general solution of the equation without a right-hand side member:

[8] In fact, terms in $\sqrt{j\omega}$ will be found, that correspond to a derivative of time order $1/2$: about this topic, the reader should refer to [7, 20, 21, 37].

$$V_x = AJ_0(k_v r) + BN_0(k_v r) + \frac{1}{\mu k_v^2}\frac{dP}{dx},$$

where A and B are two constants. J_0 and N_0 are the Bessel functions of first and second kinds, respectively. Considering that N_0 tends towards infinity for $r = 0$, the boundary condition is $B = 0$ since the field must be finite in $r = 0$. It remains to write the condition on the wall ($v_x = 0$ in $r = R$), from which the coefficient A is derived, which gives

$$V_x = -\frac{1}{j\omega\rho}\frac{dP}{dx}\left[1 - \frac{J_0(k_v r)}{J_0(k_v R)}\right]. \tag{5.111}$$

Figure 5.11 shows the velocity profile obtained. $r_v = |k_v R|$ is an essential parameter (as well as the parameter r/R) representing the ratio of the radius to the boundary layer thickness, where the axial velocity decreases quickly towards zero. It is called the *Stokes number*. Using the asymptotic expansion for large[9] pipes near the walls, the following result is obtained (for large values of $k_v r$):

$$V_x = -\frac{1}{j\omega\rho}\frac{dP}{dx}\left[1 - \exp\left[jk_v(r - R)\right]\right]. \tag{5.112}$$

The exponential term, corresponding to the solenoidal velocity, has an argument proportional to $(1 + j)(r - R)$, which has a real negative part as $r < R$. It decreases therefore quickly as r decreases away from the wall, as is expected for the solution of a diffusion equation. If the boundary layer thickness E_v is defined as the value of $(R - r)$ for which the modulus of the exponential is $1/e$, it is equal to

$$E_v = \sqrt{2\mu/\omega\rho}. \tag{5.113}$$

The boundary layer thickness is inversely proportional to the square root of frequency, because attenuation increases with frequency. When the Stokes number is large, the total velocity linearly increases from the wall:

$$V_x \simeq \frac{1}{\omega\rho}\frac{dP}{dx}k_v(r - R)\,. \tag{5.114}$$

Conversely, if the boundary layer thickness is the same order of magnitude as the radius, which occurs at low frequency, then the two boundary layers on opposite sides of the pipe overlap and phenomena change. Writing $J_0(x) = 1 - x^2/4 + O(x^4)$, this leads to

[9] To calculate the Bessel function, it should be noticed that it is function of an argument of type $z\sqrt{-j}$, where z is real: it is a Kelvin function, denoted $\mathrm{ber}_0(x) + j\mathrm{bei}_0(x)$, already met for shell vibrations in Chap. 3, and for which asymptotic expansion can be found in tables [1].

$$V_x = -\frac{1}{\mu}\frac{dP}{dx}\frac{R^2 - r^2}{4}. \tag{5.115}$$

The velocity profile becomes parabolic. For this case, the flow is laminar and is called Poiseuille flow. For (low) audible frequencies, this behavior is met only for pipes with a very small diameter (less than a tenth of a mm) that are called capillaries. This is also true for very narrow slits, e.g., leak interstices in a wind instrument. Musicians want to avoid such leaks, because they strongly disturb the input impedance. This behavior is also met in static regime for a viscous fluid flow, for which the viscosity effects overcome the convection effects (which are zero in linear acoustics without mean flow). In fact it should not be forgotten that in Eq. (5.108), the convection terms of the Navier–Stokes equation have been ignored (as done for Euler Equation (1.101)). As a dimensionless number, the Stokes number is the ratio of the unsteadiness term to the viscosity term.[10]

5.4.2.3 Averaged Axial Velocity

Going back to a one-dimensional system, the average of Eq. (5.111) remains to be calculated, which is equivalent to calculating the axial flow rate $u = 2\pi \int_0^R v_x r dr$. This provides the first of the two required equations. It replaces the one-dimensional Euler Equation, with a kind of effective density, that we will denote $\rho_v(\omega)$, which depends on both viscosity and frequency. Its behavior will be studied further. As $\int xJ_0(x)dx$ is equal to $xJ_1(x)$, it is written as:

$$U = -\frac{S}{j\omega\rho_v}\frac{dP}{dx} \quad \text{where} \quad \frac{1}{\rho_v(\omega)} = \frac{1}{\rho}\left[1 - \frac{2}{k_v R}\frac{J_1(k_v R)}{J_0(k_v R)}\right]. \tag{5.116}$$

5.4.3 *Thermal Conduction Effects*

Thermal conduction effects are responsible for a temperature profile which is very similar to that of the axial velocity. An equation giving the effective compressibility and linking pressure and velocity can be established. Here, we start from four

[10] When a convection term exists, the *Reynolds number* ($\rho v R/\mu$) is defined as the ratio of the convection term to the viscosity one, and the *Strouhal number* ($\omega R/v$) as the ratio of the unsteadiness term to the convection one. It can be checked that the square of the Stokes number is the product of the Reynolds and Strouhal numbers.

equations with five acoustic unknowns (temperature τ, density ρ', entropy s, pressure p, and velocity v). In order to obtain one single equation for two unknowns p and v, three unknowns must be eliminated.

5.4.3.1 Thermodynamics Equations

i) Statement of the Equations

The problem with four thermodynamic variables ($P, T, \rho, and\ S$) can be reduced to two variables for a bivariant gas, depending on only two variables. T is the absolute temperature, expressed in Kelvin degrees (°K), S is the mass entropy, which is a state function. The variations $d\rho$ and dS are expressed as functions of dP and dT: four coefficients are needed, searched as functions of usual "measurable" coefficients. By definition [see Eq. (1.95)]:

$$c^2 = \left(\frac{\partial P}{\partial \rho}\right)_S.$$

Then the isothermal and isentropic compressibilities are used

$$\chi_T = \frac{1}{\rho}\left(\frac{\partial \rho}{\partial P}\right)_T \text{ and } \chi_S = \frac{1}{\rho}\left(\frac{\partial \rho}{\partial P}\right)_S = \frac{1}{\rho c^2},$$

as well as the specific heats at constant pressure and volume:

$$C_p = T\left(\frac{\partial S}{\partial T}\right)_P \text{ and } C_v = T\left(\frac{\partial S}{\partial T}\right)_V;$$

and the coefficient of bulk thermal expansion:

$$\beta = -\frac{1}{\rho}\left(\frac{\partial \rho}{\partial T}\right)_P.$$

Therefore, by definition:

$$d\rho = \rho\chi_T dP - \rho\beta dT. \tag{5.117}$$

This is the first equation needed. It is classically shown that:[11]

[11] In fact

$$\gamma = \left(\frac{\partial S}{\partial T}\right)_P \left(\frac{\partial T}{\partial S}\right)_\rho$$

and

$$\frac{\chi_T}{\chi_S} = \left(\frac{\partial \rho}{\partial P}\right)_T \left(\frac{\partial P}{\partial \rho}\right)_S = \left(\frac{\partial \rho}{\partial S}\right)_T \left(\frac{\partial S}{\partial P}\right)_T \left(\frac{\partial P}{\partial T}\right)_S \left(\frac{\partial T}{\partial \rho}\right)_S.$$

It remains to use, for (ρ, S, T) and (S, P, T), the following relationship valid for any three variables

$$\left(\frac{\partial x}{\partial y}\right)_z \left(\frac{\partial y}{\partial z}\right)_x \left(\frac{\partial z}{\partial x}\right)_y = -1.$$

$$\chi_T = \gamma \chi_s \text{ hence } \rho \chi_T = \gamma / c^2. \tag{5.118}$$

In a similar way to (5.117), this gives

$$d\rho = \frac{1}{c^2} dP + \left(\frac{\partial \rho}{\partial S} \right)_P dS. \tag{5.119}$$

Eliminating $d\rho$ between (5.117) and (5.119), yields

$$dS = \left(\frac{\partial S}{\partial \rho} \right)_P \left[-\rho \beta dT + \frac{\gamma - 1}{c^2} dP \right].$$

Finally, using coefficients C_p and β, the second equation is found:

$$dS = \frac{C_p}{T} \left[dT - \frac{1}{\rho \beta} \frac{\gamma - 1}{c^2} dP \right]. \tag{5.120}$$

Back to the Isentropic Approximation (Chap. 1)

Under the assumption of isentropic transformation, Eq. (5.120) gives the proportionality coefficient between acoustic temperature and pressure (see Chap. 1):

$$\tau = \frac{1}{\rho \beta} \frac{\gamma - 1}{c^2} p \text{ where } \tau = \frac{\beta T}{\rho C_p} p,$$

the second expression being obtained using Maxwell law $(\partial S / \partial P)_T = -\beta / \rho$. If the gas is now supposed to satisfy a law $p/\rho = f(T)$, by using the definition of χ_T, the equilibrium coefficients are found:

$$\chi_T = \frac{1}{p_0} \text{ hence } \chi_S = \frac{1}{p_0 \gamma} \text{ and } c^2 = \frac{p_0 \gamma}{\rho_0}. \tag{5.121}$$

If, finally, $f(T)$ is the ideal gas law, $MP = RT\rho$, the sound speed is

$$c^2 = \gamma \frac{RT_0}{M}; \tag{5.122}$$

this formula is widely used for sound speed calculation (see a discussion in [36], and for numerical values of some useful constants, in Sect. 5.5.2): it is thus proportional to the square root of the absolute temperature. Moreover $\beta = 1/T$, and the acoustic temperature τ is also given by:

(continued)

$$\frac{\tau}{T_0} = \frac{\gamma - 1}{\gamma} \frac{p}{p_0}.$$

Finally, with Eqs. (1.95) and (5.121), the well-known formula for isentropic motion is also found: $dP/P = \gamma d\rho/\rho$, or, after integration:

$$P\rho^{-\gamma} = \text{constant} = P_0 \rho_0^{-\gamma} . \tag{5.123}$$

ii) Linearization

It remains to linearize Eqs. (5.117) and (5.120). We write $dS = s$, $d\rho = \rho'$, $dT = \tau$, $dP = p$, and for averaged quantities, we again use ρ instead of ρ_0. This gives

$$s = \frac{C_p}{T_0}(\tau - \alpha_s p) \quad \text{with } \alpha_s = \frac{1}{\rho\beta}\frac{\gamma - 1}{c^2}, \tag{5.124}$$

and

$$\rho' = \frac{\gamma}{c^2}\left[p - \frac{\beta\rho c^2}{\gamma}\tau\right]. \tag{5.125}$$

5.4.3.2 Heat Equation and Solution

We start from the Fourier-Kirchhoff heat equation, (see for instance [36]), linearized for a fluid at rest:

$$\kappa \Delta\tau = T_0 \rho \partial s/\partial t,$$

where κ is the thermal conductivity coefficient, T_0 and ρ being the average values of temperature and density. Using the state relationship for entropy (5.124), it gives in the frequency domain (for the temperature, τ_ω is the transform of $\tau(t)$) :

$$\Delta\tau_\omega + k_t^2 \tau_\omega = -j\omega \frac{\alpha_s \rho C_p}{\kappa} P, \quad \text{where} \tag{5.126}$$

$$k_t = \sqrt{-j\omega\rho\frac{C_p}{\kappa}}. \tag{5.127}$$

k_t is the thermal diffusion wavenumber. Assuming P to be plane, and, again, that the Laplacian is almost radial, an equation very similar to (5.110) is obtained. The boundary conditions are given by the requirement to have a finite solution at $r = 0$, and by a condition proposed by Kirchhoff: $\tau = 0$ on the wall. This imposes that the temperature does not vary at the wall. Therefore a heat flow exists inside the wall. Furthermore the product of the heat capacity by the thermal coefficient needs to be larger in the wall than in the fluid [6]. The solution is written:

$$\tau_\omega = \alpha_s P \left[1 - \frac{J_0(k_t r)}{J_0(k_t R)} \right]. \tag{5.128}$$

Therefore the temperature profile is similar to that of the axial velocity, since the wavenumber k_t is very close to k_v. The temperature is the sum of the acoustic temperature, which is planar, and of a temperature linked to the entropy variation, the sum of these two temperatures vanishing at the wall.

It remains to find the relationship between temperature and axial velocity; to achieve this, both the state equation (5.125) and mass conservation (1.108) are used, assuming again that the term of axial velocity variation is predominant in the divergence

$$\rho \frac{\partial V_x}{\partial x} = -j\omega\rho', \tag{5.129}$$

and in the state equation (5.125). Finally:

$$\frac{\partial V_x}{\partial x} = -\frac{j\omega}{\rho c^2} P \left[1 + (\gamma - 1) \frac{J_0(k_t r)}{J_0(k_t R)} \right].$$

It remains to calculate the average of V_x on the section, or the flow U. We obtain the equation giving an effective compressibility, noted $\chi_t(\omega)$, completing Eq. (5.116):

$$\frac{dU}{dx} = -j\omega S \chi_t P \quad \text{where} \quad \chi_t(\omega) = \chi_s \left[1 + (\gamma - 1) \frac{2}{k_r R} \frac{J_1(k_t R)}{J_0(k_t R)} \right]. \tag{5.130}$$

5.4.4 Radiation Dissipation at the Open End of the Pipe

A detailed presentation of the radiation is proposed in the 4th part of this work. However, an approximated formula of the radiation impedance Z_R is needed from now in order to determine the field in the pipe. The effect of a length correction to the imaginary part of Z_R has already been seen in Eq. (4.67). Dissipation adds a real part to it. Restricting ourselves to the case of low frequencies (transverse dimension very small compared to the wavelength, i.e., $kR \ll 1$), the radiation impedance is written:

$$Z_R = Z_c \left[jk\Delta\ell + \frac{1}{4}(kR)^2 \right], \tag{5.131}$$

where R is the radius, and $\Delta\ell \cong 0.6R$. This formula is satisfactory as long as $kR < 1$. Although smaller in relative value than the imaginary part, the real part is qualitatively the most important, because it ensures the energy radiation all the way to our ears.

5.5 Transmission Line Equations

5.5.1 General Equations and Solutions

The description of the cylindrical pipe has been previously obtained in the form:

$$\frac{dP}{dx} = -Z_v U \quad \text{and} \quad \frac{dU}{dx} = -Y_t P \tag{5.132}$$

where

$$Z_v = \frac{j\omega\rho}{S}\left[1 - \frac{2}{k_v R}\frac{J_1(k_v R)}{J_0(k_v R)}\right]^{-1} ; \tag{5.133}$$

$$Y_t = j\omega\chi_s S\left[1 + (\gamma - 1)\frac{2}{k_t R}\frac{J_1(k_t R)}{J_0(k_t R)}\right] . \tag{5.134}$$

Equations (5.132) are of the transmission line type, and are called telegraphist's equations. Z_v and Y_t are the impedance in series and the admittance in parallel, both being expressed per unit length, corresponding to viscous and thermal conduction effects, respectively (J_0 and J_1 are the Bessel functions). The terms "series" and "parallel" are justified as follows: if one of these quantities does not vary, integrating on x, the Ohm's law is obtained (see Chap. 1, Sect. 1.5) as

$$\begin{aligned} \text{either} \quad & p_1 - p_2 = (x_2 - x_1) Z_v \, u, \\ \text{or} \quad & u_1 - u_2 = (x_2 - x_1) Y_t \, p \, . \end{aligned} \tag{5.135}$$

By analogy between electric voltage and current, and acoustic pressure and flow rate, the impedance Z_v per unit length is said to be in series, and admittance Y_t per unit length in parallel. It is convenient to use two characteristic lengths, ℓ_v and ℓ_t, in order to define the viscous and thermal diffusion wavenumbers k_v and k_t:

$$\ell_v = \frac{\mu}{\rho c} \, ; \, \ell_t = \frac{\kappa}{\rho c C_p} \, ; \, k_v = \sqrt{-\frac{j\omega}{c\ell_v}} \, ; \, k_t = \sqrt{-\frac{j\omega}{c\ell_t}}. \tag{5.136}$$

In air, these lengths are very small,[12] as ℓ_v is equal to 4×10^{-8} m, and their ratio, called *Prandtl number* : $\ell_v/\ell_t = P_r$, is equal to 0.71.

For sinusoidal signals, assuming without proof, that the acoustic intensity in each segment at every time is given by the product Spv, the average intensity over a period is $I = \frac{1}{2}\Re e(PU^*)$, and its derivative is

$$\frac{dI}{dx} = -\frac{1}{2}\Re e(Y_t)\,|P|^2 - \frac{1}{2}\Re e(Z_v)\,|U|^2\,. \tag{5.137}$$

Energy must be dissipated. Thus $\Re e(Y_t)$ and $\Re e(Z_v)$ must be positive. Thus viscous effects are important when flow rate is large, while thermal effects are important when the pressure is large. Standard solutions of line equations are written as:

$$P = P^+ e^{-\Gamma x} + P^- e^{\Gamma x} \text{ and } U = Y_c\left[P^+ e^{-\Gamma x} - P^- e^{\Gamma x}\right] \tag{5.138}$$

$$\text{where } \Gamma = \sqrt{Z_v Y_t} \text{ and } Z_c = 1/Y_c = \sqrt{Z_v/Y_t}. \tag{5.139}$$

Γ is the propagation constant ($\Gamma = jk_c$, where k_c is the wavenumber) and Z_c is the characteristic impedance. Notice that when boundary layers are taken into account, the characteristic impedance differs slightly from the lossless value, that we used in Chap. 4 or in Eq. (5.131). Both are complex, and the chosen square root is such that the real part is positive: for Γ, this is due to the fact that waves must be attenuated when they propagate, and, for Z_c, this is due to the fact that they must carry energy in their propagation direction.[13]

Another expression of these solutions is obtained using transfer matrices [see Eq. (4.28)]:

$$\begin{pmatrix} P_1 \\ U_1 \end{pmatrix} = \begin{pmatrix} \cosh \Gamma(x_2 - x_1) & Z_c \sinh \Gamma(x_2 - x_1) \\ Y_c \sinh \Gamma(x_2 - x_1) & \cosh \Gamma(x_2 - x_1) \end{pmatrix} \begin{pmatrix} P_2 \\ U_2 \end{pmatrix}. \tag{5.140}$$

The projected impedance formula can be deduced immediately, and will not be reproduced here [see Eq. (4.29)].[14]

[12] The validity of these formulas is very broad: solving completely the Kirchhoff theory, the following conditions are found: $\ell_v \ll R$, and $\omega\ell_v/c \ll 1$, which is not cause for concern for audible frequencies and for musical instruments. Another condition enables to be sure that attenuation effects in the volume are very weak: $[\omega R/c]\sqrt{\omega\ell_v/c} \ll 1$, and which, again, does not pose any problem [24, 40].

[13] In fact, the first expression of Z_c, when Γ is chosen, is Z_v/Γ and thus the choice of Γ implies the choice of Z_c.

[14] Notion of wall admittance: in 1948, another simplification of the Kirchhoff theory has been proposed by Cremer [14]. He dealt with the reflection of a wave incoming to a wall with an incidence angle θ with respect to the normal. He has shown that the boundary layer effect can be replaced by an equivalent admittance:

5.5.2 Numerical Values of Main Constants in Air

The numerical values of the main constants useful to calculate propagation in a pipe filled with air are given, with indication of the uncertainty. t is the temperature in Celsius degrees, and T the absolute temperature. Thus for $t_0 = 0\,°\mathrm{C} : T_0 = 273.16\,°\mathrm{K}$. It should be noticed that the three last quantities do not vary substantially with temperature (see for instance [9]). Finally, air humidity plays a role that has received little attention so far [12].

Sound velocity: $c = 331.45\sqrt{T/T_0}\ \mathrm{ms}^{-1}\ (\pm 0.015\,\%)$
Density: $\rho = 1.2929\,T_0/T\ \ \mathrm{kg\,m}^{-3}\ (\pm 0.01\,\%)$
Viscosity: $\mu = 1.708 \times 10^{-5}(1 + 0.0029t)\ \mathrm{kg\,m}^{-1}\,\mathrm{s}^{-1}\ (\pm 2\,\%)$
Thermal conductivity: $\kappa = 5.77 \times 10^{-3}(1 + 0.0033t)\ \mathrm{Cal/(m\,s\,°C)}\ (\pm 2\,\%)$
Specific heat with constant pressure: $C_p = 240\ \mathrm{Cal/(kg\,°C)}\ (\pm 0.1\,\%)$
Ratio of specific heats: $\gamma = C_p/C_v = 1.402\ (\pm 0.1\,\%)$
Prandtl number: $P_r = \ell_v/\ell_t = (r_t/r_v)^2 = 0.71.$ (5.142)

5.5.3 "Wide" Pipes

5.5.3.1 Expression of Parameters

The expression of the parameters Z_v and Y_t involves the Stokes number $r_v = |k_v R|$, which is the ratio of the radius to the boundary layer thickness. When pipes are

$$Y_p = -\frac{v_\perp}{p} = \frac{1}{\rho c}\sqrt{\frac{j\omega}{c}}\left[\sin^2\theta\sqrt{\ell_v} + \sqrt{\ell_t}\right]. \tag{5.141}$$

This quantity is the specific admittance; $v_\perp$ is the velocity projected on the outgoing normal of the wall. The thermal effects do not depend on incidence, in contrast to viscous effects: for a wave coming perpendicularly to the wall, there can be no shear effects. A new problem can be solved for a large pipe considering a propagation without losses with wall admittance, and the former results would be obtained again. To this end, as plane waves in a pipe propagate parallel to the wall, $\theta = \pi/2$ must be chosen. Conversely this formula is also useful at the end of a stopped pipe (i.e., an organ pipe closed at its passive end), with this time $\theta = 0$, and Y_p will be used as a termination admittance. In fact it can be shown that the total dissipation is linked to the total surface, and the terminal surface of a stopped pipe is clearly smaller than the surface of the side walls, which legitimates to ignore this effect, considering further that only thermal effects occur then.

It can be finally added that this notion can be generalized to a porous wall. The Cremer theory assumes that the wall is perfectly smooth, but experimental results show that this is very satisfactory.

wide, i.e., when the Stokes number is large (typically larger than 10), the asymptotic expansion of the Kelvin functions is made. The second-order approximation is largely sufficient for musical instruments, and even the first order is often useful (see [22] for more general formulas). The following expressions are obtained:

$$Z_v = \frac{j\omega\rho}{S}\left[1 + \frac{2\sqrt{-j}}{r_v} - \frac{3j}{r_v^2}\right] \text{ and } Y_t = j\omega\chi_s S\left[1 + (\gamma-1)\left(\frac{2\sqrt{-j}}{r_t} + \frac{j}{r_t^2}\right)\right] \tag{5.143}$$

with $\sqrt{-j} = \dfrac{1-j}{\sqrt{2}}$; $r_v = |k_v R| = R\sqrt{\dfrac{\omega}{c\ell_v}}$; $r_t = R\sqrt{\dfrac{\omega}{c\ell_t}} = \nu r_v$ where $\nu = \sqrt{P_r}$.

Thus, expanding again to the second-order, the propagation constant is

$$\Gamma = j\frac{\omega}{c}\left[1 + \frac{\alpha_1\sqrt{-2j}}{r_v} - j\frac{\alpha_2}{r_v^2}\right], \tag{5.144}$$

with: $\alpha_1 = \dfrac{1}{\sqrt{2}}\left[1 + \dfrac{\gamma-1}{\nu}\right] = 1.044$ and $\alpha_2 = 1 + \dfrac{\gamma-1}{\nu} - \dfrac{\gamma-1}{2\nu^2} - \dfrac{(\gamma-1)^2}{2\nu^2} = 1.080$.

For numerical values, the properties for air have been used, i.e., $\nu = 0.843$ and $\gamma = 1.402$, which vary very little with temperature. Exhibiting the damping α and the phase velocity v_φ, it is obtained

$$\Gamma = \alpha + \frac{j\omega}{v_\varphi} \text{ where } \alpha = \frac{\omega}{c}\left[\frac{\alpha_1}{r_v} + \frac{\alpha_2}{r_v^2}\right] \quad \text{and} \quad \frac{\omega}{v_\varphi} = \frac{\omega}{c}\left[1 + \frac{\alpha_1}{r_v}\right]. \tag{5.145}$$

Finally:

$$Z_c = \frac{\rho c}{S}\left[1 + \frac{\overline{\alpha_1}(1-j)}{r_v} - \frac{\overline{\alpha_2} j}{r_v^2}\right] \tag{5.146}$$

where

$$\overline{\alpha_1} = \frac{1}{\sqrt{2}}\left(1 - \frac{\gamma-1}{\nu}\right) = 0.370 \ ; \ \overline{\alpha_2} = 1 - \frac{\gamma-1}{\nu} + \frac{\gamma-1}{2\nu^2} + \frac{3(\gamma-1)^2}{2\nu^2} = 1.147.$$

Some comments on the values obtained are useful:

- The damping α increases with the square root of frequency, and with the inverse of the radius; visco-thermal losses are generally much higher than radiation "losses," except at high frequencies. The wind instrument efficiency is therefore quite low. This enables, as a first approximation, to study their functioning independently of their radiation, as the sound production mainly depends on low frequencies (see Chaps. 9 and 10).
- The phase velocity v_φ slightly decreases from the isentropic value c when frequency decreases, and all the more that radius is small. For a low note of a narrow instrument, such as the bassoon (a conical instrument), the variation

of low resonance frequencies can reach 4 %, which is nearly to a semitone. This variation of sound speed with frequency yields inharmonicity and has some significant consequences on the functioning, as it will be seen in the third part.

- For the characteristic impedance Z_c, as viscous and thermal effects are subtracted from each other, the first-order coefficient is weak; this is a first reason for which the characteristic impedance is often assumed to keep the isentropic value. A second reason is that, at resonances, there is equipartition of total energy in the pipe, i.e., equality between kinetic and potential energies (see [26]).

A simple approximated formula for a pipe is often needed; it is thus chosen:

$$\Gamma = j\frac{\omega}{c} + (1+j)3 \times 10^{-5}\frac{\sqrt{f}}{R}\,;\, Z_c = \frac{\rho c}{S}, \tag{5.147}$$

where f and R are frequency and pipe radius expressed in MKS units. In the present work, the dispersion effect will often be ignored, replacing factor $(1+j)$ by 1 in Eq. (5.147).

5.5.3.2 Propagation of an Impulse

The propagation constant Γ (or the complex wavenumber) depends on frequency. Thus a monochromatic wave is attenuated and distorted because of dispersion. Let us consider the case of an impulse. Using the result (5.144), the inverse transform of the following quantity can be calculated

$$\exp(-\Gamma x) = \exp\left[-\left(j\frac{\omega}{c} + B\sqrt{j\omega} + \alpha_2\frac{\ell_v}{R^2}\right)x\right] \text{ where } B = \alpha_1\frac{1}{R}\sqrt{\frac{2\ell_v}{c}}.$$

The first term in the exponential corresponds to propagation, the second to a pure diffusion (wave in $\sqrt{j\omega}$), the third to a simple attenuation independent of frequency. In the time domain, the first is a delay of x/c, the second is the impulse response of the diffusion equation (such as the heat equation), which is known analytically. The inverse Fourier transform can thus be calculated and it gives [32, 38]:

$$TF^{-1}\left[\exp(-\Gamma x)\right] = H(t-x/c)\frac{D}{\pi^{1/2}}\frac{\exp\left[-D^2/(t-x/c)\right]}{(t-x/c)^{3/2}}\exp\left[-\alpha_2\frac{x\ell_v}{R^2}\right]. \tag{5.148}$$

$D = Bx/2$ has the same dimension as $\sqrt{t}$. This function replaces the simple delay $\delta(t-x/c)$ when there is no dissipation. For a fixed x, the maximum is $0.2313/D^2$ and is obtained for $t = x/c + 2D^2/3$. It takes place thus just after the signal arrival at $t = x/c$, and is large. The longer the traveled distance, the more attenuated the wave, the rise being decreasingly steep [29]. Figure 5.13 shows the reflection function at the input of an open cylindrical pipe. If we assume that radiation does not occur because the pipe is quite narrow, the reflection function is nothing else

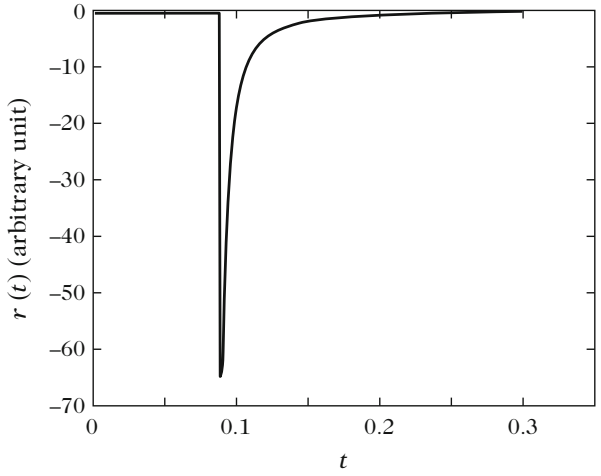

Fig. 5.13 Reflection function for a long open cylindrical pipe of radius 4 mm and length 15 m [Eq. (5.148), first-order calculation ($\alpha_2 = 0$)]. The second-order calculation would multiply the curve by a factor 0.93. The slow decrease after the maximum can be observed

that this transfer function for $x = 2\ell$, with a negative sign for the reflection at the output. Two facts are essential: no signal is arriving quicker that the sound (the arrival time is thus exactly $2\ell/c$), and the rate of decrease is very slow. We notice that the dimensionless parameter is $\ell\ell_v/R^2$, where ℓ is the traveled distance, corresponds to the inverse of the Stokes number $|k_v R|$, in which the wavelength has been replaced by the propagation distance. It can also be seen in Fig. 4.2 how the different reflections are added for the response in pressure to a flow rate impulse.

5.5.3.3 Input Impedance of a Cylinder

In the previous chapter, it was seen that the input impedance characterizes the wind instrument response. The calculation can now be made precisely for a cylinder:

$$Z_e = Z_c \tanh[\Gamma\ell + \arg\tanh(Z_R/Z_c)] \,. \tag{5.149}$$

If Formula (5.131) is used, to the second-order in kR, $\arg\tanh(Z_R/Z_c)$ can be replaced by Z_R/Z_c, and this gives

$$Z_e \simeq Z_c \tanh\left(\Gamma\ell + Z_R/Z_c\right) = Z_c \tanh\left[j\frac{\omega}{v_\varphi}L + \alpha\ell + \frac{1}{4}(kR)^2\right] \,. \tag{5.150}$$

where $L = \ell + \Delta\ell$ (the sound speed on the length $\Delta\ell$ is considered to be v_φ, instead of c, which is a small approximation). If the quantity $\tanh\left[\alpha\ell + \frac{1}{4}(kR)^2\right]$,

which is smaller than unity, and the phase velocity are assumed to slowly vary with frequency, the maxima can be shown to be obtained for an infinite value of $\tan\left[\omega L/v_\varphi\right]$, and the minima for zero $\tan\left[\omega L/v_\varphi\right]$. The extrema of the modulus are therefore obtained for

$$f_n = (2n-1)v_\varphi/4L \text{ and } f_n = nv_\varphi/2L, \tag{5.151}$$

respectively (v_φ is calculated for the value of frequency without dispersion), and are

$$|Z_e|_{\max} \simeq Z_c/\tanh\left[\alpha\ell + \tfrac{1}{4}(kR)^2\right] \text{ and } |Z_e|_{\min} \simeq Z_c \tanh\left[\alpha\ell + \tfrac{1}{4}(kR)^2\right]. \tag{5.152}$$

Nothing forbids the numerical calculation of the exact formula, but these approximations are convenient. For the extrema, the impedance is real, as for a one-degree-of-freedom oscillator. The term $\alpha\ell + \frac{1}{4}(kR)^2$ corresponds to dissipation, as previously shown. When dissipation is large, extrema tend towards the characteristic impedance. At low frequencies, maxima decrease as the square root of frequency, while minima increase as the square root of frequency. These calculations can be shown to be valid to the first-order of the Stokes number. The second-order calculation can be found in [23], but the differences with the previous result are quite small for wind instruments.

The property that the first peaks are proportional to $\omega^{-\frac{1}{2}}$ is important. If rules for pipe ranks are desired (for an organ or a panpipe for instance), the first idea that comes to mind to keep a similar behavior is to maintain the same dimensionless parameter $\alpha(f_n)\ell$, i.e., the inverse of the Stokes number written as $\sqrt{\ell\ell_v}/R$. In other words, if the pipe length is multiplied by 2, its radius is multiplied by $\sqrt{2}$. This rule was used by the Chinese in very ancient times. In practice, this question is very complex, and organ makers have quite different rules. To go further, radiation [18] and excitation parameters must be taken into account. Nevertheless, a first very simple approach of the problem is obtained here.

Figure 5.14 shows an input impedance curve, in modulus, calculated at the first-order of the Stokes number. This is the same curve as the one given in Fig. 4.5, but in a log-log scale. The logarithmic scale exhibits in ordinate the symmetry between peaks and dips, and in abscissa the relative width of the peaks, which decreases with frequency. As a consequence, the quality factor increases with frequency. Its calculation is done in Sect. 5.6.

Approximated Calculation of the Radiated Power: Boundary Conditions Corresponding to a Weak Coupling

In Chap. 4, the successive or closed-form reflection formulas were found to be valid for arbitrary boundary conditions, which can be absorbing, and

(continued)

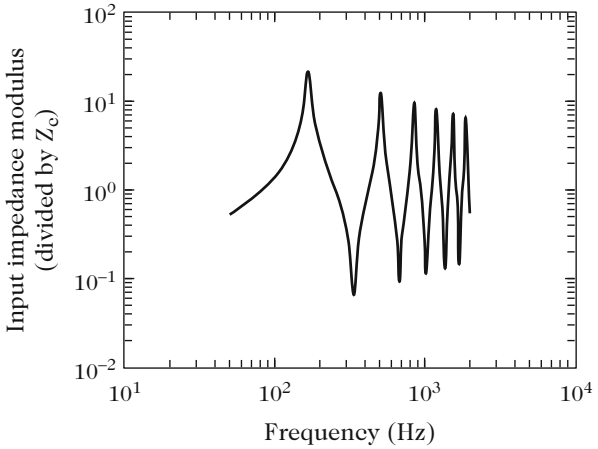

Fig. 5.14 Input impedance modulus of a cylinder terminating in a zero impedance, in a log-log scale. It is the same curve as in Fig. 4.5. For higher notes, peaks are lower, but sharper (their relative width decreases, in other words their quality factor increases)

therefore can be in particular a radiation impedance condition. The next section will focus on the difficult question of modal expansion.

At low frequencies, the real part of the radiation impedance and therefore the radiated power are very weak. In other words, the coupling between pipe and surrounding space is very weak. This is why calculating the radiated field by perturbation is legitimate, beginning by ignoring it, then deducing it from the obtained flow rate.

We consider a termination corresponding to an impedance Z_ℓ, which is small or at least has a small real part. The condition is sought for which the output flow rate U_ℓ can be calculated as if the impedance was zero (implying $P_\ell = 0$), then the approximated value $P_\ell = Z_\ell U_\ell$ can be deduced. For stringed instruments, this will also be the case for a small bridge admittance, when the coupling between a string and the soundbox is weak. This kind of reasoning can be iterated, enabling convergence to the exact result. For the particular case of a homogeneous one-dimensional medium, the limits of this method can be exactly determined. If a source U_s is given, it is known that it can be expressed as a function of two constants.[15] It can be written as:

$$U_s = Y_t P_\ell + F_t U_\ell \tag{5.153}$$

where Y_t and F_t are two coefficients depending on frequency. In the case where the source is at the input, they are easily deduced from the transfer

(continued)

matrices (4.28) or (5.140). In the most general case, Eqs. (4.42) and (4.58) can be used, and a zero output impedance is obtained (it is recalled that η_0 corresponds to the input boundary condition):

$$Y_t = -j\frac{1}{Z_c}\frac{\cos(k\ell+\eta_0)}{\sin(kx_s+\eta_0)} \;;\; F_t = \frac{\sin(k\ell+\eta_0)}{\sin(kx_s+\eta_0)}. \tag{5.154}$$

The iterative calculation is done by writing successively:

$$P_\ell^{(0)} = 0 \;;\; U_\ell^{(0)} = U_s/F_t; \tag{5.155}$$

$$P_\ell^{(1)} = Z_\ell U_\ell^{(0)} \;;\; U_\ell^{(1)} = \left[U_s - Y_t P_\ell^{(1)}\right]/F_t \;\text{; etc.} \tag{5.156}$$

This calculation is equivalent to expanding the exact result in series:

$$U_\ell = \frac{U_s}{F_t(1+Z_\ell Y_t F_t^{-1})}, \tag{5.157}$$

the validity condition being $Z_\ell Y_t F^{-1} < 1$. In fact, when there is no dissipation, the resonance frequencies are indeed given by Eq. (5.157), when the denominator vanishes. Consequently, in this case this method has no practical interest, because then $Z_\ell Y_t F_t^{-1} = -1$! On the contrary, if there is some dissipation, the situation can be quite different. Losses are considered during propagation and at both ends, which means that the wavenumber and coefficients η_0 and η_ℓ are complex. As the considered domain is the Fourier one, there is no limit to this reasoning, as all coefficients can depend on frequency without additional complexity.

Let us consider the case where the impedance Z_ℓ is real, thus $\eta_\ell = -j\varphi_\ell$, where φ_ℓ is real (and positive, if the output impedance is passive). $|Z_\ell| < \left|Y_t^{-1}F_t\right|$ is wanted, i.e., $\tanh\varphi_\ell < |\tan(k\ell+\eta_0)|$. Expanding complex quantities into real and imaginary parts, it can be written as: $k\ell+\eta_0 = k\ell - ja\ell + \eta_0' - j\eta_0''$, and if $(\alpha\ell+\eta_0'')$ is small (weak losses) and does not vary too much with frequency, quantity $|\tan(k\ell+\eta_0)|$ is a classical resonance term, which minimum is about $\alpha\ell+\eta_0''$. As a result this perturbation reasoning has a meaning provided that $\varphi_\ell < \alpha\ell+\eta_0''$, which simply means that output losses in ℓ are smaller than other losses. In order to stop the perturbation at the first-order, these losses in ℓ must be much smaller than other losses. This is the case for a cylindrical pipe, except at very high frequencies: radiation losses at an open end are smaller than losses during propagation.

As a conclusion, in this case, it is valid to calculate the transfer function U_ℓ/U_s ignoring losses at the pipe output (or at the string end), then deducing losses using the calculation of the power $\frac{1}{2}\Re e(Z_\ell)\,|U_\ell|^2$. This is quite general

(continued)

because often the power radiated by an instrument is very small, although it is essential! The previous analysis could be generalized when the impedance Z_ℓ also has an imaginary part. This means that the real part can be ignored to calculate the transfer function, but obviously the imaginary part cannot. The difficulty would be the same as the previous one, i.e., the shift of resonance frequencies, resulting in a great change of the results around the resonances. The case of a strong coupling will be studied in Chap. 6.

[15] As a matter of fact Eq. (4.34) is a second-order equation; taking into account dissipation does not change the formulas of the frequency domain of Chap. 4, except for the complex character of the wavenumber.

5.5.4 *"Narrow" Pipes*

We will not fully develop the case of narrow pipes, i.e., of capillary pipes at very low frequencies. However, the main results will be given, corresponding to the results of Eq. (5.143) and following. They are obtained by doing the series expansion with respect to the Stokes number of Eqs. (5.133) and (5.134) that are valid for $|k_v R| < 1$. At the fourth order this gives

$$Z_v = \frac{\rho c}{S}\frac{8\ell_v}{R^2}\left[1 + \frac{1}{6}jr_v^2\right] = \frac{\rho c}{S}\left[\frac{8\ell_v}{R^2} + j\frac{4}{3}\frac{\omega}{c}\right] \quad \text{and} \tag{5.158}$$

$$Y_t = j\omega\gamma\frac{S}{\rho c^2}\left[1 - \frac{\gamma-1}{8\gamma}jr_t^2\right] = j\omega\chi_t S\left[1 - \frac{\gamma-1}{8\gamma}jR^2\frac{\omega}{c\ell_t}\right]. \tag{5.159}$$

It is noticed that there is no thermal dissipation here as Y_t is purely imaginary. At lower frequencies, the motion is isothermal. Conversely viscous dissipation is significant, because it is proportional to the real part of Z_v, inversely proportional to the fourth power of the radius. It can be shown that frequency variations of reactive terms are very weak throughout the audible frequency range (the acoustic mass decreases monotonously from a coefficient $4/3$ at low frequencies to 1 at higher frequencies, and the compliance from $\gamma = 1.4$ to 1). The calculation of the propagation constant Γ shows that a diffusion wave occurs, as it is proportional to $\sqrt{j\omega}$. In the time domain, this leads to a shape of the kind (5.148), but without delay of the signal arrival. An impulsive diffusion wave is immediately spread out in the entire space. In fact taking the higher order terms into account includes the delay, no signal propagating with a speed faster than sound speed [29].

The main conclusion is that a small open pipe behaves as a resistance equal to $8\ell\ell_v\rho c/\pi R^4$, if its length ℓ is small enough with respect to the diffusion wavelength

($|\Gamma\ell| \ll 1$, see Chap. 1, Sect. 1.5 for the behavior of lumped elements systems). For other slit shapes, the coefficients are different, but the behavior is the same: pressure and velocity fields obey the Poiseuille law (5.115).

When the frequency increases, it is possible to find a continued fraction expansion for the equations of Zwikker and Kosten (5.132) [4, 25, 42]. This can avoid the use of the asymptotic expansion at high frequencies, which involves terms with square roots of frequency.

5.6 Modes of a (Reed) Cylindrical Instrument

5.6.1 Presentation

The modal expansion is now given for the input impedance of a pipe with visco-thermal effects and radiating into infinite space. The Green's function is calculated considering a flow rate source for reed instruments. The different case of instruments with a flute mouthpiece will be addressed in Chap. 7. There it will be seen that radiation by the mouth, with a section smaller than that of the pipe, complicates the problem.

We start again in the frequency domain: damping during propagation depends on frequency, which is not really a cause for concern, as seen in Sect. 5.2.2.1. Conversely the fact that radiation impedance does depend on frequency is a difficulty: exact solutions have been found if this impedance is equivalent to a mass termination [see Eq. (4.73)], or to a resistive one (see Sect. 5.2.2.3). But the radiation resistance is proportional to the square of frequency.

The advantage of modal expansion for self-oscillating instruments is to largely simplify the oscillation analysis (see third Part). As mostly low frequencies are involved in self-oscillation production, some low-frequency approximations can be made, especially for the radiation impedance. In fact, even this basic problem requires a numerical approach or tedious analytical calculation. In the following, the essential phenomena will be highlighted using a method that could be easily generalized in the case of non-cylindrical instruments.

To simplify the calculation, we study first the approximation for which radiated power is ignored (and thus also the real part of Z_R), and where the pipe length ℓ includes the length correction $\Delta\ell$: that is, $L = \ell + \Delta\ell$. This simplifies the understanding of the boundary layer effects: the dependency on frequency is a problem that is significantly simplified by the nature of the boundary conditions considered. The method used is that of Sect. 5.2.2.1. Then the result taking the radiated power into account is given.

5.6.2 Modes Orthogonality Method (Without Radiation)

For reed instruments, a flow rate source is considered. For any position x_s we can write (see Chap. 4, Sect. 4.6.1):

$$U_s = U_s^+ - U_s^- = -\frac{1}{Z_v}\left[\left(\frac{dP}{dx}\right)^+ - \left(\frac{dP}{dx}\right)^-\right].$$

For the propagation, $\Gamma = jk_c(\omega)$ is given by (5.144); for the sake of simplicity, visco-thermal effects will be limited to the first-order:

$$k_c(\omega) = \frac{\omega}{c}\left[1 + \frac{\alpha_1(1-j)}{r_v}\right]. \tag{5.160}$$

Remembering that r_v depends on frequency, the equation to be solved and the boundary conditions are written as:

$$\left[\frac{d^2}{dx^2} + k_c^2\right] P = -Z_v U_s \delta(x - x_s), \tag{5.161}$$

$$\frac{dP}{dx} = 0 \quad \text{for} \quad x = 0 \quad ; \quad P = 0 \quad \text{for} \quad x = L. \tag{5.162}$$

The input condition is necessary to calculate the input impedance as the limit when the source tends towards the input (see Chap. 4, Sect. 4.6.3). The modes on which the solution is projected are solutions of:

$$\left[\frac{d^2}{dx^2} + k_n^2\right] \Phi_n = 0$$

and of the boundary conditions (therefore modes do not depend on damping during propagation). Thus:

$$\Phi_n(x) = \cos k_n x \ ; \tag{5.163}$$

$$\cot k_n \ell = 0, \text{ hence } \ k_n \ell = (2n-1)\frac{\pi}{2} \ ; \tag{5.164}$$

$$\int_0^\ell \Phi_n(x)\Phi_m(x)dx = \frac{\ell}{2}\delta_{mn}. \tag{5.165}$$

Using this relation as in Sect. 4.6.2.1, we obtain a formula that generalizes Eq. (4.72) of Chap. 4:

$$P = \frac{2}{\ell} Z_v U_s \sum_{n>0} \frac{\cos k_n x \cos k_n x_s}{k_n^2 - k_c^2(\omega)} \quad \text{where} \tag{5.166}$$

$$k_n^2 - k_c^2(\omega) = k_n^2 - \frac{\omega^2}{c^2}\left[1 + \frac{\alpha_1(1-j)}{r_v}\right]^2. \tag{5.167}$$

This expression is not exactly a modal decomposition, because of the variation of r_v with frequency. We will show later how to obtain this decomposition. For now, knowing that visco-thermal effects vary slowly with frequency, r_v can just be calculated for frequency ω_n in each term of the series, and the boundary layer effects in Z_v can be ignored: $Z_v = j\omega\rho/S$. Then to first order in r_v :

$$k_n^2 - k_c^2(\omega) \simeq k_n^2 - \frac{\omega^2}{c^2}\left[1 + 2\frac{\alpha_1(1-j)}{r_v(\omega_n)}\right] \simeq k_n^2 - \frac{\omega^2}{v_{\varphi n}^2}\left[1 - 2j\frac{\alpha_1}{r_v(\omega_n)}\right]$$

$$\text{with} \quad \frac{1}{v_{\varphi n}} = \frac{1}{c}\left[1 + \frac{\alpha_1}{r_v(\omega_n)}\right].$$

The expression of phase velocity v_φ is indeed the same as the one given by (5.145). It remains to approximate each term as a one-degree-of-freedom oscillator:

$$P = \frac{2c}{\ell} Z_c j\omega U_s \frac{c}{v_{\varphi n}^2} \sum_{n>0} \frac{v_{\varphi n}^2}{c^2} \frac{\cos k_n x \cos k_n x_s}{\omega_n^2 + j\omega\omega_n Q_n^{-1} - \omega^2} \text{ where} \tag{5.168}$$

$$\omega_n = k_n c\left[1 - \frac{\alpha_1}{r_v(\omega_n)}\right] \text{ and } \frac{1}{Q_n} = 2\frac{\alpha_1}{r_v(\omega_n)} \simeq 2\frac{\alpha_1}{R}\sqrt{\frac{\ell_v}{k_n}}. \tag{5.169}$$

Expressions (5.166) and (5.168) give similar numerical results, except for frequencies lower than the first resonance. In Fig. 4.5, the latter is compared with the compact formula. The truncation at 10 modes highlights the effect of higher order modes even at low frequencies. The value of peak maxima is

$$Z_{M,n} \simeq Z_c \frac{2c}{\ell}\frac{Q_n}{\omega_n}. \tag{5.170}$$

The quality factor is proportional to the square root of frequency, in contrast to the impedance peaks, which are inversely proportional to it. Finally the quality factor is proportional to the radius R, and impedance peaks are inversely proportional to R[16] (because of the characteristic impedance factor). Some practical consequences have been discussed in Sect. 5.5.3.3 (see in particular Fig. 5.14).

[16] A wide pipe has impedance peaks lower than a narrow one: this explains why the vocal tract has not much influence on the playing of reed instruments, at least for low notes.

5.6.3 Residue Calculus (Taking Radiation into Account)

Still in the frequency domain, the closed form (4.47) is used to deal exactly with the problem including radiation. The boundary conditions are written as $\eta_0 = \pi/2$ and

$$j\eta_\ell = \arg\tanh(z_R) = h(s) \tag{5.171}$$

$$\text{where } s = j\omega \text{ and } z_R = Z_R/Z_c = s\frac{\Delta\ell}{c} - \frac{1}{4}\left(\frac{sR}{c}\right)^2. \tag{5.172}$$

$P(x)$ is the solution of (5.161). After some calculations, it gives, for $x > x_s$:

$$P = U_s \frac{Z_v}{\Gamma} \frac{\sinh\left[\Gamma(\ell - x) + h(s)\right]\cosh\Gamma x_s}{\cosh\left[\Gamma\ell + h(s)\right]}, \tag{5.173}$$

where $\Gamma(s)$ is given by (5.160). As Γ and h vanish at $s = 0$, there is no constant (or "rigid") mode. Poles s_n, and thus the eigenfrequencies are a priori complex and are given by:

$$\cosh\left[\Gamma(s_n)\ell + h(s_n)\right] = 0, \text{ i.e., } \Gamma(s_n)\ell + h(s_n) = j\gamma_n \text{ where } \gamma_n = (2n-1)\frac{\pi}{2}. \tag{5.174}$$

Near the poles, the denominator is written as:

$$D = (s - s_n)\left[\Gamma'(s_n)\ell + h'(s_n)\right]\sinh\left[\Gamma(s_n)\ell + h(s_n)\right],$$

where the symbol $'$ represents the derivative with respect to the variable s. Considering expressions of Γ and h, the poles s_n occur as complex conjugate pairs.

The application of the residue theorem and some further calculations give the expansion of $P(\omega)$ as a sum of terms:

$$P_n = U_s \frac{Z_v(s_n)}{\Gamma(s_n)} \frac{\cosh\left[\Gamma(s_n)x\right]\cosh\left[\Gamma(s_n)x_s\right]}{(s - s_n)\left[\Gamma'(s_n)\ell + h'(s_n)\right]}, \text{ where } h'(s_n) = \frac{z_R'}{1 - z_R^2}. \tag{5.175}$$

It should be noted that $Z_v/\Gamma = Z_c$. Considering (5.174), the eigenmode shapes are complex, and the dependency on s is the one of a generalized Lorentzian corresponding to complex modes. This was previously seen for a resistive end (for that case $h(s)$ was a real constant). The question of the orthogonality of the modes will not be discussed here.

The relation with the particular case $z_R = 0$, treated in the former section, is sought now. If the terms corresponding to s_n and s_n^* are added, an equation similar to Eq. (5.166) is found; in fact the two equations differ because of the frequency variation of Γ. However, the modes are the same. There can thus be several kinds of expansion in the frequency domain on the same modes. It can be shown that (5.166) corresponds to the following formula, when $h(s) = 0$:

$$P_n = U_s \frac{Z_v(s)}{\Gamma(s_n)} \frac{\cosh\left[\Gamma(s_n)x\right] \cosh\left[\Gamma(s_n)x_s\right]}{\left[\Gamma\ell + h\right](s) - j\gamma_n}. \tag{5.176}$$

Expressions (5.175) and (5.176) are different, but because each term has the same residue, the inverse Fourier transform is identical. In fact the residues are unchanged if $Z_v(s_n)$ is changed in $Z_v(s)$; as for the denominators, they are, thanks to (5.174), equivalent to first-order in $(s-s_n)$. Obviously the time expression must be calculated directly with (5.175)! The fact that they are exact should be highlighted,[17] and this is true whatever are the frequency dependencies of Z_v, Γ, and h.

Approximated Expression of the Modal Expansion

In order to have an approximated formula in an analytical form, Eq. (5.176) is calculated ignoring losses (in boundary layers and by radiation), except in the resonance term. For the effects of boundary layers to first-order, Eq. (5.144) is used; in addition the imaginary part of the radiation impedance is supposed to be much larger than its real part. Given

$$C(s) = \Gamma(s)\ell + h(s) = C_0(s) + C_1(s), \tag{5.177}$$

$$\text{with } \Gamma(s) = \frac{s}{c} + \delta\sqrt{s} \text{ where } \delta = \frac{\alpha_1}{R}\sqrt{\frac{2\ell_v}{c}}.$$

where $C_0(s)$ is the term without losses and $C_1(s)$ the term with losses that are assumed to be small. These terms are

$$C_0(s) = \frac{s\ell}{c} + \delta\ell j\Im m(\sqrt{s}) + \operatorname{arg\,tanh}\frac{s\Delta\ell}{c};$$

$$C_1(s) \simeq \delta\ell(\Re e\sqrt{s}) - \frac{1}{4}\left(\frac{sR}{c}\right)^2\left[1 - \left(\frac{s\Delta\ell}{c}\right)^2\right]^{-1}.$$

Without losses, [if Eq. (5.145) is used] the eigenfrequencies, denoted $\omega_{n0} = -js_{n0}$ verify

$$C_0(s_{n0}) = \frac{s_{n0}\ell}{v_\varphi} + \operatorname{arg\,tanh}\frac{s_{n0}\Delta\ell}{c} = j\gamma_n$$

$$\text{hence } \frac{\omega_{n0}\Delta\ell}{c} = \tan\left[\gamma_n - \frac{\omega_{n0}}{v_\varphi}\ell\right] = \cot\frac{\omega_{n0}}{v_\varphi}\ell. \tag{5.178}$$

(continued)

[17] This question can be quite complicated when visco-thermal effects occur: Equation $s_n + \varepsilon\sqrt{s_n} = j\pi/2$ can have two solutions in $\sqrt{s_n}$, but one of them can be ignored, when the problem is stated completely [33]. Thus we know that only the solution near the case $\varepsilon = 0$ is interesting.

This equation, whose solutions ω_{n0} are real, is similar to the one written in Sect. 4.6.4 of Chap. 4, when $v_\varphi = c$. Now $C(s) = j\gamma_n = C_0(s_{n0})$ will be solved assuming $s_n - s_{n0}$ to be small. It gives

$$C(s) = C_0(s_{n0}) + (s_n - s_{n0})C_0'(s_{n0}) + C_1(s_{n0}), \text{ hence}$$
$$s_n - s_{n0} = -C \text{ where } C = \frac{C_1(s_{n0})}{C_0'(s_{n0})}. \tag{5.179}$$

If the variation with frequency of the phase velocity v_φ is ignored, the quantity $C_0'(s_{n0})$ which appears in the denominator of (5.175) is written:

$$C_0'(s_{n0}) = \frac{\ell}{v_\varphi(\omega_{n0})} + \frac{\Delta\ell}{c}\left[1 + \frac{\omega_{n0}^2\Delta\ell^2}{c^2}\right]^{-1}.$$

With the assumptions made, and assuming the characteristic impedance independent of the boundary layer effects, thanks to (5.175), the sum of terms in s_n and s_n^* can be calculated:

$$P = U_s Z_c \sum_{n>0} \frac{\cosh\left[\Gamma(s_{n0})x\right]\cosh\left[\Gamma(s_{n0})x_s\right]}{C_0'((s_{n0})}\left[\frac{1}{s - s_n} + \frac{1}{s - s_n^*}\right], \tag{5.180}$$

where $\cosh\left[\Gamma(s_{n0})x\right] = \cos\omega_{n0}x/v_\varphi$. Denoting $C = \frac{1}{2}\omega_{n0}Q_n^{-1}$ and neglecting the second-order terms in Q_n^{-1}, the term in brackets can be written as:

$$2\frac{s + C}{s^2 + 2sC - s_{n0}^2} = 2\frac{j\omega + \frac{1}{2}\omega_{n0}Q_n^{-1}}{\omega_{n0}^2 + j\omega\omega_{n0}Q_n^{-1} - \omega^2}. \tag{5.181}$$

This expression has the form of a generalized Lorentzian of complex modes: the denominator is the one of a usual Lorentzian, however, the numerator differs by the constant term. To second-order in Q_n^{-1}, the resonance frequency is given by $\omega_{n0}\left[1 + \frac{1}{8Q_n^2}\right]$, and the value of the maximum of the bracket modulus is then $2Q_n/\omega_{n0}$. It remains to express the quality factor:

$$\frac{1}{Q_n} = \frac{2C_1(s_{n0})}{\omega_{n0}C_0'(s_{n0})} = \frac{\frac{2\alpha_1\ell}{R}\sqrt{\frac{\omega_{n0}\ell_v}{c}} + \frac{1}{2}\left(\frac{\omega_{n0}R}{c}\right)^2\left[1 + \frac{\omega_{n0}^2\Delta\ell^2}{c^2}\right]^{-1}}{\omega_{n0}\left[\frac{\ell}{v_\varphi(\omega_{n0})} + \frac{\Delta\ell}{c}\left[1 + \frac{\omega_{n0}^2\Delta\ell^2}{c^2}\right]^{-1}\right]}. \tag{5.182}$$

(continued)

The inverse of the quality factor is proportional to the sum of terms of visco-thermal and radiation losses. They could be compared to the terms obtained by the closed-form formula of the projected impedance (Sect. 5.5.3.3).

Simplification of the Approximated Expression

Formulas (5.178) to (5.182) are valid for large quality factors. This supposes among other things that radiation remains weak ($k_n R \ll 1$). If needed, it is better to numerically calculate Expression (5.175). However, the formulae can be substantially simplified by assuming that the radius is small with respect to wavelength ($\omega_{n0}^2 \Delta\ell^2/c^2 \ll 1$), and, ignoring the dispersion ($v_\varphi = c$). Then this gives, if $L = \ell + \Delta\ell$, $k_n = \gamma_n/L$:

$$P = \frac{2}{L} j\omega \frac{\rho c^2}{S} U_s \sum_{n>0} \cos k_n x \cos k_n x_s \frac{j\omega + \frac{1}{2}\omega_{n0} Q_n^{-1}}{\omega_{n0}^2 + j\omega\omega_{n0} Q_n^{-1} - \omega^2} \text{ where}$$

$$\omega_{n0} = c k_n \quad ; \quad \frac{1}{Q_n} = \frac{2\alpha_1}{R}\sqrt{\frac{\ell}{L}}\sqrt{\frac{\ell_v \ell}{\gamma_n}} + \frac{1}{2}\frac{(k_n R)^2}{\gamma_n}. \tag{5.183}$$

where $\gamma_n = (2n-1)\pi/2$. In practice, the term in Q_n^{-1} can be ignored in the numerator. When radiation is negligible, this formula is very close to Formula (5.168), which takes the dispersion into account. It can also be shown that the three definitions of the quality factor approximately coincide for a cylindrical pipe, as for a one-degree-of-freedom oscillator (see Chap. 2).

References

1. Abramowitz, M., Stegun, I.A.: Handbook of Mathematical Functions, with Formulas, Graphs, and Mathematical Tables. Dover, New York (1972)
2. Backus, J.: Acoustic impedance of an annular capillary. J. Acoust. Soc. Am. **58**(5), 1078–1081 (1975)
3. Balmès, E.: Methods for vibration design and validation. Course notes, Ecole Centrale Paris (2006)
4. Bilbao, S., Harrison, R., Kergomard, J., Lombard, B., Vergez, C.: Passive models of viscothermal wave propagation in acoustic tubes. J. Acoust. Soc. Am. **138**, 555–558 (2015)
5. Biot, M.A.: Thermoelasticity and irreversible thermodynamics. J. Appl. Phys. **27**(3), 240–253 (1956)
6. Bruneau, M.: Fundamentals of Acoustics. Wiley-ISTE, London (2006)
7. Bruneau, M., Herzog, P., Kergomard, J., Polack, J.: General formulation of the dispersion equation in bounded viscothermal fluid, and application to some simple geometries. Wave Motion **11**, 441–451 (1989)
8. Castellengo, M., Musical listening and acoustics (in French). Eyrolles, Paris (2015)

9. Caussé, R., Kergomard, J., Lurton, X.: Input impedance of brass musical instruments - comparison between experiment and numerical models. J. Acoust. Soc. Am. **75**(1), 241–254 (1984)
10. Chaigne, A., Lambourg, C.: Time-domain simulation of damped impacted plates. I. Theory and experiments. J. Acoust. Soc. Am. **109(4)**, 1422–1432 (2001)
11. Christensen, R.M.: Theory of Viscoelasticity, 2nd edn. Dover, New York (2003)
12. Coltman, J.: Acoustical losses in wet instrument bores (l). J. Acoust. Soc. Am. **114**, 1221 (2003)
13. Crandall, S.H.: The role of damping in vibration theory. J. Sound Vib. **11**(1), 3–18 (1970)
14. Cremer, L.: On the acoustic boundary layer outside a rigid wall. Arch. Elektr. Uebertr. **2**, 235 (1948)
15. Cremer, L., Heckl, M.: Structure-Borne Sound, 2nd edn. Springer, Berlin (1988)
16. Davis, J.L.: Mathematics of Wave Propagation. Princeton University Press, Princeton (2000)
17. Ewins, D.J.: Modal Testing, Theory, Practice and Applications, 2nd edn. Research Studies Press Ltd, Baldock (2000)
18. Fletcher, N.: Scaling rules for organ pipes ranks. Acustica **37**, 131–138 (1977)
19. Géradin, M., Rixen, D.: Mechanical Vibrations: Theory and Application to Structural Dynamics. Wiley, Chichester (1999)
20. Hélie, T., Matignon, D.: Diffusive representations for the analysis and simulation of flared acoustic pipes with visco-thermal losses. Math. Models Methods in Appl. Sci. **16**(4), 503–536 (2006)
21. Hélie, T., Matignon, D.: Representations with poles and cuts for the time-domain simulation of fractional systems and irrational transfer functions. Signal Process. **86**, 2516–2528 (2006)
22. Keefe, D.H.: Acoustical wave propagation in cylindrical ducts: transmission line parameter approximations for isothermal and non-isothermal boundary conditions. J. Acoust. Soc. Am. **75**(1), 58–62 (1984)
23. Kergomard, J.: Quasi-standing waves in horns with wall visco-thermal losses: calculation of the impedance (in French). Acustica **48**(1), 31–43 (1981)
24. Kergomard, J.: Comments on wall effects on sound propagation in tubes. J. Acoust. Soc. Am. **98**, 149–155 (1985)
25. Kergomard, J.: General equivalent circuits for acoustics horns. J. Audio Eng. Soc. **36**, 948–955 (1988)
26. Kergomard, J.: Elementary considerations on reed-instrument oscillations. In: Weinreich, A.H.J.K.G. (ed.) Mechanics of Musical Instruments. CISM Courses and Lectures, vol. 335, pp. 229–290. Springer, Wien (1995)
27. Kergomard, J., Caussé, R.: Measurement of acoustic impedance using a capillary: an attempt to achieve optimization. J. Acoust. Soc. Am. **79**(4), 1129–1140 (1986)
28. Kergomard, J., Debut, V., Matignon, D.: Resonance modes in a one-dimensional medium with two purely absorbing boundaries: calculation methods, orthogonality and completeness. J. Acoust. Soc. Am. **119**(3), 1356–1367 (2006)
29. Kergomard, J., Polack, J., Gilbert, J.: Propagation velocity of a plane impulse wave in a sound pipe (in French). J. Acoust. **4**, 467–483 (1991)
30. Kirchhoff, G.: Ueber die Einfluss der Warmeleitung in einem Gase auf die Schallbewegung. Annalen der Physik Leipzig **134**, 177–193 (English translation 1974. In: Lindsay, R.B. (ed.) Physical Acoustics. Dowden, Hutchinson and Ross, Stroudsburg) (1868)
31. Krenk, S.: Complex modes and frequencies in damped structural vibrations. J. Sound Vib. **270**, 981–996 (2004)
32. Martinez, J., Agulló, J., Cardona, S.: Conical bores. Part II: multiconvolution. J. Acoust. Soc. Am. **84**(5), 1620–1627 (1988)
33. Matignon, D., D'Andréa-Novel, B.: Spectral and time-domain consequences of an integro-differential perturbation of the wave PDE. In: Third International Conference on Mathematical and Numerical Aspects of Wave Propagation Phenomena, Mandelieu, France, pp. 769–771. INRIA, SIAM (1995)

34. Matignon, D., Montseny, G. (eds.): Fractional Differential Systems: Models, Methods and Applications (in French). European Series on Applied and Industrial Mathematics, vol. 5. ESAIM, Paris (1998)
35. Meirovitch, L.: Computational Methods in Structural Dynamics. Sijthoff and Noordhoff, Alphen aan den Rijn, The Netherlands (1980)
36. Pierce, A.D.: Acoustics: An Introduction to its Physical Principles and Applications. Acoustical Society of America, Melville (1989)
37. Polack, J.: Time domain solution of Kirchoff's equation for sound propagation in viscothermal gases: a diffusion process. J. d'Acoust. **4**, 46–67 (1991)
38. Polack, J.D., Meynial, X., Kergomard, J., Cosnard, C., Bruneau, M.: Reflection function of a plane sound wave in a cylindrical tube. Rev. Phys. Appl. **22**(5), 331–337 (1987)
39. Salençon, J.: Handbook of Continuum Mechanics: General Concepts, Thermoelasticity. Springer, Berlin (2001)
40. Scheichl, S.: On the calculation of the transmission line parameters for long tubes using the method of multiple scales. J. Acoust. Soc. Am. **115**(2), 534–555 (2004)
41. Stokes, G.G.: On the effect of internal friction of fluids on the motion of pendulums. Trans. Camb. Philos. Soc. **9**, 8 (1851)
42. Thompson, S., Gabrielson, T., Warren, D.: Analog model for thermoviscous propagation in a cylindrical tube. J. Acoust. Soc. Am. **135**, 585–590 (2014)
43. Valette, C., Cuesta, C.: Mechanics of the Vibrating String (in French). Hermès, Paris (1993)
44. Zener, C.: Internal friction in solids - I. Theory of internal friction in reeds. Phys. Rev. **32**, 230–235 (1937)
45. Zwikker, G., Kosten, C.: Sound absorbing materials. Elsevier, Amsterdam (1949)

Chapter 6
Coupled Systems

Antoine Chaigne and Jean Kergomard

Abstract As a natural continuation of the previous chapters, this chapter is devoted to the description of some important coupling phenomena in musical acoustics. The presentation starts with the basic coupling between a SDOF oscillator and a one-dimensional pipe. This example illustrates the modifications of the eigenfrequencies due to coupling, and allows fundamental concepts to be introduced such as added mass and stiffness. It is then generalized to the coupling between soundboard and cavity observed in stringed instruments. As a second example, the coupling of piano strings at the bridge is examined extensively. It is shown, in particular, how the tuning of the strings and the bridge admittance affect the temporal evolution of piano tones. Another example of coupling between a damped string and a dissipative soundboard yields useful light on the effects of "strong" and "weak" coupling observed in violins and guitars, respectively. The chapter ends with a description of the soundboard–bridge coupling in violins, and on its consequence on the observed input admittance.

6.1 Introduction

String and percussive instruments can be viewed as the assembly of different elementary structures. Some of these are designed to vibrate and, in turn, to radiate acoustic energy into the surrounding air, while others are not. In the case of timpani, for example, the objective is to control and enhance the vibrations of the membrane while minimizing those of the bowl. In most cases, these instruments show a closed, or semi-open, air cavity whose acoustic function is essential.

A. Chaigne (✉)
Institute of Music Acoustics, University of Music and Performing Arts Vienna (MDW), Anton-von-Webern-Platz 1, 1030 Vienna, Austria
e-mail: antchaigne@gmail.com

J. Kergomard
CNRS Laboratoire de Mecanique et d'Acoustique (LMA), 4 impasse Nikola Tesla CS 40006, 13453 Marseille Cedex 13, France
e-mail: kergomard@lma.cnrs-mrs.fr

A. Chaigne, J. Kergomard, *Acoustics of Musical Instruments*, Modern Acoustics and Signal Processing, DOI 10.1007/978-1-4939-3679-3_6

For these instruments, a number of different couplings can be exhibited, with variable proportions, depending on the instrument:

1. Multiple degrees of freedom structural coupling between two elements (e.g., string–soundboard coupling);
2. Coupling between a mechanical structure and an air cavity (e.g., timpani drumhead–cavity, or soundboard–soundbox coupling in a violin);
3. Coupling between a structure and an infinite or semi-infinite space filled with air: this is the case for almost all instruments, if room (bounded space) effects are ignored;
4. Coupling between a vibrating structure and a passive resonator located in its vicinity: case of keyboard percussive instruments (marimba, xylophone, and vibraphone).

General structural–acoustic coupling with applications to musical instruments, including the effect of passive resonators in the sound field, is presented in the fourth part of this book. The acoustical coupling between resonators of simple form is treated in Chap. 7. The present chapter is limited to the description of some selected simple coupling situations between structural elements, with or without a closed cavity, in order to emphasize their physical meaning. The consequences of these couplings are of several kinds:

- The coupling between attached structures modifies the natural frequencies and damping factors of the constitutive parts of the system.
- In the case of a vibrating structure coupled to a cavity, *structural-acoustic* modes can be observed. In addition, for some frequencies, the cavity affects the structure either as an added mass or as an added stiffness.
- When the cavity is open (which is generally the case of stringed instruments), radiation through the holes can extend the frequency range in which radiation is efficient.
- When a vibrating structure is surrounded by air, the reaction of the fluid changes the structural modes: the in vacuo modes of the structure are coupled together.
- A concert hall also is an acoustic cavity whose modes are coupled to the instrument.
- Finally, the sound field that reaches the ears of a listener can be modified by the presence of other vibrating structures, typically passive resonators, placed in the vicinity of a given instrument and excited by its radiated field.

6.2 Structure–Cavity Interaction

6.2.1 Mechanical Oscillator Coupled to a Pipe

The simple example presented in this section aims at illustrating the influence of the coupling between an air cavity and an elastic structure. This situation is encountered in almost all stringed instruments and can also be found in a significant

number of percussion instruments, as the membranophones (drums and timpani). To simplify the presentation, the structure is modeled here by a single-degree-of-freedom oscillator, while the cavity is assumed to be one-dimensional. The system is composed by a pipe with cross-section S and length L excited at one end by a mechanical oscillator of mass M, angular frequency ω_0, and reduced damping ζ_o (see Chap. 2). The term $f(t)$ is the excitation force of the oscillator. Visco-thermal losses are ignored in the pipe, for simplicity (Fig. 6.1).

It is further assumed that the pipe is closed at the other end by a mechanical impedance Z_L, defined in the Laplace formalism as $SP(L,s) = Z_L(s)V(L,s)$, where $P(L,s)$ and $V(L,s)$ are the Laplace transforms of sound pressure and acoustic velocity, respectively (for more details on the properties of the Laplace transform, see, for example, [11]). The other equations of the problem, written in the time domain, are

$$\begin{cases} \dfrac{1}{c^2}\dfrac{\partial^2 p}{\partial t^2} = \dfrac{\partial^2 p}{\partial x^2} \quad \text{for} \quad 0 < x < L, \\ \rho \dfrac{\partial v}{\partial t} = -\dfrac{\partial p}{\partial x}, \\ M\left(\ddot{\xi} + 2\zeta_o\omega_0\dot{\xi} + \omega_0^2\xi\right) = -Sp(x=0,t) + f(t), \\ v(0,t) = \dot{\xi}(t)\ . \end{cases} \tag{6.1}$$

This system can be solved in terms of the oscillator displacement ξ and pipe pressure p. The goal is to show, in particular, the influence of the coupling on the eigenfrequencies.

6.2.1.1 Oscillator Displacement and Pipe Pressure

The Laplace formalism is used here. Using the continuity of the displacement at $x = 0$, and the formula for the transfer impedance (4.29) leads to the expression for the input impedance of the pipe acting on the oscillator:

$$P(x=0,s) = s\rho c\Xi(s)z(s) \ \text{ where } z(s) = \frac{\tanh\frac{sL}{c} + z_L}{1 + z_l \tanh\frac{sL}{c}} \tag{6.2}$$

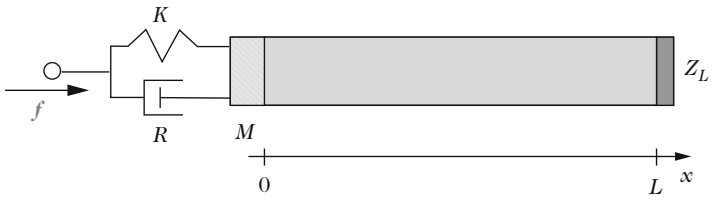

Fig. 6.1 Single-degree-of-freedom oscillator coupled to a tube of finite length loaded at one end by an impedance Z_L

with $z_L = Z_L/\rho cS$, and where $\Xi(s)$ is the Laplace transform of the displacement ξ. The equation of motion of the oscillator is written:

$$\left[s^2 + 2\zeta_o\omega_0 s + \omega_0^2\right]\Xi(s) = \frac{F(s)}{M} - s\frac{\rho cS}{M}\Xi(s)z(s). \tag{6.3}$$

The displacement of the oscillator can be written in the form:

$$\Xi(s) = \frac{F(s)}{M}\frac{1}{s^2 + 2\omega_0\left[\zeta_o + \zeta_a z(s)\right]s + \omega_0^2}, \tag{6.4}$$

with

$$2\zeta_a\omega_0 = \frac{\rho cS}{M}.$$

6.2.1.2 Discussion

A number of particular cases now deserve consideration:

- If the loading of the pipe at position $x = L$ is $Z_L = \rho cS$, there is no reflection, and $z(s) = 1$. This also corresponds to the case of an infinite pipe. Acoustic propagation in the pipe has the effect of increasing the damping of the oscillator through radiation (see also Chap. 2, Sect. 2.5.2).
- If the pipe is closed at $x = L$, then Z_L tends to infinity and $z(s) = 1/\tanh[sL/c]$. In addition, if the length L of the pipe is assumed to be small enough so that the approximation $\tanh[sL/c] \approx sL/c$ can be made, then the displacement of the oscillator becomes

$$\Xi(s) = \frac{F(s)}{M}\frac{1}{s^2 + 2\omega_0\zeta_o s + \omega_0^2 + 2\omega_0\zeta_a c/L}. \tag{6.5}$$

  The pipe thus becomes a lumped element system. It acts here as an *added stiffness*

$$K_a = \frac{2\omega_0 M\zeta_a c}{L} = \frac{\rho c^2 S^2}{\mathscr{V}}, \tag{6.6}$$

  where $\mathscr{V}$ is the volume of air enclosed in the pipe. This stiffness has an influence on the oscillator only if K_a is comparable to, or greater than, K ($K = M\omega_0^2$ is the stiffness of the oscillator). The effect is therefore significant for *flexible* structures ($K < K_a$).
- If the pipe is open at $x = L$, and if the radiation at the open end is ignored to a first approximation, then $Z_L = 0$ and $z(s) = \tanh[sL/c]$. For a pipe of short length or, more generally, for $sL/c \ll 1$ it leads to:

$$\Xi(s) = \frac{F(s)}{M}\frac{1}{s^2 + 2\omega_0\zeta_o s + \omega_0^2 + 2\omega_0\zeta_a s^2 L/c}, \tag{6.7}$$

which means that the pipe acts now as an added mass

$$M_a = \frac{2M\omega_0\zeta_a L}{c} = \rho\mathscr{V}, \tag{6.8}$$

which corresponds to the total mass of air enclosed in the pipe. As a consequence, *light* structures ($M < M_a$) are significantly affected by this coupling.

6.2.1.3 Eigenfrequencies of the Coupled System

Let us now consider the case of the pipe closed at $x = L$. The eigenfrequencies of the system are obtained by setting $s = j\omega$ and looking for the poles of the displacement, given by the roots of the real part of the denominator $\mathscr{D}(\omega)$:

$$\Re e\{\mathscr{D}(\omega)\} = (-\omega^2 + \omega_0^2)\sin\frac{\omega L}{c} + 2\omega_0\omega\zeta_a\cos\frac{\omega L}{c} = 0\,. \tag{6.9}$$

Recall that dissipation is ignored in this case (see Chap. 2). Notice that the roots of $\Re e\{\mathscr{D}(\omega)\}$ also yield the poles of the pressure. Equation (6.9) is now written in a dimensionless form, in order to show the different behaviors of the system, depending on the reduced values of the parameters. The reduced driving frequency is written $X = \omega L/c$, where L/c is the *characteristic time* of the pipe corresponding to the traveling time of a longitudinal acoustic wave between both ends. Finally, we define the dimensionless quantities $X_0 = \omega_0 L/c$ and $\varepsilon = K_a/K$. Equation (6.9) becomes

$$\frac{X^2}{X_0^2} = 1 + \varepsilon\frac{X}{\tan X} \quad \text{or equivalently} \quad \tan X = \frac{\varepsilon X X_0^2}{X^2 - X_0^2}\,. \tag{6.10}$$

The following situations can be identified, which depend on the frequency domain in which the system operates:

- If $X \gg X_0$, or, in other words, if the frequency ω is large compared to the reduced frequency ω_0 of the mechanical oscillator, then (6.10) shows that $\tan X$ is positive. The mechanical oscillator is of *mass* type. Due to the presence of the oscillator, the resonances of the tube closed at both ends are *increased*, compared to the isolated closed tube. This increase of frequency can be easily understood considering that, compared to the limiting case of an "infinite mass" at the end for the closed tube, the presence of the oscillator, of finite mass, corresponds to a decrease of the overall inertia of the system. The eigenfrequencies increase even more if ε is large. This corresponds to the case where the equivalent stiffness of the closed tube is large compared to that of the oscillator. However, for higher eigenfrequencies, the modifications are smaller. Similar results are found for a stringed instrument: the higher the frequency, the lesser the eigenfrequencies of the string are modified by the modes of the soundboard (see Chap. 3).

- Conversely, if $X \ll X_0$, $\tan X$ is negative. In this case, the eigenfrequencies of the tube are *reduced* because of the presence of the oscillator, compared to the tube closed at both ends. In fact, below its resonance frequency, the oscillator is governed by its stiffness. This stiffness is always smaller than those of perfectly rigid ends. Here again, this effect is more pronounced if ε is large.
- If $X \ll 1$, meaning that the frequency is much smaller than the characteristic frequency of the tube, there is no resonance inside the tube, and the only eigenfrequency of the system is given by $X = X_0\sqrt{1+\varepsilon}$ (which implies that $X_0 \ll 1$). Like in the previous case, the tube acts as an additional stiffness which has the effect of increasing the eigenfrequency of the mechanical oscillator.
- Suppose now that X is close to X_0, and, in addition, that these two quantities are close to a resonance of order n of the tube. In this case, the eigenfrequencies of the tube given in Eq. (6.10) are strongly modified in comparison to the solutions $X_n = n\pi$ obtained for the isolated tube (see Fig. 6.2). The difference between structural modes (S) and acoustic modes (A) cannot hold any longer. The modes are strongly coupled and are sometimes referred to as structural-acoustic modes (SA).

6.2.2 *Soundboard–Cavity Coupling in Stringed Instruments at Low Frequencies*

The coupling between soundboard and soundbox in stringed instruments is an example of structure–cavity interaction which has been extensively treated in the literature. The first models were published in the 1980s [3]. They are often limited to the interaction between the first (lowest) mode of the soundboard and the lowest acoustic mode of the cavity. Traditionally, these two modes are called $T1$ (soundboard) and $A0$ (air), respectively, when coupled together on the complete instrument. A simplified model with two degrees of freedom fairly reproduces the behavior of real instruments at low frequencies, i.e., below $T1$. It has been a source of inspiration for Hutchins in the realization of her violin octet, among other things [9].

Today, the main limitations of such models are well known: the soundbox is not only coupled to the soundboard, but also to the back plate and neck [6]. In addition, the coupling to the radiated field and the presence of holes also contribute to form a complex system: this will be discussed in detail in Chap. 14. The study is limited here to a simplified system with two degrees of freedom where the soundboard is represented by a rigid body with mass m_p of area A_p and intrinsic stiffness k_p subjected to the vertical force F of the strings. Its vertical displacement is denoted ξ_p which can be seen as the mean displacement of the attached soundboard vibrating near its first mode (see Fig. 6.3).

In this model, the soundbox is represented by a Helmholtz resonator (see Chap. 1, Sect. 1.5) with one moving wall (the soundboard). The inertial part of the resonator

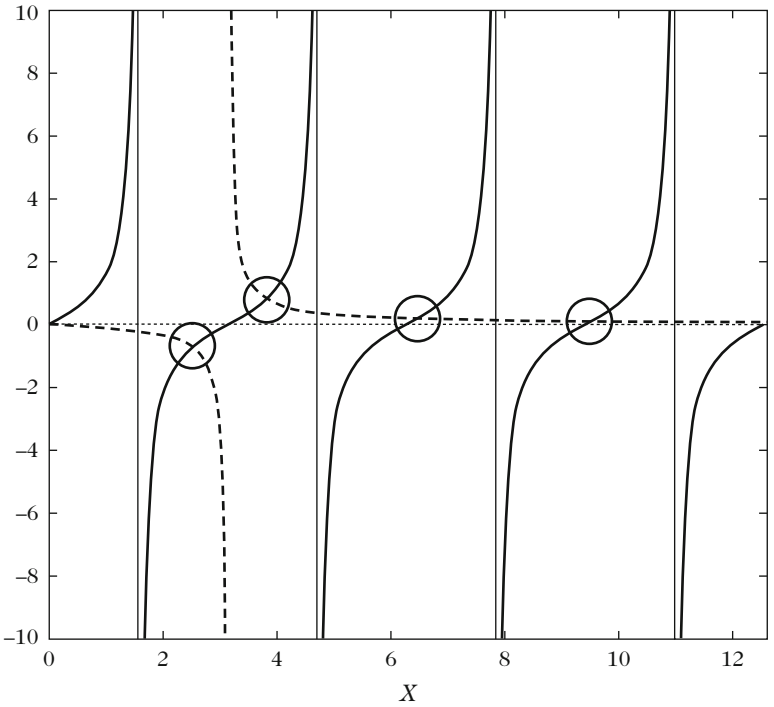

Fig. 6.2 Graphical solution for the eigenfrequencies of a 1-D acoustic tube loaded by a mechanical oscillator; $\varepsilon = 0.1$; $X_0 = \pi$. The intersections of the tan function (*solid line*) with the X-axis yield the eigenfrequencies $X = n\pi$ of the tube closed at both ends. The intersections (o) of the tan function with the expression $\varepsilon X X_0^2/(X^2 - X_0^2)$ (*dashed line*) yield the eigenfrequencies of the coupled system. The first eigenfrequency of the tube and the frequency of the mechanical oscillator, both equal to π in the decoupled case, are strongly modified by the coupling. Higher frequencies of the coupled system increase only slightly in comparison to the isolated tube

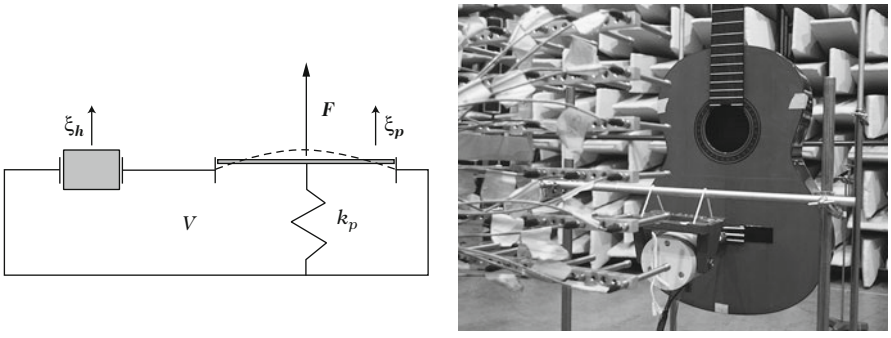

Fig. 6.3 (*Left*) At low frequencies (approximately $f < 300$ Hz), the Soundboard–cavity coupling of the classical guitar is reasonably modeled by a system with two degrees of freedom. (*Right*) Experimental vibroacoustical study of a guitar (© LAUM)

is the mass of air m_h oscillating through the holes of total area A_h, with the overall displacement ξ_h. During the motion, the change of volume in the cavity is equal to $\Delta\mathscr{V} = A_p\xi_p + A_h\xi_h$. Because of the compressibility of the air, the resulting change of pressure is $\Delta p = -\rho c^2 \Delta\mathscr{V}/\mathscr{V} = -\mu(A_p\xi_p + A_h\xi_h)$ (see Chap. 1). For simplicity the damping matrix of the system is assumed to be diagonal. The losses are modeled as resistances which remain constant over frequencies, and are here denoted R_p and R_h, respectively. Under these assumptions, the equations of motion for this system are written:

$$\begin{bmatrix} m_p & 0 \\ 0 & m_h \end{bmatrix} \begin{Bmatrix} \ddot{\xi}_p \\ \ddot{\xi}_h \end{Bmatrix} + \begin{bmatrix} R_p & 0 \\ 0 & R_h \end{bmatrix} \begin{Bmatrix} \dot{\xi}_p \\ \dot{\xi}_h \end{Bmatrix} + \begin{bmatrix} k_p + \mu A_p^2 & \mu A_h A_p \\ \mu A_h A_p & \mu A_h^2 \end{bmatrix} \begin{Bmatrix} \xi_p \\ \xi_h \end{Bmatrix} = \begin{Bmatrix} F \\ 0 \end{Bmatrix} . \tag{6.11}$$

This is a system coupled through the stiffness terms $\mu A_h A_p$, and the matrix $\mathbb{K}$ is not diagonal. In what follows, the eigenfrequencies of the coupled system are compared to some specific frequencies:

- Without an aperture in the soundboard (closed hole: $A_h = 0$), it can be seen from (6.11) that the box acts on the board as a spring of added stiffness μA_p^2. Its angular eigenfrequency (without damping) becomes $\omega_p = \sqrt{(k_p + \mu A_p^2)/m_p}$.
- If, in addition, the board has no stiffness ($k_p = 0$), this angular frequency becomes $\omega_a = \sqrt{\mu A_p^2/m_p}$.
- If now the board with an open hole is rigidly maintained, a classical case of Helmholtz resonator is obtained with angular eigenfrequency $\omega_h = \sqrt{\mu A_h^2/m_h}$.

In what follows, the coupled system will be conveniently expressed in terms of these three particular frequencies (ω_p, ω_a, and ω_h).

The eigenfrequencies of the associated conservative system are obtained from $\det[\mathbb{K} - \omega^2\mathbb{M}] = 0$ which can be written as:

$$\mathscr{D} = (\omega_p^2 - \omega^2)(\omega_h^2 - \omega^2) - \omega_{ph}^4 = 0 \quad \text{where} \quad \omega_{ph}^4 = \omega_a^2\omega_h^2 . \tag{6.12}$$

With typical numerical values for a classical guitar (see Fig. 6.4), the eigenfrequencies of the coupled system are equal to $f_1 = 86$ Hz and $f_2 = 206.5$ Hz. The frequency f_1 corresponds to the coupled acoustic mode $A0$, while f_2 is the eigenfrequency of the coupled mode $T1$. A main effect of the coupling is to move the frequencies apart compared to the uncoupled case (here $f_h = 100$ Hz and $f_p = 200$ Hz).[1] These frequencies also have the following mathematical property:

$$\omega_1^2 + \omega_2^2 = \omega_p^2 + \omega_h^2, \tag{6.13}$$

[1] Unfortunately, f_1 is often referred to as the Helmholtz frequency, however, this is an error that should not be made. Although f_1 and f_h are usually close in frequency, they correspond to opposite physical facts: the first frequency is related to a maximum, whereas the second is related to a minimum displacement for a given force. The latter is obtained by replacing the flow rate excitation of the cavity (upper Fig. 1.27) by a force excitation.

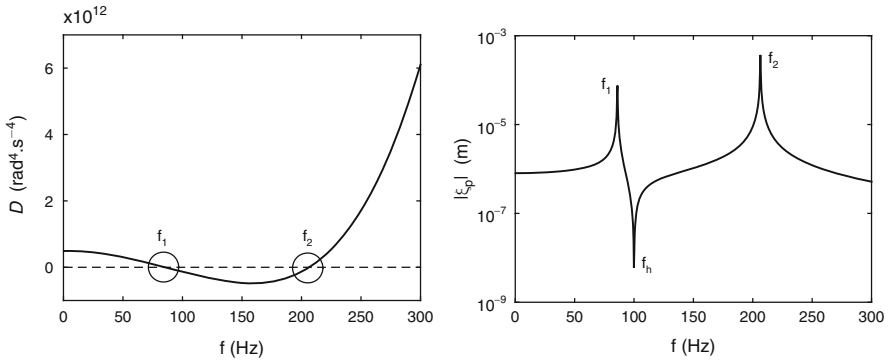

Fig. 6.4 Model of structure–cavity coupling with two degrees of freedom. (*Left*) Characteristic equation $\mathscr{D}$ as a function of frequency. (*Right*) Amplitude of soundboard displacement $|\xi_p|$ as a function of frequency. $f_h = 100\,\text{Hz}$; $f_p = 200\,\text{Hz}$; $m_p = 0.2\,\text{kg}$; $A_p = 0.3\ \text{m}^2$; $\mathscr{V} = 0.014\ \text{m}^3$; $\gamma_h = 1\,\text{s}^{-1}$; $\gamma_p = 2\,\text{s}^{-1}$

which is of particular interest, for example, in order to estimate the parameters of a given instrument experimentally.

The eigenvectors $\boldsymbol{\Phi_i}$ $(i = 1, 2)$ are obtained from the equation $[\mathbb{K} - \omega_i^2 \mathbb{M}]\boldsymbol{\Phi_i} = 0$. Whatever the parameters values, the two components of $\boldsymbol{\Phi_1}$ are opposite in sign, which means that the respective displacements of soundboard and hole have opposite signs, at the lowest coupling frequency f_1. Conversely, they are in phase at frequency f_2.

The interested reader can pursue this modal approach, using the method presented in Chap. 3. The modal projection $\boldsymbol{\xi} = \sum_i \boldsymbol{\Phi}_i q_i(t)$ is written here:

$$\begin{Bmatrix} \xi_p \\ \xi_h \end{Bmatrix} = \begin{Bmatrix} \Phi_{11} \\ \Phi_{12} \end{Bmatrix} q_1(t) + \begin{Bmatrix} \Phi_{12} \\ \Phi_{22} \end{Bmatrix} q_2(t), \tag{6.14}$$

where $q_i(t)$ are solutions of the system of uncoupled equations:

$$m_i \ddot{q}_i + k_i q_i = 0 \quad \text{with} \quad m_i = {}^t\boldsymbol{\Phi}_i \mathbb{M} \boldsymbol{\Phi}_i \quad \text{and} \quad k_i = {}^t\boldsymbol{\Phi}_i \mathbb{K} \boldsymbol{\Phi}_i = \omega_i^2 m_i\,. \tag{6.15}$$

The displacements obtained from (6.15) are approximate since the damping terms are ignored. These approximations may be sufficient in some situations, for example, when the goal is to predict acoustic or structural modifications required to modify the eigenfrequencies of the system (see Sect. 6.2.2.1 below).

However, the approximations (6.15) are not accurate enough if the evolution of the displacements with frequency needs to be known and, in particular, when one has to estimate their maximum (resp. minimum) values. In these cases, it is necessary to take the damping terms into account. One can use, for example, the method

of complex modes explained in Chap. 5. In the present simple example, with two degrees of freedom only, another relatively straightforward (and equivalent) solution is to solve the linear system (6.11) directly. This gives

$$\begin{cases} \xi_p = \dfrac{F}{m_p}\dfrac{\omega_h^2 - \omega^2 + j\omega\gamma_h}{D_c}, \\ \xi_h = \dfrac{F}{m_p}\dfrac{A_p}{A_h}\dfrac{\omega_h^2}{D_c} \\ \text{with} \quad D_c = (\omega_p^2 - \omega^2 + j\omega\gamma_p)(\omega_h^2 - \omega^2 + j\omega\gamma_h) - \omega_{ph}^4, \end{cases} \tag{6.16}$$

where $\gamma_h = R_h/m_h$ and $\gamma_p = R_p/m_p$.

Figure 6.4 shows the amplitude $|\xi_p|$ of the soundboard displacement versus frequency. Considering the low values chosen for γ_p and γ_h in our example, the maxima for $|\xi_p|$ are obtained for frequencies very close to the eigenfrequencies f_1 and f_2. It is found that the minimum is obtained for $f = f_h = 100\,\text{Hz}$, which corresponds exactly to the frequency of the Helmholtz resonator. This is consistent with the fact that f_h corresponds to the case of a resonator with fixed walls, when the displacement of the soundboard is equal to zero. It can be noted that the determination of this minimum is a very good way to experimentally estimate the Helmholtz frequency of a string instrument.

6.2.2.1 Structural Modifications of the Instrument: The Art of the Maker

A model of soundboard coupled to the soundbox like the one shown in (6.11) allows estimating the effects of structural modifications (mass of the board, soundbox volume, hole area, stiffness of the board,...) on the eigenfrequencies of the system. Such a procedure is similar to the skilled practice of a maker. However, the model presented above is elementary, and one should keep in mind that the requirements that govern the making of an instrument are not limited to the prediction of eigenfrequencies. Within this restrictive framework, the approach proposed below, inspired by French [7], illustrates a good example of the use of physics in instrument design.

As a starting point, we use the eigenvectors equation $[\mathbb{K}]\boldsymbol{\Phi} = \lambda[\mathbb{M}]\boldsymbol{\Phi}$ where $\lambda = \omega^2$. The matrices $\mathbb{K}$ and $\mathbb{M}$ are symmetric. Mathematically speaking, we are interested in the so-called *sensitivity* $\partial\lambda/\partial a$ of the eigenvalues λ with respect to a physical or a geometric parameter of the system, denoted a. Through derivation, we get

$$\left[\frac{\partial\mathbb{K}}{\partial a}\right]\boldsymbol{\Phi} + \mathbb{K}\left[\frac{\partial\boldsymbol{\Phi}}{\partial a}\right] = \frac{\partial\lambda}{\partial a}\left[\mathbb{M}\right]\boldsymbol{\Phi} + \lambda\left[\frac{\partial\mathbb{M}}{\partial a}\right]\boldsymbol{\Phi} + \lambda\mathbb{M}\left[\frac{\partial\boldsymbol{\Phi}}{\partial a}\right]. \tag{6.17}$$

Multiplying by the transposed eigenvector and using the symmetry properties of the matrices yields

$$\frac{\partial \lambda}{\partial a} = \frac{{}^t\boldsymbol{\Phi}\left[\frac{\partial \mathbb{K}}{\partial a}\right]\boldsymbol{\Phi} - \lambda\, {}^t\boldsymbol{\Phi}\left[\frac{\partial \mathbb{M}}{\partial a}\right]\boldsymbol{\Phi}}{{}^t\boldsymbol{\Phi}\left[\mathbb{M}\right]\boldsymbol{\Phi}} \,. \tag{6.18}$$

To illustrate the use of this general formula, some examples of structural changes are presented below.

Effect of Variation of the Soundboard Mass

In this case $a = m_p$. Equation (6.11) gives

$$\left[\frac{\partial \mathbb{M}}{\partial m_p}\right] = \begin{bmatrix} 1 & 0 \\ 0 & 0 \end{bmatrix} . \tag{6.19}$$

Since the vectors $\boldsymbol{\Phi_i}$ are known, the resulting changes of the eigenvalues are derived from (6.18):

$$\frac{\partial \lambda_i}{\partial m_p} = -\frac{\lambda_i \Phi_{1i}^2}{m_p \Phi_{1i}^2 + m_h \Phi_{2i}^2} \,. \tag{6.20}$$

It can be seen that if the mass of the soundboard is increased, then the eigenfrequencies of the system are lowered. The effects of such changes on the acoustic radiation will be examined in Part IV of this book.

Effect of Soundbox Volume Modification

The previous method is again applied, by setting now $a = \mathscr{V}$. Only the stiffness matrix is affected by a change in volume, which gives

$$\left[\frac{\partial \mathbb{K}}{\partial \mathscr{V}}\right] = -\frac{c^2 \rho}{\mathscr{V}^2} \begin{bmatrix} A_p^2 & A_h A_p \\ A_h A_p & A_h^2 \end{bmatrix} , \tag{6.21}$$

from which the sensitivity can be obtained

$$\frac{\partial \lambda_i}{\partial \mathscr{V}} = \frac{{}^t\boldsymbol{\Phi}\left[\frac{\partial \mathbb{K}}{\partial \mathscr{V}}\right]\boldsymbol{\Phi}}{{}^t\boldsymbol{\Phi}\left[\mathbb{M}\right]\boldsymbol{\Phi}} = -\frac{(c^2\rho/\mathscr{V}^2)(A_p^2 \Phi_{1i}^2 + 2A_p A_h \Phi_{1i}\Phi_{2i} + A_h^2 \Phi_{2i}^2)}{m_p \Phi_{1i}^2 + m_h \Phi_{2i}^2} \,. \tag{6.22}$$

It can be seen that an increase of the soundbox volume lowers the eigenfrequencies. This corresponds to one major structural changes in guitar making at the end of the nineteenth century, when the romantic guitar has evolved to the Torres guitar, which is still a reference model today for classical guitars [14].

Modification of the Hole Area

The average thickness of the hole is denoted h, taking the end corrections into account.[2] The mass of air in the hole is written: $m_h = \rho h A_h$. Therefore a perturbation of A_h induces changes both in stiffness and mass matrices. It gives

$$\left[\frac{\partial \mathbb{K}}{\partial A_h}\right] = \mu \begin{bmatrix} 0 & A_p \\ A_p & 2A_h \end{bmatrix} \quad \text{and} \quad \left[\frac{\partial \mathbb{M}}{\partial A_h}\right] = \begin{bmatrix} 0 & 0 \\ 0 & \rho h \end{bmatrix} . \tag{6.23}$$

which leads to:

$$\frac{\partial \lambda_i}{\partial A_h} = \frac{2\mu(A_p \Phi_{1i}\Phi_{2i} + A_h \Phi_{2i}^2) - \lambda_i \rho h \Phi_{2i}^2}{m_p \Phi_{1i}^2 + m_h \Phi_{2i}^2} . \tag{6.24}$$

Thus, an increase in the area of the openings induces an increase of the eigenfrequencies, while an increase in thickness causes the opposite effect.

Modification of the Soundboard Stiffness

The makers modify the overall stiffness of the soundboard either by varying the thickness or by adding stiffeners (bracing), or both. When the thickness e of the board is modified, the mass varies in proportion to it, but the stiffness varies as e^3, so significantly more strongly (see Chap. 1). For simplicity, it is assumed here that only the stiffness k_p is changed, but not the mass m_p whose effects were studied above. We obtain

$$\frac{\partial \lambda_i}{\partial k_p} = \frac{\Phi_{1i}^2}{m_p \Phi_{1i}^2 + m_h \Phi_{2i}^2} . \tag{6.25}$$

It can be seen that a decrease of the soundboard thickness lowers the eigenfrequencies. To be more rigorous, the model should be refined by writing m_p and k_p as functions of the thickness e and recalculating the sensitivities $\frac{\partial \lambda}{\partial e}$ in order to simultaneously show the influence of mass and stiffness matrices, as it was done for the area A_h of the holes.

[2] The thickness to be considered is the sum of the geometric height and length corrections due to radiation, at both sides of the hole. The origin of these corrections is due to the radiation impedance of the hole. See Chaps. 7 and 12.

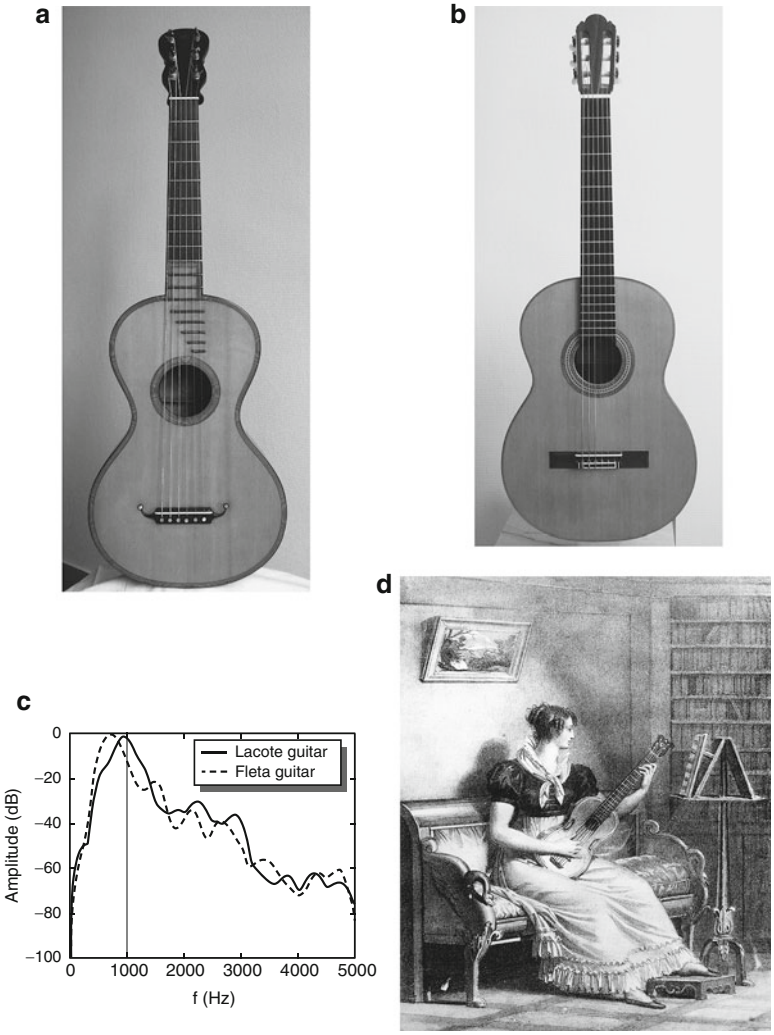

Fig. 6.5 Comparison between (**a**) a romantic guitar (René Lacote 1828) and (**b**) a contemporary guitar (Fleta 1977). The dimensions of the second one, including soundboard thickness, are larger than those of the first one. (**c**) The spectral balance shows a clear shift of the average spectrum of the second guitar in the direction of low frequencies: the spectral envelopes above were obtained by averaging over the same piece of music (*Ejercicio* by Jose Ferrer) played by the same musician (Bruno Marlat) successively on both guitars. These changes correspond to an aesthetic evolution due to the repertoire, the art of playing and musical taste between the nineteenth and the twentieth century. (**d**) shows the romantic guitar in real playing situation around the year 1820. (**a**) and (**b**): © Bruno Marlat; (**d**) Danielle Ribouillaut

6.3 Coupling of Piano Strings

Except at low frequencies, piano notes are obtained by striking a doublet or a triplet of strings. The listening experience shows that the sound is significantly changed if one string (of a doublet) or two strings (of a triplet) are damped, with only one vibrating string left. There are many coupling phenomena between strings that contribute to characterize the piano sound strongly. These properties are confirmed by experiments: the beat phenomenon[3] and double decay[4] have been highlighted by several authors [5].

The first theoretical and experimental comprehensive study on coupled piano strings is due to Weinreich [16]. The model developed in his study uses the formalism of dynamic matrices, which is a standard tool in solid-state physics, especially for studying the vibrations of atomic chains [4]. In order to make the link between this approach and the physics of strings described in this book, a detailed presentation of the problem studied by Weinreich is made below, starting from general equations, and discussing then the approximations made by this author systematically.

Fig. 6.6 Inside view of a piano showing string doublets (*far left*) and string triplets struck by the same hammer. © Pleyel

[3] A beat is a pronounced amplitude modulation at low frequency (less than a dozen Hz) due to the juxtaposition of very close frequencies f_1 and f_2.

[4] The double decay characterizes free oscillations where the temporal evolution of the amplitude shows two successive parts with different time constants. In piano tones, the amplitude decay most often shows first a short time constant followed by a longer one.

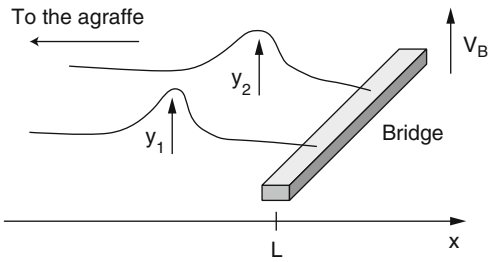

Fig. 6.7 Two strings coupled to the bridge of a piano. For simplicity, the motion of the string is assumed to be vertical only

N.B. *For consistency with other chapters in this book, some notations have been changed below compared to the cited paper by Weinreich. All changes are indicated in the text.*

6.3.1 General Equations of the Problem

In what follows, the problem is simplified by considering the coupling between two strings of identical length, mass, and cross-sectional area, and differing by their tensions only. We consider the linear transverse vibrations of both strings only, in vertical polarizations $y_1(x,t)$ and $y_2(x,t)$ with regard to bridge and soundboard plane (see Fig. 6.7). The lateral and longitudinal components are ignored, as well as dissipative and intrinsic stiffness effects. The free regime is considered, immediately after the interaction with the hammer. Therefore, the action of the hammer is ignored in the equations. With ρS the mass per unit length of both strings, the equations of motion are written:

$$\begin{cases} \rho S \dfrac{\partial^2 y_1}{\partial x^2} - T_1 \dfrac{\partial^2 y_1}{\partial t^2} = 0, \\ \rho S \dfrac{\partial^2 y_2}{\partial x^2} - T_2 \dfrac{\partial^2 y_2}{\partial t^2} = 0\,. \end{cases} \tag{6.26}$$

Both strings are assumed to be rigidly fixed at the one end, at the agraffe side, so that we can write $y_1(0,t) = y_2(0,t) = 0$. At the other end (at $x = L$), the strings are attached to the bridge, which is here symbolically represented by the impedance Z_B (or, equivalently, by the admittance Y_B). The validity of this representation is justified in Sect. 6.3.1.2. At the attachment point, the displacements of both strings are equal to the displacement $q_B(t)$ of the bridge, so that we have $y_1(L,t) = y_2(L,t) = q_B(t)$. Finally, the total force exerted by the strings on the bridge is written:

$$f_B = f_1 + f_2 = -T_1 \left(\frac{\partial y_1}{\partial x} \right)_{x=L} - T_2 \left(\frac{\partial y_2}{\partial x} \right)_{x=L}\,. \tag{6.27}$$

6.3.1.1 Two-Mode Approximations

Assuming the linearity of the problem, the transverse displacements of the strings can be expanded onto their eigenmodes:

$$y_1(x,t) = \sum_{i=1}^{n} \Phi_{1n}(x) q_{1n}(t) \quad \text{and} \quad y_2(x,t) = \sum_{i=1}^{n} \Phi_{2n}(x) q_{2n}(t) \; . \tag{6.28}$$

The bridge mobility is assumed to be small, which is consistent with experiments. In this case, it is justified to expand the string displacements onto the series of modes obtained for strings fixed at both ends: $\Phi_n(x) = \sin k_n x$ with $k_n L = n\pi$. As a consequence, all perturbation terms resulting from departure from the ideal case are found in the expressions of generalized displacements $q_n(t)$.

Since the fundamental frequencies of the strings of a given doublet are very close to each other in a piano, the general system can be represented as a set of modes coupled by pairs (one mode per string). Our study is then restricted to the coupling between one pair of two modes, without loss of generality. We focus below on the coupling between the fundamental frequencies, but the results are generalizable to any pair of modes of higher rank. This corresponds to seeking solutions to the following problem:

$$y_1(x,t) \simeq \Phi_1(x) q_1(t) \quad \text{and} \quad y_2(x,t) \simeq \Phi_2(x) q_2(t), \tag{6.29}$$

where

$$\begin{cases} \ddot{q}_1 + \omega_0^2 q_1 = g_1(q_i), \\ \ddot{q}_2 + \omega_0^2 q_2 = g_2(q_i) \; . \end{cases} \tag{6.30}$$

In (6.30), the left-hand side terms represent the temporal evolution of the oscillators, without coupling, loaded by an infinite impedance, and in unison. The perturbations of the system are grouped in the terms $g_1(t)$ and $g_2(t)$ on the right-hand side: detuning (departure from unison) and finite impedance at the bridge. These are functions of q_i and of their time derivatives.

6.3.1.2 Complex Notation

The goal is now to determine the oscillation frequencies and damping rates of the freely vibrating strings coupled at the bridge and slightly detuned. The mechanical quantities are defined as the real part of complex quantities. The solutions are of the form $e^{j\beta t}$ where the variable β is complex, and where the imaginary part represents the attenuation of oscillations in time, resulting from damping at the bridge. As in the paper by Weinreich, the displacements are denoted: $q_i = \Re e\{\psi_i\}$. Equation (6.30) becomes

$$\begin{cases} (\omega_0^2 - \beta^2)\psi_1 = \gamma_1(\psi_i), \\ (\omega_0^2 - \beta^2)\psi_2 = \gamma_2(\psi_i) \end{cases} \tag{6.31}$$

where γ_1 and γ_2 are the complex quantities associated to g_1 and g_2. For the strings, the notations $v_i(t) = \Re e\{V_i\}$ and $f_i(t) = \Re e\{F_i\}$, are used, where V_i and F_i are the complex quantities associated with velocities and forces at the bridge, respectively. Since the detuning between the two strings is assumed to be small, the angular frequencies of the coupled system are close to the fundamental frequency $\omega_0 = \sqrt{T/\rho S}$ corresponding to tuned strings in unison. Over this small frequency range, the complex impedance of the bridge at the attachment point Z_B can therefore be regarded as constant ($Z_B(\omega) \simeq Z_B(\omega_0)$), and the following equation can be written as:

$$F_B = F_1 + F_2 = Z_B V_B. \tag{6.32}$$

This yields the admittance matrix at the bridge:

$$\begin{pmatrix} V_1 \\ V_2 \end{pmatrix} = \begin{pmatrix} Y_B & Y_B \\ Y_B & Y_B \end{pmatrix} \begin{pmatrix} F_1 \\ F_2 \end{pmatrix}. \tag{6.33}$$

This admittance matrix is not invertible since its determinant is zero. Still following Weinreich's approach, Y_B is normalized with respect to the characteristic impedance of the strings in unison, denoted $Z_c = Z_0 = \sqrt{\rho S T}$ ($T_1 = T_2 = T$), so that the following expression is obtained:

$$Y_B = \frac{\pi}{j\omega_0 Z_0}\zeta = \frac{\pi}{jZ_0}\chi = \frac{\pi}{jZ_0}(\xi + j\eta), \tag{6.34}$$

where ξ and η are dimensionless quantities.[5]

Because of the presence of dissipative phenomena at the bridge, η is always positive or null. The case $\eta = 0$ corresponds to a purely reactive bridge. The motion of the bridge has the effect of shifting the eigenfrequencies of the strings (see Chap. 3). The particular case $\xi = 0$ corresponds to a string with purely dissipative ends (see Chap. 5).

Example of a Simplified Model of a String

In order to illustrate the expression of g_i in (6.30) with a practical example, one can see the fundamental mode as the oscillation of a mass M concentrated

(continued)

[5] Warning! In Weinreich's paper [16] these quantities have the dimension of a frequency. Here, they are divided by ω_0.

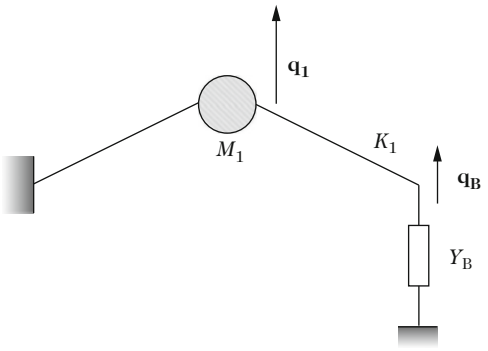

Fig. 6.8 Simplified scheme of a string vibrating at its fundamental frequency and loaded by a finite impedance at the bridge

in the middle of the string of stiffness K. In the case of two oscillators, we write $M = M_1 = M_2$ and $K_2 = K_1(1 + 2\varepsilon)$, which accounts for a slight difference of tension between both strings. With the assumptions of small mobility at the bridge, the displacement $q_B(t)$ is small compared to q_1 and q_2 (see Fig. 6.8).

With $\omega_0^2 = K_1/M$, the equations are written:

$$\begin{cases} \ddot{q}_1 + \omega_0^2 q_1 = \omega_0^2 q_B, \\ \ddot{q}_2 + \omega_0^2 q_2 = \omega_0^2(1 + 2\varepsilon) q_B - 2\varepsilon\omega_0^2 q_2, \end{cases} \tag{6.35}$$

where the displacement at the bridge q_B is linked to q_1 and q_2 by the boundary condition:

$$f_1 + f_2 = K_1(q_1 - q_B) + K_2(q_2 - q_B)\,, \tag{6.36}$$

or, equivalently, in terms of impedance:

$$F_1 + F_2 = K_B Q_B\,, \tag{6.37}$$

where K_B represents the dynamic stiffness of the bridge defined by $Z_B V_B = K_B Q_B$. With the previous notations, Eq. (6.36) is rewritten:

$$Q_B = \frac{\psi_1 + \psi_2(1 + 2\varepsilon)}{2(1 + \varepsilon) + \frac{K_B}{M\omega_0^2}}\,. \tag{6.38}$$

The model can be further simplified, taking the small detuning between both strings into account ($\varepsilon \ll 1$). Equation (6.35) becomes

(continued)

$$\begin{cases} (\omega_0^2 - \beta^2)\psi_1 = \omega_0^2 \dfrac{\psi_1 + \psi_2}{2 + \frac{K_B}{M\omega_0^2}}, \\ (\omega_0^2 - \beta^2)\psi_2 = \omega_0^2 \left[\dfrac{\psi_1 + \psi_2}{2 + \frac{K_B}{M\omega_0^2}} - 2\varepsilon\psi_2 \right], \end{cases} \tag{6.39}$$

where the expressions for g_1 and g_2 are exhibited.

6.3.2 Formulation of the Problem in Terms of Forces

The model presented in Sect. 6.3.1 has direct applications in sound synthesis and in experimentation. However, the formulation in terms of displacements is not convenient for obtaining the dynamical matrices. Another elegant method to obtain the equations whose solutions are the (complex) eigenfrequencies of coupled strings is to formulate the problem in terms of forces. The assumption is based primarily on the calculation of the transfer impedance Z in $x = L$ of a string with characteristic impedance $Z_c = \sqrt{T\rho S} = T/c$ fixed at $x = 0$. From (4.29), the transfer impedance is equal to:

$$Z = jZ_c \cot kL \,. \tag{6.40}$$

At this stage, it is interesting to use the series expansion of the cotangent function [1]:

$$\pi \cot \pi z = \frac{1}{z} + 2z \sum_{n=1}^{\infty} \frac{1}{z^2 - n^2}, \tag{6.41}$$

from which we derive

$$Z = j\frac{T}{\omega L} + j\frac{2\omega T}{L} \sum_{n=1}^{\infty} \frac{1}{\omega^2 - \omega_n^2}, \tag{6.42}$$

where $\omega_n = ck_n = n\pi c/L$ are the eigenfrequencies of the string rigidly fixed at both ends. One can here recognize some expressions seen in Chap. 4. If the angular frequency ω is close to one eigenfrequency ω_n, Eq. (6.42) can be simplified as:

$$Z \simeq j\frac{2\omega T}{L} \frac{1}{\omega^2 - \omega_n^2} = \frac{F}{V_B} \,. \tag{6.43}$$

and we have

$$\left(\omega_n^2 - \omega^2\right) F = -\frac{2T}{L} j\omega V_B \,. \tag{6.44}$$

Returning now to the time domain, the equations that describe the string forces $f_i(t)$ at the bridge are obtained

$$\ddot{f}_i + \omega_i^2 f_i = -\frac{2T_i}{L}\, \dot{v}_B \;\text{ with }\; i = [1, 2] \,. \tag{6.45}$$

With the notations defined above, this yields

$$\begin{cases} (\omega_1^2 - \beta^2) F_1 = -\dfrac{2T_1}{L} j\beta Y_B (F_1 + F_2), \\ (\omega_2^2 - \beta^2) F_2 = -\dfrac{2T_2}{L} j\beta Y_B (F_1 + F_2) \,. \end{cases} \tag{6.46}$$

The detuning of the strings is modeled by setting $\omega_1 = \omega_0$ and $\omega_2 = \omega_0(1 + 2\varepsilon)$, where $\varepsilon \ll 1$ (notice that ε is here a dimensionless quantity, whereas in Weinreich's paper [16], this term has the dimension of an angular frequency). In terms of tension, we have $T_2 = T_1(1 + 4\varepsilon)$. A first-order approximation of (6.46) then gives

$$\begin{cases} j\left[\beta - \omega_0\right] F_1 = j\zeta (F_1 + F_2), \\ j\left[\beta - \omega_0\right] F_2 = j\zeta (F_1 + F_2) + 2j\varepsilon\omega_0 F_2, \end{cases} \tag{6.47}$$

where ζ is given by (6.34). These equations can be further simplified if the variables are defined as differences, compared to the unison reference case, and if the admittance at the bridge is written in dimensionless form [see Eq. (6.34)]. Thus, we write $\beta = \alpha + \omega_0$ and $a = \frac{\alpha}{\omega_0}$. After calculations, the following differential system is obtained:

$$ja \begin{pmatrix} F_1 \\ F_2 \end{pmatrix} = j\boldsymbol{\Omega} \begin{pmatrix} F_1 \\ F_2 \end{pmatrix} = j \begin{bmatrix} \chi & \chi \\ \chi & \chi + 2\varepsilon \end{bmatrix} \begin{pmatrix} F_1 \\ F_2 \end{pmatrix} \,. \tag{6.48}$$

where $\boldsymbol{\Omega}$ is the dynamical matrix of the coupled system.

6.3.3 Eigenvalues of the Strings-Bridge Coupled System

The forces F_1 and F_2, solutions of the system (6.48), are linear combinations of $\exp\{ja_+ t\}$ and $\exp\{ja_- t\}$, where a_+ and a_- are solutions of the characteristic equation:

$$a^2 - 2(\chi + \varepsilon)a + 2\varepsilon\chi = 0, \tag{6.49}$$

from which we get the following roots:

$$a_{\pm} = \chi + \varepsilon \pm \mu \quad \text{with} \quad \mu = (\varepsilon^2 + \chi^2)^{1/2} . \tag{6.50}$$

6.3.3.1 Discussion

To illustrate this result, Fig. 6.9 shows the variations of the coupled frequencies with respect to string detuning ε for some selected values of the bridge admittance.

- When the admittance is purely reactive [$\chi = \xi$, see Eq. (6.34)], we have $a_{\pm} = \xi + \varepsilon \pm (\xi^2 + \varepsilon^2)^{1/2}$. Figure 6.9a shows the representative curve of $b_{\pm} = a_{\pm} - \xi$ with respect to $\omega_0\varepsilon$. When ε is large, the eigenfrequencies of the strings are close to those obtained in the uncoupled case. As ε tends to zero (unison), the bridge coupling is important and moves the eigenfrequencies apart from each other.

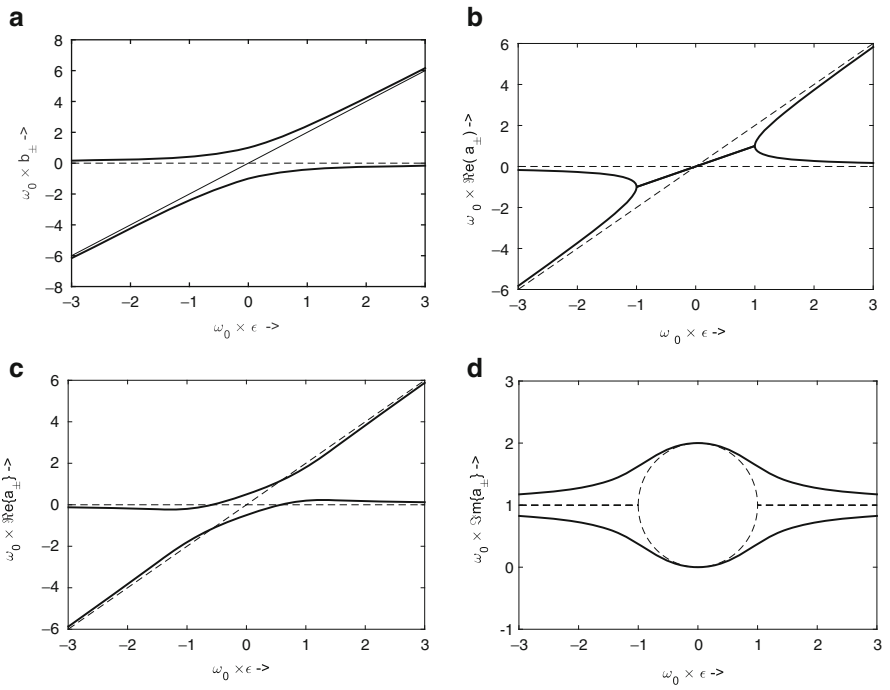

Fig. 6.9 Eigenvalues of the system of strings coupled to the bridge. (**a**) Reactive end ($\omega_0\xi = 1$, $\eta = 0$); $b_{\pm} = a_{\pm} - \xi$. (**b**) Resistive end ($\omega_0\eta = 1$, $\xi = 0$): real part. (**c**) Particular case ($\omega_0\xi = 1/2$, $\omega_0\eta = 1$): real part. *Solid lines*: solutions of the coupled system; *dashed lines*: uncoupled case. (**d**) End with nonzero resistive part: imaginary part. *Solid line*: $\omega_0\xi = 1/2$, $\omega_0\eta = 1$; *dashed line*: $\omega_0\eta = 1$, $\xi = 0$

- When the bridge admittance is purely resistive ($\chi = j\eta$), two cases must be discussed depending on whether η is smaller or larger than ε. The first case yields $a_\pm = \varepsilon + j\eta \pm \sqrt{\varepsilon^2 - \eta^2}$. The real part of the solution is represented by two branches of hyperbola in Fig. 6.9b. The imaginary part is represented by two segments $\Im m(a_\pm) = \eta =$ cst (see Fig. 6.9d).

  In the case where $\eta > \varepsilon$, we get $a_\pm = \varepsilon + j\eta \pm j\sqrt{\eta^2 - \varepsilon^2}$. The real part is represented by the line segment $\Re e(a_\pm) = \varepsilon$, and the imaginary part is the circle with center $\mathscr{C} = (0, \eta)$ and radius η.
- In the general case ($\chi = \xi + j\eta$), one can observe intermediate situations compared to the previous particular cases (see Fig. 6.9c, d). The eigenfrequencies and damping factors of the strings are modified by the coupling, essentially for small values of ε. In this case, one string of the pair is damped much faster than the other: it can be observed on Fig. 6.9d, for $\omega_0\varepsilon$ between $+1/2$ and $-1/2$, that $\omega_0\Im m(a)$ is close to 2 for one string, which corresponds to a damping rate twice as high as for an isolated string, while for the other string $\omega_0\Im m(a)$ is less than 0.1. For the particular case $\varepsilon = 0$, it can be seen that one string is no longer damped at all. Everything happens as if the energy dissipated in the bridge is fully "pumped" by one string of the doublet.

6.3.4 Bridge Motion

The expressions for the forces are obtained by solving the system (6.47). The values of the integration constants are given by the initial conditions. Setting, for example, $f_1(0) = f_2(0) = F_0$ and using dimensional quantities for the frequencies, we get

$$\begin{cases} F_1 = \dfrac{F_0}{2\mu}\left[(\chi - \varepsilon + \mu)e^{ja+t} + (\varepsilon - \chi + \mu)e^{ja-t}\right], \\ F_2 = \dfrac{F_0}{2\mu\chi}\left[(\varepsilon + \mu)(\chi - \varepsilon + \mu)e^{ja+t} + (\varepsilon - \mu)(\varepsilon - \chi + \mu)e^{ja-t}\right], \end{cases} \tag{6.51}$$

where $\mu = \sqrt{\varepsilon^2 + \chi^2} = \sqrt{\varepsilon^2 + \xi^2 - \eta^2}$. From these expressions, the bridge velocity is derived [see Eq. (6.32)]:

$$V_B = Y_B(F_1 + F_2) = \frac{2\pi F_0 \chi}{\mu Z_0} e^{j(\varepsilon+\chi)\omega_0 t}\left[\mu \cos \mu\omega_0 t + j\chi \sin \mu\omega_0 t\right] e^{j\omega_0 t}. \tag{6.52}$$

The temporal evolution of forces and velocities is obtained by taking the real parts of Expressions (6.51) and (6.52).

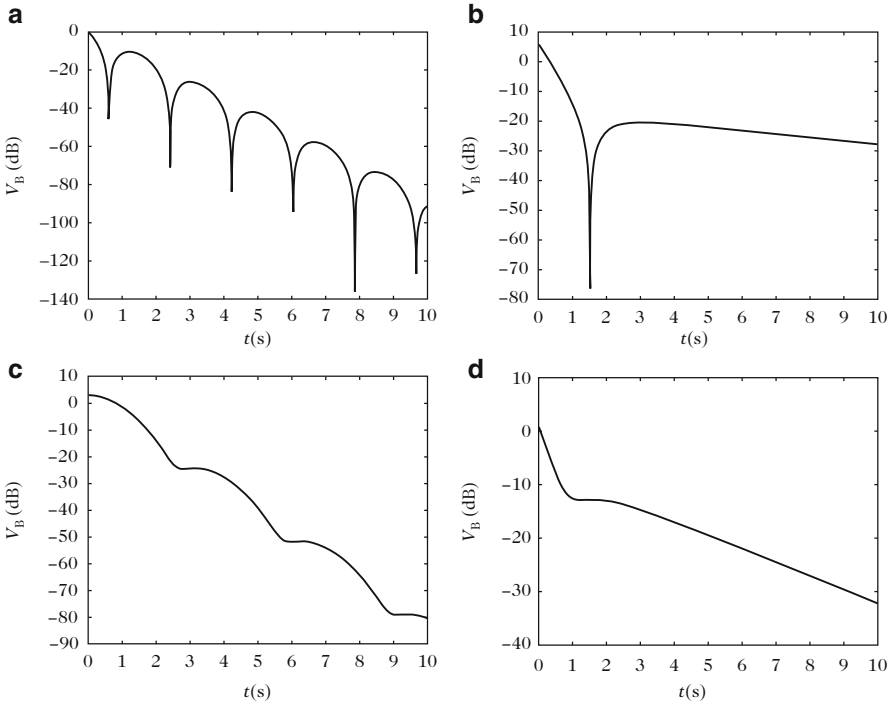

Fig. 6.10 Temporal envelope of the bridge velocity. (**a**) Coupling of strings with a purely resistive admittance at the bridge and $\varepsilon > \eta$. (**b**) Same situation with $\varepsilon < \eta$. (**c**) Coupling of strings with a complex admittance at the bridge and $\varepsilon^2 + \xi^2 > \eta^2$. (**d**) Same case with $\varepsilon^2 + \xi^2 < \eta^2$

6.3.4.1 Discussion

Figure 6.10 shows the envelopes of the bridge velocity for some special cases of bridge admittance and string detuning.

- The case (a) corresponds to a coupling with a purely resistive admittance where $\varepsilon > \eta$. A single decay of the velocity is observed with a time constant $1/\eta$ with superimposed beats of frequency $\mu = \sqrt{\varepsilon^2 - \eta^2}$.
- The case (b) again corresponds to a purely resistive coupling, but with $\varepsilon < \eta$. In this case, the velocity modulus is written:

$$|V_B| = \frac{2\pi F_0 \eta}{|\mu| Z_0} e^{j(\varepsilon+\chi)\omega_0 t} \left[|\mu| \cosh |\mu| \omega_0 t - \eta \sinh |\mu| \omega_0 t \right] . \tag{6.53}$$

  The beats disappear and the velocity envelope shows a double decay: a rapid initial decay followed by a slower decay that arises after a strong minimum.
- The case (c) corresponds to a bridge admittance with both a resistive and a reactive part, and where the detuning between the strings is such that the quantity

μ is real, or, equivalently, $\varepsilon^2 + \xi^2 > \eta^2$. As for case (a), oscillations are superimposed to a single decay. However, the amplitude of the beats is less pronounced here.

- Finally, the case (d) also corresponds to a common admittance, but with the condition $\varepsilon^2 + \xi^2 < \eta^2$, which implies $\mu = j|\mu|$. As for the case (b), a double decay is observed, though with a less pronounced minimum.

All these regimes are commonly observed on real pianos. We are now able to better understand the role of the piano tuner, who does not only adjust the pitch, but also the temporal envelope of sound.

6.3.4.2 Limiting Case of a Single String

In the particular case of a single string coupled to the soundboard, Eq. (6.47) becomes

$$\beta - \omega_0 = \zeta = j\frac{Y_B Z_0 \omega_0}{\pi} \,. \tag{6.54}$$

Setting $Y_B(\omega_0) = G_B + jB_B$, Eq. (6.54) gives the frequency shift and the damping factor of the string due to coupling, which is

$$\begin{aligned} &\beta = \omega_0 + \delta\omega_0 + \alpha, \\ &\text{with} \quad \frac{\delta\omega_0}{\omega_0} = -\frac{B_B Z_0}{\pi} = -\frac{Z_0 \Im m\{Y_B\}}{\pi}, \\ &\text{and} \quad \alpha = \frac{\omega_0 G_B}{\pi} = \frac{\omega_0 Z_0 \Re e\{Y_B\}}{\pi} \,. \end{aligned} \tag{6.55}$$

These are the classical formulas established by several authors [12]. They are similar in form to those obtained for a lossless tube loaded by a radiation impedance.

6.4 String–Soundboard Coupling

In Sects. 6.2 and 6.3, two examples of coupling were studied and illustrated by simple models with two degrees of freedom. In this section, the purpose is extended by considering the more general coupling between N_s string modes and N_b board modes. The damping coefficients are still considered as small, which allows for some approximations (see Chap. 5). The approach presented below is based on a study by Woodhouse in the case of the guitar [17]. In a first step, both string and soundboard kinematics are formulated. Then the mass and stiffness matrices are derived, using energetic considerations. The eigenvalues and eigenvectors of the associated conservative system are obtained using the general method described in Chap. 3.

For real systems, it has been seen in Chap. 5 that the dissipation matrix is generally not diagonal, and that an exact resolution requires the calculation of complex modes. Here, the presentation is simplified by assuming that this matrix is diagonal. In what follows, complex eigenfrequencies are thus considered, but with real mode shapes.

6.4.1 Determination of Mass and Stiffness Matrices

The string of length L is assumed to be fixed at $x = 0$ and moving at $x = L$ with $y(L, t) = q_0(t)$ (see Fig. 6.11).

Only the vertical displacement of the string is considered. The amplitude of q_0 is assumed to be small compared to the transverse displacement of the string, so that its eigenmodes $\Phi_n(x)$ (with $n \geq 1$) are assumed to be given by $\sin \frac{n\pi x}{L}$ with $k_n L = n\pi$. Finally, the string displacement is written in the form:

$$y(x, t) = q_0(t)\frac{x}{L} + \sum_{n=1}^{N_s} q_n(t) \sin \frac{n\pi x}{L}, \tag{6.56}$$

where q_0 appears as the generalized displacement of the rigid mode (case $n = 0$), corresponding to an overall rotation of the string around the end $x = 0$, whereas q_n (for $n \geq 1$) are the eigenmodes of a string simply supported at both ends.

The modal displacements of the N_b soundboard modes at the attachment point of the string are denoted $r_m(t)$. The continuity of displacement at this point imposes the condition:

$$q_0(t) = \sum_{m=1}^{N_b} r_m(t) \, . \tag{6.57}$$

In what follows, $B = EI$ is the string's bending stiffness, T its tension, and $k_m = m_m \omega_m^2$ the modal stiffness of the soundboard mode m. The elastic potential energy of the coupled system is written (see Chap. 1):

$$E_p = \frac{1}{2}\left[\sum_{m=1}^{N_b} k_m r_m^2 + T\int_0^L \left(\frac{\partial y}{\partial x}\right)^2 dx + B\int_0^L \left(\frac{\partial^2 y}{\partial x^2}\right)^2 dx\right] . \tag{6.58}$$

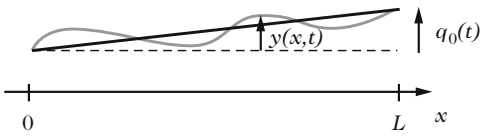

Fig. 6.11 Kinematics of a string coupled to a soundboard. N.B. For better clarity, the displacement $q_0(t)$ of the soundboard at one end of the string is intentionally drawn with an amplitude comparable to the transverse motion of the string $y(x, t)$, although it is much smaller in reality

Given (6.57) and (6.56), Eq. (6.58) can be rewritten as:

$$E_p = \frac{1}{2}\left[\sum_{m=1}^{N_b} k_m r_m^2 + \frac{T}{L}\left(\sum_{m=1}^{N_b} r_m\right)^2 + \frac{T\pi^2}{2L}\sum_{n=1}^{N_s} n^2 q_n^2 + \frac{B\pi^4}{2L^3}\sum_{n=1}^{N_s} n^4 q_n^2\right]. \tag{6.59}$$

The vector $\boldsymbol{X}$ of the generalized coordinates is defined as:

$$\boldsymbol{X} = {}^t[q_1, \ldots, q_{N_s}, r_1, r_2, \ldots, r_{N_b}] \tag{6.60}$$

so that the stiffness matrix $\mathbb{K}$ is given by:

$$E_p = \frac{1}{2}{}^t\boldsymbol{X}\mathbb{K}\boldsymbol{X}\,. \tag{6.61}$$

Finally $\mathbb{K}$ is written in the form:

$$\mathbb{K} = \begin{bmatrix} \mathbb{K}_{11} & 0 \\ 0 & \mathbb{K}_{22} \end{bmatrix}, \tag{6.62}$$

with

$$\mathbb{K}_{11} = \frac{\pi^2}{2L}\text{diag}\left\{T + \frac{B\pi^2}{L^2}, 4T + 16\frac{B\pi^2}{L^2}, \ldots, N_s^2 T + \frac{N_s^4 B\pi^2}{L^2}\right\}, \tag{6.63}$$

and

$$\mathbb{K}_{22} = \begin{bmatrix} k_1 + T/L & T/L & \ldots & T/L \\ T/L & k_2 + T/L & \ldots & T/L \\ \ldots & \ldots & \ldots & \ldots \\ T/L & T/L & \ldots & k_{N_b} + T/L \end{bmatrix}. \tag{6.64}$$

Similarly, the mass matrix $\mathbb{M}$ is obtained from the kinetic energy of the system:

$$E_c = \frac{1}{2}\left[\sum_{n=1}^{N_s} m_n \dot{r}_m^2 + \mu\int_0^L \dot{y}^2 dx\right], \tag{6.65}$$

where $\mu = \rho S$. E_c is written in the quadratic form:

$$E_c = \frac{1}{2}{}^t\dot{\boldsymbol{X}}\mathbb{M}\dot{\boldsymbol{X}}, \tag{6.66}$$

from which $\mathbb{M}$ is derived in the form

$$\mathbb{M} = \begin{bmatrix} \mathbb{M}_{11} & \mathbb{M}_{12} \\ {}^t\mathbb{M}_{12} & \mathbb{M}_{22} \end{bmatrix}. \tag{6.67}$$

The reader will check that the different sub-matrices defined in (6.67) are written:

$$\mathbb{M}_{11} = \frac{\mu L}{2}\text{diag}\left\{1, 1, \ldots, 1\right\}, \tag{6.68}$$

$$\mathbb{M}_{22} = \begin{bmatrix} m_1 + \frac{\mu L}{3} & \frac{\mu L}{3} & \ldots & \frac{\mu L}{3} \\ \frac{\mu L}{3} & m_2 + \frac{\mu L}{3} & \ldots & \frac{\mu L}{3} \\ \ldots & \ldots & \ldots & \ldots \\ \frac{\mu L}{3} & \ldots & \frac{\mu L}{3} & m_{N_b} + \frac{\mu L}{3} \end{bmatrix}, \tag{6.69}$$

$$\mathbb{M}_{12} = \frac{\mu L}{\pi}\begin{bmatrix} 1 & 1 & \ldots & 1 \\ -1/2 & -1/2 & \ldots & -1/2 \\ \ldots & \ldots & \ldots & \ldots \\ (-1)^{N_s+1}/N_s & \ldots & (-1)^{N_s+1}/N_s & (-1)^{N_s+1}/N_s \end{bmatrix}. \tag{6.70}$$

The coupling affects here the mass matrix only, through the sub-matrices $\mathbb{M}_{12}$ and $\mathbb{M}_{21} = {}^t\mathbb{M}_{12}$ (inertial coupling). The stiffness matrix remains diagonal.

6.4.2 Mode Crossing

In order to illustrate the previous results by a particular case, the coupling between a string mode and a soundboard mode is solved below analytically. Special attention is paid to the damping coefficients of these modes, which determine the temporal evolution of the free system. Using the results obtained in Sect. 6.4.1, the reduction of the system to two modes leads to the following mass matrix:

$$\mathbb{M} = \begin{bmatrix} m_{11} & m_{12} \\ m_{21} & m_{22} \end{bmatrix} = \begin{bmatrix} \frac{\mu L}{2} & \frac{\mu L}{\pi} \\ \frac{\mu L}{\pi} & m_1 + \frac{\mu L}{3} \end{bmatrix}. \tag{6.71}$$

The reduced stiffness matrix becomes

$$\mathbb{K} = \begin{bmatrix} k_{11} & 0 \\ 0 & k_{22} \end{bmatrix} = \begin{bmatrix} \frac{\pi^2}{2L}\left(T + \frac{B\pi^2}{L^2}\right) & 0 \\ 0 & k_1 + \frac{T}{L} \end{bmatrix}. \tag{6.72}$$

In stringed instruments, the quality factors of the string modes are generally higher (significantly much higher, most of the time) than those of the soundboard (see Chap. 2). In what follows, all quality factors are also assumed to be significantly larger than unity, which means $Q_i = 1/2\zeta_i \gg 1$ where ζ_i are the damping coefficients. The damping matrix, which is assumed to be diagonal, is written:

$$\mathbb{C} = \begin{bmatrix} c_{11} & 0 \\ 0 & c_{22} \end{bmatrix} = \begin{bmatrix} 2\zeta_1\omega_1 m_{11} & 0 \\ 0 & 2\zeta_2\omega_2 m_{22} \end{bmatrix}, \tag{6.73}$$

where $\omega_1 = \sqrt{m_{11}/k_{11}}$ and $\omega_2 = \sqrt{m_{22}/k_{22}}$ are the uncoupled eigenfrequencies of string and soundboard, respectively. Altogether, this reduced coupled system takes the standard form:

$$\mathbb{M}\ddot{q} + \mathbb{C}\dot{q} + \mathbb{K}q = 0\,. \tag{6.74}$$

The (complex) eigenfrequencies of the uncoupled system are given by the roots of the characteristic equation:

$$\left(\omega_1^2 + 2j\omega\zeta_1\omega_1 - \omega^2\right)\left(\omega_2^2 + 2j\omega\zeta_2\omega_2 - \omega^2\right) = \omega^4\lambda^2\,. \tag{6.75}$$

where $\lambda^2 = \frac{m_{12}m_{21}}{m_{11}m_{22}}$ is the mass coupling coefficient. It is explicitly written here:

$$\lambda^2 = \frac{2\mu L}{\pi^2(m_1 + \mu L/3)}\,. \tag{6.76}$$

It is easy to show that its generalization to the coupling between the p-th string mode and the n-th board mode is given by:

$$\lambda^2 = \frac{2\mu L}{p^2\pi^2(m_n + \mu L/3)}\,. \tag{6.77}$$

We restrict ourselves to the frequency range where the angular frequency ω remains close to ω_1, itself close to ω_2, or, in other words, when string and soundboard resonances are comparable. As a consequence, the calculations can be simplified by setting $\omega\zeta_1\omega_1 \simeq \omega_1^2\zeta_1$ and $\omega\zeta_2\omega_2 \simeq \omega_2^2\zeta_2$ in (6.75). With $\gamma = (\omega_2/\omega_1)^2$, the roots of Eq. (6.75) are given by:

$$\frac{\omega_\pm}{\omega_1} = \Omega^{1/2} \quad \text{with} \quad \Omega = \frac{1 + \gamma + 2j(\zeta_1 + \gamma\zeta_2) \pm \sqrt{\Delta}}{2(1-\lambda^2)}$$
$$\text{and} \quad \Delta = [1 + \gamma + 2j(\zeta_1 + \gamma\zeta_2)]^2 - 4(1-\lambda^2)\gamma[1 - 4\zeta_1\zeta_2 + 2j(\zeta_1 + \zeta_2)]\,. \tag{6.78}$$

Figure 6.12 shows that for fixed values of ζ_i, either the real part or the imaginary part of the eigenfrequencies cross each other, depending on the values of the coupling parameter λ.

These figures show, among other things, that crossing can occur in the vicinity of $\omega_2 = \omega_1$. As a consequence, the value $\gamma = 1$ will be now imposed in the following equations. Thus, the frequencies are written:

$$\omega_\pm = \Omega^{1/2} \quad \text{with} \quad \Omega = \frac{1 + j(\zeta_1 + \zeta_2) \pm \sqrt{\Delta'}}{1-\lambda^2}$$
$$\text{and} \quad \Delta' = \lambda^2[(1 + 2j\zeta_1)(1 + 2j\zeta_2)] - (\zeta_1 - \zeta_2)^2\,. \tag{6.79}$$

Given the fact that $\zeta_i \ll 1$ (nearly 10^{-2} for the board modes and 10^{-3} for the string modes), one can write:

$$\Delta' \simeq \lambda^2 - (\zeta_1 - \zeta_2)^2 \,. \tag{6.80}$$

Discussion

- For $\lambda^2 > (\zeta_1 - \zeta_2)^2$, the determinant Δ' is positive and its square root is real. In this case, both values of Ω have the same imaginary part, and differ only by the real part. To the first order, the same result applies to the eigenfrequencies $\omega_\pm$ since their imaginary parts are small compared to their real parts. For quality factors such as $Q_1 = 3500$ and $Q_2 = 100$, and with $\lambda = 0.01$, this leads to the results shown in Fig. 6.12a, b where a crossing exists for the imaginary part

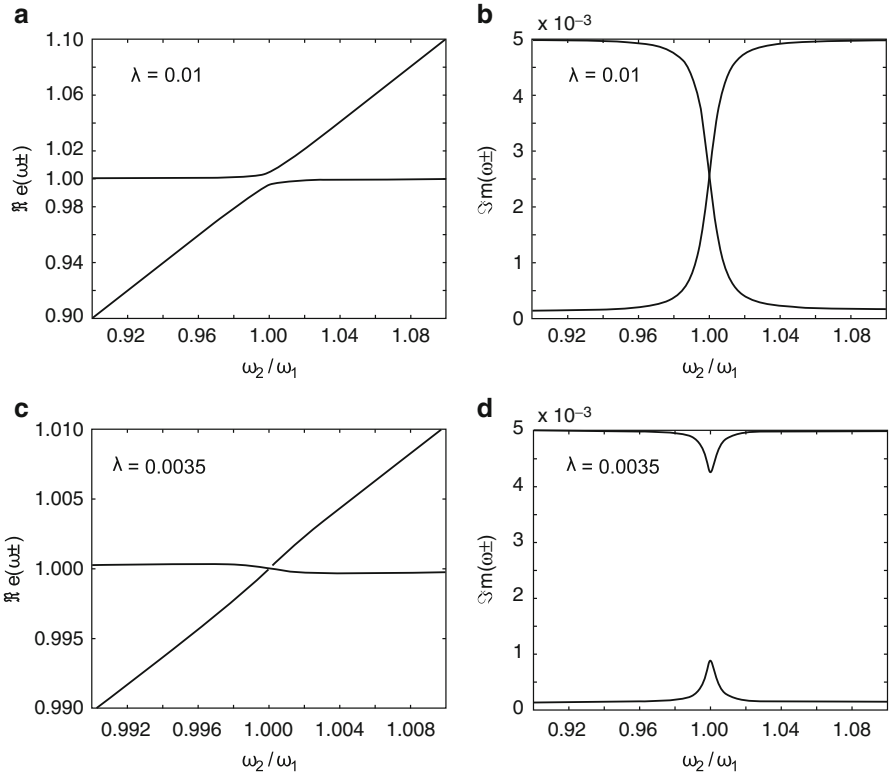

Fig. 6.12 Real and imaginary parts of the eigenfrequencies of the coupled system as a function of ω_2/ω_1 for two different values of the mass coupling parameter λ between string and soundboard, exhibiting crossing and non-crossing situations for the modes. Q_1=3500; Q_2=100. (**a**) and (**b**): $\lambda^2 > (\zeta_1 - \zeta_2)^2$; (**c**) and (**d**): $\lambda^2 < (\zeta_1 - \zeta_2)^2$

only in the vicinity of $\gamma = 1$. This situation occurs when the modal mass of the soundboard mode is comparable to the total mass of the string, or lower [see Eq. (6.76)]. The coupling moves the eigenfrequencies of string and board apart from each other, compared to the uncoupled case. However, the two modes oscillate with the same damping rate.

- For $\lambda^2 < (\zeta_1 - \zeta_2)^2$, the determinant is negative and its square root is purely imaginary. Both values of Ω have now the same real part and different imaginary parts. It is also the case, to the first order, for the eigenfrequencies $\omega_\pm$. With the same quality factors, and with $\lambda = 0.0035$, the situation shown in Fig. 6.12c, d occurs, characterized by a crossing of the real part only, in the vicinity of $\gamma = 1$. From a physical point of view, this is a situation where the modal mass of the soundboard mode is large compared to the total mass of the string. The main consequence of this property is that even if the eigenfrequencies of string and soundboard are close, the string has a low damping and therefore oscillates for a long time while the vibration of the soundboard is damped more rapidly.

Figure 6.13 illustrates both regimes, when the quality factor of one of the two modes varies, the real parts of the uncoupled eigenfrequencies remaining equal ($\omega_1 = \omega_2$). This figure shows that, as long as the ratio Q_1/Q_2 remains small (less than nearly 7 in our example, see Fig. 6.13b), the imaginary parts of both coupled modes are comparable. This means these two modes have the same decay time. However, within the same range, the real part (the oscillation frequencies) of the modes are moved apart from each other because of the coupling.

Conversely, if the ratio Q_1/Q_2 is larger than the threshold value defined by $\Delta' = 0$, the real parts (and thus the oscillation frequencies) of the modes coincide. In this range, their imaginary parts differ significantly. The string damping remains significantly smaller than the board damping. This is a remarkable and not really intuitive result: in fact, one might think (but it is wrong!) that a string mode tuned

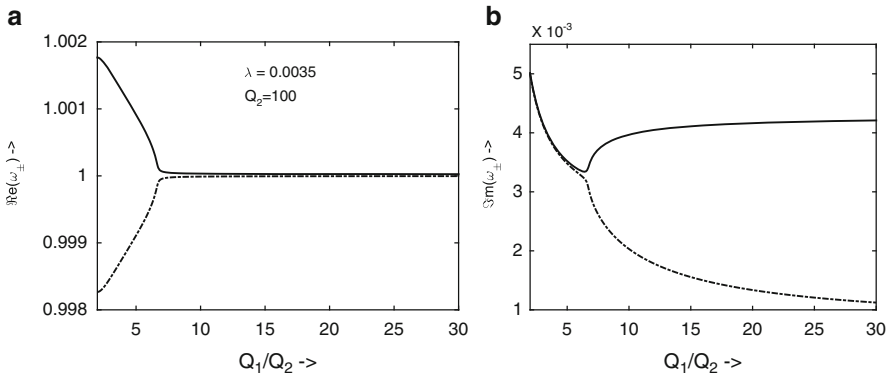

Fig. 6.13 Variations of the eigenfrequencies of the coupled string-soundboard system as a function of the ratio between the quality factors of both elements. (**a**) Real part and (**b**) Imaginary part

to a soundboard mode always contributes to increase the energy transfer from string to soundboard, and thus increase the damping coefficients. One can see, through the example presented above, that it is by no means the case: the quality factors of both elements must be taken into account, showing two clearly different behaviors.

6.4.3 Musical Consequences of the Coupling

In the case of the guitar, Woodhouse has shown experimentally that only a few modes, below 300 Hz approximately, fulfill the condition $\lambda^2 > (\zeta_1 - \zeta_2)^2$ [17], which Gough earlier describes as a "strong" coupling condition [8].[6] The upper range of the guitar corresponds to the opposite case (or "low" coupling). String modes are not strongly coupled to the board, which ensures a sufficient duration of sound.

The comparison with the violin case is instructive: a strong coupling at low frequencies for the violin comparable to the one observed in guitars would cause significant problems, due to the possible apparition of the "wolf tone".[7] Conversely, with a strong coupling between string and board as for the violin, the guitar notes would be too short, and the instrument would sound like a "pizzicato" violin. Why do these differences exist between these two instruments? It is essentially because the violinist, unlike the guitar player, can continuously introduce mechanical power to the instrument with the bow. As a consequence, the primary problem here is to allow an efficient acoustic radiation, and thus it is preferable to ensure a good impedance matching between string and board.

In contrast, because of sound duration, the guitar string should not be too strongly coupled to the instrument body. The energy must be confined long enough in the string and this is why, in turn, the radiated sound power of this instrument is small compared to a violin or a cello. To ensure a weak coupling, the impedance ratio between the string and the board (at the attachment point) must be high. It can be seen from Eq. (6.77) that increasing the mass of the bridge helps in decreasing the coupling, since this leads to increase m_n while keeping other parameters unchanged. One exception can be made for jazz guitars and mandolins, since for these instruments the sound power during the attack transient is musically more important than the sound duration. Conversely, the bridge mass of a violin has to remain small.

[6] In general, a strong coupling is expressed by a large coefficient C/D, where C is a coupling coefficient, and D is a coefficient that characterizes a difference between specific parameters of two elements of the system.

[7] Bowed string players know (and do not like!) this phenomenon. It can lead to an abrupt jump of one octave for a given note, or even give rise to an uncontrolled rough and pulsating sound. Several authors, including Raman [13] and Schelleng [15], have shown that this phenomenon occurs when the fundamental of the string is close to a resonance with high quality factor of the instrument body; see, for example, the discussion of Benade [2] on this problem.

6.5 Soundboard–Bridge Coupling in Violins

The bridge of bowed string instruments is the component that realizes the coupling between strings and soundboard. Players and makers are aware of its particular significance. A number of admittance measurements at the bridge were carried out by several authors, on violins in particular (see, for example, the work by Jansson [10]). All measurements show a relatively wide "peak" between 2 and 3 kHz, and most authors agree that this peak is due to the bridge: this is why it is usually referred to as the *bridge hill*. This observation is well known, however, its theoretical explanation is more recent. The presentation below is largely inspired by Woodhouse [18]. The general idea is that the board and the bridge can no more be considered globally, in contrast to what has been implicitly done in the previous examples treated in this chapter. This refinement is aimed at clarifying the filtering performed by the bridge between string and soundboard.

In fact, the term *bridge hill* can be misleading since the shape of this peak on the admittance curve not only depends on the bridge itself, but also on the coupling between bridge and body. This property is identical to that of a filter whose input impedance (or admittance) depends on the load at the output. The simplified model that serves here as a guideline is drawn in Fig. 6.14. The string action is represented by a force $F \exp j\omega t$ applied to a mass-spring system (m, k) representing the bridge, itself loaded by the admittance $Y(\omega)$ of the board at the attachment point on the body. Denoting by V_b the bridge velocity at the junction with the string, and V_t the velocity of the vertical translation of the board, the equations of motion are written:

$$\begin{cases} -m\omega^2 V_b + k(V_b - V_t) = j\omega F, \\ V_t = YF_t = \dfrac{kY}{j\omega}(V_b - V_t)\,. \end{cases} \tag{6.81}$$

The equivalent circuit with "impedance" notations for this system is shown in Fig. 6.14. When the bridge is fixed on its base (mobility $Y = 0$, or infinite board impedance $Z = 1/Y$), there is a series resonant circuit corresponding to the bridge eigenmode. In all other cases, the input admittance $Y_b = V_b/F$ seen from the string depends on Y. From (6.81), the input admittance of the system can be derived:

$$Y_b(\omega) = \frac{kY(\omega) + j\omega}{k - m\omega^2 + j\omega kmY(\omega)}\,. \tag{6.82}$$

Figure 6.15 shows a comparison between an arbitrary board admittance Y and the corresponding input admittance Y_b for a bridge of mass $m = 1.5$ g with a resonance tuned to $f = 3$ kHz. The admittance Y is simply described as the sum of a few identical and regularly spaced modal contributions. The parameters chosen to calculate Y as shown in Fig. 6.15 are based on the paper by Woodhouse [18] and are such that $f_n = n \times 500$ Hz, $Q_n = 1/2\zeta_n = 50$, $m_n = 0.1$ kg. The eigenvectors

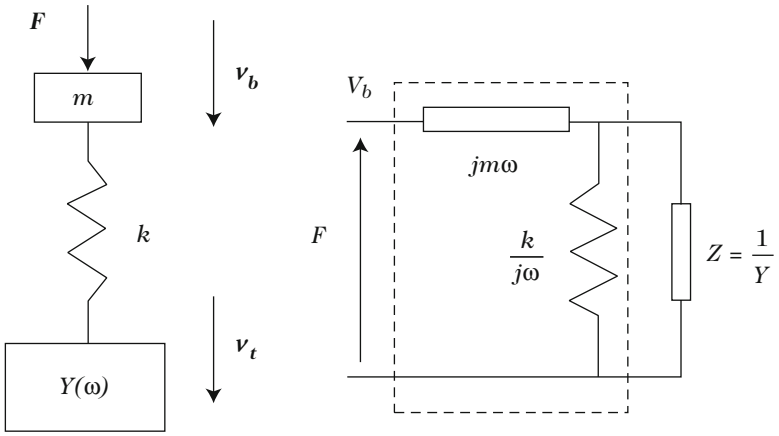

Fig. 6.14 Simplified model of a violin bridge coupled to the body (model 1). From [18]

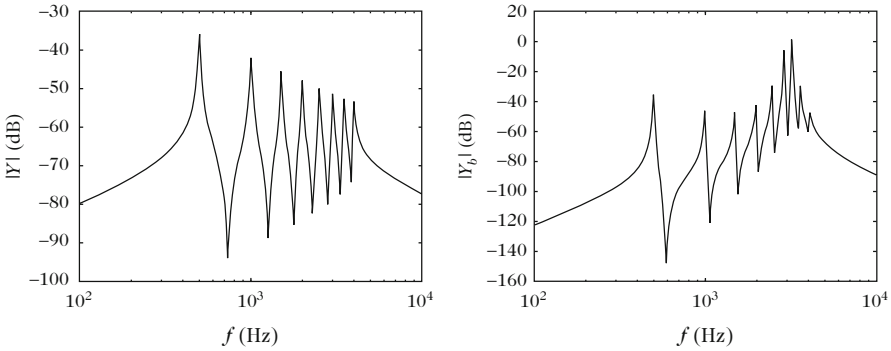

Fig. 6.15 Comparison between the modulus of a simplified board admittance Y and the modulus of a bridge input admittance Y_b for the case of the simplified model 1 presented in Fig. 6.14. From [18]

are normalized to unity. The filtering effect of the bridge can be seen on the graph of the admittance modulus Y_b, which shows a peak around 3 kHz, similar to the one observed in measurements on a violin.

In the cited paper [18], the author develops several successive models to improve the description of the coupling between bridge and soundboard. Here, we restrict ourselves to the model described in Fig. 6.16 which is more realistic than the model 1 shown in Fig. 6.14. The model 2 takes the bridge rotation due to the horizontal force F resulting from the action of the bow into account. This system also serves as a good example of a coupled system in rotation and translation, which illustrates a number of concepts discussed in previous chapters.

In this model, our interest is first focused on the *rotational admittance* defined as the ratio between the angular velocity of rotation θ of the bridge and the momentum $\mathscr{M} = Fa$ of the horizontal force applied by the string during its motion $Y_r = \theta/\mathscr{M}$.

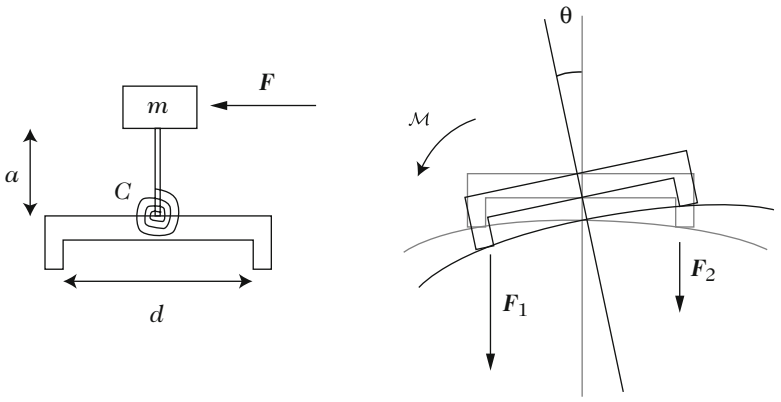

Fig. 6.16 Advanced model of a violin bridge coupled to the board, taking the bridge rotation into account (model 2). From [18]. m is the bridge mass and C its torsional stiffness. d is the distance between the two legs of the bridge, and a is the mean lever arm between the attachment point of the string and the base of the bridge

The parameter a is the mean lever arm and C is the torsional stiffness of the bridge (see Fig. 6.16). The equation of motion for the bridge fixed at its feet is

$$\mathscr{M} = ma^2\ddot{\theta} + C\theta, \tag{6.83}$$

showing the angular eigenfrequency $\omega_b = \sqrt{\frac{C}{ma^2}}$. The bridge is connected to the board by two feet separated from each other by a distance d. Under the action of the transverse forces F_1 and F_2, these feet take the velocities V_1 and V_2 defined by the admittance matrix (see Chap. 3):

$$\begin{pmatrix} V_1 \\ V_2 \end{pmatrix} = \begin{bmatrix} Y_{11} & Y_{12} \\ Y_{21} & Y_{22} \end{bmatrix} \begin{pmatrix} F_1 \\ F_2 \end{pmatrix}. \tag{6.84}$$

Consider now the second foot (right foot, over the soundpost) as fixed. Under the action of a moment $\mathscr{M}$ applied to the bridge, Foot 1 (left foot, on the bass bar side) takes the rotational velocity $\dot{\theta}_1$. Reciprocally, $\dot{\theta}_2$ is the rotational velocity of the right foot, when Foot 1 is fixed (see Fig. 6.16). Given (6.84), this yields the following matrix:

$$\begin{pmatrix} \dot{\theta}_1 \\ \dot{\theta}_2 \end{pmatrix} = \begin{bmatrix} Y_{11} & Y_{12} \\ Y_{21} & Y_{22} \end{bmatrix} \begin{pmatrix} \frac{\mathscr{M}}{d^2} \\ -\frac{\mathscr{M}}{d^2} \end{pmatrix}, \tag{6.85}$$

where $Y_{12} = Y_{21}$. The rotational velocity of the system is $\dot{\theta} = \dot{\theta}_1 - \dot{\theta}_2$, and thus the bridge rotational admittance is written:

$$Y_r = \frac{\dot{\theta}}{\mathscr{M}} = \frac{Y_{11} + Y_{22} - 2Y_{12}}{d^2}. \tag{6.86}$$

It has been shown in Chap. 3 that all terms of the admittance matrix can be written as a modal expansion:

$$Y_{ij}(\omega) = \sum_n j\omega \frac{\Phi_n(x_i, y_i)\Phi_n(x_j, y_j)}{m_n(\omega_n^2 + 2j\omega\omega_n\zeta_n - \omega^2)}, \tag{6.87}$$

where Φ_n is the eigenshape associated to the mode of frequency ω_n, m_n the modal mass, and ζ_n the modal damping. The coordinates of the bridge feet on the board are denoted (x_1, y_1) and (x_2, y_2). From (6.86) and (6.87), we get

$$Y_r(\omega) = \frac{j\omega}{d^2} \sum_n \frac{[\Phi_n(x_1, y_1) - \Phi_n(x_2, y_2)]^2}{m_n(\omega_n^2 + 2j\omega\omega_n\zeta_n - \omega^2)}. \tag{6.88}$$

Finally, the balance of moments around the axis of rotation of the bridge loaded by the board is written:

$$\begin{cases} \mathcal{M}_b = Fa = ma^2\ddot{\theta}_b + C(\theta_b - \theta_t), \\ \mathcal{M}_t = C(\theta_b - \theta_t) = \dfrac{\dot{\theta}_t}{Y_r}, \end{cases} \tag{6.89}$$

where θ_b and θ_t are the rotation angles of bridge and soundboard, respectively, and where $\mathcal{M}_b$ and $\mathcal{M}_t$ are the applied angular momenta. From these relations, the input admittance at the string is derived:

$$Y_b(\omega) = \frac{V_b}{F} = \frac{a^2\dot{\theta}}{\mathcal{M}_b} = \frac{a^2\left[CY_r(\omega) + j\omega\right]}{C - ma^2\omega^2 + j\omega Cma^2 Y_r(\omega)}. \tag{6.90}$$

This model is significantly more accurate than the previous one. In addition to its more refined kinematics, it can be seen that (6.90) allows taking significant manufacturing parameters, such as the bridge height a and the distance d between the feet, into account. In the cited paper, Woodhouse pursues the calculation further using the expressions obtained in the case of simply supported rectangular plates for the eigenshapes Φ_n and eigenfrequencies ω_n [18]. The values of the elastic and geometrical parameters correspond to typical values (see Chap. 13). This model can be further improved by taking not only the upper board into account, but also the back of the instrument coupled to the soundboard by the soundpost. The reader will find in Chap. 7 the analysis of a similar problem: a trumpet mouthpiece coupled to a pipe.

References

1. Abramowitz, M., Stegun, I.A.: Handbook of Mathematical Functions, with Formulas, Graphs, and Mathematical Tables. Dover, New York (1972)
2. Benade, A.H.: Fundamentals of Musical Acoustics. Oxford University Press, London (1976)
3. Christensen, O., Vistisen, R.B.: Simple model for low-frequency guitar function. J. Acoust. Soc. Am. **68**, 758–766 (1980)
4. Dove, M.T.: Introduction to Lattice Dynamics. Cambridge Topics in Mineral Physics and Chemistry. Cambridge University Press, Cambridge (1993)
5. Félix, S.: Vibrations and tuning of the triplets of piano strings (in French). Master thesis, IRCAM (1999)
6. Fletcher, N.H., Rossing, T.D.: The Physics of Musical Instruments. Springer, New-York (1991)
7. French, M.: Structural modifications of stringed instruments. Mech. Syst. Signal Process. **21**, 98–107 (2007)
8. Gough, C.E.: The theory of string resonances on musical instruments. Acustica **49**, 124–141 (1981)
9. Hutchins, C.M.: A 30-year experiment in the acoustical and musical development of violin-family instruments. J. Acoust. Soc. Am. **92**(2), 639–650 (1992)
10. Jansson, E., Niewczyk, B.: On the acoustics of the violin: bridge or body hill. J. Catgut Acoust. Soc. Ser. 2 **3**, 23–27 (1999)
11. Kuo, F.D.: Network Analysis and Synthesis, 2nd edn. Wiley International Edition, New York (1966)
12. Morse, P.M.: Vibration and Sound. Acoustical Society of America, Melville (1981)
13. Raman, C.V.: On the wolf note in the bowed strings instruments. Philos. Mag. **32**, 391–395 (1916)
14. Ribouillault, D.: The guitar technique in France in the first half of the 19th Century (in French). Ph.D. thesis, Université de Paris Sorbonne (1980)
15. Schelleng, J.C.: The violin as a circuit. J. Acoust. Soc. Am. **35**, 326–338 (1963)
16. Weinreich, G.: Coupled piano strings. J. Acoust. Soc. Am. **62**, 1474–1484 (1977)
17. Woodhouse, J.: On the synthesis of guitar plucks. Acta Acust. United Acust. **90**, 928–944 (2004)
18. Woodhouse, J.: On the "bridge hill" of the violin. Acta Acust. United Acust. **91**, 155–165 (2005)

Chapter 7
Wind Instruments: Variable Cross Section and Toneholes

Jean Kergomard

Abstract Wind instruments are studied in two steps. In the first step, one-dimensional models are presented. The horn equation is equivalent to the heterogeneous string studied in Chap. 3. It can either be used for tubes with discontinuities, such as chimney pipes, flutes, or trumpet mouthpieces, or for tubes with a continuous change in cross section, such as conical instruments or bells of brass instruments. The natural modes are calculated with some approximations for several basic shapes of wind instruments. The geometry has an important and complex effect on eigenfrequencies and on amplitudes of input impedance peaks. The role of dissipation is more simple, because it can be averaged over the length of the instrument. However, it depends on the radius, and this yields non-proportional damping. In the second step, it is investigated how to reduce three-dimensional geometric elements, such as toneholes or bends, to lumped elements. For this purpose, the definition of duct modes is given, and the mode-matching method is presented. The basis is a general formulation of the junction of several waveguides at low frequencies. Useful formulas are given for many elements of this kind. The chapter ends with the use of the theory of periodic media in order to analyze the tonehole lattice, with the explanation of important features that distinguish baroque from modern instruments. Attempt is made to give the most recent formulas of use for designing the resonators of wind instruments.

7.1 Introduction

In Chap. 3 we already have dealt with inhomogeneous media, in particular with strings. A whole chapter is dedicated to pipes of varying cross section, possibly with toneholes, because what most distinguishes the wind instruments among themselves is their geometry (along with their excitation system). Several sections are devoted to what does not require three-dimensional theory: the approximation

J. Kergomard (✉)
CNRS Laboratoire de Mécanique et d'Acoustique (LMA), 4 impasse Nikola Tesla, CS 40006, 13453 Marseille Cedex 13, France
e-mail: kergomard@lma.cnrs-mrs.fr

A. Chaigne, J. Kergomard, *Acoustics of Musical Instruments*, Modern Acoustics and Signal Processing, DOI 10.1007/978-1-4939-3679-3_7

called matched planar waves, applied to cross section discontinuities and to horns, as well as the study of cones, for which an exact solution of the sound equation exists.

Then the limits of this approximation are studied, by treating the step discontinuities, and the generalization to the essential issue of toneholes. Finally the problem of periodic media is treated, leading to an analogy between pipes with open holes and pipes with bells.

This chapter is concerned with linear effects only, therefore by low levels of sound. It focuses on eigenfrequencies and response to a given excitation, assuming that this latter is known: we will focus on excitation in the third part. For a given fingering, the input impedance gives a useful approximation of the playing frequencies, even if losses are ignored, as well as a good approximation of the ease of emission.

7.2 Pipes with Variable Cross Section: General Equations

7.2.1 Horn Equation

Early work on pipes with varying cross section (see Fig. 7.1), or with sharp cross section discontinuities, goes back to the eighteenth century, according to Bernoulli and Lagrange. The basic idea is that when a change in cross section area occurs, both flow rate and pressure, once averaged over the cross section, are continuous: this will be discussed in Sect. 7.6. We first give the general equations that will be useful later, although their presentation seems a bit tedious at first glance. Then we focus on important features for wind instruments.

In Chap. 1, two possible analogies between pipes and strings have been established. In Chap. 3, Eq. (3.25) describes inhomogeneous string vibrations when continuity of forces and displacements is assumed. The validity of such an approximation will be discussed below: for now the flow rate and (average) pressure are assumed to remain continuous at a change of cross section. This implies that the

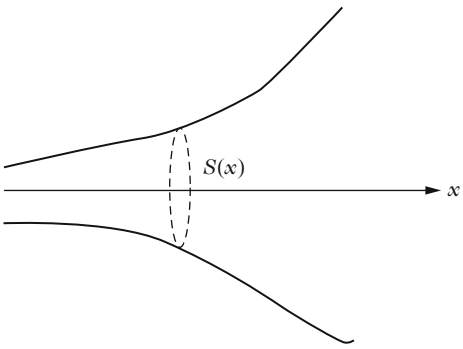

Fig. 7.1 Pipe of variable cross section $S(x)$

two equations of the transmission line (see Table 1.1, Chap. 1) remain valid when the parameters depend only slowly on x:

$$\frac{\partial p}{\partial x} = -\frac{\rho(x)}{S(x)}\frac{\partial u}{\partial t} + \rho(x)F \; ; \; \frac{\partial u}{\partial x} = -S(x)\,\chi_s \frac{\partial p}{\partial t} + q, \tag{7.1}$$

where $\rho(x)F = f_{\text{ext}}/S(x)$ (f_{ext} is an external force per unit length and q a flow rate per unit length). The temperature can vary within the pipe, and so does the density $\rho(x)$, which is inversely proportional to the absolute temperature. On the other hand, the spatial dependence of the compressibility can be ignored, because it is nearly temperature independent. Retaining only the flow source for the equation of pressure (useful for reed instruments) and the force source for the equation of flow (useful for flutes), the wave equations are obtained as follows:

$$\chi_s S\frac{\partial^2 p}{\partial t^2} - \frac{\partial}{\partial x}\left[\frac{S}{\rho}\frac{\partial p}{\partial x}\right] = \frac{\partial q}{\partial t} \; ; \tag{7.2}$$

$$\frac{\rho}{S}\frac{\partial^2 u}{\partial t^2} - \frac{\partial}{\partial x}\left[\frac{1}{S\chi_s}\frac{\partial u}{\partial x}\right] = \rho\frac{\partial F}{\partial t}. \tag{7.3}$$

In the case of a uniform temperature, one obtains, respectively:

$$\frac{S}{c^2}\frac{\partial^2 p}{\partial t^2} - \frac{\partial}{\partial x}\left[S\frac{\partial p}{\partial x}\right] = \rho\frac{\partial q}{\partial t} \; ; \tag{7.4}$$

$$\frac{1}{S}\frac{\partial^2 u}{\partial t^2} - c^2\frac{\partial}{\partial x}\left[\frac{1}{S}\frac{\partial u}{\partial x}\right] = \frac{\partial F}{\partial t}. \tag{7.5}$$

In the absence of sources, Eq. (7.4) is often called the "Webster's horn equation" because of an article published in 1919 [84], even if it is much older [28]. We will call this equation the *horn equation*. One can also write:

$$\frac{\partial^2 p}{\partial x^2} + \frac{S'}{S}\frac{\partial p}{\partial x} - \frac{1}{c^2}\frac{\partial^2 p}{\partial t^2} = -\frac{1}{S}\rho\frac{\partial q}{\partial t}. \tag{7.6}$$

Another expression of Eq. (7.1), often useful, consists in replacing the pressure and flow rate variables by the pR and vR variables, where $R(x)$ is the radius (we consider the case without sources only):

$$\frac{\partial(pR)}{\partial x} = -\rho\frac{\partial(vR)}{\partial t} + \frac{R'}{R}(pR) \; ; \; \frac{\partial(vR)}{\partial x} = -\chi_s\frac{\partial(pR)}{\partial t} - \frac{R'}{R}(vR). \tag{7.7}$$

We can derive from (7.6) another form of the horn equation with no source:

$$\frac{\partial^2(pR)}{\partial x^2} - \frac{1}{c^2}\frac{\partial^2(pR)}{\partial t^2} - \frac{1}{R}\frac{\partial^2 R}{\partial x^2}(pR) = 0\,. \tag{7.8}$$

In the Fourier domain, if $R'' = \partial^2 R/\partial x^2$, it can be written as:

$$\frac{\partial^2 (PR)}{\partial x^2} + \left[k^2 - \frac{R''}{R}\right](PR) = 0 \tag{7.9}$$

Literature on horns is extremely abundant (see [28]). It concerns in particular the solving of the (approximate) plane wave equation, written in one of the forms (7.6) or (7.8): it can be solved either analytically for some geometries defined by the area function $S(x)$, or numerically. Many other studies of the literature are concerned with the possibility of increasing the validity range of the horn equation. This question will be studied in Sect. 7.6.3.5.

7.2.2 Orthogonality of Modes

There is no need to consider all the properties of these equations. One can simply use the analogy with the string equation (3.25). Thus, for simple boundary conditions (Neumann or Dirichlet conditions), assuming that ρ and χ_s remain uniform, the modes $\Phi_n(x)\exp(j\omega_n t)$ are orthogonal for the following scalar product:

$$\int_0^\ell S(x)\Phi_n(x)\Phi_m(x)dx = 0 \text{ for } n \neq m, \tag{7.10}$$

for Eq. (7.4). For Eq. (7.5):

$$\int_0^\ell S^{-1}(x)\Phi_n(x)\Phi_m(x)dx = 0 \text{ for } n \neq m. \tag{7.11}$$

These relationships remain valid when there are discontinuities in cross section. This can be verified by integrating by parts and using the continuity conditions. Pyle [71] noted that all properties which are valid for the pressure in a pipe with cross section area $S(x)$ are valid also for the flow rate in a pipe with cross section area $S'(x) = 1/S(x)$. This duality is useful for certain reasoning. We finally note that if we consider the modes $\Phi_R(x) = \Phi(x)R(x)$ corresponding to the quantity (pR), the scalar product (7.10) does not contain the factor $S(x)$.[1]

[1]This simple result follows the fact that, mathematically, the Fourier transform of Eq. (7.6) is a Sturm-Liouville equation, i.e., an ordinary differential second-order equation with variable coefficients. Making the change of variable $p \longrightarrow pR$ to obtain the transform of (7.8) is equivalent to make canonical the Sturm–Liouville equation by eliminating the term containing the derivative of order 1 with respect to x. This is a general result.

7.2.3 Horn Equation with Boundary Layer Effects

We can generalize these results when the effects of boundary layers are taken into account. In harmonic regime, we assume that the changes in cross section do not influence these effects, which implies that they are slow enough. Thus, using Eq. (5.132) to replace Eq. (7.1), the following equation is obtained:

$$\frac{\partial^2 P}{\partial x^2} - \frac{Z_v'}{Z_v}\frac{\partial P}{\partial x} - Z_v Y_t P = 0, \tag{7.12}$$

as well as a similar equation for the flow rate. We can make use of the concepts of effective density ρ_v (5.116) and effective compressibility χ_t (5.130), that vary with respect to the radius:

$$\rho_v = \rho\left[1 + 2\sqrt{-j}/r_v\right] \; ; \; \chi_t = \chi_s\left[1 + 2(\gamma - 1)\sqrt{-j}/r_t\right]. \tag{7.13}$$

(these expressions, derived from (5.143), are limited to the first order of the ratio boundary layer thickness/radius). We then modify Eq. (7.12) as follows:

$$\frac{\partial^2 P}{\partial x^2} + \left[\frac{S'}{S} - \frac{\rho_v'}{\rho_v}\right]\frac{\partial P}{\partial x} - \Gamma^2 P = 0 \tag{7.14}$$

where the propagation constant Γ is given by (5.144). Two ideas come from this equation: the first one is that if the effects of boundary layers do not strongly vary with the radius, or if the effects are calculated for a kind of average radius, we can solve the horn equation with losses as soon as we know the solution without losses (we just need to consider the effective density and effective compressibility for this average radius). The second idea is that a rigorous solution of this equation is hampered by the problems of non-proportional damping, i.e., damping varying with the space coordinate (see Chap. 5). Illustrations are given for chimney pipes (Sect. 7.3.3) or conical tubes (Sect. 7.4).

7.2.4 Lumped Elements of Horns

We now consider pipes shorter than the wavelength, with "lumped elements" (see Sect. 1.5 in Chap. 1). We will ignore the sources and assume a uniform temperature, and we will start by ignoring losses. If in Eq. (7.1) the flow rate (in the first equation) and the pressure (in the second one) are assumed to be uniform between two abscissae x_1 and $x_2 = x_1 + \ell$, we obtain

$$p(x_2) - p(x_1) = -M_a\frac{\partial u}{\partial t} \; ; \; u(x_2) - u(x_1) = -C_a\frac{\partial p}{\partial t}, \text{ where} \tag{7.15}$$

$$M_a = \rho\int_{x_1}^{x_2}\frac{1}{S(x)}dx \; ; \; C_a = \chi_s\int_{x_1}^{x_2} S(x)dx. \tag{7.16}$$

The expression of the acoustic compliance C_a involves the volume; this expression is exact, i.e., the same result is obtained when starting from the equations in three dimensions, due to the law of mass conservation [Eq. (1.154)].

What happens when losses are considered? In harmonic regime, ignoring dispersion, (only the imaginary part of $\sqrt{-j}$ in (7.13) is retained, see remark (5.147)), we can write after some calculations:

$$p(x_2) - p(x_1) = -(R_a + j\omega M_a)u \; ; \; u(x_2) - u(x_1) = -(G_a + j\omega C_a)p, \text{ where}$$
$$R_a = \rho\sqrt{\omega\ell_v c}\int_{x_1}^{x_2} \frac{1}{\pi R^3(x)}dx \; ; \; G_a = \chi_s(\gamma-1)\sqrt{\omega\ell_t c}\int_{x_1}^{x_2} \pi R(x)dx. \qquad (7.17)$$

This applies to pipes we called "wide." The resistance R_a and the conductance G_a are not "pure" in the sense that they vary with frequency, which would not be the case for "narrow" pipes or capillaries.

7.2.5 *Modal Expansion of the Input Impedance*

In Chap. 3, we derived in the frequency domain, the shape of the modal expansion for the driving-point admittance of a general structure. For a tube with varying cross section, we have to use the analogy between tubes and strings given in Table 1.1 in Chap. 1. Then we can use the formulas (3.105) and (3.39) for the driving-point impedance,

$$Z_{ij}(\omega) = j\omega\sum_{n=1}^{N}\frac{\Phi_n(x_i)\Phi_n(x_j)}{m_n(\omega_n^2 + j\omega\omega_n Q_n^{-1} - \omega^2)},$$
$$m_n = \int_0^L \Phi_n^2(x)\chi(x)S(x)dx. \qquad (7.18)$$

We have directly added the damping term, where $Q_n^{-1} = 2\zeta_0$. As we learned in Chap. 5, this formula is valid for certain boundary conditions, and under the condition that the damping is proportional, so that the mode shape is real. For simple boundary conditions, if we ignore damping, and if in addition we consider a cylindrical tube with uniform parameters $\rho(x)$ and $\chi(x)$, we obtain Eq. (4.57).

In the present chapter, we are often interested in the input impedance, denoted $Z(\omega)$, and for that case, Eq. (7.18) becomes

$$Z(\omega)/Z_{c0} = j\omega\sum_{n=1}^{N}\frac{F_n}{\omega_n^2 + j\omega\omega_n Q_n^{-1} - \omega^2}, \text{ with}$$
$$Z_{c0} = \frac{\rho c}{S(0)} \; ; F_n = c\frac{\Phi_n^2(0)S(0)}{\int_0^L \Phi_n^2(x)S(x)dx}. \qquad (7.19)$$

For a cylindrical tube, $F_n = 2c/\ell$ for all modes. However, the visco-thermal losses depend on the radius, therefore in horns the damping is not proportional. Nevertheless we will see for the example of a conical tube that this formula is sufficiently accurate if we use the average value of damping, i.e., the average value of the inverse of the radius.

Now, what happens when the damping is not proportional and/or when the boundary conditions are not of simple kind, in particular when they are dissipative, such as the radiation condition? We saw in Chap. 5 that we can use the residue calculus see Eq. (5.175), and therefore may write the following general formula:

$$Z(s)/Z_{c0} = \sum_n \left[\frac{C_n}{s - s_n} + \frac{C_n^*}{s - s_n^*} \right], \tag{7.20}$$

where $s = j\omega$ and $s_n = j\widetilde{\omega_n} - \alpha_n$. The complex natural frequencies are $\widetilde{\omega_n} + j\alpha_n$. The coefficients C_n are complex, because the modes are complex. In order to compare Eqs. (7.19) and (7.20), we write

$$Z(s)/Z_{c0} = \sum_n \frac{s(C_n + C_n^*) - (C_n s_n^* + C_n^* s_n)}{s^2 + 2\alpha_n s + |s_n|^2} \tag{7.21}$$

The identification yields

$$F_n = 2\Re e(C_n)\ ;\ \frac{\omega_n}{Q_n} = 2\alpha_n\ ;\ \omega_n^2 = \ |s_n|^2 = \widetilde{\omega_n}^2 + \alpha_n^2. \tag{7.22}$$

However, it is observed that the identification can be done only if $\Re e(C_n s_n^*)$ is small enough, or:

$$|s| >> \left| \Re e(C_n s_n^*)/\Re e(C_n) \right| \ . \tag{7.23}$$

We will often use the simple formula (7.19), but it is important not to forget that difficulties can occur at very low frequencies.

7.3 Pipes with Cross Section Discontinuities: First Approximation

7.3.1 Elementary Model: Example of the Eigenfrequencies Equation: the Helmholtz Resonance

Discontinuities in cross section were treated in an approximated way by Bernoulli, who studied chimney organ pipes: these pipes, consisting of two consecutive cylinders, are used to obtain formants in the spectrum, i.e., some strengthened

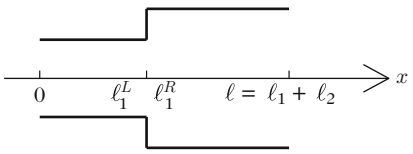

Fig. 7.2 Chimney pipe, consisting of tube 1 (length ℓ_1 and cross section area S_1) and a tube 2 (length ℓ_2 and cross section area S_2). $\sigma = S_2/S_1$. The superscripts $+$ and $-$ refer to the quantities on either side of the discontinuity

frequency ranges. This is a simple interesting case, because it allows an easy understanding of the effect of a deviation from the cylindrical shape. This can also regarded as an example of a coupled system, such as those studied in Chap. 6. An example is the effect of a brass instrument mouthpiece. Moreover this study allows finding a simple formula for the study of a cylindrical flute, the mouthpiece hole being considered as a small pipe.
We will study the eigenfrequencies, then the successive reflections, and finally the modes, for the following boundary conditions: zero pressure at the output, and zero velocity at the input.

- Let us consider a sequence of two pipes with different cross sections (see Fig. 7.2). We will examine this example in detail, but many conclusions will remain valid for other configurations. Bernoulli admitted that at the discontinuity, at any time, one could write the flow conservation, at $x = \ell_1$, $u_1^L = u_1^R$. In Sect. 7.6.3.2 we will show that, because of the mass conservation, this equation is rigorous. Bernoulli also considered that the pressure is continuous, i.e., $p_1^L = p_1^R$: this is an approximation, which we will also discuss. In fact the pressure is not plane near the discontinuity, but this approximation is quite satisfactory for the pressure averaged over the section, especially if one takes a small length correction to the pipe into account, as discussed further in Sect. 7.6.3.3. For the moment, we ignore this correction.

Under these conditions, the acoustic impedance is continuous at the cross section discontinuity: this is the reason why pressure and flow rate are preferred as basic variables, and this choice implies the definition of the acoustic impedance. In order to find the eigenfrequencies of such a pipe, we use the projected impedance (ignoring losses). Let us consider a pipe closed at $x = 0$ and "open" at $x = \ell = \ell_1 + \ell_2$ (the length ℓ includes the radiation length correction). We have, taking carefully the direction in which we project the impedances into account:

$$Z_1^R = j\rho c S_2^{-1} \tan k\ell_2 \; ; \; Z_1^L = j\rho c S_1^{-1} \cot k\ell_1. \tag{7.24}$$

Hence the equation for the eigenfrequencies is given by $Z_1^R = Z_1^L$:

$$\tan k\ell_1 \tan k\ell_2 = \sigma \quad \text{where } \sigma = S_2/S_1. \tag{7.25}$$

Notice that another method, similar but heavier, is to project the impedance from $x = \ell$ to $x = \ell_1$, then to deduce Z_1^R, then project Z_1^R until $x = 0$ where the impedance is infinite. The transcendental equation (7.25) can be solved in several ways, e.g., using a graphical method. Furthermore if the length ℓ_2 is small, and the ratio σ is large, we can write $\cot k\ell_1 \simeq k\ell_2/\sigma \simeq \tan(k\ell_2/\sigma)$, which yields an approximate analytical solution: $k(\ell_1 + \ell_2/\sigma) = (n - 1/2)\pi$. Nevertheless we wrote: "if the length ℓ_2 is small," without giving any reference length. The latter is actually the wavelength $2\pi/k$, corresponding to the frequencies obtained, and we see that the condition implies $\ell_2 \ll \ell_1$, and n should be not too large. Similarly if the two lengths are "small," we get

$$k^2 = \sigma/\ell_1\ell_2. \tag{7.26}$$

The corresponding frequency is nothing else than the resonance frequency of a Helmholtz resonator (see Chap. 1, Sect. 1.5 and Chap 2). The conditions on the lengths imply:

$$\sigma\ell_1/\ell_2 \ll 1 \; ; \sigma\ell_2/\ell_1 \ll 1.$$

This requires that σ is small: thus the resonance frequency is very low, much lower than the frequencies for which the wavelengths are related to the geometric dimensions. A (more or less) sudden cross section discontinuity is therefore necessary to build a Helmholtz resonator, which has the behavior of a *system with lumped elements for its (first) resonance*. If the discontinuity is small, this behavior is not possible at resonance, and the resonance wavelength is of the order of magnitude of the lengths. A more complete (linear) model of a Helmholtz resonator is discussed in Sect. 7.6.3.4.

- A general method to solve Eq. (7.24) is the iterative one (or perturbation method): let us try to determine the length $\Delta\ell$ to be added to the total length ℓ so that the resonances are those of a closed/open tube of length $\ell + \Delta\ell$ with no discontinuity. We must have

$$\tan k\ell_2 = \cot k(\ell_1 + \Delta\ell) \text{ , hence } \cot k(\ell_1 + \Delta\ell) = \sigma \cot k\ell_1.$$

  Using $\tan k\Delta\ell$ as unknown, and denoting $\sigma = 1 - 2\varepsilon$, the following result is derived:

$$\Delta\ell = \frac{1}{k}\arctan\left[\frac{\varepsilon \sin 2k\ell_1}{1 - 2\varepsilon\cos^2 k\ell_1}\right]. \tag{7.27}$$

  For this problem, the two lengths are playing the same role in (7.25), and we might equivalently have written $\cot k\ell_1 = \tan k(\ell_2 + \Delta\ell)$: therefore Formula (7.27) remains valid by just interchanging the two lengths (but without changing σ). So the formula with the shortest length will be preferred, so that the arguments of the trigonometric functions are smaller. This yields a simple

result for the first order in ε (weak discontinuity): $\Delta\ell \simeq (\varepsilon/k)\sin 2k\ell_1 \simeq (\varepsilon/k)\sin 2k\ell_2$. In addition we notice that $\Delta\ell$ depends on frequency, which induces an iterative method of calculation: we first determine k for $\varepsilon = 0$, resulting in $k^{(0)} = (n-1/2)\pi/\ell$. We therefore deduce $\Delta\ell^{(0)}$, then $k^{(1)} = (n-1/2)\pi/(\ell+\Delta\ell^{(0)})$, etc. The method converges even more quickly for smaller values of ε. This method can be used for any type of discontinuity in a pipe, and obviously it is very interesting when there are N small discontinuities. In this case, the total correction length is simply the sum of the corrections due to each one of the discontinuities.

- The fact that $\Delta\ell$ depends on frequency implies that the eigenfrequencies are not harmonically related, which has several consequences on the produced sounds. First, this raises tuning problems during a register change, and then this implies that the playing frequency evolves with the excitation level, which is problematic for the musician, as discussed in Chap. 9. Finally the sound spectrum is strongly affected. For the case of a small perturbation (ε small), where $\ell_1 \ll \ell_2$, we may perform a series expansion of the function $\sin k\ell_1$, in order to know the direction of inharmonicity: $\Delta\ell = 2\varepsilon\ell_1(1-2k^2\ell_1^2/3)$. If $S_2 > S_1$, ε is negative, the lengths corrections also are negative, and the first resonance frequency increases. Moreover the absolute value of $\Delta\ell$ decreases with frequency, so the second resonance increases less than the first one, resulting in negative inharmonicity. On the other hand, if $S_2 < S_1$, ε is positive, the length corrections are positive and the first resonance frequencies become smaller; otherwise, $\Delta\ell$ decreases with frequency, so the second resonance decreases less than the first one, which results in positive inharmonicity.

7.3.2 *Waves: Successive Reflections*

We could generalize all the results in Chap. 4 to a chimney pipe. We simply look at what is new, i.e., the equations at the cross section discontinuity, and treat a simple example, that of the reflection function at the entrance of such a pipe. Instead of writing the equations at the discontinuity in terms of pressure and flow rate, we describe them using the incoming and outgoing waves [see Eqs. (4.1) and (4.7)]. Thus we can write for Pipe 1, at any time, at $x = \ell_1$:

$$p = p^+ + p^- \; ; \quad u = (S_1/\rho c)(p^+ - p^L).$$

When the wave p^+ reaches the discontinuity, it is partly reflected and partly transmitted into Pipe 2 as if it was infinite, before other reflections arrive. So at the time of arrival, we have: $p/u = \rho c/S_2$. This gives the very simple following results, valid until the arrival of other reflected waves:

$$\frac{p^-}{p^+} = \frac{S_1 - S_2}{S_1 + S_2} = R_1 \; , \; \frac{p}{p^+} = 1 + R_1 = \frac{2S_1}{S_1 + S_2} = T_1. \tag{7.28}$$

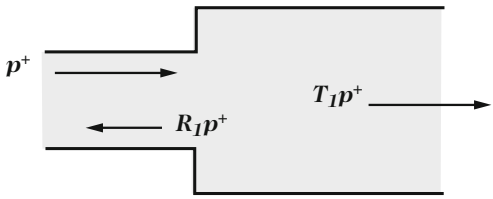

Fig. 7.3 First reflection $p^- = R_1 p^+$ and transmission $p = T_1 p^+$ at the discontinuity for a pressure wave p^+ coming from Pipe 1

R_1 is the reflection coefficient at the discontinuity, and T_1 the transmission coefficient into Pipe 2 (see Fig. 7.3). Of course, we check that if the sections are equal, $R_1 = 0$, $T_1 = 1$. If S_2 is smaller than S_1, the reflection occurs with no sign change, as in the case of a closed pipe (at $x = \ell_1$); however, if S_2 is larger than S_1, reflection occurs with a sign change, as if Pipe 1 was opened on a large space (very small pressure).

When Pipe 2 is finite, we can follow the successive reflections of the reflected and transmitted waves at both ends of the chimney pipe, and obtain expressions generalizing Expression (4.13). Consider the simple example of the reflection function, which is the value of the returning pressure p^- when considering an impulse of pressure p^+ (see Chap. 4). The round trip of the wave transmitted in Pipe 2, with reflections at the open end of Pipe 2, yields an incoming wave arriving at $x = \ell_1$, which is $T_1 r_L(t)$, where $r_L(t) = -\delta(t - 2\ell_2/c)$. This incoming wave is partially reflected back into Pipe 2 at $x = \ell_1$ and is partially transmitted into Pipe 1, with the reflection and transmission coefficients obtained when Pipe 1 is infinite, i.e.,

$$R_2 = \frac{S_2 - S_1}{S_1 + S_2}\,; \quad T_2 = \frac{2S_2}{S_1 + S_2}. \tag{7.29}$$

Finally, for an incident impulse wave p^+, there are the following incoming waves in Pipe 1: R_1, then $T_1 r_L T_2$, then $T_1 r_L R_2 * r_L T_2$, then $T_1 r_L R_2 * r_L R_2 * r_L T_2$, etc. There is no outgoing wave in Pipe 1, since the incoming wave is an impulse, so it is zero for positive t; and the incoming waves in Pipe 1 are the waves having already done some round trips in Pipe 2.

- Let us go now in the Fourier domain. The incident wave P^+ is equal to unity. The Fourier transform of $r_L(t)$ is $R_L(\omega) = -\exp(-2jk\ell_2)$. Hence, paying attention to the terms in chronological order:

$$P^- = R_1 + T_1 R_L T_2 + T_1 R_L R_2 R_L T_2 + T_1 R_L R_2 R_L R_2 R_L T_2 + \cdots,$$

that we can factorize as follows:

$$P^- = R_1 + T_1 R_L (1 + R_2 R_L + (R_2 R_L)^2 + \cdots) T_2 = R_1 + \frac{T_1 R_L T_2}{1 - R_2 R_L}, \tag{7.30}$$

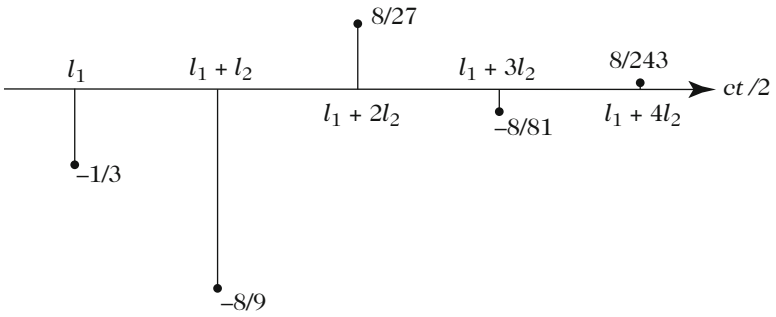

Fig. 7.4 Reflection function (response in incoming wave to an impulsive outgoing pressure wave) for a chimney pipe [Eq. (7.30)]. The calculation is done at the entrance of the pipe 1, for the case $S_2 = 2S_1$ and $R_L = -1$, $\ell_2 = 2\ell_1$. One can easily check the sign of each reflection, knowing that a widening (or radiation) requires a change of sign, while a narrowing does not imply a change in sign

provided that $|R_2 R_L|$ is smaller than unity (the latter expression is what we call a closed-form expression).

We can multiply this kind of calculations to switch from the closed-form to successive reflections, or vice versa. Some concluding remarks:

- What we calculated is the reflection in Pipe 1 at $x = \ell_1$; of course, to get the reflection at the entrance ($x = 0$), we have to multiply the result (7.30) by $\exp(-2jk\ell_1)$; Fig. 7.4 schematically shows the result of the reflection function at the entrance of Pipe 1, for an impulsive excitation, both pipes being lossless.
- The absolute value of quantity $R_2 = (S_2 - S_1)/(S_2 + S_1)$ is always smaller than unity, which ensures the convergence of the series, and validates the closed-form (7.30).
- The amplitude of the reflected waves rapidly decreases with time, since the modulus of each reflection is obtained from the previous one by multiplying it by R_2.
- Furthermore, we could be interested in the input impedance, but this requires reflections at the entrance of the instrument to be taken into account, and thus the formulas quickly become cumbersome: the reflection function is much simpler.
- The successive reflections corresponding to the input impedance would decrease much more slowly. This can be understood as a simple exercise (notice that this observation is obvious in the case of a simple cylindrical pipe, see Chap. 4, because there is only one reflected wave for the reflection function!). This property makes the reflection function very useful for calculating oscillations in a self-sustained oscillations instrument (bowed strings or woodwinds), as shown by Schumacher [76]. However, for certain kinds of pipes, the reflection function can last a very long time, more than the impulse response corresponding to the input impedance [33].

- Measuring successive reflections can allow the inverse problem to be solved [4, 24, 32], i.e., deducing the geometry from the measured impulse response for horns of any kind.[2]

7.3.3 *Modes of a Chimney Pipe: The Case of a Reed Instrument*

7.3.3.1 General Expression

We continue to treat the example of a chimney pipe (Fig. 7.2), an archetype of tube with variable cross section. It is easy to obtain a closed-form formula using transfer matrices, but the modal expansion can also give an expression of the height of impedance peaks (input or transfer impedance). To do this, we seek the Green's function (or transfer impedance) for the case studied above (closed/open pipe), taking into account the dissipation in boundary layers, and using the mode-orthogonality method of the lossless problem.[3]

A pressure mode $\Phi_n(x)$ satisfies: (1) the Helmholtz equation in the two pipes; (2) the two boundary conditions; (3) the condition of continuity at $x = \ell_1$; (4) the flow rate continuity condition, which is written, according to the Euler equation[4]:

$$S_1 \frac{d\Phi_n(x)}{dx}(l_1^L) = S_2 \frac{d\Phi_n(x)}{dx}(l_1^R). \tag{7.31}$$

We choose in Pipe 1: $\Phi_n(x) = \cos k_n x$ (to take into account the infinite impedance at $x = 0$), so the amplitude will be 1 at $x = 0$, at the reed location. The exit condition $x = \ell$ and continuity at $x = \ell_1$ impose

$$\Phi_n(x) = \cos k_n x \quad \text{if } x \leq \ell_1 \tag{7.32}$$

$$\Phi_n(x) = a_n \sin k_n(\ell - x) \text{ , where } a_n = \frac{\cos k_n \ell_1}{\sin k_n \ell_2} \text{ if } x \geq \ell_1. \tag{7.33}$$

[2] An alternative method is the optimization in the frequency domain [13, 39, 40]: it is sought to minimize the error between the impedance of a target shape and an estimate thereof, based on a number of geometrical parameters.

[3] For the sake of simplicity, radiation will be ignored, thus results are limited to not too high frequencies. Dispersion is ignored as well. One difficulty is that the modes of the problem with losses are not quite orthogonal, because damping is varying with the radius. This can be avoided by applying the residue calculus (see Chap. 4, Sect. 4.6.2) to the closed-form expression, which exists, but this leads to heavier calculations.

[4] We will assume that there is no influence coming from boundary layers ($Z_v = j\omega\rho/S(x)$ on both sides), although this is not strictly true.

Using the flow rate continuity (7.31), we again obtain the eigenfrequencies equation (7.25):

$$\tan k_n \ell_1 \tan k_n \ell_2 = S_2/S_1 = \sigma. \tag{7.34}$$

Now consider the Helmholtz equation with source (5.161), assuming $Z_v = j\omega\rho/S$ (as explained in Chap. 5, Sect. 5.6) and:

$$k_c = \frac{\omega}{c}\left[1 - j\alpha_1 \frac{1}{R(x)}\sqrt{\frac{c\ell_v}{\omega}}\right]. \tag{7.35}$$

[see (5.160), (5.144)]. What is new compared to a simple cylindrical pipe is the variation of the wavenumber with the space coordinate. We denote

$$k_c = \frac{\omega}{c} - j\frac{\kappa}{R(x)} \text{ where } \kappa = \alpha_1\sqrt{\frac{\omega\ell_v}{c}}. \tag{7.36}$$

The injection of $P(x) = \sum_n A_n \Phi_n(x)$ in Eq. (5.161) gives at the first order of losses:

$$\sum_n A_n \left[k_n^2 - \frac{\omega^2}{c^2} + 2j\frac{\omega}{c}\frac{\kappa}{R(x)}\right]\Phi_n(x) = j\omega\rho\frac{1}{S(x)}U_s\delta(x - x_s).$$

In order to use orthogonality, we need to calculate two quantities:

$$\Lambda_{nm} = \int_0^\ell S(x)\Phi_n(x)\Phi_m(x)dx \text{ and } \Lambda'_{nm} = \pi\int_0^\ell R(x)\Phi_n(x)\Phi_m(x)dx. \tag{7.37}$$

Λ_{nm} is zero for $n \neq m$ [see Eq. (7.10)], but this is different for Λ'_{nm} (here the notation $'$ does not represent the derivative), which corresponds to the term $\kappa/R(x)$. This is due to the non-proportional damping (see Chap. 5, Sect. 5.2.1.2): in the computation of inter-modal scalar products, the term $R(x)$ prevents the mode separation. But as shown in Chap. 5, Sect. 5.2.1.1, for discrete systems, the equations can be decoupled at the first order of damping, and we can ignore the cross terms. Thus, we obtain

$$P = j\omega\rho c^2 U_s \sum_{n>0}\frac{1}{\Lambda_n}\frac{\Phi_n(x)\Phi_n(x_s)}{\omega_n^2 + j\omega\omega_n\frac{1}{Q_n} - \omega^2} \tag{7.38}$$

$$\text{where } \frac{1}{Q_n} = 2\kappa\frac{\Lambda'_n}{\Lambda_n}\frac{c}{\omega_n}, \tag{7.39}$$

where $\Lambda_n = \Lambda_{nn}$, and similarly for Λ'_n. For each mode, the transfer impedance is the product of a factor, $\Phi_n(x)\Phi_n(x_s)/\Lambda_n$, related to geometry, i.e., related to wave reflections, and a factor, related to dissipation, which is the response of a single-degree-of-freedom oscillator. For the input impedance $\Phi_n(x)\Phi_n(x_s) = 1$: we find

a formula similar to that for a cylindrical pipe, but the quantities Λ_n and Λ'_n vary with the eigenfrequency number n. We will show below that the ratio Λ'_n/Λ_n varies much more slowly than Λ_n. It can be concluded that the peak height of the input impedance[5] is approximately the product:

- of factor Q_n/ω_n, which decreases as the square root of n, because of the coefficient $\kappa(\omega_n)$, and depends little on the geometric shape;
- and the factor Λ_n^{-1}, which heavily depends on the geometrical shape, because of the reflections at cross section changes: it is constant only for a cylinder, and does not depend on dissipation.[6] In other words, the height of the input impedance peaks is approximately that of a cylinder modulated by a purely geometric factor, Λ_n^{-1}. This result would be exact if damping was independent of the radius;
- in order to calculate the factor Λ_n, taking into account the conditions at both ends, we use the equivalent of Eq. (3.33), which means nothing else than the equipartition of energy:

$$\omega_n^2 \mathscr{P}_M(n,n) = \mathscr{P}_T(n,n)$$

$$\text{where } \mathscr{P}_M(n,n) = \chi_s \Lambda_n \text{ and } \mathscr{P}_T(n,n) = \frac{1}{\rho}\int_0^\ell S(x)\left[\frac{d}{dx}\Phi_n(x)\right]^2 dx,$$

$$\text{thus } 2\Lambda_n = \int_0^\ell S(x)\left[\Phi_n^2(x) + k_n^{-2}\Phi_n'^2(x)\right] dx. \tag{7.40}$$

This equation, in which we use the notation $'$ for the derivation with respect to x, is valid when the boundary conditions are of Neumann or Dirichlet type (zero or infinite impedance). Apart from a factor, the integral represents the total energy. Because in both pipes the function $\Phi_n(x)$ is a sine function, the function to integrate is a constant in each cylinder. (This is due to the fact that the total energy density of a plane wave, either traveling or standing, is constant in space.) Using (7.25), it is found:

$$2\Lambda_n = S_1\ell_1 + S_2 a_n^2 \ell_2 \tag{7.41}$$

$$\text{where } a_n^2 = \cos^2 k_n\ell_1 / \sin^2 k_n\ell_2 = \cos^2 k_n\ell_1 + \sigma^{-2}\sin^2 k_n\ell_1. \tag{7.42}$$

Depending on the application to be studied, we can use the eigenfrequency equation (7.25) in order to remove one of the terms $\tan k_n\ell_1$ or $\cot k_n\ell_2$. Here we have eliminated $\cot k_n\ell_2$. Indeed, we consider a long pipe of length ℓ_2, perturbed by a small pipe of length ℓ_1; the quantity $\tan k_n\ell_2$ varies much faster than the

[5] Remember that strictly speaking, as the peaks are finite, all modes have to be taken into account at a given resonance frequency. However, we will consider that dissipation is low enough in order to consider in the infinite series only the mode whose eigenfrequency is the considered resonance frequency.

[6] More accurately, only Λ_n occurs far from the resonances, and Λ'_n occurs near the resonances.

quantity $\tan k_n \ell_1$ in the frequency interval considered. Eliminating the rapidly varying quantities therefore gives access to an envelope of the input impedance curve, with rich information. Thus, if $V = S_1\ell_1 + S_2\ell_2$ is the total volume:

$$2\Lambda_n = V + \ell_2 S_2 \sin^2 k_n \ell_1 \left[\sigma^{-2} - 1\right]. \tag{7.43}$$

Therefore, if $\sigma = S_2/S_1 < 1$, Λ_n varies between minima equal to $V/2$, as for a cylinder, and maxima given by

$$\frac{\min \Lambda_n}{\max \Lambda_n} = \left[1 + \frac{\ell_2}{\ell_1}\sigma\right] : \left[1 + \frac{\ell_2}{\ell_1}\frac{1}{\sigma}\right]. \tag{7.44}$$

The interpretation of the frequencies corresponding to the extrema is simple: for the case where σ tends to 0, the input impedance (without dissipation) is proportional to $\cot k\ell_1$. The maxima of the input impedance are obtained for $\sin k\ell_1 = 0$ (eigenfrequencies of Pipe 1 closed at its two ends), and the minima occur for $\sin k\ell_1 = \pm 1$ (Pipe 1 open at the entrance, closed at $x = \ell_1$). The maxima and minima are achieved at the same frequencies as those of Λ_n^{-1}, but their values differ from these of Λ_n^{-1}.[7] However, it is remarkable that in Eq. (7.43) the frequencies of Pipe 1 only appear, whatever the ratio of the cross sections: this can be regarded as a kind of "decoupling" of the two pipes, although it is obviously false for the eigenfrequencies of the whole system.

- Studying variations of Λ_n', if $S_2 < S_1$, bounds can be found, starting from:

$$\Lambda_n = \pi \int_0^\ell R^2(x)\Phi_n^2(x)dx > \pi R_2 \int_0^\ell R(x)\Phi_n^2(x)dx = R_2\Lambda_n'.$$

Using this, and doing a similar calculation with R_1, it is obtained

$$\frac{1}{R_1} < \frac{\Lambda_n'}{\Lambda_n} < \frac{1}{R_2}. \tag{7.45}$$

Variations of Λ_n'/Λ_n are much smaller than those of Λ_n, especially if one pipe is much longer than the other one, which justifies the result (7.39). Figure 7.5 shows the input impedance of a chimney pipe, compared to the same pipe without discontinuity at the entrance ($S_2 = S_1$), as well as the same curve multiplied by the factor $1/\Lambda_n$ calculated above.

[7] The extrema of these two curves are different, as those of the input impedance of Cylinder 1 depend on dissipation, while the modulation factor Λ_n is "reactive," independent of dissipation. The result cannot be the product of the input impedances of two cylinders: we can never have the product of two damping factors. The simple sentence "the first cylinder impedance modulates that of the second" is therefore improper.

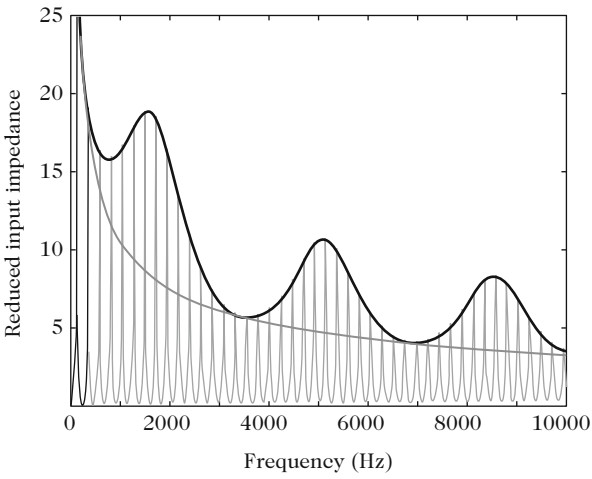

Fig. 7.5 Input impedance (divided by of $\rho c/S_1$) of a chimney pipe and its envelope. Dimensions are $\ell_1 = 5\,\text{cm}$; $r_1 = 6\,\text{mm}$; $\ell_2 = 70\,\text{cm}$; $r_2 = 7.5\,\text{mm}$, Pipe 2 ends in a zero impedance. The maximum of the envelope corresponds to $\sin^2 k\ell_1 = 1$. We superimposed the curve of a cylinder of the same length and its envelope, which is simply decreasing

7.3.3.2 Discussion on the Effects of a Discontinuity in Cross Section

In Sect. 7.3.1 we examined the effects of inharmonicity. What about the changes in peak height of the input impedance? We will see in Part III that playing a note whose fundamental corresponds to a given peak is easier when the peak is higher. Moreover what is primarily relevant is the height of the peak, not its quality factor.

It may also be interesting to consider the spectrum of the radiated sound, whose pressure is roughly proportional to the time derivative of the output flow rate. We therefore calculate the ratio between output flow rate and input pressure. In the studied case, it is for the mode n:

$$\frac{U(\ell)}{P(0)} = -\frac{S_2}{\rho c}\frac{1}{\Phi_n(0)}\frac{1}{jk_n}\frac{d}{dx}\Phi_n(\ell) = -j\frac{S_2}{\rho c}a_n. \tag{7.46}$$

where a_n is given by (7.42). The transfer function has a maximum value for frequencies for which the input impedance of Pipe 1 has a minimum value, and has a minimum value for the opposite case. The existence of formants in the sound around these frequencies could be deduced, but it is not so simple, because a part of the spectrum of the inlet pressure itself depends on the input impedance, and thus on the same coefficient a_n. Moreover inharmonicity plays an important role, and radiation depends on frequency in a complicated way. The question is in general very intricate, since harmonics of the fundamental frequency can be very far from a resonance frequency. Nevertheless this study reveals that the geometry influences the notes which can be played (both their frequency and ease of playing). These ideas will be developed in the third section (see also a study on chimney organ pipes in [50]). The present study may apply to the role of a clarinet mouthpiece or

of the saxophone, which correspond respectively to a cross section expansion and narrowing (but the shape of the saxophone is conical).[8] We discuss later a similar case for a trumpet mouthpiece.

7.3.4 Brass Instrument Mouthpiece

7.3.4.1 General Approach: Effect of Pipe with Variable Section Located at the Entrance of a Cylinder

An example of generalization of the chimney pipe is a brass instrument with a mouthpiece (see Fig. 7.6). Pipe 1 (Fig. 7.2) is replaced by a resonator consisting of a cavity with a large enough volume, on which the lips come to rest, and a backbore. The backbore is a rather narrow pipe which fits into the instrument, which is at first cylindrical for a trumpet or trombone. As the backbore does not have the same section as that of the instrument pipe, a decoupling effect can be found as described above. A resonance of the mouthpiece, whose backbore would be open into an infinite space, produces a modulation of the pipe input impedance. One can hear this frequency when hitting with a flat hand on the cup: the resulting sound is "pop," hence the name given to this frequency by Benade, the *popping frequency*. We will now study how the mouthpiece acts on the resonance frequencies, and on the input impedance curve, making easier emission of certain notes. We use the same method as for the chimney pipe. For the sake of simplicity, we still do not take dissipation by radiation into account and, as well, we do not take the existence of the bell into account, which will be discussed later.

- Consider first the general problem of a Pipe 1 of length ℓ_1 and variable cross section area $S(x)$: we return to the problem described in Sect. 7.3.3. There is a cross section discontinuity at $x = \ell_1$, which is S^L on the left and $S^R = S_2$ on the right. We assume for the moment that the mode shapes $\Phi_n(x)$ are known, for $0 \leq x \leq \ell_1$, and that they satisfy $\Phi_n'(x) = 0$ at the opening, i.e., zero flow, because we are looking again for the input impedance maxima of the whole instrument. For the Pipe number 2, between ℓ_1 and $\ell = \ell_1 + \ell_2$, we have

$$\Phi_n(x) = a_n \sin k_n(\ell - x) \text{ for } \ell_1 \leq x \leq \ell. \tag{7.47}$$

  The conditions at the discontinuity give

$$\Phi_n(\ell_1) = a_n \sin k_n \ell_2 \; ; \; S^L \Phi_n'(\ell_1) = -a_n S_2 k_n \cos k_n \ell_2. \tag{7.48}$$

[8] An interest of the above-discussed problem is that it can be treated as a limiting case of the mass-type or compliance-type termination, while maintaining simple boundary conditions (zero or infinite impedance). The idea has already been touched on when considering the radiation impedance of a pipe as a length correction (see Chap. 4). This can be advantageous for the sake of simple calculations.

The eigenwavenumbers are solutions of:

$$j\frac{\rho c}{S_2}\tan k_n\ell_2 = -\frac{\rho c}{S^L}jk_n\frac{\Phi_n(\ell_1)}{\Phi_n'(\ell_1)}. \tag{7.49}$$

The right-hand side of the equation is the input impedance at $x = \ell_1$ of the pipe with variable cross section, seen from Pipe 2. At lower frequencies, because the condition at input is a zero flow condition, the impedance is that of a volume with lumped elements, $-\rho c^2/(j\omega V_1)$, where V_1 is the total volume of Pipe 1. We search for the eigenfrequencies using a length correction for Pipe 2, writing the second member of (7.49) as [72]:

$$j\frac{\rho c}{S_2}\cot k_n\Delta\ell = -\frac{\rho c}{S^L}jk_n\frac{\Phi_n(\ell_1)}{\Phi_n'(\ell_1)}. \tag{7.50}$$

This is not the definition adopted for chimney pipes, because here the correction is the length to be added to the length of Pipe 2, and not to the total length. At low frequencies, we have $\Delta\ell = V_1/S_2$, which is the length of a section of Pipe 2 of volume V_1. For the eigenfrequency f_r of the "closed/open" Pipe 1, with zero impedance at $x = \ell_1$, we have $\Delta\ell = \pi/2k_r = c/4f_r$.

Considering the modes, they are orthogonal since the flow vanishes at $x = 0$, and:

$$2\Lambda_n = \int_0^{\ell_1} S(x)\left[\Phi_n^2(x) + k_n^{-2}\Phi_n'^2(x)\right]dx + S_2a_n^2\ell_2 \tag{7.51}$$

[see Eq. (7.40)]. Using Eq. (7.48), the rapidly varying functions can be eliminated (since we suppose $\ell_2 \gg \ell_1$, they are functions of $k_n\ell_2$), and we obtain

$$a_n^2 = \Phi_n^2(\ell_1) + \left(\frac{S^L}{S_2}\right)^2\frac{1}{k_n^2}\Phi_n'^2(\ell_1). \tag{7.52}$$

Equation (7.38) remains valid, and for the same reasons as above, we assume that $\Lambda_n' = \Lambda_n/R_2$ [see Eqs. (7.37) and (7.45)]. The input impedance envelope curve is approximately given by the ratio $E_n = \Phi_n^2(0)/\Lambda_n$, multiplied by the damping function, Q_n/ω_n, decreasing as $\sqrt{\omega}$. At lower frequencies, the pressure field must be constant throughout the pipe, so we simply have

$$2\Lambda_n = V_1 + V_2,$$

which is the total volume of the instrument. The frequency variation of the quantity given in Eq. (7.51) is difficult to analyze in general, but if the ratio S^L/S_2 is small, we can simplify Expression (7.52), ignoring the second term. On the other hand, when Pipe 2 is narrower, we could ignore the first term. If S^L/S_2 is small, the

"amplification" effect is maximized when, roughly, $\Phi_n^2(\ell_1)$ is minimized, i.e., for frequencies corresponding to the eigenfrequencies of Pipe 1, closed at the entrance $x = 0$ and open at the end $x = \ell_1$. This "amplification" of the input impedance (the quotations marks are essential here, because of course the mouthpiece does not create energy, but simply strongly reflects energy at its resonance) facilitates the playing of the notes near the mouthpiece resonance. If the volume increases, the peak is shifted to lower frequencies and low notes are enhanced.[9]

7.3.4.2 Case of a Mouthpiece Similar to a Helmholtz Resonator

The previous study holds for an arbitrarily shaped Pipe 1. We suppose now (see Fig. 7.6) that Pipe number 1 is a Helmholtz resonator, the dimensions of which being small compared to the wavelength, with a uniform pressure in the cup[10] ($0 \leq x \leq \ell_0$), of volume V_0, and a constant flow rate in the backbore ($\ell_0 \leq x \leq \ell_1$). So, the backbore length is equal to $\ell_1 - \ell_0$. We will discuss below the validity of this model for a trumpet mouthpiece. We must calculate the function $\Phi_n(x)$ in the mouthpiece, by integrating Eq. (7.1) in their version without source and with lumped elements (7.15). For the cup, we obtain

$$\Phi_n(x) = 1 \text{ for } 0 \leq x \leq \ell_0 \text{ and } U_n(x) = -jk_n c\chi_s \int_0^x S(x)dx, \tag{7.53}$$

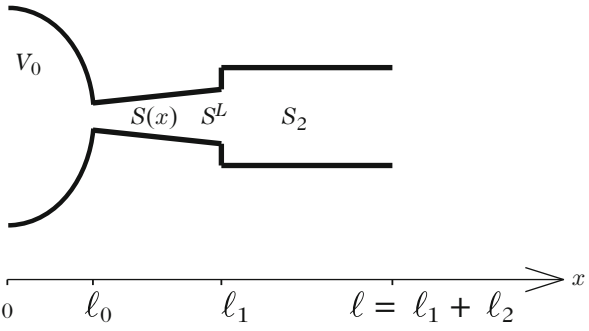

Fig. 7.6 Scheme of a brass instrument mouthpiece and notations. The mouthpiece is Pipe 1, with variable cross section, and with total length ℓ_1

[9] We can presume that enhancing the impedance peaks also enhances the harmonics of lower notes whose frequency is close to the mouthpiece resonance: this is a delicate issue, because resonance inharmonicity explains why the frequencies of the harmonics rarely coincide with those of the peaks, and consequently why their impedance can be small (with a large imaginary part compared to the real part).

[10] Notice that if the cup is cylindrical, Eq. (7.32) yields a pressure uniform within the cup if $k_n\ell_1 << 1$. Moreover notice that we choose to consider here the pressure as dimensionless; therefore the flow rate has the dimension of an admittance.

where $U_n(x)$ is the flow rate, and then $U_n(\ell_0) = -jk_nV_0/\rho c$. For the backbore we obtain

$$\Phi_n(x) - 1 = -jk_n\rho c U_n(\ell_0) \int_{\ell_0}^{x} S^{-1}(x)dx \,, \text{ for } \ell_0 \leq x \leq \ell_1, \text{ or} \tag{7.54}$$

$$\Phi_n(x) = 1 - k_n^2 V_0 M_1(x) \text{ where } M_1(x) = \int_{\ell_0}^{x} S^{-1}(x)dx. \tag{7.55}$$

The quantity $\rho M_1(x)$ is the acoustic mass[11] located between ℓ_0 and x. So in the backbore, if we denote $M_1 = M_1(\ell_1)$:

$$\Phi_n'(x) = -k_n^2 V_0/S(x) \text{ and } \Phi_n(\ell_1) = 1 - k_n^2 V_0 M_1 \,. \tag{7.56}$$

For $k_n^2 = k_r^2 = 1/V_0M_1$, there is a resonance of the mouthpiece. We first consider the length correction, given by (7.50):

$$\cot k_n \Delta\ell = S_2 \left[(k_n V_0)^{-1} - k_n M_1\right]. \tag{7.57}$$

We have already given the low frequency value, V_1/S_2: here we get V_0/S_2, which is consistent, provided that the backbore volume is small compared to that of the cup, and that the flow rate is constant in the backbore. When the frequency increases, $\Delta\ell$ also increases, which produces *negative* inharmonicity: the resonance value was given above ($c/4f_{res}$). Beyond this frequency, we can write

$$k_n \Delta\ell = \frac{\pi}{2} + \arctan S_2 \left[k_n M_1 - (k_n V_0)^{-1}\right], \tag{7.58}$$

and show, using a Taylor expansion around the resonance, that the length correction continues to grow to a maximum, before decaying. We do not detail this aspect here, when the lumped elements model loses its validity; we will see later how this correction can compensate for that due to the bell shape.

- In order to calculate the impedance maxima, we calculate the envelope $E_n = 1/\Lambda_n$ for the input impedance, according to (7.51). We obtain, if $\rho M_2 = \rho\ell_2/S_2$ is the acoustic mass of Pipe number 2:

$$2\Lambda_n = V_0 + k_n^2 V_0^2 (M_1 + M_2) + V_2 (1 - k_n^2 V_0 M_1)^2. \tag{7.59}$$

  At low frequencies this quantity is $V_0 + V_2$, the total volume of the instrument, because the volume of the backbore has been ignored. The minimum of this function is obtained for a frequency very close to the resonance frequency, because the volume V_2 of Pipe number 2 is very large:

[11] Remember that the dimension of an acoustic mass is kg m^{-4}.

$$k_{\max}^2 = k_r^2 \left[1 - \frac{1}{2}\frac{V_0}{V_2}\left(1 + \frac{M_2}{M_1}\right)\right] \simeq k_r^2$$

$$\text{with} \quad 2\Lambda_n \simeq V_0 + V_0\left(1 + \frac{M_2}{M_1}\right). \tag{7.60}$$

It turns out that the ratio M_2/M_1 is in practice around 3 for a trumpet. The "amplification" factor is therefore about $V/4V_0$, i.e., the total volume V of the instrument divided by four times that of the cup.[12] Of course, this conclusion is mainly qualitative. It is also not certain that the maximum of the envelope is reached, because for that there must be a resonant frequency of Pipe 2 coinciding with the resonance of the mouthpiece, which depends on the length ℓ_2, see Eq. (7.49).

- It turns out that the above model is very approximate: it neglects the potential energy in the backbore with respect to that of the cup. And this is exaggerated, because *in practice the backbore has a volume larger than that of the cup*. We therefore do not really have a Helmholtz resonator. An easy correction can be made: at low frequencies, this consists in retaining the total volume of the mouthpiece for the calculation of both the length correction and the peaks envelope curve. It can be shown [54] that a satisfactory approximation of the peak curve is obtained simply by adjusting the volume in the first term of (7.59), after the determination of M_1 from the knowledge of the resonance frequency of the mouthpiece and the volume of the cup:

$$2\Lambda_n = V + k_n^2 V_0^2 (M_1 + M_2) + V_2 (1 - k_n^2 V_0 M_1)^2. \tag{7.61}$$

The minimum of this quantity is: $2\Lambda_n \simeq V + V_0\,[1 + M_2/M_1]$, which reduces the amplification factor found above. Figure 7.7 shows the corresponding envelope curve, the mode expansion obtained with the same approximation, and the numerical calculation of the impedance curve of the instrument (as explained below in Sect. 7.5.2), for a trumpet without bell. The figure shows that the approximations are quite satisfactory. At higher frequencies, the envelope is steadily decreasing, but formula (7.61) becomes less and less acceptable, which shows the limits of the model.

To conclude, we refer the reader to detailed discussions found in [8, 52]. Recall that the instrument studied here consists of a cylindrical Pipe (2) open at $x = \ell$, which is obviously far from a real brass instrument, since the bell has an important role. However, it is easily verified that the results remain valid for

[12] If Pipe 2 had a large section, the ratio M_2/M_1 could be neglected with respect to unity, and this would lead to $V/2V_0$. In this ratio, the value of the numerator comes from the fact that at zero frequency, there is only potential energy in the entire instrument, since the flow is zero at the input, and therefore everywhere! Otherwise the value of the denominator arises from the fact that at the mouthpiece resonance, we have equipartition of energy (hence the factor 2) in the mouthpiece, and very low energy in the main part of the instrument.

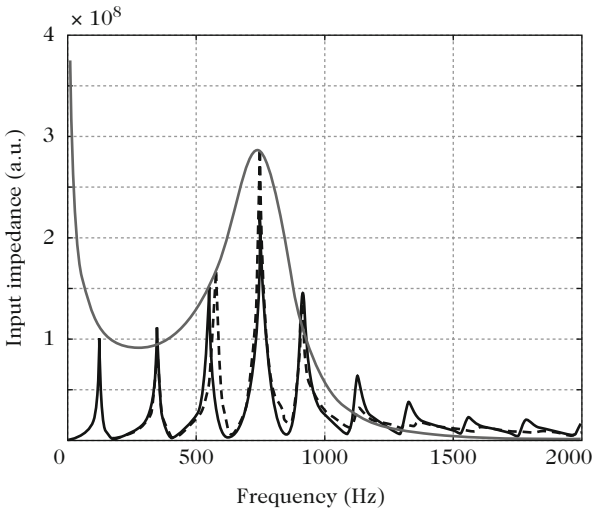

Fig. 7.7 Input impedance of a cylinder with a brass mouthpiece: the *dashed curve* is the approximate mode expansion; both the envelope and the numerical curve are in *solid lines* (according to [54])

a closed cylindrical Pipe (only the equation of resonances (7.49) is changed), and we show that, concerning the resonance frequencies, the role of the bell, except at lower frequencies, is close to that of a closed cylinder. The numerical results show that the shape of the envelope is preserved.

7.3.5 Cylindrical Instrument with Flute Mouthpiece

For reed instruments, we considered a flow rate source, U_s, at the entrance of the instrument.[13] For instruments with a flute mouthpiece, we consider the dual of the previous problem: on both sides of the edge, the flow rate produces a pressure difference, ΔP, which in the linear view can be seen as a source (see Chap. 10). The important point is to actually know the flow responses to this source. As in the previous sections, we study the eigenfrequencies, then the modes.

We limit ourselves to the case of open flutes, leaving aside the closed flutes (stopped pipes, Pan flutes, slide flutes, ...). Concerning open flutes, at least two radiating openings exist: the hole of the mouthpiece and the passive end of the pipe.

[13]Considering this source as the one that produces the sound is adopting a linear point of view, which is wrong. Actually, it is not the player who sets this source because we are dealing with a closed loop system, which will require knowledge of another equation. The important thing for reed instrument is to know the ratio P/U_s, in particular at the entrance.

The knowledge of the modes enables us to find the amplitude ratio between these two openings, a key element regarding directionality, which will be studied in the fourth part.

7.3.5.1 The Model: Closed-Form of the Response

We restrict ourselves to the basic shape, the cylindrical one. We consider the mouthpiece as a lumped element system, with a uniform flow rate, denoted $U(0)$. The change in cross section between the mouthpiece hole, of area S_m, and the pipe, of area S, is an important parameter. The mouthpiece hole is parallel to the axis of the pipe: this represents a bend effect, the effect of which will be studied in Sect. 7.6.3.2: We will show that it is the effect of an added mass, equivalent to a cross section discontinuity. Therefore for the sake of simplicity we can represent the mouthpiece by a small tube in the axis of the main pipe (see Fig. 7.8), i.e., by a kind of chimney pipe [82].

We are searching for the response in flow rate to an excitation force, i.e., a source of pressure difference, denoted by $\Delta P = P_s^+ - P_s^-$, placed at the location of the edge, in $x = 0$ (ignoring the thickness of the edge, i.e., the length of mouthpiece hole). At low frequencies, the radiation impedance of the mouthpiece hole can be written as [see Eq. (5.131)]:

$$Z_m = \frac{\rho c}{S_m}\left[j\frac{\omega}{c}\Delta\ell_m + \frac{1}{4}(\omega R_m/c)^2\right], \tag{7.62}$$

where R_m is the equivalent radius (the hole has often a roughly rectangular shape). For the sake of simplicity we assume that $\Delta\ell_m = 0.7R_m$. The real part of Z_m is in fact independent of the size (and shape) of the hole: this will be discussed in

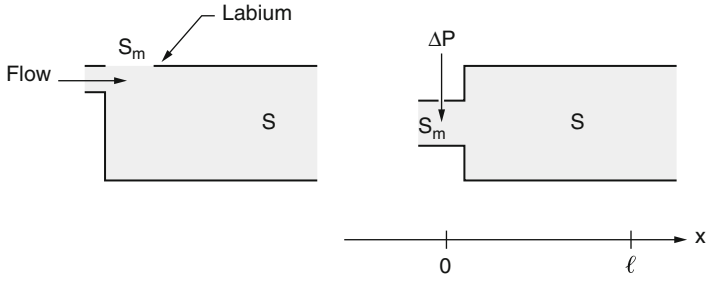

Fig. 7.8 Diagram of an instrument with a flute mouthpiece and equivalent representation. The opening of the mouthpiece is represented by a small pipe of cross section area S_m. Although this pipe has a very small length, its presence causes significant length corrections due to radiation and cross section discontinuity. The flow arrives almost facing the edge, and produces a source of pressure difference, ΔP

the fourth part. If we consider the "incoming" flow rate in the pipe,[14] we write: $P_s^- = -Z_m U(0)$. On the other side, the small pipe opens into a pipe of cross section S and length ℓ: if Z_p is the input impedance of this pipe,[15] we can write $P_s^+ = Z_p U(0)$. The response we seek is the flow rate response $U(x)$ at point x of the main pipe to the excitation ΔP. At the input $x = 0$, the response is the following admittance:

$$U(0)/\Delta P = (Z_p + Z_m)^{-1}. \tag{7.63}$$

In the main pipe, we must solve the dual equation of (5.161), the source being included in the boundary condition (7.63):

$$\left[\frac{\partial^2}{\partial x^2} + k_c^2\right] U = 0. \tag{7.64}$$

The ratio $U(x)/U(0)$, as well as the input impedance Z_p, only depends on the main pipe and its radiation impedance, denoted $Z_\ell = Z_c j \tan \eta_\ell$, where $Z_c = \rho c/S$:

$$\frac{U(x)}{U(0)} = \frac{\cos\left[k_c(\ell - x) + \eta_\ell\right]}{\cos\left[k_c \ell + \eta_\ell\right]} \; ; Z_p = Z(0) = Z_c j \tan\left[k_c \ell + \eta_\ell\right] \; . \tag{7.65}$$

These relationships are obtained, e.g., by using the transfer matrix of the pipe. Knowing the ratio $U(0)/\Delta P$, the sought response is found in closed-form, if $Z_m = Z_c j \tan \eta_0$:

$$\frac{U(x)}{\Delta P} = -jY_c \frac{\cos\left[k_c(\ell - x) + \eta_\ell\right] \cos \eta_0}{\sin\left[k_c \ell + \eta_\ell + \eta_0\right]} \; . \tag{7.66}$$

7.3.5.2 Resonance Frequencies

The resonance frequencies are sought by ignoring dissipation (k_c, η_0, and η_ℓ are real), and also, for the sake of simplicity, dispersion: then $k_c = k = \omega/c$. At resonances the denominator of (7.66) vanishes, implying the relationship:

$$n\pi = k\ell + \eta_0 + \eta_\ell \simeq k\ell + \arctan \eta_0 + \arctan \eta_\ell = k\left[\ell + \Delta\ell + \frac{S}{S_m}\ell_m\right], \tag{7.67}$$

[14] Of course the flow oscillates and thus goes in and out of the pipe, but we define it as the volume flow rate through the pipe surface, the vector $d\overrightarrow{S}$ being here oriented to the right.

[15] The discontinuity between the mouthpiece hole and the pipe requires adding a series impedance of acoustic-mass type, denoted by $Z_d = j\omega\rho\Delta\ell_{dm}/S_m$ at the input impedance of the pipe Z_e. This will be explained in Sect. 7.6.3.2. The order of magnitude of the length $\Delta\ell_{dm}$ is similar to that of $\Delta\ell_m$. Since in the mouthpiece hole there is flow rate continuity (the fluid being considered to be incompressible), we can simply add this acoustic mass to the radiation acoustic mass, and replace in the radiation impedance Z_m the length $\Delta\ell_m$ by the equivalent total length of the mouthpiece hole, ℓ_m, whose order of magnitude is 1.5 times the radius R_m.

where $\Delta\ell$ is the radiation length correction for $x = \ell$, and ℓ_m the total equivalent height of the mouthpiece hole. Therefore at low frequencies:

$$f_n \simeq nc/2L\,, \text{ where } L = \ell + \Delta\ell + \ell_m S/S_m. \tag{7.68}$$

As a matter of fact, overblowing in an open flute gives an octave (the first two resonances are distant by an octave): the frequencies of the main regimes correspond to the frequency $c/2L$ and its harmonics. The length correction due to the mouthpiece hole, $\ell_m S/S_m$, is larger than that of the end ℓ because the mouthpiece hole has a smaller area than the pipe. Approximation (7.68), however, is not valid at high frequencies and the frequencies of higher regimes are shifted upwards. To verify this, Eq. (7.67) can be solved using the length correction method: we assume that $k\Delta\ell \ll 1$, and write (7.67) in the form $\tan k(\ell + \Delta\ell) = -\tan(k\ell_{\text{eff}})$, where ℓ_{eff} is unknown. The latter is

$$\ell_{\text{eff}} = \frac{1}{k}\arctan\left[\frac{S}{S_m}k\ell_m\right] = \ell_m\frac{S}{S_m}\left[1 - \frac{1}{3}\left(\frac{S}{S_m}k\ell_m\right)^2\right]. \tag{7.69}$$

The second expression, obtained from a Taylor expansion to the third order, shows that the length correction decreases with frequency, and hence the resonance frequencies are higher than those given by (7.68), the discrepancy increasing with n. A simple interpretation is the following: if the surface of the mouthpiece hole gradually decreases and tends to 0, the frequencies tend to those of a closed–open pipe, in a succession $1, 3, 5\ldots$ instead of $1, 2, 3\ldots$: so the interval between two successive frequencies increases.

7.3.5.3 Modal Expansion

We use the method used for the reeds (see Chap. 5, Sect. 5.6.3). We write again (7.66), with obvious notations ($h_i = j\eta_i$, where $i = 0$ or ℓ):

$$\frac{U(x)}{\Delta P} = Y_c\frac{\cosh\left[\Gamma(\ell - x) + h_0 + h_\ell\right]\cosh h_0}{\sinh\left[\Gamma\ell + h_0 + h_\ell\right]}.$$

The poles and the modal expansion can be written as:

$$(\Gamma\ell + h_0 + h_\ell)(s_n) = j\gamma_n, \text{ where } \gamma_n = n\pi\ ; \tag{7.70}$$

$$\frac{U(x)}{\Delta P} = Y_c\sum_n \frac{\cosh\left[\Gamma(s_n)x + h_0(s_n)\right]\cosh h_0(s_n)}{(s - s_n)\left[\Gamma'\ell + h_0' + h_\ell'\right](s_n)}\,. \tag{7.71}$$

In contrast to what happens for reed instruments, the zero-frequency pole exists here, $s_0 = 0$, which is a constant mode: $\Gamma(s_0) = 0$. Indeed, for this mode, it is obvious to show that the differential equation is satisfied, as well as the boundary

conditions, which are close to Neumann conditions for the flow rate (see Eq. (4.57) for the dual case, this of pressure in a closed–closed pipe). The constant mode needs to be taken into account.

It has no physical meaning because the model used is certainly not valid at zero frequency, but it is essential to ensure the series convergence to the right result for nonzero frequencies. Nevertheless it is certain that there is a zero-frequency flow rate (as in reed instruments!), but it has been ignored in the wave equation (7.64). We have already encountered a similar issue in Chap. 6, to treat the coupling between a string and a resonant cavity (for this case we had chosen a mode $\Phi = ax/L$ to reflect the fact that one end of the string might move).

We do not comment further on the result (7.71): it could be possible to simplify it as was done in Chap. 5 for reed instruments, with very similar calculations.

7.3.5.4 Relationship Between the Two Radiating Apertures of a Flute

Assuming that near the eigenfrequencies a single mode contributes to the response, we derive from Eqs. (7.70) and (7.71) the (complex) ratio of the two radiating aperture flow rates. Assuming that these openings have small dimensions compared to the wavelength, the ratio is simply[16] $-U(\ell)/U(0)$. We therefore find:

$$-\frac{U(\ell)}{U(0)} = -\frac{\cosh\left[\Gamma(s_n)\ell + h_0(s_n)\right]}{\cosh h_0(s_n)} = (-1)^{n+1}\frac{\cosh h_\ell(s_n)}{\cosh h_0(s_n)}\,. \tag{7.72}$$

The last expression is obtained using (7.70). If we had the same terminal impedances, so $h_0 = h_\ell$, the ratio would be ± 1, because the field would be perfectly symmetrical or anti-symmetric. This result could be considered in detail: we only note that for the first modes, the functions $h_0(s_n)$ and $h_\ell(s_n)$ are small, and the amplitude ratio is very close to unity.[17] Regarding the phase difference between the two openings, the following result is obtained: for mode $n = 1$, the two openings are in phase, while for $n = 2$, they are opposite in phase. $n = 1$ corresponds to the first playing frequency, and $n = 2$ to the second playing frequency, or to a frequency near the second harmonic of the first playing frequency. The consequences of these phase differences on the directivity are important: we will analyze them in the fourth part.

[16] Why the $-$ sign? In order to find the phase difference of the radiated pressures, we must consider the flow rate "outgoing" from the instruments (see fourth Part).

[17] Actually it can be shown that the ratio increases with frequency, because, if $jk_n = s_n/c$:

$$-\frac{U(\ell)}{U(0)} \simeq \frac{1 + k_n^2\ell_m^2(S/S_m)^2}{1 + k_n^2\Delta\ell^2}\,.$$

We have seen that the mouthpiece-hole length correction is significantly larger than that of the end ℓ.

7.4 Conical Instruments

Conical instruments play a major role in music, and, for the case of reed instruments, conical instruments have taken the biggest rise before cylindrical instruments. The reason is that overblowing gives octaves, instead of twelfths for clarinets. Therefore fewer holes and keys are required: the first register contains 12 semitones only (i.e., one octave) instead of 18 (i.e., one twelfth). This issue is discussed at the end of this chapter, in Sect. 7.7.5.5. The conical shape, although basic, gives rise to a number of complicated behaviors compared to that of the cylindrical shape.

7.4.1 Equations and Solutions for a Lossless Conical Resonator

Let us consider a truncated cone, for example, a saxophone without toneholes. At low frequencies, only planar waves can propagate in a cylindrical pipe with perfectly reflecting walls (see below Sect. 7.6.2). Similarly only spherically symmetrical waves can propagate in a cone. The spatial coordinate is denoted r, and is counted from the apex (see Fig. 7.9). The waves are solutions of the 3D wave equation (1.111); the operators are written in spherical coordinates and if spherical symmetry is assumed, the particle velocity has only a radial component, v_r, denoted v for the sake of simplicity. In order to later introduce dissipation by simply making the density and compressibility complex, we start from the two Eqs. (1.109) and (1.110):

$$\frac{1}{r^2}\frac{\partial(r^2 v)}{\partial r} + \chi_s \frac{\partial p}{\partial t} = q_V(r,t) \tag{7.73}$$

$$\frac{\partial p}{\partial r} + \rho \frac{\partial v}{\partial t} = \rho F_r \,. \tag{7.74}$$

The spherical wave equation is deduced

$$\frac{\partial^2 p}{\partial r^2} + \frac{2}{r}\frac{\partial p}{\partial r} - \frac{1}{c^2}\frac{\partial^2 p}{\partial t^2} = \rho\left[\frac{1}{r^2}\frac{\partial(r^2 F_r)}{\partial r} - \frac{\partial q_V}{\partial t}\right] . \tag{7.75}$$

Using the variable pR, which was already used for (7.8), or better here the variable pr, since the radius R is proportional to the distance r, the equation becomes

$$\frac{\partial^2 (pr)}{\partial r^2} - \frac{1}{c^2}\frac{\partial^2 (pr)}{\partial t^2} = \rho r\left[\frac{1}{r^2}\frac{\partial(r^2 F_r)}{\partial r} - \frac{\partial q_V}{\partial t}\right].$$

The equation for pr with no source is simply the planar wave equation, the solution being written as:

$$p = \frac{f^+(t - r/c) + f^-(t + x/c)}{r} \tag{7.76}$$

The factor $1/r$ is the geometrical divergence factor, ensuring that the average power of a wave through a surface defined by constant r is independent of r. Apart from this factor, the propagation is similar to that of a planar wave. But the reflection of pressure waves is modified, because the acoustic velocity does not verify this simple equation. It is solution of the Euler equation:

$$\rho\frac{\partial v}{\partial t} = -\frac{\partial p}{\partial r} = \frac{1}{rc}[f^{+\prime}(t - r/c) - f^{-\prime}(t + x/c)] + \frac{p}{r} \tag{7.77}$$

where $f'(x)$ is the derivative of $f(x)$. The first term is similar to that of a planar wave, but the second is new, and we see that an impulsive pressure wave gives rise to an acoustic velocity that is spread over time. In the Fourier domain, we have

$$P = \frac{a^+ e^{-jkr} + a^- e^{jkr}}{r}\ ; \tag{7.78}$$

$$V\rho c = -\frac{1}{jk}\frac{\partial P}{\partial r} = \frac{a^+ e^{-jkr} - a^- e^{jkr}}{r} + \frac{P}{jkr}. \tag{7.79}$$

Specific admittances of outgoing and incoming waves therefore are (we define in the propagation direction $Y_c^+ = V/P$, and $Y_c^- = -V/P$):

$$Y_c^{\pm} = \frac{1}{\rho c}\left[1 \pm \frac{1}{jkr}\right] \tag{7.80}$$

(for the acoustic admittance, we multiply by $S(r)$). The two admittances vary with r, and moreover they are different, which is characteristic of asymmetric transmission lines (it is obvious that in a truncated cone, unlike in a cylinder, the input and output cannot play the same role!). A key point is the appearance of the parameter kr, i.e., the ratio of distance to the apex to wavelength. If it is large, spherical waves are similar to planar waves: a sphere with large radius is locally similar to a plane, and if the wavelength is small, the wave does not "see" the curvature.
In Expression (7.79), the term p/jkr is large near the apex at low frequencies, and thus velocity and pressure are almost in quadrature, regardless of boundary conditions. There is no average power: we can say that the energy is stationary and, in addition, it is primarily kinetic since the velocity/pressure ratio is quite large. This phenomenon is characteristic of flow rate sources of dimensions small compared to the wavelength, when they radiate into a large space (here the truncated cone).

Finally, if we change the variable V and the admittance Y in

$$\tilde{V} = V - \frac{P}{jkr\rho c}\ ;\ \tilde{Y} = Y - \frac{S(r)}{jkr\rho c}, \tag{7.81}$$

all calculations valid for planar waves (transfer matrices, projected impedances, etc.) can be extended to the pair P and $\tilde{V}$ (one can call the velocity $\tilde{V}$ the "symmetric"

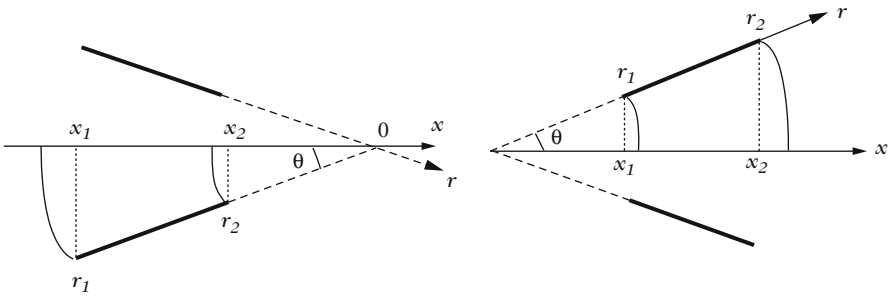

Fig. 7.9 Geometry of diverging and converging truncated cones. We carefully notice the choice used to define directions. We denote: $\ell = r_2 - r_1$; $\tan\theta = R_1/x_1 = R_2/x_2 \simeq (R_2 - R_1)/\ell$; $\sin\theta = R_1/r_1 = R_2/r_2 = (R_2 - R_1)/\ell$

velocity, and the admittance $\tilde{Y}$ the "symmetric" admittance). Thus, if r_1 is the input coordinate of the truncated cone, and $r_2 = r_1 + \ell$ that of the end [see, (4.28)], the following result is obtained:

$$\begin{pmatrix} Pr \\ \tilde{V}r\rho c \end{pmatrix}_1 = \begin{pmatrix} \cos k\ell & j\sin k\ell \\ j\sin k\ell & \cos k\ell \end{pmatrix} \begin{pmatrix} Pr \\ \tilde{V}r\rho c \end{pmatrix}_2 . \tag{7.82}$$

7.4.2 *Validity of the Horn Equation for a Truncated Cone*

It is interesting to compare Eqs. (7.75) and (7.6). On one hand $q_V = q/S$ (because q_V is the flow rate per unit volume) and, on the other hand, $S(x) = \pi R(x)^2$ is proportional to x^2. Both equations are identical, but the space coordinate is not the same. For (7.6), it is the distance r from the apex of the cone to the portion of the sphere that limits it, while x is the projection of r on the cone axis, with $x = r\cos\theta$, where θ is the apex half-angle (see Fig. 7.9).

The horn equation is derived by matching planar waves, thus the spherical wavefront is assimilated to a plane wavefront. Intuitively this is valid if the distance between these two surfaces is small compared to the wavelength. More specifically, for a traveling (pressure) wave, the amplitude ratio between the output and input of the truncated cone is independent of the choice made: $r_1/r_2 = x_1/x_2 = R_1/R_2$. However, there is a phase difference, i.e., if θ is small: $k(r_2 - r_1) - k(x_2 - x_1) = k\ell\theta^2/2 = k(R_2 - R_1)^2/2\ell$ (in this expression, $\ell = r_2 - r_1 \simeq x_2 - x_1$). For conical instruments, we can show that this quantity is actually small for audible range frequencies. Therefore, what follows is valid for r as well as for x. We choose, for the sake of simplicity, the coordinate x, so the planar wave approximation. Unlike a cylindrical tube, the origin of the x-axis is fixed here (at the apex of the cone). Moreover, *for a convergent cone, it is convenient to choose the direction to the apex,* so that if the input and output keep the same subscripts, there is always the relation $\ell = r_2 - r_1$, with ℓ positive: we therefore have negative r_2, r_1, x_2, x_1 (see Fig. 7.9).

7.4.3 Transfer Matrix of a Truncated Cone

We want to derive from (7.82) the pressure/flow transfer matrix by replacing the lengths r by lengths x. After some tedious calculations, we get, between the two abscissae of index 1 and 2:

$$\begin{pmatrix} P_1 \\ U_1 \end{pmatrix} = \begin{pmatrix} A & B \\ C & D \end{pmatrix} \begin{pmatrix} P_2 \\ U_2 \end{pmatrix} \quad \text{where}$$

$$A = \frac{R_2}{R_1}\cos k\ell - \frac{\sin k\ell}{kx_1}\ ; B = j\frac{\rho c}{\pi R_1 R_2}\sin k\ell\ \ ; D = \frac{R_1}{R_2}\cos k\ell + \frac{\sin k\ell}{kx_2}\ ;$$

$$C = \frac{\pi R_1 R_2}{\rho c}\left[j\sin k\ell\left[1 + \frac{1}{k^2 x_1 x_2}\right] + \frac{\cos k\ell}{jk}\left(\frac{1}{x_1} - \frac{1}{x_2}\right)\right]. \tag{7.83}$$

We easily check the result for a cylinder ($R_1 = R_2$; x_1 and x_2 infinite). It can be shown that the determinant of this transfer matrix is always equal to 1, which corresponds to the reciprocity property. This property is equivalent to the symmetry of the Green's function (the equivalence is standard, and we will not prove it here). This kind of calculation can also be done using equivalent electrical circuits [9].[18]

7.4.4 Eigenfrequencies: Elementary Approximations

- As a first application of the obtained solutions, we look for eigenfrequencies. Consider an "open–open" pipe, with a zero-impedance condition at both ends, which is the extreme simplification of a flute. The symmetric admittance $\tilde{Y}$ is infinite, so there is no effect of the taper: to a first approximation, a convergent or divergent conical flute has the same eigenfrequencies as cylindrical flute of the same length.

  Let us more precisely consider a pipe terminated in the radiation impedance, assuming that the taper does not affect the previously used value (5.131). For the calculation of the eigenfrequencies, we can simply take the imaginary part of the impedance into account, and write $Z_R = \rho c S_2^{-1} jk\Delta\ell$, where S_2 is the output section, and $\Delta\ell = 0.6R_2$, R_2 being the output radius. For the symmetric acoustic admittance we get

$$\widetilde{Y_R} = \frac{S_2}{\rho c}\left[\frac{1}{jk\Delta\ell} - \frac{1}{jkx_2}\right]. \tag{7.84}$$

[18] If the frequency tends to 0 in (7.83), we find, (after some calculations): $A = D = 1$, $B = j\omega L_a$, $C = j\omega C_a$, where L_a and C_a are the mass and the acoustic compliance found in (7.16), respectively. We find that the cross section of the cylinder equivalent to a truncated cone of length ℓ is: for the acoustic mass $S = \pi R_1 R_2$; and for the acoustic compliance: $S = \pi(R_1^2 + R_1 R_2 + R_2^2)/3$. This type of result is useful, e.g., for sizing a conical tonehole, by calculating the equivalent cylindrical hole.

We derive the effective correction to the radiation length that can be used in (7.82): $\Delta\ell_{\text{eff}}^{-1} = \Delta\ell^{-1} - x_2^{-1}$. The effect of the taper is negligible if $x_2 \gg \Delta\ell$, which is a condition often satisfied for a diverging truncated cone; the length correction is therefore the same as for a cylindrical pipe. For a truncated converging cone, however, the radiation length correction may be substantially modified by the taper.

- Let us now consider a (diverging) conical reed instrument, such as an oboe, a bassoon, or a saxophone. The frequencies played by the instrument are close to the eigenfrequencies of a "closed–open" (conical) pipe. The input admittance is zero, therefore the admittance after symmetrization is $\widetilde{Y}_e = -S(x_1)/jkx_1\rho c$, where x_1 is the input radius. By projecting the symmetric admittance from the output to the input, we obtain, as for a cylinder,

$$\widetilde{Y}_e = -\frac{S_1}{\rho c} j \cot k\ell \tag{7.85}$$

where the length ℓ includes the radiation length correction. We can therefore infer the eigenfrequency equation:

$$\tan k\ell = -kx_1. \tag{7.86}$$

This type of equation is familiar in musical acoustics and was encountered for certain cases of vibrating strings. If the distance from the apex of the cone to the entrance of the truncated cone, x_1, is small compared to the wavelength, we can write

$$kx_1 \simeq \tan kx_1 \quad \text{therefore} \tag{7.87}$$

$$f = nc/2(\ell + x_1). \tag{7.88}$$

Thus the eigenfrequencies of conical reed instruments are thus nearly harmonically related, and are multiple of the fundamental frequency corresponding to a wavelength equal to twice the length of the instrument, extended up to its apex. At low frequencies, the cone can be seen as a cylinder of length $\ell + x_1$ with two zero-impedance conditions at the ends. A soprano saxophone with a length comparable to that of a clarinet cannot produce notes that are so low. Notice that Eq. (7.86) remains valid for a cylinder (x_1 infinite!); however, this it not the case for Formula (7.88).

Actually, the approximation (7.87) is equivalent to the approximation of the conical instrument by a "cylindrical saxophone," which would be a cylinder of length $\ell + x_1$, with the mouthpiece located at a distance x_1 from the input (see Fig. 7.10). This gives a number of qualitative ideas, that we will use and discuss (in Sect. 9.4.8, Chap. 9), in analogy with a bowed string [65], when excited at a given location. The ratio $x_1/(\ell + x_1)$ is often written β.

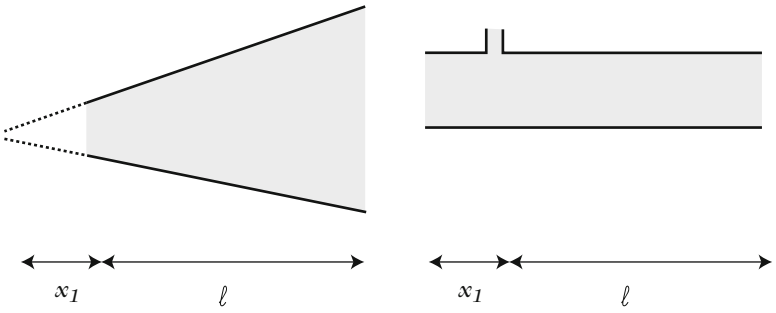

Fig. 7.10 Cylindrical saxophone equivalent, at low frequencies, to a conical saxophone: the mouthpiece is placed on the side of a cylindrical pipe. The eigenfrequencies of the two pipes are the same

Conical reed instruments therefore present overblowing conditions which differ from those of a clarinet (they play octaves and not twelves). Actually, the validity of the approximation decreases when the frequency number increases: as is gets larger, the frequency spacing approaches a series $1, 3, 5, ..(2n+1)\ldots$ [as for a cylinder, see Eq. (4.50)]. So the second frequency is higher than two times the first, and the shift from the series $1, 2, 3 \ldots n \ldots$ increases with the frequency number. And of course the more x_1 increases, the more the shift increases, until we find the behavior of the cylinder.

- To be more accurate, we can use a method similar to that which led to Formula (7.27), and slightly complicate the problem to take into account the existence of a mouthpiece, of volume V, whose dimensions are small compared to the wavelength. Since at the origin the input admittance is zero, the admittance at the output of the mouthpiece is: $Y = -j\omega V/\rho c^2$ [see Eq. (1.154)]. So, we have at x_1, $\tilde{Y} = -j\omega V/\rho c^2 - S_1/jkx_1\rho c$, that must match the value (7.85), hence:

$$\cot k\ell = \frac{kV}{S_1} - \frac{1}{kx_1}. \tag{7.89}$$

If we write that the second member is $-\cot k\Delta\ell$, we deduce that at the third order in kx_1:

$$\Delta\ell = \frac{1}{k}\arctan\left[\frac{kx_1}{1-k^2x_1V/S_1}\right] \simeq x_1\left[1+k^2x_1^2\left(\frac{V}{x_1S_1}-\frac{1}{3}\right)\right]. \tag{7.90}$$

If the mouthpiece volume is zero or small, we conclude that the length correction due to the finite length of x_1 decreases with frequency, so that high frequencies are indeed too high compared to the series $1, 2, 3 \ldots n \ldots$ To improve the harmonicity of the eigenfrequencies, we see that it is desirable to have a mouthpiece volume equal to $x_1S_1/3$, which is the volume of the missing part of the truncated cone. Indeed, the surface S_1 is πR_e^2 and the volume of a cone $\pi R_e^3/3$; in spherical coordinates, we would have $2\pi r^2(1-\cos\theta)$ and $2\pi r^3(1-\cos\theta)/3$, respectively.

This mouthpiece volume is what is approximately found for the saxophones, but the real volume may be smaller due to the effects of the reed (see Chap. 9). For an oboe, it was shown that the makers had also introduced a change in taper in the upper part of the instrument. This further improves harmonicity of eigenfrequencies and offsets the effect of the 5th order in kx_1 [12, 22].

- Which parameters characterize a conical instrument? The input and output radii, and the length. However, as the actual length depends on the note, and on the effective output radius, a better choice is the apex angle 2θ and the input radius R_1. The distance from the apex, x_1, can be employed to evaluate the inharmonicity (this distance is close to R_1/θ). There are dimension data in [60], for several woodwinds. It may be noticed that, for an oboe, the angle 2θ is about 0.026 radians (1.5°), much less than for a soprano saxophone, of comparable range, for which it is about 0.07 (4°). For a bassoon, a much lower pitched instrument, the angle 2θ is 0.014 (0.8°); for a tenor saxophone, 0.054 (3°). The apex angles of the instruments of the same family are larger for a high-pitched instrument than for a low-pitched instrument. It is also noticeable that in the modern saxophone family, the angle is wider than that of the family created by Sax. The choice of dimensions is even more complicated than for a cylindrical instrument family, and remains to be elucidated (Fig. 7.11).

7.4.5 *Equations with "Averaged" Losses, Transfer Matrices*

A rigorous treatment including boundary layers would take us far. Solving equations with boundary layers in spherical coordinates is possible [19], but because the apex angle is low, we accept the validity of Eq. (7.12), which is based on the planar waves matching. This equation has no analytical solution. Before showing that an approximate calculation method is the calculation of the modes, we first investigate an even more approximate solution: we calculate the transfer matrix of a conical tube in which losses are calculated for an "average" radius, denoted r_m, assuming that the quantities r_v and r_t involved in (7.13) are independent of x, and calculated for this radius r_m.

Equations (7.83) remain valid if ρ is replaced by ρ_v, given by (7.13) and, as well, χ_s by χ_t. This gives a new value of the sound speed and therefore of the wavenumber [see, (5.144)]:

$$k = \frac{\omega}{c}\left[1 + \alpha_1 \frac{\sqrt{-2j}}{r_v}\right]. \tag{7.91}$$

We can further simplify the result by assuming that, as well as for cylinders, the characteristic (specific) impedance ρc, given by (5.146) is not affected by losses. When there are no losses, the coefficients of the transfer matrix have the following properties: A and D are real, and B and C are purely imaginary. This is due to the

Fig. 7.11 Soprano, tenor, and baritone saxophones. Notice that the apex angle is higher for high-pitched instruments than for low-pitched instruments

fact that the incoming power must be equal to the outgoing power whatever the end conditions. When there are losses the 4 coefficients are complex, but the determinant remains equal to unity.

The use of the transfer matrix (7.83) with constant losses is discussed for the numerical calculation of horns, in Sect. 7.5.2.

7.4.6 Modal Expansion for a Conical Reed Instrument

After the determination of the eigenfrequencies, we seek the modal decomposition as for the other geometries, in order to know the impedance peaks. Because losses vary with the radius, a closed-form solution of (7.12) is not available. Perturbation methods have been employed [44, 60]. Before showing that the modal decomposition is also a method to solve this problem, we study the cylindrical saxophone, which provides interesting qualitative information.

7.4.6.1 Modes for a Cylindrical Saxophone

We have solved a similar problem in Chap. 5, with the simplified formula (5.183). This time the source is not located at the entrance, but at $x = x_1$, and both ends are open: the calculation is exactly the same, but there is a zero-impedance boundary condition at $x = 0$. This gives for the impedance at $x = x_1$, excited at the same point:

$$P = \frac{2}{L} j\omega \frac{\rho c^2}{S} U_s \sum_{n>0} \sin^2 k_n x_1 \frac{j\omega + \frac{1}{2}\omega_{n0} Q_n^{-1}}{\omega_{n0}^2 + j\omega\omega_{n0}\frac{1}{Q_n} - \omega^2} \,. \tag{7.92}$$

The eigenfrequencies ω_{n0} have already been studied, while the modal factor is proportional to: $\sin^2 k_n x_1$. Using the approximation (7.87), this quantity can be written as:

$$\frac{\tan^2 k_n x_1}{1 + \tan^2 k_n x_1} = \frac{1}{1 + 1/(k_n x_1)^2}. \tag{7.93}$$

Consequently, at low frequencies, the input impedance is much lower than for a cylinder excited at the entrance. Therefore the lowest notes of the saxophone are difficult to play, especially since the second peak is higher than the first one, which causes a tendency to overblow. Actually, there is competition between the evolution of this factor and the damping factor, proportional to Q_n/ω_n, which decreases as $\sqrt{\omega}$. For notes corresponding to a shorter length, the first peak becomes larger than the second one (we will analyze the sound production in Chap. 9). How to choose the length of x_1 when designing a conical reed instrument? At first, by maintaining the same pipe (with same length, apex angle, and output radius), it is possible to extend the length of the truncated cone without changing the total length $\ell + x_1$, thus without changing the playing frequency. This means reducing the length x_1, and thus reducing the input impedance at low frequencies, which will certainly not benefit the emission of low notes. Conversely, reducing the length of the truncated cone may seem like a good solution, but this implies an enlargement of the mouthpiece, and thus an increase of inharmonicity. There is probably a good compromise, which to our knowledge remains to be investigated more deeply. The parameter $k_n x_1 = \pi x_1/(\ell + x_1)$ for the fundamental frequency of the lowest note is probably an important parameter for making the instrument: for a bassoon, it is approximately 0.3; for a bass saxophone, of comparable range, it is about the double of this value. Consequently low notes are more easily played on an oboe or bassoon than on high taper instruments such as saxophones.

7.4.6.2 Equation to be Solved

Now we seek the input impedance without using the approximation of the cylindrical saxophone. We use the same method as the one used for chimney pipes, ignoring the dispersion and the radiated power (for the sake of simplicity), but we will see how to add them at the end. The equation for the pressure response to a source of flow rate yields [compare with (5.161)]:

$$\frac{\partial^2 P}{\partial x^2} + \left[\frac{2}{x} - \frac{\rho_v'}{\rho_v}\right]\frac{\partial P}{\partial x} + k_c^2 P = -\frac{j\omega\rho}{S} U_s \delta(x - x_s) \tag{7.94}$$

where

$$k_c^2 = k_s^2\left[1 - j\alpha_1 \frac{\kappa}{x}\right] \text{ where } k_s^2 = \frac{\omega^2}{c^2} \; ; \rho_v = \rho\left[1 - j\frac{1}{\sqrt{2}}\frac{\kappa}{x}\right]. \tag{7.95}$$

κ is a length proportional to the thickness of the boundary layer:

$$\kappa = \frac{2}{\tan\theta}\sqrt{\frac{c\ell_v}{\omega}}. \tag{7.96}$$

7.4.6.3 Modes and Modal Expansion

The modes $\Phi_n(x)$ are solutions of the equation without losses, and are therefore of the form: $(\sin k_n x + B\cos k_n x)/x$. For a complete cone, the condition at the apex would be to have a field of finite pressure, or $B = 0$ (see on this subject [6]). For a truncated cone (with reed!), we write: $\partial\Phi_n(x)/\partial x = 0$ at $x = x_1$ (see Fig. 7.9). The other boundary condition is: $\Phi_n(x) = 0$ at $x = x_2$. We therefore have:

$$\Phi_n(x) = \frac{\sin k_n(x_2 - x)}{x}. \tag{7.97}$$

The input condition gives Eq. (7.86) for the eigenwavenumbers k_n. We now search for the solution of (7.94) written as: $P(x) = \sum_n A_n \Phi_n(x)$. This gives

$$\sum_n A_n(k_s^2 - k_n^2)\Phi_n(x) - j\frac{\kappa\alpha_1}{x}k_s^2\sum_n A_n\Phi_n(x) - j\frac{\kappa}{\sqrt{2}x^2}\sum_n A_n\frac{d\Phi_n(x)}{dx} = -\frac{j\omega\rho}{S}U_s\delta(x - x_s). \tag{7.98}$$

To use the mode orthogonality, we start from (7.10), up to the factor $\pi\tan^2\theta$. Since $S(x) = \pi R^2 = \pi x^2\tan^2\theta$, we multiply both members of (7.98) by $x^2\Phi_m(x)$, and integrate over the length. With orthogonality, the first term on the left involves

$$\Lambda_n = \int_{x_1}^{x_2} x^2 \Phi_n^2(x) dx = \int_{x_1}^{x_2} \sin^2 k_n(x_2 - x) dx = \frac{1}{2}\left[\ell + \frac{x_1}{1 + k^2 x_1^2}\right]. \tag{7.99}$$

This result is achieved by eliminating the trigonometric functions, using the eigenfrequency equation (7.86). But for other terms, proportional to x^{-1} and x^{-2}, there is no orthogonality, because, as for the chimney pipe, damping depends on the radius. It is not proportional (see Chap. 5, Sect. 5.2.1.2). We shall use again the approximation consisting of forgetting the inter-modal coupling terms. We obtain two other integrals:

$$\Lambda_n' = \int_{x_1}^{x_2} x \Phi_n^2(x) dx = \int_{x_1}^{x_2} \frac{\sin^2 k_n(x_2 - x)}{x} dx \tag{7.100}$$

$$= \frac{1}{2}\int_{x_1}^{x_2} \frac{1 - \cos 2k_n(x_2 - x)}{x} dx = \frac{1}{2}\ln\frac{x_2}{x_1} + \frac{1}{2} I_n \tag{7.101}$$

where I_n is an integral involving the functions *cosine integral* and *sine integral* [1]. The last integral to calculate reads

$$\Lambda_n'' = \int_{x_1}^{x_2} \Phi_n(x) \frac{\partial \Phi_n(x)}{\partial x} dx = \frac{1}{2}\left[\Phi_n^2(x_2) - \Phi_n^2(x_1)\right] = -\frac{1}{2}\frac{k_n^2}{1 + k_n^2 x_1^2}. \tag{7.102}$$

The expression is not simple, but if the expression of k_n is taken into account, it is found that the sum of terms corresponding to I_n and Λ_n'' can be ignored (for a detailed analysis, see [44]). We extract from this the A_n coefficient, and obtain the following expression:

$$\frac{P(x)}{U_s} = \frac{j\omega\rho}{\pi R(x) R(x_s)} \sum_n \frac{\sin k_n(x_2 - x) \sin k_n(x_2 - x_s)}{\Lambda_n\left[(k_n^2 - k_s^2) + j k_s k_n / Q_n\right]}$$

$$\text{where } \frac{1}{Q_n} = \frac{1}{k_n \Lambda_n}\left[k_n \frac{\kappa}{2}\alpha_1 \ln\frac{x_2}{x_1} + \frac{1}{4}(k_n r_2)^2\right]. \tag{7.103}$$

In the expression of the quality factor, we write $k_s = k_n$, since the corresponding term occurs only near the resonance frequencies; and radiation has been taken into account, without proof [44]. For the input impedance, we derive the expression:

$$Z_1 = \frac{j\omega\rho}{\pi R_1^2} \sum_n \frac{k_n^2 x_1^2}{\ell(1 + k_n^2 x_1^2) + x_1} \frac{1}{k_n^2 - k^2 + j k k_n / Q_n}. \tag{7.104}$$

Unlike the cases discussed above for a chimney pipe with pipe of length ℓ_2 much longer than pipe of length ℓ_1, we cannot separate the reactive and dissipative effects, because the quality factor Q_n depends on the geometry. Indeed it has a complicated form, involving the norm Λ_n. In other words, the factor $k_n^2 / \left[\ell(1 + k_n^2 x_1^2) + x_1\right]$ represents well enough the effect of the geometry away from resonances, but near

the resonances the envelope curve of the impedance peaks is related to another factor. For the peaks ($k_s = k_n$), we obtain after some calculations:

$$Z_{1\mathrm{Max}} = \frac{\rho c}{\pi R_1^2} \frac{k_n^2 x_1^2}{1 + k_n^2 x_1^2} : \left[\alpha_1 \frac{x_1}{R_1} \sqrt{k_n \ell_v} \ln \frac{x_2}{x_1} + \frac{1}{4} (k_n r_2)^2 \right]. \tag{7.105}$$

The term of visco-thermal losses is equal to that of a cylinder of equal length and equivalent radius of R_{eq} satisfying

$$\frac{\ell}{R_{eq}} = \frac{x_1}{R_1} \ln \left(1 + \frac{\ell}{x_1} \right). \tag{7.106}$$

At the limit of a cylinder (x_1 tends to infinity), we find the result obtained for a cylinder [see Eq. (5.183) in Chap. 5]. We can deduce important results from this analysis:

- the factor $F_n = k_n^2 x_1^2 / (1 + k_n^2 x_1^2)$ is what most distinguishes a truncated cone and a cylinder. An approximation was found in the approximate model of the cylindrical saxophone [see Eq. (7.93)]. At low frequencies, it significantly reduces the peak height, because of reactive effects (i.e., because of the wave reflection due to changes in cross section). For a trumpet mouthpiece, we had an "amplification," here we observe a reduction. It could be shown that the presence of the mouthpiece does not essentially change this result. The factor F_n^{-1} is simply the squared modulus of the characteristic (specific) impedance (7.80) at the entrance of the truncated cone, divided by ρc: the kinetic energy at the entrance of the truncated cone is so large compared to the potential energy that the impedance can never be very large.
- As the radius is much larger than that of a cylinder, the radiated power is much greater in a conical instrument than in a cylindrical instrument, and since the power dissipated in the boundary layers is of the same order of magnitude, the radiation of a cone is very efficient at high frequencies. This could be shown directly from a power analysis. The term of visco-thermal losses is simply what we would have obtained using a constant damping, calculated for *average losses*, i.e., the average of the inverse of the radius.
- The same analysis was done for the impedance minima [44]. It was shown that the dissipative term is complicated, but the factor F_n is does not depend on frequency. This explains why the tapered flutes have a behavior similar to that of cylindrical flutes, as opposed to reed instruments (we already saw that a first approximation is that the flute eigenfrequencies are not influenced by the taper).

About mode expansion, we already know that truncating the series and keeping only one mode in the modal series, for frequencies close to its natural frequency, makes sense only for frequencies which are very close to it. As soon as the frequency is closer to impedance valleys, all other modes are involved. This is even more true for a truncated cone with a reed, as we see in Fig. 7.12: the first peak is very asymmetrical, the frequency of the first valley being very close to that of the first

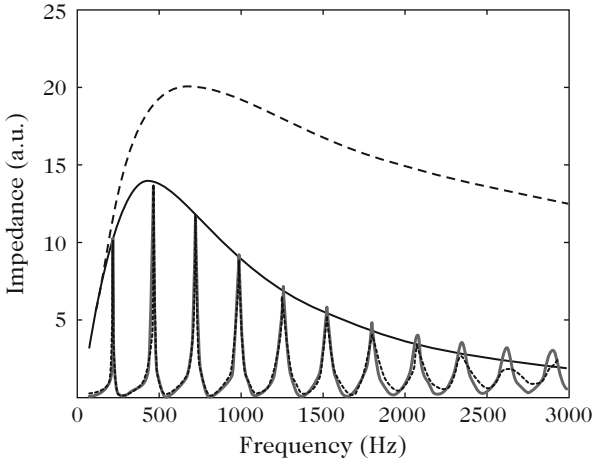

Fig. 7.12 Input impedance modulus of a truncated cone similar to a soprano saxophone ($r_1 = 4.6\,\text{mm}$; $r_2 = 24.7\,\text{mm}$; $\ell = 61\,\text{cm}$). The *solid line curve* is calculated using transfer matrices, taking dissipation in the wavenumber k [Eq. (7.83)] into account. The *dashed curve* is the modal calculation truncated at 11 modes. The envelope is calculated by (7.105), and the *dashed envelope* by the same formula without radiation

peak. The valley frequency is $c/2\ell$, while the peak frequency is $c/2(\ell + x_1)$. The ratio between the two is often close to 1.1, instead of 2 for a cylinder! Such an asymmetry shows the importance of higher modes near the valleys. It can be shown that adding only the second peak would be largely insufficient.

Figure 7.12 shows these results for a truncated cone of the size of a soprano saxophone. The calculation of wavenumbers k_n has been done taking radiation into account, by solving Eq. (7.86), with a length including the correction $0.61r_2$. Then dispersion has been taken into account using Eq. (5.169) for the average radius. The envelope curves with and without radiation show the importance of radiation above the second peak (we remind that in principle the values of k_n are not needed to calculate the envelope curve).

7.4.7 Changes in Conicity

We have treated discontinuities of cross section areas. What happens when there is a discontinuity in the derivative of the section, for example, between two truncated cones of different tapers—a case that is usually found?

If we choose the exact solution in spherical waves for each cone, there is a junction volume (see Fig. 7.13) between two spherical surfaces. In order to built a model, we can take the flow rate conservation between the two surfaces into account. A question remains: how can the pressure on those two surfaces be matched?

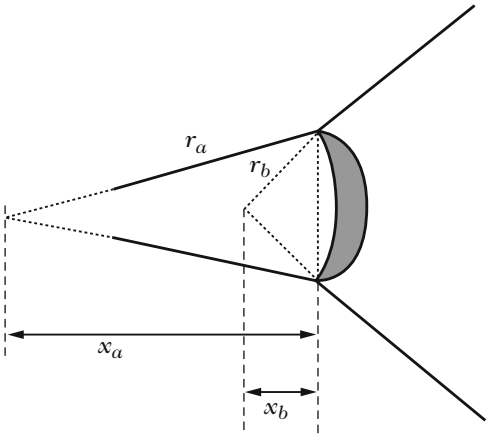

Fig. 7.13 Matching of two truncated cones (case of an increasing flare). Between the two spheres of radii r_a and r_b the junction zone, in *gray*, has a nonzero volume, and the spherical wave description is insufficient. In order to avoid this problem planar waves can be chosen, but, a priori the validity of this model is not improved (see Sect. 7.6.3.5)

This question is difficult [48], and is similar to the question of the exact solution of the field in a horn. At low frequencies, we can assume that the pressure is uniform in the cavity between the two surfaces. In order to go further we can use the same type of assumption as the one made so far, i.e., plane wave matching. This avoids the necessity to consider the volume of the junction cavity. The calculation of a complete instrument can then be done by multiplying matrices of the type (7.83), as explained in Sect. 7.5.2.1. To project the impedances, it can be even easier to use the symmetric admittances, defined by Eq. (7.82). If we call x_a the distance of the transition point to the apex of the cone on the left, and x_b to the apex of the cone to the right (see Fig. 7.13), the continuity of the admittance can be expressed in term of symmetric admittances, as follows:

$$\tilde{Y}_a + S/jkx_a\rho c = \tilde{Y}_b + S/jkx_b\rho c \tag{7.107}$$

where S is the cross section at the junction (for the sake of simplicity, we ignore here viscous effects). Everything happens for the symmetric admittance as if an acoustic mass was inserted in parallel, between the two admittances:

$$\tilde{Y}_a = \tilde{Y}_b + \frac{1}{j\omega M} \text{ where } M^{-1} = \frac{S}{\rho}\left[\frac{1}{x_b} - \frac{1}{x_a}\right]. \tag{7.108}$$

For the case shown in Fig. 7.13 ($x_a > x_b$), the mass is positive, and *plays approximately the same role as that of an open tonehole*, which will be studied below (Sect. 7.7.5.3). On the other hand, if the cone with index b is less open than the cone with index a, the mass is negative, which raises causality issues [2, 34]. This makes the computation difficult, especially in discrete time (discrete time computation will be presented in Sect. 7.5.2.2 using cylinder sections).

We treat here the particular problem of the reflection function of a cylinder (x_a infinite) ending in an infinite flared cone. Since the cone b is infinite, the symmetric

admittance at the entrance is $\tilde{Y}_b = S/\rho c$. The symmetric admittance $\tilde{Y}_a$ is simply the admittance for a cylinder, which is

$$\tilde{Y}_a = S/\rho c + S/jkx_b\rho c.$$

Using Eq. (4.32), we derive the reflection coefficient in the cylinder and, using the Fourier transform, we find the reflection function:

$$R = -\frac{\alpha}{j\omega + \alpha} \text{ where } \alpha = \frac{c}{2x_b};$$
$$r(t) = -H(t)\alpha e^{-\alpha t}. \tag{7.109}$$

What would happen for a converging cone? A first observation is that it would be finite, and thus multiple reflections would exist. For the first of them, it can be shown that Formula (7.109) remains valid, the coefficient α becoming negative. There is therefore a growing exponential function, but the pressure never goes to infinity because the successive reflections are limiting the effect of the first one. This issue has prompted a number of works [2, 34] because, since each term tends to infinity, it is not possible to calculate the Fourier transform of such a reflection function by isolating the different reflections. A method is to determine an appropriate Laplace transform in order to avoid having a growing exponential function in the integral. Thus one can make calculations of multiple reflections in the Laplace domain, as we have done in the Fourier domain for the reflections in a cylinder (see Eq. (4.38) and after).

7.5 Tubes with Variable Cross Section

We will now analyze bells of brass instruments, for which an analytical solution exists, and later we will explain some numerical methods for the treatment of shapes of any kind.

7.5.1 Bells of Brass Instruments: Analytical Solution

The shape of brass bells is fairly complicated. We will discuss later a simple numerical-solving method. However, Benade noticed that their shape was close to a power function of x, which allows an approximation using Bessel functions. This allows us to understand some basic phenomena, in particular the resonance frequencies of brass instruments. The interest is in impedance maxima, since they are reed instruments. The radius $R(x)$ can be written as [52]:

$$R(x) = \frac{b}{(x_a - x)^v} \tag{7.110}$$

Fig. 7.14 Geometry of a "Bessel horn," for different values of ν. x_i and x_o are the abscissae of the input and output, while x_a is that of the asymptote

where the three constants b, x_a, and ν are obtained by a fitting procedure. The abscissa x_a is therefore outside the bell, at a distance of about a few centimeters [see Fig. 7.14], and the flare grows rapidly when x approaches the exit.

The coefficient ν lies between 0.5 and 0.65 for trumpets and trombones, which corresponds to a very rapid widening of bell extremity. For some instruments, such as French horns or cornets and saxhorns, the widening of the bell is more gradual, and ν can be larger than unity. The shape is indeed very different from that of a cylinder ($\nu = 0$) or of a cone ($\nu = -1$).

We use Eq. (7.8), in harmonic regime. It is written, if we denote $X = x_a - x$ to simplify the expressions, as:

$$\frac{d^2(PR)}{dX^2} + \left[k^2 - \frac{\nu(\nu+1)}{X^2}\right] PR = 0. \tag{7.111}$$

With a change in variable $z = kX$, the equation is reduced to a Bessel equation for $q(X) = PR/\sqrt{X}$, hence the general solution is[19]

$$PR = \sqrt{X} q(X) \text{ where } q(X) = \left[a_1 J_{\nu+\frac{1}{2}}(kX) + a_2 Y_{\nu+\frac{1}{2}}(kX)\right]. \tag{7.112}$$

From Eq. (7.7), the velocity can be derived, after some calculations:

$$VR = \tilde{q}(X)\sqrt{X} \text{ where } j\rho c\tilde{q}(X) = \frac{dq}{dz} + \frac{q}{z}\left[\upsilon + \frac{1}{2}\right].$$

Using the derivation relation between Bessel functions

$$J_{\nu-1}(z) = J'_\nu(z) + \nu J'_\nu(z)/z,$$

we find that the function $j\rho c\tilde{q}(X)$ satisfies the same expression as $q(X)$, changing $\nu + 1/2$ in $\nu - 1/2$. Moreover, the functions of the 2nd kind can be written as a combination of functions of the first kind (the proof not being given here). Hence the expression of the impedance at the point X is

$$Z = j\frac{\rho c}{S}\frac{J_{\nu+\frac{1}{2}}(kX) + BJ_{-\nu-\frac{1}{2}}(kX)}{J_{\nu-\frac{1}{2}}(kX) - BJ_{-\nu+\frac{1}{2}}(kX)}. \tag{7.113}$$

[19] In the case of a cylinder or a cone, these functions can be expressed using trigonometric functions.

The coefficient B can be obtained using the radiation impedance Z_o at $x = x_o$:

$$B = \frac{\widehat{Z}_o J_{\nu-\frac{1}{2}}(kX_o) - J_{\nu+\frac{1}{2}}(kX_o)}{\widehat{Z}_o J_{-\nu+\frac{1}{2}}(kX_o) + J_{-\nu-\frac{1}{2}}(kX_o)} \text{ where } \widehat{Z}_o = \frac{Z_o S}{j\rho c}.$$

It turns out that $kX_o = k(x_a - x_o)$ is small, because the output is close to the asymptote, and the Bessel function $J_\nu(z)$ is proportional to $z^\nu(1 + O(z^2))$ when z tends to 0. Therefore B is proportional to $Z_o(kX_o)^{2\nu}$, and for $\nu > 0$, the coefficient B tends to 0 when X_o tends to 0 : it can be approximated by 0 when the frequency is not too high, provided that $\nu > -1/2$ for a given X_o. This means that the impedance in the bell does not depend on the exact position of the output, provided that it is fairly close to the abscissa of the asymptote $x = x_a$ ($X = 0$). At the entrance of the bell, we therefore have

$$Z_i = j\frac{\rho c}{S_i}\frac{J_{\nu+\frac{1}{2}}(kX_i)}{J_{\nu-\frac{1}{2}}(kX_i)}. \tag{7.114}$$

This expression is exact for $X_o = 0$, i.e., for strongly flared bells. Nevertheless for that case the plane wave model is not valid at higher frequencies, therefore these results must be handled with caution. As all the types of losses (either near the walls or by radiation) have been ignored, the input impedance Z_i is a purely imaginary number. If kX_i is large enough, we can use the asymptotic expansion of Bessel functions: $J_n(z) \simeq \sqrt{2}/\sqrt{\pi z}\cos\left[z - (n + \frac{1}{2})\frac{\pi}{2}\right]$, valid if $\arg(z) \neq \pi$. For sufficiently high, and positive frequencies, the final result is

$$Z_i = j\frac{\rho c}{S_i}\tan\left[kX_i - \nu\frac{\pi}{2}\right]. \tag{7.115}$$

For many brass instruments, the bell is attached at the end of a long cylinder, whose length ℓ can be modified, using either a slide (for trombones) or pistons (e.g., for trumpets). The impedance given by Eq. (7.114) can be projected to the instrument input [Eq. (4.29)]. If the simplified formula (7.115) is used, the result at the instrument input is

$$Z_0 = \frac{\rho c}{S} j\tan\left[k(\ell + X_i) - \nu\frac{\pi}{2}\right], \tag{7.116}$$

where the length $\ell + X_i$ is fairly close to the total length of the instrument (without mouthpiece), since $X_i = x_a - x_i$ is apart from a few centimeters the length of the bell. The approximated resonance frequencies, corresponding to the impedance maxima are

$$f_n = \frac{c}{2(\ell + X_i)}\left[n - \frac{1-\nu}{2}\right]. \tag{7.117}$$

Remind that this equation, derived from Eq. (7.115), is valid for sufficiently high frequencies. At the input of the bell (i.e., if $\ell = 0$), it is rather satisfactory, but at the instrument input, the first resonance frequencies are very low, and this formula becomes less satisfactory.[20]

Equation (7.117) can be further discussed. For a bell with a flare such as $\nu = 1$, a series corresponding to that of a closed–closed pipe is obtained. Notice that the horn with $\nu = 1$ is simply the dual of the cone, as defined in Sect. 7.2.2 [see, Eq. (4.50)]. For an instrument with a low exponent (for example, $\nu = 0.63$ for a trombone), the series is close to the same series for high frequencies (n large). For this example, the series is 0.815; 1.815; 2.815, etc. After dividing by the first frequency, we obtain the ratios 1; 2.23; 3.45; 4.68, etc. This series seems to be very far from a harmonic series, but this comparison is not very relevant. Considering the ratio between successive frequencies, we have: 2.23 instead of 2 for a closed cylinder (or a full cone !); 1.55 instead of 1.5; 1.35 instead of 1.33, etc. So the harmonic series of a closed cylinder is quickly approached.

To summarize the previous discussion, let us look at the impedance curve of a complete trombone (Fig. 7.15): apart from the first, the spacing between resonance frequencies is quite regular. It can be shown that the low value for the first resonance is explained by the validity limit of Eq. (7.114). The resonance

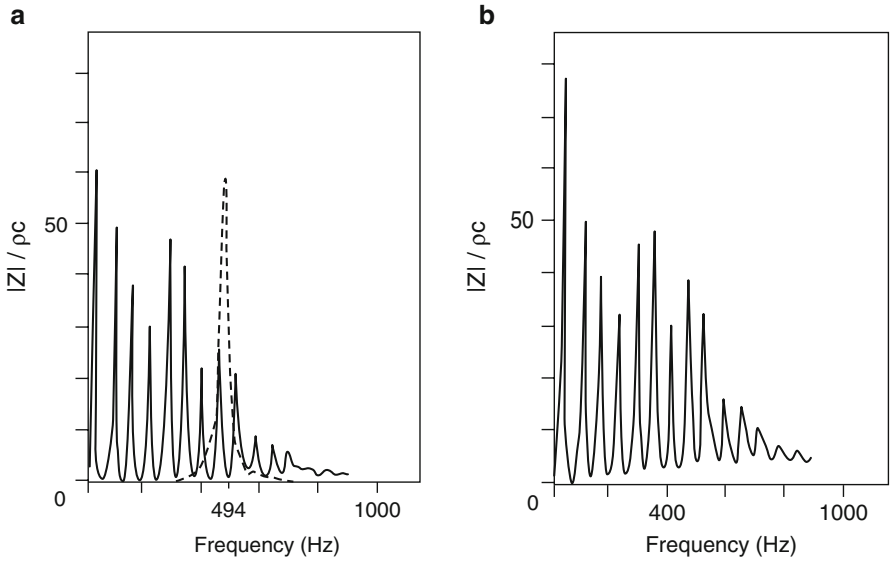

Fig. 7.15 Input impedance of a trombone, (**a**) experiment (**b**) theory. On the experimental curve, the input impedance curve of the mouthpiece alone is superimposed (*dashed curve*, from [20])

[20]Moreover let us not forget that is only an approximation, because Eq. (7.114) does not depend on the termination of the bell, and the geometrical shape is not an exact power law.

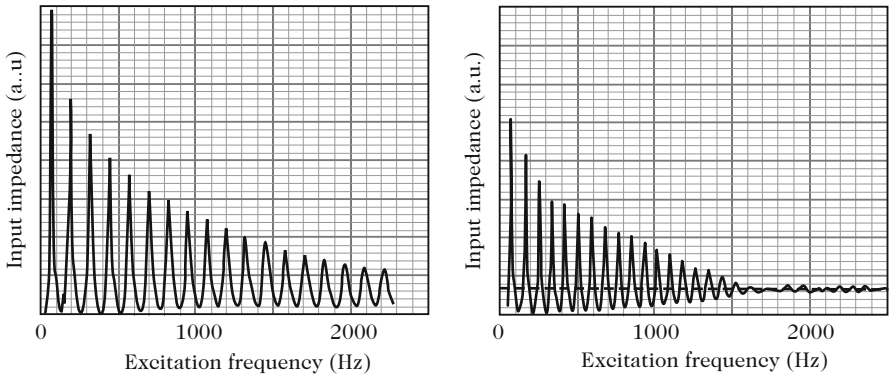

Fig. 7.16 Effect of a trumpet bell on the resonances of a cylinder (see [8, p. 398]). (**a**) Cylinder alone; (**b**) Cylinder + bell. We can notice that the bell approximately transforms the odd resonance series in a complete series, while the higher impedance peaks collapse

frequencies above the first one are close to a series $2, 3, 4, \ldots$. We can say that the gap between the first and second, much larger than 2, is a secondary consequence of the fact that the pipe is cylindrical over most of its length. We will see in Part III the consequences on the various possible oscillation regimes. Compared to the series $1, 2, 3, 4, \ldots$, for the cylinder plus bell there is positive inharmonicity, and it turns out that the mouthpiece, below its Helmholtz resonance, compensates for this effect: we saw in Sect. 7.3.4.2 that it produces negative inharmonicity.[21] For a tuba, the frequencies are fairly harmonically related, and the same type of results is found. However, the first resonance frequency is higher than half of the second one [20].

Now let us go back to the role of the bell, which is primarily to increase the radiation efficiency of higher frequencies (see Fig. 7.16). Beyond a certain frequency, about 1500 Hz, there are no more significant impedance peaks, because dissipation by radiation becomes very important. This is due to the size of the terminal cross section, as we will see in the fourth part. A bell, with a gradual transition of cross section, improves the transfer of higher frequencies to the outside: this property is called impedance matching. At low frequencies, peaks have a significantly reduced height compared to those of a single cylinder, because of both losses near the walls inside the bell and radiation losses, that are added to the losses inside the cylinder.

In practice it is important to estimate the frequency above which resonances disappear. This frequency is related to both the bell shape and the value of the output radius: here its order of magnitude is $kR_o = 1$ for the output radius. The theoretical

[21] One can say that everything is for the best: the mouthpiece, used to improve the emission of quite high notes, offsets the effect of the bell. A more human point of view is that makers have succeeded after years of trials and errors to find well-adapted shapes for the mouthpiece and the bell. However, Bouasse [15, p. 308] noted that in any case, at higher frequencies, the ratio between successive harmonics for the two basic series (odd or complete) tends towards the same values!

determination would require an accurate calculation of both the propagation inside the bell and the outside radiation. For higher frequencies, the calculation is beyond the theory we develop here.

The above described behavior is interesting for the two frequency ranges of wind instruments, because low frequencies are essential for the sound production (see third Part). The high impedance peaks at lower frequencies allow sustaining oscillations, while effective radiation at higher frequencies is important so that the ear has a perception of loud sound power.

7.5.2 Numerical Solution of the Horn Equation for Woodwinds and Brass Instruments

Analytical calculation of some archetypal pipe geometries can be used to understand some basic phenomena. In practice, we often need to perform numerical calculations. For most shapes, there are no exact analytical solutions to the horn equation. For instruments with a shape that is mainly cylindrical or conical, one may use perturbation methods, such as length corrections, to describe the small deviations from a perfectly cylindrical or conical shape. Instruments with this type of shape, however, almost always feature short bells and/or toneholes. For brass instruments, the "Bessel" shape is an approximation, and it is better to use a discretization calculation to take into account the profile as accurately as possible. As this equation is one-dimensional, numerous numerical methods are available, starting with the most general ones, like the finite difference or finite element methods [7]. Nevertheless these methods are especially interesting for 2D or 3D problems [14, 51].

We present below the most usual methods: the product of matrices in the frequency domain, and delay methods in the time domain.

7.5.2.1 Matrix Products

We can consider that a horn is a succession of small portions of cylinders. The solution of the Helmholtz equation is correct for each of them: it is a discretization method which gives an exact result for a perfect cylinder, unlike the finite difference method, for example (except for certain specific choices). If we choose a succession of portions of cones, we simply have to multiply the transfer matrices of the type set out in Eq. (7.83). This method has been used for a long time (see, e.g., [69]), and when there are toneholes, we just insert a special matrix that will be defined later.[22]

[22]We can improve the convergence by dividing the instrument into small cone portions, but then, because of the variation of boundary layers thicknesses with the radius, analytical solutions exist

At the limit of a division into infinitely small segments, the method converges to the correct result. We therefore calculate

$$\begin{pmatrix} P \\ U \end{pmatrix}_{\text{input}} = \mathbb{T} \begin{pmatrix} P \\ U \end{pmatrix}_{\text{output}} \quad \text{where } \mathbb{T} = \prod_i \begin{pmatrix} A_i & B_i \\ C_i & D_i \end{pmatrix} \tag{7.118}$$

This system with an input and an output port is named two-port. If required, the product of matrices can be calculated. Alternatively, an output impedance and an output vector of the type ${}^t(Z, 1)$, where t indicates the transpose of the vector, can be set and ratios of input values to the output flow rate can be deduced: this reduces the number of calculations by a factor 2. A less advantageous variant is to project impedances using homographic relations (like $(AZ + B)/(CZ + D)$), but this only gives the impedances, and cannot provide the transfer functions.

The inverse of a transfer matrix is written, because of reciprocity (the determinant is unity):

$$\begin{pmatrix} A_i & B_i \\ C_i & D_i \end{pmatrix}^{-1} = \begin{pmatrix} D_i & -B_i \\ -C_i & A_i \end{pmatrix}.$$

There are a large number of matrix types related to the transfer matrices, allowing equivalent calculations. For example, an admittance matrix $\mathbb{Y}$ can be defined for the segment $(i-1, i)$ of cross section S_i (assigning the index 0 to the horn entrance, and N to the end). If P_i and U_i are the pressure and flow rate at the output of the segment (similarly for the input with the subscript $i-1$), it can be expressed as:

$$\begin{pmatrix} U_{i-1} \\ \widetilde{U}_i \end{pmatrix} = \begin{pmatrix} Y_i & Y_{\mu,i} \\ Y_{\mu,i} & Y'_i \end{pmatrix} \begin{pmatrix} P_{i-1} \\ P_i \end{pmatrix} \tag{7.119}$$

where $Y_i = D_i/B_i$; $Y'_i = A_i/B_i$; $Y_{\mu,i} = -1/B_i$; $\widetilde{U}_i = -U_i$. The sign $-$ before U_i symmetrizes the input and output, and thus the coefficients of the second diagonal of the admittance matrix are equal, which corresponds to reciprocity.[23] It can be deduced, considering two consecutive segments, that this corresponds to a kind of second-order equation:

$$Y_{\mu,i+1}P_{i+1} + (Y'_i + Y_{i+1})P_i + Y_{\mu,i}P_{i-1} = 0 \tag{7.120}$$

only when calculating the visco-thermal effects for a fixed equivalent radius [see Eq. (7.106)]. This method has been used for the calculation in Fig. 7.12.

[23] Changing U_i in $\widetilde{U}_i$ is equivalent to consider the flow rate at the output along the axis opposite to that of the input, and thus to consider the two ends of a two-port in a symmetrical way. Conversely the orientation chosen for a transfer matrix distinguishes input and output, and is obviously essential in order to juxtapose a sequence of cascaded two-ports.

which can be put in matrix form:

$$\begin{pmatrix} P_{i-1} \\ P_i \end{pmatrix} = \begin{pmatrix} a_i & b_i \\ 1 & 0 \end{pmatrix} \begin{pmatrix} P_i \\ P_{i+1} \end{pmatrix} \tag{7.121}$$

where the writing of the coefficients a_i and b_i is obvious. Again, matrix products can be used to switch from the output to the input or vice versa, starting from known boundary conditions.[24]

Another type of matrix that can be used operates on the incoming/outgoing waves pair, instead of the pressure/flow rate pair. It allows using of successive reflections, simplifying the calculation in the time domain, as we will see in Sect. 7.5.2.2. However it is easier to use for cylindrical portions than for conical portions (see Sect. 7.4.7).

Riccati Equation for the Impedance and Continued Fractions

Another expression of the horn equation is an equation for the impedance. This is a first-order differential equation (once we know the impedance at a point, it is known everywhere), but it is also nonlinear. Starting from Eq. (5.132), and calculating the derivative of $P/U = Z$, or of $U/P = Y$, one obtains

$$\frac{dZ}{dx} = -Z_v(x) + Y_t(x)Z^2 \; ; \; \frac{dY}{dx} = -Y_t(x) + Z_v(x)Y^2. \tag{7.122}$$

This type of equation, called Riccati equation, can be solved very simply by a numerical method for first-order equations, e.g., the Runge–Kutta method. We note first that if the impedance at a point is very small, the equation for Z becomes linear, and the same happens if the impedance is very large for the equation for Y: we find the same results as when using the system with lumped elements (see Sect. 7.2.4). Moreover a remarkable property of the Riccati equation is that it can be solved using another method, the method of continued fractions expansion [46]. This method consists in finding a series of functions of the geometry, $g_n(x)$, according to a very particular recurrence law: $g'_n(x) = 1/g'_{n-1}(x)$: increasing the index n corresponds to increasing the frequencies, as for a series expansion. We give a simple example of continued fraction result for an open cylinder:

(continued)

[24]Note: for a segment without losses, it is easy to show that the coefficients A and D are real numbers, and B and C purely imaginary. Furthermore the coefficients of the admittance matrix are all purely imaginary numbers.

$$\tan kx = \cfrac{1}{\cfrac{1}{kx} + \cfrac{1}{-\cfrac{3}{kx} + \cfrac{1}{\cfrac{5}{kx} + \text{etc}\ldots}}}} \tag{7.123}$$

At the order 3, this result is equivalent to:

$$\tan kx = \frac{kx}{1 - \dfrac{k^2x^2}{3}} \simeq kx\left[1 + \frac{k^2x^2}{3}\right]. \tag{7.124}$$

This shows the relationship with the series expansion. The formula is equivalent to the series expansion to the third order: $\tan kx = kx\left[1 + (kx)^2/3\right]$, at the same approximation order. Its domain of validity in kx is much wider, however, and includes a pole that the series expansion cannot have (as the latter cannot be valid above the resonance $\pi/2$). This pole is obtained when $kx = \sqrt{3}$. We can compare it to the exact value of the first pole of the tangent function, $\pi/2$. Valid approximations beyond the poles can be found. They converge rapidly when the number of terms taken into account increases. The numerical calculation for any shape of horn is very rapid, even when losses are taken into account [46]. This type of expansion can be put in the form of electrical circuits with lumped elements (equivalent to masses and springs). The convergence is faster than that of a modal expansion.

7.5.2.2 Discrete-Time Computation

The purpose of discrete time computing is numerical calculation in the time domain, especially in real time. Let us restrict ourselves to the calculation of the lossless horn equation using a succession of cylinder portions.[25] All calculations reduce to a series of operations involving simple delays, as we did in Chap. 4 for the successive reflections (see also Sect. 7.3.2 of current chapter). A significant simplification is to choose portions whose length is a multiple of an elementary length, equal to $\ell = c/f_e$, (f_e being the sampling frequency). Delays appear in the incoming and outgoing wave variables [see Eq. (4.1)], i.e., the eigenvectors of the transfer matrices of planar waves.

The problem to be solved is that of a cross-section discontinuity, since the corresponding equations are written for the values of pressure and flow rate.

[25] To take visco-thermal effects (losses and dispersion) into account, we replace the delays $\delta(t - T)$ by digital filters, which represent these effects in an approximate way.

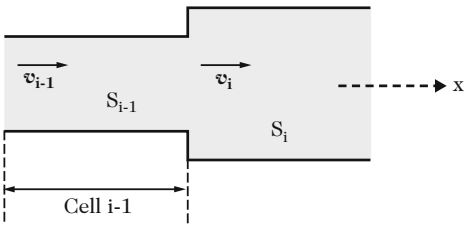

Fig. 7.17 Horn divided in cylinder portions. The considered cell goes from the input of Portion $i-1$ to the input of Portion i

We consider a discontinuity between the pipes of subscripts 1 and 2 in Fig. 7.17 (here $i = 2$, so that the chosen elementary cell goes from the entrance of the Pipe 1 to the entrance of the Pipe 2, just after the discontinuity). In terms of incoming and outgoing waves (we choose $x = 0$ at the discontinuity), continuity of pressure and flow rate is written as (see Sect. 7.3.2):

$$\begin{aligned} p_1^+ + p_1^- &= p_2^+ + p_2^- \ ; \\ S_1(p_1^+ - p_1^-) &= S_2(p_2^+ - p_2^-). \end{aligned} \tag{7.125}$$

Using a simple causal logic, we seek the outgoing waves of a system with respect to the incoming waves. Here p_1^+ and p_2^- are incoming, and p_1^- and p_2^+ are outgoing (considering the chosen orientation);

$$p_2^+ = p_2^- + (1+K)(p_1^+ - p_2^-) \text{ where } K = \frac{S_1 - S_2}{S_1 + S_2} \ ; \tag{7.126}$$

$$p_1^- = p_1^+ + (K-1)(p_1^+ - p_2^-). \tag{7.127}$$

This arrangement of variables gives rise to the scattering matrix method. For sound synthesis, this arrangement leads to the so-called Kelly-Lochbaum junction [37, 43, 55, 74, 75, 78, 79, 81]. One just needs to juxtapose such schemes to treat the whole horn. The use of outgoing and incoming waves in the discrete time domain is called the waveguide technique, and gave rise to an abundant literature [78], for the synthesis of both speech and musical instruments.[26]

Furthermore, in order to minimize the number of multiplications, we prefer to write another kind of relationship:

$$p_2^+ = p_2^- + (1+K)(p_1^+ - p_2^-) \ ; \tag{7.128}$$

$$p_1^- = p_2^+ - (p_1^+ - p_2^-). \tag{7.129}$$

[26]We should pay attention to notations: we use the symbol K for the reflection coefficient, while Smith [78] uses k (he uses R for the characteristic impedance, inversely proportional to the cross section area).

At any time there is only one multiplication to be done, to switch from incoming waves to outgoing waves, by solving the first equation and then the second one.

In order to connect the input of Cell 1 to the input of Cell 2 (which is the output of Cell 1), we consider propagation in the Pipe 1 over the length ℓ, then the discontinuity, expressing the incoming and outgoing waves at the input of cylinder 1 with respect to the same quantities at the discontinuity. At $x = 0$, the outgoing wave is delayed by a time $T = \ell/c = f_e^{-1}$ from its value at the input of the cell at $x = -\ell$. It is a function of $t - x/c$, so it has the same value in $x = -\ell$ at time $t - T$ as in $x = 0$, at time t. Conversely the incoming wave is a function of $x + ct$, and has the same value in $x = -\ell$ at time $t + T$ as in $x = 0$ at time t. In order to find the desired result, these expressions are simply used in Eqs. (7.128) and (7.129). In the cascade of segments (or cells) including a length ℓ and a discontinuity, we denote $i - 1$ the index of the input of Pipe 1 ($x = -\ell$) and i the entrance of Pipe 2 ($x = 0$):

$$p_i^+(t) = p_i^-(t) + (1 + K_i)\left[p_{i-1}^+(t - T) - p_i^-(t)\right]\ ; \tag{7.130}$$

$$p_{i-1}^-(t + T) = p_i^+(t) - \left[p_{i-1}^+(t - T) - p_i^-(t)\right]. \tag{7.131}$$

$K_i = (S_{i-1} - S_i)/\ (S_{i-1} + S_i)$ is the reflection coefficient of a wave in segment $i - 1$ incident on segment i. To proceed to the time discretization, we denote the time domain sample number at time t as n such that $n/pm1$ corresponds to t/pmT. Finally:

$$p_i^+(n) = p_i^-(n) + (1 + K_i)\left[p_{i-1}^+(n - 1) - p_i^-(n)\right]; \tag{7.132}$$

$$p_{i-1}^-(n + 1) = p_i^+(n) - \left[p_{i-1}^+(n - 1) - p_i^-(n)\right]. \tag{7.133}$$

7.5.2.3 How to Measure the Input Impedance of a Wind Instrument?

The input impedance is the ratio of two quantities of a linear passive system, i.e., a transfer function, which depends only on the properties of the passive system downstream from the source. In principle, to obtain the input impedance of a pipe, one just has to excite it using any source, and to measure both the pressure with a microphone and the average particle velocity (or the acoustic flow rate) using a velocity sensor. In practice this solution is rarely used because the acoustic velocity or flow rate sensors are sometimes difficult to use.[27]

For this reason an indirect determination of the velocity is generally preferred. For instance, two microphones located one next to each other make a pressure gradient sensor from which the velocity can be deduced. This method has the

[27] One solution is the hot wire anemometer, which, however, implies that there is a mean flow, or better the Microflown probe that was developed to measure low particle velocity. More complex methods, such as the Laser Doppler Anemometry can also be considered.

drawback of being usable over a limited range of frequencies,[28] necessitating the use of more than one pair of microphones. The signal from the source can also be used directly, because it is connected to the velocity: a condenser microphone used as a source produces, as a first approximation, a displacement proportional to the applied voltage. The reader will find summaries on this topic in several articles (see especially [21, 26], and also [83]). A general difficulty is the calibration, which can be done from theoretical knowledge, either of the measurement system itself or, better, of the input impedance of particular test objects, such as cylindrical pipes.

7.6 Duct Modes and Simple Discontinuities

So far we have treated modes in one-dimensional systems, and rarely in systems with multiple dimensions, with the exception of material on from membranes and plates (See Chap. 3). In resonators, there are discontinuities such as toneholes that require three dimensions to be taken into account: that is the purpose of this section. We first define the cavity modes, which make use of concepts seen before, then the concept of duct modes. We will see that duct modes are a generalization of one-dimensional waves: they are waves in one direction, and modes in the two others. They allow writing the formulas in closed-form (See Chap. 4) in one direction, and to expand into modes in the other two. These concepts are more easily introduced in Cartesian geometry. We then discuss the cylindrical geometry, which is of course the most usual.

We do not consider any dissipation or mean flow effects: this limits the validity of our analysis, but still yields quite useful results, especially for calculating the effect of toneholes on the resonance frequencies. Flow effects, which are nonlinear, are discussed in Chap. 8.

7.6.1 Cavity Modes and Duct Modes: Cartesian Geometry

7.6.1.1 Cavity Modes: The Example of a Closed Cavity

For an acoustic cavity (in three dimensions), a triple infinity of modes is found. They are solutions of the wave equation without sources, for given boundary conditions. We can then show that any solution of the wave equation (with sources) can be written as a linear combination of modes, which are valid solutions *apart from a multiplicative constant*.

[28] On the one hand, at lower frequencies, the gradient is small and, on the other hand, at higher frequencies, the gradient can vanish when the distance is equal to one half wavelength. In both cases, accuracy is poor.

Let us consider the simple example of a closed, rectangular, perfectly reflective cavity with rigid walls, of dimensions L_x, L_y, L_z. The corresponding modes can be easily calculated by using the separation of variables. We look for solutions of the wave equation with no source in the form $p(\boldsymbol{r}, t) = X(x)Y(y)Z(z)T(t)$, with the vector $\boldsymbol{r} = (x, y, z)$. Dividing the wave equation by $p(\boldsymbol{r}, t)$, we obtain

$$\frac{1}{X}\frac{\partial^2 X}{\partial x^2} + \frac{1}{Y}\frac{\partial^2 Y}{\partial y^2} + \frac{1}{Z}\frac{\partial^2 Z}{\partial z^2} = \frac{1}{c^2}\frac{1}{T}\frac{\partial^2 T}{\partial t^2}.$$

The left-hand member depends on space only, and the right-hand member on time only, therefore both must be equal to a constant (i.e., *a space and time independent constant*). We write it $-k^2 = -\omega^2/c^2$. Both notations are convenient, especially for conservative boundary conditions, for which we find that k and ω are real numbers. The time solution of the equation is $T(t) = \exp(\pm j\omega t)$. Then we particularize the direction x, writing:

$$\frac{1}{X}\frac{\partial^2 X}{\partial x^2} = -\frac{1}{Y}\frac{\partial^2 Y}{\partial y^2} - \frac{1}{Z}\frac{\partial^2 Z}{\partial z^2} - k^2 = -k_x^2.$$

Similarly, the constant (independent of x on one side, and of y and z on the other) is denoted $-k_x^2$ (in the present case, it is positive, but we will see a case where it is negative). Neumann boundary conditions are assumed for $x = 0$ and $x = L_x$. The x equation has the solution $X(x) = \cos k_x x$, where $k_x = n_x\pi/L_x$. n_x is an integer. One can do a similar operation for the coordinate y, which is separated from z, and we obtain for Neumann conditions at $y = 0$ and $y = L_y$: $Y(y) = \cos k_y y$, where $k_y = n_y\pi/L_y$. Finally for z, we made a last operation, but this time the constant, denoted $-k_z^2$, is *already fixed*:

$$\frac{1}{Z}\frac{\partial^2 Z}{\partial z^2} = -k^2 + k_x^2 + k_y^2 = -k_z^2. \tag{7.134}$$

This equation is the *dispersion* equation. Also for Neumann conditions in $z = 0$ and $z = L_z$: $Z(z) = \cos k_z z$, where $k_z = n_z\pi/L_z$. Eventually, for our rectangular cavity, we have the following solutions, written apart a multiplicative constant:

$$p(\boldsymbol{r}, t) = \cos k_x x \cos k_y y \cos k_z z \; e^{j\omega t}, \text{ with} \tag{7.135}$$

$$\omega^2/c^2 = (n_x\pi/L_x)^2 + (n_y\pi/L_y)^2 + (n_z\pi/L_z)^2. \tag{7.136}$$

Solutions using $\exp(-j\omega t)$ would produce the same real quantities, and are therefore excluded. The functions given by (7.135) are the modes of the cavity, which are consistent with the entirety Chap. 3. As the medium is limited, the eigenfrequencies are quantized: they can only take a number of values corresponding to the integers n_x, n_y, n_z, satisfying (7.136). For the particular case of the boundary conditions chosen, there is a uniform mode of zero frequency, such as $n_x = n_y = n_z = 0$: it is

obvious that $p(\boldsymbol{r}, t)$= constant is a solution of the wave equation, satisfying Neumann conditions on the walls, since its gradient vanishes. We can finally show that the modes we found are orthogonal in the case of conservative walls, whose admittance is purely imaginary, the conditions of Neumann or Dirichlet being a special case.

7.6.1.2 Duct Modes (Rectangular Geometry)

The separation of variables can also be done for an infinite medium. This was the case in one dimension for the general decomposition in the form of outgoing and incoming waves in sinusoidal regime [see Eq. (4.24)]. Hence all frequencies can exist. Compared to the modal expansion for a finite domain, this formulation has the advantage of avoiding the infinite series, thanks to the closed-form solutions. If we take the three dimensions of a duct into account, we still have the choice between the modes of the duct regarded as a cavity, and a different kind of modes, called *duct modes or waveguide modes*, which are the solutions for a bounded medium in the directions transverse to the axis of the duct and unbounded in this axis. So let us suppose that the rectangular cavity is unbounded along the x-direction. The solutions for separate variables are written as:

$$p(\boldsymbol{r}, t) = \left[a^{+} e^{-jk_x x} + a^{-} e^{jk_x x}\right] \Phi_{n_y,n_z}(y, z) e^{j\omega t} \tag{7.137}$$

$$\text{where } \Phi_{n_y,n_z}(y, z) = \cos k_y y \cos k_z z \ ; \ k_x^2 = \omega^2/c^2 - k_\perp^2 \tag{7.138}$$

$$\text{with } k_\perp^2 = (n_y \pi/L_y)^2 + (n_z \pi/L_z)^2. \tag{7.139}$$

The modal shape $\Phi_{n_y,n_z}(y, z)$ is solution of the Helmholtz equation:

$$(\Delta_\perp + k_\perp^2)\Phi = 0, \tag{7.140}$$

where $\Delta_\perp$ is the two-dimensional Laplacian on y and z. The values of $k_\perp$ are the eigenwavenumbers of a specific problem in two dimensions, which are quantified by (7.139).

- The mode discussed in Chap. 4 is the planar mode, denoted $(0, 0)$, for which $n_y = n_z = 0$. It is the equivalent of a uniform mode $(0, 0, 0)$ for a cavity. This property exists whatever the geometry, provided that the conditions on the walls are Neumann conditions. Acoustic quantities are uniform, or "planar," in a section of the duct perpendicular to the x-axis.
- The other modes depend on the geometry, and present an important feature: depending on the sign of k_x^2, they can be either *propagating* (real k_x) or *evanescent* (purely imaginary k_x). In this case waves are exponentially decreasing

or increasing in the x direction.[29] The frequency at the limit $k_x = 0$ is called the "cutoff frequency," and is simply a eigenfrequency of the two-dimensional problem on y and z. It satisfies $\omega/c = k_\perp$, and its values are given by (7.139). Therefore, for a given frequency, there are a finite number of propagating modes.

Thus, at lower frequencies, when ω/c is smaller than any nonzero value of $k_\perp$, only the planar mode propagates. Suppose that the section of the duct is such that $L_y \ll L_z$. The lowest non-planar modes of wavenumber $k_\perp$ are obtained for $n_y = 0$ and $n_z = 1, 2, 3 \ldots$ For $n_z = 1$, $\Phi_{0,1}(y, z) = \cos(\pi z/L_z)$: this is an anti-symmetric mode with respect to $z = L_z/2$. For $n_z = 2$, $\Phi_{0,2}(y, z) = \cos(2\pi z/L_z)$: this mode is symmetrical with respect to $z = L_z/2$. If the instrument under consideration (including the excitation) is fully symmetrical, the mode $(0, 1)$ cannot exist, and therefore the first non-planar mode is $(0, 2)$ and appears for $kL_z = 2\pi$. Below this frequency, only the planar mode can propagate, and, because evanescent modes are located near the cross section changes, this is a justification for the approximation of plane waves, widely used so far. In practice, the instrument is not symmetrical, and the frequency given by

$$kL_z = \pi, \text{ or } L_z = \lambda/2, \tag{7.141}$$

is the limit of validity (corresponding to the so-called half-wavelength resonance). As the transverse dimensions are small compared to the wavelength ($L_z < \lambda/2$), the waves are assumed to be planar. This is a very common situation for wind instruments. However some mouth organ pipes have a section large enough for the appearance of modes called "upper modes" at audible range frequencies, which are important in the spectrum. A similar phenomenon exists at higher frequencies in the vocal tract, when the transverse dimensions are large compared to the wavelength [67]: a dimension of 4 cm gives a first cutoff frequency at approximately 4000 Hz, a high though significant frequency for the voice. In addition, near the transverse resonance, we can understand intuitively that the air can excite the walls in a non-negligible way, which can cause coupling phenomena.

- As for the cavity modes, the duct modes are orthogonal when the wall conditions are conservative (i.e., purely imaginary normal impedance). To show this we use the divergence theorem for the two-dimensional Helmholtz equation in the case of a constant section, (See [18]):

$$\int_S \Phi_{n_y,n_z}(y, z)\Phi_{m_y,m_z}(y, z)dS = 0 \text{ if } n_y \neq m_y \text{ or } n_z \neq m_z. \tag{7.142}$$

[29] Physically, the modes can only decrease on both sides of a discontinuity or of a source, the existence of growing modes is thus linked to a choice of orientation of the x axis. Such modes are typically found near the open end of a tube.

This allows, if the pressure profile on a section is known, the coefficients of the modal expansion to be determined. We deduce in particular that since the planar mode exists, all non-planar modes have averages equal to zero. *In other words, the planar mode represents the average field pressure*.

- The (specific) characteristic impedance of a mode traveling in the x-direction is obtained from the Euler equation:

$$Z_x = \frac{p}{v_x} = -j\omega\rho\frac{p}{\partial p/\partial x} = \rho c\frac{k}{k_x}. \tag{7.143}$$

For an evanescent mode this is a purely imaginary number: the mode does not transport energy.[30] Moreover, at very low frequencies, such as

$$jk_x = \left[(n_y\pi/L_y)^2 + (n_z\pi/L_z)^2\right]^{1/2},$$

the impedance is mass-like: energy of evanescent modes is kinetic. We will later study their role near a change in cross section: the field is far from being plane, thus all modes, whether propagating or evanescent, exist. Notice that if the first higher mode is obtained for $n_y = 0$, $n_z = 1$, the mode in a long enough pipe decreases as $\exp(-\pi x/L_z)$ at lower frequencies, so we can ignore it as long as x reaches the order of magnitude of the transverse dimension L_z; and since the higher modes decrease more quickly, this gives an intuitive idea of the distance over which the evanescent modes can be significant close to an obstacle or a discontinuity (this type of reasoning is only qualitative, because it covers an infinity of modes, but numerical calculations confirm the correctness of this assertion).

7.6.2 Cylindrical Duct Modes

Circular cross sections are the most common in wind instruments. Everything we have written above can be transposed by replacing the coordinates (y, z) by the polar coordinates (r, θ). The equation we need to solve, (7.140), is written as:

$$\left[\frac{\partial^2}{\partial r^2} + \frac{1}{r}\frac{\partial}{\partial r} + \frac{1}{r^2}\frac{\partial^2}{\partial\theta^2}\right]\Phi(r,\theta) + k_\perp^2 = 0, \tag{7.144}$$

which is similar to the Fourier transform of the membrane equation (3.143). The separation of variables can be done by requiring that the field is finite at $r = 0$ (first boundary condition), and therefore the solutions only involve the Bessel functions of the first kind:

[30] The superposition of increasing and decreasing modes, which occurs, for example, between two close discontinuities, can transport energy if they are not in phase, which is equivalent to the tunneling effect in quantum mechanics.

$$\Phi_{mn}(r,\theta) = J_n(\gamma_{mn} r)\cos n\theta \quad \text{and} \quad \Phi_{mn}(r,\theta) = J_n(\gamma_{mn} r)\sin n\theta,$$
$$\text{where} \quad \gamma_{mn}^2 = \omega^2/c^2 - k_x^2 \quad \text{and } m \text{ and } n \text{ are positive integers.} \tag{7.145}$$

These solutions are written apart from a multiplicative constant. The values of γ_{mn} are given by the other boundary condition, i.e., the condition at the wall $r = R$: this distinguishes these modes from those of membranes, because here the condition is a Neumann condition and not a Dirichlet condition. We must therefore have

$$J_n'(\gamma_{mn} R) = 0. \tag{7.146}$$

For $n = 0$ (modes of radial symmetry), it is found: $\gamma_{m0} R = 0$ (this is the planar mode!); 3.83; 7.02; 10.17, etc. (to 2 decimal points). For $n = 1$, it is found $\gamma_{m1} R = 1.84$; 5.33; 8.54, etc. Figure 7.18 shows the shape of the nodal lines (zero pressure) for the first modes.

Among the modes without radial symmetry, only the $\cos n\theta$ modes are shown. If the instrument had a radial symmetry, only modes such as $n = 0$ would exist, and the first cutoff frequency would be given by $kR = 3.83$. In practice this is not the case, and the first cutoff frequency is given by:

$$kR = 1.84. \tag{7.147}$$

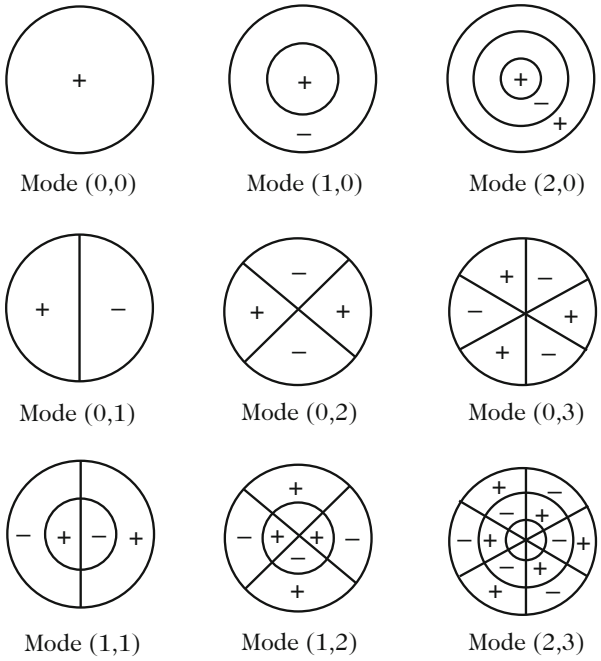

Fig. 7.18 Nodal lines for the first modes of a cylindrical tube; for modes without radial symmetry. Modes with $\cos n\theta$ are chosen

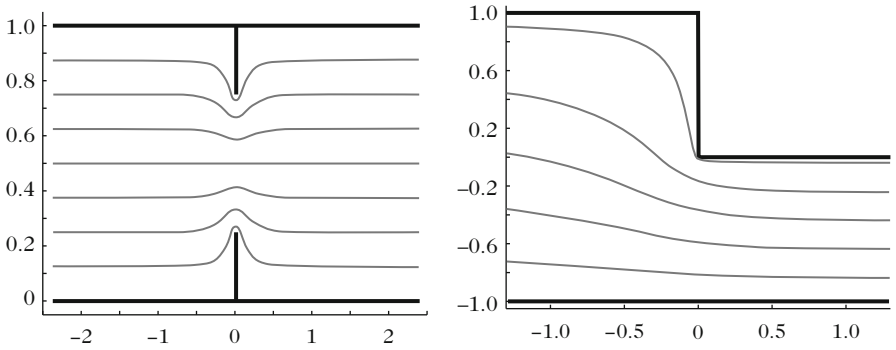

Fig. 7.19 Potential flow in the presence of a zero-thickness diaphragm (*on the left*) or at a change in cross section (*on the right*) (the calculation is made by a conformal mapping of the complex plane for a rectangular geometry, see [59])

Writing the same expression with the diameter $D = 2R$ reads: $kD = 3.68$. This is the same order of magnitude as for the rectangular geometry, when compared to Eq. (7.141), replacing the transverse dimension L_z by the diameter.

7.6.3 Cross Section Discontinuities and Diaphragms

7.6.3.1 Problem Statement

The theory we used for chimney pipes is a simplification, because pressure continuity of the planar mode is not satisfied. Since Bernoulli's work, the theory has been employed for the analysis of many situations, starting with the case of a horn. A difficulty when using this approximation clearly appears for a diaphragm without thickness (see Fig. 7.19): assuming continuity of both the planar mode pressure and flow rate, we cannot "see" the diaphragm, whereas when the opening goes to 0, the impedance must tend to infinity, and therefore strongly disturbs the field!

Actually, even at very low frequencies, the field is not uniform near the discontinuity, i.e., higher modes are present: they are evanescent and disappear when the distance from the junction increases. At very low frequencies, the field is a solution of the Laplace equation. Assuming that there is a compact region of space, i.e., a region small compared to the wavelength, we can consider the flow as incompressible. Moreover it is irrotational (we are still considering the linear approximation, without mean flow or dissipation); the problem to be solved is that of a potential flow. At any times the velocity is parallel to the streamlines shown in Fig. 7.19.

When the streamlines become narrower, there is an increase of the total kinetic energy due to the presence of the diaphragm. Therefore there is an additional

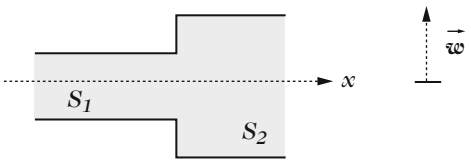

Fig. 7.20 Notations for a discontinuity between a small guide (*1*) and a large guide (*2*)

acoustic mass.[31] It can be shown that this extra mass tends to infinity when the radius of the diaphragm tends to zero, which is equivalent to closing the pipe.

However, this type of discontinuity does not induce any additional compressibility effect, as we will show later: this is because the mass conservation equation is scalar, and the acoustic compliance of a volume V of any shape is always $\chi_s V = V/\rho c^2$ [Eqs. (1.154) and (1.96)]. The volume to be considered is that of a certain portion of the pipe, but the exact shape does not affect the result.

7.6.3.2 Solving the Problem of a Discontinuity in Cross Section

There are many methods for solving the problems of discontinuities [57]. The only analytical method for solving the Laplace equation is that of conformal mapping, but it is limited to the rectangular, two-dimensional geometry [27, 59]. We present below a quite natural method, based on the modal expansion in each of the guides, by treating the simple case of a discontinuity in cross section (see Fig. 7.20). A numerical calculation yields the solutions for some geometries.

We have to solve the three-dimensional sound equation exactly. For this purpose, we decompose the field in each waveguide in modes of the form (7.137) and use a matrix notation. $(x, \boldsymbol{w})$ are the coordinates in a guide: $\boldsymbol{w}$ is a 2D vector, denoted (y, z) and (r, θ) for the two above-discussed geometries. An index refers to each of the Pipes (1 or 2), and the origin is at the discontinuity. The modal decomposition is known for certain geometries for which coordinates are separable. We assume here that there is a (double) infinity of modes that are solutions of (7.140).[32] In the general case, however, we sort modes using a single index, for example, using increasing cutoff frequencies. For each of the guides, the field is decomposed as follows, preferably using a vector notation for the pressure and the projection of velocity along the x-axis, defined below:

[31] This mass is added to that due to the planar mode, which is $\rho\ell/S$ for a small tube of length ℓ and section S, and we will see that its order of magnitude is the mass of air in a pipe whose cross section is that of the diaphragm and the length is that of the radius.

[32] If the guides have a common symmetry, the double infinity can be reduced to a simple infinite: in the circular case, if both guides are concentric, we have a radial symmetry, and the azimuth θ is not relevant. Similarly for the case of a 2D rectangular geometry, if the two guides have a common transverse dimension, the discontinuity cannot create any higher order modes in the common dimension.

Scalar notation	Vector notation
$p(x,\boldsymbol{w}) = \sum_{i=0}^{+\infty} \Phi_i(\boldsymbol{w}) P_i(x)$	$p(x,\boldsymbol{w}) = {}^t\boldsymbol{\phi}(\boldsymbol{w})\boldsymbol{P}(x)$
$v(x,\boldsymbol{w}) = S^{-1} \sum_{i=0}^{+\infty} \Phi_i(\boldsymbol{w}) U_i(x)$	$v(x,\boldsymbol{w}) = S^{-1}\, {}^t\boldsymbol{\phi}(\boldsymbol{w})\boldsymbol{U}(x)$
$\int_S \Phi_i(\boldsymbol{w})\Phi_k(\boldsymbol{w})dS = S\delta_{ik}$	$\int_S \boldsymbol{\phi}(\boldsymbol{w}){}^t\boldsymbol{\phi}(\boldsymbol{w})dS = S\mathbb{I}$
$P_i(x) = S^{-1}\int_S \Phi_i(\boldsymbol{w}) p(x,\boldsymbol{w})dS$	$\boldsymbol{P}(x) = S^{-1}\int_S \boldsymbol{\phi}(\boldsymbol{w}) p(x,\boldsymbol{w})dS$
$U_i(x) = \int_S \Phi_i(\boldsymbol{w}) v(x,\boldsymbol{w})dS$	$\boldsymbol{U}(x) = \int_S \boldsymbol{\phi}(\boldsymbol{w}) v(x,\boldsymbol{w})dS$

where $\mathbb{I}$ is the identity matrix. The normalization chosen for the modes is such that they are dimensionless (so that the planar mode is $\Phi_i(\boldsymbol{w}) = 1$). Vectors $\boldsymbol{P}$, $\boldsymbol{U}$, and $\boldsymbol{\phi}$, are column vectors, and are therefore of infinite dimension for the first step. We omit the time dependence $\exp(j\omega t)$. For the velocity, the vector $\boldsymbol{U}(x)$ (given the factor S^{-1}) is chosen to obtain the flow rate in the case of a uniform velocity. We can write for Pipe 2, according to Eq. (7.137) and Euler's equation, apart from a multiplicative constant:

$$\begin{aligned} P_{2,i}(x) &= A_2\left[e^{-jk_{2,i}x} + R_{2,i}e^{jk_{2,i}x}\right]; \\ U_{2,i}(x) &= A_2 Z_{2,i}^{-1}\left[e^{-jk_{2,i}x} - R_{2,i}e^{jk_{2,i}x}\right], \end{aligned} \tag{7.148}$$

with, according to (7.143), $Z_{2,i} = \rho ck/(k_{2,i}S_2)$. The reflection coefficient $R_{2,i}$ depends on the conditions at the end. Similarly for the Pipe 1, we have

$$\begin{aligned} P_{1,i}(x) &= A_1\left[e^{jk_{1,i}x} + R_{1,i}e^{-jk_{1,i}x}\right] \\ U_{1,i}(x) &= -A_1 Z_{1,i}^{-1}\left[e^{jk_{1,i}x} - R_{1,i}e^{-jk_{1,i}x}\right], \end{aligned} \tag{7.149}$$

with $Z_{1,i} = \rho ck/(k_{1,i}S_1)$. The reflection coefficient $R_{1,i}$ depends on the conditions at the entrance of the Pipe 1. A_1 and A_2 are complex amplitudes. Considering the set of two pipes shown in Fig. 7.20 between two given abscissae, we have what is called a multi-port system with two infinities of ports. A port is defined by two scalar quantities: pressure and velocity (projected on the axis). For a unique mode in a tube of given length, we therefore have a two-port, see Sect. 7.5.2.1. For n modes, we have $2n$ ports. In order to find the field everywhere, we have to find a characterization of the multi-port that enables us to move from the left to the right

of the cross section discontinuity. Between two given abscissas of a straight guide, the relationships are well known, each mode being characterized by a transfer matrix of order 2.

- The problem is to find the relationship between the vector pressures, $\boldsymbol{P}_1(x)$ and $\boldsymbol{P}_2(x)$, and the velocity vectors, $\boldsymbol{U}_1(x)$ and $\boldsymbol{U}_2(x)$, on the two sides of the discontinuity (the approximation made in Sect. 7.3 was the truncation of these vectors to a single component, considering only the planar mode, with continuity of average pressure and flow rate). The first step is to find a matrix to represent this multi-port with two infinities of ports. To do this, we use the continuity conditions at each point $\boldsymbol{w}$ of the matching section. At every time and every point continuity of the pressure and particle velocity on the common section needs to be satisfied (i.e., the section S_1 of the small duct). Furthermore the normal velocity vanishes on the vertical wall surface $S_2 - S_1$. This is written as follows:

$$\begin{aligned} &p_1(0,\boldsymbol{w}) = p_2(0,\boldsymbol{w}) \text{ and } v_1(0,\boldsymbol{w}) = v_2(0,\boldsymbol{w}) \text{ if } \boldsymbol{w} \in S_1 \ ; \\ &v_2(0,\boldsymbol{w}) = 0 \text{ if } \boldsymbol{w} \in S_2 - S_1. \end{aligned} \tag{7.150}$$

  The projection of these conditions on the modes allows us to find the desired relationship. This is called the method of *mode matching*: since there is a surface where the two modal decompositions are possible, we can therefore match them.
- The second step is based on the fact that among the infinity of modes, there are a finite number that propagate (and at low frequencies only one, the planar mode). We assume that the discontinuity is sufficiently far from any other discontinuity. Thus the two pipes are infinite for the evanescent modes (i.e., the exponentials decrease on both sides of the discontinuity, because growing exponentials could appear only if there were a second discontinuity close to the first one). With this hypotheses, the coefficients $R_{1,i}$ and $R_{2,i}$ are zero for all subscripts i corresponding to evanescent modes and the impedances of evanescent modes are known to be given by their characteristic impedances $Z_{1,i}$ and $Z_{2,i}$. This means that all corresponding ports are closed on a known impedance (one can eliminate the pressure and flow rate vectors of evanescent modes), and that the *multi-port dimension is reduced to the number of propagating modes*. The only condition is that on each side there is a long enough pipe length without discontinuity. In practice, it is sufficient that, for each duct, this length has the order of magnitude of the transverse dimensions, as we intuitively explained at the end of Sect. 7.6.1.2.

  Now, projecting the conditions (7.150) on both modal bases, we have

$${}^t\boldsymbol{\phi}_1(\boldsymbol{w})\boldsymbol{P}_1(0) = {}^t\boldsymbol{\phi}_2(\boldsymbol{w})\boldsymbol{P}_2(0) \ \text{ for } \ \boldsymbol{w} \in S_1,$$

hence projecting on the basis of the Pipe 1 (and from now on omitting abscissa $x = 0$):

$$\boldsymbol{P}_1 = \mathbb{F}\boldsymbol{P}_2 \ \text{ where } \ \mathbb{F} = S_1^{-1} \int_{S_1} \boldsymbol{\phi}_1(\boldsymbol{w}) {}^t\boldsymbol{\phi}_2(\boldsymbol{w}) dS. \tag{7.151}$$

For the velocity, we get

$$S_1^{-1t}\boldsymbol{\phi}_1(\boldsymbol{w})\boldsymbol{U}_1 = S_2^{-1t}\boldsymbol{\phi}_2(\boldsymbol{w})\boldsymbol{U}_2 \text{ for } \boldsymbol{w} \in S_1$$
$$\int_{S_2} \boldsymbol{\phi}_2(\boldsymbol{w})v(0,\boldsymbol{w})dS = \int_{S_1} \boldsymbol{\phi}_2(\boldsymbol{w})v(0,\boldsymbol{w})dS$$

since the velocity vanishes on $S_2 - S_1$. The projection on the basis of the Pipe 2 is used to take into account these conditions, and we obtain

$$\boldsymbol{U}_2 = {}^t\mathbb{F}\boldsymbol{U}_1. \tag{7.152}$$

The appearance of the transpose matrix of $\mathbb{F}$ is due to reciprocity: this is not explained here. Equations (7.151) and (7.152) are used to represent the change in cross section by a generalized transfer matrix:

$$\begin{pmatrix} \boldsymbol{P}_1 \\ \boldsymbol{U}_1 \end{pmatrix} = \begin{pmatrix} \mathbb{F} & \mathbf{0} \\ \mathbf{0} & {}^t\mathbb{F}^{-1} \end{pmatrix} \begin{pmatrix} \boldsymbol{P}_2 \\ \boldsymbol{U}_2 \end{pmatrix}. \tag{7.153}$$

Unfortunately this writing is valid only formally, and is not usable: the inverse of the matrix $\mathbb{F}$ is difficult to obtain numerically. In particular it is assumed that $\mathbb{F}$ is square, and that the vectors are truncated to the same number of modes on the two sides (of course the actual calculation assumes a vector truncation!). In theory this means that the field is more "detailed" on the left than on the right, as the guide on the left is smaller and therefore the above description of the singularity (the right angle) is not satisfactory. This issue is complicated. We notice that in general for a large number of modes, if the large guide is q times larger than the smaller one, we must take q times more modes in the large guide [57].

Formally, the first step is achieved. Now, using Eqs. (7.151) and (7.152) at low frequencies, we ensure that the evanescent modes in the two guides obey the relevant characteristic impedance. To do this, we decompose the vectors and matrices into sub-vectors and sub-matrices, corresponding to the propagating mode(s) and to the evanescent modes. For the calculation of products, the sub-matrices will be used as ordinary matrices. If only the planar mode propagates, one of the sub-vectors is a scalar, and for each of the ducts it can be written as:

$$\boldsymbol{P} = \begin{pmatrix} p \\ \boldsymbol{P}' \end{pmatrix} \; ; \; \boldsymbol{U} = \begin{pmatrix} u \\ \boldsymbol{U}' \end{pmatrix} \; ; \boldsymbol{\phi} = \begin{pmatrix} 1 \\ \boldsymbol{\phi}' \end{pmatrix}. \tag{7.154}$$

The matrix $\mathbb{F}$ can be written as:

$$\mathbb{F} = \begin{pmatrix} 1 & {}^t\boldsymbol{f} \\ \mathbf{0} & \mathbb{F}' \end{pmatrix}. \tag{7.155}$$

The first column has a very particular form, because of the existence of a mode common to the two guides, i.e., the planar mode (1 is a scalar, $\mathbf{0}$ a zero column vector). This is an essential feature of acoustic waveguides with Neumann conditions. $\boldsymbol{f}$ is a vector of the following form: $\boldsymbol{f} = S_1^{-1}\int_{S_1}\boldsymbol{\phi}_2'(\boldsymbol{w})dS$, and the matrix $\mathbb{F}'$ is the reduction of the matrix $\mathbb{F}$ once the planar mode is removed. The decomposition of Eqs. (7.151) and (7.152) gives

$$p_1 = p_2 + {}^t\boldsymbol{f}\boldsymbol{P}_2' \; ; \boldsymbol{P}_1' = \mathbb{F}'\boldsymbol{P}_2', \tag{7.156}$$
$$u_2 = u_1 \; ; \boldsymbol{U}_2' = \boldsymbol{f}u_1 + {}^t\mathbb{F}'\boldsymbol{U}_1'.$$

We have seen that because of the existence of the planar mode, it is the only mode to have a nonzero average: this means that only the planar mode contributes to the flow rate. As the vertical wall does not contribute to the flow, a key equation, used since the beginning of this chapter up to the horn equation, is verified: this is flow rate conservation ($u_2 = u_1$) at a change in cross section, due to the fact that the matching occurs on a surface of zero volume. Now we need to force the evanescent modes to obey the relevant characteristic impedance, using (7.148) and (7.149):

$$\boldsymbol{P}_1' = -\mathbb{Z}_1'\boldsymbol{U}_1' \; ; \boldsymbol{P}_2' = \mathbb{Z}_2'\boldsymbol{U}_2', \tag{7.157}$$

where the matrices $\mathbb{Z}'$ are the characteristic impedance matrices, which are diagonal. Then, after a simple calculation, using the characteristic admittance matrices $\mathbb{Y}' = \mathbb{Z}'^{-1}$, we obtain

$$p_1 = p_2 + Z_d u \; ; u = u_1 = u_2 \text{ where} \tag{7.158}$$
$$Z_d = {}^t\boldsymbol{f}(\mathbb{Y}_2' + {}^t\mathbb{F}'\mathbb{Y}_1'\mathbb{F}')^{-1}\boldsymbol{f}. \tag{7.159}$$

Here we mention only what is relevant to the planar mode. Z_d, which is scalar, is called the discontinuity impedance. To obtain it, we have to find the inverse of a matrix. But an excellent approximation is often used: evanescent modes in the small pipe are ignored ($\boldsymbol{P}_1' = \boldsymbol{U}_1' = 0$), and thus at the discontinuity the pressure field is plane, which yields

$$Z_d = {}^t\boldsymbol{f}\mathbb{Z}_2'\boldsymbol{f}, \tag{7.160}$$

This gives the single infinite series, and is the well-known plane piston approximation.[33] It is best when the guide 1 is small. However, when the guide 1 is not

[33]The approximation of the plane piston can be generalized. We write in (7.159):

$$\mathbb{Y}_2' + {}^t\mathbb{F}'\mathbb{Y}_1'\mathbb{F}' = \mathbb{Y}_2'(\mathbb{I} + \mathbb{Q}) \text{ where } \mathbb{Q} = \mathbb{Z}_2'{}^t\mathbb{F}'\mathbb{Y}_1'\mathbb{F}',$$

and we use the Neumann series expansion, valid if the matrix norm of $\mathbb{Q}$ is less than unity $(\mathbb{I} + \mathbb{Q})^{-1} = \mathbb{I} - \mathbb{Q} + \mathbb{Q}^2 - \mathbb{Q}^3 + \ldots$ The characteristic impedances are inversely proportional to the

small, i.e., for a small discontinuity, the impedance Z_d is small, and it is not very significant to make a relatively large percentage error on a small quantity. This is the reason for the success of the approximation. The next section yields the values obtained by a numerical calculation for the cylindrical geometry. Because the matrix $\mathbb{F}$ is independent of frequency, the frequency dependence of the discontinuity impedance Z_d is related to that of the characteristic impedances. For evanescent modes, when the frequency tends to zero, these impedances are of the acoustic-mass type, i.e., proportional to $j\omega$. The discontinuity impedance is therefore an added acoustic mass: $Z_d = j\omega M_d$.

7.6.3.3 Results for a Discontinuity in Cross Section and a Diaphragm: Added Mass

We will not give further detail on calculation methods. For rectangular and cylindrical geometries, approximate results can be found in [47], which depend on frequency: indeed the characteristic impedances of evanescent modes are frequency dependent, especially near their cutoff frequency. A useful formula for cylindrical geometry, valid at lower frequencies for concentric ducts of radii R_1 and R_2, with $\alpha = R_1/R_2$, is

$$M_d R_1/\rho = 0.26164 - 0.353\alpha + 0.0809\alpha^3 + O(\alpha^5), \tag{7.161}$$

when $\alpha \leq 0.55$. When $\alpha \geq 0.55$, the following formula can be used if $\varepsilon = 1 - \alpha$:

$$M_d R_1/\rho = 4\varepsilon^2\pi^{-2}\left[-0.49198\ln(\varepsilon) + 0.50349 - 0.376246\varepsilon^2 - 0.852222\varepsilon^2\ln(\varepsilon)\right] \tag{7.162}$$

Regarding the approximation of the plane piston, when $\alpha \leq 0.55$ we have

$$M_d R_1/\rho = 8/3\pi^2 - 0.3525\alpha + 0.0643\alpha^3 + O(\alpha^5). \tag{7.163}$$

These formulas are valid both for an enlargement and a constriction. For a diaphragm without thickness, which can be seen as a double discontinuity, we can also use modal matching, but paying attention to some subtleties. Of course the approximation of the plane piston is the same, apart from a factor 2. The exact result was obtained using an analytical method by Fock [31]:

$$M_d R_1/\rho = 2\left[0.25 - 0.3523\alpha + 0.0848\alpha^3 + O(\alpha^5)\right]. \tag{7.164}$$

sections, so $\mathbb{Q}$ is proportional to S_1/S_2: intuitively, we therefore understand that the convergence is even better when this ratio is small. The plane piston approximation is the zeroth order of the expansion.

The similarity of these results can be explained by utilization of variational principles, example of which is the method due to Rayleigh (see [68]).[34] We note that the acoustic mass is always of the order of magnitude of the planar mode in the small waveguide, extended with a length equal to the radius: $\rho R_1/S_1 = \rho/(\pi R_1)$. In this regard, we often write $M_d = \rho\Delta\ell/S_1$, where $\Delta\ell$ is called length correction, as is done for the acoustic mass of radiation in infinite space.[35]

However, this notion of length correction needs to be discussed. Suppose that the planar mode in the guide 2 has an input impedance equal to Z_2. According to (7.158), the output impedance of the guide 1, near the left side of the discontinuity is: $Z_1 = Z_2 + j\omega M_d$. If the discontinuity plays exactly the role of a length correction to the guide 2, we must find, using the reduced impedance formula:

$$\frac{Z_1 S_1}{\rho c} = \frac{j \tan k\Delta\ell + Z_2 S_1/(\rho c)}{1 + (Z_2 S_1/(\rho c)) j \tan k\Delta\ell}. \tag{7.165}$$

If $k\Delta\ell$ is small, in addition to $Z_2 S_1/(\rho c)$, we do obtain $j\omega M_d = j\rho c k\Delta\ell/S_1$, and so, for a strong discontinuity (7.163): $\Delta\ell = 0.26164\pi R_1 \simeq 0.822 R_1$. This concept of length correction is of great practical interest,[36] but we see that here it is only valid if Z_2 is not too large compared to the characteristic impedance of the small tube, which may not be the case if the large tube 2 presents resonances at its input. It is worth noting this when incorporating the length correction in the length of the small tube, as we did earlier in this chapter, more or less explicitly[37]! Notice that when the frequency increases, the mass M_d increases up to a very high value at the cutoff frequency of the first higher mode, which produces a kind of transverse resonance. However, the nature of this resonance is very different from a classical resonance of a single-degree-of-freedom oscillator, especially since the M_d value is finite, even when there are no losses.

In conclusion, for the assessment of orders of magnitude, we can say that the effect of the acoustic mass is a simple length correction of the small pipe, such as $\Delta\ell = 0.822 R_1$ for a strong cross section discontinuity (and $\Delta\ell = 0.85 R_1 = 8R_1/3\pi$ for the plane piston approximation). These values were already given by

[34] The value of 0.25 for a zero-thickness diaphragm instead of 0.26164 for a discontinuity reveals the (weak) interaction effect between the input and output of the diaphragm. This interaction is that of decreasing and increasing evanescent modes in the diaphragm, when the latter has a very small thickness.

[35] When the radius R_2 tends to infinity, the discontinuity mass is the same as that of the low frequency radiation, provided that the pipe radiates in an infinite screen. The case of tube radiation is covered in Chap. 12.

[36] We can also mention that we could have chosen to find a length correction for guide 2, assuming that the input impedance of guide 1 is not too large. If we label it $\Delta\ell^{(2)}$, where obviously $\Delta\ell^{(2)} = \Delta\ell S_2/S_1$, we see that it has a more complicated relationship with the radii, particularly for large discontinuities, where $\Delta\ell$ is simply proportional to the radius of the small guide.

[37] A simple way to summarize the discussion is as follows: a short length of pipe corresponds to the effects of a mass and a spring. Assimilating a mass added to a length correction therefore yields the addition of a spring that does not exist.

Rayleigh for a pipe radiating into an infinite flange. For a numerical calculation, however, it is better not to use the length correction approximation, but rather to use an added mass in series with the input impedance of Pipe 2 [Eq. (7.158)].

7.6.3.4 Linear Model of a Helmholtz Resonator: An Attempt of Overview

We have treated the Helmholtz resonator in several places. Let us try to give an overview, because now we do have almost all the ingredients for a satisfactory model, at least in a linear regime. From a geometrical point of view, it is the assembly of a cavity and a neck. As explained in Sect. 7.3.1 (when both elements are cylindrical), the first resonance is such that the corresponding wavelength is large compared to the dimensions: this essential property could be the definition of a Helmholtz resonator, as the expression "resonant acoustic circuit with lumped elements." A condition for achieving this property relates to the discontinuity in cross section between cavity and neck: it must be strong (see Sect. 7.3.1).
The resonator can be excited by two types of sources [See Chap. 1, Eq. (1.156)]. We still have to describe as precisely as possible the acoustic elements that compose it. The acoustic compliance C_a is very simple, since it is given by the volume of the cavity. More complicated is the value of the acoustic-mass M_a. It can be written as the sum of:

- the mass of the planar mode in the neck, given by Eq. (7.55):

$$M_p = \rho \int_{\text{neck}} S^{-1}(x)dx\,; \tag{7.166}$$

- the mass of the internal discontinuity, which is roughly:
  $M_{\text{int}} = 0.26\rho/R_{\text{int}} = 0.82\rho R_{\text{int}}/S_{\text{int}}$, if the cavity/neck discontinuity is strong, where R_{int} is the radius of the neck on the side of the cavity;
- the radiation mass, which is roughly:
  $M_{\text{ext}} = 0.19\rho/R_{\text{ext}} = 0.61R_{\text{ext}}/S_{\text{ext}}$, if the neck has no thickness, or $M_{\text{ext}} = 0.26\rho/R_{\text{ext}}$ if the neck radiates into a thick flange (we will be more precise when considering radiation).

These expressions are often used as length corrections and apply to cylindrical ducts; for other geometries, a simple approximation is to calculate the equivalent radii. If the neck is very short, the total mass slightly decreases because of the interaction between input and output [see Eq. (7.164)]. Finally, when there are several necks, which is the case of an ocarina, we just consider that they are in parallel, so if they are identical, the equivalent mass is the mass of a neck divided by the number. However, the internal and radiation masses can be modified by the interaction between the necks. For instance, considering the case of two identical necks side by side, the mass M_{int} is inversely proportional not to the surface, but to

the square root of it. In practice, one can consider that the interaction is negligible when the distance between two necks is much greater than their radius.[38]

We still have to consider dissipation: as the neck is much narrower than the cavity, dissipation is preponderant in it, and because the inertial effect is predominant in the neck, we just add a resistance in series with the mass M_a . Its value is given by Eq. (5.143) with an integration over the length of the neck:

$$R_v = \rho c \sqrt{\frac{2\omega \ell_v}{c}} \int_{\text{neck}} S(x)^{-1} R(x)^{-1} dx. \tag{7.167}$$

Finally at high amplitudes, nonlinear effects can appear in the neck (Fig. 7.21). They are discussed in Chap. 8.

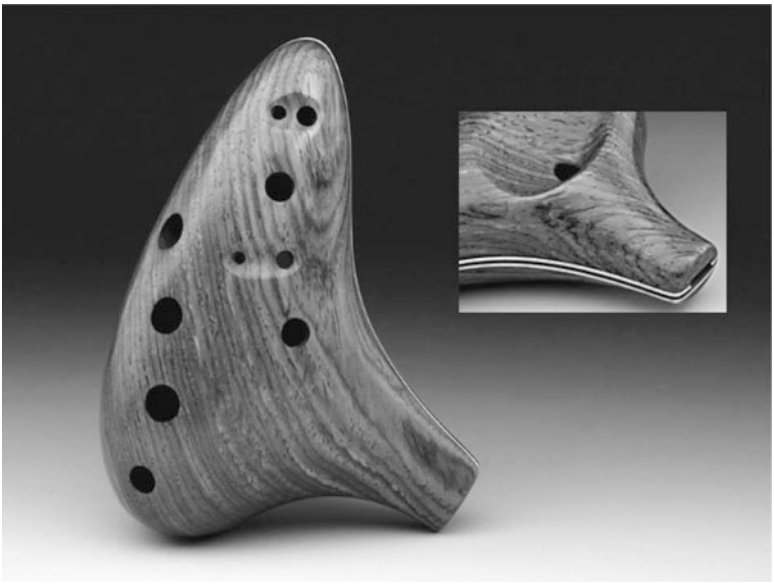

Fig. 7.21 The ocarina is a flute made of a Helmholtz resonator with several holes. Different notes are obtained by closing of one or more holes. (Instrument made by Charlie Hind, South Carolina, United States, www.hindocarina.com)

[38]We can refine the effect of the compliance and mass using continued fraction expansions (Sect. 7.5.2.1). Let us take the example of a cylindrical cavity of length ℓ and of section S. Its resonance frequency is given by $\rho c S^{-1} \cot k\ell = \omega M_a$. We can always write $M_a = \rho L_a / S_{\text{int}}$, where L_a is a length. Expanding the function $\cot k\ell$ to the third order, the approximate solution is written:

$$k\ell = 1/\sqrt{\frac{SL_a}{S_{\text{int}}\ell} + \frac{1}{3}}.$$

7.6.3.5 Discussion About the Validity of the Horn Equation: Exact Methods

The error made when assuming continuity of the average pressure at a cross section discontinuity is due to ignoring the acoustic mass. It is the same kind of error as the one made for the horn equation when we indicate plane wave matching. Indeed if we consider a horn as a series of stepped cylinders whose length tends to zero, an exact representation must take the mass associated with the discontinuity into account. In fact since the length tends to zero, the masses of two successive discontinuities interact: we cannot treat a discontinuity as if it was far from another (as it was our hypothesis in stating that the evanescent modes were terminated on their characteristic impedance). A formulation exhibiting this approximation was performed by the method of matched asymptotic expansion [73].

It is possible to find an exact modal formulation based on segmentation into cylinder sections, provided that we do not make the assumption of average pressure continuity: the calculation is done numerically by truncating the number of evanescent modes [66]. Instead of projecting scalar impedances, an impedance matrix is defined whose order is the number of modes considered, and then a Riccati matrix equation is solved. It is shown that taking into account a single evanescent mode can satisfy the condition of a zero velocity perpendicular to the wall (which is not horizontal) and to approach the exact result. This numerical method is of course in competition with all the discretization methods, such as the boundary elements method. It can also be coupled with the numerical calculation of radiation [5]; a great difficulty for understanding the validity of the horn equation arises because the radiation impedance is not known except in the simplest cases.

Another approach to solve the problem of horns is to find a coordinate system appropriate to yield a one-dimensional equation. For a truncated cone, the exact solution of the wave equation is based on spherical waves. We can look for other geometries for which an exact solution exists [70], using the mathematical results on separable coordinate systems. One can also seek a coordinate system that approximately satisfies the sound equation [36, 38, 56] or try to solve the problem by matching spherical waves [3, 10, 62].

Finally, it is interesting to know what the validity condition is for the horn equation based on plane waves. For a cone, a condition is that the phase shift between a planar wavefront (which is approximate) and the spherical wavefront (which is exact) should be small compared to the wavelength. This is written, using the notations of Sect. 7.4.2: $k(R_2 - R_1)^2/\ell \ll 1$. If this result is integrated for any horn shape by writing $\ell = dx$, $R_1 = R(x)$, $R_2 = R(x + dx)$, the equation yields

$$\frac{1}{2}\int_0^\ell kR'^2(x)dx \ll 1. \tag{7.168}$$

This condition, though very approximate, seems quite satisfactory for instruments like the trombone (the validity limit being 750 Hz), as shown by the comparison between experiment and theory for the input impedance [20] (see also [29, 38]).

7.7 Generalized Junction of Waveguides: Application to Toneholes

7.7.1 Overview

After considering a simple junction of two guides, we go one step further in the generalization, to treat the case of toneholes, fundamental elements of the instruments called "woodwind instruments." Toneholes can be seen as small ducts, and therefore we consider a junction between three guides. We could start as for chimney pipes through intuitive results with conservation of flow rate in a small junction volume where the pressure is uniform, and we could then apply a length correction to the small pipe of the hole towards its junction with the main pipe (the other end of the pipe being described by a radiation impedance). Many results could then be shown, but in fact the problem of side holes is a little more complicated. We prefer using a more complete theory, taking into account the three-dimensional effects, without giving all the milestones.

Let us consider any junction between n guides (see Fig. 7.22 for $n = 3$). We set straight pipe sections as close as possible to the junction, on which the expansion of the field in duct modes is possible. What follows is also valid away from the connection, but it is better to choose a connection volume as small as possible, with dimensions small compared to the wavelength. The straight sections of pipe, as well as the rigid walls of the connection, define a volume V bounded by a total surface S. The system is a multi-port with n infinities of ports. The calculation is based upon the same steps we used for two ducts:

1. Modal expansion for each duct;
2. Connection of all the modes [see Eqs. (7.151) and (7.152)] defining a super-matrix of n infinities of dimensions; for two pipes, there is a transfer matrix (7.153), but in general it is more convenient to seek an impedance matrix

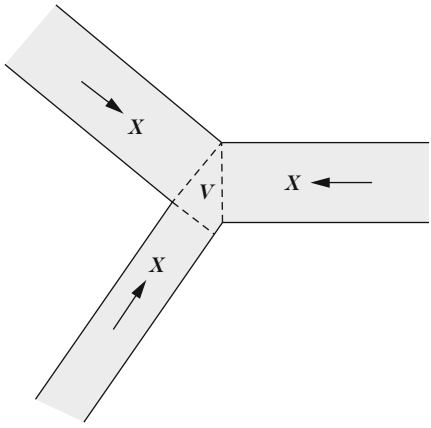

Fig. 7.22 Example of junction of several guides. For each of them, we know a cross section beyond which there is a straight duct, and the orientation of abscissa X is chosen towards the junction. A tonehole is a special case of a junction between three guides. V is the volume of the cavity of the junction

linking the vectors $\boldsymbol{P}_i$ to vectors $\boldsymbol{U}_i$ (in the case of a cross section discontinuity, such a matrix does not exist: it would have infinite elements, because the transfer matrix has two zero elements).

3. The impedances of all evanescent modes are set equal to the characteristic impedances, provided that the junction is not close to another discontinuity in one of the guides, assuming that each guide has a length greater than its transverse dimensions;
4. Separation of the propagating modes from evanescent, and reduction of the super-matrix impedance to a matrix with a finite number of ports. The number corresponds to that of the propagating modes in each of the guides. So at least n ports are considered if there are n guides with perfectly reflecting walls, since the planar mode exists in each of them.

The difference with the previously studied case lies in the second step: since there is no common surface where one can perform the modal decomposition corresponding to different guides, one should use an integral equation (that we will write in Chap. 12) involving an appropriate three-dimensional Green's function. Details can be found in [48]. We decompose the Green's function according to increasing frequencies,[39] and we obtain the following final result, written for the case of three guides, generalizing Eq. (7.158):

$$\begin{pmatrix} p_1 \\ p_2 \\ p_3 \end{pmatrix} = \left[\frac{\rho c^2}{j\omega V} \begin{pmatrix} 1 & 1 & 1 \\ 1 & 1 & 1 \\ 1 & 1 & 1 \end{pmatrix} + j\omega \begin{pmatrix} M_{11} & M_{12} & M_{13} \\ M_{21} & M_{22} & M_{23} \\ M_{31} & M_{32} & M_{33} \end{pmatrix} + O(\omega^3) \right] \begin{pmatrix} u_1 \\ u_2 \\ u_3 \end{pmatrix} \tag{7.169}$$

where p_i and u_i are the pressure and flow rate going out of the guides into the cavity (for the planar mode of the guide i). We denote the second matrix by $\mathbb{M}$ (multiplied by $j\omega$). The first two terms of this expansion are particularly interesting:

- The first term is the approximation valid at the lowest frequencies. The pressure is uniform across the junction and the flow rate is conserved (the pressure uniformity yields the flow conservation, see Chap. 1). This term is also the result we would have for a compressible but massless gas, since the matrix $\mathbb{M}$ is proportional to ρ;
- the second term corresponds to the inertial effects. The Green's function symmetry leads to the symmetry of the matrix $\mathbb{M}$ (reciprocity). The matrix $\mathbb{M}$ does not depend on frequency.

In general the above scheme is not a calculation method because the Green's function of the cavity is not known. This is only a proof of the impedance matrix

[39] In the case where we can use a Green's function expanded in the modes of the cavity volume V, we can get an idea of the method. The shape of this function is given by (4.52), replacing the simple sum by a triple sum. The expansion can be done on the increasing frequencies: the term of lowest order is in brackets, corresponding to the uniform mode of the cavity, which explains the simplicity of the first term of Eq. (7.169).

shape for a general junction. How can the result for a cross section discontinuity, studied in detail in the previous section, be deduced? This is a special case where the junction volume can be chosen as zero. It follows that the compliance corresponding to the first term of the expansion vanishes, therefore, in order for the pressure to be finite, the sum of the flow rates $u_1 + u_2 + u_3$ needs to vanish. This gives a new equation, which replaces one of the three Eqs. (7.169). We must rewrite the two others by subtracting Eq. (7.169) two by two, which gives, for example:

$$u_1 + u_2 + u_3 = 0$$

$$\begin{pmatrix} p_1 - p_3 \\ p_2 - p_3 \end{pmatrix} = j\omega \begin{pmatrix} M_{11} - M_{31} & M_{12} - M_{32} & M_{13} - M_{33} \\ M_{21} - M_{31} & M_{22} - M_{32} & M_{23} - M_{33} \end{pmatrix} \begin{pmatrix} u_1 \\ u_2 \\ u_3 \end{pmatrix}. \quad (7.170)$$

Using the zero sum of the flow rates, we see that the mass matrix has only three independent elements, instead of 6 in the general formulation.[40] In the case of a cross section discontinuity, Eq. (7.170), written for two guides only, this can be simplified as:

$$p_1 - p_2 = j\omega \left[(M_{11} - M_{21}) - (M_{12} - M_{22}) \right] u_1 \; ; \quad u_1 = -u_2 \; . \quad (7.171)$$

As a consequence there is a single term of acoustic mass to calculate, and this is consistent with the result (7.158).

7.7.2 Two Waveguides Converging Into a Third

Now consider the case of two guides converging into a third, without junction volume (see Fig. 7.23). By eliminating u_3, Eq. (7.170) can be written as follows:

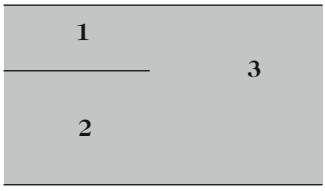

Fig. 7.23 Two waveguides converging into a third

[40] This simplification can be applied to a cavity of zero volume, but also to an incompressible fluid. The various elements of the new mass matrix can be calculated using the incompressible fluid approximation simply verifying the Laplace equation. In particular for two-dimensional geometry, this allows the conformal mapping technique to be used in different termination cases to obtain the various terms of the matrix [17, 49].

$$\begin{pmatrix} p_1 - p_3 \\ p_2 - p_3 \end{pmatrix} = j\omega \begin{pmatrix} m_{11} & m_{12} \\ m_{21} & m_{22} \end{pmatrix} \begin{pmatrix} u_1 \\ u_2 \end{pmatrix} \tag{7.172}$$

$$u_3 = -u_1 - u_2 \,.$$

where the relationship between the masses m and masses M is easy to determine. Thus, $m_{12} = M_{33} - M_{13} + M_{12} - M_{32} = M_{33} - M_{23} + M_{21} - M_{31} = m_{21}$. The two masses are equal because of reciprocity. We therefore can write

$$p_1 - p_3 = j\omega \left[(m_{11} - m_{12})u_1 - m_{12}u_3 \right],$$

and a similar relationship for $p_2 - p_3$, or

$$p_1 - j\omega(m_{11} - m_{12})u_1 = p_3 - j\omega m_{12}u_3 = p_2 - j\omega(m_{22} - m_{12})u_2 \,. \tag{7.173}$$

This expression is interpreted as follows: in addition to the flow rate conservation, the pressure are equal, up to the length corrections, corresponding to the masses $(m_{11} - m_{12})$ for guide 1, $(m_{22} - m_{12})$ for guide 2, and m_{12} for guide 3. For instance, for the guide 1, we obtain $\rho \Delta \ell_1 / S_1 = m_{11} - m_{12}$. It can be shown that it is sufficient to offset the guides junction by $\Delta \ell_1$ in order to write the pressure continuity, which generalizes the length correction notion for a cross section discontinuity. Such a problem is a schematization of the U-shaped pipe encountered in the boot of a bassoon of French type, to connect the ascending and descending branches of the instrument (if the taper of the branches is ignored).

7.7.3 Right-Angle Bends

Now consider another configuration: that of a right-angle bend (see Fig. 7.24). The matching volume $V = \ell S_1$ a priori is not zero, and we must use the expressions (7.169). However it can be shown quite generally that it is possible to use a zero matching volume, leading to much simpler expressions, of type (7.171). We demonstrate this here within the low frequency approximation. Suppose that the surface of guide 1 defining the junction volume is extended from $x = -\ell$ to the vertical wall $x = 0$, so that this volume vanishes. In principle it is not possible to use our general result, because the modal expansion in guide 1 is not valid in the extension of the volume V, since there is no wall. Nevertheless it is possible, by using the quantities (p_1, u_1) known at the entrance of volume V $(x = -\ell)$ as a function of (p_2, u_2), to determine the values (p_1', u_1') which are at the other end of this volume $(x = 0)$, and which would correspond to the plane propagation over the length ℓ. These are quantities whose physical meaning is not direct, but which are then used to calculate the planar mode in guide 1 as we would have

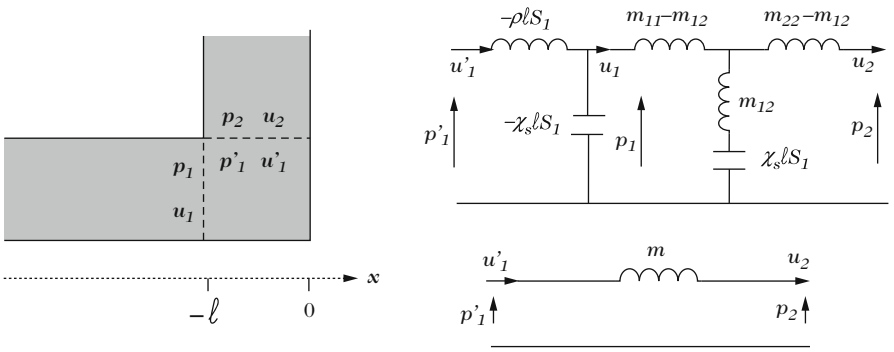

Fig. 7.24 Geometry of a bend; equivalent electrical circuit (see Fig. 7.23), and its approximation with a zero matching volume

done with (p_1, u_1), but for another abscissa. If the length ℓ is small compared to the wavelength, the transfer of values (p'_1, u'_1) to (p_1, u_1) is done by using an acoustic mass in series, $\rho\ell/S_1$ and an acoustic compliance, $\chi_s \ell S_1$:

$$p'_1 = p_1 - j\omega\rho\ell S_1^{-1} u_1 \; ; \quad u'_1 = u_1 - j\omega\chi_s \ell S_1 p_1.$$

For the proof, one can calculate the transfer matrix equivalent to the relation (7.169) reduced to two guides and then multiply the transfer matrix with the one we just found: this allows us to verify that the compressibility effect disappears at the same order in the frequency expansion.

However, this type of calculation is cumbersome, despite the simplicity of its principle, and it is more convenient to use an equivalent circuit diagram, as shown in Fig. 7.24. We can move the branch where the compliance is to the other side of the mass $m_{11} - m_{12}$: to invert an impedance in series and an admittance in parallel, it is sufficient that their product is much lower than unity. At low frequencies, this is verified by the product $j\omega\chi_s\ell S_1 j\omega(m_{11} - m_{12})$. Then we can calculate the admittance sum for the two adjacent branches in parallel, one with $-\chi_s\ell S_1$ and one with $\chi_s\ell S_1$, which is in series with the mass m_{12}. This sum yields a term featuring ω^3, that we ignore, and therefore the two branches disappear. Finally, we obtain a result with a simple acoustic mass in series for the junction:

$$\begin{aligned} p'_1 - p_2 &= j\omega m\, u \\ u'_1 &= -u_2 = u, \end{aligned} \tag{7.174}$$

where $m = -\rho\ell/S_1 + m_{11} - m_{12} + m_{22} - m_{12}$. This result greatly simplifies the description of such a junction, since there is only one mass to determine, for example, with the incompressibility hypothesis. The calculation of the right-angle bend effect can be done by calculating the planar mode on the vertical wall $x = 0$, and taking into account a single acoustic mass, which may be viewed as a length

correction, either for guide 1 or guide 2. Of course the same treatment is possible by extending the planar mode of waveguide 2 instead of that of waveguide 1. Values of m are given in the next section, since it is twice the mass m_s of a side hole. Other types of bends have been studied with other methods [61] and also give rise to added masses.

7.7.4 Bends in Cylindrical Tubes

The effect of bends is rather weak, but it cannot be ignored. It is often encountered in brass instruments, as well as in saxophones or bass clarinets. As explained above, at low frequencies a right angle acts as an added acoustic mass. For a bend in a cylindrical tube, the effect is also of inertial type, modifying the density ρ, which becomes ρ_{eff}. The effect on compressibility is weak. But the effect on the density is frequency dependent and distributed over the length of the bend. It is equivalent to a temperature increase at low frequencies and a temperature decrease at high frequencies. Recent works have allowed the determination of an approximate formula which is very satisfactory (see [30]).

We denote R_0 the radius of curvature and a the radius of the cylinder, with $K = a/R_0$. The formula is as follows:

$$\frac{\rho_{\text{eff}}}{\rho} = 1 + \beta^2 K^2 + \frac{1}{2}\left[\sqrt{\left(\frac{\gamma_{10}}{ka}\right)^4 - 8\beta^2 K^2\left[\left(\frac{\gamma_{10}}{ka}\right)^2 - 2\right]} - \left(\frac{\gamma_{10}}{ka}\right)^2\right] \tag{7.175}$$

with $k = \omega/c$, $\gamma_{10} = 1.8412$ and

$$\beta = \frac{1}{\gamma_{10}}\sqrt{\frac{2}{\gamma_{10}^2 - 1}} \simeq 0.5. \tag{7.176}$$

The effect vanishes for $\rho_{\text{eff}} = \rho$, or:

$$f = \frac{\gamma_{10}}{4\pi a} c\sqrt{1 - \frac{\beta^2 K^2}{4}}. \tag{7.177}$$

The sound speed c_{eff} is equal to $c\sqrt{\rho/\rho_{\text{eff}}}$ and the bent tube is equivalent to a straight tube with a modified wavenumber k_{eff} and a characteristic impedance Z_{eff} given by:

$$\frac{k_{\text{eff}}}{k} = \frac{Z_{\text{eff}}}{Z_c} = \sqrt{\frac{\rho_{\text{eff}}}{\rho}}. \tag{7.178}$$

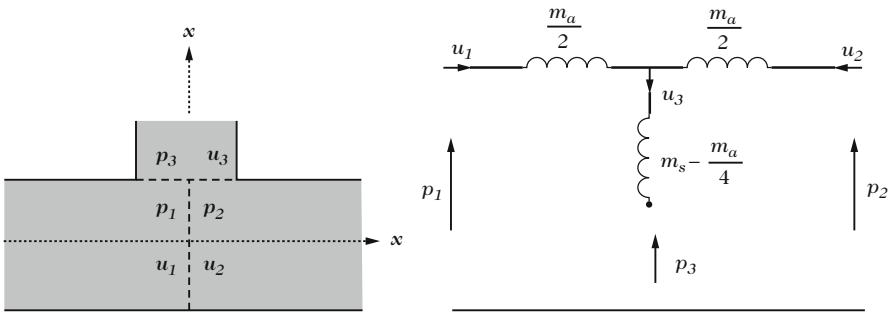

Fig. 7.25 Tonehole on a cylindrical pipe, and electrical circuit equivalent to an open hole at low frequencies. The field is matched at the median plan of the hole, with a zero matching volume (at least in rectangular geometry). For the circular geometry, a and b are the radii of the main duct and the hole, respectively, h the height of the chimney, $S_1 = S_2 = S = \pi a^2$; $S_3 = \pi b^2$

7.7.5 Toneholes and Derivations

7.7.5.1 General Model

Now consider the problem of toneholes (see Fig. 7.25). We generalize, without proof, what we wrote concerning right-angle bends. The modes of the main pipe, calculated on the median plane of the hole (assumed to be symmetrical; for a non-symmetrical hole, see [27]), can be linked to the planar mode in the pipe made by the hole, which is called the *chimney*. This is again a *3 port*. If the main pipe is rectangular, its upper wall perpendicularly intersects the chimney in a surface where we can decompose the field into modes of the chimney: the matching volume is zero, which is a strong simplification. However, in the most common case, the main pipe and the chimney are cylindrical, and the matching surface has a saddle shape: if we cut the hole chimney as close as possible to the pipe, we will still have a very small matching volume, with a complex shape.

We will first ignore this problem. If index 3 is assigned to the chimney, and subscripts 1 and 2 to the two sides of the hole axis, Eq. (7.172) apply. By choosing the outgoing axis (rather than the incoming one) for the hole chimney, we have: $u_1 + u_2 = u_3$. The hole being symmetrical, it is deduced that: $m_{11} = m_{22}$. Expressing u_1 and u_2 as a function of their half-difference and half-sum, the first two equations can be rewritten as:

$$\begin{aligned} p_1 - p_3 &= \frac{1}{4} j\omega m_a (u_1 - u_2) + j\omega m_s (u_1 + u_2) \\ p_2 - p_3 &= \frac{1}{4} j\omega m_a (u_2 - u_1) + j\omega m_s (u_1 + u_2) \end{aligned} \tag{7.179}$$

where $m_a = 2(m_{11} - m_{12})$ and $m_s = (m_{11} + m_{12})/2$. Notations m_a and m_s are

chosen to be consistent with existing literature. This shows the contributions of the anti-symmetric and symmetrical velocity field, in the midplane of the hole (taking care not to confuse the symmetry of the geometry and that of the field!).

- When the field is anti-symmetric, we have $u_1 = -u_2$, and u_3 vanishes (there cannot be any flow rate in the chimney), and the element m_a is characteristic of the anti-symmetric field. This corresponds to the interaction of anti-symmetric modes in the chimney with the modes of the main pipe. But, in the chimney, the planar mode is symmetrical, so if we seek an approximation similar to that of the plane piston, we will not find this element. As for a discontinuity between a small pipe (here the hole) and a larger pipe, the planar piston approximation is quite satisfactory, therefore it is expected that m_a is small.
- When the field is symmetrical, $u_1 = u_2 = u_3/2$, and the important element is m_s. This corresponds to the interaction of symmetrical modes in the chimney, including the planar one, with the modes of the main pipe. We will see that it acts as a length correction to the chimney, and we expect it to be of the order of magnitude of the radius of the hole.

When calculating the elements using a modal method, the elements m_a and m_s are found, separately. A numerical approximation of these elements is given below. An electrical circuit equivalent to a hole is given in Fig. 7.25. This corresponds to Eq. (7.173), that are written here as:

$$p_1 - j\omega u_1 m_a/2 = p_2 - j\omega u_2 m_a/2 = [Z_3 + j\omega m_{12}]\,(u_1 + u_2), \tag{7.180}$$

where $m_{12} = m_s - m_a/4$ and $Z_3 = p_3/u_3$. These various representations have the disadvantage of not directly revealing the pressure-flow rate duality. However, this duality is clearly exhibited if we write (7.179) as:

$$\begin{aligned} p_1 - p_2 &= \frac{1}{2} Z_a (u_1 - u_2) \\ p_1 + p_2 &= 2(Z_s + Z_3)(u_1 + u_2), \end{aligned} \tag{7.181}$$

where $Z_a = j\omega m_a$ and $Z_s = j\omega m_s$. In doing so, we reduced the three-port to a two-port device, replacing the chimney with a known impedance. The known impedance is the chimney input impedance, Z_3, which depends on the termination, either open or closed.

This theory assumes that the chimney of the hole is long enough for evanescent modes at the input and output (which is radiating when the hole is open) not to interfere. Actually, this is not always the case, and we can take the finite length of the chimney into account along with the type of termination (open or closed). However, the effect is not very strong, especially concerning the impedance Z_s. The following results are extracted from the publications [23, 27, 63], (see also the first article on this topic [41]), which give very similar results, valid at low frequencies,

i.e., roughly up to half of the first cutoff frequency of the main pipe ($ka = 1.8$). Below are the formulas, [for symmetry reasons, the mass m_s is half of that found for a right bend (7.174)]:

$$m_s = \rho \frac{t_s}{\pi b^2} \text{ with } \frac{t_s}{b} = 0.82 - 0.193\delta - 1.09\delta^2 + 1.27\delta^3 - 0.71\delta^4 \quad (7.182)$$

$$m_a = \rho \frac{t_a}{\pi a^2} \text{ with } \frac{t_a}{b} = [-0.37 + 0.087\delta]\,\delta^2, \quad (7.183)$$

where $\delta = b/a$ is the radius ratio (b and a are the radii of the hole and the main duct, respectively). For the case of a rectangular geometry, i.e., a rectangular hole of width b located on a rectangular duct of height a, with a common dimension denoted d, calculations by a conformal mapping gives the following results [27], if $\delta = 2b/a$:

$$m_s = \frac{\rho}{\pi d}\left[\ln\frac{1+\delta^2}{\delta} + \frac{1}{\delta}\left(1-\delta^2\right)\arctan\delta\right] \simeq \frac{\rho}{\pi d}\left[-\ln\delta + 1 - \frac{\delta^2}{3} + O(\delta^4)\right];$$

$$m_a = \frac{2\rho}{\pi d}\left[\ln\left(1+\delta^2\right) - 2\delta\arctan\delta\right] \simeq -\frac{2\rho}{\pi d}\left[\delta^2 + O(\delta^4)\right].$$

7.7.5.2 Closed Chimney

If the chimney is closed, with a length h, the impedance of the planar mode in the chimney pipe is written as:

$$Z_3 = -j\rho c S_3^{-1}\cot\left[k(h + t_w)\right], \quad (7.184)$$

where the wavenumber k may include visco-thermal effects in the chimney [see, for example, Eq. (5.147)] and t_w is the length corresponding to the matching volume between the surfaces on which the modal expansions are known. We find that the length is equal to [63]:

$$t_w = \frac{b\delta}{8}\left[1 + 0.207\delta^3\right]. \quad (7.185)$$

i) Low Frequencies

If the chimney is short, its input impedance verifies $Z_3^{-1} = j\omega V/\rho c^2$, with $V = S_3(h + t_w)$. In this case the expression (7.184) is exact since the effect of compressibility is exactly proportional to the total volume of the hole. The effect of the mass $m_s - m_a/4 = m_{12}$ in Eq. (7.180) can be neglected and we obtain a transfer matrix from the right to the left of the hole. Keeping only the terms corresponding to low frequencies, we get

$$p_1 = p_2 - j\omega m_a u_2 \; ;$$
$$u_1 = p_2 j\omega V/\rho c^2 - u_2. \tag{7.186}$$

Within the incompressibility hypothesis, only the element m_a exists, and this helps to explain why it is negative: the streamlines do not follow straight lines in the main pipe to enter the closed chimney, and therefore there is a kinetic energy decrease. In practice, for a compressible gas, the effect of compressibility of the enclosed volume is predominant, and thus should be taken into account when calculating the effect of toneholes. The effect of the negative mass is often ignored because it is very low [42]; however, it was shown that the cumulative effect of many closed holes could significantly shift the resonance frequencies [25]. The reader familiar with the use of equivalent circuits (electric or mechanical) may prefer them to equations, because they allow a more direct relative evaluation of elements.

ii) High Frequency and Rejection

When the frequency increases, the wavelength may be comparable to the height h of the chimney, and another consequence of the closed holes is the production of a filtering effect. Suppose that we have a "quarter wavelength" resonance of the chimney (very small value of Z_3, $f \simeq c/\left[4(h + t_w)\right]$), or rather that we have a resonance of the parallel branch of the circuit, $Z_3 + j\omega m_{12}$. It follows that the resonance frequency is given by ($f \simeq c/\left[4(h + t_w)\right] + \Delta\ell$), where $m_{12} = \rho\Delta\ell/S_h$ and m_{12} is equivalent to a length comparable to the magnitude of the hole radius. So if the part 1 of the main pipe is upstream and contains the source (a reed, for example), the impedance p_2/u_2 is determined by the geometry of the downstream part 2, and, necessarily, p_2 is very small. Let us calculate the impedance upstream of the hole, according to the electrical circuit of Fig. 7.25, or to Eq. (7.180), writing $Y_3' = 1/(Z_3 + j\omega m_{12})$ and $Y_2' = 1/(Z_2 + j\omega m_a/2)$, with $Z_2 = -p_2/u_2$ (the minus sign being due to the orientation in the Pipe 2):

$$Z_1 = j\omega m_a/2 + (Y_2' + Y_3')^{-1}. \tag{7.187}$$

If the admittance Y_3' becomes very large, the impedance Z_1 is small regardless of the admittance of the branch 2, which is in short circuit. Transmitted power is very low at the corresponding frequencies. This is what happens for an instrument like the bassoon: in order to allow closer finger holes to compensate for the large size of the instrument, the makers produced oblique and long chimneys, of about 4 cm in length. This results a rejection in the emitted sound spectrum around 2000 Hz. This frequency belongs to the more sensitive range for the ear. The rejection is all the more marked when there are many closed chimneys, and disappears for note F#3, obtained when all holes are open, as seen on the spectrogram of Fig. 7.26. Thus there is an "anti-formant," i.e., a very attenuated frequency range whatever the note, which is a characteristic of the spectrum of this instrument.

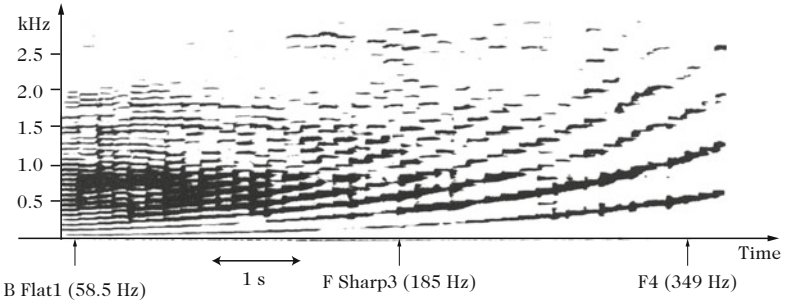

Fig. 7.26 Spectrogram of a chromatic scale of a bassoon (three reference times corresponding to $B\flat 1$, F#3, and F4 are indicated). The abscissa is time and the ordinate is frequency. It can be noticed that there is a hole in the spectrum around 2000 Hz produced by the quarter wavelength resonance of the closed tonehole chimneys. This is an anti-formant. For note F#3, in the middle of the range, all holes are open, and we note that there is no rejection

iii) Mutes

The principle of brass mutes is first to limit the radiation by limiting the output surface of the bell. The most common mute, called the "straight" mute, is a closed truncated cone [77], which has some input admittance maxima in the frequency range of the spectrum, typically between 1000 and 5000 Hz. As for the closed chimney above, the duct formed by the remaining space between the bell and the mute is in parallel with the mute itself. There is therefore a rejection in the spectrum of the radiated sound, which is highly modified. For low frequencies, the mute should be designed so as not to change the input impedance too much, so as not to disturb the production of sound.

7.7.5.3 Open Chimney

When they are open, the chimneys have of course their key role, for which they are designed: to change the pitch. A rejection phenomenon exists also, but for a half-wavelength resonance, since the extremity of the hole radiates, and thus this happens at frequencies around two times higher than when chimneys are closed. For an open hole,[41] the input impedance of the chimney is: $Z_3 \simeq j\rho c S_3^{-1} \tan\left[k(h + t_w + \Delta\ell_{\text{ray}})\right]$). In general this phenomenon is not very important, and moreover, the rejection is effective for the sound radiated by the main pipe, but

[41]The calculation is similar to that of a closed pipe [See. Eq. (7.184)]. Here, we focus on the resonance frequencies, and therefore ignore the real part of the radiation impedance.

the hole itself radiates[42]! When a quarter wavelength matches the effective length of the pipe, Z_3 goes to infinity and thus the open hole behaves like a closed wall. The behavior at low frequencies is essential. It can be shown that the effect of the "anti-symmetric" masses is very low [25], and the effect of an open hole is essentially the effect of a mass in parallel, which is obtained using (7.180):

$$p_1 = p_2 = (u_1 + u_2) j\omega\rho L_3/S_3, \text{ with } L_3 = h + t_w + \Delta\ell_{\text{ray}} + \Delta\ell_{\text{int}}, \tag{7.188}$$

where $\rho\Delta\ell_{\text{int}}/S_3 = m_s$. We will discuss the value of the correction due to radiation in the fourth part; the total effective length L_3 of a hole is around $h + 1.6b$. At very low frequency, the effect of the open hole is to impose a short circuit to the downstream part of the instrument (see the circuit in Fig. 7.25). The pressure value is close to zero near the location of the hole, and therefore it is as if the pipe was cut at this location. This approximation is very useful, and has been used by many makers (see, for example, [53]), and is even more satisfactory when the cross section of the hole, S_3, is large (but it is bad for the so-called register holes, see below in Sect. 7.7.5.5). A better approximation is to consider the role played by the downstream portion of the main pipe: if the main pipe with cross section S is terminated in the radiation impedance (including the radiation length correction into the total length ℓ_2 of the tube between the hole and the end), we write

$$Y_1 = Y_2 + Y_3 = -j\frac{S}{\rho c}\cot[kl_2] - j\frac{S_3}{\omega\rho L_3}. \tag{7.189}$$

We seek the length correction due to the tone hole compared to the pipe cut at the location of the hole, writing $Y_1 = S/(j\omega\rho\Delta\ell)$. This yields, using the expansion of the cotangent function:

$$\frac{1}{\Delta\ell} = \frac{1}{\ell_2(1 + k^2\ell_2^2/3)} + \frac{S_3}{SL_3}. \tag{7.190}$$

The length correction is therefore positive at lower frequencies, and it increases with frequency, because the downstream pipe plays an increasingly significant role. Two parameters are the key: the height of the chimney and the ratio of its cross section to that of the main pipe. An important consequence is that, unexpectedly for the uninitiated, the effect of a long chimney pipe is smaller than that of a short chimney! Of course, there is rarely a simple cylinder portion after a hole, since there are several holes. This issue is discussed below.

[42] Similar phenomena are encountered in connection with speech production, with the effect of the nasal tract: for producing the nasal vowels, the velum is lowered to connect the nasal and vocal tracts, thereby producing rejections in the sound radiated from the mouth.

The previous discussion applies to an open hole placed on a cylinder. On a cone, without lengthy developments, we will just be making the following observation: many phenomena that exist in a cylinder still exist in a cone provided we consider the symmetric admittance. As a tonehole essentially acts as a derivation, it has the same consequences on the symmetric admittance as on the admittance itself if there is no taper change at the location of the hole. So, basically, the valid reasoning for a hole on a cylinder remains valid for a hole on a cone.

7.7.5.4 Hole with Variable Cross Section

The holes do not always present a perfect cylindrical shape. One reason is that the instrument makers chamfer the edges to avoid any flow separation phenomena that would produce nonlinear losses (see Chap. 8). We can keep most of the results, using equivalent masses and compliances of a pipe with variable cross section to replace, at low frequencies, those of a cylinder (see Sect. 7.2.4).

7.7.5.5 Fingerings for Instruments with Toneholes

Without going into details of the making of instruments with toneholes, it is useful to give here the main principles of their construction.

- The *basis* of a baroque instrument is a diatonic scale: for each note a hole can be opened. For a given note, there are consequently, starting from the entrance of the instrument, first a number of closed holes, then a number of open holes. Semitones are obtained either by holes controlled by "closed" keys, i.e., that are closed except for a given note, or by fork fingerings[43]; or else by the use of half-holes.

  The instruments called Boehm instruments[44] have a basis of the same type, but some semitones are obtained by additional open holes, like the notes of the diatonic scale: the basis is therefore almost chromatic. Another key feature is that the Boehm instrument holes are large, and require the use of keys to be closed by the fingers.

  The instrument basis provides a given scale, e.g., C for the flute or oboe, or F for the bassoon. Some instruments are transposing, such as the saxophone, whose basis is a C-scale for the player, but actually a scale of $B\flat$ or $E\flat$ for the listener. The clarinet is also normally a transposing instrument, but as the second modes

[43]They are made by not only closing the holes upstream of the first open hole, but also by closing one or two holes downstream. The case of the recorder is typical.

[44]Theobald Boehm (1794–1881) redesigned the flute, now often called the Boehm flute, and his invention had repercussions for many "woodwind instruments," including the saxophone, invented by Adolphe Sax in 1846.

correspond to the frequency triple of the fundamental one, the basis has a longer compass, of an octave and a fifth, instead of an octave for the other instruments.

- The basis is the essence of what we call the first register, this register being defined as a set of notes whose fundamental corresponds to the first pipe mode. Thanks to *register holes*, playing the frequency set whose fundamental frequency corresponds to the second mode of the pipe is made easier. Taking the example of the Boehm flute, the basis goes from D4 to C#5, and when opening a small hole, the production of notes an octave higher than those in the basis becomes easier: this point will be discussed in Chap. 9, concerning reed instruments. In principle there should be a register hole for each note, but this is not useful, because a single hole can act for several notes, even if this imposes slight corrections in the lower octave fingering. However, saxophones have two register holes which, thanks to a mechanical system, are driven by a single key, the change from one to the other being automatic, depending on the fingering. On the bassoon, there are four register holes for an octave, including the hole located on the crook (i.e., the top of the instrument), but it is the player who directly controls them with the thumb. It is all the more remarkable that an instrument like the clarinet has a single register hole. However in order to play the twelfths of the higher notes of the first register, one instead uses the third mode (corresponding to fingerings of lower notes of the first register, but with corrections nonetheless).
- Notice that the register hole is often also used as a tonehole, and for certain instruments like the recorder, a half- closed hole (half-hole) is used as a register hole. It remains to mention two other types of holes: those of the "extension," corresponding to very low notes of the first register whose octave or twelfth are not used (this is the case for C3 and C# 3 for the Boehm flute), and those designed for trills. These correspond to a higher extension of the first register: the sound is not very good but acceptable for very fast passages like trills (it is difficult to produce trills between the last note of the first register and the first of the second one, because then alternately opening and closing all the holes would be needed).

This set of holes, either closed or open, needs to be optimized in a refined manner to obtain a satisfactory precision, even though the musician may adjust the pitch of a note using their playing parameters.

7.8 Lattice of Toneholes

When observing a quasi-cylindrical instrument with toneholes, one notices a certain regularity of the holes in their size and spacing. But when looking more precisely, we see that on a clarinet the holes away from the reed are slightly larger and more spaced, and on a Boehm flute slightly further spaced. Because the equal tempered

scale is logarithmic, we can expect to find this increase in the position of the holes[45]; concerning their diameter, it affects radiation [35], and for low notes, one can expect to have larger holes for a similar radiation. The problem of optimal position and size is actually very complex [64].

To study their effect, Benade [8] proposed to study a pipe with a tonehole lattice as an approximation of a periodic medium. To some extent, the idea of periodicity allows an interesting qualitative analysis, which remains valid under certain conditions. When a deviation exists from the exact periodicity, as noted by Benade, one can distinguish the acoustic regularity and geometric regularity, which is discussed later. For a conical instrument, the ratio of the diameter of a hole to that of the pipe at the hole location varies little. If also the chimney height remains constant, the relevant parameter of an open hole varies little on a conical instrument. This, using the idea of symmetric admittance [Eq. (7.81)], allows an analysis similar to that which follows for a cylindrical pipe.

7.8.1 Generalities About the Waves in a Periodic Medium

Let us consider a periodic lattice of symmetrical cells made of a cylinder with identical and equally spaced holes, as shown in Fig. 7.27. The length between holes is denoted $L = 2\ell$. The basic idea is that only discrete points in the lattice are considered.[46] Between two adjacent points, the field may undergo complicated variations, but we assume the variations are known.

The basic calculation is done using the transfer matrix of a cell, which is the product of three matrices: that of a cylindrical section of length ℓ, that of a hole, and

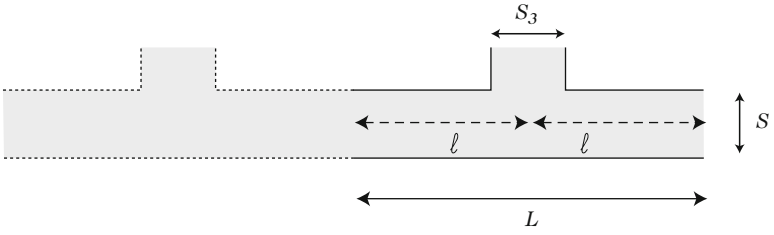

Fig. 7.27 Cell of a periodic lattice of open tone holes

[45]This reasoning is based on the first approximation of the model of a hole, which assumes equivalence with the effect of cutting the pipe where it is located, and ignores the effect of closed holes.

[46]One might just as well choose either another symmetrical cell, of length 2ℓ, ended by two half-holes or an asymmetrical cell.

that of a cylindrical section of length ℓ. We used already the products of matrices in Sect. 7.5.2.1. For the cell corresponding to the nth hole we write[47]

$$\begin{pmatrix} p_n \\ u_n \end{pmatrix} = \begin{pmatrix} A & B \\ C & D \end{pmatrix} \begin{pmatrix} p_{n+1} \\ u_{n+1} \end{pmatrix} \tag{7.191}$$

from which we derive an equation equivalent to (7.120) for two successive cells:

$$p_{n+1} + p_{n-1} = (A + D)p_n = 2Ap_n \tag{7.192}$$

(the selected cell is symmetrical, $A = D$, therefore the lattice is "symmetrical"). This equation looks like a difference equation, but the coefficient A may possibly vary in complicated ways with frequency. Using the classical theory (see, e.g., [16, 80]), we seek solutions for p_n as a superposition of two propagating waves:

$$p^{\pm} \exp(\mp n\Gamma), \text{ hence } \quad \cosh \Gamma = A \, . \tag{7.193}$$

Γ is called the propagation constant: apart from the j factor, Γ is a wavenumber, which is dimensionless. In the simplest case of a pipe without toneholes, it is: $\Gamma = 2jk\ell$. Using the transfer matrix, the characteristic admittance Y_c of the outgoing wave, such that $u_{n+1} = Y_c p_{n+1}$, is given by:

$$Y_c = \sinh \Gamma / B \, , \qquad \text{or} \tag{7.194}$$

$$Y_c^2 = \frac{A^2 - 1}{B^2} = \frac{C}{B} = \frac{C^2}{A^2 - 1}. \tag{7.195}$$

For the incoming wave, the characteristic admittance is the same (provided the reverse orientation is chosen), due to the symmetry of the cell. In what follows, limited to a lossless two-port, the coefficients A and D are real, and B and C are pure imaginary numbers (see Sect. 7.5.2.1). We deduce that:

- either $|A| < 1$: Γ is a pure imaginary number, and Y_c is real;
- or $|A| > 1$: if $A > 1$, Γ is real; if $A < -1$, Γ=real$+j\pi$. Y_c is a pure imaginary number.

This kind of behavior has been observed for modes in a duct (Sect. 7.6.1.2), which are propagating (first case) or evanescent (second case). The cutoff frequencies are given by $A = \cosh \Gamma = \pm 1$, either $\Gamma = 0$ or $j\pi$, hence $\exp(\Gamma) = \pm 1$. To study them, we can calculate the evolution of the coefficient A with frequency, or calculate the frequency values for which there is a change of sign in the square of the characteristic admittance. A more interesting method is to exploit the symmetry

[47] To multiply the transfer matrices, we use the same orientation for both ends of the two-port, u_n and u_{n+1}; we must be careful when using the results for a tonehole, obtained with the other orientation convention (see Fig. 7.25).

of the lattice ($A = D$). Using the definition (7.191), and the relation $A^2 - BC = 1$ (reciprocity), we have for the cutoff frequencies, $A = \pm 1$, hence $BC = 0$:

- either $C = 0, Y_c = 0$, so $u_n = 0\ \forall n$, and $p_n = \pm p_{n+1}$: If the pressure value is nonzero and equal at both ends of the cell, the pressure field in the cell is symmetrical; if the pressure value is nonzero and opposite at the two ends of the cell, the field pressure in the cell is anti-symmetric. In both cases the flow rate is zero at the ends.
- or $B = 0, Y_c = \infty$, therefore $p_n = 0\ \forall n$, and $u_n = \pm u_{n+1}$: because of duality, it is enough to replace the flow rate by the pressure (and vice versa) in the previous sentences.

The cutoff frequencies therefore correspond to the frequencies for which we impose Dirichlet or Neumann conditions at both ends of the cell. All this is perfectly general for a symmetrical lattice.

7.8.2 *Periodic Lattice of Open Holes*

7.8.2.1 Cutoff Frequencies

For our particular case of a pipe with toneholes, the four kinds of cutoff frequencies are

(a) If the impedance is infinite at the ends (case $C = 0$), we can deduce the impedance of both sides of the hole: on the right, $Z = -j\rho c S^{-1} \cot k\ell$. On the left, the value is the same but opposite. To use Eq. (7.181), written with a symmetrical orientation convention for the flow rates, we change the impedance sign on the right, and therefore the two impedances on both sides of the hole are: $Z = j\rho c S^{-1} \cot k\ell$. If the pressure field is symmetrical, the first Eq. (7.181) confirms that the flow rate field is symmetrical too (for this choice of orientation), and we therefore have

$$j\rho c S^{-1} \cot k\ell = 2(Z_s + Z_3) = 2j\omega m_t \text{ with } \cosh\Gamma = 1, \tag{7.196}$$

where $Z_s + Z_3 = j\omega m_t = j\omega\rho L_3/S_3$ [L_3 is the total effective length of the hole, see (7.188)]. If the pressure field is anti-symmetric, we similarly have

$$j\rho c S^{-1} \cot k\ell = Z_a/2 = j\omega m_a/2 \quad \text{with } \cosh\Gamma = -1. \tag{7.197}$$

(b) If the impedance is zero at the ends (case $B = 0$), the same type of reasoning gives the two other cases:

$$-j\rho c S^{-1} \tan k\ell = 2j\omega m_t \text{ with } \cosh\Gamma = -1. \tag{7.198}$$

$$-j\rho c S^{-1} \tan k\ell = j\omega m_a/2 \text{ with } \cosh\Gamma = 1. \tag{7.199}$$

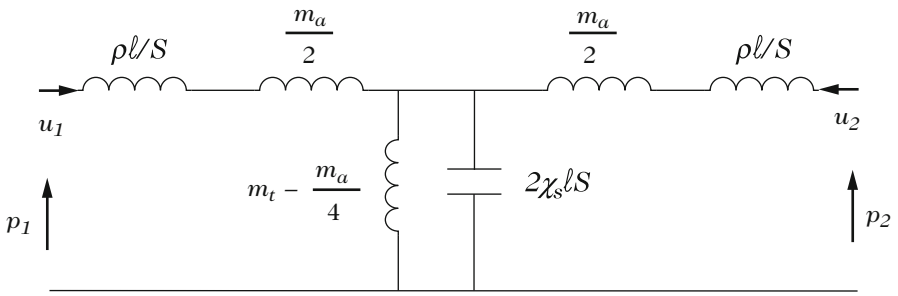

Fig. 7.28 Equivalent circuit for a cell of a periodic array of open toneholes, when the length is small compared to the wavelength. The description of the hole is given by Fig. 7.25, and the mass m_t is given by (7.196)

These equations involve one of the two masses only, either the "symmetrical" mass or the "anti-symmetric" one, but not both. This is consistent with the use of symmetry in our reasoning. To find the frequencies where the waves are propagating or evanescent, we must study the variations of $\cosh \Gamma$ with frequency, distinguishing the case of open or closed chimneys. We start with the behavior at low frequencies.

7.8.2.2 Low Frequency Behavior

At low frequencies, the length ℓ, half of the distance between two holes, is small compared to the wavelength, and we therefore have the circuit shown in Fig. 7.28. To make the following easier, we ignore the "anti-symmetric" masses, as for an isolated open hole. The hole has an admittance $1/[j\omega m_t]$, and the pipe is represented by two masses $m = \rho\ell/S$ and a compliance $C_a = 2\ell S/\left[\rho c^2\right]$. The coefficients of the transfer matrix of a cell can be written as:

$$A = D = 1 + Yj\omega m \; ; B = j\omega m(2 + Yj\omega m) \tag{7.200}$$

$$C = Y \;\text{ where } Y = j\omega C_a + 1/[\omega m_t] \; . \tag{7.201}$$

At lower frequencies, we have seen that the parallel branch has a very high admittance ($Y \simeq 1/[j\omega m_t]$); so each portion of the main pipe acts only as a mass, the effect of compressibility being negligible. We only have inertia effects, in series and in parallel, and this prohibits any wave propagation (since there is no spring effect). The coefficient $A = 1 + m/m_t$ is greater than unity. Waves are therefore evanescent: we again find that at very low frequencies, an open hole produces a strong attenuation, by strongly reflecting the energy (the phenomena considered here are without dissipation). For an infinite lattice of open holes, waves attenuate exponentially, but the effect of finite size (i.e., the existence of an exponentially

increasing wave near the end) is very low, and just two open holes are sufficient so that the amplitude at lower frequencies is negligible downstream of these holes. We will see in the fourth part what this means in terms of radiation.

To show that the lattice effect is a simple length correction, we calculate the characteristic impedance at these frequencies, using (7.194):

$$Z_c = \frac{(A^2-1)^{1/2}}{C} = j\omega m\sqrt{1+\frac{2m_t}{m}}.$$

Assuming that the lattice is infinite, Z_c is the input impedance of the array, i.e., the terminal impedance of the upstream pipe portion without open holes. It is mass-like, as for other types of evanescent waves and one can therefore set a length correction to the main pipe at the location of the first open hole:

$$\Delta\ell = \ell\sqrt{1+\frac{2L_3}{\ell}\frac{a^2}{b^2}} - \ell. \tag{7.202}$$

This result differs from that obtained for a single tonehole (7.188). At low frequencies, and apart from this length correction, it is as if the pipe was cut at the first open hole.

7.8.2.3 Pass Bands and Stop Bands

When the frequency increases, the coefficient A decreases until it reaches $+1$, at the first cutoff frequency. The remaining question is which cutoff it is, either the first given by (7.196) or the first given by (7.199): to compare the frequencies given by Eqs. (7.196)–(7.199), we can graph (as a function of frequency), the functions $\cot k\ell$ and $-\tan k\ell$; a straight line $\omega m_a/2$, having a negative slope; and a straight line $2\omega m_t$, having a positive slope. It appears that the first is a solution of (7.196), which will get our full attention in the next section. The two following frequencies, depending on the value of the slopes, are those for which $A = -1$. Actually, the function $A(\omega)$ is continuous, and after it crosses the value -1 for the first time when decreasing, it must re-cross the same value in the other direction before finding the value $A = 1$, and we can continue this reasoning further.

Considering (7.197), as m_a is very small (in absolute value), the second cutoff frequency is very close to the half-wavelength resonance of the interval between two holes ($2k\ell = \pi$). For most high-pitched instruments, this corresponds to a fairly high frequency, typically 5000 Hz. However, this is not the case of low-pitched instruments such as the bassoon or the bass clarinet.

Let us focus on the first cutoff that separates the first two frequency bands: below the first cutoff the waves are evanescent (the corresponding band is called the *stop band*, or the *forbidden band* by analogy with the problem of conduction in solids). Above the first cutoff the waves propagate (the band is called the *pass band*, or the

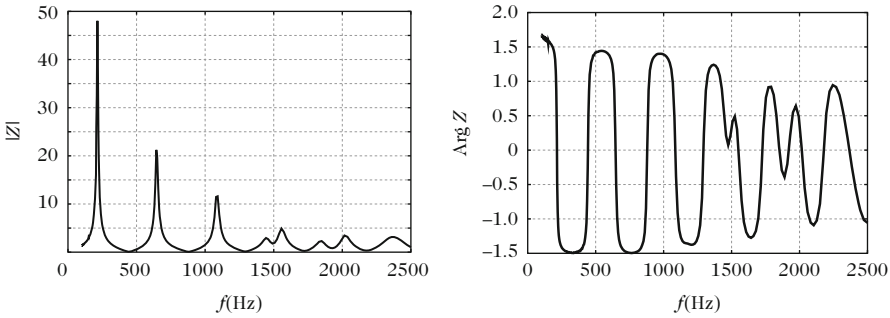

Fig. 7.29 Measured dimensionless input impedance (modulus and argument) for a clarinet, for the lower note B (corresponding to A4 440 Hz; 4 open holes). Above about 1300 Hz a significant change in behavior can be noticed, when the waves reach the end of the pipe

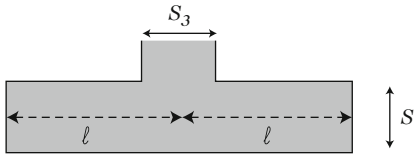

Fig. 7.30 First cutoff frequency of a periodic lattice of open toneholes: it is the eigenfrequency of the resonator formed by a cell closed at its both ends

allowed band). In the pass band, waves propagate to the end of the instrument, where they are reflected. The instrument therefore comprises two sections with different wave phase velocity v_φ: the upstream section, with no toneholes (or with closed toneholes, of fairly small influence), where the speed is the regular sound speed in tubes, and the downstream section, where the phase velocity is very large just above the cutoff, when $\Gamma = j\omega/v_\varphi$ is very small, then decreases when frequency increases. As with the case of a chimney pipe, the resonance frequencies are irregular and, as dissipation occurs over a greater length, the impedance peaks are smaller (Fig. 7.29). In fact, we see that because of radiation, they are often very small, with the impedance being close to the characteristic impedance of the pipe.

7.8.2.4 Study of the First Cutoff Frequency

The first cutoff frequency, given by (7.196), is none other than the the eigenfrequency of a cell *closed* at both ends (see Fig. 7.30). If the length ℓ is small compared to the wavelength, it is *the eigenfrequency of a Helmholtz resonator* and is

$$f_c = \frac{c}{2\pi\ell}\frac{1}{\sqrt{2(L_3/\ell)(a/b)^2 + 1/3}} \simeq \frac{c}{2\pi}\frac{b}{a}\frac{1}{\sqrt{2L_3\ell}} \tag{7.203}$$

The term $1/3$ comes from a refinement of the calculation, by expanding the cotangent function to the third order, but the second expression is often sufficient.

Notice that for a periodic lattice, the cutoff frequency shown in Fig. 7.29 *does not depend on the number of open holes*, unless there are only one or two, in which case this theory is meaningless. The cutoff frequency must be identical when measuring the input impedance for several fingerings. This can be a cause for the existence of *formants* in the sound, characteristic of the timbre independent of the note played. This also explains another essential feature of toneholes instruments: their compass. Above the cutoff, it is difficult to produce sounds at frequencies corresponding to the impedance peaks, primarily because they are very small, and secondly because the resonances are highly inharmonic. The resonance of a Helmholtz resonator is highest if:

- the neck is wide,
- the neck is short,
- the volume is small (and therefore the spacing between holes is small).

Thus an instrument designed to play a diatonic scale has a cutoff frequency lower than an instrument designed to play a chromatic scale; it is the same difference for an instrument with narrow holes compared to an instrument with wide holes, which need to be closed with keys. These two effects combine when comparing "baroque" and modern instruments, such as the recorder and the Boehm flute, respectively.

Another comparison is interesting: that of fingerings of the diatonic scale on a baroque instrument, with fingerings of the flat and sharp notes, which use forks (see Sect. 7.7.5.5): a fork means a great distance between two open holes, which produces a very low cutoff. The inhomogeneity of sound is also a feature of baroque instruments. All of this is schematic and simplified (see in particular the following section), but gives an idea of general trends (Fig. 7.31).

We also understand why it is much easier to play higher notes whose fundamental is a resonance frequency of an instrument with all finger holes closed than for the same instrument with one or more holes open. Thus for a bassoon, it is very easy to get a long harmonics series of the lowest note, $B\flat 1$, which is 59 Hz (three octaves, or eight quasi-harmonics, which are almost well tuned,[48] because the resonances are very harmonic due to the lack of open holes). On the contrary, for a fingering with many open holes, a maximum of 2 or 3 notes may be sounded, and the help of a register hole is still required, as well as small fingering adjustments to ensure fine tuning.

[48] However, these notes are not used because they are too isolated. Raising the pitch by a tone, for example, requires some complicated movements, and furthermore a register hole would still be required to completely remove the fundamental frequencies from the sound. We will discuss this issue in the third Part.

Fig. 7.31 The holes of the Boehm flute (*below*) are larger and closer together than those of the baroque flute

7.8.2.5 Deviation from Periodicity

Let us summarize and specify what we have learned on the periodic media: if a lattice is periodic, lossless, and finite, the waves either exponentially attenuate from the entrance (and grow again towards the exit), or propagate until the end where a reflection happens. When dissipation is taken into account, the cutoff frequency cannot be defined precisely (the propagation constant is always complex), but there is still a significant change in behavior around the cutoff frequency of the lossless lattice. Moreover, for the pass band, dissipation, including radiation, becomes so large that the waves are attenuated and are very weak when they reach the end. This attenuation is due to dissipation, while in the stop band, it is related to the wave reflection at the holes.[49]

However, we must try to have a less simplistic approach, since obviously the toneholes are neither identical nor equidistant.[50] Can we suppose that the ideal behavior discussed above can be generalized thanks to a concept of averaging? We will see that another interpretation holds.[51]

[49] In the latter case the attenuation is called "reactive" attenuation, which does not correspond to dissipation. This is the type used in automotive mufflers, where the aim is essentially to prevent the source from emitting power by presenting to it a purely imaginary impedance, rather than to dissipate energy.

[50] In addition there are bore deviations from perfectly cylindrical or conical shapes, and the effect of the closed holes.

[51] A general theoretical result is known for random lattices, that can be obtained by randomizing, for example, the diameters of the holes or their spacing. It has been shown that when the number of

For all notes, except those where only one or two holes are open, two frequency bands can be distinguished on the input impedance curve (see Fig. 7.29): for one band the resonances are fairly harmonic and well marked, while for the other, resonances are very inharmonic, and very slightly marked, because of dissipation due to radiation through the toneholes. Benade proposed a practical definition of the cutoff frequency using the input impedance, and showed that in practice the cutoff frequency depends very little of the played note, even for an instrument as irregular as the bassoon (the cutoff occurs around 500 Hz). This practical definition is *global* and it is not accurate, and must be distinguished from a *local* definition which would be based on the eigenfrequencies of successive cells of an almost periodic medium. For a truly periodic medium, the two definitions coincide (see Sect. 7.8.2.4). We will see that they can coincide also for a non-periodic lattice, if the lattice is composed of cells with the same eigenfrequency, provided that the cells are small compared to the wavelength.

Using the transfer matrix of a cell [Eqs. (7.200) and (7.201)], and exhibiting the cutoff frequency for which $Y = 0$, we can write

$$Y = j\omega C_a \left[1 - k_c^2/k^2\right], \tag{7.204}$$

where $k_c^{-1} = c(m_t C_a)^{1/2}$ corresponds to the approximate formula (7.203). Using $\cosh \Gamma = A = 1 + j\omega m Y$, we obtain

$$\sinh^2(\Gamma/2) = -\ell^2(k^2 - k_c^2), \tag{7.205}$$

from which :

$$\Gamma \simeq 2\ell j k_1 \text{ and } Z_c = \sqrt{\frac{B}{C}} \simeq \frac{\rho c}{S}\frac{k}{k_1}\text{, where } k_1 = \sqrt{k^2 - k_c^2}. \tag{7.206}$$

These results assume $k_1\ell \ll 1$, as well as the initial assumption $k\ell \ll 1$. The transfer matrix of our cell may ultimately be written, using (7.193) and (7.194), as follows:

$$\begin{pmatrix} A & B \\ C & D \end{pmatrix} = \begin{pmatrix} \cos(k_1 L) & Z_c j \sin(k_1 L) \\ Z_c^{-1} j \sin(k_1 L) & \cos(k_1 L) \end{pmatrix}, \tag{7.207}$$

if $L = 2\ell$. Now consider several cells with the same cutoff frequency ω_c: they have the same characteristic impedance and wavenumber. The product of the corresponding transfer matrices has the same form as that of a single matrix, by changing the length L of a cell to the total length. Thus we have generalized the behavior of a periodic medium, with a stop band followed by a pass band (for higher frequencies, the restrictive assumptions are no longer satisfied).

cells (i.e., of holes) increases to infinity, there are no longer any pass bands, all frequencies being exponentially attenuated. But in practice this result does not apply for wind instruments, because the deviation from periodicity (the "disorder") is too low.

Consequently, the global cutoff frequencies measured via the input impedance are independent of the notes, although the geometry is irregular. Two cells of different lengths must have different hole diameters to have the same cutoff frequency [see Eq. (7.203)]. It is a trend we find for the real instruments: the hole spacing increases with the distance from the entrance, and this is compensated by the hole size, which increases so that the cutoff frequency remains independent of the notes. It would certainly still remain to interpret this (coarse) observation, by examining the work of makers, who have many constraints, in particular finding the correct tuning over several registers.

In any case the assumptions necessary to have a (first) global cutoff frequency independent of the played note have been greatly expanded. This validates the theorized possibility of an acoustical regularity (at low frequency) more general than the geometrical one [58].

7.8.2.6 Toneholes and Bells

To conclude, let us compare a pipe with toneholes and a pipe ending with a bell. In both cases, above a certain frequency, resonances are strongly attenuated (see Figs. 7.16 and 7.29). However, for a "Bessel horn," the resonances below this frequency are quite regular, without being harmonics of a fundamental, while for a pipe with open holes, the resonances are harmonics of a fundamental, because at low frequencies there is very little energy in the open hole lattice.

However, a thorough analogy can be found between an open-hole periodic lattice and an *exponential* horn. Let us consider Eq. (7.9). For a particular type of horn, R''/R is a constant, and an evident analytical solution can be found. If $R'' > 0$, such horns are flared, of exponential or catenoid type (the function being a hyperbolic cosine); if $R'' < 0$ the horns are of the sinusoidal type, and if $R'' = 0$, we find a conical horn.[52]

Let us study flared horns, with positive curvature. A horn can be seen as a succession of small truncated cones whose length tends to zero (see, Sect. 7.5.2.1). Each change of taper is equivalent to a mass in parallel (see Sect. 7.4.7), as well as an open hole (when we forget the effect of the anti-symmetric mass). In order to find an analogy, the masses must be positive, and the conicity changes must be flaring. Now it is easily shown that an exponential horn is the limit, when the length tends to 0, for a horn consisting of truncated cones with the same length, and presenting taper changes with the same mass. Therefore the exponential horn is analogous to a cylindrical pipe (or tapered pipe!) drilled with identical and equidistant, open holes.

[52]Some horn shapes, which are duals of the previous ones, also give rise to an analytical solution [71], such as $(1/R)''/(1/R) =$ constant, for which the flow rate is easily calculated (see Sect. 7.2.2).

We could write this analogy in great detail, but we simply examine the solution for the exponential horn: $R(x) = R(0)\exp(mx)$. The general solution is written:

$$PR = a^+ e^{-jk_1 x} + a^- e^{jk_1 x} \text{ where } k_1 = \sqrt{k^2 - m^2}. \tag{7.208}$$

A key point is that k_1 is independent of x. The first term corresponds to an outgoing wave and the second to an incoming wave. If $k > m$, waves are propagating, while if $k < m$, the exponential functions are real, and there is a superposition of a decreasing exponential and a growing exponential (see the analogous situation of the modes in a duct, Sect. 7.6.1.2).

We can now calculate the velocity from (7.208), which satisfies

$$\widetilde{V}R = VR - \frac{1}{j\omega\rho}\frac{R'}{R}(PR) = \frac{k_1}{k\rho c}\left[a^+ e^{-jk_1 x} - a^- e^{jk_1 x}\right]. \tag{7.209}$$

Defining $Z_c = k\rho c/Sk_1$, we obtain a transfer matrix identical to (7.207) for the vector defined by the quantities PR and $S\widetilde{V}R$. The difference between the two systems lies in the difference between the velocity V and the velocity $\widetilde{V}$, which we call the "symmetric" velocity for a cone. This difference lies in the fact that the horn has a nonzero slope at the entrance. But its behavior is identical to that of the tonehole lattice with a constant cutoff frequency, and when located at the end of a cylindrical pipe, it has the same behavior. And the analogy goes quite far, because thanks to the flare, the radiation is strong above the cutoff, resulting in low and irregular peaks.

To compare the bells of brasses to acoustically regular open hole lattices, for which we noted a difference in behavior, we can compare these horns to an exponential horn. Looking at the horn equation (7.9), applied to Bessel horns [Eq. (7.110)], we might think of determining a *local* cutoff frequency defined as (see [10]):

$$k^2 = \frac{R''}{R} = \frac{\upsilon(\upsilon+1)}{(x_a - x)^2}.$$

This frequency is very low at the horn entrance, because the denominator is large, and very high at the end. We intuitively understand that for this medium the regularity is qualitatively very different from that of an exponential horn. Therefore it is very difficult to define a relationship between these local frequencies and the *global* cutoff frequency, that we can measure on the input impedance curve.[53] The problem is further complicated by the fact that the models that would be useful to us are necessarily very complicated, i.e., three-dimensional!

[53] Strictly speaking, the existence of a cutoff frequency between propagating waves and evanescent waves is a global limit property of a medium with uniform characteristics, like an exponential, infinite, and lossless horn. The only thing that is easy to show in the case of a horn of arbitrary shape, is that for the horn alone, there will be no resonance below the lowest local cutoff,

The comparison between tonehole lattices and bells, that both favor the emission of higher frequencies, also explains one of the roles of the (short) bell of a clarinet: without bell, the note for which all holes are closed may have a sound quite different from that of other notes. One way to make this note homogeneous with others is to lengthen the pipe, and to drill other holes that will always be open: this solution is encountered in some traditional instruments. Another option is flaring the pipe termination, in order to form a bell which will play the same role [11], the higher frequencies being strengthened.

Another role of this flare is to compensate for the inharmonicity of resonances. We can succeed, by various means, to make the resonances of individual notes rather harmonic, correcting the effect of open holes. In doing so we also increase the resonance inharmonicity of the lowest note, and there is a choice in terms of what to correct.

References

1. Abramowitz, M., Stegun, I.A.: Handbook of Mathematical Functions, with Formulas, Graphs, and Mathematical Tables. Dover, New York (1972)
2. Agulló, J., Barjau, A., Martínez, J.: On the time-domain description of conical bores. J. Acoust. Soc. Am. **91**(2), 1099–1105 (1992)
3. Agulló, J., Barjau, A., Keefe, D.: Acoustic propagation in flaring, axisymmetric horns: I. A new family of unidimensional solutions. Acust. Acta Acust. **85**, 278–284 (1999)
4. Amir, N., Rosenhouse, G., Shimony, U.: A discrete model for tubular acoustics systems with varying cross-section - the direct and inverse problem. Parts I and II: theory and experiments. Acustica **81**, 450–474 (1995)
5. Amir, N., Pagneux, V., Kergomard, J.: A study of wave propagation in varying cross-section waveguides by modal decomposition. Part II. Results. J. Acoust. Soc. Am. **101**(5), 2504–2517 (1997)
6. Ayers, R., Eliason, L., Mahgerefteh, D.: The conical bore in musical instruments. Am. J. Phys. **53**, 528–537 (1985)
7. Barjau, A., Gibiat, V.: Delay lines, finite differences and cellular automata: three close but different schemes for simulating acoustical propagation in 1*d* systems. Acta Acust. United Acust. **88**, 554–566 (2002)
8. Benade, A.H.: Fundamentals of Musical Acoustics. Oxford University Press, London (1976)
9. Benade, A.H.: Equivalent circuits for conical waveguides. J. Acoust. Soc. Am. **88**(5), 1764–1769 (1988)
10. Benade, A., Jansson, E.: On plane and spherical waves in horns with nonuniform flare. Acustica **31**, 80–98 (1974)
11. Benade, A.H., Kouzoupis, S.N.: The clarinet spectrum: theory and experiment. J. Acoust. Soc. Am. **83**(1), 292–304 (1988)
12. Benade, A.H., Richards, W.B.: Oboe normal mode adjustment via reed and staple proportioning. J. Acoust. Soc. Am. **73**(5), 1794–1803 (1983)
13. Béngtsson, E., Noreland, D., Berggren, M.: Shape optimization of an acoustic horn. Comput. Methods Appl. Mech. Eng. **192**, 1533–1571 (2003)

corresponding to the horn entrance [45]. But this leads to nothing more, for a Bessel horn, than Eq. (7.117)!

14. Bilbao, S., Chick, J.: Finite difference time domain simulation for the brass instrument bore. J. Acoust. Soc. Am. **134**, 3860–3871 (2013)
15. Bouasse, H.: Wind instruments. Metallic and Membranous Reeds, Reed and Flue Pipes, Organ, Instruments with Horn Mouthpiece (in French), vol. 1, 2nd edn. Librairie Scientifique et Technique, Paris (1986)
16. Brillouin, L.: Wave Propagation in Periodic Structures. Dover, New York (1953)
17. Bruggeman, J.: The propagation of low-frequency sound in a two-dimensional duct system with T joints and right angle bends: theory and experiment. J. Acoust. Soc. Am. **82**(3), 1045–1051 (1987)
18. Bruneau, M.: Fundamentals of Acoustics. Wiley-ISTE, London (2006)
19. Bruneau, M., Herzog, P., Kergomard, J., Polack, J.: General formulation of the dispersion equation in bounded viscothermal fluid, and application to some simple geometries. Wave Motion **11**, 441–451 (1989)
20. Caussé, R., Kergomard, J., Lurton, X.: Input impedance of brass musical instruments - comparison between experiment and numerical models. J. Acoust. Soc. Am. **75**(1), 241–254 (1984)
21. Dalmont, J.: Acoustic impedance measurement, part I: a review. J. Sound Vib. **243**, 427–439 (2001)
22. Dalmont, J.P., Gazengel, B., Gilbert, J., Kergomard, J.: Some aspects of tuning and clean intonation in reed instruments. Appl. Acoust. **46**, 19–60 (1995)
23. Dalmont, J.P., Nederveen, C.J., Dubos, V., Ollivier, S., Méserette, V., te Sligte, E.: Experimental determination of the equivalent circuit of an open side hole: linear and non linear behaviour. Acta Acust. United Acust. **88**, 567–575 (2002)
24. Dalmont, J., Curtit, M., Yahaya, A.F.: On the accuracy of bore reconstruction from input impedance measurements: application to bassoon crook measurements. J. Acoust. Soc. Am. **131**, 708–714 (2012)
25. Debut, V., Kergomard, J., Laloë, F.: Analysis and optimisation of the tuning of the twelfths for a clarinet resonator. Appl. Acoust. **66**, 365–409 (2005)
26. Dickens, P., Smith, J., Wolfe, J.: Improved precision in measurements of acoustic impedance spectra using resonance-free calibration loads and controlled error distribution. J. Acoust. Soc. Am. **121**(3), 1471–1481 (2007)
27. Dubos, V., Kergomard, J., Khettabi, A., Dalmont, J.P., Keefe, D.H., Nederveen, C.: Theory of sound propagation in a duct with a branched tube using modal decomposition. Acust. Acta Acust. **85**, 153–169 (1999)
28. Eisner, E.: Complete solutions of the "Webster" horn equation. J. Acoust. Soc. Am. **41**(4B), 1126–1146 (1967)
29. Eveno, P., Petiot, J., Gilbert, J., Kieffer, B., Caussé, R.: The relationship between bore resonance frequencies and playing frequencies in trumpets. Acta Acust. United Acust. **100**, 362–374 (2014)
30. Felix, S., Dalmont, J., Nederveen, C.J.: Effects of bending portions of the air column on the acoustical resonances of a wind instrument. J. Acoust. Soc. Am. **131**(5), 4164–4172 (2012)
31. Fock, V.: A theoretical investigation of the acoustical conductivity of a circular aperture in a wall put across a tube. C. R. Acad. Sci. U.R.S.S. (Doklady Akad. Nauk. SSSR) **31**, 875–878 (1941)
32. Forbes, B., Sharp, D., Kemp, J., Li, A.: Singular system methods in acoustics pulse reflectometry. Acta Acust. United Acust. **89**, 743–753 (2003)
33. Gibiat, V.: Physical Characterization of Wind Instruments: Impedance Measurements and Phase Trajectories (in French). Thèse d'État, Université du Maine, Le Mans, France (1990)
34. Gilbert, J., Kergomard, J., Polack, J.D.: On the reflection functions associated with discontinuities in conical bores. J. Acoust. Soc. Am. **87**(4), 1773–1780 (1990)
35. Guilloteau, A., Guillemain, P., Kergomard, J., Jousserand, M.: The effect of the size of the opening on the acoustic power radiated by a reed woodwind instrument. J. Sound Vib. **343**, 166–175 (2015)

36. Hélie, T.: Unidimensional models of acoustic propagation in axisymmetric waveguides. J. Acoust. Soc. Am. **114**(5), 2633–2647 (2003)
37. Hélie, T., Mignot, R., Matignon, D.: Waveguide modeling of lossy flared acoustic pipes: derivation of a Kelly-Lochbaum structure for real-time simulations. In: 2007 IEEE Workshop on Applications of Signal Processing to Audio and Acoustics, New Paltz, NY, pp. 293–296 (2007)
38. Hélie, T., Hezard, T., Mignot, R., Matignon, D.: One-dimensional acoustic models of horns and comparison with measurement. Acta Acust. United Acust. **99**, 960–974 (2013)
39. Kausel, W.: Optimization of brass instruments and its application in bore reconstruction. J. New Music Res. **30**, 69–82 (2001)
40. Kausel, W.: Bore reconstruction of tubular ducts from its acoustic input impedance curve. IEEE Trans. Instrum. Meas. **53**, 1097–1105 (2004)
41. Keefe, D.H.: Theory on the single woodwind tone hole. J. Acoust. Soc. Am. **72**(3), 676–687 (1982)
42. Keefe, D.H.: Woodwind air column models. J. Acoust. Soc. Am. **88**(1), 35–51 (1990)
43. Kemp, J., Bilbao, S., McMaster, J., Smith, R.: Discrete-time modeling of woodwind instrument bores using wave variables. J. Acoust. Soc. Am. **134**, 1395–1406 (2013)
44. Kergomard, J.: Quasi-standing waves in horns with wall visco-thermal losses: calculation of the impedance (in French). Acustica **48**(1), 31–43 (1981)
45. Kergomard, J.: Wave propagation in lines of finite length: notions of evanescent wave and cutoff frequency (in French). Rev. Phys. Appl. **17**, 307–327 (1982)
46. Kergomard, J.: General equivalent circuits for acoustics horns. J. Audio Eng. Soc. **36**, 948–955 (1988)
47. Kergomard, J., Garcia, A.: Simple discontinuities in acoustic waveguides at low frequencies: critical analysis and formulae. J. Sound Vib. **114**, 465–479 (1987)
48. Kergomard, J., Lefebre, A., Scavone, G.: Matching of fundamental modes at a junction of a cylinder and a truncated cone; application to the calculation of some radiation impedances. Acta Acust. United Acust. **101**, 1189–1198 (2015)
49. Khettabi, A.: Studies of discontinuities in acoustic 2*D* waveguides by using modal expansion and conformal mapping (in French). Ph.D. thesis, Université du Maine (1994)
50. Kokkelmans, S.J.M.F., Verge, M.P., Hirschberg, A., Wijnands, A., Schoffelen, R.: Acoustic behavior of chimney pipes. J. Acoust. Soc. Am. **105**(1), 546–551 (1999)
51. Lefebvre, A., Scavone, G.: Characterization of woodwind instrument toneholes with the finite element method. J. Acoust. Soc. Am. **131**, 3153–3163 (2012)
52. Lurton, X.: Analytic study of the input impedance of brass instruments (in French). Acustica **49**, 142–151 (1981)
53. Mahillon, V.: Elements of Musical and Instrumental Acoustics (in French), Première édition 1874. Les amis de la musique, Bruxelles (1984)
54. Mallaroni, B.: Effect of the geometry of a trumpet mouthpiece on the impedance spectrum (in French). Master's thesis, Master in Acoustics, Marseille University (2006)
55. Markel, J.D., Gray, A.: Linear Prediction of Speech. Springer, New York (1976)
56. Mignot, R., Hélie, T., Matignon, D.: From a model of lossy flared pipes to a general framework for simulation of waveguides. Acta Acust. United Acust. **97**, 477–491 (2011)
57. Mittra, R., Lee, S.: Analytical Techniques in the Theory of Guided Waves. Macmillan, New York (1971)
58. Moers, E., Kergomard, J.: On the cutoff frequency of clarinet-like instruments. geometrical versus acoustical regularity. Acta Acust. United Acust. **97**, 984–996 (2011)
59. Morse, P.M., Ingard, K.: Theoretical Acoustics. McGraw Hill, New York (1968)
60. Nederveen, C.J.: Acoustical Aspects of Woodwind Instruments, New edition, 1998. Northern Illinois University Press, Illinois (1969)
61. Nederveen, C.: Influence of a toroidal bend on wind instrument tuning. J. Acoust. Soc. Am. **104**(3), 1616–1626 (1998)
62. Nederveen, C., Dalmont, J.: Mode locking effects on the playing frequency for fork fingerings on the clarinet. J. Acoust. Soc. Am. **131**, 689–697 (2012)

63. Nederveen, C.J., Jansen, J.K.M., Van Hassel, R.R.: Corrections for woodwind tone-hole calculations. Acustica **84**, 957–966 (1998)
64. Noreland, D., Kergomard, J., Laloë, F., Vergez, C., Guillemain, P., Guilloteau, A.: The logical clarinet: numerical optimization of the geometry of woddwind instruments. Acta Acust. United Acust. **101**, 279–291 (2013)
65. Ollivier, S., Dalmont, J.P., Kergomard, J.: Idealized models of reed woodwinds. Part I: analogy with the bowed string. Acta Acust. United Acust. **90**(6), 1192–1203 (2004)
66. Pagneux, V., Amir, N., Kergomard, J.: A study of wave propagation in varying cross-section waveguides by modal decomposition. Part I. Theory and validation. J. Acoust. Soc. Am. **100**(4), 2034–2048 (1996)
67. Pelorson, X., Motoki, K., Laboissiére, R.: Contribution to the three-dimensional analysis of the vocal tract acoustics. In: Actes du 5e Congrès Français d'Acoustique, pp. 514–517. Presses Polytechniques et Universitaires Romandes, Lausanne (2000)
68. Pierce, A.D.: Acoustics: An Introduction to Its Physical Principles and Applications. Acoustical Society of America, Melville (1989)
69. Plitnik, G., Strong, W.: Numerical method for calculating input impedances of the oboe. J. Acoust. Soc. Am. **65**(3), 816–825 (1979)
70. Putland, G.: Every one-parameter acoustic field obeys Webster's horn equation. J. Audio Eng. Soc. **6**, 435–451 (1993)
71. Pyle, R. Jr.: Duality principle for horns. J. Acoust. Soc. Am. **37**(6), 1178–1178 (1965)
72. Pyle, R. Jr.: Effective length of horns. J. Acoust. Soc. Am. **57**(6), 1309–1317 (1975)
73. Rienstra, S.: Webster's horn equation revisited. SIMA J. Appl. Math. **65**, 1981–2004 (2005)
74. Rochesso, D., Smith, J.O.: Generalized digital waveguide networks. IEEE Trans. Speech Audio Process. **123**, 242–254 (2003)
75. Scavone, G.: An acoustic analysis of single-reed woodwind instruments with an emphasis on design and performance issues and digital waveguide modeling techniques. Ph.D. thesis, Stanford university (1997)
76. Schumacher, R.T.: Ab Initio calculations of the oscillations of a Clarinet. Acustica **48**(2), 71–85 (1981)
77. Sluchin, B., Caussé, R.: Brass Instrument Mutes (in French). Edition de la Maison des Sciences de l'Homme, Paris (1991)
78. Smith III, J.O.: Principles of digital waveguide models of musical instruments. In: Kahrs, M., Brandenburg, K. (eds.) Applications of DSP to Audio and Acoustics, pp. 417–466. Kluwer, Dordrecht (1998)
79. Smith, J.O.: Virtual acoustic musical instruments: review and update. J. New Music Res. **33**, 283–304 (2004)
80. Stewart, G., Lindsay, R.: Acoustics. Van Nostrand, New York (1930)
81. Välimäki, V., Pakarinen, J., Erkut, C., Karjalainen, M.: Discrete-time modelling of musical instruments. Rep. Prog. Phys. **69**, 1–78 (2006)
82. Verge, M., Fabre, B., Mahu, W., Hirschberg, A., van Hassel, R., Wijnands, A., de Vries, J., Hogendoor, C.: Jet formation and jet velocity fluctuations in a flue organ pipe. J. Acoust. Soc. Am. **95**, 1119–1132 (1994)
83. van Walstijn, M., Campbell, M., Kemp, J., Sharp, D.: Wideband measurement of the acoustic impedance of tubular objects. Acta Acust. United Acust. **91**, 590–604 (2005)
84. Webster, A.: Acoustical impedance, and the theory of horns and the phonograph. Proc. Nat. Acad. Sci. U. S. A. **5**, 275–282 (1919)

Part III
Nonlinearities and Self-Oscillations

This third Part is devoted to nonlinear oscillations. In Chap. 8, an overview of the domain is given, with application to free nonlinear oscillations of gongs, cymbals and strings, and on the nonlinearities in wind instruments due to propagation and dissipation. A number of general methods used for the analysis of nonlinear systems are detailed. In the following chapters, the production of sound due to self-oscillations both in wind and bowed strings instruments is analyzed. These oscillations are intrinsically nonlinear. Thus, the three main families of self-oscillating musical instruments are presented: the reed instruments (in Chap. 9), the flute-like instruments (in Chap. 10) and the bowed string instruments (in Chap. 11).

Chapter 8
Nonlinearities

Antoine Chaigne, Joël Gilbert, Jean-Pierre Dalmont, and Cyril Touzé

Abstract In the previous chapters, it was assumed that the amplitude of both air and structural oscillations in musical instruments were sufficiently small so that the assumption of linearity for their underlying models was fulfilled. However, this assumption is no longer valid in a number of situations encountered in musical acoustics, and a nonlinear approach becomes necessary for describing the observed phenomena. This chapter starts with the presentation of a simple example of nonlinear oscillator, the interrupted pendulum, whose aim is to introduce some fundamental properties of nonlinear systems, such as the dependence of resonance frequency on amplitude. The generic Duffing equation, which is found in many areas of nonlinear physics, is then examined. Musical applications are found first in piano strings, where the transverse-longitudinal coupling and the presence of additional partials in the spectrum (or "phantom" partials) are the consequence of nonlinearity due to high amplitude motion (geometric nonlinearity). In brass instruments, high values of the acoustic pressure induce nonlinear propagation which, in turn, might give rise to shock waves. In gongs and cymbals, a strong excitation produces the so-called bifurcations materialized by the emergence of new frequencies in the spectrum, which ultimately can lead to chaos. Specific methods are used for characterizing chaotic signals, such as the Lyapunov exponents. New emerging tools, such as the nonlinear normal modes (NNMs), appear to be very efficient for describing the dynamics of nonlinear systems with a reduced number of degrees of freedom. Self-sustained oscillations of reed, flute-like and bowed string instruments are treated in the three following chapters.

A. Chaigne (✉)
Institute of Music Acoustics, University of Music and Performing Arts Vienna (MDW), Anton-von-Webern-Platz 1, 1030 Vienna, Austria
e-mail: antchaigne@gmail.com

J. Gilbert • J.-P. Dalmont
Laboratoire d'Acoustique de l'Université du Maine (LAUM), Avenue Olivier Messiaen, 72085 Le Mans Cedex 09, France
e-mail: joel.gilbert@univ-lemans.fr; jean-pierre.dalmont@univ-lemans.fr

C. Touzé
Institute of Mechanical Sciences and Industrial Applications (IMSIA), ENSTA ParisTech, Université Paris-Saclay, 828 Boulevard des Maréchaux, 91762 Palaiseau Cedex, France
e-mail: cyril.touze@ensta-paristech.fr

A. Chaigne, J. Kergomard, *Acoustics of Musical Instruments*, Modern Acoustics and Signal Processing, DOI 10.1007/978-1-4939-3679-3_8

Most of the concepts on waves and modes presented in Parts I and II imply that the basic conditions of linearity are fulfilled. This requires first that the perturbations of the physical quantities involved in the models remain "small": there will be many opportunities to clarify what is meant by "small" in the following sections. The present chapter intends to show how to analyze and model the phenomena observed when the assumption of linearity is not valid anymore, which implies, in turn, that the effects of finite amplitude need to be considered (geometric nonlinearity). It is also important to know whether or not the constitutive equations of the materials remain linear. When stretching a rubber ribbon, for example, the relation between stress and strain significantly depends on the amplitude, even for a small tensile strength. This property is referred to as material nonlinearity.

Finally, and this is fundamental for the physics of musical instruments, the conditions for maintaining permanent oscillations in bowed stringed and wind instruments can be fulfilled only if a nonlinear element is introduced in the system loop. In fact, it would not be possible otherwise to transform a continuous source of energy, such as a static blowing pressure for the flute player, or a constant bow velocity for the violin player, into periodic oscillations. In this context, the purpose of the three following chapters is to give a detailed analysis of the instruments governed by self-sustained oscillations.

This chapter starts with the illustration of some fundamental concepts of geometric nonlinearity. Usual methods for studying nonlinear equations are introduced, including harmonic balance, iteration method, and the multiple scales method. Using simple examples, basic phenomena observed in nonlinear systems are introduced, such as eigenfrequencies depending on the amplitude, jumps, and hysteresis.

8.1 An Example of Asymmetry: The Interrupted Pendulum

First, a simple example of asymmetrical system is studied: the interrupted pendulum (see Fig. 8.1). The system is composed by a point mass m suspended on a massless string of length L at rest, attached to a pulley, and subjected to the action of gravity g. When the pendulum is set into motion, the string length changes over time: it increases when the weight moves away from the pulley of radius R, and it becomes shorter in the opposite case, when the string is wrapped around it. This elementary system illustrates several situations of asymmetry encountered in musical acoustics, for example, scrolling of the reed on the clarinet mouthpiece, boundary condition of a string on the tambura,[1] or geometric nonlinearity in gongs and cymbals (see Sect. 8.5). In the latter case, the curvature can be viewed as a stiffness asymmetry, where the rigid pulley adds some "stiffness" to the system during the time interval when the string is wrapped around it, compared to the free string case. This example is not only relevant in musical acoustics but also in other domains of physics. It has been used, for example, to understand complex nonlinear systems such as the propagation of compressional waves in rocks [22].

[1] The tambura is an Indian plucked stringed instrument.

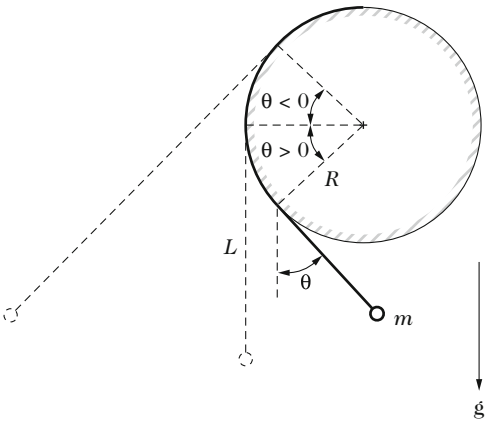

Fig. 8.1 Interrupted pendulum (from Denardo [22]). A point mass m is suspended to a massless string, forming a pendulum with a varying length during the motion due to the presence of the pulley which forms an obstacle

8.1.1 Equation of Motion

The equation of motion for the interrupted pendulum can be derived from the Lagrange equations [6]. The main variable is the angle θ made between the pendulum and the vertical axis. The instantaneous kinetic energy of the system is written $E_c = \frac{1}{2}m(L - R\theta)^2\dot{\theta}^2$. After some calculations, the equation of motion is found to be

$$\ddot{\theta} + \omega_0^2 \sin\theta = \rho\frac{d}{dt}(\theta\dot{\theta}), \tag{8.1}$$

where $\omega_o^2 = g/L$ and $\rho = R/L$. As R tends to zero in (8.1), the well-known equation of a simple pendulum is found where the unique nonlinear term is $\sin\theta$. The right-hand side of the equation represents the nonlinearity introduced by the obstacle. Equation (8.1) is valid for $\theta \in [0, \theta_{\max}]$ where $\theta_{\max} = \min(1/\rho, \pi/2)$. In what follows, the pendulum is assumed to be released at the initial time ($t = 0$) from a position θ_0 with zero initial velocity.

8.1.2 Solution by a Perturbation Method

For low and medium amplitudes, and with ρ less than or equal to unity, it is observed experimentally that the solution is periodic (see Fig. 8.2) and that the period of the oscillation depends on the amplitude. It is also observed that the oscillation increasingly departs from the linear sinusoidal reference solution as the amplitude increases.

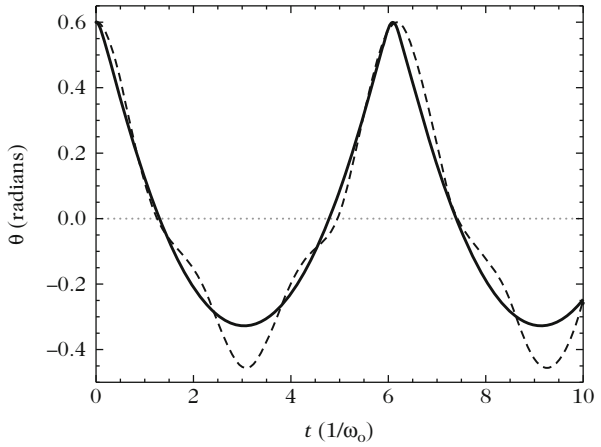

Fig. 8.2 Oscillations of the interrupted pendulum (from Denardo [22]). Displacement waveform of the mass *m*. *Solid line*: exact solution. *Dashed line*: perturbative solution to the third order

These observations incite us to look for solutions under the following form:

$$\begin{cases} \theta = \varepsilon A\cos\omega t + \varepsilon^2 B\cos 2\omega t + \varepsilon^3 C\cos 3\omega t + \cdots = \varepsilon\theta_1 + \varepsilon^2\theta_2 + \varepsilon^3\theta_3 + \cdots, \\ \omega^2 = \omega_0^2 + \varepsilon\omega_1^2 + \varepsilon^2\omega_2^2 + \varepsilon^3\omega_3^2 + \cdots \end{cases} \tag{8.2}$$

In Eq. (8.2), the solution is written in terms of a Fourier series where the amplitudes of the respective coefficients are arranged in increasing powers of the dimensionless parameter $\varepsilon \ll 1$. Similarly, the oscillation frequency ω is expanded as a series of terms of increasing powers of ε to account for variations with amplitude. The principle of the calculation consists in substituting the expansion (8.2) into (8.1) and in calculating the unknowns of the problem (A, B, C, ω_1, ω_2, ω_3) separately [22]. For the sake of simplicity, the expansion is limited here to the third order in ε. In order to deal with dimensionless equations, the change of variable $\tau = \omega t$ is made.

Since the problem is of the third order, it is justified here to replace the term in $\sin\theta$ in (8.1) by the first two terms of its Taylor expansion: $\sin\theta \simeq \theta - \theta^3/6$. Equation (8.1) becomes

$$\omega^2\frac{d^2\theta}{d\tau^2} + \omega_0^2\left(\theta - \theta^3/6\right) = \rho\omega^2\frac{d}{d\tau}\left(\theta\frac{d\theta}{d\tau}\right). \tag{8.3}$$

Inserting (8.2) in (8.3) and making the term ε equals to zero, leads to

$$\frac{d^2\theta_1}{d\tau^2} + \theta_1 = 0, \tag{8.4}$$

which has a solution of the form $\theta_1 = A\cos\tau$, in view of the initial conditions. Setting the term in ε^2 to zero, we have

$$\frac{d^2\theta_2}{d\tau^2} + \theta_2 = \frac{\omega_1^2}{\omega_0^2}\theta_1 + \rho\frac{d}{d\tau}\left(\theta_1\frac{d\theta_1}{d\tau}\right). \tag{8.5}$$

By replacing the angular variables by their approximate expressions, one finds that Eq. (8.5) provides the following relation between the parameters:

$$-3B\cos 2\tau = \frac{\omega_1^2}{\omega_0^2}A\cos\tau - \rho A^2\cos 2\tau. \tag{8.6}$$

The basic principle of the method is then to set to zero the respective terms of each *harmonic* $n\tau$ (*harmonic balance*), which gives here:

$$\omega_1 = 0 \quad \text{and} \quad B = \frac{\rho A^2}{3}. \tag{8.7}$$

At this stage, one can check that Eq. (8.1) suggests that the obstacle formed by the pulley of radius R causes a quadratic nonlinearity since an harmonic of order two is exhibited. This effect disappears if $\rho = 0$, i.e., without any obstacle. However, this nonlinearity causes no change in the angular frequency, at least at the first order. Continuing further by eliminating the terms of power 3 in ε, we get

$$\frac{d^2\theta_3}{d\tau^2} + \theta_3 = \frac{\omega_2^2}{\omega_0^2}\theta_1 + \frac{\theta_1^3}{6} + \rho\frac{d^2}{d\tau^2}(\theta_1\theta_2). \tag{8.8}$$

Replacing, as previously, the angular variables by their approximate expressions in (8.8), and eliminating further the terms in $n\tau$, leads to:

$$C = \frac{A^3}{192}\left(36\rho^2 - 1\right) \quad \text{and} \quad \frac{\omega_2^2}{\omega_0^2} = \frac{A^2}{24}\left(4\rho^2 - 3\right). \tag{8.9}$$

Finally, defining $\theta_{10} = \varepsilon A$ as the fundamental amplitude of the oscillation, the solution to the problem is written at the order 3:

$$\begin{cases} \theta = \theta_{10}\cos\omega t + \dfrac{\rho\theta_{10}^2}{3}\cos 2\omega t + (36\rho^2 - 1)\dfrac{\theta_{10}^3}{192}\cos 3\omega t, \\ \text{and} \\ \omega^2 = \omega_o^2\left[1 + \dfrac{\theta_{10}^2}{24}\left(4\rho^2 - 3\right)\right]. \end{cases} \tag{8.10}$$

This result suggests the following comments:

- At the third order, the fundamental amplitude is linked to the initial condition by the relation:

$$\theta_0 \simeq \theta_{10} + \frac{\rho\theta_{10}^2}{3} + (36\rho^2 - 1)\frac{\theta_{10}^3}{192}. \tag{8.11}$$

- Figure 8.2 shows that the third-order approximation yields a fair estimation of the oscillation period and waveform when θ is positive, i.e., when the string is in contact with the obstacle. However, it is necessary to expand the solution to higher orders in order to account for the observed oscillation when θ is negative.
- When $\rho = 0$, we have $\omega \simeq \omega_0(1 - \theta_{10}^2/16)$, and the term in $\cos 2\omega t$ is equal to zero. This yields a case of cubic nonlinearity due to gravity, through the term in $\sin\theta$. The tension of the string decreases as the amplitude of the motion increases, and it vanishes when the string reaches the horizontal plane, which corresponds to a decrease in the overall stiffness of the system.
- For $0 < \rho < \sqrt{3}/2$, the frequency decreases with the amplitude of the oscillation. The oscillator is said to show a *softening* behavior.
- For $\rho > \sqrt{3}/2$, the oscillator is of the *hardening* type. The stiffness provided by the obstacle becomes larger than the increase in softness due to gravity.
- When $\rho = \sqrt{3}/2$, the period of the oscillation is independent of the amplitude. This gives the particular case of an *isochronous pendulum*. This result remains true to the fourth order, since $\omega_3^2 = 0$ in the series expansion of ω^2. Both softening and hardening effects are compensating one another.

In conclusion, it can be noticed that most nonlinear phenomena exhibited in this simple example also occur in more complex systems: frequency dependence with regard to the amplitude, softening or hardening behavior of some structural modes, etc. The method presented to solve this particular case is also applicable to other nonlinear systems. Gilbert et al. used a similar approach, for example, to predict the steady-state amplitude of sound pressure in a clarinet [29]. Before studying specific nonlinear phenomena of musical acoustics in subsequent sections more closely, the Duffing equation will first be examined in detail, as it is an equation frequently encountered in nonlinear dynamics.

8.2 Duffing Equation

Duffing equation is a generic nonlinear equation of an oscillator which includes a cubic term. It is found in many areas of physics, and therefore it has been the subject of extensive study. In mechanics, it is a good model for phenomena that occur for large amplitude oscillations when the elastic restoring force can no longer be considered as proportional to the displacement. In musical acoustics, this model is used for explaining the presence of phantom partials in the spectrum of piano strings, and the enrichment of spectrum due to increasing amplitudes in gongs and cymbals, as it will be seen later in this chapter.

The main properties of the Duffing equation will be first illustrated from the example of the elastic pendulum. This example can be considered as a simplified case, with one degree of freedom, of the increase in stiffness due to the extension of length in vibrating strings (see Sect. 8.3).

Another type of nonlinear equation frequently encountered in physics is the Van der Pol equation. It differs from Duffing equation by the fact that the nonlinearity is included in the dissipative term, and not in the stiffness term. It can lead to self-sustained oscillations, which correspond to oscillations that occur without an oscillating forcing term. The Van der Pol equation is not studied in this chapter, but it will serve as a basic simplified model of some instruments, such as the clarinet, and treated in detail in Chap. 9.

8.2.1 Example

Let us now consider the oscillator drawn in Fig. 8.3. The rigid mass M is moved horizontally apart of a distance x from its initial equilibrium position, under the effect of a sinusoidal force $F\cos\Omega t$. This mass is attached to two springs of stiffness k, with free length L_0. This length becomes equal to L after stretching at rest. We denote $\lambda = L_0/L < 1$ and $y = x/L$.

During the motion, the spring length becomes $\ell(y) = L\sqrt{1+y^2}$ and the elastic potential energy stored in each spring is $\mathscr{E}_p = \frac{1}{2}k(\ell - L_0)^2$. Differentiating this expression with respect to y, the expression of the elastic restoring force exerted on the spring is obtained, from which the equation of motion is derived:

$$M\frac{d^2y}{dt^2} + 2ky\left[1 - \frac{\lambda}{\sqrt{1+y^2}}\right] = \frac{F}{L}\cos\Omega t. \tag{8.12}$$

Under the assumption of "small" displacements ($y \ll 1$), and setting $\omega_0^2 = 2k/M$, we obtain a first-order approximation:

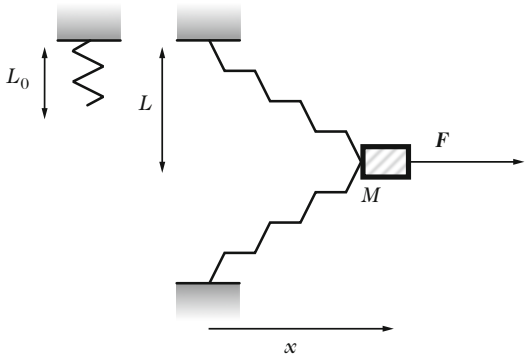

Fig. 8.3 Elastic pendulum

$$\frac{d^2y}{dt^2} + \omega_0^2(1-\lambda)y + \frac{\omega_0^2\lambda}{2}y^3 = \frac{F}{ML}\cos\Omega t, \tag{8.13}$$

or, equivalently, in dimensionless form, with $\tau = \omega t$, $\omega^2 = \omega_0^2(1-\lambda)$ and $\gamma = \Omega/\omega$:

$$\frac{d^2y}{d\tau^2} + y + \eta y^3 = \alpha\cos\gamma\tau, \tag{8.14}$$

where $\eta = \frac{\lambda}{2(1-\lambda)}$ and $\alpha = \frac{F}{ML\omega^2}$. Equation (8.14) is a Duffing equation with a forcing term. In the example above, the coefficient η is positive. An equation similar to the case of the interrupted pendulum is obtained (with $R = 0$ and θ small), though with a change of sign for η.

8.2.2 Solutions for the Forced Duffing Oscillator

In what follows, both coefficients η and α defined in (8.14) are assumed to be small compared to unity. In addition, η is positive (equivalent to $\lambda \ll 1$ in the previous example), which corresponds to the case of an *hardening* oscillator. The Duffing equation is solved by the *iteration method*, whose principle is to look for step-by-step refined approximations of the solution. Considering the solution obtained in the case of the linear oscillator (see Chap. 2), the solution $y_1(t) = A\cos\gamma\tau$ is selected as a starting approximation, where A is the unknown. The coefficient A can be positive or negative, depending on whether the solution is in phase or in antiphase with the force. The approximation of order 2 is sought in the form:

$$y_2(\tau) = A\cos\gamma\tau + B\cos 3\gamma\tau. \tag{8.15}$$

Now, y_2 is inserted in (8.14). Using the trigonometric identity

$$4\cos^3\gamma\tau = 3\cos\gamma\tau + \cos 3\gamma\tau, \tag{8.16}$$

and writing down the condition for which the amplitude of the term $\cos\gamma\tau$ is equal to zero, we have

$$(1-\gamma^2)A + \frac{3\eta A^3}{4} = \alpha. \tag{8.17}$$

Note To obtain the amplitude B of the term $\cos 3\gamma\tau$, the calculation must be continued with an approximation of order 3, and so on.

If the nonlinearity coefficient η is equal to zero in (8.17), then the resonance curve of the linear oscillator in forced oscillations is found: $A = \frac{\alpha}{1-\gamma^2}$, or, equivalently,

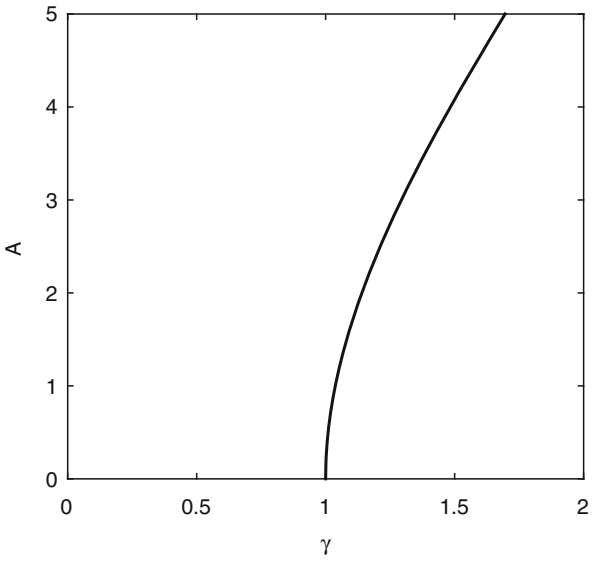

Fig. 8.4 Backbone curve for the Duffing equation with $\eta > 0$; $\gamma = \Omega/\omega$

$X = AL = \frac{F}{M}\frac{1}{\omega^2 - \Omega^2}$ using the dimensional quantities. Another method for obtaining the result (8.17) will be presented later in this chapter. To plot the resonance curves in the general case, it is convenient to write (8.17) under the form

$$\gamma^2 - 1 = \frac{3\eta A^2}{4} \pm \frac{\alpha}{|A|}. \tag{8.18}$$

- When $\alpha = 0$, the limiting case (the so-called backbone curve) is obtained (see Fig. 8.4). In the quarter plane ($\Omega^2 > 0, |A| > 0$), this curve is parabola with its concavity facing upwards, which corresponds here to the *hardening* case, i.e., to an increase of frequency with amplitude.
- When $\alpha \neq 0$, two branches of solution are obtained depending on whether A is positive or negative. In the first case, the resonance curve is located above the parabola. In the second case, it is located below.

To find the standard resonance curves, the x-axis and y-axis need to be reversed, after calculating the square root of Ω^2. If $\eta < 0$, the limiting curve of free oscillations in the quarter plane ($\Omega^2 > 0, |A| > 0$) is a parabola of concavity facing downwards, which corresponds to the case of a *softening* oscillator, where the eigenfrequency decreases with amplitude. With $\alpha \neq 0$, both branches of the curve are obtained with (8.18). If a viscous damping is introduced in the Duffing equation, it can be written in dimensionless form:

$$\frac{d^2y}{d\tau^2} + \beta\frac{dy}{d\tau} + y + \eta y^3 = \alpha \cos \gamma\tau. \tag{8.19}$$

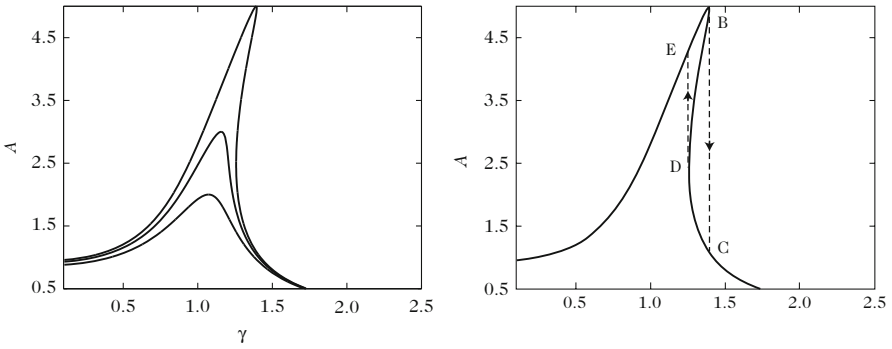

Fig. 8.5 (*Left*) Resonance curves of the damped Duffing equation for different values of the damping: the bending of the curves is more pronounced for low damping. (*Right*) Hysteresis loop: when γ increases, the operating point jumps from B to C; when γ decreases, the operating point jumps from D to E

With a similar approach as above, it is found that the resonance curves are governed by the equation:

$$\left[(1-\gamma^2)A + \frac{3\eta A^3}{4}\right]^2 + \beta^2 A^2 = \alpha^2 \tag{8.20}$$

which corresponds to the curves shown in Fig. 8.5.

8.2.2.1 Jump and Hysteresis Phenomena

The resonance curves of the nonlinear Duffing oscillator are bent to the left or to the right (see Fig. 8.5). As a consequence, a frequency domain exists (delimited by dotted lines in the figure) where one value of γ may correspond to three values of $|A|$. Through a rigorous mathematical reasoning, it can be shown that the extreme values obtained for $|A|$ are stable, while the states corresponding to the middle curve portion are unstable. In Sect. 8.5.4.1, a general method for determining the stability of oscillators will be studied. Experimentally, the consequences of these stability properties are the following:

1. If the frequency increases (resp. decreases) regularly, the intersection point in the middle curve does not stay fixed, and it "jumps" from one stable curve to the other as soon as the point on one stable curve reaches its limit (see Fig. 8.5).
2. The closed curve built up by the two jumps and the two stable portions of both upper and lower curves forms a *hysteresis loop*.

8.2.2.2 Secular Terms

Let us now return to the generic Duffing equation under forced oscillations, written in dimensionless form as follows:

$$\ddot{q} + q + \varepsilon q^3 = F \cos \Omega t, \tag{8.21}$$

with

$$F = \varepsilon F_0, \ \Omega^2 = 1 + \varepsilon \omega_1^2. \tag{8.22}$$

Note With these notations, all quantities q (and its derivatives), F, Ω are dimensionless. Thus, the eigenfrequency of the linear oscillator is now denoted 1 instead of ω_0. The dimensionless parameter ω_1 quantifies the difference between the oscillator's eigenfrequency and the forcing frequency. The expressions (8.22) indicate first that the study is restricted here to forcing frequencies close to the oscillator's eigenfrequency and, secondly, that the forcing amplitude is low.

Let us look for solutions in the form of an expansion in ε, as in the case of free oscillations for the interrupted pendulum:

$$q(t) = q_0(t) + \varepsilon q_1(t) + \cdots \tag{8.23}$$

By replacing the quantity q by its first-order expansion, we have

$$\ddot{q}_0 + \varepsilon \ddot{q}_1 + \left(\Omega^2 - \varepsilon \omega_1^2\right)(q_0 + \varepsilon q_1) + \varepsilon (q_0 + \varepsilon q_1)^3 = \varepsilon F_0 \cos \Omega t. \tag{8.24}$$

At zero order, this yields immediately

$$\ddot{q}_0 + \Omega^2 q_0 = 0, \tag{8.25}$$

from which we derive $q_0(t) = A \cos \Omega t$. At the order one, we have

$$\ddot{q}_1 + \Omega^2 q_1 = \left[\left(\omega_1^2 - \frac{3}{4}A^2\right)A + F_0\right] \cos \Omega t - \frac{1}{4}A^3 \cos 3\Omega t. \tag{8.26}$$

Here, the important point to consider is that an equation is obtained where the frequency of one forcing term (at the right-hand side) is equal to the oscillator eigenfrequency Ω. As shown in the first part of this book, this resonance case leads to an continuous increase of the amplitude of the solution with time, in $t \cos \Omega t$. These terms, called secular terms,[2] must be eliminated here, since stationary

[2]The origin of this denomination is due to the fact that these terms were highlighted as first in the field of celestial mechanics, where the time scales are of the order of centuries rather than of milliseconds!

solutions are sought. The amplitude of the term $\cos \Omega t$ in the right-hand side is thus put equal to zero, which leads to the condition

$$\left(\omega_1^2 - \frac{3}{4}A^2\right)A + F_0 = 0, \tag{8.27}$$

and, in turn, to the relation between amplitude and forcing parameters

$$\frac{3}{4}\varepsilon A^3 - A(\Omega^2 - 1) = F. \tag{8.28}$$

In conclusion, the result obtained for the forced spring pendulum in Eq. (8.17) is found again here, though with another method. For a forcing amplitude equal to zero ($F = 0$), the case of free oscillations is recognized. With $\varepsilon = 0$, we obtain the linear case.

8.2.3 Generation of Subharmonics

Nonlinear oscillators have the property to generate spectral components which are not included in the excitation spectrum. This section examines under which conditions a Duffing oscillator subjected to forced oscillations can generate subharmonics, i.e., spectral components of frequency equal to a submultiple of the excitation frequency or, equivalently, whose period is a multiple of the forcing period. Let us consider the forced Duffing equation with a source term of reduced frequency 3γ :

$$\frac{d^2y}{d\tau^2} + y + \eta y^3 = \alpha \cos 3\gamma\tau, \tag{8.29}$$

with $\eta \ll 1$. We look for the solutions that can be expanded in the form:

$$y(\tau) = y_0(\tau) + \eta y_1(\tau) \quad \text{with} \quad \gamma^2 = 1 + \eta\gamma_1^2. \tag{8.30}$$

Inserting the expressions (8.30) in (8.29), and eliminating the terms of order 2 in η (and higher), we get

$$\frac{d^2y_0}{d\tau^2} + \gamma^2 y_0 - \eta\gamma_1^2 y_0 + \eta\frac{d^2y_1}{d\tau^2} + \eta\gamma^2 y_1 + \eta y_0^3 = \alpha \cos 3\gamma\tau. \tag{8.31}$$

The linear solution (term of order 0) is obtained by setting $\eta = 0$ in (8.31) which yields

$$\frac{d^2y_0}{d\tau^2} + \gamma^2 y_0 = \alpha \cos 3\gamma\tau, \tag{8.32}$$

which, under the additional assumption of zero initial velocity, leads to a solution of the form $y_0(\tau) = A\cos\gamma\tau + C\cos 3\gamma\tau$. Finally, inserting the latter expression in (8.32) leads to $C = -\frac{\alpha}{8\gamma^2}$.

In the next step, the term in η is set to zero in (8.31), to ensure compatibility of the equation, which provides the term of order 1 of the solution:

$$\frac{d^2y_1}{d\tau^2} + \gamma^2 y_1 = \gamma_1^2 y_0 - y_0^3. \tag{8.33}$$

Now, by substituting in (8.33) the expression for $y_o(\tau)$, and after some trigonometric calculations, it is found that $y_1(\tau)$ must satisfy the equation:

$$\begin{aligned}\frac{d^2y_1}{d\tau^2} + \gamma^2 y_1 = A\left[\gamma_1^2 - \frac{3}{4}\left(A^2 + \frac{3\alpha^2}{64\gamma^4} - \frac{A\alpha}{8\gamma^2}\right)\right]\cos\gamma\tau \\ + \text{ terms in } 3\gamma,\ 5\gamma,\ 7\gamma,\ 9\gamma.\end{aligned} \tag{8.34}$$

Equation (8.34) shows that if the forcing amplitude of the γ term is not equal to zero, then we again face a situation where the amplitude of an oscillator, excited at its eigenfrequency, increases continuously in time. After removing the secular terms, we get

$$\gamma_1^2 = \frac{3}{4}\left(A^2 + \frac{3\alpha^2}{64\gamma^4} - \frac{A\alpha}{8\gamma^2}\right). \tag{8.35}$$

After some algebraic rearrangement, Eq. (8.35) provides the condition of existence for subharmonics of order 3 in the form of a relation between the amplitude A and the reduced frequency γ, for a given cubic nonlinearity coefficient η:

$$\gamma^6 - \gamma^4 - \frac{3\eta}{256}\left(64A^2\gamma^4 - 8A\alpha\gamma^2 + 2\alpha^2\right) = 0. \tag{8.36}$$

Finally, let us indicate that any oscillator governed by the Duffing equation may also exhibit *harmonics of higher order*. To demonstrate this, the previous calculation must be carried out again, with an forcing term in γ, and with the objective of obtaining conditions of existence for solutions in 3γ (or higher).

8.3 Nonlinear Vibrations of Strings

The models of strings presented in the previous chapters do not take the variations of tension consecutive to length fluctuations during the motion into account. This assumption is not justified anymore when the ratio between the transverse displacement and the string's length becomes large. In several stringed instruments (electric guitar, gypsy guitar, double bass played pizzicato,...) such variations of

tension are responsible for perceptually and musically relevant nonlinear effects: pitch glide (think of the well-known initial "twang" in the attack!), coupling between modes, and elliptical polarization of the string. One particular effect of nonlinear coupling between modes lies in the ability to excite a string at a fraction L/n of its length without canceling the harmonics of order n, in contradiction with the linear theory. The elliptical polarization of a string also is a consequence of the nonlinearity due to variations of tension.

The forced vibrations of an elastic string are examined below for large amplitude oscillations. These will be focused on two transverse components of the string's motion, denoted $y(x,t)$ and $z(x,t)$. Torsional vibrations and longitudinal vibrations are ignored [49, 73]. One may refer to the paper by Watzky for a more complete description of the nonlinear dynamics of a vibrating string [75].

8.3.1 Simplified Equations of Motion

Let T_0 be the initial tension of the string at rest. During the string motion, the relative increase in length λ of a small element of initial length dx is given by:

$$ds - dx = \lambda dx, \tag{8.37}$$

where ds is the current length (at time t) of the element (see Fig. 8.6).

For an elastic string of Young's modulus E and cross-section A (in m^2), the tension at time t during the motion becomes

$$T = T_0 + EA\lambda\,. \tag{8.38}$$

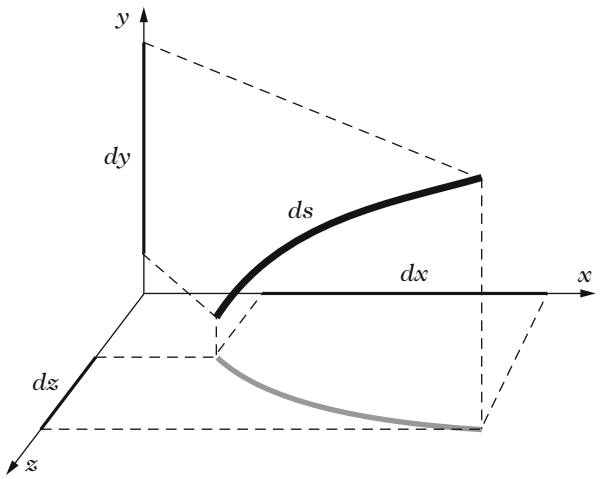

Fig. 8.6 Geometry of a nonlinear string element

It is assumed that the components of the strain tensor (see Chap. 1) remain small compared to unity so that it can be written that $ds = [dx^2 + dy^2 + dz^2]^{1/2}$. A second-order Taylor expansion of this equation gives

$$ds = dx \left\{ 1 + \frac{1}{2}\left[\left(\frac{\partial y}{\partial x}\right)^2 + \left(\frac{\partial z}{\partial x}\right)^2 \right] - \frac{1}{8}\left[\left(\frac{\partial y}{\partial x}\right)^2 + \left(\frac{\partial z}{\partial x}\right)^2 \right]^2 + \cdots \right\}. \tag{8.39}$$

Inserting this expression in (8.38) and assuming also that $EA \gg T_0$, it can be shown that the potential energy of the string of length L fixed rigidly at both ends is written [49]:

$$E_p = \int_0^L \left\{ \frac{T_0}{2}\left[\left(\frac{\partial y}{\partial x}\right)^2 + \left(\frac{\partial z}{\partial x}\right)^2 \right] + \frac{EA}{8}\left[\left(\frac{\partial y}{\partial x}\right)^2 + \left(\frac{\partial z}{\partial x}\right)^2 \right]^2 \right\} dx. \tag{8.40}$$

The kinetic energy is written:

$$E_c = \frac{\mu}{2}\int_0^L \left[\left(\frac{\partial y}{\partial t}\right)^2 + \left(\frac{\partial z}{\partial t}\right)^2 \right] dx. \tag{8.41}$$

By using the Hamilton's principle, and considering that a sinusoidal force $f(x)\cos\omega t$ is applied to the string in the transverse direction y, the following coupled equations are obtained (where the subscript letters refer to partial derivatives):

$$\begin{cases} y_{tt} - c_o^2 y_{xx} = \dfrac{c_1^2}{2}\left[3y_{xx}y_x^2 + \dfrac{\partial}{\partial x}(y_x z_x^2) \right] + \dfrac{f(x)}{\mu}\cos\omega t, \\ z_{tt} - c_o^2 z_{xx} = \dfrac{c_1^2}{2}\left[3z_{xx}z_x^2 + \dfrac{\partial}{\partial x}(z_x y_x^2) \right], \end{cases} \tag{8.42}$$

where $c_o = \sqrt{T_0/\mu}$ and $c_1 = \sqrt{EA/\mu}$ are the transverse and longitudinal velocities in the linear case, respectively. In Eq. (8.42) the left-hand sides correspond to the linear case, while nonlinear terms are the terms in brackets on the right-hand side. These terms can be ignored as long as the gradients y_x and z_x remain weak. Otherwise, they are responsible for a coupling between y and z. Thus, a force applied in the direction y is likely to generate a motion in the perpendicular direction z. This explains why an initially plane motion of the string does not remain plane during the motion.[3]

[3] Let us recall (see Chap. 6) that the boundary conditions at the bridge are another cause of coupling between y and z in the linear case. In the general complex case of a real stringed instrument during normal playing, these two factors coexist and it is often difficult to separate them.

8.3.2 Forced Vibrations

As a result of the large amplitude displacement of the string, it is usually not justified to neglect the nonlinear terms in (8.42) close to resonances. In what follows, it is assumed that the forcing frequency ω is close to one particular eigenfrequency $\omega_n = \frac{n\pi c_0}{L}$ of the string. It is further assumed, for simplicity, that the mode n is not coupled to other modes, which is not the case in practice. In fact, if the modes are close together and/or if there are some algebraic relations between the eigenfrequencies (see below, Sect. 8.5), then intermodal coupling must be taken into account. To a first approximation, let us consider the two transverse components of the string for the mode n:

$$y(x,t) = a_{ny} \sin\frac{n\pi x}{L} \cos\omega t \quad \text{and} \quad z(x,t) = a_{nz} \sin\frac{n\pi x}{L} \sin\omega t. \tag{8.43}$$

Inserting the expressions (8.43) in (8.42), the amplitudes a_{ny} and a_{nz} satisfy the following relations:

$$\begin{cases} (\omega_n^2 - \omega^2)a_{ny} + \dfrac{9c_1^2}{32}\left(\dfrac{n\pi}{L}\right)^4 a_{ny}^3 + \dfrac{3c_1^2}{32}\left(\dfrac{n\pi}{L}\right)^4 a_{ny}a_{nz}^2 = \dfrac{\alpha_n}{\mu}, \\ (\omega_n^2 - \omega^2)a_{nz} + \dfrac{9c_1^2}{32}\left(\dfrac{n\pi}{L}\right)^4 a_{nz}^3 + \dfrac{3c_1^2}{32}\left(\dfrac{n\pi}{L}\right)^4 a_{nz}a_{ny}^2 = 0, \end{cases} \tag{8.44}$$

where α_n is the projection of the excitation force on the mode n of the string.

8.3.2.1 Planar Motion

The case of a planar motion is obtained by setting $a_{nz} = 0$ in (8.44). In this case, the amplitude in the y-direction is governed by the nonlinear equation:

$$(\omega_n^2 - \omega^2)a_{ny} + \frac{9c_1^2}{32}\left(\frac{n\pi}{L}\right)^4 a_{ny}^3 = \frac{\alpha_n}{\mu}, \tag{8.45}$$

which is similar to Eq. (8.17) obtained for a Duffing oscillator under forced oscillations. Therefore, all results presented in Sect. 8.2.2 for Duffing oscillators of "hardening" type are valid here, including bending of resonance curves, jumps, and hysteresis.

8.3.2.2 Out-of-Plane Motion

Eliminating a_{nz} between both Eq. (8.44), yields for a_{ny}:

$$(\omega_n^2 - \omega^2)a_{ny} + \frac{3c_1^2}{8}\left(\frac{n\pi}{L}\right)^4 a_{ny}^3 = \frac{\alpha_n}{\mu}. \tag{8.46}$$

This expression is similar to (8.45), though the nonlinear term is now multiplied by a factor $4/3$, compared to the case of a planar motion. The second equation becomes

$$a_{nz}^2 = a_{ny}^2 - \frac{16}{3}\frac{\alpha_n}{\mu c_1^2 \left(\frac{n\pi}{L}\right)^4 a_{ny}}. \tag{8.47}$$

It proves that the string is likely to have an elliptical motion at a given point of abscissa x, under the condition:

$$a_{ny} > a_{ny}^{\text{crit}} = \left[\frac{16\alpha_n}{3\mu c_1^2 \left(\frac{n\pi}{L}\right)^4}\right]^{1/3}. \tag{8.48}$$

The condition (8.48) shows that increasing the forcing amplitude facilitates the emergence of such motion. For plucked, and struck, string instruments, the elliptical polarization has important consequences on the sound. In fact, each polarization is "loaded" by a specific impedance at the bridge. Consequently, the detuning and damping of both polarizations, due to these boundary conditions, are slightly different. This, in turn, induces beats and complex decay history, which are particularly sensitive to the attack time, when the amplitude is the largest. In the spectral domain, these nonlinear phenomena take the form of "double peaks" of very close frequencies.

In conclusion, it has been shown here that a single nonlinear string shows some characteristics observed in the case of linear coupled strings in pianos (see Chap. 6). However, it is important to notice that the underlying physical phenomena at the origin of these temporal and spectral properties are fundamentally different: amplitude nonlinearity in the first case, moving end in the linear case. Both phenomena exist in the vibrations of real piano strings, so that it is sometimes hard to separate them experimentally.

8.3.3 Transverse-Longitudinal Coupling: Simplified Approach

In the previous section, the coupling between transverse and longitudinal motion of the string is ignored. However, in many string instruments and, in particular, in pianos, such coupling is clearly visible and has a perceptual relevance [15]. To illustrate this, Fig. 8.7 shows the recorded acceleration at the bridge of a piano. It highlights the existence of the so-called precursor, that precedes the transverse vibration. Spectral analysis of this precursor shows that it is mainly due to longitudinal vibration of the string, caused by its elongation during the attack [2].

This section is dedicated to the analysis of this coupling. It is restricted to the description of the coupling between one transverse polarization $y(x,t)$ and the longitudinal (or axial) motion $\xi(x,t)$. The string is assumed to be homogeneous, lossless, and rigidly fixed at both ends. Finally, it is assumed that both transverse

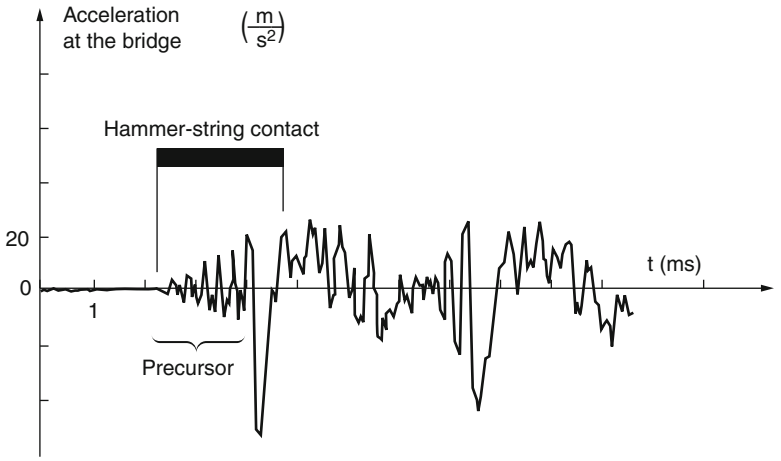

Fig. 8.7 Acceleration at the bridge of a piano. A precursor is clearly visible in the initial part of the waveform. It is due to the longitudinal vibration of the string struck by the hammer. The duration of hammer-string contact is indicated by a *black rectangle*, for comparison. From [2]

and longitudinal modes are integer multiples of their respective fundamentals. The proposed approach used below is close to the one used by Bank [7], and inspired by Morse [46]. We start from Eq. (8.38) where the extension ds, for a given axial displacement $\xi(x,t)$, is written:

$$\mathrm{d}s = dx\sqrt{\left(1+\frac{\partial\xi}{\partial x}\right)^2+\left(\frac{\partial y}{\partial x}\right)^2}, \tag{8.49}$$

from which a first-order expression of string tension is derived

$$T = T_0 + EA\left[\frac{\partial\xi}{\partial x}+\frac{1}{2}\left(\frac{\partial y}{\partial x}\right)^2\right]. \tag{8.50}$$

Thus the longitudinal force exerted on the string element ds is written:

$$F_x = \frac{\partial T}{\partial x}dx = EA\left[\frac{\partial^2\xi}{\partial x^2}+\frac{1}{2}\frac{\partial}{\partial x}\left(\frac{\partial y}{\partial x}\right)^2\right]dx. \tag{8.51}$$

This yields the equation that governs the longitudinal displacement of the string:

$$\mu\frac{\partial^2\xi}{\partial t^2} = EA\left[\frac{\partial^2\xi}{\partial x^2}+\frac{1}{2}\frac{\partial}{\partial x}\left(\frac{\partial y}{\partial x}\right)^2\right]. \tag{8.52}$$

The equation that governs the transverse string component y is written:

$$\mu \frac{\partial^2 y}{\partial t^2} = T_0 \frac{\partial^2 y}{\partial x^2} + EA \frac{\partial}{\partial x} \left\{ \frac{\partial y}{\partial x} \left[\frac{\partial \xi}{\partial x} + \frac{1}{2} \left(\frac{\partial y}{\partial x} \right)^2 \right] \right\}. \tag{8.53}$$

It should be noticed in Eq. (8.52) that the coupling term due to transverse motion is quadratic in y, while in (8.53) the coupling term due to longitudinal motion is cubic in y. Under the assumptions of fixed boundary conditions and homogeneous string, the transverse motion is expanded in the form:

$$y(x,t) = \sum_{n=1}^{\infty} y_n(t) \sin \frac{n\pi x}{L}. \tag{8.54}$$

At this step, the goal is to define the conditions of existence for longitudinal motion of the string and quantify it (this will be referred to as transverse-longitudinal, or TL, mode coupling). The inverse problem, namely the generation of a transverse motion induced by a longitudinal motion (longitudinal-transverse, or LT, mode coupling) is intentionally left aside. Both couplings exist simultaneously in reality, but the description of the TL coupling is sufficient to bring out the essential principles. Starting from (8.54), the longitudinal force per unit length of the string is written, from (8.51)

$$\begin{aligned} f_{\mathrm{TL}}(x,t) &= \frac{EA}{2} \frac{\partial}{\partial x} \left(\frac{\partial y}{\partial x} \right)^2 = \frac{EA}{2} \frac{\partial}{\partial x} \left[\sum_{n=1}^{\infty} y_n(t) \frac{n\pi}{L} \cos \frac{n\pi x}{L} \right]^2 \\ &= \frac{EA\pi^3}{4L^3} \sum_{m=1}^{\infty} \sum_{n=1}^{\infty} y_m(t) y_n(t) mn \left[(m+n) \sin \frac{(m+n)\pi x}{L} \right. \\ &\quad \left. + (m-n) \sin \frac{(m-n)\pi x}{L} \right]. \end{aligned} \tag{8.55}$$

Under the assumptions of fixed boundary conditions and no dissipation, the longitudinal displacement becomes

$$\xi(x,t) = \sum_{k=1}^{\infty} \xi_k(t) \sin \frac{k\pi x}{L} = \sum_{k=1}^{\infty} \xi_k(x,t). \tag{8.56}$$

The component $\xi_k(x,t)$ will be excited under the condition that the projection of f_{TL} on this component is not equal to zero. This is checked by calculating the scalar product:

$$f_{\mathrm{TL},k}(t) = \int_0^L f_{\mathrm{TL}}(x,t) \sin \frac{k\pi x}{L} dx. \tag{8.57}$$

The calculation (8.57) then shows that the only cases where $f_{\mathrm{TL},k} \neq 0$ are obtained under the following conditions:

$$m + n = k \quad \text{or} \quad |m - n| = k. \tag{8.58}$$

In the first case (or "+" case), we have

$$f^{+}_{\mathrm{TL},k}(t) = -\frac{EA\pi^3}{8L^2} \sum_{n=1}^{k-1} y_{k-n}(t) y_n(t) k(k-n)n, \tag{8.59}$$

and, in the second case (or "−" case):

$$f^{-}_{\mathrm{TL},k}(t) = -\frac{EA\pi^3}{4L^2} \sum_{n=1}^{\infty} y_{k+n}(t) y_n(t) k(k+n)n. \tag{8.60}$$

From a spectral point of view, the previous equations yield the conditions that govern the occurrence of frequencies due to longitudinal vibrations of the string. For harmonic spectra, it can be checked (8.59) and (8.60) that these conditions are written:

$$\begin{cases} \text{for } f^{+}_{\mathrm{TL},k}(t) \ : \ f_n + f_{k-n} = f_k \ \text{ and } \ f_n - f_{k-n} = f_{|2n-k|}, \\ \text{for } f^{-}_{\mathrm{TL},k}(t) \ : \ f_n + f_{k+n} = f_{2n+k} \ \text{ and } \ f_n - f_{k+n} = f_k. \end{cases} \tag{8.61}$$

Such selection rules were applied successfully by Valette and Watzky to account for the generation of longitudinal modes in harpsichord strings [73]. They also account for "phantom partials" observable in piano sounds [17]. In the case of the piano, Bank and Sujbert made systematic measurements of real sounds that helped in enlarging the validity of relations (8.61) to the case of slightly inharmonic signals [7].

8.3.4 *Exact Geometrical Model of Piano Strings with Intrinsic Stiffness*

The general considerations on the nonlinear properties of strings presented in Sects. 8.3.1–8.3.3 above were based on simplified models of geometric nonlinearity and, in particular, on first-order approximations of the nonlinear terms in the wave equations. However, it has recently been demonstrated that the numerical simulations based on these approximate models can lead to errors, and even to instabilities [12]. In addition, as mentioned in several chapters of this book, and, particularly, in Chap. 3, the intrinsic stiffness of strings is an essential property, with significant audible consequences for the piano [26]. As shown below, the association of nonlinearity and stiffness is necessary in order to obtain a realistic model of piano

string. It is also preferable to use a geometrically exact model of string vibrations. Such a model has recently been developed by Chabassier et al., who write the nonlinear piano string's equations [13]:

$$\begin{cases} \rho A \dfrac{\partial^2 u_s}{\partial t^2} - \dfrac{\partial}{\partial x}\left[EA \dfrac{\partial u_s}{\partial x} - \dfrac{(EA - T_0)\, \dfrac{\partial u_s}{\partial x}}{\sqrt{\left(\dfrac{\partial u_s}{\partial x}\right)^2 + \left(1 + \dfrac{\partial v_s}{\partial x}\right)^2}} \right] + AG\kappa \dfrac{\partial}{\partial x}\left(\varphi_s - \dfrac{\partial u_s}{\partial x}\right) = S, \\ \rho A \dfrac{\partial^2 v_s}{\partial t^2} - \dfrac{\partial}{\partial x}\left[EA \dfrac{\partial v_s}{\partial x} - \dfrac{(EA - T_0)\left(1 + \dfrac{\partial v_s}{\partial x}\right)}{\sqrt{\left(\dfrac{\partial u_s}{\partial x}\right)^2 + \left(1 + \dfrac{\partial v_s}{\partial x}\right)^2}} \right] = 0, \\ \rho I \dfrac{\partial^2 \varphi_s}{\partial t^2} - EI \dfrac{\partial^2 \varphi_s}{\partial x^2} + AG\kappa \left(\varphi_s - \dfrac{\partial u_s}{\partial x}\right) = 0. \end{cases} \tag{8.62}$$

In this system, u_s is the transverse component of the string's displacement, v_s is the longitudinal component, and φ_s is the angle of rotation of the cross-sections (see Fig. 8.8).[4] ρ is the density of the string. For an homogeneous steel string, the string density is equal to the density of the material ρ_c, where the index "c" means "core." Similarly, the area of the cross-section is $A = A_c$. For the wrapped bass strings, where the wrapping (usually in copper) is aimed at increasing the mass without altering too much the stiffness, the density can be written $\rho = \rho_c F$, where F is the wrapping factor defined as [15] :

$$F = 1 + \frac{\rho_w A_w}{\rho_c A_c}. \tag{8.63}$$

[4]Strictly speaking, the model should contain an additional horizontal component. In fact, it is observed experimentally that the polarization of most piano strings changes with time. It is often almost vertical during the initial transient, due to the action of the hammer, and is then evolving progressively towards a horizontal motion, even for small amplitudes. It can be demonstrated mathematically that such a polarization change can only occur if some asymmetry exists in the system that allows a transfer of energy from one component to the other. If the string is assumed to be homogeneous and perfectly rectilinear, with ideal boundary conditions (assuming a vertical motion of the bridge, for example), then the string will keep the initial polarization induced by the hammer during its motion. In [13], the authors made such assumptions, with a vertical initial motion of the hammer, and this is the reason why only one transverse component of the string is considered here. Revisiting the bridge model would be necessary for allowing a horizontal component.

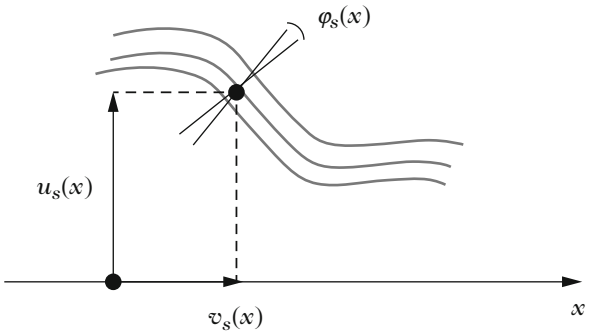

Fig. 8.8 Variables for the nonlinear planar motion of a stiff string: u_s is the transverse component, v_s is the longitudinal component, and φ is the angle of rotation of the cross-section due to shear stress

In this expression, A_w is the cross-sectional area and ρ_w the density of the wrapping. The other parameters (Young's modulus E, tension at rest T_0, torsional modulus G, and shear coefficient κ) are related to the core. The stiffness model in Eq. (8.62) is a Timoshenko model. Its main property follows from the coupling between transverse and shear waves. Accounting for shear yields accurate estimation of the string's eigenfrequencies in the audible range. In addition, the Timoshenko model has desired mathematical properties for the simulations. As shown in Chap. 3, for example, the transverse velocity in a Timoshenko beam tends to an asymptotic value as the frequency increases, whereas it tends to infinity for an Euler–Bernoulli beam, which is unsatisfactory from both a physical and numerical point of view. The source term S in (8.62) accounts for the action of the hammer. To be complete, the model must also contain damping terms, which are not written here for the sake of simplicity.

The motion of the string imparts transverse and longitudinal forces at the bridge (see Fig. 8.9). These forces are transmitted to the soundboard, as a result of the particular geometry of the system and, also probably, because of the complex motion of the bridge. This motion is left aside here, since it is still not completely understood today, and subjected to some controversy. Considering then the angle between the string and the horizontal plane, only, then the two components of the string force at the bridge (in $x = L$) can be written as:

$$F_b(t) = \cos\alpha \left[EA\,\partial_x u_s + AG\kappa\big(\partial_x u_s - \varphi_s\big) - (EA - T_0)\frac{\partial_x u_s}{\sqrt{(\partial_x u_s)^2 + (1 + \partial_x v_s)^2}} \right](x = L, t)$$
$$+ \sin\alpha \left[EA\,\partial_x v_s + (EA - T_0)\big(1 - \frac{1 + \partial_x v_s}{\sqrt{(\partial_x u_s)^2 + (1 + \partial_x v_s)^2}}\big) \right](x = L, t). \tag{8.64}$$

The nonlinear string force (8.64) is the exact expression to be used in simulations. However, it is interesting to examine lower-order expansions of this force for the purpose of a physical interpretation. We get

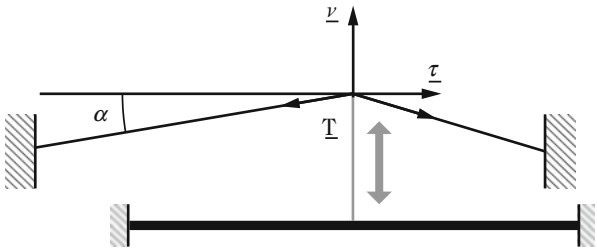

Fig. 8.9 String–soundboard coupling at the bridge, allowing the transmission of the transverse and longitudinal components of the string force

$$
\begin{aligned}
F_b(t) \approx \cos(\alpha) \Big[& T_0\, \partial_x u_s + AG\kappa \big(\partial_x u_s - \varphi_c\big) \\
& + (EA - T_0) \partial_x u_s\, \partial_x v_s + (EA - T_0) \frac{(\partial_x u_s)^3}{2} \Big] (x = L, t) \\
& + \sin(\alpha) \left[EA\, \partial_x v_s + (EA - T_0) \frac{(\partial_x u_s)^2}{2} \right] (x = L, t).
\end{aligned}
\tag{8.65}
$$

In (8.65), the term $(T_0 + AG\kappa)\partial_x u_s$ contains the linear components of higher magnitude. The following term refers to the shear wave, and has no effect on the piano sound since the corresponding spectrum is beyond the audible range. The term $(EA - T_0)\partial_x u_s\, \partial_x v_s$ shows the possible existence of spectral combinations between transverse and longitudinal modes. The term $(EA - T_0)\frac{(\partial_x u_s)^3}{2}$ accounts for cubic transverse nonlinearities. The term $EA\, \partial_x v_s$ accounts for the longitudinal components. Finally, the term $(EA - T_0)\frac{(\partial_x u_s)^2}{2}$ accounts for quadratic transverse nonlinearities. This last term is comparable to the one discussed in Sect. 8.3.3. This shows that the nonlinear expression of the force transmitted from string to soundboard accounts for the richness of piano sounds. In addition to transverse and longitudinal partials, which are easily seen on real piano spectra because of their relative high amplitudes, the spectral analysis of piano tones show many other peaks due to combinations of order 2 or 3 between all components. These combinations are nothing but the famous *phantom* partials, as designated in the literature [16].

The experimental identification of these phenomena is shown in Fig. 8.10. The transverse partials are the peaks of highest amplitude: they are designated by a single number. On the top figure, the spectral peaks of smaller amplitude located between the transverse partials are the result of quadratic nonlinearity: they are designated by the sum of two numbers. The frequency of the phantom partial "14+16," for example, is equal to the exact sum (within 1 Hz, which corresponds to the accuracy of the spectral analysis) of the respective frequencies of partials 14 and 16. Here, one can realize the importance of inharmonicity: with a perfect harmonic transverse series of partials, it would be impossible to detect the phantom partials. In the previous example, the phantom partial "14+16" would be then superimposed to the 30th harmonic component. As shown in Chap. 3, the inharmonicity (due to stiffness)

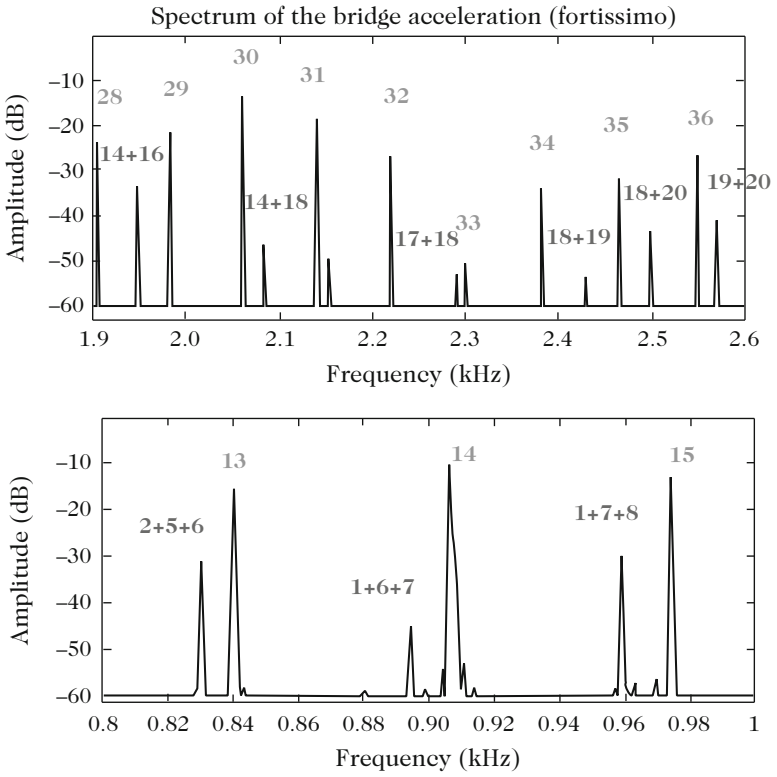

Fig. 8.10 Experimental identification of phantom partials due to quadratic (*top*) and cubic (*bottom*) nonlinearities in the bridge acceleration spectrum, at the attachment point of string C2 (fundamental $f = 65.4$ Hz) of an upright piano

increases as the square of the partial's rank. Thus, the 30th transverse partial has a frequency higher than the "14 + 16" phantom partial. Similar comments can be made for the bottom figure where the added phantom partials are due to cubic nonlinearity. As a consequence, their frequencies are the combinations of three different frequencies of transverse partials. Zooming on other parts of the spectrum (not shown here) would illustrate other types of combinations, where the frequencies of some phantom partials are the sum of transverse and longitudinal frequencies, for example.

The issue of frequency combinations and added partials due to geometric nonlinearity will be addressed again in Sect. 8.5 devoted to gongs and cymbals. The mechanisms of instability at the origin of these new frequencies and the conditions for their existence will be analyzed and discussed.

8.4 Nonlinearities in Wind Instruments Resonators

In the previous chapters, the propagation of sound in wind instruments was based on the wave equation (cf. Chap. 1) obtained from basic equations (conservation equations, adiabatic behavior of ideal gas), through linearization of acoustic quantities with regard to the fluid at rest, considered as a reference state. The so-called small perturbations hypothesis is no longer justified in situations with high levels of sound, as the acoustic pressure amplitude inside the tube can reach 1–10 % of the atmospheric pressure. In this case, the phenomena must be analyzed with nonlinear propagation equations. The purpose of this section is to present basic tools of weakly nonlinear acoustics applied to one-dimensional waveguides (case without source, fluid at rest), and to discuss one particularly impressive wave distortion phenomenon, the so-called brassy sounds, observed in brass instruments.[5] In addition to brassy sounds, the nonlinear localized dissipation found in side-hole instruments, will also be examined (Sect. 8.4.5).

8.4.1 Nonlinear Propagation

8.4.1.1 From Basic Equations to the Weakly Nonlinear Wave Equation

A criterion for evaluating the relevance of the linear approximation consists in checking that the (dimensionless) acoustic Mach number $M = v_a/c$ is small compared to unity (v_a is the amplitude of the acoustic velocity, whereas c is the speed of sound). Reciprocally, in the case of very intense sound level (with M of the order of unity), which corresponds to highly nonlinear acoustics, the basic equations cannot be linearized anymore! In fact, even for small acoustic Mach number, it is possible to observe pronounced nonlinear distortion phenomena. These effects are negligible on a small spatial scale: for distances small compared to the wavelength, it is possible to assume $p = \rho c v$ (as for a simple traveling wave). However, these effects are cumulative in space, for distances corresponding to a significant number of wavelengths, and can then generate highly distorted waves, and even shock waves.[6] This area of study is referred to as "weakly nonlinear" acoustics.

Nonlinear Equation of Wave Propagation

In the simple case of 1D linear acoustics, the propagation equation can be put in the form of two traveling wave equations of order 1, without a source: $\partial p/\partial t \pm$

[5] For a more detailed study of fundamental nonlinear acoustics, the reader may refer, for example, to the following authors: [18, 34, 54, 57].

[6] A shock wave is a pressure field which has an abrupt, and almost discontinuous, transition.

$c\partial p/\partial x = 0$. To generalize this, one can start from the basic equations of mass conservation (1.107) and momentum conservation (1.101), so that the quadratic nonlinear terms appear

$$\frac{\partial \rho}{\partial t} + \frac{\partial(\rho v)}{\partial x} = 0 \ ; \rho\left(\frac{\partial v}{\partial t} + v\frac{\partial v}{\partial x}\right) = -\frac{\partial P}{\partial x}. \tag{8.66}$$

Here, the initial symbols of the basic acoustic equations are used (i.e., before linearization), where ρ and P are the density and total pressure, respectively. Under the assumption of adiabaticity, ρ depends only on P, or vice versa (adiabaticity is defined in Chap. 1). In addition, the velocity v is also assumed to be a function of pressure P. The following system of equations is derived

$$\begin{aligned} \frac{d\rho}{dP}\frac{\partial P}{\partial t} + \frac{d(\rho v)}{dP}\frac{\partial P}{\partial x} &= 0 \\ \rho\frac{dv}{dP}\frac{\partial P}{\partial t} + \left(\rho v\frac{dv}{dP} + 1\right)\frac{\partial P}{\partial x} &= 0. \end{aligned} \tag{8.67}$$

It has nontrivial solutions for $\partial P/\partial t$ and $\partial P/\partial x$ if the determinant associated with the system of these two equations is equal to zero, which gives

$$\frac{d\rho}{dP}\left(\rho v\frac{dv}{dP} + 1\right) - \frac{d(\rho v)}{dP}\rho\frac{dv}{dP} = 0 \ \text{, equivalent to } \frac{d\rho}{dP} = \rho^2\left(\frac{dv}{dP}\right)^2.$$

By definition, we have $c^2 = dP/d\rho$. This leads to two solutions: "outgoing" and "incoming" traveling waves, respectively, corresponding to $dP/dv = \pm\rho c$. In the particular case of the outgoing wave, using the first Eq. (8.67), the so-called nonlinear propagation equation of the simple wave [24] is obtained

$$\frac{\partial P}{\partial t} + (c + v)\frac{\partial P}{\partial x} = 0. \tag{8.68}$$

This equation, obtained without any approximation, is nonlinear. Now, the speed of sound has to be expressed. In Chap. 5 the following nonlinear state equation was established in the case of an ideal adiabatic fluid:

$$\frac{P}{P_0} = \left(\frac{\rho}{\rho_0}\right)^\gamma \ \text{ from which } \ c^2 = \frac{dP}{d\rho} = \gamma\frac{P_0}{\rho_0}\left(\frac{\rho}{\rho_0}\right)^{\gamma-1}.$$

Weakly Nonlinear Acoustics Assumption

Under the assumption of weakly nonlinear acoustics, an approximate version of the simple wave equation (8.68) is now derived. Restricting the study to quadratic terms,

it is sufficient to write a first-order approximation of the speed of sound as a function of density, which gives

$$c \simeq c_0 \left[1 + \frac{\gamma - 1}{2} \frac{\rho'}{\rho_0}\right] \quad \text{with } c_0^2 = \gamma \frac{P_0}{\rho_0}. \tag{8.69}$$

ρ' is still the acoustic density: $\rho = \rho_0 + \rho'$. The pressure is also assumed small, using the following notation (see Chap. 1): $P = P_0 + p$. Thus, we have $p/P_0 = \gamma \rho'/\rho_0$. Again to the first order, we have $p = \rho_0 c_0 v$, which yields

$$c_0 \frac{\rho'}{\rho_0} = \frac{c_0}{\gamma} \frac{p}{P_0} = v, \text{ and then } \; c = c_0 + \frac{\gamma - 1}{2} v. \tag{8.70}$$

Finally, the nonlinear equation (8.68) is approximated as follows:

$$\frac{\partial p}{\partial t} + (c + v) \frac{\partial p}{\partial x} = \frac{\partial p}{\partial t} + \left[c_0 + \frac{\gamma + 1}{2} v\right] \frac{\partial p}{\partial x} = 0. \tag{8.71}$$

This wave equation also remains valid, if we replace p by v or ρ'. In summary, Eqs. (8.68) and (8.70) account for the causes of nonlinearity present in both the conservation and the state equations:

- the convection effects (due to flow velocity). For a fixed observer, each point of the wave, instead of moving at the same speed c_0 is moving in fact at speed $c + v$, so faster at the maxima of the acoustic velocity, and slower at the minima.
- variations in the sound pressure induce compression and expansion zones that increase and decrease with temperature, respectively. Since the local speed of sound c depends on temperature, it is also a function of the acoustic velocity.

As discussed in Sect. 8.4.2, the nonlinear traveling wave equation obtained above can be solved accurately by the method of Riemann invariants, also called the method of characteristics. The wave equation can also be established in the general case (non-traveling wave case), but it cannot be solved accurately. Notice that losses were not considered in the previous developments. If losses are taken into account, approximate methods, using perturbation calculus, should be used. Burgers equation mentioned in the following Sect. 8.4.1.2 is the result of such methods.

8.4.1.2 Burgers Equation

The exact solution of nonlinear acoustics including losses is not possible. An approximate way to tackle the problem is to use a perturbation method: the method of "multiple scales".[7] This method is based on the presence in the equation of a

[7] This method is detailed in Sect. 8.5 devoted to nonlinear vibrations of gongs and cymbals.

small parameter, compared to unity: in our case, the selected parameter is the Mach number defined in the vicinity of the acoustic source of the system. This number serves as a basis for the definition of different scales: a short spatial scale (or "fast" scale) that describes the wave propagation locally, and a long spatial scale (or "slow" scale) that represents the cumulative effects of nonlinear distortion and losses. After some mathematical operations, that will not be detailed here, the weakly nonlinear lossless wave equation (8.71) is approximated by the following so-called Burgers equation:

$$\frac{\partial q}{\partial \sigma} - q\frac{\partial q}{\partial \theta} = 0, \tag{8.72}$$

where q is a dimensionless velocity, σ is a long spatial quantity, and θ is a dimensionless delayed time quantity. For more details, the reader may consult [57] or [19]. If the Burgers equation above is valid for the speed of sound, it is also applicable to other acoustic quantities, such as density and pressure. Equation (8.72) has an exact solution for $\sigma < 1$. For the particular case of a sine wave at the input ($\sigma = 0$), Fubini has obtained the solution [25]:

$$q(\sigma, \theta) = 2\sum_{n=1}^{\infty} \frac{J_n(n\sigma)}{n\sigma} \sin(n\theta), \tag{8.73}$$

where J_n is the Bessel function of order n. "Generalized" Burgers equations exist, that take additional physical phenomena into account. As a consequence, the nonlinear differential equation that follows has two terms on the right-hand side, the first corresponding to volume visco-thermal phenomena, and the second to visco-thermal losses localized near the walls[8]:

$$\frac{\partial q}{\partial \sigma} - q\frac{\partial q}{\partial \theta} = A\frac{\partial^2 q}{\partial \theta^2} + B\frac{\partial^{1/2} q}{\partial \theta^{1/2}}, \tag{8.74}$$

where A and B are constants depending on the thermodynamic constants of both the gas and geometric characteristics of the system under study. In practice, the volume losses term can be ignored almost everywhere (i.e., outside the shock zone[9]) in the "sound pipes" application. Nevertheless, it is possible to separate and measure the relative influence of all these effects, using dimensional analysis (see, for example, [44]).

[8] So far, the volume visco-thermal losses, proportional to ω^2, were ignored because in a wind instrument they are very low compared to losses in the boundary layers, proportional to $\sqrt{\omega}$. However, volume losses are essential in free space. Equation (8.74) including only the volume loss term ($B = 0$) is the equation called "Burgers equation," referring to the similar nonlinear equation used by the Dutch physicist J.M. Burgers in his work on turbulence.

[9] The shock zone is the zone where sudden changes of pressure, acoustic velocity, and temperature may occur.

8.4.2 Nonlinear Distortion and Shock Waves, Method of Characteristics

The nonlinearity of Burgers equation allows us to understand the origin of abrupt changes in pressure, which will be assumed to be discontinuous to a first approximation, although strictly discontinuous phenomena do not exist in real life.

To build simple analytical solutions to this equation, the mathematical method known as the method of characteristics (or *Riemann invariants method*) is used (however, this method will not be detailed here [34]). In what follows, we restrict ourselves to a qualitative description. Notice that this method is applicable to other discontinuous phenomena such as road traffic or the formation of tidal bores.

Losses are ignored in a first step. From the weakly nonlinear equation (8.71), it is derived that the velocity of a signal point propagating along the x-axis for a fixed observer is $c = c_0 + \frac{1}{2}(\gamma + 1)v$. The maximum of the acoustic wave propagates faster than the minimum. The wave becomes distorted during the propagation (see Fig. 8.11). Under the assumption of weak nonlinearity, any signal (plane wave) is necessarily transformed into a shock wave, even if the sound level at the source is low, as long as the dissipative phenomena are not taken into account, as is done here. The higher the amplitude of the wave at the origin, the faster the wave is distorted, and the shorter is the distance x_c where the shock wave grows [54]. Using the method of characteristics, one can show that this distance is written:

$$x_c = \frac{2\gamma P_0 c_0}{(\gamma + 1)\,[\mathrm{d}p/\mathrm{d}t]_{\max}} \text{ where } [\mathrm{d}p/\mathrm{d}t]_{\max} \text{ at } x = 0. \tag{8.75}$$

From (8.75), it turns out that x_c also depends on the shape of the signal, through the term $[\mathrm{d}p/\mathrm{d}t]_{\max}$. Thus, for an initially sinusoidal signal, x_c is a decreasing function of frequency.

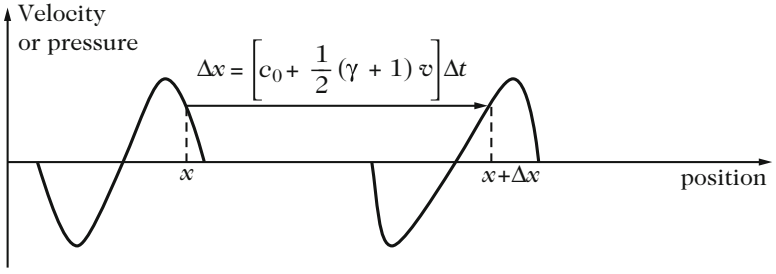

Fig. 8.11 Wave distortion: evolution of a sinusoidal signal for a traveling plane wave (pressure or velocity) governed by the weakly nonlinear equation. Each point of the waveform travels with a given characteristic velocity that depends of the amplitude, which distorts the signal

Equation (8.68), with (8.70), implies that the acoustic velocity v is constant over time ($dv/dt = 0$) along some lines (the so-called characteristics) of slope $c = c_0 + \frac{1}{2}(\gamma + 1)v$ in the (x, t)-plane. The method of characteristics illustrates the "cumulative" effect of the nonlinear distortion during wave propagation. The intersection of two characteristics in this plane corresponds to two possible values of sound pressure at the same point simultaneously: this corresponds to the formation of a shock wave. The first intersection yields an estimation for the shaping distance of the shock wave x_c. Beyond this point, the method of characteristics implies the existence of multivalued solutions, which is non-physical! It becomes then necessary to introduce a new condition to describe the shock. This condition is given by writing the conservation of mass across the shock wave, the so-called law of equal areas. It follows that the structure of the wave has a "sawtooth" shape, with a decreasing amplitude in the subsequent propagation. This wave is also called the "N-wave" (see, e.g., [54]).

The distortion of an initially sinusoidal wave is shown in the frequency domain as an energy transfer from the fundamental component of the signal to higher order harmonics [this is illustrated quantitatively by the Fubini equations (8.73)].

8.4.3 Competition Between Nonlinear Effects and Dissipation

In the absence of losses, the model systematically predicts wave distortion and N-wave formation. The amplitude of this wave decreases, regardless of the intensity of the source signal (even if it is very low), and whatever the shape of the signal, as long as the wave propagates far enough! This is in contradiction with experiments showing that the initial amplitude of the source signal influences the nature of the produced sound. The model is therefore incomplete.

Taking the losses into account helps in obtaining a model which is closer to reality. The goal here is to a priori estimate the order of magnitude of competing phenomena: nonlinear effects and visco-thermal losses. As a consequence, losses may damp the signal before it has time to distort. In this case, the context of linear acoustics is sufficient to model the phenomena. For strong nonlinear phenomena, a possibility exists when the amplitude of the N-wave becomes low enough so that the dissipative effects are dominant. Since the visco-thermal losses at walls are an increasing function of frequency, the N-wave is damped and deformed over time to tend ultimately to a sinusoidal signal of very low amplitude. Notice that, during the formation of the shock wave, both the volume visco-thermal losses (usually ignored in the pipe) and visco-thermal losses in the boundary layer describe the shock wave shape correctly. In practice, the angles of the shock wave are "rounded" by dissipation.

8.4.4 *Shock Waves and Brassy Sounds*

The sound levels inside wind instruments can be very high (about 130–170 dB), and only a small part of the acoustic energy is transmitted to the external air. One way to a priori notice the presence, or the absence, of nonlinear phenomena, consists in estimating the distance of shock formation from the source signal. This procedure has been used for pressure signals measured inside a trombone mouthpiece [35]. The measured distance is of the order of magnitude of several meters, which suggests the presence of spectacular nonlinear effects in the instrument (recall that the length of the cylindrical part of the trombone, the main slide, is between 2 and 3 m).

Internal acoustic pressures corresponding to a high F (F4—frequency 350 Hz) were measured at the input of a trombone slide and at the slide end, for various sound levels (see Fig. 8.12). It is observed that the input signal is slightly distorted for increasing amplitudes, and that a spectacular distortion is visible on the signal at the output of the slide. If a note is played at the sixth position (for a slide near its maximum length, 2.8 m, which enhances the cumulative effect of nonlinear propagation), the distortion is such that shock waves are visible. The resulting spectral enrichment of the higher harmonics is also found in the sound radiated by the instrument. These sounds with a specific tone color are often called "brassy sounds" by the players.

The question of the propagation in bells is not discussed here (see Chap. 7). Outside the instrument, the radiated sound looks like a series of pulses generated at the frequency of the played note (it is calculated in the model by deriving the flow rate at the output). These high frequencies are totally transmitted to the external air and do not return to the lips of the player. Thus, they are not involved in the

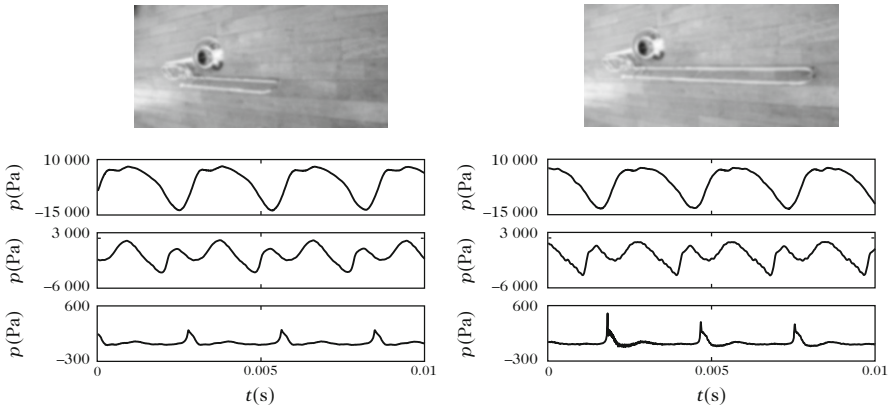

Fig. 8.12 Shock waves in a trombone illustrated by pressure signals measured at the input of the instrument, at the slide output, and 20 cm outside the bell, respectively (*from top to bottom* on the figure). The note F4 (350 Hz) is played fortissimo in first (*left*) and in sixth position (*right*), the length of the cylindrical part being 1.80 and 2.80 m, respectively

self-sustained oscillations. This is an additional argument to justify the use of a linear propagation model (input impedance) for the analysis of sound production, which is the topic of the next chapter. In addition, this also justifies the following simplification currently used for synthesized sounds: in a first step, the synthesized sounds are obtained from a model of linear resonator, in a second step the sounds obtained at the input of the instrument propagate nonlinearly and radiate [47, 65, 74]. Such synthesized sounds simulate "brassy sounds" in a very realistic manner.

Only trombone brassy sounds were presented here, but in fact these "brassy sounds" are characteristics of all brass instruments, including those with predominantly conical bore. Nevertheless, the nonlinear distortion phenomenon is less pronounced in cones than in cylinders. We can probably see there an explanation for the distinction used by musicians between "bright brass" with a preponderant cylindrical bore (trumpet and trombone), and "soft brass" with a preponderant conical bore (cornet, flugelhorn, French horn, and tuba) (see Fig. 8.13) [50]. Another distinction between these types of instruments is due to the shape of the mouthpiece [28].

Woodwind instruments do not produce "brassy sounds," and it seems also that they are not subjected to, even small, nonlinear distortion effects [30]. However, nonlinear phenomena of a different nature can be seen, which are located at open holes, as it will be discussed in the next section.

Fig. 8.13 Two examples of brass instrument families, each having one cylindrical bore instrument and another with a conical bore. *Left*: trumpet (*cylindrical*) and bugle (*cone*). *Right*: trombone (*cylindrical*) and low saxhorn (*cone*)

8.4.5 *Localized Nonlinear Dissipation*

When the particle velocity is high, jet separation phenomena at geometric singularities, like openings, may occur (see, for example, Chap. 10, Sect. 10.3.1.2). These phenomena, which are standard in fluid mechanics, occur less frequently in acoustics since they only appear for velocities larger than or equal to nearly 1 m/s, which corresponds to very intense sound levels.[10] However, these velocities correspond to a rather weak acoustic Mach number, which explains why these separation phenomena, when they occur, are generally more pronounced than the nonlinearity due to propagation. The phenomenon of jet separation may be of little consequence if it sticks quickly back to the wall. Otherwise, the interaction of the jet with the external fluid at rest generates vortices, because of shear effects. Part of the kinetic energy of the jet is absorbed by the vortices and further dissipated as heat by friction. This effect will be discussed in the next chapter where the output jet of a reed canal is examined. Finally, dissipation of acoustic energy exists, and the nonlinearity can be reasonably modeled as a nonlinear resistance.

8.4.5.1 Simple Quasi-Static Model for the End of a Pipe

Consider the end of a tube, assuming zero impedance, in which a periodic flow has the form $v = v_0 \sin \omega t$. Assuming that a proportion of the kinetic energy is dissipated, the required pressure p_s to maintain the flow is written:

$$p_s = c_d \frac{1}{2} \rho v \, |v| \, . \tag{8.76}$$

In fact there is no reason for the coefficient c_d to be independent of speed. Atig et al. [5], in particular, have shown that this coefficient is larger when $v > 0$ (outgoing jet) that when $v < 0$ (incoming jet) and the value of this coefficient becomes larger as the radius of curvature at the pipe output decreases (see Fig. 8.14).

The same authors have shown elsewhere [4, 10] that considering either c_d as a constant value, or two different values for the outgoing and incoming flows, respectively, has little influence on the oscillation of a clarinet, the relevant parameter being the average value of the coefficient. Therefore a model with one constant parameter, though very approximate, may lead to satisfactory results. In this case, we have

$$p_s = c_d \frac{1}{2} \rho v_0^2 \sin \omega t \, |\sin \omega t| = c_d \frac{1}{2} \rho v_0^2 \, \frac{8}{3\pi} \sin \omega t, \tag{8.77}$$

[10] For a pure traveling plane wave, a particle velocity of 1 m/s corresponds to a level of 400 Pa, or 146 dB SPL.

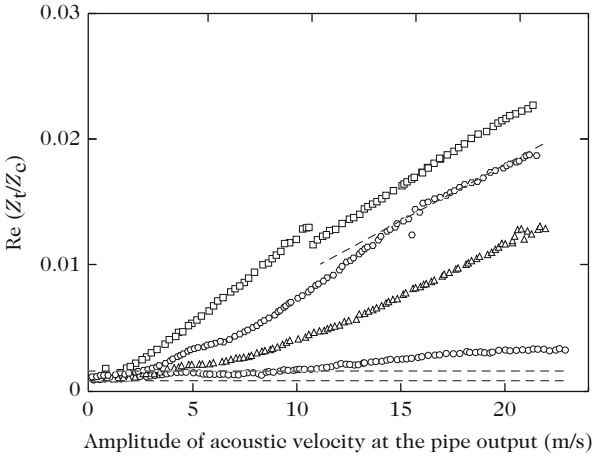

Fig. 8.14 Real part of the normalized end impedance Z_t/Z_c as a function of the velocity v_0 at the output of the pipe, for various radii of curvature r: *open circle* $r = 4$ mm; *triangle symbol*: $r = 1$ mm; *asterisk symbol*: $r = 0.3$ mm; *square symbol*: $r = 0.01$ mm. The inclined *straight dashed line* corresponds to the model of pressure losses for the outgoing jet with $c_d = 13/9$, and the two *horizontal dashed lines* correspond to the linear losses with and without screen, respectively. From [3]

if only the first term of the Fourier series is kept (first harmonic approximation). The power dissipated over a period is then:

$$P = \overline{p_s v} S = \frac{2c_d}{3\pi} \rho v_0^3 S. \tag{8.78}$$

Within the framework of the first harmonic approximation, assuming that the end impedance is real, it is found equal to:

$$Z_t = \frac{4c_d}{3\pi} M Z_c, \tag{8.79}$$

where $M = v_0/c$ is the acoustic Mach number. Experiments show that this simple model reflects the asymptotic behavior of nonlinear impedance fairly well (within the context of the first harmonic method). In practice, it is valid for high velocities (typically $v_0 > 10$ m/s, see Fig. 8.14). The definition of impedance in a nonlinear regime would deserve much more care, but if one satisfies with a perturbation approach (the linear speed is calculated, and injected in the "nonlinear" impedance expression), the validity of (8.79) can be assumed. The value of the coefficient c_d is difficult to predict theoretically and it is easier to determine it experimentally.

8.4.5.2 Side Hole

In the case of a side hole one can expect to see nonlinear resistances both in series and in parallel branches of the tube model (see Chap. 7). Dalmont et al. were able to highlight these resistances, however, they also have shown that the resistance in series could reasonably be neglected when the diameter of the side hole is significantly smaller than the diameter of the main guide [20]. Again here, the parameters are highly dependent on the radii of curvature at the junction and at the output of the hole. The use of nonlinear impedance in a calculation of input impedance, or of reflection impedance, can be done simply with perturbation methods.

The influence of high sound level (up to 10 kPa, or nearly 174 dB) on the self-sustained oscillations of a clarinet type instrument has been investigated ([4], see Chap. 9, Sect. 9.4.6) for a cylinder. It shows the importance of nonlinear losses at the end on sound pressure level. One can also show that losses in a side hole reduce the playing frequency, which is easily understood: if the, even real, impedance of a side hole, increases notably, it may eventually act as a closed end for the hole! The conventional calculation of playing frequency that ignores the losses and uses purely imaginary impedances, shows here an obvious limit. Debut et al. [21] proposed an approximate formula to account for this.

8.5 Geometric Nonlinearities in Gongs and Cymbals

Gongs and cymbals perfectly illustrate a number of fundamental properties of nonlinear systems: sensitivity to initial conditions, bifurcations, hysteresis, and routes to chaos. Geometric nonlinearities are also present in other instruments, such as the steelpan [45].

By striking an orchestral gong (also called a Chinese tam-tam, see Fig. 8.15) gently near its center with a mallet, one can clearly hear the excited modes and their extinction. The vibration is then adequately described by a linear model. If one hits harder, other frequencies appear, and a simple linear analysis does not account for them.

The vibration spectrum (and, consequently, that of the produced sound) can only be explained with the help of nonlinear theories that predict the existence of *combinations of resonances*. These combinations contribute to enrich the number of emitted frequencies considerably.

Finally, if one hits even stronger, this yields a continuous spectrum. In other words, the excited frequencies are no longer separable from one another. A detailed analysis performed on the obtained signals shows that *chaotic* oscillations are

Fig. 8.15 Orchestral gong, or Chinese tam-tam. Courtesy © Rythmes et Sons

obtained (see Fig. 8.16).[11] The strict definition of this term will be specified later. Notice that, although the spectrum of the sound obtained at strong impact is continuous, it is not that of a random noise.

In this section, the nonlinear phenomena that are the origin of the specific sounds of those instruments are described. We show, in particular, that they are due to the *geometric nonlinearity* caused by large amplitude motion of the structure, when subjected to a strong impact. To facilitate the understanding, a simplified mathematical description of a subsystem composed of a small number of nonlinearly coupled oscillators will be conducted. Finally, the generalization to nonlinear continuous systems with a large number of degrees of freedom will be made. Spherical shells subjected to large amplitude oscillations will serve as an example of a structure for which an analytical description of such phenomena is possible.[12]

[11]The definition of chaos, as well as the method used for analyzing and quantifying such oscillations, will be presented throughout this chapter (see Sect. 8.6, in particular). Here, we can see some first properties of chaotic oscillations: irregularity in the time-domain, and a broadband spectrum where it is not possible to discriminate individual spectral peaks anymore. Sensitivity to initial conditions is another essential feature of chaotic oscillations, which will be discussed later in detail.

[12]An important part of the topics presented in this section are the results of new insights on the nonlinear vibrations of thin structures which were published during the last 15 years. See, in particular, the Ph.D. thesis by O. Thomas, and his joint work with colleagues [8, 11, 60, 61, 64, 68].

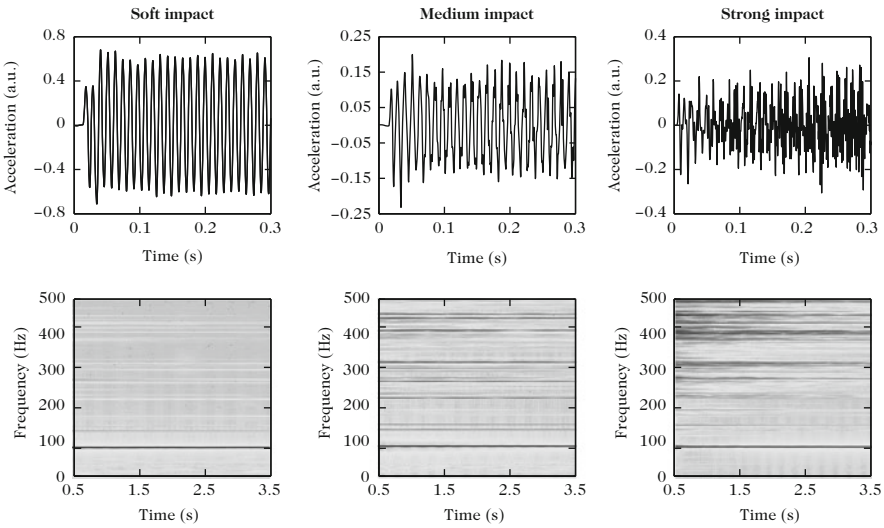

Fig. 8.16 Vibration waveforms and spectra of a gong struck with increasing impact force. The three *upper figures* show the vibration signals delivered by an accelerometer glued to a gong excited near its center with a mallet. The three figures at the *bottom* show the corresponding spectrograms, which represent the spectral content of these signals over time. The *dark lines* corresponds to high level, the *light gray lines* to low level. For a "soft" impact, the vibration signal is almost sinusoidal, the spectrum shows an intense spectral line around 90 Hz, and only a few lines at higher frequencies, at a lower level. For a "medium" impact, the intensity of the 90 Hz component decreases, whereas the level of higher frequencies increases. Simultaneously, new components with a significant energy appear in the higher range of the spectrum. For a "strong" impact, the energy is still increasing in the high frequency range (between 200 and 500 Hz in the spectrogram), the spectrum becomes continuous, and it is no longer possible to separate the spectral lines. The waveform loses its periodic nature and becomes chaotic (see Sect. 8.6)

8.5.1 Sinusoidal Forced Excitation

Impact clearly corresponds to the standard use for gongs and cymbals. However, it is difficult to analyze the phenomena, because of the large bandwidth of the excitation spectrum. For this reason, it is preferable to observe the phenomena experimentally with a forced sinusoidal excitation. This procedure has the advantage of presenting the main phenomena, and thus allowing easier modeling. Nevertheless, recall that, unlike the case of linear systems, one cannot conclude here that the oscillations obtained through normal impact are the superposition of the oscillations obtained by summing the results obtained for each frequency of the excitation spectrum, since the superposition principle is not anymore valid for nonlinear oscillations.

Figure 8.17 shows an example of experiments where the amplitude of the excitation force gradually increases at a given point of a gong. Similar experiments were conducted on cymbals. An excitation frequency close to one natural frequency of the structure is selected, in order to generate high amplitude. The vibration velocity is

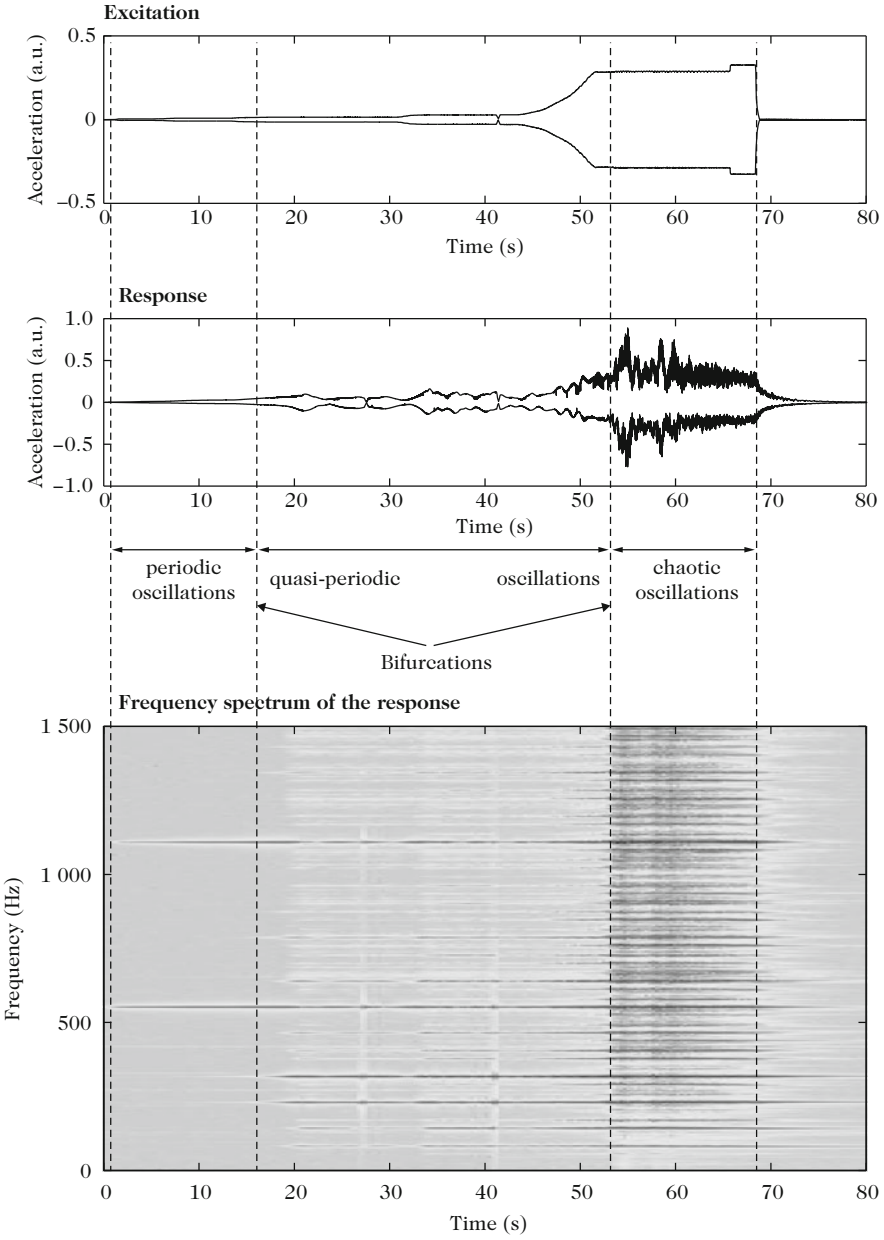

Fig. 8.17 Forced sinusoidal excitation of a gong. (See [60] and Sect. 8.5.1 in the text for a detailed description of this experiment)

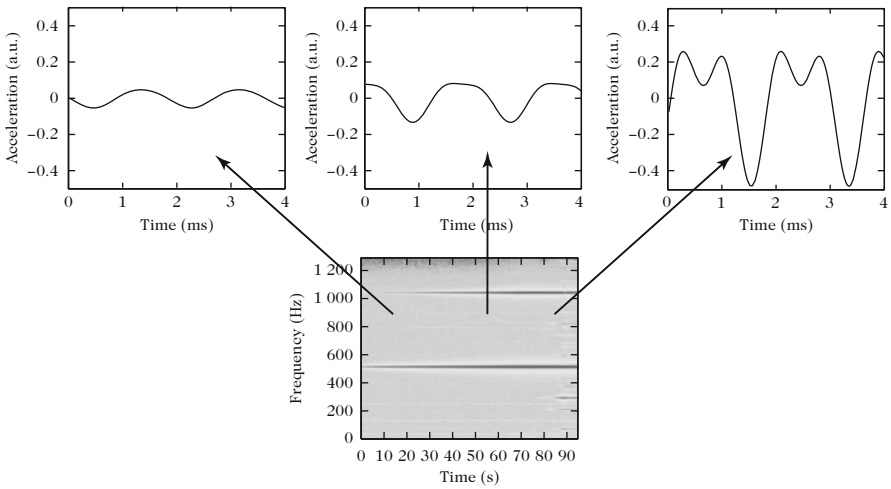

Fig. 8.18 (*Top*) Vibration acceleration at a given point of the gong for increasing amplitude of the sinusoidal excitation force. (*Bottom*) Corresponding spectrogram. One can see an increasing distortion of the wave and an enrichment in harmonics in the spectrum over time. For reasons of clarity, the frequency scale on the spectrogram is intentionally reduced and does not show the higher harmonics 2Ω, 3Ω, 4Ω,... which are nonetheless present in the vibration spectrum

measured at a point on the structure with the help of a laser vibrometer. It is observed that the obtained waveform is, first, a sine wave. Some harmonics gradually appear as the amplitude of the excitation further increases (see Fig. 8.18). For a particular value of this amplitude (or *threshold*), additional frequencies suddenly appear in the spectrum and are inserted between the harmonics. A detailed examination of the values of these frequencies shows that they are algebraically related to the harmonic excitation. Moreover, they correspond to other eigenmodes of the structure than the one initially excited (see the next section). The emergence of these new frequencies is characteristic of what is called a *bifurcation*. Mathematically, we will see in the next sections that such a bifurcation corresponds to a loss of stability for the system, and that the stability domain depends on both the amplitude and frequency of the excitation.

When the amplitude of the exciting force continues to increase, there is a new threshold that causes a second bifurcation. For slightly damped systems, such as metallic percussion instruments, one reaches a chaotic regime on this second bifurcation. It can be seen in Fig. 8.17 that the vibration spectrum beyond this threshold is so dense that there it is almost continuous. When listening, the characteristic shimmering sound of a gong (or a cymbal) is easily recognized, although the instruments are excited with a single frequency.

8.5.2 Internal Resonances

To explain these phenomena, a brief return back to the linear case presented in Chap. 3 is necessary, where it was established that the vibrations of a conservative finite structure can be represented as a projection onto a eigenmodes basis. In what follows, we will see that the nonlinear behavior of gongs can be described with the help of their linear modal properties. As seen in Chap. 3, the linear motion of a structure, which is assumed to be non dissipative so far, can be written in the following generic form:

$$\mathscr{L}(\boldsymbol{\xi}) + \ddot{\boldsymbol{\xi}} = 0$$
$$+ \text{boundary conditions}, \tag{8.80}$$

where $\mathscr{L}$ is a *linear operator* involving the displacement field $\boldsymbol{\xi}$ of the structure and its spatial derivatives. Then, this motion can be decomposed on the basis of its own eigenmodes, each mode being characterized by an eigenfrequency and an associated eigenshape.

Thus, for a given material, geometry (thickness, curvature, size,...) and boundary conditions, the eigenfrequencies and eigenmodes of the structure are fully determined. If some algebraic relations exist between the eigenfrequencies, such as:

$$\sum_{i=1}^{L} m_i \omega_i = 0, \tag{8.81}$$

where m_i is an integer (positive or negative), the structure is said to have *internal resonances*. Some relations of the following types, for example:

$$\omega_1 + \omega_2 = \omega_3 \quad \text{or} \quad 2\omega_3 - \omega_1 = \omega_5. \tag{8.82}$$

can be exhibited.

In the case of structures with a circular geometry, some other interesting properties are observed: one can discriminate between the *asymmetric* modes, and the *axisymmetric* modes which show a symmetry with regard to the revolution axis (see Fig. 8.19).

In fact, the *asymmetric* modes are grouped by pairs, whose mode shapes are identical, showing only a phase shift of $\pi/2p$, where p is the number of nodal diameters. If the structure is perfectly homogeneous, the eigenfrequencies, denoted here, for example, ω_{n1} and ω_{n2}, are theoretically identical. In practice, measurements show that these frequencies differ slightly, as a result of some unavoidable imperfections in the structure (which may include residual stresses), and because of the attachment system. For inhomogeneous structures (such as gongs), one can observe some important differences between both frequencies of a mode pair. An important subset of the relations (8.81) are those where:

$$m_k \omega_k = m_i \omega_i + m_j \omega_j \quad \text{with} \quad |m_i| + |m_j| = 2, \tag{8.83}$$

This type of internal resonance is of prime importance in the case of *quadratic nonlinearities*, which govern the physical behavior of gongs and cymbals.

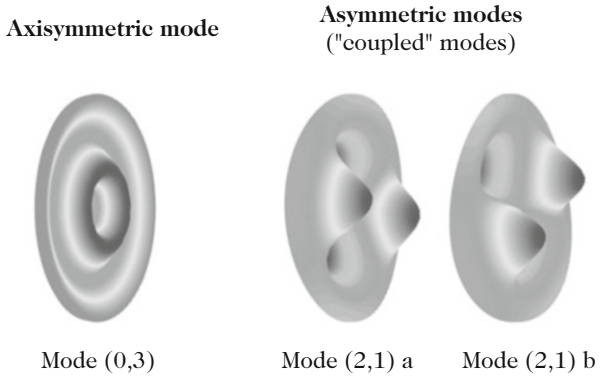

Fig. 8.19 Examples of axisymmetrical modes and asymmetrical modes of a gong

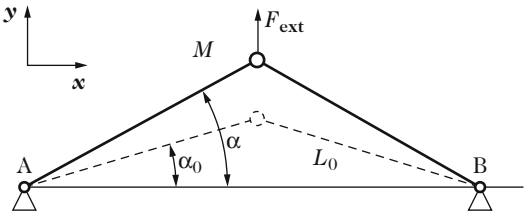

Fig. 8.20 Set of two joint articulated bars illustrating an example of geometrical nonlinearity

8.5.3 Weakly Nonlinear Regime

Structures such as gongs, cymbals, and thin spherical shells, show an asymmetry due to curvature. In fact, the transverse motion is easier in the direction of the hollow side than in the rounded one. This is an example of geometrical nonlinearity, which is comparable to the case of the interrupted pendulum seen in Sect. 8.1. Another qualitative interpretation of such a geometrical nonlinearity can be made for a simple system of two articulated rods oscillating around a position defined by an initial angle α_0 that represents the curvature (see Fig. 8.20) [62].

Let E be the Young's modulus of the rods, A their cross-sectional area, and L_0 their length at rest. It can be shown that, under the action of a vertical force with amplitude F, the transverse displacement y of the joining point of the rods is linked to the force by the relation:

$$F = 2EA \left\{ \frac{y}{L_0} \sin^2 \alpha_o + \frac{3}{2} \sin \alpha_0 \left(\frac{y}{L_0} \right)^2 + \frac{1}{2} \left(\frac{y}{L_0} \right)^3 \right\} . \tag{8.84}$$

Quadratic terms in y^2 are seen in Eq. (8.84). This equation also shows the presence of cubic terms: this result can be generalized to more complex curved structures,

something that we will admit here without proof.[13] Let us now return to the experiments of the gong excited at its center by a sinusoidal force of frequency Ω close to the eigenfrequency of one particular *axisymmetric* mode. As shown in Fig. 8.18, the increase of the excitation amplitude results in an asymmetry in the vibration waveform where the oscillations are more distorted for positive values of the acceleration than for negative values. It is an example of quadratic nonlinearity, which, in the spectral domain, is characterized by the presence of even harmonics $(2\Omega, 4\Omega, \ldots)$.

Beyond the first bifurcation, a fine frequency analysis shows that the new frequencies arising in the spectrum are related to the driving frequency by the following combination rules, also called *combination of resonances*:

$$m_k \Omega = m_i \omega_i + m_j \omega_j \quad \text{with} \quad |m_i| + |m_j| = 2. \tag{8.85}$$

where m_k is a positive integer, and m_i and m_j positive (or negative) integers. These combination rules are the result of both the internal resonances of the structure (particular relationships between eigenfrequencies) and quadratic nonlinearity. One practical consequence of the excitation of such frequencies is, for example, the possibility of exciting asymmetric modes with a shaker attached at the center of symmetry of the structure. This would never be possible in the linear regime (see Chap. 3) since this point corresponds to a node for asymmetric modes. A nonlinear coupling only can explain such a phenomenon. An experimental illustration of these resonances is described in Sect. 8.5.5.

8.5.4 Energy Transfer Through Combination of Resonances

To analyze the phenomena described above, a simple example of nonlinear quadratic coupling between two discrete oscillators will be used. The method of *multiple scales* is used for solving the problem [51]. The system under consideration is the following:

$$\begin{cases} \ddot{x}_1 + \omega_1^2 x_1 = \varepsilon \left[-\beta_{12} x_1 x_2 - 2\mu_1 x_1 \right], \\ \ddot{x}_2 + \omega_2^2 x_2 = \varepsilon \left[-\beta_{21} x_1^2 - 2\mu_2 x_2 + P \cos \Omega t \right]. \end{cases} \tag{8.86}$$

The variables x_1 and x_2 are the displacements of the oscillators. The frequencies ω_1 and ω_2 are the eigenfrequencies of each oscillator in its linear regime. In the absence of driving force, damping and nonlinearities, the system (8.86) reduces to the free oscillations of two independent linear oscillators. The right-hand sides of

[13] In this example, the terms in y^2 and y^3, respectively, are comparable as long as α_o is not supposed to be small. We will see later that the quadratic terms are predominant in thin shells.

the differential system (8.86) represent the perturbation terms with regard to this ideal linear case. The dimensionless quantity $\varepsilon \ll 1$ indicates that these terms are small. The quadratic nonlinear coupling is ensured by the terms $\beta_{12}x_1x_2$ and $\beta_{21}x_1^2$. It can be shown, and this will be assumed here, that these two terms are sufficient for guaranteeing the generality of quadratic coupling. In other words, it is not necessary to add a term in x_2^2, for instance, in the first equation, since an appropriate change of variables would yield a formulation similar to (8.86) (see a justification for this property in Sect. 8.7 devoted to nonlinear normal modes). As an example, a system with an internal resonance $\omega_2 = 2\omega_1 + \varepsilon\sigma_1$ is studied, where σ_1 is the parameter of *internal detuning*. The driving frequency Ω is chosen close to ω_2 so that one can write $\Omega = \omega_2 + \varepsilon\sigma_2$ where σ_2 is the parameter of *external detuning*.

8.5.4.1 Solution by the Method of Multiple Scales

In this section, we want to obtain the expressions of both amplitudes a_1 and a_2 of x_1 and x_2, respectively, as a function of frequency, or, equivalently, in terms of the external detuning parameter σ_2. We also want to determine the threshold values for which bifurcations occur. In the example presented here, this implies, in practice, to calculate the amplitude of the forcing term for which a subharmonic of order two of the driving frequency Ω just appears.

Principle and Main Steps of the Calculation

The example presented here is very rich, since it contains the essential concepts and methods used in the study of nonlinear oscillators. To assist the reader, we start by presenting a summary of the main steps of the calculation with their respective goals.

1. Definition of the time scales, and general form of the solution.
2. Solvability conditions. Elimination of the secular terms.
3. Autonomous system and fixed points.
4. Stability of the system.
5. Amplitudes and phases of the solution.

Time Scales and General Form of the Solution

The time scales are defined as:

$$T_j = \varepsilon^j t \quad \text{with} \quad j \geq 0, \tag{8.87}$$

and the solutions are expanded in increasing power of ε

$$\begin{cases} x_1(t) = x_{10}(T_0, T_1) + \varepsilon x_{11}(T_0, T_1) + O(\varepsilon^2), \\ x_2(t) = x_{20}(T_0, T_1) + \varepsilon x_{21}(T_0, T_1) + O(\varepsilon^2), \end{cases} \tag{8.88}$$

In what follows, the expansion is limited to the first order in ε. In (8.87), notice that the differentiation operators with respect to time are such that:

$$\begin{cases} \dfrac{\partial}{\partial t} = \dfrac{\partial}{\partial T_0} + \varepsilon \dfrac{\partial}{\partial T_1}, \\ \dfrac{\partial^2}{\partial t^2} = \dfrac{\partial^2}{\partial T_0^2} + 2\varepsilon \dfrac{\partial}{\partial T_0} \dfrac{\partial}{\partial T_1}. \end{cases} \tag{8.89}$$

From here, we use the notation $D_j = \frac{\partial}{\partial T_j}$. Inserting (8.89) in (8.86), and identifying the terms of identical power in ε, yields

- to order $\varepsilon^0 = 1$:

$$\begin{cases} D_0^2 x_{10} + \omega_1^2 x_{10} = 0, \\ D_0^2 x_{20} + \omega_2^2 x_{20} = 0, \end{cases} \tag{8.90}$$

- to order ε:

$$\begin{cases} D_0^2 x_{11} + \omega_1^2 x_{11} = -2D_0 D_1 x_{10} - \beta_{12} x_{10} x_{20} - 2\mu_1 D_0 x_{10}, \\ D_0^2 x_{21} + \omega_2^2 x_{21} = -2D_0 D_1 x_{20} - \beta_{21} x_{10}^2 - 2\mu_2 D_0 x_{20} + P \cos \Omega t. \end{cases} \tag{8.91}$$

The solutions of the system (8.90) are written in general form:

$$\begin{cases} x_{10}(t) = A_1(T_1) e^{j\omega_1 t} + A_1^\star(T_1) e^{-j\omega_1 t}, \\ x_{20}(t) = A_2(T_1) e^{j\omega_2 t} + A_2^\star(T_1) e^{-j\omega_2 t}, \end{cases} \tag{8.92}$$

where the exponent (*) indicates the complex conjugate.

Solvability Conditions

The complex quantities $A_1(T_1)$ and $A_2(T_1)$ are functions of $T_1 = \varepsilon t$, and are still unknown at this stage of the solving. To determine them, the expressions (8.92) are inserted in (8.91), and we derive the conditions for avoiding *secular terms* in the solution. This yields the so-called *solvability conditions* which are written here:

$$\begin{cases} -2j\omega_1\left(\dfrac{\partial A_1}{\partial T_1}+\mu_1 A_1\right)-\beta_{12}A_1^* A_2 e^{j\sigma_1 T_1}=0, \\ -2j\omega_2\left(\dfrac{\partial A_2}{\partial T_1}+\mu_2 A_2\right)-\beta_{21}A_1^2 e^{-j\sigma_1 T_1}+\dfrac{P}{2}e^{j\sigma_2 T_1}=0. \end{cases} \tag{8.93}$$

These Eqs. (8.93) are usually solved in the following polar form:

$$\begin{cases} A_1(T_1)=\dfrac{a_1}{2}e^{j\theta_1}, \\ A_2(T_1)=\dfrac{a_2}{2}e^{j\theta_2}, \end{cases} \tag{8.94}$$

where both the amplitudes a_i and phases θ_i are functions of T_1. Substituting these expressions in (8.93), we get the dynamic system that governs the evolution of amplitudes and phases of the oscillators at the time scale T_1, corresponding to *slow* changes in the system. It is written here:

$$\begin{cases} \dfrac{\partial a_1}{\partial T_1}=-\mu_1 a_1-\dfrac{\beta_{12}a_1 a_2}{4\omega_1}\sin(\sigma_1 T_1+\theta_2-2\theta_1), \\ a_1\dfrac{\partial \theta_1}{\partial T_1}=\dfrac{\beta_{12}a_1 a_2}{4\omega_1}\cos(\sigma_1 T_1+\theta_2-2\theta_1), \\ \dfrac{\partial a_2}{\partial T_2}=-\mu_2 a_2+\dfrac{\beta_{21}a_1^2}{4\omega_2}\sin(\sigma_1 T_1+\theta_2-2\theta_1)+\dfrac{P}{2\omega_2}\sin(\sigma_2 T_1-\theta_2), \\ a_2\dfrac{\partial \theta_2}{\partial T_2}=\dfrac{\beta_{21}a_1^2}{4\omega_2}\cos(\sigma_1 T_1+\theta_2-2\theta_1)-\dfrac{P}{2\omega_2}\cos(\sigma_2 T_1-\theta_2). \end{cases} \tag{8.95}$$

Autonomous System and Fixed Points

In order to determine the conditions for obtaining solutions to the nonlinear coupled system (8.86), it is necessary to express first Eq. (8.95) as an *autonomous system* or, equivalently, in the form $\dot{X}=F(X)$ where the time variable T_1 is no longer present in the right-hand side. In practice, this procedure is equivalent to using the variables $\gamma_1=\sigma_2 T_1-\theta_2$ and $\gamma_2=\sigma_1 T_1+\theta_2-2\theta_1$, which yields

$$\begin{cases} \dfrac{\partial a_1}{\partial T_1} = -\mu_1 a_1 - \dfrac{\beta_{12} a_1 a_2}{4\omega_1} \sin\gamma_2, \\ \dfrac{\partial \gamma_1}{\partial T_1} = \sigma_2 - \dfrac{\beta_{21} a_1^2}{4\omega_2 a_2} \cos\gamma_2 + \dfrac{P}{2\omega_2 a_2} \cos\gamma_1, \\ \dfrac{\partial a_2}{\partial T_2} = -\mu_2 a_2 + \dfrac{\beta_{21} a_1^2}{4\omega_2} \sin\gamma_2 + \dfrac{P}{2\omega_2} \sin\gamma_1, \\ \dfrac{\partial \gamma_2}{\partial T_2} = \sigma_1 - \dfrac{\beta_{12} a_2}{2\omega_1} \cos\gamma_2 + \dfrac{\beta_{21} a_1^2}{4\omega_2 a_2} \cos\gamma_2 - \dfrac{P}{2\omega_2 a_2} \cos\gamma_1. \end{cases} \tag{8.96}$$

The so-called *fixed points* are obtained by eliminating the time derivatives in (8.96). This corresponds to the stationary solutions of the system, i.e., those of interest in the case of a forced oscillations. We get

$$\begin{cases} a_1 \left(\mu_1 + \dfrac{\beta_{12} a_2}{4\omega_1} \sin\gamma_2 \right) = 0, \\ \sigma_2 - \dfrac{\beta_{21} a_1^2}{4\omega_2 a_2} \cos\gamma_2 + \dfrac{P}{2\omega_2 a_2} \cos\gamma_1 = 0, \\ -\mu_2 a_2 + \dfrac{\beta_{21} a_1^2}{4\omega_2} \sin\gamma_2 + \dfrac{P}{2\omega_2} \sin\gamma_1 = 0, \\ \sigma_1 + \dfrac{\beta_{21} a_1^2}{4\omega_2 a_2} \cos\gamma_2 - \dfrac{P}{2\omega_2 a_2} \cos\gamma_1 - \dfrac{\beta_{12} a_2}{2\omega_1} \cos\gamma_2 = 0. \end{cases} \tag{8.97}$$

Note Setting $a_1 = 0$ in (8.97) gives the expression for the amplitude a_2 of the second oscillator:

$$a_2 = \frac{P}{2\omega_2 \sqrt{\sigma_2^2 + \mu_2^2}}. \tag{8.98}$$

Recall that σ_2 is here the difference between the loading frequency and the oscillator's frequency, and that μ_2 is the "fluid" damping parameter. Thus, the variation of amplitude with frequency of a forced linear oscillator is obtained (see Chap. 2).

Stability of the Nonlinear Coupled System

Intuitively, the concept of instability can be represented by a physical system, slightly pushed aside from its equilibrium position, that continues to increasingly depart from equilibrium instead of returning back to it. In the case of gongs and cymbals, it is observed that, under a sufficient level of excitation, new frequencies

appear and, through a process of instability cascade (previously called nonlinear coupling), may lead to other components to form the richness of the sound.

From a mathematical point of view, the departures from equilibrium for a system of equations of several variables similar to (8.97) are calculated from the partial derivatives of each equation with respect to each variable. This yields what is called the *Jacobian matrix* or, more simply, the *Jacobian* of the system. Let f_1, f_2, f_3, f_4 be the four equations and $a_1, \gamma_1, a_2, \gamma_2$ the four variables of interest. The Jacobian is written:

$$\mathscr{J} = \begin{bmatrix} \frac{\partial f_1}{\partial a_1} & \frac{\partial f_1}{\partial \gamma_1} & \frac{\partial f_1}{\partial a_2} & \frac{\partial f_1}{\partial \gamma_2} \\ \frac{\partial f_2}{\partial a_1} & \frac{\partial f_2}{\partial \gamma_1} & \frac{\partial f_2}{\partial a_2} & \frac{\partial f_2}{\partial \gamma_2} \\ \frac{\partial f_3}{\partial a_1} & \frac{\partial f_3}{\partial \gamma_1} & \frac{\partial f_3}{\partial a_2} & \frac{\partial f_3}{\partial \gamma_2} \\ \frac{\partial f_4}{\partial a_1} & \frac{\partial f_4}{\partial \gamma_1} & \frac{\partial f_4}{\partial a_2} & \frac{\partial f_4}{\partial \gamma_2} \end{bmatrix}. \tag{8.99}$$

Each term of the Jacobian represents a small deviation from equilibrium. In order to calculate the stability of the equilibrium at point $a_1 = 0$, which corresponds to the conditions of appearance for oscillator 1, a standard method is used, where the eigenvalues λ_i of $\mathscr{J}$ are calculated. These eigenvalues are the roots of the determinant $\mathscr{J} - \lambda\mathscr{I}$, where $\mathscr{I}$ is the identity matrix. The following four eigenvalues are found:

$$\begin{cases} \lambda_1 = -\mu_2 + j\sigma_2, & \lambda_2 = -\mu_2 - j\sigma_2, \\ \lambda_3 = -\dfrac{\beta_{12} a_2}{4\omega_1} \sin\gamma_2 - \mu_2, & \lambda_4 = \dfrac{\beta_{12} a_2}{2\omega_1} \sin\gamma_2. \end{cases} \tag{8.100}$$

The system will be *unstable* if the real part of at least one root is positive, since, in this case, the general solution includes an exponential term that grows with time. Notice that λ_1 and λ_2 always have a negative real part, due to the presence of the damping term $\mu_2 > 0$ of the oscillator 2. These two roots are independent of oscillator 1, and correspond to the case of oscillator 2 in linear forced oscillations. It is therefore natural to have conditions of stability for these two roots. However, if one calculates the product of the other two roots:

$$\lambda_3\lambda_4 = -\frac{\mu_2\beta_{12} a_2}{2\omega_1} \sin\gamma_2 - \frac{\beta_{12}^2 a_2^2}{8\omega_1^2} \sin^2\gamma_2, \tag{8.101}$$

and considering the first equation in (8.97) we see that some situations may occur where the product $\lambda_3\lambda_4$ is strictly less than 0, i.e., where at least one of these two (real) roots is positive. A detailed calculation shows that this instability condition is satisfied if:

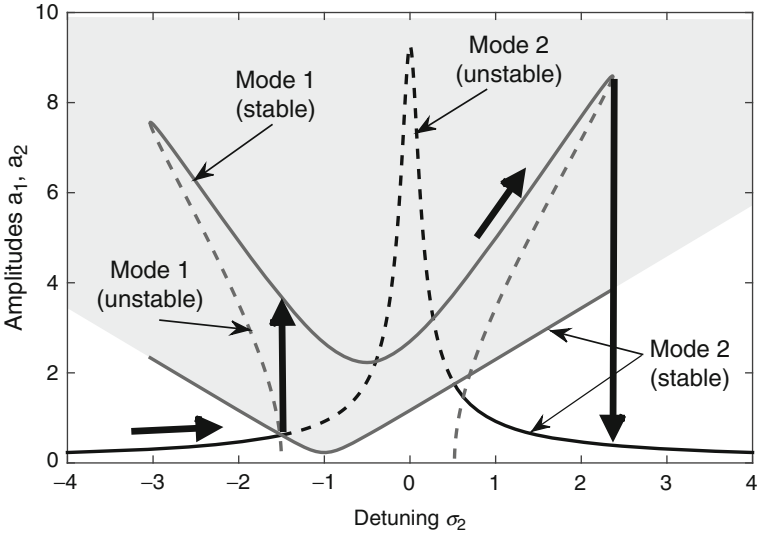

Fig. 8.21 Amplitudes a_1 and a_2 of two nonlinearly coupled oscillators, as a function of the external detuning parameter σ_2. The *gray area* represents the instability domain. The *arrows* indicate the path of the running point when moving on the frequency axis (σ_2) from left to right. The *dashed lines* correspond to unstable parts of the resonance curves, and the *solid lines* to stable parts

$$a_2 > \frac{2\omega_1}{|\beta_{12}|}\sqrt{4\mu_1^2 + (\sigma_1 + \sigma_2)^2}. \tag{8.102}$$

The instability zone corresponding to (8.102) is shown in gray color in Fig. 8.21. Notice that the amplitude threshold increases with the damping of oscillator 1, and as the frequency moves away from ω_2 ($\sigma_2 = 0$).

Amplitudes and Phases of the Solution

After this analysis, we are now able to complete the study by calculating the amplitudes a_1 and a_2, and the phases θ_1 and θ_2. As a result, the zero-order solution is obtained, whose general form was specified in (8.92). Combining (8.92) with (8.94), and considering the definitions of T_1, σ_1, σ_2 γ_1 and γ_2, we get

$$\begin{cases} x_{10} = a_1 \cos(\omega_1 t + \theta_1) = a_1 \cos\left(\dfrac{\Omega}{2}t - \dfrac{\gamma_1 + \gamma_2}{2}\right), \\ x_{20} = a_2 \cos(\omega_2 t + \theta_2) = a_2 \cos\left(\Omega t - \gamma_1\right). \end{cases} \tag{8.103}$$

By solving the system (8.97) corresponding to stationary solutions, the amplitudes are finally obtained as a function of the input parameters:

$$\begin{cases} a_2 = \dfrac{2\omega_1}{|\beta_{12}|}\sqrt{(\sigma_1+\sigma_2)^2+4\mu_1^2}, \\ a_1 = 2\left[-\Gamma_1 \pm \sqrt{\dfrac{P^2}{4\beta_{21}^2}-\Gamma_2^2}\right]^{1/2}, \\ \text{with} \quad \Gamma_1 = \dfrac{2\omega_1\omega_2}{\beta_{12}\beta_{21}}\left[2\mu_1\mu_2-\sigma_2(\sigma_1+\sigma_2)\right], \\ \text{and} \quad \Gamma_2 = \dfrac{2\omega_1\omega_2}{\beta_{12}\beta_{21}}\left[2\mu_1\sigma_2-\mu_2(\sigma_1+\sigma_2)\right]. \end{cases} \tag{8.104}$$

The expressions (8.103) show an important result, as expected: for steady-state oscillations, the frequency of the oscillator 2 is equal to the excitation frequency Ω, and the frequency of the oscillator 1 is exactly $\Omega/2$. This result is in accordance with the properties of internal resonance of the structure.

Figure 8.21 shows the curves of the amplitudes a_1 and a_2 of the coupled oscillators, as a function of the external detuning parameter σ_2, all other parameters being assumed to be constant. If the driving frequency increases (from left to right on the frequency axis), the following phenomena are observed:

1. First, the amplitude a_2 of oscillator 2 is examined. As long as the operating point is below the zone of instability, there is no subharmonic.
2. For the threshold value corresponding to the instability limit given by (8.102), the oscillator 1 suddenly appears. In the example shown, the amplitude a_1 is larger than a_2, and this remains true as long as the running point stays above the limiting instability curve.
3. As the maximum of the oscillator 1 curve is reached, the running point jumps back to the oscillator 2 curve, and the oscillation at $\Omega/2$ disappears.
4. If the frequency axis is described in the opposite direction by gradually reducing the excitation frequency, one observes qualitatively similar phenomena, but, in this case, the threshold values for which oscillator 1 appears are different. This is a characteristic *hysteresis* phenomenon.

8.5.5 Nonlinear Mechanical Model

8.5.5.1 Introduction

The purpose of this section is to show that the fundamental properties of gongs and cymbals can be described by a set of nonlinearly coupled oscillators, similar to the above-presented example. To do this, the study starts by examining a nonlinear model of flexural vibrations for a spherical shallow shell. In fact, almost all gongs and cymbals show a rotational symmetry, and a more or less pronounced curvature. A spherical cap has similar properties and is a suitable approximation of real shapes

observed in gongs and cymbals. Compared to real instruments, some discrepancies will be observed on modal frequencies and shapes, but the general results will be preserved. In addition, the spherical shape has the advantage of providing an analytic reference model.

The case of thin spherical shallow shells is considered here in the context of large amplitude oscillations. The same notation as in Sect. 3.5.4 of Chap. 3 is used. These assumptions form the basis of the Von Kármán equations (also called, sometimes, equations of Marguerre or Koiter in the specialized literature) [1, 63]. Hamdouni and Millet, in particular, have shown that these equations can be obtained from an asymptotic method applied to the general equations of elasticity [33]. As in the linear case (see Sect. 3.5.4 in Chap. 3), the equations of motion are written in polar coordinates, where (r, θ) are the coordinates of one current point of the shell, after projection on the horizontal plane. These equations are written [63]:

$$\begin{cases} \nabla^4 w + \dfrac{\nabla^2 F}{R} + \rho h \ddot{w} = L(w, F) - \mu \dot{w} + p, \\ \nabla^4 F - \dfrac{Eh}{R} \nabla^2 w = -\dfrac{Eh}{2} L(w, w), \end{cases} \tag{8.105}$$

where F is the Airy stress function, and L a bilinear quadratic operator, written in polar coordinates:

$$L(w, F) = w_{rr} \left(\frac{F_r}{r} + \frac{F_{\theta\theta}}{r^2} \right) + F_{rr} \left(\frac{w_r}{r} + \frac{w_{\theta\theta}}{r^2} \right) - 2 \left(\frac{w_{r\theta}}{r} - \frac{w_\theta}{r^2} \right) \left(\frac{F_{r\theta}}{r} - \frac{F_\theta}{r^2} \right). \tag{8.106}$$

In Eq. (8.105), F contains both linear and quadratic terms in w. As a consequence, $L(w, F)$ contains quadratic terms and cubic terms in w. Finally, the equation of flexural motion contains linear terms, quadratic terms and cubic terms in w. When $R \to \infty$, Eq. (8.105) represents the nonlinear flexural vibrations of a flat plate. In this case, the quadratic terms disappear, and only the cubic terms remain. To examine the relative significance of the different terms in these equations, it is necessary to write them in dimensionless form using the following variables [63]:

$$\begin{aligned} &r = a\overline{r}\,, \quad t = a^2 \sqrt{\rho h / D}\,\overline{t}\,, \quad w = h^3 / a^2 \overline{w}\,, \quad F = Eh^7 / a^4 \overline{F}\,, \\ &\mu = [2Eh^4 / Ra^2] \sqrt{\rho h / D}\,\overline{\mu}\,, \quad p = Eh^7 / Ra^6 \overline{p}. \end{aligned} \tag{8.107}$$

Thus Eq. (8.105) becomes[14]

[14]For the sake of clarity, the overlinings are now removed from the equations.

$$\begin{cases} \nabla^4 w + \varepsilon_q \nabla^2 F + \ddot{w} = \varepsilon_c L(w, F) + \varepsilon_q \left[-\mu \dot{w} + p \right], \\ \nabla^4 F - \dfrac{a^4}{Rh^3} \nabla^2 w = -\dfrac{1}{2} L(w, w). \end{cases} \tag{8.108}$$

Equations (8.108) contain a quadratic perturbation coefficient $\varepsilon_q = 12(1-\nu^2)h/R$ and a cubic perturbation coefficient $\varepsilon_c = 12(1-\nu^2)h^4/a^4$. Within the framework of "thin shell" approximations, i.e., $h \ll a$ and $hR \ll a^2$, one can see that the cubic terms are significantly smaller than the quadratic terms. In practice, this means that even a very small curvature of the structure allows the quadratic nonlinearities to dominate. This may explain why it is extremely difficult, or even impossible, to experimentally exhibit the phenomena of cubic nonlinearity on a plate: even the slightest flatness defect has such effect that the cubic nonlinear term is masked by the quadratic one.

The nonlinear solution is now expanded onto the basis of the eigenmodes, taking advantage of their orthogonality properties[15]:

$$w(r, \theta, t) = \sum_n \Phi_n(r, \theta) q_n(t). \tag{8.109}$$

As a consequence, all nonlinear terms will appear in the time functions (generalized displacements). These functions form a system of coupled differential equations:

$$\ddot{q}_n + \omega_n^2 q_n = \varepsilon_q \left[-\sum_p \sum_q \alpha_{npq} q_p q_q - \mu \dot{q} + p_n \right] + \varepsilon_c \sum_p \sum_q \sum_r \beta_{npqr} q_p q_q q_r, \tag{8.110}$$

which highlights the simultaneous existence of cubic and quadratic coupling terms. For a plate, the coefficients α_{npq} are all equal to zero. For a shell, we note a formal analogy between these results and those obtained for the pendulum (see Sect. 8.1). The quadratic nonlinearity here results from the asymmetry due to the curvature.

The expansion of the shell motion in terms of eigenmodes is only one possible way of representing the solution, and this does not imply any linearity of the problem. In contrast to the linear case, it is not possible to decouple the differential equations that govern the time functions $q_n(t)$. In addition, this representation does not imply at all that the deflection shape of the shell for $\omega = \omega_n$ is the (linear) mode shape $\Phi_n(r, \theta)$. This can be seen, for example, by rewriting Eq. (8.110) under forced oscillations at this frequency. In general, the vibratory motion of the shell for a given frequency depends on the amplitude. Because of intermodal couplings (see Sect. 8.5.4), the deflection shape of the shell, for given loading frequency and amplitude, is a complex combination of several mode shapes (see Fig. 8.24 in the next section).

[15] Details on numerical methods for solving the von Kármán plate equations can be found in [8].

8.5.5.2 Truncation

If the nonlinearities are weak, and if the forcing frequency is close to one particular eigenfrequency, it is legitimate to truncate the system (8.110) by keeping only the equations that govern the main excited modes, and those associated with them through internal resonances. Let us illustrate this by the example of a thin spherical shell shown in Fig. 8.22. This example shows a situation where the structure is excited at its center with frequency $f \simeq f_3 = 224\,\text{Hz}$, corresponding to the

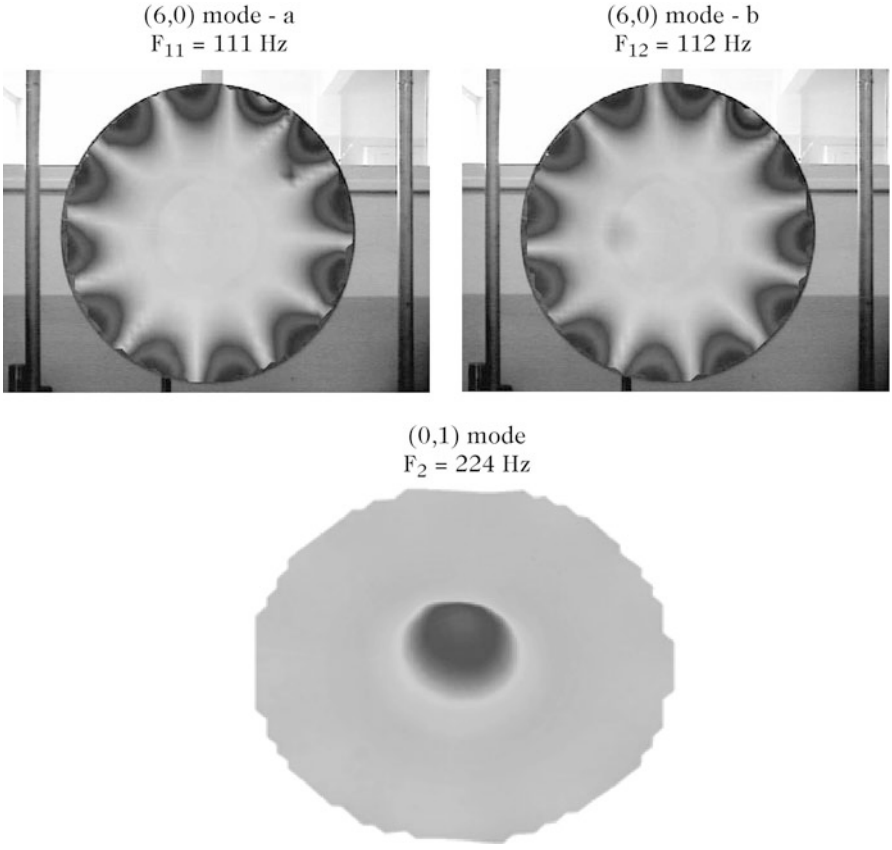

Fig. 8.22 Examples of some particular modes of a spherical shell subjected to internal resonance (see also [64])

symmetric mode (0,1).[16] For this particular shell, it turns out that the frequency of the mode (0,1) corresponds to twice the asymmetric modal frequencies (6,0), approximatively: $f_1 = 111\,\text{Hz}$ and $f_2 = 112\,\text{Hz}$.

In order to observe the phenomena caused by a forcing in the vicinity of f_{01}, then it can be assumed that the displacement is written in the approximated form:

$$w(r,\theta,t) \simeq \Phi_{60}(r)\left[q_1(t)\cos 6\theta + q_2(t)\sin 6\theta\right] + \Phi_{01}(r)q_3(t). \tag{8.111}$$

where q_1 and q_2 are the generalized displacements corresponding to the two configurations in quadrature for the asymmetric modes (6,0), and where q_3 governs the temporal evolution of the axisymmetric mode (0,1). As a consequence of the modal truncation, the system (8.110) is written in reduced form as follows:

$$\begin{cases} \ddot{q}_1 + \omega_1^2 q_1 = \varepsilon_q\left[-\beta_{13}q_1q_3 - 2\mu_1\dot{q}_1\right], \\ \ddot{q}_2 + \omega_2^2 q_2 = \varepsilon_q\left[-\beta_{23}q_2q_3 - 2\mu_2\dot{q}_2\right], \\ \ddot{q}_3 + \omega_3^2 q_3 = \varepsilon_q\left[-\beta_{11}q_1^2 - \beta_{22}q_2^2 - 2\mu_3\dot{q}_3 + P_3(t)\right]. \end{cases} \tag{8.112}$$

where $P_3(t)$ represents the forcing term, and where terms of modal damping of the form $-2\mu_i\dot{q}_i$ are added. The cubic terms are ignored because of the "thin shell" assumptions, as discussed previously. The intermodal coupling coefficients β_{ij} depend on both the geometrical and material properties of the shell. These parameters can be calculated explicitly [63]. The resolution of the nonlinear system (8.112) can be made using the method of multiple scales presented in Sect. 8.5.4.

Figure 8.23 shows the stability curve obtained for the truncated system (8.112). The theoretical results are represented by solid lines (where the states are stable) or dotted lines (when unstable). The experimental points are represented by triangles and circles. One sees at the center of the figure the classical resonance curve of a forced isolated oscillator close to its eigenfrequency. This is the curve that would have been obtained for an isolated oscillator (0,1), with no internal resonances related to other modes. By changing the driving frequency, one obtains different coupling situations of this mode with one configuration of the two asymmetric modes (6,0). Figure 8.24 illustrates these nonlinear couplings for a spherical shell excited at its center: in each case, one can see the simultaneous contributions of the axisymmetric mode and an asymmetric mode.

[16] As shown in Chap. 3 for the circular membrane (see Fig. 3.32), a mode (n, m) of a structure with a circular geometry is characterized by n nodal diameters and m nodal circles. However, in contrast to the case of stretched membranes described in Chap. 3, the outer edge of the spherical shells considered here are free, so that the lowest number of nodal circles is zero.

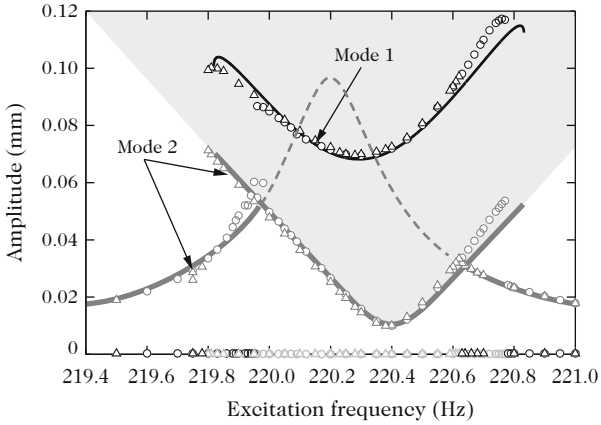

Fig. 8.23 Stability curve for a thin spherical shell excited close to the frequency of mode (0,1). *Black*: response of mode (0,1). *Gray*: responses of both configurations for the mode (6,0). *Solid lines and dotted lines*: theoretical model (8.112). *Triangles and circles*: experimental points. After [64]

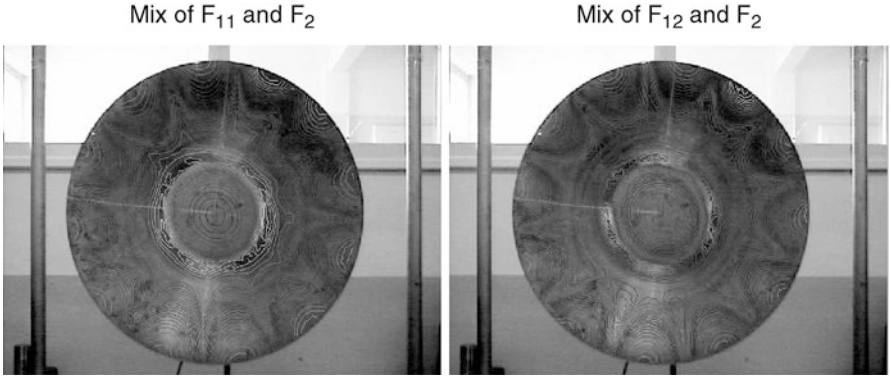

Fig. 8.24 Examples of large amplitude deflection shapes of a spherical shell driven at its center. This figure shows two situations of coupling between the axisymmetric mode (0,1) and one configuration of the asymmetric modes (6,0) shown in Fig. 8.22. See also [64]

8.5.5.3 Generalization and Musical Interest

The previous section allows us to understand a key aspect of sound generation in gongs and cymbals where the spectrum shows new components above a given threshold of amplitude, as a consequence of geometric nonlinearity. At the end of the Sect. 8.5.5 the presentation was deliberately focused on the interaction between a small number of modes. However, these results can be quantitatively generalized to a non-sinusoidal periodic forcing, which is coherent with the reality as one observes in practice the distortion of the response even for low excitations (see Sect. 8.5.1).

In this case, the enrichment of the spectrum is due to combinations of modes around each harmonic of the driving signal. Sound synthesis of gongs and cymbals based on these methods were made by Ducceschi and Touzé [23].

As said earlier, the normal excitation of a cymbal or a gong is a force impulse, communicated to the structure by the impact of a mallet (or a stick). The spectrum of the impact force is analogous to that of a low pass filter, whose bandwidth increases with the hardness of the mallet's head. For a pulse excitation, the system (8.112) can only be solved numerically, since the nonlinearities do not obey the principle of superposition. At this stage, one can imagine that each component of the excitation spectrum gives rise to a local spectral broadening and that, in total, there is an energy transfer to the high frequencies, beyond the initial spectrum. That is what is audibly observed, and confirmed by experiments.

8.6 Chaotic Regime

Let us now return to the fundamental experience described in Fig. 8.17. In the previous sections, the phenomena observed between the two bifurcations were studied. Beyond the second bifurcation, the observed acceleration of the gong (or of the cymbal) shows a broadband spectrum where it is no longer possible to discriminate between the discrete frequency peaks. The Fourier transform is not the right tool to describe the dynamics of the system properly, and other methods of analysis must be considered. Details of the transition to chaos in thin structures can be found in [69].

Among the possible strategies, observing the signal in the phase space is an effective and recognized method for analyzing the dynamics of nonlinear systems [27, 48]. Starting from a given time series $s(t)$, the phase space trajectory is obtained by representing the set of points with coordinates $[x_1 = s(t), x_2 = s(t+T)]$ where T is a time delay whose value obeys selection criteria that are beyond the scope of the present book. One can remember that a widely used method consists of choosing T as equal to the first zero of the autocorrelation function of the signal. Another possibility is to select the first minimum of the mutual information function. The reader interested in these questions can see for instance [40].

Figure 8.25 shows a comparison between a standard spectral representation and a phase space representation, for a cymbal vibration signal, where the instrument is excited by a sinusoidal force, for three different forcing amplitude, successively. As long as the amplitude remains weak, the spectrum is harmonic, and the trajectory takes the form of a closed curve. When the forcing amplitude increases, one can see an inharmonic spectrum due to the multiple combinations of resonances whose origin has been described earlier in this chapter. Here, the phase space trajectory shows typical foldings, which are known to indicate a possible route to chaos. Finally, after a second bifurcation, the spectrum is almost continuous, and the phase space representation takes the form of a blurring structure, which is difficult to analyze visually. We will see below how to draw valuable information from this signal.

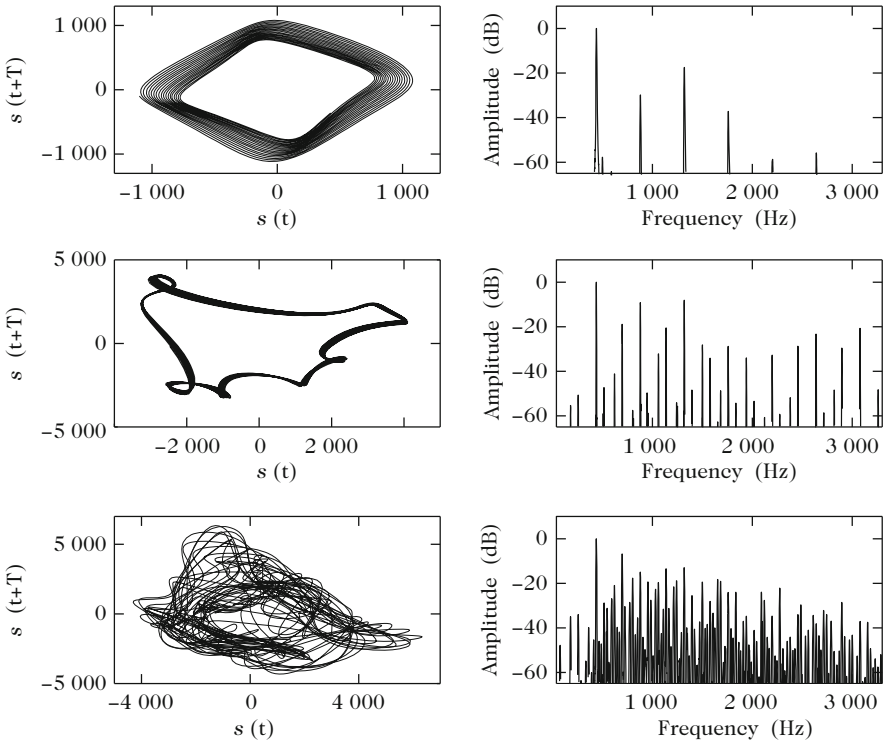

Fig. 8.25 Phase space and spectrum of a sound for a cymbal under sinusoidal forcing excitation at 440 Hz. *Top line*: quasi-linear oscillations. *Medium line*: weakly nonlinear oscillations. *Bottom line*: chaotic regime

8.6.1 Degrees of Freedom

The erratic structure of the cymbal vibrations at the bottom of Fig. 8.25 looks like a random signal. However, random signals are characterized by a lack of correlation between successive time windows of the signal. Therefore, it is of interest to check whether or not such a correlation exists here. For this purpose, the signal $s(t)$ is sampled at regular intervals $t_n = nT_e$ (where n is a positive integer), and the obtained time series is denoted $s(n)$. N indicates the length of $s(n)$. Then, a set of vectors $y(n)$ is built, defined by:

$$\begin{aligned} &y(n) = [s(n), s(n + n_T), s(n + 2n_T), \ldots, s(n + (d-1)n_T)] \\ &\text{with } n = 1, \ldots, N - (d-1)n_T, \end{aligned} \tag{8.113}$$

where the parameter d is called the *embedding dimension* of the vectors $y(n)$, and where the index n_T corresponds to the time delay T used for representing the signal

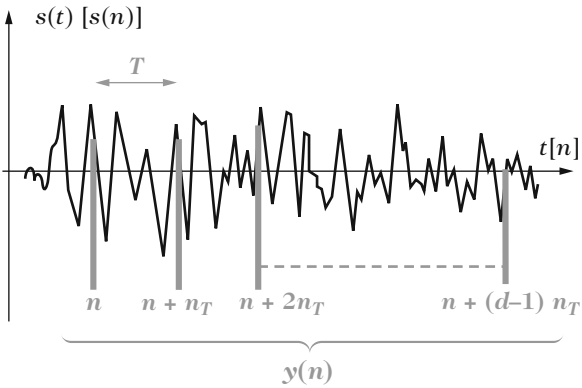

Fig. 8.26 Creation of a multivariate set from a time series

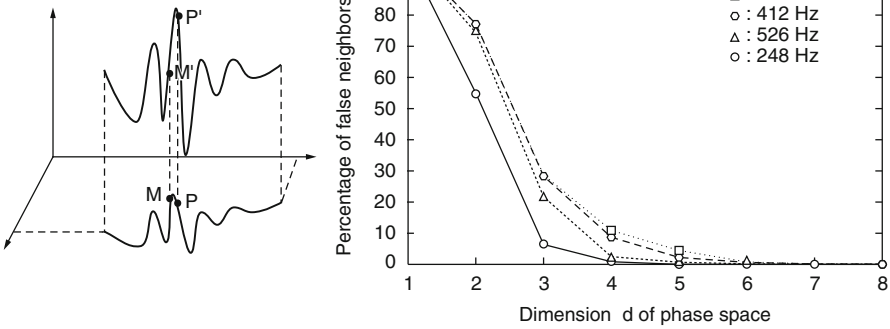

Fig. 8.27 (*Left*) Principle of signal "unrolling" in phase spaces of increasing sizes: the points M and P are neighbors in dimension 2, but are no longer neighbors in dimension 3. (*Right*) Percentage of false neighbors as a function of the dimension d of the space for cymbal vibrations, at different excitation frequencies

in phase space. In total, the length of $s(n)$ required for the construction of each vector y is equal to dn_T. If we want to explore $s(n)$ entirely, it is necessary to make n varying within the interval 1 to $N-(d-1)n_T$. Figure 8.26 illustrates the partition of the initial series $s(n)$.

This partition might seem arbitrary at first sight. In practice, it will be used to check whether $s(n)$ is random or deterministic. We will also derive a first estimate of the number of degrees of freedom of the underlying mechanical system from this analysis.

A first method is presented, called *method of false nearest neighbors*. To illustrate it, let us examine the case $d = 2$. This corresponds to the case of the phase space shown in Fig. 8.25, where the components of vector $y(n)$ are $s(n)$ and $s(n + n_T)$. These components are the coordinates of a point M on the trajectory (see Fig. 8.27). Let us consider this point and another *neighbor* point P on the same trajectory.

Imagine now that we examine the case $d = 3$: for that purpose, the cymbal motion is now represented in a three-dimensional space, where the vector $y(n)$ has three components $s(n)$, $s(n+n_T)$, and $s(n+2n_T)$. One can see this procedure as unrolling a 2-D "ball of wool" into 3D! The central question is to know if, during this operation, M and P will remain close neighbors or not. In the case of a random signals, it can be shown that close neighbors in dimension d never stay close in dimension $d + 1$. This is a property of *false nearest neighbors*. With a deterministic signal, similar to those we are interested in here, the number of false neighbors regularly decreases as d increases (see Fig. 8.27).

Figure 8.27 shows that the percentage of false neighbors is practically zero beyond a certain value of d ($d = 8$ here). This means that, for this dimension, the trajectory is completely unrolled, and that the projection into a space of higher dimension does not provide any additional information: for $d > 8$, all neighbors are "true neighbors" which stay close if d increases. This is also the case for a mechanical system of finite dimension m: if one attempts to use $m + 1$ variables to describe this system, it necessarily leads to a set of equations where one variable is expressed as a function of the m others, and we have only m independent equations. To sum up, the method of false nearest neighbors described here gives an upper boundary for the dimension of the system from which the time series $s(n)$ was extracted. According to this estimation, we would derived here $m \leq 8$ for the cymbal dynamics.

An estimation of the lower boundary of m can be obtained by calculating the *correlation dimension*. This is obtained by determining the number of pairs of points whose mutual distance is smaller than a certain quantity ε. For a series of points N, the discrete formulation of the *correlation integral* is written:

$$C(\varepsilon) = \frac{1}{N(N-1)} \sum_{i \neq j} H\left(\varepsilon - \|y(i) - y(j)\|\right), \tag{8.114}$$

where the vectors y of dimension d are calculated like as the method of false neighbors described above. H is the Heaviside function.

Figure 8.28b represents, in logarithmic coordinates, the correlation integral $C(\varepsilon)$ depending on ε for increasing values of the dimension d, in the case of cymbal vibrations. It can be seen that the slope of this curve increases, and tends to a limiting value from a given value of d (around $d = 6$ in this figure). This is a general result, which is also valid for other dynamical systems [31]. This property means that, beyond this limiting value, the number of pairs of points increases exponentially with a constant exponent d_c ($C(\varepsilon) \sim \varepsilon^{d_c}$), regardless of the value of d. This also means that the relative increase $\mathrm{d}dC/C$ is proportional to the relative increase of the "radius" $\mathrm{d}d\varepsilon/\varepsilon$. The asymptotic value d_c of the slope is the *correlation dimension of the system*.

This behavior characterizes a deterministic dynamical system with a finite number of degrees of freedom. In the case of a random signal, a white noise, for

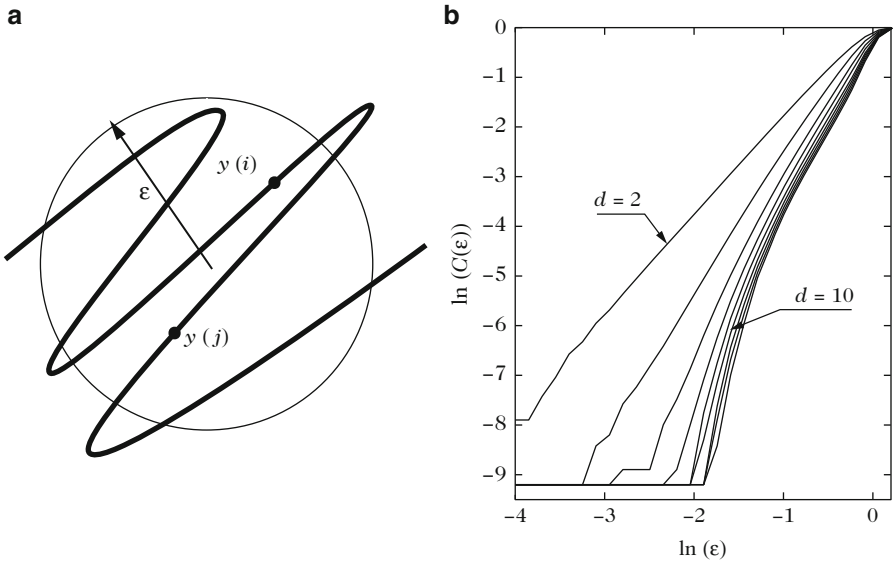

Fig. 8.28 Correlation integral. (**a**) Principle of the calculation: for a given dimension d, the number of pairs of points is evaluated whose distance is less than a given quantity ε. (**b**) Correlation integral $C(\varepsilon)$ of cymbal vibrations, for d varying between 2 and 10

example, we would observe that the slope of $\ln[C(\varepsilon)]$ continues to increase with increasing values of d. This would mean, in practice, that the relative increase in the number of pairs of neighboring points within a hypersphere of radius ε continues to grow faster than the relative increase of the radius when the signal is observed in spaces of increasing dimensions.

Figure 8.29 shows a range of estimates of d_c obtained from multiple vibration recordings of the same cymbal, for various forcing frequencies and excitation positions. We note that the correlation dimension converges for all signals, which is a clear indication of a deterministic process governed by a small number of degrees of freedom (DOF). However, we note that d_c is not identical in all cases, suggesting that the number of DOF depends on both the driving frequency and excitation position. This result is in accordance with the mechanical analysis of the problem made earlier in this chapter.

In conclusion, is has been shown in this section that some analysis tools exist for extracting information from signals governed by highly nonlinear process, for which conventional spectral analysis is no more applicable. From a practical point of view, the quality of the estimates can be rapidly affected if the signal is corrupted by noise. In addition, it is often necessary to analyze signals of long duration (N large) in order to obtain results with a sufficient accuracy. In any case, the estimation of the dimensions should be connected to a physical analysis of the phenomena, in order to avoid hazardous interpretations.

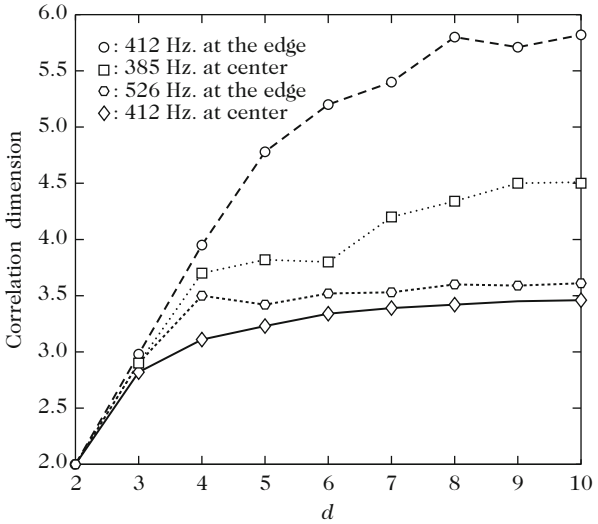

Fig. 8.29 Correlation dimension of some cymbal vibration signals as a function of the dimension d, for various driving frequencies and observation positions. Notice that the correlation dimensions d_c of all signals converge to an asymptotic value

8.6.2 Characterization of Chaos: Lyapunov Exponents

In the previous sections, the term "chaotic" was used to characterize the vibratory oscillations of cymbals and gongs subjected to strong nonlinear oscillations. This concept will be now made clearer and a method will be presented for quantifying the chaos.

A chaotic system is mainly characterized by its sensitivity with regard to the initial conditions. For a deterministic system, one can exactly reproduce the temporal variations of a variable, provided that the same initial conditions are given. With a chaotic system, even a small perturbation of these conditions is sufficient for the system to operate on a completely different trajectory in the phase space. The *Lyapunov exponents*, which are calculated from measured samples of a time series $s(n)$ (see the next section), are quantities that measure the divergence rate of small perturbations around a given trajectory in phase space accurately, and are recognized as pertinent to quantify the chaos. Only one positive exponent is sufficient for the trajectory to diverge, which proves the sensitivity of the system to initial conditions.

8.6.2.1 Calculation of the Lyapunov Exponents

The presentation below is inspired by Manneville [43]. As for the estimation of dimensions discussed above, we start from a time series $s(n)$ (with $n = 1, \ldots, N$) from which a set of vectors $y(n)$ is constructed, using the procedure described

in (8.113). At a future time $T_F = n_F T_e$, which is assumed to be small, the vectors $y(n)$ are transformed into another set $y(n + n_F)$. The calculation of the Lyapunov exponents is then made on the function $\mathbf{F}$ which characterizes the evolution of $y(n)$ to $y(n + n_F)$, which can be written symbolically[17]:

$$y(n + n_F) = \mathbf{F}\{y(n)\}. \tag{8.115}$$

As an illustration, let us consider the simple case of a single variable with initial condition y_0. First, we choose $n_F = 1$. Introducing a small initial perturbation, we obtain the adjacent trajectory $\tilde{y}_0 = y_0 + \delta y_0$. From (8.115) it gives

$$\begin{aligned} \tilde{y}_1 &= y_1 + \delta y_1 = \mathbf{F}(\tilde{y}_0 = y_0 + \delta y_0) \\ &= \mathbf{F}(y_0) + \mathbf{F}'(y_0)\delta y_0. \end{aligned} \tag{8.116}$$

Thus, the distance $|\delta y_1|$ between two trajectories is given by $|\delta y_1| = |\mathbf{F}'(y_0)||\delta y_0|$. Pursuing the same calculation to the next iteration gives

$$|\delta y_2| = |\mathbf{F}'(y_1)||\mathbf{F}'(y_0)||\delta y_0|. \tag{8.117}$$

Finally, after n_F iterations, we get

$$|\delta y_{n_F}| = \left(\prod_{k=0}^{k=n_F-1} |\mathbf{F}'(y_k)| \right) |\delta y_0|. \tag{8.118}$$

It can be seen in (8.118) that the required quantity is obtained, namely a measure of the evolution of the perturbation. This evolution can be quantified by a global coefficient γ defined as follows:

$$\gamma^{n_F} = \frac{|\delta y_{n_F}|}{|\delta y_0|}. \tag{8.119}$$

Finally, the Lyapunov exponent λ is defined as the logarithm of γ, which yields

$$\lambda = \ln(\gamma) = \frac{1}{n_F} \sum_{k=0}^{n_F-1} \ln |\mathbf{F}'(y_k)| \tag{8.120}$$

for an estimation on n_F iterations. If the exponent λ defined in (8.120) is positive, this means that, for different initial conditions, the trajectories diverge as $e^{\lambda n}$, or, equivalently, as $e^{\lambda t}$ using the dimensional quantities.

[17] The choice of T_F determines the accuracy of the estimated Lyapunov exponents. These very technical considerations will not be detailed here, and we invite the interested reader to refer to the specialized literature [40, 43]. We simply recommend to choose $T/2 \leq T_F < T$, where T is the time interval chosen for the construction of the vectors y [see Eq. (8.113)].

The previous calculus can be generalized to higher values of the dimension d (dimension of vectors y) without any difficulties. In this case, several Lyapunov exponents are obtained. This is known as the *Lyapunov spectrum*. These exponents are calculated from the Jacobian of the transformation $\mathbf{F}$ [43, 67]. Only one Lyapunov exponent needs to be positive for the trajectories to diverge, and one can then conclude that the system is chaotic. Such properties are observed in the case of cymbals and gongs, and this result comes in addition to other analysis methods (mechanical model, phase space, bifurcations,...) to explain the scenario of routes to chaos for these instruments, subjected to large amplitude oscillations [14].

Finally, since the transformation for vibrations to acoustic waves is linear for percussion instruments, all nonlinearities are contained in the vibrations. In other words, the considerations presented in this chapter remain valid to explain the observations made on the sounds of cymbals and gongs. On the experimental point of view, it is preferable to perform the analysis on the vibration of one particular point of the structure rather than on the radiated sound. In fact, the combinations of modes and the number of degrees of freedom vary from one point to another of the structure. As the sound pressure results from an integration over the whole geometry, it is understandable that the corresponding signals are therefore more difficult to analyze.

8.7 Nonlinear Normal Modes

8.7.1 Introduction

As soon as the nonlinearities are considered in a physical problem, then the evolution equations of the variables are coupled together. This has been seen on several occasions in this chapter, as, for example, in Eq. (8.110) for gongs and cymbals. The superposition theorem, which enables us to solve several simple problems independently, and then to reconstruct the overall response by summing individual responses, is no longer valid. As a consequence, it becomes also difficult, or even impossible, to make truncations in the system. Terms that would be otherwise neglected could be responsible for major changes in the evolution of the system, whereas such simplifications are perfectly justified in the linear case. Direct solving of nonlinear problems is often impossible analytically. It thus implies long and heavy numerical calculations, which are very demanding in terms of computational resources. However, in many situations, the dynamics observed in real cases seem to be relatively simple. This is, for example, the case for a structure forced near its resonance frequency, at moderate amplitudes. Even if nonlinearity is present, yielding higher harmonics and bending of resonance curves like those shown in Sect. 8.2, the dynamic behavior remains rather simple to describe.

In order to propose effective methods to reduce the nonlinear dynamics in specific cases, the concept of *nonlinear normal mode*, or NNM, was introduced.

This concept is briefly presented below, for the particular case of a vibrating structure under large amplitude, i.e., for geometric nonlinearities. It is assumed that the modes of the system were calculated in a previous step, and that the equation of motion was projected onto these modes, so that the starting point of this presentation is a dynamical system of the form shown in (8.110), i.e., an infinite number of nonlinearly coupled oscillators. Damping and forcing terms are left aside in this presentation.

8.7.2 First Approach of Nonlinear Normal Modes

To make the reader understand the interest of NNMs, we will present this concept on a simple case. The selected example is the dynamics of a mass subjected to elastic restoring forces by two springs whose extensions are not considered as small, so that linear approximations are not justified here (Fig. 8.30).

l_0 is the length of the springs at rest. The coordinates of the point mass m at time t are $l_0 + x_1$ and $l_0 + x_2$, respectively. The problem is expressed in terms of the dimensionless variables $X_1 = x_1/l_0$ and $X_2 = x_2/l_0$. We denote $\omega_1^2 = k_1/m$ and $\omega_2^2 = k_2/m$ the square of the natural angular frequencies of the system, corresponding to purely horizontal and vertical motions in the physical space (X_1, X_2), respectively. The elastic potential energy W of the system is given by:

$$W = m\left\{\frac{1}{2}\omega_1^2\left[X_1 + \frac{1}{2}\left(X_1^2 + X_2^2\right)\right] + \frac{1}{2}\omega_2^2\left[X_2 + \frac{1}{2}\left(X_1^2 + X_2^2\right)\right]\right\}. \tag{8.121}$$

The equations of motion are then obtained by:

$$m\ddot{X}_i + \frac{\partial W}{\partial X_i} = 0, \qquad \text{for} \quad i = 1, 2. \tag{8.122}$$

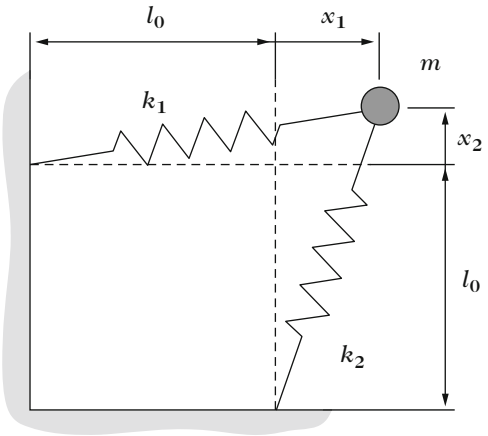

Fig. 8.30 A point mass m is fixed at two springs of stiffness k_1 and k_2, respectively. Each spring is rigidly fixed to the other end of the walls, which are perpendicular to each other

Finally, the equations governing the dynamics of the system are written:

$$\begin{aligned}
&\ddot{X}_1 + \omega_1^2 X_1 + \frac{\omega_1^2}{2}(3X_1^2 + X_2^2) + \omega_2^2 X_1 X_2 + \frac{\omega_1^2 + \omega_2^2}{2} X_1 (X_1^2 + X_2^2) = 0, \\
&\ddot{X}_2 + \omega_2^2 X_2 + \frac{\omega_2^2}{2}(3X_2^2 + X_1^2) + \omega_1^2 X_1 X_2 + \frac{\omega_1^2 + \omega_2^2}{2} X_2 (X_1^2 + X_2^2) = 0.
\end{aligned} \tag{8.123}$$

Notice that both equations are decoupled in the linear regime, which is due to the fact that the modal variables, X_1 and X_2 were chosen to describe the system.

Truncation problems mentioned in the previous section can be easily illustrated with these equations. Suppose that we want to study the motion of the first mode, simplifying the system (8.123) by writing $X_2 = 0$. The dynamical problem that governs X_1 then yields an inconsistent result. In fact, if $X_1 \neq 0$, the term in X_1^2 of the second equation of (8.123) yields energy to the second oscillator, so that we no longer have $X_2 = 0$!

However, if the system is linear, a motion initiated with the first eigenmode, taking as initial conditions $X_1 \neq 0$ and $X_2 = 0$, is such that X_2 remains equal to zero. This is the property of *invariance* of eigenmodes for a linear system. This is no longer true for nonlinear systems, because of the presence of terms such as X_1^2 in the second equation of (8.123). We are now able to define NNMs more accurately, but before that we need to specify the general framework.

8.7.3 Invariant Manifolds

Consider the dynamics of the system in phase space. For that purpose, the system (8.123) is written in first order, by using the velocities $Y_1 = \dot{X}_1$ and $Y_2 = \dot{X}_2$ as additional independent variables. The phase space thus is four-dimensional, and the dynamics can be rewritten as:

$$\begin{cases}
\dot{X}_1 = Y_1, \\
\dot{Y}_1 = f_1(X_1, Y_1, X_2, Y_2), \\
\dot{X}_2 = Y_2, \\
\dot{Y}_2 = f_2(X_1, Y_1, X_2, Y_2).
\end{cases} \tag{8.124}$$

The eigenmodes correspond to two hyperplanes defined by: $X_2 = Y_2 = 0$ for the first mode, $X_1 = Y_1 = 0$ for the second mode. These are two-dimensional subspaces of the phase space. These subspaces are not *invariant* (see the end of the previous section), this property being true if the dynamics is linear, only. This is illustrated in Fig. 8.31, where the system (8.123) is solved numerically for three different initial conditions on the first eigenmode, respectively: $X_1 = 0.01$, $X_1 = 0.025$,

and $X_1 = 0.05$, respectively (all other coordinates being equal to zero), and for an integration time T corresponding to 12 times the period $T_1 = 2\pi/\omega_1$ of the first oscillator.

It is found that the first orbit (or periodic solution) is almost included in the plane defined by the first eigenmode. This trajectory was calculated for a small amplitude, $X_1 = 0.01$, the nonlinearities do not appear and the loss of invariance is almost not visible. This is not the case for the other two orbits, which are no longer included in the plane. The significant contribution that can be observed on the coordinate X_2 is entirely due to the coupling term in X_1^2 on the second equation that induces an energy transfer from the first to the second mode.

Let us now observe the computed trajectories for other initial conditions, selected at well-chosen locations in phase space. Figure 8.32 shows three trajectories, computed for the same observation time T, and which initial conditions are: (X_1, X_2)=(0.01,0) ; $(0.025, 2.3 \times 10^{-5})$ and $(0.05, 1.8 \times 10^{-4})$, respectively. Selected values of X_2 are small compared to those of X_1, and appear as small corrections brought for recovering out closed periodic orbits. These initial conditions have been selected onto the first NNM, and this allows us to define the NNM by two equivalent formulations. First, they can be defined as the family of periodic orbits existing in the vicinity of the origin. Existence of these periodic orbits are guaranteed by a theorem due to Lyapunov [42], and one can see in Figs. 8.31 and 8.32 that they are not confined into the linear eigenspaces but are slightly aside. This definition is however limited to the conservative case, as periodic orbits are no longer solutions of the dynamical system as soon as dissipation comes into play. To overcome

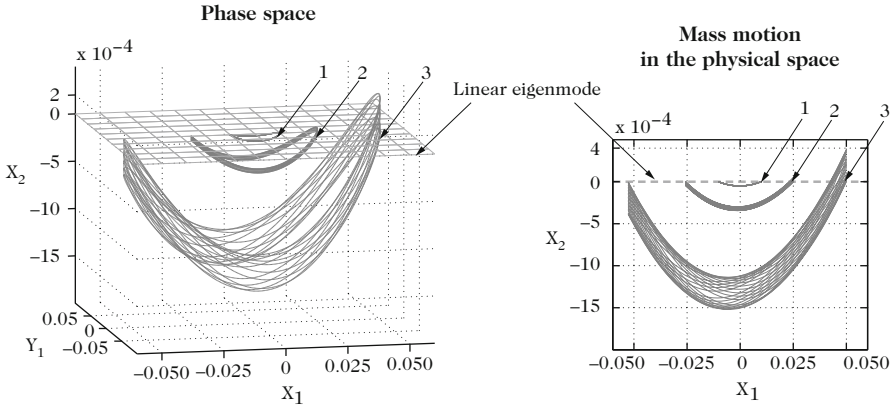

Fig. 8.31 Non-invariance of the first eigenmode. The figure on the *left* shows the trajectories of the system in phase space (X_1, Y_1, X_2). The plane $X_2 = 0$ corresponds to the first eigenmode. Three initial conditions were taken (numbered 1, 2, and 3), for $X_1 = 0.01$, $X_1 = 0.025$, and $X_1 = 0.05$. We see that the corresponding trajectories are located out of the plane defining the first eigenmode. The figure on the *right* shows the motion of the mass in the physical space (X_1, X_2). Here, we have: $\omega_1 = 1$, $\omega_2 = \sqrt{2}$

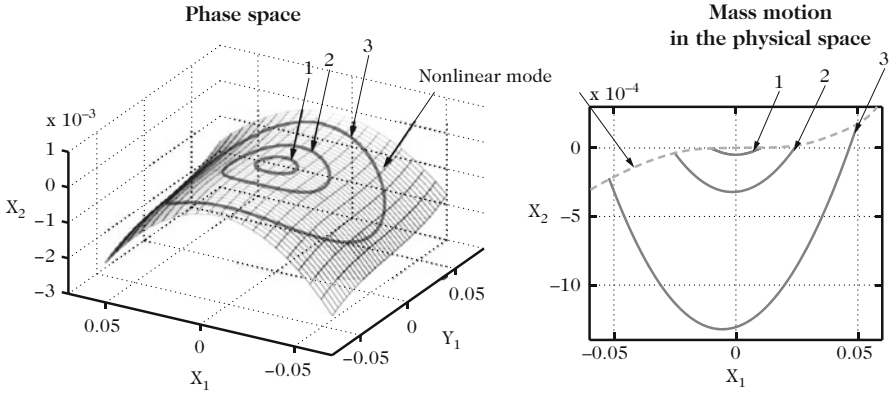

Fig. 8.32 First nonlinear normal mode. On the *left*: representation in phase space, showing the invariance property of the nonlinear normal mode. For three different initial conditions (numbered 1, 2, and 3) taken on the manifold, the periodic orbits are entirely contained within the nonlinear normal mode. On the *right*: representation of the mass motion in the physical space (X_1, X_2). The consequence of the invariance is that the motion of the mass occurs along a line and not on a blurred trajectory

this limitation, an NNM can be defined as the set of initial conditions giving rise to trajectories that are contained in a two-dimensional surface, or manifold in mathematical terms. By doing so, one introduces the fundamental notion of invariance. For a conservative system, the NNM can be viewed as the manifold generated by all the periodic orbits. This manifold is invariant because any initial condition taken on it will give rise to a trajectory that will stay on the manifold, for any time. This definition in terms of invariant manifold is more general and will be retained in the following.

We are now able to define an NNM:

Definition. An NNM is an invariant manifold (a surface) in the phase space, which is tangent to the corresponding eigenspace at the origin (corresponding to the position at rest). This definition ensures the following properties:

- Imposing that the manifolds be tangent at the origin to the eigenmode can help in recovering the linear results. The nonlinear modes are thus defined as an extension of the eigenmodes, where the invariance property is retained.
- The invariant manifolds are in fact minimal surfaces that allow us to capture existing trajectories of the phase space: making projections on these surfaces is therefore a priori the best possible reduction, which is their fundamental interest.
- With this notion, we are able to compute reduced-order models that retain the essential properties of the observed dynamics. We thus find the issue raised in the introduction: the apparent complexity of the equations, which needs to retain a large number of oscillators, is included in the curved geometry of the manifold. Now, the dynamics of that manifold is relatively simple, since it is governed by a single oscillator, that we will specify in the next section.

8.7.4 Calculation of Nonlinear Normal Modes

Several methods exist to calculate the NNMs. In this presentation, two of them are selected, that use powerful mathematical tools (encountered elsewhere in many other areas of physics) and that fully exploit the notions of invariance. The first work introducing the concept of NNM is due to Rosenberg [56], although without the more general interpretation in terms of invariant manifolds that was introduced here.

One first approach consists in calculating the geometry of the invariant manifold in the phase space, and then to project the equations of motion onto the manifold. To do this, a very general theorem of dynamical systems is used: the *center manifold* theorem. The results given by this theorem are of great significance, since it provides the best means of reducing nonlinear dynamics. The basic idea is to separate the very damped modes, which have a very short lifetime and have therefore little influence on long-term dynamics, from the lightly damped modes, which are primarily responsible for the dynamics over long duration. Once these two families are separated, it is shown that the center manifold of the phase space, which contains the amplitudes of the master (lightly damped) modes only, exists. The theorem then provides an explicit method for calculating it [32, 43]. Applying this method to vibrating systems with nonlinear geometries is discussed in numerous papers [9, 38, 39, 53, 58, 59]. In the conservative case considered here, one can use the center manifold reduction method without making references to slightly and little damped variables. We then simply choose an eigenmode for which we want to extend the invariance property to the nonlinear regime.

Let us now examine the first NNM of the system (8.124): (X_1, Y_1) is chosen arbitrarily as the pair of *master* variables, while (X_2, Y_2) is the so-called pair of *slave* variables. The equation that defines the geometry of the manifold in phase space is obtained through a functional link between master and slave variables. We therefore write:

$$\begin{aligned} X_2 &= u(X_1, Y_1), \\ Y_2 &= v(X_1, Y_1), \end{aligned} \tag{8.125}$$

where $u(X_1, Y_1)$ and $v(X_1, Y_1)$ are the unknown functions to be determined. Equation (8.125) defines a two-dimensional manifold in phase space, and the invariance is ensured by expressing X_2 and Y_2 as functions of X_1 and Y_1. To find the unknowns u and v, Eq. (8.125) is differentiated with respect to time:

$$\begin{aligned} \dot{X}_2 &= \frac{\partial u}{\partial X_1}\dot{X}_1 + \frac{\partial u}{\partial Y_1}\dot{Y}_1, \\ \dot{Y}_2 &= \frac{\partial v}{\partial X_1}\dot{X}_1 + \frac{\partial v}{\partial Y_1}\dot{Y}_1. \end{aligned} \tag{8.126}$$

Finally, all time derivatives in (8.126) are replaced by their expressions given in (8.124). This leads to a nonlinear equation where the time variable has been removed, and which describes the geometry of the first NNM in phase space:

$$\begin{aligned} v(X_1, Y_1) &= \frac{\partial u}{\partial X_1} Y_1 + \frac{\partial u}{\partial Y_1} f_1(X_1, Y_1, u(X_1, Y_1), v(X_1, Y_1)), \\ f_2(X_1, Y_1, u(X_1, Y_1), v(X_1, Y_1)) &= \frac{\partial v}{\partial X_1} Y_1 + \frac{\partial v}{\partial Y_1} f_1(X_1, Y_1, u(X_1, Y_1), v(X_1, Y_1)). \end{aligned} \tag{8.127}$$

Solving these two partial differential equations yields $u(X_1, Y_1)$ and $v(X_1, Y_1)$, and thus the position of the invariant manifold. The major issue is that the analytical solution of these equations is never known in the general case. Thus, asymptotic or numerical methods are used to determine u and v. The dynamics on the manifold is given by replacing u and v by their expressions in (8.124). It can be written with a single oscillator equation, hence giving rise to a reduced-order model. The efficiency of the method might seem relatively insignificant in the particular example treated here, where the reduction of complexity is of only one equation. However, this method yields appreciable results if dynamical systems with a large number N of oscillators can be reduced to one, which is the case when dealing with continuous structures.

The second method is based on the *normal forms* theory. Again, the mathematical tool that is used is very powerful, and is used in almost all branches of physics. The basic ideas of normal forms were developed by Henri Poincaré [55]. The goal is to simplify the dynamics of a system as much as possible, using a well-chosen nonlinear change of variables. In fact, one can show that some nonlinear terms of a dynamical system are essential for obtaining the main features of the dynamics (number and nature of the fixed points, bifurcations), while others can be eliminated without changing its characteristics. These terms, or the so-called non-resonant terms, can be thus eliminated with an appropriate change of variables. Finally, the *normal form* of the system is obtained, that contains the resonant terms only.[18] Returning to our example, we therefore look for a change of variables of the form:

$$\begin{aligned} X_1 &= R_1 + \mathscr{P}_1(R_1, S_1, R_2, S_2), \\ Y_1 &= S_1 + \mathscr{Q}_1(R_1, S_1, R_2, S_2), \\ X_2 &= R_2 + \mathscr{P}_2(R_1, S_1, R_2, S_2), \\ Y_2 &= S_2 + \mathscr{Q}_2(R_1, S_1, R_2, S_2). \end{aligned} \tag{8.128}$$

(R_1, R_2, S_1, S_2) are the new variables, having dimensions of displacements and velocities, respectively. The change of variables is chosen as tangent to the identity:

[18] New results on the use of normal form theory can be found in [41].

the first term indicates that, for small displacements, $R_1 = X_1$, $R_2 = X_2$, $S_1 = Y_1$, and $S_2 = Y_2$, which allows the recovery of the linear results. $\mathscr{P}_1, \mathscr{Q}_1, \mathscr{P}_2, \mathscr{Q}_2$ are unknown functions that are determined iteratively: these quantities are expressed as polynomial functions with unknowns (R_1, S_1, R_2, S_2), whose coefficients are found at each iteration, by eliminating non-resonant terms [37, 66, 70, 71]. Replacing (8.128) in (8.123), one obtains the dynamics expressed in (R_1, S_1, R_2, S_2), i.e., in a curved reference frame generated by the invariant manifolds. In the next step, the appropriate truncations can be made since the invariance is recovered. To study the first NNM, for example, the coordinates corresponding to the second NNM are set equal to zero: $R_2 = S_2 = 0$. After substitution into the last two equations of (8.128), the geometry of the first invariant manifold in phase space is found, which corresponds to Eq. (8.125). Finally, it is found that the dynamics of the first NNM, up to order three, is governed by:

$$\ddot{R}_1 + \omega_1^2 R_1 + \left(\frac{\omega_1^2 + \omega_2^2}{2} + A_1 \right) R_1^3 + B_1 R_1 \dot{R}_1^2 = 0, \tag{8.129}$$

where A_1 and B_1 arise from the elimination of the non-resonant terms. These coefficients account for the effect of the second linear mode that would have been otherwise abruptly neglected by imposing $X_2 = 0$ in (8.123). These two coefficients are written explicitly:

$$\begin{aligned} A_1 &= -\frac{3\omega_1^2}{2} + \frac{\omega_2^2(2\omega_1^2 - \omega_2^2)}{2(\omega_2^2 - 4\omega_1^2)}, \\ B_1 &= -3 + \frac{\omega_2^2}{\omega_2^2 - 4\omega_1^2}. \end{aligned} \tag{8.130}$$

In total, the nonlinear dynamics is described by a single oscillator, which is able to predict the behavior of the entire system with a good accuracy. It can be shown, for example, that the hardening, resp. softening, behavior of the system, (i.e., the dependence of the frequency with amplitude), is correctly predicted by the dynamics on the manifold (8.129), whereas an erroneous result is obtained if the system (8.123) is simplified in a crude manner by putting $X_2 = 0$ [70].

8.7.5 Conclusion

The derivations presented here with the help of a simple system with two degrees of freedom naturally extend to N degrees of freedom, with N arbitrarily large. The influence of damping terms has not been treated, but this question is addressed, for example, in [39, 59] and [66]. Taking also external forces for the calculation of invariant manifolds into account is a more difficult problem, since the invariant manifold then depends on time. One can find an example of such cases in [39].

A nonlinear normal mode (NNM) was defined as an invariant manifold of phase space, tangent at the origin to the corresponding eigenmode, which allows us to consider it as an extension of the eigenmode for which the invariance property is maintained. This property is a key point to adequately reduce nonlinear dynamics. Using NNMs, one can derive reduced-order models, with a small number of degrees of freedom, that contain the main properties of the original dynamics. These methods can be applied to the sound synthesis of nonlinear percussion instruments, in particular. Notice also that the computation of NNMs with application to self-sustained oscillations of the clarinet was made by Noreland et al. [52].

Finally, recent results show that the dynamics of nonlinear thin structures can gain in being examined in light of the wave turbulence theory [36, 72].

References

1. Amabili, M., Paidoussis, M.P.: Review of studies on geometrically nonlinear vibrations and dynamics of circular cylindrical shells and panels, with and without fluid-structure interaction. ASME Appl. Mech. Rev. **56**(4), 349–381 (2003)
2. Askenfelt, A.: Observations on the transient components of the piano tone. STL-QPSR **34**(4), 15–22 (1993)
3. Atig, M.: Acoustical nonlinearity localised at the open-end of a tube. Measurement, modeling and application to woodwind instruments (in French). Ph.D. thesis, Université du Maine, Laboratoire d'acoustique de l'université du Maine (2004). http://tel.archives-ouvertes.fr/
4. Atig, M., Dalmont, J., Gilbert, J.: Saturation mechanism in clarinet-like instruments, the effect of the localised nonlinear losses. Appl. Acoust. **65**, 1133–1154 (2004)
5. Atig, M., Dalmont, J., Gilbert, J.: Termination impedance of open-ended cylindrical tubes at high sound pressure level. C. R. Acad. Sci. Paris Ser. II **332**, 299–304 (2004)
6. Axisa, F.: Modelling of Mechanical Systems. Discrete Systems, vol. 1. Kogan Page Science, London (2003)
7. Bank, B., Sujbert, L.: Generation of longitudinal vibrations in piano strings: from physics to sound synthesis. J. Acoust. Soc. Am. **117**(4), 2268–2278 (2005)
8. Bilbao, S., O.Thomas, Touzé, C., Ducceschi, M.: Conservative numerical methods for the full von Kármán plate equations. Numer. Methods Partial Differ. Equ. **31(6)**, 1948–1970 (2015)
9. Boivin, N., Pierre, C., Shaw, S.W.: Nonlinear normal modes, invariance, and modal dynamics approximations of non-linear systems. Nonlinear Dyn. **8**(3), 315–346 (1995)
10. Buick, J., Atig, M., Skulina, D., Campbell, D., Dalmont, J., Gilbert, J.: Investigation of non-linear acoustic losses at the open end of a tube. J. Acoust. Soc. Am. **129**, 1261–1272 (2011)
11. Camier, C., Touzé, C., Thomas, O.: Non-linear vibrations of imperfect free-edge circular plates and shells. Eur. J. Mech. A Solids **28**(3), 500–515 (2009)
12. Chabassier, J., Joly, P.: Energy preserving schemes for nonlinear Hamiltonian systems of wave equations. Application to the vibrating piano string. Comput. Methods Appl. Mech. Eng. **199**, 2779–2795 (2010)
13. Chabassier, J., Chaigne, A., Joly, P.: Modeling and simulation of a grand piano. J. Acoust. Soc. Am. **134**(1), 648–665 (2013)
14. Chaigne, A., Touzé, C., Thomas, O.: Nonlinear vibrations in gongs and cymbals. Acoust. Sci. Technol. **26**(5), 403–409 (2005)
15. Conklin, H.A.: Design and tone in the mechanoacoustic piano. Part III. Piano strings and scale design. J. Acoust. Soc. Am. **100**, 1286–1298 (1996)
16. Conklin, H.A.: Piano strings and "phantom" partials. J. Acoust. Soc. Am. **102**(1), 659–659 (1997)

17. Conklin, H.A.: Generation of partials due to nonlinear mixing in a stringed instrument. J. Acoust. Soc. Am. **105**, 536–545 (1999)
18. Coulouvrat, F.: On the equations of nonlinear acoustics. J. Acoust. **5**, 321–359 (1992)
19. Crighton, D.: Nonlinear acoustics. In: Modern Methods in Analytical Acoustics (Lecture Notes). Springer, London (1992)
20. Dalmont, J.P., Nederveen, C.J., Dubos, V., Ollivier, S., Méserette, V., te Sligte, E.: Experimental determination of the equivalent circuit of an open side hole: linear and non linear behaviour. Acustica Acta Acustica **88**, 567–575 (2002)
21. Debut, V., Kergomard, J., Laloë, F.: Analysis and optimisation of the tuning of the twelfths for a clarinet resonator. Appl. Acoust. **66**, 365–409 (2005)
22. Denardo, B.: Nonanalytic nonlinear oscillations: Christiaan Huygens, quadratic Schroedinger equations, and solitary waves. J. Acoust. Soc. Am. **104(3)**, 1289–1300 (1998)
23. Ducceschi, M., Touzé, C.: Modal approach for nonlinear vibrations of damped impacted plates: Application to sound synthesis of gongs and cymbals. J. Sound Vib. **344**, 313–331 (2015)
24. Earnshaw, S.: On the mathematical theory of sound. Philos. Trans. R. Soc. Lond. **150**, 133–148 (1860)
25. Fubini, E.: Anomalies in the propagation of acoustic waves of great amplitude. Alta Frequenza **4**, 530–581 (1935)
26. Galembo, A., Askenfelt, A., Cuddy, L., Russo, F.: Perceptual relevance of inharmonicity and spectral envelope in the piano bass range. Acustica Acta Acustica **90**, 528–536 (2004)
27. Gibiat, V.: Phase space representations of acoustical musical signals. J. Sound Vib. **123**(3), 529–536 (1988)
28. Gilbert, J.: Differences between cylindrical and conical brass instruments; the nonlinear propagation point of view from experiments and simulations. J. Acoust. Soc. Am. **120**, 3332 (2006)
29. Gilbert, J., Kergomard, J., Ngoya, E.: Calculation of the steady-state oscillation of a clarinet using the harmonic balance method. J. Acoust. Soc. Am. **86**, 35–41 (1989)
30. Gilbert, J., Dalmont, J.P., Guimezanes, T.: Nonlinear propagation in woodwinds. In: Proceedings of Forum Acusticum, Budapest (2005)
31. Grassberger, P., Procaccia, I.: Measuring the strangeness of strange attractors. Phys. D **9**, 189–208 (1983)
32. Guckenheimer, J., Holmes, P.: Nonlinear Oscillations, Dynamical Systems and Bifurcations of Vector Fields. Springer, New York (1983)
33. Hamdouni, A., Millet, O.: Classification of thin shell models deduced from the nonlinear three-dimensional elasticity. Part I: the shallow shells. Arch. Mech. **55**(2), 135–175 (2003)
34. Hamilton, M., Blackstock, D. (eds.): Nonlinear Acoustics. Academic Press, New York (1998)
35. Hirschberg, A., Gilbert, J., Msallam, R., Wijnands, A.: Shock waves in trombones. J. Acoust. Soc. Am. **99**, 1754–1758 (1996)
36. Humbert, T., Cadot, O., Düring, G., Josserand, C., Rica, S., Touzé, C.: Wave turbulence in vibrating plates: the effect of damping. Europhys. Lett. **102**(3), 30002 (2013)
37. Jézéquel, L., Lamarque, C.H.: Analysis of nonlinear dynamical systems by the normal form theory. J. Sound Vib. **149**(3), 429–459 (1991)
38. Jiang, D., Pierre, C., Shaw, S.W.: The construction of nonlinear normal modes for systems with internal resonance. Int. J. Nonlinear Mech. **40**(5), 729–746 (2005)
39. Jiang, D., Pierre, C., Shaw, S.W.: Nonlinear normal modes for vibratory systems under harmonic excitation. J. Sound Vib. **288**(4–5), 791–812 (2005)
40. Kantz, H., Schreiber, T.: Nonlinear Time Series Analysis. Cambridge University Press, Cambridge (1997)
41. Lamarque, C.H., Touzé, C., Thomas, O.: An upper bound for validity limits of asymptotic analytical approaches based on normal form theory. Nonlinear Dyn. **70**(3), 1931–1949 (2012)
42. Lyapunov, A.M.: General problem of motion stability (in French). Annales de la faculté des sciences de Toulouse **9**, 203–474 (1907)
43. Manneville, P.: Instabilities, Chaos and Turbulence. Imperial College Press, London (2010)

44. Menguy, L., Gilbert, J.: Gas oscillations in air-filled tubes, solutions and experiments. Acustica Acta Acustica **86**, 798–810 (2000)
45. Monteil, M., Thomas, O., Touzé, C.: Identification of mode couplings in nonlinear vibrations of the steelpan. Appl. Acoust. **89**, 1–15 (2015)
46. Morse, P.M.: Vibration and Sound. Acoustical Society of America, Melville (1981)
47. Msallam, R., Dequidt, S., Caussé, R., Tassart, S.: Physical model of the trombone including nonlinear effects; application to the sound synthesis of loud tones. Acustica Acta Acustica **86**, 725–736 (2000)
48. Müller, G., Lauterborn, W.: The bowed string as a nonlinear dynamical system. Acustica Acta Acustica **82**(4), 657–664 (1996)
49. Murthy, G.S.S., Ramakrishna, B.S.: Nonlinear character of resonance in stretched strings. J. Acoust. Soc. Am. **38**, 461–471 (1965)
50. Myers, A., Pyle, R., Gilbert, J., Campbell, D., Chick, J., Logie, S.: Effects of nonlinear sound propagation on the characteristic timbres of brass instruments. J. Acoust. Soc. Am. **131**, 678–688 (2012)
51. Nayfeh, A.H., Mook, D.T.: Nonlinear Oscillations. Wiley, New York (1979)
52. Noreland, D., Bellizzi, S., Bouc, R., Vergez, C.: Nonlinear modes of clarinet-like musical instruments. J. Sound Vib. **324**, 983–1002 (2006)
53. Peshek, E., Pierre, C., Shaw, S.: A new galerkin-based approach for accurate non-linear normal modes through invariant manifolds. J. Sound Vib. **249**(5), 971–993 (2002)
54. Pierce, A.D.: Acoustics: An Introduction to Its Physical Principles and Applications. Acoustical Society of America, Melville (1989)
55. Poincaré, H.: Sur les propriétés des fonctions définies par les équations aux différences partielles. Gauthier-Villars, Paris (1879)
56. Rosenberg, R.M.: On non-linear vibrations of systems with many degrees of freedom. Adv. Appl. Mech. **9**, 155–242 (1966)
57. Rudenko, O., Soluyan, S.: Theoretical Foundations of Nonlinear Acoustics. Consultant Bureau, New York (1977)
58. Shaw, S.W., Pierre, C.: Nonlinear normal modes and invariant manifolds. J. Sound Vib. **150**(1), 170–173 (1991)
59. Shaw, S.W., Pierre, C.: Normal modes for nonlinear vibratory systems. J. Sound Vib. **164**(1), 85–124 (1993)
60. Thomas, O.: Analysis and modeling of nonlinearly vibrating thin elastic structures. Application to percussion instruments (in French). Ph.D. thesis, Telecom ParisTech (2001). https://hal.archives-ouvertes.fr/
61. Thomas, O., Bilbao, S.: Geometrically non-linear flexural vibrations of plates: in-plane boundary conditions and some symmetry properties. J. Sound Vib. **315**(3), 569–590 (2008)
62. Thomas, O., Touzé, C., Chaigne, A.: Nonlinear behavior of gongs through the dynamics of simple rods systems. In: Bonsi, D. (ed.) Proceedings of the International Symposium on Musical Acoustics, vol. 1, pp. 173–178, Perugia (2001)
63. Thomas, O., Touzé, C., Chaigne, A.: Non-linear vibrations of free-edge thin spherical shells: modal interaction rules and 1:1:2 internal resonance. Int. J. Solid Struct. **42**(1), 3339–3373 (2005)
64. Thomas, O., Touzé, C., Luminais, E.: Non-linear vibrations of free-edge thin spherical shells: experiments on a 1:1:2 internal resonance. Nonlinear Dyn. **49**(1–2), 259–284 (2007)
65. Thompson, M., Strong, W.: Inclusion of wave steepening in a frequency-domain model of trombone sound production. J. Acoust. Soc. Am. **110**, 556–562 (2001)
66. Touzé, C., Amabili, M.: Nonlinear normal modes for damped geometrically nonlinear systems: application to reduced-order modeling of harmonically forced structures. J. Sound Vib. **298**(4–5), 958–981 (2006)
67. Touzé, C., Chaigne, A.: Lyapunov exponents from experimental time series: application to cymbal vibrations. Acustica Acta Acustica **86**, 557–567 (2000)
68. Touzé, C., Thomas, O.: Non-linear behaviour of free-edge shallow spherical shells: effect of the geometry. Int. J. Nonlinear Mech. **41**(5), 678–692 (2006)

69. Touzé, C., Thomas, O., Amabili, M.: Transition to chaotic vibrations for harmonically forced perfect and imperfect circular plates. Int. J. Nonlinear Mech. **46**(1), 234–246 (2011)
70. Touzé, C., Thomas, O., Chaigne, A.: Hardening/softening behaviour in nonlinear oscillations of structural systems using non-linear normal modes. J. Sound Vib. **273**(1–2), 77–101 (2004)
71. Touzé, C., Thomas, O., Huberdeau, A.: Asymptotic nonlinear normal modes for large-amplitude vibrations of continuous structures. Comput. Struct. **82**(31–32), 2671–2682 (2004)
72. Touzé, C., Bilbao, S., Cadot, O.: Transition scenario to turbulence in thin vibrating plates. J. Sound Vib. **331**(2), 412–433 (2012)
73. Valette, C.: The mechanics of vibrating strings. In: Hirschberg, A., Kergomard, J., Weinreich, G. (eds.) Mechanics of Musical Instruments. CISM Courses and Lectures, vol. 355, pp. 115–183. Springer, Wien (1995)
74. Vergez, C., Rodet, X.: New algorithm for nonlinear propagation of a sound wave. Application to a physical model of a trumpet. J. Signal Process. **4**, 79–87 (2000)
75. Watzky, A.: Non-linear three-dimensional large-amplitude damped free vibration of a stiff elastic string. J. Sound Vib. **153**(1), 125–142 (1992)

Chapter 9
Reed Instruments

Jean Kergomard

Abstract This chapter deals with self-sustained oscillations created by reed instruments. Single, double, and lip-reed instruments (lip reeds are encountered in brass instruments) are presented. A basic model is proposed, the reed being regarded as a single-degree-of-freedom oscillator. Single and double reeds are shown to be inward-striking reed, while for the simplest model of lips the reeds are striking outward. The consequences of this difference are analyzed at the end of the chapter, when the effects of the reed dynamics, especially the role of the reed damping, are investigated. Because these effects are complicated, focus is given to the oscillation threshold (frequency and mouth-pressure thresholds). However, for single and double reed instruments, many useful results can be obtained with a simpler model, by ignoring the reed dynamics, i.e., equating the reed with a spring without mass. A large part of the chapter is devoted to this model. This is relevant because the resonance frequency of the resonator, and therefore the playing frequency, is much smaller than that of the reed. The different regimes for cylindrical and conical resonators are analyzed, with the nature of bifurcations. Playing frequencies, amplitudes, and spectra are found to depend on the excitation parameters, which are mainly the mouth pressure, the reed opening at rest and the reed compliance. In order to obtain insights in the behaviors, cylindrical resonators with single reed can be simplified to archetypes of nonlinear systems, either iterated map systems or Van der Pol oscillators. Simple conclusions can be drawn. Unfortunately, this is not possible for a lip-reed instruments because, for outward-striking reeds, the playing frequency is slightly higher than the reed resonance frequency.

This chapter deals with reed instruments. Single, double, and lip-reed instruments (lip reeds are encountered in brass instruments) are presented. This chapter and the following chapter, dedicated to flutes, will therefore encompass most types of wind instruments.

J. Kergomard (✉)
CNRS Laboratoire de Mécanique et d'Acoustique (LMA), 4 impasse Nikola Tesla CS 40006, 13453 Marseille Cedex 13, France
e-mail: kergomard@lma.cnrs-mrs.fr

A. Chaigne, J. Kergomard, *Acoustics of Musical Instruments*, Modern Acoustics and Signal Processing, DOI 10.1007/978-1-4939-3679-3_9

9.1 Background on Self-Sustained Oscillations

The first study related to wind instruments was carried out by Mersenne [80] and Bernoulli [15] who focused on the resonance frequencies of the tube. This topic, which is still being investigated nowadays, led to a fundamental understanding of several manufacturing parameters related to the resonator: cross-section variations, location and diameter of the toneholes, height of the chimney, etc. This was developed in detail in Chap. 7. For bowed-string instruments, a seminal work was also carried out by Mersenne. Following Mersenne's work, the next step was to understand the excitation of the system. The first attempts appeared at the end of the nineteenth century (Helmholtz [68] and Rayleigh [93]) and were further investigated during the twentieth century. Today, many questions remain open concerning this complex subject.

Self-sustained oscillations were introduced in Chap. 8. They are encountered in three kinds of instruments: reed instruments (including brass instruments), flutes, and bowed-string instruments. It is noteworthy that the last family can also produce sound with free oscillations (pizzicati). The fundamental research question is the understanding of the sound production, and therefore the oscillation *regimes*, as well as the conditions at which they can be obtained. For wind instruments, it is well known that several regimes with different frequencies can be obtained for a given fingering.

The study of musical instruments does not deal only with the conditions for oscillations to emerge, but deal mainly with the kind of oscillation which can exist. This differs from problems of practical interest such as Larsen effect, or oscillations of piping systems: the problem is not to product these oscillations, but to prevent them. Self-sustained oscillations are produced by an energy source, which is continuous, or rather slowly varying, a linear resonator, such as a tube or a string, and a feedback mechanism (Fig. 9.1). The feedback is very rapid, because it happens at the playing frequency, which in general is related to the reflections in the resonator (if no reflections occur in the resonator, the playing frequency cannot be related to the resonator length). The feedback mechanism is therefore much more rapid than the control loop of the energy source by the instrumentalist, via the force feedback and the sound hearing.

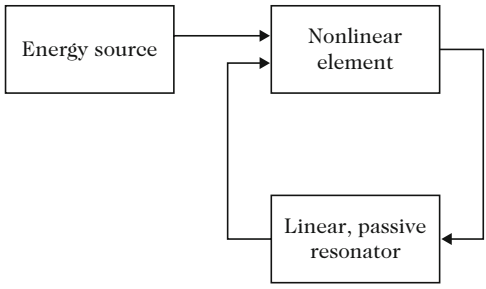

Fig. 9.1 Elementary block diagram of the loop of a self-sustained oscillation instrument

The simplest models assume that the nonlinearity, which is essential for the conversion of a continuous excitation into steady oscillations, is localized at the input of the resonator. This input is the entry of the tube for reed instruments, and the contact between the string and the bow for bowed-string instruments. This assumption markedly simplifies the analysis. In a well-known 1983 paper, Mc Intyre et al. [79] attempted to unify the three kinds of self-sustained instruments by using two elements only: the localized nonlinearity and the resonator. Obviously this assumption implies some simplifications (and is questionable for flute-like instruments), but provides initial elements of understanding. The authors demonstrated in particular the utility of the reflection function instead of the impulse response (which corresponds in the frequency domain to the input admittance or impedance of the resonator, see Chap. 4). However, for certain purposes, it is necessary to consider a non-localized nonlinearity. Moreover the models describing the transients can slightly differ from the models for the steady-state regime: this remark demonstrates the complexity of the phenomena. The following three chapters are of unequal length: a "preferential" treatment has been given to reed instruments, because today we have a model both simple and rather reliable. This allows presenting different approaches, in both time and frequency domains, for both transient and steady-state regimes. These methods help explain how the sound is produced, even if several problems remain open. Some analogies given by the table of Chap. 1 can sometimes be used, but obviously this is not always possible, because important differences exist between the nonlinearities.[1] The physics of reed instruments is based on the effect of a valve, which is a solid element (of the wall) modulating a flow, and the playing frequencies are close to the maxima of the input impedance. On the contrary the sound production of flute-like instruments is based on the instability of an air jet, without significant wall vibration, and the playing frequencies correspond to the maxima of the input admittance. In addition a significant broadband noise due to turbulence exists in flue instruments.

The outline of the present chapter is as follows: the models are first described in Sect. 9.2. Models without reed dynamics are then explored in Sects. 9.3 and 9.4 with a focus on emergence and stability of regimes. Finally the effect of the reed dynamics is investigated in Sect. 9.5.

[1] The bowed-string instruments can be compared to cylindrical reed instruments with an excitation at a certain distance of the extremities; it is well known that the harmonics whose number is multiple of n disappear in the spectrum when the string is excited at a distance equal to the nth part of the length. The clarinet is equivalent to the string bowed at its middle: the two parts of the string play the same role, and are equivalent to a unique string, with a double characteristic impedance. The excitation parameters can also be compared: the bow velocity is equivalent to the mouth pressure, while the bow force is equivalent to the reed-mouthpiece parameter defined hereafter. Nevertheless the nonlinearity of reed instruments and bowed strings is extremely different, and that of the bowed string poses very difficult problems concerning stability.

9.2 Reed Instruments Models

9.2.1 Introduction

A reed is a type of valve, capable of modulating the air flow rate produced by a pressure difference between the upstream (the instrumentalist mouth) and the downstream (the instrument mouthpiece). This principle is common to all kinds of reed instruments, either with a (single or double) cane reed, a metallic reed, or a lip reed. The main distinction between this different instruments is based on the shape of the resonator, and the ratio between the natural frequencies of the reed and those of the resonator. Similar types of sources can be found in an industrial setting, such as electro-pneumatic loudspeakers with an electrically controlled valve. Their main advantage lies in the capacity to produce very loud sounds. Converting a static (dc) pressure into an alternating (ac) one with the same energy can produce extremely loud sounds, which are difficult to generate with linear sources.

In the case of reed instruments, the energy source is the flow itself, and the measurement of acoustic pressures within the mouthpiece requires particular microphones (170 dB is rather usual!). Fortunately the radiation has a very low efficiency and cannot damage our ear. The external sound is much less loud, because of the strong reflection at the end of the tube (which allows the sound production). A reed can be modeled as a flexible structure, such as an elastic beam, with a pressure difference acting of the two faces. The real boundary conditions can be rather complicated. As a first approximation, the beam can be considered as a cantilever beam with one fixed end and one free end, but its displacement can be limited by another reed (for double reeds) or by the mouthpiece (for single reeds). This kind of boundary conditions exists also for stringed instruments: it is called "conditional" [111], and produces strong nonlinearities. When the reed closes the mouthpiece, it is called a "beating reed." When no obstacle stops the displacement, the reed is "free"; it is the case of the accordion and harmonica. For cane reed, the lips strongly damp the reed vibration, and limit the amplitude of the vibration between lip and the ligature (but this amplitude does not vanish). In Chap. 5 an example of localized damping has been studied; to produce an accurate model for the reed is not easy. In particular the lips have complex geometrical and mechanical characteristics. For organ reeds, the tuning wire plays the role of the lower lip of the clarinettist. Its position allows the tuning of the pipe, and this fact demonstrates the weak coupling between reed and pipe in reed organs.

Some instruments have (single or double) reeds which are encapsulated and this causes difficulties in playing: the damping and vibrating length of the reed cannot be controlled during playing. This is the case of crumhorns and bagpipes. The difficulty of creating a model is even greater for lip reeds. Often a simple, global model is used, based on an experimental modal expansion of the reed vibration. To take into account one vibration mode only gives very useful information, even if it is not sufficient at higher frequencies (some authors proposed more precise models [5, 40, 44]). In what follows, we consider a single mechanical reed oscillation mode.

In order to understand the fundamental physical features, which are essentially nonlinear, it is necessary to introduce major simplifications, even if details related to sound quality are lost. For single reed instruments, we therefore first assume that the reed is a spring without dynamics (without neither mass nor damping), and obtain first results concerning the sound production.

9.2.2 Mechanical Response of a Reed: Experimental Data

9.2.2.1 General Considerations

A major obstacle to the study of the characteristics of a reed instrument is the number of parameters that influence sound production. Moreover when carrying out a measurement involving an instrumentalist, it is not easy to be sure that he or she does not influence, either consciously or not, the result of a given task. For this reason, the artificial mouth is a very useful device: it acts as a good surrogate for an instrumentalist.[2] Using artificial blowing it is possible to measure the reed mechanics in the form of a mechanical response to a pressure excitation (see, e.g., [47]). If this pressure is assumed to be almost uniform on each of the two sides of the reed (see discussion hereafter), the frequency response is defined as follows:

$$H_{\mathrm{mr}}(\omega) = \frac{\mathscr{Y}(\omega)}{\Delta P(\omega)}, \tag{9.1}$$

where $\mathscr{Y}(\omega)$ is the reed displacement at low excitation level and $\Delta P(\omega)$ the pressure difference across the reed. The subscript m stands for mechanical, and the subscript r for reed. Obviously the reed displacement is not uniform, thus the response measurement should be completed by the measurement of the reed deformation. However, we assume that the displacement of the reed extremity represents the reed displacement, at least when the reed does not beat. Another difficulty of the measurement lies in the control of the pressure difference $\Delta P(\omega)$ (see [29]). Figures 9.2 and 9.3 show two examples of responses for a single reed and lips, respectively.

Concerning a single reed, the support of the lip plays a significant role for reducing the vibrating length of the reed, and mainly a role of reed damping. For the example shown in Fig. 9.2, it can be seen that the first reed resonance lies close to 2000 Hz. The response argument is $+\pi/2$ at the resonance; this is evident in particular for the reed without lip of Fig. 9.2. Consequences will be analyzed in Sect. 9.2.3.2. For the lips of a trombonist, a precise analysis of the figure shows the

[2] This kind of device is based upon an old idea. For instance during the eighteenth century the Kempelen machine imitated the voice. There are also numerous more recent works: we cite [6, 70, 109] for the clarinet, and [58, 114] for brass instruments. The organ obviously is a kind of artificial mouth!

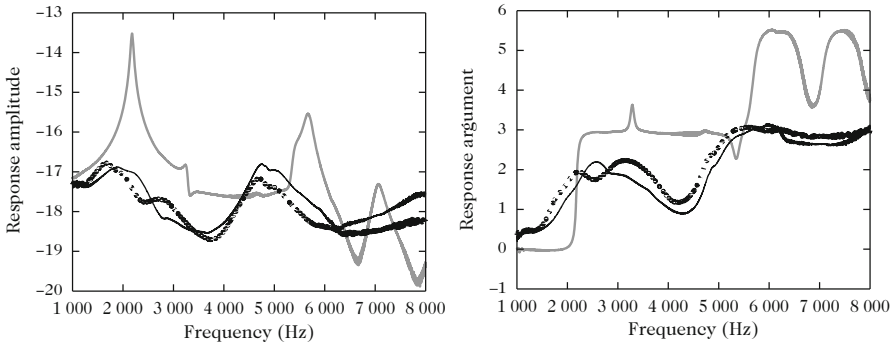

Fig. 9.2 Response of a single clarinet-like reed of to an oscillating pressure differences: without support of the lip (*gray* curve) and for two lip forces pressing on the reed (*black curves*). The amplitude scale is arbitrary, the argument is in radians (after [66])

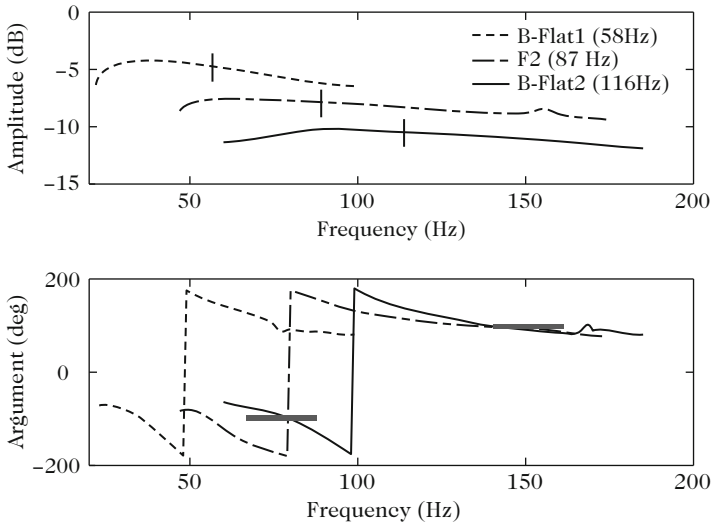

Fig. 9.3 Mechanical response of human lips (modulus and argument) to an oscillating pressure difference for three different notes of a tenor trombone: Bflat1 is the "pedal" tone. Its harmonics correspond to a series of impedance peaks, but the fundamental of the note does not correspond to a peak. The playing frequency is noted with a *small vertical dash* on the amplitude curve. For clarity the amplitude curves of the two highest pitches are shifted by 3 dB and 6 dB, respectively. The amplitude scale is arbitrary. The two *horizontal lines* on the argument curve at $\pm 90°$ indicate the resonances (after [88])

existence of two resonances which are close together. The argument is $-\pi/2$ for the first one while for the second, which is strongly damped, it is $+\pi/2$.

9.2.2.2 Single Reed of Clarinet–Reed Kind

The response shown in Fig. 9.2 corresponds to a given "embouchure" of the player. What we call embouchure corresponds to a particular setting of both the lip position and the force applied by the lips on the reed. Several resonances appear. Recent theoretical or experimental works analyzed these resonances, either without or with lip [92, 102, 106, 112]. From the first resonance of the response, it is possible to extract several parameters, which will be important for our simple model: (1) the static stiffness (per unit area), K_s, depending of the reed "hardness" (reeds are commonly classified using a single parameter, the "hardness," given by the reed makers); (2) the first resonance frequency, f_r, which allows deducing the modal mass (per unit area) of the first mode, $m_s = K_s/\omega_r^2$ (see Chap. 3, Sect. 3.3.1). So we obtain a single-degree-of-freedom model:

$$\frac{d^2y}{dt^2} + q_r\omega_r\frac{dy}{dt} + \omega_r^2 y = \frac{f_s}{m_s}, \tag{9.2}$$

where $y(t)$ is the tip displacement of the reed (at low excitation level), the origin being the value of y at rest (when $f_s = 0$), $q_r\omega_r$ is the damping coefficient, $q_r = 1/Q_r$ is the inverse of the quality factor of the reed, which depends on the positioning of the lips (q_r is equal to $2\zeta_0$, as defined in Chap. 2). ω_r is the resonance angular frequency and $f_s(t)$ is the force per unit area due to the acoustic pressure. For a clarinet reed, this force can be written as:

$$f_s = -\Delta p, \text{ where } \Delta p = p_m - p. \tag{9.3}$$

Δp is the difference of the pressure applied on the two faces (p_m is the mouth pressure, p is the pressure on the other face). The minus sign is explained as follows: if Δp increases, the reed will be closed (see Fig. 9.4).

The fundamental frequency of the played notes is assumed to be very close to the natural frequencies of the resonator and much lower than the resonance frequency of the reed, f_r. This is not true for very high notes and even wrong for the squeaks, but this assumption allows large simplifications for the study of this kind of instruments. Ignoring the reed dynamics leads to the simple equation:

$$K_s y = -\Delta p. \tag{9.4}$$

The quantity K_s can be measured, via the measurement of the ratio $\Delta p/y$. The "closure pressure" p_M, is the mouth pressure for which the reed remains closed in the static regime (then $y = -H$, and the mouthpiece pressure vanishes)[3]:

$$p_M = K_s H. \tag{9.5}$$

[3]The stiffness of the reed depends on the closure of the reed, and therefore varies with the pressure difference, because of the curvature of the mouthpiece lay. However, the closure pressure p_M varies very little [30].

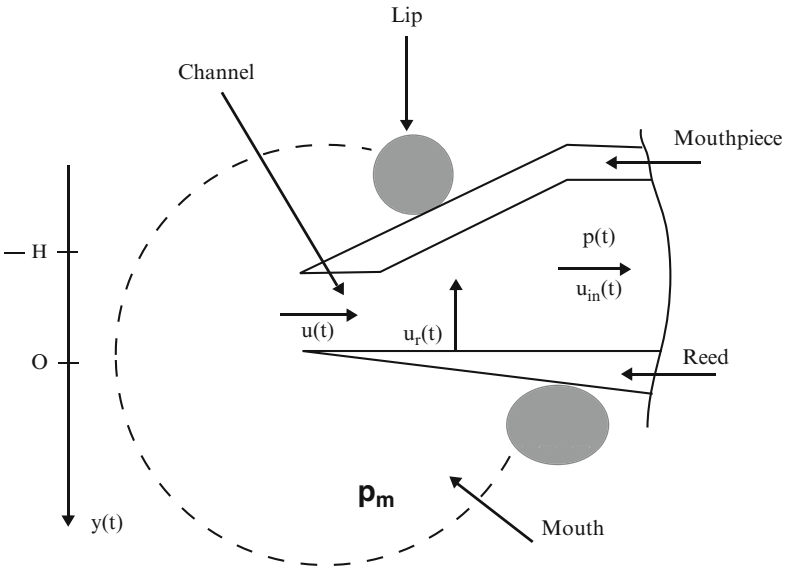

Fig. 9.4 Schematic representation of a clarinet mouthpiece with a single reed, and choice of orientations. The lower lip restricts the vibrating length and provides its damping. The model assumes a two-dimensional geometry, with a rectangular reed of width w. The definition of the flow rates is given in Sect. 9.2.4

Figure 9.5 shows simultaneous signals for the mouthpiece pressure and the reed displacement. On the left part, it is observed that the two signals are in phase and almost proportional: this justifies the assumption (9.4). Nevertheless an asymmetry is more noticeable for the displacement signal than for the pressure one. This indicates the presence of even harmonics. Here the spectra are not shown, but they exhibit a maximum of the response close to the harmonic 21, i.e., 2800 Hz: this frequency is the first resonance of the reed. On the right part of the figure, a limit of the displacement can be seen: it corresponds to the beating state of the reed. This is a nonlinear phenomenon. The linear frequency response (9.1) loses significance, because Eq. (9.2) needs to be completed by the following nonlinear condition:

$$y > -H. \tag{9.6}$$

9.2.2.3 Lip Reed

For instruments with a cane reed, the playing frequency is mainly controlled by one of the natural frequencies of the resonator, and the influence of the reed is small. This is different for lip-reed instruments. The lip resonances of a "brass" instrument player are crucial in order to obtain correct playing frequencies, which

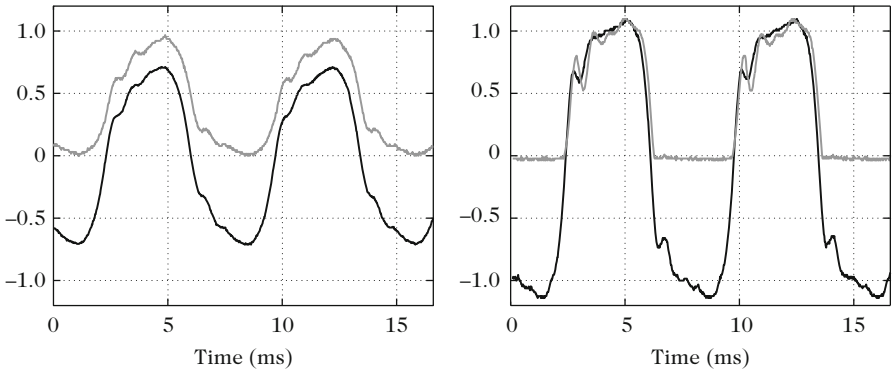

Fig. 9.5 Reed displacement (*gray curve*) and mouthpiece pressure (*black curve*) for a non-beating reed (on the *left*) and for a beating reed (on the *right*): for the latter case, a plateau of the displacement signal is visible, when the reed closes the mouthpiece. The scale is arbitrary. The instrument is a cylindrical tube with a clarinet mouthpiece (From [89])

are also related to the resonator natural frequencies. As a consequence, the coupling between reed and resonator is strong. The instrumentalist has to learn the control of his lips to get the correct mechanical resonance frequency which allows using a given resonance of the resonator. Thus the learning curve to obtain a "correct sound" is arduous. It requires a significant muscular training. Some instruments have a range of four octaves! In contrast to skilled players, the artificial mouths are similar to a beginner: it is difficult to dynamically control the artificial lip tension, and the compass is limited to two octaves.

It is therefore impossible to ignore the lip dynamic when trying to explain the brass instrument properties. Equation (9.2) with one reed mode is the simplest model and allows obtaining rather realistic synthesized sounds [64, 116]. Nevertheless it is sometimes better to take two modes into account, by using the so-called two-mass model. This is often done for the modeling of the vocal folds (the main difference between brass instruments and the voice lies in the degree of coupling between the "lips" and the resonator; the coupling between the folds and the vocal tract is weak).[4] Figure 9.3 shows that the two-mode model probably is more realistic for brass instruments, because two resonances appear: they are close together, with a strong attenuation for the second one. These twin resonances can be sharper with an artificial mouth, as reported in [88].

[4] In singing it is possible to continuously change in notes without changing the length and the shape of the vocal tract. The skilled brass instrument players can also play without instrument, but the timbre is strongly modified.

9.2.3 *Dynamic of the Fluid Passing the Reed*

9.2.3.1 Pressure Field, Flow Separation, Valve Effect (Single Reed)

Now we need to find a relationship between the pressure and velocity of the fluid, by investigating the properties of the flow which enters the resonator. Figure 9.4 shows a schematic representation of the mouthpiece of a single reed instrument. We remark the localized constriction at the extremity of the reed. Its length has an order of magnitude of 1 mm. The constriction can be regarded as a channel located between a "pressure reservoir" (i.e., the player mouth) and the entry of the clarinet mouthpiece (for lip-reed instruments, the channel consists of the space between the lips of the musician). The cross section of the channel is time-varying, and it is controlled by the reed (or lips) position during an oscillation. The flow at the entry of the instrument has the form of a jet at the channel exit: for a detailed description of the jet and the underlying hypotheses, the reader is referred to the Chap. 10 about flute-like instruments (see Sect. 10.3.1). The main result is that for $\Delta p > 0$ the velocity v_j at the end of the constriction (i.e., of the channel) is given by:

$$v_j = \sqrt{2\Delta p/\rho}. \tag{9.7}$$

Δp is defined by Eq. (9.3). The pressure at the instrument inlet is assumed to be equal to that in the channel. The above result is based upon a very simplified description of the flow separation, which is assumed to be localized at the channel exit. However, the precise determination of the separation point is not easy. It depends on the detail of geometry of the channel exit, i.e., on the channel flare and on the flow rate. The higher are the flare and the flow rate, the more upwards is the separation point (see [43, 69], pp. 311 and the following). An air jet is intrinsically unstable (see Sect. 10.3.2 in Chap. 10 on flutes), and becomes turbulent. Turbulence implies a fast mixing of the jet with the surrounding air, and consequently an abrupt deceleration happens without pressure recovery at the mouthpiece inlet. Without dissipation, it could be possible to apply the Bernoulli law, and a pressure increase would result from the velocity decrease. Actually dissipation "compensates" for the non-recovery of pressure in the mixing zone. When the turbulent mixing is over, the decelerated flow is assumed to be spread over the complete cross section of the mouthpiece (typically 15 mm in diameter) and to be almost uniform. Finally the nature of the acoustic source in reed instruments can be summarized as follows: it is a flow source using the valve effect. The fluctuating volume flow entering the instrument is the product of a velocity and a fluctuating cross-section area. The flow rate is mainly controlled by the pressure difference Δp, and the cross-section area by that of the channel exit.

Each quantity is the sum of an average part (over time) and a fluctuating part. The mouth pressure is assumed to be constant, i.e., the input impedance of the vocal tract at non-zero frequencies is negligible compared to that of the instrument. This will be discussed in Sect. 9.4.7 of this chapter. Conversely, the time-average static

pressure at the inlet of the instrument is assumed to be negligible compared to the mouth pressure. In other words the input impedance of the resonator is very small at zero frequency. Indeed an order of magnitude of the time-average flow resistance of the pipe can be estimated by ignoring the inflow effect and assuming a Poiseuille flow [Eq. (5.115)]. It is found to be less than 1 % of the characteristic impedance of the clarinet tube at the playing frequency [73, p. 251]. Concerning the estimation of the flow velocity at the inlet of the tube, the use of the previous model leads to a Mach number (the ratio of the velocity to the sound speed) significantly lower than 1 %. Such a value for the Mach number allows neglecting convective effects on wave propagation. This is valid as long as nonlinear propagation is not considered (see Chap. 8).

9.2.3.2 Inward- and Outward-Striking Reeds

For the last two centuries many authors have tried to characterize the reeds according to the effect of the pressure difference across the reed. For inward-striking reeds an increase in the pressure difference Δp tends to close the reed channel, while for outward-striking reeds, it tends to open the reed channel. The behavior of the two kinds of reeds is very different, as demonstrated by the differences in playing frequencies. This will be explained in Sect. 9.5 of this chapter. Figure 9.6 gives a schematic representation of this difference [50]. The clarinet reed therefore is an inward-striking reed, and is described by Eq. (9.3): for a positive pressure difference, the force is exerted upward[5] (see Fig. 9.4). Fletcher [49] proposed a finer distinction for the reeds, by distinguishing the mean pressure on the two faces of the reed. We do not go further on this difficult subject.

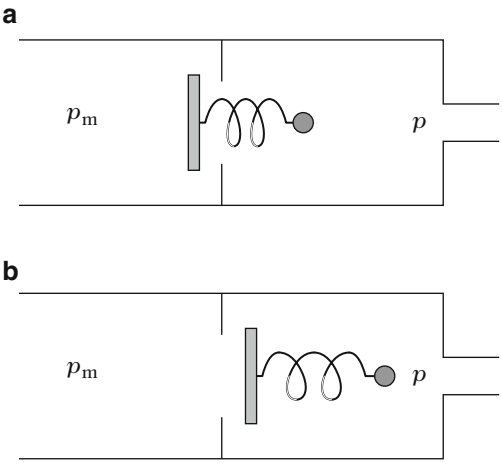

Fig. 9.6 Principle of an inward-striking reed (**a**) and an outward-striking reed; (**b**) after Fletcher [50]. A positive pressure difference $\Delta p = p_m - p$ tends to close the reed for the case (**a**) and to open the reed for the case (**b**)

[5]This is consistent with the value of the response argument $H_{mr}(\omega)$ around the resonance, as given by Eq. (9.1). We saw that it is equal to $+\pi/2$: using Eq. (9.2), the argument of the ratio $\mathscr{Y}(\omega)/F(\omega)$ is $-\pi/2$, thus that of the ratio $\mathscr{Y}(\omega)/\Delta p(\omega)$ is $+\pi/2$.

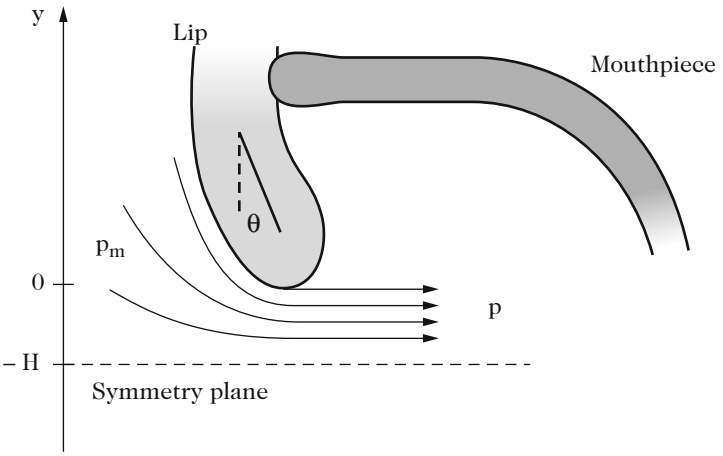

Fig. 9.7 Lip reed seen as a swinging door. The two lips are assumed to be symmetrical. The point $y = -H$ corresponds to the closure of the lips

9.2.3.3 The Case of the Lip Reed

The case of the lip reed is more complicated than that of the single reed with a mouthpiece. The geometry and the mechanical structure of the lips and their surrounding (the "embouchure") are complex. A drastically simplified geometry is often considered in order to describe the valve effect. It is possible to use a model of a "swinging door" (see Fig. 9.7), for each lip, assuming a perfect symmetry between the two lips.

The lips are again approximated by a one-degree-of-freedom oscillator: a rotation abound an equilibrium position defined by an angle θ, with respect to the vertical axis [1]. For this simplified geometry, there is a localized constriction at the end of the lip, and it is possible to apply the air flow description used for cane reeds. We assume rather arbitrarily that flow separation occurs at the neck of the channel formed between the lips, with a jet velocity given by Eq. (9.7). After a certain distance into the mouthpiece, the jet rapidly expands and produces a zone of turbulent mixing. After this zone, the velocity field is supposed to be uniform over a cross section of the mouthpiece, and the pressure in the lip channel is equal to the pressure in the mouthpiece. For a trombone, the diameter of the mouthpiece is around 30 mm, and it is much larger than the lip opening.

Therefore at the extremity of the lip, the upstream pressure is the mouth pressure, p_m, and the downstream pressure is the mouthpiece pressure. Thus it is reasonable to consider that the force exerted on the lip is proportional to the pressure difference, Δp. With this model, the lip enters the mouthpiece for an increasing pressure difference, and this corresponds to an outward-striking reed. With an orientation convention similar to that used for the clarinet reed, the force projection on the axis can now be written as:

$$f_s = +\Delta p. \tag{9.8}$$

There is a great similarity with the model of a clarinet reed, but the force is given by the previous equation. Figure 9.7 depicts a very simplified schematic representation. A static closure pressure can again be defined, but *it is now negative*, because we should inhale to close the lips. For the sake of simplicity, the closure pressure will be denoted $-p_M$, where p_M is given again by Eq. (9.5).

Other models can be found in the literature. Some of them take into account both the vertical and the horizontal movements of the lips. A review is given in [24], with a discussion of the link to the models of singing voice and speech. Some models can also consider an inward-striking behavior under certain conditions.

Figure 9.8 shows an example of lip movement [22, 23]. We will not go further in the discussion of the model. We conclude that it is difficult to develop an accurate and reliable model. In fact the first resonance probably corresponds to a mode of an outward-striking reed. In this chapter, we limit our study to the latter case.

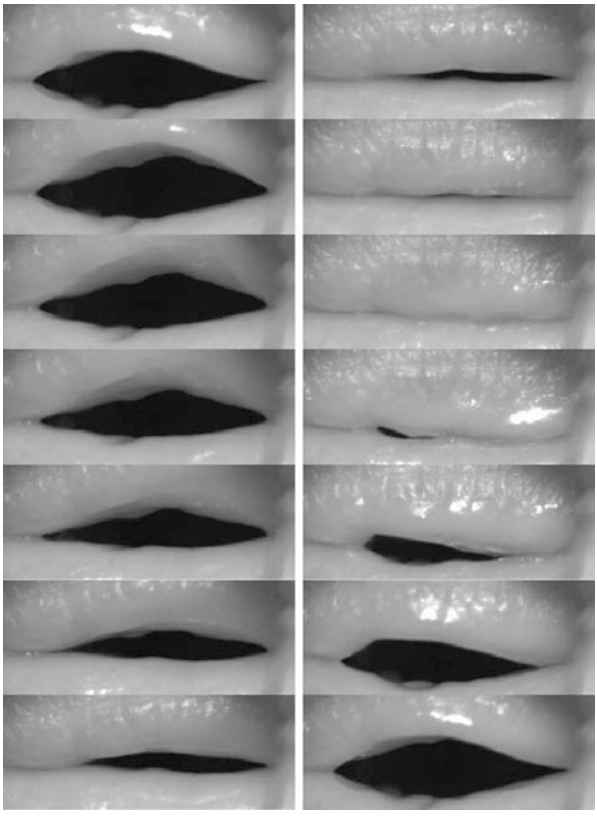

Fig. 9.8 Movement of the upper lip during one period [21]

9.2.4 Reed Opening Area and Flow Rate

9.2.4.1 Outgoing Channel Flow Rate

Let us first estimate the flow rate u entering the resonator. The jet velocity is assumed to be equal to that at the output of the reed channel. The flow rate can therefore be simply expressed with respect to the cross-section area of the jet S_j, i.e., that of the reed channel:

$$u = v_j S_j. \tag{9.9}$$

S_j plays a major role for the control of the flow valve effect. In a two-dimensional flow, we get a very simple linear relation between the opening area and the channel height:

$$S_j = (y + H)w, \tag{9.10}$$

where w is the effective width (see Fig. 9.4 for the definition of y and H). This linearity was experimentally verified by Dalmont et al. [34]. However, Backus [7] experimentally found an area depending on the height with a power q, $S_j \propto (y+H)^q$, where $q = 4/3$, and this dependence has been used by many authors. For reasons that will be explained soon, we keep the linear dependence for the single reed.

A similar debate exists for the double reed. If the shape to the reed end is seen as two circle arcs, it should be found a power $q = 1.5$ or more (see [8]), but authors found [117] a linear dependence on the reed opening. For lip reeds, many authors investigated this issue, and they found a power between 1 and 2, for instance, by graphical inspection (see, e.g., Fig. 9.8).

9.2.4.2 Flow Rate Due to the Reed and Total Flow

Equation (9.9) gives the flow rate passing through the reed channel. However, another source of flow, of secondary importance, exists: it is the flow produced by the reed vibration, which is similar to the flow produced by any vibrating surface, such as a loudspeaker membrane. The reed pushes and pulls out air inducing a flow rate u_r equal to:

$$u_r = -S_r \frac{dy}{dt}, \tag{9.11}$$

where S_r is the effective area of the reed. The sign $-$ comes from the orientation choice in Fig. 9.4: the reed produces a flow entering the resonator when y decreases (in the figure it is not obvious that this displacement flow enters the resonator, however, it might be clearer that an equivalent flow induced by the top of the reed "leaves" the mouth, which surrounds the mouthpiece! There is actually no creation

of volume by the reed movement). The total flow rate entering the instrument is therefore:

$$u_{\text{in}} = u + u_r. \tag{9.12}$$

If plane waves are assumed at the instrument inlet, this flow rate is related to the input impedance, or, in time domain, to the impulse response $h(t)$, which is the inverse Fourier Transform of the input admittance (this has been largely studied in Part II):

$$u_{\text{in}}(t) = [h * p](t).$$

It is often convenient to choose the flow passing through the channel as the unknown u, which is related to the impulse response $h(t)$ by the following equation:

$$u = [h * p](t) + S_r \frac{dy}{dt}. \tag{9.13}$$

The flow created by the reed movement is responsible for the added term. The effect of this term was studied in [86]. For frequencies much lower than the reed resonance, there is a simple interpretation to this term. The reed stiffness K_s is equivalent to a small volume V_{eq} added at the input of the instrument. For a constant mouth pressure p_m and a non-beating reed:

$$\frac{dy}{dt} = -\frac{1}{K_s}\frac{d(\Delta p)}{dt} = \frac{1}{K_s}\frac{dp}{dt} = \frac{H}{p_M}\frac{dp}{dt}. \tag{9.14}$$

Combining Eqs. (9.11) and (9.14):

$$u_r = -\frac{V_{\text{eq}}}{\rho c^2}\frac{dp}{dt} \quad \text{where} \quad V_{\text{eq}} = \frac{\rho c^2}{p_M} S_r H; \tag{9.15}$$

$$u = u_{\text{in}} + \frac{V_{\text{eq}}}{\rho c^2}\frac{dp}{dt}. \tag{9.16}$$

Thus the flow due to the reed is equivalent to adding a compliance in parallel to the pipe input impedance, V_{eq}. It is that of an air volume localized at the instrument input if the frequency is sufficiently low [see Chap. 1 Sect. 1.5, Eq. (1.154)].[6] In general it is easy to correct the mouthpiece volume by the volume V_{eq}. This correction is independent of the fingering, and can be measured.

[6] V_{eq} differs from the air volume displaced by the reed, $S_r H$. Furthermore this description assumes that the stiffness by unit area K_s does not vary with the pressure level. In practice when the reed progressively closes the mouthpiece, the stiffness varies, as well as V_{eq}, and consequently the playing frequency.

If the mouthpiece is almost cylindrical, the addition of a closed volume in parallel with the pipe input impedance implies a shift of the impedance maxima which corresponds to an extension of the cylinder by a length $\Delta\ell$. This length is defined such as $V_{\text{eq}} = S\Delta\ell$, where S is the cross-section area of the tube, therefore:

$$\Delta\ell = \frac{\rho c^2}{p_M}\frac{S_r}{S}H. \tag{9.17}$$

Measurement results give a length of about 10 mm added to that of a clarinet mouthpiece [32].

9.2.5 Basic Model (Clarinet-Like Reed)

9.2.5.1 Three-Equation Model

By gathering the different equations discussed above one obtains a basic model. We use the length correction defined by Eq. (9.17).[7] in the general Eq. (9.13):

$$u = [h * p](t) + \frac{S\Delta\ell}{H}\frac{p_M}{\rho c^2}\frac{dy}{dt}. \tag{9.18}$$

When using the closure pressure p_M, Eq. (9.2) becomes

$$\frac{d^2y}{dt^2} + q_r\omega_r\frac{dy}{dt} + \omega_r^2 y = -H\omega_r^2\frac{\Delta p}{p_M}. \tag{9.19}$$

Now we can suppose that the flow separation situation is reversible when the pressure difference is inverted,[8] and that the area of the reed channel depends linearly on its height. Equations (9.7) and (9.10) yield

$$u = u_A\left(1 + \frac{y}{H}\right)\sqrt{\frac{|\Delta p|}{p_M}}\text{sign}(\Delta p) \quad \text{if} \quad y > -H \tag{9.20}$$

$$\text{and} \quad u = 0 \quad \text{if} \quad y < -H \quad \text{(beating reed)}, \tag{9.21}$$

[7] Here it is a notation only, because the interpretation as a length correction is limited to low frequencies and cylindrical mouthpieces.

[8] All above-mentioned hypotheses are satisfied again, but in the reverse sense: the cross section of the tube is much larger than that of the reed channel, then there is a jet formation at the output of the channel (in the mouth), and there is no pressure recovery. This is somewhat arbitrary, but the situation with a flow entering the mouth seems to be quite extreme, and was never observed experimentally.

where the flow rate u_A is given by:

$$u_A = wH\sqrt{\frac{2}{\rho}p_M} = wH^{3/2}\sqrt{\frac{2}{\rho}K_s}. \tag{9.22}$$

Equations (9.18)–(9.20) form a system of three equations with three unknowns, u, the flow rate going out to the channel into the resonator p, the pressure at the input of the resonator and y the vertical displacement of the reed. The two first equations are linear, and can be described in the frequency domain, while the third is nonlinear (remember that a necessary condition for the production of steady self-sustained oscillations is the existence of a nonlinearity which limits the amplitude).

9.2.5.2 Simplified Two-Equation Model

A useful approximation consists in approximating the reed with a simple static spring. This is a good approximation when the natural angular frequency ω_r is much higher than the (angular) playing frequency. In this case $y = -H\Delta p/p_M$, and Eq. (9.19) can be eliminated together with the unknown y:

$$u = u_A\left[1 - \frac{\Delta p}{p_M}\right]\sqrt{\frac{|\Delta p|}{p_M}}\text{sign}(\Delta p). \tag{9.23}$$

For a non-beating reed, the condition (9.6) needs to be added. This condition can be also written as: $\Delta p < p_M$. For a beating reed, when the channel is closed, the flow rate vanishes

$$u = 0 \text{ if } \Delta p > p_M. \tag{9.24}$$

Such a model is not completely satisfactory because it implies a discontinuity of the flow rate derivative. It should be completed by a transition with a very narrow channel and, for instance, a Poiseuille flow [115]. The curvature of the mouthpiece lay should be also taken into account. These subtle phenomena are not investigated in this book. Furthermore the discontinuity in derivative yields difficulties in the numerical treatment [16, 72].

These simplifications lead to a characteristic function $u(\Delta p)$, which has been measured for a stationary flow [34], with positive pressure differences only. Figure 9.9 shows the result, which is perfectly in accordance with the law (9.23), except for the highest pressures. For these pressures, there is no abrupt transition to a beating reed, and the flow does not vanish completely, because the reed does

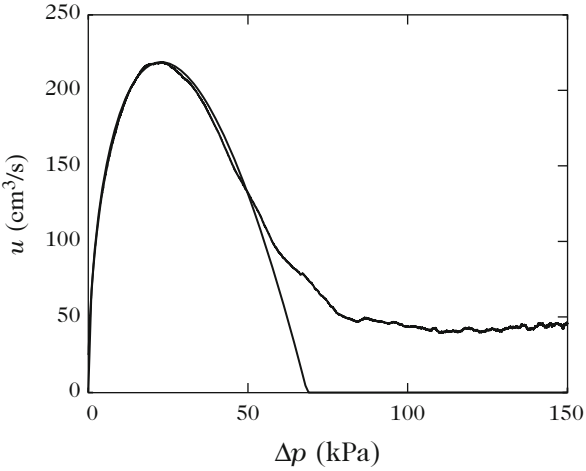

Fig. 9.9 Nonlinear characteristic measured (*thick line*) and calculated (*thin line*) based on (9.23) and (9.51). The increasing portion of the curve is close to a square root of the pressure difference, because the displacement of the reed is very small. In the decreasing portion the progressive closure of the reed becomes dominant. The experiments do not exhibit any beating of the reed, because the flow does non vanish for large pressure differences

not entirely closes the mouthpiece.[9] The measurement of the characteristic function leads to the values of two essential excitation parameters, p_M and u_A: however, their values obviously cannot satisfy all our hypotheses. As an example, if the jet cross section is not strictly equal to that of the reed channel, the formula (9.23) remains identical, but the value of u_A can be changed based on experiments.[10]

The global shape of the curve is rather intuitive: the flow rate first increases when the pressure difference increases, but it is expected to almost vanish for high pressure differences. Hence a saturation occurs, then a decrease. If the mouth pressure p_m does not depend on time, it is possible to write a function $u = F(p)$ which does not depend on the parameter p_m, deduced from the function

[9]In the two-dimensional model we ignored that the air can pass through the sides of the reed, because the mouthpiece lay is curved, and the reed does not perfectly wrap the lay. Moreover the extremity of the mouthpiece is not planar. The air can also flow between the reed and the mouthpiece; the reed does not remain perfectly planar, and twisting can occur. For a double reed, such as a bassoon reed, the way the reed is pressed by the fingers at its extremity is a quality criterion for instrumentalists, which are sanding their reed. When the reed closes linearly (the sides are closed simultaneously with the center), the closure is rather sudden, and the spectrum is rich in harmonics; on the contrary if the sides are closed before the center, the closure is more progressive, and the spectrum is poorer [67].

[10]A validation of the dynamic model can be obtained from a simultaneous measurement of the flow rate and the pressure. For instance it has not been proved that taking into account an unsteady term in the Bernoulli equation would improve the model; however, because of the effect of the reed dynamic, such a simultaneous measurement cannot give a quasi-static curve, as shown by Meynial [81]. He compared experiment and theory by measuring the velocity with a hot wire anemometer at several places in order to deduce the flow rate, and by measuring the pressure with a microphone. Another method could consist in measuring the pressure at several places in the tube, then deducing the input quantities from the knowledge of theoretical transfer functions. Similar ideas have been utilized for bowed strings [123], but it is tedious for a reed instrument, because the input impedance for the even harmonics is highly sensitive to the mouthpiece shape.

$u(\Delta p)$ (9.23): the modification of p_m leads to a simple translation of the curve. The other parameter of the function, u_A, which is a composite parameter, characterizes the amplitude of the curve. It depends on both the reed opening, that the musician can adjust when playing, and the reed stiffness, which is chosen a priori by the musician. This parameter is related to the maximum flow rate that can enter the tube: the maximum of the function $u(\Delta p)$, obtained for $\Delta p = p_M/3$, is

$$u_{\max} = u_A \frac{2}{3\sqrt{3}}. \tag{9.25}$$

Experiments compare very well with the model for the non-beating reed of a clarinet [30]. For an oboe reed, there is a significant difference between measurement and model, because the increase of the curve at low Δp is steeper. This observation was related to the jet behavior in the conical part which is the channel output of the double reed [3, 34, 61].

9.2.5.3 Dimensionless Equations

In order to draw general conclusions, it is convenient to make the three basic equations dimensionless. It is logical to divide the reed displacement by the height of the opening at rest, H, and the pressures by the closure pressure p_M. The flow rates are divided by p_M/Z_c, where $Z_c = \rho c/S$ is the characteristic impedance of the tube. Thus the following definitions are chosen for the unknowns and the parameters:

$$\tilde{y} = y/H;\ \ \tilde{p} = p/p_M;\ \ \tilde{u} = uZ_C/p_M; x = \tilde{y} + \gamma$$

$$\gamma = \frac{p_m}{p_M}\ ;\quad \zeta = Z_c \frac{u_A}{p_M} = Z_c w H \sqrt{\frac{2}{\rho p_M}} = \frac{wH}{S}\sqrt{2\frac{C_p}{C_v}\frac{p_0}{p_M}}.$$

In the last expression of ζ, the compressibility $1/\rho c^2$ has been replaced by its value with respect to the atmospheric pressure p_0 [see Eq. (1.98)]. Typical values of the reed parameter ζ are of the order of 0.3–0.4 [52, 89]: it will be seen that this parameter has a strong influence on the attack transients, while the mouth pressure dictates the amplitude and the spectrum of the sound. The input admittance, and therefore the function $h(t)$, is multiplied by Z_c. Introducing dimensionless variables and removing the superscripts (for the sake of simplicity), Eqs. (9.18)–(9.20) become

$$u = [h * p] + \frac{\Delta \ell}{c}\frac{dx}{dt}; \tag{9.26}$$

$$\frac{1}{\omega_r^2}\frac{d^2x}{dt^2} + \frac{q_r}{\omega_r}\frac{dx}{dt} + x = p; \tag{9.27}$$

$$u = \zeta(1 + x - \gamma)\sqrt{\gamma - p} \text{ if } 1 + x - \gamma \geq 0\,, \text{ or} \tag{9.28}$$

$$u = 0 \text{ if } 1 + x - \gamma \leq 0. \tag{9.29}$$

(One can assume that Δp is positive, because in practice the mouth pressure is almost always higher than the mouthpiece pressure, at least for quasi-cylindrical instruments). Using this hypothesis the two-equation model (9.23) is given by:

$$u = F(p), \text{ where} \tag{9.30}$$

$$F(p) = \zeta(1 - \gamma + p)\sqrt{\gamma - p} \text{ if } \gamma - p \leq 1; \tag{9.31}$$

$$F(p) = 0 \text{ if } \gamma - p \geq 1. \tag{9.32}$$

9.2.6 Basic Model (Lip Reed)

9.2.6.1 Three-Equation Model

The basic model for a lip reed (or more precisely for an outward-striking reed) is now given. Obviously we cannot reduce the 3-equation model to 2-equation model, because the reed dynamics play an essential role.

$$u = [h * p](t) + \frac{S\Delta\ell}{H}\frac{p_M}{\rho c^2}\frac{dy}{dt}; \tag{9.33}$$

$$\frac{d^2y}{dt^2} + q_r\omega_r\frac{dy}{dt} + \omega_r^2 y = H\omega_r^2\frac{\Delta p}{p_M}; \tag{9.34}$$

$$u = u_A\left(1 + \frac{y}{H}\right)\sqrt{\frac{|\Delta p|}{p_M}}\text{sign}(\Delta p), \tag{9.35}$$

where the coefficient u_A is given by:

$$u_A = wH\sqrt{\frac{2}{\rho}p_M} = wH^{3/2}\sqrt{\frac{2}{\rho}K_s}. \tag{9.36}$$

9.2.6.2 Dimensionless Equations

All dimensionless parameters are defined in the same way. Nonetheless here the closure pressure is negative, equal to $-p_M$, and we write

$$x = y - \gamma.$$

This yields

$$u = [h * p](t) + \frac{\Delta\ell}{c}\frac{dx}{dt}; \tag{9.37}$$

$$\frac{1}{\omega_r^2}\frac{d^2x}{dt^2} + \frac{q_r}{\omega_r}\frac{dx}{dt} + x = -p; \tag{9.38}$$

$$u = \zeta(1 + x + \gamma)\sqrt{\gamma - p}. \tag{9.39}$$

Here the flow rate is assumed to always enter the resonator. Moreover, the reed is assumed to be not beating, because this would imply that the mouth pressure γ should be negative (more exactly $\gamma + x < -1$). Brass instruments are played by blowing and not by inhaling!

9.3 Behavior of the Two-Equation Model (Regimes, Existence and Stability, Transients) Without Reed Dynamics

9.3.1 Introduction

For a reed instrument such as a clarinet or a saxophone, the playing frequencies and their first harmonics are lower than the first reed resonance frequency, except for the highest notes. This allows using the two-equation model. This approximation is considered to be valid in Sects. 9.3 and 9.4, and its limitations will be discussed in Sect. 9.5. Moreover, we assume that the reed displacement yields a simple correction to the length of the resonator, included in the total length, as well as the radiation length correction. The equation to be solved is Eq. (9.26) with $\Delta\ell = 0$:

$$u = [h * p](t) \quad \text{or} \tag{9.40}$$

$$U(\omega) = Y(\omega)P(\omega). \tag{9.41}$$

With Eq. (9.30), this is the two-equation model. Figure 9.10 shows the nonlinear function (9.30) for several values of the mouth pressure γ. For some approaches, we will further simplify this function. Several versions of the model of resonator can exhibit different aspects of the main phenomena. In some calculations, it will be assumed to be purely cylindrical, for other purposes it will be sufficient that it is quasi-cylindrical; for certain calculations, losses will be taken into account, but not always. Starting from the two-equation model, we first solve a system for the input variables only, then investigate the transfer functions, which allow deducing all quantities in the tube and outside. In the present analysis the control parameters are supposed to be time-independent: this obviously is far form real playing conditions, when the player modify these parameters at every time for expression purposes.

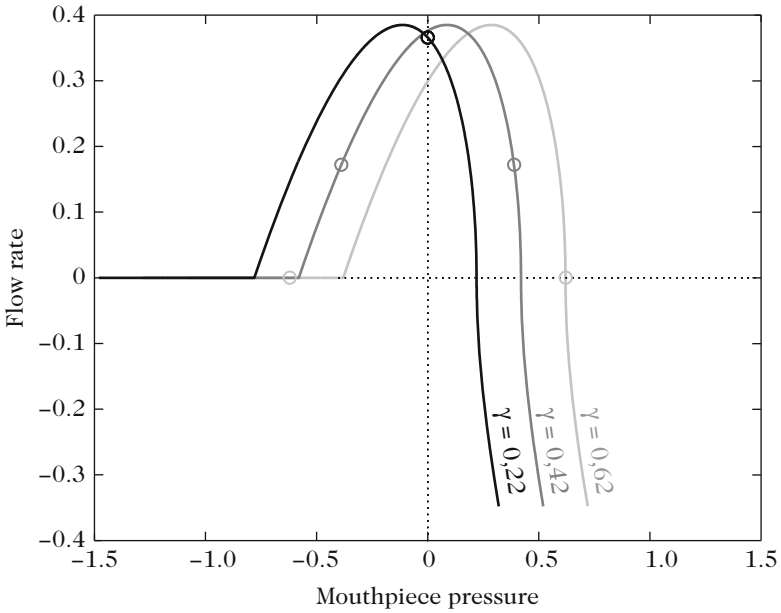

Fig. 9.10 Examples of flow curves [Eq. (9.30)] with respect to the pressure p in the mouthpiece for three values of the static pressure in the mouth. The variables are dimensionless: *from left to right* γ=0.22; 0.42; 0.62. When the pressure p is very low (and negative), the reed closes the mouthpiece. The limit points of the lossless approximation correspond to the two states of the square signal (see Sect. 9.3.3); they are denoted by *circles*. For the static regime, they coincide. The regime is static for $\gamma = 0.22$, while it is oscillating and non-beating for $\gamma = 0.42$, and oscillating and beating for $\gamma = 0.62$, with a zero flow rate. Here the flow rate has been divided by ζ, and the maximum value is $2/(3\sqrt{3})$

9.3.2 Static Regime and "Ab Initio" Method

9.3.2.1 Static Regime

A trivial solution for the system of Eqs. (9.40) and (9.30) can be found for the static regime, when the unknowns do not depend on time. If the pipe input impedance is assumed to be zero at zero frequency, the input pressure is zero as well at every time t, and the flow rate is $F_0 = F(0) = \zeta(1-\gamma)\sqrt{\gamma}$. For this situation, no sound is produced (when the reed closes the mouthpiece, if $\gamma > 1$, $F_0 = 0$). However, even for this regime, a transient exists if the mouthpiece pressure is not zero when the musician blows. Moreover the excitation pressure γ does not change instantaneously from 0 to a finite, stable value. After the transient, if the input pressure converges to 0, the regime is stable. In order to study the stability, one can imagine a deviation from the equilibrium, which yields a variation of the acoustic quantities. The outline of the study is as follows: if we are searching for a periodic steady-state regime, which is called "limit cycle" for dynamical systems (for the static regime the limit

cycle is a fixed point), the problem can be greatly simplified, e.g., by the use of the Fourier series. However, if we are searching for either the shape of a transient or the stability of the regime, the problem is much more complicated. In what follows, we present the most general method for solving the problem, including the transient; the solution is called "ab initio" and depends on known initial conditions.

9.3.2.2 "Ab Initio" General Method of Calculation

The system of Eqs. (9.30) and (9.40) can be solved by starting from the initial conditions. The impulse response $h(t)$ can be used, but its duration is very long, as explained in Chap. 4. It is better to modify the system, choosing as variables the outgoing and incoming pressure waves instead of the pressure and flow rate [99]. Using dimensionless variables, in the case of a perfect cylinder we have

$$p = p^+ + p^- \; ; u = p^+ - p^- \;\text{ with} \tag{9.42}$$

$$p^+ = \frac{1}{2}(p+u) \; ; p^- = \frac{1}{2}(p-u). \tag{9.43}$$

One can relate p^+ and p^- through a nonlinear function G:

$$p^+ = G\left[-p^-\right]. \tag{9.44}$$

It is obtained by a rotation of the function F by 45° (see [78] and Fig. 9.11). Equations (9.40) and (9.41) become, respectively:

$$\begin{aligned} p^-(t) &= \left[r * p^+\right](t) \\ P^-(\omega) &= R(\omega)P^+(\omega), \end{aligned} \tag{9.45}$$

where $R(\omega)$ is the classical reflection coefficient and $r(t)$ is the reflection function defined in Chap. 4. This formulation is possible whatever the shape of the resonator: the reflection function $r(t)$ is in general much shorter than the impulse response $h(t)$, and it can be used also for a numerical computation. Starting from Eqs. (9.43) and (9.45), the following useful equation is obtained

$$p(t) = u(t) + \left[r * (p+u)\right](t) = u(t) + \int_0^t r(t')\left[p(t-t') + u(t-t')\right]dt'. \tag{9.46}$$

The integral corresponds to the past time, which is known, and the use of the nonlinear equation (9.30) leads to the variables $p(t)$ and $u(t)$ when the initial conditions are defined. The integral is limited to 0 and t because the functions $r(t)$, $p(t)$, and $u(t)$ are causal. In general, in order to solve Eq. (9.46), time needs to be discretized.

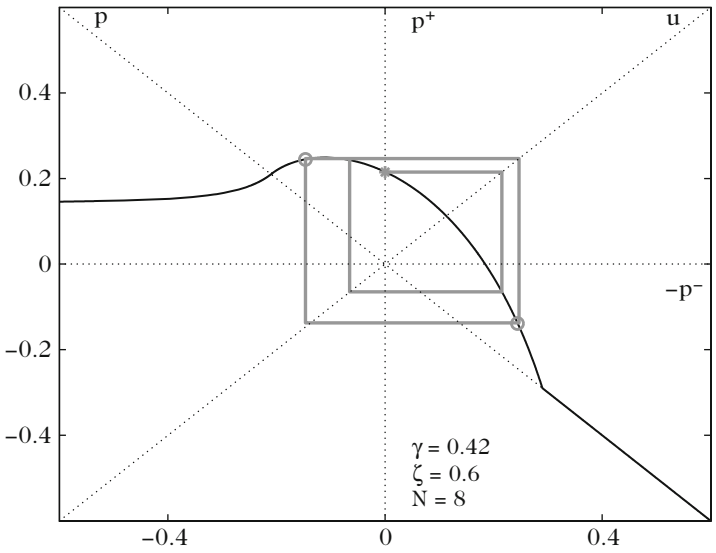

Fig. 9.11 The function G [see Eq. (9.44)] links the outgoing and incoming waves. The figure shows the principle of the iterative calculation of an ab initio solution when no losses are taken into account. *Circles* are the limit points. The values of the parameters are: $\zeta = 0.6$; $\gamma = 0.42$. Signals of pressure and flow rate are shown in Fig. 9.13a

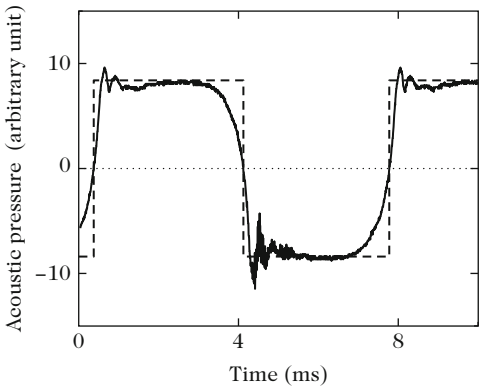

Fig. 9.12 Periodic signal for the internal pressure of a clarinet note, and its approximation by a square signal

The problem can be simplified, considering two types of approximations for the resonator: (1) the lossless approximation, (see Sect. 9.3.3), which leads to square signals for a cylinder (the pressure oscillates between two values, called "states"), and (2) the one-mode approximation for the resonator (Sect. 9.3.4), which leads to a Van der Pol equation. These approximations do not give all useful information: for instance, the spectrum of a square signal is not realistic compared to a real spectrum (Fig. 9.12). Nevertheless, essential conclusions related to sound production are reached.

9.3.3 *Lossless Approximation for a Cylinder: Helmholtz Motion*

9.3.3.1 Ab Initio Solution

For a perfect cylinder, the reflection function has a very short duration, because it corresponds to a simple delay of one round trip in the tube, with a convolution due to the visco-thermal losses and radiation effect. As a first approximation the latter is reduced to a change in sign and losses are ignored:

$$r(t) = -\delta(t - \tau), \tag{9.47}$$

where $\tau = 2\ell/c$ is the time of a round trip in the tube. Therefore:

$$p^-(t) = -p^+(t - \tau). \tag{9.48}$$

Equation (9.46) can now be written in the form:

$$p(t) = u(t) - p(t - \tau) - u(t - \tau). \tag{9.49}$$

If the pressure p^+ deviates from 0 at $t = 0$ and has the value $p^+(0) = p_0^+$, the problem is that of a sequence of unknowns when the time is discretized by intervals τ. Denoting for each variable $p(n\tau) = p_n$, the following system is obtained

$$p_n^- = -p_{n-1}^+; \tag{9.50}$$

$$p_n^+ = G(-p_n^-) = G(p_{n-1}^+). \tag{9.51}$$

This very simple sequence allows determining the solution at each time step $n\tau$. It corresponds to an elementary dynamical system called "iterated map." Each value of the sequence is obtained from the previous one by the iteration of a function. This implies that p^+ suddenly deviates from 0 at a point instant, because we consider a discrete time. This is not realistic, but allows finding basic solutions, with a steady-state regime having two states.[11] This shape is a particular case of the so-called Helmholtz motion, which was discovered experimentally by Helmholtz in the context of the bowed string, and will be discussed in Sect. 9.4.8.3. Notice that during the first round trip, from 0 to τ, the incoming wave is necessarily zero, because no wave comes back faster than the speed of sound. The solution of Eq. (9.51) can be found using a graphical method [78], as shown in Fig. 9.11. Starting from the

[11] In this section we implicitly assume that the mouth pressure suddenly goes from 0 to a non-zero value, then remains constant: $p = p_0^+$ until $\tau > t$. Thus the mouthpiece pressure is constant during the first round trip, and consequently, constant as well during every successive half-periods, resulting in a square signal shape, with two states. Other kind of initial conditions will be investigated further.

value $p_0^- = 0$, the value of p_0^+ corresponding to the imposed control parameters is deduced using Eq. (9.44). The next value $-p_1^- = p_0^+$ is determined, then the nonlinear function is applied, and so on. After a transient, the signal converges to two limit points, opposite in sign, which are the values of the two states of the square signal. Figure 9.13 shows the corresponding signals $p(t)$ and $u(t)$, as well as the result for other values of the parameters: the convergence can occur to the static regime (a unique limit point), or even to other regimes. This is studied in the following sections.

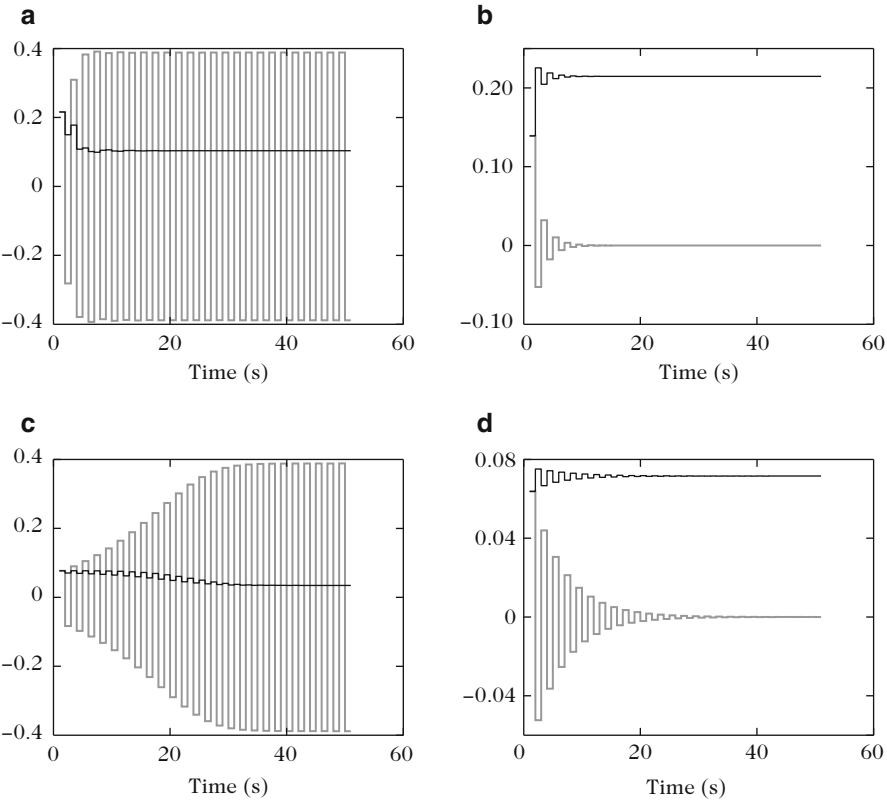

Fig. 9.13 Transients in square signals for two values of the reed parameter and the mouth pressure. In *gray*, the pressure; in *black*, the flow rate. (**a**) $\zeta = 0.6$, $\gamma = 0.42$; (**b**) $\zeta = 0.6$, $\gamma = 0.2$; (**c**) $\zeta = 0.2$, $\gamma = 0.42$; (**d**) $\zeta = 0.2$, $\gamma = 0.2$. The larger is the parameter ζ, the shorter is the transient. When γ is small, the signal converges to the static regime

9.3.3.2 Stability of the Static Regime; Start of the Transient

We continue the analysis of the solutions, and examine the stability of the regimes, the transients and the steady-state regime. Consider first an idealized attack, when the mouth pressure suddenly jumps from zero to a finite value, γ. Starting from the static regime, the pressure $p(t)$ remains small for the first time intervals and it is possible to linearize [Eq. (9.30)]:

$$u_n = F_0 + Ap_n \text{ ; with } F_0 = \zeta(1-\gamma)\sqrt{\gamma},\ \ A = \zeta\frac{3\gamma-1}{2\sqrt{\gamma}}. \tag{9.52}$$

where $F_0 = F(0)$ and $A = dF/dp$ at $p = 0$. Equation (9.49) gives

$$p_n - u_n = -(p_{n-1} + u_{n-1}). \tag{9.53}$$

It is the equation of the resonator, and it yields:

$$p_n = -p_{n-1}\frac{1+A}{1-A}\ ;\ p_n = p_0(-1)^n\left(\frac{1+A}{1-A}\right)^n, \tag{9.54}$$

where $p_0 = p_0^+ = F_0/(1-A)$. Expression (9.54) is obtained from Eq. (9.52) because $p_0^- = 0$.

If the factor raised to the power n is smaller than unity, the pressure p_n tends to 0 when n increases, otherwise it increases exponentially. The two cases correspond to a coefficient A which is negative or positive, respectively. If A is negative, the pressure converges to the static regime, which is stable; otherwise the static regime is unstable, see Fig. 9.13, and the pressure grows exponentially. Maybe the nonlinear terms of the function will produce a saturation to a stable oscillating solution. Given the expression of A, the threshold corresponds to a mouth pressure $\gamma = 1/3$. The larger is the reed parameter ζ (i.e., the wider is the reed opening at rest, or the smaller is the reed stiffness), the faster is the transient. From the perception point of view, this is an important characteristic of the sound.[12] Considering variables with dimensions, it can be shown that this linear problem up to a factor F_0/c stated corresponds for the tube to the calculation of the Green's function with an input admittance boundary condition: $Y = -AS/\rho c$, which is real. If the admittance Y is positive (negative A), the boundary is absorbing and the signal decreases, while if it is negative, the boundary is active and acts as a source, and the oscillation can start. Thus the problem involves a resistive termination, added to dissipation during propagation. The modal expansion shows that the complex natural frequencies are such that their real part, which is the instantaneous frequency during the transient, is higher than the frequency of the steady-state regime, which will be further studied. Thus there is a shift of the instantaneous frequency during the transient [36].

[12]For large values of ζ, and therefore for large pressure p_0, the validity of the expansion to the first order (9.52) is limited to the first values of the pressure, see, e.g., Fig. 9.13a

9.3.3.3 Simplified Model for the Non-beating Reed

For the sake of simplicity, we assume again that the pressure p does not deviate too much from the zero value (and we still assume $Z(0) = 0$; the more general case was investigated in [73]). We assume a non-beating reed which is typically obtained for a mouth pressure γ that is lower than 0.5, (see Sect. 9.4.6). A third order approximation of the flow rate gives (see [60, 124]):

$$u = F(p) \simeq F_0 + Ap + Bp^2 + Cp^3, \text{ where} \tag{9.55}$$

$$F_0 = \zeta(1-\gamma)\sqrt{\gamma},\ \ A = \zeta\frac{3\gamma-1}{2\sqrt{\gamma}},\quad B = -\zeta\frac{3\gamma+1}{8\gamma^{3/2}}\quad C = -\zeta\frac{\gamma+1}{16\gamma^{5/2}}\,. \tag{9.56}$$

In the normal range of variation for the parameter γ, the variation of the coefficient A is mainly due to the numerator, which varies almost linearly, while the parameters B and C only slightly vary. The parameters B and C are negative; this property will be shown to be essential in order for the oscillation to be saturated after the initial grow. All coefficients are proportional to the "reed opening" ζ; we conclude that A varies almost linearly with the mouth pressure; the other parameters are almost constant and negative. The series expansion allows simplifying calculations, but limits the validity of the results. However, the polynomial model can be used for a wide class of physical problems.

9.3.3.4 Existence of the Periodic Steady-State Regime

The steady-state can now be investigated if we assume a periodic behavior. The period is unknown, therefore it will be empirically determined (more straightforward methods will be further explained). It is first assumed to be equal to the round trip duration, $\tau = 2\ell/c$. Thus the variables are equal at times t and $t-\tau$:

$$p(t) = p^+(t) + p^-(t) = p^+(t) - p^+(t-\tau) = 0.$$

With this assumption, there is no non-zero periodic solution. This can be easily interpreted as follows: if a flow rate at the input of the instrument produces a positive pressure in the mouthpiece, this pressure travels to the end, then changes in sign and cannot recover the initial value after a single round trip.[13] It is easy to imagine that

[13]This kind of reasoning requires some care. For instance, why can't the same reasoning be valid for a flute-like instrument (see Chap. 10)? The reason lies in the nature of the source: for a flute, pressure and flow rate have to be inverted at the open end, and the flow-rate wave is reflected without change in sign at the end: thus the period $2\ell/c$ is possible. On the contrary a closed flute is similar to a clarinet.

with two round trips, a periodic regime is possible: if we search for a period equal to 2τ, the variables are equal at times $t+\tau$ and $t-\tau$, thus:

$$p(t+\tau) = p^+(t+\tau) - p^+(t)\ ; p(t) = p^+(t) - p^+(t-\tau). \quad (9.57)$$

$$\text{Therefore} \quad p(t) = -p(t+\tau). \quad (9.58)$$

A two-state signal is obtained, and the two values are opposite in sign. Thus the period 2τ is a solution. In order to find the two values, it is noticed that the flow rate is periodic with the period τ, because:

$$u(t+\tau) = p^+(t+\tau) + p^+(t) = p^+(t-\tau) + p^+(t) = u(t). \quad (9.59)$$

In steady-state regime, the flow rate is constant, as shown in Fig. 9.13. The limit points $\pm p_\infty$ are solutions of:

$$F(p_\infty) = F(-p_\infty), \text{ thus } A + Cp_\infty^2 = 0, \text{ and:} \quad (9.60)$$

$$p_\infty = \pm\sqrt{-\frac{A}{C}}. \quad (9.61)$$

If C is negative, this oscillating solution exists for positive A, when the static regime becomes unstable. If C were positive (it is not the case of the present model), solutions would exist when A is negative, i.e., when the static regime is stable. It is possible to theoretically show that in general the oscillating regime would be unstable, using either a perturbation method [71] or the theory of the topological degree [96]. A proof will be provided for our case in the following section. Concerning the square shape of the pressure signal and the constant value of the flow rate, it is possible to link these results to a reasoning in terms of input impedance. For a lossless cylindrical resonator open at the end, the input impedance has infinite maxima for frequencies which are odd multiple of the frequency $c/4\ell$, which corresponds to the period 2τ, and zero minima for frequencies which are even harmonics of this frequency. Consequently the pressure involves odd harmonics only, while the flow rate involves even harmonics only. Moreover the studied signals are constant during one half-period (see Sect. 9.3.3.1). Therefore during the steady-state regime, the flow rate can involve odd harmonics only, and a continuous component; finally it is constant, with neither odd nor even harmonics! These calculations can be easily generalized to the nonlinear function (9.30) [73, 76]; the two values of the pressure remain opposite, and the flow rate is constant. Figure 9.10 shows the limit(s) point(s) for three values of the pressure γ. The result is written as:

$$p_\infty = \pm\left[(3\gamma-1)(1-\gamma)\right]^{1/2} \text{ if } \gamma < 1/2;$$
$$p_\infty = \pm\gamma \text{ if } \gamma > 1/2. \quad (9.62)$$

9.3.3.5 Stability of the Periodic Oscillation Regime

How can be investigated the stability of the periodic oscillation regime? Similarly to what we did for the static regime [see Eq. (9.54)], the function F is linearized around the limit points. This time there are two limit points:

$$u_n = F(p_\infty) + (p_n - p_\infty)F'^{+}$$
$$u_{n+1} = F(-p_\infty) + (p_{n+1} + p_\infty)F'^{-},$$

where $F'^{\pm}$ is the derivative of F at $\pm p_\infty$. Using the equation of the resonator (9.53), we deduce

$$(1 - F'^{-})(p_{n+1} + p_\infty) = -(p_n - p_\infty)(1 + F'^{+}), \text{ and}$$
$$(1 - F'^{+})(p_{n+2} - p_\infty) = -(p_{n+1} + p_\infty)(1 + F'^{-}),$$

then

$$(p_{n+2} - p_\infty) = (p_n - p_\infty)\frac{(1 + F'^{-})(1 + F'^{+})}{(1 - F'^{-})(1 - F'^{+})}. \tag{9.63}$$

Stability is ensured if the factor multiplying $(p_n - p_\infty)$ has an absolute value smaller than unity. Squaring this factor, we obtain

$$(F'^{+} + F'^{-})(1 + F'^{+}F'^{-}) < 0. \tag{9.64}$$

And using Eq. (9.61):

$$A\left[1 + 4A(B^2/C + A)\right] > 0. \tag{9.65}$$

When A is small, *the stability condition* $A > 0$ *is opposite to that of the static regime*, QED. If A increases, considering the first order term in A in the bracket, it can be seen that:

– either C is negative, and the sign of the bracket can change for a non-zero, positive value of A. Beyond this threshold, it can be shown that a periodic regime exists with a double period. This kind of regimes is discussed hereafter. The most important result is that the *bifurcation* is *direct*. As a consequence the clarinet can play pianissimo. We already considered bifurcations for free oscillations (see Sect. 8.5 of Chap. 8); "direct"[14] means that after a threshold, $A = 0$, there

[14]In the literature the adjectives "normal" or "overcritical" or "supercritical" can be found instead of "direct." The contrary is "inverse," or "undercritical," and implies a discontinuity between two regimes, with a hysteresis, as it will be seen hereafter.

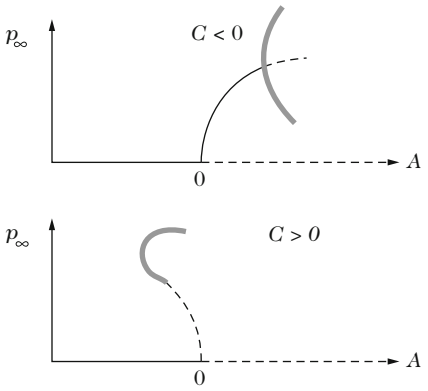

Fig. 9.14 Schematic bifurcation diagram in A $=$ 0 for the two cases positive C (inverse bifurcation) or negative C (direct bifurcation). *Solid, black line*: limit values of stable regimes, either static ($p_\infty = 0$), or oscillating (the positive value only is indicated). *Dotted, black line*: unstable regimes. Beyond the cases of calculation that are presented by the inequality (9.65), the hypotheses are as follows: for $C > O$, the unstable oscillation regime becomes stable, and for $C < 0$, there is a new bifurcation to a stable regime with four values (*lower octave*)

is continuity from a stable regime (here the static one) to another (here the oscillating one), when the control parameter (here A, or more precisely the mouth pressure) increases.

– or C is positive (this is not the case of the present model), and the solution of Eq. (9.61) exists for negative A only. It is unstable for small values of A. For a non-zero, negative value of A, it is possible to find a new periodic, stable regime, and the bifurcation is said "inverse." Figure 9.14 shows the two cases. No investigation concerning phenomena far from $A = 0$ is presented yet.

9.3.3.6 Period Doubling and Chaos: Discussion

What happens when the condition (9.65) is not fulfilled? It is possible to investigate the case when the bracket in Eq. (9.65) is negative: (1) either by computing the solution ab initio (*stable* regimes are obtained, but it is not sure that they are *all possible regimes*, because they depend on initial conditions, which are certainly not unique); (2) or by calculating the periodic steady-state regimes with a pre-supposed frequency, as above explained (but it is not possible to know whether *these regimes are stable*!). It is possible to try a period double, 4τ, and to confirm that the threshold of existence for the solutions is $A\left[1 + 4A(B^2/C + A)\right] = 0$, but the calculation is tedious. For the model (9.30), without series expansion around the static solution, the ab initio study, which corresponds to the graphical solution of Fig. 9.11, was done in [73, 105]. Frequency divisions by 2, 4, 6, 12,... are obtained, and the thresholds appearing for the mouth pressure (γ) depend of the reed parameter ζ. The weaker is the reed (large ζ), the earlier these regimes appear. When γ continues

to raise, the solution comes back to the "normal" frequency for $\gamma = 1/2$. This will be studied when looking at the beating reed behavior. For a fixed value of γ, it was possible to obtain with the same model, a complete scheme of period doubling toward a chaotic signal [77]. This scheme is called "subharmonic cascade," and was already studied for the case of a clarinet [20, 70, 78, 104, 105]. The chaos is a non-periodic regime (we could say with an infinite period), and it is called "deterministic chaos" because it is solution of a deterministic equation, while it is extremely sensitive to the initial conditions and for this reason it is unpredictable. This concept was presented in Chap. 8.

The reader can be surprised by this result of a frequency division, because this phenomenon is not common, while the frequency multiplication by a factor 3 is. This issue is treated hereafter. Actually, if realistic losses are taken into account in the model, the period doubling can disappear [35]. However, period doubling can be encountered for other reed instruments, such as the crumhorn or the bassoon [55]: the notes of a contrabassoon can be played with a bassoon.[15]

9.3.3.7 Other Types of Regimes: Twelfths

This section investigates regimes with triple frequency, also known as twelfth regimes. Equations (9.50) and (9.51) do not make any assumption concerning the variation of the signals during the time $\tau = 2\ell/c$. If the frequency is an odd multiple of $f_1 = c/4\ell$, which corresponds to the period 2τ (see the previous paragraphs), it is easy to find Helmholtz regimes (two-state signals) which satisfy Eqs. (9.58)–(9.61). It is sufficient to choose different initial conditions in order to initiate the triple frequency: we impose a non-zero value to the outgoing wave p^+ not only at $t = 0$, but also at $t = 2\tau/3$, and a zero-value at $t = \tau/3$. Therefore this regime has the same threshold than the "fundamental" regime. When it is reached it is not more difficult to sustain than the fundamental regime. A practical solution for imposing these initial conditions is easy: a small "register hole," located at the third of the length is opened, and allows emitting the twelfth. If we ignore the losses, after initialization, when closing this hole, the twelfth regime should remain stable.[16]

[15] In practice the frequency division is possible for very narrow ranges of parameters (γ or ζ), especially when approaching the chaotic regime. Consequently it is easy for an instrument maker to avoid these phenomena.

[16] In practice this is not always possible when playing a clarinet, because when closing the register hole, it is also possible to retrieve the fundamental regime. The reason is not simple. We will see that when losses are taken into account, the threshold pressure for the triple frequency is higher than that for f_1. This is not a sufficient reason, because beyond the threshold for the triple frequency, both regimes should be reachable by choosing the appropriate initial conditions. Notice that for other instruments, such as a flute or a bassoon, it is often easy to play the higher registers even without the opening of a register hole. Moreover baroque oboes have no register holes for overblowing.

9.3.4 One-Mode Approximation

The Helmholtz motion is an interesting approximation for the study of the transients, the regime stability, their frequency and their amplitude, but do not give insights into the real shape of the signal, i.e., of the spectrum: fortunately the signal is not perfectly square. In the next section (Sect. 9.4) the steady-state regime will be examined, taking losses into account. But beforehand it is interesting to make a study similar to the previous one for another approximation of the resonator, when this response is reduced to that of a single mode. This is also a rough approximation of the resonator, but it allows considering realistic losses and their frequency dependence.[17] In contrast, the previous model, "lossless model," took into account an infinity of modes with harmonically related frequencies.

9.3.4.1 Differential Equation for the Mouthpiece Pressure

In the second part of the book, the modal expansion of the dimensionless input impedance was obtained [see in particular Eq. (7.19)]:

$$Z(\omega) = j\omega \sum_n \frac{F_n}{\omega_n^2 - \omega^2 + j\omega\omega_n/Q_n}, \tag{9.66}$$

where ω_n is the frequency of the nth resonance, Q_n is the quality factor, and F_n the modal factor. The value of the (real) maximum of the impedance modulus is $Z_{Mn} = F_n Q_n/\omega_n$.[18] For a cylinder $F_n = 2c/\ell$ and $Z_{Mn} = 2cQ_n/(\ell\omega_n) = k_n/2\alpha$ (in dimensionless quantities) when radiation losses are ignored and α is given by Eq. (5.147). A great simplification is obtained by truncating the series after the first mode. For a cylinder, using a first order approximation of the losses, this is allowable near the resonance ω_1: starting from expression $Z(\omega) = j\tan(k - j\alpha)\ell$, the following equation is exact: $Z(\omega_1) = (\alpha\ell)^{-1} = 2Q_1/k_1\ell$ (for the study of a resonance peak, see Chap. 2). However, far from the resonances, the truncation strongly modifies the predicted response of the resonator. For the first register of the clarinet, the truncation is not as consequential as for conical instruments, because the second resonance frequency is far from the first one, and the first peak is dominant. Nevertheless one should not expect correct results for the spectrum.

[17] Meynial [81] studied a "monochromatic" resonator, by considering a tube with axial chimney, so that all the resonances, but the first, are strongly attenuated. Also the frequencies of the higher order modes are not multiple of the frequency of the first mode. The present model is close to this experimental realization, which produced a spectrum dominated by a single frequency, even at higher levels.

[18] We used Eq. (5.183) in dimensionless quantities, simplifying it by including the radiation length correction into the length ℓ.

Using Eq. (9.66), and truncating it to the first mode, we obtain

$$(\omega_1^2 - \omega^2 + j\omega\omega_1/Q_1)P(\omega) = j\omega F_1 U(\omega).$$

Its inverse Fourier Transform is written as:

$$\frac{d^2}{dt^2}p(t) + \frac{\omega_1}{Q_1}\frac{d}{dt}p(t) + \omega_1^2 p(t) = F_1\frac{d}{dt}u(t), \tag{9.67}$$

or, after the attack, if Eq. (9.55) is used

$$\frac{d^2}{dt^2}p(t) + F_1\frac{d}{dt}\left[(Y_{m1} - A)p(t) - Bp^2(t) - Cp^3(t)\right] + \omega_1^2 p(t) = 0. \tag{9.68}$$

$Y_{m1} = 1/Z_{M1}$ is the value of the (real) minimum of the admittance. This equation is a Van der Pol equation. It is now possible to consider the successive steps of the study of the Helmholtz motion (see Sect. 9.3.3). For the transient, approximate solutions of the Van der Pol equation can be found in the literature (see, e.g., [36]), but are not simple. We limit this section to the stability of the static regime, the early transient, and the existence of the periodic regime.

The solution of Eq. (9.68) is not sinusoidal, because of the nonlinear terms. The modal method can be generalized to an arbitrary number of modes in order to solve the exact problem; a system of nonlinear, ordinary differential equations has to be solved, and numerical methods are available for this purpose. This method is an alternative solution to the ab initio method [9, 36].

9.3.4.2 Stability of the Static Regime, Early Transient

A trivial solution is the static regime $p(t) = 0$. In order to study its stability, we linearize Eq. (9.68), by ignoring the terms with B and C. This equation becomes the equation of a linear oscillator with one degree of freedom. The damping can be negative, if A is larger than Y_{m1}. For A smaller than Y_{m1}, the oscillation is exponentially damped, and the oscillator returns to the static regime. On the contrary, the oscillation can grow exponentially, and the nonlinear terms will allow the saturation of the amplitude. This study of stability is similar to the one that leads to Eq. (9.54). The instability threshold of the static regime is now given by: $A = Y_{m1}$, instead of $A = 0$. In order to produce a sound, it is necessary to blow sufficiently hard to compensating for the losses. Notice that radiation losses have been neglected compared to the visco-thermal losses: but if they are large, the threshold is high. Paradoxically the radiation of a self-sustained oscillation instrument should not to be too efficient in order for the sound to exist (see also Chap. 7, Sect. 7.5.1).

- In the case of a cylindrical tube, by using the value of A given by Eq. (9.56), a simple result can be obtained. We simply consider that the perturbation due to

the losses is small, and replace γ by $1/3$ in the denominator of A. This yields the pressure threshold:

$$\gamma_{\text{th}} = \frac{1}{3} + \frac{\alpha\ell}{\zeta}\frac{2}{3\sqrt{3}}. \tag{9.69}$$

A typical order of magnitude for this threshold is 0.38. It is possible to derive the solution of the linearized equation (9.67), by assuming[19] $p(t) = 0$ at $t \leq 0$, and $u(t) = F_0 H(t) + Ap(t)$:

$$p(t) = \frac{4}{\pi} F_0 H(t) e^{-\alpha_o t} \sin \omega_1 t \text{ where } \alpha_0 = (Y_{m1} - A)c/\ell. \tag{9.70}$$

in the classical hypothesis of an oscillator which is either weakly damped of weakly excited, satisfying $|Y_{m1} - A| << \omega_1 \ell/c$ (see Chap. 2). If losses are ignored, this solution can be compared to that in square signals (9.54), and the two agree in both amplitude and phase.

- For a tube with an arbitrary profile, two observations can be made when looking at Eq. (9.68):
- The general expression of the modal expansion obtained in Chap. 7 [Eq. (7.38)] shows that the modal factor F_1 satisfies

$$F_1 = cS(0)\frac{\Phi_1^2(0)}{\Lambda_1} \text{ where } \Lambda_1 = \int_0^\ell S(x)\Phi_1^2(x)dx.$$

It depends on the geometry only, and is independent of losses. As a consequence, for a non-cylindrical instrument, it can strongly vary with frequency. Beyond the threshold, the amplification factor is the product of the modal factor by A [see Eq. (9.68)], and does not depend on losses. On the contrary, for free oscillations, the duration of the transient is determined by the quality factor (see Chap. 2). Similarly it is possible to show that the extinction transient when the mouth pressure decreases is not primarily linked to losses.

- The relevant quantity for the determination of the threshold is the minimum Y_{m1}, which is inversely proportional to the quality factor, but is also proportional to the modal factor. Consequently if the geometry imposes a very large impedance, it is possible to diminish the minimum Y_{m1} and therefore to lower the threshold without reduction of losses, by using the reactive effects due to reflections at cross-section changes. Thus the threshold is not only linked to losses, but mainly to the height of the impedance peak. This explains why the mouthpiece of brass instruments makes the attacks easier without reducing losses (this sentence is a

[19] The solution satisfies $p(t) = p(t)H(t)$, and the flow rate $u = H(t)\,[F_0 + Ap(t)]$ hence $u = F_0 H(t) + Ap(t)$. Thus it exists a source term in Eq. (9.68), which is equal to $2c\ell^{-1}F_0\delta(t)$. The solution is proportional to the Green's function of this equation, which was studied in Chap. 2, see Eq. (2.14).

simplified explanation, because it ignores the reed dynamic, essential for these instruments). These remarks fully justifies the importance that Benade [10] gave to the height of the impedance peaks (see Chap. 7 of the present book for a detailed study of the role of the brass instrument mouthpiece).

9.3.4.3 Negative Resistance and Energy

The term $-A$ in Eq. (9.68) can be interpreted as the energy source of the self-oscillating system: it corresponds to a negative resistance when sound is produced, i.e., when its absolute value is large enough to overcome the positive resistance of term Y_{m1} (A is the first derivative of the nonlinear function du/dp near $p = 0$). Figure 9.10 shows that for values of γ larger than $1/3$, the slope of the curve is negative and an oscillation regime with two states exists, while for $\gamma = 0.22$, the slope is negative.[20]

Extending this idea to the nonlinear operation range, we can rewrite the time derivative term of Eq. (9.68), up to the factor $\omega_1 Z_{M1}/Q_1$:

$$\frac{dp}{dt}\left[Y_{m1} - A - 2Bp - 3Cp^2\right].$$

Thus the source resistance is $R = -(A + 2Bp + 3Cp^2)$. Its instantaneous value oscillates because of the term Bp, but its absolute value diminishes with increasing p because the coefficient C is negative. Intuitively we understand that the oscillation does not continue to grow exponentially, but saturates and converges to a stable amplitude in the steady-state regime.

9.3.4.4 Existence of the Periodic Regime

In order to obtain an analytical expression for the periodic regime, we can seek an approximated solution of the nonlinear equation. To assume that the solution is sinusoidal is not rigorous, but often gives very good results. This is the simplest application of the harmonic balance technique (see the next paragraph). The result is

$$p(t) = 2\sqrt{\frac{1}{3}\frac{Y_{m1} - A}{C}}\cos(\omega_1 t + \varphi). \tag{9.71}$$

[20] The previous comment comes from the study of the function $F(p)$, where p_m (γ) is a parameter. Another way of thinking [50] considers the function $F(\Delta p)$ (see Fig. 9.9), with the following property: $(du/dp)_{p=0} = -(du/d\Delta p)_{\Delta p = p_m}$. This curve demonstrates that the oscillation threshold is obtained at the maximum of the curve, and that the increasing and decreasing parts of the curve correspond to a stable and an unstable static regime, respectively.

The phase φ of the oscillating factor is unimportant in a periodic, steady-state regime. The existence of this solution is ensured under the same condition as the instability of the static regime, $A > Y_{m1}$, because the coefficient C is negative. This confirms the direct behavior of the bifurcation. This solution can be compared to that of the lossless model, when $Y_{m1} = 0$. Starting from the square signal solution (9.61), the amplitude of the first harmonic of a square signal is calculated and the same result is obtained, up to the factor $2\sqrt{3}/\pi$. This explanation will be detailed further.

Let us summarize the present section. We compared the robustness of two approximated models: the lossless resonator and the one-mode resonator. This was easy for several features of the behavior of reed instruments, but the calculation of the stability of the oscillation regime leads to an intricate computation for the latter model [113] and is not presented here.

9.4 Away from the Reed Resonance (Two-Equation Model): Steady-State Regimes

9.4.1 Principle of the Harmonic Balance Method: First Harmonic Approximation

In order to study the spectra, we need to take into account the losses, which depend on frequency. The ab initio method (see Sect. 9.3.2.2) allows solving the problem numerically. Nevertheless another method, called "harmonic balance," is possible, at least for the steady-state regime. It was already presented in Chap. 8. It can be used numerically, but very useful analytical approximations can also be obtained. It is based upon the periodicity of the signal, which implies that it can be written in the form of a Fourier series:

$$p(t) = \sum_{n=-\infty}^{n=+\infty} P_n e^{jn\omega_1 t}, \tag{9.72}$$

where $P_{-n} = P_n^*$ since the signal is real, and ω_1 is the fundamental frequency, which is a priori unknown. P_1 can be chosen for instance as a positive, real quantity, because the phase of the signal has no significance in the steady-state regime. As a matter of fact, the relative phases are to be determined for the harmonics only (a periodic signal is invariant with respect to a temporal translation). The d.c. component P_0 is real as well. With this choice, the square signal $\pm p_\infty$ has the following spectrum:

$$P_{2\nu+1} = \frac{2(-1)^\nu p_\infty}{(2\nu+1)\pi}; \; P_{2\nu} = 0. \tag{9.73}$$

The even harmonics are zero, while the phase of the odd harmonics is alternately 0 and π. For the Helmholtz motion, the spectrum of the mouthpiece pressure is that of a square signal, and therefore it decreases with increasing frequency. When losses are taken into account, this spectrum decreases as well, but more rapidly, especially near the oscillation threshold. This allows seeking simple approximations. The simplest one is the so-called first harmonic approximation (also called in textbooks on dynamical systems the "describing function" method), for which the series (9.72) is truncated to $n = \pm 1$. Using this, we can investigate the existence of solutions, their frequency and their amplitude, by solving Eqs. (9.41) and (9.55):

$$u = F_0 + Ap + Bp^2 + Cp^3; \tag{9.74}$$

$$U(\omega) = Y(\omega)P(\omega). \tag{9.75}$$

The reed is assumed not to beat. The flow rate is also expanded in harmonics, and their amplitudes are Y_nP_n, where the Y_n are the values of the input admittance $Y(\omega)$ for the frequencies which are multiple of the frequency ω_1 (remember that this frequency is unknown). In Eq. (9.55), we keep the terms of frequency ω_1 only. The term of order 0 (a constant) and the term of order 2 of the polynomial cannot involve terms with frequency ω_1. Notice that the calculation of the powers in the polynomial is much easier with complex exponential than with trigonometric functions. If we "balance" the terms of frequency ω_1 on the left and the right of the nonlinear equation, we get

$$Y_1P_1 = AP_1 + 3CP_1^2P_1^* = AP_1 + 3CP_1^3. \tag{9.76}$$

The balance for the frequency $-\omega_1$ would not give any supplementary information, because we would obtain the complex conjugate equation. A trivial solution is $P_1 = 0$; it is the static regime. The other solution is

$$P_1^2 = \frac{1}{3}\frac{Y_1 - A}{C}. \tag{9.77}$$

- P_1 is chosen as a real quantity, therefore the imaginary part of this equation yields: $\Im m(Y_1) = 0$. Solutions exist if Y_1 is real, therefore the oscillation frequency can be calculated from $\Im m(Y_1) = 0$. As a first approximation (if the influence of visco-thermal effects on the sound speed is ignored), the first possible playing frequency for an open cylinder is $f_1 = c/4\ell$. A result of great musical importance is that the playing frequency does not depend on the amplitude. If higher harmonics are taken into account, this result is marginally modified, as explained further.[21]

[21]The oscillation condition is not given by the maximum of the input impedance modulus, but by the zero value of the imaginary part of the admittance. In Chap. 2 the difference between these two conditions was shown to be very small.

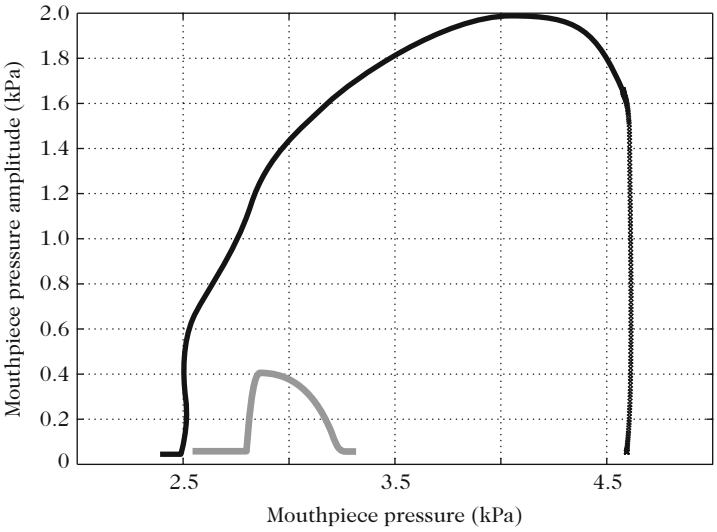

Fig. 9.15 Experimental bifurcation scheme (with artificial mouth) for a clarinet note, for two values of the reed parameter ζ. The ordinate is the root mean square (RMS) pressure. The bifurcation at the oscillation threshold is direct for both curves, while at the extinction threshold, it is inverse for the *black curve* (normal reed opening ζ), and direct for the *gray curve* (small ζ): beyond a certain value, which is called the "closure" pressure, there is no more oscillation, because the reed eventually closes the mouthpiece. This will be explained in Sect. 9.4.6, when studying the beating reed

- The real part of Eq. (9.77) gives the solution for the other unknown of the problem, i.e., the amplitude of the first harmonic. Replacing Y_1 by Y_{m1}, which is the real part of Y_1 at frequency ω_1, we found the result (9.71). Because C is negative, the solution exists only if A is larger than Y_{m1}. It is the same threshold as the instability threshold of the static regime. A diagram showing the measured amplitude for a clarinet-like instrument can be seen in Fig. 9.15: for rather weak amplitudes, the curve is similar to a square root curve. Notice that it is very delicate to measure small amplitudes near the threshold. At moderately high amplitudes, the reed begins to beat: this will be investigated in Sect. 9.4.6.

If we consider the case $Y_{m1} = 0$, we can compare the amplitude with that of a square signal [Eq. (9.61)]. The two values differ slightly. Indeed if the Eqs. (9.61) and (9.73) are combined, the following value is obtained for the Helmholtz motion: $P_1^2 = -\frac{A}{C}\frac{4}{\pi^2}$. The ratio between these two values is $2\sqrt{3}/\pi$, or 1.102 (i.e., less than 1 dB). The error is due to the truncation of the series of harmonics, and can be accepted for most applications.[22]

[22]This feature is related to the modulus of the input impedance for the different harmonics: for a cylinder, when losses are taken into account, the input impedance for the harmonic 2 is very small, and for the harmonic 3, it is approximately $\sqrt{3}$ times smaller than that of the fundamental.

9.4.2 Characteristic Equation and Instability Threshold of the Static Regime

For square signals, the instability threshold of the static regime and the threshold of the oscillation regime (stable or not) were distinguished. With the harmonic balance method, or more precisely with Eq. (9.77), the existence threshold of the oscillation regime was found. It is characterized by specific values of the frequency and of the excitation parameter A. More generally several oscillating solutions can be found: they cancel the imaginary part of $Y_1(\omega)$. For small amplitudes, Eq. (9.76) implies $Y_1 P_1 = A P_1$, thus:

$$Y(\omega) = A \text{ or } AZ(\omega) = 1. \tag{9.78}$$

This is the so-called characteristic equation, which is the equation of the linearized system. It is obtained when the nonlinear equation is linearized around the static solution. The solution of this equation is sinusoidal (but for degenerate cases, it can be a square signal [60]). This justifies the writing without the subscript 1, because there is no ambiguity. In the case of a one-mode truncation, the stability of the static regime (see Sect. 9.3.4.2) was deduced. The solution of the equation was sought in the form of a complex exponential (9.70), i.e., an exponentially increasing or decreasing sinusoid, according to the parameters of the problem. When the exponent has a zero real part, the (in)stability threshold of the static regime is found, but the existence threshold of the oscillation regime cannot be found by using the linearized equation. How is it possible to generalize this search for the instability threshold to Eq. (9.78)? We have to search for all (complex) zeros of the equation and to see if they correspond to growing exponentials or not. If all exponentials are decreasing, then the static regime is stable; if any exponential is growing, the static regime is unstable, and the solution of the nonlinear problem can be expected to be oscillating.[23] When a parameter varies and one decreasing solution switches to

This is very different for other types of instruments, such as conical instruments. This reasoning implies that losses are accounted for, because when losses are ignored, the impedance ratios are unknown (the impedance is infinite for the maxima and zero for the minima): the system is called "degenerate." In practice we have to consider losses, and make them tend to zero [60].

[23] For a more general system, the Nyquist criterion can be used: it is based on the location of the poles of the characteristic equation in the complex plane. Using the terminology of the control system theory [85], Eqs. (9.74) and (9.75) are typical of a (nonlinear) feedback loop system, functioning in free oscillations. For most industrial applications the aim is to push further the instability ranges of the feedback system, on the contrary the instrument maker and the player attempt to make the system unstable in order to produce self-sustained oscillations (see, e.g., [11, 41, 48]). The analysis of linear stability starts with the linearization of the nonlinear element of the feedback loop system (for us $u = F_0 + Ap$). In the linearized system this element is replaced by a quantity whose dimension is an admittance (the coefficient A in our equations, which is the derivative of the nonlinear function with respect to the acoustic pressure, when the latter is calculated at the operating point, i.e., at the equilibrium position of the system). Then the instability threshold is calculated by using an equation that is formally identical to Eq. (9.78).

an increasing solution, we get the instability threshold of the static regime. Exactly at the threshold, the exponent of the exponential is purely imaginary, because its real part vanishes. Therefore solving the characteristic equation for real frequencies provides the thresholds. As an example, using Eq. (9.68), it can be written as: $\omega_1^2 - \omega^2 + j\omega\omega_1 Z_{M1} Q_1^{-1}(Y_{m1} - A) = 0$. Because ω is real, this equation yields $\omega = \omega_1$, and $Y_{m1} = A$, i.e., the frequency and excitation pressure thresholds.

- Another, equivalent, formulation is often used for the study of dynamical system. Let us suppose that it is possible to write the equations of the linearized problem in the following form:

$$\frac{d}{dt}\mathbf{V} = \mathbb{M}\mathbf{V},$$

where $\mathbf{V}$ is a vector involving the physical variables of the problem, and $\mathbb{M}$ is a matrix involving the parameters of the problem.[24]

If all eigenvalues of the matrix $\mathbb{M}$ have a negative real part, the static regime is stable. If the real part of one of the eigenvalues becomes positive, this regime becomes unstable (notice that because $\mathbb{M}$ is real, the eigenvalue pairs are complex conjugate). The threshold value is given by the zero of the real part of an eigenvalue pair. This technique can be easily applied to Eq. (9.68), confirming the conclusions of Sect. 3.4.2. by writing the following relationship:

$$\mathbf{V} = \begin{pmatrix} p \\ dp/dt \end{pmatrix} \text{ and } \mathbb{M} = \begin{pmatrix} 0 & 1 \\ -\omega_1^2 & F_1(A - Y_{m1}) \end{pmatrix}.$$

9.4.3 *The Harmonic Balance Method: An Overview*

If we wish to go beyond the first harmonic approximation in order to solve Eqs. (9.55) and (9.41), we can truncate the series (9.72) to N harmonics, and increase N to infinity. When we fill the truncated series in Eq. (9.55), we obtain a set of equations corresponding to the first N harmonics. We obtain a system of nonlinear complex equations with N complex unknowns, P_n. Moreover a real equation has to be added for the d.c. component, with the real unknown P_0. Therefore the system of $2N + 1$ nonlinear real equations has $2N + 1$ real unknowns. The "balance" seems to be satisfactory. However, there is a supplementary unknown, the playing frequency,

[24] More generally, it can be written before the linearization:

$$\frac{d}{dt}\mathbf{V} = \mathbf{F}(\mathbf{V})$$

where the components of the vector function $\mathbf{F}(\mathbf{V})$ are nonlinear functions of the components of the vector $\mathbf{V}$. The matrix $\mathbb{M}$, already encountered in Chap. 8, is called "jacobian" of the function $\mathbf{F}$.

and it is solved by the possibility to impose a real P_1! In order to solve the problem numerically, the continuation method can be used: starting from a known solution, the parameters are slightly changed, and the equations linearized around the known solution. More specifically: Eq. (9.55) is treated in the time domain, while Eq. (9.41) is treated in the frequency domain, and the passage to one domain to the other is done alternately by summation and by Fourier Transform. In principle this method allows following all regimes when the parameters change, e.g., the mouth pressure γ, whatever stability of the regime is [46, 57, 98]. A free software, Harmbal, permits solving this type of problems, including the reed modes [45].

We will now investigate new simplifications, beyond the first harmonic approximation, yielding analytical results.

9.4.4 The Variable Truncation Method, and Its Application to Clarinet-Like Instruments

9.4.4.1 Odd Harmonics

Because the clarinet profile is mainly cylindrical, the even harmonics in the mouthpiece can be assumed to be much weaker than the odd ones. Thus it is interesting to split the pressure and the flow rate into a part involving even harmonics only (subscript s) and a part involving odd harmonics only (subscript a). The functions with subscript s satisfy: $f_s(t + T/4) = f_s(t - T/4)$ at every t, where $T = 2\pi/\omega_1$ is the period. The functions with subscript a satisfy: $f_a(t + T/4) = -f_a(t - T/4)$. For the product of two functions of one or another type, the following rules are applied: $f_s g_s$ and $f_a g_a$ are of type s, while $f_s g_a$ is of type a.[25] For the pressure, it can be assumed that $p_s << p_a$. Using a perturbation method, the calculation starts by ignoring the part p_s; the nonlinear equation is split into two equations:

$$u_s = F_0 + Bp_a^2; \tag{9.79}$$

$$u_a = Ap_a + Cp_a^3. \tag{9.80}$$

The second equation involves odd harmonics only, and is solved first, thanks to Eq. (9.75). The first equation gives the even harmonics of the flow rate from the odd harmonics of the pressure. Using Eq. (9.75), we finally deduce the even harmonics of the pressure, as explained hereafter. Here we solve Eq. (9.80) by truncating it to two harmonics, the first and the third. Bringing the series with terms -3, -1, 1, and 3 and equating the terms of frequency ω_1 (which is unknown) and $3\omega_1$, we obtain the equations:

[25] These rules are identical to the rules for even and odd functions. Notwithstanding the two types are not even and odd functions, in contradiction with what is written in [76]. It is possible to show that this could be true in the following case only: when the even harmonics have real coefficients P_n, and the odd harmonics have imaginary coefficients P_n. This can be checked by the reader.

$$\frac{Y_1 - A}{C} P_1 = 3(P_1^2 P_1^* + P_1^{*2} P_3 + 2P_3 P_3^* P_1); \tag{9.81}$$

$$\frac{Y_3 - A}{C} P_3 = P_1^3 + 3(P_3^2 P_3^* + 2P_1 P_1^* P_3). \tag{9.82}$$

Rejecting the solution $P_1 = 0$,[26] using the assumption that P_1 is real, Eq. (9.81) can be rewritten as:

$$\frac{Y_1 - A}{C} = 3P_1^2(1 + P_3/P_1 + 2\,|P_3/P_1|^2). \tag{9.83}$$

- Let us seek a solution to the equations, supposing that we are close to the threshold defined by Eq. (9.77). It is consistent to consider that P_1 is small, and following Eq. (9.82), P_3 is of order 3 in P_1. This solution is called "small oscillation solution." The harmonic n can be shown to be of order n in P_1. This power law for the harmonics near the threshold is very general (see [2]) and it is often called "Worman theorem" in musical acoustics (see [60, 94, 124]).[27]
- Another approximation is consistent with the previous one, but it is valid in a much wider range of pressures. It is called "Variable truncation method": the first harmonic is assumed not to be influenced by the third one, thus Eq. (9.83) is simplified into Eq. (9.77), and both the frequency and the amplitude can be determined. Consequently P_3 is deduced from Eq. (9.82) using the values of P_1 and ω_1. The higher harmonics can be successively found, and the approximation, whose accuracy decreases with the harmonic number, is very satisfactory for a clarinet-like instrument. For instance, for the lossless case, the error is 10 % for the harmonic 5 (0.8 dB) and 21 % the harmonic 11 (1.7 dB) [76]: this is due to the decrease of the spectrum of the lossless solution at high frequencies [see Eq.(9.73)] (the decrease is much more rapid when losses are introduced). For sake of simplicity, the cubic term $P_3^2 P_3^*$ is ignored, and the calculation yields

[26] What is this solution? Eq. (9.82) becomes: $(Y_3 - A)P_3/C = P_3^2 P_3^*$, and is nothing else than Eq. (9.76) written for the frequency $3\omega_1$. Two solutions are deduced: the static regime $P_3 = 0$, and the oscillating (sinusoidal) regime of frequency $3\omega_1$. The threshold for the latter is higher than that for the fundamental regime with frequency ω_1, because as a first approximation the admittances increase as the square root of frequency. As a consequence losses allow discriminating the threshold of the oscillation regimes: in order to reach the twelfth, it is required to blow harder. However, we had to avoid the fundamental regime during the attack, and this is possible thanks to the register hole, which strongly lowers the first resonance and shifts its frequency.

[27] This law also applies to the even harmonics: there is a minor difficulty, because according to the law, the second harmonic should be larger than the third, but this situation occurs for values of the mouth pressure which are extremely close to the oscillation threshold. Thus we consider that this result is not in contradiction with the ignoring of the even harmonics in Eq. (9.80) (see [76]).

$$\frac{P_3}{P_1} = -\frac{1}{3}\frac{A - Y_1}{(A - Y_1) + (Y_3 - Y_1)}. \tag{9.84}$$

- Several conclusions can be drawn:
- Because Eq. (9.77) is assumed to be valid, $Y_1 = Y_{m1}$ is real and the frequency does not depend on Y_3. When the second resonance is a perfect harmonic of the first, Y_3 also is real, but this is not the general case. For the different notes of a clarinet the inharmonicity of the resonances has been studied in detail (see, e.g., [32, 37, 86]). It is not large, because the various causes of inharmonicity are partially mutually compensating. As a reminder the following factors are influential: dispersion due to visco-thermal effects, temperature gradient, closed or open tone holes, non-uniformity of the cross section, etc. The effect of inharmonicity will be examined in Sect. 9.4.5.
- When the loss limit is approached, the admittances Y_1 and Y_3 vanish, and the Helmholtz motion is reached [see Eq. (9.73)]; this is true also when losses are independent of frequency ($Y_1 = Y_3$).
- When the amplitude becomes large (A becomes large compared to Y_1), the amplitude ratio converges to the result for the Helmholtz motion as well, because the admittances Y_1 and Y_3 have the same order of magnitude. As a consequence, the details of either the tube shape or the losses, i.e., the details of the pipe input admittance have a minor influence far from the threshold.
- Near the threshold, the denominator is almost equal to $Y_3 - Y_1$ (the reader can check that this is consistent with the power law, i.e., that P_3 is proportional to P_1^3), and all details have a significant influence. For instance, the visco-thermal dispersion leads to a complex Y_3, thus the phase of P_3/P_1 is not π, as for the Helmholtz motion.[28]
- The effective loss parameter is the ratio of the loss coefficient to the reed parameter ζ, because A is proportional to the latter. If ζ is small (small reed opening, stiff reed), the effect of losses, which increases with frequency, is significant. Therefore there are few higher harmonics, in contrast to the case of large ζ. This parameter has an effect on both the rapidity of the attacks (via the coefficient A), and the spectrum.

[28] When Y_3 is slightly larger than Y_1, the relative amplitude of the third harmonic is approximately:

$$\frac{P_3}{P_1} \simeq -\frac{1}{3}(A - Y_1)Z_3.$$

So it is nearly proportional to Z_3, which is small. For instance it is the case of a one-mode resonator: its spectrum remains close to that of a sinusoid even at high levels [82]. Nevertheless even if the conclusion were correct, the calculation would be inconsistent, because the even harmonics have been assumed to be small compared to the odd ones. Here this is not true, for example, for the second harmonic compared to the first one.

- Another important aspect of the result (9.84) is that it does not depend on the cubic coefficient of the nonlinearity. As a matter of fact it can be rigorously proved from Eq. (9.80) that the shape of the signal, which depends on ratios P_n/P_1 only, as well as the playing frequency, depend on the coefficient A and of admittances Y_n only. This relativizes the importance of the accuracy of the nonlinear model, except obviously for the amplitude, which crucially depends on the coefficient C. This simplicity stems from ignoring the terms of degree two (which are proportional to B) or higher in the polynomial $F(p)$. Yet this approximation is rather good for a clarinet, at least when the reed does not beat.

9.4.4.2 Even Harmonics

Even harmonics remain to be calculated. They are very weak in the mouthpiece, but relatively much stronger in the radiated sound field. After some calculation (details are not given here), the solution of Eq. (9.79) is obtained

$$P_2 = BZ_2(P_1^2 + 2P_1P_3 + \cdots). \tag{9.85}$$

Notice that at the threshold the power law is satisfied. As expected, the amplitude is proportional to the coefficient B of the quadratic term in the expansion (9.55) [76]. The nonlinearity plays an important role, as well as the input impedance near the dips, and therefore as the shape of the mouthpiece is also influential.

9.4.4.3 Application to a Perfectly Cylindrical Tube

In what follows we apply the previous formulas to a perfectly cylindrical tube. The coefficients A and C are written with respect to the excitation parameters γ and ζ [see Eq. (9.55)], and a model of losses is added. The threshold pressure γ_{th} is known, thanks to Eq. (9.69): because α is proportional to the square root of the frequency, which is inversely proportional to the pipe length, the correction factor in comparison to the lossless case $(1/3)$ is proportional to the square root of the length. This implies that if the tube length increases, the pressure threshold increases. We need to blow harder in order to obtain a sound. Another reasoning is the following: for a given mouth pressure γ, a length threshold exists, beyond which no oscillations are possible. Losses need to be diminished, by choosing a wider tube. This is one reason explaining why bass instruments require wider diameter. This issue was discussed in Chap. 5, Sect. 5.5.3.3. Concerning the amplitude of the first harmonic, a similar calculation can be made. Because $Y_{m1} = A_{\text{th}}$, it is found that $Y_{m1} - A = 3\sqrt{3}\zeta(\gamma_{\text{th}} - \gamma)/2$ and:

$$P_1^2 \simeq \frac{2}{3}(\gamma - \gamma_{\text{th}}). \tag{9.86}$$

For the third harmonic, by writing $Y_3 = Y_{m1}\sqrt{3}$, the following result is obtained.

$$\frac{P_3}{P_1} \simeq -\frac{1}{3}\frac{\gamma - \gamma_{\text{th}}}{\gamma - \gamma_{\text{th}} + 0.28\alpha\ell/\zeta}. \tag{9.87}$$

Finally, for the second harmonic, the impedance $Z_2 = \alpha(2\omega_1)\ell$ is very small, because it is at a minimum, and we get

$$\frac{P_2}{P_1} = -Z_2\zeta\frac{3}{2\sqrt{2}}\sqrt{\gamma - \gamma_{\text{th}}}\left(1 + 2\frac{P_3}{P_1} + \cdots\right). \tag{9.88}$$

Here the losses involve the product of α and ζ, and not their ratio as for the harmonic 3. Figure 9.16 shows experimental results in two forms, and exhibits the two ranges of amplitude for the odd harmonics. In the first range, their amplitude compared to that of the first harmonic grows according to the power law, while in the second range the amplitude is almost constant. For the harmonic 3, Eq. (9.87) is qualitatively verified. Many similar results can be found in [10]. Notice that at high level, the reed beats and the previous calculations are no longer valid.

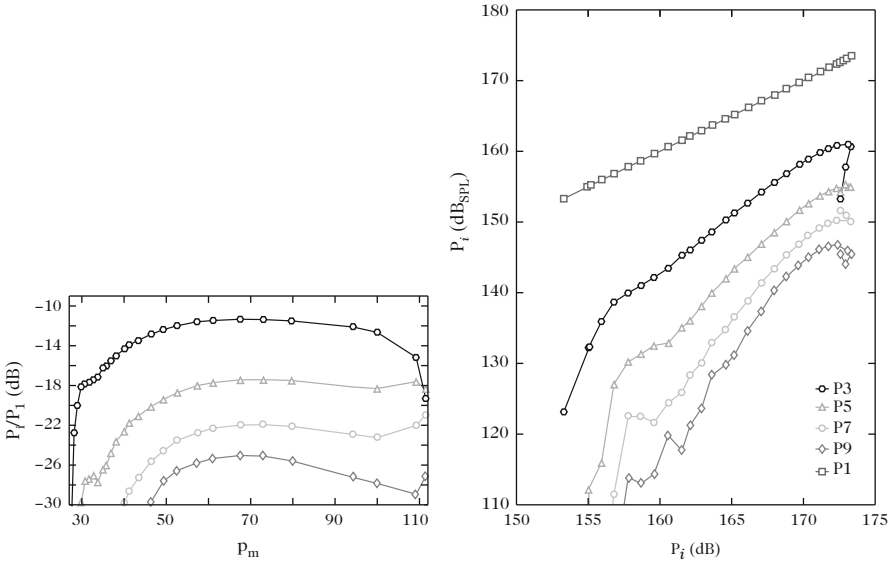

Fig. 9.16 Experimental results for a cylinder (four first odd harmonics) [89]. The *left plot* shows the amplitude ratios P_{2n+1}/P_1 as a function of the excitation pressure. The stabilization of the amplitude occurs at an amplitude level which is lower than that for a square signal, which would be $1/(2n+1)$ (i.e., in dB -9.5, -14, -17, -19, respectively). The scale for the mouth pressure p_m is in mbar. The *right plot* is an equivalent representation of the same results, which uses as an abscissa the amplitude (in dB) of the first harmonic. This representation is due to Benade [10], and provides a clear representation of the power law near the threshold

9.4.4.4 External Spectrum: Some Simple Consequences for a Cylinder at Low Frequencies

Lossless Model

At low frequencies the far-field radiated pressure p_{ext} is obtained by using a simple formula which will be detailed in the fourth part. We examine the case of a cylindrical open pipe without toneholes, which radiates in an omnidirectional way, i.e., as a monopole. The pressure p_{ext} is proportional to the time derivative of the flow rate at the output, with a delay of D/c, if D is the distance of the considered point to the tube output. According to the lossless model we used (square signals), the output pressure is zero, therefore $p_\ell^+ = -p_\ell^-$, and the output flow rate is $u_\ell = 2p_\ell^+$. Knowing how to calculate the outgoing wave at the input, we simply translate it by ℓ/c to obtain it at the output. Because the outgoing wave at the input is the half-sum of the pressure and the flow rate, the output flow rate is

$$u_\ell(t) = p(t - \ell/c) + u(t - \ell/c),$$

and, because in the lossless model the input flow rate is a constant, the external pressure is deduced as follows:

$$p_{\text{ext}} \propto \frac{du_\ell}{dt} = \frac{dp(t - \ell/c)}{dt}.$$

The interpretation of this result is easy, because for a plane wave the density of total acoustic energy in a slice of air does not depend on x: because there is no potential energy at the output and no kinetic (acoustic) energy at the input, the output flow rate is proportional to the pipe inlet pressure. Instead of a square signal, the far-field radiated pressure signal is a series of Dirac peaks which are alternately positive and negative. This is shown in Fig. 9.17. Concerning its spectrum, the ratio of the complex amplitude of the harmonics to that of the first one is $P_{\text{ext},2\nu+1}/P_{\text{ext},1} = 1$, instead of $(-1)^\nu/(2\,\nu + 1)$ [see Eq. (9.73)] for the internal spectrum.[29]

Model with Losses

When losses are taken into account (but not the dispersion), the transfer function is $U_\ell(\omega)/P(\omega) = 1/j\sin(k - j\alpha)\ell$ [see, e.g., the matrix given by Eq. (4.28)]. The external pressure is proportional to $\omega P(\omega)/\sin(k - j\alpha)\ell$, a delay function apart.

[29] This result is obtained for p_{ext} which is proportional to du_ℓ/dt. However, because of the delay due to the distance from the tube, the relative phase varies, and therefore the main conclusion concerns the real amplitude (i.e., the modulus of the complex amplitude): the ratio of the real amplitudes is 1 instead of $1/(2\nu + 1)$. Notice that the Fourier Transform of $\delta(t - \ell/c)$ is $\exp(-j\omega\ell/c)$, thus for $\omega = (2\nu + 1)\omega_1$, it is $(-1)^\nu$.

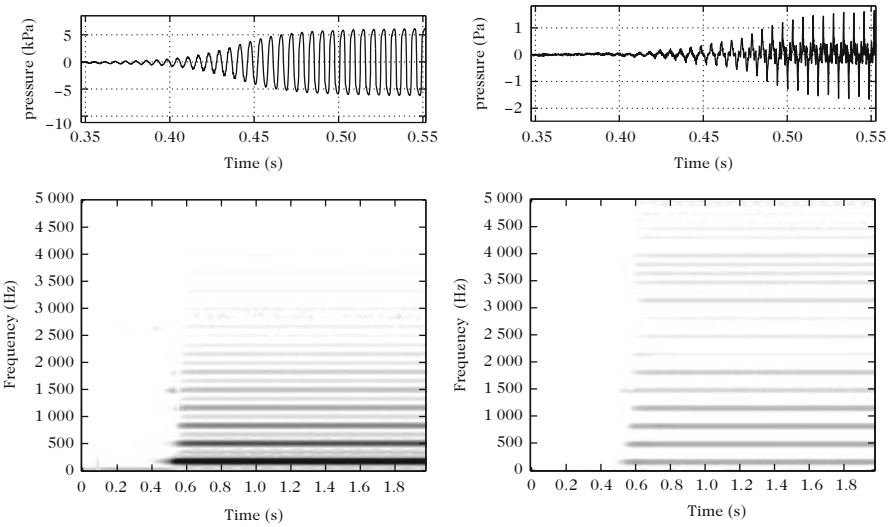

Fig. 9.17 Sound of a cylindrical tube with a clarinet mouthpiece: the internal pressure (on the *left*) is a rounded square signal (see also Fig. 9.12), the radiated pressure (on the *right*) is roughly the derivative of the previous one, because the monopole radiation at the end of the tube implies a derivative of the output flow rate, and because the latter signal is a square signal (in the lossless approximation). The time-frequency spectrograms (*bottom figures*) show that the first harmonic appears first, and confirm that the external sound is much richer in harmonics than the internal sound. The weakness of the even harmonics is also clear. Notice that the duration of the spectrogram is much longer than that of the signal

For odd harmonics $H_{2\nu+1}$, we write $\sin k\ell = (-1)^\nu$. Thus by neglecting the terms of order 2 in $\alpha\ell$, the complex amplitude with respect to that of the first harmonic is found to be equal to unity. Finally the expression (9.87) has to be multiplied by 3 and the modulus gives the result for the external pressure. For even harmonics, the situation is slightly more complicated (remind that their amplitudes are zero when losses are ignored). Limiting the calculation to the second harmonic:

$$\left|\frac{P_{\text{ext},2}}{P_{\text{ext},1}}\right| = \frac{3}{\sqrt{2}}\zeta\sqrt{\gamma-\gamma_{\text{th}}}\left[1+2\frac{P_3}{P_1}+\cdots\right]. \tag{9.89}$$

Compared to the internal spectrum, the value given by Eq. (9.88) is divided by $Z_2/2$. Curiously the harmonics 2 seems not to vanish with vanishing losses! In fact the factor in bracket is an infinite series depending on the odd harmonics of the internal spectrum, and we need to consider more and more terms when going far from the threshold...or when losses tend to zero. The Helmholtz motion in square signal does not produce even harmonics, but inversely if a signal is poor in harmonics, the even harmonics are relatively strong, as shown in Fig. 9.18.

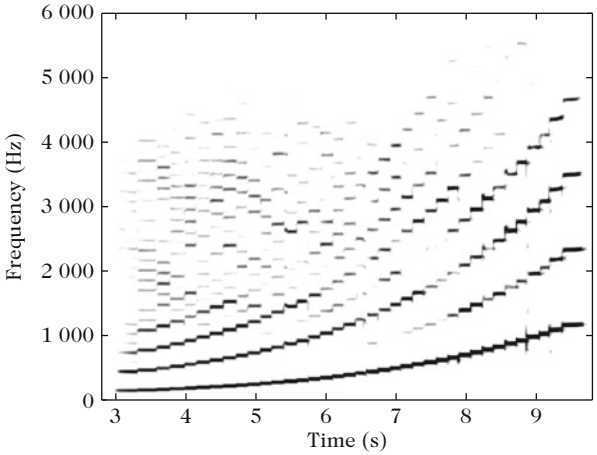

Fig. 9.18 Spectrogram of a clarinet chromatic scale (external pressure). The quasi absence of even harmonics is observed for lower notes. For higher notes their appearance is linked to the fact that the signal becomes less rich in harmonics, therefore differs from a square signal [see Eq. (9.89)]. One observes that frequencies below 1800 Hz are globally stronger than above this frequency. This corresponds to what Benade [10] called the cutoff frequency, due to the tonehole lattice (see Chap. 7)

9.4.5 *Variation of the Playing Frequency with the Excitation Level*

With the lossless model, the frequency is independent of the excitation level. In practice, it slightly varies. There are several causes, such as the reed dynamic, the flow rate due to the reed displacement, the effect of the vocal tract. This allows the player adapting the tuning with respect to what he hears, in a more or less efficient way. In this section a single cause is treated, the inharmonicity of the resonance frequencies. We limit the study to the steady-state regime. For this purpose we use the relationship obtained by Boutillon [18], which is related to the reactive power. It assumes that a nonlinear, quasi-static relationship exists between the input pressure and flow rate. Thus the reed is assumed to be without dynamic, like a massless spring, according to the model used since Sect. 9.3. In the steady-state regime, with a period T, it can be written as:

$$\int_t^{t+T} u dp = \int_t^{t+T} F(p) \frac{dp}{dt} dt = \left[F^{(-1)}(p) \right]_{p(t)}^{p(t+T)} = 0, \tag{9.90}$$

where $F^{(-1)}(p)$ is the integral of $F(p)$. If ω_p is the playing frequency, by using the expansion (9.72) and calculating the average of the product of two complex quantities (see Sect. 1.3 of Chap. 1), the following result is found:

$$\int u dp = 4\pi \sum_{n>0} n \, |P_n|^2 \, \Im m(Y_n). \tag{9.91}$$

This quantity is related to the reactive power [see Eq. (1.129)], i.e., to the derivative of the fluctuating power with respect to frequency. Therefore:

$$\Im m(Y_1) + 3\left|\frac{P_3}{P_1}\right|^2 \Im m(Y_3) + 5\left|\frac{P_5}{P_1}\right|^2 \Im m(Y_5) + \cdots = 0. \tag{9.92}$$

The advantage of this equation[30] is to provide a relation between frequency variation and the spectrum.

Denoting ω_1 the frequency of the first impedance peak, the other peaks are assumed to be at frequency $\omega_n = n\omega_1(1+\eta_n)$, where η_n measures the inharmonicity. The playing frequency is sought in the form: $\omega_p = \omega_1(1+\varepsilon)$. The input admittance is given by Eq. (9.66). We assume that for a frequency ω_n close to a resonance a single peak intervenes, thus for ω close to ω_n [see Eq. (2.39)]:

$$\Im m(Y) = 2\frac{\omega - \omega_n}{F_n}, \text{ with } F_n = \omega_n Z_{Mn}/Q_n. \tag{9.93}$$

For the frequencies ω_p and $n\omega_p$, at the first order in ε and η_n, we obtain

$$\Im m(Y_1) = 2\varepsilon\omega_1/F_1 \; ; \; \Im m(Y_n) = 2n\omega_1(\varepsilon - \eta_n)/F_n. \tag{9.94}$$

For a perfect cylinder, the modal coefficients $F_n = 2c/\ell$ are independent of n. If the cylinder is not perfect, the coefficients are assumed to remain independent of n at the first order of the perturbation. Using Eq. (9.92), we obtain

$$\varepsilon = \frac{\sigma}{1+\sigma'} \text{ where } \sigma = \sum_{n\geq 3} n^2\eta_n \left|\frac{P_n}{P_1}\right|^2 \text{ and } \sigma' = \sum_{n\geq 3} n^2 \left|\frac{P_n}{P_1}\right|^2. \tag{9.95}$$

Near the threshold, P_n/P_1 is very small, and ε vanishes. On the other hand, when we move away from the threshold, the influence of inharmonicity becomes significant. Let us consider the harmonics 1 and 3 only. In the extreme case where $|P_3/P_1| = 1/3$, the result would be the following:

$$\varepsilon = \eta/2. \tag{9.96}$$

This result provides an order of magnitude of the effect of inharmonicity, but obviously it is an approximation, because the harmonics of order higher than 3 are ignored. This is correct near the threshold only. Moreover the ratio $1/3$ was not observed for a cylindrical pipe. For $|P_3/P_1| = 0.2$, (this value seems to be encountered in practice), the result is $\varepsilon = 0.26\eta_3$. As a conclusion, if the second

[30] This equation is not an extra equation in addition to the equations harmonic balancing. The reader can check that, when limited to harmonics 1 and 3, it directly comes from Eqs. (9.81) and (9.82).

resonance frequency is 20 cents[31] too high (resp. too low) with respect to the first one, the frequency increases (resp. decreases) by around 10 cents during a crescendo. This order of magnitude is roughly confirmed by experiment, especially for a perfect cylinder, where inharmonicity is due to visco-thermal dispersion: the playing frequency increases with the excitation level. However, very close to the threshold the reed damping plays a predominant role and the frequency starts by decreasing, then increases [75, 89].

- Inharmonicity influences the playing frequency and more generally the self-sustained oscillation [87]. Benade [10] cited Bouasse [17, p. 91], who correctly felt the nonlinear character of the oscillation: *"the sustaining of the wave is made easier by the coincidence of the harmonic q of the pressure system due to the puffs with the partial $N = qn$ of the tube. Correlatively the puffs become more intense and regular: the reed is stabilized for the frequency n."* Harmonicity ensures the stability of the frequency when the level is changed, and if the peaks are of similar height, a too strong inharmonicity can lead to quasi periodic regimes (see, e.g., [56]). This phenomenon is a cause of the "wolf note" for the cellos (see Chap. 11). For the instrumentalist the quality of the different notes appear to be unequal. It is furthermore probable that harmonicity is an important element of the ease of playing.

In particular a periodic sound can be produced with a very low input impedance at the playing frequency, when the harmonics correspond to impedance peaks. Some specific cases are particularly interesting: the "pedal" sounds of brass instruments (their first harmonic is shifted with respect to the other harmonics, see Chap. 7). It is possible to produce a sound the frequency of which is the half of that of the second peak, because the resonance frequencies 3, 4, 5, etc., are harmonics of this frequency. More generally periodic "multiphonic" sounds can be produced: their frequency is generally very low, because it is the highest common factor when it exists [25]. For the point of view of perception, some sounds can have an almost vanishing at the fundamental frequency and many harmonics, and the perceived pitch corresponds to the inverse of the period. Furthermore various multiphonic regimes can be obtained on wind instruments, such as quasi-periodic, or chaotic regimes (as already mentioned) [38, 39, 107].

9.4.6 Beating Reed and Sound Extinction

9.4.6.1 Lossless Model (Steady-State Regime)

Up to now we considered that the reed does not beat, thus we supposed that the nonlinear function (9.30) is limited to low pressures. We used Eq. (9.31), or its simplified version (9.55). If the reed is allowed to beat, Eq. (9.32) needs to be used as

[31] The cent is the hundredth of a semi-tone. The latter corresponds to a frequency ratio of $2^{1/12} = 1.05946$, therefore the cent is a difference of 0.06 % in frequency.

well. This beating-reed model (see Sect. 9.2.5.2) is a rough approximation because in practice the closure is not sudden and the non-beating range becomes larger. Nevertheless it gives interesting results when they are compared to experiments. If it is assumed that a clarinettist plays as often with a non-beating reed as with a beating reed (see for a discussion [12]), the reader may be surprised by the treatment imbalance for these two types of functioning. A lot of work remains to do in order to understand the beating reed oscillation. It is actually the main operating mode of conical reed instruments (this will be seen hereafter). For a beating reed, all the analysis of small oscillations becomes useless.

We limit the analysis to the two-state approach for the steady-state regime, considering first a lossless resonator, then discussing a more general model with frequency-independent losses. We consider first the static regime: it occurs for $p = 0$ because the input impedance at zero frequency is assumed to be zero, and this implies $\gamma > 1$ for the dimensionless mouth pressure. For a mouth pressure higher than the closure pressure, the reed closes the mouthpiece: it is our definition of the closure pressure p_M. The stability of this regime is not discussed here, because the discussion should be rather long and the stability is intuitively understood. Now we search for the oscillation regime in the same way as in Sect. 9.3.3.4: because the mean pressure is zero, we search again for two opposite values of the two states: $\pm p_\infty$, with constant flow rate. If the reed beats for $p = -p_\infty$, the flow rate vanishes and, following Eq. (9.32), this implies

$$p_\infty \geq 1 - \gamma. \tag{9.97}$$

Equation (9.60) shows that the flow rate is constant, thus it also vanishes while the reed is open. If the reed was beating for both $p = p_\infty$ and $p = -p_\infty$, the regime would be the static regime). Thus, after Eq. (9.31):

$$p_\infty = \gamma. \tag{9.98}$$

So the reed does not close for the positive mouthpiece pressure and beats for the negative one, because of the large pressure difference $p_m - p$ between the mouth and the mouthpiece. The condition for this regime is given by Eq. (9.97):

$$\gamma > 1/2.$$

This solution[32] is illustrated in Fig. 9.19. This extremely simplified functioning can be described as follows: during one half-period, the mouthpiece pressure is opposite to the mouth pressure and the reed is closed, while during the other half-

[32]This solution can be easily shown to be stable whatever the value of γ is [91]. So, if the pressure increases with a non-beating reed, yielding several frequency divisions (see Sect. 9.3.3.6), then frequency multiplications occur in order to retrieve the normal frequency when the reed starts to beat (see [73]).

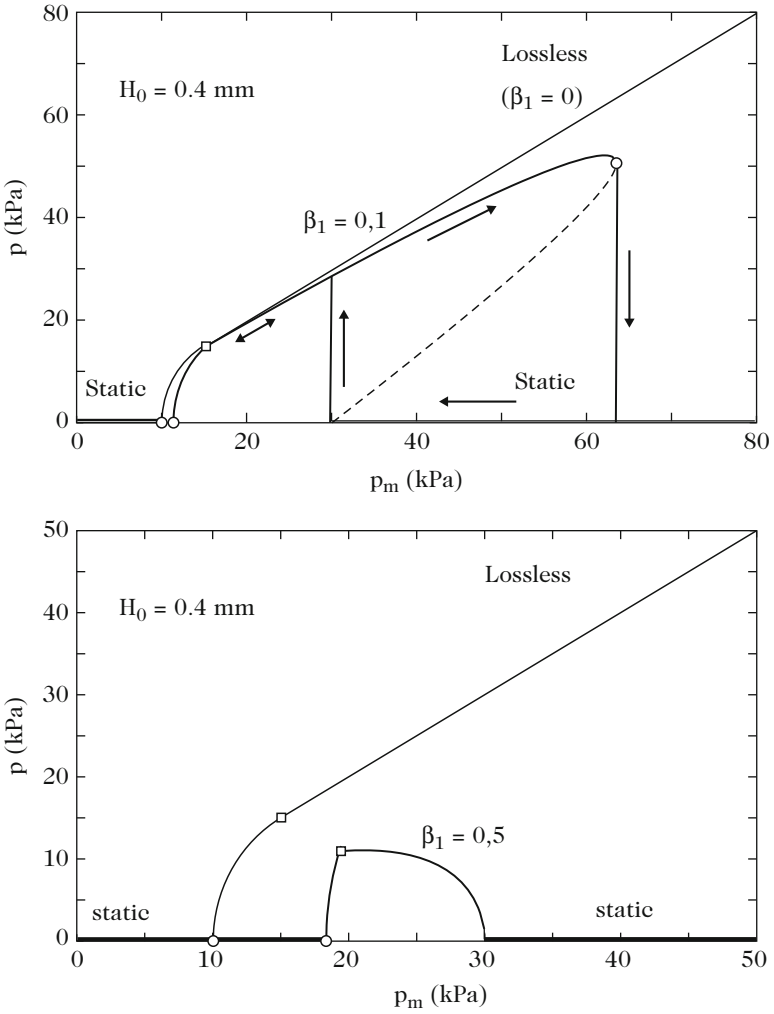

Fig. 9.19 Bifurcation schemes for the Raman model. *Top*: $\beta_1 = 0.1$, inverse bifurcation at the extinction; *bottom*: $\beta_1 = 0.5$ (very small reed opening), direct bifurcation. The reader can compare with Fig. 9.15 (experimental result)

period, it is equal to the mouth pressure and the flow rate vanishes (no pressure difference). This behavior can produce large sound levels in the mouthpiece, as explained in the introduction (Sect. 9.2.1).

9.4.6.2 "Raman Model" with Losses

A major drawback of the lossless model lies in the infinite increase of the acoustic pressure when the blowing pressure increases [see Eq. (9.98)]. A simple model can remedy this difficulty [35]: considering frequency-independent losses keeps square signals but allows finding a good agreement between experiment and model for the bifurcation schemes. This model is called "Raman model" by analogy with the model of bowed strings which was studied by the great Indian physicist at the beginning of the twentieth century. Writing the solution of the wave equation with damping in the form:

$$P = P^+ e^{-\alpha x} e^{-jk\ell} + P^- e^{\alpha x} e^{jk\ell},$$

and assuming a zero pressure at the output, it is found that the reflection coefficient at the input is $R = P^-/P^+ = -e^{-2\alpha x} e^{-2jk\ell}$. The input impedance reduced by the characteristic impedance Z_c is given by:

$$Z = j \tan(k - j\alpha)\ell. \tag{9.99}$$

Resonance frequencies are unchanged by damping and all input impedance maxima are equal to $Z_{\max} = 1/\tanh \alpha\ell$, while minima are $Z_{\min} = \tanh \alpha\ell$. The modal expansion (9.66) remains valid. It is possible to generalize the previous study of square signals, including the graphical method for building the solution. Exact calculations, which generalize the approach of Sect. 9.3.3, are tedious [35]. A significant simplification is obtained when the input impedance at zero frequency is assumed to be zero (instead of $Z_{\min}$). Then the static regime remains $p = 0$. For the instability threshold, it is not useful to make the calculation because the formula $A = Y_1$ given by the one-mode approximation remains valid, as well as Eq. (9.69). This is actually valid whatever the frequency dependence of the damping α is. When the blowing pressure increases the threshold of period doubling can be found; however, for a significant damping this threshold is larger than that of beating reed for the oscillation regime. As a consequence the rather large losses in real cylindrical instruments explains why it is very difficult to produce a period doubling.

- Now we consider the behavior of the Raman model when the reed beats. In steady-state regime, because $Z(0) = 0$, the two states (i.e., open reed and closed reed) are opposite. We write them again: $\pm p_\infty$ and expand the square signal into (odd) harmonics. For each of them the corresponding flow rate is deduced from the admittance $1/Z_{\max}$; then the oscillating part is $\pm p_\infty/Z_{\max}$. A constant (dc) flow rate denoted u_0 has to be added. Using Eq. (9.30), if $\Delta p = \gamma - p_\infty$, we find the steady-state regime:

$$\begin{aligned} &u_0 + p_\infty/Z_{\max} = \zeta(1 - \Delta p)\sqrt{\Delta p} \ \text{ with } 0 < \Delta p < 1; \\ &u_0 - p_\infty/Z_{\max} = 0 \text{ with } 1 - \gamma - p_\infty < 0 \ \text{ or } \ \Delta p \le 2\gamma - 1. \end{aligned} \tag{9.100}$$

Hence:

$$2\beta_1(\gamma - \Delta p) = (1 - \Delta p)\sqrt{\Delta p}, \tag{9.101}$$

$$\text{with } \beta_1 = \tanh \alpha\ell/\zeta \simeq \alpha\ell/\zeta. \tag{9.102}$$

We confirm that the loss parameter intervenes via the ratio α/ζ. The threshold of beating reed is given by $\Delta p = 2\gamma - 1$, therefore $\gamma = (1 + \beta_1^2)/2$. It is slightly modified by the losses if β_1 is small. Moreover by solving[33] Eq. (9.101), it can be shown that: *if γ is lower than* 1, there is always a unique solution, and it can be proved to be stable. But if *if γ is higher than* 1 when the mouth pressure is large, there are two possible cases:

- either $\beta_1 < \dfrac{1}{2}$: there are two solutions, one is stable, and the other one is unstable if γ is lower than the extinction threshold given by $\gamma_{\text{extinc}} \simeq \frac{1}{3}\left[1 + \frac{1}{\beta_1\sqrt{3}}\right]$, while there is no solution if $\gamma > \gamma_{\text{extinc}}$ (as expected this threshold tends to infinity when losses tend to 0).
- or $\beta_1 > \dfrac{1}{2}$: there is no solution.

Figure 9.19 shows the two cases: the first one corresponds to an inverse bifurcation at extinction, with hysteresis. For $\gamma > 1$, when forcing the breath, the pressure increases following the (stable) upper branch, then diminishes. Then the oscillating solution disappears abruptly and the static solution is retrieved. When the breath is diminished anew, the static solution is kept up to $\gamma = 1$, where there is a jump to the upper oscillating branch. The maximum pressure, or saturation pressure is obtained for $\gamma_{\text{sat}} \simeq \frac{1}{3}\left[1 + \frac{1}{\beta_1 3\sqrt{3}}\right]$. It is undoubtedly the most usual case.

The second case shows a direct bifurcation at extinction, which is a remarkable result: it is possible to play pianissimo at extinction also, by pinching strongly the reed! This technique is used by some instrumentalists, who reduce the reed opening and therefore the parameter ζ. Comparisons with experiment give excellent results [30], especially when nonlinear losses are taken into account at the various openings (see Chap. 8, Sect. 8.4.5), by using c_d as a fitting parameter. As a conclusion, the Raman model gives very interesting results, although the pressure signals are square signals.

9.4.7 *Miscellaneous Considerations About Clarinet-Like Instruments*

In the present chapter we did not treat the reality of the resonator geometry, with toneholes, changes in cross section, etc. As noted earlier, there is an average

[33] Equation (9.101) can be graphically solved, by seeking the intersection of the straight line corresponding to the left term with the function defined on the right-hand side and depicted in Fig. 9.9.

compensation of the action of the different elements resulting in a reduction of inharmonicity [32, 37]. When toneholes are open, one could think that the existence of cutoff frequency hampers the oscillations because the higher order peaks become low. The reduction of the compass is effective because it is difficult for the fundamental frequencies to be higher than the cutoff (from experience, players know that it is easy to obtain higher order regimes for the note with all holes closed, while it is more difficult for the other notes). But the dominant feature is that at low frequencies the effective length of the tube is shorter when opening the toneholes, thus the threshold diminishes and the oscillations become easier.

Another possibility for easing the oscillations is the use of the vocal tract: the two resonators are in series. If the player manages to have resonances of the vocal tract at medium frequencies, he can act on the tuning and tone color. Moreover he can reinforce the even harmonics of the sound, which do no longer correspond to impedance minima and can have an effect on the playing frequency (via the inharmonicity). This topic was recently investigated, and some aspects remain open. So a difficult question can be asked: what physical quantity can be regarded as a source, e.g., as imposed by the player? Up to now we assumed that it is the mouth pressure, assumed to be uniform. On this topic, we refer to the following references [26, 27, 52, 53, 63, 65, 97, 103, 120]. Another important subject is the role of the reed dynamics, that we have completely ignored up to now. We will include it in Sect. 9.5.

Finally we mention the problem of the measurement of the input impedance, considering the complicated geometry of the mouthpiece. The matching between a turbulent jet and an acoustic field is extremely complicated (see, e.g., [100]). Even when exciting the mouthpiece by an acoustic source at its output, the acoustic field is not planar, and cannot be characterized by a unique quantity such as the input impedance. Moreover the reed excite the mouthpiece on its side, therefore produces evanescent modes. The general solution chosen by several authors is to replace the mouthpiece by a cylindrical tube having the same volume, with a cross section are equal to that of the mouthpiece output. The first advantage is to be able to compare with plane-wave models of the input impedance. The second advantage is that near the first impedance maximum, the effect of the mouthpiece depends on its volume only, thus the results of the theoretical models of the nonlinear coupled system can be rather reliable. However, this is not true for the impedance minima, and more generally at higher frequencies, when the mouthpiece cannot be regarded as a lumped element. Notice that this difficulty can be anyway of minor importance when compared to the effect of the vocal tract. Remember that a one-dimensional model is a great simplification.

9.4.8 Conical Reed Instruments

The resonator of conical reed instruments such as the saxophone has been studied in Chap. 7. They are truncated cones, and have a mouthpiece similar to that of a

clarinet, but their resonators are very different from an acoustical point of view. Oboes and bassoons have a double reed with a nonlinear characteristic which slightly differs from that of single reeds (see Sect. 9.2.5.2), but what follows deals with both single and double reed instruments. Indeed it appears that the shape of the resonator plays a predominant role. As an illustration it is possible to buy a mouthpiece of sopranino saxophone type adapted to the bassoon, and it is noticeable that the sounds are rather similar to those normally obtained with a double reed [61]. For the lowest notes of a conical pipe, the first impedance peak is lower than the second. Furthermore the second peak corresponds more or less to the octave instead to the twelfth.

The resonance frequencies are approximately a complete series of harmonics (see Chap. 7). The Helmholtz motion (HM) is also for conical instruments an interesting approximation of the pressure signal (except near the oscillation threshold). We will see that the signal is a "rectangle signal," with a duration ratio of the two states equal to the length ratio of the missing cone (due to the truncation) and the truncated cone (see Fig. 9.20).

In comparison with cylindrical instruments, one supplementary parameter is needed, e.g., the apex angle, which makes the problem far more difficult. The approach without losses leading to two-state signals implies one more approximation: the length of the missing cone needs to be much smaller than the wavelength. This hypothesis is paradoxical for a rectangle signal which is rich in high harmonics!

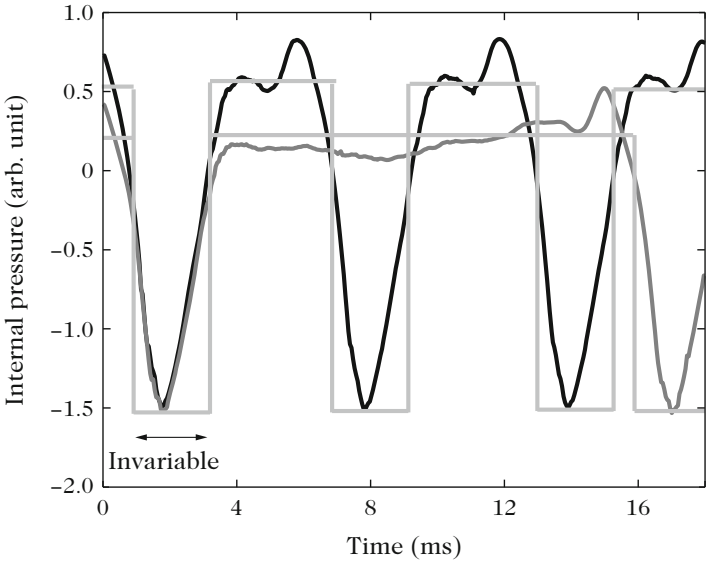

Fig. 9.20 Periodic signal of barytone saxophone, and the approximation by a rectangle signal. The signal is the internal pressure for two notes, which are the lowest and the highest of the first register. The state of negative pressure, which corresponds to a beating-reed, is common to the two notes

Moreover the "small oscillation" approach as well as the variable truncation method is not of much interest because the bifurcation at low mouth pressure is inverse. This remarks explain why many problems remain open.

9.4.8.1 Small Oscillation Solution (with Losses)

At the instability threshold of the static solution, it has been seen that oscillations can start (linearly) and are quasi sinusoidal. If the impedance of the second peak is higher than that of the first, the first oscillation threshold is that of the octave regime, not that of the fundamental one. This explains why it is difficult for beginners to play the fundamental regimes. Going further, we consider the nonlinearities in steady-state regime, using the harmonic balance for small oscillations in order to find the existence threshold of the oscillating solution [we refer to the explanation accompanying Eq. (9.83)]. Equations (9.74) and (9.75) have to be solved without hypothesis with respect to even and odd harmonics. The "small oscillation" solution is written as[34] [60]:

$$P_1^2 = \frac{Y_1 - A}{3C + \frac{2B^2}{Y_2 - A}} = \frac{(Y_1 - A)(Y_2 - A)}{3C(Y_2 - A) + 2B^2} \tag{9.103}$$

$$P_2 = \frac{BP_1^2}{Y_2 - A}. \tag{9.104}$$

For the clarinet, Y_2 is very large, $Y_2 > Y_1$, and the result (9.77) is obtained, as well as Eq. (9.85) for small oscillations.

We start the investigation with a case simpler than that of the lowest notes: the case of higher notes for which *the second peak is smaller than the first*, but has the same order of magnitude. Now Y_2 is larger than Y_1, but remains small: the second term of the denominator of Eq. (9.103) is the larger term (the term in C can be ignored). In order to find a solution, it is necessary for P_1^2 to be positive. Thus A needs to be either smaller than Y_1 or larger than Y_2 (here we assume that the two resonance frequencies are harmonic, therefore the two admittances are real for the playing frequency). Starting away from the oscillation threshold $A = Y_1$, the solution P_1^2 only exists if $A < Y_1$. The case is similar to the case of a clarinet for which C would be positive, implying an inverse bifurcation (see Fig. 9.14). Close to the threshold, the oscillating solution is unstable. The existence of a subcritical threshold can be shown. Above this threshold the oscillation becomes stable (an example is shown in Fig. 9.21). When the blowing pressure (like A) increases from 0, there is a jump at the threshold $A = Y_1$ to a finite value of the amplitude, while when the blowing pressure decreases, the player can reach the subcritical threshold, where he jumps back to the static regime.

[34] The series is truncated to harmonics 1 and 2 (and -1 and -2), and the harmonic 0 (dc component) is negligible because the input impedance at zero frequency is very small. For small amplitudes the influence of the higher harmonics is of higher order in P_1.

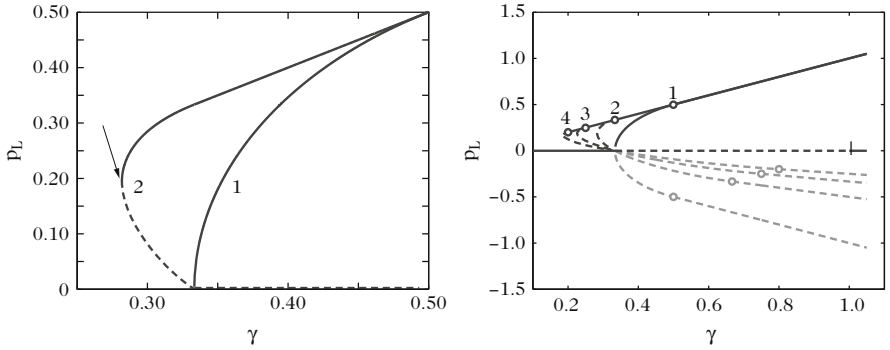

Fig. 9.21 Helmholtz motion for a cylindrical saxophone. The *right plot* shows for different values of β the values of the pressure during the long state p_L with respect to the mouth pressure γ. The increasing part corresponds to p_L^+, and the *decreasing part* corresponds to p_L^-. The stable HM is in *solid black line*, the unstable HM is in *dotted black line*, and the inverse HM is in *gray*. The integer N is related to β by $\beta = 1/(1+N)$. The *asterisk* indicates the beating thresholds. The *left plot* depicts a zoomed view for $N = 1$ and 2: the bifurcation is direct for $N = 1$ and inverse for $N = 2$. The *arrow* indicates the subcritical threshold at $\gamma = 0.28$

Therefore there is a hysteresis. It is not possible to play pianissimo, and it is easier to play with a low amplitude, when playing decrescendo than playing crescendo (if it is assumed that the player modifies the mouth pressure only). Figure 9.21 (left) shows an example of inverse bifurcation for a cylindrical saxophone, treated in the next sections.

In the case where the admittance Y_2 is smaller than the admittance Y_1, which is the general case for lower notes, the fundamental regime can exist with small oscillations only if $A < Y_2$, and it is still unstable (but the octave regime can exist and be stable), or if $A > Y_1$: however, for the latter case it can be shown that the regime is the inverse HM, discussed in the next section. The important feature is that the octave regime is favored. The previous discussion analyzed the phenomena occurring when there is a maximum input impedance at the double frequency, instead of a minimum as for the case of a clarinet.

9.4.8.2 "Cylindrical Saxophone", Statement of the Problem

Coming back to the lossless approximation, it is possible to go slightly further. On the one hand if losses are ignored, the two thresholds $A = Y_1$ or Y_2 are equal [see Eq. (9.103)], and information is lost; on the other hand, if a supplementary approximation is added, results about the amplitude can be found. Figure 9.20 shows that the internal sound of a saxophone can be loosely approximated by a rectangle signal, and this gives the idea to seek an analogy with the bowed string, which is studied in Chap. 11. For that purpose, it was seen in Chap. 7 that considering the natural frequencies, an approximation of the diverging cone is a cylinder of length

$\ell + x_1$ open at the two ends, called "cylindrical saxophone". x_1 is the distance of the input of the truncated cone to its apex, and it is assumed to be small compared to the wavelength [see Eq. (7.88), and Fig. 7.10]. So, when losses are ignored, the input admittance is written as:

$$Y = \frac{S_1}{\rho c}\left[\frac{1}{jkx_1} + \frac{1}{j\tan k\ell}\right] \quad \text{or} \tag{9.105}$$

$$Y \simeq \frac{S_1}{\rho c}\left[\frac{1}{j\tan kx_1} + \frac{1}{j\tan k\ell}\right]. \tag{9.106}$$

Formula (9.106) is analogous to the mechanical impedance of a string at the location of the bow (see the table of Sect. 1.6 of Chap. 1). The two ends of the string are in series, with the same velocity at the bow position. For the cylindrical saxophone, the two ends, of length ℓ and x_1, are in parallel, with the same pressure at their input, where the reed is located. As a first approximation, this equivalence between a conical tube and a cylindrical one remains valid for any length ℓ, and for any effective length when holes are open. In what follows, we make an analysis similar to the one we have made for the clarinet in Sect. 9.3.3. As far for the clarinet, we will not obtain much information about the spectrum, because we ignore the losses, as for the clarinet, and in addition we assume the length x_1 to be small compared to the wavelength (notice that this is wrong for higher harmonics). But many phenomena can be explained thanks to this simplified model,[35] that was proposed for the first time by Gokhshtein [59].[36]

Thus we seek a periodic solution of period $T = 2L/c$, where $L = \ell + x_1$. The pressure and the flow rate have the frequencies $f_n = nc/2L$ as *only possible components*, and they satisfy $\sin kL = 0$ (this can include the dc component). We will now investigate a particular solution, the Helmholtz motion. Beforehand we propose an analysis of the different possible solutions, for the interested reader.

[35] With this model, a clarinet is not analogous to a bowed string, because this should imply an infinite value for x_1. However, if a cylinder is excited at its middle, the two ends of the tubes play the same role, thus a clarinet is equivalent to a cylinder of double length, excited at its middle and having a half cross section. This can be checked by using Eq. (9.106) with $\ell = x_1$.

[36] Dalmont [31] showed that a step cone built with N cylindrical pipe segments of equal length x_1 and cross section $s_n = n(n+1)/2$ (where the integer n is the rank order of the cylindrical segment and s_n its cross-section area) has the same admittance [Eq. (9.106)] as a cylindrical saxophone of cross-section area $S_1 = s_1/2$ when $\ell = Nx_1$. Their realization is easier than that of a cylindrical saxophone, but is limited to the condition of integer ℓ/x_1. It is the reason why these instruments allow studying the Helmholtz motion in a precise way [90, 91]. It is noticeable that bamboo "saxophones" exist with a geometry approaching that of such step cones.

Different Possible Solutions

In order to study the different possible solutions, we rewrite Eq. (9.106) in the form:

$$U(\omega)\sin kx_1 \sin k\ell = P(\omega)\sin kL.$$

The inverse Fourier Transform of this expression is Eq. (4.65), if the analogy between stringed instruments and reed instruments is used. For frequencies f_n, equations $\sin kL = 0$ and $\sin k\ell = -(-1)^n \sin kx_1$ are valid. It is deduced that the corresponding components of the flow rate vanish, except if $\sin kx_1 = 0$, i.e., for $f_m = mc/2x_1$, where m is another integer. Now f_m can belong to frequencies f_n, thus $x_1/L = m/n$ (all integer values of m are not possible). This implies

- either the ratio $\beta = x_1/L$ is a rational number, and the flow rate can have non-zero components for frequencies $mc/2x_1$ such as $m = n\beta$. For instance if $\beta = 2/5$, the pairs $(m, n) = (2, 5),\ (4, 10)$, etc. are possible.
- or $m = n = 0$, and a priori the dc component of the flow rate does not vanish whether β is rational or not. If β is irrational, the dc component of the flow rate is the only non-zero component.

For the pressure, the component f_n vanishes if $\sin kx_1 = 0$: this can happen only if β is rational, or if $n = 0$. As a summary:

- β is irrational, and the pressure involves all harmonics f_n, except the continuous component; the flow rate is continuous (in particular when it vanishes at every time, i.e., when the reed beats!).
- β is rational, and the pressure has all harmonics f_n except harmonics f_m (they are called "missing harmonics") and among the harmonics f_n the flow rate has the harmonics f_m only. Then the flow rate is periodic with the period $2x_1/c$ or a submultiple which remains compatible with the period of the solution, $2c/L$ (if a signal is periodic with period T, it is also periodic with period pT, where p is any integer).

Therefore numerous solutions to our problem exist. A simple particular case is that where the solution has two states only. For instance the pressure has a negative value p_S during a time $T_S = \tilde{\beta}T$, and a positive value p_L during a time $T_L = (1 - \tilde{\beta})T$. The flow rate also has two states, because its values are related to those of the pressure through the nonlinear reed characteristics. If we subtract the dc component, the flow rate is proportional to the pressure, and its spectrum is proportional to the pressure spectrum. It has been seen that if β is irrational, the flow rate is continuous, with two equal states, similarly to the behavior of a clarinet. Conversely if β is rational, both the flow rate and the pressure have harmonics f_n except harmonics f_m; but the flow rate cannot

(continued)

have other harmonics than f_m, thus in this case it is continuous as well. A more straightforward proof of this result is the following: the mean pressure vanishes, thus $\tilde{\beta}p_S+(1-\tilde{\beta})p_L = 0$ (remind that the indices L and S correspond to long and short, respectively); on the other hand because the losses are ignored, the injected power needs to vanish, thus: $\tilde{\beta}p_S u_S+(1-\tilde{\beta})p_L u_L = 0$ and $u_S = u_L$. We still need to find the possible values of $\tilde{\beta}$, for a stable or unstable solution. If β is irrational, any value is possible, but if β is rational, there is a limitation because the harmonics f_m are absent of the spectrum: we need to choose a value of $\tilde{\beta}$ which suppresses these frequencies in the spectrum. This topic has been investigated by several authors [28, 119].

9.4.8.3 The Particular Case of the Helmholtz Motion

A particular solution was discovered by Helmholtz. It is called "Helmholtz motion" (HM), which describes the motion of a bowed string that players normally seek. In this case the division $\tilde{\beta} = T_s/T$ of the period is equal to the division $\beta = x_1/L$ of the length of the instrument, either a bowed string or a cylindrical saxophone. This case is shown in Fig. 9.20. Because the flow rate is constant, the two states of the pressure satisfy

$$F(p_L) = F(p_S); \tag{9.107}$$

$$\beta p_S + (1-\beta)p_L = 0. \tag{9.108}$$

We choose the function given by Eq. (9.31). When the reed does not beat, we have

$$F^2(p) = F_0^2 + A_2 p + B_2 p^2 + C_2 p^3, \text{ where } F_0 = \zeta(1-\gamma)\sqrt{\gamma}; \tag{9.109}$$

$$A_2 = \zeta^2(1-\gamma)(3\gamma-1); \quad B_2 = \zeta^2(3\gamma-2); \quad C_2 = -\zeta^2. \tag{9.110}$$

(it can be noticed that $B_2^2 = \zeta^4 + 3A_2C_2$). In the useful range of mouth pressure γ A_2 is either positive or negative, and B_2 and C_2 are negative. The flow rate being constant, we find

$$A_2(p_L - p_S) + B_2(p_L^2 - p_S^2) + C_2(p_L^3 - p_S^3) = 0. \tag{9.111}$$

The solution $p_L = p_S$ is trivial: it is the static regime, because Eq. (9.108) implies $p_L = p_S = 0$. The final result for the oscillating solutions is the following[37]:

$$p_L^{\pm} = \frac{2\beta}{1+3\chi^2}\left((2-3\gamma)\chi \pm \sqrt{\chi^2+(1-\gamma)(3\gamma-1)}\right) \tag{9.114}$$

$$p_S^{\pm} = -\frac{2(1-\beta)}{1+3\chi^2}\left((2-3\gamma)\chi \pm \sqrt{\chi^2+(1-\gamma)(3\gamma-1)}\right) \tag{9.115}$$

$$\text{where} \quad \chi = \frac{T_L - T_S}{T_L + T_S} = \frac{p_S + p_L}{p_S - p_L} = 1 - 2\beta. \tag{9.116}$$

The parameter ζ does not intervene: it intervenes in the value of the flow rate only. Thus there are two different oscillating solutions: one with a pressure p_L, which increases with the blowing pressure γ (sign $+$), the other one with a decreasing pressure (exponent $-$). An important value of γ is what it is called the subcritical threshold γ_{sc} for which the two values $p_L^{\pm}$ are equal, as well as the values $p_S^{\pm}$ (the argument of the square root vanishes):

$$\gamma_{sc} = \frac{2}{3}\left[1 - \sqrt{1-3\beta+3\beta^2}\right] \simeq \beta\left(1 - \frac{\beta}{4} + O(\beta^2)\right). \tag{9.117}$$

These results are valid when the reed does not beat. When it beats, the flow rate needs to vanish for two different values of the pressure, therefore one is γ and the other one is lower than $\gamma - 1$. Using (9.108), and the signs $+$ and $-$ for the increasing and decreasing functions of p_L, we obtain

$$\text{if } p_L^{+} = \gamma,\ p_s^{+} = -(1-\beta)\gamma/\beta; \text{ this implies: } \gamma > \beta \tag{9.118}$$

$$\text{if } p_s^{-} = \gamma, p_L^{-} = -\beta\gamma/(1-\beta); \text{ this implies: } \gamma > 1-\beta. \tag{9.119}$$

Figure 9.21 shows the solutions p_L for different values of β. Some comments can be added

[37] Starting from (9.111) for $p_L \neq p_S$, the solutions satisfy

$$A_2 + B_2(p_L + p_S) + C_2\left[\frac{3}{4}(p_L + p_S)^2 + \frac{1}{4}(p_L - p_S)^2\right] = 0. \tag{9.112}$$

This equation is solved for the unknown $\sigma = p_L + p_S$, then, because $p_L = -\beta\sigma/\chi$, it is found:

$$p_L^{\pm} = -\frac{2\beta}{C_2}\frac{1}{1+3\chi^2}\left(-B_2\chi \pm \sqrt{\chi^2(B_2^2 - 3A_2C_2) - A_2C_2}\right). \tag{9.113}$$

For the polynomial function (9.55), the expression is exactly the same, if the subscript 2 is suppressed in the coefficients, and the above result can be easily used in both cases.

- For the clarinet, χ vanishes, and the result becomes very simple [Eq. (9.62) is found].
- For conical instruments, β is small and the subcritical threshold (9.117) is very close to the beating reed threshold β: such instruments are expected to function mainly with a beating reed.
- This is true for positive values of p_L: the solution is the standard HM, analogous to the usual solution for bowed strings, and an inverse bifurcation prevails. The result of the previous section is confirmed.
- For negative values of p_L, the HM is "inverse." It seems to be produced with a direct bifurcation, but this issue is very delicate, because the losses differentiate the thresholds (Y_1 and Y_2 are different). The problem is rather simple if Y_2 is larger than Y_1, but the difficulty increases when the number of impedance peaks having an amplitude larger than that of the first peak increases. The analysis of a system with two peaks was done [33] for the different regimes (standard, inverse and octave; the latter case appears when the second peak is larger than the first). A more detailed study of the general case with N peaks (for small values of β) remains to be performed.
- A signal close to the inverted HM was obtained by experiment for saxophone-like instruments, but was not observed for bowed strings. The mouth pressure was strong, probably for pressure beyond the saturation threshold of the standard HM.
- The stability was studied for the case $\beta = 1/3$ [91]: the ab initio solution [Eq. (4.65)] can be used, by considering a small deviation from the sought solution, but difficulties can occur when two stable regimes are very close together. When $1/\beta$ is an integer, another method is the Floquet method, which generalizes what we did in Sect. 9.3.3.5, but the recurrence relationships become longer.[38]
- The bifurcation point of the static regime is obtained for $p_L = p_S = 0$. This implies $A_2 = 0$, i.e., $\gamma = 1$ or $1/3$. The value 1 for γ corresponds to a closed reed, after Eqs. (9.118) and (9.119), and the bifurcation occurs at $\gamma = 1/3$ independently of β. The interpretation is easy: when the equations are derived assuming small oscillations (see the previous section), the solution is quasi sinusoidal at the threshold limit, and the equation for the first harmonic (9.77) applies in all cases. Therefore the threshold is $A = 0$ when losses are ignored. Notice that the first harmonic approximation cannot distinguish the two HMs, because it does not provide the sign of P_1. In order to distinguish the two regimes, we have to calculate more harmonics, and this is necessary also for the distinction between square and rectangle signals.

[38]The period needs to be split into $1/\beta$ points, and high order matrices need to be studied for the position of eigenvalues with respect to unity. This issue was investigated in numerous articles about bowed strings [122].

9.4.8.4 Considerations About the Spectrum of Conical Instruments

The question of the relation between the conical shape and the sound spectrum remains largely open, in particular for the radiated sound. The simplification of the signal shape shown in Fig. 9.20 obviously yields the suppression of higher frequencies in the spectrum. However, for a clarinet we have seen that the simplified square signal yields relevant results for the signal amplitudes, the oscillation regimes, and the amplitude of the first odd harmonics far from the oscillations threshold. This simplification corresponds to a model with losses independent of frequency, or lossless. For a conical instrument, a supplementary approximation was needed. The hypothesis that it is equivalent to a cylindrical saxophone is only valid over a limited frequency range, because the length of the missing cone, denoted x_1, is assumed to be small compared to the wavelength[39] We have seen that the pressure signal when the reed is beating is common to the different notes, and we can suppose that:

- Characteristic frequencies common to different notes exist in the spectrum, including higher frequencies, and a consequence is the apparition of formants or anti-formants;
- For the lowest ones, the common frequencies are the same as those of a cylindrical saxophone

Internal Spectrum

Let us consider first the spectrum of the internal pressure at low frequencies. We can imagine without rigorous proof that the maximum of this spectrum is linked to that of the input impedance. The latter can be determined by using Eq. (7.105), which describes the envelope curve of the impedance peaks of a truncated cone. The envelope is proportional for all notes to the following function:

$$\frac{1}{1+\frac{1}{k^2x_1^2}}\frac{1}{\sqrt{kx_1}}.$$

A simple calculation gives a rough estimation for the position of this maximum: $kx_1 = \sqrt{3}$. A formant can be found around the corresponding frequency. For instance, for a soprano saxophone, it is 670 Hz. For the lowest notes of an instrument, there are few low harmonics (1 and 2) in the spectrum because of the shape of the input impedance curve.

- At higher frequency, we examine first the case of a cylindrical saxophone. The first characteristics of the spectrum is necessarily the absence of a certain

[39]Thanks to the choice of the mouthpiece dimensions and instrument input, this limit can be put off rather high, see Chap. 7. For instance, let us assume that the limit is around $kx_1 = 1$.

category of harmonics, similarly to the absence of even harmonics for the clarinet. When the ratio β ($= x_1/L$) is the inverse of an integer, the harmonics m/β should be absent. Because the fundamental of the first register is $c/2L$, this corresponds to frequencies $mc/2x_1$, which are the natural frequencies of a pipe of length x_1. As they do not depend on the played note, an anti-formant is expected at these frequencies, which are such that $kx_1 = m\pi$. The anti-formant can exists also if β is irrational, but they are less pronounced because there are no harmonics at exactly these frequencies.

- What happens for a conical instrument? Obviously if the quantity kx_1 is of order of π or larger, the use of a cylindrical saxophone model becomes meaningless. Nevertheless it is possible to find frequencies which are independent of the notes and for which the input impedance is minimum (and other frequencies for which the input impedance is maximum). We start from Eq. (9.105), and ignore the losses. As we have seen, an excellent approximation for the frequency of the first maximum at the mouthpiece input is $c/2(\ell + x_1)$. Hence $k(\ell + x_1) = \pi$. We know that it is not exactly the playing frequency, because the latter depends on the excitation level, but we assume that it is valid. The harmonics of this frequency are not necessarily resonance frequencies, because they do not satisfy the condition $kx_1 \ll 1$. However, the harmonic n satisfies

$$k(\ell + x_1) = n\pi \quad \text{thus} \quad \cot k\ell = \cot(n\pi - kx_1) = -\cot kx_1. \tag{9.120}$$

In other words, for a given frequency which exists in the spectrum, the input admittance of the truncated cone (and therefore the admittance at the input of the mouthpiece) does not depend on the fingering, i.e., on the played note. These admittances exhibit extrema which are common to the different notes, as shown in Fig. 9.22. Hence in the spectrum of the internal pressure formants and anti-formants are expected. They are the elements common to the different notes that we mentioned above. They can be calculated for a given shape of the mouthpiece, but here we do not discuss this matter further. The first anti-formant is slightly higher than that of a cylindrical saxophone ($kx_1 = \pi$). But these formants and anti-formants are less accentuated than those of a cylindrical saxophone, because losses make their presence less obvious.

External Spectrum

The previous analysis was focusing on the internal spectrum. What happens for the radiated pressure? For the lowest frequencies the previous reasoning can be extended by straightforward use of the shape of the input impedance curve. The scarcity of the lowest frequencies in the spectrum of the internal pressure is accentuated by the fact that the radiated pressure is the time derivative of the output flow rate. This is clearly observed, e.g., in the spectrogram of bassoon (see Fig. 7.26 of Chap. 7).

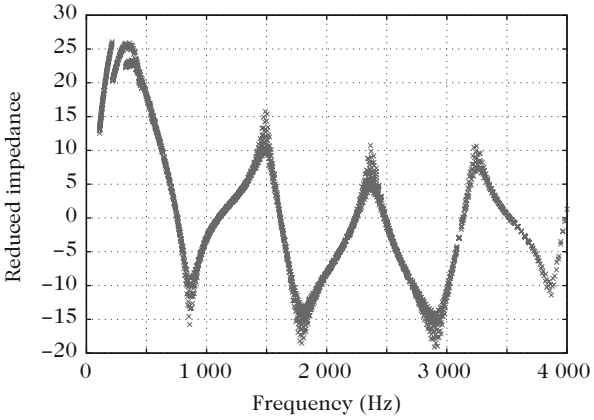

Fig. 9.22 Input impedance for 100 values of ℓ linearly distributed on one octave. The visco-thermal losses are taken into account. The points indicate the impedance modulus for the fundamental frequency and its harmonics for the notes corresponding to each length value. Above 500 Hz, extrema common to the different notes are clearly observed. Minima are found around 800, 1800, 2900 Hz. The dimensions are those of a tenor saxophone with a mouthpiece. The toneholes are ignored (the change of note is obtained thanks to a modification of ℓ). Courtesy of S. Karkar

Unfortunately for the higher frequencies we do not have much insight. Formants and anti-formants exist, but they are less pronounced and their position differs from that observed in the spectrum of the internal pressure. We saw that for a cylindrical instrument the issue of the relative amplitude of the even and odd harmonics is subtle. We imagine that this subtlety is similar for a cylindrical saxophone for the main harmonics versus the missing ones. The problem becomes even more intricate for a conical instrument.[40]

What is clear is that the level difference between formants and anti-formants is much smaller than for the internal pressure, as for the difference between even and odd harmonics of the clarinet.[41] Nevertheless, contrary to some possible hypotheses, the position of the formants is not directly linked to the length x_1 of the missing cone or to the mouthpiece shape.

The previous analysis shows that if the length x_1 of the missing cone is reduced, and then if for a given length, the apex angle is increased, the first characteristic frequencies increase. Observing the increase of the taper from the first saxophones of Adolphe Sax to modern saxophones, it is possible to explain this increase by the aim to enrich the timbre [74], as probably requested by jazz music. In comparison to a violin, this would correspond to a play closer to the bridge. It is well known

[40]Remember that this discussion ignores the existence of toneholes, which strongly complicate the sound analysis above the cutoff frequency (see Chap. 14). Moreover the reed dynamic also is ignored.

[41]This is due to the difference between the input impedance and the pressure transfer function: the first function of the frequency has poles and zeros, while the second has poles only.

that the timbre is richer in harmonics because the first missing harmonic becomes higher (similarly to what happens when playing a guitar close to the bridge).

Finally we mention the study by Benade and Lutgen [13], who measured the external spectrum averaged in a room and showed for the highest frequencies the existence of a frequency above which the amplitude of the pressure spectrum decreases as f^3: this frequency would be linked to the cutoff frequency of the toneholes lattice. Moreover they showed that minima exist in the spectrum of a given note, and that this is related to the reed beating. To our mind many issues require further studies in this matter.

9.5 Behavior of the 3-Equation Model with Reed Dynamics (Non-beating Reed)

9.5.1 Introduction

Synthetic sounds show that what instrumentalists call "squeaks" for single reed instruments are sounds with a frequency close to that of the (first) reed resonance. A beginner has to learn how to avoid them, by intuitively controlling the reed damping with his lower lip. The 3-equation model (9.26)–(9.28) can explain the relevance of this intuition. Two parameters need to be added to the study of Sects. 9.3 and 9.4: the damping factor and natural frequency of the reed, because the reed is assumed to be a single-degree-of-freedom oscillator. At the same time it is possible to study what happens when the playing frequency is close to the reed natural frequency. It is the case for reed instrument for notes belonging to the high part of the compass. It is also the case for reed organ pipes for which the reed resonance determines the playing frequency and the resonator role is limited to a coloring of the sound: these pipes are tuned by modifying a tuning spring. It can be said that the corresponding regime is the "reed regime," as opposed to the "resonator regime": this opposition was largely explored by Bouasse [17]. The case of lip-reed instruments is an intermediate case because the natural frequency of the reed (i.e., of the lips) needs to be very close to that of the resonator, yielding a strong coupling.

In order to solve the three dimensionless equations (9.26)–(9.28), the assumption of square signals is no more suitable, because the reed resonance modifies the spectrum. Notwithstanding some approximations remain possible. We start by focusing our attention on the instability threshold of the static regime, by using the characteristic equation (see Sect. 9.4.2) and supposing that the reed does not beat, because the amplitudes are extremely small near the threshold. To this end we base our study on the work by Wilson and Beavers [121], noted as WB, which is an important milestone in the research on reed instruments.[42] We first consider an

[42]What is the most important for the determination of the pitch? Is it the reed or the resonator? Historically it was one of the most important subjects of musical acoustics. We can cite Weber

inward-striking reed, later an outward-striking one. The latter was not considered up to now because they cannot function for frequencies which are very low compared to the reed natural frequency.

9.5.2 Oscillation Threshold for an Inward-Striking Reed

The previous presentation needs to be completed. Actually, two effects of the reed need to be distinguished: (1) the reed dynamics, and (2) the volume flow rate created by the reed displacement, which modifies the equation of the resonator [see Eq. (9.18)]. The distinction between these two effects is rather subtle, as this will be explained in the present section. The historical development can be summarized as follows:

Effect of the Reed Displacement

Helmholtz [68] and many authors tried to understand the effect of the flow rate in order to compare instruments such as clarinets with instruments such organ reed pipes. For the first type, the parameter defined as the ratio of the pipe resonance frequency to the reed resonance frequency is small, and the reed has a small influence on the playing frequency. Conversely for the latter type, the same ratio is large, and the playing frequency is close to the reed resonance frequency. For this study, a linear theory is used, assuming that the playing frequency is the resonance frequency of a composite resonator, i.e., the air column coupled to the reed. The reed dynamics is ignored, and therefore the reed acts as a simple spring. This leads to a simple transcendental equation, which describes the transition of the playing frequency from the pipe resonance to the reed resonance, when the pipe resonance frequency increases up to the reed resonance frequency.

Effect of the Reed Dynamics

How is it possible to proof that, when the reed dynamics is ignored, the playing frequency is the resonance of the composite resonator? Actually, this is true at the threshold of oscillation, as shown by the characteristic equation (9.78) which has been written in Sect. 9.4.2. It involves the input admittance of the composite resonator. It is obtained by linearizing the nonlinear equation of the excitor, and

[118], Helmholtz [68], and Bouasse [17], who performed a thorough literature review. He discussed all works of his time with many experimental results, which remain to be studied in detail. Works on valves with weak coupling of two resonators can also be cited [49, 108] (for us one of the resonators would be the vocal tract).

yields the value of both the operating (or playing) frequency, and the mouth pressure. For the nonlinear model proposed in this chapter, the latter is found to be equal to the third of the closure pressure p_M, whatever the ratio pipe-resonance frequency/reed-resonance frequency.[43]

One century after Helmholtz, Wilson, and Beavers were the first authors to propose a model based on the Bernoulli equation. They tried to take the reed dynamics into account, considering a single-degree-of-freedom oscillator. However, they ignored the effect of the reed flow. The solving is based anew on the derivation of the characteristic equation, which is much more complicated than when ignoring the reed dynamics. Concerning the dependence of the playing frequency with respect to the ratio pipe frequency/reed frequency, it seems to be similar to that found for the other effect (no reed dynamics, but the reed flow is considered). However, the deviation from the pipe resonance frequency is much smaller than that found for the reed flow effect. Moreover, when taken into account both effects, the effect of the reed flow appears to be dominant (this has been explained in [101]). Conversely the effect of the reed dynamics on the mouth-pressure threshold can be dominant, and is strongly influenced by the quality factor of the reed. For a strongly damped reed (for instance the clarinet reed, which is strongly damped by the player lip), the pressure threshold is close to $p_M/3$. However, for a slightly damped reed, the pressure threshold is largely lowered, and this explains why squeaks are obtained with a clarinet when the reed is insufficiently damped by the lip.

The present section considers first the two effects together.

9.5.2.1 Characteristic Equation, Real Frequency Solution for the Thresholds

We start from the three equations (9.26)–(9.28), by slightly modifying them. The two first equations can be written in the frequency domain[44]:

$$U = YP + j\omega X \Delta\ell/c \tag{9.121}$$

$$X = DP \quad \text{where } D(\omega) = \left[1 + \frac{j\omega q_r}{\omega_r} - \frac{\omega^2}{\omega_r^2}\right]^{-1}. \tag{9.122}$$

As WB did [121], we derive the characteristic equation, but we wish also to investigate the effect of the reed displacement flow rate, which is proportional to

[43]Notice that these results are valid if the threshold of oscillation is equal to the threshold of instability of the static regime, i.e., if the bifurcation is direct. This is the case for a clarinet or an organ reed pipe.

[44]Remind the notations: U is the volume flow rate, P is the pressure at the resonator inlet, X the reed displacement, Y the admittance at the resonator inlet. γ is the mouth pressure, ζ is the reed parameter. All quantities are dimensionless (see Sect. 9.2.5.3). $\Delta\ell$ is the length associated to the reed flow rate, ω_r the reed angular frequency, and q_r^{-1} its quality factor.

$\Delta\ell$, and was ignored by these authors. We linearize Eq. (9.28) around the static regime ($p = x = 0$), assuming again the zero frequency impedance to be zero:

$$u = \zeta\sqrt{\gamma}(1-\gamma)\left[1 + \frac{x}{1-\gamma} - \frac{p}{2\gamma}\right]. \tag{9.123}$$

Writing this equation in the frequency domain and limiting it to a single harmonic, using the two linear equations (9.121) and (9.122), and finally dividing the two sides of the equation by P_1, we find the characteristic equation:

$$Y + Dj\omega\frac{\Delta\ell}{c} = \zeta\sqrt{\gamma}\left[D - \frac{1-\gamma}{2\gamma}\right]. \tag{9.124}$$

This equation generalizes the relation $Y = A$ that we obtained in Sect. 9.4.2: this can be checked by writing $\Delta\ell = 0$. and $D = 1$. We determine the thresholds by solving this equation for a real frequency ω. We assumed that we are around a static, non-beating regime and have linearized the nonlinear equation: the quantities x and p being small, the non-beating reed condition for the static regime is simply[45] as $\gamma < 1$. Thus results such with $\gamma > 1$ are not relevant, even if in certain cases the following analysis can lead to such values.

9.5.2.2 Results of Wilson and Beavers for a Cylinder

We present hereafter the experimental result of WB and compare them with numerical solutions of Eq. (9.124) (see [101]). The latter slightly differs from those of WB, especially because we take into account the reed displacement flow rate. Then analytical approximate results are provided.

- The results shown in Fig. 9.23 correspond to a weak damping of the reed (of type metallic organ reed, $q_r = 0.008$). The abscissa is the product $k_r\ell$. For a given reed frequency (here $f_r = 700\,\text{Hz}$), it is proportional to the length. Thus these curves are obtained when the tube length varies, e.g., with a slide. For a given length, several solutions, which correspond to different tube modes, are possible. Only the oscillation frequency with the lowest pressure threshold is indicated. The reed parameters were measured using different techniques. The thresholds were measured by increasing the blowing pressure until a sound is produced (in this study the bifurcation is assumed to be direct).

  It can be observed that the threshold frequencies are always lower than the natural frequencies of both the reed and the resonator. The latter are given by decreasing hyperbolas (in dotted lines) by $\cot k\ell = 0$, or $k\ell = (2n-1)\pi/2$,

[45] It would be tedious to go beyond this value for solving the complete equation (9.30): indeed if for $p = 0$, the function $F(p)$ is regarded as a function of γ, its derivative is not continuous in $\gamma = 1$. Moreover we know that the model slightly disagrees with experiment.

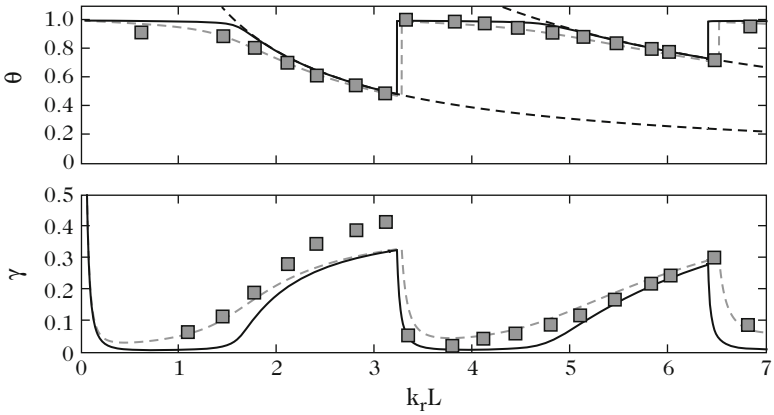

Fig. 9.23 Thresholds of frequency θ and of mouth pressure γ for a weakly damped reed. $q_r = 0.008$; $\zeta = 0.1$; $f_r = 700$ Hz ; $r = 6.4$ mm. *Solid line*: theoretical results [101] without reed displacement flow rate, corresponding to the calculation by Wilson and Beavers [121]; *dashed line*: theoretical results with the reed displacement flow rate ($\Delta\ell = 5$ mm); *dotted line*: hyperbolas of the natural frequencies of the resonator. The *squares* are the experimental results by WB

i.e., $\theta = \omega/\omega_r = (k_r\ell)^{-1}(2n-1)\pi/2$. When the length increases initially the frequencies of the first regime are obtained, then those of the second one, followed by the third one, etc. The pressure thresholds differ drastically much from the value predicted by the model without losses and reed dynamics, $\gamma = 1/3$. They can reach values smaller than $1/20$, because the reed greatly favors the oscillation when ω/ω_r is close to unity. But when $k_r\ell$ approaches the values $n\pi$ from below, the functioning is very similar to the functioning without reed dynamics, i.e., the playing frequency corresponds to a tube resonance, with a pressure threshold close to $1/3$. Then suddenly the solution corresponding to the following regime appears, because its threshold is much lower, and the playing frequency is close to the reed natural frequency. Consequently for a long tube the reed favors either "squeaks" when $k_r\ell$ is close to $n\pi$, or approaches acoustic resonance frequencies when $k_r\ell$ is far from these values.

- Now let us look at Fig. 9.24, for which the reed damping is strong, $q_r = 0.4$ (the reed is of clarinet-type). The variation of the playing frequencies is qualitatively similar to that for a weak damping but squeaks cannot be obtained, because the pressure thresholds would be very high. These thresholds are much closer to the thresholds that we have calculated without reed dynamics [Eq. (9.69)]. And the thresholds of the higher order regimes become higher than those of the first regime. This allows keeping the first acoustic regime for any length, and prevents the production of the other regimes. Because the reed is more damped than in the previous case, its role is weaker in the variation of the pressure thresholds and the resonator acoustic losses play a much greater role.[46]

[46]Notice that it is easy for a clarinet to obtain squeaks by driving the mouthpiece in the mouth in order to suppress the damping by the lip.

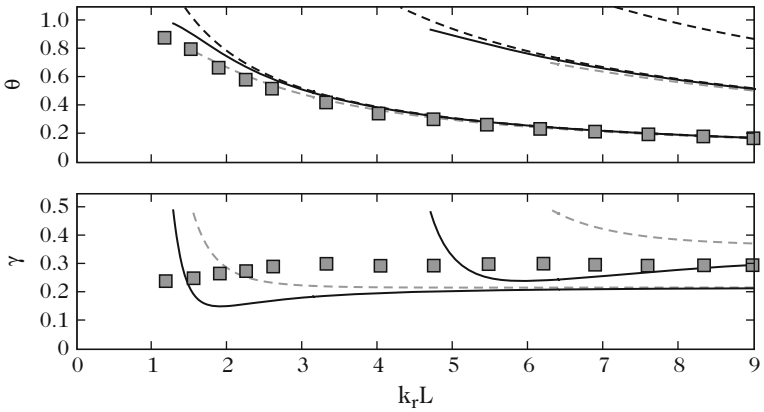

Fig. 9.24 Thresholds of frequency θ and of mouth pressure γ for a strongly damped reed. $q_r = 0.4$; $\zeta = 0.13$; $f_r = 750\,\text{Hz}$; $r = 6.4\,\text{mm}$. *Solid line*: theoretical results [101] without reed flow rate, corresponding to the calculation by Wilson and Beavers [121]; *dashed line*: theoretical results with reed flow rate ($\Delta\ell = 12\,\text{mm}$); *dotted line*: hyperbolas of the natural frequencies of the resonator. The *squares* are the experimental results by WB

9.5.2.3 Analysis of Threshold Frequencies

For the analysis we simplify the problem by ignoring (for the moment) both the reed displacement flow rate and the acoustic losses in the resonator. The admittance Y is purely imaginary. For a cylinder of length ℓ, $\Im m(Y) = -\cot k\ell$. For a resonator of arbitrary shape, we reduce the admittance to one mode, of subscript n, and even to one "single" mode, of positive frequency (see Chap. 2). This implies that we search for a frequency that is not too far from the natural frequency of the resonator. We rewrite Eq. (9.66) in the following form (see Chap. 2):

$$Y \simeq 2jF_n^{-1}(\omega - \omega_n^+) \text{ where } \omega_n^+ = \omega_n + j\omega_n/(2Q_n), \text{ thus} \quad (9.125)$$

$$\Im m(Y) \simeq 2F_n^{-1}(\omega - \omega_n) \quad (9.126)$$

(remind that for a cylinder, $2F_n^{-1} = \ell/c$). If $\Re e(Y) = 0$ and $\Delta\ell = 0$, the separation of the real and imaginary parts of the characteristic equation yields

$$\frac{1-\gamma}{2\gamma} = \Re e(D) = \frac{1}{\eta}. \quad (9.127)$$

$$\Im m(Y) = \Im m(D)\zeta\sqrt{\gamma} = -\frac{\zeta\sqrt{\gamma}\theta q_r}{\eta(1-\theta^2)}, \quad (9.128)$$

where:

$$\theta = \frac{\omega}{\omega_r} \text{ and } \eta = \frac{1}{\Re e(D)} = 1 - \theta^2 + \frac{q_r^2\theta^2}{1-\theta^2}. \quad (9.129)$$

The parameters ζ, q_r, ω_r, and those of the resonator are fixed, thus two unknowns remain for the characterization of the threshold: the threshold frequency θ and the mouth pressure γ (for the sake of simplicity, the subscript th has been omitted). The calculation seems to be tedious, but some results are surprisingly simple and informative. We first retrieve the results obtained without reed dynamic ($\theta = 0$): because in such a case $\eta = 1$, $\gamma = 1/3$ and $\Im m(Y) = 0$. Then Eq. (9.127) yields

$$\gamma = \frac{\eta}{2+\eta}. \tag{9.130}$$

This can be brought in Eq. (9.128), therefore, for a cylinder, the following result is obtained

$$-\Im m(Y) = \cot k\ell = \cot k_r \ell\theta = \zeta F(\theta) \tag{9.131}$$

$$\text{where } F(\theta) = q_r\theta\left[(1-\theta^2)^2 + q_r^2\theta^2\right]^{-1/2}\left[(3-\theta^2)(1-\theta^2) + q_r^2\theta^2\right]^{-1/2}.$$

Equation (9.131) has only one unknown, ω, or $\theta = k\ell/k_r\ell$ when $k_r\ell$ is fixed. Up to $\theta = 0.8$, the function $F(\theta)$ has a nearly linear variation with respect to $q_r\theta$, thus it is proportional to q_r. A numerical calculation shows that the increase is monotonous from 0 to $1/q_r$ when θ varies from 0 to 1 (see Fig. 9.25). Thus for two different values of q_r, the curves intersect very close to $\theta = 1$. Because $F(\theta)$ is positive, the cotangent function is always positive and the solutions are always below the hyperbolas $\cot k\ell = 0$, whose solutions are $\theta = (k_r\ell)^{-1}(2n-1)\pi/2$ (see Figs. 9.23 and 9.24). For a one-mode resonator, a similar result can be obtained: following Eq. (9.125), the solutions are smaller than the natural frequencies of the resonator:

$$\omega = \theta\omega_r = \omega_n - \frac{1}{2}\zeta F_n F(\theta). \tag{9.132}$$

The previous explanation is not a rigorous proof because the unknown ω is included in $F(\theta)$, but it is undoubtedly correct when ζ is not too large.[47]

- *For the case of a strongly damped reed*, the quantity $\zeta F(\theta)$ is rather large except near $\theta = 1$, where there is no solution. Thus the threshold frequencies are rather far from the resonator natural frequencies, roots of $\cot k\ell = 0$ (i.e., $k\ell = (2n-1)\pi/2$): it should be remembered that a weak relative difference can be important from the musical point of view, because one semitone corresponds to 6 % in the frequency. In order to calculate the threshold frequencies with a good accuracy, it is possible to use perturbations, bringing into the second member of Eq. (9.132),

[47] We know that the results with $\gamma > 1$ are not relevant, because they correspond to a complete closure of the mouthpiece. According to Eq. (9.127), this corresponds to $\eta < 0$ and therefore to $\theta > 1$. With this theory we cannot know determine whether the playing frequency can exceed the reed resonance or not.

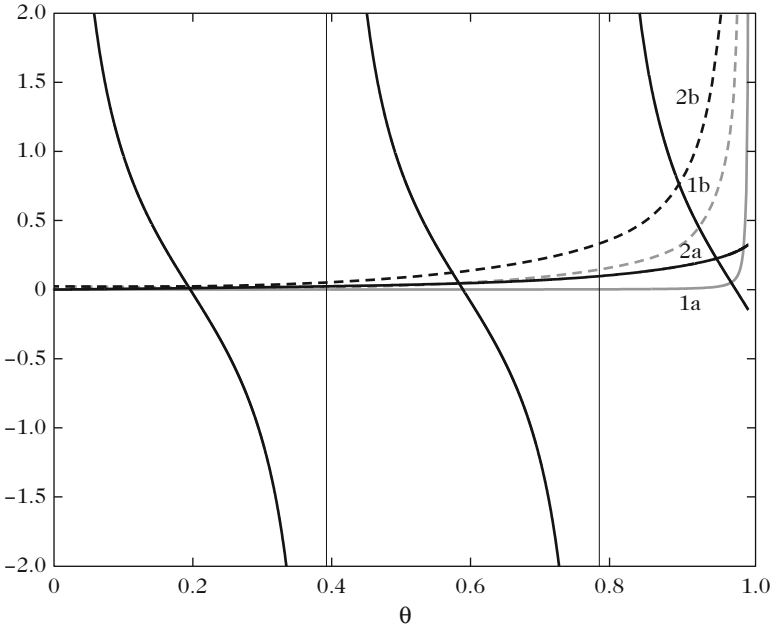

Fig. 9.25 Comparison of the function $\cot k_r \ell\theta$ for $k_r\ell = 8$ (*thin line*) and the function $\zeta F(\theta)$ for the two cases shown in Figs. 9.23 (*solid line 1a*) and 9.24 (*solid line 2a*). It is observed that the playing frequencies are smaller than the natural frequencies of the tube which cancel the cotangent function $F'(\theta)$, [Eq. (9.138)]. The latter represents the effect of the reed displacement flow rate, which is predominant near the reed resonance for both cases

the values of k we found with $\theta = k/k_r$. The variation of frequency due to damping can be written in the form of a length correction, equal to:

$$\Delta\ell = \zeta F(\theta)/k = \zeta F(\theta)/(\theta k_r).$$

Then, because in this case θ is small compared to unity, the square roots involved in $F(\theta)$ can be simplified by ignoring the terms in $q_r\theta$, giving:

$$\Delta\ell = \frac{q_r\zeta}{k_r(1-\theta_n^2)^{3/2}(3-\theta_n^2)^{1/2}}, \tag{9.133}$$

where $\theta_n = (2n-1)\pi/(2k_r\ell)$. Hence this length correction is positive. It is proportional to the reed damping and inversely proportional to the reed frequency. This was expected, because the correction needs to vanish when the latter tends to infinity. For a sufficiently high reed frequency, the denominator simplifies to $k_r\sqrt{3}$.

- *The case of a weakly damped reed* is not very different regarding frequencies: however, the quantity $\zeta F(\theta)$, which is ζ/q_r for $\theta = 1$, can be very large near

this value of θ, thus the frequencies are far from the tube natural frequencies. The quasi horizontal portion of the frequency curve starting from the values $k_r\ell = n\pi$ is longer than in the case of a strong damping. This seems to be obvious because when there is no damping the reed dynamic plays a more important role, and the threshold frequencies are more distant from the tube natural frequencies. However, for small values of the solutions θ, they are closer to the tube frequencies than for a strongly damped reed.

9.5.2.4 Threshold Pressures

For the threshold pressure, the main result is shown in Fig. 9.23: its variation is rather strong with the tube length or the reed natural frequency (parameter $k_r\ell$). When the playing frequency approaches the tube frequencies, the quantity η becomes close to unity, corresponding to a threshold pressure close to $1/3$ [in fact its value is slightly higher, because of the tube losses, see Eq. (9.69)].

The minima of threshold pressure can be easily determined because γ is a monotonously increasing function of η. The study of the function $\eta(\theta)$ [Eq. (9.129)] shows that it has one minimum, for $\theta_c^2 = 1 - q_r$. Its value is $\eta_{\min} = q_r(2 - q_r)$, and, using Eq. (9.130) the minimum of γ is

$$\gamma_{\min} = \frac{q_r(2 - q_r)}{2 + q_r(2 - q_r)}. \tag{9.134}$$

For a weak damping q_r, this expression simplifies in $\gamma_{\min} \simeq q_r(1 - 3q_r/2)$. For a strong damping, the minima $\gamma_{\min}$ are higher. However, we did not take into account the tube losses, and this expression cannot explain why the second minimum is higher than the first (see Fig. 9.24). Therefore this analysis should be refined further, because such a difference can be responsible for the jump to the second register (twelfth register), even without register hole, and consequently is important from a musical point of view.

The search for the value of $(k_r\ell)_{\min}$ at which there is a minimum of threshold pressure can be done using Eq. (9.132). The first order approximation $\theta \simeq 1 - q_r/2$ yields

$$F(\theta) = \frac{1 - 3q_r/4}{2\sqrt{q_r}}, \text{ and } \omega_n = \omega_r\left[1 - \frac{q_r}{2}\right] + \frac{\zeta F_n}{4\sqrt{q_r}}\left[1 - \frac{3q_r}{4}\right]. \tag{9.135}$$

For a cylinder:

$$k_r\ell = (2n - 1)\frac{\pi}{2}\left[1 + \frac{q_r}{2}\right] - \frac{\zeta}{2\sqrt{q_r}}\left[1 - \frac{q_r}{4}\right]. \tag{9.136}$$

For a strong damping, the second term remains small and the order of magnitude is given by $(k_r\ell)_{\min} = (2n-1)\pi/2$; when the damping decreases, the values of $(k_r\ell)_{\min}$ decrease significantly.[48]

What is the influence of resonator losses, that we have ignored up to now? A general idea can guide us: if reactive phenomena have a great influence on the frequencies, it is not the case of dissipative phenomena. However, the latter have an influence on the threshold pressure and need to be considered. A detailed calculation can be found in [101], and gives the following result:

$$\gamma_{\min} = \gamma_0 \left[1 + 2Y_{mn}\sqrt{\gamma_0}/\zeta\right]. \tag{9.137}$$

γ_0 is the value when tube losses are ignored [Eq. (9.134)], and $Y_{mn} = 1/Z_{Mn}$ [see Eq. (9.66)] is the minimum admittance of the tube, equal to $\alpha\ell$ for a cylinder (where α is the loss coefficient of the tube). As expected it appears that the minimum increases when the length increases, and that it is larger for the second register than for the first one.

9.5.2.5 Effect of the Reed Displacement Flow Rate

Figures 9.23 and 9.24 show that near the reed resonance, the effect of the reed displacement flow rate on the threshold frequencies is more important than that of damping. A complete calculation is difficult, therefore we limit the study to the threshold frequencies by ignoring the reed dynamic, in order to compare the two effects separately. Equation (9.124) shows that the reed displacement flow intervenes as a simple (reactive) modification of the input admittance of the resonator. If $q_r = 0$, the left member of (9.124) is imaginary and determines the frequencies, while the right member is real and imposes the pressure. Equation (9.131) leads to the definition of a new function, $F'(\theta)$:

$$-\Im m(Y) = k\Delta\ell\frac{1}{1-\theta^2} = F'(\theta) \quad \text{where} \quad F'(\theta) = k_r\Delta\ell\frac{\theta}{1-\theta^2}. \tag{9.138}$$

The quantity $k_r\Delta\ell$ is small.[49] For small values of θ, the right members of Eqs. (9.138) and (9.131) have the same order of magnitude. However, close to the

[48] *Above the values* $(k_r\ell)_{\min}$, Fig. 9.24 shows also the growth of the three branches of the curve $\gamma(k_r\ell)$. The second branch growths slower than the first, and the third growths slower than the second, because the frequencies are less and less remote from the reed resonance (θ does not take small values for the branches corresponding to higher regimes). *Below the values* $(k_r\ell)_{\min}$, the growth is very fast, because between θ_c and $\theta = 1$, γ increases from $\gamma_{\min}$ to a value close to 1 (infinite η).

[49] The order of magnitude of $\Delta\ell$ can be estimated to 1 cm, by measuring the playing frequencies when they are close to the resonance frequencies of the tube [32]. From the data of Figs. 9.23 and 9.24, the following values are obtained, respectively: $k_r\Delta\ell = 0.06$ and 0.16.

reed resonance ($\theta = 1$), the reed displacement flow term becomes much larger than the reed dynamics one. This is shown in Fig. 9.25. Indeed the function $\theta/(1-\theta^2)$ is increasing from 0 to infinity when θ increases from 0 to 1 (it resembles the function $F(\theta)$, but the latter is limited to a finite value, $1/q_r$).

In order to solve Eq. (9.138) in the case of a one-mode resonator, Eq. (9.126) is used

$$\theta = \theta_n - \frac{1}{2}\frac{\theta F_n \Delta\ell}{c(1-\theta^2)} \quad \text{where} \quad \theta_n = \frac{\omega_n}{\omega_r}. \tag{9.139}$$

For a cylinder, in the limit of small θ, the reed displacement flow effect is reduced to a simple length correction, as explained when defining $\Delta\ell$ [see Eq. (9.17)]. Indeed the result is $f = \dfrac{(2n-1)c}{4(\ell+\Delta\ell)}$. Obviously this can be improved by a perturbation calculation [75]. Nevertheless the problem is more complicated close to the reed resonance: if θ tends to unity, $\Im m(Y)$ tends to infinity, and we approach the anti-resonances of the tube. For certain lengths of the tube, when $k_r\ell$ corresponds to a tube anti-resonance, the playing frequency is the reed natural frequency. If θ is close to unity, the solution can be sought in the form $\theta = 1-\varepsilon$, writing $\theta_n = 1-\varepsilon_n$, and this leads to a quadratic equation in ε:

$$2\varepsilon(\varepsilon - \varepsilon_n) = \beta(1 + O(\varepsilon)),$$

where $\beta = \frac{1}{2}F_n\Delta\ell/c$ is small (it is equal to $\Delta\ell/\ell$ for a cylinder). Therefore:

$$\varepsilon = \frac{\varepsilon_n}{2}\left[1 + \sqrt{1 + \frac{2\beta}{\varepsilon_n^2}}\right]. \tag{9.140}$$

The square root comes typically from mode coupling. This explains why, as soon as we are interested in more complicated problems, it is extremely difficult to find analytical solutions. The principle of this study should be emphasized: we sought the playing frequencies at the threshold by calculating the frequencies for which the imaginary part of the passive resonator admittance vanishes. The passive resonator consists of the tube and the reed, while the effect of the flow coming from the mouth is totally ignored. Historically this approach was used by many authors (see, e.g., [83]) and give often interesting results, because the reed displacement flow has an effect preponderant over the reed dynamic. The theoretical curves of the playing frequencies can be fitted with experimental results, and a reasonable value of the reed displacement flow rate is obtained. This allows predicting threshold frequencies, but the measurement of the threshold pressure remains difficult.

9.5.3 Oscillation Threshold for an Outward-Striking Reed

9.5.3.1 Characteristic Equation

We now investigate an outward-striking reed, which is the elementary model for lip reeds. There is a major difference with respect to the previous case: the closure pressure is negative, therefore the mouth pressure is always far from this pressure. Using a 3-equation model, we will show that the playing frequency is higher than that of the reed: a functioning in square signals is not possible, and we need to take into account the reed dynamic (in order to get square signals, it would be mandatory to inhale).

Using Eqs. (9.37)–(9.39), we obtain the characteristic equation, which is the counterpart of (9.124):

$$Y + Dj\omega\frac{\Delta\ell}{c} = \zeta\sqrt{\gamma}\left[-D - \frac{1+\gamma}{2\gamma}\right]. \tag{9.141}$$

We ignore the reed displacement flow rate, although its potential importance was not studied yet, and we ignore the losses in the tube. As a result:

$$\gamma = -\frac{\eta}{2+\eta}; \tag{9.142}$$

$$\Im m(Y) = \frac{\zeta\sqrt{\gamma}\theta q_r}{\eta(1-\theta^2)}. \tag{9.143}$$

9.5.3.2 Threshold Frequencies

Because of the sign of the second member of (9.143), the quantity $\eta(1-\theta^2)$ is always positive, and the playing frequencies are always higher than the natural frequencies of the tube (see Fig. 9.26). They are also higher than those of the reed, because positive γ implies negative η. Then, by bringing Eq. (9.142) into Eq. (9.143), we obtain an equation similar to Eq. (9.131):

$$\Im m(Y) = \zeta G(\theta) \tag{9.144}$$

$$\text{where } G(\theta) = q_r\theta\left[(1-\theta^2)^2 + q_r^2\theta^2\right]^{-1/2}\left[-(3-\theta^2)(1-\theta^2) - q_r^2\theta^2\right]^{-1/2}.$$

This implies

$$(3-\theta^2)(1-\theta^2) + q_r^2\theta^2 < 0. \tag{9.145}$$

This inequality is satisfied between the two roots θ_1 and θ_2 of a second order equation. As q_r is sufficiently small: $\theta_1 \simeq 1 + q_r^2/4$ and $\theta_2 \simeq \sqrt{3}(1 - q_r^2/4)$.

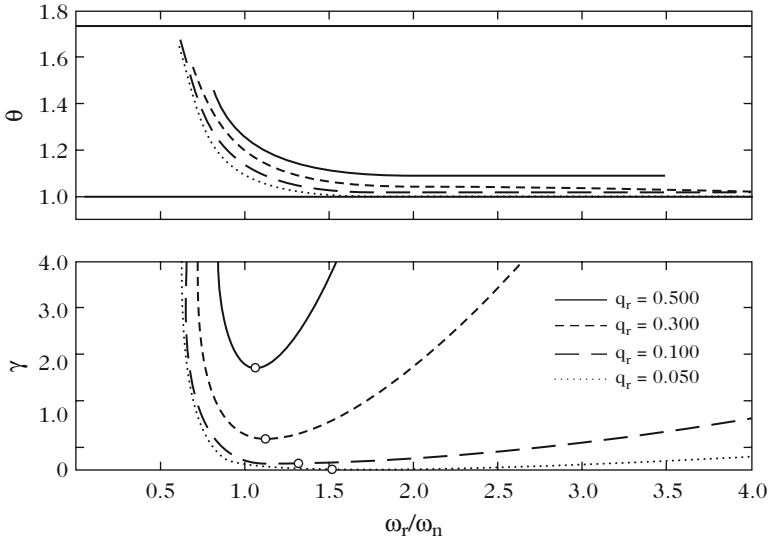

Fig. 9.26 Frequency and mouth-pressure thresholds for an outward-striking reed for different values of the reed damping

For inward-striking reeds, the value $\theta = 1$ can be reached from below. Here it cannot be reached, but θ can be rather close to unity. For the two extreme values, the tube would function at anti-resonances, but we will see that they cannot be reached. We do not write the equivalent of Sect. 9.5.2.5, but because the threshold frequency is higher than the reed frequency, the reed displacement flow produces again a cumulative effect with that of the reed dynamic. Indeed the reed flow term in Eq. (9.138) remains unchanged, but with $\theta > 1$. It increases the shift of threshold frequencies compared to the reed frequency or to the tube natural frequencies.

9.5.3.3 Threshold Pressure

Because $\theta > 1$, the quantity $\eta + 2$ needs to be positive [see Eq. (9.145)]. Thus η lies between -2 and 0. For the two limit values θ_1 and θ_2, for which $\eta = -2$, the threshold γ is infinite; therefore it is not possible, in practice, to play close to these values. For a fixed reed frequency, the interval which can be reached by changing the resonator length is significantly smaller than $\sqrt{3}$ (one sixth). Experimentally an interval of one third was found [29]. This enlightens the interest for brass instruments to have a reed with variable characteristics, that the player adapts to the tube length. This behavior greatly differs from that of an inward-striking reed, for which θ can vary from 0 to 1! The minima of γ can be calculated similarly to what was done in Sect. 9.5.2.4: according to Eq. (9.142), they correspond to maxima of η, thus to $\theta_c'^2 = 1 + q_r$, i.e., $\theta_c' \simeq 1 + q_r/2$, and they are:

$$\gamma_{\min} = \frac{q_r(2+q_r)}{2+q_r(2+q_r)}. \tag{9.146}$$

For a weak damping, this becomes $\gamma \simeq q_r(1-q_r/2)$, and is found to be slightly higher than for an inward-striking reed with the same parameters. Because the value $\theta_c'^2 = 1+q_r/2$ is quite close to θ_1, we observe that for a cylinder the curves of threshold pressure with respect to the parameter $k_r\ell$ display a strong asymmetry relative to the minimum (see Fig. 9.26). This result is in agreement with those of [29].

9.5.4 Modal Approach of the Dynamical System

In what follows we consider the analysis of the linearized system in terms of modes. An approximation of the characteristic equation (9.124) or (9.141) is obtained by expanding the input impedance in a modal series, similar to (9.66), and by truncating the series to the first mode of the resonator, as we did in Sect. 9.3.4. Considering the expression of $D(\omega)$, we obtain an equation of the fourth order in $s = j\omega$, which has real coefficients. This implies that if s is a solution, its conjugate s^* is a solution as well. Thus the four solutions are: s_1, s_1^*, s_2, s_2^*.

The characteristic equation is a polynomial, and $p(t)$ is the sum of exponentials of type $\exp(st)$. If the real part of both s_1 and s_2 are negative, the exponentials are decreasing, and the static solution $P_1 = 0$ is stable. It becomes unstable when one of the two real parts become positive. In other words if one real part is positive and the other vanishes, we get an instability threshold of the static regime. If the two real parts become positive, we have the sum of two increasing exponentials with different frequencies, which correspond to the imaginary parts of s_1 and s_2. It should be remembered that we do not know anything about the existence of oscillating solutions, because the nonlinear terms were suppressed, and obviously we do not know anything about their stability!

An approximation of the fourth order equation is obtained by ignoring the negative frequencies. This results in a quadratic equation. For the function $D(\omega)$ defined by Eq. (9.122), a treatment similar to that we did for the function $Y(\omega)$ [see Eq. (9.125)] can be done, with the following result:

$$D^{-1}(\omega) \simeq -\frac{2}{\omega_r}(\omega-\omega_r^+) \quad \text{where } \omega_r^+ = \omega_r + j\omega_r q_r/2. \tag{9.147}$$

For an inward-striking reed, the characteristic equation (9.124) becomes

$$(\omega-\omega_r^+)(\omega-\tilde{\omega}_n^+) = \frac{\omega_r F_n}{4}\left[j\zeta\sqrt{\gamma} + \frac{\omega\Delta\ell}{c}\right]$$
$$\text{with} \quad \tilde{\omega}_n^+ = \omega_n^+ + j\frac{F_n}{4}\zeta\frac{1-\gamma}{\sqrt{\gamma}}. \tag{9.148}$$

It exhibits two modes coupled by the flow from the mouth and the reed displacement flow. However, the mode of the tube itself is modified by the mouth flow, with an increase of the losses (as γ is lower than unity): this effect corresponds to the resistance due to the flow if the reed is prevented from vibrating around its average position, which is determined by the blowing pressure ($x = 0$). Therefore these two modes are passive (the imaginary parts of ω_r^+ and $\tilde{\omega}_n^+$ are positive). This approximation of the characteristic equation assumes that the playing frequency and the frequencies of both the tube and the reed do not differ much. The sum of the roots of this equation is

$$\omega_1 + \omega_2 = \omega_r^+ + \tilde{\omega}_n^+ .$$

Thus if one root, for example, ω_1, is real, the other root will have a positive imaginary part because the two modes are passive. In other words, when one of the exponentials which is decreasing becomes increasing, the other one is always decreasing. The thresholds we studied in Sect. 9.5.2.1 are *instability thresholds of the static regime*.[50] Similarly to what was done in Chap. 6 about piano strings (Sect. 6.3.2), it would be possible to discuss approximate solutions. A similar analysis can easily be done for an outward-striking reed.

9.5.5 Discussion of the Results

In the present section the role of the reed resonance has been examined together with the use of the damping for the control of the regimes for a cylindrical tube. For certain lengths of tubes, the effect of damping can be very important. This explains why it is not possible to have toneholes very close to the mouthpiece on a clarinet, because the tuning and the timbre would depend too much on the reed. The present section has been limited to the instability threshold of the static regime, for a cylindrical tube or a single-mode resonator. Implicitly the bifurcation has been assumed to be direct, while this is wrong in many cases, such as that of conical tubes. Consequently our study has drastic limitations. In addition the reduction of the reed vibration to a single mode is a supplementary limitation at higher frequencies, especially for brass instruments. No results have been obtained concerning the spectrum: the reader can refer to [110] or [54] (for results of the harmonic balance). Indeed the theoretical approach becomes much more difficult at higher frequencies, because the tube resonances become weaker and many other

[50] This does not demonstrate that considering an infinity of modes for the resonator this result would remain valid, but it is a reasonable hypothesis. Moreover we do not forget that the bifurcation can become inverse when a second mode is added to the resonator model, as it was seen for conical reed instruments, and maybe also if a second mode is added to the reed model (a reed with two modes seems to be necessary to model some behaviors of the excitor of brass instruments, see Fig. 9.3).

phenomena intervene: for instance the higher modes of the reed or the vocal tract can become important, and the radiation becomes more complicated, as it will be seen in the fourth part. However, thanks to this complexity, the playing of the higher notes is more flexible for the instrumentalist.

In the present section the addition of the two parameters of the reed dynamics implies complicated consequences on the effect of the main parameters on the playing frequency, the sound level or the spectrum. One aspect is the effect of inharmonicity of the excitation pressure (see Sect. 9.4.5), but few theoretical results has been published (see also [75]). Recently some advanced experimental studies has been published for reed instruments [4, 14, 19, 61, 62] and for brass instruments [42, 51].

The previous study gives us some insight on the free reeds (either without resonator, such as that of the accordion and harmonica, or weakly coupled to a resonator, such as organ reeds [48, 49, 84, 95, 108]). For these instruments, the playing frequencies are expected to be linked mainly to the reed resonance, and indeed the organ makers tune the reed tubes by moving the tuning spring (who plays the role of the lower lip of the clarinettists). Nevertheless they can choose a resonator with a resonance close to that of the reed. For a free reed, the damping is weak, and it can be accepted that the radiation impedance plays the role of a very short tube, and we expect that the thresholds correspond to very small values of $k_r\ell$ (see Fig. 9.23). Obviously this view is schematic, and this subject deserves longer developments.

Concerning brass instruments, it has been seen in Chap. 7 that the absence of toneholes implies the existence of a great number of significant modes for the resonator. The study of the regimes is a complex task, especially if two modes of the reed are taken into account. However, general ideas were already given by Benade [10]. The harmonicity of the impedance peaks 2, 3, 4, etc. allows playing notes without change in pitch related to the excitation level. The frequency of these notes corresponds to an impedance peak, and the harmonics to other peaks (for instance, consider peak 2, and peaks 4, 6, 8, etc. which are almost harmonically related). Moreover it is possible to play "pedal" sounds, whose harmonics correspond to a peak, except the fundamental. The theoretical study of the existence and stability of these regimes requires long computation, which is tedious but possible today.

Finally a general conclusion can be drawn concerning the influence of losses of every kind on the playing frequencies. Ignoring the losses leads to a first assessment of the frequencies, and with this approximation, the nonlinear excitation has no effect on the playing frequencies. This justifies the basic, fruitful approach (since Bernoulli): the playing frequencies were assumed to be the natural frequencies of the linear resonator. However, we have seen that for the examination of the transition between the "resonator regime" and the "reed regime," the reed damping needs to be considered and the parameters of the linearized excitation play a role [see Eq. (9.131)].

References

1. Adachi, S., Sato, M.: Trumpet sound simulation using a two-dimensional lip vibration model. J. Acoust. Soc. Am. **99**(2), 1200–1209 (1996)
2. Allwright, D.: Harmonic balance and Hopf bifurcation. Math. Proc. Camb. Philos. Soc. **82**, 453–467 (1977)
3. Almeida, A., Vergez, C., Caussé, R.: Quasistatic nonlinear characteristics of double-reed instruments. J. Acoust. Soc. Am. **121**(1), 536–546 (2007)
4. Almeida, A., George, D., Smith, J., Wolfe, J.: The clarinet: how blowing pressure, lip force, lip position and reed "hardness" affect pitch, sound level, and spectrum. J. Acoust. Soc. Am. **134**, 2247–2255 (2014)
5. Avanzini, F., Walstijn, M.V.: Modelling the mechanical response of the reed-mouthpiece-lip system of a clarinet. part i. a one-dimensional distributed model. Acta Acust. United Acust. **90**, 537–547 (2004)
   Acta Acustica united with Acustica
6. Backus, J.: Vibrations of the reed and the air column in the clarinet. J. Acoust. Soc. Am. **6**, 806–809 (1961)
7. Backus, J.: Small-vibration theory of the clarinet. J. Acoust. Soc. Am. **35**(3), 305–313 (1963)
8. Barjau, A., Agulló, J.: Calculation of the starting transients of a double-reed conical woodwind. Acustica **69**, 204–210 (1989)
9. Barjau, A., Gibiat, V.: Study of woodwind-like systems through nonlinear differential equations. Part II. Real geometry. J. Acoust. Soc. Am. **102**, 3032–3037 (1997)
10. Benade, A.H.: Fundamentals of Musical Acoustics. Oxford University Press, London (1976)
11. Benade, A.H., Gans, D.J.: Sound production in wind instruments. Ann. N. Y. Acad. Sci. **155**, 247–263 (1968)
12. Benade, A.H., Kouzoupis, S.N.: The clarinet spectrum: theory and experiment. J. Acoust. Soc. Am. **83**(1), 292–304 (1988)
13. Benade, A.H., Lutgen, S.J.: The saxophone spectrum. J. Acoust. Soc. Am. **83**(5), 1900–1907 (1988)
14. Bergeot, B., Almeida, A., Gazengel, B., Vergez, C., Ferrand, D.: Response of an artificially blown clarinet to different blowing pressure profiles. J. Acoust. Soc. Am. **135**, 479–490 (2014)
15. Bernoulli, D.: Physical, mechanical and analytical researches on sound and on the tones of differently constructed organ pipes (in French). Mem. Acad. R. Sci. **1764**, 431–485 (1762)
16. Bilbao, S., Torin, A., Chatziioannou, V.: Numerical modeling of collisions in musical instruments. Acta Acust. United Acust. **101**, 155–173 (2015)
17. Bouasse, H.: Wind instruments. In: Metallic and Membranous Reeds, Reed and Flue Pipes, Organ, Instruments with Horn Mouthpiece (in French), vol. 1, 2nd edn. Librairie Scientifique et Technique, Paris (1986)
18. Boutillon, X.: Analytical investigation of the flattening effect - the reactive power balance rule. J. Acoust. Soc. Am. **90**(2), 754–63 (1991)
19. Boutin, H., Fletcher, N., Smith, J., Wolfe, J.: Relationships between pressure, flow, lip motion, and upstream and downstream impedances for the trombone. J. Acoust. Soc. Am. **137**, 1195–1209 (2015)
20. Brod, K.: The clarinet as a bifurcation system: an application to the iterated map method(in German). Acustica **72**, 72–78 (1990)
21. Bromage, S., Campbell, D.M., Gilbert, J., Stevenson, S.: Experimental investigation of the open area of the brass player's vibrating lips. In: Forum Acusticum Budapest 2005, Budapest, Hungary, pp. 729–734 (2005)
22. Bromage, S., Campbell, D.M., Chick, J., Gilbert, J., Stevenson, S.: Motion of the brass player's lips during extreme loud playing. In: 8ème Congrès Français d'Acoustique, Tours, France, pp. 721–724 (2006)

23. Bromage, S., Campbell, D., Gilbert, J.: Open areas of vibrating lips in trombone playing. Acta Acust. United Acust. **96**, 603–613 (2010)
24. Campbell, M.: Brass instruments as we know them today. Acta Acust. United Acust. **90**, 600–610 (2004)
25. Castellengo, M.: Multiple sounds in wind instruments (in French). Report, IRCAM (1983)
26. Chen, J., Smith, J., Wolfe, J.: Pitch bending and glissandi on the clarinet: roles of the vocal tract and partial tone hole closure. J. Acoust. Soc. Am. **126**(3), 1511–1520 (2009)
27. Clinch, P.G., Troup, G.J., Harris, L.: The importance of vocal tract resonance in clarinet and saxophone performance, a preliminary account. Acustica **50**, 280–284 (1982)
28. Cremer, L.: The Physics of the Violin (Orig. "Physik der Geige"). MIT (orig.: Hirzel, 1981), Cambridge, MA (1984)
29. Cullen, J.S., Gilbert, J., Campbell, M.: Brass instruments: linear stability analysis and experiments with an artificial mouth. Acustica Acta Acustica **86**(4), 704–724 (2000)
30. Dalmont, J.P., Frappé, C.: Oscillation and extinction thresholds of the clarinet: comparison of analytical results and experiments. J. Acoust. Soc. Am. **122**(2), 1173–1179 (2007)
31. Dalmont, J.P., Kergomard, J.: Lattices of sound tubes with harmonically related eigenfrequencies. Acta Acustica **2**, 421–430 (1994)
32. Dalmont, J.P., Gazengel, B., Gilbert, J., Kergomard, J.: Some aspects of tuning and clean intonation in reed instruments. Appl. Acoust. **46**, 19–60 (1995)
33. Dalmont, J.P., Gilbert, J., Kergomard, J.: Reed instruments, from small to large amplitude periodic oscillations and the Helmholtz motion analogy. Acustica **86**, 671–684 (2000)
34. Dalmont, J.P., Gilbert, J., Ollivier, S.: Nonlinear characteristics of single-reed instruments: quasistatic volume flow and reed opening measurements. J. Acoust. Soc. Am. **114**(4), 2253–2262 (2003)
35. Dalmont, J.P., Gilbert, J., Kergomard, J., Ollivier, S.: An analytical prediction of the oscillation and extinction thresholds of a clarinet. J. Acoust. Soc. Am. **118**(5), 3294–3305 (2005)
36. Debut, V.: Two studies of a clarinet-like instrument: analysis of natural frequencies of the resonator and calculation of self-sustained oscillations by modal expansion (in French). Ph.D. thesis, Université Aix-Marseille II (2004)
37. Debut, V., Kergomard, J., Laloë, F.: Analysis and optimisation of the tuning of the twelfths for a clarinet resonator. Appl. Acoust. **66**, 365–409 (2005)
38. Doc, J., Vergez, C.: Oscillation regimes produced by an alto saxophone: influence of the control parameters and the bore inharmonicity. J. Acoust. Soc. Am. **137**, 1756–1765 (2015)
39. Doc, J., Vergez, C., Missoum, S.: A minimal model of a single-reed instrument producing quasi-periodic sounds. Acta Acust. United Acust. **100**, 543–554 (2014)
40. Ducasse, E.: Modeling and time domain simulation of wind instruments with single reed in playing situation (in French). Ph.D. thesis, Université du Maine, Le Mans (2001)
41. Elliott, S.J., Bowsher, J.M.: Regeneration in brass wind instruments. J. Sound Vib. **83**(2), 181–217 (1982)
42. Eveno, P., Petiot, J., Gilbert, J., Kieffer, B., Caussé, R.: The relationship between bore resonance frequencies and playing frequencies in trumpets. Acta Acust. United Acust. **100**, 362–374 (2014)
43. Fabre, B., Gilbert, J., Hirschberg, A., Pelorson, V.: Aeroacoustics of musical instruments. Annu. Rev. Fluid Mech. **44**, 1–25 (2012)
44. Facchinetti, M.L., Boutillon, X., Constantinescu, A.: Numerical and experimental modal analysis of the reed and the pipe of a clarinet. J. Acoust. Soc. Am. **113**(5), 2874–2883 (2003)
45. Farner, S.: Harmbal. Computer program in c (2005). Available at http://www.lma.cnrs-mrs.fr/logiciels/harmbal/
46. Farner, S., Vergez, C., Kergomard, J., Lizee, A.: Contribution to harmonic balance calculations of self-sustained periodic oscillations with focus on single-reed instruments. J. Acoust. Soc. Am. **119**(3), 1794–1804 (2006)

47. Ferrand, D., Vergez, C.: Blowing machine for wind musical instrument: toward a real-time control of the blowing pressure. In: IEEE 2008 Mediterranean Conference on Control Automation, vols. 1–4, pp. 556–561 (2008)
48. Fletcher, N.H.: Excitation mechanisms in woodwind and brass instruments. Acustica **43**, 63–72 (1979). Erratum: **50**, 155–159 (1982)
49. Fletcher, N.H.: Autonomous vibration of simple pressure-controlled valves in gas flow. J. Acoust. Soc. Am. **93**(4), 2172–2180 (1993)
50. Fletcher, N.H., Rossing, T.D.: The Physics of Musical Instruments. Springer, New-York (1991)
51. Freour, V., Lopes, N., Hélie, T., Caussé, R., Scavone, G.: In-vitro and numerical investigations of the influence of a vocal-tract resonance on lip auto-oscillations in trombone performance. Acta Acust. United Acust. **101**, 256–269 (2015)
52. Fritz, C.: Influence of musician's vocal tract on clarinet playing (in French). Ph.D. thesis, Université de Paris 6 (2004)
53. Fritz, C., Wolfe, J.: How do clarinet players adjust the resonances of their vocal tracts for different playing effects? J. Acoust. Soc. Am. **118**(5), 3306–3315 (2005)
54. Fritz, C., Farner, S., Kergomard, J.: Some aspects of the harmonic balance method applied to the clarinet. Appl. Acoust. **65**, 1155–1180 (2004)
55. Gibiat, V., Castellengo, M.: Period doubling occurrences in wind instrument musical performances. Acustica **86**, 746–754 (2000)
56. Gilbert, J.: Instruments with single reed: extension of the harmonic balance method, role of the resonance inharmonicity, measurement of the input quantities (in French). Ph.D. thesis, Université du Maine (1991)
57. Gilbert, J., Kergomard, J., Ngoya, E.: Calculation of the steady-state oscillation of a clarinet using the harmonic balance method. J. Acoust. Soc. Am. **86**, 35–41 (1989)
58. Gilbert, J., Ponthus, S., Petiot, J.F.: Artificial buzzing lips and brass instruments: experimental results. J. Acoust. Soc. Am. **104**, 1627–1632 (1998)
59. Gokhshtein, A.: Self-vibration of finite amplitude in a tube with a reed. Sov. Phys. Dokl. **24**, 739–741 (1979)
60. Grand, N., Gilbert, J., Laloë, F.: Oscillation threshold of woodwind instruments. Acustica **83**, 137–151 (1997)
61. Grothe, T.: Experimental investigation of bassoon acoustics. Ph.D. thesis, Technische Universität Dresden (2013)
62. Grothe, T., Baumgart, J.: Assessment of bassoon tuning quality from measurements under playing conditions. Acta Acust. United Acust. **101**, 238–246 (2015)
63. Guillemain, P.: Some roles of the vocal tract in clarinet breath attacks: natural sounds analysis and model-based synthesis. J. Acoust. Soc. Am. **121**(4), 2396–2406 (2007)
64. Guillemain, P., Kergomard, J., Voinier, T.: Real-time synthesis of wind instruments using nonlinear physical models. J. Acoust. Soc. Am. **105**(1), 444–455 (2005)
65. Guillemain, P., Vergez, C., Farcy, A.: An instrumented saxophone mouthpiece and its use to understand how an experienced musician plays. Acta Acust. United Acust. **96**, 622–634 (2012)
66. Guimezanes, T.: Experimental and numerical study of the clarinet reed (in French). Ph.D. thesis, Université du Maine, Le Mans (2008)
67. Heinrich, J.M., Kergomard, J.: The bassoon, history, acoustics, reed (in French). Report, Bulletin du Groupe d'Acoustique Musicale né 82–83 (1976)
68. Helmholtz, H.V.: App. VII, In the theory of pipes. In: On The Sensations Of Tone, 2nd english edn., p. 576. Dover, New York (1954)
69. Hirschberg, A.: Aero-acoustics of wind instruments. In: Mechanics of Musical Instruments. CISM Courses and Lectures, vol. 355, pp. 291–369. Springer, Wien, New York (1995)
70. Idogawa, T., Kobata, T., Komuro, K., Masakazu, I.: Nonlinear vibrations in the air column of a clarinet artificially blown. J. Acoust. Soc. Am. **93**(1), 540–551 (1993)
71. Iooss, G., Joseph, D.: Elementary Stability and Bifurcation Theory. Undergraduate Texts in Mathematics. Springer, Berlin (1980)

72. Karkar, S., Cochelin, B., Vergez, C.: A high-order, purely frequency based harmonic balance formulation for continuation of periodic solutions: the case of non-polynomial nonlinearities. J. Sound Vib. **332**, 968–977 (2013)
73. Kergomard, J.: Elementary considerations on reed-instrument oscillations. In: Weinreich, A.H.J.K.G. (ed.) Mechanics of Musical Instruments, CISM Courses and Lectures, vol. 335, pp. 229–290. Springer, Wien (1995)
74. Kergomard, J.: An acoustic revolution: the saxophone (in French). In: Colloque Acoustique et instruments anciens, Cité de la musique, Paris, pp. 237–254 (1998)
75. Kergomard J., Gilbert, J.: Analysis of some aspects of the role of the reed of a cylindrical wind instrument (in French). In: Actes du 5ème congrès Français d'acoustique, pp. 294–297 (2000)
76. Kergomard, J., Ollivier, S., Gilbert, J.: Calculation of the spectrum of the self-sustained oscillators using a variable truncation method: application to cylindrical reed instruments. Acustica **86**, 685–703 (2000)
77. Kergomard, J., Dalmont, J., Gilbert, J., Guillemain, P.: Period doubling on cylindrical reed instruments. In: 7th CFA-30th DAGA, pp. 113–114 (2004)
78. Maganza, C., Caussé, R., Laloë, F.: Bifurcations, period doubling and chaos in clarinetlike systems. Europhys. Lett. **1**, 295–302 (1986)
79. McIntyre, M.E., Schumacher, R.T., Woodhouse, J.: On the oscillations of musical instruments. J. Acoust. Soc. Am. **74**(5), 1325–1345 (1983)
80. Mersenne, M.: Harmonie Universelle, vol. 1636, Edition facsimilé. CNRS (1963)
81. Meynial, X.: Micro-interval systems for wind instruments with toneholes - oscillation of a single reed coupled with a resonator of simple shape (in French). Ph.D. thesis, Université du Maine (1987)
82. Meynial, X., Kergomard, J.: Micro-interval systems for wind instruments with toneholes (in French). J. Acoustique **1**, 255–270 (1988)
83. Miklos, A., Angster, J., Pitsch, S., Rossing, T.: Interaction of reed and resonator by sound generation in a reed organ pipe. J. Acoust. Soc. Am. **119**(5), 3121–3129 (2006)
84. Millot, L., Baumann, C.: A proposal for a minimal model of free reeds. Acta Acust. United Acust. **93**, 122–144 (2007)
85. Mira, C.: Nonlinear Controlled Systems (in French). Hermès, Paris (1990)
86. Nederveen, C.J.: Acoustical Aspects of Woodwind Instruments. Northern Illinois University Press, IL. New edition, 1998 (1969)
87. Nederveen, C., Dalmont, J.: Mode locking effects on the playing frequency for fork fingerings on the clarinet. J. Acoust. Soc. Am. **131**, 689–697 (2012)
88. Newton, M., Campbell, M., Gilbert, J.: Mechanical response measurements of real and artificial brass players lips. J. Acoust. Soc. Am. **123**, EL14–EL20 (2007)
89. Ollivier, S.: Study of wind instruments with single reed (in French). Ph.D. thesis, Université du Maine (2002)
90. Ollivier, S., Dalmont, J.P., Kergomard, J.: Idealized models of reed woodwinds. Part I: analogy with the bowed string. Acta Acust. United Acust. **90**(6), 1192–1203 (2004)
91. Ollivier, S., Kergomard, J., Dalmont, J.P.: Idealized models of reed woodwinds. Part II: on the stability of "two-step" oscillations. Acta Acust. United Acust. **91**(1), 166–179 (2005)
92. Picart, P., Leval, J., Piquet, F., Boileau, J., Guimezanes, T., Dalmont, J.: Study of the mechanical behaviour of a clarinet reed under forced and auto-oscillations with digital Fresnel holography. Strain **46**, 89–100 (2010)
93. Rayleigh, L.: The Theory of Sound, vol. 2. Dover, New York (1877). Second edition, 1945 Re-issue
94. Ricaud, B., Guillemain, P., Kergomard, J., Silva, F., Vergez, C.: Behavior of reed woodwind instruments around the oscillation threshold. Acta Acust. United Acust. **95**, 733–743 (2009)
95. Ricot, D., Caussé, R., Misdariis, N.: Aerodynamic excitation and sound production of blown-closed free reeds without acoustic coupling: the example of the accordion reed. J. Acoust. Soc. Am. **117**(4), 2279–2290 (2005)

96. Sattinger, D.: Topics in Stability and Bifurcation Theory. Lecture Notes in Mathematics. Springer, Berlin (1973)
97. Scavone, G.P., Lefebvre, A., da Silva, A.R.: Measurement of vocal-tract influence during saxophone performance. J. Acoust. Soc. Am. **123**(4), 2391–2400 (2008)
98. Schumacher, R.T.: Self-sustained oscillations of the clarinet: an integral approach. Acustica **40**, 298–309 (1978)
99. Schumacher, R.T.: Ab initio calculations of the oscillations of a clarinet. Acustica **48**(2), 71–85 (1981)
100. Silva, A.D., Scavone, G., van Walstijn, M.: Numerical simulations of fluid-structure interactions in single-reed mouthpieces. J. Acoust. Soc. Am. **122**, 1798–1809 (2007)
101. Silva, F., Kergomard, J., Vergez, C., Gilbert, J.: Interaction of reed and acoustic resonator in clarinetlike systems. J. Acoust. Soc. Am. **124**(5), 3284–3295 (2008)
102. Silva, F., Vergez, C., Guillemain, P., Kergomard, J., Debut, V.: Moreesc: a framework for the simulation and analysis of sound production in reed and brass instruments. Acta Acust. United Acust. **100**, 126–138 (2014)
103. Sommerfeldt, S.D., Strong, W.J.: Simulation of a player-clarinet system. J. Acoust. Soc. Am. **83**(5), 1908–1918 (1988)
104. Taillard, P., Kergomard, J.: An analytical prediction of the bifurcation scheme of a clarinet-like instrument: effects of resonator losses. Acta Acust. United Acust. **101**, 279–291 (2015)
105. Taillard, P., Kergomard, J., Laloë, F.: Iterated maps for clarinet-like systems. Nonlinear Dyn. **62**, 253–271 (2010)
106. Taillard, P., Laloë, F., Gross, M., Dalmont, J., Kergomard, J.: Statistical estimation of mechanical parameters of clarinet reeds using experimental and numerical approaches. Acta Acust. United Acust. **100**, 555–573 (2014)
107. Takahashi, K., Kodama, H., Nakajima, A., Tachibana, T.: Numerical study on multi-stable oscillations of woodwind single-reed instruments. Acta Acust. United Acust. **95**, 1123–1139 (2009)
108. Tarnopolsky, A.Z., Fletcher, N.H., Lai, J.C.S.: Oscillating reed valves—an experimental study. J. Acoust. Soc. Am. **108**(1), 400–406 (2000)
109. Team, N.U.: Music acoustics 'robot clarinet' (2008). http://www.phys.unsw.edu.au/jw/clarinetrobot.html
110. Thompson, S.C.: The effect of the reed resonance on woodwind tone production. J. Acoust. Soc. Am. **66**(5), 1299–1307 (1979)
111. Valette, C., Cuesta, C.: Mechanics of the Vibrating String (in French). Hermès, Paris (1993)
112. van Walstijn, M., Avanzini, F.: Modelling the mechanical response of the reed-mouthpiece-lip system of a clarinet. Part II: a lumped model approximation. Acta Acust. United Acust. **93**, 435–446 (2007)
113. Vergez, C., Lizée, A.: A frequency-domain approach of harmonic balance solutions stability. In: Forum Acusticum, Budapest, pp. 539–543 (2005)
114. Vergez, C., Rodet, X.: Experiments with an artificial mouth for trumpet. In: ISMA'98 Proceedings, pp. 153–158. Leavenworth, Washington (1998)
115. Vergez, C., Rodet, X.: Air flow related improvements for basic physical models of brass instruments. In: Proceedings of ICMC'2000, Berlin, pp. 62–65 (2000)
116. Vergez, C., Rodet, X.: Trumpet and trumpet player: physical modeling in a musical context. In: Proceedings of the International Congress of Acoustics (ICA), Rome, p. CDROM IV (2001)
117. Vergez, C., Almeida, A., Caussé, R., Rodet, X.: Toward a simple physical model of double-reed musical instruments: influence of aero-dynamical losses in the embouchure on the coupling between the reed and the bore of the resonator. Acta Acust. United Acust. **89**(6), 964–973 (2003)
118. Weber, W.: Theorie der Zungenpfeifen. Annalen der Physik und Chemie, hrsg. von J.C. Poggendorf **93**, 193–246 (1829)
119. Weinreich, G., Caussé, R.: Elementary stability considerations for bowed-string motion. J. Acoust. Soc. Am. **89**(2), 887–895 (1991)

120. Wilson, T.: The measured upstream impedance for clarinet performance and its role in sound production. Ph.D. thesis, University of Washington (1996)
121. Wilson, T.A., Beavers, G.S.: Operating modes of the clarinet. J. Acoust. Soc. Am. **56**(2), 653–658 (1974)
122. Woodhouse, J.: Idealised models of a bowed string. Acustica **79**, 233–250 (1993)
123. Woodhouse, J., Schumacher, R., Garoff, S.: Reconstruction of bowing point friction force in a bowed string. J. Acoust. Soc. Am. **108**(1), 357–68 (2000)
124. Worman, W.: Self-sustained nonlinear oscillations of medium amplitude in clarinet like-systems. Ph.D. thesis, Case Western Reserve University Cleveland (1971)

Chapter 10
Flute-Like Instruments

Benoît Fabre

Abstract This chapter deals with a second category of self-sustained oscillations produced by musical instruments and focuses on flutes with open ends. The following section presents the self-sustained oscillator as a looped system, focusing mostly on the jet and on its interaction with the acoustic field in the pipe. An integral approach, that allows to overpass the limitations of the looped system analysis, is also introduced. The three main elements that need to be described for modeling the oscillation in flutes are: (1) the perturbation of the jet by the acoustic field: the jet receptivity; (2) the evolution of the perturbation convected by the jet: the jet instability; and (3) the production of acoustical energy by the perturbed flow: the aeroacoustic sources. Models are proposed for each of these elements and compared to experiments. The jet-drive model is detailed and shown to be formally equivalent to the force source term in an aeroacoustic analogy. The main geometrical parameters that characterize a flute exciter is the ratio of the channel thickness to the distance between the flue exit and the labium, while the main parameter related to the instrumentalist is the jet Reynolds number.

10.1 Introduction and General Description

The first attempts to understand flute-like instruments from a physical point of view are found in the late nineteenth century, see, for example, the work by Helmholtz [48] and Rayleigh [36]. During the twentieth century, the development of fluid mechanics and more specifically studies on jet instability and aeroacoustics brought new insight on the physics of flute-like instruments.

Today's models allow producing realistic synthetic flute sounds, based on the physical description of the instrument. This indicates that the main physical mechanisms are now understood. However, this global understanding does not allow an accurate interpretation of the influence of some specific parameters, such as those

B. Fabre (✉)
Laboratoire LAM – Lutherie Acoustique Musique, and IJLRA – Institut Jean le Rond d'Alembert, Université Pierre-et-Marie-Curie, CNRS, ministère de la culture et de la communication, Paris, France
e-mail: benoit.fabre@upmc.fr

A. Chaigne, J. Kergomard, *Acoustics of Musical Instruments*, Modern Acoustics and Signal Processing, DOI 10.1007/978-1-4939-3679-3_10

of interest for players and instrument makers. This chapter focuses on open end flutes, excluding stopped pipes, and on quasi-cylindrical pipes. Indeed, the conical bore of flutes shows a behavior much closer to that of a cylinder than the bores of double reed instruments such as the oboe or the bassoon.

After a general description of the physics and of the different sound production mechanisms in flutes, the chapter will develop a general model of flutes (Sect. 10.2). We then focus on the most difficult parts, namely the description of the jet instability (Sect. 10.3) and of the aeroacoustic sources (Sect. 10.4). The main elements leading to a simplified model (Sect. 10.5) aiming at sound synthesis, will be discussed next.

10.1.1 The Air Jet, Driving the Oscillation in Flutes

The three main elements that need to be described for modeling the oscillation in flutes are

- the perturbation of the jet by the acoustic field: the jet *receptivity*,
- the evolution of the perturbation convected by the jet: the jet *instability*,
- the production of acoustical energy by the perturbed flow: the aeroacoustic *sources*.

The following section presents the self-sustained oscillator as a looped system, focusing mostly on the jet and on its interaction with the acoustic field in the pipe.

10.1.1.1 The Jet Instability

Observing the smoke emitted by a cigarette indicates that jets are naturally unstable. After a few centimeters, the thin smoke jet bends and oscillates, and finally looses its organized structure, ending as a wide cloud. This kind of (space-time) instability can be observed as soon as two fluids with different velocities are in contact. For example, the wind at the surface of the sea induces water waves. The surrounding air needs to be still in order to observe the evolution of the cigarette smoke described above: indeed, slight movements of the air around the cigarette or a movement of the hand holding the cigarette strongly influences the jet motion, demonstrating the high sensitivity of the smoke jet.

In a flute, the air jet is blown across an open end of the pipe resonator. When acoustic oscillation occurs within the resonator, the jet instability synchronizes on the acoustic oscillation, resulting in a “forced” oscillation of the jet. The hydrodynamic waves traveling on the jet have the same frequency as the acoustic oscillation. As for the oscillation described in the case of the cigarette smoke, the jet perturbation grows as it is carried by the flow, being convected downstream. In the case of a jet oscillation forced by a loudspeaker, Fig. 10.1 shows how the transverse displacement of the jet increases in the downstream direction.

Fig. 10.1 Photograph of the jet perturbation forced by loudspeakers placed at few centimeters apart from the flow, above and under it [$Re = 500$, 658 Hz, $U_j = 7.5$ m/s]. The jet is exhausting from the end of a 1 mm thick channel, seen on the *left side* of the picture

Two characteristics of the jet motion are important for the flute oscillation:

- the convection velocity of the perturbation, corresponding to the propagation velocity of the perturbation waves on the jet: to a first approximation, the convection velocity is equal to half the centerline jet velocity,
- the amplification of the perturbation, corresponding to a characteristic growth factor of the instability waves along the jet.

Both characteristics depend on frequency, but the amplification strongly depends on it: the jet instability is stronger in a frequency range depending on both the jet velocity and jet thickness. The strongest amplification appears for frequencies around $0.3\, U_j/h$, where U_j is the jet velocity and h is the thickness of the flue channel from which the jet is flowing.[1]

10.1.1.2 Acoustic Sources at the Labium of the Flute

Figure 10.2 illustrates the vocabulary used in the case of a recorder. The terminology changes according to the instrument studied: for instance, the foot of the organ pipe corresponds to the mouth of the recorder player, while the upper-lip of the mouth of the organ pipe corresponds to the labium or blowing edge of the recorder! In a transverse flute, the flue channel is created between the lips of the player.

Transverse perturbations of the jet are induced by the acoustic field. They are convected from the flue exit to the labium or blowing edge. As a result, the jet oscillates from one side to the other of the labium (Fig. 10.3). This induces a force on the labium due to the flow. This force is synchronized with the jet perturbation, and therefore with the acoustic oscillation. The reacting force of the labium acts as an acoustic source that sustains the acoustic oscillation, thus compensating for the various acoustic losses.

[1] Please note that in this chapter, we will denote the velocity as U, and the volume flow as Q, as it is of common use in fluid mechanics. This differs from the convention used in the other chapters of the book.

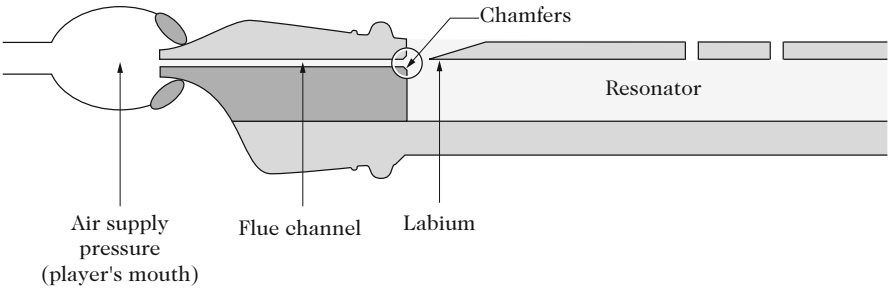

Fig. 10.2 Longitudinal sketch of a recorder, showing the terms used in this chapter. The chamfers at the flue exit can also be seen on this sketch. The opening between the flue exit and the labium is called the "mouth" in this chapter

Fig. 10.3 The acoustic field at the flue exit induces a perturbation of the jet that is amplified while it is convected towards the labium. This results into the transverse oscillation of the jet from one side of the labium to the other

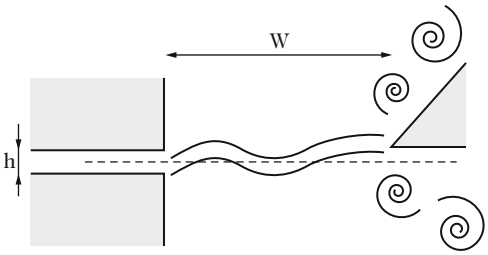

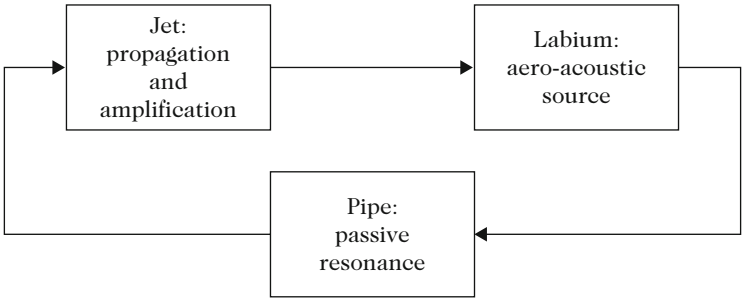

Fig. 10.4 Self-sustained oscillation in flutes can be described as a feedback loop

10.1.1.3 The Self-Sustained Oscillator as a Looped System

The acoustic field in the pipe resonator is responsible for the initial jet perturbation. This perturbation is convected and amplified downstream due to the natural jet instability. The interaction of the perturbed jet with the labium constitutes the aeroacoustic source that feeds acoustic energy into the pipe. As a response to this excitation, the acoustic energy in the pipe is associated with the acoustic flow through the mouth, that results in the jet perturbation at the flue exit. Therefore, the self-sustained oscillations in the instrument can be described as a feedback loop, as shown in Fig. 10.4.

This looped description allows to predict the oscillating frequency of the instrument. Because the pipe accumulates energy only at resonances, the oscillating frequency is close to a pipe resonance. In the looped description of the system, stationary oscillations can only occur when the total phase shift around the loop is 2π or any multiple of 2π. When blowing softly in a recorder, one can check that the time delay associated with the convection of perturbations on the jet is about half the oscillation period. The phase shift of the pipe response therefore needs to be the exact complement of one period: that is π, corresponding to another half period. If we now blow a little harder in the recorder, the jet velocity increases and the convection velocity of perturbation increases accordingly. The phase shift due to the convection of perturbations on the jet decreases and therefore the phase shift of the pipe response needs to increase: the oscillation frequency slightly increases to match the phase condition. Blowing even harder, the convection delay on the jet eventually becomes too small compared to the period of the first pipe resonance and the oscillation jumps to the second pipe resonance, for which the same convection delay represents a larger phase shift (Fig. 10.5). This is called "overblowing." For a given fingering, the player can select the oscillating regime, among the different pipe resonances, by adjusting the blowing pressure and consequently the convection jet velocity.

By blowing gently, at very low blowing pressures compared to standard playing, the player can produce very soft tones at frequencies close to the pipe resonances. This playing technique, called "whistle-tones" or sometimes "eolian tones,"

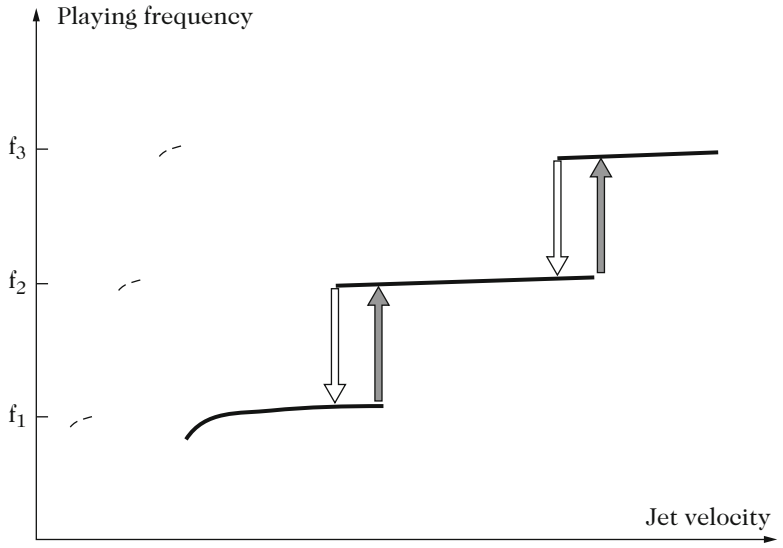

Fig. 10.5 Simplified representation of the playing frequency of a flute as function of jet velocity. The oscillation takes place at a frequency close to one of the pipe passive resonances f_1, f_2, or f_3. Regime changes do not occur at the same jet velocity for increasing (*gray arrows*) and decreasing (*white arrows*) jet velocity: a hysteresis appears. *Dotted lines* indicate whistle-tone oscillations

corresponds to convection delays on the jet that are larger than one oscillation period: one and a half or two and a half period may be observed, instead of the half period observed under standard playing conditions. These oscillations do not easily appear in recorders because of the short distance between flue exit and labium. They can appear for standard playing conditions during starting transients on some flutes and organ pipes, before the jet reaches its stationary velocity.

10.1.2 The Sounds of Flutes

10.1.2.1 The Different Elements of the Sound

Different elements are combined in the sound radiated by flutes. Using a mechanical air supply allows producing a stationary sound, as for an organ. The sound radiated by a pipe blown in such a way can be split into a deterministic part, that can be analyzed in terms of sine wave components, and a stochastic part, generated by turbulence. Indeed, turbulence produces a broadband noise, that is filtered by the pipe acoustical response. In Fig. 10.6, the FFT spectrum analysis of the stationary part of the sound of a small organ pipe shows the harmonics together with the turbulence noise filtered by the pipe. One can clearly see the shift in frequency between harmonics and pipe resonances: for example, the sixth resonance of the pipe lies between the sharp lines of the harmonics 6 and 7.

The transverse position of the labium, relative to the jet central axis, has a strong influence on the relative amplitudes of the harmonics. In the recorder, even

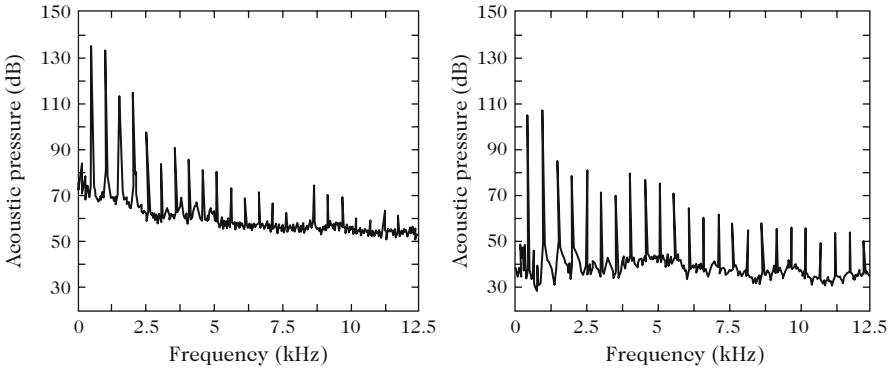

Fig. 10.6 FFT analysis of the internal pressure (*left*) and radiated pressure (*right*) at a distance of 30 cm in front of the mouth of a small organ pipe (2048 points FFT, Hanning window, averaging over 25 time slots). At frequencies higher than the fifth harmonic, (around 2.5 kHz), resonances can be identified by their filtering effect on the noise sound of turbulence, since their frequency does not coincide any more with the harmonics that correspond to the sharp peaks seen as *vertical lines* in the spectra. Radiation induces a relative amplification of the higher frequencies. From [18]

harmonics reach a minimum value for a transverse position of the labium close to the jet axis [47]. Measurements on (transverse) flute playing indicate that some players are working to enhance the amplitude of even harmonics, while some others are seeking to generate strong odd harmonics.

When the air supply comes from a player rather than from a mechanical system, pressure fluctuations modulate the sound production. Vibrato correspond to a conscious and intentional modulation of the blowing, but fluctuations are observed, even when the player aims at producing a "stable" tone. Because of these fluctuations, it is generally not possible to define a stationary part of the tone. This makes the analysis of the sound production even more difficult!

Starting transients are also quite difficult to analyze. Experiments on transients are difficult to set up, mostly because it is difficult to get an accurate and reproducible control of blowing pressure rises. Analysis is also difficult from the point of view of signal processing, while the most difficult part of the analysis of starting transients is due to the complex interaction of intricate physical phenomena [20, 46]. The different sound components, that will become the harmonics in the steady stationary part of the sound, display changing frequencies and amplitudes during the attack transient. Figure 10.7 shows the time evolution of the three first frequency components during an attack transient. In this example, the second component (with frequency close to twice that of the later fundamental) increases much faster than the first component.

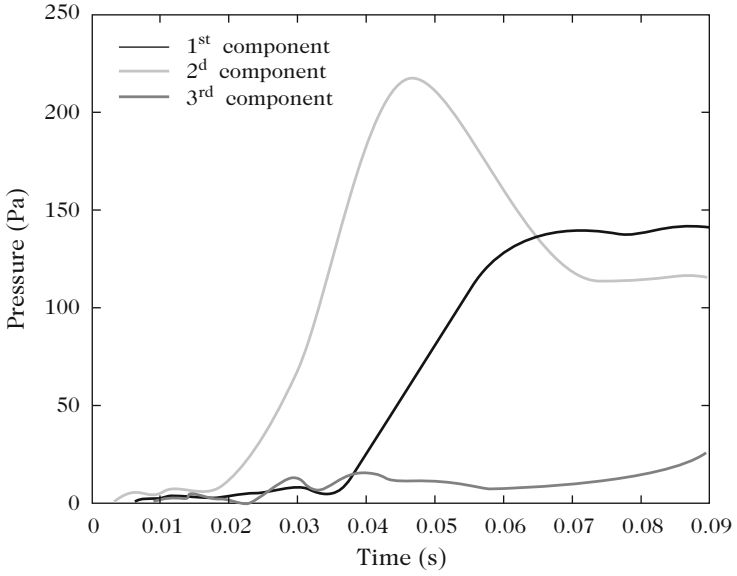

Fig. 10.7 Time evolution of the three first frequency component during the attack transient in a small organ pipe. In this case, the second component is dominating the attack transient. From [38]

10.1.2.2 Whistle-Tones or Eolian Tones

High frequency components may also appear during the attack transient [8, 20]. The frequency behavior of the so-called mouth-tones [8] shows some similarity with edge-tones. Therefore, measurements of the amplitude of these sounds (pipe internal pressure) were made under steady blowing in whistle-tone condition, showing that the amplitude is a factor 100 higher than that expected for edge-tones. Furthermore, the amplitude appears to be even higher (approximately by a factor 2) than that expected for a "normal" pipe-tone, indicating that the saturation mechanisms at work are different.

These mouth-tones, or eolian tones or whistle-tones, are relying on energy accumulation at a resonance frequency of the pipe [1]. Flute players know very well how dangerous they are because of their poor stability.

10.2 A Global Model for the Instrument

10.2.1 General Description

Before developing a physical model of a flute, the limits of the system must be clearly identified. Recall that the sound is the result of instrument–player interaction. It is therefore easier to start our description by instruments in which the player has little influence on the sound: the organ pipe, and to a lesser extend, the recorder. Both instruments have in common that the geometry of the exciter part does not change during playing, and is fully determined by the music instrument maker: jet formation channel and labium position. When the jet is blown through the lips of the player, the description is more complex because the player adapts his lip geometry during playing, in a not fully reproducible manner. A good player may aim at producing very similar sound quality when repeating a musical excerpt, but never aims at reaching the same lip geometry: the player's target is the sound, not the geometry.

Even for instruments with a fixed geometry, today's models are still very crude. They offer a good description of the physics of the instrument for a restricted range of parameters (Reynolds and Strouhal numbers, see next section). These models are only valid for specific playing techniques and fail to describe some phenomena observed during transients. Furthermore, they do not allow to include some details of the instruments such as the chamfers that are cut at the flue exit in recorders, or the nicking of some organ pipes. Direct flow simulation, solving the equations of fluid mechanics at each time step and each position in space, is still difficult nowadays when dealing with the whole instrument [31, 41], but can offer interesting answers to localized problems, providing information that can help improving simplified models [7].

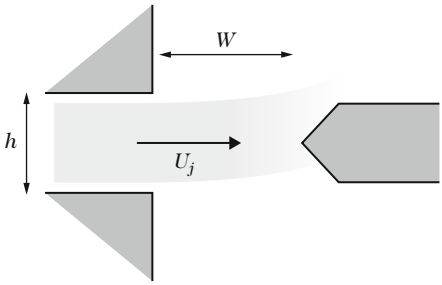

Fig. 10.8 Geometrical parameters of the exciter part. U_j is the jet central velocity at the channel exit, h is the channel thickness, and W is the flue exit to labium distance

10.2.2 Important Parameters

Oscillations in a flute can be described as the result of the coupling between a hydrodynamic mode of a jet and an acoustic mode of a pipe resonator. Different scaling parameters are useful. Figure 10.8 shows the geometrical parameters involved in this coupling.

The Reynolds number Re is used to characterize the structure of the jet: it may vary from a few hundreds (recorder) up to 10,000 in modern transverse flute playing.

$$500 < Re = \frac{U_j h}{\nu} < 10,000 \tag{10.1}$$

where U_j is the jet central velocity at the channel exit, h is the corresponding channel thickness, and ν is the kinematic viscosity of air ($\nu = 1.5 \cdot 10^{-5}$ m^2/s $= \mu/\rho$, see Sect. 5.5.2 in Chap. 5). The jet instability is characterized by the Strouhal number, corresponding to the inverse of the dimensionless frequency. Definitions of the Strouhal number may vary according to different situations and authors, from $\omega W/U_j$, with ω the angular frequency and W the flue exit to labium distance, to fh/U_j, where $f = \omega/2\pi$.

Theoretical analysis of jet instability generally uses the half-thickness parameter b of the jet, for instance, in the case of the Bickley velocity profile[2] $U(y) = U_0 \operatorname{sech}^2(y/b)$ with y the transversal coordinate [22, 34]. The relation between the experimental parameter h and the theoretical parameter b is not straightforward. To a first approximation, it can be deduced from conservation laws between the channel flow and the jet flow. For example, if the channel flow is approximated by a Poiseuille flow and the jet flow is assumed to have a Bickley velocity profile with $U_0 = U_j$, momentum conservation together with central velocity conservation lead to $b = 2h/5$ [45].

For standard blowing conditions in flutes, one half hydrodynamic wavelength λ_h can be observed on the jet between the flue exit and the labium. The wave propagation velocity on the jet is approximately equal to half the central jet velocity

[2] $\operatorname{sech} x = 1/\cosh x$

U_j, and therefore the half wavelength across the mouth width W, between flue exit and labium $W = \lambda_h/2$ corresponds to:

$$\mathrm{Str}_W = \frac{fW}{U_j} \approx 0.25 \tag{10.2}$$

which is a characteristic value in the oscillating range of the instruments [15, 21, 39, 47].

The properties of the jet instability are determined by the interaction between both shear layers, on the two sides of the jet. Therefore, the instability is often studied as function of the Strouhal number based on the transverse dimension of the jet (b or h, depending on whether the approach is theoretical or experimental): $\mathrm{Str}_h = fh/U_j$. The jet length to jet thickness ratio W/h corresponds to the ratio between the two Strouhal numbers discussed above. This ratio is an important parameter for the modeling. "Thick jets" correspond to values of this ratio smaller than 4 (in the case of transverse flute or shakuhachi, the Japanese flute, playing loud in the low register), while "thin jets" such as those found in some organ pipes are characterized by values up to 20 of the thickness ratio W/h of the jet.

Figure 10.9 shows the standard operating range of different instruments in a map representing the jet thickness W/h as function of the Reynolds number. Instruments for which the jet is formed between the lips of the player allow to vary the parameters during playing, and therefore present a wide operating range. In the case of the organ, it is the variety of pipes in the different stops that allows a wide operating range.

Models for the jet behavior need to be adapted to the specific operating range. In the organ, the same blowing system is generally used for all pipes, and the player can adjust individual blowing conditions of each pipe by varying the opening of each pipe foot. Together with different geometries of the flue and of the labium, this yields a wide operating range.

Last, the oscillating amplitude is quantified as the ratio of the acoustic velocity in the mouth of the pipe to the central jet velocity, or to the mean flow velocity of the jet. The central jet velocity is generally estimated from pressure values by applying the Bernoulli equation (see below) between the pressure reservoir and the atmospheric pressure [21, 39, 46]. The acoustic velocity in the mouth can be deduced from pressure measurement in the pipe resonator, taking the non-uniformity of the flow in the mouth [45] into account. For standard blowing conditions, oscillating amplitudes induce a transverse acoustic perturbation v_{ac} of the jet, with an amplitude V_{ac} of the order of magnitude of one-tenth of the jet velocity:

$$\frac{V_{\mathrm{ac}}}{U_j} \approx 10^{-1}. \tag{10.3}$$

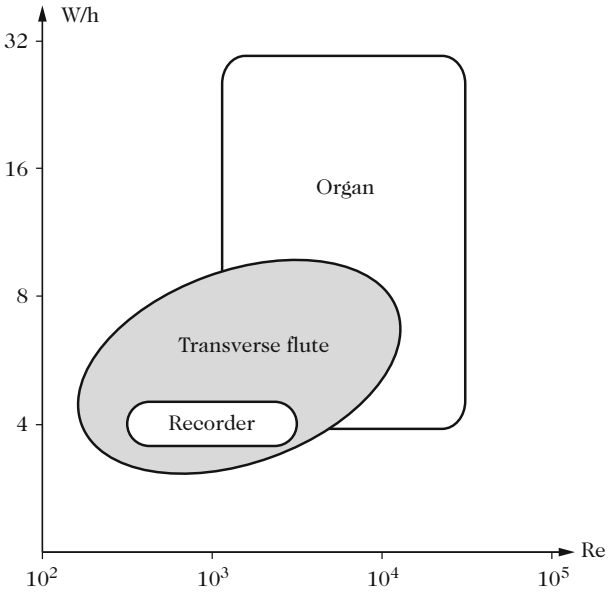

Fig. 10.9 Operating ranges of the recorder, of the transverse flute, and of the organ pipes in a map representing the jet thickness W/h as function of the Reynolds number. Transverse flute allows the player to cover a wide range on a single instrument through lip and blowing pressure adjustment, while in the case of the organ, the variety of pipes with different geometries determines the operating range

10.2.3 Localized or Distributed Interaction?

The different elements that take part in the oscillation interact in such a way that it is difficult to separate them: the acoustic resonance in the pipe cannot be separated from the radiation at the pipe ends, and the aeroacoustic source acts in the vicinity of the open end. It may seem artificial to model each element separately: the jet, the aeroacoustic sources, and the pipe resonator.

10.2.3.1 Models Assuming Localized Interaction (Lumped Models)

This separation came first from the different related scientific fields: flow instability is generally a topic of fluid mechanical studies, the pipe resonance of complex pipes is analyzed in acoustical studies, while the sound production by an unsteady flow interacting with solid boundaries is analyzed in aeroacoustical studies. Different time and space scales may allow to justify the splitting of the problem into independent problems, corresponding to different simplifications of the Navier–Stokes equation.

Jet descriptions are usually carried out under the assumption of compact flow, corresponding to small scales compared to the acoustic wavelength: the fluid is supposed to be *incompressible*[3]. In contrast, the description of the pipe acoustics usually neglects convective effects. Theses assumptions are valid, in the study of the oscillation mechanisms, only for low frequencies, corresponding to the lowest harmonics of the sound. This is justified by the fact that the oscillation mechanisms are controlled by the fundamental frequency of the oscillation, or by the two first harmonics. However, for the listener hearing the radiated sound, higher frequency components are very important. The poor radiation efficiency at low frequencies makes these two points of view compatible: low frequencies are mostly trapped inside the resonator and taking care of the self-sustained oscillation. This is because the sound waves at low frequencies are almost totally reflected at the open pipe ends, with very little radiation. The visco-thermal losses at the walls at the oscillating frequency are higher than the radiation losses. On the contrary, higher frequency components have smaller amplitudes inside the pipe, but they are much more efficiently radiated. Figure 10.6 shows the spectrum of the acoustic pressure inside the pipe, together with the spectrum of the acoustic pressure radiated at a distance of about 30 cm from the pipe mouth. Components in the frequency band from 3 to 5 kHz, corresponding to the most sensitive range of hearing, show a higher relative importance in the radiated sound than in the internal acoustic field.

10.2.3.2 Distributed Interaction Models

Lumped models with independent blocks are based on the assumption of localized interactions. The jet is supposed to be perturbed by the acoustic field at the positions of flow separation at the flue channel exit, and the sound production is supposed to be localized at the labium. The pipe resonator is then fully described by its acoustic response to this excitation at the flue exit.

A more rigorous approach can be found in analytical models, as proposed by Howe [28], Crighton [11], Elder [17], and Bechert [5]. These models describe the interaction between the flow and the acoustic field using integral formulations. These formulations can be developed for simplified geometries only, such as an infinitely thin labium, for instance, and leads to awkward mathematical developments when solving the problem. Solving is only possible under restrictive assumptions, such as infinitely thin shear layers, linear approximation of perturbations (the saturation of the oscillation is not part of the solution), or in some cases point vortices. Despite these difficulties, analytical models, together with

[3]The fluid can be considered as incompressible whenever its density ρ can be approximated to be constant. This means that the density variations induced by pressure variations can be neglected. The equation $\rho = \rho_0 =$ constant is an equation of state of the fluid, indicating that pressure changes are related to the acceleration of the fluid (Bernoulli) or to viscous forces, but not to density changes. As a consequence, one can write $\mathrm{div}(\mathbf{v}) = 0$. Of course, acoustic waves cannot be written under such an assumption. This assumption can therefore only apply within a region small compared to the acoustic wavelength, and only for flow velocities U_j that remain small compared to the velocity c of sound propagation ($M = U_j/c \ll 1$).

numerical simulation, are probably an interesting source of inspiration whenever lumped models with localized interactions fail to predict the flute's behavior. This is the reason why we will present these approaches in the following section.

10.3 A Modeling for the Jet Oscillation

The jet oscillation is described within the framework of fluid mechanics. The basic description of the flow dynamics is the same as the one used in the context of acoustics, but fluid dynamics generally focuses on different approximations. We will first discuss the jet formation at the outlet of the flue channel (in the case of a recorder) or of the lip channel (in the case of transverse flute, for example). The unstable behavior of this jet will then be addressed. The sound production associated with the interaction of the jet with the labium will be described in Sect. 10.4.

10.3.1 Jet Formation

The instrument player produces an overpressure in his mouth. As a result the air accelerates towards the low pressure area in the channel or between the player's lips. To a first approximation, our description will assume that the pressures and therefore the jet flow are constant, which correspond to stationary conditions.

10.3.1.1 The Flow in the Channel

In a frictionless approximation (inviscid flow), the circulation of the velocity round a loop is conserved (Kelvin circulation theorem). Since the circulation round a loop is related to the vorticity field, if the vorticity is zero at an initial instant, it remains zero for all subsequent times. The flow is then described as irrotational and the velocity is conservative: it is the gradient of a scalar potential $\mathbf{v} = \mathbf{grad}\,\varphi$. Starting from Euler's equation without external forces (1.101), one can write under *incompressible* assumption (mass density ρ_0 is constant, div$\mathbf{v} = 0$):

$$\rho_0 \frac{d\mathbf{v}}{dt} = -\mathbf{grad}\, p. \tag{10.4}$$

If we now assume a *stationary* flow, the time derivatives are zero. The pressure forces push the fluid into the channel in the x direction, and the velocity v_x in this direction is the only component of the flow. The previous equation then writes

$$\rho_0 v_x \frac{\partial v_x}{\partial x} = -\frac{\partial p}{\partial x}. \tag{10.5}$$

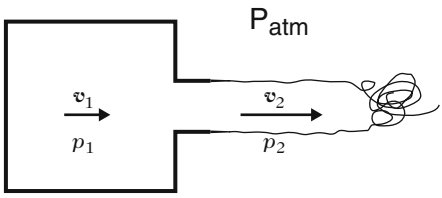

Fig. 10.10 Frictionless flow at the outlet of a pressure reservoir: application of Bernoulli's equation

The left-hand side of this equation can be written as: $\frac{1}{2}\rho_0 \partial v_x^2/\partial x$. Integrating the equation along a path from inside the pressure reservoir to a point outside in the jet yields a simplified Bernoulli equation (1.104):

$$\frac{1}{2}\rho_0(v_{x2}^2 - v_{x1}^2) = p_1 - p_2. \tag{10.6}$$

If the reservoir that accounts for the player's mouth is large enough, the integration can be carried out from a point inside the reservoir where the velocity is negligible to a point outside in the jet, where the pressure is equal to the ambient atmospheric pressure $p_2 = P_{\text{atm}}$ (Fig. 10.10). Assuming a potential flow allows this result to be independent from the path between the two considered points. A fluid particle is accelerated from the mouth (pressure higher than the atmospheric pressure, stagnant fluid, potential energy) by the pressure gradient into the flow channel down to the channel exit (atmospheric pressure and kinetic energy). The jet velocity U_j at the flue channel exit is

$$U_j = \sqrt{\frac{2\Delta p}{\rho_0}}. \tag{10.7}$$

where Δp stands for the mouth pressure relative to the atmospheric pressure: $\Delta p = p_1 - P_{\text{atm}}$.

However, this description does involve friction because of the flow separation at the channel exit. Indeed, in a strictly frictionless potential flow description, streamlines follow the walls and this would induce an infinite transverse acceleration of fluid particles at the edges of the channel exit! In an actual flow, the viscosity becomes important at this point, even if it is very small. Viscosity is responsible for flow separation and jet formation.

- *A viscous flow approach* allows describing the development of boundary layers at the channel walls. Because of viscosity, the tangential velocity is zero at the walls, and increases within a thin layer up to its nominal frictionless flow value. This transition layer is called a "boundary layer." The thickness δ of this layer grows as the flow travels downstream in the channel. The flow in the axial x direction therefore shows a transverse velocity profile $v_x(y) = U(y)$ that changes as fluid flows downstream. Friction forces due to viscosity depend on the slope

of the velocity profile $\mu(\partial U/\partial y)$, where μ is the coefficient of viscosity of the fluid. The net force on a layer of thickness dy results from viscous stresses on both sides: $\mu(\partial U/\partial y)_{y+dy}$ on one side and $-\mu(\partial U/\partial y)_y$ on the other side.

In total, the net viscous force (per unit surface $dxdz$ of the layer of thickness dy) is $\mu\partial^2 U/\partial y^2$. The momentum conservation (10.4) should take this force into consideration. Extending the viscous force in the three directions (when necessary!), leads to the Navier–Stokes equation for incompressible flows:

$$\rho_0 \frac{d\mathbf{v}}{dt} = -\mathbf{grad}\, p + \mu\nabla^2\mathbf{v}. \tag{10.8}$$

In the case of a stationary flow, this equation writes

$$\rho_0(\mathbf{v}.\mathbf{grad})(\mathbf{v}) = -\mathbf{grad}\, p + \mu\nabla^2\mathbf{v}. \tag{10.9}$$

Solving this equation in a channel is generally associated to the name of Prandtl. This is a nonlinear 2D problem. Rather than the mathematical development (see [3, 42] for reference), we now focus on its physical interpretation.

In the boundary layer along the channel walls, viscosity induces transverse transfer of momentum on a thickness that grows with time as $\delta \propto \sqrt{\nu t}$, and therefore also grows with distance x from the channel inlet. For a flow of velocity U, the boundary layer thickness can be approximated as:

$$\delta(x) \approx \sqrt{\frac{\nu x}{U}}. \tag{10.10}$$

If the channel is long enough, the two boundary layers from each side of the channel will join, resulting in the formation of a parabolic velocity profile. For a long channel of uniform thickness h, the corresponding parabolic flow velocity profile is known as the Poiseuille velocity profile[4]

$$U(y) = \frac{1}{2\mu}\frac{dp}{dx}(y^2 - h^2). \tag{10.11}$$

[4] Acoustic boundary layers discussed in Chap. 5, Sect. 5.4.2.1, are different from those studied here. In the description of the acoustic boundary layers, the linear mass acceleration $\rho_0\partial\mathbf{v}/\partial t$ takes the place of the convection term (left-hand side) in Eq. (10.9). The change between the two complementary situations is governed by the channel thickness, flow velocity, and the frequency of the acoustic phenomenon: in a cylindrical pipe, the Stokes number indicates the ratio of the pipe radius to the acoustic boundary layer thickness. The Stokes number can be seen as the combination of the Reynolds number (dimensionless flow velocity) and Strouhal number (dimensionless frequency). For a quasi-steady flow (low Strouhal) and low flow velocity (low Reynolds), the Stokes number is small and the Poiseuille velocity profile is reached, corresponding to thin pipes, also called capillaries. For high frequencies and/or wider pipes, the linear term becomes dominant and the viscous acoustic boundary layer is observed, with constant thickness as the wave travels downstream. Intermediate situations show a boundary layer that grows in space, whenever the convective term controls the development of the boundary layer.

The pressure decreases linearly with the distance x along the channel. Integrating the previous equation allows calculating the pressure gradient, as a function of the flow velocity U_0 at the channel inlet (constant velocity profile, with infinitely thin boundary layers):

$$\frac{dp}{dx} = -3\mu U_0 \frac{1}{h^2}. \tag{10.12}$$

Mass conservation between the channel inlet (uniform velocity profile) and the channel outlet yields the central velocity $U(y = 0)$ of the Poiseuille profile:

$$U(0) = 1.5U_0. \tag{10.13}$$

Before the channel exit, the flow velocity profile is determined by the time during which viscosity has smoothed the profile: for a short channel, and/or high velocity, the boundary layers are thin and the flow shows a central core with a flat velocity profile. On the opposite, a long channel, and/or a slow velocity, allows for the development of a Poiseuille-like velocity profile. In most actual applications to flute channels, the estimation of the central velocity using Bernoulli's equation (10.7) seems to be reasonable [43]. Not only the channel is relatively short, but also in the case of recorders, it is usually convergent. The decrease in channel thickness will delay the boundary layer development.

10.3.1.2 The Jet Flowing Out of the Channel

Because of viscosity, the flow separates from the walls at the channel exit in order to form a free jet.

If the end of the channel shows sharp edges, the flow separation is triggered at the edges. Indeed, a fluid particle that would stick to the walls would experience a strong localized acceleration in time and space. Even if it is low, viscosity will counteract this acceleration. This is related to the fact that edges represent singularities in a potential flow.

If the end of the channel is rounded, the flow separation point is more difficult to predict. Before the separation, the flow spreads into a divergent channel. Mass conservation indicates that the velocity in the x direction slows down as the channel gets wider. According to Bernoulli's description, this results in a rising pressure in the flow, corresponding to a change of sign of the pressure gradient in the x direction: while the pressure is decreasing in the straight part of the channel due to friction, it increases in the divergent part. The pressure in the boundary layer is equal to the pressure in the core of the flow, hence the fluid particles in the boundary layer are submitted to two opposite influences: acceleration due to viscous momentum transfer from the core of the flow to the boundary layer and deceleration due to the inverse pressure gradient. At some point in the diverging channel the balance

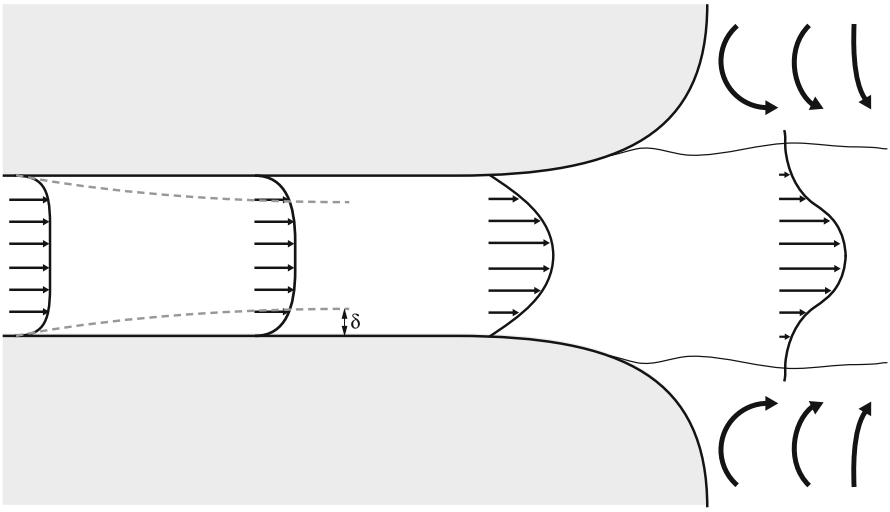

Fig. 10.11 The flow at the channel inlet has a top-hat velocity profile. As the fluid flows downstream, boundary layers get thicker because of viscosity. If the channel outlet is rounded, the flow slows down, resulting in an increase of pressure. The change of sign of the pressure gradient in the diverging part at the channel exit is responsible for flow separation. Because of viscosity, the free jet formed drags the surrounding fluid (*rounded arrows*)

between these two terms changes of sign and triggers the separation of the fluid particle at the wall, generating a stagnant fluid and/or fluid recirculation (Fig. 10.11).

In both cases (sharp or rounded edges), flow separation results in a jet that carries the memory of the channel geometry, and of upstream hydrodynamic conditions. Like a piano hammer escaping from the launching mechanism and projected against the string, the jet escapes from the control of the player. Jet characteristics such as its velocity, shape, and profile influence its behavior, like the instability that is at work in the heart of the sound production in flutes.

10.3.2 Jet Instability

An air jet flowing in air is intrinsically unstable, in the sense that any small perturbation is amplified by the jet: the example of cigarette smoke has already been discussed to illustrate this topic (see Sect. 10.1.1.1). The aim of the following section is to describe more quantitatively this instability.

10.3.2.1 Assumptions and Basic Phenomena

Assumptions

The first assumption used here is that of an inviscid fluid: as seen below, the instability of a shear flow is not driven by viscosity.[5] The second assumption is that compressibility can be ignored. This incompressibility assumption can be justified in the following cases:

- as long as the jet velocity U is kept small compared to the sound speed c,
- as long as the dimensions of the jet and sound production region are small compared to the acoustic wavelength.

Incompressibility implies a divergent free flow field div$\mathbf{v} = 0$. We will also assume for the sake of simplicity that the flow is two dimensional ($v_z = 0$). Incompressibility then writes div$\mathbf{v} = \partial v_x/\partial x + \partial v_y/\partial y = 0$. The velocity can then be written in terms of a stream function ψ:

$$v_x = \frac{\partial \psi}{\partial y} \;;\; v_y = -\frac{\partial \psi}{\partial x}. \tag{10.14}$$

Decomposition of the Velocity Field

From a general point of view, any vector field can be split into two complementary parts: a scalar potential φ part and a vector potential A part :

$$\mathbf{v} = \mathbf{grad}\,\varphi + \mathbf{curl}\,\mathbf{A}. \tag{10.15}$$

Of course, the acoustic field is part of the first contribution $\mathbf{grad}\,\varphi$ because it involves compressibility ($\nabla.\mathbf{v} = \nabla^2\varphi$). The second contribution takes into account the rotational part of the flow:

$$\boldsymbol{\omega} = \mathbf{curl}\,\mathbf{v} = \mathbf{curl}(\mathbf{curl}\,\mathbf{A}).$$

The following description is based on the evolution of the vorticity $\boldsymbol{\omega}$. This evolution can be studied by calculating the curl of the equation of motion (10.4):

$$\mathbf{curl}\left(\rho\frac{d\mathbf{v}}{dt}\right) = -\mathbf{curl}\,\mathbf{grad}\,p, \quad \text{therefore} \quad \frac{d\boldsymbol{\omega}}{dt} = 0. \tag{10.16}$$

This shows that in a frictionless flow, vorticity is conserved by the fluid particles: vorticity is convected at the local fluid velocity. In a two dimensional flow, a point

[5] Even if viscosity may be responsible for the formation of the sheared flow.

vortex of circulation Γ ($\Gamma = \oint_C v.d\ell$ on any contour C around the vortex) induces a tangential velocity field with amplitude decreasing away from the vortex. Symmetry of the flow around a point vortex allows calculating this tangential velocity v_θ induced by the vortex at a distance r from the vortex core:

$$v_\theta = \frac{\Gamma}{2\pi r}. \tag{10.17}$$

This corresponds to the Biot–Savart induction law. The instability of a shear layer can most efficiently be described starting from the flow induced by vorticity.

Kelvin–Helmholtz Instability Mechanism

Let us start the physical analysis of the jet instability with a simple case: the flow at the planar interface between two areas of the fluid with different velocities. This is known as the Kelvin–Helmholtz instability [16, 42]. This flow can be described by the relative velocity U between the two areas (see Fig. 10.12):

- $v_x = U/2$ if $y > 0$
- $v_x = -U/2$ if $y < 0$
- $v_y = 0$.

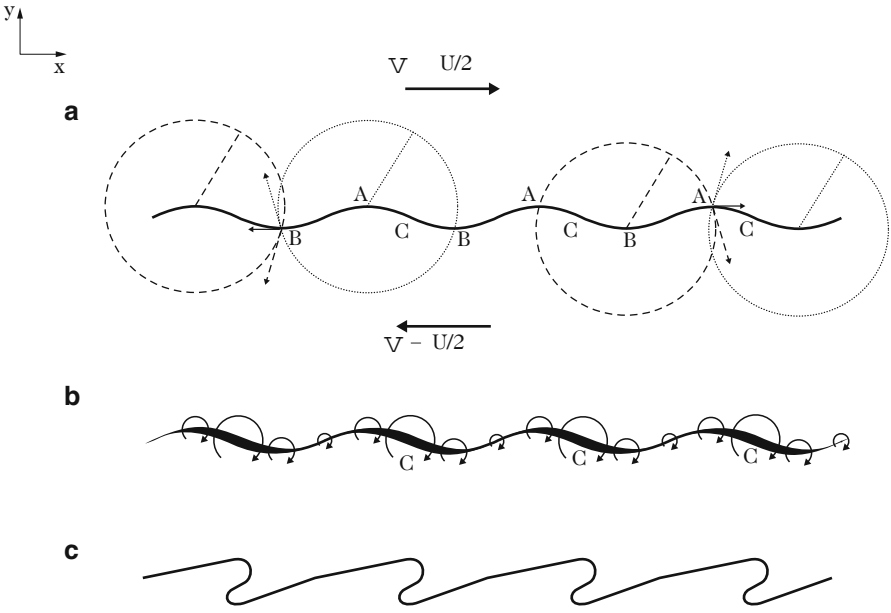

Fig. 10.12 The instability mechanism of a perturbed shear layer: (**a**) a perturbation of the interface induces local convection that concentrates (**b**) the vorticity at points C. This concentration amplifies the initial perturbation, leading to the formation of rolled structures (**c**)

The ***curl*** of the velocity field, $\boldsymbol{\omega}$, is zero everywhere except for $y = 0$: the interface is a line of vorticity. The three components of the ***curl*** are:

- $\omega_x = 0$
- $\omega_y = 0$
- $\omega_z = \partial v_y/\partial x - \partial v_x/\partial y = -\partial v_x/\partial y$.

As long as the interface remains unperturbed, the velocity field induced by the vorticity vanishes everywhere. Indeed, the transverse contributions to the velocity field at one given point of the interface due to the left side are fully compensated by the contributions on the right side. If we now assume the interface to be perturbed by a sinusoidal transverse motion, contributions from left and right sides to the local motion are no longer symmetrical. Figure 10.12 shows how this asymmetry induces a convection of vorticity of the upper parts (A) of the perturbed interface towards the right, while the lower parts (B) are convected towards the left. As a result, vorticity concentrates at the zero decreasing positions (C) of the interface.

This vorticity accumulation induces asymmetrical velocities, that contribute to the amplification of the initial perturbation, up to the point where waves break (Fig. 10.13).

10.3.2.2 Instability of an Infinite Jet

Rayleigh's Theory of an Infinite Jet

A jet can be described as two shear layers interacting with each other. The instability of an infinite jet has first been analyzed by Rayleigh [36]. The unperturbed jet in the x direction is given by:

Fig. 10.13 Wavy clouds in Wyoming, USA are induced by different wind velocities in neighboring layers (photo B.E. Martner, NOAA Environmental Technology Laboratory, Boulder)

- $v_x = U(y)$
- $v_y = 0$.

where $U(y)$ is the velocity profile of the jet. It satisfies the boundary conditions $U(\infty) = U(-\infty) = 0$ and we will further assume that the velocity profile has a single maximum. The curl of the velocity is

- $\omega_x = 0$
- $\omega_y = 0$
- $\omega_z = -\partial U(y)/\partial y = \Omega_z$.

The perturbed flow then writes

- $v_x = U + v'_x$
- $v_y = v'_y$
- $\omega_z = \Omega_z + \omega'_z$.

The vorticity conservation $d\boldsymbol{\omega}/dt = 0$ is

$$\frac{\partial(\Omega_z + \omega'_z)}{\partial t} + (U + v'_x)\frac{\partial(\Omega_z + \omega'_z)}{\partial x} + v'_y\frac{\partial(\Omega_z + \omega'_z)}{\partial y} = 0. \tag{10.18}$$

Because Ω is the steady unperturbed vorticity, it does not change in time nor in space and $\partial\Omega_z/\partial t = 0$ and $\partial\Omega_z/\partial x = 0$. For small enough perturbations, a linear approximation can be used. Products of perturbation terms are then neglected, and the previous equation becomes

$$\left(\frac{\partial}{\partial t} + U\frac{\partial}{\partial x}\right)\omega'_z + v'_y\frac{\partial\Omega_z}{\partial y} = 0 \tag{10.19}$$

where the last term shows the dependence of the jet on the second derivative of the velocity profile $\partial^2 U(y)/\partial y^2$. We now look for harmonic and propagative solutions[6] $\exp(j\omega t)\exp(-j\alpha x)$. Using $\omega'_z = \partial v'_y/\partial x - \partial v'_x/\partial y$, and the incompressibility condition $\partial v'_x/\partial x + \partial v'_y/\partial y = 0$ the previous equation turns into Rayleigh's equation:

$$\left(U(y) - \frac{\omega}{\alpha}\right)\left(\frac{\partial^2 v'_y}{\partial y^2} - \alpha^2 v'_y\right) - v'_y\frac{\partial^2 U(y)}{\partial y^2} = 0. \tag{10.20}$$

The transverse component of the perturbation v'_y is obtained by solving this equation. One needs the help of the stream function ψ' of the perturbation to calculate the longitudinal component of the perturbation. The stream function has the same harmonic propagative form $\psi'(x, y, t) = \Psi'(y)\exp(j\omega t)\exp(-j\alpha x)$.

[6]Notice that ω is the time periodicity (angular frequency) of the perturbation, while $\boldsymbol{\omega} = (0, 0, \omega_z)$ is the curl of the velocity.

All perturbation terms can be calculated from the stream function function amplitude Ψ', solution of:

$$\left(U(y) - \frac{\omega}{\alpha}\right)\left(\frac{\partial^2 \Psi'}{\partial y^2} - \alpha^2 \Psi'\right) - \Psi' \frac{\partial^2 U(y)}{\partial y^2} = 0. \tag{10.21}$$

Spatial Versus Temporal Analysis

When the jet velocity profile $U(y)$ is known, a dispersion relation is obtained, linking the time and space periodicity ω and α of the solution, by assuming boundary values $\Psi'(y) \rightarrow 0$ far from the jet ($y \rightarrow \pm\infty$). Depending on the problem studied, two resolutions can be carried out:

- the space dependence ($\alpha = \alpha_r + j\alpha_i$) of the perturbation with fixed time periodicity (ω real). Such a perturbation grows with distance as $\exp(\alpha_i x)$ with a phase velocity associated to the convection of the perturbation $c_p = \omega/\alpha_r$. A hydrodynamic wavelength $\lambda_h = 2\pi c_p/\omega = 2\pi/\alpha_r$ results from this propagation. This is a spatial analysis.
- the time dependence (ω then being complex) that results from a perturbation with specific real wavenumber α_r, corresponding to imposed geometry conditions. The perturbation then grows or vanishes in time, according to the sign of α_i. This is a temporal analysis.

The oscillating frequency in flutes is strongly dependent on the acoustic resonances of the pipe. Therefore, a spatial analysis is generally preferred.

Sinuous and Varicose Modes

If the jet velocity profile is symmetrical about $y = 0$, perturbations on both shear layers of the jet can be symmetrical or anti-symmetrical, depending on the symmetry properties of the initial perturbation of the jet. Symmetrical perturbations induce the so-called varicose oscillations of the jet, associated with a modulation of the jet thickness (see Fig. 10.14). Anti-symmetrical perturbations correspond to "sinuous" oscillations of the jet. Solving Rayleigh's equation (10.21) indicates that sinuous oscillations have a stronger amplification than varicose oscillations.

Furthermore, jet visualizations in various flute configurations indicate that the sinuous motion dominates under standard blowing conditions. In some cases, varicose contribution can be observed, which has an influence on the spectral content of the sound.

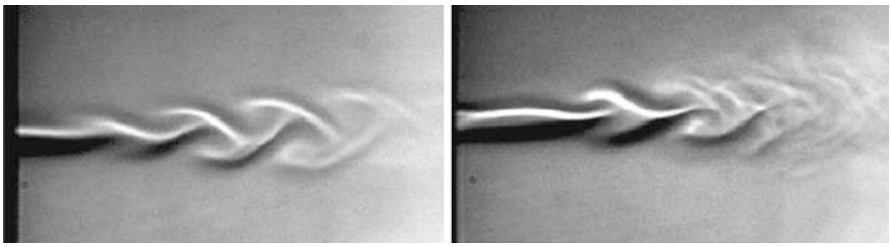

Fig. 10.14 Flow visualization of a jet submitted to an acoustic perturbation: following the initial jet perturbation, sinuous motion can be dominant (*left*) or varicose can be dominant (*right*)

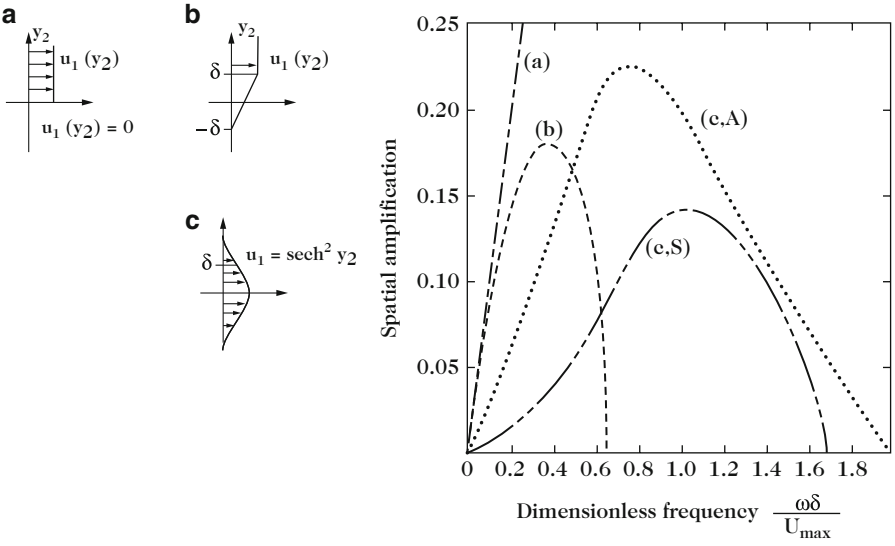

Fig. 10.15 Spatial amplification on a shear layer for different velocity profiles. (**a**), (**b**), and (**c**): simple shear layers, after Blake [6]. The amplification corresponds to anti-symmetrical jet oscillations [sinuous: (c,A)] or symmetrical [varicose: (c,S)]. Note that sinuous oscillations are better amplified than varicose oscillations

Solutions of the Rayleigh Equation

Depending on the jet velocity profile $U(y)$, Eq. (10.21) can be solved either analytically or numerically. In the case of a spatial analysis, Fig. 10.15 shows the frequency dependence of the spatial growth of perturbations on the jet. The dimensionless amplification coefficient $\alpha_i\delta$ uses the shear layer thickness δ as the spatial scale of the problem. The dimensionless frequency is the Strouhal number $\mathrm{Str}_\delta = \omega\delta/U_{\max}$, where $U_{\max}$ is the maximal value in the jet velocity profile.

It can be checked that, in the case of an infinitely thin shear layer such as the one discussed above (Kelvin–Helmholtz), the amplification increases monotonously with frequency, as already mentioned by Rayleigh. Such a thin shear layer is purely

theoretical since viscosity, even if it is very low, spreads the shear layer. All other velocity profiles with finite shear layer thickness show a maximum of amplification and then fall down below zero for Strouhal number of the order of unity. As a matter of fact, the jet does not amplify the perturbation anymore when the hydrodynamic wavelength $\lambda_h = 2\pi c_p/\omega$ gets smaller than the shear layer thickness δ.

10.3.2.3 Receptivity and Jet Oscillation in a Flute

The Jet Motion

Rayleigh's theory, presented above, is based on an infinite parallel jet flow assumption. In flutes, the jet is formed at the flue exit and flows through a window where strong transverse acoustic flows can be experienced, due to the accumulation of acoustical energy in the pipe resonator. A first step in this direction is to consider a semi-infinite jet, with negligible transverse displacement at the flue exit.

The transverse displacement $\eta(x,t)$ of the jet in the y direction can be calculated by integration of the transverse velocity from the flue exit to the actual position x. This transverse velocity is made of two components: the perturbation term v'_y exponentially growing with the distance from the flue exit, and the air displacement due to the acoustic velocity $v_{\rm ac}$:

$$\eta(x,t) = \int_{t-x/U_0}^{t} \left[v'_y(x',t') + v_{\rm ac}(x',t')\right] dt', \tag{10.22}$$

if $x' = x - (t-t')U_0$.

For long enough distances from the flue exit, one can ignore the contribution of the acoustical displacement. The transverse jet displacement then writes[7]

$$\eta(x,t) \approx -\int_{t-x/U_0}^{t} \frac{\partial \psi'(x',t')}{\partial x} dt'. \tag{10.23}$$

This implies a growth of the amplitude of the jet displacement η with $\exp(-\alpha x)$

Receptivity: The Jet Initial Perturbation

The sinuous jet motion comes from the anti-symmetrical perturbation by the acoustic field. The way the acoustic field produces the initial jet perturbation is called the *receptivity*. To a first approximation, we will assume that the initial perturbation is localized at the flue exit. In an incompressible inviscid flow approximation, this can

[7]Indeed $v'_y = -\partial\psi'(x',t')/\partial x$, which may be the reason why some authors make a confusion between the jet transverse displacement η and the stream function ψ' of the perturbation.

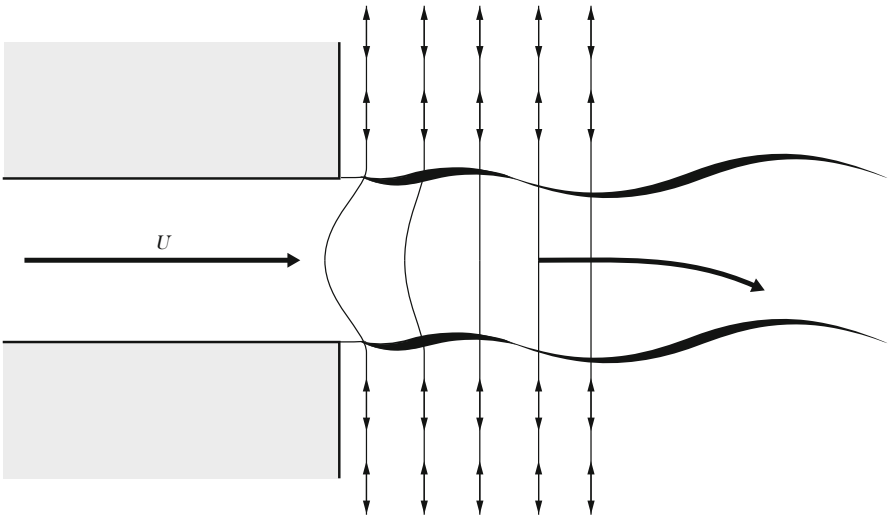

Fig. 10.16 The initial jet perturbation by the acoustic field is localized at the flow separation points where the jet is formed

be justified by the vorticity conservation in the flow. The jet perturbation can be represented as a modulation of the vorticity in the flow. Because of the vorticity conservation, such a vorticity modulation can only be injected at the separation points of the flow, due to local viscous effects. The amplification that occurs downstream is only a consequence of the jet instability, in terms of redistribution of the initial vorticity (Fig. 10.16).

Details of the geometry and of the flow in the vicinity of the flow separation points can strongly affect the receptivity [7]: boundary layer thickness in the channel just upstream from the flue exit and the geometry of the channel exit are of great influence. This is in line with the observation of recorder makers who give great care to the cutting of chamfers at the end the channel, as well as with the transverse flute players' claim that small irregularities on the player's lips strongly affect the tone quality.

Receptivity: An Empirical Model

A simplified description of the jet oscillation is generally considered for the global analysis of the oscillation in flutes. The description integrates some of the results of the analysis presented and, in particular, the exponential spatial growth α_i of the perturbation together with the convection of the perturbation. In the case of a harmonic perturbation, the transverse jet displacement η at a distance x from the flue exit is written as:

$$\eta(x,t) \approx \eta_0 e^{\alpha_i x} e^{j\omega(t-x/c_p)}. \tag{10.24}$$

Even if this description cannot fulfill the initial condition $\eta(0,t) = 0$, it offers a fairly good approximation of the jet displacement for distances from the flue exit larger than the channel thickness ($x \geq h$), provided that the initial value η_0 is correctly chosen. The perturbation being triggered by the acoustic velocity, the initial jet displacement is expected to be proportional to V_{ac}/U_j and h:

$$\eta_0 \approx \frac{V_{\mathrm{ac}} h}{U_j}. \tag{10.25}$$

Experimental data [14] indicate that the receptivity of the jet can be interpreted in terms of the relative thickness of shear layers in the jet $\delta_j = L/\sqrt{Re}$, where L is the flue channel length, and acoustic boundary layers $\delta_{\mathrm{ac}} = \sqrt{2\nu/\omega}$ as follows:

$$\eta_0 = \frac{V_{\mathrm{ac}} h \delta_j}{U_j \delta_{\mathrm{ac}}}. \tag{10.26}$$

This approach allows the dependence of the receptivity on both the frequency and jet velocity to be introduced. More recent studies by Blanc [7] indicate that the effect of chamfers found in recorders can be split into two complementary contributions: a protection effect reducing the effective V_{ac}/U_j due to the standing back of the flow separation points and an orientation of the perturbative acoustic velocity, locally following the wall geometry.

The Upper Limit of the Linear Analysis: Jet Roll Up and Vortex Formation

Rayleigh's description of the evolution of a perturbation on the jet uses a linearization of the equations [see Eq. (10.19)]. From a physical point of view, the accumulation of the shear layers' vorticity at the inflexion points in the shear layer is responsible for the growth of the perturbation. For transverse jet displacement of the same order of magnitude as the jet thickness, the jet appears to roll up and break down into discrete vortices.

The flow can then be described as an alternate vortex street, as described by Von Kármán. In order to be stable, the vortex street needs to follow the correct relation between the hydrodynamic wavelength λ_h, the street width b, the circulation Γ of vortices, and the convection velocity c_{Vx} of the street:

$$c_{Vx} = \frac{\Gamma \pi}{\lambda_h} \tanh\left(\frac{\pi b}{\lambda_h}\right). \tag{10.27}$$

Experiments show that the amplitude of the transverse jet displacement for which the linear behavior (exponential growth) turns into a vortex street is close to the jet thickness. However, this amplitude does not depend on the distance between the flue exit and the transition point, while this distance depends on the perturbation amplitude (see Fig. 10.17).

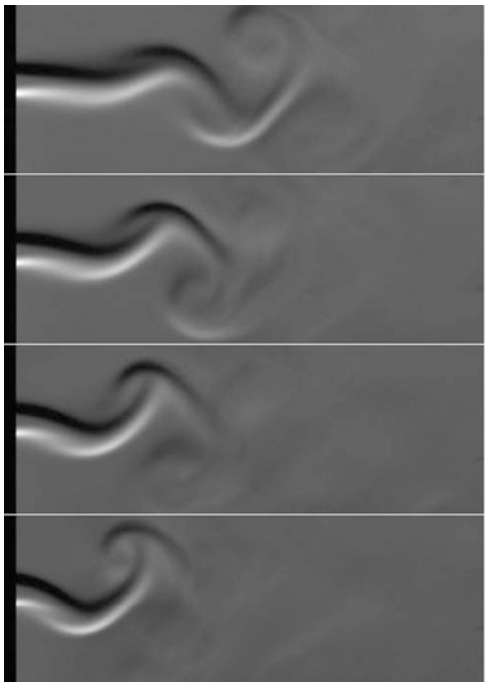

Fig. 10.17 Visualization of a jet submitted to a transverse acoustic field. From *bottom* to *top*, the excitation amplitude V_{ac} grows from 0.5 to 6.5 % of the jet velocity U_j. The jet transverse displacement grows linearly, up to the point where the jet breaks down into a row of alternate vortices, forming a vortex street. The formation of the vortex street occurs closer to the flue exit when the excitation amplitude is increased. From [14]

10.3.3 Turbulent Jet

As the jet velocity increases, its structure becomes chaotic. For values higher than a threshold, the jet is disorganized and spreads rapidly with distance. This chaotic behavior is called turbulence. This threshold depends on the geometry of the jet as well as on the fluid viscosity. It is expressed in terms of the Reynolds number $Re = U_j h/\nu$, where h is the jet channel thickness, and ν is the kinematic viscosity of air. While turbulence always develops sooner or later on the jet (see Fig. 10.18), for values of the Reynolds number smaller than 2000, the jet remains laminar for a short distance. For values above 3000, the jet becomes turbulent immediately downstream the flue exit. Estimations under playing conditions for different recorders indicate that the Reynolds number varies between 700 and 2000.

In order to produce loud sounds with flutes, the instrument and the blowing technique must allow to blow hard, that is to blow large air flows. Therefore, in most of the flutes intended for outdoor playing, one finds high values of the Reynolds number, sometimes higher than 10^4. The jet then becomes rapidly turbulent and the above description of the jet instability becomes inaccurate.

Several aspects are to be considered in this case:

- a strong decrease of the jet velocity with distance,
- a strong spreading of the jet,
- kinetic energy dissipation.

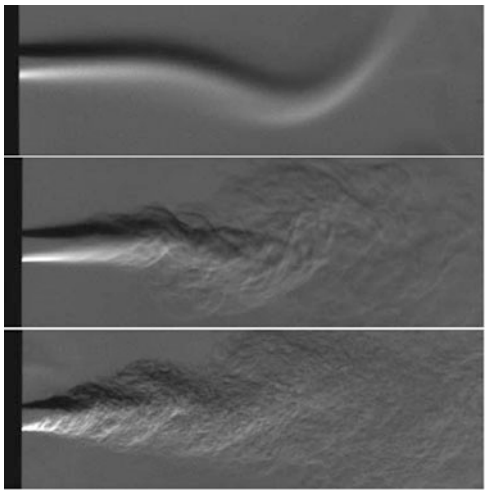

Fig. 10.18 Jet perturbed by an acoustic field. The Reynolds number in the jet increases from 200 (*top*) to 500 (*middle*) up to 3000 (*bottom*). The jet remains laminar all along the observation window for $Re = 200$. On the opposite, turbulence develops rapidly downstream of the flue exit for $Re = 3000$

A consequence of the turbulent structure of the jet is a wideband noise production. This is well known in the case of traditional instruments for outdoor music, for which a loud sound is required. The associated strong wideband noise is a part of the sounding aesthetics of these instruments. In the case of the modern Boehm flute, the quest for a "pure" tone in the sounding aesthetics of the instrument at the beginning of the twentieth century, until 1935, is challenging for the player since he has to handle a tricky compromise between sound power and tone purity (Fig. 10.19).

10.4 Aeroacoustic Sound Sources

The interaction of the oscillating jet with the labium produces the acoustic energy that sustains the oscillation in the resonator. The largest jet oscillation takes place at a position where the resonator shows a strong reaction: the labium is an edge at an open pipe end, where the acoustic velocity is maximum. Furthermore, a sharp labium induces a local singularity in the acoustic field. The same jet oscillation in free field or at less reactive position in the resonator would not produce as much sound.

Helmholtz was the first to describe the sound production by the end of the nineteenth century. In the first edition of his book [48], the jet oscillation is described as injecting fluid in the pipe at each period of the oscillation. Rayleigh argued to Helmholtz that the labium is at an open end of the pipe, where acoustic pressure fluctuations p_a are small. The mechanical work associated to volume flow injection Q is therefore weak:

$$W = \int_T p_a Q dt. \tag{10.28}$$

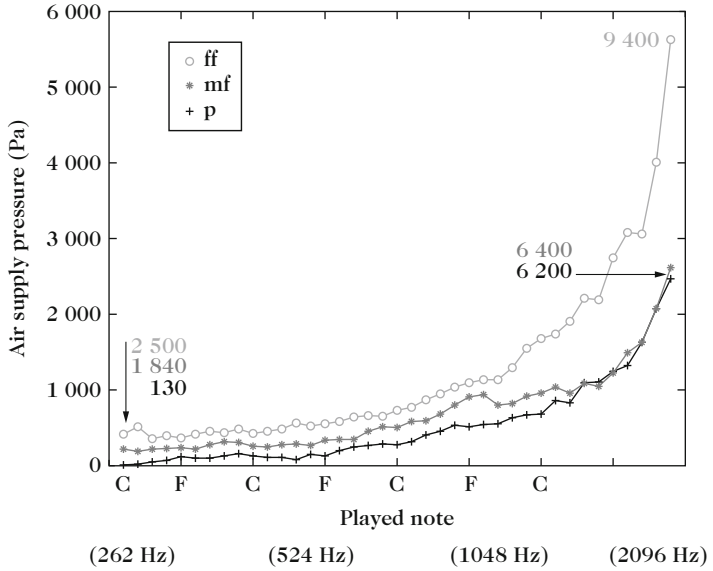

Fig. 10.19 Mouth pressure in modern Boehm flute playing as function of the pitch, for three different dynamics: *plus symbol*, *p*; *filled circle*, *mf*; *open circle*, *ff*. Estimated values of the Reynolds number are added on the plot

Conversely, the acoustic velocity is maximum at the open pipe end, therefore Rayleigh suggests that the acoustic source is a force F_a acting on the acoustic field. Such a source is more efficient since the work is then proportional to the local acoustic velocity v_a:

$$W = \int_T F_a v_a dt. \tag{10.29}$$

However, Rayleigh does not give any clue on the physical origin of this force. Several mechanisms may contribute to this force, such as the jet oscillation and the turbulence. Estimations of the acoustical power produced shows an order of magnitude of 10 mW [20].

10.4.1 The Jet-Drive Model

This model is based on Helmholtz's description: indeed, he modified his text in the second edition, taking Rayleigh's arguments into consideration! Developing Helmholtz's idea, the model takes the two flow injections on both sides of the labium into account. The two sources Q_{in} and Q_{out}, placed a small distance δ_d from each other, have fluctuating parts Q_1 and Q_2 with opposite phases ($Q_1 = -Q_2$). Therefore, they generate a pressure difference (see Fig. 10.20).

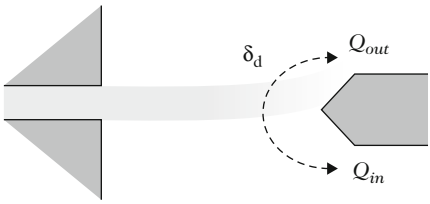

Fig. 10.20 The jet oscillation can be described as two flow injections on both sides of the labium. The fluctuating parts of the two volume flows show opposite phases $Q_1 = -Q_2$, at a short distance δ_d. In a low frequency approximation, the two sources are separated by a short distance in a small pipe. It can be represented by an equivalent pressure difference given in Eq. (10.30)

The model is developed in a low frequency approximation. Plane waves propagate in the resonator, which is therefore represented as a 1D transmission line. Assuming that the source dimensions are small compared to the acoustic wavelength, the resonator is described as a main pipe and a short thinner pipe since the open end in the mouthpiece always has a smaller cross-section area than the pipe. In this 1D representation, the two sources with opposite phases Q_1 and Q_2 are placed in the thin short pipe, at a short distance δ_d from each other (see Fig. 10.21). They constitute a dipole confined in the small pipe of cross section S_m, and produce an alternate motion of the air mass $\rho\delta_d S_m$ between the two sources.[8] The acceleration of this air mass generates the force acting on the acoustic field. This force can be written in terms of a pressure difference acting across the mouth of the pipe:

$$\Delta p = -\frac{\rho}{S_m}\delta_d \frac{d}{dt} Q_1, \tag{10.30}$$

that the source maintains between both sides of the labium. Therefore, the source can be seen as a localized pressure step across the mouth, even if both volume flow injection points are at a small distance.[9]

[8]Please note that the initial model by Helmholtz took only the inner volume flow injection into account, leaving the outer volume flow injection Q_{out} aside. However, even if the outer volume flow injection appears to be outside the pipe from a geometrical point of view, it definitely is inside the instrument from the acoustic point of view, since the limit between inner and outer field is not clearly defined from the acoustic point of view, that is within the scale of the acoustic wavelength.

[9]In Chap. 1, sources in a pipe have been discussed, using Eqs. (1.134) and (1.135). The source term in (1.134) can be written as:

$$-\frac{\rho}{S_m}\frac{d}{dt}\left[Q_1\delta(x-x_1) + Q_2\delta(x-x_2)\right] = -\frac{\rho}{S_m}\frac{d}{dt}Q_1\delta_d\frac{d}{dx}\delta(x-x_1).$$

The second expression uses the Taylor development at x_1, since $x_2 = x_1 - \delta_d$ and $Q_1 = -Q_2$. Equation (1.135) gives the equivalent force:

$$f = -\rho\frac{d}{dt}Q_1\delta_d.$$

this force balances the pressure difference $f = S_m(p_1 - p_2) = S_m\Delta p$, and corresponds to (10.30).

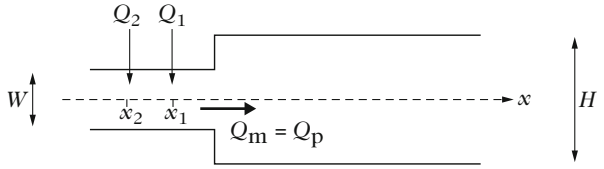

Fig. 10.21 Simplified model of a flute. Injection of two volume flows sources is equivalent to a pressure step, in a l ow frequency approximation. W and H are the flue exit to labium distance and the pipe height: in a 2D geometry, they are proportional to the areas S_m and S of mouth and pipe, respectively. The distance between the sources is $x_1 - x_2 = \delta_d$. The flow rates Q_m and Q_p through mouth and in the pipe, (that are used in the simplified model in Sect. 10.5.4) are equal since the pressure difference source *does not affect the flow rates*

The distance δ_d corresponds to the distance between the injection points Q_1 and Q_2: it corresponds to the distance associated with the potential difference in a potential theory. It can be calculated from the estimated injection positions, using conformal mapping for idealized geometries [35] (see also Chap. 7, Sect. 7.6.3.2).

10.4.2 A Discrete Vortex Model

As discussed earlier in this chapter, the jet oscillation results from the perturbation of the vorticity in the shear layers: the velocity field can be described as a potential flow on top of which two films of vorticity are added, which are modulated at the flue exit by the acoustic perturbation. The transverse motion of the jet results from the progressive concentration of vorticity at specific points, and the jet can therefore be described as a succession of line vortices shifted between the two shear layers. In such as description, the sound production can be seen as the work performed on the acoustic field by the Coriolis force associated with the convection of vortices. The force per unit volume f generated by a vortex of vorticity $\boldsymbol{\omega}$ and moving at the local fluid velocity $\boldsymbol{v}$ is given by:

$$\mathbf{f} = -\rho_0(\boldsymbol{\omega} \wedge \boldsymbol{v}). \tag{10.31}$$

The acoustic power produced per unit volume is the scalar product $\mathbf{f}.\mathbf{v}_{\mathrm{ac}}$, where $\mathbf{v}_{\mathrm{ac}}$ is the acoustic velocity. In this approach, the velocity field $\mathbf{v}$ is split into two contributions: the potential and the rotational components [see Eq. (10.15)]. The acoustic velocity then corresponds to the fluctuating part of the potential component of the field:

$$\mathbf{v}_{\mathrm{ac}} = \mathbf{grad}\varphi - \langle \mathbf{grad}\varphi \rangle. \tag{10.32}$$

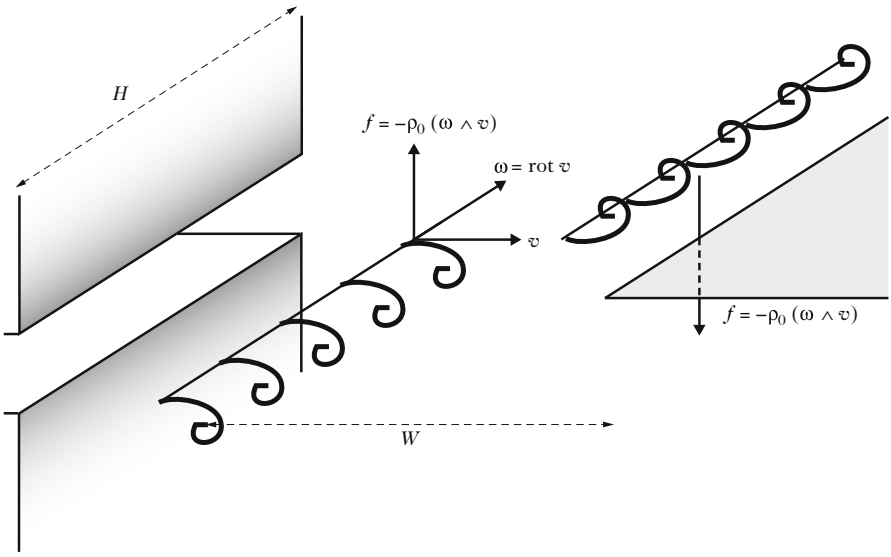

Fig. 10.22 The sound production is represented as the work performed on the acoustic field by the Coriolis force associated with the convection of vortices

where the brackets $\langle x \rangle$ indicate the time average of x. The acoustic power produced becomes

$$P_{\text{vortex}} = \frac{1}{T} \int_T \int_{\text{vol}} -\rho_0 (\boldsymbol{\omega} \wedge \boldsymbol{v}).\mathbf{v}_{\text{ac}} dV dt, \tag{10.33}$$

where vol is the volume where the source term $(\boldsymbol{\omega} \wedge \boldsymbol{v}).\mathbf{v}_{\text{ac}}$ is not vanishing (Fig. 10.22).

Sound production is restricted to areas where the force is parallel to the acoustic field, which of course corresponds to a condition for accelerating the acoustic motion. This is why the sound production is dominated by the vortex line the closest to the labium edge: indeed, the acoustic velocity is maximum around the labium edge because of the singularity associated with a sharp edge in a potential flow. Estimation of the sound power in the case of edge-tones [26] as well as in the case of flutes [15] shows that the sound production can be reasonably estimated taking only the vortex line closest to the edge into account. This explains why the sound quality is very sensitive to the shape of the edge of the labium. Vortices carried further downstream into the pipe have a velocity $\boldsymbol{v}$ parallel to the acoustic velocity $\mathbf{v}_{\text{ac}}$ so that the source term $(\boldsymbol{\omega} \wedge \boldsymbol{v}).\mathbf{v}_{\text{ac}}$ vanishes.

10.4.3 Aeroacoustic Formulation

The modeling of the acoustic source presented in the previous sections is based on the assumption that the source mechanism is localized in the vicinity of the labium edge. In a complementary approach, sound production can be described through an integral description. Several frameworks can be found, called aeroacoustic analogies: the one that is behind the description using discrete vortex lines presented above is basically the description used by Howe [28]. The following section presents the approach by Lighthill (see, for example, [12, 23, 25, 37]).

10.4.3.1 Lighthill's Analogy

In the analogy of Lighthill, one assumes a spatially limited region of sound production by the flow. The sound generated propagates to an observer located outside the source region, in a stagnant uniform fluid of density ρ_0 and sound velocity c_0. The flow at the observer's position is assumed to be described by the acoustic approximation.

Lighthill's analogy is obtained by rewriting the basic equations of flow motion. It is based on the time derivative of the mass conservation[10]:

$$\frac{\partial}{\partial t}\left[\frac{\partial \rho}{\partial t}+\frac{\partial \rho v_i}{\partial x_i}\right]=0, \tag{10.34}$$

and on the divergence of the momentum conservation equation:

$$\frac{\partial}{\partial x_i}\left[\frac{\partial \rho v_i}{\partial t}+\frac{\partial \rho v_i v_j}{\partial x_j}\right]=-\frac{\partial}{\partial x_i}\left[\frac{\partial P_{ij}}{\partial x_j}\right], \tag{10.35}$$

where P_{ij} is the stress tensor, due to pressure p and viscous stresses τ_{ij} ($P_{ij} = p\delta_{ij} - \tau_{ij}$).[11]

The fluid density ρ is split into its mean value ρ_0 at the observer's position and fluctuating component $\rho = \rho_0 + \rho'$ with $\partial^2\rho/\partial t^2 = \partial^2\rho'/\partial t^2$. Subtracting the two equations above and subtracting $c_0^2\partial^2\rho/\partial x_i^2$ on both sides of the equation yields

$$\frac{\partial^2 \rho'}{\partial t^2}-c_0^2\frac{\partial^2 \rho'}{\partial x_i^2}=\frac{\partial^2 T_{ij}}{\partial x_i \partial x_j}, \tag{10.36}$$

[10] The following equations use the so-called Einstein summation convention: when an index variable appears twice in a single term it implies summation of that term over all the values x, y, z of this index. For example, $\frac{\partial v_i}{\partial x_i}$ means $\frac{\partial v_x}{\partial x}+\frac{\partial v_y}{\partial y}+\frac{\partial v_z}{\partial z}$.

[11] τ_{ij} is defined as [3]:

$$\tau_{ij}=\mu\left[\frac{\partial v_i}{\partial x_j}+\frac{\partial v_j}{\partial x_i}\right]-\frac{2}{3}\mu \text{ div } \boldsymbol{v}.\delta_{ij}$$

As it is, (10.35) is the divergence of the Navier–Stokes equation.

where T_{ij} is the Lighthill tensor:

$$T_{ij} = \rho v_i v_j + (p' - c_0^2 \rho')\delta_{ij} - \tau_{ij} \simeq \rho v_i v_j + (p' - c_0^2 \rho')\delta_{ij}, \tag{10.37}$$

if $p = p_0 + p'$. This last expression is obtained assuming that the forces induced by the fluid viscosity are negligible compared to the convection forces: τ_{ij} can therefore be neglected. This assumption is based on an estimation of the Reynolds number in flute jets, as a ratio between inertial and viscous forces in the flow. In this approach, the equations above describing the basic fluid properties of mass and momentum conservation are subtracted to produce a left-hand term of the equation corresponding to an acoustic wave equation. All the other terms, pushed on the right-hand side are acoustic sources.

This can also be written in terms of the pressure fluctuations p', showing four source terms:

$$\frac{1}{c_0^2}\frac{\partial^2 p'}{\partial t^2} - \Delta p' = \frac{\partial^2 \rho v_i v_j}{\partial x_i \partial x_j} + \frac{\partial^2}{\partial t^2}\left(\frac{p'}{c_0^2} - \rho'\right) + \left[\rho \frac{\partial q_m}{\partial t} - \rho \frac{\partial F_i}{\partial x_i}\right]. \tag{10.38}$$

The first source term is a quadrupole, and corresponds to nonlinear convective terms like vortices and turbulence. The second source term is a monopole and corresponds to entropy fluctuations. The last two terms are not in Eq. (10.36) but have already been discussed for stagnant fluid [see Eq. (1.111)]. They have been added here. The third term is a monopole and corresponds to a mass injection ρq_m, while the last term, dipolar, describes the effect of an external force field density ρF_i acting on the fluid.

An integral formulation of this analogy has been proposed by Curle [13], in order to take the presence of walls with surface S into account, delimiting a volume V.

Sources will be discussed in Chap. 12, but the integral description presented here already introduces this discussion. The acoustic pressure in a given geometry can be written using the Green's function that describes the acoustic response of the system. This function $G(\mathbf{x}, t|\mathbf{y}, \tau)$ corresponds to the acoustic pressure at time t and position $\mathbf{x}$ observed for an impulsive source at time τ and position $\mathbf{y}$. The Green's function is solution of [see, for instance, (4.19)]:

$$\frac{\partial^2 G}{\partial t^2} - c_0^2 \Delta G = \delta(\mathbf{x} - \mathbf{y})\delta(t - \tau). \tag{10.39}$$

Applying this formalism to Lighthill's source terms yields

$$\begin{aligned} p'(\mathbf{x}, t) = &\int_{-\infty}^{t}\int_{V} T_{ij}\frac{\partial^2 G}{\partial y_i \partial y_j} dy d\tau \\ &+ \int_{-\infty}^{t}\int_{S} \rho v_i \frac{\partial G}{\partial \tau} n_i dS d\tau + \int_{-\infty}^{t}\int_{S} \frac{\partial G}{\partial y}(p'\delta_{ij} + \rho v_i v_j) n_j dS d\tau, \end{aligned} \tag{10.40}$$

where V is the volume in which all sources are located, S is the surface bounding volume V, with n_i the outgoing normal. While the last equation is an exact solution that helps to improve our understanding of the sound production mechanisms, it can only be applied to the modeling at the expense of severe simplifications, regarding both the acoustic response of the system (Green's function) and the flow, as illustrated in the following paragraphs.

10.4.3.2 Low Frequency Approximation

At frequencies lower than the pipe cutoff frequency, only plane waves propagate (see Chap. 7) and the Green's function of a 1D infinite pipe can be used

$$G(x_1, t|y_1, \tau) = \frac{c}{2S} H(t^* - \tau), \tag{10.41}$$

where $H(t)$ is the Heaviside step function, the index "1" indicates the pipe direction and $t^* = t - \frac{x_1 - y_1}{c}$ is the retarded time, taking the sound propagation from source to observer into account.[12] Using the symmetry properties of the Green's function $\partial G/\partial x_1 = -\partial G/\partial y_1$, the derivatives of the Green's function $\partial G/\partial y_1 = 1/2\,\mathrm{sgn}(x_1 - y_1)\delta(t^* - \tau)$ and $\partial G/\partial t = -c/2\delta(t^* - \tau)$, and assuming further that the volume is small compared to the acoustic wavelength λ (compact source assumption, $\partial/\partial t << c/\lambda$), the pressure then writes [12]

$$\begin{aligned} p_1'(x_1, t) = &-\frac{c}{2S}\int_S [\rho v_i]_{t^*} n_i dS \\ &- \frac{1}{2S}\,\mathrm{sgn}(x_1 - y_1)\int_S p'(y_1, t^*) n_1 dS - \frac{1}{2S}\,\mathrm{sgn}(x_1 - y_1)\int_S \left[\rho v_1 v_j\right]_{t^*} n_j dS. \end{aligned} \tag{10.42}$$

The first term describes the mass flow going out of the source volume V, while the second term describes the pressure forces acting on the surface bounding the source volume, and the third term corresponds to nonlinear convective contributions in the flow (turbulence and vortices).

In the application to sound production in flutes, if the total jet volume flow is assumed to be constant (see Sect. 10.5.2 for a discussion on this topic), the first term does not produce any sound. Furthermore, for values of the Reynolds number less than a few hundreds, the sound produced by turbulence is negligible. The main source terms then lie in the pressure term and in the vortices.

A similar analysis developed by Powell [34] in the case of edge-tones, i.e., a jet flowing towards a labium without acoustic resonator, shows that the dominant term is the unsteady force exerted by the flow on the labium. This force corresponds to

[12] It is in fact the first term of (4.20) and (4.21), since the infinite pipe does not show any reflection.

the stagnation pressure of the jet and the amplitude of the oscillating force is (H is the width of the jet in the transverse direction):

$$F_a = \frac{1}{2}\rho H \int U(y)^2 dy, \tag{10.43}$$

which has been confirmed by experiments [40].

Finally, in the case of edge-tones, the source term can be written in terms of a dipole, such as the one written in Sect. 10.4.1, provided that the potential distance δ_d between source and sink is a function of the jet velocity, or of the hydrodynamic wavelength $\lambda_h = 2\pi c_p/\omega$ of the perturbations on the jet:

$$\delta_d \approx \lambda_h/2. \tag{10.44}$$

Both approaches, the aeroacoustic and the more acoustically intuitive presented in Sect. 10.4.1 are in line, provided that the source-sink distance in the jet-drive model corresponds to half the hydrodynamic wavelength, and therefore depends on the jet velocity and on the frequency.

10.4.3.3 Increasing the Jet Velocity

The analysis presented above is restricted to relatively low Reynolds numbers and low frequencies. When the jet velocity is increased, sound production by turbulence becomes more and more important. Verge [44] presented a study of sound production by turbulence of a jet impinging on a labium in an infinite pipe, assuming no synchronized jet oscillations. The two first terms in Eq. (10.42) vanish and the pressure is written as:

$$p'(x_1, t) = -\frac{1}{2S}\,\mathrm{sgn}(x_1 - y_1) \int_S \rho v_{1_{t^*}}^2 dS, \tag{10.45}$$

showing that the acoustic power ranges as the fourth power of the jet velocity or of the Mach number $M = U_0/c$:

$$P_{\mathrm{ac}} \propto M^4. \tag{10.46}$$

In a sound synthesis by physical modeling, adding to the source terms a broadband noise that follows this power law improves the realism of the synthesis. This shows how important the turbulence noise is for the perception of the sound identity of flutes.

10.4.3.4 Vortex Shedding at the Labium

In a theoretical analysis of the problem, Howe [28] proposes a model for the sound production in flutes based on the vortex sound theory. The sound production is due to the action of the Coriolis force on the acoustic field [see Eq. (10.33)]. In this model, the sound is generated at each period by a vortex shed at the labium, triggered by the flow induced by the acoustic resonance in the pipe. This vortex is then convected by the jet (see Fig. 10.23). In this framework, the sound production in a flute has been estimated, based on flow visualizations that show the exact phase of the triggering of this vortex. It appears that, due to the phase relation between the different terms, the sound production is negative [21]: the vortex does not produce sound as was assumed by Howe [28] but rather absorbs acoustic energy. Furthermore, the analysis of the different losses, under standard blowing conditions in a recorder, indicates that the losses induced by the vortex shedding at the labium is one of the dominant mechanism that limits the oscillation amplitude.

The vortex sound theory of Howe is also interesting for thick jet configurations. The vorticity in the jet shear layers is represented as discrete vortices, triggered by the acoustic perturbation. These vortices are convected at a constant velocity of approximately half the main flow velocity, with a circulation that grows linearly with time.[13] Notice that the vortices considered here are not those shed at the labium like in Howe's model [28], but those formed at the flue exit, corresponding to the jet shear layers. The model proposed by Meissner for a whistle is built with this description. It seems to give an accurate prediction of the oscillating frequency

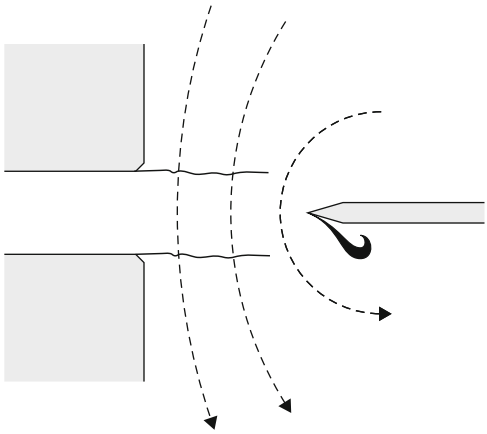

Fig. 10.23 Vortex shedding at the labium, due to the separation of the flow induced by the acoustic field. *Dashed lines* indicate streamlines of the potential flow associated with the acoustic velocity

[13] See, for example, the work by Meissner [32] in the case of a whistle and Dequand [15], inspired by Nelson's [24, 33] and Holger's [27] descriptions. A difference between the two models is that Dequand assumes that the circulation of each vortex grows during one oscillating period only, while Meissner assumes that the circulation grows without saturation, but only takes the vortices between the flue exit and the labium into account.

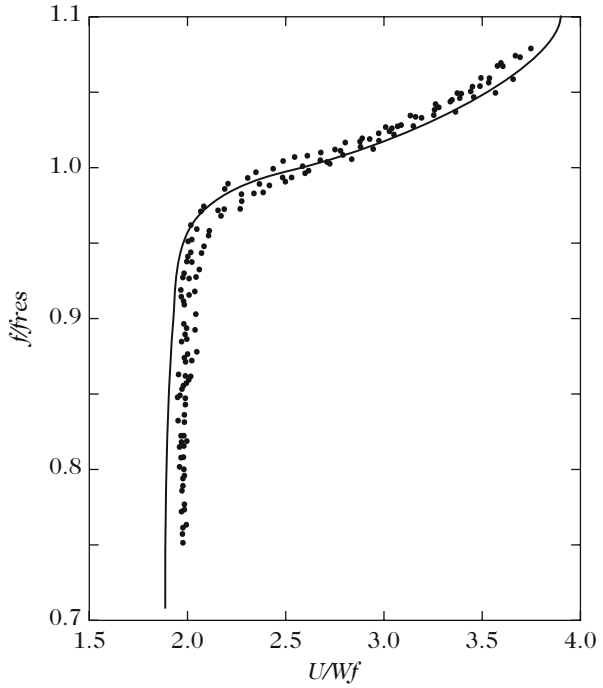

Fig. 10.24 Dimensionless frequency f/f_{res} of the oscillation in a Helmholtz resonator (f_{res} is the passive resonance frequency) as function of the dimensionless jet velocity (or inverse Strouhal number) $\text{Str}^{-1} = U/Wf$, U is the jet velocity, W is the flue exit to labium distance. For low jet velocities, the oscillation appears at frequency lower than the resonance frequency. It corresponds to a constant Strouhal number, indicating that the frequency is proportional to the jet velocity. After [32]

(Fig. 10.24) but not of the amplitude. This indicates that even if phase terms are well described in the model, losses are still difficult to estimate.

The oscillating frequency in flutes and organ pipes on the first regime shows a double slope behavior:

- for low jet velocities and oscillation at frequency lower than the pipe resonance, the oscillation appears to be at constant Strouhal number, that is at frequency proportional to the jet velocity.
- For higher jet velocities, the frequency grows much slower, due to the strong phase rotation with frequency of the acoustic response of the pipe, as shown by Auvray [2].

The frequency behavior at low jet velocities is responsible for the so-called mouth-tones observed in some organ pipes [19], during attack transients, or for low blowing conditions [8]. Notice that these mouth-tones are quite different from edge-tones, since they rely on the pipe resonance: Auvray showed that they are accurately

predicted using a model considering only the feedback of the pipe, while edge-tones rely on a direct hydrodynamic feedback [27], because there is no pipe in the edge-tone configuration.

10.5 A Lumped Model of the Oscillation in a Flute

A simplified description of the self-sustained oscillation in the flute has been presented in Sect. 10.1.1. This description can now be improved by including the aspects presented in the previous sections. In order to achieve this, we first need to describe complementary aspects:

- nonlinear losses at the window;
- jet velocity fluctuations;
- direct hydrodynamic feedback of the sources on the jet.

These three points are developed in the following section to be later integrated in lumped description of the self-sustained oscillator.

10.5.1 Nonlinear Losses at the Blowing Window

The blowing window is an open end of the pipe. The area of this window is smaller than the main pipe cross section, resulting in an increased acoustic velocity as compared to the other pipe end. Under standard blowing conditions, the acoustic velocity in the blowing window is about one-tenth of the jet velocity. The labium edge is generally sharp, at least sharper than the other edges in the instrument, and a nonlinear behavior of the flow induced by the acoustic resonance is expected: velocities are high enough to trigger flow separation at the edge of the labium, as a consequence of viscosity. Several models can be used to describe the losses induced by this flow separation [21]. We will focus on the most simple one, inspired from [30] (see also Chap. 8, Sect. 8.4.5). If we first assume an inviscid 2D incompressible flow, the flow can be described as a potential flow (see Fig. 10.25 left) and the fluid acceleration in the window is associated with a pressure decrease. After the window, the fluid slows down and the pressure rises to its initial value. Notice that, when passing close to the labium edge, the fluid is submitted to strong accelerations: a sharp edge induces a singularity in a potential flow.

If we no longer assume the flow to be inviscid, viscosity induces the flow separation, resulting in a jet formation (see Fig. 10.25 right). The initial pressure drop induced by the flow acceleration is no longer compensated: flow separation can be modeled as a pressure difference between the two sides of the labium:

$$\Delta p_{\text{sep}} = p_p - p_m = -\frac{1}{2}\rho \left(\frac{v_{\text{ac}}}{\alpha_v}\right)^2 \text{sgn}(v_{\text{ac}}), \tag{10.47}$$

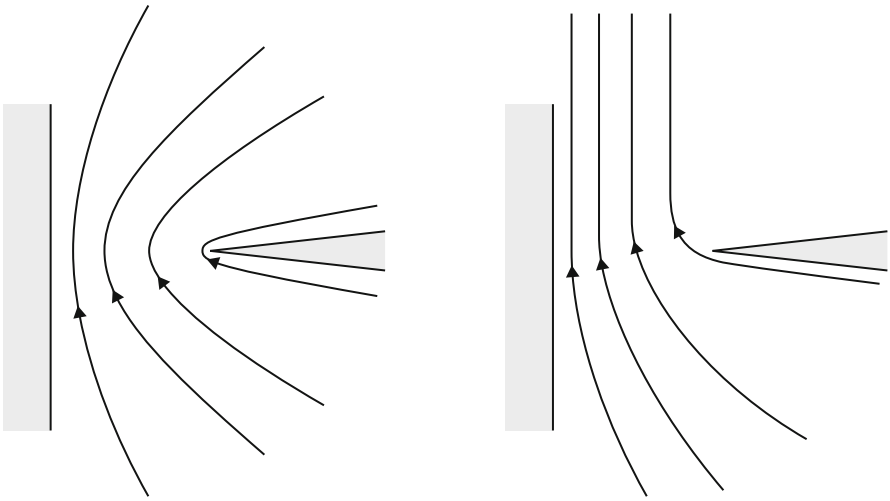

Fig. 10.25 Influence of viscosity on the flow induced by the acoustic resonance : without viscosity (*left*), the flow is potential and strong acceleration appear near the tip of the labium. Viscosity (*right*) is responsible for the flow separation and jet formation

where α_v corresponds to the *vena contracta*[14] with values $\alpha_v \approx 0.6$; v_{ac} is the acoustic velocity in the window, oriented towards the inside, while p_p and p_m are the pressures on both sides of the window. The pressure difference changes in sign with the acoustic velocity in the window, and depends on the square of the oscillating amplitude. It is therefore a dominant mechanism in the amplitude saturation of the oscillation in steady oscillation [21]. This was first observed and described in terms of a nonlinear "impedance" by Coltman [9]. It is the reason why the dimensionless oscillating amplitude does not depend on the frequency [47] (see Fig. 10.26): indeed, viscous, thermal, and radiation losses are frequency dependent and the oscillating amplitude would be frequency dependent if they were dominant!

This mechanism is the same as the one discussed in Sect. 10.4.3 of the present chapter, and also in Chap. 8 (Sect. 8.4.5).

10.5.2 Jet Velocities Fluctuations

All models presented above assume that the jet velocity is constant. The jet flow has been shown to be induced by the pressure in the player's mouth, accelerating the

[14]Inertia of the fluid particles induces flow separation in the direction given by the wall from which the flow separates. This results in a jet with a smaller width than the actual size of the window, smaller by a factor α_v.

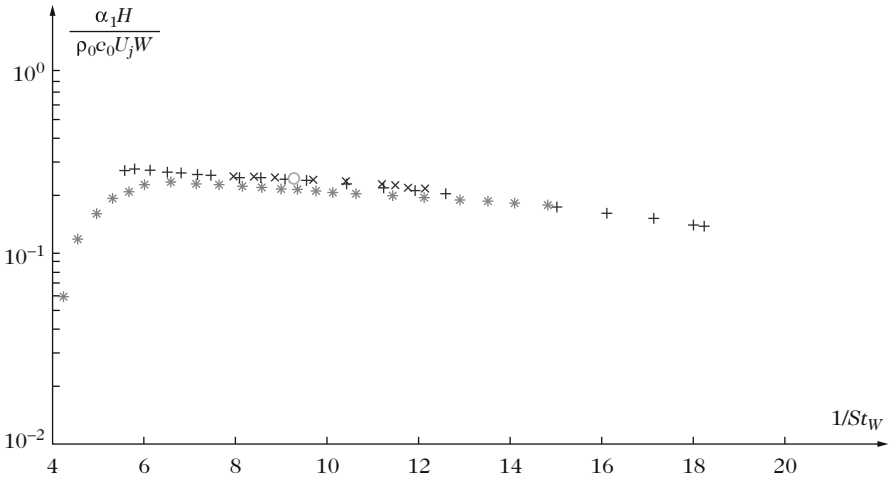

Fig. 10.26 The oscillating amplitude in a small organ pipe (square cross section (2 cm × 2 cm), 28 cm length and $W = 4$ mm flue exit to labium distance) is here presented in a dimensionless form for the four first oscillating regimes, corresponding to the four first pipe resonances: *asterisk symbol*, 1st, *plus symbol*, 2nd, *cross symbol*, 3rd, *open circle*, 4th. The amplitude of the fundamental is made dimensionless as the ratio of the acoustic velocity in the blowing window to the jet velocity, plotted as function of the dimensionless jet velocity U_j/fW. After [47]

flow into the channel. But, until now, we did not take the pressure fluctuations at the flue exit into account, due to the pipe resonance, added to the mean (atmospheric) pressure. Indeed, the flue exit is close to the open end of the pipe, but acoustic pressure at this position can still be around 60 % of the mode amplitude, depending on the end correction [10].

For a flue channel of length L, the jet velocity U_j can be estimated using the unsteady Bernoulli equation:

$$\rho l_c \frac{dU_j}{dt} + \frac{1}{2}\rho U_j^2 = p_{\text{res}} - p_{\text{exit}}, \tag{10.48}$$

where p_{res} is the reservoir pressure in the player's mouth and p_{exit} is the pressure at the channel exit.

The average jet velocity can be approximated as $\langle U_j \rangle = \sqrt{2p_{\text{res}}/\rho}$ and the total jet velocity is $U_j = \langle U_j \rangle + U_j'$. Because of the jet velocity fluctuations, the reservoir pressure can also fluctuate around its average value $p_{\text{res}} = \langle p_{\text{res}} \rangle + p'_{\text{res}}$, and the jet velocity fluctuations at the fundamental frequency ω of the oscillation can be written as:

$$U_j' \approx \frac{p'_{\text{res}} - p_{\text{exit}}}{\rho(j\omega L + \langle U_j \rangle)}. \tag{10.49}$$

For a short channel, jet velocity fluctuations are in opposite phase with the acoustic pressure at the flue exit: the instantaneous velocity increases when the pressure decreases. The acoustic work performed is therefore negative, and the jet velocity fluctuations act as losses. Air inertia in the channel becomes important when the channel is longer, and $\rho j\omega L$ becomes more important: jet velocity fluctuations are reduced and the phase shift relative to the acoustic pressure increases. A simple description can be used to describe the jet velocity fluctuations, by adding a volume flow source term $Q'_j = S_{\text{lum}} U'_j$ at the end of the resonator. In a more developed description, the jet velocity fluctuations can be integrated directly in the source mechanism as proposed by Auvray [2] with interesting influence on the balance between odd and even harmonics that affect the timbre.

Jet velocity fluctuations can be modulated by the player, adjusting mouth resonances: the jet velocity fluctuations are responsible for acoustic pressure in the mouth cavity, and the player has therefore control on the jet fluctuations. According to players, this is an important element of the control of the tone quality.

Pressure signals recorded in the foot of a small organ pipe and in the pipe, close to the labium, are presented in Fig. 10.27.

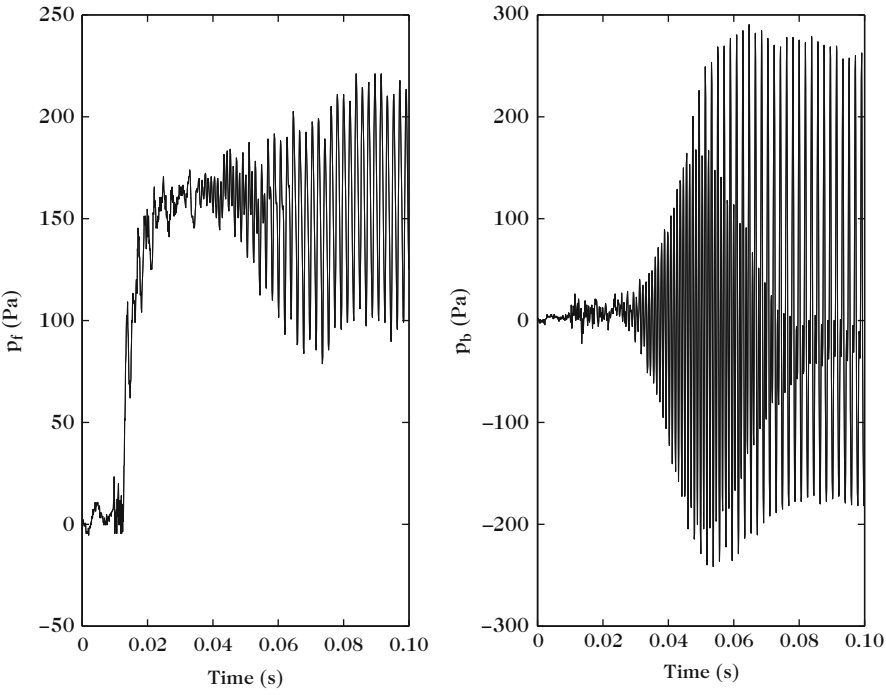

Fig. 10.27 Pressure signal in the foot (P_f) and close to the labium P_b of a small organ pipe. Strong pressure fluctuations appear in the foot, induced by the acoustic pressure in the pipe. Please note that the mean pressure in the foot and the amplitude of the acoustic pressure in the pipe are of the same order of magnitude. The pressure drop between foot and flue exit shows fluctuations that may become larger than the mean pressure: the jet velocity fluctuates around its mean value. After [47]

10.5.3 Direct Hydrodynamic Feedback

Aeroacoustic sources associated with the jet oscillation have been presented as two volume flow injections with opposite phases. While this source sustains the acoustic oscillation in the pipe, it also induces a local velocity field, that may contribute to the jet perturbation. This is a hydrodynamic direct feedback, which controls the oscillation in edge-tones. For self-sustained oscillation under normal playing conditions in a flute, this hydrodynamic feedback is negligible during steady-state oscillation, compared to the feedback from the resonator (about 4 % of the perturbation coming from the resonator [45]).

10.5.4 The Minimal Oscillator

All the different elements can be lumped to build a simple model for self-sustained oscillations in a flute, as presented in Fig. 10.4. Basic hypothesis for the model of the excitation are

- a constant jet velocity U_j, as estimated following Bernoulli (10.7),
- an exponential growth of the jet transverse displacement, independent of frequency,
- a convection velocity of perturbations on the jet, estimated as $c_p \approx 0.4U_j$,
- a dipole source associated to the jet oscillation at the labium.

The model is then described by the following equations:

- the jet transverse displacement at the labium is written as:

$$\eta(W,t) = \frac{h}{U_j} v_{\text{ac}}(t - W/c_p) e^{\alpha_i W}; \tag{10.50}$$

  where α_i comes from the resolution of Rayleigh's equation (10.21).
- the aeroacoustic source at the labium acts as a pressure step:

$$\Delta p_{\text{dip}} = -\frac{\rho \delta_d}{S_m} \frac{dQ_1}{dt}; \tag{10.51}$$

  where Q_1 is the part of the jet volume flow passing under the labium:

$$Q_1 = H \int_{y_0}^{\infty} U(y - \eta) dy, \tag{10.52}$$

where y_0 is the transverse position of the labium, relative to the jet and channel symmetry axis, and H is the jet width. For smooth velocity profiles induced by viscous spreading of the jet, the volume flow Q_1 is a smoothly nonlinear function, as for instance $U_0 H \tanh(2y/h)$. The main difference between flute models and models for simple reed instruments is the delay induced by convection of perturbations on the jet.

- losses induced by flow separation of the labium:

$$\Delta p_{\text{sep}} = -\frac{1}{2}\rho \left(\frac{v_{\text{ac}}}{0.6}\right)^2 \text{sgn}(v_{\text{ac}}). \tag{10.53}$$

This nonlinear loss term is very important for the saturation of the oscillating amplitude, but is not necessary during the starting transient of the oscillation. Please note that this pressure difference, as the one in (10.51), is a pressure step between the inside and the outside of the blowing window $\Delta p = p_p - p_m$.

- the acoustic response of the pipe is build in the frequency domain, using a low frequency 1D approximation (see Fig. 10.21). The source is introduced using mass conservation in the blowing window $Q_m = S_m v_{\text{ac}} = Q_p$ and adding the two pressure steps (dipolar source and losses). The acoustic response of the pipe is then[15]:

$$Q_m = \frac{\Delta p_{\text{tot}}}{Z_m + Z_p}, \tag{10.54}$$

where Z_m and Z_p are the acoustic impedances of the blowing window (to a first approximation, this is a mass, equivalent to a length correction) and of the resonator (input impedance).[16]

All the different elements are lumped as shown in Fig. 10.28. Time domain simulation of the equations of the model has been proposed by several authors (for instance, [14, 44]), allowing sound synthesis by physical modeling. The sound quality and realism of the synthesis is greatly enhanced by adding a wideband noise scaling with the jet velocity to the source terms, in order to model the turbulence. Some other aspects presented in the previous sections can also be integrated in order to provide a more complex model. This allows to take some important aspects for instrument makers into account, such as the channel shape and the chamfers at the flue exit.

[15]The same development is presented in Eq. (7.63) in Chap. 7, where the flow rate is written as U instead of Q.

[16]Please remind that impedances are defined as passive systems, that is with positive real part (see Sect. 1.3.3.1 in Chap. 1). We therefore have: $Q_m = -Z_m p_m$ and $Q_p = Z_p p_p$.

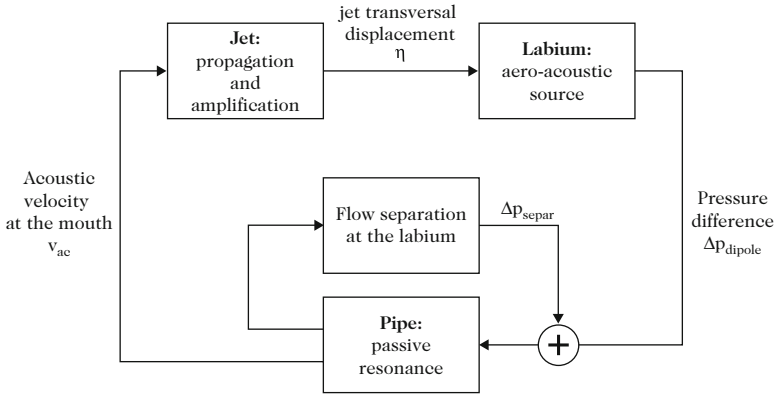

Fig. 10.28 Simplified model for self-sustained oscillations in a flute-like instrument. The nonlinear element that initiates the sound production is the saturation of the source at the labium, the other nonlinear element modeling the flow separation at the labium is essential for saturating the oscillation at a reasonable amplitude

10.6 Discussion About the Model

Different approaches to describe the elements of a model were presented in the previous sections. Each approach has its own limitations and ranges of validity, that would be interesting to point out, together with common ranges and transitions between models. A summary is presented below with regard to the sources, the instability and the receptivity.

- The *sources* can be described, to a first approximation, as a pressure step with an amplitude depending on the exact position of the flow injection points, or rather on the equivalent distance between them. Several clues indicate that this position may vary with the hydrodynamic wavelength on the jet. This wavelength does not vary much under standard blowing conditions of the instrument, and therefore, a fixed position of the injection points is fair as a first approximation. This model is restricted to low values of the Strouhal number, for which the jet does not break down into discrete vortices, typically $\mathrm{Str} = Wf/U_j < 0.3$ [15]. The amplitude of the pressure source Δp can be deduced from the transverse jet displacement η at the labium. For displacement larger than the jet thickness, Δp is a saturated function of the displacement η. When the displacement η is smaller or similar to the jet thickness, the integration of the jet velocity profile is necessary to calculate the pressure source Δp from the jet displacement η. It can be linearized for small amplitudes.

  For small amplitudes of the jet transverse displacement, in the case of a short distance W from flue exit to labium, for example, the instability does not have space to develop enough. In such a case, a better candidate is the model of Dequand [15], following [29, 33], in which the aeroacoustic source is the Coriolis

force due to the vortices that model the shear layer. This corresponds to "thick" jets, with values of W/h smaller than 2 [15]. This kind of model can also apply to thin jets ($W/h > 5$ typically) with high values of the Strouhal number, where the jet breaks into discrete vortices [26].

Finally, for turbulent jets and low values of the Strouhal number (or thick jets), the model by Howe [28] of sound production by vortices shed at the labium should still be evaluated. Even for values of the Reynolds number smaller than 2500, turbulence can significantly affect the behavior of the instrument, at least through the broadband noise generated. The first transverse acoustic resonance of the pipe seems to be strongly coupled to turbulent sources. This affects the sound quality of instruments with large bores like the bass flute of some organ pipe stops.

- The *instability* of the jet can be studied, in the case of laminar jets, through three different approaches: using a linear theory (Rayleigh), using discrete vortices to describe each shear layer of the jet, or using an alternate vortex street (Holger [26]).

  The linear model, inspired by Rayleigh, is well adapted to thin jets, with less than a half hydrodynamic wavelength between flue exit and labium. This corresponds to low values of the Strouhal number. When this condition is not fulfilled, a better candidate is Holger's model, which turns the thin jet into an alternate vortex street. In the case of very thick jets, the model of Dequand should be used since it better describes the vorticity in each shear layer. It is interesting to recall that Holger's model assumes an initial linear growth of vorticity in the shear layers before the jet breaks into a vortex street.

  For turbulent jets, the work of Bechert [4] is an interesting direction. Turbulence is not fully developed, and the study of the triggering of the turbulence, including geometrical aspects of the reservoir, would be very interesting.
- Receptivity still remains a very difficult problem. Flute makers and players as well as experiments [7, 40] on this subject indicate that the geometry of the flue exit strongly influences the receptivity. The work by Blanc [7] suggests that the chamfers in a recorder control both a protection effect due to the standing back of the flow separation points and a relative orientation of the perturbative acoustic velocity compared to the jet flow. This work should be continued in the future.
- In this chapter, the analysis focused on open pipe flutes. Closed pipe instruments have special sounding qualities, mostly because of the spectral content of the sound they produce, dominated by odd harmonics: closed organ pipes, Pan flutes... From the physical point of view, some specificities should be included in the model. First, these instruments are most often played with a turbulent jet. Second, the closed end of the pipe induces a recirculation of the air flow. As a consequence, the jet, submitted to a cross flow, bends towards the outside of the pipe.

References

1. Artaud, P., Geay, G.: Present Day Flutes (in French). Ed Jobert/Transatlantiques, Paris (1980)
2. Auvray, R., Fabre, B., Lagrée, P.: Regime change and oscillation thresholds in recorder-like instruments. J. Acoust. Soc. Am. **131**(2), 1574–1585 (2012)
3. Batchelor, G.: An Introduction to Fluid Dynamics. Cambridge University Press, Cambridge (1976)
4. Bechert, D.: The control of a plane turbulent free jet by a lateral flow generated in a sound field (in German). Z. Flugwiss. **24**, 25–33 (1976)
5. Bechert, D.: Excitation of instability waves in free shear layers part I. Theory. J. Fluid Mech. **186**, 47–62 (1988)
6. Blake, W.K.: Mechanics of Flow Induced Sound and Vibration. Academic, London (1986)
7. Blanc, F., Francois, V., Fabre, B., de la Cuadra, P., Lagrée, P.: Modeling the receptivity of an air jet to transverse acoustic disturbance with application to musical instruments. J. Acoust. Soc. Am. **135**, 3221–3230 (2014)
8. Castellengo, M.: Acoustical analysis of initial transients in flute like instruments. Acustica Acta Acustica **85**, 387–400 (1999)
9. Coltman, J.: Sounding mechanism of the flute and organ pipe. J. Acoust. Soc. Am. **44**, 983–992 (1968)
10. Coltman, J.W.: Jet drive mechanisms in edge tones and organ pipes. J. Acoust. Soc. Am. **60**(3), 725–733 (1976)
11. Crighton, D.: The edgetone feedback cycle. Linear theory for the operating stages. J. Fluid Mech. **234**, 361–391 (1992)
12. Crighton, D.: Nonlinear acoustics. In: Modern Methods in Analytical Acoustics (Lecture Notes). Springer, London (1992)
13. Curle, N.: The influence of solid boundaries upon aerodynamic sound. Proc. R. Soc. Ser. A **231**, 505–514 (1955)
14. De la Cuadra, P.: The sound of oscillating air jets: physics, modeling and simulation in flute-like instruments. Ph.D. thesis, Stanford University (2005)
15. Dequand, S.: Simplified models of flue instruments: influence of mouth geometry on the sound source. J. Acoust. Soc. Am. **113**(3), 1724–1735 (2003)
16. Drazin, P.: Introduction to Hydrodynamic Stability. Cambridge University Press, Cambridge (2002)
17. Elder, S.: The mechanism of sound production in organ pipes and cavity resonators. J. Acoust. Soc. Jpn. (E) **13**(1), 11–23 (1992)
18. Fabre, B.: Sound production in flute-like instruments: aeroacoustic modeling and time domain simulation (in French). Ph.D. thesis, Université du Maine, le Mans (1992)
19. Fabre, B., Castellengo, M.: Transients in flue organ pipes: experiments and modeling. In: Proceedings of the 17th ICA, Roma (2001)
20. Fabre, B., Hirschberg, A., Wijands, A., van Steenbergen, A.: Attack transients in flute-like instruments (in French). In: de Physique, L.E. (ed.) 2ème Congrès Français d'Acoustique, vol. C1, pp. 67–70 (1992)
21. Fabre, B., Hirschberg, A., Wijnands, A.: Vortex shedding in steady oscillation of a flue organ pipe. Acustica Acta Acustica **82**, 811–823 (1996)
22. Fletcher, N.H., Rossing, T.D.: The Physics of Musical Instruments. Springer, New York (1991)
23. Goldstein, M.: Aeroacoustics. McGraw-Hill, New York (1976)
24. Hirschberg, A.: Aero-acoustics of wind instruments. In: Mechanics of Musical Instruments, pp. 291–369. CISM Courses and Lectures, vol. 355. Springer, New York (1995)
25. Hirschberg, A., Rienstra, S.: An Introduction to Aeroacoustics. Eindhoven University of Technology, The Netherlands (2004)
26. Holger, D., Wilson, T., Beavers, G.: Fluid mechanics of the edge-tone. J. Acoust. Soc. Am. **62**, 1116–1128 (1977)

27. Holger, D., Wilson, T., Beavers, G.: The amplitude of edge-tone sound. J. Acoust. Soc. Am. **67**, 1507–1511 (1980)
28. Howe, M.: Contributions to the theory of aerodynamic sound, with applications to excess jet noise and the theory of the flute. J. Fluid Mech. **71**, 625–673 (1975)
29. Howe, M.: Acoustics of Fluid Structures Interactions. Cambridge University Press, Cambridge (1998)
30. Ingard, U., Ising, H.: Acoustic nonlinearity of an orifice. J. Acoust. Soc. Am. **42**, 6–17 (1967)
31. Kühnelt, H.: Vortex sound in recorder- and flute-like instruments: Numerical simulation and analysis. In: International Symposium on Musical Acoustics, pp. Paper 1–S1–6, Barcelona (2007)
32. Meissner, M.: Aerodynamically excited acoustic oscillations in cavity resonator exposed to an air jet. Acustica Acta Acustica **88**, 387–400 (2002)
33. Nelson, P., Halbiwell, N., Doak, P.: Fluid dynamics of flow excited resonance Part 2: theory. J. Sound Vib. **91**, 375–402 (1983)
34. Powell, A.: On the edgetone. J. Acoust. Soc. Am. **33**(4), 395–406 (1961)
35. Prandtl, L., Tietjens, O.: Fundamentals of Hydro and Aeromechanics. Dover, New York (1934)
36. Rayleigh, L.: The Theory of Sound, vol. 2. Dover, New York (1877). Second edition, 1945 re-issue
37. Rienstra, S., Hirschberg, A.: An Introduction to Acoustics. Eindhoven University of Technology, Eindhoven (2006)
38. Ségoufin, C.: Sound production by flow/acoustical resonator interaction: influence of the upstream system - application to the recorder (in French). Ph.D. thesis, University Paris 6 (2000)
39. Segoufin, C., Fabre, B., Verge, M., Hirschberg, A., Wijnands, A.: Experimental study of the influence of the mouth geometry on sound production in a recorder-like instrument: windway length and chamfers. Acustica Acta Acustica **86**, 599–610 (2000)
40. Ségoufin, C., Fabre, B., de Lacombe, L.: Experimental investigation of the flue channel geometry influence on edge-tone oscillations. Acustica Acta Acustica **90**(5), 966–975 (2004)
41. Skordos, P.A.: Modeling flue pipes: subsonic flow, lattice Boltzmann, and parallel distributed computers. Ph.D. thesis, Massachusetts Institute of Technology, Cambridge (1995)
42. Tritton, D.: Physical Fluid Dynamics, 2nd edn. Oxford University Press, Oxford (1995)
43. van Zon, J., Hirschberg, A., Gilbert, J., Wijnands, A.: Flow through the reed channel of a single reed music instrument. J. Phys. IV Colloques **51**(C2), 821–824 (1990)
44. Verge, M.P.: Aeroacoustics of confined jets, with application to the physical modeling of recorder-like instruments. Ph.D. thesis, TU Eindhoven (1995)
45. Verge, M., Caussé, R., Fabre, B., Hirschberg, A., Wijnands, A., van Steenbergen, A.: Jet oscillations and jet drive recorder-like instruments. Acustica Acta Acustica **2**, 403–419 (1994)
46. Verge, M., Fabre, B., Mahu, W., Hirschberg, A., van Hassel, R., Wijnands, A., de Vries, J., Hogendoor, C.: Jet formation and jet velocity fluctuations in a flue organ pipe. J. Acoust. Soc. Am. **95**, 1119–1132 (1994)
47. Verge, M., Fabre, B., Hirschberg, A., Wijnands, A.: Sound production in recorder-like instrument I. Dimensionless amplitude of the internal acoustic field. J. Acoust. Soc. Am. **101**, 2914–2924 (1997)
48. Von Helmholtz, H.: On the Sensation of Tones (orig. “Lehre von den Tonempfindungen”, 1862). Engl. translation: Dover, New York (1954) (1877)

Chapter 11
Bowed String Instruments

Xavier Boutillon

Abstract This chapter focuses on the interaction between a bow and a string, and on the resulting self-sustained oscillations. It starts with the presentation of the friction phenomena and tribology of the rosin, which play a major role in the dynamics of the bowed string. Among the variety of possible dynamical regimes induced by the stick-slip mechanism on a string, the so-called Helmholtz motion (HM) deserves particular attention because it is the most widely used in the musical context. First, the kinematical and dynamical characteristics of the ideal HM are described. It is followed by the presentation of some more realistic features of the HM observed on real strings, such as the flattening effect, the wolf note, and the anomalous low frequency (ALF) tones.

11.1 Introduction

After the reed- and the flute-mechanisms, the bowed string is the third example of self-sustained oscillations that we examine among musical instruments. The vibration of the instrument body and, ultimately, the radiated sound are generated by the force exerted by the string on the bridge. The purpose of this chapter is thus to analyze the dynamical characteristics of the bowed string: frequency, amplitude, and stability. Among the various regimes that can be sustained under friction by the bow, the so-called Helmholtz motion of the string is highly privileged in musical usage. It is therefore the main focus of this chapter. Other regimes will be presented at the end. We will analyze

- how the motion is initiated and sustained by the bow,
- how the mechanical and dynamical parameters under control by the luthier and by the player influence the motion characteristics (frequency, amplitude, and spectrum) and may eventually destabilize it.

Bending and torsion waves are the most important waves in a bowed string. A linear analysis of these waves has been presented in Sect. 3.4.9 (Chap. 3).

X. Boutillon (✉)
Laboratory for Solid Mechanics, CNRS and École Polytechnique, 91128 Palaiseau Cedex, France
e-mail: boutillon@lms.polytechnique.fr

A. Chaigne, J. Kergomard, *Acoustics of Musical Instruments*, Modern Acoustics and Signal Processing, DOI 10.1007/978-1-4939-3679-3_11

Several local models for the interaction between the surface of the string and the bow hair are presented in Sect. 11.2. The approximations relative to the bow are given in Sect. 11.3. In Sect. 11.4, we describe the Helmholtz motion (HM) and its relationships to the physics of the system where a linear multimodal string is associated with a nonlinear, local, or narrow bow. We also analyze the influence of the violin characteristics and of the parameters controlled by the musician on the HM or pseudo-Helmholtz motion.

Since the most recent and insightful contributions to the knowledge of the bowed string are due to Jim Woodhouse and his students, this chapter is largely inspired by their work (see References).

When it comes to the perception of a musical instrument, two aspects must be distinguished: the perception of the instrument by the player, which may be summarized by "ease of playing," and the "quality" of the sound reaching the listeners' ears, including those of the player. Science has not yet fully elucidated the physical–perceptual relationships. This chapter is an attempt to describe the current physical knowledge that underlies these relationships.

Nomenclature

a: Radius of the string

c_{T}: Speed of transverse waves in a perfectly flexible string (no stiffness)

c_{R}: Speed of torsional waves

F: Force exerted by the bow on the string (also: $F_{\mathrm{b/s}}$)

F_0: Force exerted by the end of the string on the bridge

F_{P}: Vertical (pressing) component of the force of the bow on the string (static)

T: Tension of the string

v_{b}: Bow speed

v_{H}: Velocity of the string due to the history of the wave (that is: if the bow were instantly removed)

v_{s}: Velocity of the surface of the string ($= \dot{\xi}(x,t)$ for a null-diameter string)

$Y_0(\omega)$ and $Y_L(\omega)$: Point-mobilities in the Oy-direction at the bridge-end and at the finger end

Y_{c}: Characteristic mobility of the torsion and transverse waves associated at the string periphery

$Y_{\mathrm{c,T}}$: Characteristic mobility of the transverse wave on a perfectly flexible string

$Z_{\mathrm{c,T}}$: Characteristic impedance of the transverse wave on a perfectly flexible string (reciprocal of $Y_{\mathrm{c,T}}$)

$Z_{\mathrm{c,R}}$: Characteristic impedance of torsion waves in a string

β: Position of the bow, normalized by the string length L

ϵ: Mass per unit length of string

μ_{s} and μ_{d}: Static and dynamic friction coefficients of rosin on the surface of the string (strictly speaking: depend on the string material)

$\xi(x,t)$: Displacement of the string axis in the direction of the bow (Oy)

11.2 Bow–String Interaction

As seen in Chaps. 9 and 10, the system must include one nonlinear element for self-sustained oscillations to take place. In the violin case, this element is given by the friction between the bow and the string. Friction is governed by the properties of rosin, an organic adhesive material which is spread by the player on the bow hair, which otherwise would have no adhesion properties (see Fig. 11.1).

In this section, we describe the local interaction between the string and the bow, independently of the dynamical characteristics of each of these systems. The physical quantities for this description are the velocity of the string at the contact with the bow $v_s(t)$, the bow velocity $v_b(t)$, their difference $\Delta v = v_s - v_b$ and the local or distributed force $F(t) = F_{b/s}(t)$ exerted by the bow on the string. The point (or possibly the line) of contact of the string with the bow is not on its axis but at the periphery of the string. Its velocity is the sum of the velocity given by the transverse waves $\dot{\xi}$ and by the torsion wave $a\dot{\psi}$ [see Eq. (3.114)].

11.2.1 Quasi-Static Models of Friction

The simple models that describe friction are based on two hypotheses: the area of contact is reduced to one point and the relationship between $F(t)$ and the velocity difference $\Delta v = (v_s - v_b)(t)$ is time-independent. The most simple model is that of Coulomb and the corresponding force–velocity relationship is given by the dashed line in the left diagram of Fig. 11.2.

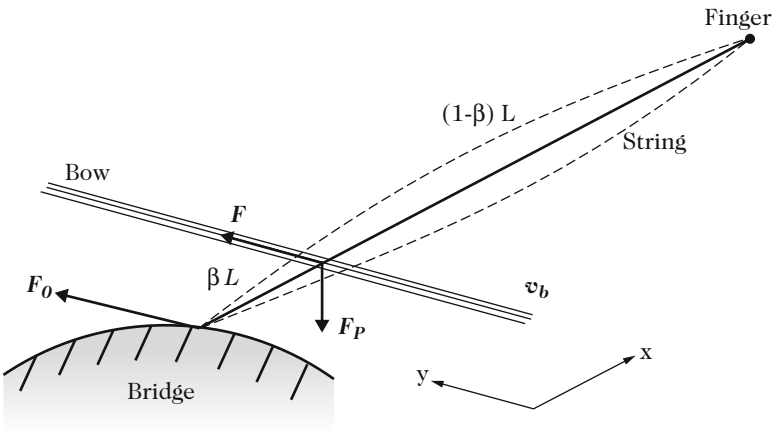

Fig. 11.1 Bowed string

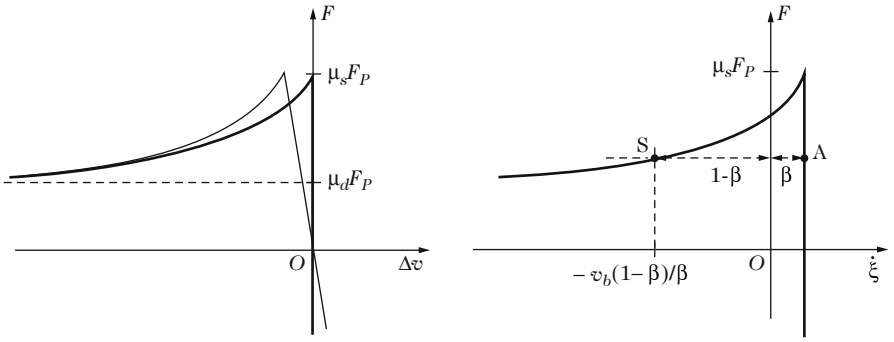

Fig. 11.2 *Left diagram*: friction models of the bow on the string. *Dashed line*: Coulomb model. *Thick solid line*: modified Coulomb model. *Thin solid line*: modified Coulomb model taking into account two outgoing torsion waves [see Eq. (11.1)]. *Right diagram*: ideal Helmholtz motion as a solution of the modified Coulomb model associated with a perfectly flexible string (see Sect. 11.4.1.2, p. 618). The solution points *A* (adhesion) and *S* (sliding) must have the same ordinate $F =$ const. and share the friction characteristics in a ratio $(1-\beta)/\beta$. After [36]

Even though this model is not commonly used in the bowed string context, it remains a conceptual reference throughout this chapter.[1] The two states of the system are (a) sliding with a constant-force $\mu_\mathrm{d} F_\mathrm{P}$ (where F_P is the pressing force of the bow on the string in the direction normal to the motion) and (b) sticking where $v_\mathrm{s} = v_\mathrm{b}$ and the force takes any value between $\pm\mu_\mathrm{s} F_\mathrm{P}$. Typical values for the dynamical and statical friction coefficients μ_d and μ_s are 0.2 and 0.7, respectively (see also Chap. 1). Noting that sticking and sliding refer to a point at the string periphery, it becomes clear that the transition from one state to the other depends on the value of the torsion and transverse waves when they reach the string point under the bow.

A model which is commonly used in a number of studies on the bowed string derives from the strict Coulomb model: the sliding force is considered as dependent on the relative velocity (solid line in Fig. 11.2). One can take for $F(\Delta v)$ a hyperbolic dependence and parameterize it by the slope at $\Delta v = 0$. It will be seen further on that this slope acquires an important physical significance when it is compared to $2Z_\mathrm{c} = 2/Y_\mathrm{c}$, where Y_c is the sum of characteristic mobilities of the transverse and torsion waves, given by Eq. (3.116). The validity of this model has been checked by Lazarus by means of experiments on the static contact between a bow and a string [20]. It is correct as long as the quantities involved do not depend on time and the bowed point is at a thermo-mechanical equilibrium. However, contrary to what has

[1]The formal analogy between strings and pipes presented in Chap. 1 can be extended by considering a reed instrument. The bow velocity v_b corresponds to the pressure p_m inside the mouth, the string velocity v_s to the pressure p in the mouthpiece, and the force $F_\mathrm{b/s}$ to the air flow u input in the mouthpiece. The pressing force of the bow onto the string, a control parameter of the player, may even be associated with the maximum flow u_A that can enter in the pipe [Eq. (9.22)].

been taken for granted for a long time, friction of the bow on a vibrating string cannot be considered as a quasi-static phenomenon (see Sect. 11.2.2).

This model can be slightly modified by including some of the torsional dynamics in the friction characteristics. Since the torsion waves are generally much more rapidly attenuated than the transverse waves, one may consider that they are generated by the bow (since it exerts a force at the periphery of the string) but that they are not reflected by the ends of the string. Within this approximation, these waves constitute a local reaction of the string which does not depend on time. They comply with the above hypothesis on friction and can therefore be included in the friction curve. A new relative velocity is considered: $\Delta v' = \dot{\xi} - v_b$, where ξ is the motion of the central axis of the string in the (Oy-)direction of the bow. The summation on waves yields $v_s = \dot{\xi} + a\dot{\psi}$. Using Eq. (3.117):

$$\begin{aligned} F(\Delta v') &= F(v_s - a\dot{\psi} - v_b) = F(\Delta v - a\dot{\psi}) \\ &= F(\Delta v - \frac{F}{2Z_{c,R}}) \end{aligned} \tag{11.1}$$

Graphically, this equation yields the thin solid line in the left frame of Fig. 11.2 which can be obtained from the thick line by shifting each point horizontally by the quantity $\frac{1}{2}F/Z_{c,R}$. The infinite slope at $\Delta v = 0$ becomes finite and, according to [25], the self-sustained oscillation of the system is more stable.

11.2.2 Tribology of Rosin

At the end of the 1980s, the models described above were challenged by experiments on the tribology of rosin [34]. The string was replaced by a simple harmonic oscillator with a resonance factor close to that of the string and this system was rubbed by a glass rod covered with rosin. It appeared that the friction curve was not single-valued: different states of the system could have the same velocity difference between the "bow" and the "string" (Fig. 11.3). Later, it was confirmed on a complete string that an additional state variable must be considered in the dynamical description of the system.

Microscopic photography (Fig. 11.4) of the rosin covering a rod "bowing" the string or its substitute revealed two possible regimes of sliding:

- when the local temperature (in the friction zone) is sufficiently high (wood rod, which conducts heat poorly), rosin melts at the string passage and becomes solid again afterwards;
- with a copper rod, the temperature does not reach the melting point but rosin encounters a considerable strain (plastic deformation) at the passage of the string.

Two thermo-mechanical models have been proposed to describe what happens in the contact zone (Fig. 11.5), with thickness δ and area A. When the temperature

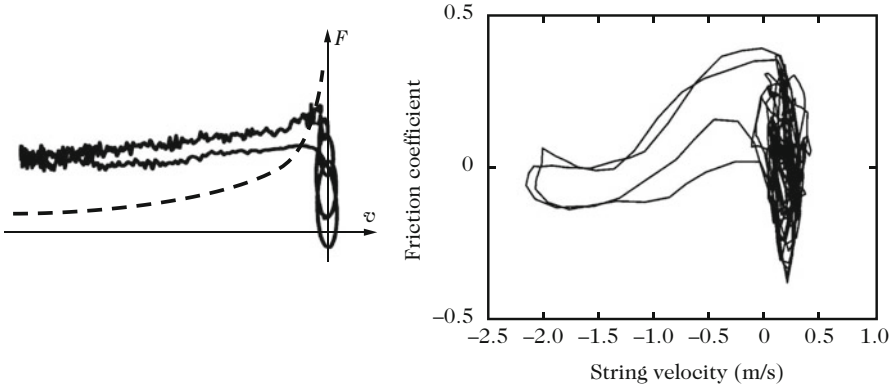

Fig. 11.3 (*Left*) Trajectory in the $(\Delta v, F)$-plane of the point representing friction of a glass rod on a small portion of string attached to a cantilever (after [34]). *Dashed line*: quasi-static friction curve. (*Right*) Friction coefficient of a glass rod bowing a vibrating string. The velocity was measured directly and the force was determined indirectly from measurements at the string ends (cf. [42])

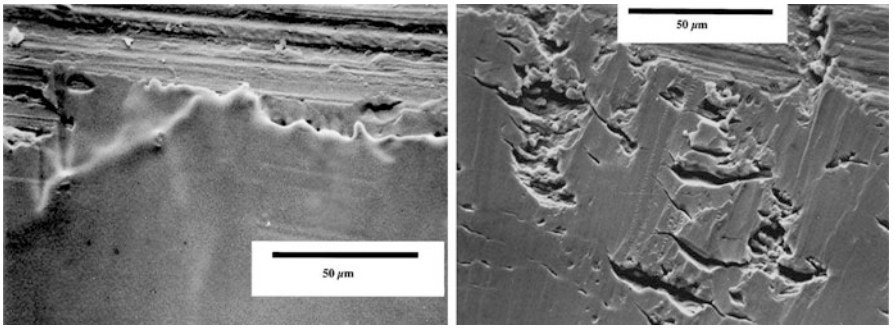

Fig. 11.4 Surface of the rosin coating a wood rod (*Left*) or a copper rod (*Right*) after friction with the string (after [34]). Fusion (*Left*) or plastification (*Right*) can be distinctly observed

variation θ induced by the mechanical work of the friction force F is large enough to melt the rosin, the force F now describes a viscous flow, with a viscosity depending on temperature:

$$F = -\nu(\theta)\, A \frac{v_\mathrm{s} - v_\mathrm{b}}{\delta}. \tag{11.2}$$

When the temperature change does not initiate melting, the shearing stress in the rosin layer is considered to cause an ideal plastic strain:

$$F = A\, k(\theta)\, \mathrm{sign}(v_\mathrm{s} - v_\mathrm{b}). \tag{11.3}$$

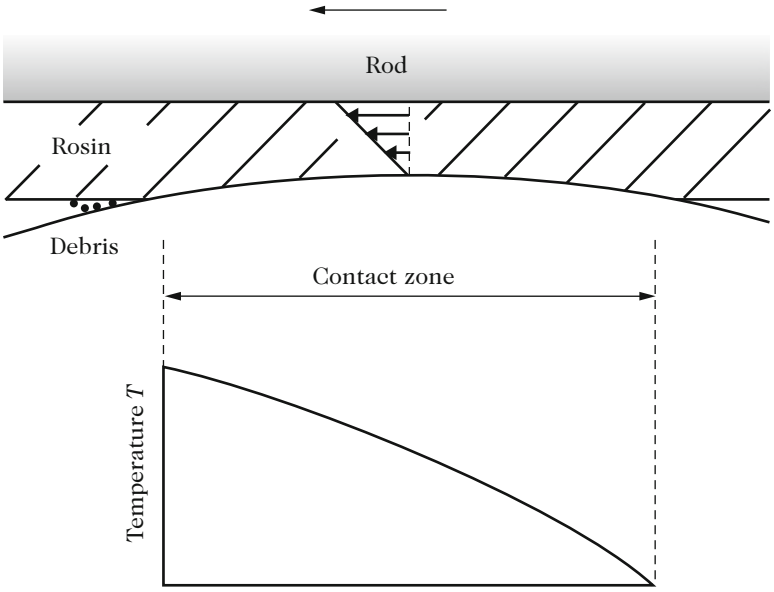

Fig. 11.5 A rod (*top gray area*) covered with rosin is driven at constant speed in contact with the string. The rosin layer (hatchings) is deformed in the contact zone. Heat flow and temperature change appear, changing in turn the adhesion properties of the rosin (after [34])

11.3 Bow Models

Violin bows have not undergone major changes for about 150 years. One of the most famous bow makers was François Tourte (1747–1835). Among other achievements, he recommended Pernambuco wood for the bow stick, which is still much praised by today's players. It is thought that this choice is motivated by mechanical properties such as a high Young's modulus [2] and a high resistance to shearing [21].

A bow must sustain a high level of hair[2] tension without being subject to buckling instability[3] [6]. This is the reason for the inverse curvature of modern violin bows, compared to ordinary (and ancient musical) bows.

In the rest of the chapter, the bow model is based on the following approximations:

- point friction,
- imposed velocity at the friction point.

[2] Bow hair are made from horse tails.

[3] Buckling refers to the deformation of beams subject to an axial compressing force.

This bow model corresponds to a zero-width bow with stiff hair. The changes induced by more realistic bow models are indicated at the end of the chapter (Sect. 11.4.2.5).

11.4 Dynamical Regimes of the Bowed String

Almost systematically, the motion of the string desired by musicians is quasi-periodic and consists of the succession, within a period, of one sticking phase and one sliding phase only (Figs. 11.6 and 11.7). In its idealized form, it was observed and described by Helmholtz in 1862 [35]. It is certainly not the only motion, periodic or not, that can be obtained by bowing a string: the sounds produced by beginners testify to the great variety of achievable motions! In a corner-stone study (difficult to read, though), Raman [29] analyzed a large number of other periodic motions that are admissible on a bowed string.[4,5]

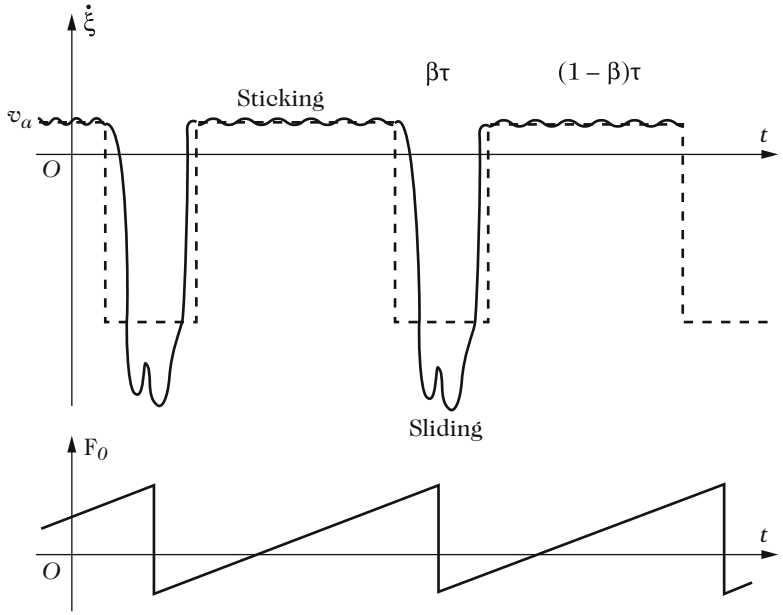

Fig. 11.6 *Top*: velocity of the center of the string at the bowing point. In the ideal HM, of period τ (*dashed line*), $\dot{\xi}$ is the same as v_s and takes successively two constant values. In a real HM (*solid line*), $\dot{\xi}$ is mainly due to transverse waves, almost following v_b during the sticking phase, with deviations due to torsion waves. *Bottom*: force exerted by the string on the bridge, for the ideal HM. Since a constant force is exerted by the bow on the string, a constant component in F_0 is superimposed to the varying force given by Eq. (11.5)

[4] A similar discussion has been given in Sect. 9.4.8 of Chap. 9 about conical woodwinds.

[5] Later on, Raman received the Nobel Prize in physics for his work in spectroscopy.

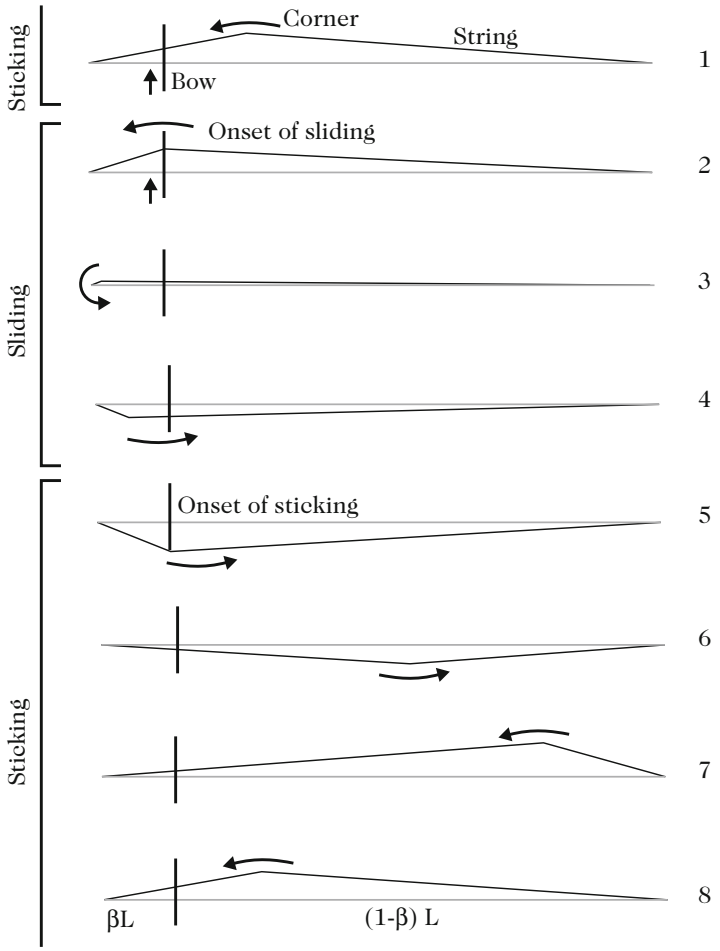

Fig. 11.7 Ideal Helmholtz motion. The bow splits the string in a $\beta/(1-\beta)$ ratio. A corner travels on the string (diag *1*), initiates sliding of the string under the bow (*2*) until (*3, 4*) sticking occurs again (*5*). This explains why the $\beta/(1-\beta)$ ratio is also the ratio between the respective durations of the sliding and sticking phases in Fig. 11.6

The characteristics of the motions of musical interest are described next. The ideal Helmholtz motion (HM) — that would be encountered by a perfectly flexible string with fixed ends, where only non-dispersive and non-dissipative transverse waves travel — is distinguished from the real HM. Of particular interest are the lower and upper limits of the bowing parameters beyond which the HM cannot be sustained, the perturbations of the HM, its stability and the frequency deviations of the real motion.

Other regimes will be evoked: either reached by mistake or imposed by the violin (wolf note) or looked after for special effects (Anomalous Low Frequency "ALF" notes).

11.4.1 The Ideal Helmholtz Motion

11.4.1.1 Kinematic Characteristics

The ideal Helmholtz motion is a periodic motion that is compatible with the propagation equation of transverse waves and with the friction condition imposed by bowing (see the right diagram in Fig. 11.2). Kinematically, the ideal HM can be represented by the propagation of a corner along the string (Fig. 11.7), at the celerity of transverse waves $c_T = \sqrt{T/\epsilon}$. Anticipating the demonstration, the period of this motion is therefore $\tau = 2L/c_T$. The shape taken by the string during one period is represented in Fig. 11.7: coming from the finger side toward the bow sticking on the string (1), the corner triggers sliding (2), reaches the bridge (3) where it is reflected with a sign change (4), goes back to the sliding bow (5) and initiates a new sticking phase, goes to the finger (6) where it is reflected (7), travels again toward the bow (8), etc.

The ideal HM can also be represented as the propagation of a velocity discontinuity $\Delta\dot{\xi} = v_b/\beta$ along the string (Fig. 11.8). This representation will be used in the rest of this section. A geometrical representation of the HM is that of two straight lines rotating around the string ends.

The velocity at the bowing point is v_b during the sticking phase which lasts $(1-\beta)\tau$, the time for the corner to travel from the bow to the bridge and back (Fig. 11.7). The velocity value during the sliding phase is given by the null average velocity condition (the string does not go away!) which yields $-(1-\beta)v_b/\beta$ (straight dashed lines of the top diagram in Fig. 11.6). At the bowing point, the amplitude of the velocity waveform is therefore v_b/β and one must notice that it does not depend on F_P.

Examining now what happens at $x = \beta' L$ ($\beta' \neq \beta$), one can derive from the various representations given above that the velocity of *each* point of the string alternates between two values in one period:

- When a point belongs to the same "velocity line" (middle frame in Fig. 11.8) as the bowing point, $\dot{\xi}(\beta' L, t)$ takes the value $v_b\beta'/\beta$ during $(1-\beta')\tau$;
- When this point is on the other side of the velocity corner, compared to the bowing point, $\dot{\xi}(\beta' L, t)$ takes the value $-v_b(1-\beta')/\beta$ during $\beta'\tau$ (by virtue of the same reasoning as before on the average velocity).

The maximum displacement of a given string point can be computed by temporal integration of the velocity during the "pseudo-sticking phase" (see above and Fig. 11.8):

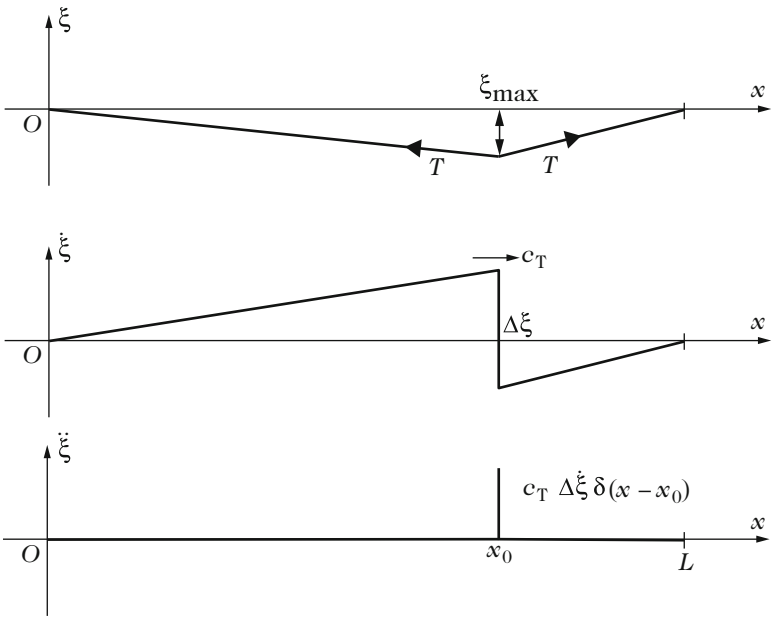

Fig. 11.8 Kinematical conditions (*from top to bottom*: position, velocity, and acceleration) on the string at $t = 0$, corresponding to frame 6 in Fig. 11.7. Such initial conditions generate an ideal HM: at point x_0, a corner and a discontinuity of velocity $\Delta\dot{\xi} > 0$ propagate a transverse wave toward the right of the string at c_T. Dynamically, the corner corresponds to an acceleration impulse $c_T \Delta\dot{\xi}\, \delta(x - x_0)$. Since $\dot{\xi}$ and $\ddot{\xi}$ are *temporal* derivatives, notice that the *middle and bottom* frames are not derived from the top and middle frames, respectively, by space derivation

$$\xi_{\max} = \frac{1}{2}\int_0^{(1-\beta')\tau} \dot{\xi}(\beta' L, t)\, dt = \frac{1}{2}\frac{\beta'(1-\beta')}{\beta} v_b\, \tau\ , \tag{11.4}$$

hence the parabolic shape of the envelope of the string motion. The force $F_0(t)$ exerted by the string on the bridge can be easily derived. Near the bridge, at $\beta' = dx/L$, the velocity is almost always $\dfrac{v_b}{\beta}\dfrac{dx}{L}$ since $\beta' \ll 1$. Therefore, the displacement is $d\xi(0^+, t) = \dfrac{v_b}{\beta}\dfrac{dx}{L}\, t$ for $t \in [-\tau/2, \tau/2]$ (choosing appropriately the origin of time), where the integration constant satisfies the null average displacement condition. The force is

$$F_0(t) = T\frac{\mathrm{d}\xi}{dx}(0, t) = \frac{v_b}{\beta}\frac{T}{L} t, \tag{11.5}$$

as represented in Fig. 11.6. Its maximum value is

$$F_{0\max} = \frac{v_b}{\beta c_T} T. \tag{11.6}$$

11.4.1.2 Dynamical Characteristics

The ideal HM is a solution of the following dynamical problem: ideal string (infinitely thin so that neither torsion waves nor dispersion of transverse waves are involved, without losses, with fixed ends) to which a bow at $x = \beta L$ imposes a friction curve corresponding to the modified Coulomb model (thick line in the left diagram of Fig. 11.2). We show below that the ideal HM is one of the periodic solutions of the propagation equation without the bow. We show then that this motion is compatible with the friction curve.

Considering the kinematic initial conditions given in the two top diagrams of Fig. 11.8, it is shown that the propagation equation and the end conditions generate the HM. In these conditions, the string position is a continuous piecewise linear function whereas the velocity profile is also piecewise linear but discontinuous. One define $\dot{\xi}(x = x_0, t = 0)$ as the initial velocity (here: negative) at the right side of $x_0 = \beta_0 L$.

Since the string is straight everywhere, the restoring force due to tension is zero everywhere except at x_0. Within the approximation of small angles, the force at x_0 can be derived from the expression (11.4) of the maximal displacement $\xi_{\max}$:

$$F(x_0) = T\left[\frac{\xi_{\max}}{(1-\beta_0)L} + \frac{\xi_{\max}}{\beta_0 L}\right] = T\frac{1}{2}\frac{\beta_0(1-\beta_0)}{\beta} v_b \tau \frac{1}{L\beta_0(1-\beta_0)}. \tag{11.7}$$

Using the expressions $\tau = 2L/c_T$ (see further) and $\Delta\dot{\xi} = v_b/\beta$ (see kinematic description) leads to:

$$F(x_0) = T\frac{1}{2}\Delta\dot{\xi}\, 2L\sqrt{\frac{\epsilon}{T}}\frac{1}{L} = \sqrt{\epsilon T}\,\Delta\dot{\xi}. \tag{11.8}$$

One recognizes here the expression of the forward propagating force associated with the forward propagating velocity discontinuity:

$$F(x_0) = +Z_{c,T}\,\Delta\dot{\xi}. \tag{11.9}$$

This localized force is responsible for an acceleration $\ddot{\xi}(x)$ which is null everywhere except at x_0,

$$F(x_0) = \int_{x_0-}^{x_0+} \ddot{\xi}(x)\,\epsilon\, dx. \tag{11.10}$$

The space-dependency of the acceleration becomes a pulse:

$$\ddot{\xi}(x) = c_T\,\Delta\dot{\xi}\,\delta(x - x_0). \tag{11.11}$$

With the acceleration given above, this point acquires the velocity corresponding to the left side of the velocity diagram (middle frame of Fig. 11.8). Since the

acceleration is null everywhere else, all other points keep their initial velocity. This amounts to a propagation of the velocity discontinuity toward the right side of the string. The string dynamics (given by the propagation equation of the transverse waves) implies that this propagation occurs at the celerity c_T and also that the force impulse given by Eq. (11.9) propagates toward the right side of the string.

The above reasoning implies also that the corner propagates toward the right. Since the velocity profile remains the same, except at x_0, the initial condition is simply transposed a bit to the right. Altogether, the dynamics of the string implies that a velocity discontinuity associated with an initial corner-shape propagates in a direction that is determined by the respective signs of these initial conditions.

It is now shown that this motion has a period $\tau = 2L/c_\mathrm{T}$ when the ends are fixed. In the absence of motion at the right end of the string, the reflection of the traveling acceleration impulse occurs instantaneously with a sign change and so does the force impulse.[6] It follows that the corner propagating now toward the left side of the string points toward the top of the diagram. At the instant of the reflection, all string points have a positive velocity. The acceleration impulse progressively changes the sign of this velocity: the velocity profile is therefore *the same* slightly before and slightly after the instant of reflection, that is, for a change in the propagation direction. At the time of the reflection at $x = L$, only the signs of the force, acceleration, and displacement have changed. This will be the same for reflection at $x = 0$, yielding the $2L/c_\mathrm{T}$ periodicity.

Combined with a small modification, the above solution is compatible with the friction curves in Fig. 11.2. Since the string does not absorb energy (in this ideal model), the force exerted by the bow does no work and the average power given by the bow is zero. Since the time-average of the string velocity is zero everywhere, it follows that the force $F(t)$ exerted by the bow must be *constant in time*: the power given during the sticking phase must be given back during the sliding phase.

The friction curve (left diagram of Fig. 11.2) can be redrawn as a function of the string velocity at the bow. The force takes the constant value that gives the value $v_\mathrm{b}\dfrac{1-\beta}{\beta}$ to the velocity during the sliding phase (point G). Since the force exerted by the bow is continuous, it adds a permanent deformation — a triangle with its summit at $x = \beta L$ — to the motion of the string described above. This permanent shape imposes in turn a DC component in the force $F_0(t)$ exerted on the bridge.

However, the ideal HM is not stable. A perturbation propagating on the string can meet the bow either during a sticking or during a sliding phase. Since the ends and the sticking bow have a null-mobility, it cannot lose energy in the first case. In the

[6] This result may look strange since the force exerted by the string on its ends is not identically zero in time. In reality, the force exerted at $x = L$ is exerted by the left part of the string on the right part of the string whereas the force impulse at stake here is local and results from the left *and* the right parts of the string.

second case, it will gain energy since the dynamical mobility $dv_s/dF_{s/b}$ presented by the bow during that phase is real and negative.[7] This point is discussed further in the case of a dissipative system.

11.4.1.3 Schelleng's Diagram and Generalization

The HM propagates a velocity discontinuity that can be observed and consequently a force discontinuity which is the velocity discontinuity times the characteristic impedance of transverse waves on the string. Since the propagated force moves the string downward the propagation direction, it can be observed by examining how it acts on an obstacle placed in its way.

The bow may represent such an obstacle for propagating waves: when the discontinuity of velocity reaches the sticking bow (diagram 2 in Fig. 11.7), sliding begins if the propagated force is sufficiently high to initiate it.[8] The bow is a fixed obstacle as long as the force does not exceed $\mu_s F_P$, corresponding, within the frame of the ideal HM dynamics, to a force variation $(\mu_s - \mu_d)F_P$. If the velocity discontinuity does not trigger sliding, it reflects with a sign change. The corresponding variation of force on the bow is $\Delta F = 2\,Z_{c,T}\,\Delta\dot{\xi}$. Thus, sliding is initiated if ΔF exceeds $(\mu_s - \mu_d)F_P$, corresponding to $Z_{c,T}\Delta\dot{\xi} \geq (\mu_s - \mu_d)F_P/2$. It follows that the pressing force F_P must not exceed a certain value in order to maintain the sticking/sliding transitions:

$$F_{P,max} = \frac{2\,Z_{c,T}\,v_b}{\beta(\mu_s - \mu_d)}. \tag{11.12}$$

In order to make the system more realistic, the first ingredient to add is a dissipative mobility at the bridge. As a first approximation, this mobility can be assumed independent of frequency so that: $F_0(t) = Y_0\,\dot{\xi}(0,t)$. Keeping the ideal HM as a valid approximation of the motion, the average power dissipated at the bow is obtained by using successively Eq. (11.5) and the relationships between the tension, the celerity, and the characteristic impedance of the transverse waves:

$$\begin{aligned}\langle P\rangle &= \frac{1}{\tau}\int_{-\tau/2}^{\tau/2} F_0(t)\,\dot{\xi}(0,t)dt = \frac{Y_0}{\tau}\left(\frac{v_b\,T}{\beta\,L}\right)^2\int_{-\tau/2}^{\tau/2} t^2 dt \\ &= \frac{Y_0}{\tau}\left(\frac{v_b\,T}{\beta\,L}\right)^2\frac{\tau^3}{12} = \frac{Y_0}{3}\frac{Z_{c,T}^2\,v_b^2}{\beta^2}.\end{aligned} \tag{11.13}$$

[7] This conclusion applies in the particular case $\beta = 1/2$ which corresponds to that of the clarinet: since the slope of the sticking branch is infinite, the stability condition (9.64) cannot be met. For other values of β, finding a stability condition is much more difficult, as mentioned for the cylindrical saxophones.

[8] One may think that the corresponding condition is $Z_{c,T}\Delta\dot{\xi} = (\mu_s - \mu_d)F_P$, but this is not the correct result (see below).

The energy comes from the bow. In the $(\Delta\dot{\xi}, F)$ plane, the point representing the state of the system during sliding is approximately the same as in the case of the ideal HM. During sticking, this point is confined to the vertical segment defined by the $\pm\mu_s F_P$ limits. The upper bond of the average power that the bow can impart to the string during the sticking phase is therefore:

$$P_{\text{upper}} = \frac{1}{\tau}\int_{\tau} F(t)\ \dot{\xi}(\beta L, t)\ dt, \text{ or}$$
$$P_{\text{upper}} = \frac{F_P v_b}{\tau}\left[\mu_s(1-\beta)\tau - \mu_d\frac{1-\beta}{\beta}\beta\tau\right] = F_P\ v_b\ (1-\beta)\ (\mu_s - \mu_d). \tag{11.14}$$

The bow can provide the energy absorbed by the bridge only if $P_{\text{upper}} > P$ and thus, only if the static pressing force F_P of the bow on the string exceeds

$$F_{P,\min} = \frac{v_b Y_0 Z_{c,T}^2}{3(1-\beta)\ (\mu_s - \mu_d)\beta^2}\ . \tag{11.15}$$

Schelleng reasoning on the force wave on the string [30] yields a slightly different result: the mobility at the bridge (for example) alters the force wave, compared to the ideal HM. This perturbation must not initiate sliding during the expected sticking phase. The bow must therefore be pressed sufficiently hard. Using certain approximations on the motion (first harmonic, small β and thus $1-\beta \simeq 1$), it comes that the pressing force must exceed $F_{P,\min} = v_b Y_0 Z_{c,T}^2/\left[2\ (\mu_s - \mu_d)\beta^2\right]$. This expression displays the same dependence on the playing parameters as in Eq. (11.15).

Schelleng's diagram (Fig. 11.9) is a qualitative representation of the maximal and minimal pressing forces as a function of the bowing position β. It shows in a

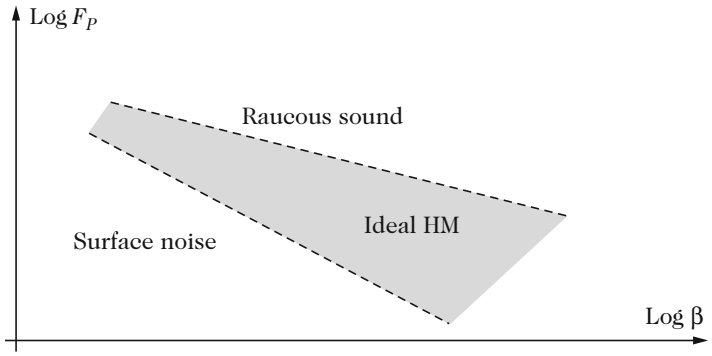

Fig. 11.9 Schelleng's diagram: minimal and maximal values of the pressing force of the bow as a function of the bowing position β. Area where a nearly ideal Helmholtz motion may take place. After [30]

simple way why it is difficult to play near the bridge, as well-known to beginners: the margin between $F_{\mathrm{P,min}}$ and $F_{\mathrm{P,max}}$ becomes progressively smaller as bowing is performed nearer to the bridge. Accordingly, the control on the bow must be more rigorous. It can also be understood why it is very difficult to play with a *pp* (pianissimo) level near the bridge, which may be desirable for sonority reasons: on one hand, v_b must be small since the amplitude of the motion is proportional to v_b/β but, on the other hand, the minimum pressing force increases accordingly (and even as β^{-2}), which makes it difficult to control a low bowing velocity v_b.

More realistic models for the bridge mobility have been proposed by Woodhouse, with a frequency-dependent reactive part. At the playing frequency ω_p, the minimal pressing force becomes [38]

$$F_{\mathrm{P,min}} = \frac{2\ v_\mathrm{b} Z_{\mathrm{c,T}}^2}{\pi^2\ (\mu_\mathrm{s} - \mu_d)\ \beta^2} \times \left[\Re e \sum_{n=1}^{\infty} \frac{Y_0(n\omega_\mathrm{p})}{n^2} \ + \ \max_t \left\{ \Re e \sum_{n=1}^{\infty} \frac{(-1)^{n+1} Y_0(n\omega_\mathrm{p})}{n^2} \exp(ni\omega_\mathrm{p} t) \right\} \right]. \tag{11.16}$$

The dependency of $F_{\mathrm{P,min}}$ on the playing parameters remains similar to that in Eq. (11.15).

11.4.2 Real Helmholtz Motion

11.4.2.1 Observations—Definition

The real motion of the bowed string in musical playing is apparently significantly different from the ideal HM, as exhibited, for example, by Fig. 11.6:

- Torsion of the string induces a difference between the motion of the center of the string — characteristic of transverse waves — and that of its surface, where the succession of sliding and sticking phases occurs. Consequently, the velocity of the center of the string encounters oscillations during the sticking phase.
- The stiffness of the string is responsible for some dispersion of the transverse waves so that the Helmholtz corners are gradually smoothened during their propagation along the string.
- If the energy dissipation that occurs in a string depends on frequency, which is generally the case, the corner is even further (generally) smoothened in the course of its propagation.
- Reactive end conditions are also a cause of a change in the shape of the corner when it reflects at the end of the string.

However, the ideal HM remains a good approximation and the family of periodic motions that are characterized by the occurrence of only one sticking phase (and

thus one sliding phase) will still be labeled as Helmholtz motions. The following paragraphs show how the string dynamics can be treated in the non-ideal case.

As shown in Sect. 3.4.9 of Chap. 3, the velocity v_s at the surface of the string interacting with the bow results from the combination of torsion and transverse waves: $v_s = \dot{\xi} + a\dot{\psi}$. The characteristic mobility of this combined wave, as seen at the surface of the string, is $Y_c = Y_{c,T} + a^2/(I\, c_R)$ [see Eq. (3.116)].

11.4.2.2 Simplified Dynamics of the Bowed String

A simplified treatment of the dynamics of the bowed string is allowed due to the following properties of the system: the string is linear whereas the nonlinear phenomenon (friction) is restricted to one point and is *instantaneous*. In order to obtain the two independent variables $v_s(t)$ and $F(t)$, two equations are required

$$v_s(t) = [F * v_\delta]\,(t); \tag{11.17}$$

$$F(t) = \mathscr{F}_{\mathscr{N}\mathscr{L}}\left[v_s(t) - v_b\right], \tag{11.18}$$

where $v_\delta(t)$ is the impulse response of the string and $\mathscr{F}_{\mathscr{N}\mathscr{L}}$ is a friction curve independent of time. In order to solve this system, Friedlander [11] suggested the construct represented in Fig. 11.11, taking advantage of the string linearity. The velocity at the bowing point $v(t)$ is split into two components as shown in Fig. 11.10 and according to the following equations:

$$v_s(t) = v_H(t) + v_{\infty,\infty}(t) \text{ with } v_{\infty,\infty}(t) = \frac{F(t)}{2Z_c} = \frac{Y_c}{2}F(t)$$

$$\Rightarrow \qquad v_s(t) = v_H(t) + \frac{Y_c}{2}F(t), \tag{11.19}$$

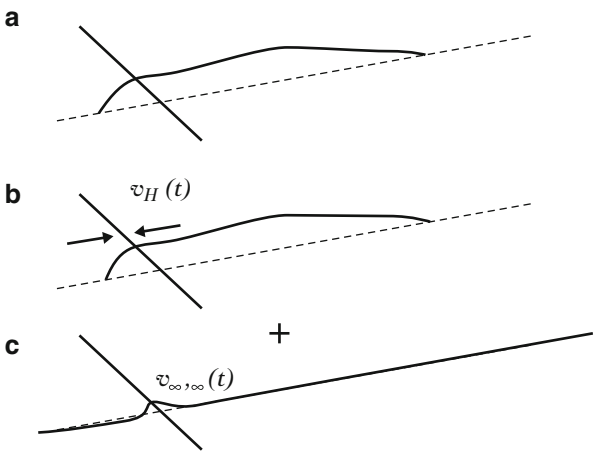

Fig. 11.10 (**a**) Decomposition of the incoming and outgoing velocity waves at the bowing point. (**b**) The incoming waves $v_H(t)$ are due to the *history* of the waves along the string. (**c**) The outgoing waves $v_{\infty,\infty}(t)$, at a given instant, are due to the instantaneous force exerted by the bow and are the same as if the string were infinite on both sides of the bow

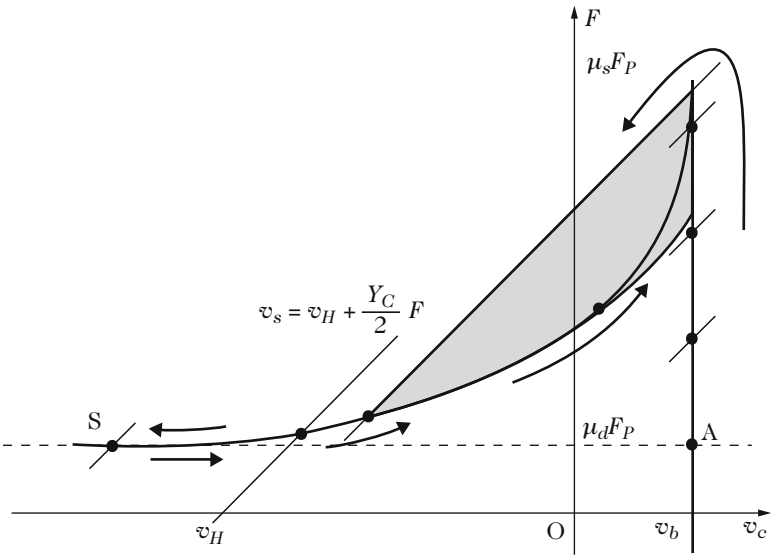

Fig. 11.11 The Friedlander resolution of a simplified dynamics of the bowed string. The point representing the dynamical state of the system in the $(v_s, F_{b/s})$-plane alternates between sticking (point A, "adhesion") and sliding (point S, "sliding"). It follows the friction curve, belongs to a line with slope $2/Y_c$ and its time evolution is governed by the history of the waves on the string (v_H)

where v_H is the velocity caused by the history of the waves along the string and $v_{\infty,\infty}(t)$ is the velocity caused by the *instantaneous* action of the bow[9] At a given time, the latter is the same as if the string were infinite on both sides, hence the notation.

The graphical resolution of these equations is given in Fig. 11.11. The point representing the dynamical state of the system, of coordinates $(v_s(t), F_{b/s}(t))$, is at the intersection of the straight line given by Eq. (11.19) and the friction curve. This point follows a closed line in the $(v_s, F_{b/s})$-plane since the motion is periodic. When the pressing force F_P is small enough, the slope of all the points of the friction curve is less than $2/Y_c$ and there is only one intersection. When F_P exceeds a certain threshold, $2/Y_c$ becomes less than the steepest slope of the friction curve so that, between points A ("really" sticking) and G ("really" sliding), the running point there is a zone with three intersection points. Switching between the two branches is done according to the following rule: the point representing the dynamical state of the system stays on the same branch as long as possible, as illustrated in Fig. 11.11. The hysteresis in the periodic cycle goes along with a slight flattening of the playing frequency, compared to the "natural" value $c_T/2L$ of the period of the HM.

[9]This equation can also be obtained from (4.64) with the following equivalence: in the case of the string, the source and the receptor are located at the same place ($x = x_S$), with p_H being the sum of all terms generated by reflections, in other words by convolutions with $r_0(t)$ and $r_\ell(t)$. Equation (4.65) is written for quantities pertaining to a string, in the Raman model.

11.4.2.3 The Flattening Effect

The flattening effect is the result of pressing the string with the bow beyond a certain force threshold: for a given bow velocity and bow position, the playing frequency goes slightly down.[10] Numerical simulations in the time-domain have shown [22, 32] that this effect appears along with a hysteresis in the sticking-sliding cycle (see above). More recent observations and simulations suggest that the flattening effect may also appear in the absence of a threshold in the pressing force and increases with the pressing force, particularly when the friction model depends on temperature, which induces almost inevitably a hysteresis cycle [33, 40].

It is also possible to analyze this effect in the frequency-domain, with the advantage of an analytical approach [4]. For a periodic motion, the Fourier components of the force exerted by the bow and of the velocity at the bowing point are

$$F(t) = \sum_n F_n \sin(\omega_n t + \psi_n) \tag{11.20}$$

$$v_s(t) = \sum_n V_n \sin(\omega_n t + \psi_n + \varphi_n), \tag{11.21}$$

where the ψ_n are chosen so that F_n are positive. Since the string absorbs energy from the bow, choosing the φ_n in the $[-\pi/2, \pi/2]$ interval also guarantees positive values for the V_n. The mechanical mobility presented by the (linear) string to the bow is therefore:

$$Y_n = \frac{V_n}{F_n} e^{j\varphi_n}. \tag{11.22}$$

This mobility combines the mobility of transverse waves with that of torsion waves (depending on the string model). These mobilities can be obtained by transporting the end mobilities along the string.[11] The area A of the hysteresis cycle in the (v_s, F)-plane is

$$\begin{aligned} A &= \int_\tau F(t)\, dv(t) \\ &= \sum_n n\, \pi\, F_n\, V_n\, \sin\varphi_n = \sum_n n\, \pi\, \frac{V_n^2}{|Y_n|}\, \sin\varphi_n \end{aligned} \tag{11.23}$$

[10] An early scientific observation of the effect has been reported by H. Bouasse [3] in an experiment which he had designed for demonstrating the stability of the playing frequency of a bowed string.

[11] A first approximation of the stiff string case is treated in [4].

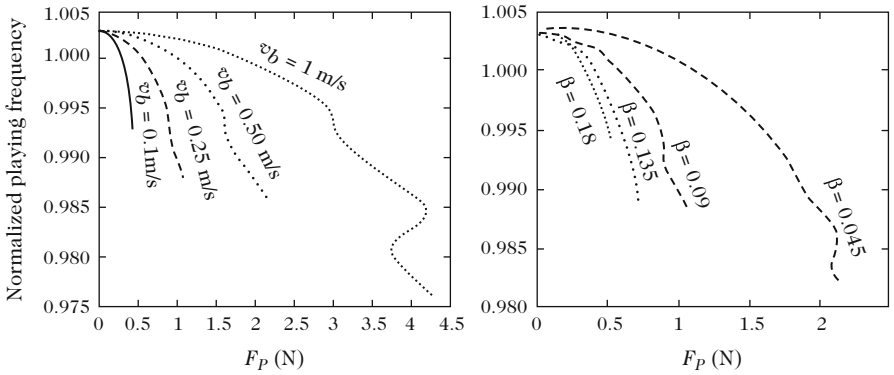

Fig. 11.12 Flattening of the playing frequency as a function of the bow pressing force F_P for a nearly ideal HM. The string has some stiffness and dissipative ends and torsion is included in the model. The friction curve is given by the modified Coulomb model. *Left diagram*: flattening effect for various bow velocity values. *Right diagram*: flattening effect for various bowing position β. After [4]

where the terms of the discrete sum can be interpreted as *reactive powers*.[12] Here, the Fourier components V_n must be determined independently. It appears in Fig. 11.11 that A is positive so that, according to Eq. (11.23), the φ_n must generally be positive. The phase of a mobility is positive below resonance and negative above. Since the playing frequency is near resonance (low inharmonicity), the appearance of the hysteresis implies flattening, compared to the non-hysteresis situation. Precise measurements of the motion of a bowed calibrated string [9] are in good quantitative agreement with this analysis.

Taking advantage of the analytical approach, the dependence of the effect on the playing parameters is displayed in Fig. 11.12: the effect is more marked for low bow velocity and when bowing closer to the bridge. This is consistent with the observation of a marked effect in attack transients and during a change in the bow direction.[13]

11.4.2.4 Stability of the Helmholtz Motion

As explained earlier, the ideal HM is not stable because the corresponding dynamical model does not include energy dissipation. Instabilities appear as growing subharmonics superimposed onto the HM [23] (Fig. 11.13).

[12]This quantity is labeled in contrast to the active power $F_n\ V_n\ \cos\varphi_n$. The principle of this computation has been used in Chap. 9 (Sect. 9.4.5) with a different objective: when there is no hysteresis, the area A is zero, which yields a relationship between the imaginary parts of the admittances (or mobilities) and the amplitudes of the harmonics.

[13]Michèle Castellengo, personal communication.

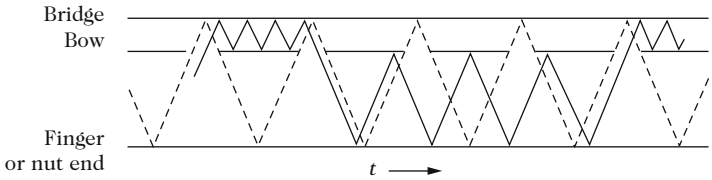

Fig. 11.13 Space-time diagram of the propagation of the Helmholtz corner (*dashed line*) and of a perturbation (*solid line*) along the string. The perturbation follows a periodic path at a frequency lower than the main motion (after [23])

Such subharmonics can indeed be heard, and even be annoying, in the real HM for specific values of β. They appear in the simulations of more realistic models with dissipation in the bow, at the string ends and in the string itself, mostly as non-reflecting torsion waves [11, 23].

Several studies on the stability of more realistic string models confirm the idea that the longer the sticking phase is, the more stable is the motion [5]. This is consistent with the fact that the instability comes from the negative dynamical resistance offered by the sliding branch of the friction curve. Also, it turns out that torsion waves are generally fairly dissipative and that they are generated when a perturbation meets the sticking bow. However, not all perturbations can be stabilized by dissipation at the bow: those which reach the bow during sliding would remain unstable without further refinements of the string model [36]. The stability of a wide range of periodic motions, including the HM, has been studied in various situations, more or less idealized [39]. It appears that the duration of the reflection functions at the string ends (whether the bridge, the finger, or the nut) tends to stabilize the motion.

11.4.2.5 Modifications Induced by a More Realistic Bow Model

In reality, the bow has a finite extension and a number of different hairs simultaneously bow the string at slightly different locations. Keeping the scheme of a corner propagating along the string as a good approximation of the motion, it follows that the sliding phases of the various hairs are initiated at slightly different instants, depending on their location on the string. The effects of such a differential slipping have been extensively studied [23, 24, 26–28], the latest of these articles also including some more realistic characteristics (elasticity of the hair, etc.). Among the consequences, one can note the altered duration of the travel of the corner under a reactive bow and the appearance of jitter, a small amount of aperiodicity of the motion. These works show that experimental and simulation results are better fit if one takes an apparent static friction coefficient μ_s for the whole bow with a smaller value than that of an individual: 0.6 instead of 0.8.

It also appears that the finite bow model provides a more gradual transition between the values of bowing parameters that lead, after some transient regime, to a

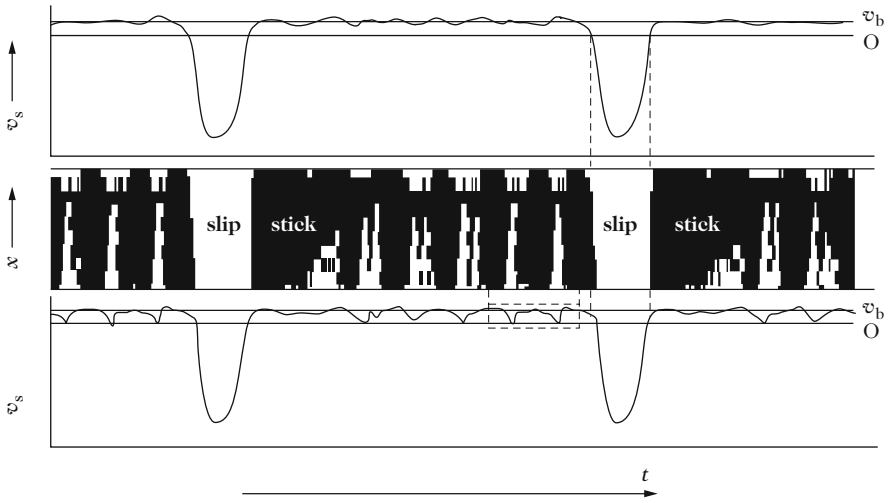

Fig. 11.14 Simulated motion of a string under a bow with finite width, as a function of time. *Top diagram*: velocity of the string at the bow edge nearest to the finger. *Bottom diagram*: velocity of the string at the bow edge nearest to the bridge. *Middle diagram*: position of the bow hair (in ordinates, the *lowest line* of the diagram corresponds to the bow edge nearest to the bridge), whether slipping (*white areas*) or sliding (*black areas*). Partial slipping is initiated mostly on the bridge side; however, these partial slipping events are not successful in breaking sticking on the full bow width and the motion remains a HM (after [27])

musically acceptable motion and the values that fail to do so. When the bow pressing force increases, some hair initiate slipping during the sticking phase (see the middle diagram in Fig. 11.14), as in the case of an ideal bow, leading to the breaking in the HM. For a finite bow, the level of the bow pressing force for which *all* the bow hair initiate slipping during the sticking phase is significantly larger. Conversely, some wiggles appear in the waveform (see bottom diagram in Fig. 11.14) which may become unfavorable to the musicality of the sound.

The dynamics of the bow stick (flexibility and damping) and of the bow hair (longitudinal flexibility) plays an important role in the physics of the bow–string contact but also, according to the makers and players, in the appreciation of the violin itself. A detailed sensitivity analysis of the bowing parameters [28] shows that partial slipping during the sticking phase is less frequent with more flexible and damped hair. As evoked above, the possible consequence of an increased reactive mobility of the bow, seen by the string, is an increase in the frequency variations of the HM. An example of simulations of the string motion under a finite-width bow made of finite-compliance hair, is displayed in Fig. 11.14.

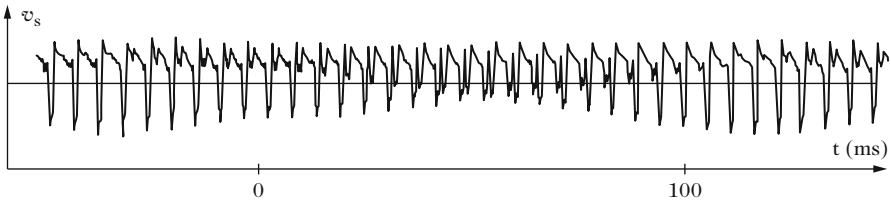

Fig. 11.15 Observation of a wolf note on a cello (after [10])

11.4.3 Other Regimes

11.4.3.1 Wolf Note

The so-called wolf note is an amplitude modulation of the note which appears during a stable bowing gesture, out of the player's control. This occurs on some notes of the cello and viola, rarely on violins (Fig. 11.15). Dynamically, this corresponds to a stable, biperiodic regime, which is not acceptable for musicians. When the fundamental (or pitch) of the note corresponds to a resonance of the instrument body, sustaining the tone goes along with a slow (because the coupling remains weak, altogether) growth of the amplitude of the bridge motion. In turn, this end motion generates a perturbation to the HM (see also Chap. 6). Beyond a certain level of the bridge motion, this perturbation is sufficiently large to trigger a second slip in the middle of the sticking phase. The primary HM is gradually destroyed, which decreases the amplitude of the bridge motion, and a new HM appears with a phase difference relative to the primary motion corresponding to the time shift of the (new) slipping phase. This secondary HM increases, thereby increasing the bridge motion and has the same fate as the primary HM, etc.

Musicians can attenuate this modulation amplitude by pressing the bow harder or by changing the bowing position. Mechanical devices to be added on the "dead" part of the string, between the bridge and the tailpiece, have been proposed in order to alter the bridge mobility. For a more precise analysis of this question, as well as others, we refer the reader to papers by McIntyre and Woodhouse and to the book by Cremer [5].

11.4.3.2 Anomalous Low Frequency (ALF) Tones

An interesting regime has been independently (re?)discovered in the early 1990s by a violinist, Mari Kimura,[14] a bassist and acoustician, Knut Guettler [18] and a physicist, Roger Hanson together with Frederick Halgedahl, a violinist [19]. Later documents report the use of the technique by Paganini. The main characteristic of

[14]The reader may consult her website for examples of musical usage.

the regime is to be periodic at a *lower* frequency than that of the HM. In other words, it is possible to play a third, an octave, a ninth, a twelve, and even two octaves below G3 on a violin! In effect, an appropriate bowing technique, requiring careful control, adjusts the cooperation of the torsion and the transverse waves so that the traveling corner does not trigger slipping each time it reaches the bow. Because the period of ALF tones is not a multiple of the "normal" period of the string, this regime is not to be mistaken with genuine subharmonics which can sometimes be heard, as mentioned above, *together with* the "normal" Helmholtz motion.

11.5 Recent Results

In recent years, a number of new results were published on the physics of violins. Studies of the violin bow were made by Gough [16, 17], Ablitzer et al. [1], and Demoucron [7]. Bowed string transients were investigated by Galluzzo [15]. A method was developed by Schoonderwaldt and Demoucron for extracting bowing parameters from bow performance [31]. Measurements of input admittance of bowed string admittance were discussed by Zhang and Woodhouse [43]. Bridge transfer mobility measurements were performed by Elie et al. [8]. Finally, a significant number of papers were published by Fritz and colleagues on the links between physical properties and perception of violin tones [12–14, 37]. One can also refer to the review by Woodhouse [41].

References

1. Ablitzer, F., Dauchez, N., Dalmont, J.: A predictive model for the adjustment of violin bows. Acta Acust. United Acust. **98**(4), 640–650 (2012)
2. Askenfelt, A.: Observations on the violin bow and the interaction with the string. STL-QPSR **36**(2–3), 23–42 (1995)
3. Bouasse, H.: Bowed string motion (in French). Strings and Membranes. Delagrave, Paris (1926)
4. Boutillon, X.: Analytical investigation of the flattening effect - the reactive power balance rule. J. Acoust. Soc. Am. **90**(2), 754–763 (1991)
5. Cremer, L.: The Physics of the Violin (orig. "Physik der Geige") . MIT Press, Cambridge (1984) (orig.: Hirzel, 1981)
6. Dauchez, N., Génevaux, J., Brémaud, I.: Quality of a violin bow and instability of buckling type (in French). In: Actes du 8ème Congrès Français d'Acoustique, Tours (2006)
7. Demoucron, M.: The performance of bow changes: some mechanical aspects. Acta Acust. United Acust. **101**(2), 331–346 (2015)
8. Elie, B., Gautier, F., David, B.: Acoustic signature of violins based on bridge transfer mobility measurements. J. Acoust. Soc. Am. **136**(3), 1385–1393 (2014)
9. Faure, C., Boutillon, X.: Determination and experimental study of the oscillation frequency of a bowed string (in French). C. R. Acad. Sci. Paris, Série II **t. 317**(11), 1377–1382 (1993)
10. Firth, I.M.: Action of cello at wolf tone. Acustica **39**(4), 252–263 (1978)

11. Friedlander, F.G.: On the oscillations of a bowed string. Proc. Camb. Philos. Soc. **49**(3), 516–530 (1953)
12. Fritz, C., Cross, I., Moore, B.C., Woodhouse, J.: Perceptual thresholds for detecting modifications applied to the acoustical properties of a violin. J. Acoust. Soc. Am. **122**(6), 3640–3650 (2007)
13. Fritz, C., Woodhouse, J., Cheng, F.P.H., Cross, I., Blackwell, A.F., Moore, B.C.: Perceptual studies of violin body damping and vibrato. J. Acoust. Soc. Am. **127**(1), 513–524 (2010)
14. Fritz, C., Blackwell, A.F., Cross, I., Woodhouse, J., Moore, B.C.: Exploring violin sound quality: investigating english timbre descriptors and correlating resynthesized acoustical modifications with perceptual properties. J. Acoust. Soc. Am. **131**(1), 783–794 (2012)
15. Galluzzo, P.M., Woodhouse, J.: High-performance bowing machine tests of bowed-string transients. Acta Acust. United Acust. **100**(1), 139–153 (2014)
16. Gough, C.: The violin bow: Taper, camber and flexibility. J. Acoust. Soc. Am. **130**(6), 4105–4116 (2011)
17. Gough, C.: Violin bow vibrations. J. Acoust. Soc. Am. **131**(5), 4152–4163 (2012)
18. Guettler, K.: Wave analysis of a string bowed to anomalous low frequencies. J. Catgut Acoust. Soc. II **2**(6), 8–14 (1994)
19. Hanson, R., Schneider, A., Halgedahl, F.: Anomalous low-pitched tones from a bowed violin string. J. Catgut Acoust. Soc. II **2**(6), 1–7 (1994)
20. Lazarus, H.: The treatment of the self-excited relaxation oscillations of the bowed string using the finite Laplace transform (in German). Ph.D. thesis, Technische Universität Berlin (1972)
21. Matsunaga, M., Minato, K.: Physical and mechanical properties required for violin bow materials II: comparison of the processing properties and durability between Pernambuco and substitutable wood species. J. Wood Sci. **44**, 142–146 (1998)
22. McIntyre, M., Woodhouse, J.: Fundamentals of bowed-string dynamics. Acustica **43**(2), 93–108 (1979)
23. McIntyre, M.E., Schumacher, R.T., Woodhouse, J.: Aperiodicity in bowed-string motion. Acustica **49**(1), 13–32 (1981)
24. McIntyre, M.E., Schumacher, R.T., Woodhouse, J.: Aperiodicity in bowed-string motion - on the differential-slipping mechanism. Acustica **50**(4), 294–295 (1982)
25. McIntyre, M.E., Schumacher, R.T., Woodhouse, J.: On the oscillations of musical instruments. J. Acoust. Soc. Am. **74**(5), 1325–1345 (1983)
26. Pitteroff, R., Woodhouse, J.: Mechanics of the contact area between a violin bow and a string. part I: reflection and transmission behaviour. Acust. Acta Acust. **84**(3), 543–562 (1998)
27. Pitteroff, R., Woodhouse, J.: Mechanics of the contact area between a violin bow and a string. part II: simulating the bowed string. Acust. Acta Acust. **84**(4), 744–757 (1998)
28. Pitteroff, R., Woodhouse, J.: Mechanics of the contact area between a violin bow and a string. part III: parameter dependence. Acust. Acta Acust. **84**(5), 929–946 (1998)
29. Raman, C.: On the mechanical theory of vibrations of bowed strings. Assoc. Cult. Sci. Bull. **15**, 1–158 (1918)
30. Schelleng, J.C.: The bowed string and the player. J. Acoust. Soc. Am. **53**(1), 26–41 (1973)
31. Schoonderwaldt, E., Demoucron, M.: Extraction of bowing parameters from violin performance combining motion capture and sensors. J. Acoust. Soc. Am. **126**(5), 2695–2708 (2009)
32. Schumacher, R.T.: Self-sustained oscillations of the bowed string. Acustica **43**(2), 109–120 (1979)
33. Schumacher, R.: Measurements of some parameters of bowing. J. Acoust. Soc. Am. **96**(4), 1985–1998 (1994)
34. Smith, J., Woodhouse, J.: The tribology of rosin. J. Mech. Phys. Solids **48**(8), 1633–1681 (2000)
35. Von Helmholtz, H.: On the Sensation of Tones (orig. "Lehre von den Tonempfindungen", 1862) (Engl. translation: 1954). Dover, New York (1877)
36. Weinreich, G., Caussé, R.: Elementary stability considerations for bowed-string motion. J. Acoust. Soc. Am. **89**(2), 887–895 (1991)

37. Wollman, I., Fritz, C., Poitevineau, J.: Influence of vibrotactile feedback on some perceptual features of violins. J. Acoust. Soc. Am. **136**(2), 910–921 (2014)
38. Woodhouse, J.: On the playability of violins. Part II: minimum bow force and transients. Acustica **78**(3), 137–153 (1993)
39. Woodhouse, J.: On the stability of bowed string motion. Acustica **80**(1), 58–72 (1994)
40. Woodhouse, J.: Bowed string simulation using a thermal friction model. Acta Acust. United Acust. **89**, 355–368 (2003)
41. Woodhouse, J.: The acoustics of the violin: a review. Rep. Prog. Phys. **77**(11), 115901 (2014)
42. Woodhouse, J., Schumacher, R., Garoff, S.: Reconstruction of bowing point friction force in a bowed string. J. Acoust. Soc. Am. **108**(1), 357–368 (2000)
43. Zhang, A., Woodhouse, J.: Reliability of the input admittance of bowed-string instruments measured by the hammer method. J. Acoust. Soc. Am. **136**(6), 3371–3381 (2014)

Part IV
Radiation and Sound–Structure Interaction

Musical instruments are complex systems in which numerous acoustical and vibratory phenomena are intrinsically mixed together. Since this book is devoted not only to research, but also to teaching, it seemed necessary to us in this fourth part to start with the description of the main phenomena on simple examples. Thus, the main results on elementary sources (monopoles, dipoles, quadrupoles,...), which might be of use in the accurate description of musical instrument in the next chapters, are presented in Chap. 12. Here, we do not demonstrate all results mathematically, because these sources are largely described in the literature, and we invite the reader to consult specialized textbooks for more details.

Chapter 13 is entirely devoted to the radiation of structures. The presented results are aimed at providing an understanding on how a sound is produced by stringed and percussive instruments. The main concepts are introduced through the example of the radiation of thin elastic plates, which offers the advantage to give an pertinent analytical reference.

Finally, with the purpose to illustrate the basic concepts on complete instruments, the last chapter is devoted to the detailed presentation of the radiation of some selected instruments: vibraphone, timpani, guitar, piano and wind instruments.

Chapter 12
Elementary Sources and Multipoles

Antoine Chaigne and Jean Kergomard

Abstract Elementary sources, such as monopoles and dipoles, are described in this chapter in order to introduce the basic concepts of radiation applicable to musical instruments. In each case, the radiation field is characterized in terms of sound pressure, directivity, acoustic intensity, and sound power. The dependence of the pressure amplitude with respect to distance and frequency is highlighted. Pulsating and oscillating spheres are used as reference examples to illustrate these concepts. Another interest of the elementary sources follows from the fundamental Kirchhoff–Helmholtz theorem, which states that any extended source can be represented as a distribution of elementary sources. This result forms the basis of the calculation of the acoustic field radiated by a musical instrument with arbitrary geometry. Particular attention is also paid to the radiation of sound tubes, either isolated or with mutual influence due to their proximity.

12.1 Introduction: Acoustical Radiation of Musical Instruments

Musical instruments are primarily designed for radiating sound power: this is a necessary condition for allowing the audience to listen to music! A good knowledge on the radiation mechanisms is also essential for the sound engineer, who is in charge of recording a concert with only a finite number of microphones. The sound that reaches the listener (or the microphones) not only depends on the properties of the sources (the musical instruments), but also on the properties of the listening space, and on the position of the listener (resp. the microphones) in the room.

A. Chaigne (✉)
Institute of Music Acoustics, University of Music and Performing Arts Vienna (MDW), Anton-von-Webern-Platz 1, 1030 Vienna, Austria
e-mail: antchaigne@gmail.com

J. Kergomard
CNRS Laboratoire de Mécanique et d'Acoustique (LMA), 4 impasse Nikola Tesla CS 40006, 13453 Marseille Cedex 13, France
e-mail: kergomard@lma.cnrs-mrs.fr

A. Chaigne, J. Kergomard, *Acoustics of Musical Instruments*, Modern Acoustics and Signal Processing, DOI 10.1007/978-1-4939-3679-3_12

In this fourth part of the book, we limit ourselves to the physical description of the radiation of the instruments, leaving aside the questions linked to the acoustics of the room and on the psychoacoustical aspects of the sound perceived by the listeners. However, before starting this study, a rapid overview is made on the parameters to be considered, alternatively from the point of view of the player, the listener, and the sound engineer.

An instrument has to be heard. From the point of view of the physicist, this implies that it can produce sufficient sound power. In an orchestra, or in a chamber music ensemble, another linked question is the level balance between all sections of instruments. This, in turn, determines, for example, the total number of violin players compared to the number of trumpet or clarinet players in an orchestra. We will not go further into these considerations which, as one can imagine, also largely depend on aesthetic choices and on the work performed.

The spatial distribution of the radiated sound and the directivity of the instrument also are important aspects of radiation. During a concert, some instruments, such as the trumpet or the trombone, for example, radiate in restricted emitting cones. In what follows, we will see that the directivity of a given instrument strongly depends on frequency, and thus varies substantially from bass to treble range.

For the player, one important feature of the instrument is the ratio between the input mechanical power and the acoustical power at the "output." This determines the playability of the instrument: in a number of situations, some notes are more difficult to play than others. As a consequence, the sound level can be very heterogeneous over the complete frequency range of the instrument. In terms of physics, attempt will be made to model the relationships between the input mechanical quantities (blow velocity, plucking force, bow pressure, key velocity,...) and the sound pressure.

These are also central questions for the instrument maker. The physical approach of the instrument must serve as a guide for the selection of construction parameters (geometry, materials,...). The function of the developed models is to establish clear links between these parameters and the sound qualities of the instrument: sound level, dynamic range, directivity, homogeneity, and playability.

To finish with this preamble, let us add a few words on contemporary music, with focus on those which make a large use of virtual instruments and synthesizers. In this case, the sound does not result from structural-acoustics coupling between instrument's body and air, but is rather obtained by transduction through loudspeakers. The question of sound level is less critical here, since it is always possible to amplify the electric signal, within the limits imposed by the linear range of the transducers. However, the problem of directivity is still present as well as the question of distribution of these virtual sources in a symphonic orchestra.

12.1.1 General Problem of Radiation

12.1.1.1 Musical Sound Sources

The radiation mechanisms are specific for each musical instrument. However, three basic mechanisms (or source types) are present, to a lesser or greater extent, in each family of instruments [10]:

1. For the sources of **type 1**, the sound results from the variation with time of a *volume flow*. The academic example is the *pulsating sphere* that can be illustrated by the oscillations of a air bubble in water. In musical acoustics, the lowest mode of a kettledrum struck by a mallet in its center, or the radiation at the end of a tube (below the cut-off frequency), are examples of such sources (see Fig. 12.1). In this case the continuity equation (1.109), presented in Part I of this book, is written:

$$\frac{1}{c^2}\frac{\partial p}{\partial t} + \rho \,\mathrm{div}\, \boldsymbol{v} = m, \tag{12.1}$$

   where $m = \rho q$ represents the *mass flow*, or, equivalently, the volume and time density of mass injected in the surrounding fluid.
2. In **type 2** sources, the sound results from local variations of forces exerted on the particles of the fluid, with a zero volume velocity. The standard models of such sources are the *oscillating disk* or the *oscillating sphere*. In musical acoustics, the lowest flexural mode of a xylophone beam, the 11 mode of a kettledrum or of a guitar plate are examples of type 2 sources (see the Fig. 12.1). In general, external force densities are present not only on oscillating sources, but also when sound waves are reflected on a rigid surface. One example was given in Chap. 10 for the flutes. In the presence of external force density $\boldsymbol{f}$, the linearized Euler equation in the fluid becomes

$$\rho \frac{\partial \boldsymbol{v}}{\partial t} + \mathbf{grad}\, p = \boldsymbol{f}\,. \tag{12.2}$$

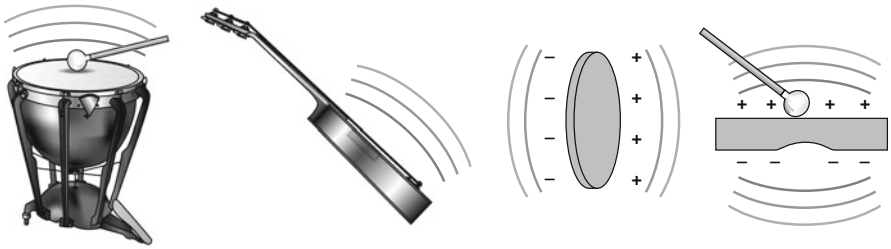

Fig. 12.1 (*Left*) Examples of sources of type 1: lowest modes of a kettledrum and of a guitar plate. (*Right*) Examples of sources of type 2: oscillating disk, first flexural mode of a xylophone beam, without its resonator

where $\boldsymbol{f} = \rho \boldsymbol{F}$ ($\boldsymbol{F}$ is a mass density of force). Eliminating the acoustic velocity $\boldsymbol{v}$ between these two equations yields the heterogeneous wave equation (i.e., with a source term):

$$\frac{1}{c^2}\frac{\partial^2 p}{\partial t^2} - \Delta p = \frac{\partial m}{\partial t} - \operatorname{div} \boldsymbol{f} \,. \tag{12.3}$$

In Eq. (12.3), the two types of sources are present in the right-hand side. It can be seen that the mass term produces sound only if it varies with time. Conversely, the force term produces some sound under the condition of spatial variation.

3. Finally, sources of **type 3** exist in a viscous fluid, and are due to the presence of shear stresses. The formulation of these source terms is obtained by taking the viscosity forces and the convective acceleration (nonlinear terms) in the equations. These terms govern, for example, the origin of jet noise in aeroacoustics [see Eq. (10.30) and Sect. 10.4 in Chap. 10] [26].

12.2 Elementary Sources

Elementary sources are limiting cases that are often very useful, to a first approximation, in order to describe complex sources such as musical instruments.

The pulsating sphere is a good archetype of a perfectly omnidirectional source, which means that the amplitude of the sound pressure only depends on the distance from the source, and not on the angle of observation. The example of the air bubble in water was given in the previous paragraph, but it is not very "musical"! In musical acoustics, the radiation of the guitar soundhole, or of the end of a tube, also can be considered as omnidirectional, at least in a given frequency range. If the radiation field is omnidirectional in an half-space (or in the fraction of the acoustic space), then models of pulsating half-sphere or fractional pulsating spheres can be applied. In what follows, this simple model will be used to introduce the basic concepts of acoustic intensity, radiating power and impedance, and to define the concepts of both near and far fields.

A *monopole*, or point source, can be viewed as the theoretical limit of a pulsating sphere, when its radius tends to zero. It is an idealized system which is not feasible in practice. However, one can build reasonable approximate monopole sources under the condition that their dimensions are kept small compared to the wavelength and/or the distance to the observer (listener).

In contrast with the pulsating sphere (source of type 1), the volume of an oscillating sphere (or of an oscillating disk) does not change during its motion and it will be seen below in this chapter that it corresponds to a type 2 source. The limiting case of such sources yields another elementary source called *dipole*. A dipole is a directional source. It will be shown that a dipole with the same amplitude as the one of a monopole radiates the low frequencies less efficiently. In musical acoustics a xylophone beam, or an oscillating string, can be conveniently described by linear arrays of dipoles [15].

One major interest of such point sources lies in the fact that extended sources can be viewed as distribution of elementary sources. This is one essential result of the Kirchhoff–Helmholtz theorem that will be demonstrated at the end of the present chapter. This theorem also forms the theoretical basis of numerical techniques such that the *Boundary Element Method* which are of current use for the computation of acoustic radiation.

In this chapter, the main properties of the elementary acoustic sources are reviewed, without the details of the mathematical derivations. The reader is invited to consult the numerous textbooks available on these topics (see, for example, [31]). Emphasis is put instead on the consequences of these properties in the particular cases of musical instruments. Most derivations are made in the frequency domain, although some examples are intentionally treated in the time domain.

12.3 Pulsating Sphere

The most simple example of a "type 1" source is the pulsating sphere. Due to the spherical symmetry of the problem, the radiation phenomena can be described analytically with only one spatial coordinate. A sphere with radius a and given radial velocity $V_a(\omega)$ along its periphery (S) is described here in the frequency domain (Fig. 12.2). The amplitude of the radial motion is supposed to be small compared to the radius.

12.3.1 Pressure and Velocity Fields

Using the wave equation expressed in spherical coordinates, as seen in Sect. 7.4.1 in Chap. 7, we get the expression of the radiated pressure field at a distance r from the center of the sphere. In what follows, the pressure field inside the sphere is ignored (it might lead to nonlinear effects in the vicinity of the center whose is beyond the

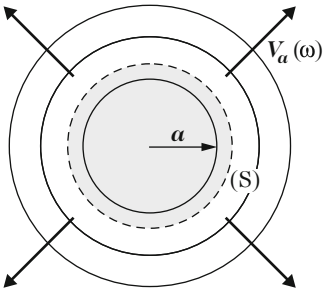

Fig. 12.2 A pulsating sphere of radius a is vibrating radially with angular frequency ω and velocity $V_a(\omega)$ along its periphery (S): the resulting pressure at a given distance from the center of the sphere is identical in all directions

scope of this book) and we concentrate on the outside pressure in free space. From the general solution, the pressure at a distance r can be expressed as a function of the surface pressure $P(a)$ as follows[1]:

$$P(r) = P(a)\frac{a}{r}e^{-jk(r-a)}. \tag{12.4}$$

Using the specific admittance in a [Eq. (7.79)], we get the pressure $P(r)$ as a function of the acoustic velocity which is, by continuity, equal to V_a. Introducing the volume velocity of the sphere $U = 4\pi a^2 V_a$, we get

$$P(r) = \frac{\rho c}{4\pi a^2}\frac{a}{r}U\frac{jka}{1+jka}e^{-jk(r-a)}\ . \tag{12.5}$$

The first term in this expression is the *characteristic acoustical impedance* of the source $Z_c = \frac{\rho c}{4\pi a^2}$. The second term a/r characterizes the *spherical expansion in free field* (or $1/r$ law). The term $\frac{jka}{1+jka}$ governs the frequency dependence of the pressure. If the characteristic dimension of the sphere (the radius a, here) is small compared to the acoustical wavelength ($ka \ll 1$), then the magnitude of the sound pressure is of the same order as ka. Conversely, for the "small" wavelengths ($ka \gg 1$), in the "high" frequency range, the magnitude of P becomes independent of frequency. Finally, the exponential term expresses the delay of propagation between the vibrating surface of the sphere and the observation point. This delay takes the form of a phase shift in the frequency domain. Figure 12.3 shows the variations of the squared pressure modulus as a function of frequency for a given source at a given fixed point in space.

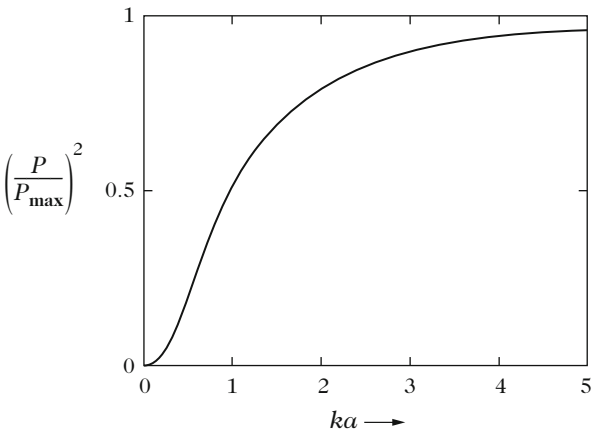

Fig. 12.3 Squared modulus of the pressure radiated by a pulsating sphere as a function of the dimensionless frequency ka

[1] In all the following expressions, the time dependence of the acoustical quantities are omitted, for simplicity. Thus, $P(r, \omega)$ is denoted $P(r)$.

Using again the expression of the admittance in r [Eq. (7.79)] now yields

$$V(r) = \frac{U}{4\pi a^2}\frac{a^2}{r^2}\frac{1+jkr}{1+jka}e^{-jk(r-a)} . \tag{12.6}$$

It can be checked in (12.6) that the continuity condition of the radial velocity is fulfilled in $r = a$. When the observation point is located far from the source ($kr \gg 1$, in terms of wavelength), then the modulus of the acoustic velocity decreases proportionally to $1/r$ as the sound pressure. In this case $P(r) \simeq \rho c V(r)$, which means that the radiated wave at a large distance from the source behaves like a plane wave. In contrary, if $kr \ll 1$ (in the near field of the source), the acoustic velocity decreases as $1/r^2$.

These results illustrate different important cases of approximations which are frequently encountered when studying the radiation of sound sources:

- *Approximation at the emission* depending on the ratio between the dimensions of the source and the acoustic wavelength (discussion on the parameter ka in the case of the pulsating sphere)
- *Approximation at the reception* depending on the ratio between the source-receiver distance and the wavelength (discussion on the parameter kr in the case of the pulsating sphere)

In some case, we might also consider *purely geometrical* approximations, for a given wavelength, where a comparison has to be made between the source-receiver distance and the characteristic dimension of the source. For the pulsating sphere, for example, this refers to approximations involving the ratio a/r.

12.3.2 Acoustic Intensity and Sound Power

From the expressions of pressure and acoustic velocity in the frequency domain, the mean value of the acoustic intensity is derived.[2] In the case of the pulsating sphere, the acoustic intensity is radial (as the velocity) and its modulus is equal to:

$$I(r) = \frac{1}{2}\Re e\{P(r)V^*(r)\} = \frac{|U|^2}{4\pi r^2}\frac{\rho c}{2S}\frac{k^2a^2}{1+k^2a^2}, \tag{12.7}$$

where $S = 4\pi a^2$ is the emitting surface.

One can see that the mean acoustic intensity decreases in $1/r^2$, which is in accordance with the property of spherical expansion. The mean acoustic power corresponds to the flow of the acoustic intensity vector through a closed surface surrounding the source. Taking advantage of the spherical symmetry, the power is computed on a spherical surface Σ with radius r, which yields

[2] In this chapter, capital letters are used for all quantities expressed in the frequency (Fourier) domain. Recall that the concept of mean power only has a signification in the frequency domain.

$$\mathscr{P}_r = \int_\Sigma I(r) d\Sigma = 4\pi r^2 I(r) = \frac{\rho c\,|U|^2}{2S} \frac{k^2a^2}{1+k^2a^2}\,. \tag{12.8}$$

The quantity $\mathscr{P}_r$ is independent of r, which is in accordance with the principle of energy conservation, since no dissipation has been introduced in the model, neither on the source, nor during the propagation. The evolution of the acoustic power with the reduced number ka is identical to the squared modulus of the pressure (see the Fig. 12.3). For a given volume velocity U, the sound power radiated by the spherical sphere is proportional to the square of frequency as long as $ka \ll 1$, and tends to the asymptotic limit $\mathscr{P}_{\max} = \frac{\rho c |U|^2}{2S}$ for $ka \gg 1$.

12.3.3 Force Exerted by the Fluid on the Sphere: Radiation Impedance

Let us now examine the different acoustic quantities in the vicinity of the pulsating sphere. The *radiation impedance* is defined as the ratio between the surface pressure and the volume velocity in $r = a$. We have

$$Z_r = \frac{P(a)}{SV(a)} = \frac{\rho c}{S} \frac{jka}{1+jka} = \frac{\rho c}{S}\left[\frac{k^2a^2}{1+k^2a^2} + j\frac{ka}{1+k^2a^2}\right] = R_r + jX_r\,. \tag{12.9}$$

Comparing (12.9) and (12.8), one can see that the acoustic power can be written equivalently:

$$\mathscr{P}_r = \frac{|U|^2}{2} R_r\,. \tag{12.10}$$

In other words, the acoustic power radiated by the sphere is proportional to the real part of the radiation impedance (or *radiation resistance*) R_r. The imaginary part of the radiation impedance (or *reactance*) X_r is written:

$$X_r = \frac{\rho c}{S} \frac{ka}{1+k^2a^2}\,. \tag{12.11}$$

One can see that X_r has the form of an acoustic mass. This mass depends on frequency, except for $ka \ll 1$. In this latter case, the mass is constant and is equal to $\frac{\rho a}{S}$. The reactance corresponds to the inertial forces that are to be overcome by the sphere during its motion, and to the fluctuating power exchanged between the source and the near field (see Chap. 1). In summary, the radiation impedance yields useful information on the radiated sound power and on the reaction of the fluid on the acoustic source. If the sphere radiates in a finite space (room, cavity), then the reactance might also contain an elastic term which represents the influence of the compressibility of the enclosed fluid.

12.3.4 Concept of Point Source

12.3.4.1 First Approach

Imagine now that the radius of the pulsating sphere vanishes, while keeping a constant volume velocity U. As a result, we obtain a omnidirectional point source, centered at point $r = 0$, called *monopole*. The pressure (12.5) becomes

$$P(r) = j\omega\rho U G(r) \quad \text{with} \quad G(r) = \frac{e^{-jkr}}{4\pi r} . \tag{12.12}$$

The function $G(r)$ is the *Green's function* in free space. More generally, if $\boldsymbol{r}'$ denotes the position of the point source and $\boldsymbol{r}$ the one of the observer ($\boldsymbol{r}$ and $\boldsymbol{r}'$ are vectors), one writes

$$G(\boldsymbol{r}|\boldsymbol{r}') = G(\boldsymbol{r}'|\boldsymbol{r}) = \frac{e^{-jk|\boldsymbol{r}-\boldsymbol{r}'|}}{4\pi|\boldsymbol{r}-\boldsymbol{r}'|} . \tag{12.13}$$

This expression shows the important *reciprocity* property of the Green's function which means that the expression of the pressure is unchanged through permutation of the respective coordinates of both the source and receiver.

In the time-domain, the operator $j\omega$ corresponds to a time derivative, while the operator $\exp(-jkr)$ corresponds to a delay r/c. As a consequence, the pressure $p(r,t)$ generated by the monopole is written:

$$p(r,t) = \frac{\rho}{4\pi r}\frac{d}{dt}u\left(t - \frac{r}{c}\right) . \tag{12.14}$$

In Eq. (12.14), one can see that an acoustic pressure exists only if the *time derivative of the volume velocity* is different from zero. A sphere moving at constant speed, for example, does not create sound.[3] It is also observed that the pressure still decreases in $1/r$. It is finally not surprising to see that the pressure (which is nothing but a surface force density) is proportional to an acceleration, following Newton's second law.

12.3.4.2 Second Approach

The mathematical tool that describes the point source is the Dirac delta distribution δ. Imagine now that a point source with volume velocity $u(t)$ is placed at the origin of the axes (in $r = 0$). In order to establish a link with the wave

[3]This remark might be surprising and seems to contradict everyday experience where a vehicle rolling at constant speed creates aerodynamical noise. In fact, this noise is due to the viscous forces in the fluid, which are not taken into account in the present model.

equation (12.3), one can write that the mass flow is defined as:

$$m = \rho\, u(t)\, \delta(r)\ . \tag{12.15}$$

The Helmholtz equation is then written:

$$\Delta P + k^2 P = -j\omega\rho U(\omega)\delta(r)\ . \tag{12.16}$$

In order to solve (12.16), this equation is integrated on a sphere of radius ε with $\varepsilon \to 0$ (see Fig. 12.4). Due to the spherical symmetry, one can write $P(r) = \frac{A}{r}\exp(-jkr)$, for $r \neq 0$. Denoting $\mathcal{V}$ the volume of the sphere around the source, the integration of (12.16) is written:

$$A\int_{\mathcal{V}} \Delta\left(\frac{e^{-jkr}}{r}\right) d\mathcal{V} + A\int_{\mathcal{V}} k^2 \frac{e^{-jkr}}{r} d\mathcal{V} = -j\omega\rho U\ . \tag{12.17}$$

After some manipulations, this equation can be transformed as follows:

$$A\int_S \mathbf{grad}\left(\frac{e^{-jkr}}{r}\right).\boldsymbol{n}\, dS + A\int_0^{\varepsilon} k^2 4\pi r e^{-jkr} dr = -j\omega\rho U, \tag{12.18}$$

where (S) is the surface of the sphere of radius ε and $\boldsymbol{n}$ the normal vector oriented towards the external field (see Fig. 12.4). As ε tends to zero, the first integral in (12.18) tends to -4π, and the second integral vanishes. One obtains

$$A = \frac{j\omega\rho}{4\pi} U \quad \text{and} \quad P(r) = j\omega\rho U G(r)\ . \tag{12.19}$$

One find then again the intuitive solution previously obtained for a finite pulsating sphere as the radius tends to zero. By the way, one shows that if P is a solution of (12.16), then the Green's function $G(\boldsymbol{r}|\boldsymbol{r'})$ is a solution of the equation:

$$\Delta G(\boldsymbol{r}|\boldsymbol{r'}) + k^2 G(\boldsymbol{r}|\boldsymbol{r'}) = -\delta(\boldsymbol{r} - \boldsymbol{r'})\ . \tag{12.20}$$

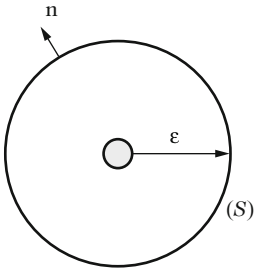

Fig. 12.4 Integration of the Helmholtz equation with a point source

In what follows, the set of both Eqs. (12.16) and (12.20) will be used for calculating the pressure field radiated by any source.

12.3.4.3 Acoustic Power Radiated by a Monopole

In order to calculate the sound power radiated by a monopole, the acoustic intensity is integrated over a spherical surface around the source, as it has been done for the pulsating sphere. Alternatively, one can also use the expression (12.8) and calculate its limit when $ka \ll 1$. In both cases, one gets

$$\mathscr{P}_r = \frac{\rho c k^2 |U|^2}{8\pi} = \frac{\rho \omega^2 |U|^2}{8\pi c} . \tag{12.21}$$

which indicates, among other things, that the power radiated by a monopole is proportional to the square of frequency.

12.3.5 Monopole Arrays

In order to extend the results of the previous paragraph, let us now consider a discrete set of monopoles distributed in space (see Fig. 12.5). This array can be seen as a cloud of active points. Applying the principle of superposition which is valid in linear acoustics, one can derive the resulting field at a given point M of coordinates $\boldsymbol{r}$ just by summing the contributions of the n sources of volume velocities U_n:

$$P(\boldsymbol{r}) = \frac{j\omega\rho}{4\pi} \sum_n U_n \frac{e^{-jkR_n}}{R_n} = \frac{j\omega\rho}{4\pi} \sum_n U_n \frac{e^{-jk|\boldsymbol{r}-\boldsymbol{r_n}|}}{|\boldsymbol{r}-\boldsymbol{r_n}|} . \tag{12.22}$$

This result can be generalized to the case of a continuous distribution of monopoles with elementary volume velocities UdS distributed over a surface $\mathscr{S}$:

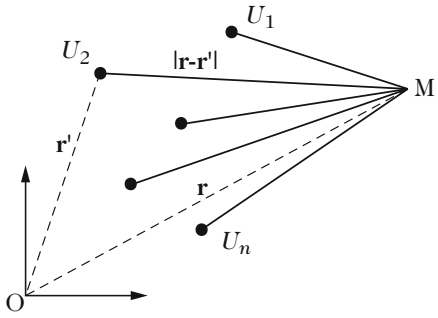

Fig. 12.5 Discrete arrays of monopoles

$$P(\boldsymbol{r}) = \frac{j\omega\rho}{4\pi}\int_{\mathscr{S}} U(\boldsymbol{r}')\,\frac{e^{-jk|\boldsymbol{r}-\boldsymbol{r}'|}}{|\boldsymbol{r}-\boldsymbol{r}'|}d\mathscr{S}, \tag{12.23}$$

whose equivalent time-domain formulation is given by:

$$p(\boldsymbol{r},t) = \frac{\rho}{4\pi}\frac{d}{dt}\int_{\mathscr{S}} \frac{1}{|\boldsymbol{r}-\boldsymbol{r}'|}\,u\left(\boldsymbol{r}', t-\frac{|\boldsymbol{r}-\boldsymbol{r}'|}{c}\right)\,d\mathscr{S}\,. \tag{12.24}$$

Important Remark Equation (12.24) is not valid if $\mathscr{S}$ corresponds to the surface of a finite structure with a finite volume. In this latter case, the waves radiated by the structure are reflected by its own surface, and this phenomenon has to be taken into account.

12.3.5.1 Large Distance Approximations

let us denote L a characteristic dimension of the monopolar distribution. For $r \gg L$, the pressure at a distance r from the source in (12.24) can be simplified, considering that $|\boldsymbol{r}-\boldsymbol{r}'| \simeq r$. A first level of approximation (we will denote it *modulus* approximation) is obtained by simplifying the denominator only:

$$p(\boldsymbol{r},t) = \frac{\rho}{4\pi r}\frac{d}{dt}\int_{\mathscr{S}} u\left(\boldsymbol{r}', t-\frac{|\boldsymbol{r}-\boldsymbol{r}'|}{c}\right)d\mathscr{S}\,. \tag{12.25}$$

For rapidly varying signals (with significant energy in the "high" frequency range) the phase terms can be significant and cannot be neglected, even in the case of small propagation delays between the sources. These delays may alter the waveform at the receiver substantially. Conversely, for slowly varying signals with a significant energy level in the "low" frequency range, an higher level of approximation (let us denote it *phase* approximation) leads to the expression:

$$p(\boldsymbol{r},t) = \frac{\rho}{4\pi r}\frac{d}{dt}\int_{\mathscr{S}} u\left(\boldsymbol{r}', t-\frac{\boldsymbol{r}}{c}\right)d\mathscr{S}\,. \tag{12.26}$$

In this case, the pressure is equivalent to the one radiated by a unique monopole whose total volume velocity is the sum of all elementary volume velocities. However, one should keep in mind that this equivalence is only valid in restrictive situations which depend on the assumptions made on the geometry of the source distribution and on the properties (spectral content) of the emitted signal.

12.3.5.2 Acoustic Power Radiated by a Set of Coherent Monopoles

For a set of sources radiating coherent acoustic signals simultaneously, the acoustic power radiated by each source is affected by the presence of the other sources (see, for example, [14]).

One can think, for example, of the simultaneous emission of pressure by the two main sources of a flute (mouth and open end) for a given note, as seen in Chap. 7. This phenomenon is now illustrated in a simple case involving two monopoles S_1 and S_2 separated by a distance d, and with given volume velocities U_1 and U_2. The results can be generalized to the case of multiple sources.[4]

The far field pressure (at point M) can be calculated using an approximation of the type (12.26). We denote θ the angle between the vector $\boldsymbol{OM} = \boldsymbol{r}$ and the source axis (see the Fig. 12.6). With a first-order expansion (in terms of the ratio d/r), the distance between the source S_1 and the observation point M is $|r - r_1| \simeq r + \frac{1}{2} d \cos\theta$, whereas it is equal to $|r - r_2| \simeq r - \frac{1}{2} d \cos\theta$ for the distance between S_2 and M.

$$P(r) = \frac{j\omega\rho}{4\pi r} e^{-jkr} U(\theta) \text{ where } U(\theta) = U_1 e^{-j\frac{kd}{2}\cos\theta} + U_2 e^{+j\frac{kd}{2}\cos\theta} . \qquad (12.27)$$

Fig. 12.6 Two monopoles.
For a dipole: $U_2 = U = -U_1$

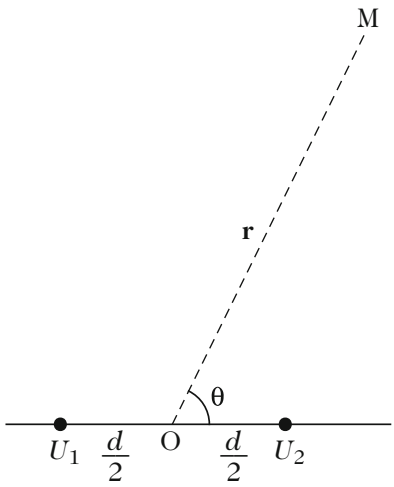

[4]For the sake of simplicity, the following derivations are made in the case of given volume velocities. However, one has to be aware of the fact that, in numerous cases, the two sources are not independent and are linked together by means of a transfer function. This is, for example, the case for the side holes of wind instruments interacting through the resonator, or for the volume velocities of plate and sound hole in stringed instruments that are coupled by the air cavity (see Chap. 6).

The far field behavior of these two sources is thus equivalent to the one of a single monopole, though with a directivity $U(\theta)$ depending on the reduced wavenumber kd. In order to calculate the total acoustic power radiated by both sources, one has to calculate[5] the acoustic intensity on a sphere with radius r. Using the notations $U_{1,2} = |U_{1,2}| \exp(j\varphi_{1,2})$ and $\varphi = \varphi_2 - \varphi_1$, we have

$$\mathscr{P}_r = \frac{\rho c k^2}{8\pi} \left[|U_1|^2 + |U_2|^2 + 2|U_1||U_2| \frac{\sin kd}{kd} \cos\varphi \right] . \tag{12.28}$$

The power is always positive, because the free field can be seen as an absorbing medium at the infinity, and thus the outgoing pressure never comes back to the source. The term in $|U_1||U_2|$ is the *interaction* term. Let us first consider two sources of identical amplitudes in the low-frequency range ($kd \ll 1$). if the sources are in phase, the interferences are constructive, and the sound power is equal to four times the power radiated by a single source ($+ 6\,\mathrm{dB}$). If these sources are in antiphase ($\varphi = \pi$), the sound power is close to zero. By expanding $\sin kd$ to the third order in kd, we then find the expression of the sound power radiated by a dipole (see the next section). One well-known illustration is the case of two loudspeaker systems in antiphase.

Let us now examine how the power is distributed among both sources [14]: depending on the values taken by φ, the sound power due to the presence of the second monopole can either increase or decrease. Moreover, is the amplitude ratio $|U_2/U_1|$ is larger than unity, the power can even become negative, which means that the second monopole is absorbing part of the acoustic energy: it behaves then like a *sink* and not like a source.

Directivity of a Linear Array of Monopoles

One main consequence of linear arrays of monopoles is that the directivity increases compared to the case of a single monopole. One can take benefit of this property in electroacoustics: an antenna of microphones is used, for example, if the purpose is to record a source in a restrictive solid angle. Such a process is very useful in order to record situated at a large distance from the microphones, since it reduces the influence of sideways ambient noise considerably. Reciprocally, loudspeakers arrays are used with the purpose of radiating sound in a restrictive region of space. The directivity of arrays is a joint property of both sources and receivers.

[5] On should integrate over the surface $r =$constant :

$$I(r,\theta) = \frac{1}{2} \frac{k^2 \rho c}{(4\pi r)^2} |U(\theta)|^2 \quad \text{where} \quad |U(\theta)|^2 = |U_1|^2 + |U_2|^2 + 2|U_1||U_2| \cos[kd\cos\theta + \varphi]$$

which amounts to calculate the integral $2\pi r^2 \int_0^\pi |U(\theta)|^2 \sin\theta d\theta$. This calculation is straightforward since $\sin\theta$ is the derivative of the θ-function appearing in $\cos[kd\cos\theta + \varphi]$.

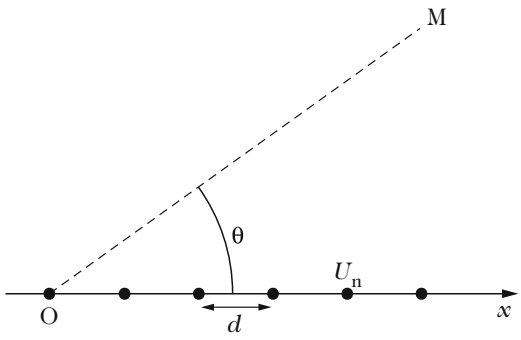

Fig. 12.7 Linear array of monopoles

Musical instruments do not escape this rule: a slender structure (like a xylophone bar) vibrating on a high flexural mode can be viewed as a linear array of sources.

Another illustrative example is the association of several regularly distributed open holes in wind instruments. In order to determine theoretically the directivity resulting from the association of point sources, we calculate it below for an array composed by N monopoles with velocities U_n, equally distributed on the x axis, with a distance d between consecutive sources (see Fig. 12.7). It is assumed here that all sources have the same amplitude, but that there is a constant phase shift between consecutive sources:

$$U_n = U \exp\left[-j(n-1)\varphi\right].$$

Using a first-order expansion of $|\boldsymbol{r} - \boldsymbol{r}_n|$ in (12.22), and defining θ as the angle between the x-axis and the vector $\boldsymbol{r} = \boldsymbol{OM}$, where M is the observation point, the pressure is written:

$$P(r,\theta) = \frac{j\omega\rho_0 U e^{-jkr}}{4\pi r} \sum_{n=1}^{N} e^{j(n-1)(kd\cos\theta-\varphi)} . \tag{12.29}$$

Denoting then $\Theta = (kd\cos\theta - \varphi)$, the directivity of the array is given by:

$$\mathscr{D}(\theta) = \frac{1}{N}\frac{e^{-2jN\Theta}-1}{e^{-2j\Theta}-1} = \frac{\sin N\Theta}{N\sin\Theta} . \tag{12.30}$$

Examining (12.30) shows that the main lobe of the directivity pattern becomes narrower as N increases (see Fig. 12.8).

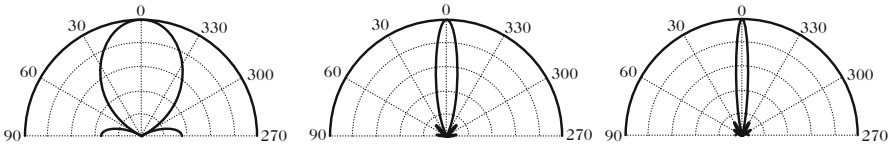

Fig. 12.8 Directivity $D(\theta)$ of the array [see Eq. (12.30)] for different numbers N of monopoles: (*left*) $N = 3$; (*center*) $N = 10$; (*right*) $N = 20$

12.4 Oscillating Sphere

We now turn to the sources with a global zero volume velocity, but which are subjected to a force density $\boldsymbol{f}$ by the surrounding fluid during their motion. In this case, the heterogeneous wave equation (12.3) shows that the divergence of the force density must be different from zero in order to generate sound. An oscillating source meets these requirements, since its motion creates an overpressure in front and a decrease of pressure at the back. In total, this produces a spatial heterogeneity of the force field in the vicinity of the source that creates a nonzero divergence term. At the same time, the total sum of the volume velocities is zero. In order to compare the properties of the oscillating sphere with those of the pulsating sphere, the main results are briefly reviewed below. As done previously, bringing the radius of the sphere close to zero allows to define a dipole, or elementary oscillating source.

12.4.1 Pressure and Velocity Field

Given $v_0(t)$ the oscillating velocity of a sphere of radius a (see Fig. 12.9), and $V_0(\omega)$ its Fourier transform. θ is the angle between the direction of the oscillation and the radial velocity at a given point of the sphere surface. The equation of continuity at the interface between fluid and solid allows to write:

$$V_r(a) = V_0 \cos\theta. \tag{12.31}$$

As for the pulsating sphere, the acoustic pressure and velocity fields are obtained by combining the wave equation with the Euler equation. We find

$$P(r,\theta) = \rho c V_0 \cos\theta \frac{a^2}{r^2}\left[\frac{jka(1+jkr)}{2+2jka-k^2a^2}\right] e^{-jk(r-a)}\,. \tag{12.32}$$

The main difference with the pulsating sphere is the presence here of the *directivity factor* $\cos\theta$ in the expression of the pressure (see Fig. 12.10). As a consequence, the pressure is maximum in the direction of the oscillation, and zero

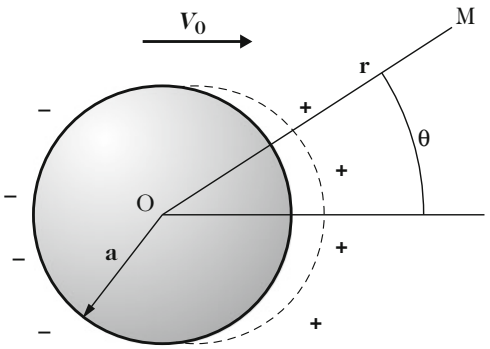

Fig. 12.9 A rigid oscillating sphere creates an overpressure in front and a decrease of pressure at the back, during its motion. In the median plane, overpressure and decrease of pressure are equal and opposite in signs, and thus the resulting pressure is equal to zero

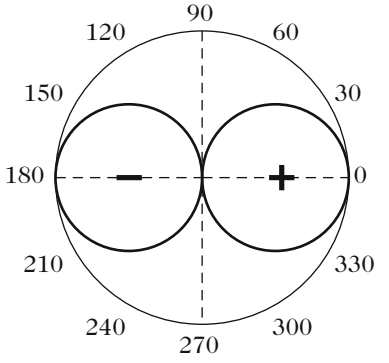

Fig. 12.10 Pressure directivity of an oscillating sphere

in the plane perpendicular to it. A small distances ($kr \ll 1$), the pressure varies as $1/r^2$, and as $1/r$ for $kr \gg 1$. Finally, we have the propagation term $\exp[-jk(r-a)]$.

The acoustic velocity vector has now two components, in the directions $\boldsymbol{e_r}$ and $\boldsymbol{e_\theta}$, respectively (see Fig. 12.11):

$$\begin{cases} V_r(r,\theta) = V_0 \cos\theta \dfrac{a^3}{r^3} \dfrac{2+2jkr-k^2r^2}{2+2jka-k^2a^2} e^{-jk(r-a)}, \\ V_\theta(r,\theta) = V_0 \sin\theta \dfrac{a^3}{r^3} \dfrac{1+jkr}{2+2jka-k^2a^2} e^{-jk(r-a)}. \end{cases} \tag{12.33}$$

In the near field ($kr \ll 1$), both components of the velocity vary as $1/r^3$. In the far field ($kr \gg 1$), the radial component varies as $1/r$. The specific impedance is equal to ρc, and the component along $\boldsymbol{e_\theta}$ varies as $1/r^2$.

12.4.2 Acoustic Intensity and Radiated Pressure

The $\boldsymbol{e_\theta}$-component of the intensity is zero. Its radial component is given by:

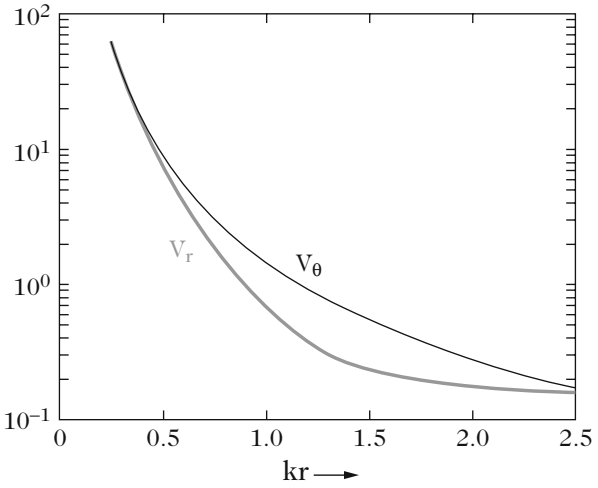

Fig. 12.11 Acoustic velocity radiated by an oscillating sphere

$$I_r(r,\theta) = \frac{1}{2} Re\{PV_r^*\} = \frac{1}{2}\rho c \, \frac{a^2}{r^2} \, \frac{k^4 a^4}{1+k^4 a^4} \, |V_0|^2 \cos^2\theta \; . \tag{12.34}$$

The radiated power is derived:

$$\mathscr{P}_r = \int_S I_r(r,\theta)\, dS = \rho c \, \frac{2\pi a^2 |V_0|^2}{3} \, \frac{k^4 a^4}{1+k^4 a^4} \; . \tag{12.35}$$

If the acoustic wavelength is larger than the dimensions of the source ($ka \ll 1$), then the radiated power is proportional to ω^4. This means that, for given radius and velocity magnitude, an oscillating sphere is less efficient for radiating sound in the low-frequency domain, compared to a pulsating sphere. Using Eqs. (12.8) and (12.35), it is found that the ratio η between both acoustic powers, for a given oscillation velocity V_0, is given by:

$$\eta = \frac{(\mathscr{P}_r)_{SO}}{(\mathscr{P}_r)_{SP}} = \frac{k^2 a^2}{3} \frac{1+k^2 a^2}{1+k^4 a^4} \; , \tag{12.36}$$

which yields $\eta \simeq k^2 a^2/3$ for the sources of small dimensions $ka \ll 1$.

This reduction of radiated power at low frequencies is the consequence of destructive interferences between the acoustic waves generated in the front and at the back, respectively. If the wave at the back is "eliminated" in an absorbing box, as made in most loudspeaker systems, the radiating properties of the system become closer to a those of a monopole and is thus more efficient at low frequencies. It is exactly what happens also in drums (timpani, bass drums,...).

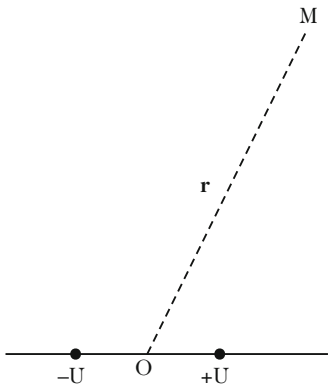

Fig. 12.12 Elementary dipole

12.4.3 Concept of Elementary Dipole

12.4.3.1 First Approach

Bringing the radius of the sphere in (12.32) close to zero yields the expression of the sound pressure generated by an oscillating point source (or dipole) (Fig. 12.12):

$$P(r,\theta) = j2\pi a^3 \omega \rho V_0 \left(jk + \frac{1}{r}\right) G(r) \cos\theta \ . \tag{12.37}$$

The reader can check that this expression is identical to the one obtained by calculating the pressure radiated by a set of two monopoles of equal volume velocity and opposite signs $+U/-U$, where $d = 2a$ is the distance between them (see Fig. 12.6) and where

$$U = \int_S \boldsymbol{V_0}.\boldsymbol{n}\, dS = \pi a^2 V_0 \ . \tag{12.38}$$

Defining now $D_d = j2a\omega\rho U = jk\rho c U d$ as the *moment* of the dipole[6] and using the definition of the Green's function in free space $G(r) = e^{-jkr}/4\pi r$ defined above, the radiated pressure can be expressed under the form:

$$\begin{aligned} P(r,\theta) &= D_d \left(jk + \frac{1}{r}\right) G(r) \cos\theta \\ &= -D_d \frac{\partial G}{\partial r} \cos\theta \ . \end{aligned} \tag{12.39}$$

[6]Notice that some authors define $D_d = Ud$ as the moment of the dipole.

In the time-domain, the pressure is written:

$$p(r,\theta,t) = \frac{\cos\theta}{4\pi r}\left[\frac{1}{r}d_d\left(t-\frac{r}{c}\right) + \frac{1}{c}\frac{d}{dt}d_d\left(t-\frac{r}{c}\right)\right]. \tag{12.40}$$

The variable d_d has the dimension of an acceleration. The pressure here results from two terms: one acceleration term and another term proportional to the time derivative of the acceleration, which corresponds to a third-order time derivative. The contribution of this second term is dominant for the rapidly varying pressure, such as those resulting from percussive impacts, for example, for which instantaneous levels can reach very high values.

Applying the same method as for the sphere, we get the radial intensity:

$$I_r = \frac{1}{2}\rho c\left(\frac{k^2\,|U|\,d}{4\pi r}\right)^2 \cos^2\theta\ . \tag{12.41}$$

The other components of the intensity vector are zero. The power radiated by the dipole [a particular case of Eq. (12.28)] is

$$\mathscr{P}_r = \rho c\frac{k^4\,|U|^2\,d^2}{24\pi} = \rho\frac{\omega^4\,|U|^2\,d^2}{24\pi c^3}\ . \tag{12.42}$$

12.4.3.2 Second Approach

As done previously for the monopole, the pressure radiated by a dipole source is directly derived from the heterogeneous wave equation. For a particle oscillating with volume velocity U at constant volume between two positions r_1 and r_2, the fluid in this region is subjected to a force $f_0 = j\omega\rho U$, according to Newton's second law of motion (see Fig. 12.13). As a consequence, the spatial derivatives (the divergence term) yield the Dirac delta functions corresponding to the discontinuities of the force field in r_1 and r_2. The heterogeneous equation becomes

$$\frac{1}{c^2}\frac{\partial^2 p}{\partial t^2} - \Delta p = -\mathrm{div}\,\boldsymbol{f} = f_0\left[\delta(\boldsymbol{r}-\boldsymbol{r_1}) - \delta(\boldsymbol{r}-\boldsymbol{r_2})\right]. \tag{12.43}$$

In the frequency domain, taking advantage of the properties of the Green's function in free space in Eq. (12.20), we derive the pressure:

$$P(\boldsymbol{r}) = \frac{j\omega\rho U}{4\pi}\left[\frac{e^{-jk|\boldsymbol{r}-\boldsymbol{r_2}|}}{|\boldsymbol{r}-\boldsymbol{r_2}|} - \frac{e^{-jk|\boldsymbol{r}-\boldsymbol{r_1}|}}{|\boldsymbol{r}-\boldsymbol{r_1}|}\right]. \tag{12.44}$$

We find again the intuitive result obtained as the radius of the oscillating sphere tends to zero. This shows that the acoustic field generated by an elementary oscillating source is equivalent to the one radiated by two monopoles of identical

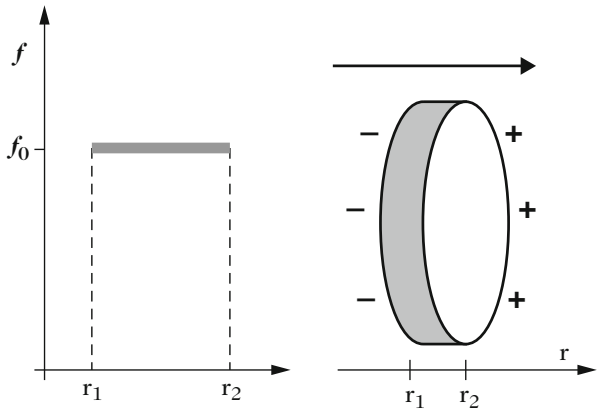

Fig. 12.13 Forces exerted on an elementary dipole

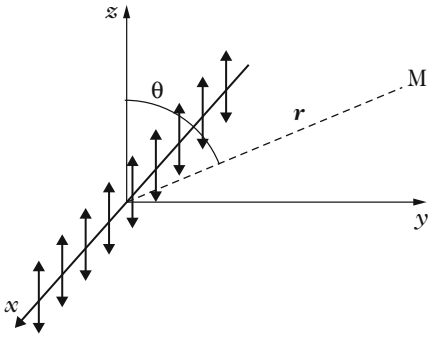

Fig. 12.14 Radiation of an isolated vibrating string. The string is stretched along the x-axis and is assumed to vibrate transversely along the z-axis. The oscillating string can thus be viewed as a linear array of dipoles oriented in the direction of the z-axis. The observation point M is located in the vertical plane, at a distance r from the string with an elevation angle θ with regard to the z-axis

volume velocity and opposite signs, where the distance between the point sources is determined by the peak-to-peak amplitude of the oscillation.

12.4.4 Distribution of Dipoles: Example of the Vibrating String

The vibrating string is a good example of a continuous distribution of dipoles. Before tackling in the next chapters the radiation of a complete stringed instrument, it is a interesting step to calculate the acoustic power radiated by an isolated string, not coupled to a soundboard. The examined configuration is shown in Fig. 12.14. The vector $\boldsymbol{D} = j\omega\rho U\boldsymbol{d}$ is the moment of the elementary dipoles oscillating along the z-axis and $\boldsymbol{d}$ is the vector oriented from $-U$ to $+U$. The pressure is calculated

at point M of coordinates (y, z) (or, alternatively, (r, θ)), with $r = \sqrt{y^2 + z^2}$ and $\cos\theta = y/r$. With $\boldsymbol{r}_1 = \boldsymbol{r}' - \boldsymbol{d}/2$ and $\boldsymbol{r}_2 = \boldsymbol{r}' + \boldsymbol{d}/2$ in (12.44), one obtains

$$P(\boldsymbol{r}) = \frac{j\omega\rho U}{4\pi}\left[\frac{e^{-jk|\boldsymbol{r}-\boldsymbol{r}'+\boldsymbol{d}/2|}}{|\boldsymbol{r}-\boldsymbol{r}'+\boldsymbol{d}/2|} - \frac{e^{-jk|\boldsymbol{r}-\boldsymbol{r}'-\boldsymbol{d}/2|}}{|\boldsymbol{r}-\boldsymbol{r}'-\boldsymbol{d}/2|}\right]. \tag{12.45}$$

If $|\boldsymbol{d}|$ tends to zero in the previous equation, we get

$$P(\boldsymbol{r}) = -j\omega\rho U\boldsymbol{d}.\mathbf{grad}\left[\frac{e^{-jk|\boldsymbol{r}-\boldsymbol{r}'|}}{4\pi|\boldsymbol{r}-\boldsymbol{r}'|}\right] = -\boldsymbol{D}.\mathbf{grad}\left[G(\boldsymbol{r}|\boldsymbol{r}')\right]. \tag{12.46}$$

One finds again the expression (12.39) obtained for an oscillating sphere whose radius tends to zero, and where θ is the angle between the vectors $\boldsymbol{D}$ and $(\boldsymbol{r} - \boldsymbol{r}')$.

Considering now the vibrating string as a linear distribution of dipoles yields the radiated pressure:

$$P(r) = -\frac{1}{4\pi}\frac{\partial}{\partial z}\left[\int_L D(x)\frac{e^{-jk\sqrt{r^2+x^2}}}{\sqrt{r^2+x^2}}\,dx\right]. \tag{12.47}$$

In this formula, $D(x)$ contains the information on the vibratory state of the string. In general, the integral in Eq. (12.47) cannot be solved analytically. However, in order to continue the calculation with the objective of highlighting some typical orders of magnitude for the radiation, two additional assumptions are made:

1. $D(x) = j\omega\rho U_0 d$; which corresponds to a uniform oscillation of the string with diameter d.
2. The string is of infinite length.

In this particular case, Eq. (12.47) becomes

$$P(r) = -\frac{j\omega\rho U_0 d}{4\pi}\frac{\partial}{\partial z}\left[\int_{-\infty}^{\infty}\frac{e^{-jkr\sqrt{1+w^2}}}{\sqrt{1+w^2}}\,dw\right], \tag{12.48}$$

with the change of variable $w = x/r$. It can be shown (see, for example, [31]) that the pressure is written:

$$P(r) = \frac{\rho c U_0 d}{4}\,k^2\,H_1^{(2)}(kr)\cos\theta, \tag{12.49}$$

where $H_1^{(2)}(kr)$ is the Hankel function of the second kind of order one[7] [2]. Another strategy for obtaining this result consists in solving the wave equation in cylindrical coordinates [20].

The acoustic power radiated per unit length of the string is derived from the calculations of pressure and acoustic velocity:

$$\mathscr{P}_r = \frac{\rho\omega^3 |U_0|^2 d^2}{16c^2} = \frac{\rho\pi^2\omega^3 |V_0|^2 d^4}{16c^2}, \tag{12.50}$$

where $U_0 = V_0 \pi dL$ with $L = 1$ m. V_0 is the oscillating velocity of the string. We can check on this expression that the radiated power varies as ω^3, which means that it increases rapidly with frequency. The strings of musical instruments generally have a small diameter (except for the low bass strings of the piano and of the double bass). According to Eq. (12.50), this means that they usually are very inefficient in terms of radiation. It is easy to make the experiment that the sound emitted by an isolated stretched string is almost inaudible, except if the string is put close to the ear.

12.4.5 Quadrupoles

Quadrupolar sources can be viewed as the association of dipoles. A few "musical" examples of such sources are presented below. The most common quadrupoles are the following:

- The *lateral* quadrupole whose plane configuration is shown in Fig. 12.15a. It corresponds to the association of four monopoles of alternate signs located at the corners of a square. The pressure radiated by this source in its plane is given by [14]:

$$P(r,\theta) = -j\rho c d^2 k^3 U \frac{e^{-jkr}}{4\pi r}\left[1 + \frac{3}{jkr} - \frac{3}{k^2 r^2}\right] \sin\theta\cos\theta\ . \tag{12.51}$$

  For a point situated outside its plane, the pressure is (see Fig. 12.16):

$$P(r,\theta,\phi) = -j\rho c d^2 k^3 U \frac{e^{-jkr}}{4\pi r}\left[1 + \frac{3}{jkr} - \frac{3}{k^2 r^2}\right] \sin\theta\cos\theta\ \cos\phi\ . \tag{12.52}$$

  The acoustic power radiated by the quadrupole is given by:

$$\mathscr{P}_r = \frac{\rho c d^4 k^6 |U|^2}{120\pi}\ . \tag{12.53}$$

[7] The Hankel functions of the first and second kind of order n are defined from the Bessel functions of the first kind J_n and from the Bessel functions of the second kind Y_n through the relation $H_n^{(1)}(z) = J_n(z) + jY_n(z)$ and $H_n^{(2)}(z) = J_n(z) - jY_n(z)$.

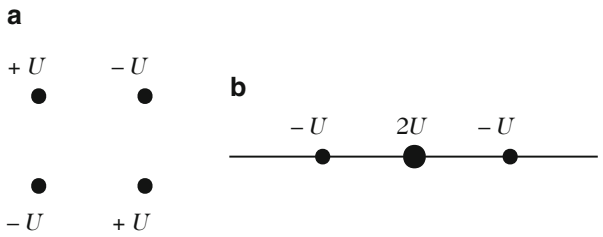

Fig. 12.15 (**a**) Lateral quadrupole. (**b**) Linear (or longitudinal) quadrupole

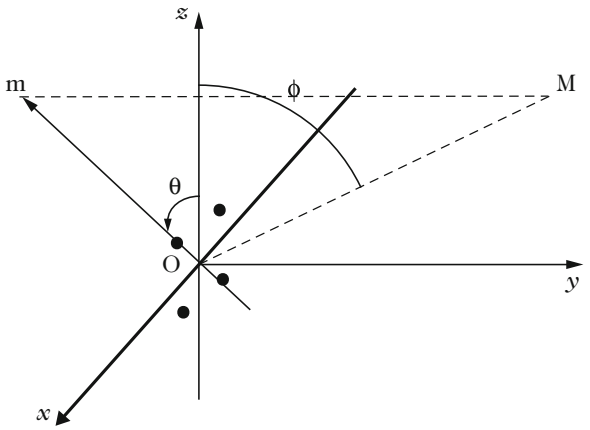

Fig. 12.16 Radiation of a lateral quadrupole: definition of the geometry outside the quadrupole plane. Point m is the projection of point M in the xOz-plane

This power is proportional to ω^6 which means that, for similar flow rate, this source is less efficient than a dipole in the low-frequency domain, though it increases more rapidly with frequency.

- The *linear (or longitudinal)* quadrupole, composed by two dipoles aligned on the same axis (see the Fig. 12.15b). The whole set is symmetrical with regard to the vertical plane, which yields a double flow rate $2U$ to the monopole in the center. In this case, the acoustic pressure is written [14]):

$$P(r,\theta) = -j\rho c d^2 k^3 U \frac{e^{-jkr}}{4\pi r}\left[\cos^2\theta\left(1+\frac{3}{jkr}-\frac{3}{k^2r^2}\right)-\frac{1}{jkr}+\frac{1}{k^2r^2}\right]. \tag{12.54}$$

Applying the same method as for the other elementary sources, the acoustic power of this quadrupole is derived:

$$\mathscr{P}_r = \frac{\rho c d^4 k^6 |U|^2}{40\pi}. \tag{12.55}$$

Compared to the lateral quadrupole, the same frequency dependence is observed (in ω^6). However, the resulting pressure (for identical flow rates) is three times higher.

12.4.5.1 Application 1: Acoustic Field Radiated by a Tuning Fork

The tuning fork is an essential device for each musician. We could have model this device as an example for illustrating the vibrations of beams in Chap. 1, but we prefer to focus here on its quadrupolar radiation properties. These properties were investigated by Russel [28]. In this study, the directivity of a tuning fork at a forced frequency around 440 Hz (note A4), and at different distances r from the source were investigated. The main results of this study are summarized below.

- At a frequency of 426 Hz (close to the nominal frequency of the fork) and at a distance $r = 5$ cm (close to the ear), we have $kr = 0.39$. On can thus reasonably consider to be in the near field. For this kr-value, it is not possible to derive from the simple observation of the directivity pattern whether the fork behaves as a lateral or as a longitudinal quadrupole, since both patterns are very similar (see Fig. 12.17). In both cases, four lobes are observed, which can be easily confirmed audibly by rotating the fork around its axis close to the ear. Notice, however, a

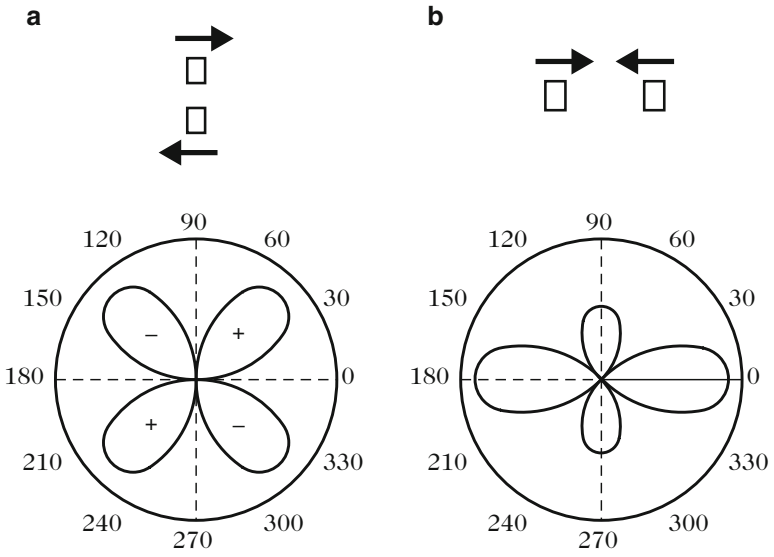

Fig. 12.17 θ- directivities of two quadrupoles for $kr = 0.39$. *Left*: (**a**) lateral quadrupole. *Right*: (**b**) longitudinal quadrupole [28]. The corresponding vibrational modes are displayed on top of each directivity pattern, as well as the motion of the tines. In the normal use of the fork, both branches vibrate at a nominal frequency of 440 Hz with the (**b**)-motion (note A4)

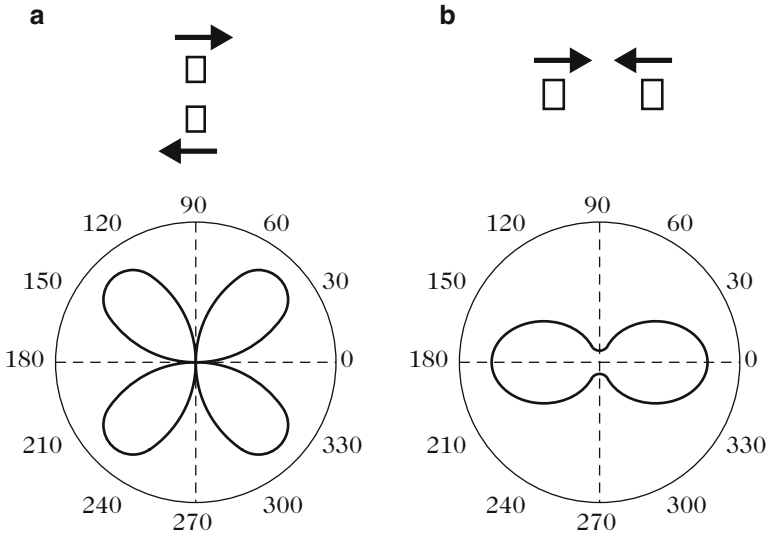

Fig. 12.18 Directivity along θ of quadrupoles for $kr = 7.8$. *Left*: lateral quadrupole. *Right*: longitudinal quadrupole. After [28]

difference of 5 dB between both models in the direction perpendicular to the axis of the fork [according to Eqs. (12.51) and (12.54)].

- If now the fork is located at a distance of 1 m from the ear ($kr = 7.8$), and slowly put into rotation around its axis, then only two maxima of the sound intensity are perceived for a complete turn, instead of four. In addition, the differences between the maximum and the minimum sound intensity level are less clearly audible than in the previous experiments. In this case, the directivity is clearly close to the one observed for the longitudinal quadrupole in the far field (see Fig. 12.18). This is coherent with the motion of the branches in the normal use of the fork.
- For $kr \gg 1$, the first-order approximation of Eq. (12.54) yields

$$P(r, \theta) \propto \frac{k^3}{r} \cos^2 \theta \ . \tag{12.56}$$

This approximation accounts for the existence of two directivity lobes. However, this approximation predicts a zero amplitude in the axis perpendicular to the fork, which is neither in accordance with the complete model in Eq. (12.54), nor to the experiments.

In conclusion, these simple, and easy-to-reproduce, experiments illustrate the fact that the directivity of multipoles not only depend on frequency, but also on the distance of observation. In addition, it shows that oversimplified models can be not sufficient (and even wrong) for interpreting the experiments.

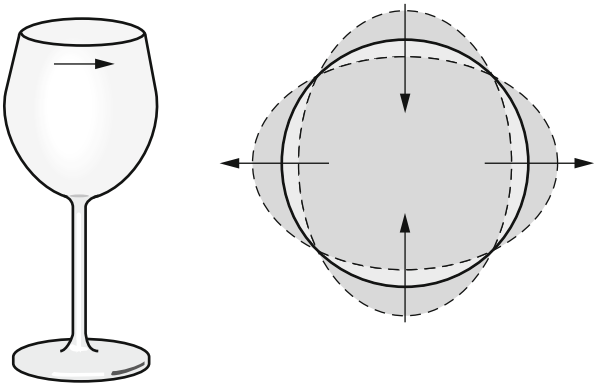

Fig. 12.19 Sliding the edge of a wine glass with a wet finger generates a self-sustained oscillation comparable to the one of a string excited by a bow. The glass vibrates close to a (2,0) mode (two nodal diameters) and the directivity of the sound field is similar to the one of a lateral quadrupole

12.4.5.2 Application 2: Radiation of Wine Glasses

Another easy to do experiments consists in sliding a wet finger on the edge of a glass. Several authors have shown that the main excited shell mode is of the $(2, 0)$-type (see Fig. 12.19). Such a mode is also often observed in the vibrations of bells [11, 27]. The excitation of this system involves typical stick-slip mechanisms, as for the bowed strings (see Chap. 11). Here, the sound is nearly a pure tone, since almost only one mode is strongly excited. The instrument called *glassharmonica* can be viewed as a generalization of this system. It has been used in the past by Mozart and other composers [4]. Figure 12.19 shows that the directivity of the sound field for this mode is analogous to the one of a lateral quadrupole, as verified experimentally by Russel [28].

12.5 Radiation of a Source with Arbitrary Shape

12.5.1 Kirchhoff–Helmholtz Integral

In this section, we are now dealing with the external field radiation of an extended acoustic source with arbitrary geometry, where a part of the external surface is subjected to a vibratory motion (see Fig. 12.20). This situation corresponds to the one encountered in most stringed and percussive instruments. Our purpose is to introduce a general formulation of the radiation, known as the Kirchhoff–Helmholtz integral. Except for very particular geometries, only numerical techniques (such as the Boundary Element Method, or BEM) can be used for solving such an integral (see Sect. 12.5.3.6 below). However, some approximations are valid, in some situations, leading to interesting results in terms of physics. Approximate

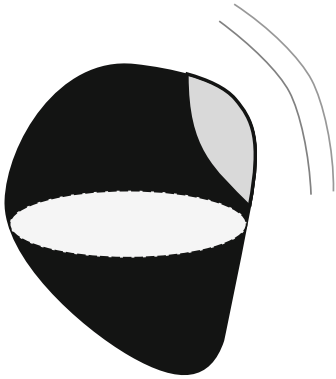

Fig. 12.20 In the most general case, an extended acoustic source is composed of both vibrating surfaces (*in grey*) and rigid parts (*in black*). The rigid parts reflect the waves emitted by the vibrating surfaces. The total resulting pressure field is the sum of the direct field radiated by the vibrating surfaces and the field reflected by the rigid passive surfaces

results can also serve as reference solutions when the purpose is to evaluate the pertinence and consistency of a numerical solution.

The pressure field radiated by an extended source such as the one shown in Fig. 12.20 is together due to the vibrating surfaces and to the waves reflected by the rigid parts. As a consequence, it will be shown that the whole source can be viewed equivalently as the association of a monopole and dipole distributions. This is one fundamental result of the Kirchhoff–Helmholtz integral. The existence of two distributions is a consequence of the fact that the Helmholtz equation itself is of the second order.

12.5.1.1 Green's Theorem

In order to introduce the Kirchhoff–Helmholtz equation, a mathematical tool is needed that allows the transformation of a volume integral into a surface integral: the Green's theorem. The interest of such a transformation will appear later, especially for the use of the integral in numerical applications.

Let us select two arbitrary functions G and Φ, assuming that these functions have the adequate properties of continuity and derivability for the problem. These functions are defined in a volume $\mathcal{V}$ bounded by a surface S with external normal vector $\boldsymbol{n}$. It can be shown that:

$$\int_{\mathcal{V}} [G\Delta\Phi - \Phi\Delta G]\, d\mathcal{V} = \int_{\mathcal{V}} \mathrm{div}\,[G\mathbf{grad}\Phi - \Phi\mathbf{gradG}]\, d\mathcal{V} = \int_S \left[G\frac{\partial\Phi}{\partial n} - \Phi\frac{\partial G}{\partial n}\right] dS\,. \tag{12.57}$$

The main interest of this theorem, which is nothing but a generalization of the divergence theorem, is the transformation of a volume integral into a surface integral, thus reducing by one the dimension of the problem. If both functions have the same impedance boundary condition on S (or on a part of S), the integral is equal to zero on this surface (or, on the considered part). Recall that the impedance is defined as the ratio between G and $\partial G/\partial n$.

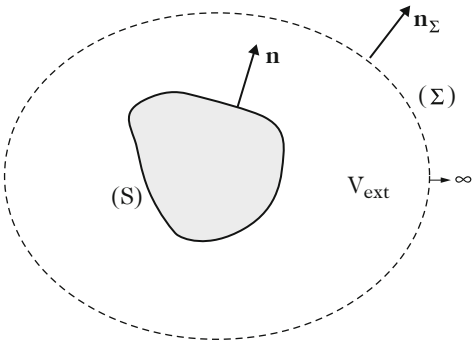

Fig. 12.21 Application of the Green's theorem to the calculation of the external pressure field

The application of the theorem (12.57) to the calculation of the external pressure field is illustrated in Fig. 12.21. The volume to consider here is the *external volume* denoted $\mathscr{V}_{\text{ext}}$ bounded by the external surface S of the source, on the one hand and, on the other hand, by the closed spherical surface Σ obtained as its radius tends to infinity:

$$\int_{\mathscr{V}_{\text{ext}}} [G\Delta\Phi - \Phi\Delta G]\, d\mathscr{V} = -\int_S \left[G\frac{\partial\Phi}{\partial n} - \Phi\frac{\partial G}{\partial n}\right] dS + \int_\Sigma \left[G\frac{\partial\Phi}{\partial n_\Sigma} - \Phi\frac{\partial G}{\partial n_\Sigma}\right] d\Sigma \,. \tag{12.58}$$

On Σ, the functions G and Φ fulfill the so-called *Sommerfeld condition* (see Sect. 12.5.1.2) and the integral vanishes. The change of sign in front of the first integral, in the right-hand side of the equation, is a consequence of the fact that the normal vector $\boldsymbol{n}$ is oriented towards the *internal part* of the volume $\mathscr{V}_{\text{ext}}$.

12.5.1.2 Calculation of the Pressure Radiated Outside the Source (External Field)

The purpose now is to determine the sound pressure $P(\boldsymbol{r})$ radiated by the acoustic source in the external field. This pressure is governed by the Helmholtz equation $\Delta P(\boldsymbol{r}) + k^2 P(\boldsymbol{r}) = 0$. In addition, the Green's function in free space is given by Eq. (12.20) where $\boldsymbol{r'}$ refers to any point on the surface S surrounding the volume $\mathscr{V}$ of the source. From these two equations, one can simply derive:

$$\Delta P(\boldsymbol{r})G(\boldsymbol{r}|\boldsymbol{r'}) - \Delta G(\boldsymbol{r}|\boldsymbol{r'})P(\boldsymbol{r}) = P(\boldsymbol{r})\delta(\boldsymbol{r} - \boldsymbol{r'}) \,. \tag{12.59}$$

Taking advantage of the reciprocity properties of the function G, Eq. (12.59) becomes

$$\Delta P(\boldsymbol{r'})G(\boldsymbol{r}|\boldsymbol{r'}) - \Delta G(\boldsymbol{r}|\boldsymbol{r'})P(\boldsymbol{r'}) = P(\boldsymbol{r'})\delta(\boldsymbol{r} - \boldsymbol{r'}) \,. \tag{12.60}$$

Finally, after integration over V_{ext} and application of the Green's theorem, we get

$$\int_{\mathscr{V}_{\text{ext}}} P(\mathbf{r}')\delta(\mathbf{r}|\mathbf{r}')d\mathscr{V} = P(\mathbf{r}) = \int_S \left[P(\mathbf{r}')\frac{\partial G(\mathbf{r}|\mathbf{r}')}{\partial n} - G(\mathbf{r}|\mathbf{r}')\frac{\partial P(\mathbf{r}')}{\partial n} \right] dS_{(\mathbf{r}')} \,. \tag{12.61}$$

The Kirchhoff–Helmholtz (KH) in (12.61) is valid for the *external* field. It shows that the pressure at any point $\boldsymbol{r}$ in the external space is obtained by means of a surface integral on the bounding surface S of the source.[8] This integral involves a distribution of monopoles (terms in $G(\boldsymbol{r}|\boldsymbol{r'})$), and a dipole distribution (terms in $\frac{\partial G(\boldsymbol{r}|\boldsymbol{r'})}{\partial n}$). In the following examples, the physical meaning of both distributions will be clarified.

Using Euler equation $\partial P/\partial n = -j\omega\rho V_n$, where V_n is the normal velocity (with regard to S), the KH-equation can be transformed into the following form[9]:

$$P(\boldsymbol{r}) = \int_S \left(-P(\boldsymbol{r'})\frac{e^{-jkR}}{4\pi R}\left[jk + \frac{1}{R} \right]\cos\theta + \frac{e^{-jkR}}{4\pi R} j\omega\rho V_n(\boldsymbol{r'}) \right) dS_{(\boldsymbol{r'})} \,. \tag{12.62}$$

Equation (12.62) shows that, for the calculation of the external pressure, knowledge of both the surface (parietal) pressure $P(\boldsymbol{r'})$ and normal velocity $V_n(\boldsymbol{r'})$ are necessary.

Sommerfeld Condition

In order to define a complete problem of radiation, initial and boundary conditions must be added to the partial differential (wave) equation. Writing in (12.58) that the integral on Σ vanishes as the observation distance tends to infinity corresponds to imposing a boundary condition at the infinity. In the far field ($r' \longrightarrow \infty$), we have $|\boldsymbol{r} - \boldsymbol{r'}| \simeq r'$. The integral then vanishes under the condition:

$$-4\pi r'^2 \left[P(\boldsymbol{r'})jk\frac{e^{-jk|\boldsymbol{r}-\boldsymbol{r'}|}}{4\pi r'} + \frac{e^{-jk|\boldsymbol{r}-\boldsymbol{r'}|}}{4\pi r'}\frac{\partial P(\boldsymbol{r'})}{\partial r'} \right] \to 0 \,. \tag{12.63}$$

Through permutation of r and r', this condition becomes

$$\lim_{r\to\infty} r\left[\frac{\partial P(r)}{\partial r} + jkP(r) \right] = 0 \,. \tag{12.64}$$

(continued)

[8] Notice that this integral is valid for any Green's function satisfying (12.20) in the external space, whatever the boundary conditions. In addition, this integral can be generalized to the case of multiple sources in the external space, due to the principle of superposition.

[9] It can be shown that the normal derivative of G is written $\frac{\partial G}{\partial n} = -G\left[jk + \frac{1}{R}\right]\cos\theta$, where $\theta = (\boldsymbol{n}, \boldsymbol{R})$.

This condition is the so-called *Sommerfeld condition*. Notice that the Green's function fulfills this condition. This amounts to assume that there is no convergent wave reflected back from infinity.

One drawback of the Sommerfeld condition is that it depends on the geometry. As a consequence, its exact formulation can be known explicitly only in a limited number of cases. An equivalent method for accounting to the zero condition at infinity is to consider that the wave is progressively damped during its propagation. This very "physical" method can be illustrated in the following 1-D case. Consider the transfer impedance [Eq. (4.29)]: if x_2 tends to infinity, the *tangent* function exhibits zeros and infinite maxima, and does not converge, which indicates the presence of reflected waves. However, if the wavenumber k becomes complex, and is written $k - j\alpha$, then the *tangent* function (of complex angle) tends to unity and the impedance tends to the characteristic impedance of a progressive wave, due to the absence of returning wave. In this case, the damping factor α can be imposed as small as we want. Finally, a Sommerfeld condition is obtained for the plane wave case: $\partial P/\partial x + jkP \longrightarrow 0$.

It will be shown in Chap. 14 that, for numerical necessity, another widely used method for simulating the radiation and propagation of waves in free space consists in imposing Absorbing Boundary Conditions at the border of a finite computational domain (such as a "virtual" anechoic chamber) in order to prevent the propagation of returning waves back to the source.

12.5.1.3 Time-Domain Formulation of the KH Integral

At this stage, a transformation of the KH integral in the time-domain can be achieved. The operator $j\omega$ corresponds to a time derivative, while $\exp(-jkr)$ corresponds to a time delay r/c. The pressure is then written:

$$p(\mathbf{r},t) = -\frac{1}{4\pi}\int_S \left[\frac{1}{Rc}\frac{\partial}{\partial t}p\left(\mathbf{r}', t-\frac{R}{c}\right) + \frac{1}{R^2}\,p\left(\mathbf{r}', t-\frac{R}{c}\right)\right]\cos\theta\; dS_{(\mathbf{r}')} + \frac{\rho_0}{4\pi}\int_S \frac{\partial v_n}{\partial t}\left(\mathbf{r}', t-\frac{R}{c}\right)\; dS_{(\mathbf{r}')}\,. \tag{12.65}$$

Equation (12.65) shows the *implicit* character of the equation, since the surface pressure p also appears under the integral. This induces some difficulties in the resolution. In addition, two terms are present in the first integral, where the magnitude of the second (in $1/R^2$) is attenuated more rapidly than the first one during the propagation. This first integral is of the dipolar type [see Eq. (12.40)]. The second integral is of the monopolar type, as in Eq. (12.14).

12.5.2 Multipolar Decomposition

Under the condition that the external surface S is sufficiently regular, it can be shown that the Kirchhoff–Helmholtz integral can be expanded as a convergent series of multipoles, whatever the size of the source. This approximation is particularly useful for the sources whose characteristic dimensions are small compared to the wavelength. Such a decomposition can be obtained using Taylor series expansion of vector functions f such as [2]:

$$f(\boldsymbol{r}-\boldsymbol{r}') = f(\boldsymbol{r}) - (\boldsymbol{r}'.\mathbf{grad})f(\boldsymbol{r}) + \frac{1}{2!}(\boldsymbol{r}'.\mathbf{grad})^2 f(\boldsymbol{r}) + \cdots \tag{12.66}$$

Applying this expansion to the function $R^{-1}p\,(\mathbf{r}', t - R/c)$, where $R = |\mathbf{r} - \mathbf{r}'|$, we get

$$\frac{p\,(\mathbf{r}', t-R/c)}{R} = \frac{1}{r}p\left(\mathbf{r}', t-R/c\right) - (\mathbf{r}'.\mathbf{grad})\frac{p\,(\mathbf{r}', t-R/c)}{r} + \frac{1}{2!}(\mathbf{r}'.\mathbf{grad})^2\frac{p\,(\mathbf{r}', t-R/c)}{r} + \cdots \tag{12.67}$$

or, equivalently:

$$\frac{p\left(\boldsymbol{r}', t-\frac{R}{c}\right)}{R} = \exp(-\boldsymbol{r}'.\mathbf{grad})\frac{p\left(\boldsymbol{r}', t-\frac{r}{c}\right)}{r} \quad \text{with}$$
$$\exp(-\boldsymbol{r}'.\mathbf{grad}) = 1 - \boldsymbol{r}'.\mathbf{grad} + \tfrac{1}{2!}(\boldsymbol{r}'.\mathbf{grad})^2 + \cdots . \tag{12.68}$$

Applying this result to both the pressure and velocity in (12.65), the KH integral is rewritten as follows:

$$p(\boldsymbol{r}, t) = -\tfrac{1}{4\pi}\int_S \exp(-\boldsymbol{r}'.\mathbf{grad})(\boldsymbol{n}.\mathbf{grad})\tfrac{p(\boldsymbol{r}', t-r/c)}{r}\, dS_{(\boldsymbol{r}')} + \tfrac{\rho}{4\pi r}\int_S \exp(-\boldsymbol{r}'.\mathbf{grad})\tfrac{\partial v_n}{\partial t}\,(\boldsymbol{r}', t-r/c)\; dS_{(\boldsymbol{r}')}\,. \tag{12.69}$$

Then, defining the following quantities:

$$\begin{cases} S(t) = \dfrac{\rho}{4\pi}\displaystyle\int_S \dot{v}_n(\boldsymbol{r}', t)\, dS, \\ \boldsymbol{D}(t) = \dfrac{1}{4\pi}\displaystyle\int_S \left[\rho\, \boldsymbol{r}'\, \dot{v}_n(\boldsymbol{r}', t) + \boldsymbol{n}\, p(\boldsymbol{r}', t)\right] dS, \\ Q_{ij}(t) = \dfrac{1}{8\pi}\displaystyle\int_S \left[\rho\, r'_i\, r'_j\, \dot{v}_n(\boldsymbol{r}', t) + (r'_i\, n_j + r'_j\, n_i)p(\boldsymbol{r}', t)\right] dS\,, \end{cases} \tag{12.70}$$

where the indices i and j refer to the vector components, the radiated pressure is expressed as follows:

$$p(r,t) = \frac{S(t-r/c)}{r} - \mathbf{grad}.\frac{\boldsymbol{D}(t-r/c)}{r} + \sum_{i,j=1}^{3} \frac{\partial^2}{\partial x_i \partial x_j}\frac{Q_{ij}(t-r/c)}{r} + \cdots . \tag{12.71}$$

In (12.71), $S(t)$ is the monopolar term, the vector $\boldsymbol{D}$ is the dipole moment, and the Q_{ij} are the quadrupolar components of the source.

12.5.2.1 Spherical Harmonics Expansion

The interest of the multipolar decomposition is to formulate the pressure field radiated by any source as a sum of elementary fields radiated by point sources of increasing order. However, from a mathematical point of view, such a decomposition might be problematic, because the selected basis is not orthogonal. For this reason, it is often preferred to expand the pressure on a spherical harmonics basis, which is orthogonal. For the external problem, and assuming no returning wave propagating towards the source, this expansion is written: [35]:

$$P(r,\theta,\phi,\omega) = \sum_{n=0}^{\infty} \sum_{m=-n}^{n} C_{mn}\, h_n(kr)\, Y_n^m(\theta,\phi), \tag{12.72}$$

where the C_{mn} are complex coefficients depending on frequency, the $h_n(kr)$ are *Spherical Hankel functions*[10], and the $Y_n^m(\theta,\phi)$ are the *spherical harmonics* [2]. These harmonics are written explicitly:

$$Y_n^m(\theta,\phi) = \sqrt{\frac{2n+1}{4\pi}\,\frac{(n-m)!}{(n+m)!}}\, P_n^m(\cos\theta)\; e^{jm\phi}, \tag{12.73}$$

where the P_n^m are the Legendre polynomials.

There is no bijection between the coefficients of the multipolar expansion and the spherical harmonics. However, it is relatively easy to express the first coefficients of the multipolar expansion in terms of spherical harmonics. The first spherical harmonic

$$Y_0^0(\theta,\phi) = \frac{1}{\sqrt{4\pi}} \tag{12.74}$$

[10]With the time convention selected throughout this book, the spherical Hankel functions here are of the second kind, defined as $h_n^{(2)}(z) = j_n(z) - jn_n(z)$, where $j_n(z)$ and $n_n(z)$ are the spherical Bessel functions of the first and second kinds, respectively. The exponent (2) is omitted for clarity.

for example, is a monopolar term. Similarly, the second spherical harmonic

$$Y_1^0(\theta,\phi) = \sqrt{\frac{3}{4\pi}}\cos\theta \tag{12.75}$$

has the directivity of an axial dipole . One can also show that the directivity of a longitudinal quadrupole can be derived from the difference $Y_2^0 - \alpha Y_0^0$ where α is a constant (see [35]).

Radiated Power

The acoustic power can be obtained through integration of the acoustic intensity on a sphere Σ of radius r_0 around the source. We obtain

$$\mathscr{P}_r(\omega) = \frac{1}{2}\int_\Sigma \Re e\left[P(r_0,\theta,\varphi,\omega)V^*(r_0,\theta,\varphi,\omega)\right] r_0^2 \sin\theta \; d\theta \; d\varphi \; . \tag{12.76}$$

Using Euler equation and the spherical harmonics expansion of the pressure, the acoustic velocity is written:

$$V(r_0,\theta,\varphi,\omega) = -\frac{1}{j\rho ck}\frac{\partial P}{\partial r} = -\frac{1}{j\rho c}\sum_{n=0}^{\infty}\sum_{m=-n}^{n} C_{mn}\, h_n'(kr_0)\; Y_n^m(\theta,\phi) \; . \tag{12.77}$$

The acoustic power can thus be rewritten as:

$$\mathscr{P}_r(\omega) = \frac{r_0^2}{2\rho c}\sum_{n=0}^{\infty}\sum_{m=-n}^{n} |C_{mn}^2| \Re e\left[h_n(kr_0)h_n'(kr_0)^*\right] \; . \tag{12.78}$$

Using one characteristic property of the spherical Hankel functions:

$$\Re e\left[h_n(kr_0)h_n'(kr_0)^*\right] = \frac{1}{k^2 r_0^2}, \tag{12.79}$$

it is found finally that the radiated power can be expressed in terms of the spherical harmonics under the form:

$$\mathscr{P}_r(\omega) = \frac{1}{2\rho ck^2}\sum_{n=0}^{\infty}\sum_{m=-n}^{n} |C_{mn}^2| \; . \tag{12.80}$$

This result shows that, due to their orthogonality property, the spherical harmonics are independent and thus the acoustic power radiated by each component only depends on the squared modulus $|C_{mn}|^2$ of its magnitude.

12.5.2.2 A Few Applications of the Spherical Harmonics in Musical Acoustics

Radiation of a Stringed Instrument with Holes

In the 1980s, Weinreich and Arnold have developed a new technique for measuring acoustic fields, based on the spherical harmonics expansion of the sound pressure. This technique was applied with success to the violin [34]. More precisely, Weinreich and his colleagues made the measurements of the *radiativities* of a stringed instrument, such as the violin, defined as the ratio between the so-called *multipolar moments* μ_{mn} and the force F_B exerted by the string at the bridge [33]. The moments defined by this author are related to the coefficients C_{mn} of the expansion in Eq. (12.72) by the relations[11]:

$$C_{mn} = \left[-j\omega\rho c \frac{k^{n+2}}{\sqrt{4\pi(2n+1)}} \frac{2^n n!}{(2n)!} \right] \mu_{mn} \,. \tag{12.81}$$

With this definition, one can show that the moments μ_{mn} for a sphere of radius a small compared to the wavelength ($ka \ll 1$) and subjected to a radial motion $\xi(r = a, \theta, \varphi)$ are given by:

$$\mu_{mn} = \frac{4\pi\sqrt{2n+1}a^{n+2}}{n+1} \int_{\varphi=0}^{2\pi} \int_{\theta=0}^{\pi} Y_n^{m*}(\theta, \varphi)\, \xi(a, \theta, \varphi) \sin\theta \, d\theta \, d\varphi, \tag{12.82}$$

due to the orthogonality properties of the spherical harmonics [35]. One can check, in particular, that for $m = n = 0$, the monopolar moment is written:

$$\mu_{00} = \int_{\varphi=0}^{2\pi} \int_{\theta=0}^{\pi} \xi(a, \theta, \varphi)\, a^2 \, \sin\theta \, d\theta \, d\varphi, \tag{12.83}$$

which corresponds to the volume variation of the sphere during its motion.

One interest of the spherical harmonics expansion is due to its rapid convergence as the order n becomes higher than ka, where a is a characteristic dimension of the source. Keeping a few terms only in the expansion (12.72) is then sufficient for obtaining a good estimate of the radiated field. Assuming a characteristic dimension of the order of 10 cm for the violin, for example, then an expansion up to the second order yields a good approximation of the radiated field between 0 and 1 kHz.

The radiativities $\Gamma_{mn} = \mu_{mn}/F_B$ are functions of frequency which can be further expanded on the eigenmodes basis (see Part II of this book):

[11] This definition by the author of the acoustic multipolar moments is dictated by analogies with corresponding definitions in electrodynamics. Let us also mention that, in the presently cited paper, the index n is replaced by the index l and the order of the indices is reversed. As a consequence, the moment μ_{mn} defined here corresponds to the moment μ_{lm} in Weinreich's paper.

$$\Gamma_{mn}(\omega) = \sum_j \frac{A^j_{mn}}{\omega - \omega_j}, \tag{12.84}$$

where the ω_j are the complex eigenfrequencies of the source (see Sect. 2.2.1 in Chap. 2), and where the A^j_{mn} are also complex constants. This expression is also written:

$$-\Gamma_{mn}(\omega) = \sum_j \frac{A^j_{mn}}{\omega_j} + \omega \sum_j \frac{A^j_{mn}}{\omega_j^2} + \omega^2 \sum_j \frac{A^j_{mn}}{\omega_j^3} + \cdots . \tag{12.85}$$

- *Back to the physics of the violin*. For $\omega \to 0$, the behavior of the instrument in *quasi-static* regime is obtained. This corresponds to very low frequencies, where the air can be considered as incompressible. In other words, applying a vertical force F_B on the soundboard, then the decrease in air volume inside the box is exactly compensated by the volume of air escaping through the f-holes. As a consequence, Eq. (12.83) indicates that the monopolar moment μ_{00} must be zero, which implies

$$\sum_j \frac{A^j_{00}}{\omega_j} = 0 . \tag{12.86}$$

This result is valid for any musical instrument made of a vibrating shell with holes (guitar, lute,...). It is the so-called *sound hole sum rule*.

Neglecting the damping terms yields real eigenfrequencies. In this case, the radiativities become

$$\Gamma_{mn}(\omega) \simeq \sum_j \frac{B^j_{mn}}{\omega^2 - \omega_j^2}. \tag{12.87}$$

These expressions can be expanded as follows[12]:

$$-\Gamma_{mn}(\omega) \simeq \sum_j \frac{B^j_{mn}}{\omega_j} + \omega^2 \sum_j \frac{B^j_{mn}}{\omega_j^3} + \omega^4 \sum_j \frac{B^j_{mn}}{\omega_j^5} + \cdots . \tag{12.88}$$

It can be seen that the terms of odd exponent in ω are not present in the expansion (12.88). As mentioned earlier, the constant term vanishes, because of the

[12]The coefficients in the numerator are denoted B^j_{mn}, in order to make the difference with the coefficients A^j_{mn}. We do not write the relationships between these two families of coefficients explicitly, since it is not necessary for the present demonstration.

sound hole sum rule. The first nonzero term is in ω^2, which corresponds to a dipole (see, for example, Eq. (12.39). As a consequence, the radiated power is proportional to ω^4.

For stringed instruments such as the violin or the guitar, the modal damping coefficients ζ_j (see the definition of these coefficients in Eq. (2.3)) generally are in average smaller than 0.05 below the lowest mode, so that the approximation (12.88) is justified. One can conclude that these instruments radiate as dipoles below the first mode.

Virtual Sources

The reproduction of the acoustic field radiated by a given source is another growing application of the spherical harmonics. In the music world, the use of synthesizers and electronic amplification leads to the question of sound diffusion through loudspeakers. In fact, recording a given instrument (flute, or violin,...) and reproducing it through a standard stereophonic apparatus composed of 3-way loudspeaker systems, then there is very little probability that the reproduced sound field will be identical to the one radiated by the original recorded instrument. Even if the human ear recognizes the type of instrument without ambiguity, the directivity of the source (and, even, its timbre) might be substantially altered by the electroacoustic system.

For many years, the research team at IRCAM (Institut de Recherche et Coordination Acoustique-Musique) in Paris have tackled that question [8]. Here again, they took advantage of the fast convergence of the spherical harmonics expansion for approximating real sources with an array of loudspeakers. The first step of the method consists in measuring the directivity $\mathscr{D}$ of a given instrument (violin and upright piano) in free field (anechoic chamber) at a given distance from the instrument, and for different frequencies. The measured directivity pattern is then decomposed on a truncated spherical harmonics basis. To a first approximation, this truncated basis contains the monopolar component and the three dipole components. This can be written formally:

$$\mathscr{D} \simeq a_1 \mathscr{D}_m + a_2 \mathscr{D}_{d1} + a_3 \mathscr{D}_{d2} + a_4 \mathscr{D}_{d3}, \tag{12.89}$$

where the $a_i(\omega)$ are the unknowns of the problem. These coefficients (or filters) can be estimated by using, for example, least square methods where the goal is to minimize the distance between measured and approximate directivity.

As soon as the filters $a_i(\omega)$ are determined, the recorded sound is played through loudspeaker arrays, where each group of loudspeakers has been first designed so that its directivity pattern corresponds either to a monopole or to one of the three dipoleterms, with one dipole oriented in each of the three directions of the coordinates. In summary, the principles of the diffusion is shown in Fig. 12.22. The recorded signal is filtered in parallel on the i channels of the expansion. The output

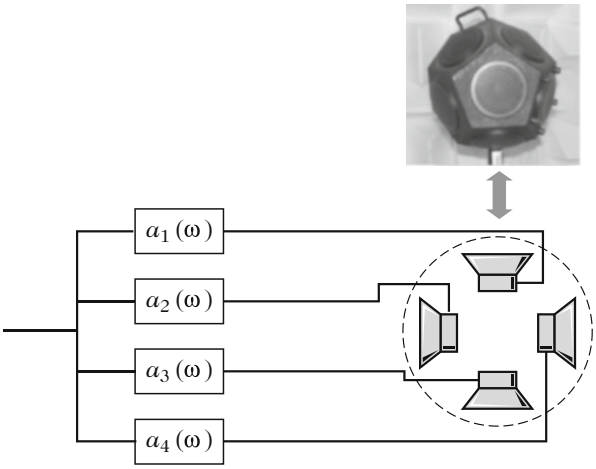

Fig. 12.22 This figure shows the basic principles of sound reproduction of a given instrument (piano and violin) by a loudspeaker array (here, a dodecahedron), so that the array has a directivity similar (or close) to the one of the real instrument. For this purpose, the sound radiated by the instrument is recorded and fed into a filter bank $a_i(\omega)$. The output signal of each filter is, in turn, fed into groups of loudspeakers, where each group has either the directivity of a monopole or the one of a dipole. The sum of all output pressure patterns must fulfills the condition (12.89), which corresponds to the directivity of the real instrument. After [8]

of each filter a_i is fed into the loudspeaker array corresponding to its directivity. The whole set of loudspeakers is usually grouped into a single extended source (cube, dodecahedron, ...).

12.5.3 Radiation of Sound in a Semi-Infinite Space

12.5.3.1 General Formulation

In the previous sections, it has been shown to what extent the acoustic pressure that reaches the ear of a listener depends on the velocity profile of the external surface of the source, and on its geometry. It has been also pointed out that the passive surfaces (without sources) contribute to the radiation field. This last property is generalized here where it is shown that the sound field is influenced by the passive surfaces situated in the vicinity of the sources. The acoustic field radiated by a loudspeaker located in the corner of a room, for example, is not the same as the one resulting from the same loudspeaker (playing the same sound) located in the center of the room. Similarly, recording an instrument (a cello, for example) in a room with a very reflective floor can be surprising! In this case, the sound that reaches the microphone is

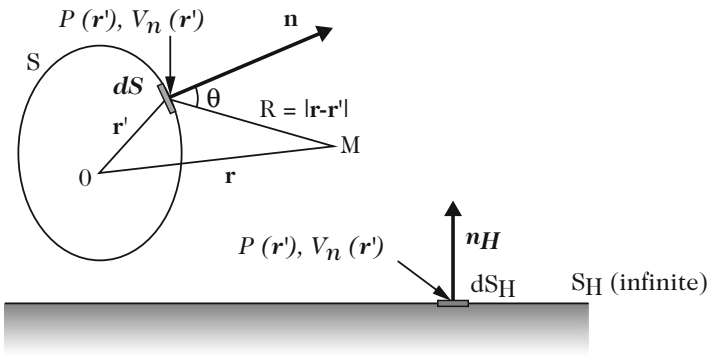

Fig. 12.23 Source in the vicinity of an infinite plane

the sum of the direct field and the field reflected by the floor. Constructive (or destructive) interferences can result from this superposition which might alter the timbre of the instrument substantially, like the well-known "comb-filter" effect. In order to address this question, we consider the simple situation, shown in Fig. 12.23 where the source is situated in the vicinity of an infinite plane S_H with normal vector $\boldsymbol{n_H}$.

As for S, $\boldsymbol{r'}$ denotes any point of S_H, where the pressure and the acoustic velocity are denoted $P(\boldsymbol{r'})$ and $V_n(\boldsymbol{r'})$, respectively. According to the superposition theorem, Eq. (12.61) becomes

$$P(\boldsymbol{r}) = \int_S \left[P(\boldsymbol{r'}) \frac{\partial G(\boldsymbol{r}|\boldsymbol{r'})}{\partial n} - G(\boldsymbol{r}|\boldsymbol{r'}) \frac{\partial P(\boldsymbol{r'})}{\partial n} \right] dS + \int_{S_H} \left[P(\boldsymbol{r'}) \frac{\partial G(\boldsymbol{r}|\boldsymbol{r'})}{\partial n_H} - G(\boldsymbol{r}|\boldsymbol{r'}) \frac{\partial P(\boldsymbol{r'})}{\partial n_H} \right] dS \,. \tag{12.90}$$

12.5.3.2 Particular Case: Half-Space Delimited by an Infinite Rigid Plane

In the particular case where an infinite plane delimiting the half-space is supposed to be rigid, then the velocity normal to this plane is supposed to be zero. Equation (12.90) can be simplified through the use of a new Green's function G_H which takes the presence of the rigid plane into account. In other words, a function $G_H(\boldsymbol{r}|\boldsymbol{r'})$ is searched which fulfills both the Sommerfeld condition and the boundary condition $V_n = 0$ on S_H. We have

$$\Delta G_H(\boldsymbol{r}|\boldsymbol{r'}) + k^2 G_H(\boldsymbol{r}|\boldsymbol{r'}) = -\delta(\boldsymbol{r}|\boldsymbol{r'}) \quad \text{with} \quad \left. \frac{\partial G_H}{\partial n_H} \right|_{S_H} = 0 \,. \tag{12.91}$$

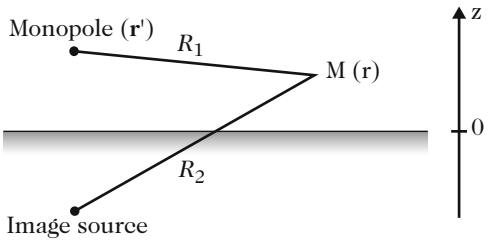

Fig. 12.24 Green's function for an half-space bounded by an infinite plane

It can be easily checked that the function:

$$G_H(\boldsymbol{r}|\boldsymbol{r'}) = \frac{e^{-jkR_1}}{4\pi R_1} + \frac{e^{-jkR_2}}{4\pi R_2}, \tag{12.92}$$

where R_1 and R_2 are the distances defined in Fig. 12.24, fulfills the required conditions of the problem.

In Cartesian coordinates, these distances are given by:

$$\begin{aligned} R_1 &= \left[(x-x')^2 + (y-y')^2 + (z-z')^2\right]^{1/2} \\ R_2 &= \left[(x-x')^2 + (y-y')^2 + (z+z')^2\right]^{1/2}, \end{aligned} \tag{12.93}$$

where R_1 is the distance between one point source and the observation point, and R_2 is the distance between the image of the source point (with regard to the plane S_H) and the observation point.

On S_H, or equivalently for $z = 0$, we have $R_1 = R_2 = R$ and $\frac{\partial R_1}{\partial z} + \frac{\partial R_2}{\partial z} = 0$. As a consequence, the expression (12.92) fulfills

$$\left.\frac{\partial G_H}{\partial n_H}\right|_{S_H} = \left.\frac{\partial G_H}{\partial z}\right|_{S_H} = 0\,. \tag{12.94}$$

Finally, G_H is obtained when the observation point $M(\boldsymbol{r})$ tends to the plane S_H, and is equal to:

$$G_{HS_H} = 2\frac{e^{-jkR}}{4\pi R} = 2G\,. \tag{12.95}$$

12.5.3.3 Radiation of a Plane Source Fixed in an Infinite Rigid Plane

The determination of the acoustic field is highly simplified in the particular case of the plane sources, especially in the far field. In this case, and under certain conditions, the implicit Kirchhoff–Helmholtz integral is transformed into the simpler explicit Rayleigh integral where the free-field pressure is derived from the velocity profile of the emitting surface.

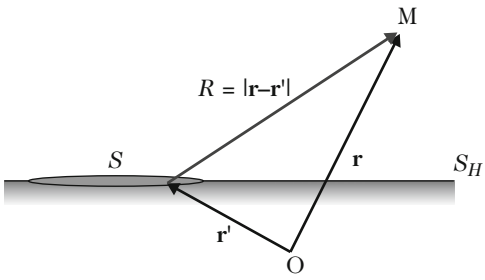

Fig. 12.25 Plane source of surface S fixed in an infinite rigid plane (S_H). The origin O is arbitrary. $\boldsymbol{r}$ is the coordinate vector of the observation point M. $\boldsymbol{r}'$ is the coordinate vector of a point on the source S

In musical acoustics, the Rayleigh integral is a convenient tool for computing, for example, the sound field radiated by a plane soundboard, to a first approximation. However, in this case, the condition of fixation in an infinite plane is not fulfilled, which leads to significant discrepancies with measurements, especially in the low-frequency range, when the acoustic wavelength is larger than the dimensions of the soundboard. The Rayleigh integral also yields wrong results in the soundboard plane and behind the source. Therefore, most precise predictive calculations applicable to real instruments will be presented in Chap. 13.

In this section, the main results for the radiation of a plane source fixed in an infinite rigid plane are briefly reviewed. More details can be found in many textbooks.

12.5.3.4 Rayleigh Integral

We consider an extended plane source with surface S fixed in an infinite rigid plane S_H (Fig. 12.25). It has been shown above that the Eq. (12.61) remains valid for any Green's function whatever the boundary conditions. We derive

$$P(\boldsymbol{r}) = \int_{S_H} \left[P(\boldsymbol{r}') \frac{\partial G_H}{\partial n_H} - G_H \frac{\partial P(\boldsymbol{r}')}{\partial n_H} \right] dS_H, \tag{12.96}$$

By definition, the normal derivative of the Green's function G_H is zero on the surface S_H. The normal derivative of the pressure $P(\boldsymbol{r})$ is also zero on S_H, except on S. We get

$$P(\boldsymbol{r}) = -\int_S G_H \frac{\partial P(\boldsymbol{r}')}{\partial n_H} dS\,. \tag{12.97}$$

Writing G_H explicitly [Eq. (12.95)], and using Euler equation, we get

$$P(\mathbf{r}) = \frac{j\omega\rho}{2\pi} \int_S \frac{V_n(\mathbf{r}')}{R}\, e^{-jkR}\, dS. \tag{12.98}$$

This last expression is the so-called *Rayleigh integral*.

12.5.3.5 Fresnel and Fraunhofer Approximations

For $|\boldsymbol{r}| \gg |\boldsymbol{r'}|$, it is useful to look for approximations of the Rayleigh integral, based on Taylor series expansion of R, as follows:

$$R = |\boldsymbol{r} - \boldsymbol{r'}| \simeq r - \boldsymbol{r'}.\boldsymbol{m} + \frac{1}{2r}\left[r'^2 - \left(\boldsymbol{r'}.\boldsymbol{m}\right)^2\right] + \cdots , \tag{12.99}$$

where $\boldsymbol{m}$ is the unitary vector $\boldsymbol{r}/r$.

In the so-called *Fraunhofer* approximation, the expansion (12.99) is truncated to the first two terms. As a consequence, the Rayleigh integral becomes

$$P(\boldsymbol{r}) \simeq \frac{j\omega\rho}{2\pi}\,\frac{e^{-jkr}}{r}\int_S V_n(\boldsymbol{r'})e^{-j\boldsymbol{k}.\boldsymbol{r'}}\,dS, \tag{12.100}$$

where $\boldsymbol{k} = k\boldsymbol{m}$. By definition, the spatial Fourier transform of $V_n(\boldsymbol{r'})$ is

$$\tilde{V}_n(\boldsymbol{k}) = \int_S V_n(\boldsymbol{r'})e^{-j\boldsymbol{k}.\boldsymbol{r'}}\,dS\,. \tag{12.101}$$

Finally, we get for the pressure:

$$P(\boldsymbol{r}) \simeq \frac{j\omega\rho}{2\pi}\,\frac{e^{-jkr}}{r}\,\tilde{V}_n(\boldsymbol{k}). \tag{12.102}$$

This result means that the magnitude of the pressure, besides the $1/r$ dependence, is fully determined by the *spatial Fourier transform* of the normal velocity field of the baffled source. Under the condition of adequate spatial discretization, this property opens a wide range of efficient methods for the calculation of radiated field, in view of the existence of numerous fast algorithms dedicated to the computation of discrete Fourier transforms.

In the *Fresnel* approximation, the first three terms of the expansion of R are kept. It is further assumed that the observation point is not too far from the x-axis or, equivalently, $r \simeq x$ (see Fig. 12.26). We can then calculate the acoustic field near the plane source and close to its axis. We have

$$R = |\boldsymbol{r} - \boldsymbol{r'}| \simeq x - \boldsymbol{m}.\boldsymbol{r'} + \frac{r'^2}{2x}\,. \tag{12.103}$$

Using the same notations as previously, the pressure is written:

$$P(\boldsymbol{r}) \simeq \frac{j\omega\rho}{2\pi}\,\frac{e^{-jkx}}{x}\int_S V_n(\boldsymbol{r'})e^{-j\boldsymbol{k}.\boldsymbol{r'}}\,e^{-\frac{jkr'^2}{2x}}\,dS\,. \tag{12.104}$$

This last expression also involves a Fourier transform. However, in the Fresnel case, the velocity field on the source has to be first multiplied by a phase factor. Denoting

V_{pn} this weighted velocity, we have:

$$V_{pn} = V_n(\boldsymbol{r'})\, e^{-\frac{jkr'^2}{2x}}, \tag{12.105}$$

and the acoustic pressure becomes

$$P(\boldsymbol{r}) \simeq \frac{j\omega\rho}{2\pi}\,\frac{e^{-jkr}}{r}\,\tilde{V}_{pn}(\boldsymbol{k})\ . \tag{12.106}$$

It can be shown that the limit between the Fresnel and the Fraunhofer zone is located at position $x = L^2/4\lambda \simeq L^2 f/4c$, where L is a characteristic dimension of the source, and λ the acoustic wavelength. This is an alternative way to define a limit between near and far field.

12.5.3.6 Source with Uniform Velocity Distribution, or "Plane Piston"

In this paragraph, the radiation of a plane circular disk of radius a subjected to a uniform velocity V_0 at frequency ω is considered. This well-known example is often called a "plane piston" (see Fig. 12.26). In the far field, it is assumed that the Fraunhofer approximation is valid, so that the pressure can be computed using (12.102). For the velocity, we have

$$V_n(r') = \begin{cases} V_0 \ \text{ for } \ 0 \le r' \le a, \\ 0 \ \text{ elsewhere}\ . \end{cases} \tag{12.107}$$

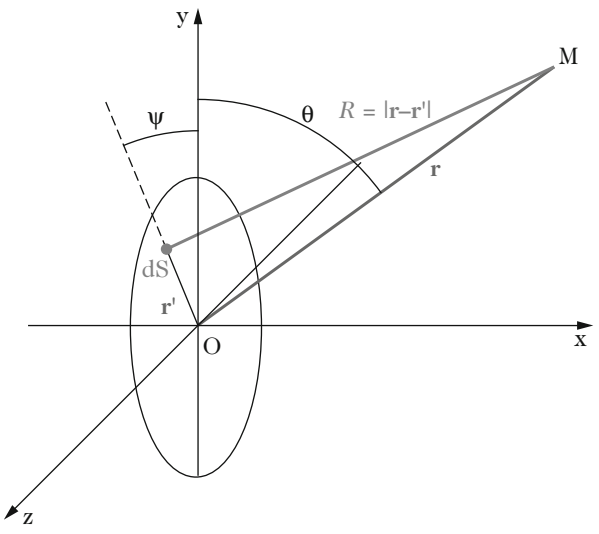

Fig. 12.26 Geometry of the plane piston. The circular disk of radius a is situated in the plane yOz and subjected to a uniform velocity V_0 oriented along the Ox-axis

As a consequence, its spatial Fourier transform is written:

$$\tilde{V}_n(\boldsymbol{k}) = U_0 \left[\frac{2J_1(ka\cos\theta)}{ka\cos\theta} \right] \tag{12.108}$$

where θ is the angle between the vector $\boldsymbol{r}$ and the source plane (see Fig. 12.26), and $U_0 = \pi a^2 V_0$ the volume velocity of the piston. The quantity $\mathscr{D}(\theta) = \frac{2J_1(ka\cos\theta)}{ka\cos\theta}$ is the *directivity* of the piston. The radiated pressure is written:

$$P(r,\theta) = \frac{j\omega\rho U_0}{2\pi} \frac{e^{-jkr}}{r} \mathscr{D}(\theta) \,. \tag{12.109}$$

Comparing this result with the pressure field radiated by a pulsating half-sphere shows that the directivity is more pronounced for an extended source than for a point source. The directivity increases with frequency. This general result can be explained as follows: at low frequencies, the different vibrating points of the surface S yield constructive interferences, whereas, with increasing frequency, the phase shifts due to the differences in the propagation distances at a given point in space are more and more pronounced, leading to destructive interferences, especially off-axis. The power radiated by the piston is equal to:

$$\mathscr{P}_r = \frac{\rho c k^2 \left|U_0\right|^2}{4\pi}, \tag{12.110}$$

which corresponds exactly to twice the sound power radiated by a monopole with identical volume velocity.[13] As a consequence of the source extension, the sound intensity is not distributed equally in all directions.

One interesting result for the circular plane piston is the calculation of the pressure on the axis since, in this particular case, an exact calculation of the pressure can be made without assuming a far field approximation. Figure 12.27 shows some examples for different values of the source radius a at various frequencies. At a frequency of 5.525 kHz and for a radius $a = 25$ cm, for example, it can be seen that the limit between near and far field is close to 1 m. below this limit, in the vicinity of the piston, the pressure shows rapid fluctuations. These fluctuations are reduced for a smaller radius, and at lower frequencies. Such properties are important to know when recording sound sources in general (including musical instruments), since the recorded signal is highly sensitive to the location of the microphone in the near field.

[13] This is due to the fact that the plane piston radiates in an half-space: the volume velocity in the complete space is $U_0' = 2U_0$, thus, expressing the power in (12.110) as a function of U_0' yields a factor 16 in the denominator. The total power in the two half-spaces is the sum of the power on each side of the rigid plane, and we find as a result the factor 8 in the denominator as in (12.21).

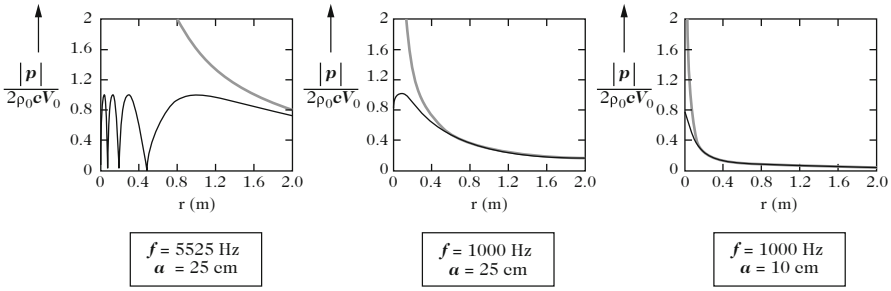

Fig. 12.27 Axial pressure field of a circular plane piston for different values of the radius a and oscillation frequency f. Comparison with the results obtained for a semi-monopole (in *grey color*). As a and f increase, more and more important amplitude fluctuations are seen in the vicinity of the piston. The monopole approximation becomes more and more relevant as both a and f decrease. However, this approximation is never realistic on the piston itself, since it predicts an infinite pressure

Boundary Element Method (BEM)

The Kirchhoff–Helmholtz (KH) integral forms the theoretical basis of the numerical *BEM: Boundary Element Method*. It mains attracting aspect lies in the fact that the KH integral is a surface integral (and not a volume integral) which contributes to reduce the computational burden substantially. In musical acoustics, this method has been applied to the guitar by Brooke [3] and Fleischer [32]. This last author also applied the BEM method to timpani. The main principles and difficulties of this method are briefly summarized below. The reader may consult specialized textbooks on this topic for more information [36].

In Eq. (12.61), the expression of $P(\boldsymbol{r})$ was given for an observation point situated in free space outside the external bounding surface S of the source. For an observation point situated on the surface S, one can show that the equation becomes

$$\frac{1}{2}P(\boldsymbol{r}) = \int_S \left[P(\boldsymbol{r}')\frac{\partial G(\boldsymbol{r}|\boldsymbol{r}')}{\partial n} - G(\boldsymbol{r}|\boldsymbol{r}')\frac{\partial P(\boldsymbol{r}')}{\partial n} \right] dS_{(\boldsymbol{r}')} \,. \tag{12.111}$$

The physical meaning of the factor $1/2$ can be explained by the fact that, on the surface, we have to define a Green's function in 2π steradians, and not in 4π steradians. The use is to group (12.61) and (12.111) in a single expression:

(continued)

$$\int_S \left[P(\boldsymbol{r}') \frac{\partial G(\boldsymbol{r}|\boldsymbol{r}')}{\partial n} - G(\boldsymbol{r}|\boldsymbol{r}') \frac{\partial P(\boldsymbol{r}')}{\partial n} \right] dS_{(\boldsymbol{r}')} = \epsilon P(\boldsymbol{r}) \quad \text{with} \quad \begin{cases} \epsilon = 1 \ \text{ for } \ M \in V_{\text{ext}}, \\ \epsilon = \dfrac{1}{2} \ \text{ for } \ M \in S\,. \end{cases} \tag{12.112}$$

The first level of approximation of the BEM method is of the *geometrical* type. It is due to the fact that the discretization of (12.112) requires a subdivision of the surface (or boundary) S in a number N_e of finite elements, so that:

$$\sum_{j=1}^{N_e} S_j \simeq S\,. \tag{12.113}$$

In (12.113), the symbol "$\simeq$" means that some fine details of the edges, and/or of the curvature of the surface, cannot be taken into account by such a discretization. Equation (12.112) becomes

$$\epsilon P(\boldsymbol{r}) = \sum_{j=1}^{N_e} \int_{S_j} \left[P(\boldsymbol{r}') \frac{\partial G(\boldsymbol{r}|\boldsymbol{r}')}{\partial n} - G(\boldsymbol{r}|\boldsymbol{r}') \frac{\partial P(\boldsymbol{r}')}{\partial n} \right] dS_{(\boldsymbol{r}')}\,. \tag{12.114}$$

For approximating the surface, one can use simple elements, such as triangles, or other geometrical forms of higher order (spline functions). The degree of accuracy of the approximation increases with the number of elements N_e and with the order of the surface elements.

The second level of approximation in the BEM method is of the *functional* type. This level govern how the variables P and G inside a given surface element are expressed as functions of their values in a number of fixed points called *nodes*. In the simplest case, it is assumed that these variables are approximated by piecewise constant functions. In this case, Eq. (12.114) is written:

$$\epsilon P(\boldsymbol{r}) = \sum_{j=1}^{N_e} P(r'_j) \int_{S_j} \frac{\partial G(\boldsymbol{r}|r'_j)}{\partial n} dS_{(\boldsymbol{r}')} - \sum_{j=1}^{N_e} \frac{\partial P(r'_j)}{\partial n} \int_{S_j} G(\boldsymbol{r}|r'_j) dS_{(\boldsymbol{r}')}, \tag{12.115}$$

and the number of nodes is equal to the number of elements. The expression of the pressure at points r_i becomes

$$\epsilon P(r_i) = \sum_{j=1}^{N_e} P(r'_j) M_{ij} - \sum_{j=1}^{N_e} \frac{\partial P(r'_j)}{\partial n} L_{ij} \tag{12.116}$$

(continued)

or, equivalently, in matrix form:

$$\epsilon \boldsymbol{P} = \mathbb{M}\, \boldsymbol{P}_S - \mathbb{L}\, \frac{\partial \boldsymbol{P}_S}{\partial n}\,. \tag{12.117}$$

In general, the normal velocity is a given parameter, so that $\frac{\partial \boldsymbol{P}_S}{\partial n}$ is known. The unknowns are $\boldsymbol{P}$ in free space and $\boldsymbol{P}_S$ on the surface S. In a first step, it is necessary to determine $\boldsymbol{P}_S$ in order to solve Eq. (12.117). This quantity is obtained as the observation point converges to the surface S, which means that $\boldsymbol{r}$ tends to $\boldsymbol{r}'$. Equation (12.117) becomes

$$[\mathbb{M} - \epsilon \mathbb{I}]\ \boldsymbol{P}_S = \mathbb{L}\, \frac{\partial \boldsymbol{P}_S}{\partial n}, \tag{12.118}$$

where $\mathbb{I}$ is the identity matrix. At this stage, one of the main difficulties of the BEM method is a consequence of the non-uniqueness of the solution observed for the eigenvalues of the operator $[\mathbb{M} - \epsilon \mathbb{I}]$. A physical meaning for this eigenvalues is difficult to find, since they result from a purely mathematical singularity problem. Some methods exist today, such as the *CHIEF* (or *Combined Helmholtz Integral Equation Formulation*), for overcoming such difficulties [32]: this last method is based on the idea to formulate (12.118) in the form of a overdetermined system which is solved by means of a least square method.

12.6 Radiation of Sound Tubes

The complexity of the radiation by wind instruments is mainly due to the existence of orifices, which can be large compared to the wavelength for brass instruments or saxophones. Moreover for woodwinds they can have a significant external interaction. Hereafter we give the main elements (i.e., the radiation impedance, which represents the effect inside the tube, and directivity of the radiated field outside) for the end of a tube, and we explain the principle of the interaction of two orifices. The radiation of instruments with several sources will be investigated in Chap. 14.

12.6.1 Radiation Impedances

12.6.1.1 First Approach

In what follows we consider the radiation by tubes without mean flow, in the linear approximation. An analysis of the flow influence can be found in the literature [6, 21, 24], and the issue of high levels is treated in Chap. 8 (Sect. 8.4.5) of the present book. Moreover we consider low Helmholtz number ka, where a is the tube radius, when only the planar mode propagates.[14] Results concerning non-planar modes of the tube can be found in [13]. We start with a very qualitative approach, which allows understanding the tube radiation phenomenon, and gives already a correct value for the real part of the input impedance at low frequencies. Indeed for a tube radiating into the infinite space, radiation is a particular case of discontinuities such as those studied in Chap. 7.

- Let us consider an abrupt change in cross section (Fig. 7.20): at low frequencies, the fluid can be regarded as incompressible (cf. Chap. 1, Sect. 1.5), thus there is flow rate conservation from one side of the discontinuity to the other side. If in addition the pressure is uniform in a straight cross section of each duct, the energy conservation yields

$$\Re e(Z_{\text{left}}) = \Re e(Z_{\text{right}}). \tag{12.119}$$

  (here the impedances are the acoustic impedances, i.e., a ratio pressure/flow rate). Close to the discontinuity, the pressure is not uniform, but if the straight cross sections are chosen at a certain distance of the discontinuity (i.e., one or two diameters), only the planar mode is present, and this expression is valid. Otherwise the discontinuity impedance Z_d is purely imaginary [see Eq. (7.158)], and the Expression (12.119) remains valid at the discontinuity. This is exactly what we need to match the internal and external fields.

If the tube on the right is infinite, the impedance to the right is: $\rho c/S_{\text{right}}$, and we have found a first expression of the real part of the radiation impedance Z_{left} of the left tube into an infinite tube. The reflection coefficient R_ℓ at the end of this tube is found to be:

$$|R_\ell|^2 = \frac{(R_R - 1)^2 + X_R^2}{(R_R + 1)^2 + X_R^2} \simeq \left(\frac{R_R - 1}{R_R + 1}\right)^2,$$

[14] This means $ka < 1.8$ [cf. Eq. (7.147)]. For a clarinet this gives $f < 14$ kHz, but for tapered instruments, the limit frequency can be much lower. The following equation can be used up to $ka = 3.8$ for the case of a perfect axisymmetry (see Chap. 7), but it is not the case of wind instruments, because of the exciter geometry and of the existence of toneholes.

if we denote $Z_{\text{right}} S_{\text{left}}/\rho c = R_R + jX_R$ (see Sect. 7.3.2 in Chap. 7). Indeed at low frequencies the effect X_R of the added mass tends to 0. Therefore, the larger the cross section discontinuity, the stronger the reflection.

- This reasoning can be extended to the case where the left tube is terminated in an infinite cone (with index b): there is a matching volume, as shown in Fig. 7.13, where pressure and velocity have complicated profiles, but, at low frequencies, the flow rate is conserved. The field can be expanded in the cone by using spherical Bessel functions. The fundamental mode is the mode with a spherical symmetry. Its characteristic admittance (ratio pressure/flow rate) is given by:

$$Y = \frac{S_b}{\rho c}\left[1 + \frac{1}{jkr_b}\right].$$

  [see Eq. (7.79)]. At low frequencies, this implies

$$\Re e(Z_{\text{right}}) = \frac{\rho c}{S_b}\frac{k^2 r_b^2}{1 + k^2 r_b^2} \tag{12.120}$$

$$\simeq \frac{\rho c}{S_b} k^2 r_b^2 = \frac{\rho c k^2}{2\pi(1 - \cos\theta_b)}. \tag{12.121}$$

  Here, θ_b is the apex semi-angle of the cone, because the impedance is defined on a spherical cap.[15] When the cone is opened up to become an infinite flange, θ_b tends to $\pi/2$, and the real part of the radiation impedance decreases down to:

$$\Re e(Z_R) = \frac{\rho c k^2}{2\pi}. \tag{12.122}$$

  The explanation of the decrease is intuitive, because the discontinuity increases, thus the reflection coefficient increases and the reflection tends to be total.
- The latter result can be obtained directly if we assume that the tube radiates with an infinite flange and that waves are spherical far enough from the tube end (Fig. 12.28). This assumption is confirmed by the fact that the result does not depend on the radius of the hemisphere. And for an unflanged tube (i.e., with a zero thickness) the surface where waves are spherical is a sphere,[16] and we obtain

$$\Re e(Z_R) = \frac{\rho c k^2}{4\pi}. \tag{12.123}$$

[15] Formula (12.121) is not valid for a cone with weak taper: when r_b tends to infinity, the impedance should tend to $\rho c/S_{\text{left}}$, which is the characteristic impedance of the cylindrical tube. In order to find this result, we must keep the expression (12.120) with $S_{\text{gauche}} = S_b$, because the matching volume tends to zero.

[16] In fact, we have here a complete sphere reduced by the external cross section of the tube. Nevertheless, because the radius is small compared to the wavelength, this reduction may be ignored.

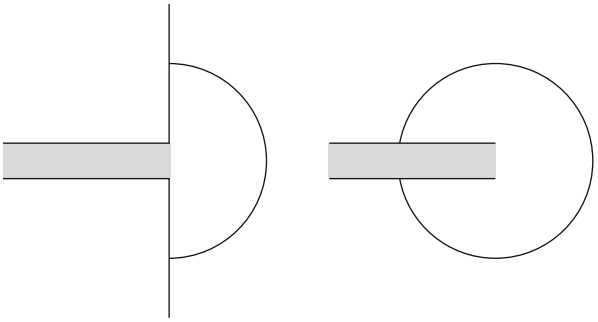

Fig. 12.28 Radiation of a tube with an infinite flange (*left*) and of an unflanged tube (*right*). The flow rate and power are conserved on a hemisphere and a quasi-complete sphere, respectively. The radius of the sphere is sufficiently large for waves to be spherical on it

Therefore the previous approach allows determining the real part of the radiation impedance at low frequencies. It is nothing but that of a monopole radiating into the infinite space expressed in (12.12). Incidentally we notice that, using the same argument, the radiation of a diverging conical tube produces a reflection smaller than the one of a cylinder. In what follows, the formulas are limited to cylindrical tubes, because there are no known formulas for a cone or a flared bell. As to the termination of a bell, i.e., the shape of the flange, plays a determinant role on radiation and, as one can imagine, there are no simple formulas for these cases. The matching of the field between the bell and the infinite space presents a difficulty of a nature similar to that of the field analysis inside the bell. The case of the Bessel horns (see Sect. 7.5.1 in Chap. 7) illustrates the fact that the separation between the tube and the flange is less relevant than for a cylinder.

12.6.1.2 Radiation Impedance of a Cylinder with an Infinite Flange

Now we wholly treat a rather simple case, that of a cylinder radiating with an infinite flange. It is somewhat academic but interesting, and it can be applied as a first approximation for a side hole, when the flange is the external surface of the tube. Then the two cases of a tube without flange and with a finite flange (which can be the tube thickness) are considered. In a cylinder, where the planar mode only propagates, evanescent modes can exist near the tube end, but they all are with a radial symmetry $n = 0$, which is the symmetry of the problem. The calculation of the radiation with an infinite flange is done thanks to the Rayleigh integral (12.98) together with the modal expansion given in Sect. 7.6.3.2 of Chap. 7. Pressure and velocity are expanded in duct modes (in a vector form), and a matrix radiation impedance $\mathbb{Z}_R$ is deduced for the modes with radial symmetry $\Phi_{i0}(r) = J_0(\gamma_{i0} r)$:

$$\boldsymbol{P} = \mathbb{Z}_R \boldsymbol{U} \quad \text{where} \quad Z_{ij} = \frac{j\omega\rho}{2\pi} \frac{1}{S^2} \int_S \int_S \boldsymbol{\Phi}_{i0}(r) \Phi_{j0}(r') \frac{\exp(-jk\,|r - r'|)}{|r - r'|} dS\, dS'. \tag{12.124}$$

Similarly to the method used for a cross section discontinuity, it remains to separate the planar mode (p, u) from the higher order modes $(\boldsymbol{P}', \boldsymbol{U}')$, then to close the latter on their characteristic impedance $(\boldsymbol{P}' = -\mathbb{Z}'\boldsymbol{U}')$, because the tube end is assumed to be far from any other discontinuity. Using evident notations, we write

$$\begin{pmatrix} p \\ \boldsymbol{P}' \end{pmatrix} = \begin{pmatrix} Z_{R00} & {}^t\boldsymbol{z} \\ \boldsymbol{z} & \mathbb{Z}'_R \end{pmatrix} \begin{pmatrix} u \\ \boldsymbol{U}' \end{pmatrix},$$

where

$$p = Z_R u, \text{ with } Z_R = Z_{R00} - {}^t\boldsymbol{z}(\mathbb{Z}'_R + \mathbb{Z}')^{-1}\boldsymbol{z}. \tag{12.125}$$

In this expression the quantity Z_{R00} is the plane piston approximation, which was discussed in Sect. 7.6.3.2 of Chap. 7, and is often used since Rayleigh. This author calculated the ratio of the averaged pressure to the piston velocity starting from formula (12.98), and obtained a formula where modified Bessel functions, called Struve functions, intervene. The low-frequency approximation is the following:

$$Z_{R00} = \frac{\rho c}{S}\left[\frac{1}{2}(ka)^2 + j\frac{8}{3\pi}ka\right] + O\left[(ka)^3\right]. \tag{12.126}$$

The imaginary part corresponds to a length correction of $\Delta\ell = 8a/(3\pi) = 0.85a$ (cf. the analysis of Chap. 4, Sect. 4.6.4), and the real part is that given by Eq. (12.122).

For a tube, several authors made the computation (see, for example, [23]). At low frequencies, the result is very close to that of the plane piston, but the length correction is $\Delta\ell = 0.8216a$, as calculated by Rayleigh himself. At other frequencies, the impedance can be written with respect to the complex reflection coefficient R_ℓ:

$$Z_R = \frac{\rho c}{S}\frac{1+R_\ell}{1-R_\ell} = j\frac{\rho c}{S}\tan\left[k\Delta\ell + \frac{j}{2}\ln|R_\ell|\right] \tag{12.127}$$

$$\text{where} \quad R_\ell = -|R_\ell|\exp(-2jk\Delta\ell) \tag{12.128}$$

[cf. Eq. (4.43)]. As a consequence, both the length correction $\Delta\ell$ and the modulus of the reflection coefficient depend on frequency. Figure 12.29 shows the two results (the exact formula and the plane piston approximation). The behaviors are different at lower and higher frequencies, with a transition around $ka = 1$ or 2. At higher frequencies, the real part tends to the characteristic impedance, the imaginary part tends to 0, and the length correction decreases significantly.

An approximate formula was recently obtained [17, 30], by seeking an expansion ensuring the following properties:

- symmetry $Z(\omega) = Z^*(-\omega)$;
- causality of the reflection function (and of the inverse FT of the impedance);

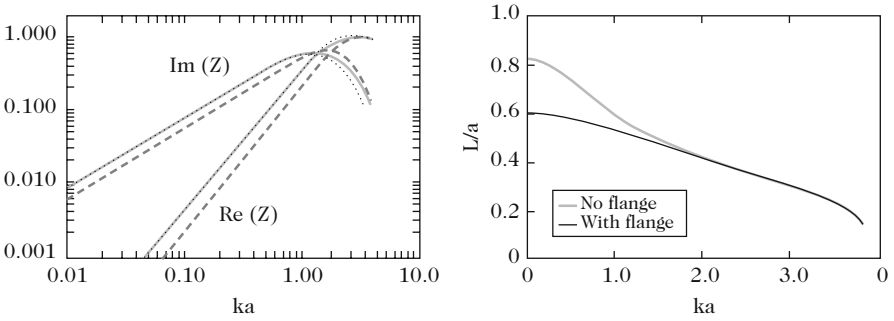

Fig. 12.29 *Left plot*: real and imaginary parts of the radiation impedance for a tube without flange (*gray dashed line*), with an infinite flange (*gray solid line*) and with an infinite flange in the approximation of the plane piston (*dotted line*). At higher frequencies, the real part tends to the characteristic impedance while the imaginary part tends to 0. *Right plot*: length correction $\Delta\ell$ with respect to frequency: with an infinite flange (*gray line*) and without flange (*black line*)

- a correct behavior of Z_R at low frequencies, with the following notation: $Z_R = Z_c\left[j\delta ka + \frac{1}{2}\beta(ka)^2\right]$;
- convergence of Z_R to the characteristic impedance at higher frequencies.

This formula is written as follows:

$$R_\ell = -\frac{1 + n_1 jka}{1 + d_1 jka + d_2(jka)^2}\ , \text{where} \tag{12.129}$$

$$n_1 = 0.182;\ d_1 = 2\delta + n_1 = 1.825\ ;\ d_2 = \frac{1}{2}\left(d_1^2 - n_1^2\right) - 2\beta = 0.649 \tag{12.130}$$

$$\delta = 0.8236;\ \beta = \frac{1}{2}. \tag{12.131}$$

The inverse FT of $R_\ell(\omega)$ can be deduced: for $t > 0$, it is the superposition of two real decreasing exponentials, because the poles of the polynomial $1 + d_1 x + d_2 x^2$ are real. The corresponding formula for the impedance is

$$Z_R = Z_c \frac{j\delta ka + \frac{1}{2}d_2(jka)^2}{1 + \frac{1}{2}(n_1 + d_1)jka + \frac{1}{2}d_2(jka)^2}. \tag{12.132}$$

12.6.1.3 Radiation Impedance of an Unflanged Tube

The calculation for an unflanged tube is significantly more complicated. It was done by using the analytic continuation in the complex plane (i.e., the Wiener–Hopf method) by Levine and Schwinger [18]. At low frequencies the result is the following:

$$Z_R = \frac{\rho c}{S}\left[\frac{1}{4}(ka)^2 + 0.6133jka\right]. \tag{12.133}$$

The real part is that given by Eq. (12.123), and the imaginary part corresponds to a length correction of $\Delta\ell = 0.6133a$. Figure 12.29 shows the comparison between this result, which is probably the most useful, with that of the previous cases. The approximate formula (12.129) can be used, with:

$$n_1 = 0.167\,;\, d_1 = 2\delta + n_1 = 1.393\,;\, d_2 = \frac{1}{2}\left(d_1^2 - n_1^2\right) - 2\beta = 0.457 \tag{12.134}$$

$$\delta = 0.6133;\ \beta = \frac{1}{4}. \tag{12.135}$$

12.6.1.4 Radiation Impedance of a Tube with a Finite Flange

The two above presented cases are extreme cases. Calculations were done for the case of a tube with a finite flange. The external diameter is denoted $2b$. Fit formulas were obtained for the reflection coefficient, based upon experimental and numerical results [7]:

$$R_\ell = R_\ell^* - 0.43\frac{a(b-a)}{b^2}\sin^2\left[\frac{kb}{1.85 - a/b}\right]e^{-jkb\left[1+a/b\left(2.3-a/b-0.3(ka)^2\right)\right]}\,; \tag{12.136}$$

$$R_\ell^* = -e^{-2jk\Delta\ell^*} \quad \Delta\ell^* = \Delta\ell_\infty^* + \frac{a}{b}(\Delta\ell_0^* - \Delta\ell_\infty^*) + 0.057\frac{a}{b}\left[1 - \left(\frac{a}{b}\right)^5\right]a. \tag{12.137}$$

The quantities $\Delta\ell_0^*$ and $\Delta\ell_\infty^*$ are complex length corrections (the indices 0 and ∞ correspond to the cases without flange and with infinite flange, respectively), and are deduced from formulas (12.129) to (12.135) by:

$$k\Delta\ell^* = k\Delta\ell + \frac{j}{2}\ln|R_\ell|\,.$$

In formula (12.136), the function $\sin^2$ evidences oscillations which are due to reflections on the external edges of the tube. Other geometrical shapes or other terminations were studied by some authors [7, 12, 24, 29]: as it was above mentioned, the issue is complicated and cannot be clearly distinguished from that of the extension of a tube into a small bell. Concerning the radiation by bells, the case of a conical horn has been treated above. If the plane wave approximation is accepted, it is consistent to choose the radiation impedance of a cylindrical tube. However, the frequency limit of validity is rather low, similarly to that of the horn

equation (cf. Sect. 7.6.3.5, Chap. 7). In order to study this matter in a more precise way, numerical methods need to be used, such as the Boundary Element Method (cf. Sect. 12.5.3.6), or experiments can be carried out.

12.6.1.5 Radiation Impedance of a Tonehole

The radiation by a tonehole is another rather complicated problem. When the radius tends to 0, the radiation is expected to become similar to that with an infinite flange, and the corresponding formula is in general satisfactory. However, holes are often provided with keys which are perforated or not and modify the radiation: some indications can be found on their effect, in particular in Refs. [9, 22].

12.6.2 Field Radiated by a Tube: Directivity

For an unflanged tube Levine and Schwinger [18] gave an approximated formula for the far field. It can be written in the following form (if $\theta = 0$ in the tube axis):

$$P(r,\theta) = j\omega\rho U_\ell \; D(\theta) \; F(\theta) \; \frac{e^{-jkr}}{4\pi r} \quad \text{where}$$
$$D(\theta) = \frac{2J_1(ka\sin\theta)}{ka\sin\theta} \text{ and } F(\theta) = 1 + \frac{Z_R S}{\rho c}\cos\theta. \qquad (12.138)$$

At the lowest frequencies the radiation is that of a monopole. The directivity factor $D(\theta)$ is that for a plane piston in an infinite baffle.

The factor $F(\theta)$, can be interpreted as the result of the superposition of a plane piston in an infinite baffle and an unflanged piston, which behaves as a dipole with the directivity factor $D(\theta)\cos\theta$: it can be shown that this superposition corresponds to a piston radiating without flange from one side only[17] [5]. The existence of this dipole makes the radiation forwardly and rearwardly very asymmetrical (notice that the result $|F(\pi)| \,/\, |F(0)| = |R_\ell|$ is exact). At higher frequencies, the factor $F(\theta)$ tends to $(1 + \cos\theta)$, which is the directivity of a cardioid.

Figure 12.30 shows the directivity of a tube for different values of ka, and a comparison with the case of a plane piston in an infinite baffle. The maximum is obtained for $\theta = 0°$, and the minimum near $\theta = 130°$. For example, for $ka = 1$, with respect to $\theta = 0°$, it is found -2.7 dB for $\theta = 90°$, -3.5 dB for $\theta = 131°$, and -3.3 dB for $\theta = 180°$. At higher frequencies, the formula (12.138) diverges from the exact value, except for 0° and 180°.

[17]For this case the imaginary part is found to be $2R/\pi = 0.6366R$, and is slightly larger than that of a unflanged tube: this difference can be compared to that between a tube and a plane piston.

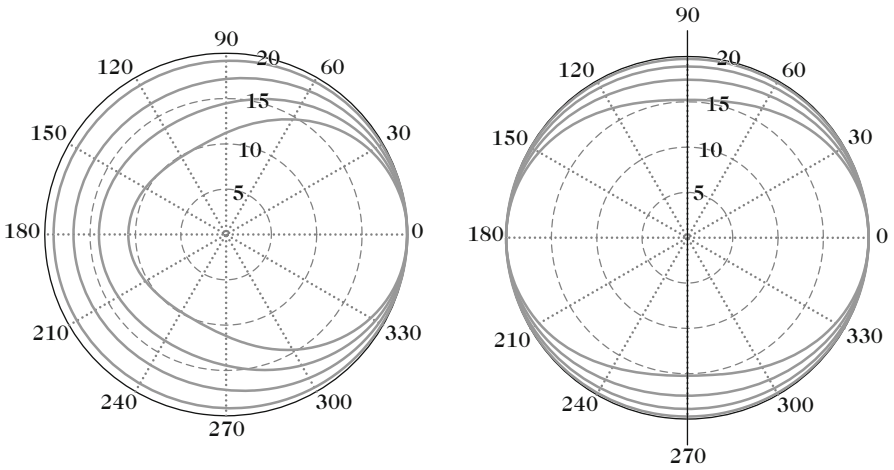

Fig. 12.30 Directivity, in decibels, of an unflanged tube (*left plot*), $D(\theta)F(\theta)$, and of a plane piston in an infinite baffle, $D(\theta)$ (*right plot*). The values of the frequency are, from the outside to the inside: $ka = 0.5; 1; 1,5; 2$

Considering now the argument of the function $F(\theta)$, we see that, for small ka, it is equal to $k\Delta\ell \cos\theta$. A geometrical reasoning shows that the acoustic center of the waves produced by the tube is located at the distance $\Delta\ell$ from the tube end: therefore the length correction is also a quantity related to the radiated field.

Finally, Ando [1] showed that the directivity is slightly modified when the tube thickness is taken into account, and that the acoustic center is no longer located exactly at a distance equal to the length correction of the tube.

For a bell, experiment shows that the directivity globally increases at higher frequencies, and is similar to that of a cylinder. Figure 12.31 shows experimental results, which are obtained by exciting a trombone with a loudspeaker at its input (the real radiation can be slightly different because of the mean flow). However, as the opening is wide, the directivity of the bell is significant even at rather low audible frequencies. This result was confirmed by Martin, who made similar measurements [19]. Such a phenomenon is very well known by the players, who modify the orientation of their instrument in order to adjust the perception of higher frequencies by the listeners.

12.6.3 Radiation by Two Tubes or Two Orifices

When two sources are close together, they have a mutual influence. From the integral formulation of type (12.61), we can calculate the average pressure on two surfaces with respect to the flow rate of each of them, and the result can be written in the general form of a radiation impedance matrix (or an admittance matrix):

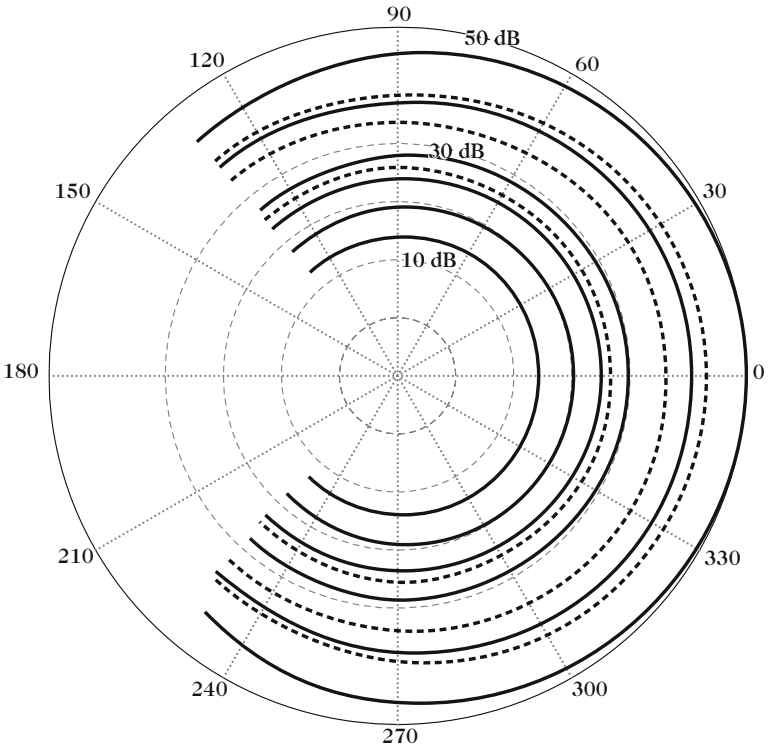

Fig. 12.31 Radiation of a trombone with closed slide excited by a loudspeaker. The directivity is measured for different harmonics of the note. The corresponding frequencies are 113; 171; 229; 294; 346; 406; 465; 521; 590 Hz. The increase from the lower frequencies to the higher ones is plotted from the inside to the outside. It can be noticed that the directivity increases with frequency. (Courtesy of R. Caussé)

$$P_1 = Z_{11}U_1 + Z_{12}U_2$$
$$P_2 = Z_{21}U_1 + Z_{22}U_2. \tag{12.139}$$

Z_{11} and Z_{22} are "self-impedances," and $Z_{12} = Z_{21}$ are mutual impedance, which are equal because of reciprocity. It can be useful to know them when the ends of two tubes are close together, or when two orifices of a tube are close together, as it is the case for open toneholes. We examine this issue in detail at lower frequencies, and focus on the power balance. A simple approximate formula can be deduced, together with a validity condition.

The mutual impedances generally are as difficult to calculate as the self-impedances, which were calculated in the previous section. The literature on this subject is wide. As an example, we can start with two pistons located in the same infinite baffle. The formula of the mutual impedances can be then directly deduced from the Rayleigh integral (12.98):

$$Z_{12} = Z_{21} = j\rho c \frac{k}{2\pi} \frac{1}{S_1 S_2} \int_{S_1} \int_{S_2} \frac{e^{-jk|\boldsymbol{r}_1 - \boldsymbol{r}_2|}}{|\boldsymbol{r}_1 - \boldsymbol{r}_2|} dS_1 dS_2. \tag{12.140}$$

We consider two elementary sources, separated by a distance d. A series expansion can be calculated if the quantity $k\,[d + (a_1 + a_2)/2]$ is assumed to be small [25]. We limit the calculation to the real part, which is the only term involved in the power balance. The result is

$$\Re e(Z_{ii}) = \rho c \frac{k^2}{2\pi} \left[1 - \frac{k^2 a_i^2}{6} + O(k^4 a_i^4) \right], \; i = 1, 2\,; \tag{12.141}$$

$$\Re e(Z_{12}) = \rho c \frac{k^2}{2\pi} \left[1 - \frac{1}{6} k^2 \left(d^2 + \frac{a_1^2 + a_2^2}{2} \right) + O\left(k^4 d^4, k^4 a_1^4, k^4 a_2^4\right) \right]. \tag{12.142}$$

The power averaged over a period is written in the following form:

$$\mathscr{P} = \frac{1}{2} \Re e(p_1 U_1^*) + \frac{1}{2} \Re e(p_2 U_2^*) \;\text{ or} \tag{12.143}$$

$$\mathscr{P} = \frac{1}{2} |U_1|^2 \Re e(Z_{11} - Z_{12}) + \frac{1}{2} |U_2|^2 \Re e(Z_{22} - Z_{12}) + \frac{1}{2} |U_1 + U_2|^2 \Re e(Z_{12}). \tag{12.144}$$

For the case of the two pistons, we derive

$$\mathscr{P} = \rho c \frac{k^2}{4\pi} |U_1 + U_2|^2 + \rho c \frac{k^4}{24\pi} |U_1|^2 \left(\frac{a_2^2 - a_1^2}{2} + d^2 \right) + \rho c \frac{k^4}{24\pi} \left[|U_2|^2 \left(\frac{a_1^2 - a_2^2}{2} + d^2 \right) - |U_1 + U_2|^2 \left(\frac{a_1^2 + a_2^2}{2} + d^2 \right) \right]. \tag{12.145}$$

For point sources, it can be checked that the result is the same than Eq. (12.28) by a factor of two, since the pistons here radiate into a half-space.

Formula (12.145) shows that at low frequencies the radiation is that of a monopole with flow rate $|U_1 + U_2|^2$, which is proportional to ω^2, but if the two sources have the same amplitude and are opposite in phase, the radiation is that of a dipole, proportional to ω^4. This kind of analysis allows understanding why a vented box loudspeaker[18] paradoxically radiates as a dipole at lower frequencies

[18]The enclosure partially separates the rear face of a loudspeaker; it has several openings, contrary to a closed box loudspeaker.

and as a monopole at higher frequencies, because the two sources are linked by a relationship of kind: $U_1 = U_2(\omega^2/\omega_r^2 - 1)$, where ω_r is the Helmholtz angular resonance frequency of the enclosure. A similar case is that of stringed instruments with openings: this was analyzed in connection with the sound hole sum rule in Eq. (12.86).

For two tubes radiating in the same plane and without flange, the approximation of the plane piston can be used [16]. By applying again the superposition principle, we obtain for the real part of the mutual impedance the Expression (12.142), divided by a factor 2. This analysis could be extended, but it is rather academic, because the two tube ends rarely are in the same plane. This result can be used, for instance for toneholes, but we can simply use the approximation, and more generally the formula of a monopole radiation:

$$Z_{12} = j\rho c \frac{k}{4\pi} \frac{e^{-jkd}}{d}. \tag{12.146}$$

In summary, the previous analysis allows understanding, at least for a particular case, under which condition this condition is valid: the distance d needs to be large compared to the source radii. This very simplified expression will be used in order to analyze the radiation of complex sources in Chap. 14.

References

1. Ando, Y.: On the sound radiation from semi-infinite circular pipe of certain wall thickness. Acustica **22**, 219–225 (1969–1970)
2. Arfken, G., Weber, H.J.: Mathematical Methods for Physicists. Elsevier, Amsterdam (2005)
3. Brooke, M.: Numerical simulation of guitar radiation fields using the boundary element method. Ph.D. thesis, University of Wales, College of Cardiff (1992)
4. Chaigne, A.: The song of wine glasses (in French). Sci. et Avenir **100**, 52–57 (1995)
5. Crane, P.: Method for the calculation of the acoustic radiation impedance of unbaffled and partially baffled piston source. J. Sound Vib. **5**, 255–277 (1967)
6. Da Silva, A., Scavone, G.: Lattice Boltzmann simulations of the acoustic radiation from waveguides. J. Phys. A Math. Theor. **40**, 397–408, et 9721 (2007)
7. Dalmont, J.P., Nederveen, K., Joly, N.: Radiation impedance of tubes with different flanges: numerical and experimental investigation. J. Sound Vib. **244**(3), 505–534 (2001)
8. Dérogis, P.: Analysis of the vibrations and radiation of an upright piano soundboard, and design of a system for reproducing its acoustic field (in French). Ph.D. thesis, Université du Maine, Le Mans (1997)
9. Dickens, P.: Flute acoustics: measurement, modelling and design. Ph.D. thesis, University of New South Wales, Australia (2007)
10. Fahy, F.: Foundations of Engineering Acoustics. Academic, London (2000)
11. French, A.P.: In vino veritas: a study of wineglass acoustics. Am. J. Phys. **51**, 688–694 (1983)
12. Hélie, T., Rodet, X.: Radiation of a pulsating portion of a sphere: application to horn radiation. Acta Acustica United with Acustica **89**, 565–577 (2003)
13. Hocter, S.: Sound radiated from a cylindrical duct with Keller's geometrical theory. J. Sound Vib. **231**, 1243–1256 (2000)

14. Jacobsen, F., Juhl, P.: Radiation of sound. Acoustic Technology, Technical University of Denmark (2006)
15. Junger, M.C.: Sound radiation by resonances of free-free beams. J. Acoust. Soc. Am. **52**, 332–334 (1972)
16. Kergomard, J.: On the response of a vented box loudspeaker system at very low frequencies. In: 75th Convention of the Audio Engineering Society (preprint 2060), Paris (1984)
17. Kergomard, J., Lefebre, A., Scavone, G.: Matching of fundamental modes at a junction of a cylinder and a truncated cone; application to the calculation of some radiation impedances. Acta Acustica United with Acustica **101**, 1189–1198 (2015)
18. Levine, H., Schwinger, J.: On the radiation of sound from an unflanged circular pipe. Phys. Rev. **73**, 383–406 (1948)
19. Martin, D.W.: Directivity and the acoustic spectra of brass wind instruments. J. Acoust. Soc. Am. **13**(3), 309–313 (1942)
20. Morse, P.M., Ingard, K.: Theoretical Acoustics. McGraw Hill, New York (1968)
21. Munt, R.: Acoustic radiation from a circular cylinder in a subsonic stream. J. Inst. Math. Appl. **16**, 1–10 (1975)
22. Nederveen, C.J.: Acoustical Aspects of Woodwind Instruments. Northern Illinois University Press, Illinois. New edition, 1998 (1969)
23. Norris, A., Sheng, I.: Acoustic radiation from a circular pipe with an infinite flange. J. Sound Vib. **135**, 85–93 (1989)
24. Peters, M., Hirschberg, A., Reijnen, A., Wijnands, A.: Damping and reflection coefficient measurements for an open pipe at low mach and low Helmholtz numbers. J. Fluid Mech. **256**, 499–534 (1993)
25. Pritchard, R.: Mutual acoustic impedance between radiators in an infinite rigid plane. J. Acoust. Soc. Am. **32**, 730–737 (1960)
26. Rienstra, S., Hirschberg, A.: An Introduction to Acoustics. Eindhoven University of Technology, Eindhoven (2006)
27. Rossing, T.D.: Acoustics of the glass harmonica. J. Acoust. Soc. Am. **95**, 1106–1111 (1994)
28. Russel, D.A.: On the sound field radiated by a tuning fork. Am. J. Phys. **68**(12), 1139–1145 (2000)
29. Selamet, A., Ji, Z.L., Kach, R.A.: Wave reflections from duct terminations. J. Acoust. Soc. Am. **109**(4), 1304–1311 (2001)
30. Silva, F., Kergomard, J., Norris, A., Mallaroni, B.: Approximation formulae for the acoustic radiation impedance of a cylindrical pipe. J. Sound Vib. **322**, 255–263 (2009)
31. Temkin, S.: Elements of Acoustics. Acoustical Society of America, Melville (2001)
32. von Estorff, O. (ed.): Boundary Elements in Acoustics: Advances and Applications. WIT Press, Southampton (2000)
33. Weinreich, G.: Sound hole sum rule and the dipole moment of the violin. J. Acoust. Soc. Am. **77**(2), 710–718 (1985)
34. Weinreich, G., Arnold, E.B.: Method for measuring acoustic radiation fields. J. Acoust. Soc. Am. **68**(2), 404–411 (1980)
35. Williams, E.G.: Fourier Acoustics: Sound Radiation and NearField Acoustical Holography. Academic, New York (1999)
36. Wu, T.W. (ed.): Boundary Element Acoustics: Fundamentals and Computer Codes. WIT Press, Southampton (2000)

Chapter 13
Radiation of Vibrating Structures

Antoine Chaigne

Abstract This chapter deals with the radiation of vibrating structures in air, with application to stringed and percussive instruments. Basic notions are first presented with the help of an introductory example of a beam coupled to an air column. The important concept of critical frequency is then introduced through the example of an infinite thin plate radiating in air. The radiation models of finite plates and their results can be applied to real musical instruments. Recent methods are then presented for calculating the radiation of unbaffled plates, structural volumes, and nonplanar sources. Finally, the questions relative to the appropriate choice of material, and to the compromise between radiation efficiency and tone duration, are illustrated on several stringed instruments.

13.1 Introduction

For a number of musical instruments, the sound results from the vibration of structures. This is the case, for example, for stringed and percussive instruments. Structural acoustics (or *vibroacoustics*) is that subdomain of acoustics dealing with the interaction phenomena between a vibrating structure and the sound field in the adjacent fluid. In what follows, the air is the considered *light* fluid interacting with the structures. The concept of *light* and *heavy* fluid will be defined more formally in this chapter.

The structures used in the making of instrument are most often *thin* structures, which means that their thickness is small compared to the other dimensions. Different types of elastic waves can propagate in these structures. Among them, the flexural waves are those which show the lowest characteristic mechanical impedance. As a consequence, these waves also are those which are the most excited by an impact, and/or by the vibrations of strings coupled to them. The normal velocity and, in turn, the acoustic pressure field, are directly linked to the mechanical vibratory field of the structure.

A. Chaigne (✉)
Institute of Music Acoustics, University of Music and Performing Arts Vienna (MDW), Anton-von-Webern-Platz 1, 1030 Vienna, Austria
e-mail: antchaigne@gmail.com

A. Chaigne, J. Kergomard, *Acoustics of Musical Instruments*, Modern Acoustics and Signal Processing, DOI 10.1007/978-1-4939-3679-3_13

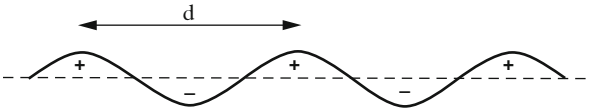

Fig. 13.1 Transverse vibrations of a plate at a frequency close to one on its eigenmodes

In musical acoustics, the most common vibrating structures are plates (guitar, harp, piano soundboards, etc.) or shells (soundboards of bowed strings instruments, bells, gongs, cymbals, etc.). The beams (xylophone, vibraphone, marimba, glockenspiel, etc.) can be considered as limiting cases of plates whose width is small compared to the length. The particular case of the membranes (timpani, drums, etc.) will be treated in detail in Chap. 14.

In contrast with the case of the plane piston seen in Chap. 12, where the surface velocity field is uniform, the vibrations of shells and plates are characterized by the juxtaposition of zones with velocity fields of alternate signs, which can be seen as the 2-D association of dipoles (pairs of monopoles of opposite signs) (see Fig. 13.1). The main effect of this situation is to globally reduce the compression of the fluid (compared to the plane piston), and thus to limit the efficiency of the radiation to the far field. Intuitively, one can feel that the dipoles will produce destructive interferences if $kd \ll 1$, where k is the wavenumber and d the distance between two consecutive "monopoles" on the plate or on the shell. Conversely, if $kd \gg 1$, the monopoles radiate more independently and the radiation efficiency is improved (see also Chap. 12).

As seen in Chap. 3, flexural waves are dispersive, where the phase and group velocities vary with frequency. It will be shown in Sect. 13.3 that the so-called *critical (or coincidence) frequency* f_c exists, for which the acoustic wavelength in the fluid is equal to the elastic wavelength in the structure. For the frequencies smaller than f_c, the sound power radiated by an infinite flat plate is zero, and is very weak for a finite plate. For the shells, and, more generally, for complex structures (such as ribbed plates, for example), the radiation properties depend on the elastic dispersion curve. The phase velocity increases by imposing a curvature to a flat plate: as a consequence, shells are generally more efficient in terms of radiation than plates of similar external surface and thickness, and made of the same material. However, this general tendency needs to be clarified for each particular geometry: in Sect. 13.5, it will be seen on a simple example that the curvature also affects the bandwidth and the directivity of the source.

13.2 Basic Concepts in Structural Acoustics

This chapter starts with the presentation of a simple 1-D example whose aim is to introduce the basic concepts in structural–acoustic coupling. The purpose is to highlight the following properties:

- Both the real and imaginary parts of the eigenfrequencies are modified by the acoustic radiation of a structure. In this section, a method is shown for calculating these modifications. In addition, approximations are presented which are justified in case of weak coupling between the structure and the fluid, as it is often the case for the air.
- Expanding the general solution of a coupled system in terms of the structural in vacuo modes shows that intermodal coupling results from the radiation. In practice, this means that if one particular mode is excited then, in turn, other coupled modes are excited. These phenomena are currently observed in stringed instruments. For a formal point of view, this coupling is indicated through the fact that the differential equations that govern the generalized displacements are not independent from each other anymore. These properties are analogous to those demonstrated in Chap. 5 for the nonproportional damping.[1]
- For a forced excitation at a given frequency ω, it is generally not possible to excite only one mode, as a consequence of the intermodal coupling. Thus, the concept of *Operating Deflexion Shape* (or ODS) needs to be introduced.
- The structural and radiation resistance matrices are introduced by means of an energy analysis of the coupled system. The radiation efficiency is derived from these definitions.

13.2.1 Vibrating Beam Coupled to an Infinite Fluid Medium: Modal Approach

A typical situation involving a vibrating structure radiating sound energy in free space is analyzed here. The simple selected system is composed of a finite elastic beam vibrating longitudinally and loaded at one end by a semi-infinite tube filled with air. This problem shows some analogies with the example of the string with dissipative end studied in Chap. 5.

The system shown in Fig. 13.2 is considered. It is composed of an elastic longitudinally vibrating 1-D beam with density ρ_s, section S, length L, and Young's modulus E. $\xi(x,t)$ is the longitudinal displacement of a current point at position x along the bar (with $0 < x < L$). This beam is coupled at one end ($x = L$) with a semi-infinite tube filled with air, and clamped at the other ($x = 0$). The motion of the beam induces a pressure $p(x,t)$ inside the tube. This pressure reacts on the beam at point $x = L$. $c_L = \sqrt{E/\rho_s}$ is the longitudinal wave speed. The coupled system is governed by the equations:

[1] In reality, the modes of the coupled system are complex, and we could think of applying the rigorous theory of complex modes presented in Chap. 5. However, since the air coupling can be most often considered as weak in musical acoustics, the method of projection on the in vacuo modes is preferred here, which corresponds to current practice.

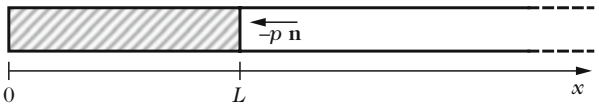

Fig. 13.2 Longitudinally vibrating beam coupled to a semi-infinite tube. In $x = L$, the cross-section of the bar is subjected to the sound pressure $-p\,\boldsymbol{n}$, where $\boldsymbol{n}$ is the unitary vector normal to the beam

$$\begin{cases} \rho_s \frac{\partial^2 \xi}{\partial t^2} = E \frac{\partial^2 \xi}{\partial x^2} \quad \text{for} \quad 0 \le x < L, \\ p(L,t) = \rho c \dot{\xi}(L,t), \\ \xi(0,t) = 0, \\ p(x,t) = \rho c \dot{\xi}(L, t - \frac{x-L}{c}) \quad \text{for} \quad L < x < \infty. \end{cases} \tag{13.1}$$

The system (13.1) is solved by expanding the sought solution $\xi(x,t)$ in terms of the in vacuo modes $\phi_n(x)$ of the beam:

$$\xi(x,t) = \sum_n \phi_n(x) q_n(t), \tag{13.2}$$

where the $q_n(t)$ are the generalized displacements. The system (13.1) is then integrated over the length of the beam (from 0 to L), after multiplication by any eigenfunction ϕ_n. This gives

$$\int_0^L \rho_s S \left(\sum_m \phi_m(x) \ddot{q}_m(t) \right) \phi_n(x)\, dx - \int_0^L ES \left(\sum_m \phi_m''(x) q_m(t) \right) \phi_n(x)\, dx$$
$$= S\rho c \left(\sum_m \phi_m(L) \dot{q}_m(t) \right) \phi_n(L). \tag{13.3}$$

Equation (13.3) expresses the energetic balance between the internal stresses inside the beam, the inertial forces, and the pressure forces applied to the beam by the exterior medium. Due to the orthogonality properties of the in vacuo modes ϕ_n, the only nonzero terms remaining in (13.3) are those for which $m = n$. Introducing further the modal mass:

$$m_n = \int_0^L \rho_s S \phi_n^2(x) dx, \tag{13.4}$$

and rewriting the second integral:

$$-\int_0^L ES \frac{\omega_n^2}{c_L^2} \left(\sum_m \phi_m(x) q_m(t) \right) \phi_n(x)\, dx = -\omega_n^2 m_n q_n(t), \tag{13.5}$$

it is found that the generalized displacements $q_n(t)$ are solutions of the coupled system:

$$m_n\ddot{q}_n(t) + m_n\omega_n^2 q_n(t) = -R_a\phi_n(L)\sum_m \phi_m(L)\dot{q}_m(t), \tag{13.6}$$

where $R_a = \rho cS$ is the radiation resistance. It is observed that one effect of the radiation is to couple together the in vacuo modes of the beam. However, under some restrictive assumptions, it will be allowed to replace the system (13.6) by an approximate uncoupled system.

After determining the generalized displacements q_n, the displacement ξ is derived from (13.2), and this allows to calculate both the velocity and the pressure field. In conclusion, all variables of the problem are known. This justifies to focus primarily on the q_n in what follows.

13.2.1.1 Systems Having a Few Number of Degrees of Freedom (dof)

In this section, coupled systems of small dimensions are examined, in order to better understand their physical meaning.

Single dof System

Let us suppose that, for various reasons, the beam can be reduced to a single mode. In this case (13.6) reduces to:

$$\ddot{q}_1(t) + \frac{R_a\phi_1^2(L)}{m_1}\dot{q}_1(t) + \omega_1^2 q_1(t) = 0. \tag{13.7}$$

This is simply the equation of a damped oscillator (see Chap. 2) where the dimensionless damping factor ζ_1 is

$$2\zeta_1\omega_1 = \frac{R_a\phi_1^2(L)}{m_1}. \tag{13.8}$$

Thus, for a single dof system loaded by a semi-infinite tube, the acoustic coupling adds a radiation damping to the structure.

2-dof System

Let us now truncate the continuous beam to its two lowest modes. In this case, (13.6) becomes

$$\begin{cases} \ddot{q}_1(t) + \omega_1^2 q_1(t) = -\frac{R_a\phi_1(L)}{m_1}[\phi_1(L)\dot{q}_1(t) + \phi_2(L)\dot{q}_2(t)], \\ \ddot{q}_2(t) + \omega_2^2 q_2(t) = -\frac{R_a\phi_2(L)}{m_2}[\phi_1(L)\dot{q}_1(t) + \phi_2(L)\dot{q}_2(t)]. \end{cases} \tag{13.9}$$

Equation (13.9) can be rewritten as:

$$\begin{cases} \ddot{q}_1 + 2\zeta_1\omega_1\dot{q}_1 + \omega_1^2 q_1 = -\frac{R_a\phi_1(L)\phi_2(L)}{m_1}\dot{q}_2 = C_{12}\dot{q}_2, \\ \ddot{q}_2 + 2\zeta_2\omega_2\dot{q}_2 + \omega_2^2 q_2 = -\frac{R_a\phi_2(L)\phi_1(L)}{m_2}\dot{q}_1 = C_{21}\dot{q}_1, \end{cases} \tag{13.10}$$

where $-m_1 C_{12} = -m_2 C_{21} = R_a\phi_2(L)\phi_1(L)$.

Several conclusions can be drawn from this result:

- Due to the acoustic radiation, damping terms $2\zeta_i\omega_i\dot{q}_i$ are introduced in both equations.
- The generalized displacements are coupled.
- In the absence of any other damping phenomena, the coupling coefficients C_{12} and C_{21} are linked by the property[2]:

$$C_{12}C_{21} = 4\zeta_1\zeta_2\omega_1\omega_2.$$

The eigenfrequencies of the system are the roots of the characteristic equation:

$$(s^2 + 2\zeta_1\omega_1 s + \omega_1^2)(s^2 + 2\zeta_2\omega_2 s + \omega_2^2) - 4\zeta_1\zeta_2\omega_1\omega_2 s^2 = 0, \tag{13.11}$$

This equation shows that the structural-acoustic coupling modifies the complex eigenfrequencies. In general, this equation can only be solved numerically. However, under the assumption of weak damping ($\zeta_1 \ll 1$ and $\zeta_2 \ll 1$), first-order approximations can be found [8].

13.2.1.2 Generalization

For a continuous system with a large number of dof, the differential system (13.6) is written:

$$\ddot{q}_n + 2\zeta_n\omega_n\dot{q}_n + \omega_n^2 q_n = \sum_{m\neq n} C_{nm}\dot{q}_m, \tag{13.12}$$

where

$$2\zeta_n\omega_n = \frac{R_a\phi_n^2(L)}{m_n} \quad \text{and} \quad C_{nm} = -\frac{R_a\phi_n(L)\phi_m(L)}{m_n}. \tag{13.13}$$

This expression shows the two main effects of the elasto-acoustic coupling seen in Fig. 13.2:

[2]Notice that this property is no longer valid if there is another structural damping inside the beam.

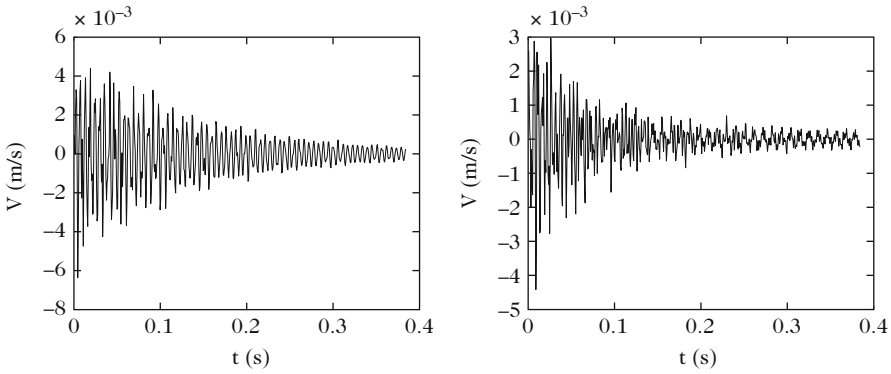

Fig. 13.3 Comparison between two velocity waveforms at a given point on a guitar soundboard (synthesis). (*Left*) Isolated mode in vacuo. (*Right*) Coupled modes due to air-soundboard coupling

1. modal damping due to radiation
2. modification of the eigenfrequencies due to intermodal coupling.

The 1-D model presented here can be further generalized to more complex systems. Figure 13.3 shows, for example, the case of a synthesized guitar tone. The picture on the left shows the time decay of an isolated mode, assuming only a modal damping in the in vacuo soundboard. The picture on the right shows the time evolution of the generalized displacement, in case of a coupling with external air and cavity. It can be seen that several other modes are excited, as a consequence of the air-structure coupling.

13.2.1.3 Reactive Effects

Imagine now that the free end of the beam subjected to longitudinal vibrations is now inserted in an infinite plane baffle, as in the case of the plane piston seen in Chap. 12. The radiation impedance now contains a real part R_a, and an imaginary part X_a.

The imaginary part corresponds to an inertial load by the fluid[3] which was not present in the case of the beam loaded by the semi-infinite tube. The main effect of X_a is to lower the eigenmodes of the structure compared to the in vacuo case.

[3] Such an effect can be taken into account as a length correction in tubes.

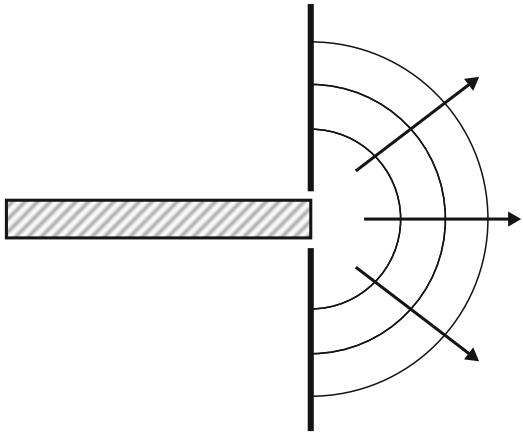

Fig. 13.4 Elastic beam vibrating longitudinally and inserted in an infinite plane baffle

13.2.2 Forced Regime

As for the harmonic oscillator in Chap. 2, the case of a forced excitation is now considered. A force $F(t)$ is applied at point $x = x_0$ with $x_0 < L$. This situation corresponds in practice to stringed instruments, where the soundboard is excited at the bridge by the vibration of a string. For a violin, the force is due to self-sustained oscillations. For a guitar or a piano, the decay times of the strings' vibrations are usually long compared to those of the soundboard, so that the excitation can be viewed as quasi-stationary. In the presence of an excitation, the energy balance (13.3) becomes

$$\int_0^L \rho_s S \left(\sum_m \phi_m(x) \ddot{q}_m(t) \right) \phi_n(x)\, dx - \int_0^L ES \left(\sum_m \phi_m''(x) q_m(t) \right) \phi_n(x)\, dx$$
$$= \int_0^L R_a \left(\sum_m \phi_m(L) \dot{q}_m(t) \right) \phi_n(x) \delta(x - L)\, dx + \int_0^L F(x_0, t) \delta(x - x_0) \phi_n(x)\, dx \tag{13.14}$$

which leads to the equations governing the generalized displacements:

$$\ddot{q}_n + 2\zeta_n \omega_n \dot{q}_n + \omega_n^2 q_n = \sum_{m \neq n} C_{nm} \dot{q}_m + F(x_0, t) \frac{\phi_n(x_0)}{m_n}, \tag{13.15}$$

or, equivalently, using the Laplace transform:

$$\tilde{q}_n(s) = H_n(s) \tilde{F}(x_0, s) + \sum_{m \neq n} K_{nm}(s) \tilde{q}_m(s), \tag{13.16}$$

with

$$H_n(s) = \frac{\phi_n(x_0)}{m_n(s^2 + 2\zeta_n\omega_n s + \omega_n^2)} \quad \text{and} \quad K_{nm}(s) = \frac{sC_{nm}}{s^2 + 2\zeta_n\omega_n s + \omega_n^2}. \tag{13.17}$$

In summary, the displacement is written:

$$\tilde{\xi}(x,s) = \sum_n \tilde{q}_n(s)\phi_n(x) = \tilde{F}(x_0,s)\sum_n \phi_n(x)H_n(s) + \sum_n \phi_n(x)\sum_{m\neq n} K_{nm}(s)\tilde{q}_m(s). \tag{13.18}$$

In matrix form, the system (13.16) is written[4]:

$$\begin{bmatrix} D_1 & -sC_{12} & \dots & -sC_{1n} \\ -sC_{21} & D_2 & \dots & -sC_{2n} \\ \dots & \dots & \dots & \dots \\ -sC_{n1} & -sC_{n2} & \dots & D_n \end{bmatrix} \begin{bmatrix} q_1 \\ q_2 \\ \dots \\ q_n \end{bmatrix} = F \begin{bmatrix} \beta_1 \\ \beta_2 \\ \dots \\ \beta_n \end{bmatrix} \tag{13.19}$$

where $\beta_n = \frac{\phi_n(x_0)}{m_n}$ and $D_n = s^2 + 2\zeta_n\omega_n s + \omega_n^2$. It is convenient to put this equation in the following form:

$$\mathbb{C}\boldsymbol{Q} = F\boldsymbol{\beta}, \tag{13.20}$$

where the displacement thus becomes

$$\xi = {}^t\boldsymbol{\phi}\boldsymbol{Q} \quad \text{where} \quad \boldsymbol{Q} = (\mathbb{C}^{-1}\boldsymbol{\beta})F. \tag{13.21}$$

Notice that, due to the sound–structure coupling, the matrix $\mathbb{C}$ is not diagonal. However, in the case of radiation in air, this coupling is generally weak and it will be justified to use approximate formulations.

13.2.2.1 Light Fluid Approximation

Several methods exist for addressing the problem of elasto-acoustic coupling in light fluid. In the method retained below, dimensionless intermodal coupling coefficients are viewed as perturbation terms, compared to the reference in vacuo case. A simple expression is then derived for the structural shapes. As previously, the presentation starts with a simple 2-dof system.

[4] In what follows, the symbols "~" will be omitted for clarity.

2-dof System

For a 2-dof system, the matrix $\mathbb{C}$ is written:

$$\mathbb{C} = \begin{bmatrix} D_1 & -sC_{12} \\ -sC_{21} & D_2 \end{bmatrix}. \tag{13.22}$$

In order to test to what extent this matrix is different from the diagonal case, we look for the diagonal matrix $\mathbb{D}$ built with the eigenvalues λ_1 and λ_2 which are solutions of the characteristic equation:

$$\begin{vmatrix} D_1 - \lambda & -sC12 \\ -sC_{21} & D_2 - \lambda \end{vmatrix} = (D_2 - \lambda)(D_1 - \lambda) - s^2 C_{12} C_{21} = 0. \tag{13.23}$$

Denoting $\mathbf{e}_i$ the corresponding eigenvectors, and $\mathbb{T} = [\mathbf{e}_1 \quad \mathbf{e}_2]$, the classical matrix relationships are obtained

$$\mathbb{T}\mathbb{D} = \mathbb{C}\mathbb{T} \quad \Leftrightarrow \quad \mathbb{D} = \mathbb{T}^{-1}\mathbb{C}\mathbb{T}, \tag{13.24}$$

where it is assumed that $\mathbb{C}$ is reversible. In the general case (without approximations), the eigenvalues of $\mathbb{C}$ are given by:

$$\lambda_{1,2} = \frac{1}{2}\left[D_1 + D_2 \pm \sqrt{(D_1 - D_2)^2 + 4s^2 C_{12} C_{21}}\right]. \tag{13.25}$$

At this stage, the following *dimensionless coupling coefficient* is defined[5]

$$\varepsilon = \frac{C_{12}C_{21}}{D_2 - D_1} = \frac{C_{12}C_{21}}{\omega_2^2 - \omega_1^2 + 2s(\zeta_2\omega_2 - \zeta_1\omega_1)}, \tag{13.26}$$

so that, for $\varepsilon \ll 1$, the eigenvalues of $\mathbb{C}$ can be written to first-order approximation:

$$\lambda_1 = D_1 - \varepsilon s^2 \quad ; \quad \lambda_2 = D_2 + \varepsilon s^2. \tag{13.27}$$

Discussion At this stage, we make the approximation of "light fluid," i.e., we assume that the coefficients C_{ij} and ζ_i are small in (13.26). As a consequence, it can be seen that the coupling parameter ε is small only under the condition that the in vacuo frequencies of the structure are sufficiently far apart from each other. If this latter condition is not fulfilled, a strong coupling can be observed, even for a light fluid. Such a situation occurs, for example, in the coupling between the fundamental mode of a head, and the lowest mode of the cavity in timpani (see Chap. 14).

[5] See also the definition of a coupling coefficient in Sect. 6.4 of Chap. 6.

Generalization

For a system with n dof, it can be shown that the first-order approximations of the eigenvalues λ_i can be written as:

$$\lambda_i = D_i + \varepsilon_i s^2 \quad \text{with} \quad \varepsilon_i = \sum_j \frac{C_{ij}C_{ji}}{D_i - D_j} \quad \text{and} \quad 1 \leq j \leq n \quad \text{and} \quad j \neq i. \tag{13.28}$$

In summary, n intermodal coupling coefficients are defined, one for each pair of modes. The conditions of weak coupling are generalized: light fluid and sufficient distance between the values of the eigenfrequencies.

13.2.2.2 Operating Deflexion Shapes

Forced excitation is often used for measurements purpose on musical instruments. In case of uncoupled modes, a forced excitation close to one particular eigenfrequency of the structure yields the corresponding modal shape. However for coupled modes, as in the case examined in this section, the observed deflexion cannot be reduced to a single modal shape. They are usually referred to as ODS.

In what follows, we content ourselves with a simplified presentation with two dof. The results can be generalized to any number n of dof. We start by writing the displacement field of the structure in vacuo:

$$\xi_0 = \phi_{10} q_{10} + \phi_{20} q_{20}. \tag{13.29}$$

For the same structure vibrating in air, and using an expansion of the displacement on the *in vacuo modes*, we get

$$\xi = \phi_{10} q_1 + \phi_{20} q_2. \tag{13.30}$$

Based on the results obtained in the previous section, we can write to the first-order:

$$\xi = \phi_{10}\left(q_{10} + \frac{sC_{12}}{D_1} q_{20}\right) + \phi_{20}\left(q_{20} + q_{10}\frac{sC_{21}}{D_2}\right), \tag{13.31}$$

or, equivalently, by grouping the terms corresponding to each generalized displacement:

$$\xi = q_{10}\left(\phi_{10} + \frac{sC_{21}}{D_2}\phi_{20}\right) + q_{20}\left(\phi_{20} + \phi_{10}\frac{sC_{12}}{D_1}\right) \quad \text{with} \quad q_{i0} = \frac{\phi_{i0}}{m_i D_i} F. \tag{13.32}$$

Let us now examine typical experimental situations where a sinusoidal force $F(t) = F_0 H(t) \sin \omega t$[6] is applied suddenly at time $t = 0$ and at point x_0.

(1) In the particular case where both the frequency and excitation point are selected so that q_{20} is negligible compared to q_{10}, the displacement becomes

$$\phi_1 = \phi_{10} + \phi_{20} \frac{sC_{21}}{D_2}. \tag{13.33}$$

After a certain amount of time, the second term in (13.33) tends to zero, and the observed deflexion corresponds to the first mode.

(2) However, in the general case, Eq. (13.32) shows that both modes are simultaneously excited. After the transient regime, the stationary solution for the displacement is given by:

$$\xi(\omega, x) = \left[\frac{\phi_{10}\beta_1}{D_1(j\omega)} + \frac{\phi_{20}\beta_2}{D_2(j\omega)} \right]. \tag{13.34}$$

The quantity enclosed in square brackets is the ODS of the structure at frequency ω.

13.2.3 Energy Approach

In the previous sections, the internal losses inside the material of the structure were not considered. However, if we take the example of a stringed instrument, only a part of the mechanical power transmitted by the string to the body is transformed into acoustic power. The difference is essentially due to dissipation in the material.

The energy balance and the acoustical efficiency of a single dof oscillator loaded by a tube filled with air were determined in Chap. 2. This example is generalized here to a structural system with multiple dof coupled to a fluid. For a better comprehension, we start with a 2-dof system. The losses in the structure itself are represented by two mechanical resistances r_1 and r_2. The resistances r_{a1} and r_{a2} account for the radiation losses. One goal is to compare the dissipated power in the structure and in air, respectively.

13.2.3.1 Structural and Acoustic Resistance Matrix

The illustrating example is still the case of a longitudinally vibrating beam radiating at one end ($x = L$) in a semi-infinite tube (see Fig. 13.2). The excitation force F is applied at point $x = x_0$. The radiation coupling coefficients are defined in (13.13).

[6] Recall that $H(t)$ is the Heaviside function.

The system is truncated to the first two modes of the beam, for simplicity. The system of equations governing the system is

$$\begin{cases} m_1\ddot{q}_1 + (r_1 + r_{a1})\dot{q}_1 + k_1 q_1 + \gamma\dot{q}_2 = \phi_1(x_0)F, \\ m_2\ddot{q}_2 + (r_2 + r_{a2})\dot{q}_2 + k_1 q_2 + \gamma\dot{q}_1 = \phi_2(x_0)F, \end{cases} \tag{13.35}$$

where $\gamma = -C_{12}m_1 = -C_{21}m_2$. The following notations are used

$$\begin{cases} 2\zeta_1\omega_1 = \frac{r_1+r_{a1}}{m_1} \quad ; \quad 2\zeta_{10}\omega_1 = \frac{r_1}{m_1} \quad ; \quad \omega_1^2 = \frac{k_1}{m_1}, \\ 2\zeta_2\omega_2 = \frac{r_2+r_{a2}}{m_1} \quad ; \quad 2\zeta_{20}\omega_2 = \frac{r_2}{m_2} \quad ; \quad \omega_2^2 = \frac{k_2}{m_2}. \end{cases} \tag{13.36}$$

The instantaneous mechanical power imparted to the beam is

$$\begin{aligned} p_m(t) &= F\frac{d\xi}{dt}(x_0, t) = F\left[\phi_1(x_0)\dot{q}_1 + \phi_2(x_0)\dot{q}_2\right] \\ &= m_1\ddot{q}_1\dot{q}_1 + (r_1 + r_{a1})\dot{q}_1^2 + k_1 q_1\dot{q}_1 + 2\gamma\dot{q}_1\dot{q}_2 \\ &\quad + m_2\ddot{q}_2\dot{q}_2 + (r_2 + r_{a2})\dot{q}_2^2 + k_2 q_2\dot{q}_2. \end{aligned} \tag{13.37}$$

In case of a periodic motion with period T, the mean value of this power is:

$$\mathscr{P}_m(T) = \frac{1}{T}\int_0^T (r_1 + r_{a1})\dot{q}_1^2 + (r_2 + r_{a2})\dot{q}_2^2 + 2\gamma\dot{q}_2\dot{q}_1\, dt, \tag{13.38}$$

It is composed of three terms:

- The mean power dissipate in the structure (material) $\mathscr{P}_s(T) = \frac{1}{T}\int_0^T r_1\dot{q}_1^2 + r_2\dot{q}_2^2\, dt$,
- The mean radiated acoustic power $\mathscr{P}_a(T) = \frac{1}{T}\int_0^T r_{a1}\dot{q}_1^2 + r_{a2}\dot{q}_2^2\, dt$,
- The mean coupling power $\mathscr{P}_c(T) = \frac{2}{T}\int_0^T \gamma\dot{q}_2\dot{q}_1\, dt$ reflecting the energy exchange between the modes.

In the particular case of sinusoidal excitation, we get

$$\mathscr{P}_m = \frac{1}{2}\left[(r_1 + r_{a1})|\dot{q}_1|^2 + (r_2 + r_{a2})|\dot{q}_2|^2 + 2\gamma|\dot{q}_2||\dot{q}_1|\right]. \tag{13.39}$$

In vacuo, this expression reduces to:

$$\mathscr{P}_{mo} = \frac{1}{2}\left[r_1|\dot{q}_{10}|^2 + r_2|\dot{q}_{20}|^2\right]. \tag{13.40}$$

In what follows, it is convenient to write these results in matrix form. Introducing the notations: $\dot{\mathbf{Q}} = \begin{bmatrix} \dot{q}_1 \\ \dot{q}_2 \end{bmatrix}$, $\mathbb{R}_s = \begin{bmatrix} r_1 & 0 \\ 0 & r_2 \end{bmatrix}$ and $\mathbb{R}_a = \begin{bmatrix} r_{a1} & \gamma \\ \gamma & r_{a2} \end{bmatrix}$, we get

$$\mathscr{P}_m = \dot{\mathbf{Q}}^H \left[\mathbb{R}_s + \mathbb{R}_a\right] \dot{\mathbf{Q}}, \tag{13.41}$$

where $\dot{\mathbf{Q}}^H$ is the Hermitian conjugate (conjugate transpose) of $\dot{\mathbf{Q}}$. $\mathbb{R}_s$ is the matrix of the structural resistances. For the sake of simplicity, it is written here in diagonal form. However, it is not the case for all causes of damping (see Chap. 5). Finally, $\mathbb{R}_a$ is the radiation resistance matrix of the beam coupled to the fluid.

13.2.3.2 Generalization and Acoustical Efficiency

Generalizing the previous results to the n dof of the beam, we find

$$\mathscr{P}_m(T) = \frac{1}{T}\int_0^T \left[\sum_{i=1}^{n}(r_i + r_{ai})\dot{q}_i^2 + \sum_{i=1}^{n}\sum_{j\neq i=1}^{n} \gamma_{ij}\dot{q}_i\dot{q}_j\right] dt \quad \text{où} \quad \gamma_{ij} = -m_i C_{ij}. \tag{13.42}$$

The resistance matrix becomes

$$\mathbb{R}_s + \mathbb{R}_a = \begin{bmatrix} r_1 + r_{a1} & \dots & \gamma_{1i} & \dots & \gamma_{1j} & \dots & \gamma_{1n} \\ \dots & \dots & \dots & \dots & \dots & \dots & \dots \\ \gamma_{i1} & \dots & r_i + r_{ai} & \dots & \gamma_{ij} & \dots & \gamma_{in} \\ \dots & \dots & \dots & \dots & \dots & \dots & \dots \\ \gamma_{j1} & \dots & \gamma_{ji} & \dots & r_j + r_{aj} & \dots & \gamma_{jn} \\ \dots & \dots & \dots & \dots & \dots & \dots & \dots \\ \gamma_{n1} & \dots & \gamma_{ni} & \dots & \gamma_{nj} & \dots & r_n + r_{an}. \end{bmatrix} \tag{13.43}$$

The radiated acoustic power is given by:

$$\mathscr{P}_a = \dot{\mathbf{Q}}^H \mathbb{R}_a \dot{\mathbf{Q}}. \tag{13.44}$$

In conclusion, for an elastic-acoustic system where the modes are coupled by the radiation, the acoustical efficiency is written:

$$\eta_m = \frac{\dot{\mathbf{Q}}^H \left[\mathbb{R}_a\right] \dot{\mathbf{Q}}}{\dot{\mathbf{Q}}^H \left[\mathbb{R}_s + \mathbb{R}_a\right] \dot{\mathbf{Q}}}. \tag{13.45}$$

Equation (13.45) is thus the generalization of the result obtained in Chap. 2 for a single oscillator coupled to the air.

Measurements conducted on a number of classical guitars have shown that the order of magnitude of the acoustical efficiency is nearly 10 % between 100 and 1000 Hz, and 5 % between 1 and 8 kHz. However, for some particular frequencies, the efficiency can reach 20 % [5].

13.3 Radiation of an Infinite Thin Plate

13.3.1 Elastic Equation

The radiation properties of a plane surface with uniform velocity profile were studied in Chap. 12. This theory is valid for the structures subjected to rigid body motion. It can also be applied to the radiation of a hole (as the soundhole of a guitar, for example), as long as the normal acoustic velocity remains constant over the cross-section.

As soon as the frequency increases, which causes in turn that the vibratory wavelength becomes comparable to (or smaller than) the dimensions of the structure, then one has to consider the propagation phenomena inside the structure. To illustrate this point, the case of flexural motion of thin plates is treated below.

The presentation starts with the case of an "infinite" plate, which amounts to neglecting the reflection of waves at the edges. The particular case of an isotropic plate subjected to a transverse velocity $V(x,\omega) = V_0(\omega)e^{-jk_B x}$ along the x-axis is studied in the frequency domain. $k_B = 2\pi/\lambda_B$ is the flexural wavenumber (see Fig. 13.5). For a given frequency ω, the phase velocity of the elastic wave in the plate is given by $c_B = \omega/k_B$.

At this stage, the internal losses in the plate, and the reaction of the acoustic pressure on it, are left temporarily aside. These features will be progressively introduced later. ρ_p is the density of the plate, E its Young's modulus, ν its Poisson's coefficient, and h its thickness. In the context of the Kirchhoff–Love assumptions, it has been shown in Chap. 1 that the governing equation of motion for the plate is given by:

$$-\omega^2\rho_p hW + D\frac{d^4W}{dx^4} = 0 \quad \text{with} \quad D = \frac{Eh^3}{12(1-\nu^2)}, \tag{13.46}$$

where $W(x,\omega)$ is the transverse displacement.

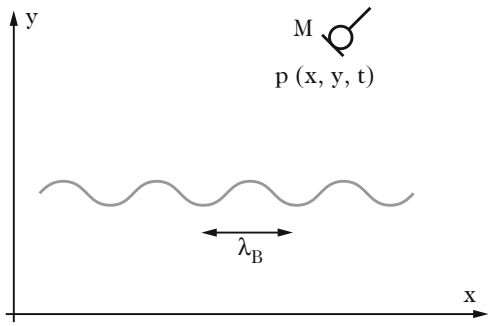

Fig. 13.5 Radiation of an infinite plate subjected to transverse flexural vibrations. The elastic flexural wavelength is λ_B. The objective is to determine the pressure p radiated by this plate in free space. For simplicity, the case of a "1D" plate (equivalent to a beam) is considered. As a consequence, the pressure only depends on two spatial coordinates: x and y

13.3.2 Acoustic Equations

The Helmholtz equation governing the sound pressure $P(x, y, \omega)$ is written:

$$\frac{\partial^2 P}{\partial x^2} + \frac{\partial^2 P}{\partial y^2} + k^2 P = 0. \tag{13.47}$$

The elasto-acoustic interaction between the plate and the air (with density ρ) is ensured by the continuity equation for the normal velocities:

$$\left.\frac{\partial P}{\partial y}\right|_{y=0} = -j\omega\rho V_0 e^{-jk_B x}. \tag{13.48}$$

13.3.3 Dispersion Equations and Critical Frequency

For any progressive flexural wave of the form $e^{j(\omega t - k_B x)}$ injected in Eq. (13.46), we get the dispersion relationship between frequency and wavenumber in the plate:

$$\omega = \sqrt{\frac{D}{\rho_p h}} k_B^2. \tag{13.49}$$

Due to the linearity of the problem, the same frequency is found in the acoustic field, which yields the acoustic dispersion relation:

$$\omega = kc. \tag{13.50}$$

where c is the speed of sound in air. Plotting both dispersion relationships (13.49) and (13.50) on the same figure (see Fig. 13.6) shows that a particular frequency exists for which the wavenumber in the plate is equal to the wavenumber in air. This so-called *critical (or coincidence) frequency* is given by:

$$f_c = \frac{\omega_c}{2\pi} = \frac{c^2}{2\pi}\sqrt{\frac{\rho_p h}{D}} = \frac{c^2}{\pi h}\sqrt{\frac{3\rho_p(1-\nu^2)}{E}}. \tag{13.51}$$

The critical frequency f_c plays a major role in elasto-acoustic coupling. In Sect. 13.3.4, it will be shown that this two distinct frequency domains are defined by this frequency: below f_c, the radiation efficiency is weak, whereas it becomes significant for frequencies higher than f_c. A maximum is obtained for the particular case $f = f_c$. This result is due to the particular shape (parabolic, here) of the plate dispersion. By contrast, for ideal membranes, the dispersion relationship is linear, and no critical frequency can be exhibited. There is only one particular case where both wave speed in air and in the membrane are equal (see the next paragraph).

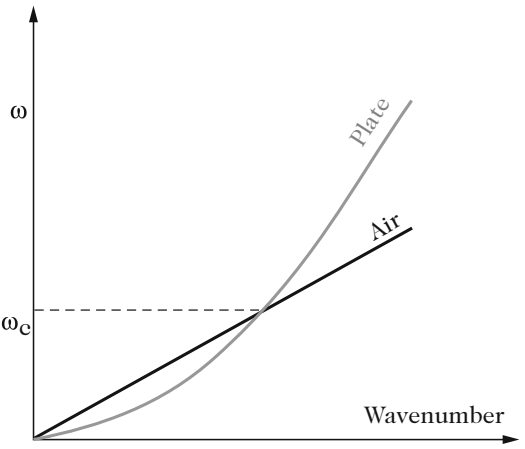

Fig. 13.6 Equations of dispersion in plate and air. The critical (or coincidence) frequency is given by the intersection of both curves

For other structures (for some shells, for example) some situations can also be observed where there are no intersections between the air and structures dispersion relationships. These features will be studied in more details in Sect. 13.5.

In Eq. (13.51), it can be seen that the critical frequency depends on the thickness of the plate and on the material properties. In summary, the critical frequency decreases as the plate becomes thicker, more dense, and more rigid.

Transposing these results to stringed instruments, one can derive that, for similar thickness and density, replacing a given material by a more rigid one contributes to lower the critical frequency which, in turn, should enhance the radiation efficiency of the lowest notes. In this context, gluing some ribs on the soundboard contributes to increase its stiffness and its mean thickness, which is coherent with a decrease of the critical frequency. However, one must be careful before concluding that these modifications will, in fact, lead to an increase in sound power. One has first to consider (and estimate) the change of velocity profile of the soundboard due to the attachment of ribs.

Critical Domain for Orthotropic Materials

For orthotropic materials (such as the wood species used for stringed instruments), the calculation (13.51) can be conducted again in the two limiting cases corresponding to the stiffer and to the more flexible directions, respectively. Two dispersion curves are then obtained from which the critical domain $[\omega_{c1}, \omega_{c2}]$ is derived (see Fig. 13.7). It has been shown in Chap. 3 that, for a finite orthotropic plate, all eigenfrequencies are situated between the two dispersion curves. Among these eigenfrequencies, those situated in the critical interval will have a particularly high radiation efficiency.

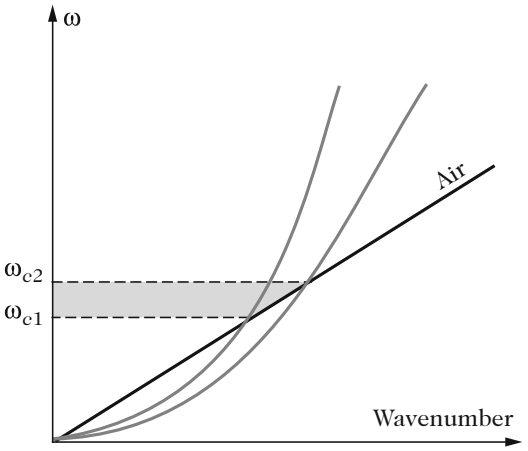

Fig. 13.7 Critical domain for the orthotropic materials. The *straight line* accounts for the air dispersion. The direction of maximal rigidity determines the frequency ω_{c1}, whereas the less stiff direction determines ω_{c2}. The "critical domain" is given by the interval $[\omega_{c1}, \omega_{c2}]$

Critical Frequency for Stiff Membranes and Prestressed Plates

The flexural motion of ideal membranes (with no damping and stiffness terms) is governed by a wave equation. As a consequence, their dispersion equation is of the form $\omega = kc_m$, where $c_m = \sqrt{\tau/\rho_m h}$ is the transverse wave speed (see Chap. 1). In timpani membranes, the tension and density are such that usually we have $c_m < c$. In practice, the wave speed is of the order of $100\,\mathrm{m\,s^{-1}}$ for timpani.

As a consequence, the dispersion curve of the membrane is a straight line with a lower slope than for the air, and there is no intersection between both curves (see Fig. 13.8). In practice, however, timpani heads (like nylon guitar strings) have a nonzero elasticity modulus. Therefore, the dispersion equation is written:

$$\omega = \sqrt{\frac{Dk^4 + \tau k^2}{\rho_m h}}, \tag{13.52}$$

and it becomes possible to define a critical frequency. The dispersion equation for a prestressed plate is written in the form similar to (13.52). If the plate is subjected to a compression ($\tau < 0$), then its critical frequency increases. Conversely, if the plate is subjected to a tension ($\tau > 0$), its critical frequency decreases. In conclusion, it is checked on this example that introducing any kind of stiffening effect in the plate globally contributes to yield favorable conditions for the radiation.

13.3.4 Pressure, Velocity, and Acoustic Power

In order to show the relevance of the critical frequency on the radiation efficiency, for the infinite plane plate in air, both the pressure and acoustic velocity in the fluid

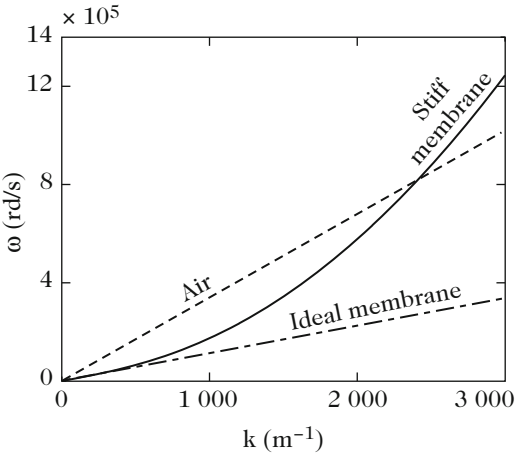

Fig. 13.8 Dispersion curves for stiff membranes and prestressed plates. *Dashed line*: air dispersion. *Dash-dotted line*: dispersion curve of an ideal membrane with density $\rho_m = 1.05 \times 10^3$ kg m^{-3}, thickness $h = 0.25$ mm, and tension $\tau = 3325$ N m^{-1}. *Solid line*: dispersion of the same membrane taking the Young's modulus $E = 3 \times 10^9$ N m^{-2} and the Poisson's coefficient $\nu = 0.4$ into account. Notice that, in this latter case, a critical frequency exists though it has a rather high frequency (127 kHz)

need to be calculated explicitly. This, in turn, will allow the calculation of sound intensity and acoustic power.

We look for a pressure field of the form $P(x, y) = P_0 e^{-j(k_x x + k_y y)}$. The Helmholtz equation (13.47) then yields $k^2 = k_x^2 + k_y^2$. In addition, the condition of continuity on the plate (13.48) imposes $k_x = k_B$, so that:

$$k_y^2 = k^2 - k_B^2 \quad \text{and} \quad P_0 = \rho c V_0 \frac{k}{k_y}. \tag{13.53}$$

As a consequence, the pressure and velocity fields are written:

$$\begin{cases} P(x, y, \omega) = \rho c V_0 \dfrac{k}{k_y} e^{-j(k_x x + k_y y)}, \\ V_x(x, y, \omega) = -\dfrac{1}{j\omega\rho} \dfrac{\partial P}{\partial x} = V_0 \dfrac{k_B}{k_y} e^{-j(k_x x + k_y y)}, \\ V_y(x, y, \omega) = -\dfrac{1}{j\omega\rho} \dfrac{\partial P}{\partial y} = V_0 e^{-j(k_x x + k_y y)}. \end{cases} \tag{13.54}$$

The first equation in (13.53) shows that the k_y component of the wavenumber is real if $k > k_B$, and purely imaginary otherwise.

For a given frequency, the first so-called *supersonic* case is obtained when the acoustic wavelength $\lambda = 2\pi/k$ is less than the elastic wavelength $\lambda_B = 2\pi/k_B$.

Figure 13.6 shows that this situation is obtained when the frequency of vibration of the plate is higher than its critical frequency. In terms of wave speed, this amounts to saying that $c_B = \omega/k_B > c = \omega/k$, which justifies the designation of *supersonic*. Conversely, when the acoustic wavelength $\lambda = 2\pi/k$ is higher than the elastic wavelength in the plate $\lambda_B = 2\pi/k_B$ or, equivalently, when the driving frequency is less than the critical frequency, the elastic wave speed is lower than the speed of sound, and this corresponds to the so-called *subsonic* case. These two situations are now examined with more details.

13.3.4.1 Supersonic Case

The supersonic case is illustrated in Fig. 13.9. With $k_y = \sqrt{k^2 - k_B^2}$, the pressure is written:

$$P(x, y) = \rho c V_0 \frac{k}{\sqrt{k^2 - k_B^2}} e^{-j(k_B x + \sqrt{k^2 - k_B^2} y)}. \tag{13.55}$$

The wave vector (indication the direction of propagation) is given by the angle θ defined by:

$$\sin\theta = \frac{k_B}{k} = \sqrt{\frac{\omega_c}{\omega}}. \tag{13.56}$$

As the frequency increases, the angle θ between the direction of propagation and the vector normal to the plate decreases. The direction of propagation then tends

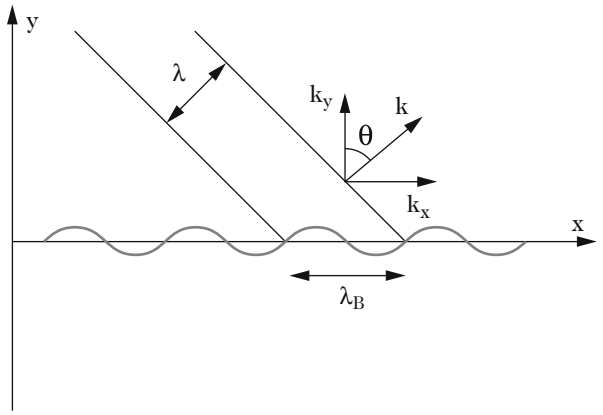

Fig. 13.9 Supersonic case. When the acoustic wavelength λ is less than the elastic wavelength λ_B in the plate, the acoustic wave radiated by the plate propagates in the direction θ. As the frequency increases, the angle θ decreases, and thus the propagation tends to be more and more perpendicular to the plate

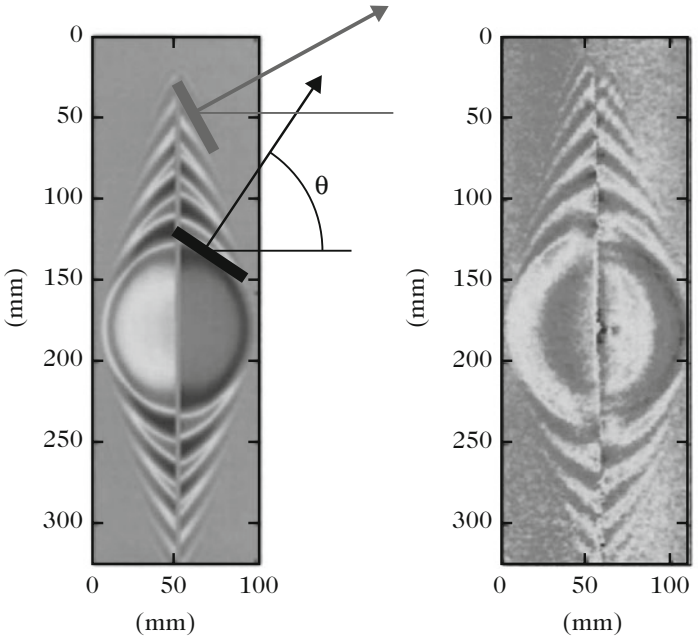

Fig. 13.10 Radiation of a plate excited by an impact in its center. (*Left*) simulation. (*Right*) measurements. The plate is perpendicular to the plane of the figure. The angle θ between the direction of propagation and the vector normal to the plate decreases from the center to the edges, consecutive to the increase of propagation speed with frequency. See also the insert on the "optical measurements of sound fields" in the next section. After [32]

to become progressively perpendicular to the plate. In contrast, as the vibration frequency decreases and tends to the critical frequency of the plate (with $f \geq f_c$), then the acoustic wave progressively tends to be confined to the plate plane.[7]

This property is clearly visible in Fig. 13.10 which shows a comparison between measurements and simulation for a plate excited by an impact in its center. As a

[7]Here, an interesting link can be made with the linear array of monopoles shown in Fig. 12.7. It was shown in the previous chapter that, as the number N of monopoles tend to infinity, then the direction of radiation tends to $\Theta = 0$, which is equivalent to $kd\cos\theta = \varphi$. This can only occur under the condition $|\varphi| < kd$. In the present example of the plate, the definition of the angle θ is modified, so that we must here convert the $\cos\theta$ of the monopole array in $\sin\theta$, which yields

$$\sin\theta = \frac{\varphi}{kd}.$$

For the plate, the phase shift φ between two consecutive "monopoles" is given here by $k_B d = \varphi$. As d tends to zero, we find Eq. (13.56) again. This shows that the linear array of monopoles is of the *supersonic* type. We can further add that if a condition such as $|\varphi| > kd$ would have been obtained as N tends to infinity, then no radiation would have exist in the far field, because Θ could not be zero. This remark will be useful in Chap. 14 to understand why there is no critical frequency in wind instruments.

result of the impact force, flexural waves propagate from the center to the edges. According to the elastic dispersion relationship, the high frequencies propagate faster than the low frequencies. For this reason, the angle θ between the vector normal to the plate and the direction of propagation decreases from the impact point to the edge.

The mean value of the acoustic power radiated per unit area is obtained by a classical method:

$$\langle \mathscr{P}_a \rangle = \frac{1}{2}\mathscr{R}e\{PV_y^\star\} = \frac{1}{2}\rho c V_0^2 \frac{k}{\sqrt{k^2 - k_B^2}} = \frac{1}{2}\rho c V_0^2 \frac{1}{\sqrt{1 - \frac{\omega_c}{\omega}}}. \tag{13.57}$$

The *radiation efficiency* $\sigma(\omega)$ is defined as the ratio between the mean value of the power radiated by the plate and the power obtained for an identical plate with the same area vibrating with a uniform velocity V_0. Here, we have (see Fig. 13.11):

$$\sigma = \frac{\langle \mathscr{P}_a \rangle}{\frac{1}{2}\rho c V_0^2} = \frac{k}{\sqrt{k^2 - k_B^2}} = \frac{1}{\sqrt{1 - \frac{\omega_c}{\omega}}}. \tag{13.58}$$

In summary, it has been shown that the infinite plate can radiate acoustic energy for the frequencies above the critical frequency. As the frequency $f > f_c$ becomes closer to the critical frequency, then the radiation efficiency increases and the direction of propagation tends to the plate plane. Notice that the simple theory presented here predicts that $\langle \mathscr{P}_a \rangle$ can tend to infinity. In the reality, the acoustic power is bounded both by the internal losses and by the finite size of the plate, as shown in the next sections.

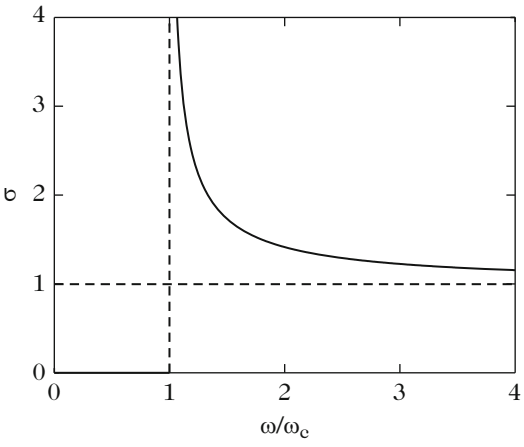

Fig. 13.11 Radiation efficiency of the infinite plate as a function of frequency

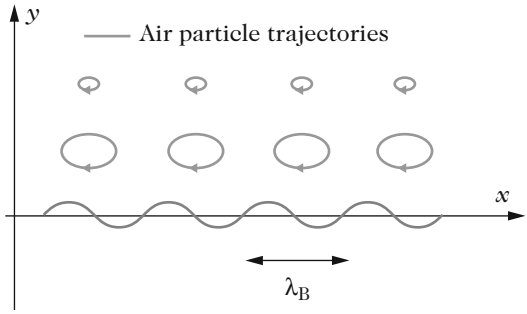

Fig. 13.12 Subsonic case. The trajectories of the air particles are elliptic, with axes decreasing exponentially with the distance from the plate plane

13.3.4.2 Subsonic Case

The subsonic case corresponds to the situation shown in Fig. 13.12. In this case, we have $k_y = -j\sqrt{k_B^2 - k^2}$, and the acoustic variables are written:

$$\begin{cases} P(x,y) = j\rho c V_0 \dfrac{k}{\sqrt{k_B^2 - k^2}} e^{-jk_B x} e^{-\sqrt{k_B^2 - k^2}\,y}, \\ V_x(x,y) = jV_0 \dfrac{k_B}{\sqrt{k_B^2 - k^2}} e^{-jk_B x} e^{-\sqrt{k_B^2 - k^2}\,y}, \\ V_y(x,y) = V_0 e^{-jk_B x} e^{-\sqrt{k_B^2 - k^2}\,y}. \end{cases} \tag{13.59}$$

The pressure modulus decreases exponentially with the distance y. The exponent increases with the ratio between the acoustic wavelength and the elastic wavelength. From a physical point of view, this means that there is destructive interferences between the neighboring "dipoles" of the plate over one given acoustic wavelength λ.

Examining now the acoustic velocity sheds useful light on the underlying physics of the subsonic case. It is seen in Eq. (13.59) that both components of the velocity vector are in quadrature and, in general, with different amplitudes. As a consequence the trajectories of the particles are elliptic. The motion is then confined locally and there is no transmission of energy from plane to plane as in the propagative case. In addition, the area of the ellipses decrease exponentially with the distance to the plate. The quantity $1/\sqrt{k_B^2 - k^2}$ gives a measure of the "thickness" of this evanescent field. It can be seen that this thickness decreases as the two wavelengths (elastic and acoustic) are more and more apart from each other. Finally, one can easily check that the mean value of the acoustic power $\langle \mathscr{P}_a \rangle$ is zero in the subsonic case, since the product $PV_y^\star$ is purely imaginary.

Let us now conclude this paragraph with the description of an experiment. It can be observed that if a second plate made of porous (absorbing) material is

placed close to the first vibrating plate, then the radiation losses increase, which induces an increase of damping for the elastic vibrations in the first plate. In order to demonstrate this phenomenon in a rigorous manner, the reader is invited to reconsider the previous mathematical derivations with a complex structural wavenumber k_B [10]. In short, this additional damping is due to the fact that, close to the plate, the energy contained in the elliptic motion of the particles is transformed into heat in the porous material. Benefit of this well-known phenomenon was taken, for example, in the plate reverberators used in the past in the recording studio for adding artificial reverberation effects [2].

Optical Measurements of Sound Fields

The figure shown in Fig. 13.10-(right) was obtained by means of optical measurements of the acoustic pressure [32]. A first instantaneous image of the sound field is made with a laser, for the air at rest. In this case, the optical index is n_0. A rubber bullet then hits the plate: as a result a transient sound pressure p is generated in the vicinity of the plate. A second image is recorded with the same laser, at a very short time t after the impact. In accordance with the Gladstone–Dale law, the optical index field is then governed by the equation:

$$n - 1 = K\rho, \tag{13.60}$$

where K is the Gladstone constant, and ρ the density of the fluid. The density is linked to the sound pressure by the adiabatic equation of state (see Chap. 1). Due to the index variation consecutive to the propagation of the sound wave, the optical path in the z-direction (the plane of Fig. 13.10) is modified by the quantity:

$$\Delta L = \int [n(x, y, z) - n_0]\ dz. \tag{13.61}$$

As a consequence, the phase shift undergone by the laser beam with wavenumber k_l is $\Delta\Phi = k_l \Delta L$. The superposition of both images generates the fringes of interference shown in Fig. 13.10.

13.3.5 Acoustic Loading of the Plate

As for the pulsating sphere in the previous chapter, the radiation impedance (or acoustic loading impedance) per unit area of the plate is defined by the ratio of the pressure divided by the normal acoustic velocity in the plate plane (in $y = 0$). For the supersonic case, Eq. (13.55) yields

$$Z(x,0) = \rho c \frac{k}{\sqrt{k^2 - k_B^2}} = \rho c \frac{1}{\sqrt{1 - \frac{\omega_c}{\omega}}}, \tag{13.62}$$

Since k is larger than k_B, the radiation impedance is purely resistive and equal to $R_a = \rho c \sigma(\omega)$. This radiation resistance is thus proportional to the radiation efficiency. Conversely, in the subsonic case, a purely imaginary radiation impedance is obtained

$$Z(x,0) = \rho c \frac{jk}{\sqrt{k_B^2 - k^2}} = j\rho\omega \frac{1}{\sqrt{k_B^2 - k^2}}. \tag{13.63}$$

which corresponds to an acoustic mass of the form:

$$M_a = \rho \frac{1}{\sqrt{k_B^2 - k^2}}, \tag{13.64}$$

This result quantifies the inertial loading of the fluid on the plate.

Remark. In this paragraph, only the radiation on one side of the plate was considered, in the positive half-space. In reality, notice that the infinite plate also radiates another sound field, in opposite phase, in the negative half-space.

13.3.6 Dispersion Equation for the Acoustically Loaded Plate

In order to evaluate and quantify the influence of the acoustic field on the plate, its flexural equation of motion needs to be modified through introduction of the pressure forces on each side of the plate, as follows:

$$-\omega^2 \rho_p h W + D \frac{d^4 W}{dx^4} = -P(x, 0^+, \omega) + P(x, 0^-, \omega). \tag{13.65}$$

As previously, the pressure terms are governed by the Helmholtz equation, and the continuity of the normal velocity is expressed by means of the Euler equation. These classical derivations are not detailed here. It is assumed that the plate radiates in the air on both sides.

The demonstration is conducted in the case of a forcing frequency ω. The unknown is the flexural wave number, denoted γ_B in order to make a distinction with the case presented in Sect. 13.3.4 where the acoustic loading was ignored. According to the results obtained in Eq. (13.54), the equation of dispersion becomes

$$D(\gamma_B, \omega) = -\frac{2j\rho}{\sqrt{k^2 - \gamma_B^2}} + \rho_p h \left(1 - \frac{D\gamma_B^4}{\rho_p h \omega^2}\right) = 0. \tag{13.66}$$

The first term in Eq. (13.66) accounts for the acoustic loading of the fluid. If the plate radiates in a light fluid (which is usually the case for a fluid with a "small" density ρ compared to the density of the plate), then we have $\gamma_B \simeq k_B$ (see Sect. 13.3.3).

It is often of interest to write the equation of dispersion (13.66) in a dimensionless form, using the following reduced variables:

$$\Omega = \frac{\omega}{\omega_c} \quad ; \quad \tau = \sqrt{\frac{c^2}{c_b^2} - 1} \quad ; \quad \varepsilon = \frac{2\rho c}{\omega_c \rho_p h}, \tag{13.67}$$

where $c_b = \omega/\gamma_B$ is the speed of the flexural waves for the acoustically loaded plated. After some derivations, the following equation is obtained [21]:

$$\tau^5 + 2\tau^3 + \left(1 - \Omega^{-2}\right)\tau - \varepsilon\Omega^{-3} = 0. \tag{13.68}$$

It can be shown that Eq. (13.68) has five roots. Only two of them are physically relevant for the radiation of the loaded plate. Compared to the supersonic case presented in Sect. 13.3.4, these roots are complex, with a positive imaginary part. This means that the elastic wave is damped in the plate, due to the radiation losses.

For stringed instruments, the order of magnitude for the physical parameters are the following: $f_c = 1\,\text{kHz}$, $\rho_p = 10^3\,\text{kg/m}^3$, $h = 1\,\text{mm}$, $\rho = 1.2\,\text{kg/m}^3$, and $c = 340\,\text{m/s}$. As a consequence, the parameter ε which quantifies the acoustic loading is equal to 0.15.

13.3.7 Radiation of a Point-Excited Plate

13.3.7.1 One Step Backwards: Back to the Plate Vibrations, Ignoring the Acoustic Loading

The particular case of an infinite point-excited plate is examined below. This is a very pertinent example in musical acoustics, since it accounts well for the practical situation of a soundboard excited by a string, at least during the time interval before the first reflections at the boundaries.

The geometry of the problem is shown in Fig. 13.13. For convenience, the problem is solved in polar coordinates, taking advantage of the axial symmetry. In the Fourier domain, the flexural equation of motion is written:

$$D\left(\frac{d^2}{dr^2} + \frac{1}{r}\frac{d}{dr}\right)^2 W - \rho_p h\omega^2 W = Q(r), \tag{13.69}$$

where the source term $Q(r)$ has the dimension of a surface density of force and is defined by:

$$\int_0^{2\pi} \int_0^{\infty} Q(r) r dr d\theta = F_0, \tag{13.70}$$

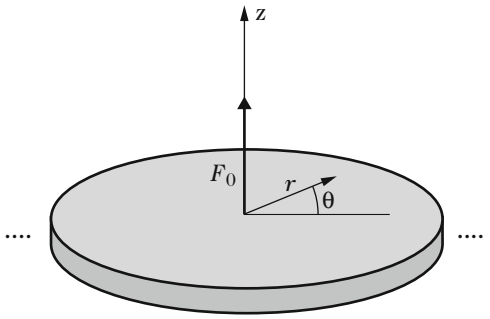

Fig. 13.13 Point-excited vibrating plate

which yields

$$Q(r) = \frac{F_0 \delta(r)}{2\pi r}. \tag{13.71}$$

This class of axisymmetrical problem can be solved with the Hankel transform of zero-order, defined as:

$$\hat{f}(\gamma) = \int_0^\infty f(r) r J_0(\gamma r) dr, \tag{13.72}$$

where J_0 is the zero-order Bessel function of the first kind [1]. Applying this transform to the equation of motion of the plate (13.69) yields the Hankel function of the displacement:

$$\hat{W}(\gamma) = \frac{F_0}{2\pi} \frac{1}{D\left(\gamma^4 - k_B^4\right)} \quad \text{with} \quad k_B^4 = \frac{\rho_p h \omega^2}{D}. \tag{13.73}$$

The plate displacement is derived from the inverse Hankel transform:

$$W(r) = \int_0^\infty \hat{W}(\gamma) \gamma J_0(\gamma r) d\gamma, \tag{13.74}$$

which yields, finally:

$$W(r) = \frac{F_0}{2\pi D} \int_0^\infty \frac{J_0(\gamma r)}{\gamma^4 - k_B^4} \gamma d\gamma. \tag{13.75}$$

The integral in (13.75) yields: (see [21, 31, 40]):

$$W(r) = \frac{j F_0}{8\omega \sqrt{\rho_p h D}} \left[H_0^{(2)}(k_B r) - \frac{2j}{\pi} K_0(k_B r) \right], \tag{13.76}$$

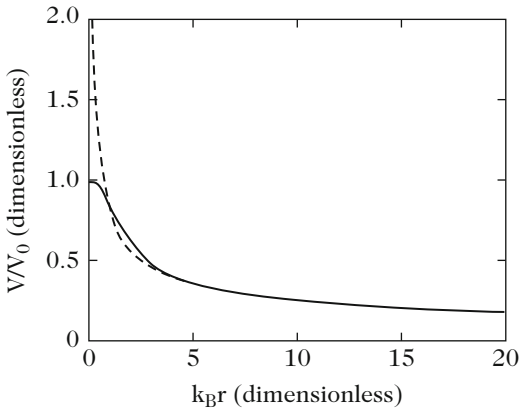

Fig. 13.14 Point-excited infinite plate at constant frequency. Modulus of the plate velocity V as a function of the distance from the excitation point. *Dotted line*: approximate solution, valid for $k_B r > 4$. $V_0 = |j\omega W(0)|$

where $H_0^{(2)}$ is the zero-order Hankel function of the second kind defined by:

$$H_0^{(2)}(x) = J_0(x) - jY_0(x). \tag{13.77}$$

In this expression, $Y_0(x)$ is the zero-order Bessel function of the second kind, and $K_0(x)$ is the modified zero-order Hankel function [1].

Figure 13.14 shows the modulus $V = j\omega W$ of the plate velocity as a function of the normalized distance $k_B r$, and the approximate solution:

$$V \simeq \frac{F_0}{\sqrt{\rho_p h D}} \sqrt{\frac{2}{\pi k_B r}}, \tag{13.78}$$

which is valid for $k_B r > 4$.

At the excitation point, the term between square brackets in Eq. (13.76) is equal to one. The driving impedance is defined by the fraction:

$$Z_p(0) = \frac{F_0}{j\omega W(0)} = 8\sqrt{\rho_p h D} = 4h^2 \sqrt{\frac{\rho_p E}{3(1-\nu^2)}}. \tag{13.79}$$

The remarkable result here is that this impedance is real and does not depend on frequency. It depends on the thickness and on the material properties of the plate, only. Notice, however, that this result is only true for a thin plate (Kirchhoff–Love model). The driving admittance (or mobility) is given by $Y_p(0) = 1/Z_p(0)$.

The expression (13.79) can be used for validating measurements of driving impedance (or admittance) of finite damped isotropic thin plates, in the high frequency range. In general, the losses increase with frequency, so that the returning waves reflected at the boundaries can be neglected. Equation (13.79) can then be viewed as an asymptotic limit. Benefit will be taken from this expression at the end

of the chapter for defining a "merit index" for stringed instruments, whose interest is to help in the selection of appropriate materials for the soundboard.

A similar expression can be found for anisotropic plates [4, 7]. For an orthotropic plate, for example, the following approximation is usually admitted:

$$Z_p(0) \simeq 4h^2 \sqrt{\frac{\rho_p [E_1 E_2]^{1/2}}{3(1-\nu^2)}}, \tag{13.80}$$

where E_1 is the Young's modulus in the direction of the fibers, and E_2 the modulus perpendicular to the fibers [19].[8]

Taking further the structural losses into account, then the Young's modulus becomes complex of the form $E[1 + j\eta(\omega)]$. For most materials used in instrument making, η increases with frequency. As a consequence, the modulus $|Z(\omega)|$ increases and the admittance $|Y(\omega)|$ decreases with frequency.

Most soundboards of musical instruments are not homogeneous, due to the presence of ribs glued on one side. The driving-point mobility of isotropic plates reinforced by periodic ribs was investigated by Nightingale and Bosmans [28]. One conclusion of this study is that the measured mobility greatly depends on the distance between the driving point and the closest rib, as long as this distance is small compared to the flexural wavelength. For a driving-point close to a rib, the measured real part of $Y_p(0)$ corresponds to the mobility of the rib (beam). As soon as the rib-driving-point distance becomes larger than the wavelength, then the measured mobility tends to the theoretical value obtained for a plate with constant thickness. These results are of interest for understanding and interpreting the driving-point mobility measurements performed on a piano, for example.

Impulse Excitation

For a given load $q(r, t)$ in the time domain, the governing equation for the plate displacement $w(r, t)$ is

$$D\left(\frac{\partial^2}{\partial r^2} + \frac{1}{r}\frac{\partial}{\partial r}\right)^2 w + \rho_p h \frac{\partial^2 w}{\partial t^2} = q(r, t). \tag{13.81}$$

Let us assume that the plate is initially at rest ($w(r, 0) = \dot{w}(r, 0) = 0$). Denoting $b^2 = D/\rho_p h$, the particular case of an impulse excitation of the form:

(continued)

[8] In this expression, it is assumed that the Poisson's coefficients are identical in both directions.

$$q(r,t) = 8b\rho_p h f(r)\delta(t), \quad \text{where} \quad \int_0^\infty 2\pi r f(r) dr = 1 \quad \text{so that} \quad f(r) = \frac{\delta(r)}{2\pi r}. \tag{13.82}$$

is examined. The full calculation was done by Graff [17]. The following solution is obtained

$$w(r,t) = \frac{2}{\pi}\int_0^t \frac{u}{t-u} \sin\left[\frac{r^2}{4b(t-u)}\right] du. \tag{13.83}$$

The displacement can be rewritten in the form:

$$w(r,t) = 1 - \frac{2}{\pi}\mathrm{Si}\left(\frac{r^2}{4bt}\right) \quad \text{where} \quad \mathrm{Si}(x) = \int_0^x \frac{\sin z}{z} dz, \tag{13.84}$$

and where $\mathrm{Si}(x)$ denotes the *sine integral* function.

Figure 13.15 shows the motion of the plate at a given fixed time t_0, and the temporal evolution of one particular point. It shows, among other things, the presence of a precursor where the most rapid oscillations arrive first, due to the properties of the dispersion equation.

13.3.7.2 Fluid-Loaded Plate

The purpose of this paragraph is to evaluate the influence of the fluid (acoustic field) on the plate for a harmonic excitation on a single point. The results presented below should be compared to those obtained for a plate in vacuo (see Sect. 13.3.7.1).

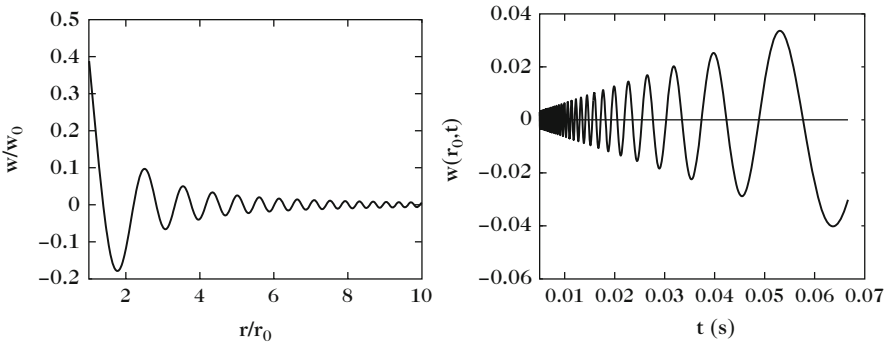

Fig. 13.15 Impulse excitation of a plate. (*Left*) Global motion of the plate at a fixed time $t = t_0$. (*Right*) Temporal evolution of the plate displacement at a given point $r = r_0$

Taking now the radiated pressure exerted on both sides of the plate into account, the equation of motion is modified as follows:

$$D\left(\frac{d^2}{dr^2}+\frac{1}{r}\frac{d}{dr}\right)^2 W-\rho_p h\omega^2 W=\frac{F_0\delta(r)}{2\pi r}-P(r,z=0^+)+P(r,z=0^-), \tag{13.85}$$

where the z-axis is perpendicular to the plate. The plate is located in the plane $z=0$. As in Sect. 13.3.7.1, this equation can be solved by means of the Hankel transform [17, 40]. Denoting $\hat{P}(\gamma,0)$ the Hankel transform of the pressure, and $\hat{W}(\gamma)$ the transform of the displacement, we get

$$D\left(\gamma^4-k_B^4\right)\hat{W}(\gamma)=-\hat{P}(\gamma,0^+)+\hat{P}(\gamma,0^-)+\frac{F_0}{2\pi}. \tag{13.86}$$

Noticing that the first term in the left-hand side of Eq. (13.86) has the dimension of a pressure, the Hankel transform of the driving-point impedance of the plate can be defined as:

$$\hat{Z}_p(\gamma)=\frac{D\left(\gamma^4-k_B^4\right)}{j\omega}. \tag{13.87}$$

According to (13.62), the pressure is written:

$$\hat{P}(\gamma,0)=j\omega\hat{Z}_a(\gamma)\hat{W}\quad\text{with}\quad\hat{Z}_a(\gamma)=\rho\frac{\omega}{\sqrt{k^2-\gamma^2}}. \tag{13.88}$$

Equation (13.86) becomes

$$j\omega\hat{W}(\gamma)=\frac{F_0}{2\pi}\frac{1}{\hat{Z}_p(\gamma)+2\hat{Z}_a(\gamma)}. \tag{13.89}$$

Through inverse Hankel transform, the displacement of the plate is derived

$$W(r)=\frac{F_0}{j2\pi\omega}\int_0^\infty\frac{\gamma J_0(\gamma r)}{\hat{Z}_p(\gamma)+2\hat{Z}_a(\gamma)}d\gamma. \tag{13.90}$$

This last equation can be solved using contour integration in the complex plane, or numerically [21]. The Hankel transform of the radiated pressure is obtained through the Helmholtz equation combined with the continuity of the normal velocities on the plate, as in Sect. 13.3.4. These derivations are not detailed further here. Finally, we obtain

$$\text{for } z>0\quad\hat{P}(\gamma,z)=j\omega\hat{Z}_a(\gamma)\hat{W}(\gamma)e^{-jz\sqrt{k^2-\gamma^2}}, \tag{13.91}$$

which yields, in turn:

$$P(r,z) = \frac{F_0}{2\pi}\int_0^\infty \frac{\hat{Z}_a(\gamma)}{\hat{Z}_p(\gamma)+\hat{Z}_a(\gamma)}\gamma J_0(\gamma r)e^{-jz\sqrt{k^2-\gamma^2}}d\gamma. \tag{13.92}$$

The far field pressure $P(r,z)$ can be derived by using the method of stationary phase [21]. With the change of coordinates $r = R\sin\theta$ and $z = R\cos\theta$, the following expression is obtained for the half-plane $z > 0$, and for $kR \gg 1$:

$$P(R,\theta) = \frac{jkF_0e^{-jkR}}{2\pi R}\frac{\cos\theta}{1+jkh\frac{\rho_p}{\rho}\cos\theta\left[1-\frac{\omega^2}{\omega_c^2}\sin^4\theta\right]}. \tag{13.93}$$

Discussion

A few remarks can be made with regard to the expression of the far field pressure calculated in (13.93):

- In the direction perpendicular to the plate ($\theta = 0$), the pressure reduces to:

$$P(R,0) = \frac{jkF_0e^{-jkR}}{2\pi R}\frac{1}{1+jkh\frac{\rho_p}{\rho}}. \tag{13.94}$$

  This result shows that, due to the loading, the pressure is multiplied by a correcting factor which depends on the surface density $\rho_p h$ of the plate only (in particular, this factor does not depend on the plate rigidity D). In other words, *the far field pressure of a plate is similar to the one radiated by a membrane with the same surface density*.
- In addition, if the plate can be considered as sufficiently thin or, equivalently, that the frequency is sufficiently small so that one can assume that $kh\frac{\rho_p}{\rho} \ll 1$, then we have

$$P(R,0)_{\text{lim}} \approx \frac{jkF_0e^{-jkR}}{2\pi R}. \tag{13.95}$$

  Under these assumptions, it can be seen that the pressure is equivalent to the one radiated by a point source with imposed force F_0.
- For frequencies below the critical frequency, $P(R,0)$ is the maximum of the pressure. In contrast, in the supersonic range, pressure maxima can exist with larger amplitudes than $P(R,0)$ in some particular directions θ_c defined by the condition:

$$\theta_c = \sin^{-1}\left(\frac{\omega_c}{\omega}\right)^{1/2}. \tag{13.96}$$

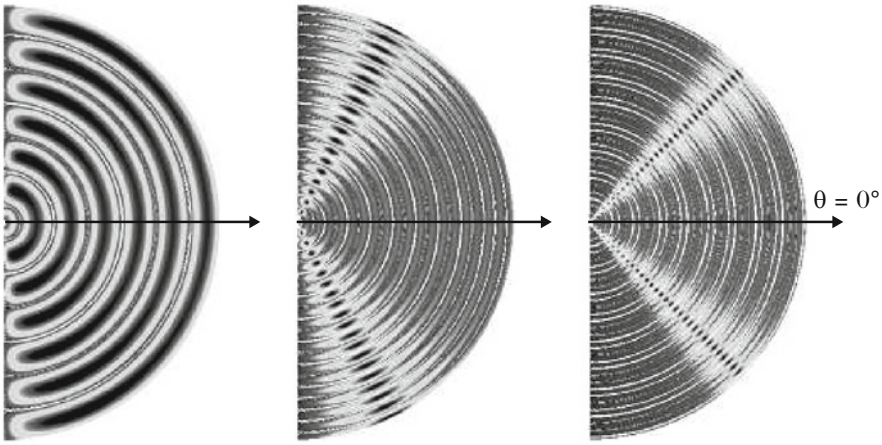

Fig. 13.16 Pressure field radiated by a thin isotropic plate loaded by the air. (*Left*) $f = 0.4f_c$; (*Center*) $f = 1.2f_c$; (*Right*) $f = 2.0f_c$. The horizontal arrow is perpendicular to the plate plane and corresponds to the direction $\theta = 0$. The *light-gray* zones (for $f > f_c$, *middle and right* figures) indicate the directions of maximum pressure. For $f < f_c$ (*left* figure), there are no preferential directions, and the directivity pattern is close to the radiation pattern of a dipole [31]

Figure 13.16 shows the sound pressure radiated by an isotropic plate, for different frequencies (below and above the critical frequency of the plate).

- In practice, the magnitude of the pressure is limited by the internal damping inside the plate. This is particularly true in the supersonic range, above the critical frequency.

13.4 Radiation from Finite Plates

In a number of past studies, it has been shown that finite plates are relevant to account for the radiation of stringed instruments, at least to a first approximation (see Fig. 13.17) [11]. In fact, it is plain that guitar, violin or piano soundboards cannot be strictly modeled as plates. Other components such as the ribs, the sound holes and the bridge, for example, and geometrical factors such as the curvature contribute to add perturbations in the model [15, 16]. However, the finite plate model is a good reference for presenting the basic principles that govern the structural acoustics of stringed and percussive instruments. It also yields interesting reference solutions which might be helpful in case of numerical approach. This explains why the radiation of finite plates is presented in detail below. The application of the results to real instruments, as well as the study of some particular modifying features will be examined later in this section.

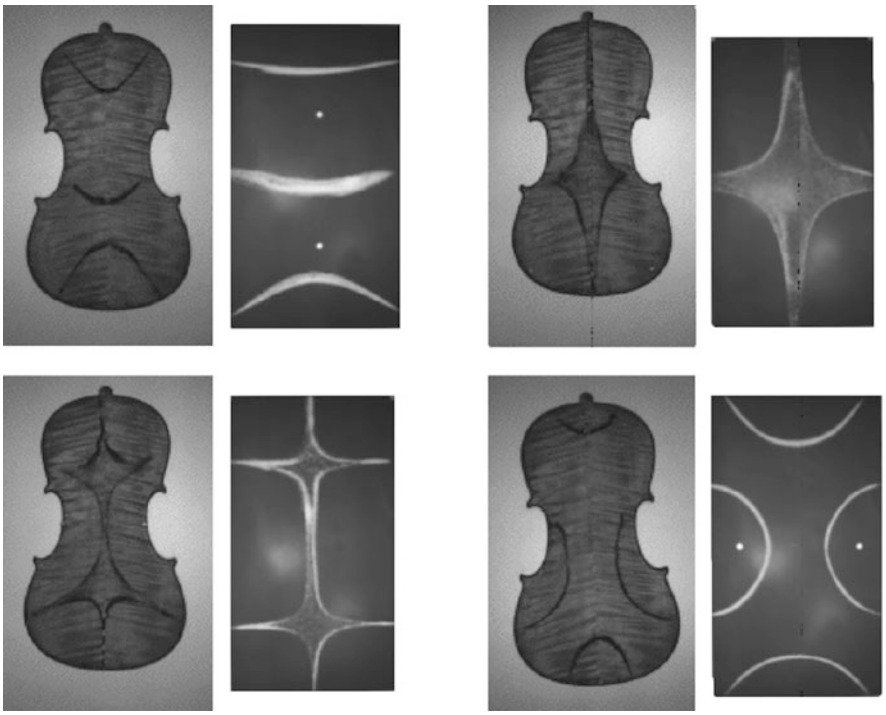

Fig. 13.17 Relevance of the plate model in the case of violin plates. A few low-order modal shapes of violin back plates are presented. These shapes are very similar to those of a metallic plate of comparable dimensions. The Chladni patterns were obtained in a similar way as for the guitar modes in Chap. 3. After [41]

13.4.1 Spatial Fourier Transform

The purpose of this section is to calculate the acoustic field radiated by a thin rectangular isotropic vibrating plate, simply supported along its edges. The vibratory properties of such a plate were presented in Chap. 3. It is assumed that the plate is inserted in an infinite rigid baffle, so that the Rayleigh formula presented in Chap. 12 can be used. It is also assumed that the observation point is located at a sufficiently large distance from the plate, in order to take advantage of the Fraunhofer approximation defined in the same chapter. The geometry of the problem is shown in Fig. 13.18. W denotes the flexural displacement of the plate. Cartesian coordinates are used. All derivations are made for an harmonic excitation of the plate with frequency ω. The radiated pressure is written:

$$P(\mathbf{r},\omega) = -\frac{\omega^2\rho}{2\pi r}\int_S W(x',y',\omega)e^{-jk|\mathbf{r}-\mathbf{r}'|}dS_{(\mathbf{r}')}, \tag{13.97}$$

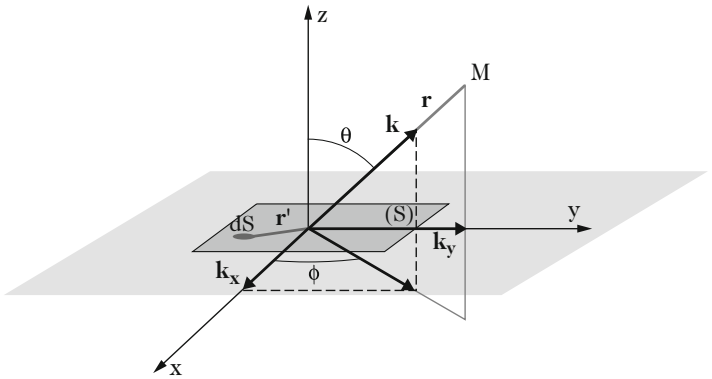

Fig. 13.18 Geometry used for calculating the radiation of a rectangular plate inserted in an infinite baffle. $k_x = k \sin\theta \cos\Phi$ and $k_y = k \sin\theta \sin\Phi$

which can be written, equivalently:

$$P(r, \theta, \Phi, \omega) = -\frac{\omega^2 \rho}{2\pi r} e^{-jkr} \int_S W(x', y', \omega) e^{+j(k_x x' + k_y y')} dx' dy', \tag{13.98}$$

with $k_x = k \sin\theta \cos\Phi$ and $k_y = k \sin\theta \sin\Phi$. A fundamental result is found in Eq. (13.98): if the distance between the observation point and the plate is large compared to the dimensions of the plate, then the radiated pressure is proportional to the *spatial Fourier transform* of the plate displacement:

$$P(r, \theta, \Phi, \omega) = -\frac{\omega^2 \rho}{2\pi r} e^{-jkr} \tilde{W}(k_x, k_y, \omega). \tag{13.99}$$

This property can be viewed as a generalization of the previously obtained result for the plane piston in Chap. 12.

13.4.2 Contribution of the Vibrating Modes to the Radiated Pressure

In what follows, the internal damping in the plate material and the reaction of the acoustic field against the plate are left temporarily aside. The displacement field if the plate is projected onto the its eigenmodes basis:

$$W(x, y, \omega) = \sum_{m=1}^{\infty} \sum_{n=1}^{\infty} A_{mn}(\omega) \phi_{mn}(x, y). \tag{13.100}$$

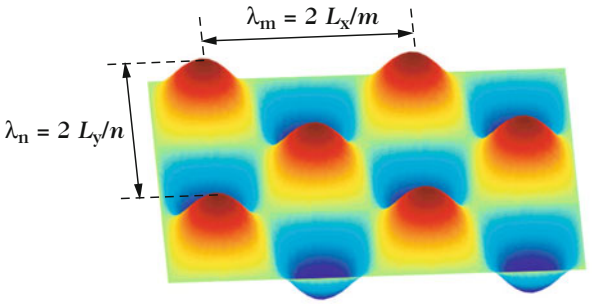

Fig. 13.19 Modal shape of a simply supported rectangular plate for ($m = 4, n = 3$). The respective quantities λ_m and λ_n determine the spatial periodicity along the x and y axis

For a simply supported plate of length L_x and width L_y, the eigenmodes are written:

$$\phi_{mn}(x,y) = \frac{2}{\sqrt{L_x L_y}} \sin\left(\frac{m\pi}{L_x}x\right) \sin\left(\frac{n\pi}{L_y}y\right) \tag{13.101}$$

where the normalization factor has been selected so that $\int_S \phi_{mn}^2 dS = 1$. An example of modal shape is shown in Fig. 13.19.

The contribution P_{mn} of the mode (m,n) to the total sound pressure is defined by:

$$P_{mn}(r,\theta,\Phi) = -\frac{\omega^2\rho}{2\pi r} e^{-jkr} A_{mn}\, \tilde{\phi}_{mn}(k_x,k_y,\omega). \tag{13.102}$$

Thus, the problem reduces to calculating the spatial Fourier transform of the modal shape $\phi_{mn}(x,y)$. This calculation is rather tedious by hand, though it becomes straightforward with currently available numerical tools. The result in the simple case presented here is written [40]:

$$P_{mn}(r,\theta,\Phi,\omega) = -\frac{\omega^2\rho}{r} e^{-jkr} A_{mn}\, \pi mn \sqrt{L_x L_y} \left[\frac{(-1)^m e^{+jk_x L_x} - 1}{(k_x L_x)^2 - m^2\pi^2}\right] \left[\frac{(-1)^n e^{+jk_y L_y} - 1}{(k_y L_y)^2 - n^2\pi^2}\right]. \tag{13.103}$$

For a given angular frequency ω, Eq. (13.103) shows that particular directions exist in space where the modal contribution P_{mn} is high. These directions fulfill the conditions $k_x L_x \approx m\pi$ and $k_y L_y \approx n\pi$.[9] The corresponding directions θ_{mn} and Φ_{mn} (also called *directions of spatial coincidence*) are given by:

[9] These values correspond to the maxima of the functions $\left|\frac{(-1)^m e^{+jk_x L_x}-1}{(k_x L_x)^2 - m^2\pi^2}\right|$ and $\left|\frac{(-1)^n e^{+jk_y L_y}-1}{(k_y L_y)^2 - n^2\pi^2}\right|$. Except for the lowest values of m and n, these maxima are close to $m\pi$ and $n\pi$.

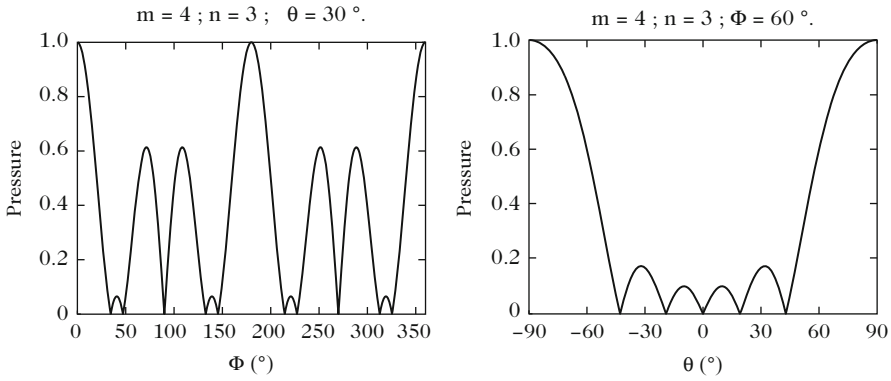

Fig. 13.20 Examples of spatial coincidence for the plate mode $m = 4$; $n = 3$, at a frequency of 1 kHz. $L_x = 1\,\text{m}$; $L_y = 0.6\,\text{m}$

$$k \sin\theta_{mn} \cos\Phi_{mn} = k_m = \frac{m\pi}{L_x} \quad \text{and} \quad k \sin\theta_{mn} \sin\Phi_{mn} = k_n = \frac{n\pi}{L_y}. \tag{13.104}$$

Examples of spatial coincidence are shown in Fig. 13.20. In addition, the pressure components P_{mn} are subjected to *frequency coincidence* through the expression of the modal amplitudes A_{mn}. In Chap. 3, it was shown that, for a plate excited with a force F at point (x_0, y_0), this amplitude is

$$A_{mn} = \frac{F}{\rho_p h} \frac{\phi_{mn}(x_0, y_0)}{\omega_{mn}^2 - \omega^2 + 2j\zeta_{mn}\omega\omega_{mn}}, \tag{13.105}$$

where the ω_{mn} are the eigenfrequencies of the plate, and ζ_{mn} the modal damping factors which are assumed to be small compared to unity. For simply supported rectangular plates, the eigenfrequencies are given by:

$$\omega_{mn} = \sqrt{\frac{D}{\rho_p h}} \left[\frac{m^2\pi^2}{L_x^2} + \frac{n^2\pi^2}{L_y^2} \right] = \sqrt{\frac{D}{\rho_p h}} \left[k_m^2 + k_n^2 \right]. \tag{13.106}$$

In summary, situations may occur where a plate mode is vibrating with high amplitude (frequency coincidence), although the corresponding sound pressure is low, if the condition of spatial coincidence is not fulfilled. In other words, resonant modes might not be always efficient in terms of radiated power. Different particular cases are now examined.

13.4.2.1 Radiated Sound Pressure

- For large wavelengths, i.e., for $k \to 0$ in (13.103), the pressure becomes

$$P_{mn} \to B_{mn} \frac{e^{-jkr}}{r}, \tag{13.107}$$

where B_{mn} depends only on ω. This means that the directivity index is constant. The pressure is similar to the one radiated by a pulsating sphere.

- In Eq. (13.104), one can see that the coincidence angles exist only if $k_n < k$ and $k_m < k$, since the sine and cosine functions are bounded by one. In terms of wavelengths, this means that the acoustic wavelength λ has to be smaller than $\lambda_m = 2L_x/m$ and $\lambda_n = 2L_y/n$ (see Fig. 13.19). For subsequent discussion, it is convenient to introduce the *structural* wavenumber $k_{mn} = \sqrt{k_m^2 + k_n^2}$. From Eq. (13.104), the directions θ_{mn} are given by:

$$\theta_{mn} = \sin^{-1} \frac{k_{mn}}{k}. \tag{13.108}$$

This shows that θ_{mn} exist under the additional condition $k_{mn} < k$, i.e., when the acoustic wavelength is smaller than the elastic wavelength in the plate. This is a generalization of the result obtained for an infinite plate. This condition can occur only for frequencies beyond the critical frequency defined in (13.51). It can be also checked that:

$$\Phi_{mn} = \tan^{-1} \frac{k_n}{k_m}. \tag{13.109}$$

Examples of two cases ($k_n < k$ with $k_m < k$ and $k_{mn} > k$, part; $k_n < k$ with $k_m < k$ and $k_{mn} < k$) are shown in Fig. 13.21.

- Some intermediate configurations also exist, corresponding to the cases where $k_n < k$ and $k_m > k$, or $k_n > k$ and $k_m < k$. In these cases, there are no maxima for Φ. However, one can observe maxima for the angles θ which fulfill the conditions:

$$\begin{cases} \text{for } k_n < k \text{ and } k_m > k \ : \ \theta_n = \sin^{-1}\left(\dfrac{k_n}{k\cos\Phi}\right), \\ \text{for } k_m < k \text{ and } k_n > k \ : \ \theta_m = \sin^{-1}\left(\dfrac{k_m}{k\cos\Phi}\right). \end{cases} \tag{13.110}$$

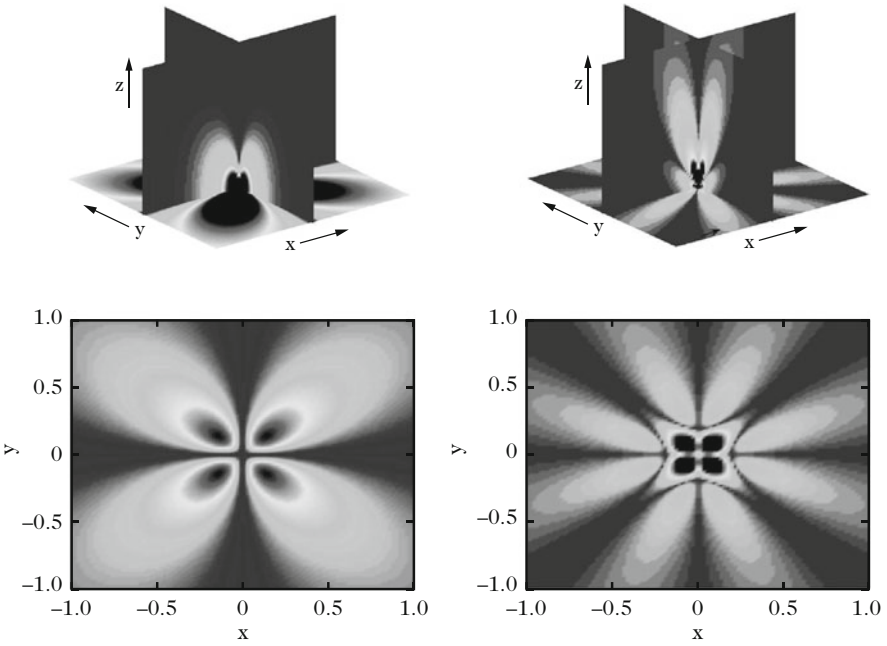

Fig. 13.21 Pressure radiated by some particular modes (m, n) of a simply supported rectangular plate. (*Left*) $k_n < k$ and $k_m < k$ and $k_{mn} > k$: the pressure vanishes in some directions (Φ) of the *horizontal* plane, but not in the *vertical* plane (θ). (*Right*) $k_n < k$ and $k_m < k$ and $k_{mn} < k$: the pressure vanishes for some particular directions in *both* the *horizontal* and *vertical* planes

13.4.2.2 Intermodal Radiation Impedances

Using the spatial Fourier transform of the displacement, the radiated pressure can be written alternatively [26]:

$$P(x, y, z, \omega)) = j\frac{\rho\omega^2}{4\pi^2}\int_{-\infty}^{+\infty}\int_{-\infty}^{+\infty}\frac{\tilde{W}(k_x, k_y)}{k_z}e^{-jk_z z}e^{j(k_x x + + k_y y)}\, dk_x dk_y,$$

$$\text{where} \quad k_z = \sqrt{k^2 - k_x^2 - k_y^2}. \tag{13.111}$$

Based on the modal expansion of the displacement (13.100), one can derive the surface pressure (in the plate plane $z = 0$):

$$P(x, y, 0, \omega) = \sum_{m,n}\sum_{r,s} j\omega A_{mn}(\omega) Z_{mnrs}(\omega)\phi_{rs}(x, y), \tag{13.112}$$

(continued)

where the Z_{mnrs} are the intermodal radiation impedance given by:

$$Z_{mnrs}(\omega) = \frac{\rho\omega}{4\pi^2}\int_{-\infty}^{+\infty}\int_{-\infty}^{+\infty}\tilde{\phi}_{mn}(k_x,k_y)\,\tilde{\phi}_{rs}(-k_x,-k_y)\,dk_x dk_y. \qquad (13.113)$$

The real part of the Z_{mnrs} corresponds to the dissipated acoustic power. The imaginary part accounts for the fluid loading. In free field, the imaginary part is positive and, in turn, the eigenfrequencies of the plate decrease compared to the in vacuo case. These expressions generalize the result obtained in Chap. 12 in the case of the plane piston. For "light" fluids, the reactive effects are often negligible, except for light and flexible structures (see Chap. 14).

In this section the comparison between acoustic and elastic wavenumber presented in Sect. 13.3 for infinite plates has been generalized to finite plates. The main difference between both cases is due to the fact that the elastic wavenumber can take only discrete values for finite plates. In addition, as a consequence of the spatial periodicity of the vibratory field on the plate, the magnitude of the pressure field is subjected to strong variations with regard to the direction of propagation in the air in the supersonic range. These directions vary a lot with the geometry of the mode. During normal playing of an instrument, different modes are excited successively. Consequently, the directivity of the instrument changes continuously.

13.4.3 Radiated Acoustic Power

13.4.3.1 Single Modal Contribution

The radiated acoustic power is calculated by integration of the flow of the acoustic intensity vector through a closed surface at a given distance r from the plate. The calculation is simple for a spherical surface in the far field. We get

$$\langle \mathscr{P}_a|_{mn}(\omega)\rangle = \frac{1}{2\rho c}\int_0^{2\pi}\int_0^{\pi/2}|P_{mn}(r,\theta,\Phi,\omega)|^2\, r^2\sin\theta\, d\theta\, d\Phi, \qquad (13.114)$$

where P_{mn} is given by (13.103). As for the infinite plate, the radiation efficiency is defined by the ratio:

$$\sigma_{mn}(\omega) = \frac{\langle \mathscr{P}_a|_{mn}(\omega)\rangle}{\frac{1}{2}\rho c L_x L_y \langle|\dot{W}_{mn}|^2\rangle}, \qquad (13.115)$$

where $\langle|\dot{W}_{mn}|^2\rangle$ is the mean quadratic velocity defined as:

$$\langle |\dot{W}_{mn}|^2 \rangle = \frac{1}{L_x L_y} \int_0^{L_x} \int_0^{L_y} |\dot{W}_{mn}(x, y, \omega)|^2 \, dxdy. \tag{13.116}$$

The efficiency σ_{mn} is proportional to the radiation resistance of the mode mn:

$$R_{amn}(\omega) = \frac{\langle \mathscr{P}_a|_{mn}(\omega) \rangle}{\frac{1}{2}\langle |\dot{W}_{mn}|^2 \rangle} = \rho c L_x L_y \sigma_{mn}(\omega). \tag{13.117}$$

In the particular case of the simply supported rectangular plate, the calculation based on (13.103) leads to the expression:

$$\sigma_{mn}(\omega) = \frac{16k^2 L_x L_y}{\pi^6 m^2 n^2} \int_0^{2\pi} \int_0^{\pi/2} \left(\frac{\left\{ \begin{matrix} \cos \\ \sin \end{matrix} \right\} \frac{k_x L_x}{2} \left\{ \begin{matrix} \cos \\ \sin \end{matrix} \right\} \frac{k_y L_y}{2}}{\left[\left(\frac{k_x L_x}{m\pi} \right)^2 - 1 \right] \left[\left(\frac{k_y L_y}{m\pi} \right)^2 - 1 \right]} \right)^2 \sin\theta d\theta d\phi. \tag{13.118}$$

In (13.118), the *cosine* function is used for odd values of m (resp. n), and the *sine* function is used for even values of these indices.

Figure 13.22 shows some examples of radiation efficiencies of a rectangular plate [38], as a function of the ratio:

$$\gamma = k/k_{mn} = \frac{k}{\sqrt{\left(\frac{m\pi}{L_x} \right)^2 + \left(\frac{n\pi}{L_y} \right)^2}}$$

For $k > k_{mn}$, the modal efficiencies tend to unity, as for the limiting case of the infinite plate.

For $k < k_{mn}$, σ_{mn} is weak but nonzero (as it was the case for infinite plates: see Fig. 13.11). Close examination shows that, depending on the values taken by m and n, two different situations may occur, depending whether the plate radiates by the edges or by the corners, as shown in the next section.

13.4.3.2 Edge and Corner Radiation

Figure 13.23 (left) shows a typical situation of corner radiation. This corresponds to the vibration of the plate at a frequency ω so that the following conditions are fulfilled:

$$k < k_{mn}, \; k_m = \frac{m\pi}{L_x} > k \quad \text{and} \quad k_n = \frac{n\pi}{L_y} > k.$$

In the case presented in Fig. 13.23, the contributions of the elementary "dipoles" on the plate to the radiated power are close to zero (see Chap. 12), except for the

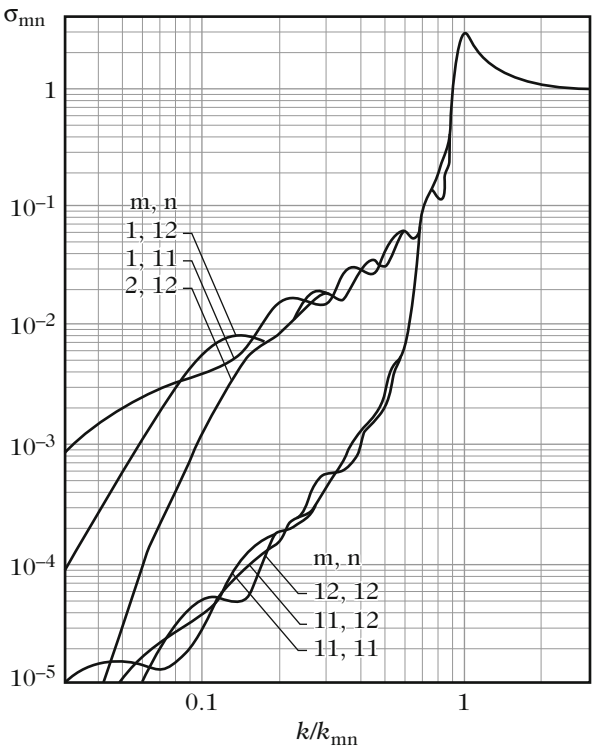

Fig. 13.22 Examples of modal radiation efficiencies σ_{mn} as a function of $\gamma = k/k_{mn}$ for a rectangular plate, after Wallace [38]. For $\gamma < 1$, the modes (1, 12), (1, 11), and (2, 12) are radiating only by the edges, whereas the modes (12, 12) (11, 11), and (11, 12) are radiating by the corners

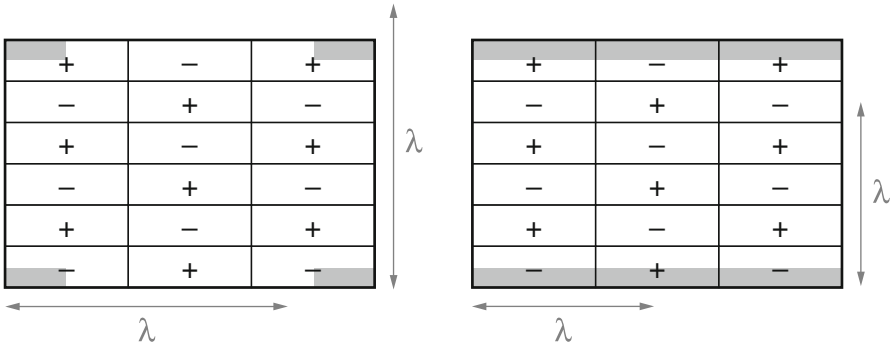

Fig. 13.23 (*Left*) Corner radiation of a rectangular plate: $\lambda > \lambda_m$ ($k < k_m$) and $\lambda > \lambda_n$ ($k < k_n$). (*Right*) Edge radiation of a rectangular plate: $\lambda < \lambda_m$ ($k > k_m$) and $\lambda > \lambda_n$ ($k < k_n$). Only the *gray* zones are efficient in terms of radiation. The radiation efficiency is close to zero in the other parts of the plate, since the distance between the centers of the zones (with opposite signs) is less than one wavelength. This is a consequence of the dipole properties demonstrated in Chap. 12

four zones at the corners since, in this latter case, the distance between the zones is larger than an acoustic wavelength. Similarly, the edge radiation corresponds to the conditions:

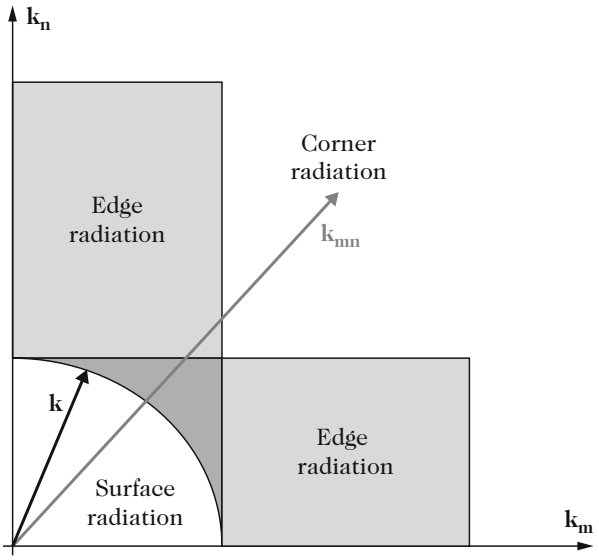

Fig. 13.24 Surface, edge, and corner radiation

$$k < k_{mn} \quad \text{and}$$
$$\left(k_m = \frac{m\pi}{L_x} < k \quad \text{and} \quad k_n = \frac{n\pi}{L_y} > k\right) \quad \text{or} \quad \left(k_m = \frac{m\pi}{L_x} > k \quad \text{and} \quad k_n = \frac{n\pi}{L_y} < k\right).$$

Here a similar situation as for the corner radiation is obtained, along the y axis only. The radiation efficiency only results from the gray zones situated close to the edges in $y = 0$ and $y = L_y$. In the case shown in Fig. 13.23, the acoustic wavelength λ is smaller than the spatial periodicity $\lambda_m = 2L_x/m$ of the mode along the x axis and, as a consequence, the different contributions to the radiation do not cancel each other in this direction.

A summary of all possible situations is shown in Fig. 13.24. In addition to the cases of edge and corner radiation, the third case corresponds to the conditions

$$k_{mn} < k, \; k_m = \frac{m\pi}{L_x} < k \quad \text{and} \quad k_n = \frac{n\pi}{L_y} < k,$$

where the whole surface contributes to the radiation. The corresponding zone in the k-plane is inside the quarter circle of radius k.

The dark gray zone located between the quarter circle of radius k and the square of side k corresponds to particular edge modes where the periphery of the whole surface contributes to the radiation efficiently. The width of the radiating zone increases progressively as the operating point comes closer to the quarter circle (see Fig. 13.25).

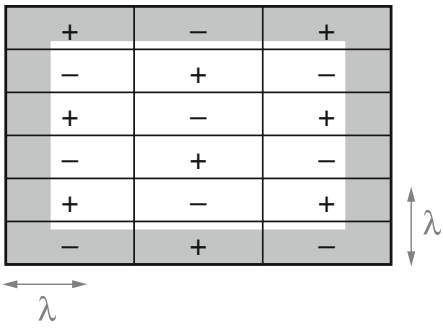

Fig. 13.25 Edge radiation in x and y directions simultaneously, or "incomplete" surface modes. $\lambda < \lambda_m$ ($k > k_m$) and $\lambda < \lambda_n$ ($k > k_n$) and $k < k_{mn}$

In summary, surface modes are the most efficient in terms of radiation, followed by the edge, and then by the corner modes.

13.4.3.3 Forced Excitation of a Rectangular Plate

In the previous paragraph, the different possible situations governing the radiation of finite rectangular plates were presented. This allows us now to address the case of the forced excitation of a plate at a given frequency ω. Such situation is close to the real case of a guitar or piano string excited by a particular frequency component of the string's vibration. In fact, the decay time of plucked and struck strings is usually much larger than the one of the body, and thus, to a first approximation, the string excitation can be considered as "forced."

Subsonic Case

Figure 13.26, inspired by Williams [40] shows an example where the excitation frequency is less than the critical frequency of the plate (*subsonic* case), which corresponds to the condition $k_B > k$ in terms of wavenumber (see Fig. 13.6). In this figure, the bullets "•" indicate the eigenmodes of the plate in terms of wavenumber.

- For a given frequency ω, the geometric locus of k_B is a "structural" quarter circle with radius larger than the "acoustic" quarter circle of radius $k = \omega/c$.
- Considering the modal vibration amplitudes A_{mn} [see Eq. (13.105)], one can derive that all modes close to the "structural" quarter circle are likely to be excited, which corresponds to the condition $\omega \approx \omega_{mn}$. This region of modal excitation is shown as a gray zone in Fig. 13.26. The width of this zone increases with the modal damping, which means that the resonance peaks are wider.
- As a consequence of the spreading of this zone, three family of modes can be excited by the forcing frequency ω: edge, corner, and surface modes. The surface modes (which are the most efficient in terms of radiation) correspond to the

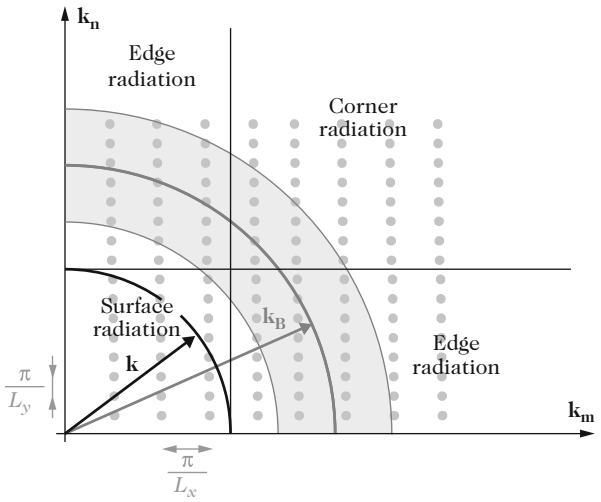

Fig. 13.26 Subsonic forced excitation of a rectangular plate. After Williams [40]

smallest values of the wavenumber in the zone (m and n such as $k_{mn} < k$). As a result, even if the vibratory magnitude A_{mn} of these surface modes is smaller than the one of the corner and edge mode at this forcing frequency, because of the distance between ω_{mn} and ω, their acoustical efficiency is higher since k_{mn} are closer to k.

For the instruments for which a plate radiation model is pertinent (piano or guitar soundboard, for example), the immediate practical consequence of the property presented above is that, in the subsonic case, the lowest modes may contribute to the radiation significantly, even if the excitation frequencies of the strings are relatively well apart from the corresponding modal frequencies of these modes.

Supersonic Case

In view of the usual order of magnitude for the soundboard materials and geometry used in stringed instruments, the elasto-acoustic interaction can be considered as subsonic below 1–5 kHz, depending on the practical case. As a consequence, almost all fundamental frequencies belong to this interval. However, it is not the case for the higher partials of the notes, which can have frequencies up to 20 kHz (and even more, in the case of the cembalo, for example). Thus, for these higher partials, the *supersonic case* also has to be examined.

Both the structural and acoustic wavelengths decrease as the forcing frequency increases. Because of the dispersion properties of the plate, the acoustic wavelength decreases faster, and thus, above the so-called critical frequency (see Sect. 13.3), the acoustic wavelength becomes smaller than the structural one. It has been shown

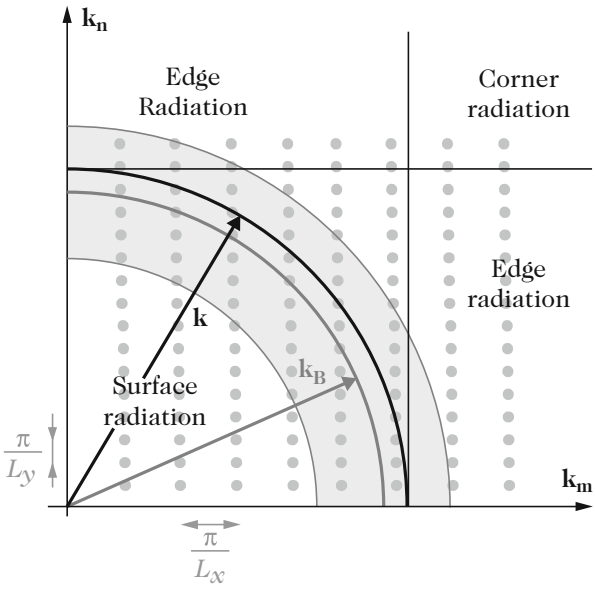

Fig. 13.27 Forced supersonic excitation of a rectangular plate

previously in this chapter that we are then in the case of a supersonic regime where the complete surface of the plate radiates efficiently. In terms of wavenumber, this case is shown in Fig. 13.27. The modes inside the gray ring in the vicinity of the quarter circle of radius k_B are together highly resonating (ω close to ω_{mn}) and radiating modes ($k_{mn} < k$).

The radiation efficiency defined in (13.115) is close to unity for all surface modes (see Fig. 13.22). recall that this quantity is normalized by the quadratic mean velocity $\langle|\dot{W}_{mn}|^2\rangle$, and thus, in turn, by the square of the modal amplitude A_{mn}. For stringed instruments, these amplitudes are rapidly decaying with the rank of the partial, so that, to a certain extent, one can say that the radiation efficiency compensates the reduction of magnitude due to the vibration.

Finally, we should bear in mind that, due to the spatial coincidences, the radiated acoustic energy is concentrated in narrow directivity lobes in the supersonic case.

13.4.3.4 Generalization to Multimode Systems

In Sect. 13.4.3.1, the radiated power was calculated for a single mode. We consider now a general motion of the plate expanded onto its in vacuo eigenmodes basis, and written in the form:

$$W(x,y,\omega) = \sum_{m=1}^{\infty}\sum_{n=1}^{\infty} A_{mn}(\omega)\phi_{mn}(x,y) \;=\; {}^t\boldsymbol{A}(\omega)\boldsymbol{\phi}(x,y). \tag{13.119}$$

In what follows, it is assumed that the far field conditions are valid, so that the spatial Fourier transform can be used. Advantage will be taken, in particular, of Parseval's theorem which states that the mean radiated power $\langle \mathscr{P}_a(\omega) \rangle$ can be calculated in the wavenumber space as follows [40]:

$$\langle \mathscr{P}_a(\omega) \rangle = \frac{1}{8\pi^2} \int_{S_r} \mathscr{R}e \left\{ \tilde{P}(k_x, k_y, \omega) \dot{\tilde{W}}^\star(k_x, k_y, \omega) \right\} dk_x dk_y, \tag{13.120}$$

where the "$\star$" symbol designates the conjugate of a variable. For simplicity, the calculation of the power in (13.120) is restricted here to a summation over the quarter circle S_r, which corresponds to the surface modes. In practice, this means that the power radiated by the edge and corner modes are neglected. Using Euler equation, $\langle \mathscr{P}_a(\omega) \rangle$ can be expressed in terms of pressure:

$$\langle \mathscr{P}_a(\omega) \rangle = \frac{1}{8\omega\rho\pi^2} \int_{S_r} |\tilde{P}(k_x, k_y, \omega)|^2 \, k_z \, dk_x dk_y, \tag{13.121}$$

where $k_z = \sqrt{k^2 - k_x^2 - k_y^2}$.

Radiation Resistances Matrix

The radiated power can also be expressed in terms of plate velocity:

$$\langle \mathscr{P}_a(\omega) \rangle = \frac{\omega\rho}{8\pi^2} \int_{S_r} \frac{|\dot{\tilde{W}}(k_x, k_y, \omega)|^2}{k_z} \, dk_x dk_y. \tag{13.122}$$

Using the modal expansion (13.119), the square modulus of the velocity is written equivalently:

$$|\dot{\tilde{W}}(k_x, k_y, \omega)|^2 = |{}^t\dot{\boldsymbol{A}}(\omega)\tilde{\boldsymbol{\phi}}(k_x, k_y)|^2 = \dot{\boldsymbol{A}}^H(\omega) \, \tilde{\boldsymbol{\phi}}^\star(k_x, k_y) \, \widetilde{{}^t\boldsymbol{\phi}}(k_x, k_y) \, \dot{\boldsymbol{A}}(\omega), \tag{13.123}$$

where the exponent "H" accounts for the Hermitian (conjugate transpose) operator. Finally, we get the (supersonic) radiated acoustic power:

$$\langle \mathscr{P}_a(\omega) \rangle = \dot{\boldsymbol{A}}^H(\omega) \mathbb{R}_a(\omega) \dot{\boldsymbol{A}}(\omega), \tag{13.124}$$

where $\mathbb{R}_a(\omega)$ is the *radiation resistance matrix* defined as:

$$\mathbb{R}_a(\omega) = \frac{\omega\rho}{8\pi^2} \int_{S_r} \frac{\tilde{\boldsymbol{\phi}}^\star(k_x, k_y) \, \widetilde{{}^t\boldsymbol{\phi}}(k_x, k_y)}{\sqrt{k^2 - k_x^2 - k_y^2}} dk_x dk_y. \tag{13.125}$$

Notice that this expression is similar to the one obtained in Sect. 13.2.3 for the elementary case of a beam coupled to a semi-infinite tube.

Each term $(R_a)_{ij} = (R_a)_{mn,m'n'}$ of the matrix $\mathbb{R}_a$ quantifies the *mutual radiation resistance* resulting from the interference between the sound fields created by the modes (m, n) and (m', n'). For (m, n)=(m', n'), the *eigen radiation resistance* are obtained, which are identical to those obtained for isolated modes, and which form the diagonal of the matrix $\mathbb{R}_a$.

For a simply supported rectangular plate, it can be shown that [21]:

$$(R_a)_{mn,m'n'} = \frac{mm'nn'\omega\rho\pi^2}{8L_x^2L_y^2} \times \int_{S_r} \frac{f_{mm'}(k_xL_x)\, f_{nn'}(k_yL_y)dk_xdk_y}{[k_x^2 - (m\pi/L_x)^2)][k_x^2 - (m'\pi/L_x)^2][k_y^2 - (n\pi/L_y)^2)][k_y^2 - (n'\pi/L_y)^2]}, \tag{13.126}$$

where the functions $f_{mm'}(k_xL_x)$ are equal to:

$$f_{mm'}(k_xL_x) = \begin{cases} 2(1 - \cos k_xL_x) & \text{for } m \text{ even}, \quad m' \text{ even}; \\ 2(1 + \cos k_xL_x) & \text{for } m \text{ odd}, \quad m' \text{ odd}; \\ 2\sin k_xL_x & \text{for } m \text{ odd}, \quad m' \text{ even}; \\ 2\sin k_xL_x & \text{for } m \text{ even}, \quad m' \text{ odd}. \end{cases} \tag{13.127}$$

Recall that, so far, the action of the sound field on the plate is ignored. This assumption is justified for a light fluid. However, as seen for the infinite plate, the dispersion equation of the plate is otherwise modified (as for a thin and flexible plate, for example). This, in turn, modifies the real and imaginary part of the wavenumbers, due to both the inertia of the fluid and radiation losses. In Chap. 14, the action of the sound field on timpani membranes will be presented, showing substantial modifications of the eigenmodes, compared to the in vacuo case.

13.4.3.5 Radiation Modes of a Plane Plate

The radiation matrix $\mathbb{R}_a(\omega)$ defined in Eq. (13.125) contains the eigenresistances of each structural mode on its diagonal and, on both sides, the mutual radiation resistances. As a consequence, it is not possible to control the power radiated by each structural mode independently from the others, because of the intermodal coupling. The problem of the vibratory and acoustic control of musical instruments is a rapidly evolving field [18], and thus it is worth to take time for addressing this question. In addition, this problem yields important theoretical results.

The goal is to determine whether velocity distributions exist on the plate so that the power radiated by each of them is independent from the others. These velocity distributions are the *radiation modes* of the plate [12]. Since $\mathbb{R}_a(\omega)$ is symmetrical,

definite and positive, it can be decomposed as follows:

$$\mathbb{R}_a = {}^t\mathbb{P}\mathbb{L}\mathbb{P}, \tag{13.128}$$

where $\mathbb{L}$ is a diagonal matrix whose elements on its diagonal are the eigenvalues of $\mathbb{R}_a$. The matrix $\mathbb{P}$ is the transfer matrix (the matrix of the eigenvectors). Following (13.124), the radiated acoustic power can be rewritten as follows:

$$\langle P_a(\omega)\rangle = \mathbf{b}^H\mathbb{L}\mathbf{b} \quad \text{where} \quad \mathbf{b} = \mathbb{P}\dot{\mathbf{A}}. \tag{13.129}$$

One can check that Eq. (13.129) is written explicitly:

$$\langle P_a\rangle = \sum_n L_n|b_n|^2, \tag{13.130}$$

which shows that the radiating modes b_n are independent from each other. L_n is the radiation efficiency associated to the n-th radiated mode.

One difficulty in the use of the radiation modes is due to the dependence of $\mathbb{R}_a$ with frequency. This means that the calculation of these variables has to be made again for each frequency of interest. However, several authors have shown that, for $ka \ll 1$ where a is a characteristic dimension of the plate, the radiation modes are reasonably well independent of frequency. Figure 13.28 shows the six first radiation modes of a baffled plane plate, calculated by Elliott and Johnson [12]. The first mode is identical to the mode of a plane piston. It corresponds to the monopole component of the plate whose flow rate is given by the product of the surface by the mean velocity. The detailed calculation of the eigenvalues and eigenvectors show that this lowest mode contains the main part of the radiated power. The radiation efficiency of the higher-order radiation modes is much lower.

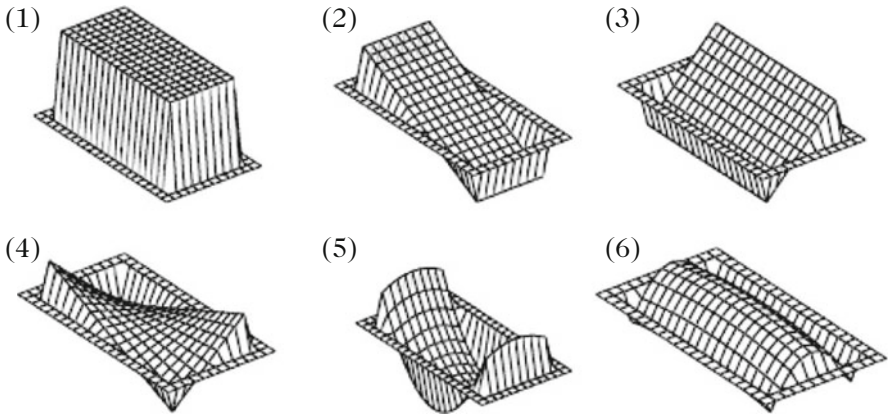

Fig. 13.28 First radiation modes for a rectangular baffled plate. $kL \approx 0.1$. After [12]

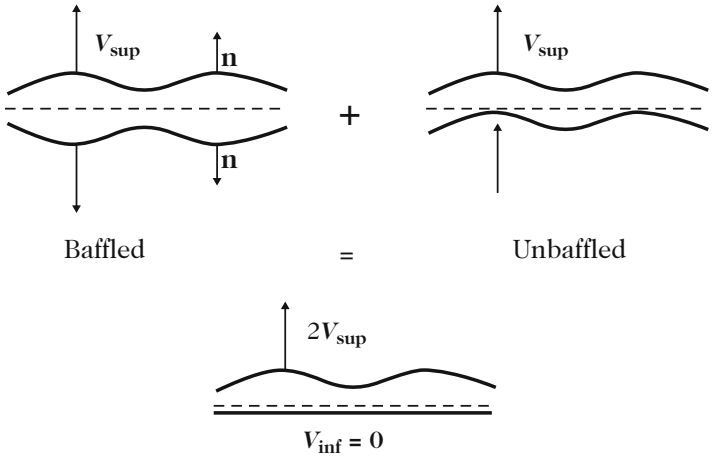

Fig. 13.29 Decomposition of a volume with plane walls into several planar sources. After [24]

13.4.4 Radiation of Unbaffled Plates and Structural Volumes

To a first approximation, stringed musical instruments can be viewed as structural volumes with one (or more) vibrating sides. For simplicity, it is assumed here that the vibrating parts of the volume are plane surfaces. Figure 13.29 shows a particular case where only the upper surface of the volume vibrates, all other surfaces remaining at rest. This simplified model is close to the case of a guitar where the vibrations of neck, sides, and back plate would be neglected compared to the vibrations of the soundboard.

The radiation of a volume composed of planar walls can be decomposed into two parts: a *baffled* plate part and an *unbaffled* plate part. As seen in Chap. 12, a baffled source has a condition of zero velocity on the rigid baffle containing the source, and thus the system is equivalent to two moving plates with symmetrically opposite velocities on both sides of the baffle. In contrast, an oscillating unbaffled source can be viewed as the association of two plates moving in phase. As a consequence, as shown in Fig. 13.29, the pressure radiated by a volume with one moving plane wall is the sum of two contributions: one pressure p_b generated by the baffled component, and a pressure p_u radiated by the unbaffled component. This property incited us to study first the radiation of unbaffled plates, for which the direct use of the Rayleigh integral is not valid anymore.

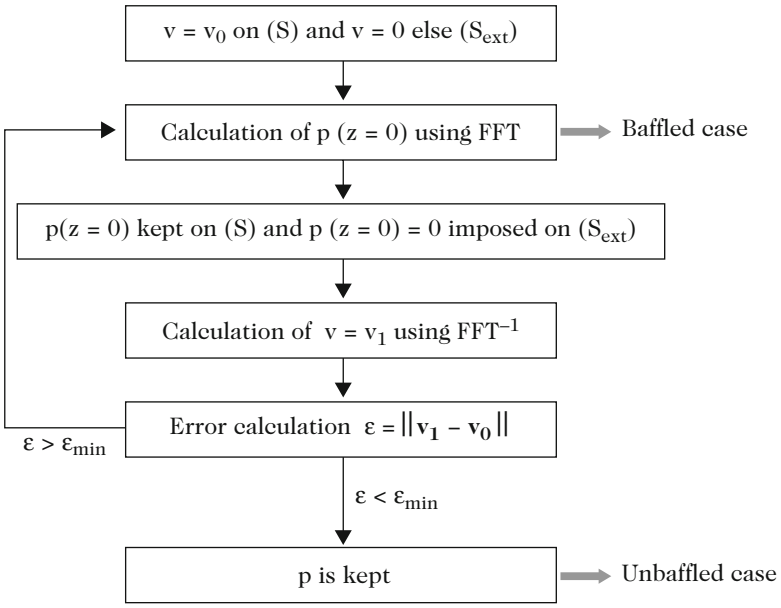

Fig. 13.30 Iterative algorithm for the calculation of the pressure radiated by an unbaffled plane plate. After [39]

13.4.4.1 Radiation of an Unbaffled Source: Iterative Algorithm

The method presented below was developed in the 1980s by Williams and Maynard [39]. This method takes advantage of the spatial Fourier transform presented in Sect. 13.4, which means that it is restricted to the prediction of far field radiation. In practice, the Fourier transforms are calculated numerically on a discrete mesh of the structure and, in turn, on a discrete set of wavenumbers. Using rapid and appropriate tools, such as the Fast Fourier Transform (FFT), a good estimate of the pressure can be rapidly obtained, even in the case of complex vibration patterns. The successive steps of the iterative algorithm used for the computation of the sound field are shown schematically in Fig. 13.30.

(1) Let us denote v_0 the velocity imposed on the baffled plate. The remaining part of the infinite plane (baffle) is supposed to be perfectly rigid ($v = 0$). In a first step, the radiated pressure field p_0 in the space is then calculated by means of the Rayleigh integral (using, for example, the FFT).
(2) In a second step, the pressure field p_0 is retained, except on the baffle, where the condition $p = 0$ is imposed. Through inverse Fourier transform, the velocity field v_1 is calculated corresponding to this modified pressure distribution.
(3) The velocity field v_1 is compared to the initial (given) velocity profile v_0. If the relative error ε between these two velocity fields is larger than an arbitrarily

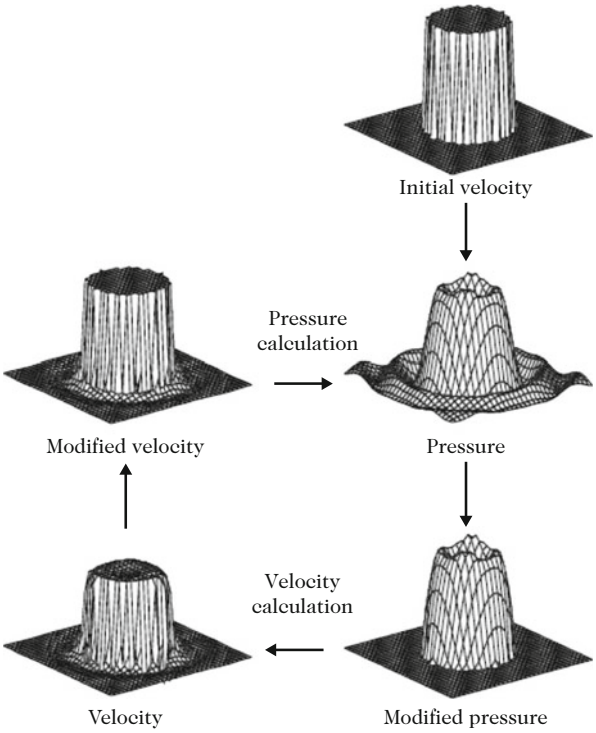

Fig. 13.31 Iterative calculation of the pressure radiated by an unbaffled plane piston of radius a, for $ka = 4$. After Le Pichon [24]

imposed limit $\varepsilon_{\min}$, then another iteration occurs. Otherwise, it is considered that the result corresponds to the imposed boundary conditions, and the calculation stops.

In practice, it is observed that the algorithm converges rapidly for $ka > 1$, where a is a characteristic dimension of the plate. Figure 13.31 shows, for example, the results obtained for a unbaffled plane piston for $ka = 4$.

13.4.4.2 Application to the Guitar

The previous method was successfully applied to the guitar by Le Pichon [25]. First, the velocity profile of both the soundboard and back plate of the instrument were measured. For each of these two vibrating surfaces, the radiated sound field was calculated by summing two contributions: the first (for the baffled component) with the Rayleigh integral, and the second (unbaffled component) by means of the iterative algorithm presented above.

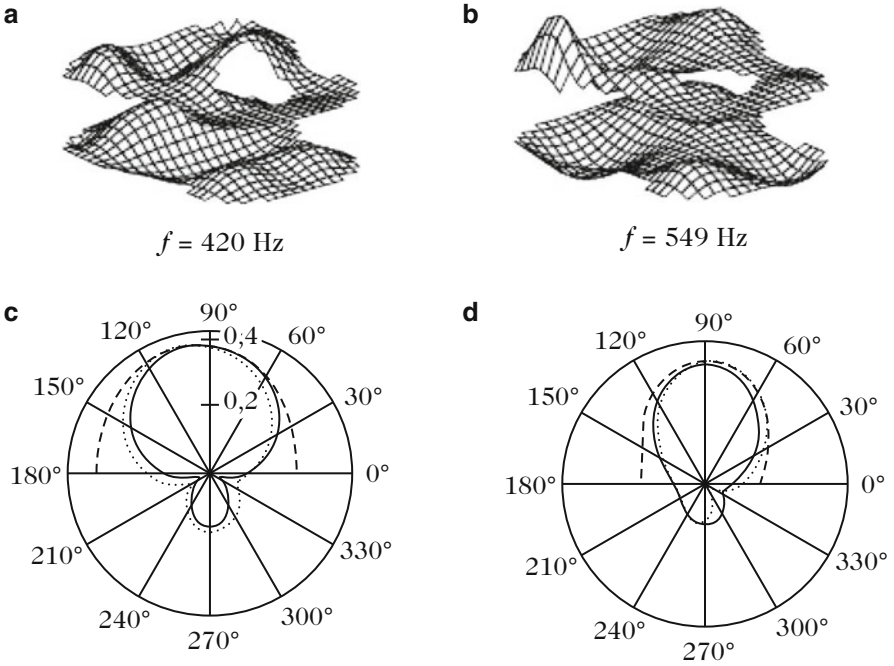

Fig. 13.32 Comparison between measurements and prediction of guitar directivity patterns at two frequencies: 420 and 549 Hz. The measured velocity profiles of soundboard and back plates are shown in (**a**) and (**b**). The corresponding directivity patterns are shown in (**c**) and (**d**). On these two diagrams, the directivity predicted by the Rayleigh integral applied to the soundboard only is represented with a *dashed line*. The directivity patterns predicted by the volume model, taking both plates into account are drawn with *solid lines*. Finally, the directivity patterns measured in an anechoic chamber are in *dotted lines*. After [25]

Figure 13.32 shows the calculated directivity patterns, and the comparison with measurements performed in an anechoic chamber. It can be seen, among other things, that the baffled plate model (Rayleigh integral) yields erroneous predictions, especially on the back of the instrument. In contrast, the measured directivity is well predicted by the *volume* model. In accordance with the properties of the iterative algorithm, the results obtained with this method are deteriorated in the low frequency range (for $ka < 1$). For a guitar, the typical frequency limit is around 60 Hz. Also recall that the method is not applicable in the near field.

13.5 Radiation of an Axisymmetrical Nonplanar Source

For a number of instruments, the radiating body is not a plate but a shell which is, by definition, a nonplanar source. Such a shape is justified by several reasons. It was shown, for example, in Chap. 8 that the curvature of gongs and cymbals is

the prime origin of the quadratic nonlinearities observed in the sounds of these instruments, in case of large amplitude motion. In bowed strings instruments, the curvature of the soundboard allows the conversion of the vertical static loading due to the tension of the strings into a "membrane-like" prestress in the soundboard. As a consequence, the soundboard is more rigid, which contributes to increase the radiation efficiency, and, in addition, this geometry yields a better contact between the bridge and the strings. Finally, in wind instruments, several authors have shown that, in some situations, a coupling exists between the sound field and the structure [13, 14, 22, 27, 29]. In this case, the tubular geometry of the tubes also is described by a shell model.[10]

In this section, the influence of the curvature on the radiation properties of a source are examined, and the differences with the case of planar sources are highlighted. First, some simple rules are derived from the dispersion curves, which show the effect of the curvature on the radiation efficiency. In a second step, it is shown to what extent the curvature modifies the radiated pressure, compared to the case of a plate. A simplified model is presented, in case of shallow shells, which can be used for many instruments. Based on a modal approach, the notion of *Spatial impulse response* is presented. The general concepts are illustrated on the particular case of the spherical shallow shell, which is typical example of practical use in many percussive instruments, and which can also account for the radiation of some loudspeakers and stringed instruments. The effect of the curvature on both the directivity of the source and cutoff frequency are particularly emphasized.

13.5.1 Dispersion Curves for Shells and Critical Frequency

Figure 13.33 shows an example of spherical shell with radius of curvature R, and the associated dispersion curve. For thin shallow shells, the dispersion relation is given by [34]:

$$\rho_s h\omega^2 = Dk^4 + \frac{Eh}{R^2}, \tag{13.131}$$

where ρ_s is the density of the shell, and h its thickness. It can be seen in Fig. 13.33 that the dispersion curve is shifted up, compared to the case of plates [Eq. (13.49)]. The shift of the curve increases when R decreases. The curvature tends to make the structure stiffer. As a consequence, the critical frequency decreases, which is shown by the position of the intersection point between both dispersion curves. In addition, due to the presence of a constant term in (13.131), another intersection point appears near the origin of the axes. This indicates that the second effect of the

[10]The issue of the material choice for wind instruments is a very intricate and controversy matter. Two different materials handled by the same tool do not produce the same geometry, and the nature of the material intervenes also by its porosity, the state of its surface, its heat capacity, etc.

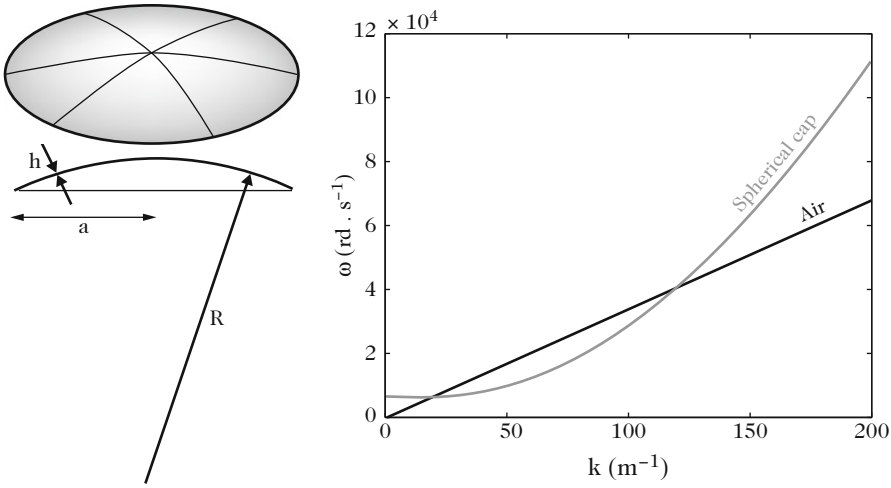

Fig. 13.33 Spherical cap and its associated dispersion curve. The *straight line* in the (ω, k)-diagram accounts for the air dispersion. The numerical values selected for this example are: $E = 2 \times 10^{11}\,\mathrm{N\,m^{-2}}$, $\rho_s = 7.8\,\mathrm{kg\,m^{-3}}$, $R = 0.8\,\mathrm{m}$, $h = 2\,\mathrm{mm}$, and $\nu = 0.3$

curvature is to enhance the radiation efficiency in the low-frequency range. For a small radius of curvature, a situation may occur where the dispersion curve of the shell is completely above the dispersion curve of the air: in this case, there is no critical frequency anymore and all structural modes are radiating.

Similar results are obtained for thin cylindrical shallow shells, such as the one shown in Fig. 13.34, where a is the radius of curvature. Denoting ω_p the corresponding plate modes (obtained in the limiting case of an infinite radius of curvature), it can be shown that the cylindrical shell modes fulfill the relation [34]:

$$\omega_s^2 = \omega_p^2 + \frac{E}{a^2 \rho_s (1 - \nu^2)}. \tag{13.132}$$

As a consequence, similar conclusions as for the spherical shell can be drawn here. In particular, all modes will be radiating when the dispersion curve of the cylindrical shell is located above the air dispersion curve, which can occur for a small radius of curvature.

13.5.2 Radiated Pressure

Let us now turn to the exact calculation of the pressure radiated by shells. For simplicity, we limit ourselves here to axisymmetrical shells. Figure 13.35 shows that, by contrast to the case of plane plates, the structural velocity might not be normal to the structure. In the general case, we have to take both the normal v_n and

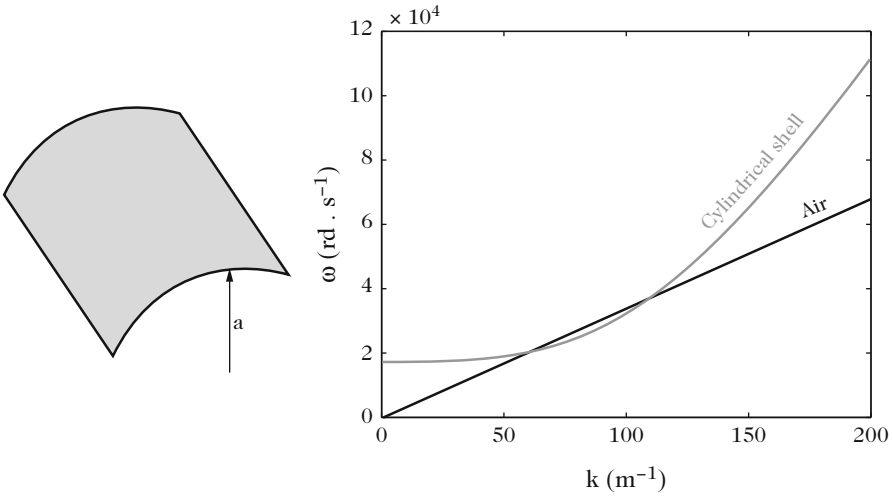

Fig. 13.34 Cylindrical shell and its associated dispersion curve. $E = 2 \times 10^{11}\,\mathrm{N\,m^{-2}}$, $\rho_s = 7.8\,\mathrm{kg\,m^{-3}}$, $a = 0.3\,\mathrm{m}$, $h = 2\,\mathrm{mm}$, and $\nu = 0.3$

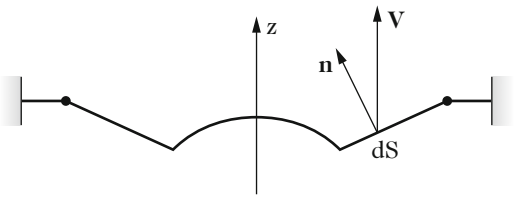

Fig. 13.35 Example of an axisymmetrical structure of axis z

the tangential v_t velocity into account. The complete calculation of the Kirchhoff–Helmholtz integral in this case was done by Hu and Wu [20]. These authors show that the pressure is then given by the sum of four terms:

$$p(\mathbf{r},t) = \mathscr{M}_n(\mathbf{r},t) + \mathscr{M}_t(\mathbf{r},t) + \mathscr{D}_n(\mathbf{r},t) + \mathscr{D}_t(\mathbf{r},t), \tag{13.133}$$

where $\mathscr{M}_n$ and $\mathscr{D}_n$ are the monopole and dipole contributions of the normal velocity, respectively, whereas $\mathscr{M}_t$ and $\mathscr{D}_t$ are the monopole and dipole contributions of the tangential velocity. For a shallow shell inserted in an infinite baffle, this sum reduces to the first term, which is of the Rayleigh type, though with a nonplanar integration surface. This term is written in the time-domain:

$$p(\mathbf{r},t) = -\rho \int_0^t \int_S g(\mathbf{r},\mathbf{r}',t,\tau)\frac{\partial v_n(\mathbf{r}',\tau)}{\partial \tau} dS_{\mathbf{r}'} d\tau, \tag{13.134}$$

where $g(\mathbf{r},\mathbf{r}',t,\tau)$ is the space-time Green's function. For a known (imposed) normal velocity v_n, the problem reduces to the appropriate determination of the Green's function g. This function is here different from the one defined in Chap. 12

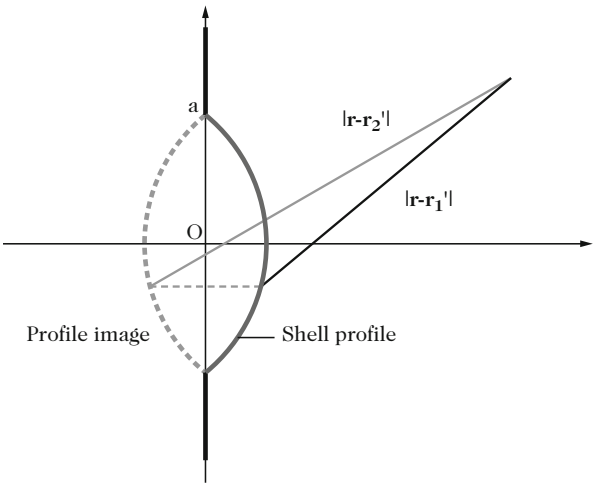

Fig. 13.36 Construction of the Green's function for a spherical cap

for the plane piston, because of the curvature of the source. Figure 13.36 shows a example of graphical construction of a Green's function for a spherical cap, using the method of images.

For a shell inserted in an infinite rigid baffle, the condition of zero velocity on the baffle imposes

$$\begin{aligned} g(\mathbf{r},\mathbf{r}',t,\tau) &= g_1(\mathbf{r},\mathbf{r}',t,\tau) + g_2(\mathbf{r},\mathbf{r}',t,\tau) \\ &= \frac{\delta(t-\tau-|\mathbf{r}-\mathbf{r}'_1|/c)}{4\pi|\mathbf{r}-\mathbf{r}'_1|} + \frac{\delta(t-\tau-|\mathbf{r}-\mathbf{r}'_2|/c)}{4\pi|\mathbf{r}-\mathbf{r}'_2|}, \end{aligned} \quad (13.135)$$

where the first term g_1 is the contribution of the direct sound, while the second term g_2 is the contribution of the reflection from the source. Once the Green's function is known, the calculation continues by using a modal approach. The transverse displacement w of the shell is expanded onto its in vacuo eigenmodes basis. We write

$$w(\mathbf{r},t) = \sum_{p=0}^{\infty} \Phi_p(\mathbf{r}) q_p(t), \quad (13.136)$$

where $q_p(t)$ are the generalized displacements. The modal decomposition of the pressure is derived

$$p(\mathbf{r},t) = -\rho \sum_{p=0}^{\infty} \int_0^t \int_S g(\mathbf{r},\mathbf{r}',t,\tau)\Phi_p(\mathbf{r}')\ddot{q}(\tau)\, \mathbf{e_z}.\mathbf{dS}_{\mathbf{r}'}\, d\tau, \quad (13.137)$$

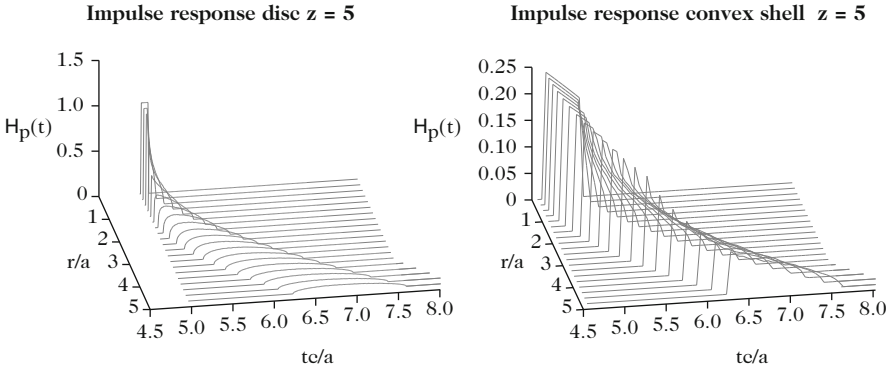

Fig. 13.37 Spatial impulse response for the planar piston (*left*) and a convex spherical cap (*right*)

in the particular case of a velocity profile of the shell oriented in the direction $\mathbf{e_z}$ of the shell axis (see Fig. 13.35). One main interest of the expression (13.137) is that it remains valid even for nonlinear vibrations, which is usually the case for gongs and cymbals, as shown in Chap. 8 [30]. This property results from the fact that no particular condition is given above on the displacements $q(t)$. Another interesting property results from the grouping of the terms g and Φ under the integral, which yields, after integration, to the following transformation:

$$p(\mathbf{r}, t) = -\rho \sum_{p=0}^{\infty} \int_0^t \mathscr{H}_p(\mathbf{r}, \tau) \ddot{q}(\tau) d\tau. \tag{13.138}$$

This method was originally developed by Stepanishen [35]. The function $\mathscr{H}_p$ was called *Spatial Impulse Response, or SIR* for the mode p by the author. This function contains together the information on the modal shape for the mode p and on the observation point $\mathbf{r}$, for a given shell profile.

Figure 13.37 shows a comparison between two spatial impulse responses, for the plane piston and a convex spherical cap. These plots show the spreading of the response over time when the observer moves in a vertical plane at a fixed distance from the source plane (baffle). One can see, in particular, that this spreading is more pronounced for the spherical cap than for the plane piston, which, as we will show in the next paragraph, implies that the cutoff frequency of the pressure spectrum is lower for the cap, compared to a piston of the same size.

13.5.3 Influence of the Source Shape

The shape of a source influences both the directivity and bandwidth of its radiated sound pressure. These effects can easily be shown in the frequency domain, through calculation of the Fourier transform of the spatial impulse response. Figure 13.38

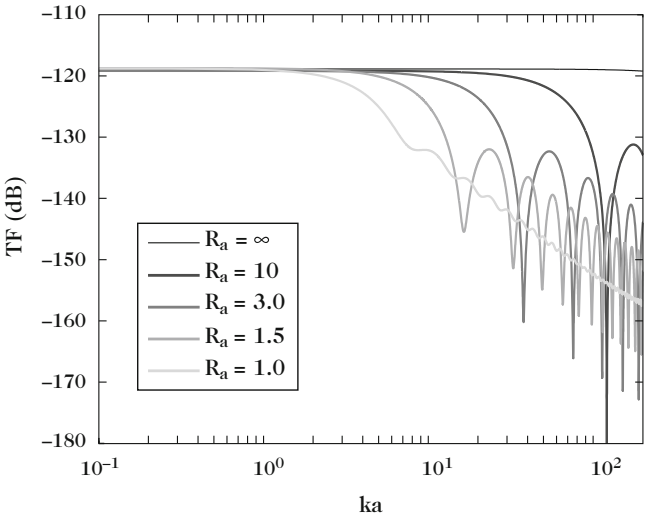

Fig. 13.38 Far field pressure response curves on the axis for different spherical caps with different radii of curvature. $R_a = R/a$ is the dimensionless ratio between the radius of curvature and the radius of the circle obtained through projection of the cap on a plane. The cutoff frequency decreases as the radius of curvature decreases. The curvature has thus a *lowpass filter* effect on the radiated pressure. After [30]

shows, for example, the frequency response of the far field pressure on the axis (at a distance equal to 100 times the radius of the source) for a spherical cap with different radii of curvature. One can see that the cutoff frequency of the response decreases as the radius of curvature increases.[11] Another feature to notice is that a kind of *comb filter* effect appears in the attenuated band.[12]

In contrast, Fig. 13.39 shows that the directivity in the far field is less pronounced for convex spherical caps, at a given frequency, as the radius of curvature decreases. The convexity of the source thus spreads the acoustic pressure more uniformly in space, the price to pay being a reduction of the pressure magnitude with frequency. These properties have direct consequences from the point of view of sound distribution and sound reproduction in a room: a source with a curvature seems to be more appropriate if the purpose to insonify a zone for a large audience.

[11] By analogy with the electric filters, this cutoff frequency can be defined as the value for which the pressure is reduced by a factor of −3 dB compared to its low-frequency asymptotic value (see Fig. 13.38).

[12] Similar results were obtained by Suzuki and Tichy [37], using the theory of spherical harmonics for expanding the pressure (see Chap. 12). These authors report that, due the diffraction effects, an attenuation of the order of −5 dB between $ka = 0.4$ and $ka = 4$ is obtained for the convex caps, whereas an amplification of 4 dB is obtained for the concave case.

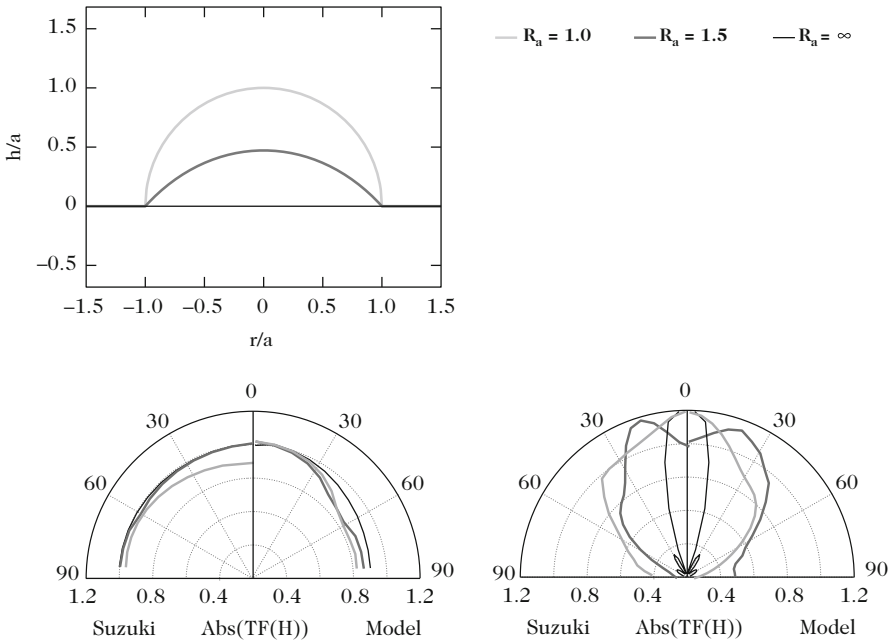

Fig. 13.39 Far field directivity patterns of some convex spherical caps at two frequencies corresponding to $ka = 1$ and $ka = 10$. The profile of the caps are drawn in *black* and *gray* colors in figure (**a**) (*top*). The model presented in this chapter is compared to the work by Suzuki [37]. (**b**) and (**c**) (*bottom*) are symmetrical about the axis $\theta = 0°$. The Suzuki model is on the *left* side of the axis and the present model on the *right*

13.6 Application to Stringed Instruments

In this section, the purpose is to show how some fundamental results of vibroacoustics can be applied to stringed instruments. The presentation starts by specifying to what extent the concepts of critical frequency and modal density, together with the mechanical impedance of the soundboard, are of help in selecting the appropriate materials for enhancing the acoustical efficiency of the instrument. It is followed by the experimental analysis of a piano soundboard which illustrates the analytical results on efficiency and radiation resistance. Finally, the necessary compromise that is to be found between loudness and tone duration for free oscillations systems, such as the piano or the guitar, is discussed.

13.6.1 Selection of Materials and Merit Index

The addressed question here is how to select the appropriate material for building stringed instruments. The demonstration below is inspired from the work by Barlow [4]. First, we focus on the acoustical efficiency of stringed instruments. The underlying idea is to show under which conditions the mechanical power transmitted by the strings to the bridge can be usefully converted into acoustical power. This imposes to lower the critical frequency while keeping the real part of the admittance at the bridge as high as possible. In Sect. 13.3.3, the critical frequency was calculated in the case of an isotropic material [see Eq. (13.51)], and the usually admitted approximate formula for orthotropic materials also was indicated

$$f_c \approx \frac{c^2}{\pi h}\sqrt{\frac{3\rho_p(1-\nu^2)}{[E_1E_2]^{1/2}}}. \tag{13.139}$$

In Sect. 13.3.7.1, the driving-point impedance was calculated for an infinite isotropic plate, and the approximate expression for an orthotropic plate also was given. In terms of admittance (or mobility), this quantity is written:

$$Y_p \approx \frac{1}{4h^2}\sqrt{\frac{3(1-\nu^2)}{\rho_p[E_1E_2]^{1/2}}}. \tag{13.140}$$

Recall that Eq. (13.140) also corresponds to the mean (and asymptotic) value of the admittance for a finite plate [33] and this is the reason why it is well adapted to our problem. Assuming further that the Poisson's coefficients have a minor effect on the admittance, one can see that both quantities in Eqs. (13.139) and (13.140) basically depend on the thickness h and density ρ, and on the Young's moduli of the plate.

First of all, it is reasonable to consider that the thickness h of the soundboard is selected in such a manner that the spectral domains of strings and soundboard, respectively, coincide. Otherwise, the instrument would not have the possibility to enhance the vibrations of the strings. Once the thickness has been fixed, then only the two parameters of the soundboard material remain to be optimized. By eliminating h between both quantities Y_p and f_c, a *merit index* is obtained

$$\mathrm{M_e} = \frac{Y_p}{f_c^2} = \frac{\pi^2}{4c^2\sqrt{3(1-\nu^2)}}\frac{[E_1E_2]^{1/4}}{{\rho_p}^{3/2}}. \tag{13.141}$$

Equation (13.141) shows that, in order to maximize the acoustical power radiated by the plate, the quantity $[E_1E_2]^{1/2}/\rho_p^3$ needs to be maximized also. For an isotropic plate, this quantity reduces to E/ρ_p^3. One convenient strategy to make the most of this result is to use the well-known Ashby diagram [3] shown in Fig. 13.40.

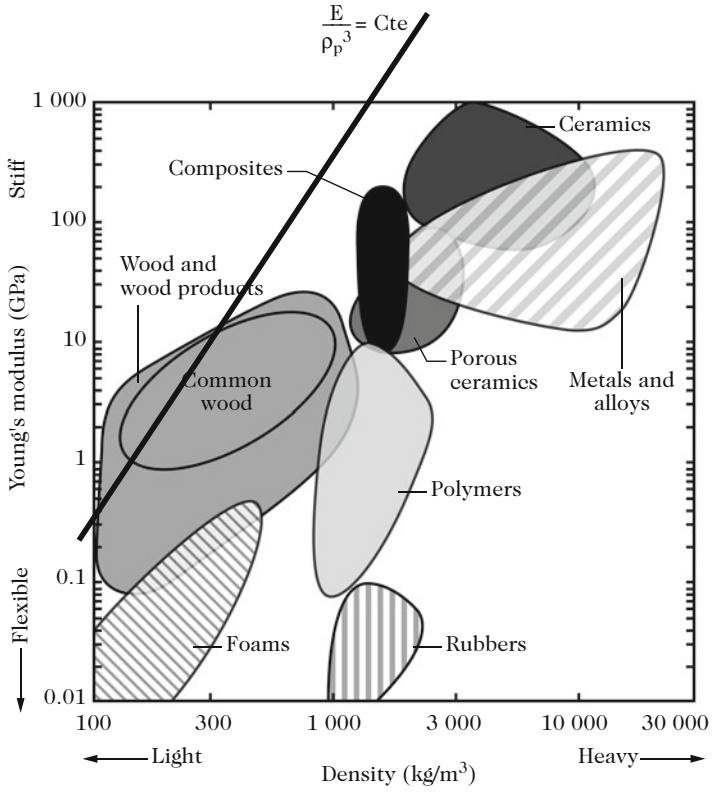

Fig. 13.40 Ashby diagram. After [3]

In this diagram, the density is represented on the horizontal axis, while the Young's modulus is shown on the vertical axis, in logarithmic coordinates, for a large class of materials. For the purpose of the demonstration, a zone called *mean wood* is added on the diagram, where the elastic moduli are the mean values $E_{moy} = [E_1 E_2]^{1/2}$ of the usual wood species used in lutherie. Imagine now a line of constant slope $E/\rho_p{}^3$ translating on this diagram. It can be seen that this quantity is maximized in the region of the diagram corresponding to low density and high moduli: as a conclusion the best candidate to build an instrument . . . is the wood !

Examining the Ashby diagram more closely shows that the "winner," for this merit index, is the balsa wood. However, this result needs to be tempered, since other criteria have to be considered in instrument making. The yield strength, in particular, imposes maximal values for the stresses in the structure in terms of traction, compression and shear. Other Ashby materials are available where such a criterion is taken into account. In practice, breakable wood species, such as balsa wood, are not appropriate for soundboard, in view of the usual static loading they have to withstand. For more information on the properties of wood in string instruments, one can refer to [6].

Function of the Modal Density

In the previous paragraph, the selection of materials for stringed instruments was based on the critical frequency. Another alternative for the reasoning is to use the concept of modal density, which yields another appropriate criterion in the case of finite plates. In Chap. 3, it was shown that the radiated acoustical power is proportional to the real part of the admittance and, in turn, to the modal density of the plate. For an orthotropic rectangular plate of surface S, the following approximate formula was obtained

$$D(f) \approx \frac{S}{h}\sqrt{\frac{3\rho_p(1-\nu^2)}{[E_1E_2]^{1/2}}}, \tag{13.142}$$

which is proportional to the critical frequency. Bringing together Eqs. (13.140) and (13.142), we get

$$D(f) = 4Y_pSh\rho_p = 4Y_pM_{\text{tot}}, \tag{13.143}$$

where M_{tot} is the total mass of the plate. For a finite plate, Y_p should be here considered as the (real) asymptotic value of the admittance in the high frequency range or, equivalently, as the mean value of the admittance over the frequency range of interest radiated by the plate [33].

In Chap. 6, it was shown that the power transmitted from the strings to the soundboard to the real part of the admittance, for a given transverse force. Equation (13.143) shows, in addition, that this admittance's real part is proportional to the modal density and inversely proportional to the total mass of the plate.

13.6.2 Example of the Piano Soundboard

The concepts of radiated power, radiation resistance, and acoustical efficiency are now illustrated by using the piano soundboard as an example. We take advantage here of the experimental results obtained by Suzuki [36].

Figure 13.41 shows the results of measurements conducted with wideband excitation. The mean radiated power was calculated by means of the flow of the acoustic intensity vector through a surface S of the soundboard $I = 1/2\mathscr{R}e\{PV^\star\}$. In these experiments, the pressure is measured in the near field, close to the soundboard, and the acoustic velocity V is derived from the measurements of the soundboard velocity. The excitation force is normalized to 1 N. Between 50 and 500 Hz, the radiated power is weak, except at some frequencies corresponding to the eigenmodes of the soundboard. The power increases progressively between 500 and 2000 Hz, with a maximum in the range 1800–2000 Hz. The power remains constant above 2 kHz. It is interesting to compare the power to the radiation efficiency shown

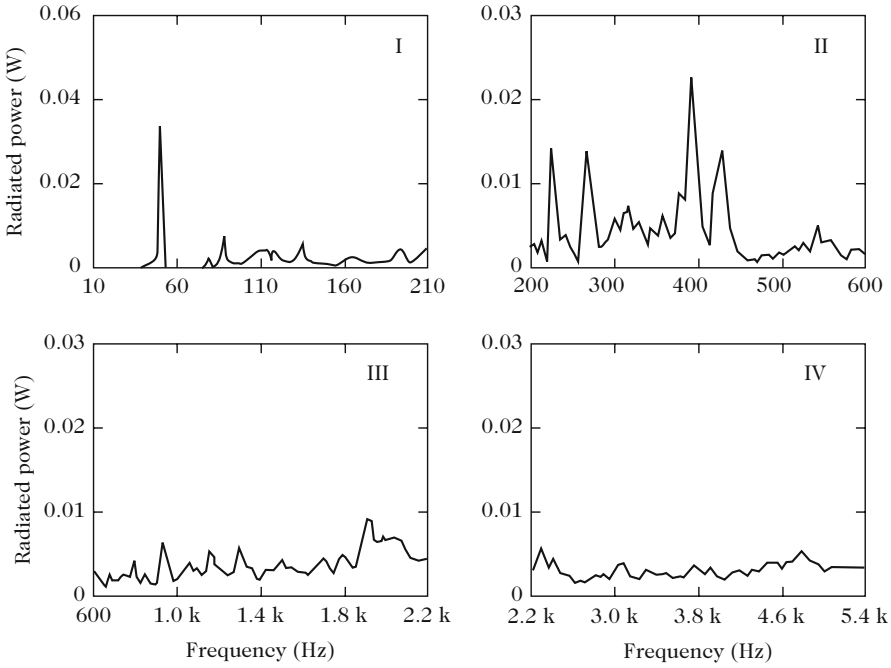

Fig. 13.41 Measurements of the acoustical power radiated by a soundboard, in four different frequency bands. After [36]

in Fig. 13.42. Recall that the efficiency is defined as the ratio between acoustical power and the mechanical power at the input. Some differences exist between both curves, although the general tendency is comparable. The efficiency is almost constant above 1.4 kHz, and decreases slightly above 3.5 kHz. By comparison with the theoretical results, one can reasonably estimate on these figures that the critical zone is approximately situated between 1.2 and 1.6 kHz. In addition, an estimation based on typical values, such as $E = 1.4 \times 10^{10}\,\mathrm{N/m^2}$ for the mean Young's modulus, $\rho_p = 400\,\mathrm{kg/m^3}$ for the density, and a mean thickness equal to 9 mm yields a critical frequency equal to 1.2 kHz, which is coherent. One can assume, in addition, that the internal losses in the wood increase above 3.5 kHz, thus contributing to reduce the efficiency in this range. Another explanation given by the author is based on the experimental conditions, as a result of the distance (a few centimeters) between the measurements points of velocity and pressure, respectively.

The Suzuki paper also shows the input power versus frequency (not shown here). This shows, in particular, that the input power is high around the eigenmodes of the soundboard, especially in the low-frequency range. One can remark that this situation is rather fortunate since, in this range, the rather high level of vibration is compensated by a smaller efficiency, compared to the high frequency range (above

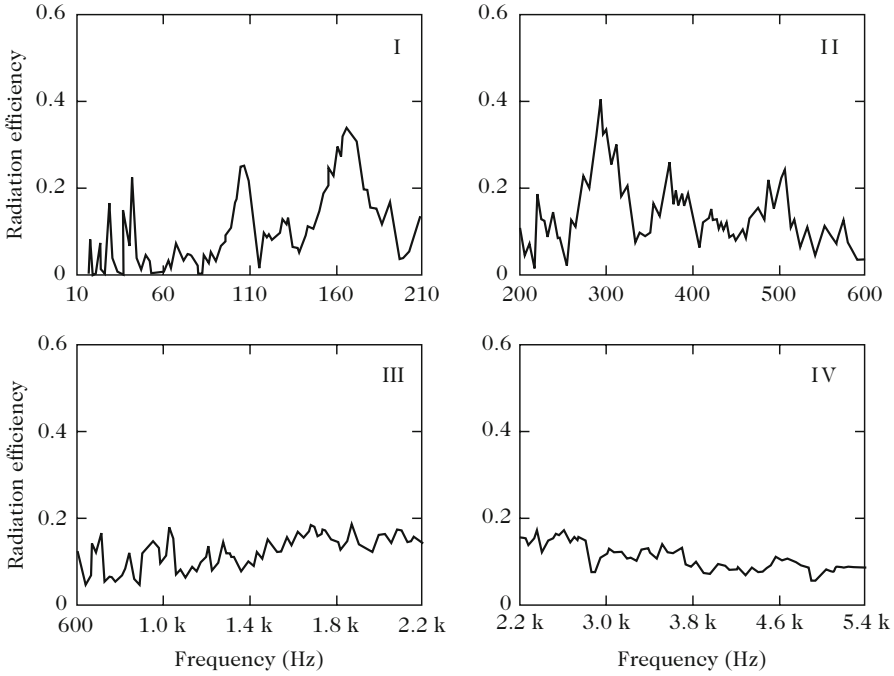

Fig. 13.42 Measurements of the radiation efficiency of a piano soundboard in the same frequency range as in Fig. 13.41. After Suzuki [36]

the critical frequency). As a result, the sound power in the complete range of the piano tends to be rather uniform. At this stage, one must add that one of the main difficulty for piano makers is to obtain a sufficiently high acoustic level for the highest notes of the instrument. The limitations here can be due to three possible phenomena: first, the mechanical energy imparted to the string is usually weak in this range. Second, the coupling between string and bridge is strong thus reducing the tone duration (see the next paragraph below). Third, the zone of effective vibration of the soundboard is restricted to a small area (see the paragraphs dealing with the localization of modes in Chap. 3).

Finally, as seen in Eq. (13.117), the normalized radiation resistance $R_a/\rho c$ is defined as the product of the radiation efficiency by the radiating area. This quantity then yields useful information on the radiation efficiency for a given vibrating part of the instrument. In the cited Suzuki paper, the resistance R_a of the piano is presented for the area corresponding to the medium and high frequency range of the instrument (see Fig. 13.43). In this figure, the increase of R_a between 0.6 and 1.8 kHz is seen more clearly than on the complete instrument. Again, a clear negative slope is seen beyond 3.5 kHz.

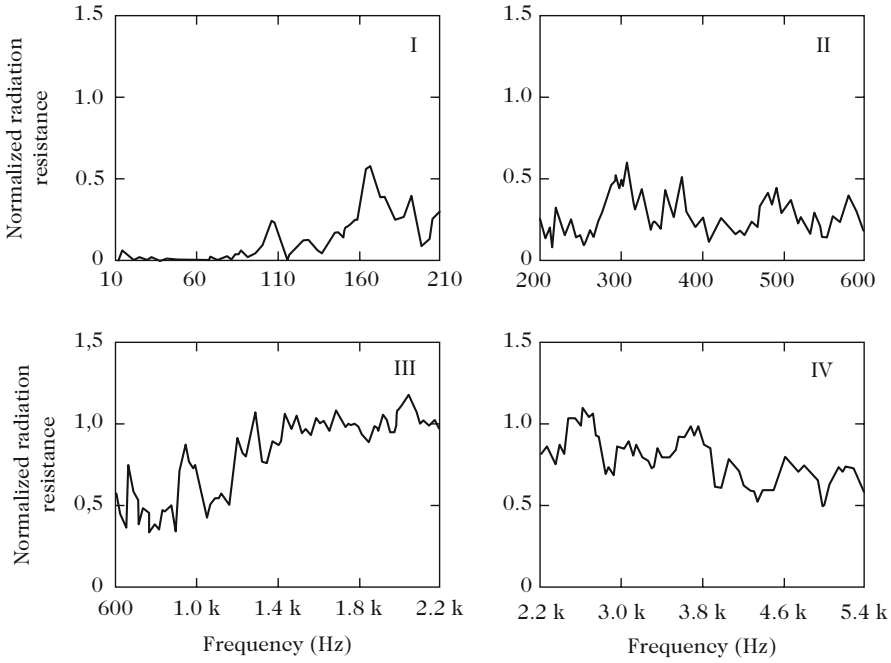

Fig. 13.43 Measurement of the radiation resistance of a piano soundboard, in the restricted area corresponding to the medium and high range of the instrument. After Suzuki [36]

Numerical methods are necessary to calculate the radiation efficiency of a piano accurately (see Chap. 14). However, it has been shown here that qualitative results and relevant trends can be obtained from general considerations based on simple plate models.

13.6.3 Compromise Between Loudness and Tone Duration

In the foregoing, simple criteria were established as guidelines for the selection of materials used for soundboards. These criteria are based on the following quantities: critical frequency, driving-point admittance at the coupling point between soundboard and strings, modal density of the soundboard. The calculations were made with the underlying goal to maximize the radiated power. In the reality, this objective has to be more flexible for free oscillations instruments, such as the piano, the cembalo, or the guitar, for example. This follows from the fact that the tone duration decreases as the radiated power increases, since the radiation damping factor of the soundboard is proportional to the radiated power (see Chap. 6). This situation might, or might not, be desirable, depending on the musical context.

Let us take the example of the piano again. In Chap. 6, it was shown that the damping factor of an isolated string with tension T and length L loaded at one end by an admittance $Y(\omega)$ was given by:

$$\alpha(\omega) = \frac{1}{\tau} = \frac{T}{L}\mathscr{R}e\{Y(\omega)\}. \tag{13.144}$$

In the upper range of a grand piano, the tension T is almost constant and equal to 800 N (see [9]). As a consequence, the damping factor increases if the string's length is reduced, for a given admittance. To compensate this phenomenon, the driving-point mobility should be reduced. This means, for example, in practice that, for a given material, and according to (13.140), the thickness and the rigidity of the soundboard increase near the coupling point. Such an achievement needs a special design, and attention must be paid to the fact that these modifications do not induce other unwanted and unanticipated effects.

In a real instrument, the tone duration is governed by additional phenomena. It was shown in Chap. 6, for example, that both the vertical and horizontal motion of the string are coupled by the motion of the bridge. The input admittance corresponding to the horizontal motion is significantly smaller than the one of the vertical motion (see, for example, [23]). As a consequence, the decay time of the horizontal component of the string is higher that the one of the vertical component, which contributes to increase the tone duration. Other coupling phenomena, such as the coupling of the triplets of strings of a given piano note, influence the duration of a tone significantly.

References

1. Abramowitz, M., Stegun, I.A.: Handbook of Mathematical Functions, with Formulas, Graphs, and Mathematical Tables. Dover, New York (1972)
2. Arcas, K.: Physical model of plate reverberation. In: Proceedings of the 19th International Congress on Acoustics, Madrid (2007)
3. Ashby, M.F.: Materials Selection in Mechanical Design. Butterworth-Heinemann, Oxford (2004)
4. Barlow, C.Y.: Materials selection for musical instruments. In: Proceedings of the Institute of Acoustics, ISMA'97, pp. 69–78 (1997)
5. Boullosa, R.R., Orduna-Bustamante, F., Lôpez, A.P.: Tuning characteristics, radiation efficiency and subjective quality of a set of classical guitars. Appl. Acoust. **59**, 183–197 (1999)
6. Brémaud, I.: Acoustical properties of wood in string instruments soundboards and tuned idiophones: biological and cultural diversity. J. Acoust. Soc. Am. **131**(1), 807–818 (2012)
7. Busch-Vishniac, I.J.: Drive point impedance of an infinite orthotropic plate under tension. J. Acoust. Soc. Am. **71**(1), 368–371 (1982)
8. Chaigne, A.: Structural acoustics and vibrations. In: Springer Handbook of Acoustics, pp. 901–960. Springer, New York (2007)
9. Conklin, H.A.: Design and tone in the mechanoacoustic piano. Part III. Piano strings and scale design. J. Acoust. Soc. Am. **100**, 1286–1298 (1996)

10. Cummings, A.: Sound radiation from a plate into a porous medium. J. Sound Vib. **247**(3), 389–406 (2001)
11. Dérogis, P.: Analysis of the vibrations and radiation of an upright piano soundboard, and design of a system for reproducing its acoustic field (in French). Ph.D. thesis, Université du Maine, Le Mans (1997)
12. Elliott, S.J., Johnson, M.E.: Radiation modes and the active control of sound power. J. Acoust. Soc. Am. **94**(4), 2194–2204 (1993)
13. Gautier, F., Tahani, N.: Vibroacoustic behavior of a simplified musical wind instrument. J. Sound Vib. **213**(1), 107–125 (1998)
14. Gautier, F., Nief, G., Gilbert, J., Dalmont, J.: Vibro-acoustics of organ pipes-revisiting the Miller experiment. J. Acoust. Soc. Am. **131**, 737–738 (2012)
15. Gough, C.: Violin plate modes. J. Acoust. Soc. Am. **137**(1), 139–153 (2015)
16. Gough, C.E.: A violin shell model: vibrational modes and acoustics. J. Acoust. Soc. Am. **137**(3), 1210–1225 (2015)
17. Graff, K.F.: Wave Motion in Elastics Solids. Dover, New York (1991)
18. Griffin, S., Lane, S.A., Clark, R.L.: The application of smart structures towards feedback suppression in amplified acoustic guitars. J. Acoust. Soc. Am. **113**(6), 3188–3196 (2003)
19. Heckl, M.: Vibrations of one- and two- dimensional continuous systems. In: Encyclopaedia of Acoustics, vol. 2, pp. 735–752. Wiley, New York (1997)
20. Hu, Q., Wu, F.: An alternative formulation for predicting sound radiation from a vibrating object. J. Acoust. Soc. Am. **103**(4), 1763–1774 (1998)
21. Junger, M.C., Feit, D.: Sound, Structures and Their Interaction. Acoustical Society of America, Melville (1993)
22. Kausel, W., Chatziioannou, V., Moore, T., Gorman, B., Rokni, M.: Axial vibrations of brass wind instrument bells and their acoustical influence: theory and simulations. J. Acoust. Soc. Am. **137**, 3149–3162 (2015)
23. Lambourg, C., Chaigne, A.: Measurements and modeling of the admittance matrix at the bridge in guitars. In: Proceedings of the SMAC 93, pp. 448–453 (1993)
24. Le Pichon, A.: Method for predicting the acoustic radiation of volumic structures composed of one or several vibrating surfaces. Application to stringed musical instruments (in French). Ph.D. thesis, Université Paris 11 (1996)
25. Le Pichon, A., Berge, S., Chaigne, A.: Comparison between experimental and predicted radiation of a guitar. Acust. Acta Acust. **84**, 136–145 (1998)
26. Lesueur, C.: Acoustic radiation of structures (in French). Collection de la direction des études et recherches d'Electricité de France. Eyrolles, Paris (1988)
27. Nederveen, C.J., Dalmont, J.: Pitch and level changes in organ pipes due to wall resonances. J. Sound Vib. **27**, 227–239 (2004)
28. Nightingale, T.R.T., Bosmans, I.: On the drive-point mobility of a periodic rib-stiffened plate. Tech. Rep. NRCC-45609, National Research Council Canada, Ottawa (2006)
29. Pico, R.: Vibroacoustics of slightly bent cylindrical tubes. influence of the wall vibrations on the oscillations of wind musical instruments (in French). Ph.D. thesis, Universités du Maine (France) et de Valence (Espagne) (2004)
30. Quaegebeur, N.: Nonlinear vibrations and acoustic radiation of thin loudspeaker-like structures (in French). Ph.D. thesis, ENSTA ParisTech (2007)
31. Ruzzene, M.: Structural acoustics. Class notes, School of Aerospace Engineering, Georgia Institute of Technology (2003)
32. Schedin, S., Lambourg, C., Chaigne, A.: Transient sound fields from impacted plates: comparison between numerical simulations and experiments. J. Sound Vib. **221**(3), 471–490 (1999)
33. Skudrzyk, E.: The mean value method of predicting the dynamic response of complex vibrators. J. Acoust. Soc. Am. **67**(4), 1105–1135 (1980)
34. Soedel, W.: Vibrations of Shells and Plates, 3rd edn. Marcel Dekker, New York (2004)
35. Stepanishen, P.R.: Transient radiation from piston in an infinite baffle. J. Acoust. Soc. Am. **49**(5B), 1629–1638 (1971)

36. Suzuki, H.: Vibration and sound radiation of a piano soundboard. J. Acoust. Soc. Am. **80**(6), 1573–1582 (1986)
37. Suzuki, H., Tichy, J.: Diffraction of sound by a convex or a concave dome in an infinite baffle. J. Acoust. Soc. Am. **70**(5), 1480–1487 (1981)
38. Wallace, C.E.: Radiation resistance of a rectangular panel. J. Acoust. Soc. Am. **51**, 946–952 (1972)
39. Williams, E.G.: Numerical evaluation of the radiation from unbaffled finite plates using the FFT. J. Acoust. Soc. Am. **73**, 343–347 (1983)
40. Williams, E.G.: Fourier Acoustics: Sound Radiation and Nearfield Acoustical Holography. Academic, New York (1999)
41. Wolfe, J.: Music acoustics web page, the University of New South Wales. http://www.phys.unsw.edu.au/music/ (2007)

Chapter 14
Radiation of Complex Systems

Antoine Chaigne and Jean Kergomard

Abstract The fundamental properties of the constitutive elements of musical instruments were presented in the previous chapters: vibrating systems, holes, and air columns. Some fundamental coupling situations between such elements, as well as their radiation in free space were also described. In this last chapter, a detailed presentation of some selected instruments is given (vibraphone, timpani, guitar, and piano). In the previous approach made on simple systems, one goal was to give a general view on several order of magnitudes for the involved physical quantities, in order to identify general laws in terms of time, space, and frequency. Here, a complementary point of view is adopted: the geometry, material and frequency range of a given instrument are fixed, and the interaction between its elements is examined for this particular configuration. The objective is to build a complete model of an instrument and to study the vibratory and acoustical phenomena from the initial excitation (mallet impact, struck or plucked string) to the acoustic radiation. The modeling complexity of these sound sources is due to several causes: complex structural geometry, coupling between different components with distinct mechanical properties, broad frequency range, and required accuracy. Finally, the previous presentation of wind instruments is supplemented here by the analysis of radiation by both the tone holes and apertures, and by the resulting interferences.

A. Chaigne (✉)
Institute of Music Acoustics, University of Music and Performing Arts Vienna (MDW), Anton-von-Webern-Platz 1, 1030 Vienna, Austria
e-mail: antchaigne@gmail.com

J. Kergomard
CNRS Laboratoire de Mecanique et d'Acoustique (LMA), 4 impasse Nikola Tesla CS 40006, 13453 Marseille Cedex 13, France
e-mail: kergomard@lma.cnrs-mrs.fr

A. Chaigne, J. Kergomard, *Acoustics of Musical Instruments*, Modern Acoustics and Signal Processing, DOI 10.1007/978-1-4939-3679-3_14

14.1 Example of the Vibraphone

14.1.1 Introduction

The vibraphone belongs to the family of mallet percussion instruments, as the xylophone, the marimba, and the glockenspiel [47]. All these instruments work in a similar way: horizontal beams are excited by the impact of a mallet and radiate sound. In most cases, a tubular resonator is put under each beam. The function of such resonators is to capture a fraction of the sound energy radiated by the beam and, in turn, to radiate again after amplification and filtering of some frequencies. The instruments of this family differ from each other both by their geometry (size) and material. A vibraphone is made of metallic beams, whereas marimba and xylophone beams are usually made of wood. The case of the vibraphone, which is presented here, can be generalized to the other mallet instruments.

From the point of view of radiation, the vibraphone is a typical example of interaction between a field radiated by an impacted beam and a tubular resonator placed in its vicinity (see Fig. 14.1).[1]

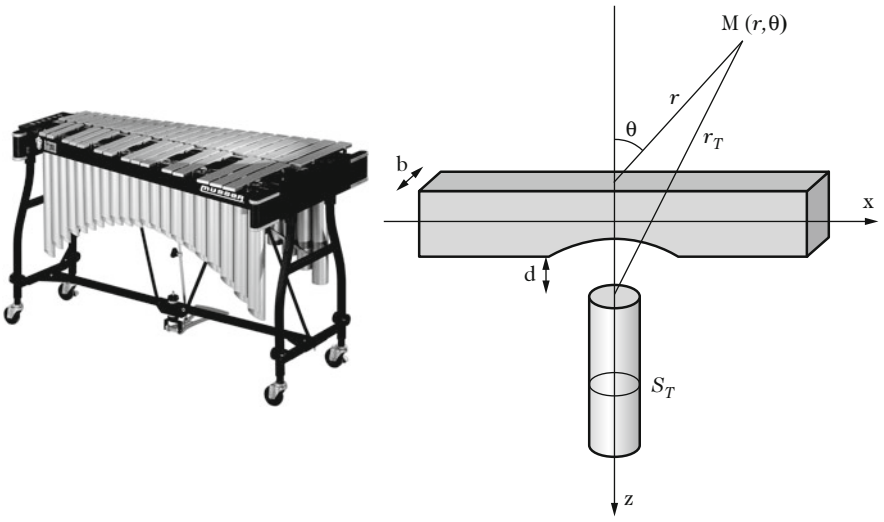

Fig. 14.1 *Left*: vibraphone (Courtesy of Rythmes et Sons). *Right*: schematic representation of a vibraphone beam and tube. The pressure at point $M(r, \theta)$ is the sum of the pressure radiated by the beam and the pressure radiated by the open end of the tube at a distance r_T

[1] In some instruments, both ends of the tube are open. In the present chapter, the example of a resonator with an open end on the beam side, and a closed end at the bottom, is investigated.

In Chap. 1, the flexural equations of motion for an Euler–Bernoulli beam were presented. The eigenmodes were calculated in Chap. 3, for beams of constant and variable sections. The damping mechanisms in both the tubes and beam materials were presented in Chap. 5. Here, the radiation of the complete instrument is described. According to the usual geometry and materials of the instrument, the following simplifying assumptions are made:

1. The vibrations of the beam are not affected by the radiated field. It has been shown in the previous chapters that this assumption is reasonable, as long as the ratio between air and material density is small and, in addition, for a sufficiently rigid beam, as it is the case here. This amounts to assuming that the coefficient ε in Eq. (13.67) is small compared to unity.
2. The transverse dimension (width) b of the beam is small compared to the acoustic wavelength: $kb \ll 1$. For a typical beam of width $b = 3\,\text{cm}$, this yields an upper limit of 11 kHz for the frequency. In most mallet instruments, the spectral energy is below this limit, except for the highest notes of the xylophone. In what follows, this condition is assumed to be fulfilled, so that some approximations can be made for calculating the radiated pressure field, according to the results presented in Chap. 12.
3. The radiation of the tube, at its open end, is not affected by the presence of the beam. It has been shown experimentally that this assumption remains valid as long as the end-beam distance remains small: $d/b \gg 1$. Otherwise, the eigenfrequencies of the tube might be modified, due to the change in the boundary conditions [25].
4. Only the flexural vibrations of the beam contribute to the radiation significantly. This is almost true in practice, except if the impact is located near the corners. In this latter case, additional torsional vibrations are generated. These vibrations are generally unpleasant and unwanted, since they are not in harmonic relationships with the flexural modes. In what follows, it is thus assumed that the vibraphone is struck by a talented player who is able to control the impact point of the mallets with precision! Denoting y_0 the distance between the symmetry axis of the beam and the impact point, the condition $y_0/b \ll 1$ is assumed (see Fig. 14.2).
5. Finally, it is assumed that the diameter D of the tube is sufficiently small so that only the longitudinal modes exist. This is true under the condition $D/\lambda \ll 1$, where λ is the acoustic wavelength (see Chap. 7). It is also admitted that the walls of the tube are rigid and do not contribute to the radiation.

Fig. 14.2 Excitation of the beam near the symmetry axis, in order to avoid the generation of torsional waves ($y_0 \ll b$)

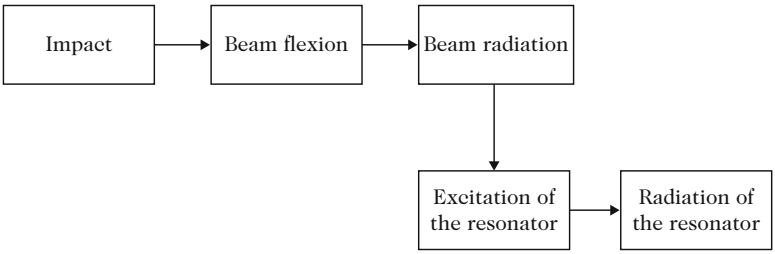

Fig. 14.3 Physical principles of the vibraphone. The beam radiates due to the impact of the mallet. A part of the radiated field excites the air column in the tubular resonator. The resonator radiates, in turn, a sound field where its own eigenfrequencies are dominant in the spectrum. The beam-tube coupling is efficient only if the tube is tuned so that some of its eigenfrequencies are close to the eigenfrequencies of the beam (see Fig. 14.4)

The physical behavior of the vibraphone can be summarized as follows (see Fig. 14.3):

- The impact of the mallet induces flexural vibrations in the beam . The excited eigenfrequencies are close to those of a beam with free boundary conditions. The suspension of the beam by a cord can be viewed as a flexible spring, so that the eigenfrequency of the oscillator made of the complete beam mass and the cord is equal to a few Hz, and thus is far below the first flexural mode. This rigid-body mode is very weakly coupled to the flexural modes, and does not radiate sound.
- From the point of view of radiation, the oscillating beam can be viewed as a linear array of dipoles (see the next section).
- A fraction of the acoustic energy radiated by the beam is captured by the tubular resonator. This resonator acts as an acoustic *filter*. Only the spectral components of the input field which are close to the eigenfrequencies of the tube can persist. The other components are subject to destructive interferences inside the tube, and are attenuated progressively.
- A fraction of the acoustic energy stored in the tube is radiated to the external field through the open end. The resonator thus acts as a secondary source. An observer in space receives the pressure contributions of both the beam and tube. The spectral content of the tube pressure is dominated by the eigenfrequencies of the tube: the amplitude of these components is significant only if some of the input components (the eigenfrequencies of the beam) coincide with some eigenfrequencies of the tube: the tube is then said to be tuned to the beam (see Fig. 14.4).

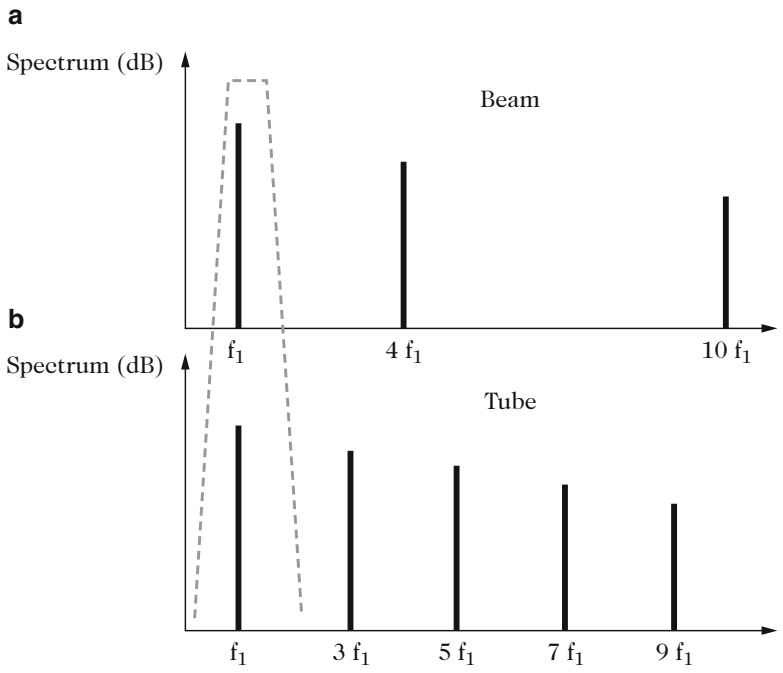

Fig. 14.4 Basic principles of tuning between a beam and a tubular resonator. (**a**) shows the spectral content of a tuned beam where the three first flexural modes are tuned to f_1, $4f_1$, and $10f_1$, respectively. (**b**) shows the spectrum of a tube closed at one end and open at the other, for which only the odd harmonics exist. It can be seen on this example that the beam and the tube are tuned if both fundamental frequencies are equal. The upper harmonics of the beam do not excite the tube

14.1.2 Radiation of the Beam

If the acoustic wavelength λ is large compared to the width b of the beam, then the reflection of waves radiated by the beam on its surface is negligible. As a consequence, it has been shown in Chap. 12 that the monopolar terms can be neglected in the Kirchhoff–Helmholtz integral (12.61). The only remaining terms are the dipolar terms due to the oscillation of the beam [34]. The total field radiated by the beam is then the sum of elementary dipoles distributed along its length L. A discrete formulation of this sum is given below. Each elementary dipole has a width $\Delta x = L/N$, where N is the number of elements, length b, and thickness $h(x)$ (see Fig. 14.5).

In order to benefit from simple known results, it is convenient to represent each element of the beam by an equivalent oscillating sphere. This is achieved by considering each element as a sphere with identical volume. The error made by using such an approximation becomes noticeable when the acoustic wavelength is less than or equal to Δx, which corresponds here to typically 1–5 mm. The radius

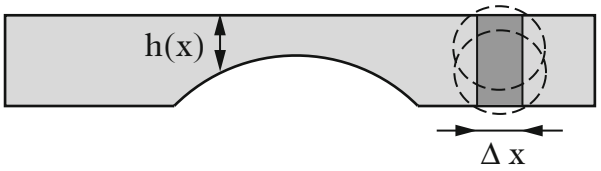

Fig. 14.5 Decomposition of the beam into an equivalent linear array of elementary oscillating spheres

$a(x)$ of the equivalent sphere is given by:

$$\frac{4}{3}\pi a^3(x) = bh(x)\Delta x = \Delta V(x), \tag{14.1}$$

where $x \in [0, L]$. Under the assumptions of far field, as seen in Chap. 12, the field radiated by each equivalent oscillating sphere is written in the time domain [see Eq. (12.40)]:

$$\Delta p[r(x), \theta(x), t] = \frac{3\rho \Delta V(x) \cos\theta(x)}{8\pi r(x)} \times \left[\frac{1}{r(x)}\gamma\left(x, t - \frac{r(x)}{c}\right) + \frac{1}{c}\frac{\partial \gamma}{\partial t}\left(x, t - \frac{r(x)}{c}\right)\right], \tag{14.2}$$

where γ is the beam acceleration at point x, $r(x)$ and $\theta(x)$ are the polar coordinates of the listening point. In total, the pressure field p_B radiated by the beam is written

$$p_B(r, \theta, t) = \sum_x \Delta p[r(x), \theta(x), t], \tag{14.3}$$

where the reference coordinates r and θ correspond to the location of the listening point with regard to the center of the beam (see Fig. 14.1). One main property of the dipole array lies in the pronounced directivity of the radiated pressure along the axis $\theta = 0$ (see also the discussion on the linear arrays in Chap. 12), which is confirmed experimentally. Another property is that the pressure is zero in the beam plane.

14.1.3 Radiation of the Resonator

The tubular resonator with cross-section S_T is oriented along the z-axis (see Fig. 14.6). $v(0, t)$ and $p(0, t)$ are the acoustic velocity and sound pressure at the open end, respectively, and $p_T(r_T, t)$ is the pressure radiated by the open end at a given point in space (see Fig. 14.6).

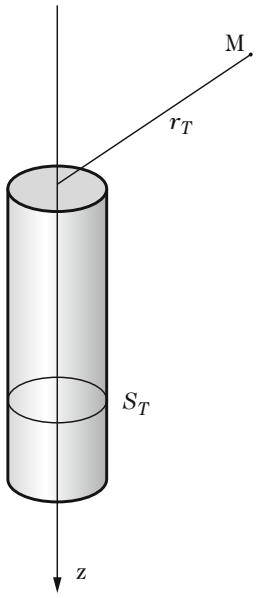

Fig. 14.6 Tubular resonator

It is assumed that the pressure radiated by the tube is similar to the one of a monopole, as long as the diameter of the tube remains smaller than the acoustic wavelength. In what follows, the diffraction of the tube is also ignored. Using the results demonstrated in Chap. 12, the pressure radiated by the tube is written

$$p_T(r_T, t) = \frac{\rho S_T}{4\pi r_T} \frac{\partial v}{\partial t} \left(0, t - \frac{r_T}{c}\right), \tag{14.4}$$

or, equivalently, using Euler equation:

$$p_T(r_T, t) = \frac{S_T}{4\pi r_T} \frac{\partial p}{\partial z} \left(0, t - \frac{r_T}{c}\right) . \tag{14.5}$$

The pressure can be determined at any point in space provided that the pressure at the end of the tube is known. This end tube pressure is the sum of both the beam pressure p_B and the tube pressure p_T. Such a superposition corresponds to the case of two tubes explained in Sect. 12.6.3 of Chap. 12.

In the frequency domain, denoting $Z_r(\omega)$ the radiation impedance of the tube, and taking further the orientation of the z axis into account, we get

$$P(0, \omega) = -Z_r(\omega) S_T V(0, \omega) + P_B(\omega) . \tag{14.6}$$

where $P(r, \omega)$ is the Fourier transform of $p(r, t)$. Since the tube is unbaffled and radiates in the unbounded space, we can use the Levine–Schwinger expression for the impedance (see Chap. 12).

Converting Eq. (14.6) into the time domain is not an easy task [26]. One possible method consists in expressing the impedance under the form of a fraction of two polynomials in $j\omega$ of the form:

$$Z_r(\omega) = \frac{\rho c}{S_T} \frac{b_0 + b_1 j\omega + b_2 (j\omega)^2 + \cdots}{a_0 + a_1 j\omega + a_2 (j\omega)^2 + \cdots}, \tag{14.7}$$

as it has already been done for Eq. (12.132). As a result, a time-domain formulation of Eq. (14.6) is obtained

$$\left[a_0 + a_1 \frac{\partial}{\partial t} + a_2 \frac{\partial^2}{\partial t^2} \right] (p_B(t) - p(0,t)) = \rho c \left[b_0 + b_1 \frac{\partial}{\partial t} + b_2 \frac{\partial^2}{\partial t^2} \right] v(0,t) \, . \tag{14.8}$$

Finally, the time-domain evolution of both internal and external tube field can be obtained by combining the boundary condition (14.8), the boundary condition at the other end of the tube (either closed end or another open end though without interaction with beam), and the wave equation inside the tube (1.111). In contrast with the beam field, the tube field is almost omnidirectional.

Figure 14.7 shows, on the left, an example of recorded pressure waveform radiated by a vibraphone beam tuned to its resonator and struck by a mallet. The measurements were made in an anechoic chamber. This waveform is compared (on the right) with the pressure waveform simulated with the help of the model presented above, using finite differences [24]. One can see on this figure that the contribution of the beam reaches first the observation (listening) point, and that the tube contribution arrives a few milliseconds later. This delay is due to the fact that the resonator behaves here like an harmonic oscillator forced in the vicinity of its eigenfrequency. As a consequence (as seen in Chap. 2), a rather slow growth is observed. Contrary to what is usually thought, this delay is not due to the

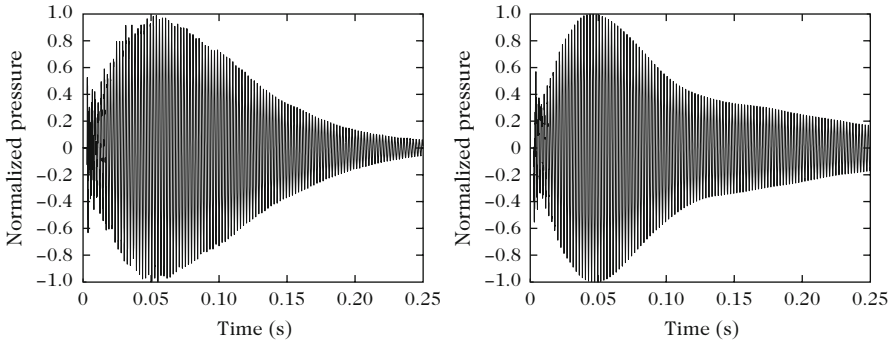

Fig. 14.7 Pressure waveform radiated by a vibraphone beam with a tuned tubular resonator. (*Left*) Measurements. (*Right*) Simulation. One can see an abrupt initial pressure jump due to the beam, followed by a slow growth due to the resonator and a slow decrease due to damping

propagation between the beam and the open end. The beam-tube distance is usually equal to a few centimeters: thus, the propagation delay should be equal to 1 or 2 ms. This value is about ten times smaller than the observed delay.

From a musical viewpoint, tubular resonators should be used if slowly growing "aftersound" is wanted. In contrast, the tubes should be (totally or partially) closed if the purpose is to emphasize the clarity and suddenness of the initial transients. Finally, it should be noticed that, in the complete instruments, the tubes are very close to each other and that the differences in tuning are only one semitone. As a consequence, they often interact together (see also Sect. 4.3), which contribute to enrich the sound of the instrument.

14.2 Example of the Kettledrum

14.2.1 Introduction

The kettledrums (or timpani), as other drums like the snare drums or the bass drums, belong to family of membranophones. As indicated in this classification name, these instruments are made of one (or two) membrane(s) (or head(s)) stretched over a cavity filled with air and struck by a mallet. Originally, the heads were made of calfskin. Today, Mylar (polyethylene terephthalate) is the most common material used for the heads, because of its better homogeneity, tensile strength, and relatively smaller sensitivity to humidity changes. However, a number of orchestras today still prefer using timpani with calfskin heads, especially for playing music of the past centuries, because of their characteristic tone color. One physical property of calfskin lies in its higher internal damping, compared to Mylar. An interesting feature of timpani is due to the fact that these instruments together have a decisive rhythmic function and a well-defined pitch.

The equations of motion for a stretched membrane were presented in Chap. 1. Their modes of vibration were calculated in Chap. 3 for a homogeneous circular membrane in vacuo. However, in order to understand the observations and experiments made on timpani, it is necessary to take further the coupling of the membrane with both external air and cavity into account. One-dimensional examples of coupling between a vibrating structure and a cavity were presented in Chap. 6. Here, the example of timpani gives us the opportunity to generalize these results to the case of a 2-D structure (the membrane) coupled to a 3-D cavity (Fig. 14.8). In Chap. 13 it was shown, in addition, to what extent the vibrations of a structure are modified by its radiated field. The case of timpani yields a situation where the density, the rigidity, and thickness of the membrane are relatively small, so that the reaction of the acoustic field cannot be neglected. One can easily be convinced of this fact by

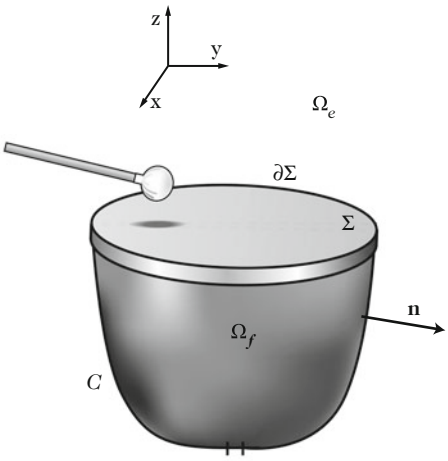

Fig. 14.8 Geometry of the kettledrum, and notations. The head Σ is bounded by its contour $\partial\Sigma$. $\mathscr{C}$ is the external surface of the bowl with normal vector $\boldsymbol{n}$. Ω_i is the internal volume delimited by the bowl and the membrane. Ω_e is the external volume

doing the simple experiments which consist in speaking (or singing!) in front of a timpani head: by lightly touching the head with the fingers, the vibrations of the membrane are clearly felt. In addition, the modifications of the tone color due to the additional sound field of the membrane excited by the speech also are clearly heard.

The joint action of both external and internal (cavity) pressure on the membrane also contributes to modify its eigenfrequencies compared to the in vacuo case. Since the membrane oscillates freely after the impact of the mallet, the spectrum of the emitted sound is composed of the eigenfrequencies of the complete coupled system (see Fig. 14.15).

It has been shown in Chap. 3 that the eigenfrequencies of a circular membrane in vacuo are not integer multiples of a fundamental frequency. In contrast, the spectral content of timpani sounds shows that the eigenfrequencies of timpani sounds, for an impact excitation close to the edge, are almost integer multiples of a missing fundamental (2f, 3f, 4f, 5f,...) as shown in Fig. 14.15. This is the reason why the instrument has a well-defined pitch, though it is a bit less clearly defined as, for example, the pitch of a violin or of a piano sound.[2] A number of authors have shown that both the external and internal pressure field acting on the membrane are responsible for these frequency shifts (see, for example, [5]). However, due to mathematical difficulties, accurate calculations of the coupled modes of the complete instruments were obtained only recently [44, 45]. In what

[2]Notice that the perceived pitch rather fits with the frequency of the first partial (at 2f) than with the missing fundamental (f). This *octave ambiguity* has several reasons: first, the lowest partial usually has the highest amplitude and, secondly, the frequency of the missing fundamental is usually low (less than 100 Hz), and thus the human ear is less sensitive in this frequency domain, from the point of view of pitch perception.

follows, emphasis is put on the physical modeling of the kettledrum and on its corresponding time-domain numerical formulation. Notice that another technique is possible, based on the use of Green's functions [18]. However, the use of this technique is restricted to simple geometrical shapes of the bowl (cylinder or half-sphere) with standard systems of coordinates.

In the following paragraph, it is also shown, as an interesting application, how to take advantage of the air-membrane-cavity coupling for determining the tension of the membrane experimentally. This determination is based on the simple measurements of the eigenfrequencies, when direct mechanical measurements of the tension usually are cumbersome and not very precise. Finally, a perturbation method is briefly presented, whose aim is to obtain a direct approximation of the eigenfrequencies of the instrument. This method can be viewed as a generalization of the results presented in Chap. 13.

14.2.2 Presentation of the Physical Model

It is supposed here, as a simplifying assumption, that only the head of the kettledrum vibrates, consecutive to the impact of the mallet, and not the bowl. In the reality, vibrations of the bowl can be sometimes observed, especially for light bowls in fiberglass. A small hole is drilled at the bottom of the cavity (with a diameter of typically 1–2 cm) in order to equalize the static pressure on both sides of the membrane. This hole plays the same role as the Eustachian tube in the middle ear: a difference in static pressure on both sides would restrict the motion of the membrane [31]. Apart from this function, the hole has no effect on the acoustic behavior of the instrument, because of its small dimensions compared to the acoustic wavelengths of the main spectral components. It is currently observed that timpani spectra do not have significant energy above 1 kHz, which corresponds to an acoustic wavelength of 34 cm.

Another function of the cavity is to enclose the acoustic wave generated by the membrane on its back side, as it is observed on other systems like loudspeaker cabinets, for example. This prevents the system from destructive interferences between forward and backward sound fields, which would otherwise reduce its acoustical efficiency.

In what follows, $m_s = \rho_s h$ denotes the surface density of the membrane of density ρ_s and thickness h, and $c_f = \sqrt{\frac{\tau}{m_s}}$ is the wave speed of the flexural waves on the membrane for a tension τ in $\mathrm{N\,m^{-1}}$ (see Chap. 1). In timpani, a typical order of magnitude for c_f is 100 m/s, and the surface density of Mylar is $0.1\,\mathrm{kg/m^2}$.

14.2.2.1 Equations of Vibrations

To a first approximation, one can consider that the initial velocity condition for the displacement $\xi(t)$ of the mallet's center of gravity reduces to $\dot{\xi}(0) = -V_0$, where the origin of time is taken as the mallet just reaches the membrane.[3] In addition, we have $\xi(0) = \delta$, where δ is the thickness of the felt before the compression (see Fig. 14.9). During the contact phase, the mallet's head of mass m is subjected to the compression force $F(t)$ resulting from its interaction with the membrane which yields (if we neglect the gravity force):

$$m\frac{d^2\xi}{dt^2} = F(t)\ . \tag{14.9}$$

$F(t)$ can be conveniently described by a nonlinear function of the felt compression of the form (see Chap. 1):

$$F(t) = K\left[(\delta - \xi(t) + W(t))^+\right]^\alpha \tag{14.10}$$

where K is a stiffness coefficient, and α an exponent. Both constants are derived from experiments by curve-fitting procedures. For typical timpani mallets, α usually

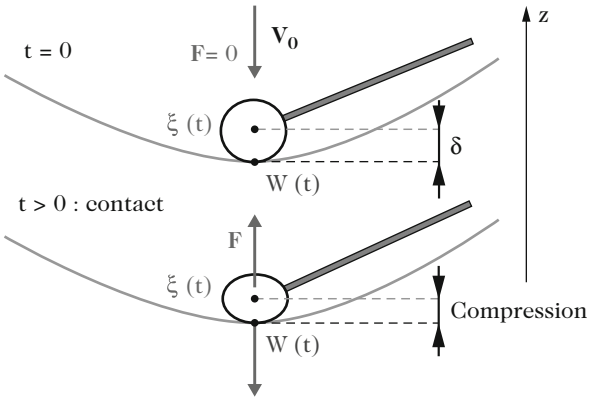

Fig. 14.9 Impact of the mallet on the membrane. At time $t = 0$, the mallet comes in contact with the membrane with an initial normal velocity V_0. At this time, both the compression of the felt and the interaction force are assumed to be zero. δ denotes the thickness of the felt before its compression. During the contact phase, this thickness decreases and becomes equal to $(W - \xi)(t)$, where W is the mean displacement of the membrane on the contact area, and ξ the center of gravity of the rigid mallet's head. An interaction force then exists between mallet and membrane

[3]The negative sign is coherent with the orientation of the vertical z axis.

lies in the range 2–4 [13]. The symbol "+" in Eq. (14.10) means that the force is zero in the absence of contact. $W(t)$ is the mean value of the membrane's displacement over the contact area, defined as:

$$W(t) = \int_{\Sigma} w(x, y, t) g(x, y)\, dS. \tag{14.11}$$

In (14.11), $w(x, y, t)$ is the transverse displacement of a given point of the membrane of surface Σ, and $g(x, y)$ is a normalized distribution function so that $\int_{\Sigma} g(x, y)\, dS = 1$. In practice, a good approximation of the size of g can be obtained experimentally by measuring the spot drawn on the head by a felt pre-soaked with dark ink.[4] Strictly speaking, this function g should vary with time, since the felt does not press instantaneously on the head. This effect is not taken into account here.[5]

The model presented below is restricted to the linear transverse vibrations of a damped membrane without stiffness. The assumption of linearity might be questionable during the impact since a motion with an amplitude 10–100 times higher than the thickness of the membrane can be observed as the mallet is in contact with it. The linear equation of motion is written [45]:

$$m_s \frac{\partial^2 w}{\partial t^2} = \operatorname{div}\left[\tau \nabla \left(w + \eta \frac{\partial w}{\partial t}\right)\right] - f(t) g - [p]\,|_{\Sigma}, \tag{14.12}$$

where $[p]\,|_{\Sigma} = (p_e - p_i)_{\Sigma}$ is the pressure jump acting on the membrane. In comparison with the membrane model presented in Chap. 1, notice the introduction of the force density $f(t)$ which represents the action of the mallet and, in addition, the viscoelastic damping coefficient η which accounts for the average losses in polymer (such as the Mylar, commonly used for timpani heads). The viscoelastic term yields an increase of damping with frequency, as observed experimentally. For nonuniform membranes, m_s and τ depend on the spatial coordinates. The tension then becomes a tensor of order 2 (as seen in Chap. 1). The force density $f(t)$ is related to the interaction force by the relation:

$$F(t) = f(t) \int_{\Sigma} g(x, y)\, dS = f(t)\,. \tag{14.13}$$

It is further assumed that the membrane is fixed at its periphery, which implies

$$w(x, y, t) = 0 \quad \forall (x, y) \in \partial\Sigma, \quad \forall t > 0\,. \tag{14.14}$$

[4]The function g is a smooth and normalized version of the indicator function, which is equal to 1 in the contact area, and 0 outside.

[5]Taking further the flexibility of the mallet's stick would also contribute to improve the model: this flexibility certainly has an influence on the contact time.

The condition (14.14) does not account for the losses at the boundary. This is probably wrong, since the head of a kettledrum is usually stretched over a dissipative rubber ring, and should be revisited in future models. In order to calculate the time evolution of the motion, starting from the membrane at rest, we write the initial conditions:

$$w(x,y,0) = \frac{\partial w}{\partial t}(x,y,0) = 0 \quad \forall (x,y) \in \partial\Sigma \ . \tag{14.15}$$

14.2.2.2 Acoustic Equations

Both the internal (inside the cavity Ω_i) and external acoustic field (in Ω_e) are governed by the basic linear acoustic equations (see Chap. 1):

$$\begin{cases} \dfrac{\partial p}{\partial t} = -c^2 \rho \ \mathrm{div}\boldsymbol{v}_j & \text{in } \ \Omega_j, \quad \text{for } j = e,i \ ; \\ \rho \dfrac{\partial \boldsymbol{v}_j}{\partial t} = -\mathbf{grad} p_j & \text{in } \ \Omega_j, \quad \text{for } j = e,i \end{cases} \tag{14.16}$$

where $\boldsymbol{v}_j$ is the acoustic velocity.

The problem imposes boundary conditions on the surface Γ of the kettledrum composed of the membrane Σ and the bowl $\mathscr{C}$, so that $\Gamma = \Sigma \cup \mathscr{C}$. On the surface Σ (in the plane $z = 0$) we write the continuity equation for the normal velocity:

$$\boldsymbol{v}_j(x,y,0,t).\mathbf{n} = \frac{\partial w}{\partial t}(x,y,t) \ \ \forall (x,y) \in \Sigma, \ \ \forall t > 0, \quad \text{for } j = e,i. \tag{14.17}$$

It is supposed, in addition, that the bowl with surface $\mathscr{C}$ delimiting the air cavity is perfectly rigid, which can be considered as justified for copper bowls. However, it is observed experimentally that fiberglass bowls (used for study instruments) vibrate significantly, especially during the impact. The assumption made here imposes the condition:

$$\boldsymbol{v}_j(x,y,z,t).\boldsymbol{n} = 0 \quad \forall (x,y,z) \in \mathscr{C}, \ \ \forall t > 0, \quad \text{for } j = e,i, \tag{14.18}$$

where $\boldsymbol{n}$ is the unitary vector normal to $\mathscr{C}$ (see the Fig. 14.8). Finally, the following initial conditions are imposed:

$$p_j(x,y,z,0) = 0, \ \ \boldsymbol{v}_j(x,y,z,0) = 0 \ \text{ in } \ \Omega_j, \quad \text{for } j = e,i \ . \tag{14.19}$$

14.2.2.3 Energy Balance

The system of coupled equations presented above has the property that the total energy decreases with time. Through integration of Eq. (14.9) to Eq. (14.18), it can be shown that the different contributions of the system to the total energy are written [44]:

$$\begin{cases} \text{for the mallet :} \quad E_m(t) = \dfrac{m}{2}\left(\dfrac{d\xi}{dt}\right)^2 + \dfrac{K}{\alpha+1}\left[(\delta - \xi(t) + W(t))^+\right]^{\alpha+1}, \\ \text{for the undamped membrane :} \quad E_w(t) = \dfrac{1}{2}\displaystyle\int_\Sigma m_s \left(\dfrac{\partial w}{\partial t}\right)^2 ds + \dfrac{1}{2}\int_\Sigma \tau\, (\mathbf{grad}\, w)^2\, ds, \\ \text{for the air :} \quad E_a(t) = \dfrac{1}{2}\displaystyle\int_{\mathbb{R}^3} \rho \boldsymbol{v}^2 d\Omega + \dfrac{1}{2}\int_{\mathbb{R}^3} \dfrac{p^2}{\rho c^2} d\Omega\ . \end{cases} \tag{14.20}$$

Adding now a viscoelastic damping term with coefficient η in the membrane equation, then the total energy $E = E_m + E_w + E_a$ is governed by [44]:

$$\frac{dE}{dt}(t) = -\eta \int_\Sigma \tau \left(\mathbf{grad}\frac{\partial w}{\partial t}\right)^2 ds\ . \tag{14.21}$$

In practice, as shown in Fig. 14.10, a slow decrease of the total energy is observed, starting from the initial value $E(0) = \frac{1}{2} m V_0^2$. This initial energy is transferred from the mallet to the air-membrane system. Beyond its physical interest, this continuous energy balance is a necessary preliminary step for guaranteeing the stability of the numerical approximation [44].

14.2.3 Eigenfrequencies, Damping Factors, and Tuning of the Instrument

For an undamped membrane in vacuo, it was shown in Chap. 3 that the eigenfrequencies are real solutions of the equation:

$$-c_f^2 \Delta w_{mn} = \omega_{mn}^2 w_{mn}, \tag{14.22}$$

(with a condition of nullity for the displacement at the edge), and the eigenfrequencies were calculated for a circular membrane, explicitly. In the case of a kettledrum, the coupling of the membrane with both the external air and cavity has to be taken into account [18]. As a consequence, the eigenfrequencies become complex, and their imaginary part represents the time decay of the spectral components. In what follows, $\omega_0 = 2\pi f_0$ denotes any eigenfrequency of the undamped membrane in vacuo, and $\tilde{\omega} = \omega + j\alpha = 2\pi\tilde{f} = 2\pi(f + j\alpha/2\pi)$ is the corresponding complex

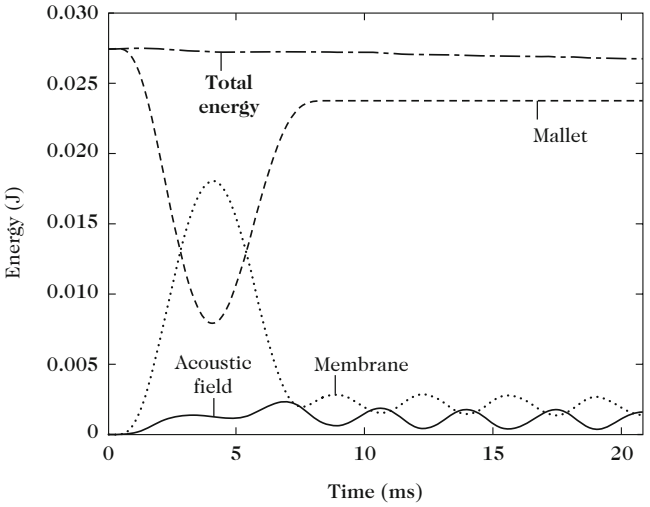

Fig. 14.10 Energy balance for the kettledrum. A time evolving energy exchange is observed between the mallet (*dashed line*), the membrane (*dotted line*), and the acoustic field (*solid line*) during the first 20 ms of the sound. The total energy of the system (*dash-dotted line*) is slowly decreasing with time

frequency when the same membrane is coupled to external air and cavity.[6] In order to characterize the time decay of the eigenmodes, some authors use the quantity τ_{60} (decay time of a free oscillation corresponding to an attenuation of -60 dB of the amplitude), whose definition is identical to the *reverberation time* in room acoustics [18]. We have

$$\tau_{60} = -\frac{\ln 10^{-3}}{\alpha} = \frac{6,9}{\alpha} \,. \tag{14.23}$$

In summary, the practical consequences of air coupling are the following:

1. The real part of the eigenfrequencies are modified substantially. In timpani, these real parts are almost harmonically related (though with a missing fundamental), whereas it is not the case for in vacuo membranes (see Chap. 3). These modifications are clearly seen in Table 14.1, which shows that the real parts of the eigenfrequencies are lowered consecutive to the air loading. In some cases, a reduction of 50 % can be observed.
2. The radiation of the instruments induces an additional damping (radiation losses) to the internal losses of the membrane. As shown in Table 14.1, the radiation

[6]The imaginary part $\alpha/2\pi$ is usually small compared to the real part f (see Table 14.1). Thus the modulus $|\tilde{f}|$ is not very different from f, which explains why the distinction between both quantities is not always mentioned in the literature.

Table 14.1 Typical eigenfrequencies for the first ten modes of a kettledrum (Premier 25″)

Mode (mn)	f_0 (in vacuo) (Hz)	f measured (Hz)	τ_{60} measured (s)	f calculated (Hz)	τ_{60} calculated (s)
01	139	139	0.4	136	0.8
11	222	147	2.8	147	2.4
02	319	221	0.5	221	0.25
21	297	245	4.2	248	5.0
31	369	288	8.4	288	6.0
12	406	315	2.4	315	2.0
41	439	355	4,6	357	4.8
22	487	395	0.9	395	1.3
03	500	408	1.0	403	0.6
51	507	419	5.2	424	3.4

Row 1: references of the modes; row 2: calculated in vacuo eigenfrequencies; row 3: real parts of the measured eigenfrequencies on the kettledrum; row 4: measured decay times τ_{60} of the timpani modes; row 5: calculated real parts of the eigenfrequencies; row 6: calculated decay times τ_{60} of the timpani modes. The calculated eigenfrequencies are the results of a time-frequency analysis performed on simulated tones based on the model presented in Sect. 14.2.2

yields decay times which do not vary monotonically with the rank of the partial. This is a consequence of the fact that the radiation losses depend on the eigenvalue. Notice that a simple structural damping is not able to take such variations into account. One can see, for example, that the symmetrical modes 01, 02, and 03 with a strong monopolar character radiate quite efficiently and, in turn, have a smaller decay time than the anti-symmetrical modes 11, 21, 31, 41, and 51.

Determination of the Eigenfrequencies Using a Perturbation Method

In Table 14.1, the eigenfrequencies were obtained by time-frequency analysis performed on the simulated pressure based on the time-domain model described in Sect. 14.2.2. However, it might be also interesting to calculate these frequencies directly, without the intermediate step of time-domain computation.

For bowls of simple shapes (cylindrical, hemispherical, parabolic,...), the eigenfrequencies of the complete system can be obtained with the help of Green's functions [18]. Alternatively, a general method based on perturbation theory is presented here [44].[7] As for the nonlinear vibrations shown in Chap. 8, the leading idea consists in expanding the eigenfrequencies in series of terms with increasing power of a small dimensionless parameter ε. Here, this parameter is defined as the ratio between air and membrane densities:

$$\varepsilon = \frac{\rho}{\rho_s}\,. \tag{14.24}$$

For Eqs. (14.12) and (14.16), leaving aside the source term due to the action of the mallet, we search solutions of the form $e^{j\tilde{\omega}t}$. As a consequence, the dispersion relation for the membrane loaded on both sides by air and cavity, respectively, is given by[8]:

$$-c_f^2 \Delta w = \tilde{\omega}^2 w + \varepsilon \tilde{\omega}^2 D(\tilde{\omega}) w, \tag{14.25}$$

(continued)

[7] Other methods exist, as the one which consists in expressing the system in terms of matrices, and in calculating the eigenfrequencies by using singular value decomposition (SVD) techniques [30].

[8] A similar example was given in Chap. 13 for the loaded plate.

where $\tilde{\omega}$ is complex. $D(\tilde{\omega})$ is an operator accounting for the radiation. Both the eigenshapes and the eigenfrequencies are expanded onto the in vacuo modes as follows:

$$\begin{cases} \tilde{w}^{\varepsilon}_{mn} = w_{mn} + \varepsilon \sum_{kl \neq mn} \lambda^{mn}_{kl} w_{kl} + \varepsilon^2 \sum_{kl \neq mn} \gamma^{mn}_{kl} w_{kl} + o(\varepsilon^3), \\ \tilde{\omega}^{\varepsilon}_{mn} = \omega_{mn} + \varepsilon\, \tilde{\omega}^{a}_{mn} + \varepsilon^2 \tilde{\omega}^{b}_{mn} + O(\varepsilon^3)\,. \end{cases} \tag{14.26}$$

where we limit ourselves here to the order 2, for simplicity. As mentioned previously in Chap. 5, the eigenmodes also become complex: therefore, we write $\tilde{w}$. Inserting (14.26) in (14.25), and taking advantage of the orthogonality of the in vacuo modes (see the general method in Chaps. 3 and 13), the coefficients of order 1 of the expansion are given by:

$$\begin{cases} \lambda^{mn}_{kl} = \dfrac{\omega^2_{mn}}{\omega^2_{kl} - \omega^2_{mn}} \langle D(\omega_{mn}) w_{mn}, w_{kl} \rangle \quad \forall (k,l) \neq (m,n), \\ \omega^{a}_{mn} = -\dfrac{\omega_{mn}}{2} \langle D(\omega_{mn}) w_{mn}, w_{mn} \rangle, \end{cases} \tag{14.27}$$

where the scalar products are indicated by the usual symbol $\langle\ \rangle$. The reader can refer to [44] for the coefficients of order 2. For the example reported in Table 14.1, the results of this perturbation method are in excellent agreement with the values obtained by time-frequency analysis [44].

Application: Experimental Determination of a Timpani Head's Tension

One interesting application of the dispersion relation of the air-loaded membrane is the experimental determination of its tension τ. It is assumed here that the membrane is uniform.

The direct static measurements of the tension are usually difficult to achieve, and suffer from insufficient precision. Its main principle is based on the vertical deflexion η of a weight M put in the center of the membrane. With a the radius of the membrane and b the radius of the cylindrical mass, we have (see Fig. 14.11) [39]:

$$\eta(b) = \frac{Mg}{2\pi\tau} \ln \frac{a}{b}\,. \tag{14.28}$$

One drawback of the static method is that η must be kept sufficiently small so that the assumption of linearity is fulfilled and, in turn, that the increase of the tension due to the vertical deflexion η is negligible (see Chap. 8). In addition, it was shown that the deflexion must be measured with a precision equal at least to 0.1 mm, for a typical 1 % accuracy on the tension [12].

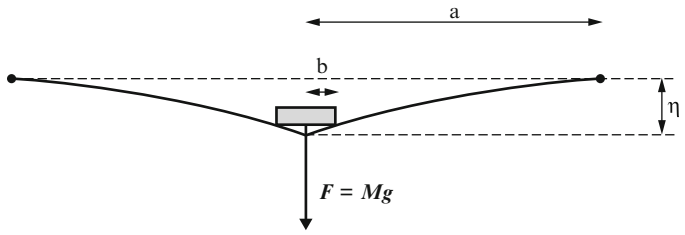

Fig. 14.11 Static determination of the tension for a circular membrane. The deflexion η is measured, consecutive to the action of a mass M put at the center. The size of the mass is assumed to be small compared to the radius of the membrane

The alternative method presented below is based on a comparison between the wave velocity on the air-loaded membrane and the wave velocity in vacuo. The tension can be then estimated from the measurements of the eigenfrequencies of the air-loaded membrane, which corresponds to the real conditions of use of the instrument.

The dispersion relation for the infinite membrane loaded by the air on both sides is written

$$\tau = c_F^2(\omega)\left[m_s + \frac{2\rho}{\omega\sqrt{\frac{1}{c_F^2(\omega)} - \frac{1}{c_f^2}}}\right], \tag{14.29}$$

where c_F is the flexural wave speed in the presence of fluid, and $c_f = \sqrt{\tau/m_s}$ the wave speed in vacuo. For typical values of kettledrum's parameters, the dispersion curve of the membrane takes the shape shown in Fig. 14.12. One can check that the fluid–structure coupling primarily affects the wave speed of the lowest frequencies. As the frequency f increases, the speed c_F asymptotically tends to c_f while remaining always smaller. Returning now to (14.29), one can see that the tension can be estimated from the estimation of c_F. One remaining question is to know to what extent the model of an infinite membrane loaded on both sides can be applicable to the case of timpani. The answer is given by examining the perturbation terms calculated in (14.27). These terms show that:

- The presence of the cavity primarily affects the axisymmetrical modes ω_{0n} of the membrane which produces a change of volume in the cavity and, in turn, a stiffness-like effect. In contrast, the model (14.29) well accounts for the asymmetrical modes and, in particular, for the modes ω_{m1} (simply denoted $m1$-modes hereinafter) which are dominant in the pressure spectrum.
- The coefficients λ_{kl}^{mn} are small for the asymmetrical modes, which means that the modal shapes are weakly perturbed by the fluid.

As a consequence, provided that only the asymmetrical modes are considered, the following relation (3.147) obtained in Chap. 3 can be used:

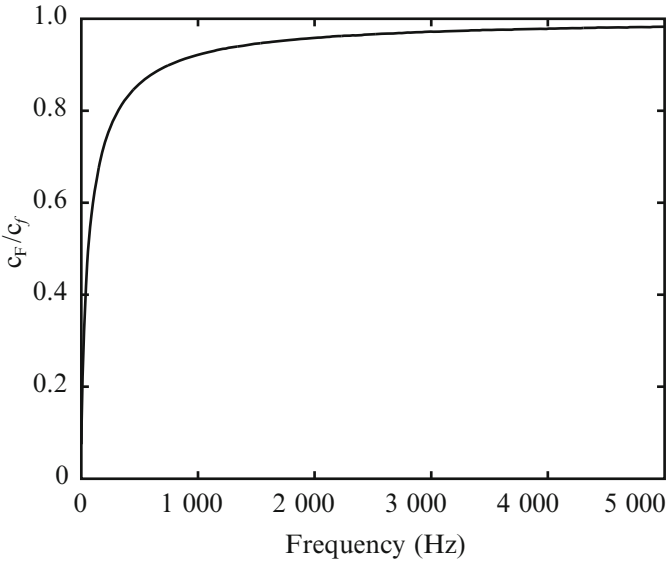

Fig. 14.12 Dispersion curve for an infinite membrane. The effect of the fluid loading is essentially pronounced in the low-frequency range

$$c_F(\omega_{mn}^{\varepsilon}) = \frac{\omega_{mn}^{\varepsilon}}{\beta_{mn}}, \tag{14.30}$$

where the coefficients $\beta_{mn}a$ are the roots of the Bessel functions, with a the radius of the membrane.

As shown in Fig. 14.13, it can be seen that an almost constant value of the tension is derived from the measurements of the asymmetrical modes of the kettledrum. However, a small increase of the estimate with frequency is to be noted.[9]

14.2.4 Acoustic and Vibratory Fields: Time-Domain Analysis

14.2.4.1 Vibration of the Head

The fictitious domain method (see Sect. 14.2.6) is a convenient tool for solving the complete set of equations that govern the kettledrum model (14.9)–(14.18). The results of these simulation were validated by comparisons with measurements performed on real instruments [45]. A few representative examples of these

[9] In practice, comparisons between measurements and simulations using the estimated values of the tension show that the error made on the determination of the tension with this method is of the order of 1–3 % [12].

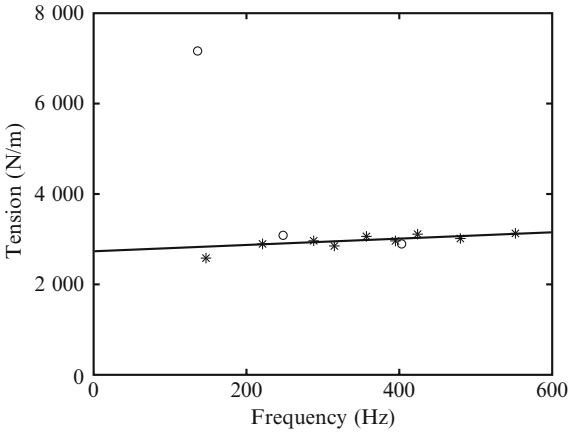

Fig. 14.13 Estimation of the tension of a kettledrum's head from measurements of its eigenfrequencies. The symbols *open circle* designate the axisymmetrical modes, and the symbols *asterisk* the asymmetrical modes

Fig. 14.14 Profile of the timpani's head during the first 12 ms of the sound. The successive vibratory states of the displacement are separated by a time interval of 2 ms (increasing time scale *from left to right*)

comparisons are described below. These examples illustrate the vibroacoustics of timpani in the time domain, from the initial impact of the mallet on the head taken as the origin of time.

Figure 14.14 shows the vibrations of the head during the first 12 ms of the sound. It is assumed that the head is uniformly stretched, and at rest at the origin of time. Due to the impact, transversal waves propagate on the membrane and are reflected at the edge with change of sign. During this period of time, the felt of the mallet is decompressing, and the mallet's head is pushed back by the waves returning from the edge: this succession of stages is similar to the interaction between hammer and string in a piano (see Chaps. 1 and 3). Here, the interaction between the mallet and the membrane ends approximately 12 ms after the initial impact (see the picture on the right in Fig. 14.14). Then, the transverse waves evolve freely on the membrane. Due to the interferences between outgoing and returning waves, only a few number of discrete frequencies are present in the vibration (and in the acoustic) spectrum. The usual bandwidth of the sound radiated by timpani is usually restricted to the interval [0, 1] kHz, due to the combined effects of excitation spectrum, internal and radiation damping.

For a uniformly stretched circular membrane, the observed modes are modes correspond to those listed in Table 14.1. In practice, it is difficult to obtain a perfectly uniform tension, because this implies to have a perfect control on the boundary conditions at the edge. As an illustration, Fig. 14.15 shows an example of heterogeneous tension field obtained on a kettledrum tuned with the help of six

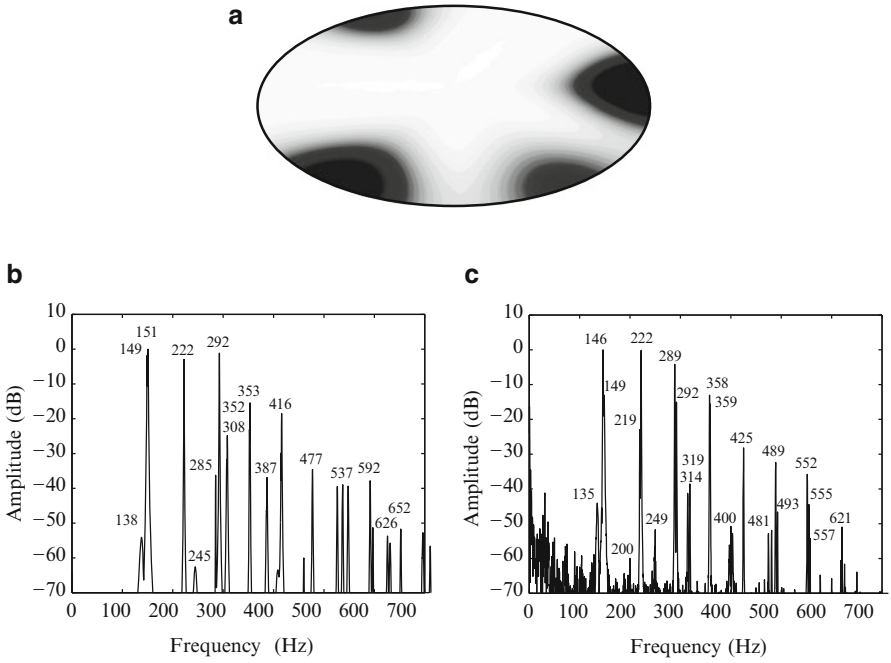

Fig. 14.15 (**a**) Heterogeneous distribution of tension of the membrane of a kettledrum. (**b**) Simulated spectrum. (**c**) Measured pressure spectrum radiated by a real kettledrum

screws equally distributed on the edge. In this particular simulated case, two of the screws were deliberately more tightened than the four others: as a consequence, the tension field shows a nonuniform tension field, between $3100\,\mathrm{N\,m^{-1}}$ (in white) and $3317\,\mathrm{N\,m^{-1}}$ (in dark grey).

Simulating a kettledrum with such a tension distribution yields the spectrum shown in Fig. 14.15.

- One can check that the simulation yields a spectrum which is very close to the measured spectrum.
- Here, the membrane is struck close to its edge. In all, the frequencies with the highest amplitude correspond to the modes $m1$ (11, 21, 31,...), which is in accordance with the prediction of small damping factors for these modes (see Table 14.1). Recall that these modes are characterized by a single nodal circle ($n = 1$) at the edge, and m nodal diameters.
- As predicted by the simulation of the air-membrane-cavity coupling, the eigenfrequencies ω_{m1} form a quasi-harmonic series with a missing fundamental (around 75 Hz).
- Finally, the heterogeneous tension is reflected in the spectrum by a number of peak doubling. In the time domain, these peak doubling result in clearly

audible beats. Systematic and progressive canceling of these beats is one of the techniques used by the percussionists for tuning their instruments.

14.2.4.2 Internal and External Acoustic Fields

The time-domain evolution of both the internal and external pressure fields are shown in Fig. 14.16. The successive snapshots are synchronized with the representations of the membrane vibrations in Fig. 14.14.

- At the time of impact, an overpressure is generated inside the air cavity, due to the reduction of air volume. As a consequence, a reduction of pressure is generated outside the bowl.
- Both the internal and external acoustic waves propagate at sound speed c, which is approximately three times faster than the elastic waves on the membrane. It can be seen on the second picture from the left (4 ms after the impact), for example, that the pressure inside the cavity already has reached the other side of the instrument, while the elastic wave on the membrane did not even reach its center.
- Due to the rigidity of the bowl, the internal wave is restrained by the shape of the cavity. Microphone measurements show that the internal pressure field is significantly more intense than the outside pressure. This property is confirmed by the representations of the pressure jump in Fig. 14.17.
- Finally, during this transient regime, it is observed that the external radiated field is subjected to significant and rapid variations of directivity.

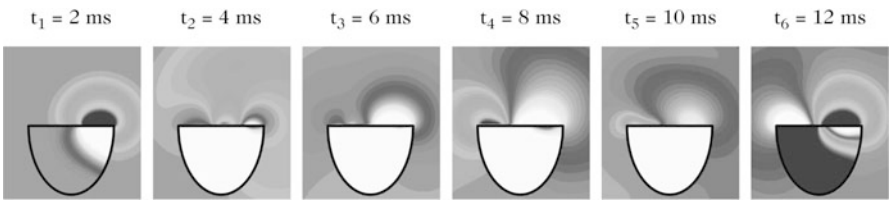

Fig. 14.16 Simulated pressure field inside and outside the cavity of the bowl, during the first 12 ms of the sound

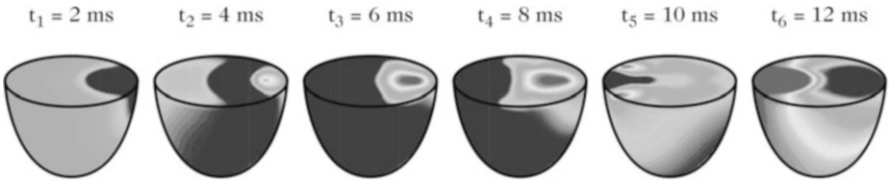

Fig. 14.17 Pressure jump between external air and cavity at the surface of the membrane during the first 12 ms of the sound

14.2.5 Spatial Distribution of the Radiated Pressure. Radiation Efficiency

After the transient regime, only a limited number of modes contribute to the radiation. Ignoring the damping temporarily, then one can admit that the oscillations of the membrane are almost stationary. Under this assumption, the method presented in Chap. 13 for calculating the power radiated by the instrument, and its associated directivity, can be applied.

As for the finite plates in Chap. 13, we consider first the radiation of a single isolated mode, assuming that it is decoupled from the others. It is also assumed hereafter that the observation (listening) point is in the far field, and that the membrane is inserted in a rigid baffle.[10] The radiated pressure is then given by:

$$P(r,\theta,\Phi,\omega) = -\rho\,\omega^2 \frac{e^{-jkr}}{2\pi r} \int_{\Sigma} W(x',y',\omega) e^{j(k_x x' + k_y y')} dx'dy', \tag{14.31}$$

with $k_x = k\sin\theta\cos\Phi$ and $k_y = k\sin\theta\sin\Phi$ which yields

$$P(r,\theta,\Phi,\omega) = -\frac{\omega^2\rho}{2\pi r} e^{-jkr} \tilde{W}(k_x,k_y,\omega), \tag{14.32}$$

where $\tilde{W}(k_x,k_y,\omega)$ is the spatial Fourier transform of the head's transverse displacement. From these expressions, all the radiation properties of the membrane can be calculated. One can get, in particular, the radiated pressure per unit solid angle at a given angular frequency ω [21]:

$$\frac{d\langle \mathscr{P}_a\rangle(\omega)}{d\Omega} = \frac{r^2}{2\rho c} |P(r,\theta,\Phi)|^2 = \frac{\rho\omega^4}{8\pi^2 c} \left|\tilde{W}(k_x,k_y,\omega)\right|^2. \tag{14.33}$$

The radiated pressure then is written

$$\langle \mathscr{P}_a\rangle(\omega) = \frac{\rho\omega^4}{8\pi^2 c} \int_{\Sigma} \left|\tilde{W}(k_x,k_y,\omega)\right|^2 \sin\theta\, d\theta\, d\Phi\ . \tag{14.34}$$

Finally, the radiation efficiency is obtained in a similar way as for the radiating plate in Chap. 13:

$$\sigma(\omega) = \frac{\langle \mathscr{P}_a\rangle(\omega)}{\frac{1}{2}\rho c \langle |\dot{W}|^2\rangle(\omega)}\ . \tag{14.35}$$

[10] This latter assumption is certainly wrong for the lowest modes of the kettledrum, for which the acoustic wavelength is larger than the diameter of the membrane. However, in this case, other methods such as the iterative algorithm presented in Sect. 13.4.4 can be applied.

Compared to plates, the main difference here is due to the fact that both the air and membrane are non dispersive media, if the stiffness of the membrane is ignored. As a consequence, no critical frequency exists, since both dispersion curves do not cross each other. Following situations can occur:

- The wave speed c_F of the flexural waves on the membrane is smaller than the speed of sound c. This is the most common case for timpani, where c_F is of the order of magnitude of $100\,\mathrm{m\,s^{-1}}$. In this case, the radiation efficiency is weak [21]. As for the plate, this follows from the fact that, over a distance corresponding to one acoustic wavelength, the different spatial contributions of the membrane (due to each elementary dipole) interfere in a destructive way. The radiation field is almost omnidirectional.
- $c_F > c$: this case can be observed in some drums, or, more generally, for instruments with stiff skins and under high tensions. This is a situation of strong radiation efficiency with $\sigma \approx 1$. The instrument radiates in a cone with an half top angle equal to $\theta = \arccos \frac{c}{c_F}$ [21].
- c_F is close to c. Here, the acoustic wavelength is close to the elastic wavelength. This corresponds to an hyper-radiating case. The radiation efficiency might take values higher than unity. The radiation field is concentrated in the plane tangent to the membrane.

For timpani, a compromise must be found between sound power and tone duration. In particular, the duration must be sufficient (i.e., a sufficiently high number of oscillations) so that the human ear can attribute a pitch to the tone. This explains why a *weakly radiating* case is preferred for this category of instruments. In such a situation, the radiated energy at each cycle is relatively small so that the vibrational energy of the flexural waves on the membrane can last longer. For some other drums (toms, djembe,...) it is either the emergence of the sound over a whole orchestra which is sought, or the transmission of the sound at a large distance (notice that the sound of a djembe in free field can be heard at distances up to hundred of meters). In this latter cases, the head is heavily stretched so that the instrument is strongly radiating.

14.2.6 Numerical Simulation of the Coupled Problem

The numerical resolution of the coupled system composed of the mallet, the membrane, the cavity, and the external air might pose a number of practical difficulties.

1. The first difficulty is due to the size of the problem. Since the wanted accuracy requires a 3D-modeling, the number of elements rapidly increases with the considered volume of space and with the refinement of the spatial mesh. In addition, for a radiation in free space, the required volume increases with the propagation of the wavefront (theoretically, there is no limit for this!). Then,

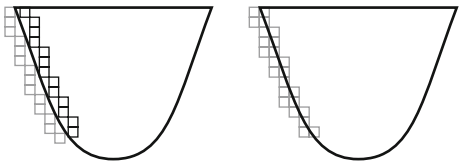

Fig. 14.18 Mesh of the kettledrum. (*Left*) Separated meshes yielding numerical diffraction. (*Right*) Fictitious domains method

in order to restrict the volume, a cube of air of $1\,\mathrm{m}^3$ is selected around the instrument. Absorbing Boundary Conditions (ABC) are simulated on the edges of the cube, in order to suppress the reflected waves, and thus to simulate a free field. The size of the mesh inside the cubic domain is directly linked to the maximum frequency $f_{\max}$ of the calculated variables. With a spatial step equal to 2.5 cm, and assuming the currently admitted accuracy criterion of 10 points per wavelength, then $f_{\max} = 340/0.25 = 1360\,\mathrm{Hz}$. This value is compatible with timpani sound spectra, which do not contain significant energy above 1 kHz, as seen in Fig. 14.15.[11]

2. A second difficulty is due to the approximation made of the shape of the bowl. In order to keep a regular mesh, defined in a simple system of coordinates (Cartesian coordinates, for example), one could imagine to use different discretization schemes for the internal and for the external pressure field, respectively (see Fig. 14.18).

However, this solution must be rejected because it generates spurious diffraction effects due to the discontinuous ("staircase") approximation of the bowl's shape. In order to overcome this difficulty, it is preferable to use the fictitious domain method [32]. In this method (see below) the acoustic variables are calculated in a unique domain Ω, instead of the two separated domains Ω_i and Ω_e, thanks to the introduction of a new "pressure jump" variable across the boundary of the instrument.

14.2.6.1 Fictitious Domain Method

The fictitious domain method is based on a variational formulation of the problem. Multiplying Eq. (14.12) by an admissible test function w^*, and integrating it over the surface Σ of the membrane, we get

$$\frac{d^2}{dt^2}\int_\Sigma m_s w w^* dS = \int_\Sigma \mathrm{div}\left[\tau\nabla\left(w+\eta\frac{d}{dt}\right)\right] w^* dS - \int_\Sigma f(t) g w^* dS - \int_\Sigma [p]|_\Sigma w^* dS\,. \tag{14.36}$$

[11] In the context of musical sound synthesis, one might prefer referring to a dispersion criterion: since the ear is very sensitive to slight differences in frequency, it is justified to select a mesh density so that the frequencies can be estimated with an accuracy smaller than 1 % [45].

Since the test function w^* must fulfill the boundary conditions of the problem, this function vanishes on the edge $\partial\Sigma$ of the membrane. It can then be checked that the integration by parts of (14.36) yields

$$\frac{d^2}{dt^2}\int_\Sigma m_s w w^* dS = \int_\Sigma \tau\nabla\left(w + \eta\frac{d}{dt}\right)\nabla w^* dS - \int_\Sigma f(t) g w^* dS - \int_\Sigma [p]|_\Sigma w^* dS. \tag{14.37}$$

A similar method is applied to the acoustic equations (14.16), through introduction of the test functions p^* and v^*, for both the pressure and velocity, for which the boundary conditions are fulfilled. After integration by parts, we get (see [45]):

$$\rho\frac{d}{dt}\int_\Omega \boldsymbol{v}\boldsymbol{v}^* d\mathscr{V} - \int_\Omega p\ \mathrm{div}\boldsymbol{v}^* d\mathscr{V} = \int_\Gamma [p]|_\Gamma \boldsymbol{v}^*.\boldsymbol{n}\ dS \tag{14.38}$$

and

$$\frac{1}{\rho c^2}\frac{d}{dt}\int_\Omega p p^* d\mathscr{V} + \int_\Omega \mathrm{div}v\ p^* d\mathscr{V} = 0\,, \tag{14.39}$$

where $\Gamma = \Sigma \cup \mathscr{C}$ is the total surface of the kettledrum (membrane + bowl), and Ω is the complete space $\mathbb{R}^3$. A new variable $\lambda = [p]|_\Gamma$ appears in Eq. (14.38). This variable is the pressure jump across the surface of the instrument with normal vector $\boldsymbol{n}$. Thanks to the introduction of this new variable, it is as if the unknown pressures p_i and p_e were replaced by the unique variable p and, similarly, the unknown velocities $\boldsymbol{v}_i$ and $\boldsymbol{v}_e$ were replaced by the unique velocity field $\boldsymbol{v}$. The formulation of the problem is completed by expressing the boundary conditions on the surface Γ:

$$\begin{cases} \boldsymbol{v}.\boldsymbol{n} = \dfrac{\partial w}{\partial t} & \text{in} \quad \Sigma, \\ \boldsymbol{v}.\boldsymbol{n} = 0 & \text{in} \quad \mathscr{C}\,. \end{cases} \tag{14.40}$$

Through integration on Γ, with the introduction of another test function λ^*, we get

$$\frac{d}{dt}\int_\Sigma w\lambda^* dS - \int_\Gamma \boldsymbol{v}.\boldsymbol{n}\lambda^* dS = 0\,. \tag{14.41}$$

In summary, the fluid–structure problem corresponding to the acoustics of timpani is entirely defined by the system of four equations (14.37)–(14.39) and (14.41), where the four unknowns are the displacement w of the membrane, the pressure p and the acoustic velocity v in space, and the pressure jump λ across the surface of the instrument. The numerical formulation of this problem is presented later in this section.

14.2.6.2 Absorbing Boundary Conditions

The purpose of ABC is to simulate a free space. In this context, the leading idea consists of inserting artificial absorbing conditions at the border of the computational domain. The basic principles of this method are presented here, for the simple case of an half-space. For a cube, additional conditions on the edges and on the corners are necessary [19]. The posed problem is the following: given the wave equation

$$\frac{\partial^2 p}{\partial t^2} - c^2 \left(\frac{\partial^2 p}{\partial x^2} + \frac{\partial^2 p}{\partial y^2} + \frac{\partial^2 p}{\partial z^2} \right) = 0 \quad \forall (x, y, z) \in \mathbb{R}^3, \tag{14.42}$$

the aim is to limit the computation in the half-plane $z < 0$ by imposing a perfectly (totally, or transparent) absorbing condition in $z = 0$ (see Fig. 14.19). Denoting $\tilde{P}(k_x, k_y, z, \omega)$ the Fourier transform of the pressure (in time and space), the conditions amounts to impose:

$$\frac{\partial \tilde{P}}{\partial z} + j\frac{\omega}{c}\sqrt{1 - \frac{c^2(k_x^2 + k_y^2)}{\omega^2}}\tilde{P} = 0 \quad \text{in} \quad z = 0\,. \tag{14.43}$$

One drawback of the formulation (14.43) is that it is nonlocal in time and space (x, y). As a consequence, the ABC cannot be expressed in the time domain using partial differential equations. In order to overcome this difficulty, the function $\sqrt{1-u}$ (where $u = c^2(k_x^2 + k_y^2)/\omega^2 < 1$) is expanded onto a series of rational functions:

$$\sqrt{1-u} \simeq 1 - \sum_{l=1}^{L} \beta_l \frac{u}{1 - \alpha_l u} = \gamma - \sum_{l=1}^{L} \frac{\beta_l}{\alpha_l} \frac{1}{1 - \alpha_l u} \quad \text{with} \quad \gamma = 1 + \sum_{l=1}^{L} \frac{\beta_l}{\alpha_l}, \tag{14.44}$$

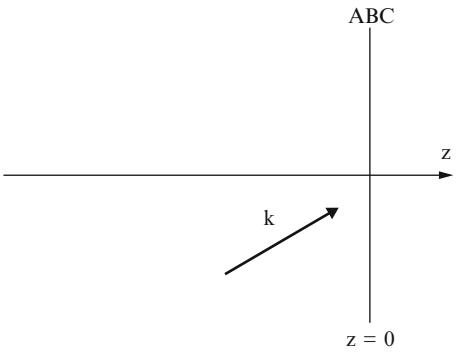

Fig. 14.19 Principle of absorbing boundary conditions (ABC) on an half-space

where, for stability reasons, the parameters α_l and β_l must fulfill the conditions

$$\alpha_l > 0, \quad \beta_l \geq 0, \quad \sum_{l=1}^{L} \frac{\beta_l}{1-\alpha_l} < 1 \, . \tag{14.45}$$

One possible alternative consists of selecting the Padé coefficients defined by:

$$\beta_l = \frac{2}{2L+1} \sin^2\left(\frac{l\pi}{2L+1}\right) \text{ and } \alpha_l = \cos^2\left(\frac{l\pi}{2L+1}\right) . \tag{14.46}$$

Auxiliary variables are the defined:

$$\tilde{\Phi}_l = \frac{\omega^2}{\omega^2 - \alpha_l c^2 (k_x^2 + k_y^2)} \tilde{P} \, . \tag{14.47}$$

The ABC can then be rewritten on the form of the following system:

$$\begin{cases} \dfrac{d\tilde{P}}{dz} + j\dfrac{\omega}{c}\left(\gamma \tilde{P} - \displaystyle\sum_{l=1}^{L} \frac{\beta_l}{\alpha_l} \tilde{\Phi}_l\right) = 0 \\ \left[\omega^2 - \alpha_l c^2 (k_x^2 + k_y^2)\right] \tilde{\Phi}_l = \omega^2 \tilde{P} \, . \end{cases} \tag{14.48}$$

Finally, returning back to the time domain through inverse Fourier transform, we get

$$\begin{cases} c\dfrac{\partial p}{\partial z} + \gamma \dfrac{\partial p}{\partial t} - \displaystyle\sum_{l=1}^{L} \frac{\beta_l}{\alpha_l} \frac{\partial \phi_l}{\partial t} = 0, \\ \dfrac{\partial^2 \phi_l}{\partial t^2} - \alpha_l c^2 \left(\dfrac{\partial^2 \phi_l}{\partial x^2} + \dfrac{\partial^2 \phi_l}{\partial y^2}\right) = \left.\dfrac{\partial^2 p}{\partial t^2}\right|_{z=0} \quad \text{for } l = 1, \ldots, L \, . \end{cases} \tag{14.49}$$

In practice, approaching the condition of perfect transparency (i.e., no wave returning from $z = 0$) as close as possible depends on the order L of the expansion (the higher the number of auxiliary variables ϕ_l, the better the approximation). The system (14.49) can be seen as a transport equation along z coupled to L 2-D wave equations in the plane $z = 0$.

14.2.6.3 Numerical Discretization

The numerical resolution of the timpani model consists of seeking for discrete approximations $(p_h, \mathbf{v_h}, w_h, \lambda_h, \xi_h)$ for the variables of the problem: the pressure p, the acoustic velocity $\mathbf{v}$, the displacement of the membrane w, the pressure jump

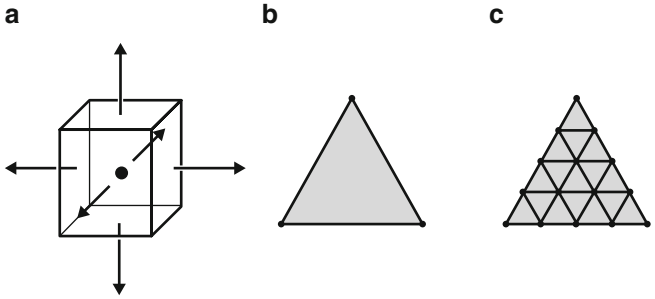

Fig. 14.20 Mesh of the different constitutive elements of the kettledrum. (**a**) Cubic mesh for the pressure p_h and the acoustic velocity $\mathbf{v_h}$. (**b**) Finite elements P1 for the pressure jump λ_h. (**c**) Refine previous P1 mesh for the displacement w_h on the membrane

λ, and the mallet's displacement ξ. The index h indicates that we are dealing here with a spatial discretization obtained from the meshes of the constituting elements of the the kettledrum coupled to the free space. For these approximations, the finite element method is used (see Chap. 1).

Figure 14.20 shows the meshes used by Rhaouti [44]. The space Ω is discretized with a cubic mesh. The pressure p_h and the velocity $\mathbf{v_h}$ are associated with each elementary cube. For the pressure jump λ_h, P1 finite elements are used. These elements can be viewed as a 2-D generalization of the *hat* functions presented in Chap. 1. A triangular mesh is selected on the surface of the instrument. Finally, a triangular mesh and P1 finite elements also are used for the displacement w_h of the membrane. Since the speed of the flexural waves is usually three to four times smaller than the speed of sound, the elastic wavelength also is three to four times smaller than the acoustic wavelength, for a given frequency. In order to ensure the coherence between all numerical schemes, a similar ratio between wavelength and mesh size must be selected for the variables. For this reason, the size of the mesh elements on the surface for w_h is selected here so that the spatial step is four times smaller than for the pressure jump λ_h.

After the space discretization, the equations of the problem are reduce to a matrix system of time differential equations, similar to the example shown in Chap. 1. We have

$$\begin{cases} f_h = K\left[(\delta - \xi_h + \mathbf{G^t} w_h)^+\right]^\alpha, \\ m\dfrac{d^2\xi_h}{dt^2} = f_h, \\ \mathbb{M}_w \dfrac{d^2 w_h}{dt^2} + \mathbb{R}_w w_h + \eta \mathbb{R}_w \dfrac{dw_h}{dt} + \mathbb{A}_w \lambda_h = -\mathbf{G} f_h, \\ \mathbb{M}_p \dfrac{dp_h}{dt} + \mathbb{D}_v^t \mathbf{v_h} = 0, \\ \mathbb{M}_v \dfrac{d\mathbf{v_h}}{dt} - \mathbb{D}_v p_h - \mathbb{B}_v \lambda_h = 0, \\ \mathbb{B}_v^t \mathbf{v_h} - \mathbb{A}_w^t \dfrac{dw_h}{dt} = 0, \end{cases} \tag{14.50}$$

where $\mathbb{M}_w$, $\mathbb{R}_w$, $\mathbb{M}_v$, $\mathbb{D}_v$, $\mathbb{B}_v^t$, and $\mathbb{A}_w^t$ are matrices, and where $\mathbf{G}$ is a vector accounting for the spatial extent of the mallet's impact on the membrane. This system can be discretized in time using finite differences, as seen in Chap. 1.

14.3 Example of the Guitar

14.3.1 Introduction

Various aspects of the acoustics of guitars have been addressed a number of times in the previous chapters of this book. The vibrations of plucked strings, for example, were presented in detail in Chap. 3. In Chap. 5, the dissipation mechanisms encountered in the different constitutive parts of the instruments were analyzed. The coupling between string and soundboard, and the soundboard-cavity coupling were studied in Chap. 6. Finally, the general results on the radiation of plates, and the plate-air interaction studied in Chap. 13 are also applicable to the guitar. These previous investigations are pursued here where the interaction between air and soundboard is now extended to the whole spectrum of the instrument (up to 5 kHz) and not only limited to the low-frequency range as in Chap. 6.[12] Another new feature of the model presented here is that the complex interactions between cavity, soundboard, and the external air are taken into account. This additional feature is made possible through application of the fictitious domain method (presented in the previous section devoted to the timpani), which allows to consider the fluid domain (internal cavity and external space of the guitar) as a whole.

The classical guitar (in contrast to the electric guitars without an air cavity) has the particularity to show a sound hole in the soundboard. As a consequence,

[12]Notice that the simplified 2 dof air-plate model presented in Chap. 6 will appear as the low-frequency limit of the general model presented here.

the air cavity is not closed, and the acoustic field has no discontinuity between inside and outside. An appropriate model should account for this specificity. The average diameter of the sound hole is 10 cm, which corresponds to an half acoustic wavelength at a frequency of 1.7 kHz. In comparison, the spectrum of guitar sounds usually shows significant energy up to 5 kHz. Thus, it is not possible to ignore the presence of this hole, in contrast with the previous case of timpani where the diameter of the hole was significantly smaller than the smallest acoustic wavelength of timpani sounds.

As for timpani, we have to consider the interaction between the vibrating parts of the guitar and the acoustic field. The soundboard is the main radiating part of the instrument, though, in some circumstances, the back plate also might contribute to the total sound. The radiation of the other parts will be ignored in this section. Compared to a membrane, the guitar soundboard is heavier and stiffer. However, as discussed later, the acoustic pressure can affect its vibratory behavior. It should be noticed that the pressure inside the cavity can be very high.[13]

In what follows, a recent guitar model is presented [22]. This presentation is complemented by considerations on the acoustic intensity radiated by the instrument [1]. Finally, a summary of power balance between all the constitutive parts of the instrument is conducted. In this section, the equations of the model that present similarities with the timpani model are not detailed. We content ourselves with the presentation of the specificity of the guitar model, and we rather focus on the significant physical results of the instrument (admittance, intensity, sound power, damping factors, and decay times) that the model is able to account for. The relevance of fluid–structure interaction in the case of the guitar is particularly emphasized. Most of these results can be generalized to other stringed instruments.

14.3.2 Physical Model

In the guitar model presented below, several elements are coupled together:

- The string(s). The flexural motion of the string is assumed to be perpendicular to the soundboard plane (one polarization). The internal damping is represented by the association of a viscous ("fluid") damping term and a viscoelastic term (see Chap. 5). The excitation of the string by the finger is represented by a idealized impulse localized in time $h(t)$ and space $g(x)$, see Fig. 14.21. The impulse $h(t)$ is made of the association of two cosine functions accounting for a slow increase followed by a fast decrease, and is inspired by experimental results (see [11]). Is also accounts, to a first approximation, for stick-slip mechanisms between the

[13] Putting a microphone inside the cavity shows that the sound pressure level can reach 130 dB!

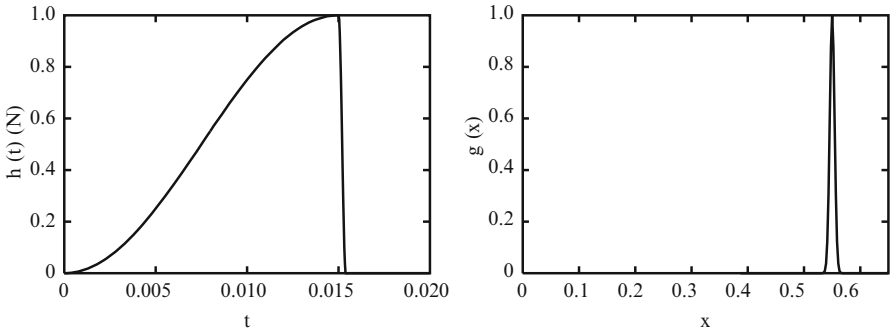

Fig. 14.21 Idealized force impulse on the string. (*Left*) Time dependence $h(t)$. (*Right*) Spatial extent $g(x)$

finger and the string (see Chap. 1). The function $g(x)$ is here a Gaussian function (though other smooth functions could be used) and accounts for the finite width of the finger on the string [23].

- The soundboard. An orthotropic plate model is used for the soundboard (see Chap. 1). The shape of the plate is that of a standard guitar. The presence of the bridge and of the ribs is represented by spatial heterogeneities of both the density $\rho_p(x, y)$ and thickness $h(x, y)$. The amount of internal damping depends on the material, and is derived from experiments. The soundboard is assumed to be clamped at its periphery, and free on the edge of the sound hole. Considering the small mean value of the thickness, it is further assumed that the Kirchhoff–Love model is applicable. The soundboard is excited by the force transmitted by the string to the bridge, and by the pressure force on its both sides. The other parts of the instrument are supposed to be perfectly rigid.
- The acoustic field. Here, the model is close to the one presented in Sect. 14.2 for timpani [see Eq. (14.16)]. A condition of continuity for the velocity normal to the soundboard is added, as well as a null condition for the normal velocity on the other constitutive parts of the instrument.

Limitations of the Present Model

The present coupled model shows an additional degree of complexity, compared to other elementary models where each constitutive part (soundboard, cavity, ...) is treated separately. In this chapter, attention is put on radiation, and thus we focus on the soundboard-acoustic field coupling. However, with the objective to model a real instrument more accurately, then several refinements should be added. Without pretending to be exhaustive, several possible additional features are the following:

(1) As indicated in the previous Chaps. 6 and 8, the motion of the string is complex and cannot be reduced to a single polarization perpendicular to the soundboard.

Several factors also induce a parallel component: the motion of the bridge, the slipping of the string along the fret, and nonlinearities due to large amplitude motion.

(2) The modal analysis of a guitar shows that one of the lowest modes corresponds to a flexural mode of the neck (free at one end, and loaded by the body at the other end). The corresponding eigenfrequency is of the order of magnitude of a few Hz. As a consequence, this mode does not directly contribute to the audible radiated acoustic pressure. However, the flexion of the neck induces fluctuations of length (and, in turn, fluctuations of tension) in the attached strings. In conclusion, the coupling between the neck and the strings should be taken into account in a future model.

14.3.3 Specificity of the Numerical Guitar Model

14.3.3.1 Spatial Discretization

A six strings guitar model that couples the soundboard with the air has been solved numerically with a method similar to the one used for timpani [3]. Both models are briefly compared and summarized below.

- The main difference between both instruments is due to the presence of a plate operator for the guitar soundboard, compared to a 2-D wave equation in the case of timpani membrane. This operator contains fourth-order space derivatives (see Chaps. 1, 3 and 13). In order to use standard finite elements, the fourth-order equations are replaced by second-order systems of equations where the new variables are the velocity and the flexural moment.
- As for the kettledrum, the fluid–structure interaction problem is solved with the fictitious domain method. For the guitar, this method has two main advantages: it allows to avoid distinct pressures meshes inside and outside the cavity and, in addition, it facilitates the treatment of the pressure continuity through the sound hole. In this context, the present method is more efficient than those where the cavity is considered separately (see, for example, [46]), or those requiring an artificial ectoplasm (a massless vibrating element) at the sound hole [6].

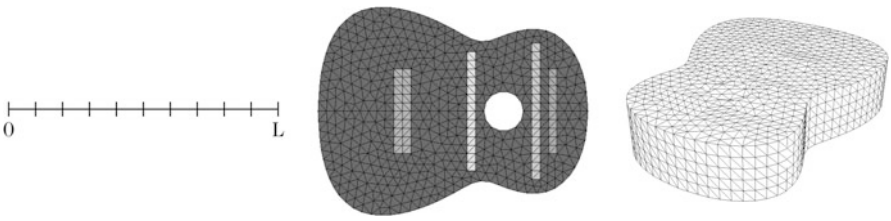

Fig. 14.22 Mesh used for the string, the soundboard and the pressure jump

- The string equation is replaced here by a system of first-order partial differential equations, where both unknowns (force and velocity) are discretized with finite elements.
- The acoustic field (inside and outside the cavity) is discretized with the same scheme as for the kettledrum.

14.3.3.2 Time-Domain Discretization

The time-domain discretization of both the string and acoustic equations is achieved with second-order centered finite difference schemes, as for the kettledrum. The main difficulty arises from the soundboard equation.

The stability condition for the plate, with explicit second-order finite differences, is of the form $\Delta t \leq A/h_p^2$, where A is a parameter depending on the material used for the plate, and h_p is the spatial step. This means, for example, that the sampling frequency must be multiplied by 4, if the spatial mesh is refined by a factor 2. Such a condition rapidly becomes very cumbersome as soon as the objective is to extend the spectral domain of the sound to be simulated. By comparison, we have the condition $\Delta t_{\max} \propto 1/h$ for the wave (or the string) equation, which is less demanding.

In order to overcome this difficulty, one can use a pseudo-spectral method [22]. The method consists, first, in calculating the in vacuo modes of the soundboard, using spatial finite elements. This yields a system of decoupled differential equations where the damping terms can be added separately for each mode. For each damped oscillator equation, the source term is the projection of the forces exerted by the string and the pressure on the soundboard. These source terms are updated at each time step. Notice that the time step for the soundboard must be compatible with the time steps selected for the other constitutive parts of the instrument (string and air).

In practice, computing the first 50 modes of the soundboard yields a satisfactory simulation of the sound field up to 3 kHz. The average distance between consecutive modes is then $\Delta f = 60\,\text{Hz}$. As an illustration, Eq. (13.142) in Chap. 13 yields $\Delta f = 57\,\text{Hz}$ with the following data: $\rho_p = 350\,\text{kg/m}^3$, $E_1 = 15.10^9\,\text{Pa}$, $E_2 = E_1/17$, $\nu = 0.3$, $h = 2.9\,\text{mm}$, $S = 0.1\,\text{m}^2$.

14.3.4 Admittance at the Bridge

The admittance at the bridge is a key variable influencing the coupling between the "engine" of the instrument (the strings) and the resonator (the soundboard coupled to both the air cavity and external air). Therefore, computing this quantity is an appropriate means of quantifying the effects of coupling. The following results were obtained by using Derveaux's model described in Sect. 14.3.2. The values of the geometrical and material parameters are extracted from the literature (see, for example, [28, 29]). One advantage of the model is to compare the behavior of the guitar successively in vacuo and in air.

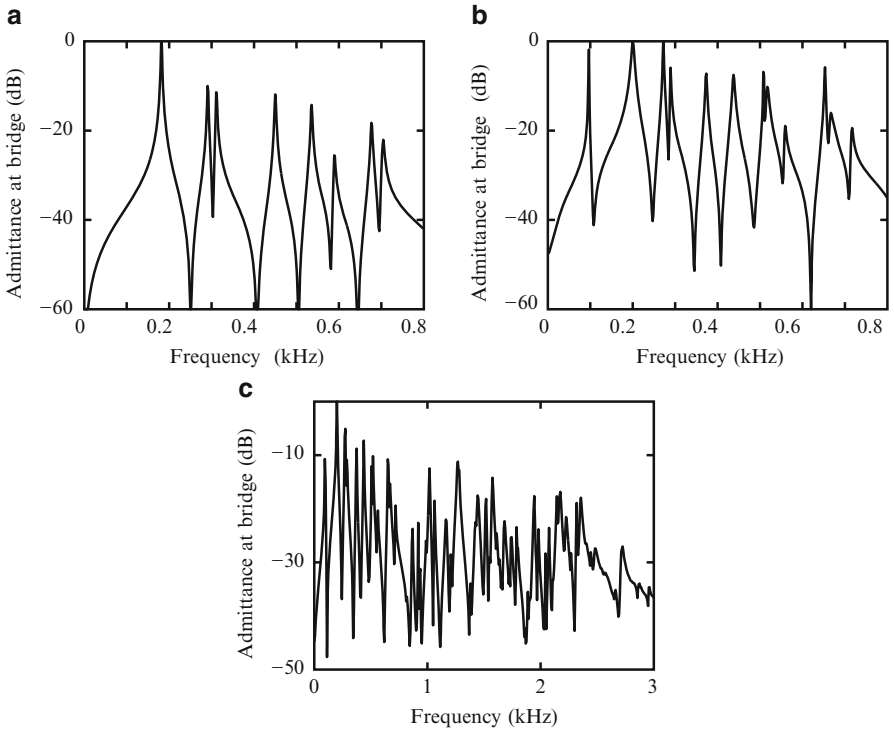

Fig. 14.23 Admittance at the bridge of a guitar at the attachment point of the 6th E-string (83 Hz). (**a**) In vacuo soundboard. (**b**) Soundboard coupled to air and cavity: [0–800] Hz. (**c**) Soundboard coupled to air and cavity: [0–3000] Hz. Simulation based on the model by Derveaux et al. [23]

Figure 14.23 shows the simulated admittances at the bridge for a guitar with a soundboard of thickness 2.9 mm, and a cavity of height 10.4 cm. The two first figures show a comparison between the simulated admittances between 0 and 800 Hz, at the point of the bridge corresponding to the position of the lowest E-string (with fundamental 83 Hz), in vacuo and in air, respectively. One can see that the influence of both external air and cavity is reflected in a shift of the spectral peaks, and by the emergence of additional peaks.

Below 250 Hz, the admittance curve in air shows the same shape as for the simplified low-frequency two-oscillators model presented in Chap. 6 [17]. The third figure shows the simulated admittance up to 3 kHz. Its general shape is similar to those observed experimentally (see, for example, [8] or [49]). With the selected parameters, the mean value of the admittance between 0 and 1 kHz is approximately 10 dB above its mean value between 1 and 2.5 kHz, which shows a higher mobility in the low-frequency domain. The peaks are clearly separated for $f < 1$ kHz, whereas they overlap more and more with increasing frequency. This overlapping can be attributed to both the air-structure coupling and damping phenomena (material damping and radiation). The imbalance between low and high

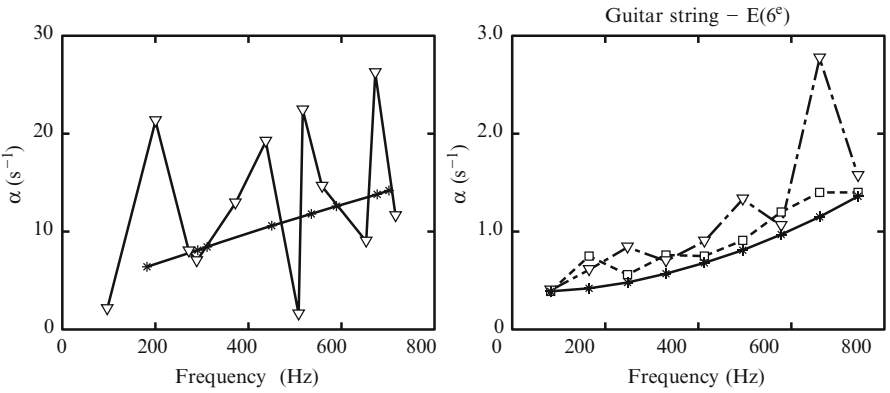

Fig. 14.24 Damping factors α (in s^{-1}). (*Left*) Comparison between the damping factors of the in vacuo soundboard modes (*asterisk symbol*), and of the soundboard coupled to external air and cavity (*inverted triangle symbol*). (*Right*) Comparison between the damping factors of the isolated open E2 string modes (*asterisk symbol*), the string modes coupled to the in vacuo soundboard (*square symbol*), and the string modes coupled to the complete guitar (*inverted triangle symbol*). Simulations based on the model by Derveaux et al. [23]

frequency domains is reinforced if the thickness of the soundboard decreases. With an average thickness divided by a factor of 2 (1.45 mm), the mean value of the admittance between 0 and 500 Hz is roughly 15 dB below its mean value between 500 and 2500 Hz [23].

14.3.5 Damping Factors

The admittance curves are complemented by the damping factors shown in Fig. 14.24. These factors are the imaginary parts of the eigenfrequencies which govern their decay times. The damping factors α of the in vacuo soundboard (asterisk symbol), and of the soundboard coupled to air and cavity (inverted triangle symbol), are represented on the left figure. These values are derived from time-frequency analysis of the impulse responses of the bridge velocity, at the attachment point of the 6th E-string (83 Hz). Not surprisingly, the curve $\alpha(f)$ for the in vacuo soundboard is in accordance with the linear law selected for the structural damping in the model. For the soundboard coupled to external air and cavity, the mean value of the damping factors is higher than in the previous case. However, the variations from one mode to the next is more erratic. Due to multiple coupling between soundboard and air modes, some of the modes even show a smaller global damping factor than the structural damping factor (at the same frequency), whereas the neighboring frequencies are more damped. It is as if some of the modes receive energy from their neighboring modes through air-structure coupling.

Similar conclusions can be drawn for the strings. Figure 14.24 (right) shows a comparison between the damping factors α of a isolated open E2 string (asterisk symbol), with fundamental 83 Hz, and of the same string coupled to the in vacuo soundboard (square symbol) and to a complete guitar (inverted triangle symbol), successively. The curve $\alpha(f)$ is a parabola, which is coherent with the selected damping model made of the association of a fluid damping term and a viscoelastic damping term. Due to the coupling of the string with the in vacuo soundboard, the damping factors globally increase. However, the increase in damping fluctuates from one mode to the next, depending on the degree of proximity between soundboard and string modes (see Chap. 6). Finally, the coupling of the soundboard with air and cavity yields an additional increase of the average damping, though with significant variations from one mode to the next. Such fluctuations are currently observed on real guitars [50].

14.3.6 Radiated Sound Field

Figure 14.25 shows five successive snapshots of the pressure field radiated by a simulated guitar in its symmetry plane, right after the initial plucking of the 1st open string (E4: fundamental 330 Hz). The delay between consecutive snapshots is 0.36 ms. At first (snapshots 1 and 2), the pressure field is omnidirectional and is mainly due to the vibration of the soundboard. In the meantime, the magnitude of the pressure field inside the cavity increases progressively. From snapshot 3, the cavity radiates through the sound hole. The internal field is partially in phase with the motion of the soundboard, and partially in antiphase. On snapshots 4 and 5, the cavity field progressively becomes in total antiphase with the external field. As a result, a decrease of pressure followed by an inversion of the outside pressure is observed. The instantaneous directivity of the pressure field is complex and evolves rapidly with time. This is a consequence of the large number of excited modes (between 0 and 3 kHz), where each mode has its own directivity pattern and its own temporal evolution. As observed in timpani, the global directivity of the instrument stabilizes after a certain amount of time (typically within one second). At this time, the sound of the guitar is governed by a relatively low number of string's partials.

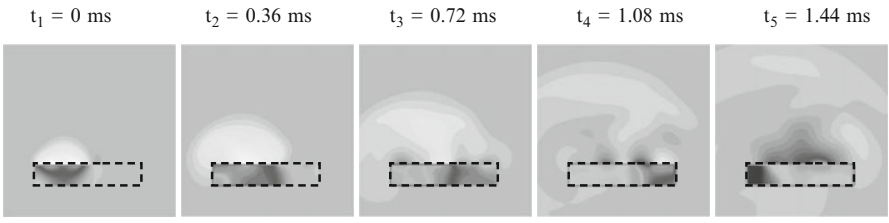

Fig. 14.25 Successive snapshots of the pressure field radiated by the guitar, right after an initial pluck of the 1st open string (E4: fundamental 330 Hz). Simulations based on the model by Derveaux et al. [22]

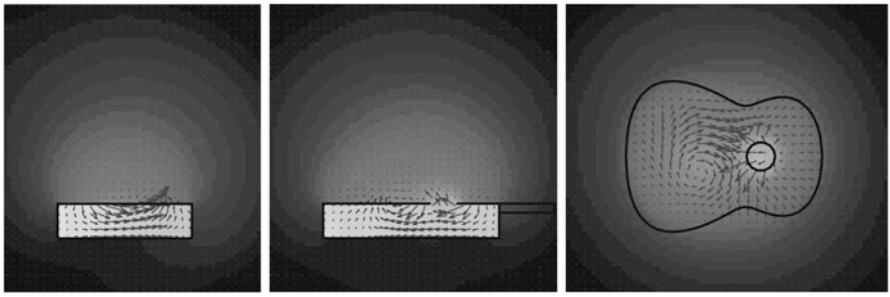

Fig. 14.26 Acoustic intensity for the guitar mode at 272 Hz. (*Left*) Plane perpendicular to the neck. (*Middle*) Symmetry plane of the guitar. (*Right*) Horizontal plane, 1 cm above the soundboard. After [1]

14.3.7 Acoustic Intensity and Power Balance

14.3.7.1 Acoustic Intensity

In the model used in the section for illustrating the acoustics of guitars through simulations, we take benefit from having at our disposal both the pressure and the acoustic velocity field to compute the acoustic intensity $\mathbf{I} = p\boldsymbol{v}$. Figure 14.26 shows an example of the useful information provided by this variable. In this Figure, the intensity $\mathbf{I}$ is shown in three perpendicular planes, successively: the symmetry plane of the instrument, one horizontal plane close to the soundboard, and one vertical plane perpendicular to the neck and passing through the box. The acoustic intensity is here averaged over one period, for a forced sinusoidal excitation close to one mode of the complete guitar (272 Hz). As shown in Chap. 1, the acoustic intensity is linked to the energy density through its divergence. As a consequence, the intensity vectors are oriented towards the regions of space with increasing acoustic energy. A "source" is characterized by a set of diverging vectors, whereas a "sink" is a region where the intensity vectors converge. In Fig. 14.26, one can see both the internal and external sources and the regions of space (above the soundboard, in particular) where the energy density vanishes, due to opposition of phase between sources.

14.3.7.2 Radiated Power and Acoustical Efficiency

At this point, we are now able to compute the acoustical efficiency of the guitar (see also Chaps. 2 and 13), defined as:

$$\zeta = \frac{\langle \mathscr{P}_a \rangle}{\langle \mathscr{P}_i \rangle}, \tag{14.51}$$

where $\mathscr{P}_a$ is the mean value of the radiated power, and $\mathscr{P}_i$ is the mean value of the total power dissipated in the instrument. For simplicity, only one string is considered. We have

$$\langle \mathscr{P}_i \rangle = \langle \mathscr{P}_a \rangle + \langle \mathscr{P}_c \rangle + \langle \mathscr{P}_s \rangle \tag{14.52}$$

where $\langle \mathscr{P}_c \rangle$ is the mean power dissipated in the string, and $\langle \mathscr{P}_s \rangle$ is the mean power dissipated in the body.

Let us now consider one particular frequency component ω_n of the string's spectrum for which the mean power dissipated over one period $T_n = 2\pi/\omega_n$ is calculated. We denote V_n the modal amplitude of the string's velocity, and r_n the modal resistance corresponding to the internal losses. The quality factor is then given by $Q_n = \omega_n m_n / r_n$, where m_n is the modal mass [33]. The mean power dissipated in the string for this partial is written

$$\langle \mathscr{P}_c \rangle(\omega_n) = \frac{1}{2} r_n V_n^2 \,. \tag{14.53}$$

When the string is coupled to the soundboard (at position $x = L$), it was shown in Chap. 6 that the mean power dissipated at the end (or, equivalently, the power transferred from string to soundboard) is written

$$\langle \mathscr{P}_L \rangle(\omega_n) = \frac{1}{2} Z_c^2 \Re e \left\{ Y(\omega_n) \right\} V_n^2 \,. \tag{14.54}$$

In (14.54), Y is the driving point admittance of the bridge at the attachment point, for the soundboard loaded by the air. $\langle \mathscr{P}_L \rangle$ accounts for all acoustic and structural losses in the loaded body at frequency ω_n: $\langle \mathscr{P}_L \rangle = \langle \mathscr{P}_a \rangle + \langle \mathscr{P}_s \rangle$. In summary, the mean power dissipated in the guitar at frequency ω_n is written

$$\langle \mathscr{P}_i \rangle(\omega_n) = \langle \mathscr{P}_c \rangle(\omega_n) + \langle \mathscr{P}_L \rangle(\omega_n) \,. \tag{14.55}$$

Experimentally, r_n can be derived from measurements performed on an isolated string, or, alternatively, on a guitar where the soundboard is blocked. The quantity $Y(\omega)$ can be obtained from standard admittance measurements (see Chap. 3). Using finally Eqs. (14.53) and (14.54), one can calculate the efficiency for a given ω_n.

Table 14.2 shows the values obtained for the acoustical efficiency, at some particular frequencies, using the guitar model by Derveaux et al. These values are coherent with measurements performed on real guitars by Boullosa et al. These authors have shown, among other things, that a link exists between the acoustical efficiency of the guitar and the subjective evaluation of its quality for both the players and listeners. From the point of view of the player, the input mechanical energy that can be transmitted to the guitar is limited in terms of maximum force and string displacement. Thus, it is essential that a significant part of this energy can be converted into sound power without excessive effort that would deteriorate

Table 14.2 Acoustical efficiency of the guitar

Frequency (Hz)	200	272	289	372	437	508
ζ (in %)	40.8	3.96	0.9	8.8	7.8	4.09

Simulations based on Derveaux's model [14]

the sound quality. A noticeable efficiency is necessary so that the guitarist can have enough dynamic range at its disposal in order to introduce subtleties in the played music. However, one must keep in mind that other quality factors of the instrument are essential for playing "good" music, such as the spectral balance between bass and treble sounds, and the clarity of the attack. Last but not least, the talent of the player cannot be ignored!

In conclusion, a guitar tone is a free oscillation: the total dissipated power is the sum of the power dissipated by both the strings and the air-loaded body. The power dissipated by the soundboard modes takes place during the initial part of the sound, since their quality factors are significantly smaller than those of the strings (see Chap. 6). After this transient part, the main part of the radiated power is concentrated in the partials of the strings. Audibly, a guitar tone is schematically made of a short "body" sound followed by a long "string" tone.

In this section, attention was mostly paid on classical guitars with nylon strings. Electric guitars are characterized, in particular, by a more massive body and the use of steel strings, which induce a significantly different tone quality. For more information on electric and steel strings guitars, one can refer to [38, 40–42].

14.4 Example of the Piano

14.4.1 General Presentation of the Model

A piano sound is the result of free oscillations, as for guitars and timpani in their normal use. As the player presses a key, a complex mechanism is activated whose main effect is to project the hammer against the strings with an impact velocity that depends on the depression conditions of the key [48]. In what follows, the key mechanism is ignored. The consecutive vibrations of the hammer shank also are ignored. A recent study by Chabassier and Duruflé highlights the relevance of these vibrations [10].

The model starts as the very instant where the hammer hits the strings, taken as the origin of time. The purpose is to model the succession of vibratory and acoustic phenomena in hammer, strings, soundboard, and surrounding air.

The strings are set into motion by the blow of the hammer. Their motion is a combination of transverse and longitudinal waves. These waves are nonlinearly coupled, due to the variation of the tension with amplitude, as shown in Chap. 8. These nonlinear phenomena greatly influence the properties of piano sounds: they are responsible for the presence of pitch glide and phantom partials. In this section,

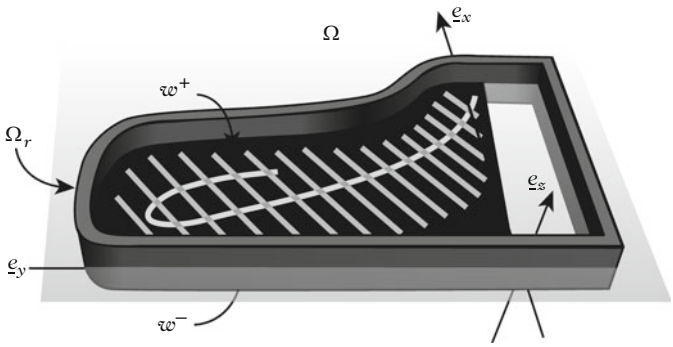

Fig. 14.27 General configuration of the piano model

the nonlinear equations of strings presented in Eq. (8.62) will be used. Another nonlinear feature exists in the hammer–string interaction, due to the compression of the felt, as seen in Chap. 1. The interaction force is modeled here as a power law, as for the interaction between a mallet and a timpani head. The main consequence of this nonlinearity is to widen the excited spectral domain (due to shortening of the force impulse) as the hammer impact velocity increases.

An orthotropic Reissner–Mindlin (or *thick* plate) model is selected for the piano soundboard [9]. Such a model can be viewed as equivalent to the Timoshenko model for plates, in the sense that it accounts for the shear stresses, so that the transverse displacement is coupled to the rotation of the cross-sections [43]. Such a model, which is more complex than the Kirchhoff–Love model used for the guitar, is firstly justified by the spectral extent of most piano sounds (up to 15 kHz and even more) and, secondly, because of the presence of bridge and ribs. Due to these elements, the assumption of *thin* plate is no longer valid. The ribs and the bridge are taken into account as heterogeneities in thickness and material properties of the soundboard, as for the guitar model presented in the previous section. Figure 14.28 illustrates this method in the case of a grand piano (Steinway D).

The coupling between the soundboard and a string has to be expressed by dual conditions, in order to conserve the energy: one condition for the force and another for the velocity. The force exerted by the string is given in Eq. (8.64) in Chap. 8. Assuming that the motion of the bridge is purely vertical (an assumption that could eventually be revised), then one has to write a condition of continuity for the vertical components of both string and bridge velocities, and a condition of nullity for the horizontal motion of the bridge.

The conditions of coupling between the structure of the piano and the acoustic field can be written with a similar method as for the guitar and the kettledrum. The linear acoustic equations in the surrounding air are the same as in Eq. (14.16). It is supposed here that only the soundboard vibrates, all other parts of the instrument remaining rigid. Thus, a continuity of the normal velocity is written on the soundboard, and a condition of nullity of the normal acoustic velocity is written

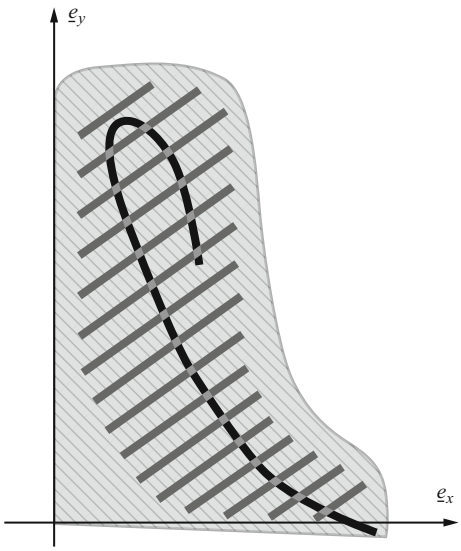

Fig. 14.28 Grand piano soundboard model. The *thin grey stripes* indicate the direction of the fibers. The ribs (*in dark grey*) and the bridge (*in black*) are treated as heterogeneities

on the other parts. We are aware of the fact that this is an approximation since, in reality, one can clearly feel with the fingers that the rim of a grand piano vibrates, especially when playing notes in the bass range.

The free space is simulated here using perfectly matched layers (PML). The method consists of simulating a fictitious layer of absorbing material along the boundaries of the computational domain, in order to limit as much as possible the reflected waves [2].

An equation of energy conservation can be written for the complete model composed by the hammer, the strings, the soundboard, and the acoustic field, as illustrated in Fig. 14.29. This energy conservation is then used for deriving numerical schemes with the guarantee of stability.

14.4.2 Modal Analysis of the Soundboard

The dynamics of the soundboard is governed by a plate operator. As for the guitar [23], it is preferable to solve this part of the model in two steps because of the required accuracy in the calculation of the frequencies (numerical dispersion). In a first step, a modal analysis is conducted on the undamped soundboard (i.e., the terms of losses are not considered in the equations). The soundboard equations are discretized in space, using high-order finite elements. For a grand piano, typically 2400 modes are necessary for predicting accurately the vibrations of the soundboard between 0 and 10 kHz.

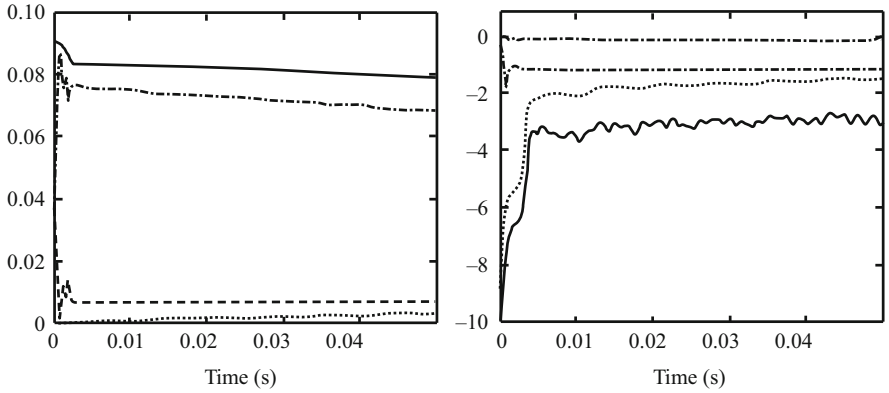

Fig. 14.29 Temporal evolution of the energy for note *C2* (fundamental $f = 65.4$ Hz). *Thin solid line*: total energy; *dashed line*: hammer energy; *dash-dotted line*: string energy; *dotted line*: soundboard energy; *thick solid line*: air (acoustic) energy. (*Left*) Linear scale; (*Right*) logarithmic scale

Figure 14.30 shows a few calculated modes for a Steinway D soundboard, with fourth-order finite elements and 450,000 degrees of freedom. Examining the shapes of the higher modes confirms the results presented in Chap. 3 for an upright piano: here also, the vibrational energy is localized in relatively narrow areas, frequently bounded by the ribs and/or the bridge.

In a second step, once the soundboard modes are obtained, each modal amplitude $X_n(t)$ associated to the modal frequency f_n is governed by a second-order differential equation, as shown several times in Chap. 3. Then, a convenient way to account for the observed damping in the soundboard material (wood) is to introduce in these oscillator equations a damping term whose value is derived either from experiments or from available data in the literature for the appropriate species. We get

$$\frac{d^2X_n}{dt^2} + \alpha(f_n)\frac{dX_n}{dt} + (2\pi f_n)^2 X_n = F_n, \tag{14.56}$$

where the terms F_n are the modal projections of the source terms. These terms are composed by both the string forces and acoustic pressure due to the radiated field. Recall that introducing a posteriori damping terms in the decoupled equations (14.56) is justified as long as the damping factors are reasonably small compared to the eigenfrequencies (see Chap. 5). Usually, this assumption of *diagonal damping* is justified for the wood species of current use for making the soundboard, for which the damping coefficients are of the order of a few percents [27].

The damped oscillator equations (14.56) yield analytical solutions which can be discretized with any time step, without altering the dispersion, and with no risk of instability. The appropriate selected time step must be synchronized with those used for the other constitutive parts of the piano (strings and acoustic space).

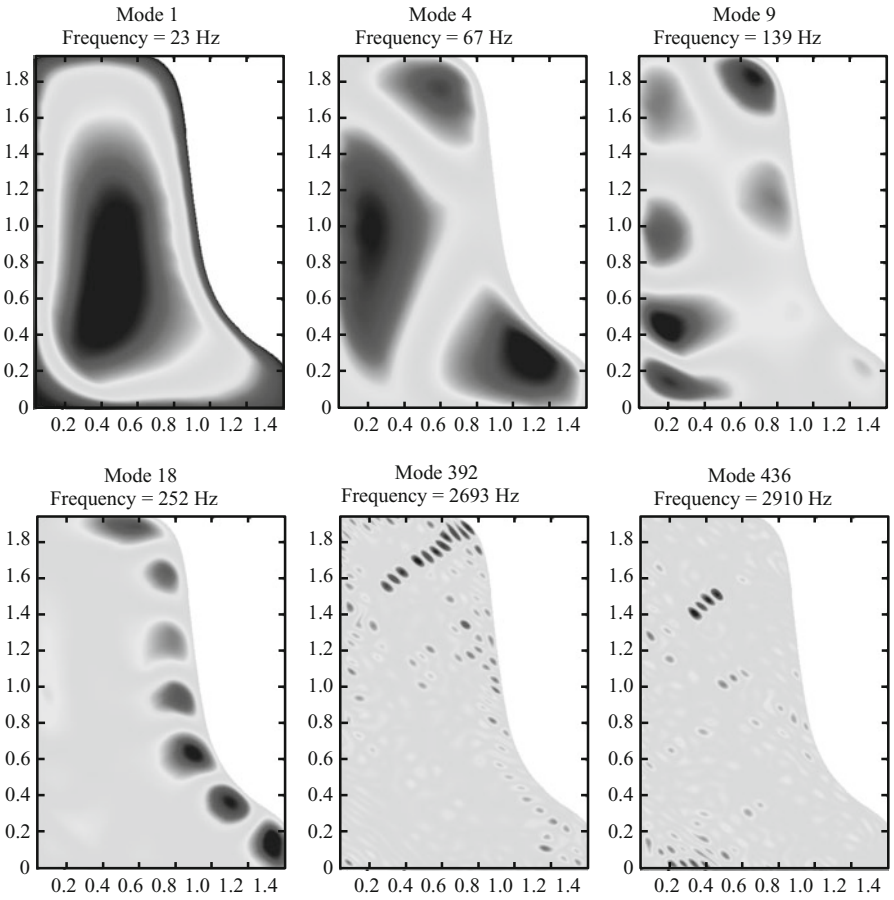

Fig. 14.30 Examples of some simulated modes of a grand piano soundboard (Steinway D)

Recent studies on the vibroacoustics of the piano soundboard were made by Boutillon and Ege [7]. Mamou-Mani et al. investigated the influence of prestress on the eigenfrequencies of piano soundboards [37].

14.4.3 Results of the Simulations

Figure 14.31 shows the temporal evolution of some simulated variables for the note *C2* (fundamental $f = 65.4$ Hz) during the first milliseconds of the sound, using the piano model presented above [9].

The transverse displacement of the string is shown on the top of the figures, the longitudinal displacement is drawn in gray color in the line thickness. It can be seen that the longitudinal perturbation reaches the end (bridge side) well before the transverse wave, in accordance with the ratio between the speed of these waves

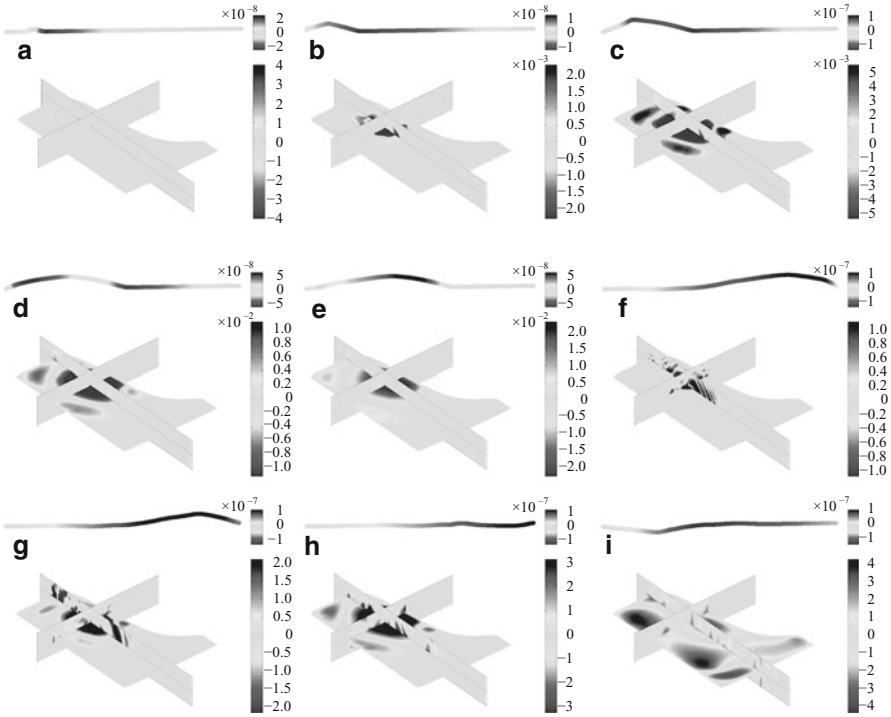

Fig. 14.31 Temporal evolution of some simulated variables for the note *C2* (fundamental $f = 65.4$ Hz) using a grand piano model (Steinway D). The transverse displacement of the string is shown on the top of the figures, the longitudinal displacement is drawn in *gray color* in the line thickness. The displacement field of the soundboard is shown in the bottom of the figures, and the pressure field is shown in two planes perpendicular to the soundboard. The snapshots are calculated at the successive instants of time: (**a**) 0.4 ms; (**b**) 1.1 ms; (**c**) 2.1 ms; (**d**) 3.1 ms; (**e**) 4.1 ms; (**f**) 5.1 ms; (**g**) 7.1 ms; (**h**) 8.1 ms; (**i**) 16.1 ms

(around 14). The displacement field of the soundboard is shown in the bottom of the figures, and the pressure field is shown in two planes perpendicular to the soundboard. These planes cross at the attachment point of the string (*C2*) on the bridge. It can be seen that the soundboard starts to vibrate in picture (b), approximately one millisecond after the impact of the hammer: this initial vibration is due to the longitudinal wave, since the transverse wave has not reached the bridge at that time. From Fig. 14.31b–f, the longitudinal wave excites the soundboard modes, which yield a significant contribution to the attack of piano tones. On the waveforms, this contribution takes the form of the so-called *precursor* whose magnitude increases with the loudness of the tone, which is in accordance with the nonlinear model of the string [15]. This property is illustrated in Fig. 14.32, for the note D♯1.

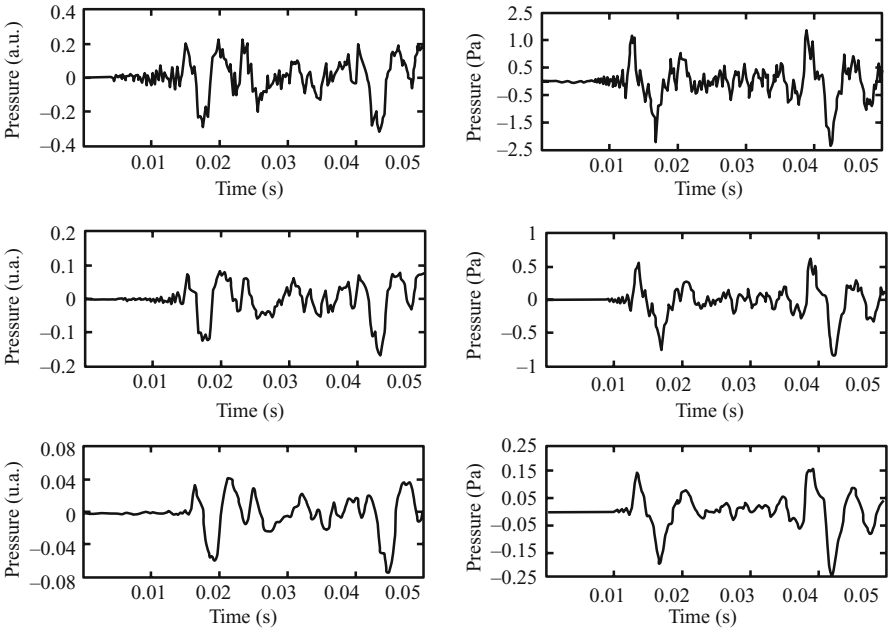

Fig. 14.32 (*Left*) Measurements and (*Right*) simulations of the acoustic pressure radiated by a grand piano (Steinway D) for different levels of excitation: (*top*) *forte*; (*middle*) *mezzoforte*; (*bottom*) *piano*. Note D♯1 (fundamental $f = 39$ Hz)

Figure 14.33 shows the spectral analysis of measured and simulated piano tones for the note D♯1 played on a Steinway D, for different levels of attack.

It can be seen first that the domain of excited frequencies increases towards the high frequencies as the initial velocity of the hammer increases. This is a consequence of the decrease of the impulse duration due to stiffening of the hammer's felt. In each spectrum, the presence of a dense *packet of frequencies* between 0 and 800 Hz superimposed to the string's partials is also observed. This *packet*, which remains almost unchanged from one spectrum to another, is made of the lowest modes of the soundboard. These modes are excited by the strings: the lowest soundboard modes are less damped than those in the medium and high range, and this is the reason why they are more visible on the spectra. Although all soundboard modes are significantly more damped than the strings' modes, they are clearly audible during the attack transients. Cutting artificially the first milliseconds of a piano tone, then a rather poor "string" tone is obtained. Finally, Fig. 14.33 shows that the spectra are enriched in some specific frequency bands, as the amplitude increases. In the present case, such an enrichment is visible around 1.2, 1.7, 2.3, 2.8, 3.3, 3.7, and 3.9 kHz. As shown in Chap. 8, these additional peaks are phantom partials, due to nonlinear combination of both the transverse and longitudinal waves on the string.

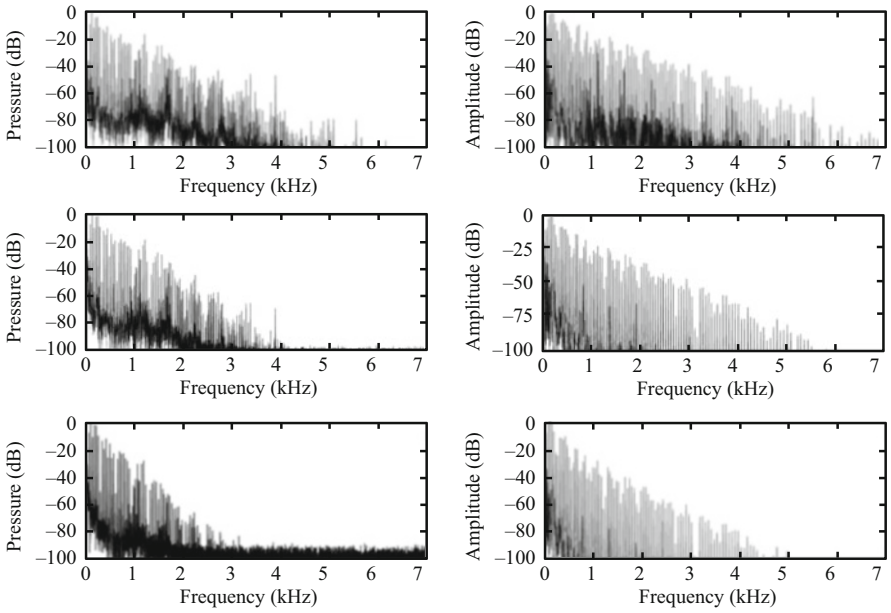

Fig. 14.33 Spectra of the sound pressure radiated by a Steinway D grand piano for different levels of excitation: (*top*) *forte*; (*middle*) *mezzoforte*; (*bottom*) *piano*. Note D♯1 (fundamental $f = 39$ Hz). *Left*: measurements; *Right*: simulations

14.4.4 Radiation and Directivity of the Piano

In this section, the purpose is to investigate the influence of ribs and bridge on the radiation of the piano, with special emphasis on the directivity of the instrument in the medium and high frequency range. This study is related to the localization of modes presented in Chap. 3 [16].

The problem is illustrated here by simulations of directivity performed on a model of upright piano soundboard with equally spaced ribs, without the bridge. Figure 14.34 shows the directivity of the pressure field in two (almost perpendicular) particular planes in the direction of the ribs, and in the direction of the fibers, respectively. At frequency $f = 2078$ Hz, the inter-ribs distance corresponds here exactly to the half of a vibratory wavelength. The sound field is calculated on a hemisphere with radius $r = 3$ m. Both directivity patterns show a number of narrow peaks, which means that the radiated energy is concentrated in narrow solid angles. This is nothing but a particular case of *antenna* effect, comparable to those seen in the previous chapters for plates and wind instruments: in all these situations, the directivity is reinforced for equally spaced arrays of identical sources.

By contrast, Fig. 14.35 shows the directivity patterns obtained from a measured velocity field on an upright piano soundboard, at a forcing frequency $f = 1542$ Hz. The real soundboard here has a slightly irregular distribution of ribs and two

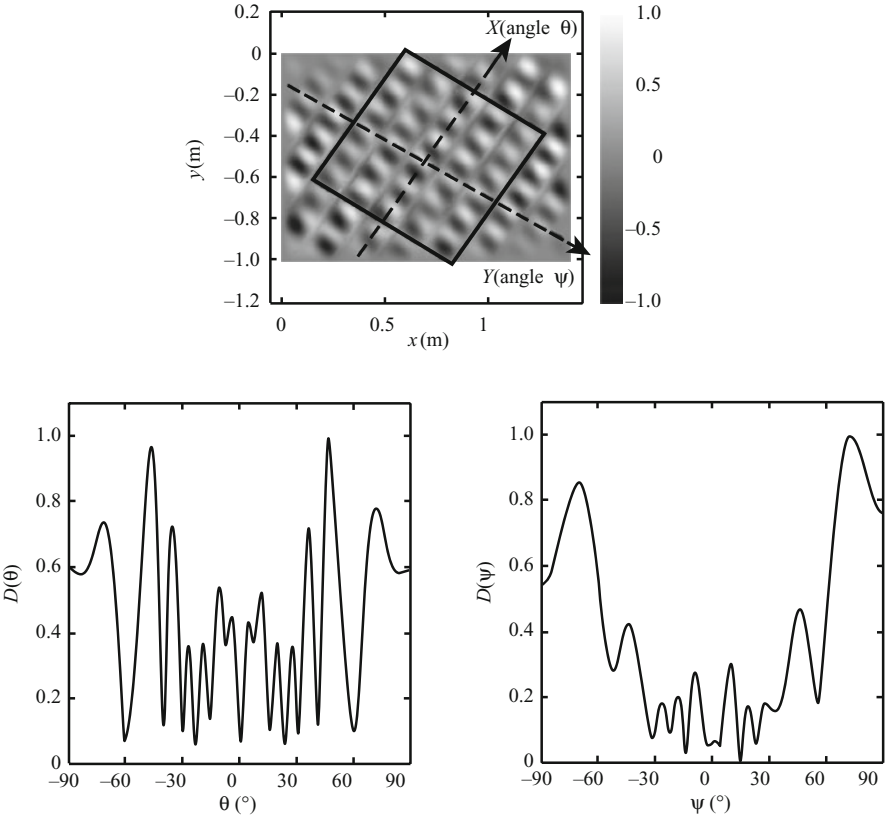

Fig. 14.34 (*Top*) Calculated displacement field for an upright piano soundboard with equally spaced ribs, at frequency $f = 2078$ Hz. (*Middle*) Directivity $D(\theta)$ in the direction of the ribs (X axis). (*Bottom*) Directivity $D(\psi)$ in the direction of the fibers (Y axis)

bridges. As a consequence, localized modes, and also localized operating deflexion shapes (ODS) are observed. Recall that ODS are combination of modes with close eigenfrequencies, that are currently observed for forced excitation (see Chap. 3). Due to damping, the modes of a real structure generally cannot be separated beyond a certain frequency (usually beyond 1–1.2 kHz for piano soundboards), and ODS are measured. In a recent paper, it was shown that the localization of modes also can lead to localization of ODS, which corresponds to experiments [16]. As a result of this localization, the array equivalent to the soundboard is made of a significantly small number of sources, compared to the case presented in Fig. 14.34. Thus, the directivity patterns show only one main lobe (along ψ) and two main lobes (along θ). In addition, these calculated patterns are very well predicted by those resulting from an equivalent array of 4×2 monopoles (see Fig. 14.35). In conclusion, one practical result of mode localization in the piano, which occurs primarily in the medium and high frequency range, is that the opening of the main lobe is wider as

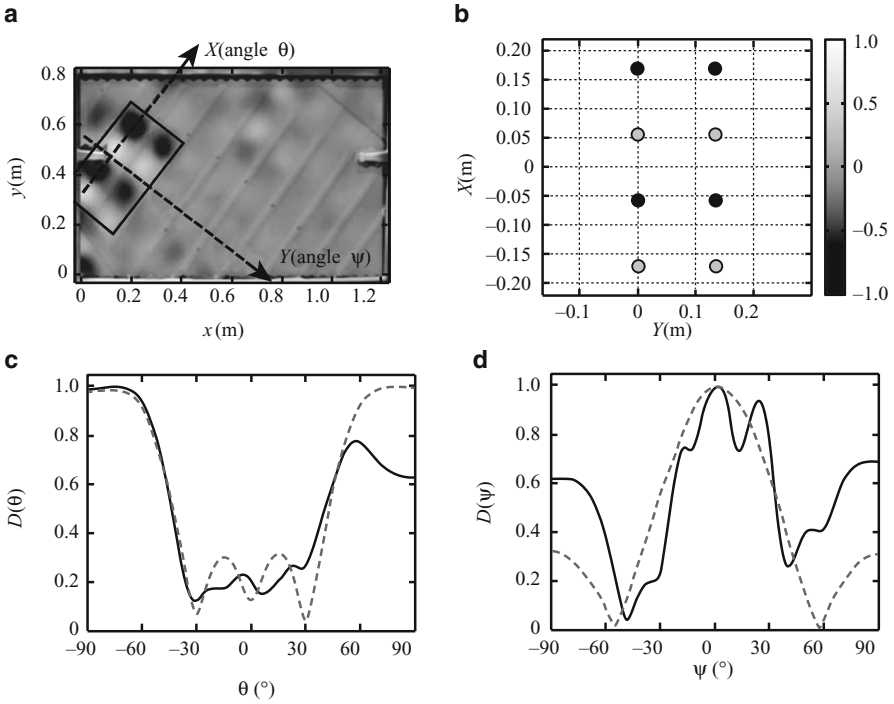

Fig. 14.35 (**a**) Measured velocity field on an upright piano at $f = 1542$ Hz. (**b**) Array of 4×2 monopoles presenting the same geometrical properties as the vibratory zones of the soundboard. (**c**) Directivity pattern $D(\theta)$ along the X-axis (direction of the ribs) and (**d**) along the Y-axis (direction of the fibers): these patterns were calculated from the measured velocity field (*solid line*) and from the array of monopoles (*dashed line*), respectively

with a regularly spaced ribs pattern. In consequence, the spectral distribution of the radiated sound is not subjected to strong variations, as the direction of observation changes around the instrument, which is rather a favorable property. At this stage, one remaining question is to know whether this interesting effect is really wanted (and controlled) by the piano makers.

14.5 Radiation of Wind Instruments with Several Orifices

In Chap. 12, we explained that at low frequencies the orifices of wind instruments radiate as monopoles, because their dimensions are small compared to the wavelength. This is true, in particular, for woodwinds, even for saxophones which belong to this category, although these instruments have rather wide orifices. The present section aims to show how multiple sources can radiate. Two simple examples are considered: the two orifices of an open flute, which are rather far apart from each

other, and the lattice of woodwind toneholes, which are close to each other. We add the problem, which is slightly different in nature, of two tubes having their radiating ends close to each other; this allows a global understanding of the sound production and radiation for a self-oscillation instrument.

As mentioned in the introduction of Chap. 12, we do not study the effect of the room, or even the reflection on the floor, and assume that instruments radiate into an anechoic room. Indeed it is useful, if only for the sound engineers, to understand the essentials of the interference fields created by wind instruments, before studying how they are modified by the rooms.

14.5.1 Open Flute at Low Frequencies

Among woodwinds the flutes are a particular case, because the exciter system directly radiates. For a Boehm flute, radiation is due at least to two sources.[14] We choose to investigate the particular case of an open flute without toneholes, with a limitation to low frequencies. In chap. 7 we obtained the amplitude ratio of the two sources for the mode n [Eq. (7.72)], and here we simplify this ratio. At low frequencies, it is approximately equal to:

$$\frac{U_2}{U_1} \simeq (-1)^{n+1}. \tag{14.57}$$

For clarity we deliberately changed the notation: the outgoing flow rates from the orifices are considered as positive[15]: for the mouth-hole $U_1 = -U(0)$ and for the passive end of the instrument $U_2 = U(\ell)$. We are interested in the playing frequencies and in their harmonics, assuming that they are very close to the modal frequencies: as an example, the mth harmonic of the playing frequency n is at the frequency mn.

- In Chap. 12 (Sect. 12.6.3), we examined the problem of the *interaction* of orifices of two tubes, and here we discuss it for the present case by choosing the example of the passive end, with flow rate U_2. The pressure created by this flow rate at this end is equal to $P_{22} = Z_{22}U_2$, where Z_{22} is the (self-)impedance of this source, while the pressure created by the mouth-hole, which is at the distance ℓ, is given by $P_{21} = Z_{21}U_1$. The mutual impedance Z_{21} is given in Eq. (12.146), with $d = \ell$. The determination of the influence of one source on the other is reduced to the ratio $|Z_{21}/Z_{22}|$, because the two flow rates have the same order of magnitude.

[14] We wish to emphasize different meanings of the word "source": in Chap. 10, aeroacoustic sources were defined as the origin of the sound production. Here the considered sources are the orifices, which are the sources of acoustic radiation.

[15] Remind that in Chap. 10, we denoted $U(0) = Q_m$.

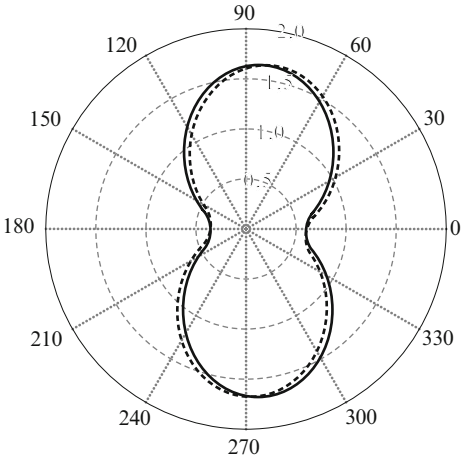

Fig. 14.36 Directivity of a Boehm flute near the fundamental frequency of the lowest note, *C*4, 261 Hz (there are two sources only: the mouth-hole and the open end). *Solid line*: theoretical result; *dotted line*: experimental result when exciting the instrument with a small loudspeaker at the location of the head joint cork. The scale is linear. The angles $\theta = 180°$ and $\theta = 0°$ correspond to the mouth-hole and the open end, respectively (Courtesy of R. Caussé)

This ratio is equal to $R/(2.4\ell)$, where R is the tube radius, and therefore it is small (in general $R/\ell < 10$, and it is possible to ignore the interaction between the two sources).

- In order to calculate the directivity in the far field (the distance being much larger than the tube length), we can directly use Eq. (12.27), with the following result (see Fig. 12.6):

$$U(\theta) = (U_1 + U_2)\cos\left[\frac{k\ell}{2}\cos\theta\right] - j(U_1 - U_2)\sin\left[\frac{k\ell}{2}\cos\theta\right],$$

or, alternatively, if Eq. (14.57) is used

$$|U(\theta)|^2 = 2\,|U_1|^2\,[1 - (-1)^n\cos(k\ell\cos\theta)]\,. \tag{14.58}$$

Because the distance of the sources is not small compared to the wavelength, the behavior is very different to that of a simple monopole (for odd n) or dipole (for even n). Figure 14.36 shows an experimental result, obtained with a loudspeaker excitation, and the corresponding theoretical result. The interference field created by an open flute is very complicated, even for the lowest playing frequencies, and even when the toneholes are closed.

For the lowest playing frequency around $k\ell = \pi$, the radiation is maximum in the direction which is transverse to the instrument ($\theta = 90°$), and minimum in the longitudinal direction. Measurements during playing were made for an organ pipe [20], with an excellent agreement with theory, which shows the very weak influence of the mean flow at low frequencies.

14.5.2 Instruments with Tonholes

In order to analyze the radiation by a lattice of toneholes, we first ignore the external interaction, starting from the approach of Chap. 7, then we show how to state the numerical problem when interaction is taken into account.

14.5.2.1 Radiation of a Regular Lattice of Toneholes Without External Interaction

The theory proposed by Benade [4] for a periodic lattice of toneholes allows showing the behavior difference between the frequency ranges below and above the cutoff, when the lattice is supposed to be infinite.[16] If the lattice is infinite, all quantities of the cell n (see Fig. 7.27) are proportional to $\exp(-n\Gamma)$, where the propagation constant $\Gamma(\omega)$ is real in the stop band and purely imaginary in the pass band [see Eq. (7.193)]. This applies in particular to the flow rate of the holes, arranged in a regular antenna of monopoles, studied in Chap. 12 (see Fig. 12.7). We denote the flow rate of the hole n $U_n = U\exp[-(n-1)\Gamma]$. The pressure produced is given in Eq. (12.29), with $\Gamma = j\varphi$; in the far field, it is proportional to $U\exp[(n-1)(2jk\ell\cos\theta - \Gamma)]$, where 2ℓ is the hole interval, and θ is the azimuth of the considered point with respect to the tube axis.

- Below the cutoff, Γ is real and the flow rates decrease exponentially from the first open hole. If it is assumed that the distance between two holes is smaller than the wavelength ($2k\ell << 1$), the superposition of the different monopoles is still a monopole and there is no directivity. Thus the woodwinds (except the flutes!) radiate in an omnidirectional way at low frequencies. The first open hole plays the main role: this is consistent with the analysis given in Chap. 7: to a first approximation, it is if the tube was cut at the first open hole.
- The case of frequencies above cutoff is more complex: Eq. (12.30) can be used for the directivity pattern:

$$D(\theta) = \frac{\sin N\Theta}{N\sin\Theta} \text{ where } \Theta = k\ell\cos\theta - \frac{\varphi}{2}. \tag{14.59}$$

  Therefore there are directivity lobes, corresponding to $\Theta = 0$; if we write $\varphi = 2\ell\omega/v_\varphi$, where v_φ is the phase velocity inside the lattice, they are obtained in particular for[17]:

[16] Here we treat the case of reed instruments, in order to separate the problem of tonehole radiation from that of the flute mouth-hole.

[17] The relationship between a monopole lattice and an infinite plate has been seen [see the note after Eq. (13.56)]. Above cutoff the wavenumber $k_1 = \varphi/2\ell$ is equal to $\sqrt{k^2 - k_c^2}$; it is therefore smaller than the wavenumber k in free space, and this corresponds to the supersonic case. The wavenumber tends to k at higher frequencies, thus there is no critical frequency and the subsonic

$$\cos\theta = c/v_\varphi. \tag{14.60}$$

When the frequency decreases to the cutoff, φ tends to 0 (v_φ tends to infinity), and the lobe angle tends to $\theta = \pi/2$ perpendicularly to the tube axis. When the frequency increases beyond cutoff, it can be shown that the phase velocity becomes close to the free space sound velocity and that the lobe becomes close to the tube axis. At very high frequencies, it can be observed that the radiation mainly occurs from the tube end: this explains why saxophonists, when playing with amplification, play with a microphone close to the instrument bell in order to reinforce the highest frequencies.

- In the stop band, the behavior of a finite lattice is rather similar to that of an infinite lattice, because the amplitude of the growing exponential is significant near the end only and is often negligible as explained in Chap. 7. Conversely, above the cutoff, the incoming wave term needs to be added to $D(\theta)$, but with a multiplication factor corresponding to the flow rate reflection coefficient, and an angle $\Theta_R = k\ell\cos\theta + \frac{\varphi}{2}$. Therefore we find lobes that are symmetrical to the lobes of the outgoing wave with respect to the vertical axis, though with a slightly smaller amplitude because the modulus of the reflection coefficient is less than unity.

  Figure 14.37 shows an example of result with front and rear lobes. The discrepancies between theory and experiment can be explained by the difficulty to obtain an accurate computation at higher frequencies, but the qualitative agreement between the results is rather satisfactory. However one difference between theory and experiment is understood: the amplitude difference between the front and rear lobes is underestimated by the theory, because the external interaction of the holes is ignored, as explained in the next paragraph.
- Beforehand we notice that the generalization presented in Sect. 7.8.2.5 of Chap. 7 cannot be easily applied to radiation. For a lattice built with cells of different geometry but with equal cutoff frequency, the input and output quantities (pressure and flow rate) remain proportional to $\exp(\mp n\Gamma)$, and it can be shown that this is also true for the pressures at the input of the holes. However, the relevant quantity for the radiated pressure is the flow rate: it is proportional to the pressure at the input of a hole divided by the hole impedance, $j\omega m_t$ [see Eq. (7.196)], and this impedance is not constant in the considered lattice. In the pass band, the modulus of $\exp(\mp n\Gamma) = \exp(\mp jn\varphi)$ is unity, and the flow rates therefore are inversely proportional to the total mass of a hole, which decreases with the hole radius. Consequently the flow rates increase with the hole radius, and the analysis requires the examination of each particular case. The considered lattice behaves as a periodic lattice for the internal field of the tube, but not for the radiated pressure field. Nevertheless we conclude that qualitatively the radiation structure keeps directivity lobes above the cutoff.

case does not exist. Below cutoff the wavenumber is purely imaginary: this case differs from both cases supersonic and subsonic, with radiation into the far field.

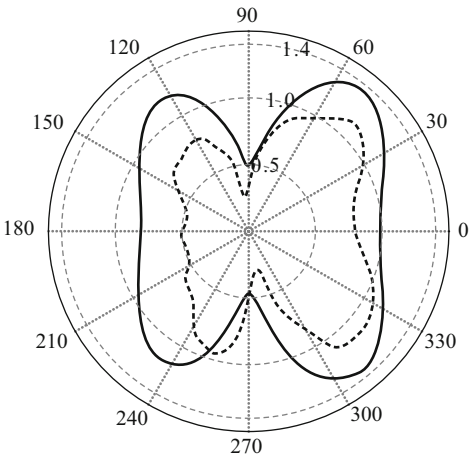

Fig. 14.37 Directivity of an oboe, at $f = 2366$ Hz near the 9th harmonic of one of the lowest notes ($C4$, fundamental 261 Hz): two holes are open, in addition to the bell. *Solid line*: theoretical calculation. *Dotted line*: experiments (which was done by exciting the instrument with a small loudspeaker at its input). The scale is linear. The angle $\theta = 0°$ corresponds to the instrument bell (Courtesy of R. Caussé)

14.5.2.2 Radiation of a Tonehole Lattice with External Interaction

The previous analysis assumes that the holes radiate in separate spaces. A method of computation of the interaction is given hereafter (see [35]; notice that another method can be found in [36]). We start by giving the main qualitative results as obtained by a numerical computation.

- In the stop band, the main attenuation from one hole to the following one is not exactly exponential because the radiation is inversely proportional to the hole spacing and comes to compensate the exponential attenuation. Thus, the attenuation is rather linear and slow.
- In the pass band, there is a reflection at the end of the tube, and therefore there are maxima and minima (i.e., antinodes and nodes) of flow rate. In other words there is a non-zero standing wave ratio. A perturbation reasoning is possible: because of the external interaction the strong flow rates compensate for the weak flow rates, and the standing wave ratio decreases. This yields a small effective reflection coefficient. The following phenomena result:
  - The input impedance peaks are very attenuated above cutoff. Thus the experimental determination of the cutoff frequency is justified. When interaction is ignored, it has been seen in Chap. 7 that, on the one hand, the peaks are very inharmonic above cutoff, and, on the other hand, they are rather low in amplitude since the attenuation near the walls occurs over the whole tube length (instead of below the first open hole as in the stop band). When interaction is considered, the magnitude of the peaks is even lower.
  - As the effective reflection coefficient is low because of external interaction, the rear lobes are smaller than when interaction is ignored. It is a part of the explanation of the discrepancy between the theory (without interaction) and the experiments shown in Fig. 14.37.

Above cutoff, we conclude that there are directivity lobes mainly in the front direction, and their orientation comes closer to the axis perpendicular to that of the tube as frequency tends to cutoff. It should be specified that this analysis is linear and ignores the particular effects existing at high level for narrow holes (see Chap. 8).

Computation Method for the External Interaction of Toneholes

The flow rates of the toneholes are sought with respect to one input reference quantity, such as the input flow rate, denoted U_{s0}, the subscript s indicating a source. In order to generalize the calculation, we assume that there is also a flow rate source U_{sn}, emitting inside the tube at tonehole n (this can be a small loudspeaker). The principle presented hereafter does not assume any particular regularity of the holes. We also assume that it is a flute, which radiates by the mouth with a flow rate U_0 (the handling of the reed instrument case is easy). For the sake of simplicity, we consider each hole as a shunt admittance, ignoring the effect of the anti-symmetrical masses. For each hole the flow rate conservation is written as:

$$U_{sn} = U_n + U_{rn} + U_{\ell n}. \tag{14.61}$$

U_n is the flow rate which radiates from each hole and contributes to the radiated pressure. U_{rn} and $U_{\ell n}$ are the flow rates entering the main tube on the right and on the left, respectively, both defined with the orientation coming out from the hole. At the output of the main tube, with subscript N, the radiating flow rate is denoted U_N, and $U_{rN} = 0$. At the input (subscript 0), we write $U_{g0} = 0$. The flow rates U_{rn} and $U_{\ell n}$ are related to the pressure of the corresponding hole and that of the following one, p_n and p_{n+1}. Using (7.119), it can be written

$$U_{rn} = Y_n p_n + Y_{\mu n} p_{n+1}. \tag{14.62}$$

$$U_{\ell n} = Y_{\mu n-1} p_{n-1} + Y'_{n-1} p_n. \tag{14.63}$$

The admittances Y are given in Eq. (7.119) with respect to the coefficients of the transfer matrix of the main tube between the two holes. A matrix relationship between flow rate vectors and pressure vectors is derived

$$\boldsymbol{U}_s = \boldsymbol{U} + \mathbb{Y}\boldsymbol{P}, \tag{14.64}$$

where the admittance matrix $\mathbb{Y}$ of the hole lattice is tridiagonal, including the known elements Y_n, $Y_{\mu n}$, and Y'_n. The dimension is equal to the radiating element number (mouth, holes, and tube end). It remains to express the radiation impedance matrix $\mathbb{Z}_R$, which generalizes the relationship (12.139)

(continued)

valid for two orifices:

$$\boldsymbol{P} = \mathbb{Z}_R \boldsymbol{U}. \tag{14.65}$$

In order to take the pressure difference between the input and output of the holes into account, Eq. (7.188) is used, and the acoustic mass which is denoted $\rho L_3/S_3$ is added to the diagonal element of the matrix $\mathbb{Z}_R$. The solution of the problem is therefore given by:

$$\boldsymbol{U} = (\mathbb{I} + \mathbb{Y}\mathbb{Z}_R)^{-1} \boldsymbol{U}_S \tag{14.66}$$

In practice there is a unique source at the input and therefore the vector U_s involves a unique non-zero element. The flow rates at every orifice is deduced with respect to U_{s0}. The method can be used also when the interaction is ignored, the matrix $\mathbb{Z}_R$ being diagonal, but it is less efficient than the transfer matrix method. Conversely, when interaction is taken into account, the matrix $\mathbb{Z}_R$ is full, and a numerical solution is required.

14.5.3 Interaction of Two Tubes

14.5.3.1 Statement of the Problem

The problem of two tubes interacting through radiation is somewhat similar to that of a vibraphone (see Sect. 14.1). A typical example is that of two juxtaposed organ pipes, which can have a mutual influence. This complex problem is interesting because it can help understanding the effect of the interaction on the sound production itself, thanks to the analysis of the input impedance and the radiation. In order to simplify the problem, we consider the example of two cylindrical tubes having a unique opening. One tube is provided with a reed, and the second one is passive, with a closed extremity (see Fig. 14.38). The distance between the two orifices is d. In order to calculate the input impedance of the reed tube, we use the formula of the impedance projected at its input, and the radiation impedance matrix which is given by Eq. (12.139).

The mutual impedance is assumed to be given in Eq. (12.146). In order to calculate the impedance at the open end of Tube 1, we simply need the knowledge of the input impedance of Tube 2:

$$Z_2 = -P_2/U_2 = j\frac{\rho c}{S_2}\cot k\ell_2. \tag{14.67}$$

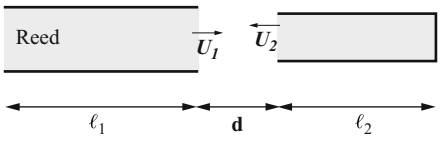

Fig. 14.38 Two tubes interacting: one is a reed tube and the other one is passive with a closed end. The lengths are ℓ_1 and ℓ_2, the radii r_1 and r_2, and the spacing of the openings d

The sign $-$ is a consequence of the orientation choice and of the definition of a passive system impedance (see Sect. 1.3.3.1, Chap. 1). The flow rate ratio and the radiation impedance of Tube 1 as modified by Tube 2 can be deduced as follows:

$$\frac{U_1}{U_2} = -\frac{Z_{22} + Z_2}{Z_{12}}; \tag{14.68}$$

$$\frac{P_1}{U_1} = Z_{11} - \frac{Z_{12}^2}{Z_{22} + Z_2}. \tag{14.69}$$

If Tube 2 was closed at its input (infinite Z_2), Tube 2 would not perturb Tube 1, because of the assumed approximations in the expression of the mutual impedance, when ignoring the diffraction effects on the external walls of the tubes. It appears that Tube 2 influences Tube 1 only if the mutual impedance is large enough, therefore if the distance d is small enough, and if the impedance $Z_{22} + Z_2$ is small enough: this corresponds to the natural frequencies of Tube 2 when open at its input. The first one is $f = c/4(\ell_2 + \Delta\ell_2)$, where $\Delta\ell_2$ is the radiation length correction of Tube 2. If the natural frequencies of Tube 2 differ from those of Tube 1, the influence of the passive tube is weak, as it is expected for two tubes of different lengths, and as it is often the case for two juxtaposed organ pipes.

14.5.3.2 Eigenmodes

The natural frequencies of the set of tubes can be calculated by considering Tube 1 closed at its input. This leads to the impedance seen from the output equal to $P_1/U_1 = j\frac{\rho c}{S_1}\cot k\ell_1 = -Z_1$ (if the orientation choice above presented for Tube 2 is used). Using (14.69), we get

$$(Z_{11} + Z_1)(Z_{22} + Z_2) = Z_{12}^2.$$

When ignoring losses, the impedances become purely imaginary, and the solution of this equation is the natural frequencies. The case of two symmetrical tubes (with the same radius and above all the same length) is especially interesting. The equation is written in the following form:

$$Z_{11} + Z_1 = Z_{22} + Z_2 = \pm Z_{12}.$$

Thus the natural frequencies are duplicated, with respect to the case where the tubes are isolated ($Z_{12} = 0$). At low frequencies the mutual impedance can be written as follows: $Z_{12} = jk\Delta\ell_{12}\rho c/S_1$, with $\Delta\ell_{12} = r_1^2/4d$. The two twin modes have the following frequencies:

$$f_n^- = \frac{(2n+1)c}{4(\ell_1 + \Delta\ell_1 + \Delta\ell_{12})} \quad \text{and} \, f_n^+ = \frac{(2n+1)c}{4(\ell_1 + \Delta\ell_1 - \Delta\ell_{12})}.$$

They are very close together and are located on both sides of the non-perturbed frequencies. Using Eq. (14.68), we find that they correspond to $U_2/U_1 = +1$ and $U_2/U_1 = -1$, respectively. The first ones correspond to a symmetrical field, while the second correspond to an anti-symmetrical field, in accordance with the symmetry of the geometry. The first ones are related to a monopole radiation, while the second are related to a dipole radiation, which is very weak. This very weak radiation corresponds to the same phenomenon than the quarter-wavelength rejection observed when a closed chimney is at its resonance (see Chap. 7).

14.5.3.3 Input Impedance

In order to interpret the theoretical result for the input impedance curve, it is not necessary to calculate the modes when losses (either visco-thermal or radiation) are taken into account. We can use the fact that the peaks are inversely proportional to the power entering the tube. Figure 14.39 shows a case where coupling is important, because the tube radii are wide, and the distance d between the two openings is small. It is limited to the first peak, which is split into two peaks. The first (sub-)peak corresponds to a symmetrical field, with a rather strong radiation, while the second (sub-)peak corresponds to an anti-symmetrical field, with a very weak radiation. This explains why the second peak is higher than the first. Moreover it can be noticed that:

- If Tube 1 does not radiate, the amplitude of the (unique) peak is almost twice that of the 2nd peak, because when interaction excites Tube 2 the boundary layer losses are equal in the two tubes. Acoustic power enters Tube 2 in order to compensate for losses;
- If Tube 1 radiates in the absence of Tube 2, the amplitude of the (unique) peak is almost twice the one of the first peak, because when interaction excites Tube 2, the boundary layer losses are equal in both tubes which radiate symmetrically in the surrounding space. The power entering Tube 2 is the difference between the compensation for the losses and the radiated power.

In practice, Tube 1 is excited by a reed and produces the frequency of the 2nd peak, which is the highest peak, and the radiation is weak. But quasi-periodic regimes can also be expected because of the proximity of both peaks. This example

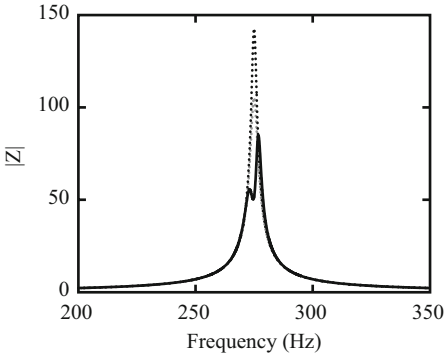

Fig. 14.39 Modification of the first impedance peak of a cylindrical tube of length $\ell_1 = 0.3\,\text{m}$, radius $r_1 = 2\,\text{cm}$, put close to another identical tube, which is closed. The extremities are set at distance $d = 5\,\text{cm}$ apart. The *solid line* shows the duplication of the peak. The *dotted lines* correspond to the case of Tube 1 with Tube 2 removed: for the higher curve, the radiation is ignored (the real part of the radiation impedance is zero), while for the lower curve, it is considered. The effect of the passive tube is very weak far from its natural frequency. The unit of $|Z|$ in ordinate is arbitrary

is particularly simple, and highlights the coupling effect of radiation. For the peaks of higher frequencies, the phenomenon is more important because the ratio of the radiated power to boundary layer losses increases and thus the first "sub-peak" strongly decreases, and might even disappear.

References

1. Balanant, N.: Numerical modeling of the acoustic guitar: applications and improvements (in French). Master thesis, ENSTA (2003)
2. Bécache, E., Fauqueux, S., Joly, P.: Stability of perfectly matched layers, group velocities and anisotropic waves. J. Comput. Phys. **188**, 399–403 (2003)
3. Bécache, E., Chaigne, A., Derveaux, G., Joly, P.: Numerical simulation of a guitar. Comput. Struct. **83**(1–2), 107–126 (2005)
4. Benade, A.H.: On the mathematical theory of woodwind finger holes. J. Acoust. Soc. Am. **32**(12), 1591–1608 (1960)
5. Benade, A.H.: Fundamentals of Musical Acoustics. Oxford University Press, Londres (1976)
6. Beslin, O.: Radiation and acoustic transparency of plates with holes (in French). Ph.D. thesis, INSA Lyon (1993)
7. Boutillon, X., Ege, K.: Vibroacoustics of the piano soundboard: Reduced models, mobility synthesis, and acoustical radiation regime. J. Sound Vib. **332**(18), 4261–4279 (2013)
8. Caldersmith, G.: Designing a guitar family. Appl. Acoust. **46**, 3–17 (1995)
9. Chabassier, J., Chaigne, A., Joly, P.: Modeling and simulation of a grand piano. J. Acoust. Soc. Am. **134**(1), 648–665 (2013)
10. Chabassier, J., Duruflé, M.: Energy based simulation of a Timoshenko beam in non-forced rotation. Influence of the piano hammer shank flexibility on the sound. J. Sound Vib. **333**(26), 7198–7215 (2014)

11. Chaigne, A.: On the use of finite differences for musical synthesis. Application to plucked string instruments. J. Acoustique **5**, 181–211 (1992)
12. Chaigne, A.: Determining the surface tension of a kettledrum head experimentally (in French). In: Actes du 5ème Congrès Français d'Acoustique, pp. 251–253 (2000)
13. Chaigne, A., Ramdane, A.: Numerical simulations of membrane-mallet interaction in kettledrums. Tech. Rep. 98D010, ENST Paris (1998)
14. Chaigne, A., Derveaux, G., Balanant, N.: Sound power and efficiency in stringed instruments. In: Proceedings of the 18th ICA, Kyoto (2004)
15. Chaigne, A., Chabassier, J., Burban, N.: Acoustics of pianos: physical modeling, simulations and experiments. In: Proceedings of SMAC'13. Stockholm, Sweden (2013)
16. Chaigne, A., Cotté, B., Viggiano, R.: Dynamical properties of piano soundboards. J. Acoust. Soc. Am. **133**(4), 2456–2466 (2013)
17. Christensen, O., Vistisen, R.B.: Simple model for low-frequency guitar function. J. Acoust. Soc. Am. **68**, 758–766 (1980)
18. Christian, R.S., Davis, R.E., Tubis, A., Anderson, C.A., Mills, R.I., Rossing, T.D.: Effects of air loading on timpani membrane vibrations. J. Acoust. Soc. Am. **76**, 1336–1345 (1984)
19. Collino, F.: Higher-order absorbing boundary conditions for the 3D wave equation (in French). Research report 2932, INRIA (1996)
20. Coltman, J.: Sound radiation from the mouth of an open pipe. J. Acoust. Soc. Am. **46**, 477 (1969)
21. Delande, D., Sornette, D.: Acoustic radiation from membranes at high frequencies: the quantum chaos regime. J. Acoust. Soc. Am. **101(4)**, 1793–1807 (1997)
22. Derveaux, G.: Numerical modeling of the acoustic guitar (in French). Ph.D. thesis, Ecole polytechnique (2002)
23. Derveaux, G., Chaigne, A., Joly, P., Becache, E.: Time-domain simulation of guitars: model and method. J. Acoust. Soc. Am. **114**(6), 3368–3383 (2003)
24. Doutaut, V.: Experimental study and numerical simulation of keyboard percussion instruments (in French). Ph.D. thesis, ENST Paris (1996)
25. Doutaut, V., Chaigne, A., Bedrane, G.: Time-domain simulation of the sound pressure radiated by mallet percussion instruments. In: Proceedings of the International Symposium on Musical Acoustics, pp. 518–524 (1995)
26. Doutaut, V., Matignon, D., Chaigne, A.: Numerical simulations of xylophones. II. Time-domain modeling of the resonator and of the radiated sound pressure. J. Acoust. Soc. Am. **104(3)**, 1633–1647 (1998)
27. Ege, K., Boutillon, X., Rébillat, M.: Vibroacoustics of the piano soundboard: (non)linearity and modal properties in the low- and mid-frequency ranges. J. Sound Vib. **332**, 1288–1305 (2013)
28. Elejabarrieta, M.J., Santamaria, C.: Air cavity modes in the resonance box of the guitar: the effect of the sound hole. J. Sound Vib. **252**(3), 584–590 (2002)
29. Elejabarrieta, M.J., Ezcurra, A., Santamaria, C.: Coupled modes of the resonance box of the guitar. J. Acoust. Soc. Am. **111**(5), 2283–2292 (2002)
30. Fahnline, J.B.: Computing fluid-coupled resonance frequencies, mode shapes, and damping loss factors using the singular value decomposition. J. Acoust. Soc. Am. **115**(4), 1474–1482 (2004)
31. Fastl, H., Zwicker, E.: Psychoacoustics: Facts and Models. Springer, Berlin (1990)
32. Glowinski, R., Pan, T.W., Periaux, J.: A fictitious domain method for Dirichlet problem and applications. Comput. Methods Appl. Mech. Eng. **111**, 283–304 (1994)
33. Gough, C.E.: The theory of string resonances on musical instruments. Acustica **49**, 124–141 (1981)
34. Junger, M.C.: Sound radiation by resonances of free-free beams. J. Acoust. Soc. Am. **52**, 332–334 (1972)
35. Lefebvre, A., Scavone, G., Kergomard, J.: External tonehole interactions in woodwind instruments. Acta Acust. United Acust. **99**, 975–985 (2013)
36. Leppington, F.: On the theory of woodwind finger holes. J. Sound Vib. **83**, 521–532 (1982)

37. Mamou-Mani, A., Le Moyne, S., Ollivier, F., Besnainou, C., Frelat, J.: Prestress effects on the eigenfrequencies of the soundboards: experimental results on a simplified string instrument. J. Acoust. Soc. Am. **131**(1), 872–877 (2012)
38. Mansour, H., Fréour, V., Saitis, C., Scavone, G.P.: Post-classification of nominally identical steel-string guitars using bridge admittances. Acta Acust. United Acust. **101**(2), 394–407 (2015)
39. Morse, P.M., Ingard, K.: Theoretical Acoustics. McGraw Hill, New York (1968)
40. Paté, A., Le Carrou, J.L., Fabre, B.: Predicting the decay time of solid body electric guitar tones. J. Acoust. Soc. Am. **135**(5), 3045–3055 (2014)
41. Paté, A., Le Carrou, J.L., Navarret, B., Dubois, D., Fabre, B.: Influence of the electric guitar's fingerboard wood on guitarists' perception. Acta Acust. United Acust. **101**(2), 347–359 (2015)
42. Paté, A., Le Carrou, J.L., Teissier, F., Fabre, B.: Evolution of the modal behaviour of nominally identical electric guitars during the making process. Acta Acust. United Acust. **101**(3), 567–580 (2015)
43. Reissner, E.: The effect of transverse shear deformation on the bending of elastic plates. J. Appl. Mech. **12**, 69–77 (1945)
44. Rhaouti, L.: Fictitious domains for the modeling of a fluid-structure interaction problem. simulation of a kettledrum (in French). Ph.D. thesis, Université Paris Dauphine (1999)
45. Rhaouti, L., Chaigne, A., Joly, P.: Time-domain simulation and numerical modeling of the kettledrum . J. Acoust. Soc. Am. **105**(6), 3545–3562 (1999)
46. Richardson, B.E., Brooke, M.: Modes of vibration and radiation fields of guitars. In: Proceedings of the I. O. A., vol. 15(3), pp. 686–696 (1995)
47. Rossing, T.D.: Science of Percussion Instruments. World Scientific, Singapore (2000)
48. Thorin, A., Boutillon, X., Lozada, J.: Modelling the dynamics of the piano action: Is apparent success real? Acta Acust. United Acust. **100**(6), 1162–1171 (2014)
49. Woodhouse, J.: Plucked guitar transients: comparison of measurements and synthesis. Acta Acust. United Acust. **90**, 945–965 (2004)
50. Wright, H.: The acoustics and psychoacoustics of the guitar. Ph.D. thesis, University of Wales, College of Cardiff (1996)

Glossary

Acoustic Compliance An acoustic compliance is defined as the ratio of an acoustic-flow-rate difference to the time derivative of the acoustic pressure. It is the product of a mechanical compliance by the square of a cross-section area.

Acoustic Impedance An acoustic impedance is the ratio of an acoustic pressure to an acoustic flow rate (acoustic quantities are variations of physical quantities around a mean value). It is equal to the *mechanical impedance* divided by the square of the cross-section area. A *specific acoustic impedance* is a local quantity, i.e., the ratio of an acoustic pressure to an acoustic velocity, equal to an acoustic impedance multiplied by a cross-section area.

Acoustic Mass An acoustic mass is defined as the ratio of the acoustic pressure difference to the time derivative of the acoustic flow rate. It is the ratio of a mechanical compliance to the square of a cross-section area.

Acoustic Power The instantaneous acoustic power through a given surface is the product of an acoustic pressure and an acoustic flow rate. The *acoustic intensity* is a local vector, which is the product of an acoustic pressure by an acoustic velocity; the flow of an acoustic intensity through a surface is the acoustic power.

Duct Modes Duct eigenmodes are modes of a cavity of infinite extend in the longitudinal direction. The eigenfrequency spectrum is continuous. Their *cutoff frequency* is the eigenfrequency of the 2D transverse area. Above this frequency, the modes are *propagating*, while below this frequency, they are *evanescent*. A planar mode (with a zero cutoff frequency) exists when the walls are rigid.

Eigenmodes and Eigenfrequencies Eigenmodes are eigenfunctions of the linear operator that describes the vibrations, the domain of solutions being defined by the boundary conditions. Modes are functions of space (the so-called *modal shapes*, defined with a relative amplitude, only) multiplied by sinusoidal functions

A. Chaigne, J. Kergomard, *Acoustics of Musical Instruments*, Modern Acoustics and Signal Processing, DOI 10.1007/978-1-4939-3679-3

of time. The frequencies of these time functions are called the *eigenfrequencies* and correspond to the eigenvalues of the operator. For conservative systems, eigenmodes and eigenfrequencies are real. All points of the structure vibrate either in phase or in antiphase. In general, the eigenfrequencies are not harmonic, and thus the spectrum of the physical quantities (in free oscillations) contains partials. For a rigid-walled cavity, an acoustic uniform exists, with a zero eigenfrequency.

Field A variable *field* corresponds to the values of this variable taken at all points in space at a given time.

Forced Oscillations A vibrating structure is subjected to *forced oscillations* when it is excited by a source imposing a time dependence to (at least) one physical quantity in (at least) one point.

Free Oscillations A vibrating (or oscillating) structure is subjected to *free oscillations* if no source interacts with this structure, after cessation of an excitation. For a linear structure, the physical quantities can then be decomposed into *eigenmodes*.

Harmonics The harmonic components of a signal (or "harmonics") are integer multiples of a fundamental frequency. The graphical representation of the magnitude spectrum of a periodic signal shows equally spaced vertical lines. The period of the signal is equal to the inverse of its fundamental frequency or, if the amplitude of the fundamental frequency is zero, to the inverse of the distance between two consecutive harmonics.

Modal Expansion For a linear structure, one can expand the motion onto the modal shapes of the structure. The associated time functions are the generalized displacements (or modal participation factors).

Modes of Dissipative Systems For a dissipative system, the eigenfrequencies are complex, the time dependence of each mode is a damped sinusoid, and the modes are either real or complex. In the complex case, the structure points do not vibrate in phase and the shapes are not fixed in time (see Chap. 5).

Partials In general, the spectrum of a non-periodic signal is continuous, with possible salient components. These components are called *partials*, and are generally not equidistant.

Resonance Frequency For a sinusoidal excitation with a given amplitude, the response (for any other physical quantity) can reach a maximum at a given frequency, called *resonance frequency*: the resonance thus corresponds to the existence of a maximum effect for a given cause.

Self-sustained Oscillations A vibrating structure is subjected to *self-sustained oscillations* when it is excited by a non-oscillating (either continuous or slowly varying) source. This is a special case of nonlinear oscillations. After a transient regime, and depending on the excitation parameters, different types of *steady-*

state regimes may exist: periodic, quasi-periodic, chaotic, etc. The oscillation frequency of the periodic regime might correspond to one particular eigenfrequency of the structure, but the spectrum is composed of exact harmonics, even if the eigenfrequencies of the structure are not harmonic.

Signal A variable *signal* (or waveform) is the time history of this variable at a given point in space.

Spectrum The *spectrum* of a signal corresponds to its Fourier transform. For a periodic signal, it contains *harmonic* components only.

Author Index

A. Chaigne, J. Kergomard, *Acoustics of Musical Instruments*, Modern Acoustics and Signal Processing, DOI 10.1007/978-1-4939-3679-3

Subject Index

A. Chaigne, J. Kergomard, *Acoustics of Musical Instruments*, Modern Acoustics and Signal Processing, DOI 10.1007/978-1-4939-3679-3